

**Proceedings
of the
First Annual
WIRELESS Symposium**

JANUARY 12-15, 1993

SAN JOSE CONVENTION CENTER, SAN JOSE, CA

Sponsored by
Microwaves & RF and Electronic Design Magazines

Conference Proceedings

RF expo

EAST *October 19-21, 1993*
Tampa Convention Center
Tampa, Florida

Sponsored by **RF design** *Magazine*



Proceedings of the First Annual *WIRELESS* Symposium

JANUARY 12-15, 1993

SAN JOSE CONVENTION CENTER, SAN JOSE, CA

Sponsored by
Microwaves & RF and Electronic Design Magazines

Copyright c 1993
Penton Publishing
All rights reserved

Penton Publishing
611 Route 46 West
Hasbrouck Heights, NJ 07604
TEL: (201) 393-6289
FAX: (201) 393-6297



Conference Proceedings

RF expo

EAST

October 19-21, 1993
Tampa Convention Center
Tampa, Florida

Copyright © 1993
Argus Business
All rights reserved

Argus Business
6300 S. Syracuse Way
Suite 650
Englewood, Colorado 80111
(303) 220-0600

Sponsored by **RF**design Magazine

SPECIAL THANKS

I would like to acknowledge the technical advisers and program chairpeople listed below. Their expertise, support, and guidance leading to and during the *WIRELESS Symposium* made the conference one of lasting technical merit and untold value to the high-frequency engineering community. I would also like to acknowledge the *WIRELESS Workshop* lecturers for their time and efforts: Richard Webb of Webb Laboratories (Hartland, WI), Donald Steinbrecher of Steinbrecher Corp. (Woburn, MA), Fred Harris of San Diego State University (San Diego, CA), and Jack Holtzman of Rutgers University WINLAB (New Brunswick, NJ).

In addition, much thanks are also owed to Paul Khanna of Hewlett-Packard/Avantek (Milpitas, CA), a friend whose help and encouragement eased the difficult days of planning prior to *WIRELESS*. Special thanks also go to a special friend, David Sprague of The Strategy Group (Martinez, CA), for helping to make *WIRELESS* successful with his characteristic display of technical knowledge and boundless energy.

Last, but certainly not least, special thanks to John Carroll, Publisher of *Electronic Design* magazine, without whom there would be no *WIRELESS Symposium and Exhibition*.

Jack Browne, Microwaves & RF
Technical Program Chairman

Technical Advisers

Raymond L. Camisa, David Sarnoff Research Center (Princeton, NJ)
Robert P. Denaro, Trimble Navigation (Sunnyvale, CA)
Jack Holtzman, Rutgers University, WINLAB (New Brunswick, NJ)
J. Eric Janson, AT&T Microelectronics (Reading, PA)
Keith Kaczmarek, NEXTEL Communications, Inc. (Fleet Call) (Lafayette, CA)
Dan Millicker, Hewlett-Packard Co. (Newark, CA)

Program Chairpeople

Ian Bruce, Analog Devices (Norwood, MA)
Robert Dietz, Microwave Printed Circuitry (Lowell, MA)
Keith Kaczmarek, NEXTEL Communications, Inc. (Fleet Call) (Lafayette, CA)
Mark McDonald, National Semiconductor (Santa Clara, CA)
Dan Millicker, Hewlett-Packard Co. (Newark, CA)
Raymond Pengelly, Compact Software (Paterson, NJ)
Randy Roberts, The Spread-Spectrum Scene (El Granada, CA)
Tim Shroyer, FEI Communications (Sunnyvale, CA)
David Sprague, The Strategy Group (Martinez, CA)
Ben Zarlingo, Hewlett-Packard Co. (Everett, WA)

Technical Proceedings of the First WIRELESS Symposium and Exhibition

ADVANCED MATERIALS FOR WIRELESS APPLICATIONS....1

Fabrication Technology for Advanced Materials, Robert Deitz, Microwave Printed Circuitry (Lowell, MA).....	2
Copper-Foil-Clad Laminates and Substrates for Commercial Applications, John Frankosky, Arlon, Microwave Materials Division (Bear, DE).....	5

FROM ANTENNA TO DSP: COMPONENTS FOR RF/IF SIGNAL PROCESSING ... 15

Analog Signal Processing: Mixers and AGC Amplifiers,* Barrie Gilbert, Eberhard Brunner, Tom Kelly, and Bob Clarke, Analog Devices, Inc. (Norwood, MA).....	16
Analog-to-Digital and Digital-to-Analog Conversion: Digitizing at IF and DDS,** Scott Behrorst, Analog Devices, Inc. (Greensboro, NC).....	N/A
Digital Signal Processing in Wireless Communications: Focus on Digital Transmitters, Dan Ash, Analog Devices, Inc. (Campbell, CA)	40

*Paper presented by Bob Clarke.

**Revised paper to appear in *Microwaves & RF*, July 1993.

LUMPED AND DISTRIBUTED CIRCUITS FOR WIRELESS COMMUNICATIONS... 48

Key Topics In Radio System Design, John G. Freed, Teletec Corp. (Raleigh, NC).....	49
A 2-GHz BiCMOS Low-Noise Amplifier and Mixer, Dave Bien, National Semiconductor, Wireless Communications Group (Santa Clara, CA).....	56
High-Efficiency Crystal Oscillator at High Frequencies, Sheng H. Lee and Alvin K. Wong, Philips Semiconductors (Sunnyvale, CA).....	62
A 2.2-GHz, PLL Frequency Synthesizer, Thom Luich, Thai Nguyen, Craig Davis, David Byrd, Eric Lindgren, Rob Rodriguez, Maggie Speers, and Eli Miller, National Semiconductor (Santa Clara, CA).....	68
A 3-V Analog Audio-Processing Chipset for Battery-Operated Systems, Omar Saleh and Saeed Navid, Philips Semiconductors (Sunnyvale, CA)	72

AUTOMOTIVE ELECTRONICS SYSTEMS AND MEASUREMENTS... 77

Coaxial Vector Network Analysis Through 67 GHz: Addressing Millimeter-Wave Commercial Applications, Todd Antes, Wiltron Co. (Morgan Hill, CA).....	78
Monolithic Components for 77-GHz Automotive Collision-Avoidance Radars, Lamberto Raffaelli, Alpha Industries (Woburn, MA).....	86
110-GHz Wafer Probe Enables Cost-Effective Millimeter-Wave Circuit Applications, Edward M. Godshalk, Cascade Microtech, Inc. (Beaverton, OR).....	92
Device Characterization with an Integrated On-Wafer Thermal Probing System, Dan d'Almeida, Cascade Microtech, Inc. (Beaverton, OR) and Robert Anholt, Gateway Modeling (Minneapolis, MN).....	103

INTEGRATED-CIRCUIT TECHNOLOGIES FOR WIRELESS APPLICATIONS... 108

Direct Versus Dual Conversion Quadrature (Vector) Modulation, Mark Rehorst, Hewlett-Packard Co., Communications Components Division (Newark, CA).....	109
Silicon Bipolar RF Integrated Circuits for Cellular Radio and Wireless Applications, Nhat Nguyen, James N. Wholey, and Madhu Avasarala, Hewlett-Packard Co., Communications Components Division (Newark, CA).....	117

TABLE OF CONTENTS

Session A-1, B-1 — Digital Communications and DSP

An ISM Band Design for WLAN and PCS
Robert J. Zavrel
GEC Plessey Semiconductors.....1

Integrated Modem/RF Design Architectures for Reduced Power, Increased Capacity F-QPSK Wireless Systems
Kamilo Feher
University of California, Davis.....N/A

A DSP Microprocessor Based Receiver for a Cosine Transition-shaped BPSK Signal
Bruce H. Williams, Roy E. Greeff
Paramax Systems Corp.....8

Designing a High Performance Monolithic Digital BPSK Modulator
Frank Hayden, Robert J. Zavrel
GEC Plessey Semiconductors.....16

Session A-2, B-2 — Test & Measurement

Methods for Estimating and Simulating the Third Order Intercept Point
Carl Stuebing, Moji C. Chian
Harris Semiconductor.....22

Low Cost Phase Noise Measurement Technique
Jim H. Walworth
Tampa Microwave Lab, Inc.....32

Externally-Induced Transmitter Intermodulation: Measurement and Control
Ernie Franke
E-Systems ECI Division.....38

A 3 GHz 50 Ohm Probe for PCB Measurements
Joel Dunsmore, Hewlett-Packard Co;
Robert Kornowski, Motorola;
Chuck Tygard, Everett-Charles Tech.....45

Low Cost RF Tuner System for JDC Load Pull and SSPA Design
Christos Tsironis, Dominique Dubouil
Focus Microwaves Inc.....65

Noise Figure and Gain Measurement on High Speed Bipolar Junction Transistors
Wayne Jung, Tektronix, Inc.;;
Paul Van Halen, Portland State Univ.....72

Session A-3, B-3 — Essential RF Circuits

The Current-Feedback Op Amp – A High-Speed Building Block
Anthony D. Wang
Burr-Brown Corporation.....82

The SLAM: A New Ultra-linear Power FET Module Concept for HF Applications
Adrian I. Cogan, Lee B. Max, Al Rosenzweig
MicroWave Technology, Inc.....92

Tradeoffs in Practical Design of Class E High-Efficiency RF Power Amplifiers
Nathan O. Sokal, Laszlo Drimusz, Design Automation;
Istvan Novak, Technical University of Budapest100

High Power, Low Frequency Microstrip Switches
S. Irons, E. Higham
M/A-COM.....N/A

Class-E Power Amplifier Delivers 24 W at 27 MHz at 89-92% Efficiency, Using One Transistor Costing \$0.85
Nathan O. Sokal, Ka-Lon Chu
Design Automation.....118

A UHF/L-Band FET Module for Pulsed Power Avionics Applications
Frank Sulak, Ken Sooknanan, Toru Nakamura,
Al Rosenzweig, Adrian I. Cogan
MicroWave Technology, Inc.....128

Session C-1, D-1 — Wireless Personal Communications

Frequency Synthesizer Strategies for Wireless
Bar-Giora Goldberg
Sciteq Electronics, Inc.....137

TDMA Transmitters — Characterizing Power, Timing and Modulation Accuracy
Helen Chen
Hewlett-Packard Co.....145

Performance Simulation of a Low-Power In-Building Wireless Centrex System
Douglas Alston
BellSouth Telecommunications.....N/A

Practical Applications of a Low Cost Low Noise GaAs PHEMT MMIC for Commercial Markets
Al Ward, Henrik Morkner
Hewlett-Packard Co.....163

Highly Integrated GaAs MMIC RF Front End for PCMCIA PCS Applications
J. Mondal, S. Geske, T. Kotsch, A. Landrie, G. Dietz,
E. Bogus, J. Blubaugh, S. Moghe
Northrop Corp.....169

Low Power Transmitter Design Using SAW Devices
Earl E. Clark
RF Monolithics, Inc.....175

Session C-2, D-2 — Specialized Design Techniques

FMCW Radar Architecture
Ken Puglia
M/A-COM.....N/A

Filter Comparator Network for Beam Position Monitoring
Michael Ferrand, Mark McWhorter
Lorch Electronics.....181

A Silicon Bipolar Mixed-Signal RFIC Array for Wireless Applications, Bob Koupal, Keith Carter, and Kevin Negus, Hewlett-Packard Co., Communications Components Division (Newark, CA).....	132
Wireless Applications for GaAs Technology, Michael Frank, Henrik Morkner, and Craig Hutchinson, Hewlett-Packard Co., Communications Components Division (Newark, CA).....	143
Low-Cost, High-Performance Receiver for Wireless Applications, Brian Kirk, California Eastern Laboratories, Inc. (Santa Clara, CA).....	154

TECHNOLOGIES FOR CELLULAR COMMUNICATIONS 159

Power Products for Cellular Telephone Handsets, William Mueller, Hewlett-Packard Co., Communications Components Division (Newark, CA).....	160
Cellular and PCS TDMA Transmitter Testing with a Spectrum Analyzer, Larry Nutting, Hewlett-Packard Co., Microwave Instruments Division (Santa Rosa, CA).....	172
Error-Free Mobile Data Communications: Principles and Protocols, Parviz Yegani, IBM Networking Systems (Research Triangle Park, NC).....	179
GaAs MESFET Direct Quadrature Modulator Integrated Circuit for Wireless Communications Systems, Chris Fisher, RF Micro Devices, Inc. (Greensboro, NC).....	200
System Aspects and RF Component Design for European Mobile Communication System, Dr. Ing. Vinod Kumar,* Alcatel Radiotelephone (Colombes, France).....	205

**Paper presented by Eric Botherel, Alcatel Radiotelephone (Colombes, France)*

VSAT, GPS, AND DBS TECHNOLOGIES.... 215

VSAT Performance Fits Market Niche Applications, Tim Shroyer, FEI Communications, Inc. (Sunnyvale, CA).....	216
The Integration of GPS and a Wide Area Cellular Packet Data Network, John Lawler, Cellular Data, Inc. (Palo Alto, CA).....	N/A
Environmental Effects on Mobile Satellite Communications, Dennis A. Jiraud, Defense Systems, Inc. (McLean, VA).....	228
Synthesizers for VSAT Applications,* Uri Yariv, Communication Techniques, Inc. (Whippany, NJ).....	N/A
A New Variable-Rate Vocoder for Wireless Communications and Voice Storage Applications, Steve Morley, QUALCOMM, Inc. (San Diego, CA).....	238

**Revised paper to appear in *Microwaves & RF*, August 1993.*

COMPUTER-AIDED ENGINEERING AND PCN COMPONENTS.... 250

Simulating Digital Radio Performance Using the HP Microwave Design System, Kirt Kisling and John Hirsekorn, Hewlett-Packard Co. (Santa Rosa, CA).....	251
The Design of Low Power Consumption RF Circuits for Digital European Cordless Telephones Using Microwave Harmonica, Raymond S. Pengelly, Compact Software (Paterson, NJ).....	275
An Integrated Microwave Radio Transceiver for WLAN Applications, David A. Williams, GEC Plessey Semiconductors (Microwave Division, Lincoln, United Kingdom).....	305
GMIC Planar Mixers for Communications Applications, Paul J. Schwab and Timothy A. Murphy, M/A-COM, Inc. (Burlington, MA).....	314
GMIC Interdigital Filters for Microwave Applications, Holly A. LaFerrara, M/A-COM, Inc., IC Design Center (Lowell, MA).....	318

DUAL-USE TECHNOLOGIES.....323

Affordable Intelligence/Direction-Finding Systems for Military and Civil Enforcement Missions, Dr. Nicholas Cianos, Delfin Systems (Santa Clara, CA).....	N/A
---	-----

<i>Digital Temperature Compensation of Oscillators Using a Mixed Mode ASIC</i> Steve Fry Murata Electronics North America	186	<i>Analysis of Transversely Coupled SAW Resonator Filters Using Coupling of Modes Technique</i> V. Narayanan and S. M. Ritchie University of Central Florida	282
<i>A Synthesizer Design Program With Detailed Noise Analysis</i> Terrence Hock National Center for Atmospheric Research	195	Session E-3 — Practical RF CAD	
<i>PLL Settling Time: Phase vs. Frequency</i> Donald E. Phillips Rockwell International	204	<i>Basics of CAD at RF for Wireless Circuits and Subsystems</i> Ray Pengelly Compact Software	N/A
<i>Linear Frequency Modulation – Theory and Practice</i> Bar-Giora Goldberg, Henry Eisenson Sciteq Electronics, Inc.	208	<i>Defining Circuit and Subsystem Specifications for Cordless Telephone Applications</i> Ray Pengelly Compact Software	N/A
Session C-3, D-3 — Analytical Methods		<i>Design Examples of Small-Signal Circuits Operating from 3.3 to 4.5-Volt Supplies</i> Ray Pengelly Compact Software	N/A
<i>RF Active Device Modeling for CAD, A Coming Necessity</i> Gary Roberts Hewlett-Packard Co.	212	<i>Design Examples of Large-Signal Circuits</i> Ray Pengelly Compact Software	N/A
<i>Regression Based Algorithms for Inductor Modeling</i> Edmund (Joe) Tillo Ford Motor Company	217	<i>Using CAD for Circuit Layout and Packaging Design</i> Ray Pengelly Compact Software	N/A
<i>Computer Aided Design Tools for Small Signal Matching Networks</i> Michael Rothery, Sam Ritchie, Madjid A. Belkerdid University of Central Florida	223	EXPO PLUS SESSION 1 — Satellite and Space Systems	
<i>SAW Resonator Oscillator Design Using Linear RF Simulation</i> Alan R. Northam RF Monolithics, Inc.	235	EXPO PLUS SESSION 2 — Components for Space Applications	
<i>Embedding RF Design Tools in an IC Design System</i> Mojoy C. Chian, Steve S. Majors, Alan G. Whittaker Harris Semiconductor	242	<i>Designing Microwave Circuits for Geosynchronous Space Applications</i> Ronald Ogan TRAK Microwave Corp.	297
<i>Electromagnetic Simulation for High-Frequency Planar Circuits</i> Daren McClearnon Hewlett-Packard Co.	250	<i>Low Cost Plated Plastic Diplexers For Use In Commercial Mobile Satellite Communications</i> Chip Scott Teledyne Microwave	301
Session E-1 — Wireless Applications		EXPO PLUS SESSION 3 — Satellite and Space Systems	
<i>A Monolithic 915 MHz Direct Sequence Spread Spectrum Transmitter</i> Stephen Press, Jeff Barry, Jim Marsh Tektronix, Inc.	259	<i>Satellite Channel Utilization in the Presence of Rain Attenuation</i> Kaivan A. Karimi, Valentine Aalo Florida Atlantic University	304
<i>A Low Power RFID Transponder</i> Raymond Page Wenzel Associates, Inc.	266	<i>Hardware Verification of Communication System Simulations</i> Henry F. Helmken Florida Atlantic University	319
Session E-2 — RF Circuits and Systems		<i>GFO Water Vapor Radiometer</i> Muhammad A. Malik E-Systems, Inc.	322
<i>Multi-Component Module for High Speed Passive Design</i> Mark Brooks Thin Film Technology	270		
<i>Design of a Search Based PLL</i> Michael F. Black Texas Instruments	275		

Microwave Instrumentation: In Transition from All Bells and Whistles to Just Enough for the Job, John Minck, Hewlett-Packard Co. (Palo Alto, CA).....	324
Applications of Microwave Power Tubes, Glen Hoffman, Varian Microwave Tube Products (Palo Alto, CA).....	N/A
Affordable MMIC Power Amplifier for 2.4 and 5.8 GHz Spread Spectrum Applications, T. Apel, R. Bhatia, H. Sun, and S. Ludvik,* Teledyne Microwave (Mountain View, CA).....	327
Affordable Dual-Use Direction-Finding (DF) Receiver, Toshikazu Tsukii, Raytheon Co., Electromagnetic Systems Division (Goleta, CA).....	N/A

**Paper presented by Ratan Bhatia.*

MEASUREMENT TECHNIQUES FOR WIRELESS SYSTEMS 337

A Better Way to Design Tomorrow's Wireless Communications Systems Using RF Analyzers with Advanced Digital Signal Processing (DSP) Ben Zarlingo, Hewlett-Packard Co., Lake Stevens Instrument Division (Everett, WA).....	338
Applying the Modulation Domain to Wireless Communication Testing, Barry Dropping, Hewlett-Packard Co., Santa Clara Div. (Santa Clara, CA).....	344
Measuring the Peak-to-Average Power of Digitally-Vector-Modulated Signals, Charles Meyer, Boonton Electronics (Randolph, NJ).....	351
Delay-Spread Measurements and Feher's Bound for Digital PCS and Mobile Cellular Systems, Dr. Kamilo Feher, DIGCOM, Inc. (El Macero, CA) and University of California at Davis (Davis, CA).....	355

PERSONAL COMMUNICATIONS SYSTEMS (PCS)367

GaAs MMICs for PCS Applications, Charles Huang, ANADIGICS, Inc. (Warren, NJ).....	368
A High-Efficiency GaAs MMIC Power Amplifier for 1.9 GHz PCS Applications, John Wachsman, Pacific Monolithics, Inc. (Sunnyvale, CA).....	372
Low-Cost Surface-Mount Mixer for PCS Applications, Shankar R. Joshi, Synergy Microwave Corp. (Paterson, NJ).....	378
Frequency Synthesizer Strategies for Wireless, Bar G. Goldberg and Henry Eisenon,* Sciteq Electronics (San Diego, CA).....	387
A 2.4-GHz Single-Chip Transceiver, L. M. Devlin, B. J. Buck, J. C. Clifton, A. W. Dearn, and A. P. Long, GEC-Marconi Materials Technology Limited (Caswell, Towcester, Northands, United Kingdom).....	395

**Paper presented by Henry Eisenon.*

WIRELESS DATA AND PERSONAL COMMUNICATIONS 403

Demodulating at 10.7 MHz IF with the NE/SA605/625, Alvin K. Wong, Philips Semiconductors (Sunnyvale, CA).....	404
Review of Technologies and Key Issues for Wireless Local Area Networks, Greg Hopkins, Windata, Inc. (Northboro, MA).....	415
A Low-Current UHF Remote-Control System Using a SAW-Based Superhet Receiver, Matthias Bopp, TEMIC Telefunken Electronic GmbH (Heilbronn, Germany).....	424
Comparison of Path Loss Performance of a Leaky Feeder Cable vs. a Distributed Antenna, Jim Ford, Robert Perelman, and D. Lang, Times Microwave Systems (Wallingford, CT).....	435
Low-Cost F-QPSK Modem Radio Solutions for Doubling the Capacity of European Standard Cellular/PCS Systems, P.S.K. Leung, Digital Communications Laboratory, Department of Electrical and Electronic Engineering, Victoria University of Technology (Footscray, Melbourne, Victoria, Australia) and Kamilo Feher, DIGCOM, Inc. (El Macero, CA) and The University of California at Davis (Davis, CA).....	443

An ISM Band Design for WLAN and PCS

Robert J. Zavrel

Worldwide Applications Manager, WLAN Products

GEC Plessey Semiconductors

1500 Green Hills Road

Scotts Valley CA 95066

1. Introduction

To realize the promise of personal wireless communications on a massive scale, a complex set of business, political, and technical issues must be resolved. New frequency allocations seem to be a certainty within the next few years. However, by using the existing ISM bands reliable and economic systems can now be configured addressing very large volume markets. This paper presents the design methodology for such a system.

The three Industrial, Scientific, and Medical band allocations (ISM bands) in North America are quite attractive for a wide range of would-be wireless services. These bands not only pose the opportunity but also design challenges to realize effective systems. FCC regulations permit up to one watt of RF output power without requiring a license. In order to facilitate *some degree* of interference rejection in a license-free environment, spread spectrum techniques are mandated. The two types of spread spectrum techniques that are permitted are frequency hopping and direct sequence. Much has been written over the past few years about these two techniques and the reader can seek the references for background information. (Ref. 1 & 2).

2. Architecture Considerations

In order to optimize an architecture one of three bands and one of two spread spectrum techniques must be chosen. A complex set of system trade-offs must be considered in this decision-making process. A review of the status of the three bands, together with design considerations can lead to a rational choice.

The 902 MHz band was recently labeled "the kitchen sink band" (Ref. 3). This is indeed an accurate description. Multiple users include radiolocation services, amateur radio, fixed and mobile services and AVM. In addition, the FCC has proposed wind profile radars and AVM for the entire band. Furthermore, the 902 MHz band is only available in North America limiting its desirability for most high volume manufacturers. This band, however, has the advantage that silicon devices can be used efficiently in both the receiver front ends and transmitter PAs. Use of this band for PCS and/or WLANs is tenuous at best.

The 2.4 GHz band is partially allocated to amateur radio. Microwave ovens also operate in this band. However, compared with the 902 MHz band, these users are comparatively benign. Another major advantage of the 2.4 GHz band is that allocations exist within the 2.4 to 2.5 GHz band in North America, Europe, and Japan. For these reasons the 2.4 GHz band was chosen for our design solution.

The 5.8 GHz band is also attractive, but the higher operating frequency offers greater design and manufacturing problems and higher power consumption. This band might be quite interesting for future generation products, if exclusive PCS/WLAN bands are not allocated in the near future.

Having chosen the 2.4 GHz ISM band the question of which spread spectrum technique remains. There are two basic spread spectrum techniques: direct sequence and frequency hopping. In contrast to direct sequence systems, frequency hopping systems offer better immunity to interference. In short, a direct sequence system relies totally upon processing gain (and the resulting jamming margin specifications) to reject in-band interference.

$$G(p) = 10 \log B_s/R_d$$

where $G(p)$ is the processing gain, B_s is the spreading bandwidth, and R_d is the data rate and

$$M_j = G(p) - (L + (S/N))$$

where M_j is the jamming margin, L is system losses, and S/N is the signal-to-noise ratio necessary to maintain a given bit error rate (BER) or error probability (P_e).

These equations are fundamental to direct sequence systems. Indeed, even low data rate direct sequence systems mandate the use of sophisticated power level control of all transmitters operating in band. The unpredictability of the ISM band environment typically renders direct sequence systems unreliable for use in these bands. There may be some special circumstances where direct sequence can be the technique of choice, but the interference trade-off is

omnipresent. Perhaps the most important mitigating circumstance is for data rates exceeding about 2 Mb/sec. It is difficult to achieve over 2 Mb/sec. with frequency hoppers while maintaining the initial advantages of the hopping system. However, as data rates increase in the direct sequence system, the vulnerability also increases. Furthermore, for each doubling of data rate, the system noise figure increases by 3 dB resulting in a net reduction in range. These might be an acceptable trade-offs, particularly if communications is intended for very short ranges, perhaps under 3 meters. However, for most practical applications, the data rate in ISM applications is limited to about 2 Mb/sec.

Frequency hopping systems rely upon the more traditional techniques of radio receiver design: dynamic range, sensitivity and selectivity. These basic specifications, in turn, reflect such specifications as noise figure, local oscillator spectral purity, filter skirts, and intermodulation. In contrast, in-band selectivity in direct sequence systems relies completely upon processing gain.

For example, in a typical ISM direct sequence system, 5 dB of jamming margin is typical (for 800 kb/sec data rates, $10E-5$ BER, operating in the US 2.4 GHz ISM band). In contrast, frequency hopping systems easily provide 60 dB of ultimate rejection by using cascaded SAW filters. Under some circumstances the LO phase noise can become more constraining than the IF filter skirts. In frequency hopping systems, a narrow-band interferer might "wipe out" several hopping channels. With proper coding, however, individual "packets" can be recovered despite the loss of a considerable number of hopping channels (Reference 4). In the direct sequence case, if the interferer exceeds the jamming margin of the system, the bit error rate (BER)

Advanced Materials for Wireless Applications

Session Chairperson: Robert Deitz,
Microwave Printed Circuitry (Lowell, MA)

Fabrication Technology for Advanced Materials, **Robert Deitz,**
Microwave Printed Circuitry (Lowell, MA)..... **2**

Copper-Foil-Clad Laminates and Substrates for Commercial
Applications, **John Frankosky,** Arlon, Microwave Materials
Division (Bear, DE)**5**

begins to increase. Further reduction in interference will upset the link and communications will be lost completely rather than a percentage of packets. Some direct sequence systems combine frequency channelization to provide filter selectivity in addition to processing gain. However, it is our conclusion that once frequency division schemes must be employed, the designer might as well limit bandwidth to the baseband and realize the full advantages narrow-band systems offer. In other words, use frequency hopping.

Direct sequence systems can be very attractive *only* in a pristine wide band where all in-band transmitters are rigidly controlled. Direct sequence systems **must** control all transmitters' power output in real time, or one or more transmitters are likely to interfere with each other. Thus, direct sequence systems must assume that all users of the spectrum within range will conform to that system's control mechanisms. If any signal source appears in-band that exceeds the jamming margin of a receiver, the bit error rate or the link itself will be compromised. Of course, this premise is not possible to attain within the ISM bands. Indeed, even with exclusive use of a band complex control mechanisms are required to control the real-time power outputs of the transmitters. Furthermore, these control mechanisms compromise the power consumption and price of the system. The ISM bands are anything but pristine. Indeed the ISM bands are hostile communications environments requiring excellent interference-avoidance techniques. The ISM band environment is not unlike circumstances presented to electronic warfare (EW) designers. It is interesting to note that tactical military communications systems typically use frequency hopping techniques to mitigate enemy jammers. Figure 1 shows in-band equivalent selectivity for the 83 MHz-wide 2.4 GHz band for various data rates of direct sequence systems

contrasted against a frequency hopping system. The jamming margin numbers are based on 10 dB necessary C/N ratio for 10 E-5 BER and 5 dB system loss.

3. System Requirements

Having settled upon 2.4 GHz frequency hopping as the architecture of choice, a detailed design analysis can now proceed. In order to "open" the very high volume data and voice communications markets certain criteria must be met in the design solution:

Power consumption: about 350 mW in receive mode

Cost: under \$100.00 for high volume (>500K/year)

Size: PCMCIA form factor (about 2x3 inch circuit board)

Performance:

A. Data Rate: up to 1 Mbit/second

B. Dynamic range: >60 dB (defined by filter skirts, noise figure, and compression point)

C. Dual antenna diversity

D. Receiver noise figure: <10 dB

E. double conversion superhet design for outstanding adjacent channel rejection

F. Tx-to-RX and RX-to-TX time <4 uS

G. Hopping settling time: <100uS

H. RF Power Output: selectable 10 or 100 mW.

The extremely fast transmit-receive transition time and hopping speed permits the use of state-of-the-art control algorithms and excellent acquisition times. Double conversion minimizes image response, permits the use of two SAW filters for outstanding selectivity, and permits limiting and detection at the optimum frequency.

REVIEW OF FABRICATION TECHNOLOGY FOR ADVANCED MATERIALS

ROBERT DEITZ
MPC, INC
LOWELL, MA

1. MATERIALS FOR HIGH FREQUENCY USES

- A. Frequency ranges 500 MHz - above 20 GHz
- B. Dielectric constant control
- C. Low loss tangent
- D. Uniform properties
- E. Comparison to standard PCB materials

2. ARTWORK PREPARATION

- A. Rubylith - cut and peel method, accurate but more expensive these days.
- B. Hand taping not recommended for microwave applications due to rough edges and tape overlaps.
- C. 1:1 film - prepared by either a reduction of rubylith or from photoplot.
- D. Film or Glass - Must use stable polyester based film. OK for short runs, but for long term stability should be put onto glass. Use as a master.
- E. Laser plotting - fast and reasonably inexpensive. Plotter should have at least a $\frac{1}{4}$ mil pixel size. Must examine corners carefully, no stairstep around the radius.
- F. Etch compensation - needs to be added to compensate for etch factor. Can be added by micro-modification, or when plotting or cutting the master. Typically will use a $\frac{1}{4}$ mil per side for $\frac{1}{2}$ oz. copper and a $\frac{1}{2}$ mil per side for 1 oz. copper. This would be for straight print and etch. For plated through boards little or no compensation is needed due to the plating used as an etch resist.

3. IMAGING

- A. Two types of resist available - dry film photoresist and wet, dip coated photoresist. Method of application is different for each resist.
- B. Dry film photoresist is used for plated-through hole boards, or when plating from an alkaline plating bath.
- C. Wet film photoresists are used primarily for print and etch processes or when plating certain acid plating baths.
- D. Due to the thinner coating of the wet film resist, it has better resolution capabilities than the dry film resists. With wet resists it is possible to etch a 2 mil line or space on $\frac{1}{2}$ oz. copper which would be difficult with dry film resists.

Most of the end-use system requirements such as range, BER, data rate, and reliability reduce to the set of RF specifications listed above. These specifications, in turn, must conform to the power, cost and form factor requirements. These combined specifications reflect a fairly high performance microwave transceiver built on a credit card from full custom devices, selling for under \$100.00. This challenge has been met with the GEC Plessey DE6003. A microwave transceiver on a credit card sized circuit board with the above set of specifications speaks for itself as a state-of-the art design.

4. RF Transceiver Description

The DE6003 represents the most advanced license-free radio data transceiver available for low power, low cost, miniature packaged and high performance applications. These transceiver modules are designed for portable battery-operated data or voice communications equipment. For example, lap-top and hand-held computers, cordless telephones, point-of-sale, inventory, security, and medical equipment can utilize these modules to great advantage. Figure 2 shows an interface block diagram of the DE6003 with power supply, antenna, and digital control bus.

Figure 3 shows an RF functional diagram with divisions of the integrated circuits delineated. Three PLL synthesizers run continuously to provide the very high hopping and TX/RX speeds. A patented divide-by-two switch is used in the transmit loop to prevent interference into the receiver IF. Dual conversion facilitates excellent selectivity and image rejection.

The DE6003 covers 2.400 to 2.500 GHz and utilizes a binary Gaussian frequency shift keying modulation scheme (GFSK). GFSK has several distinct

advantages over alternative baseband schemes. The IF systems do not require linearity and the complications involving AGC design. Limiters are easy to design and manufacture and signal strength indication (RSSI) is also relatively easy to realize. In the hostile ISM environment with interference and multipath distortion, GFSK also provides a effective and simple solution. Simplicity, manufacturability, low cost, and low power consumption are all inherent characteristics of GFSK systems. The main disadvantage of GFSK is a comparatively low bit/Hz/sec specification (typically 0.7 bits/Hz/sec.). Also, M-ary FSK, particularly 4FSK can be used to increase data rates well above 1b/Hz/sec. and is being investigated for second generation products. However, most of the current high volume market applications require well under 1Mb/sec. rates, reflecting the DE6003 specifications.

Early in the design stage of the transceiver it was realized that the effort would necessitate full custom integrated circuits. During innumerable design reviews power consumption (milliwatt by milliwatt) and cost were traded-off the various performance requirements (data rate, dynamic range, speed and others). GEC Plessey's design effort was greatly enhanced in that the IC, filter, and system designers all report through the same program manager. Consequently, optimum designs were possible from the various processes used while maintaining tight scheduling. Aggressive pricing was realized because all the critical components for the transceiver are fabricated within the same company. The radio takes full advantage of the three most important semiconductor manufacturing processes: GaAs, high speed bipolar, and CMOS.

World-class design people and facilities exist within GEC Plessey's multiple facilities. (GEC Lincoln started

4. ETCHING

- A. High frequencies require close control of line widths which in turn requires close tolerances. Standard tolerances for print and etch are $\pm \frac{1}{2}$ mil on 1 oz. copper and ± 1 mil on 1 oz. copper. For parts with plated through holes the tolerances are ± 1 mil for $\frac{1}{2}$ oz. copper and ± 1.5 mils for 1 oz. copper.
- B. The geometry of the etched line is important in that the design equations depict ideally a rectangular line where in reality the line is more trapezoidal shaped. The closer the line is held to the rectangular shape, the more closely the design parameters will be met. The importance in etching is not just the complete removal of the copper in the unwanted areas, but to do this while maintaining a good line geometry. This requires very close control of the etching and process parameters.
- C. With circuits used at microwave frequencies, the finished line width is always measured at the base of the line, not at the top surface. If the etching is properly done this should represent the true line width.
- D. Due to the dimensional stability of various materials it is necessary to use additional processes to control the movement of the substrate. During etching, the materials, particularly thinner substrates, will change dimensionally. This change causes problems when trying to maintain accurate positioning of the circuits, especially with bonded striplines. A double etching technique can be used to minimize this change. This involves a two step etching process. The first etch is with an oversize artwork to remove the bulk of the copper to be etched. This is followed by a heat cycle to further stabilize the material. The final circuit pattern is then etched. This process will generally stabilize most materials and prevent further movement.

5. PLATING

- A. Drilling and machining parameters have a direct effect on the plating of the PTFE based materials. Different speeds and feed rates must be used than are used for epoxy based materials. Due to the variety of materials, woven, non-woven, and ceramic filled, the parameters need to be adjusted for each of the materials. It is best to determine empirically the best parameters for your companies equipment and processes.

in the microwave business during World War II manufacturing point contact diodes for early radar sets.) Since then, the company has built a very impressive array of RF integrated circuits encompassing markets from consumer to space qualification. Traditional strengths have included synthesizers and low power RF integrated circuits, both critical to successful specification conformance.

The WLAN development program was broken into three stages:

1. Proof of concept (completed March, 1992)
2. System development "Alpha" units (completed September, 1992, DE6002)
3. Production prototype samples (available February 1994, DE6003)

"Beta" units of the DE6003 are currently being evaluated and design-ins are taking place in many companies.

The next generation of specifications will require MCM (multi-chip module) technology. The notion of a monolithic WLAN radio with the above specifications is currently not possible. Optimum performance must be realized by using optimum processes and designs for each function. There are no silicon processes currently available that meet all these requirements. Furthermore, Bi-MOS processes have limited advantages in meeting overall system objectives.

5. Digital Control Interface

Table 1 shows the details of the digital control interface. All interface functions to the DE6003 use standard CMOS levels. All the interface connections are digital except where otherwise noted. The digital control interface allows direct control of the radio's

functions. The digital hardware that interfaces to the radio can be tailored to any specific application and any set of regulations. Consequently the DE6003 affords the system designer great flexibility for data, voice, and even video transmission systems. All the remaining circuitry to complete a data communications transceiver can be implemented in a CMOS ASIC.

TABLE 1

TXD: Serial data input to the transmitter

RXD: Serial data output from the receiver

SYNLOCK: Indicates when all PLL synthesizers are locked

RADON: On/off switch for the radio

PLC: Power level control selects either 10 or 100 mW transmitter RF output

DSEL: Diversity select one of the two antennas

PAON: On/off switch for the PA transmitter stage

TXB/RX: Selects either transmit or receive modes

CLK: 10 MHz clock output (200 mV PTP)

RSSI: Received signal strength indicator (analog voltage proportional to dB received signal level).

LOADBAR: Loads frequency channel select

CHANNEL SELECT: Parallel seven bit word defines frequency used by the radio from 2.4 to 2.5 GHz.

6. Antenna and EMI Considerations

Placing the antenna on the circuit board is not acceptable because the radio would require shielding to prevent unwanted radiation from the radio circuitry. Also, the optimum placement of the antenna is typically not the optimum place for the radio proper. Maximizing receiver and transmitter performance only to compromise the effort by poor antenna placement is an illadvised proposition. Most antenna problems can be minimized if external antennas are permitted. At 2.4

The main thing object is to obtain good clean holes with no smear. PTFE smear cannot be removed by chemical means and will affect the reliability of the through hole plating.

- B. Because PTFE resins are non-wettable special treatments must be utilized to make the surface wettable in order to accept plating deposition. This is generally done using a form of sodium etchant. These etchants are available commercially. Any PTFE surface exposed to the sodium etch will be made wettable and therefore plateable.
 - C. Once the surface has been properly treated it is possible to use any of the standard PWB processes such as plated through holes or plated edges. The holes can be plated to meet the requirements of Mil-P-55110. Wrap around plating of the edges to establish good grounds is also feasible. Most of the plated holes and edges are used to establish ground connections.
 - D. Plating finishes available are: copper, tin/lead, tin, electroless copper, electroless nickel, and gold. New processes have been developed for plated through holes on aluminum backed materials. (Heavy metal backed) With these processes it is possible to plate any of the above metals on aluminum.
6. BONDED SUBSTRATES
- A. Differences between microstrip and stripline
 - B. Bonding films available - 6700, Polyguide, FEP, Pyralux, conductive films (SRS and Ablestik)
 - C. Preparation prior to bonding - sodium etch or bond without, direct fusion bonding
 - D. Special bonding applications - conductive bonding to aluminum, curved (conformal) bonding
7. SUMMARY

As frequencies increase and control of electrical parameters become more important the use of PTFE based materials will grow due to the excellent electrical properties. It will become necessary to be able to process these materials and hold the tolerances required.

GHz external antennas can assume small profiles, with helical configurations fitting into one or two inch plastic hemispheres.

Incorporation of these microwave radio transceivers into portable computer-based hardware will require some new approaches to hardware design. Electromagnetic considerations, up to now, have been limited to electromagnetic interference (EMI) issues in computer hardware design. Extensive shielding is required to keep unintentional RF noise produced by high speed computer clocks from escaping the computer and interfering with radios, televisions, and other equipment. With radios and antennas "inside" the electromagnetic considerations become far more complex. Indeed, shielding will remain critical, but at the operating frequencies (2.4 GHz) the "unit" must provide the opposite function: transmit and receive antenna. Indeed, electromagnetic issues necessitate new ways of thinking about computer product engineering. Handheld and laptop microprocessor based equipment must now be considered complex electromagnetic devices.

7. Protocols, control, and standards

It is one problem to build an optimum radio for the above given constraints. It is another problem to control the radio, control the communications link, provide for clock recovery, synchronization, and interface to the data bus and networks. This is the work of the protocol circuit. GEC Plessey is developing several protocols and is providing interfaces to many of the important data communications standards: ISA, ETHERNET, PCMCIA, and others. Much of this work is covered by NDAs (non-disclosure agreements) in place with major customers. Consequently details cannot as yet be published. Suffice it to say that the

protocol and interface considerations are not trivial and that a complete solution (antenna to data communications standard socket) will be available in early 1994. However, the key to opening the ISM and other radio bands is to build adequate radios.

The entire question of protocols begs the introduction and adoption of standards for WLANs. These standards will have to embrace not only ISM band radios but also IR and other radio band systems as well. The *IEEE 802.11* group and the new *IEEE Communications Society Technical Committee on PCS* are working on such standards. In addition, ETSI is working on European standards and *WINForum* (an industry group) is dealing with securing new bands and writing an etiquette for these bands' use. Clearly, convergence on standards will occur within the next year, either through these and other standards groups or by de-facto standards.

8. Conclusions

Efficient, reliable, and cost effective wireless digital communications systems are now possible to address the high volume portable markets. The opening of this market has been accomplished by providing good microwave transceiver specifications derived from exhaustive market analysis and design processes. Reliable use of the difficult ISM environment has been accomplished with designs that can be translated to new WLAN/PCS frequencies quickly when these bands become available. Effective use of these radios requires interface CMOS circuits currently under development. Standards must also be set and accepted. Electromagnetic issues for antennas and shielding must also be rectified. A comprehensive program to address WLAN and PCS radio applications is in place at GEC Plessey Semiconductors. Standard

Copper-Foil-Clad Laminates and Substrates for Commercial Applications

John Frankosky, Arlon, Microwave Materials Divison, 1100 Governer Lea Road, Bear, DE 19701; (302) 834-2100, FAX: (302) 834-2574.

Applications for PTFE based laminates continue to grow in number. As a material supplier in a more competitive market, Arlon is challenged in both the manufacture of existing products and the development of innovative products to satisfy today's and tomorrow's designs.

Woven fiberglass reinforced PTFE and nonwoven fiberglass reinforced PTFE are most widely available. The market for these PTFE based substrates has traditionally been military microwave applications, where the electrical performance of the laminate is absolutely critical. Some of the technology from the military applications has been adapted to applications for commercial and consumer products. This growth has allowed PTFE laminate manufacturers certain economies of scale, making the laminates and their encompassing technology available outside the military.

With the introduction of various ceramic fillers into the PTFE matrix, several new avenues are opened to designers in different fields. Grades are available which allow a choice of circuit miniaturization, temperature stable electrical performance or pricing comparable to high performance thermoset laminates.

The first two of the ceramic loaded PTFE laminates are high performance (and high cost) materials, with requirements as stringent as those for the mature technology of "conventional" PTFE based laminates. The third, which was most recently developed, has been introduced for applications extending from high speed digital to commercial microwave devices.

Early evolution of the PTFE based laminate was lead by the need for better performance at the available (higher) frequencies. Designs called for lower dielectric constants and lower dissipation factors. Low dielectric constants allow faster signal propagation in traditional wiring board applications.

Printed wiring boards were replaced by printed circuit boards, where the length of a circuit element was based on the wavelength at that frequency. As the frequencies increased, the traces on the PTFE based substrates were, indeed, transmission lines. The low dissipation factor (loss tangent) would yield higher signal to noise ratios for these transmission lines.

Using a conventional epoxy/fiberglass laminate, the electrical package designer is required to route all of the wiring traces such that all of the discreetly mounted components are included in the scheme. The only requirement for the epoxy/fiberglass laminates is that they are electrical insulators.

In applications which would use the PTFE laminate, tighter tolerances are required for both dielectric constant and thickness. Here, the laminates, were not going to be used as ordinary printed wiring boards; they would be used as components themselves. Increasing performance requirements has provided the impetus for the manufacture of "conventional" PTFE based laminates to "component" standards.

products that solve all problems between the data communications interface and the antenna will soon be available on the open market.

9. References

1. *Spread Spectrum Systems*, Robert C. Dixon, John Wiley & Sons, 1984
2. *Spread Spectrum Communications, Volumes 1, 2, & 3*. Marvin K. Simon, Jim K. Omura, Robert A. Scholtz, Barry K. Levitt, Computer Science Press, 1985
3. *The Kitchen-Sink Band: 902 MHz, "It Seems to Us..."*, *QST*, David Sumner, American Radio Relay League, June, 1993
4. *Wireless Access Methods and Physical Layer Specifications*, Ed Geiger, IEEE 802.11 Document number IEEE P802.11-93/104, July, 1993

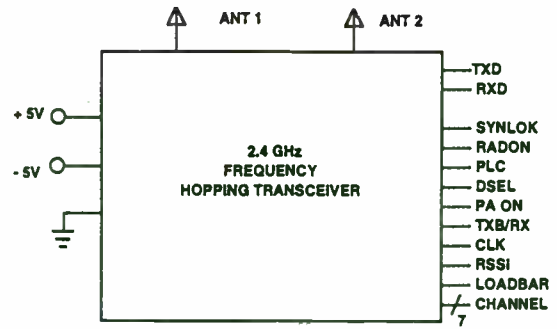


FIGURE 2
Functional Block Diagram of DE6003

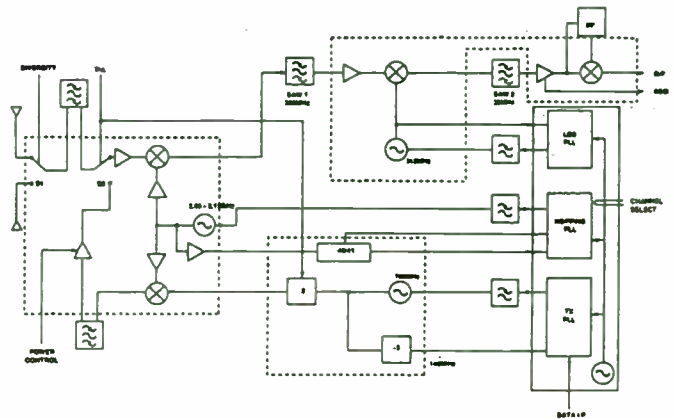


FIGURE 3
Detailed Block Diagram of DE6003

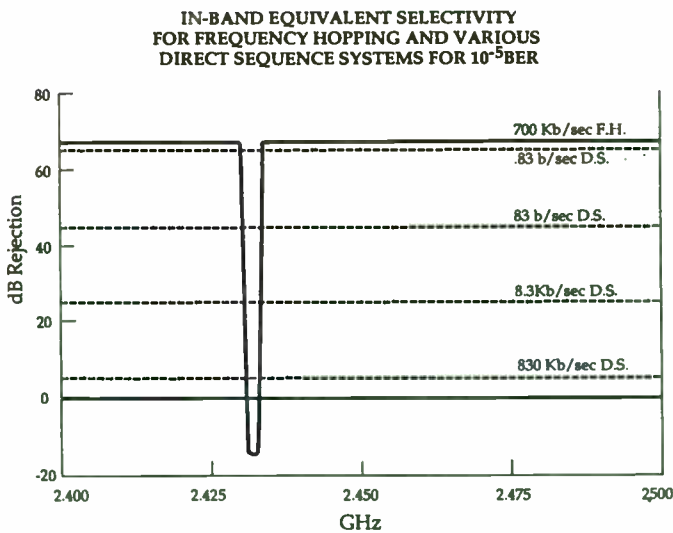


FIGURE 1.

Components which can be integrated into the circuitry would not have to be mounted discreetly upon the substrate. This capability of PTFE based laminates reduces the system cost and improves reliability.

Several types of PTFE based laminates are available to the designer for commercial signal processing components. The fundamental groupings include woven fiberglass reinforced PTFE, nonwoven fiberglass reinforced PTFE and ceramic loaded PTFE. In short, a complete product range is available for engineers to optimize their designs on PTFE based laminates.

Woven Fiberglass Reinforced PTFE:

The most common PTFE based laminates are woven fiberglass reinforced. These have been produced since the early 1950's. The first laminates of this type generally had a dielectric constant of about 2.7 to 2.8, relatively low compared to a typical laminate of epoxy/fiberglass ($\epsilon_r = 4.6$). Today, the company names have changed, but the product lines DiClad® (from Continental Diamond Fiber) and CuClad® (from 3M) are now manufactured by Arlon's Microwave Materials Division.

In addition to the electrical applications, many of the early PTFE laminates were also used in mechanical or chemical applications. Bearing pads for shifting loads and chemically inert gaskets were common uses for reinforced PTFE. These applications did not use copper foil.

With copper foil laminated to each side, the woven fiberglass/PTFE provided several advantages over its epoxy counterparts. The low dielectric constant allowed much faster propagation of signal in circuits where speed was essential. In addition, the dissipation factor was an order of magnitude lower, even as tested at 1 megahertz (MHz). More signal would be carried faster with less electrical loss.

Control of the PTFE resin coating of the fiberglass cloth is unmatched by epoxy/fiberglass laminators. The coating weight is controlled to well within one percent. This allows PTFE laminators to achieve the tight mechanical (thickness) and electrical (dielectric constant) tolerances which are necessary in the application of these substrates.

Woven fiberglass/PTFE remains the most proliferate among the varieties of PTFE based laminates. But, even within this general category, there are several distinctions to be made, each with its own advantages.

Among the first distinctions between laminate grades is that made on the basis of dielectric constant. By itself, PTFE has a dielectric constant of 2.07; electrical grade fiberglass has a dielectric constant of 6.0. The dielectric constant of the composite laminate is a function of the PTFE resin to fiberglass weight ratio. This ratio is manipulated to achieve laminates with dielectric constants ranging from 2.15 to 2.70; laminate base thicknesses range from as little as 0.002" (0.05 mm) or greater than 1 inch (25 mm).

A DSP Microprocessor Based Receiver for a Cosine Transition-shaped BPSK Signal

Roy E. Greeff and Bruce H. Williams
 Unisys Government Systems Group
 640 N. 2200 W. MS-F1E03
 Salt Lake City, UT 84116

In a previous paper (RF EXPO East 92) we discussed a cosine transition-shaping BPSK modulator implemented by direct digital synthesizers. This waveform has advantages over conventionally filtered BPSK in that filter distortion effects can be tightly controlled and reproduced consistently. This paper continues with the development of a system utilizing the shaped BPSK signal. This paper discusses a DSP microprocessor receiver for the cosine transition-shaped BPSK signal.

Modulation Waveform

By shaping NRZ data transition shapes one can effectively filter the spectrum. Figure 1 shows an "eye-pattern" for the shaped NRZ signal.

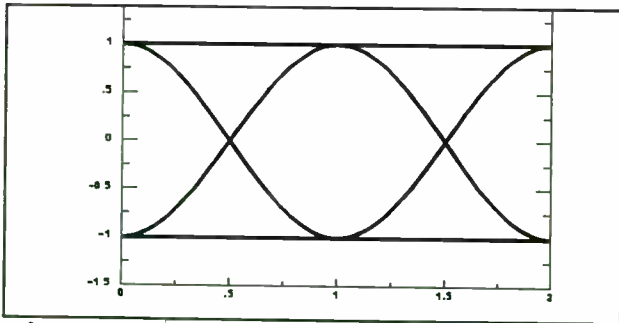


Figure 1 Transmitter Equivalent Eye Pattern

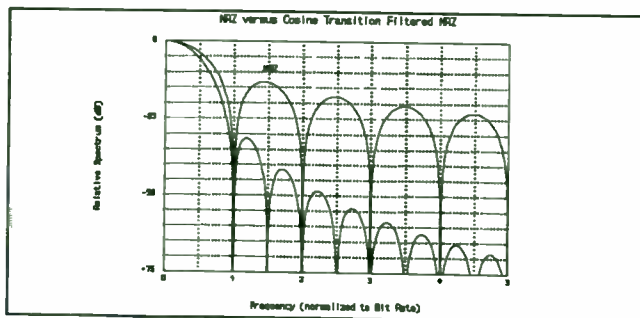


Figure 2 Relative Power Spectral Densities (dB/Hz)

Figure 2 demonstrates the effect of cosine transition shaping on the spectrum. Energy in the sidelobes is significantly reduced.

The receiver necessary to optimally demodulate this signal differs from conventional BPSK demodulators in that the matched filters are combined with intersymbol interference (ISI) canceling filters.

Main Receiver Functions

Figure 3 shows a block diagram of the main receiver functions necessary for PSK demodulation.

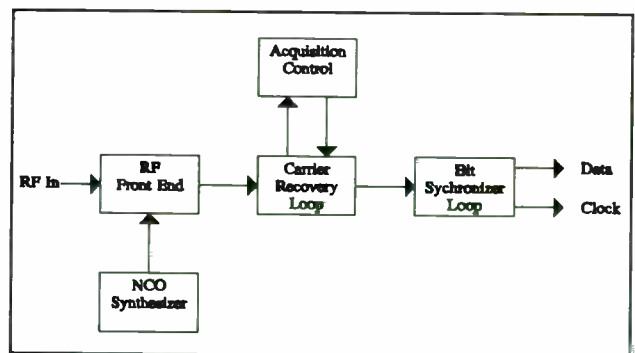


Figure 3 Main Receiver Functions

The RF front end consists of filters, the AGC, downconverter, and the A/D converters. The rest of the functions are implemented using DSP products. These functions in the past have been implemented using analog circuits. With the advent of higher speed DSP products (such as the Texas Instruments TMS320C40) these functions can now be implemented digitally for low data rates. The receiver built at UNISYS implements the Data Recovery Loop, acquisition control, and the bit

The military specification document MIL-P-13949 recognizes type GT as having a dielectric constant up to 2.8; GX laminates have a dielectric constant between 2.40 and 2.60, inclusive. In choosing between type GT and GX for an application, they are typically differentiated by the test method, amount of testing and acceptable tolerances.

GT material is tested for dielectric constant and dissipation factor at 1 MHz by a two fluid capacitance cell (well below microwave frequencies). The tolerance for the dielectric constant is ± 0.05 or about a four percent range. Dissipation factor for GT grade laminates is about 0.001 by the same test. This compares to a dissipation factor of 0.02 for epoxy/fiberglass at the same frequency.

GX grade, on the other hand, while it is essentially the same material, is tested for dielectric constant and dissipation factor at 10 gigahertz (GHz), well in the scope of microwave frequency. The standard tolerance for the dielectric constant is ± 0.04 , 20 percent tighter than the tolerance for GT grade. The dissipation factor is also tested at X - band. The maximum allowable value is 0.0023. Typical values are about 0.0020.

GY grade materials have a dielectric constant between 2.15 and 2.40. They are tested by the same method as is used for the GX grade. Here, the dielectric constant tolerance is still ± 0.04 , but typical is ± 0.02 . This grade had typically been reserved for applications where the loss factor was most critical. Thus, the maximum allowable dissipation factor is 0.0015.

As each of these grades is a combination of PTFE and fiberglass, the electrical and mechanical properties of the laminate are related. The first important compromise is between the inherently better dimensional stability of the higher dielectric constant ($\epsilon_r = 2.4$ to 2.6) laminates versus the superior electrical loss factor of the lower dielectric constant laminates (ϵ_r less than 2.4).

GT and GX grades, with their additional fiberglass, have much better dimensional stability during processing than a GY grade laminate. These grades resist etch shrinkage and are more easily handled by equipment set for conventional laminates.

GY grade laminates tend to shrink more when the copper is etched. This may cause relative difficulty in achieving precise circuit patterns or control over relative position of machined features.

However, a typical GX laminate, with a dielectric constant of 2.50, has a loss tangent of about 0.002, while a GY laminate with a dielectric constant of 2.20 has a loss tangent of 0.0009. The additional fiberglass in the GT and GX grades, which is beneficial during fabrication, results in an electrical penalty, in that they have considerably higher loss tangents.

Another consideration is the relative cost of the different laminates. The two constituents in each of these types of laminates is PTFE and fiberglass. Fiberglass cloth is relatively inexpensive when compared to PTFE. Naturally, a GX grade laminate with a dielectric constant of 2.60 and composed of 65% PTFE, can be expected to be much less expensive than the GY grade with an dielectric constant of 2.20, which has approximately 91% PTFE.

However, there are several compromises made with regard to the laminate properties. A leading commercial application of woven fiberglass reinforced PTFE is for Low Noise Amplifier (LNA) circuits for 12 GHz Direct Broadcast Satellite (DBS) receivers. Some designs use GY grade ($\epsilon_r = 2.20$), while other designs use a GT or GX grade ($\epsilon_r = 2.60$).

In either design, the noise factor of the LNA is a measure of its performance. Each design uses

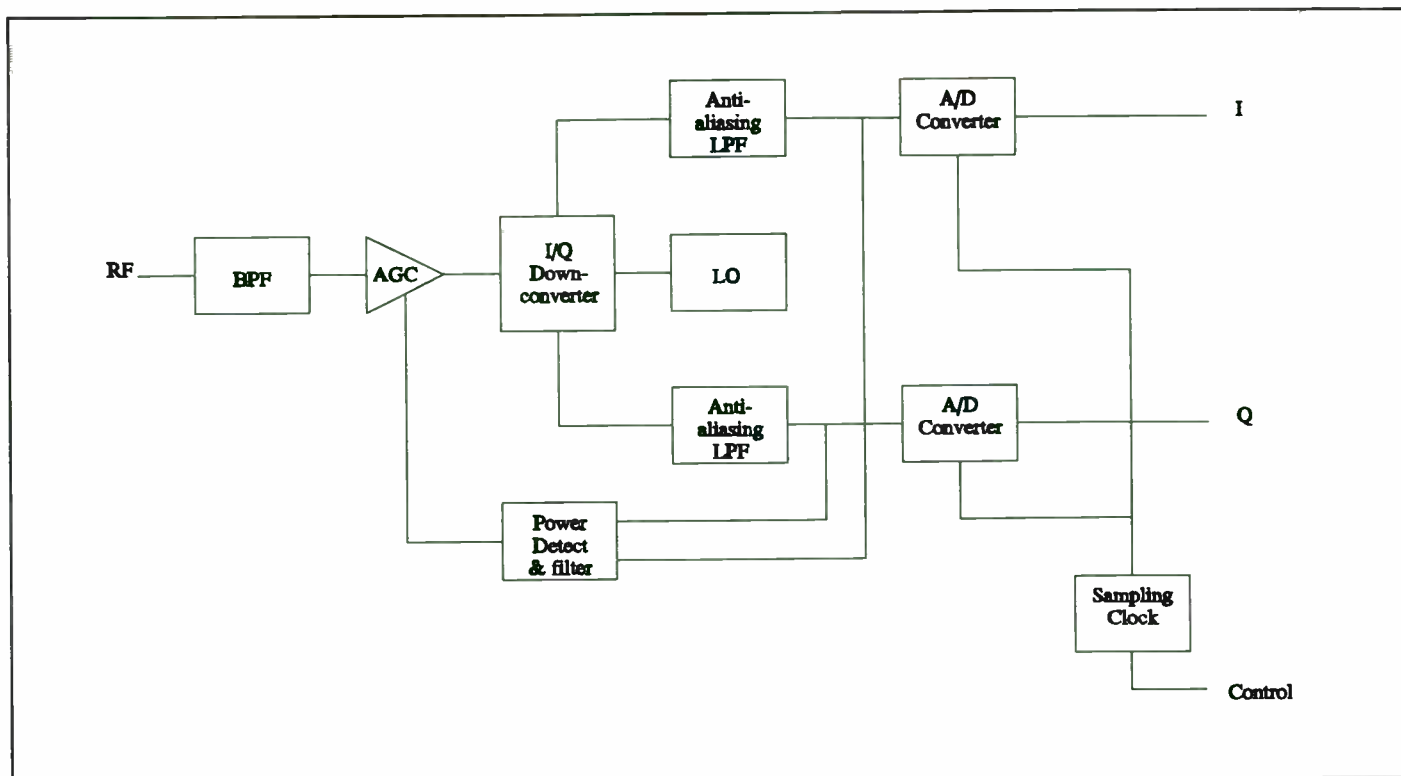


Figure 4 RF Front End

synchronizer with software loaded on a TI C40 floating point processor. Considerable flexibility is obtained by programming these functions into the C40. This flexibility is most apparent in the different algorithms that can be programmed (with no hardware changes) into the C40 for different modulation types (PSK, FSK, etc.).

RF Front End

Figure 4 shows a block diagram of the RF front end of the receiver.

The first filter is used to limit the noise bandwidth of the receiver. Its bandwidth is chosen to be only wide enough for the tuning flexibility required for multiple channels. The AGC amplifiers follow the filter. The detection of power for the AGC is at the output of the anti-aliasing filters. The power detection could occur after the baseband matched filters but if this is done too much power may be input into the I/Q downconverter. Additional AGCing is done at baseband in the demodulator algorithm. After the AGC amplifiers, the signal is downconverted as close to baseband as the frequency uncertainty of the received

signal. An NCO is used as the synthesizer for the downconversion. The resultant I and Q signal is then filtered with the anti-aliasing filters. These signals are converted to digital signals using A/D converters operating at four times the maximum data rate. The sampling rate oscillator is controlled by the demodulator algorithm. The signals are fed to the C40 processors where the samples are used to perform the appropriate demodulation. The RF circuitry can be used with many different data rates and modulation types with no changes to the hardware.

Software Carrier Recovery Loop

Using DSP techniques to perform the demodulation vs analog techniques has various advantages. A demodulator design using analog circuits may degrade over temperature, vibration or other environmental factors. The software loaded into a digital processor is immune to environmental factors. A software demodulator can be changed easily to accommodate new data rates or even new modulation types. The one advantage that analog circuits have over the same digital

several field effect transistors to amplify the incoming signal. The quality of these components, which are mounted to each substrate, are as important to the noise factor as the substrate. The field effect transistor, another significant cost item, along with choice of PTFE substrate, creates another cost versus performance trade. The designer is left to complete the exercise.

Woven Fiberglass Reinforced PTFE: Crossplied or Non-Crossplied

Compared to its epoxy/fiberglass counterpart, the range of dielectric constant within a PTFE based laminate is minimal. Some of this range owes to the directionally dependent properties of the fiberglass cloth. Dielectric constant is measured in the z direction of the laminate (that is, through its thickness). However, it is measured with respect to the x and y axes (or machine and cross-machine directions). Testing laminates for this difference shows a directional shift of about 0.010 to 0.015 depending on the amount and style of fiberglass cloth in the laminate.

Apart from the nominal dielectric constant, there is another distinction within the class of woven fiberglass/PTFE laminates. To eliminate any property changes owing to directional orientation, laminates within the CuClad® product line are manufactured with crossplied fiberglass. Alternating layers of PTFE coated fiberglass are oriented at 0° and 90° as the substrate is pre-constructed prior to lamination. This technique provides a finished substrate with isotropy of both electrical and mechanical properties with respect to the machine and cross-machine directions.

Many designers of antennas for various applications have chosen CuClad® for its electrical isotropy. The electrical length of the elements of the antenna are critical to its performance. The small change in dielectric constant associated with a directional change in a non-crossplied laminate is enough to compromise that performance.

This contrasts the manufacture of DiClad® laminates, which are not crossplied. They are, however, offered in much larger sheet sizes. DiClad® laminates are offered in a maximum sheet size of 36" x 72", while the crossplied CuClad® laminates have a maximum dimension of only 36" x 36".

Without isotropy, the electrical designer may be required to adjust lengths of electrical elements to account for dielectric constant shift depending on the element's orientation to the fiberglass weave. Elements oriented along the warp direction typically behave as if they are on lower dielectric constant material. Alternatively, the circuit or system can be designed to tolerate a larger bandwidth, but some electrical performance will be sacrificed.

To accomplish the design goal, adjusting circuit element lengths to account for the directional change in dielectric constant, the effort must be coordinated with the fabricator and the supplier of the PTFE laminate material. Both parties must track the orientation of the laminated sheet and any smaller panels cut therefrom. This practice is done regularly, but designs using CuClad® have been able to circumvent it.

The crossplied laminate obviates these considerations. Neither the laminate vendor nor the fabricator need track the orientation of panels prior to and during circuit fabrication. The engineer designs the circuit elements according to the reported nominal dielectric constant. Regardless of circuit orientation on a given panel, the performance should be equivalent.

As mentioned earlier, a disadvantage of the crossplied construction is that it limits the sheet size to a longest dimension equal to the width of the fiberglass cloth. For some applications, the circuit will be longer than a crossplied laminate; the longer dimension is absolutely critical.

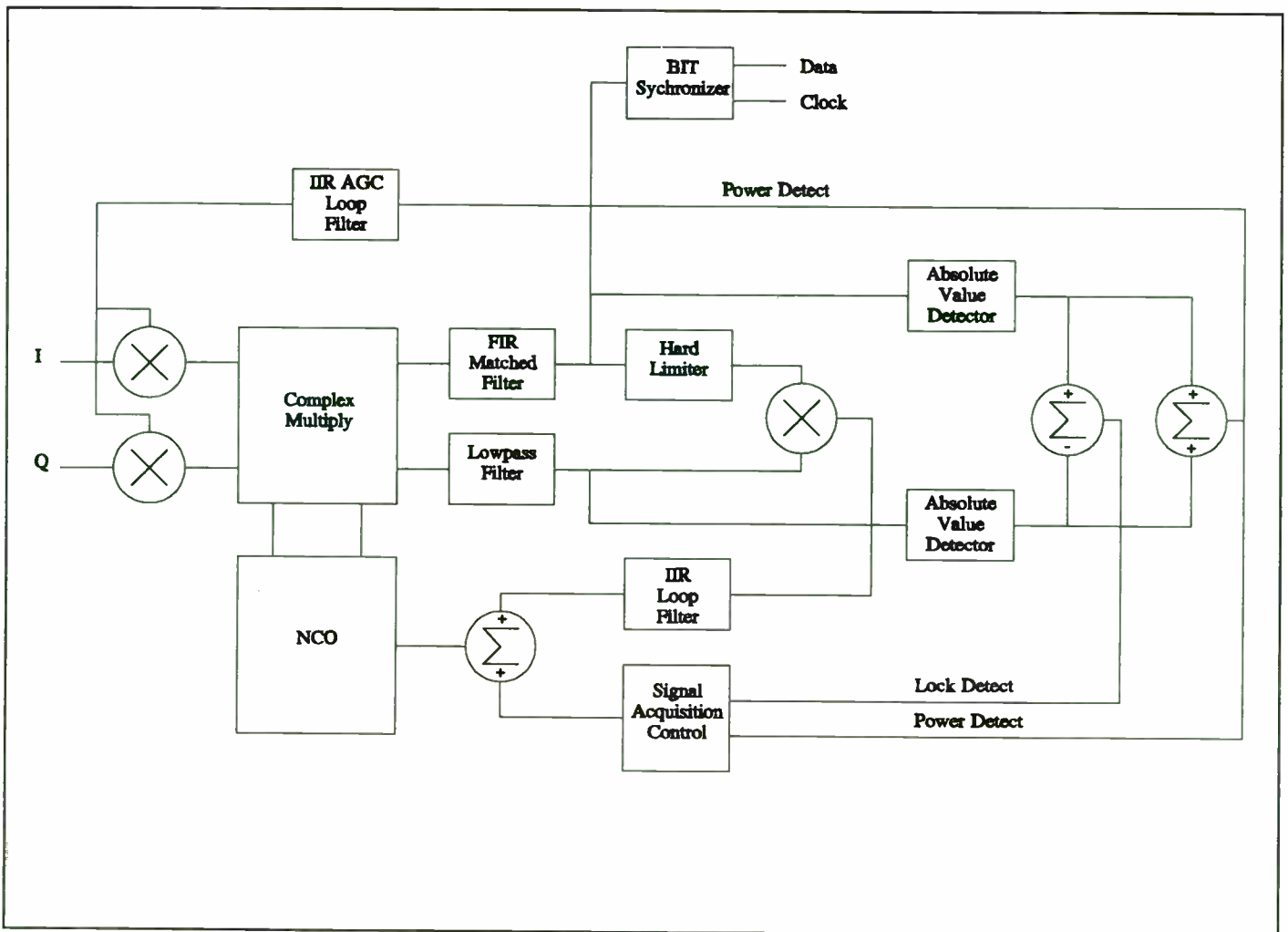


Figure 5 Demodulator Algorithm

implementation is speed. Analog circuits have the capability of operating at much higher data rates. As faster and faster digital components are developed, more and more analog systems will be replaced with digitized systems.

Figure 5 shows a block diagram of the demodulation algorithm. The algorithm is made up of three separate functions: 1) BPSK Carrier recovery loop (CRL) 2) Signal Acquisition Control for the CRL 3) clock regeneration using a bit synchronizer.

The BPSK CRL can be viewed as software implementation of a costas loop. The requirements that need to be met when a loop is designed in the analog world are the same as for loops designed in the digital world.

The digitized complex signal received from the

RF front end is demodulated using the following software functions. Refer to figure 3.

Complex Multiplier - The input complex signal received from the RF front end is first multiplied with the complex signal received from the software NCO which is phased locked to the incoming signal. The resultant signals are the I channel (data channel for BPSK) and the Q channel (the tracking channel for BPSK).

FIR Matched filters - The I channel is filtered using the FIR matched filter discussed earlier. This FIR filter spans 8 data bits or is 32 samples long for signals that are sampled 4 times per bit. The Q channel is filtered using an integrator that has the same delay as the matched filter. Filtering of the Q or tracking channel is actually not required (data aided loop) but is done to make a less noisy lock

Antennas for Personal Communications Networks (PCN) are just such an application. In other cases, the preferred panel size for fabrication can be cut more favorably from a rectangular sheet than it can from a square sheet.

Nonwoven Fiberglass Reinforced PTFE:

Historically, nonwoven fiberglass reinforced PTFE were the next class of PTFE laminates to be developed. They are available in a similar range of dielectric constants as their woven fiberglass counterparts. The exception is that ceramic filler can be more readily introduced into the nonwoven composite, allowing higher dielectric constants to be achieved. Discreet values of 2.17, 2.20 and 2.33 are standard products.

The military specification document MIL-P-13949 recognizes nonwoven fiberglass reinforced PTFE based laminates with dielectric constants between 2.15 and 2.40. The grade designations are types GP and GR. The test methods for these laminates are the same as those described earlier, in reference to type GT, GX and GY grades of woven fiberglass reinforced PTFE based laminates. Tolerances for the mechanical and electrical properties are the same as for the GY grade.

Similar to the crossplied woven fiberglass reinforced PTFE substrates, nonwoven fiberglass reinforcement offers relative isotropy in the x-y plane. The design and fabrication advantages owing to isotropy are described earlier.

Fabricators perceive a different benefit from the nonwoven fiberglass reinforcement. In machining, the cutting tool "sees" a uniform material. Woven reinforcement, in contrast, presents "hard" fiber bundles and a "soft" matrix. If proper machining parameters are not chosen for the woven fiberglass reinforced PTFE, the tool can tend to push the fiber bundles through the matrix rather than cut them. Fabricators often describe better quality holes and other machined features when they are using nonwoven fiberglass reinforced PTFE. Parameters such as RPM and feed rates may not be as critical.

Military applications of this material are numerous. Several missile programs use nonwoven fiberglass reinforced PTFE as the material for "wrap-around" antennas. These antennas are formed to the circumference of the missile.

Among commercial applications, nonwoven fiberglass reinforced PTFE is being used as the substrate material for switching circuitry in telecommunication equipment.

Ceramic Filled PTFE:

One of the advantages of PTFE as the resin system is the ability to achieve very low dielectric constants. In applications where the primary goal is high speed of signal propagation, this is especially important. Applications at microwave frequencies typically require the dissipation factor to be very low.

Mechanically, woven fiberglass and nonwoven fiberglass reinforced PTFE based laminates each have a high "z" axis thermal coefficient of expansion (TCE). The fiberglass reinforcement is oriented only in the x-y plane. Thus, with thermal expansion in the x-y plane restricted, the PTFE resin forces expansion in the "z" direction.

The choice of ceramic filler, in ceramic loaded PTFE, allows the low dissipation factor to be preserved. A choice of dielectric constants and desirable packaging, electrical, mechanical or

detect. An integrating filter is used instead of the FIR filter because the integrating filter uses less clock cycles than the FIR to implement.

Hard Limiter - The hard limiter outputs a '1' or '-1' depending on if the sample is positive or negative.

Multiplier - The multiplier simply takes two sample and does a floating point multiply.

IIR Loop Filter - Much work has already been done to analyze 2nd order type 2 loops in the analog world. This work can be used by designing the loop filter using an IIR filter. The weights for the IIR filter can be obtained by taking the transfer function of the filter and using the Bi-linear Z transform.

NCO - The software NCO (Numerically Controlled Oscillator) is basically the same as the hardware NCOs that are now available. The C40 processor keeps a record of phase using an integer 32 bits long. On each sample a delta phase is added to this integer. The first 8 bits of the integer are then used in a look up table that has the sine and cosine functions stored. Frequency is changed by changing the delta phase added to the integer.

The above software functions are all performed between adjacent samples. If the C40 operates at 40 MHz, the data rate is 50 kBs, and four samples are taken for each bit, all the above functions need to be done in 200 clock cycles or 100 instruction cycles (2 clock cycles = 1 instruction cycle). If higher speeds are desired multiple C40s operating in parallel could be used. Parallel processors can be added until the pipe line delays approach the delay of the loop filter.

Signal Acquisition Control

For low data rate systems acquisition of the signal can be a problem. Low data rate systems have small loop bandwidths in comparison with the system's frequency uncertainty. As a result some scheme to acquire the signal must be implemented. One

method is to sweep the CRL over the entire frequency uncertainty band and allow the CRL loop to lock when it finds the signal. This method can lead to false locks. A better method is to search for the maximum signal power over the band and pretune the CRL to that spot and then allow the CRL to lock. The maximum power can be found by tuning the LO over the sweep band and using an absolute value detector after the matched filter. Maximum power can also be found by using an FFT. A combination of the two techniques for finding maximum power is being implemented in UNISYS's demodulator.

Another important part of acquisition is knowing whether or not the CRL is locked or not. The lock detect indication used for the BPSK demodulator is $\text{FILTER}(\text{ABS}(I) - \text{ABS}(Q))$. This gives a good lock indication down to E_b/N_0 of 0 dB.

BIT Synchronizer

The bit synchronizer is implemented using a conventional early late type phase detector. An IIR filter is used for the loop filter and the error signal generated is sent to the Sampling Clock located near the A/D converters. This loop determines where the samples are taken during the bit period which allows for best performance.

economical advantages are offered.

Fabricators realize some benefits of the uniformly mixed ceramic loaded PTFE based laminates when machining. Usually, a wide range of speed and feed parameters can yield a high quality hole surface. However, the hardness of the ceramic particles will shorten tool life, and the bits will have to be replaced more often.

Ceramic Filled PTFE: High Dielectric Constant Laminates

Ceramic filled PTFE offers the property of a significantly higher dielectric constant than is available with either the woven or nonwoven fiberglass reinforced PTFE. The dielectric constant is higher than even epoxy/fiberglass. Arlon is offering dielectric constants of 6.0, 10.2, 10.5 and 10.8. These are the products IsoClad® GR6: $\epsilon_r = 6.0$; CuClad® Epsilam 10: $\epsilon_r = 10.2$; and DiClad® 810: $\epsilon_r = 10.2, 10.5, 10.8$.

At microwave frequencies, circuit trace lengths are specifically designed around the wavelength. At any particular frequency, the speed (C) of propagation of the signal is proportional to the speed of that signal propagating through a vacuum (C_0) divided by the square root of the dielectric constant ϵ_r :

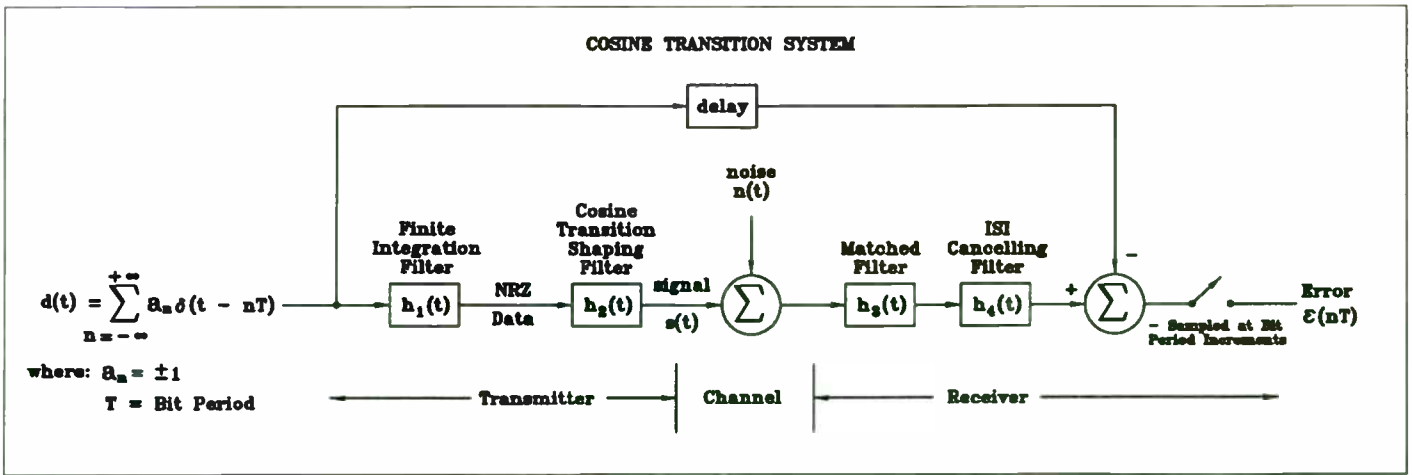
$$C = C_0 * (1/\sqrt{\epsilon_r})$$

Signal speed is also equal to the frequency (ν) multiplied by the wavelength (λ).

$$C = \nu * \lambda$$

As signal propagates through a dielectric material, the frequency of the signal does not change, but the speed of propagation, which is proportional to the inverse of the square root of the dielectric constant of the material, does. It necessarily follows that, at a particular frequency, only the wavelength can change with respect to the dielectric constant of the material through which it is propagating:

$$\nu * \lambda = C_0 * (1/\sqrt{\epsilon_r})$$



Receiver Filter Design

The transmitter filter is a combination of finite-integration filter and the filter that creates cosine transitions. The finite integration filter impulse response is:

$$h_1(t) = \begin{cases} 1, & 0 \leq t < T \\ 0, & \text{otherwise.} \end{cases}$$

The transition shaping filter impulse response is:

$$h_2(t) = \begin{cases} \frac{\pi}{2T} \sin\left(\pi \frac{t}{T}\right), & 0 \leq t \leq T \\ 0, & \text{otherwise.} \end{cases}$$

The composite transmitter filter is the convolution of $h_1(t)$ with $h_2(t)$. The effective transmitter filter impulse response is:

$$h_1(t) \otimes h_2(t) = \begin{cases} \frac{1}{2} \left[1 - \cos\left(\pi \frac{t}{T}\right) \right], & 0 \leq t \leq 2T \\ 0, & \text{otherwise} \end{cases}$$

\otimes - signifies convolution.

reversed and delayed version of the composite transmitter filter. Because the effective transmitter filter's impulse response is a real and even function, the matched filter is the same as the effective transmitter filter. By convolving the matched filter with the

$$h_3(t) = [h_1(-t) \otimes h_2(-t)]^* = h_1(t) \otimes h_2(t)$$

* - signifies complex conjugate

transmitter filter, one can determine if any intersymbol interference (ISI) has been introduced.

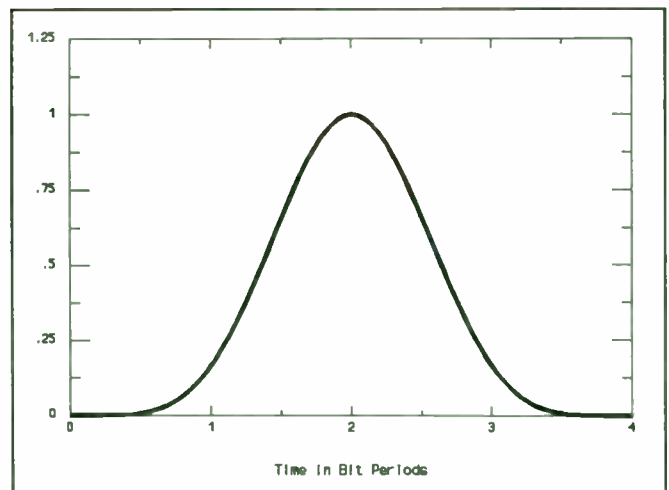


Figure 6 Impulse Response of Transmitter and Matched Filter

The matched filter is, by definition, a time

Since ν and C_0 are constants, they can be eliminated for the purpose of this discussion. Thus, the wavelength, like the speed, is inversely proportional to the dielectric constant of the material:

$$\lambda \propto (1/\epsilon_r)$$

What this means to the designer is that, using a high dielectric constant substrate, the circuit board can be miniaturized. In comparison, a board which had been designed on $\epsilon_r = 2.20$ material could be redesigned on $\epsilon_r = 10.2$ material, resulting in a circuit much less than half the length.

Holding dielectric thicknesses constant, a substrate with a dielectric constant of 10.2 also reduces the width of a constant impedance line considerably. For instance, the width of 50 Ω line, on material which is 0.025" thick, is reduced by more than a factor of three. This fact is often exploited for very low impedance lines, such as those which connect power amplifiers.

Accordingly, with both the length *and* width of the substrate reduced, the package weight is also significantly decreased. This type of substrate is used where weight and/or space are at a premium.

An important use of high dielectric constant material is for commercial aircraft. The United States Federal Aviation Administration has mandated collision avoidance systems for passenger aircraft. Engineers at Rockwell International designed the front end of the transmit/receive module of their Tactical Collision Avoidance System (TCAS II) on DiClad 810. The space and weight savings for TCAS II, an *airborne* collision avoidance system, are obvious benefits.

Another difference owing to the ceramic filler is higher thermal conductivity in comparison to other PTFE based laminates. Designers can take advantage of both miniaturization, more easily matching feed lines to low impedance power transistors, and high thermal conductivity, sinking the heat generated from a power transistor, for instance, to an integral ground plane. Westinghouse Electronics uses DiClad 810 extensively as the substrate for radar power amplifiers.

High cost is associated with high dielectric constant substrates. The manufacture of this type of substrate costs considerably more than the manufacture of conventional PTFE/fiberglass laminates. The designer will also have somewhat greater electrical loss. These cost and performance considerations limit but, as evidenced by TCAS II, do not preclude high dielectric constant substrates from the commercial market.

An important consideration for the fabricator and the designer is the fabricator's etch tolerance. This is dependent on the cladding thickness and the individual ability of the fabricator. At microwave frequencies circuit lengths and widths are critical to performance. Because the circuit dimensions on high dielectric constant substrates are less than half that on low dielectric constant substrates, the relative magnitude of the etch tolerance is more than twice.

Ceramic filled PTFE substrates are also offered with a dielectric constant of 6.0. This compromise allows some miniaturization while mitigating the negative effects of etch tolerance on the consistency of circuit performance.

The calculated weights show that the matched filter will indeed introduce ISI. The weights

$$\begin{aligned}
 h_1(t) \otimes h_2(t) \otimes h_3(t) = & \\
 & \left\{ \begin{aligned} & \frac{t}{4} + \frac{t}{8} \cos\left(\pi \frac{t}{T}\right) - \frac{3T}{8\pi} \sin\left(\pi \frac{t}{T}\right), \\ & \text{for } 0 \leq t \leq 2T, \\ & T - \frac{t}{4} - \frac{t}{8} \cos\left(\pi \frac{t}{T}\right) + \frac{T}{2} \cos\left(\pi \frac{t}{T}\right) \\ & + \frac{T}{8\pi} \sin\left(\pi \frac{t}{T}\right) + \frac{T}{4\pi} \sin\left[\pi \frac{(t-2T)}{T}\right], \\ & \text{for } 2T < t \leq 4T, \\ & 0, \text{ otherwise.} \end{aligned} \right.
 \end{aligned}$$

correspond to the impulse response of the transmitter and matched filters at plus and minus one bit period on either side of the impulse delay of 2 bit periods (see figure 6). At time T and 3T the amplitude of the impulse response is T/8; at time 2T the amplitude is 3T/4. Figure 7 shows the resulting eye pattern with ISI.

to have the following impulse response:

$$\begin{aligned}
 h_4(t) & \\
 & = \frac{4}{3T} \left[-\frac{T}{8} \delta(t) + \frac{3T}{4} \delta(t-T) \right. \\
 & \quad \left. - \frac{T}{8} \delta(t-2T) \right] \\
 & = -\frac{1}{6} \delta(t) + \delta(t-T) - \frac{1}{6} \delta(t-2T)
 \end{aligned}$$

Since $h_4(t)$ is comprised of delta functions, convolutions involving $h_4(t)$ are easily calculated:

$$\begin{aligned}
 h_4(t) \otimes \pi(t) & \\
 & = -\frac{1}{6} \int_{-\infty}^{\infty} \delta(\tau) \pi(t-\tau) d\tau \\
 & \quad + \int_{-\infty}^{\infty} \delta(\tau-T) \pi(t-\tau) d\tau \\
 & \quad - \frac{1}{6} \int_{-\infty}^{\infty} \delta(\tau-2T) \pi(t-\tau) d\tau \\
 & = -\frac{1}{6} \pi(t) + \pi(t-T) - \frac{1}{6} \pi(t-2T)
 \end{aligned}$$

The resulting system impulse response when the ISI canceling filter, $h_4(t)$, is combined with the matched filter, $h_3(t)$, is shown in Figure 8.

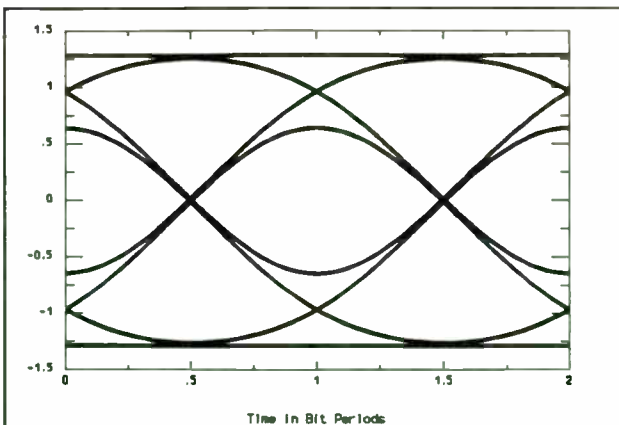


Figure 7 Eye Pattern, No ISI Canceler

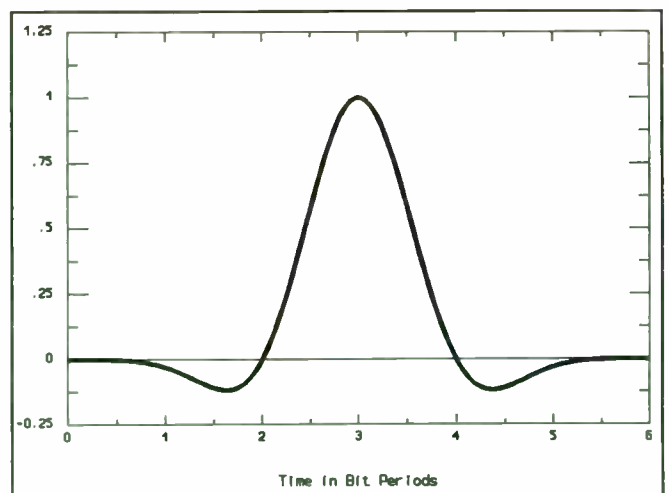


Figure 8 System Impulse Response (1st Iteration ISI canceler)

Obviously, the ISI would have a severe impact on bit error rate. Therefore, an ISI canceling transversal filter is necessary and would need

There still appears to be ISI. This is verified

Ceramic Filled PTFE:
Thermally Stable PTFE Based Laminates

The aforementioned types of ceramic filled PTFE products have been on the market for up to 20 years for the newest (ceramic filled PTFE - high dielectric constant) and 40 years for the oldest (woven fiberglass/PTFE). Among the newest PTFE based laminates are those formulated to offer superior thermal stability with regard to mechanical *and* electrical properties.

The dielectric constant of IsoClad® LTE is nominally 2.94. This is somewhat higher than the PTFE/glass laminates, but it is still lower than most thermoset based laminates. More importantly, the dissipation factor at 10 GHz is about as low as a PTFE/glass laminate with a dielectric constant of 2.33 (about 0.0013).

Previously, the electrical designer would be required to make considerations for dielectric constant change with temperature. The types of laminates discussed previously are all relatively stable with temperature in comparison to epoxy/fiberglass and most other combinations including a thermoset resin. But compared to IsoClad® LTE, the contrast to "conventional" PTFE based laminates is as striking as the comparison of the "conventional" PTFE based laminates to epoxy/fiberglass.

Both fiberglass reinforced PTFE and high dielectric constant ceramic filled PTFE have a temperature coefficient of dielectric constant (TCE_ε) which is on the order of a few hundred parts per million per degree centigrade. The coefficient is negative; ε_r decreases with increasing temperature.

In contrast, the new product has a TCE_ε which is on the order of 30 parts per million at its highest absolute value. At temperatures below 20°C the coefficient is negative, while it is positive above that temperature.

To the designer, the near zero TCE_ε of IsoClad® LTE can simplify the entire system. On conventional PTFE based laminates, given a physical length for a circuit element, its electrical length changes as the dielectric constant of the substrate changes with temperature. At a fixed frequency, the circuit will become less well matched to the wavelength. IsoClad® LTE assures, through its low TCE_ε, that the performance of the circuit remains constant as the ambient temperature changes.

The combination of raw materials which gives this substrate a low TCE_ε, also yields greater mechanical stability. This mechanical stability is manifest in its low thermal coefficient of expansion (TCE). The TCE of IsoClad LTE is just 25 parts per million per degree centigrade (ppm/°C). High dielectric constant ceramic filled PTFE based laminates also enjoy a low TCE (as low as 35 ppm/°C), just without the electrical stability (low TCE_ε).

Plated through hole reliability for IsoClad LTE is especially enhanced by the low TCE. In "conventional" PTFE/fiberglass laminates these electrical connections are often suspect. Woven and nonwoven fiberglass reinforced PTFE based laminates, especially those having the least amount of fiberglass, have up to 10 times the TCE of copper. The TCE of IsoClad LTE nearly matches that of copper (the TCE of copper used for plating through holes is 18ppm/°C), imposing little stress on that metallization through thermal cycling.

Thermal stability is manifest in both electrical and mechanical properties. Together these properties represent extraordinary reliability. Applications such as satellite communications,

by looking at the resulting eye-pattern, figure 9.

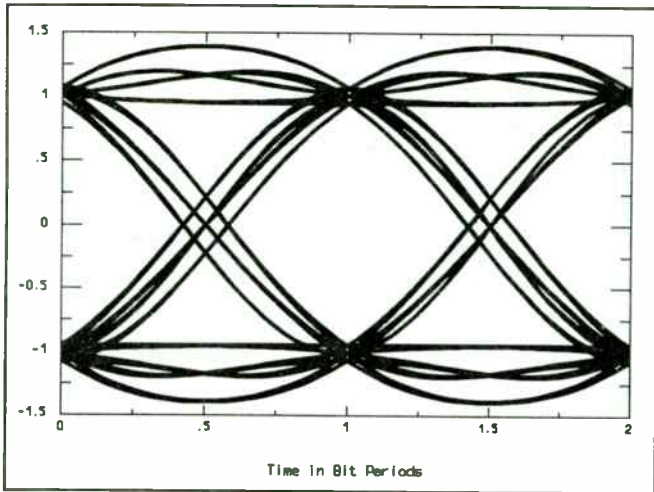


Figure 9 Eye Pattern
(1st Iteration ISI Canceler)

A modified ISI canceling filter is determined by subtracting by the correlation at 2 bit period offsets (see figure 8). The modified system impulse response is shown in figure 10:

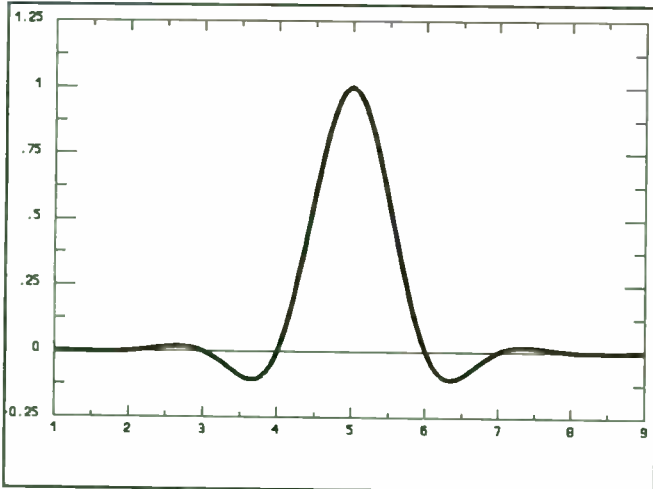


Figure 10 Impulse Response
(Modified ISI Canceler)

The correlation at bit period increments from the peak is now zero! The eye-pattern should have no ISI as shown in figure 11!

And, indeed, no ISI. The only question now to be answered is what kind degradation from ideal is the bit error rate when this system is used.

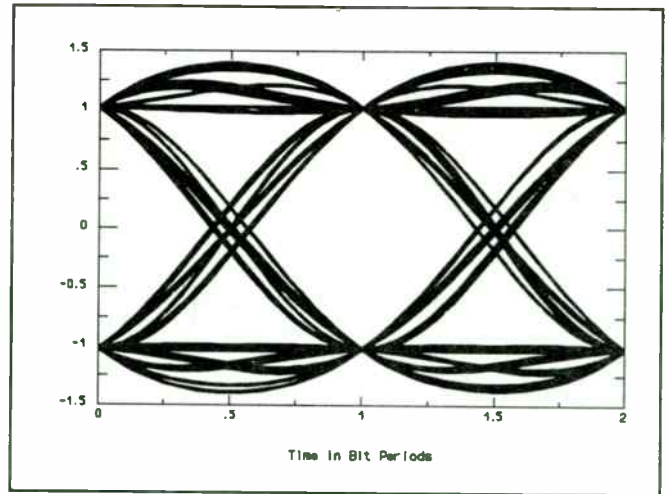


Figure 11 Eye Pattern
(Modified ISI Canceler)

Since the actual filters were implemented with digital FIR algorithms, the number of taps required and tap spacing needs to be determined. First the receiver impulse response is determined.

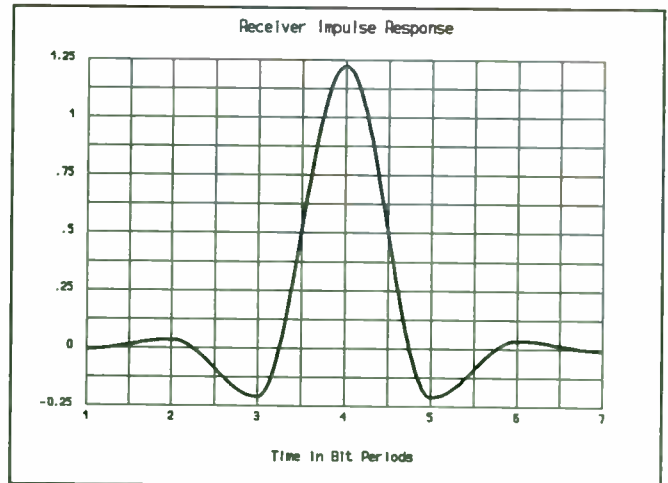


Figure 12 Receiver Impulse Response

It is advantageous to use the minimum number of taps as possible in the FIR filter. The greater the number of taps, the longer the processing time required, and the lower the data rate allowable. We analyzed a variety of spacing possibilities and ended with a sampling rate of 4 times our highest data rate. This was convenient because it allowed us to implement an early/late gate bit synchronizer with 1/2 symbol spacing. Also, by comparing

where maintenance and field repair are inconvenient, enjoy these benefits.

Ceramic Filled PTFE: Commercial Grade Laminates

Another class of new laminates is designed to offer dielectric constants similar to some thermoset laminates. Nominal dielectric constants are 3.50 and 4.50, each with a tolerance of ± 0.15 , but dissipation factors for these laminates are still similar to those of the GT and GX grades of PTFE/fiberglass.

Using coating technology from the PTFE/glass laminates, AR350L and AR450L will have much better dielectric constant uniformity, both within a sheet and between sheets, than thermoset based laminates of similar dielectric constants. To the designer, this uniformity and the aforementioned low dissipation factor allow much better impedance control and a higher signal to noise ratio.

Thermoplastic pre-pregs developed for use with AR350L and AR450L have several advantages over their thermoset based counterparts. Electrically, these "pre-pregs" AR350P and AR450P will match the performance of the laminate material for dielectric constant and dissipation factor. For the fabricator, throughput for multilayer lamination will increase dramatically.

Specifically, multilayer lamination throughput benefits significantly through the use of thermoplastic pre-pregs. Typical thermoset lamination uses longer, more complicated temperature cycles for proper cure and often requires post cure operations. Thermoplastic pre-pregs require only that a temperature high enough and a time long enough for sufficient melt be realized. Melt flow will allow the thermoplastic to wet all the surfaces to which it will bond.

A thermoplastic adhesive achieves bond as it is cooled to below its melt point. The rate at which it is cooled is insignificant to measured electrical and mechanical properties. No elaborate (and long) cure cycle is necessary. Time for multilayer lamination cycles can be reduced by as much as a factor of five.

If the designer or the fabricator prefers, conventional pre-pregs can also be used to manufacture multilayer circuits with the AR350L and AR450L laminates. They can either be used instead of the AR350P and AR450P pre-pregs or following one in sequential lamination. Circuits using only the FR-4 pre-preg have been manufactured by prototype fabricators.

Designers anticipate that this combination of materials will sacrifice some electrical performance relative to using the new materials with the pre-pregs which have been developed specifically for this application. Notwithstanding, the benefits of this new grade will demand attention.

Considerations for machining are reportedly few. However, it is imperative that holes which will be plated through do not have smeared PTFE on their walls. Accounts are that the new material is "forgiving" compared to conventional woven fiberglass or nonwoven fiberglass reinforced PTFE.

These new laminates and pre-pregs are expected to cost more than epoxy/fiberglass laminates and pre-pregs. Pricing should be competitive with high performance thermoset resins such as Bismaleimide Triazine (BT). However, much of the cost will be returned through greater fabrication throughput and reduced fabrication costs.

With superior electrical performance, it can be expected that this will allow use of AR350L and AR450L in applications where electrical performance considerations would prohibit the use of

the equivalent noise variance of an ideal finite integration filter (matched filter for non-bandlimited NRZ data) with our receiver filter, we analytically determined the implementation loss to be 0.25 dB from ideal! It later was verified through simulation.

conventional epoxy/fiberglass and many other high performance thermosets. Critical impedance matching, in higher frequency computer back planes, for instance, is expected to be an important application for this product.

Although PTFE based laminates have been in existence for much of the time that more common epoxy/fiberglass laminates have been used, they have typically been reserved for high frequency, high performance applications. The technology that used frequencies which warrant the use of PTFE based laminates were commonly in the military or research fields.

However, as more communication, data and other information is carried without wires, many of the available frequency bands for traditional transmission equipment are occupied or otherwise previously allotted. The occupied, "traditional" frequency bands seldom exceed 1 GHz.

The available frequency bands are at microwave frequencies. PTFE based laminates are designed for consistent high electrical performance at these frequencies. Specifically, PTFE has a low dissipation factor and a degree of dielectric constant control not found in the conventional thermoset based laminates. These properties are the basis on which the commercial high frequency applications will rely on and be manufacturable with PTFE based laminates.

Designing a High Performance Monolithic PSK Modulator

Frank Hayden and Robert J. Zavrel
GEC Plessey Semiconductors
1500 Green Hills Road
Scotts Valley, CA 95066

The objective of this program was to build a low power, monolithic, high performance PSK modulator. There are a wide variety of applications for such a device. The primary objectives was to fabricate a direct sequence "spreader" that could operate up to 1 GHz and provide excellent carrier suppression and combine the spreading PRN code with the data for both CDMA cellular and Part 15 applications. A second objective was to provide a high performance PSK modulator for more traditional applications, including TDMA and point-to-point microwave systems. A third objective was to facilitate derivative products that can provide QPSK, OQPSK and MSK baseband signals.

The "SL801" has been fabricated and tested. Proceeding into a true product development depends upon market acceptance of the device. Therefore, this paper represents a report on a development project and should not be considered a "product" introduction.

1. Digital Section

The SL801 is a Bi-Phase shift keyed (BPSK) modulator. The device accepts data in a digital format along with a spreading code that is used to modulate an RF carrier for transmission in spread spectrum systems. A primary performance goal was to maximize carrier suppression. The chosen circuit topology reflects this primary design objective in that two modulators are cascaded thus the carrier suppression characteristics are greatly enhanced.

Referring to the block diagram of figure 1, asynchronous data is fed into a type D flip flop at the data input. This serves to synchronize the data to the code clock. Note that the code clock is clocking all the flip flops and latches. After clock synchronization of the data, code inversion modulation is performed by modulo-2 addition of the code and the synchronized data. This takes place in exclusive OR gate G1. This serves to embed the code and data and also adds a greater level of security to the transmitted information. All the user must remember to do in the receiver is to modulo-2 add the received baseband information with the same spreading code in the receiver. This approach ensures that good auto correlation and low cross correlation are preserved.

Referring to the block diagram, Figure 1, at point A we have

$$(1) \quad A = C \oplus D$$

Where:

A is the output of exclusive OR gate G1.

C is the Spreading Code.

D is the synchronized data.

At point A the output of G1 is fed into another D type flip flop that serves to delay the code and data by one full code clock cycle. The output of the flip flop at point B may be expressed as;

$$(2) \quad B = (C \oplus D)\tau$$

Where:

B is the output of the delay flip flop L2.

τ is the clock delay through L2.

At this point in the circuit, point B is exclusive OR'ed with point A giving output C which can be expressed as;

$$(3) \quad C = (C \oplus D) \oplus (C \oplus D)\tau$$

Where:

C is the output of exclusive OR gate G2.

In order to assure proper cancellation of the undesirable terms and thus maximizing carrier suppression, the modulation inputs to the two multipliers must be correctly phased. Latches L3 and L4 assure that the modulation input signals are fed simultaneously to MOD2 and MOD1 respectively.

2. Modulator Section

The carrier input to MOD 1 and MOD 2 require a differential drive. The unbalanced input is converted to the required differential input by the carrier buffer, a unity-gain amplifier-balun with a maximum allowable input signal level of -5 dBm. The balanced modulators (MOD 1 and MOD 2) are Gilbert Cell multipliers configured such that the operation of the circuit provides balanced bi-phase modulation. Each modulator has 0 dB gain to minimize the effect of offsets that could corrupt the balance of the modulator and hence compromise carrier suppression. The modulators are cascaded so that the carrier suppression of each modulator will add to effectively double the carrier suppression (dB).

The instantaneous phase of the RF carrier is determined by the instantaneous polarity of the modulating signal. Consequently, two phase states, 0 or π radians (BPSK) are permitted. In this respect the

From Antenna to DSP: Components for RF/IF Signal-Processing

Session Chairperson: Ian Bruce,
Analog Devices (Norwood, MA)

Analog Signal Processing: Mixers and AGC Amplifiers,* **Barrie Gilbert, Eberhard Brunner, Tom Kelly, and Bob Clarke,** Analog Devices, Inc. (Norwood, MA).....16

Analog-to-Digital and Digital-to-Analog Conversion: Digitizing at IF and DDS,** **Scott Behrorst,** Analog Devices, Inc. (Greensboro, NC).....N/A

Digital Signal Processing in Wireless Communications: Focus on Digital Transmitters, **Dan Ash,** Analog Devices, Inc. (Campbell, CA).....40

**Paper presented by Bob Clarke.*

***Revised paper to appear in *Microwaves & RF*, July 1993.*

balanced BPSK modulator serves as an analog exclusive OR gate. The output of the balanced modulator can be expressed as follows;

$$(4) \quad V_{out} = \omega_c \oplus V_{data}$$

Where: V_{out} is the output voltage of the modulator.

ω_c is the RF carrier signal to be modulated. V_{data} is the modulating data signal.

To facilitate maximum carrier suppression, unity gain in the modulator path is used. Unity gain eliminates amplification of the offset voltages. Offset in the modulators leads directly to a decrease in the carrier suppression in the modulator.

The carrier buffer is simply a differential amplifier that takes a single ended input and gives a differential output. The inputs are biased at approximately 3 volts and the input impedance is approximately 10 k ohms and 2 pF. If a 50 ohm source is to be used to drive the SL801, simply terminate the input with 50 ohms and capacitively couple the signal to the input. The other differential input is AC grounded through 50 ohms in series with 10 pF. The 10 pF capacitor is connected to a pin on the package that allows the low frequency response of the input to be extended by adding a capacitor from this pin to ground. Emitter degeneration is used in the amplifier to extend the linear signal handling ability of the amplifier up to a maximum of -5 dBm.

The Gilbert cell modulator schematic is shown in Figure 2. The schematic shows the basic Gilbert cell and the level shifters at the modulating inputs and the carrier inputs. this level shifting ensures that the transistors in the cell do not saturate, which could degrade carrier suppression.

The lower two transistor pairs Q33 and Q3 are the RF input and the four upper transistors Q26, Q13 and Q4 ,Q24 are the modulating or phase reversing transistors. Emitter degeneration is used in the lower pair of transistors to extend the linear signal handling capability of the RF input. The upper four transistors in the cell have no degeneration as this would degrade the gain of the modulator.

As the upper pairs of transistors are switched the RF carrier is steered to the modulator output depending on which set of transistors in the top of the cell are biased on. For instance if Q 26 and 24 are on, then RF is passed to the output through the cascoded pair made up of Q33 and Q26 and Q3 and Q24. As Q13 and Q4 are turned on by the modulating wave form the cascode arrangement switches over to Q33 and Q13 and also Q3 and Q4. So as the modulating wave form changes state the phase of the carrier is changed 180 degrees. The gain of the modulator circuit can be approximated by the following equation;

$$(5) \quad G_v = \frac{RI}{(R_c + r_e)}$$

Where;

G_v is the voltage gain of the circuit.

RI is the collector load resistance. (R38 or R28 in the schematic)

r_e is the intrinsic emitter resistance of the transistor

$$\text{where } r_e = \frac{IC}{V_i}$$

Since the modulator path has 0 dB of gain , both of the modulators are identical. Now returning to the block diagram in Figure 1, the output of the first modulator can be expressed as follows with appropriately substituting (3) into (4);

$$(6) \quad D = \omega_c \oplus [(C \oplus D) \oplus (C \oplus D)\tau]$$

where ω_c is the RF carrier signal, and

$$(7) \quad E = \omega_c \oplus [(C \oplus D) \oplus (C \oplus D)\tau] \oplus [(C \oplus D)\tau]$$

Now using the following Boolean identity;

$$(8) \quad A \oplus B \oplus B = A$$

$$(9) \quad E = \omega_c \oplus (C \oplus D)$$

which is the desired result for the output of MOD 2.

So by using the delay component, two modulators may be cascaded together to achieve approximately twice the carrier suppression that can be achieved with one modulator. It should also be noted that the output from the first modulator is indeed a spread spectrum signal. However, there is no way that the receiver can demodulate the information that is in this signal unless the appropriate delay is generated in the receiver.

It is also worth noting that the choice of the delay component is quite critical to the success of the cascaded arrangement of modulators. It is important that the two modulating signals be as closely decorrelated as possible. Therefore, the minimum clock delay for correct operation is one, and the larger the delay, the more decorrelated the two signals become, but at the expense of added circuitry. It was felt that the minimum delay period would yield a satisfactory result.

3. Driver Section

After modulating the RF carrier, the output of the modulators is driven into a differential output 50 ohm driver. The output of this differential driver can be configured in several ways. Since the output is an

Analog Signal Processing: Mixers and AGC Amplifiers

Barrie Gilbert, Eberhard Brunner, Tom Kelly, and Bob Clarke

Analog Devices, Inc.

Overview

The invention of the superheterodyne receiver, more than sixty years ago¹, marked a major step forward in radio receiver design. It addressed basic problems associated with the then-prevalent “tuned-radio-frequency” (TRF) receiver, the most difficult of which was that of maintaining tight matching of the frequency response of many selective circuits, all operating at some *variable* frequency, as these were tuned over their full range.

The pivotal concept was to translate a selected incoming signal to a *fixed* “intermediate” frequency (IF), in order that the tuned circuits providing the all-important selectivity between closely-spaced carriers could now operate at this one optimal frequency, and be tailored to achieve very exact bandpass characteristics. For certain applications, such as the reception of code using a pulsed carrier with little sideband energy² it was for the first time possible to use very narrow-bandwidth “crystal filters” based on quartz resonators.

The key components which made the superheterodyne possible were, first, a *mixer*, which converted the incoming RF to the (usually, though not universally) lower IF, by multiplying it by a *variable* frequency from the second key element, a *local oscillator* (LO), such that

$$\begin{array}{rcccl} f_{IF} & = & f_{RF} & - & f_{LO} \\ \text{(Fixed)} & & \text{(Some} & & \text{(Variable)} \\ & & \text{range)} & & \end{array}$$

The characteristics of the mixer (chiefly, its intermodulation distortion and noise floor) and the local oscillator (its long- and short-term frequency stability) dominated the overall performance, as remains true today. This is because these critical components

¹ Armstrong, Edwin R., “The Super-Heterodyne: Its Origin, Development, and Some Recent Improvements.” Proceedings of the I.R.E., vol. 12, no. 5 (October, 1924)

² Somewhat misleadingly called “continuous-wave”, or CW, transmission.

open collector circuit, a 50 ohm resistor connected to each output and up to the supply rail will properly set the gain of the driver and allow the circuit to drive up to -5 dBm into any 50 ohm load. The output signal can also be driven into a balun and an additional 6 dB of drive obtained, less any balun losses.

The 50 ohm driver circuits are open collector differential amplifiers. A bias resistor of 50 ohms must be connected to the open collector outputs up to the 5 volt supply line. These loads can then be AC coupled to the next circuit in a single ended fashion, coupling one of the outputs to the next stage and also AC coupling the unwanted output to a 50 ohm load. This terminates the collectors with the correct differential impedance. Either output can supply -5 dBm, or if a RF balun is used correctly, the output power would increase to +1 dBm.

4. AGC Amplifier

The modulated signal is filtered externally before entering the input to the AGC amplifier. Alternatively, further processing and/or phasing with other SI801s can yield QPSK signals. The AGC amplifier has 5 dB of gain and 30 dB of AGC control range.

The AGC amplifier is also a Gilbert cell type circuit. Referring to the schematic of the amplifier in figure 3, the main portion of the amplifier is made up of transistors Q13, Q81, Q11, Q19, Q4 and Q54. In parallel with this Gilbert cell is another amplifier made up of transistors Q79, Q80, Q60 and Q33. This amplifier in parallel with the Gilbert cell serves to keep the DC point at the load resistors R55 and R53 constant as the gain control is varied by diverting current away from the collectors of Q11, Q19, Q4 and Q5.

The gain of the AGC amplifier is controlled via the differential amplifier comprised of transistors Q15 Q56. as the voltage at the AGC control input is increased above the DC bias point at the base of Q15, Q56 turns on and the current through the diode load Q57 supplies the bases of Q19 and Q4. The diode current compensates for the nonlinear control characteristic and provides a linear control characteristic over the voltage range of 2.5 to 3.5 volts.

5. Output Amplifier

The output of the AGC amplifier is fed into a differential amplifier capable of driving 0 dBm into a 50 ohm load. This differential amplifier has 0 dB gain and is similar to the 50 ohm driver at the output of the modulator section. The outputs of the amplifier are pulled up to the supply via 50 ohm resistors and capacitively coupled to the load. If a differential drive is not desired the unused output should be capacitively coupled to a 50 ohm load.

This 50 ohm driver is similar to the 50 ohm driver that is at the output of the modulators, only capable of supplying 0 dBm to the load in a single ended

application or again if an RF balun is used it is capable of delivering +3 dBm.

6. Design Considerations

On the chip are separate voltage regulators and grounds for the digital and analog functions. The chip can be put in a standby mode by supplying a TTL compatible signal that is active high.

In the digital section of the device all TTL/CMOS input levels are level translated down to a peak swing of 150 mV on chip. This is done to avoid large signal swings at the modulating inputs of the Gilbert cell and also helps with cross talk on chip.

Separate bandgap regulators for the digital and analog functions on the chip are used to set the bias point for the current sources. This was done to reduce the cross talk among the various digital and analog circuits.

In the layout of the I.C., great care was taken to match all of the transistors and metal runs in both the digital and analog sections. In the modulator section of the device all metal traces were matched to within 1 milliohm to avoid DC offsets. The carrier buffer, two modulators and the first 50 ohm driver are also surrounded with trench isolated substrate contacts to further avoid cross talk from the digital section. Both the AGC amplifier and the AGC 50 ohm driver are also surrounded with trench isolated substrate contacts to ensure that the carrier does not leak into these circuits degrading the carrier suppression after the modulator section.

7. The HE Process

Process HE is a bipolar process incorporating polysilicon base/emitter contacts, trench isolation and an advanced base/emitter structure. The process has been characterized as having a peak Ft of 14 Ghz. There are three layers of metalization available on the process.

The NPN devices are available in four different emitter lengths of 2, 5, 10 and 15 microns. There are also PNP devices available. Internitride capacitors can also be fabricated on the process with realizable values of up to 5 pF for a single capacitor. Inductors can be fabricated on the third metal layer with Q's measured at 10. There are also two different types of resistors, both of which are polysilicon. Low value resistors can be realized using 200 ohms per square polysilicon and high value resistors can be made by putting a barrier around the 200 ohms per square polysilicon increasing the sheet resistivity to 2000 ohms per square. Another feature of process HE is the ability to open selective substrate contacts around different portions of the circuitry and then surrounding these substrate contacts with walled trench isolation. This then serves to isolate portions of the circuit from other functions on the chip, thereby increasing the amount of isolation between different circuit functions.

must operate in the more difficult raw-RF domain, where little selectivity is available, and thus intermodulation between several incoming signals is more likely.

Later, as operation at higher RF frequencies grew in importance, a second advantage of the superheterodyne became apparent, namely, that high gain could be achieved more readily at a lower intermediate frequency (commonly, 455kHz, more recently, 10.7MHz). Further, to cope with a very large dynamic range of the received signal, automatic gain control (AGC) was incorporated into the multi-stage IF amplifier. More sophisticated receivers also used automatic frequency control (AFC) to cope with residual frequency drift in the LO, a practice largely eliminated by the availability of very accurate frequency-locked oscillators, nowadays using digital synthesizer techniques. Even later in the development of the superheterodyne architecture, two, or even three, stages of frequency conversion were used, to provide in effect a frequency "sieve" through which spurious by-products of the mixing processes were unlikely to pass.

This evolution has left us with a more or less standard superheterodyne architecture. In recent years, digital techniques are being found to a greater extent in the latter end of the signal processing chain. Figure 1 shows a modern dual-conversion superheterodyne receiver using linear IF amplifiers. Demodulation to baseband, and possibly some further selectivity, is here accomplished by digitizing the output of the second IF amplifier using an *analog-to-digital converter* (ADC) and applying this to a *digital signal processing* (DSP) block. AGC is effected via this DSP, but *variable-gain amplifier* (VGA) sections (usually, *voltage-controlled amplifiers*, or VCAs) are still required to compress the dynamic range to the point where a relatively low-resolution ADC (usually 8-bits, providing a theoretical dynamic range of 48dB) may be used.

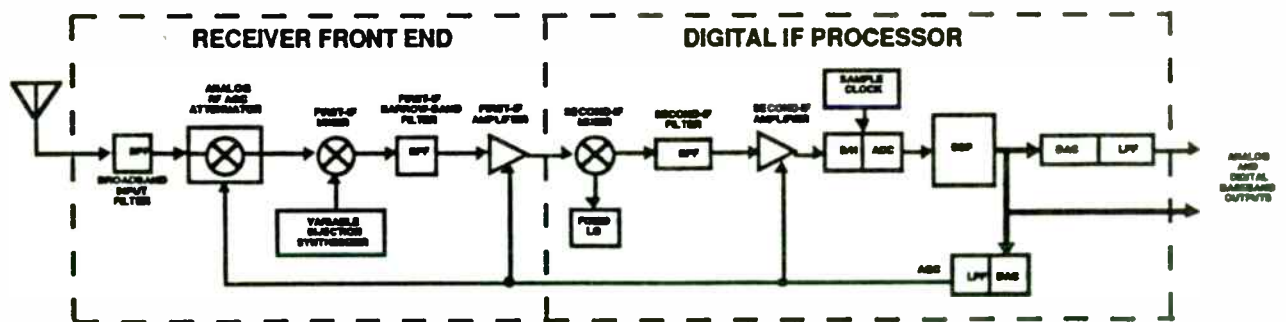


Figure 1. A Modern Superheterodyne Receiver

8. Conclusions and Further Work

The objectives of designing a high performance, low power, and convenient PSK modulator have been met. Figure 5 shows a typical output spectrum of the device.

Two SL801 circuits can be combined to produce QPSK or OQPSK signals. Furthermore, MSK can be generated with two SL801s operating in quadrature. MSK is the most likely baseband of choice for frequency hopping spread spectrum systems operating under Part 15. These applications are certainly possible using the current SL801 and/or derivative circuit configurations.

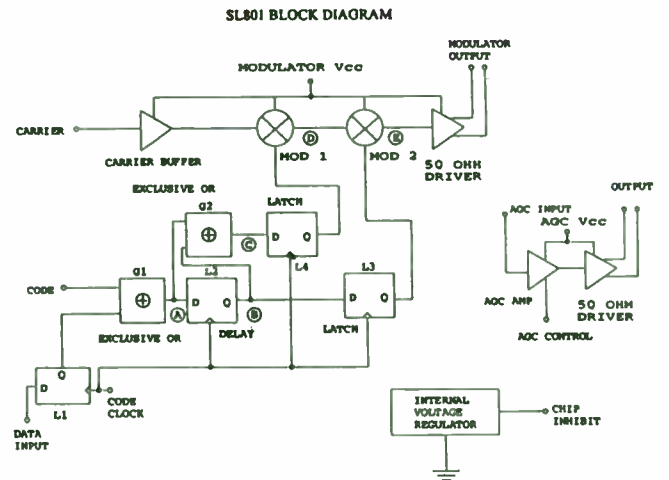


Figure 1.

MODULATOR

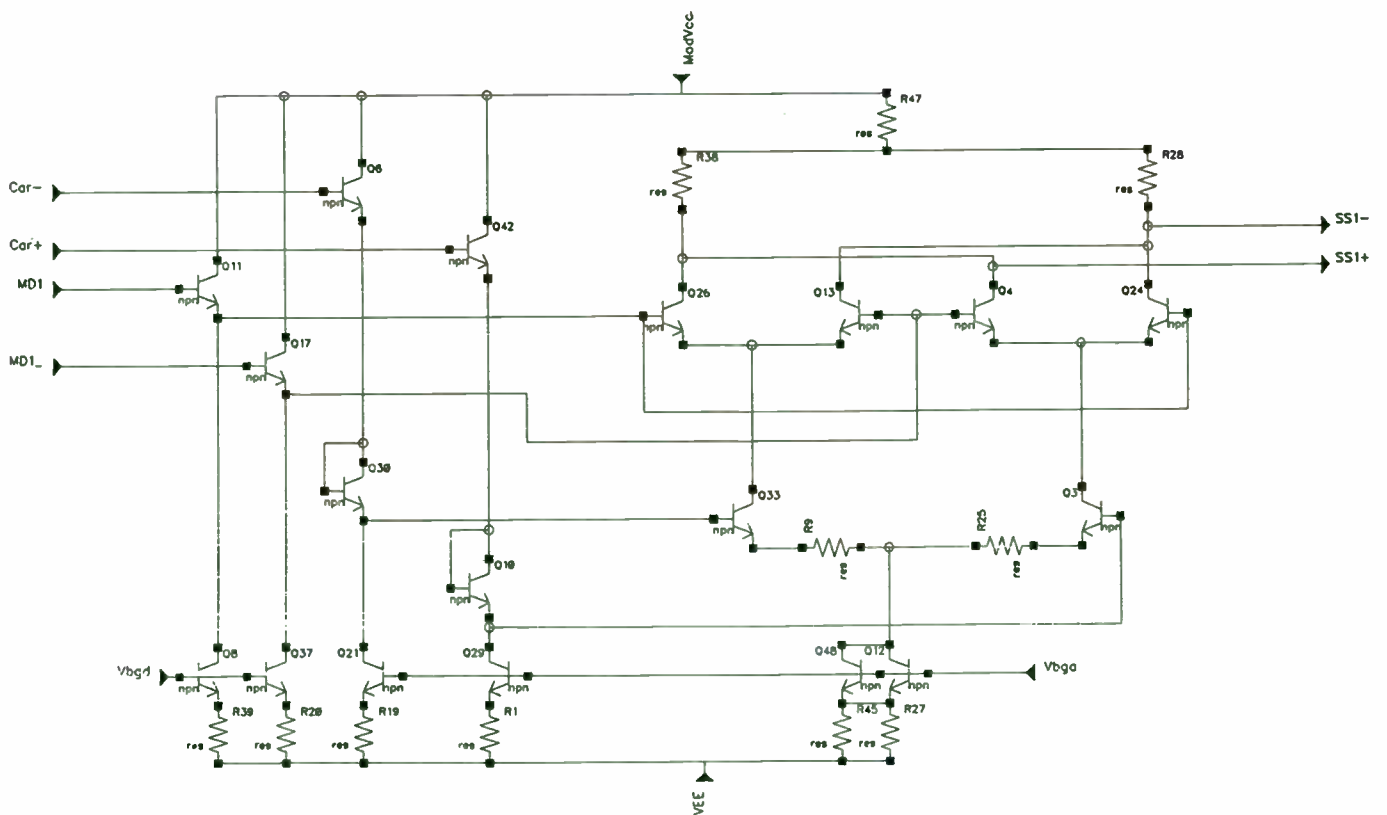


Figure 2.

Of course, many variations of this generalized theme are to be found. Depending on the application, the receiver may use single, dual, or triple conversion and either a fully-analog or DSP baseband section. Whatever the choice of architecture, however, the designer will generally need (in discrete, small-scale monolithic, or specialized ASIC form) mixers, oscillators, filters, RF and IF amplifiers (either linear, or limiting, or sometimes logarithmic), and various types of demodulator, depending on the modulation technique(s) with which the receiver must cope. Analog Devices, Inc. now supplies many of the components for use in high-performance receivers.

Mixers

A mixer³ is a nonlinear three-port element providing frequency conversion. The two input ports accept the RF and LO signals; these are subjected to multiplication, and the product at the third (output) port includes a strong component at the desired IF, along with a variety of unwanted spectral components. A linear four-quadrant multiplier⁴ could be used for this purpose, but its noise performance is much poorer than a circuit optimized for mixing, which in the simplest case provides a linear response only on the RF input, the *phase* of which is *sign-alternated* (0/180°) by the LO input. We will return to this circuit later. Nevertheless, we can understand mixer behavior more readily by assuming *linear* multiplication at this point.

Multiplication in the time domain corresponds to addition and subtraction in the frequency domain. This is easily demonstrated. Given two cisoidal⁵ input signals, say, $A\cos\alpha t$ and $B\cos\omega t$, representing the RF and LO inputs respectively, an ideal mixer (which for now is taken to mean one which exactly multiplies its RF and LO inputs) would generate the output

$$A\cos\alpha t B\cos\omega t \quad \text{Eq. (1)}$$

which can be expanded to

$$\frac{1}{2} AB \{ \cos(\alpha+\omega)t + \cos(\alpha-\omega)t \} \quad \text{Eq. (2)}$$

3 This term is also used in a video and audio context to refer to a totally different element, providing a *linear* combination of two or more inputs.

4 For example, the 500MHz current-output AD834, the 250MHz voltage-output AD835 or the general-purpose 10MHz AD734.

5 That is, either purely sinusoidal or co-sinusoidal, waveforms which differ only in phase positioning.

AGC AMP

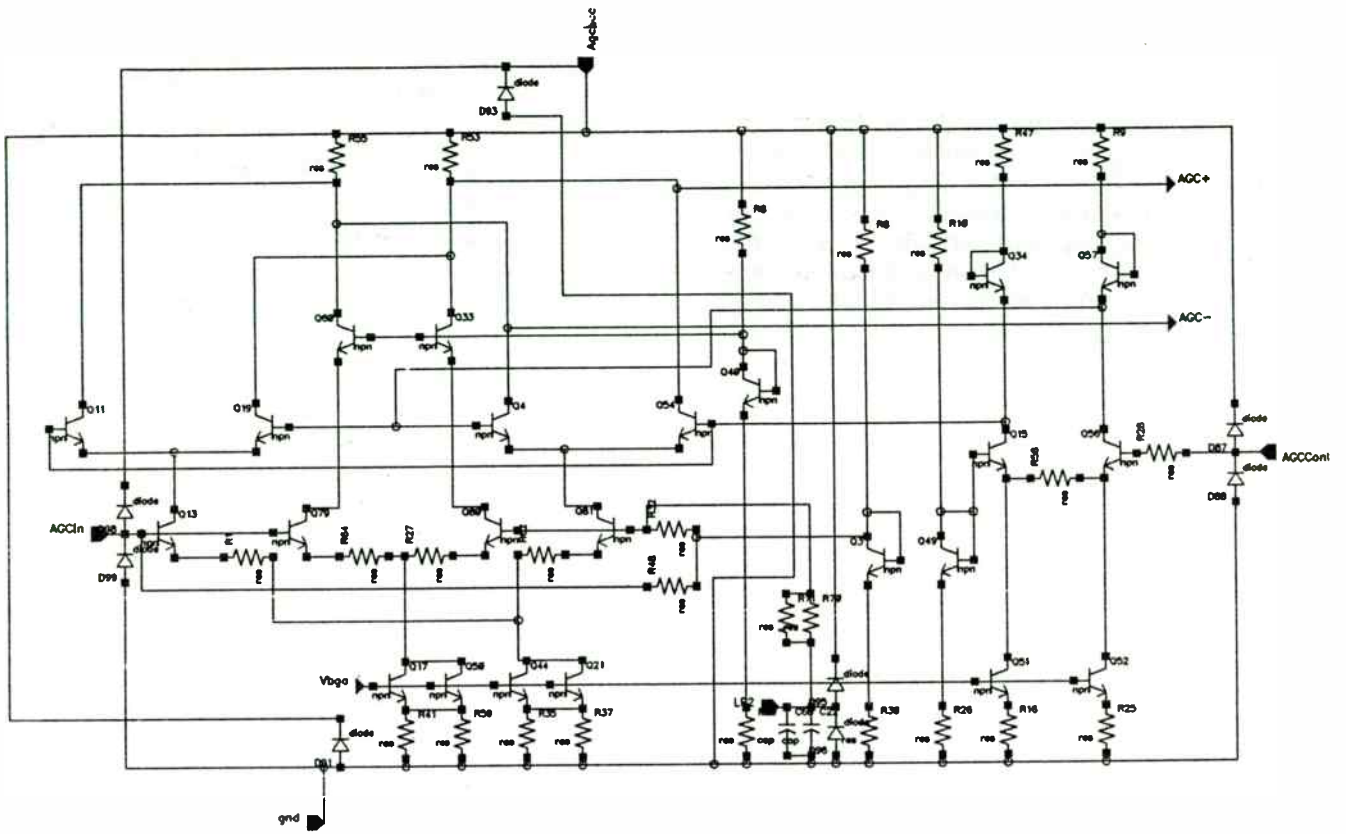


Figure 3.

50 Ohm DRIVER

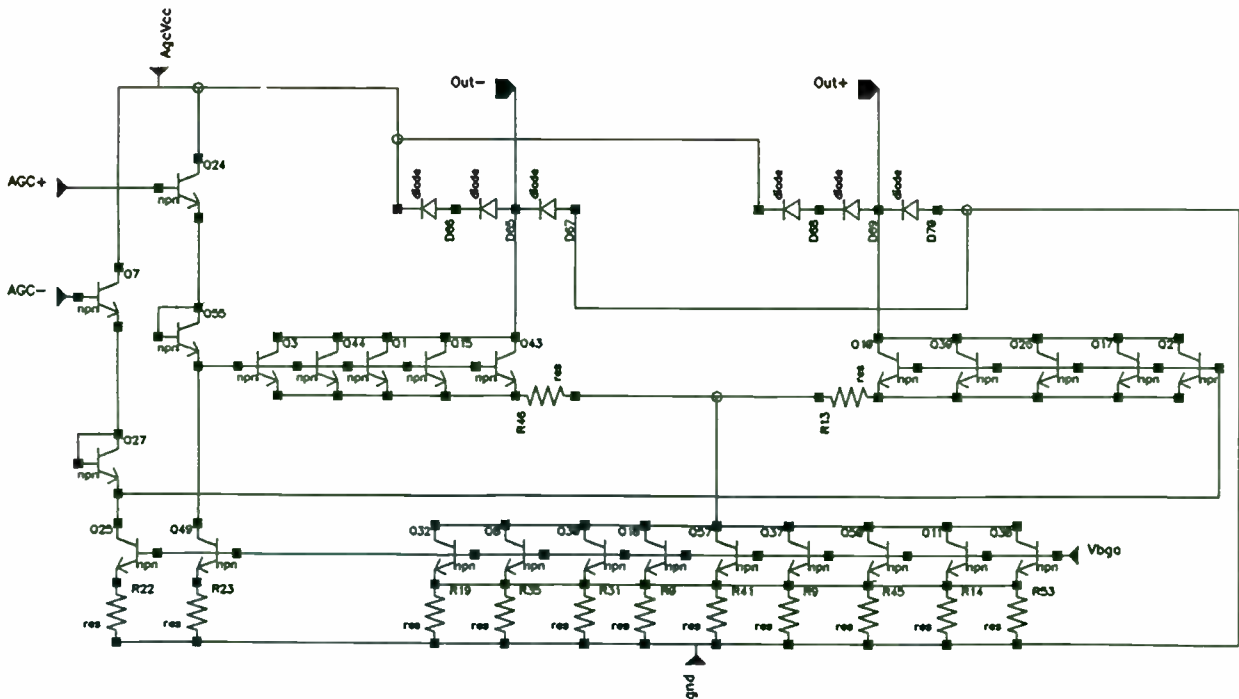


Figure 4.

The two most important features of this process are (1) the appearance of *sum* and *difference* frequencies in the output function⁶, and (2) the *fundamental* 6 dB loss (due to the factor of $1/2$ in the expansion) in the amplitude of either the sum or difference outputs. When the (usually much higher) sum frequency is used as the IF, the mixer is referred to as an *up-converter*; conversely, the term *down-converter* refers to the use of the (usually much lower) difference frequency as the IF, which is the more common situation.

Of itself, the 6 dB loss would only put an increased burden on the noise performance required of the first stage of the following IF amplifier. More problematical is the fact that, for a *down-converter*, the broadband noise at the mixer input generates an *image* (by folding of the $\alpha\text{-}\omega$ spectrum about the zero-frequency axis) at the IF, so doubling the noise power in the IF passband, leading to a 3 dB worsening of the effective mixer noise, and thus a 3 dB reduction in the dynamic range, referred to the RF port.

Practical mixers generate considerably more complex outputs because of unintentional nonlinearities in the amplitude response, as well as from many subtle mechanisms related to time-varying elements, particularly junction capacitances, within the circuit devices. It is for this reason very desirable to place the first stage of IF filtering as close as possible to the mixer output⁷.

For practical reasons (related primarily to noise performance), a linear multiplier is not ideal for mixer applications, nor is there generally any advantage to using such. One reason for this is that IF filtering must be used anyway, so the absence of strong harmonics of the IF — a possible advantage of the linear multiplier when driven by a cisoidal input at its LO port — is unimportant. Another reason is that many modern local oscillators generate square-wave outputs, which is actually desirable in achieving low mixer noise⁸.

Thus it is that high-performance mixers, such as diode-transformer (passive) and most IC (active) mixers, use essentially a *switching* (or commutating) process⁹. The *sign* of the

⁶ Note that these are not synonymous with upper and lower sidebands, which refer rather to spectral components (at both the sum and difference frequencies) which extend above (upper sideband) and below (lower sideband) the carrier frequency.

⁷ Either that, or ensure that and signal-handling stages between the raw mixer output and the filter are designed to be ultra-linear. There are many practical details which need to be considered in this regard.

⁸ Note that while *harmonic* purity is not required of a local oscillator, other types of spectral purity are.

⁹ The terms "singly-balanced modulator" and "doubly-balanced modulator" are sometimes used to describe particular integrated-circuit structures to implement the mixer function.

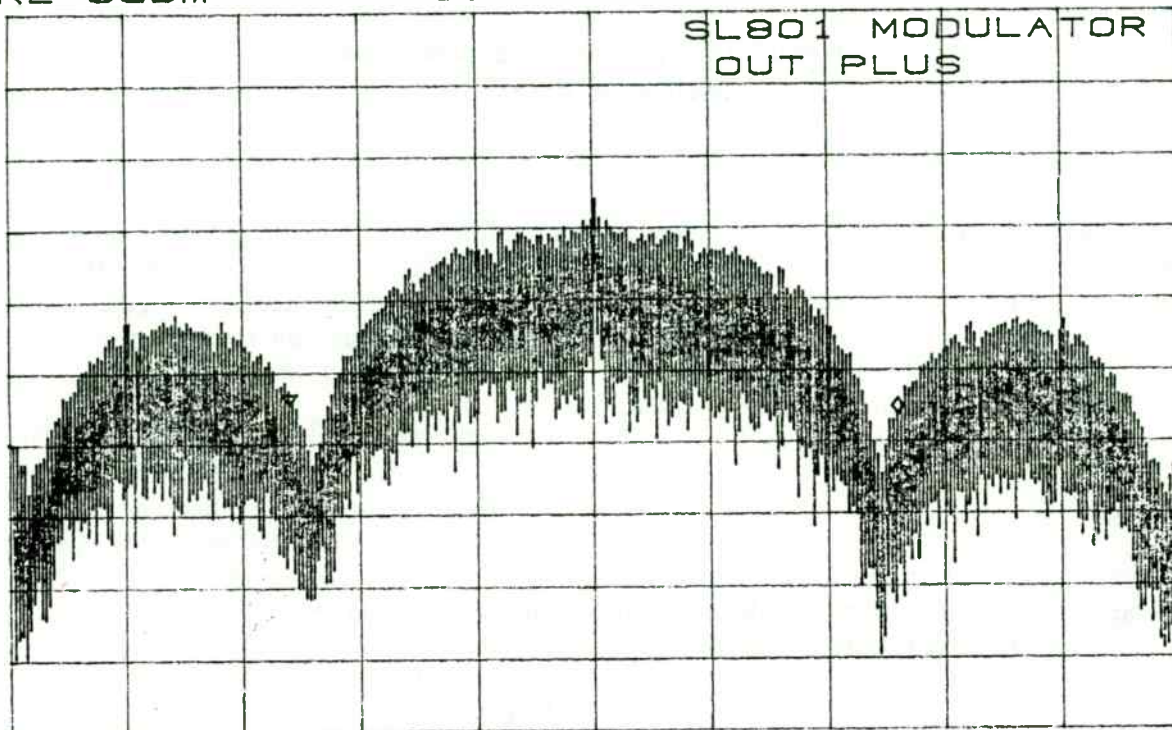
TYPICAL OUTPUT SPECTRUM

ATTEN 10dB
RL 0dBm

10dB/

Δ MKR -1.67dB
26.00MHz

SL801 MODULATOR
OUT PLUS



CENTER 915.00MHz
RBW 300kHz

VBW 300kHz

SPAN 50.00MHz
SWP 50ms

Figure 5.

signal transmission from the RF port is alternated between normalized binary values of +1 and -1, by an LO input which would ideally be a perfect square-wave. In practice, this can be approximated quite well at moderate frequencies (with today's technologies, this could mean up to about 100MHz, depending on power limitations) but the LO waveform becomes progressively more rounded, and the mixer's switching-time more pronounced, at higher frequencies.

Once again resorting to an idealization to provide rapid insight, a square-wave LO signal at an angular frequency ω can be expressed as the sum of a series of odd harmonics given by its Fourier transform, the first four terms of which are

$$\frac{4}{\pi} \left(\cos \omega t - \frac{1}{3} \cos 3\omega t + \frac{1}{5} \cos 5\omega t - \frac{1}{7} \cos 7\omega t \right). \quad \text{Eq. (3)}$$

Given an RF signal of normalized amplitude, that is, $\cos \alpha t$, the fundamental IF output (omitting the higher-order terms) has an amplitude

$$\frac{4}{\pi} \cos \omega t \cos \alpha t \quad \text{Eq. (4)}$$

which expands to

$$\frac{2}{\pi} (\cos (\omega + \alpha)t + \cos (\omega - \alpha)t) \quad \text{Eq. (5)}$$

Note that, for a switching multiplier, the normalized insertion loss is only 3.9 dB (that is, $20 \log_{10} \frac{2}{\pi}$). However, although the noise performance is much improved over a linear multiplier cell, the doubling of the output noise in a down-converter, due to the image of the noise at the RF port, remains.

The design and application of passive diode-transformer mixers has been widely treated in the literature and will not be discussed here¹⁰. Their main advantages are: (1) good linearity when properly driven and terminated; (2) high operating frequencies — to several gigahertz — using low-capacitance Schottky (sometimes, GaAs) diodes, and (3) relatively low cost due to very large manufacturing volumes. Their chief disadvantages are (a) poor isolation between ports; (b) the need for large amounts of LO power to drive

¹⁰ A good overview of practical matters is to be found in any of the annual handbooks issued by the American Radio Relay League (ARRL), 225 Main Street, Newington, CT 06111.

Methods for Estimating and Simulating the Third Order Intercept Point

Carl Stuebing and Mojoy C. Chian

Harris GCSD and Harris Semiconductor
Melbourne, FL 32901

Abstract - The third order intercept point (P_{ip3}) is a metric to quantify the nonlinearity of a circuit. P_{ip3} is used to describe the adjacent frequency isolation and gain distortion. This paper describes the concept of P_{ip3} and reviews methods to estimate and simulate it. The common simulation pitfalls are identified and practical solutions are discussed and illustrated.

I. Introduction

The nonlinearity of a radio amplifier determines its distortion. As the input signal level increases, distortion of the output signal becomes prominent and undesired harmonic products are produced.

Consider two FM carriers at 50MHz and 100MHz applied to the input of a radio amplifier. Assume that there is little filtering of the input signal and that we are interested in amplifying the 100MHz signal. However, the 50MHz signal is so strong that it drives the amplifier into distortion. In this situation, the second (2X50MHz) harmonic of the 50MHz signal would interfere with the 100MHz signal at the output of the amplifier.

Obviously, radio receivers generally do have selective filters on their signal inputs. So interference of signals is, as a practical matter, more important for signals which are close together in frequency (i.e. in band).

Nonlinearity can also cause less obvious interference problems with signals that are close together in frequency. When two in band signals are applied to a nonlinear circuit element, they will mix. This process is called intermodulation and the resultant frequency components are referred to as intermodulation products. It can be shown that the frequencies of the intermodulation products are defined by $k_1f_1 \pm k_2f_2$, where k_1 and k_2 are integers. The component with a frequency equal to $n_1f_1 \pm n_2f_2$ is defined as the n th order intermodulation product, where $n = n_1 + n_2$ [1,2].

While the two fundamental signals will typically be magnified by the amplifier, components at the sum and differ-

ence frequencies are also produced at the output. These second order intermodulation products are not usually considered to be important, because they are typically far enough out of band from the fundamentals that they can be easily suppressed with filters.

More important are the third order intermodulation products. These occur at frequencies given by the two times one frequency minus the other, and vice versa. While these parasitic signals may be smaller in amplitude than the second order products, they are more difficult to filter out. Consider two FM signals at 100 and 101 MHz. The third order parasitic tones are produced at $202-100=102\text{MHz}$ and $200-101=99\text{MHz}$. When the signal distortion is large, these products become significant since they are produced well within the band of the input frequencies.

A popular metric to quantify distortion is the Third Order Intercept Point, or " P_{ip3} ". For a two-port network excited with two sinusoidal signals with frequencies f_1 and f_2 , if the third-order intermodulation product output power ($P_{2f_1-f_2}$) and the output power at f_1 (P_{f_1}) are plotted versus the input power at f_1 , the third-order intercept point (P_{ip3}) is defined as the point where P_{f_1} and $P_{2f_1-f_2}$ intercept. The third-order intercept point is a theoretical level, however, it is a useful and popular quantity to estimate the third-order intermodulation products at different power levels (Figure 1).

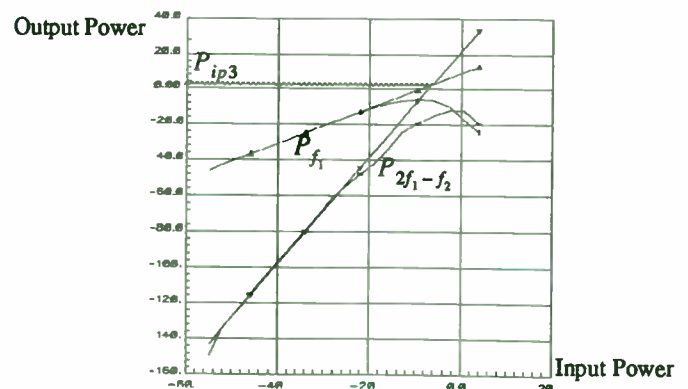


FIGURE 1. P_{f_1} , $P_{2f_1-f_2}$, and their asymptotes.

the diodes; (c) high absolute insertion loss, and (d) the requirement for very careful matching at the IF port.

Figure 3 shows a common form of diode-transformer mixer, using four diodes; two-diode forms are also used. Passive mixers generally have 8 to 10 dB of insertion loss and a similar noise figure. The signal-handling capability and the third-order distortion are roughly proportional to the LO drive level. High intercept diode-ring mixers can require +27 dBm (500 mW) or more of LO drive.

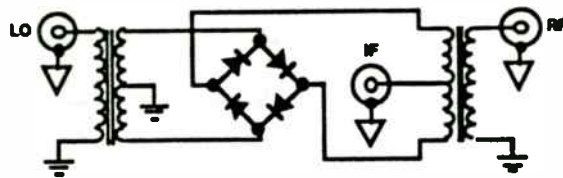


Figure 3. Typical Diode-Ring Mixer

The insertion loss of the passive mixer often requires that it be followed by a Class A low-noise amplifier, which may consume another 500 mW or even more if large signal swings are to be accommodated. The passive mixer's fussy sensitivity to termination often requires the use of a diplexer at the IF port. In some "passive" mixers, the diodes are replaced by FETs which are driven into hard conduction by the LO drive.

Discrete active mixers use transistors — most commonly FETs, sometimes double-gate devices — operating with essentially linear bias conditions. *IC mixers* generally use bipolar transistors, and comprise an RF input section which provides voltage-to-current conversion and a two- or four-transistor current-mode switching core, which introduces a more or less abrupt sign-change into the signal path between the RF input and the IF output, controlled by the LO signal. Figure 3 shows a typical IC mixer.

The power gain of the fundamental frequencies is linear and remains constant until we have a large enough input signal that clipping or gain compression occurs. However, the voltage gain of the third order products is raised to a cubed power instead of linear (as in the case of the fundamental). This means that the power gain of the third order harmonics is three times higher than that of the linear fundamental. Of course, the power level of the third order product is normally less than that of the fundamental. As the input power level increases, the ratio of the fundamental power output to the third order product output power level decreases rapidly.

The output P_{ip3} (P_{ip3o}) is defined as the point where the asymptotes of the fundamental linear power gain curve and the third order product power gain curve intersect. We can use simple trigonometry to relate this output power level to the fundamental and third order frequency gain curves. Knowing P_{ip3o} , the input power level, and the power gain, we can extrapolate the power level of the third order intermodulation products. If G is the power gain, then

$$P_{ip3o} = P_{ip3i} + G$$

When P_{ip3} is large, the power level of the third order products is suppressed, or distortion is reduced. Obviously, this is desirable. When P_{ip3} is small, the third order product power is relatively large, or distortion is increased.

While the “real world” does not consist of only two interfering radio channels, this is a convenient technique. Here we allow ourselves to define a metric for quantifying the distortion and thus the interference of radio signals.

II. Review of Some Traditional Estimation Techniques

Several “rules of thumb” exist within the RF industry for estimating P_{ip3} . Since accurate simulation of P_{ip3} can be very computer time intensive, one should attempt first to estimate this parameter. P_{ip3} is in some ways more dependent on system level considerations (such as the input termination method and available power supply voltage and current) than device design considerations (such as the geometry selected for the RF transistor). Generally, once the system determines P_{ip3} (which should be quickly albeit roughly estimated), computer simulation can be used to measure the somewhat subtle effects of transistor or integrated circuit level design on P_{ip3} .

Rule #1

The first (system level) rule of thumb is that P_{ip3} is about 6 to 10dB higher than the 1dB gain compression power level. The 1dB gain compression level refers to the signal level at which the gain at the frequency of interest has decreased due to clipping by 1dB or 12%.

There are no known elegant mathematical discussions to prove this rule. We simply have an empirical number which has been known to be a useful approximation. This is not an extremely accurate rule, but coupled with a one tone simulation is much faster than two or three tone simulations.

Rule #2

The second rule of thumb relates output power available to output intercept point. As an approximation, use the maximum (RMS) power available to the load as the 1dB compression point for output power.

This rule implies that the amplifier is piecewise linear. Thus, gain is approximated to always be equal to the (very) small signal level until the available output power level has been reached. Once the peak output power has been exceeded, the signal is suddenly clipped and incremental gain becomes zero at the maximum or minimum voltages of the output. The point at which this process starts is used to identify the approximate one dB compression point.

Real amplifiers typically demonstrate increasing compression with amplitude. Thus, 12% gain compression normally occurs below the maximum available output power level. Therefore, this rule of thumb is very rough and optimistic.

Extension #1

Some interesting results can be obtained from carrying the above assumption further. Assuming that voltage saturation of devices is not permitted, the available output power for a single collector load resistor in a common emitter amplifier is given by:

$$P_{out1dB} = \frac{I_{nom}^2 R_L}{2}$$

Where I_{nom} is the nominal DC bias current in the collector of the transistor. This is assumed to be the available zero-to-peak output current. Of course, this equation neglects the lost power output (i.e. gain) at higher frequencies due to capacitive loading.

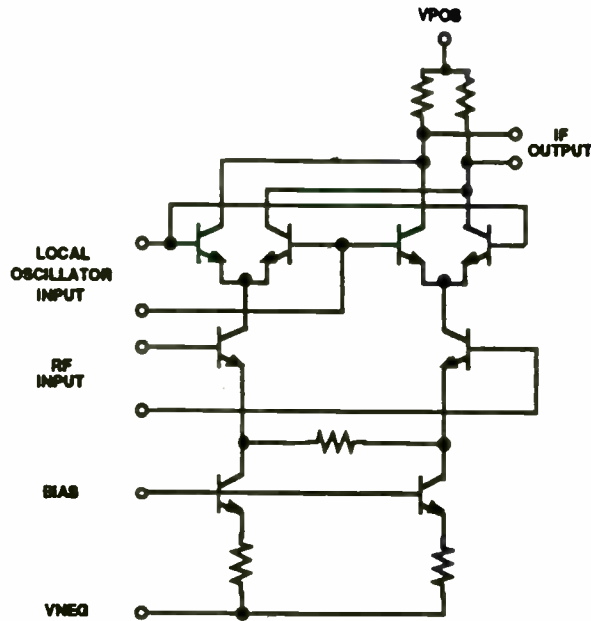


Figure 3. A Typical IC Mixer

The main advantages of active mixers are: (1) conversion gains — of typically 10 to 20 dB — can be achieved; (2) much lower local-oscillator power is needed; (3) excellent isolation between ports is achieved, resulting, for example, in very little radiation of the local oscillator signal from the RF port; (4) they can incorporate a modest amount of variable gain control for AGC purposes; (5) they are essentially termination-insensitive at the IF port; (6) an LO preamplifier can be included to lower the required LO drive to very low levels (say, -20 dBm), and, (7) they lend themselves to higher levels of system integration. The chief disadvantages are: (a) a somewhat poorer dynamic range than passives and (b) typically lower operating frequency limits. However, the advances in IC process technologies over the past decade has led to some dramatic advances in integrated-circuit mixers such that their many advantages will generally outweigh the disadvantages in future products.

The power consumption of active mixers is roughly proportional to signal handling ability — the wider the dynamic range, the higher the supply power. This is because the voltage-to-current converter section must (for almost all RF applications) be a Class-A circuit, using current-sources and resistors to define the maximum RF input, often specified in terms of the “1 dB compression point” (that level at which the output is 1 dB below the ideal value extrapolated from the small-signal response) and the “third-order

Rule #2 can now allow us to take this available output power and use it for 1dB gain compression estimates. First, we rewrite the above equation in dBm:

$$P_{out1dB} = 10\log(500I_{nom}^2 R_l)$$

Now, we apply Rule #1 to estimate Output Intercept:

$$P_{ip3o} = 10\log(500I_{nom}^2 R_l) + 6dB$$

Extension #2

A popular method for obtaining Input Intercept is to find the difference between P_{ip3o} and power gain. However, a shortcut can simplify the calculation of P_{ip3o} . Power gain depends on input impedance, output impedance, and current gain (i.e. β). This information can also be used to determine the available output power and input power levels that are associated with the estimated 1dB compressed output power. No explicit gain estimate is really necessary. This method, generally, works best at frequencies much less than the f_T of the transistor.

Thus at the 1dB compression point, output signal power can be related to input signal power. The RMS input signal power is given by:

$$P_{in} = \frac{I_b^2 R_{in}}{2}$$

where I_b is the nominal base bias current associated with I_{nom} . We observe that the input current "just below compression" (given our simplified, piecewise linear model) is simply specified by I_{nom} divided by β (which is a function of frequency). The input resistance is given by r_π and R_b :

$$P_{in1dB} = \frac{I_{nom}^2 (r_\pi + R_b)}{2\beta^2}$$

Since $r_\pi = \frac{\beta V_t}{I_{nom}}$, thus [3]:

$$P_{in1dB} = \frac{R_b I_{nom}^2}{2\beta^2} + I_{nom}^2 \left(\frac{\beta V_t}{2\beta^2 I_{nom}} \right)$$

therefore,

$$P_{in1dB} = \frac{R_b I_{nom}^2}{2\beta^2} + \frac{I_{nom} V_t}{2\beta}$$

Since we are considering frequencies much lower than the f_T of the device (where β is large and R_b should be much less than r_π), the above equation can be approximated by:

$$P_{in1dB} = \frac{I_{nom} V_t}{2\beta}$$

To convert the 1dB output compression level to P_{ip3o} , apply rule #1, and add 6 to 10 dB.

$$P_{ip3i} = 10\log\left(\frac{500I_{nom} V_t}{\beta}\right) + 6dB$$

What is particularly interesting about this result is that P_{ip3i} (in Watts, not dBm) is proportional to V_t , I_{nom} (nominal collector current) and $1/\beta$. Of all the above terms, the only process related one is β . The rest are dependent on absolute temperature and the available power supply current. So system constraints dominate this situation. Also notice that large β is "bad", because it reduces P_{ip3i} . Of course, large β tends to help noise figure.

This rough method is much faster than lengthy computer simulations, and can give us a reasonably good feel for the system level trade offs affecting P_{ip3} .

III. Simulation tools and techniques for Computing P_{ip3}

The traditional method for calculating P_{ip3} by simulation is to use a Harmonic Balance based simulator. Harmonic Balance is a frequency domain method applied to nonlinear circuits, where the computations are performed using the trigonometric-series coefficients. The approach is based on balancing of currents between the linear and nonlinear subcircuits in the frequency domain. Since nonlinear devices are generally expressed in the time domain (e.g. Gummel Poon model for a BJT) their response has to be determined using time domain techniques. First, the input signals to the nonlinear devices are converted to time domain signals (using IFFT). Second, the time domain signals (voltages) are applied to the nonlinear devices and the time domain response (currents) is determined. Third, the time domain currents are converted to the frequency domain (using FFT). Finally, the frequency domain currents of the nonlinear devices are used in a global circuit equation to satisfy KCL at each node. This process is repeated many times until a consistent solution is attained (convergence).

Harmonic Balance determines the steady state response of nonlinear circuits to sinusoidal excitations. Even

intercept" (that extrapolated input level at which the amplitude of the fundamental and the third-order products in the IF output are equal). But low noise demands the use of low-valued resistors (comparable to 50 Ω) to achieve a low noise figure, thus requiring very large bias currents (sometimes many tens of milliamperes) to support the peak inputs without significant intermodulation distortion.

The Analog Devices' AD831 is a good example of a modern high-performance mixer optimized for use in critical applications where a combination of high third-order intercept (+30dBm) and low noise figure (12dB) are essential. This IC is usable at RF inputs to 800MHz, and includes a wide-bandwidth (100MHz) low-noise IF amplifier which can be configured to provide gain. A variable bias option permits operation at lower power when relaxed performance is permissible. Figure 4 shows the general topology of the AD831.

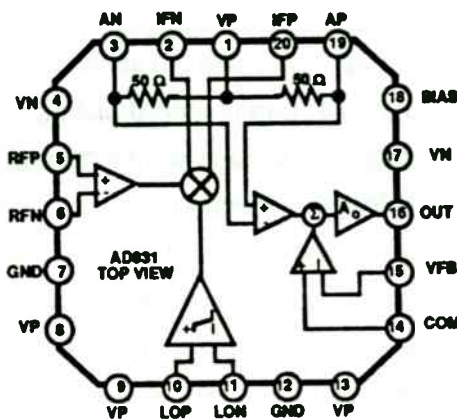


Figure 4. General Schematic of the AD831 High-Performance Mixer

Mixers are often preceded by a *low-noise amplifier* (LNA), frequently using silicon MOSFETs below 300 MHz, silicon bipolar transistors up to roughly 1 GHz, and GaAs MESFETs to over 10 GHz¹¹. The choice of gain for this amplifier is very critical: it should be just high enough so that its noise dominates the overall mixer performance, which in practice means that the output noise of the LNA needs to be about 6 dB above that of the RF port of the mixer. Any higher gain would only reduce the dynamic range.

¹¹ These ranges are very fluid as silicon IC technologies continue to broaden in applicability.

though the frequency domain response can be converted to the time domain, it does not contain the transient response of the circuit. This feature is a mixed blessing. For circuits with a very long and unwanted transient response (e.g. switching power supplies), harmonic balance is an efficient technique to bypass the transients and obtain the steady state response. For such cases, time domain based analysis algorithms can waste a lot of CPU time analyzing an undesired region of the response. On the other hand, for circuits like LNAs and comparators, it is essential to observe the transient response of the circuit to determine its effect on the frequency domain response. This issue is discussed in more detail in Section IV.

Time domain simulators (e.g. SPICE [4]), solve the global circuit equations by solving the nodal analysis matrix equation, $GV = I$, to determine node voltages (V). They solve an $n \times n$ system of equations per time step, where n is the number of nodes. Harmonic Balance simulators, on the other hand, satisfy the nodal current equations (KCL) for all harmonics in one step. This means that the system of equations to solve are $(nm) \times (nm)$. Where m is the desired number of harmonics. Since the CPU time required to solve a system of equations superlinearly increases with the size of the matrix, Harmonic Balance is expected to perform well for small circuits but not for large circuits. The large size of the system of equations also creates huge memory requirements even for moderately sized circuits by RF standards (e.g 10 transistors). As an example, a two tone RF circuit with 10 transistors may require as much as 600 MegaBytes of disk space. Additionally, since the convergence difficulty very rapidly increases with the number of equations involved, it is expected (and observed) that Harmonic Balance will have significantly more convergence problems than SPICE.

SPICE type simulators are very efficient in performing time domain analysis on large circuits. Transient analysis of circuits with many thousands of transistors is routinely performed by IC designers. In fact, RF ASICs (typically with less than 100 transistors) are considered small by IC simulation standards.

The drawback on using SPICE appears when the results are converted to the frequency domain. The typical process of performing transient analysis and then using FFT normally does not provide enough accuracy in the frequency domain. The following simple example demonstrates the lack of sufficient accuracy (also referred to as the dynamic range of FFT). Consider the following example of two series sinusoidal sources. A typical SPICE simulation, with 5005 internal time points, fol-

lowed by an FFT, with 1024 points, offers only 80db of dynamic range, Figure 2.

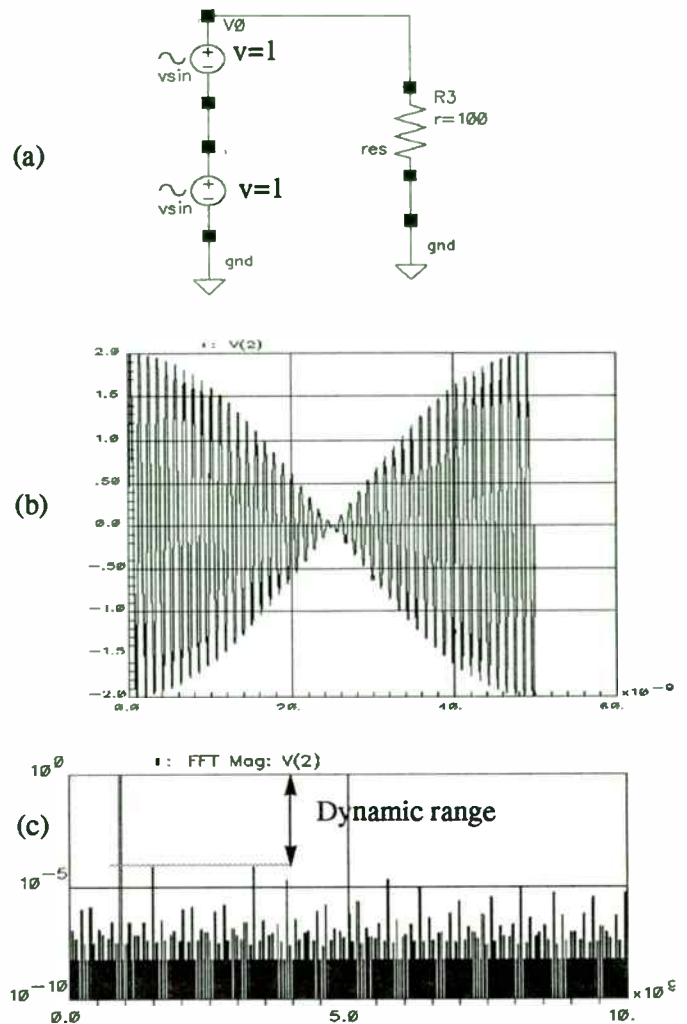


FIGURE 2. Two series sinusoidal sources (a), the time domain waveform (b), FFT results (c) with 5005 internal simulation time steps and 1024 FFT sampling points

In Section V, we will investigate the typical low dynamic range FFT and propose a technique to remedy the problem. With such a technique, the dynamic range for the same circuit and the same or less number of time points can be increased to 260 dB or more.

IV. Non Steady State and Other Pitfalls

RF circuits are traditionally designed, simulated and built with narrow band topologies. The narrow band approach is generally desirable and necessary. However, narrow band configurations, as well as time constants inherent in amplifiers, can cause design and simulation problems.

For example, consider a perfectly linear amplifier with unlimited bandwidth and no input capacitance. If we connect the amplifier to a two tone source which is AC cou-

IF Filtering

The mixer's output has one desired spectral component — the chosen IF, usually the difference frequency — and a host of undesired outputs, due to the presence of the many unwanted signals at the RF input, as well as cross-products arising from unavoidable spurious nonlinearities within the mixer. Thus, bandpass filtering is necessary to select just the desired output from the mixer.

In the case of the AD831, filtering may be added directly at the mixer's core's differential outputs. This may be as simple as shunting the internal resistive loads ($2 \times 50 \Omega$) with external capacitors, to heavily attenuate the sum component in a down-conversion application (Figure 5). The corner frequency of this one-pole low-pass filter should be placed about an octave above the difference-frequency IF. Thus, for a 70 MHz IF, a -3dB frequency of 140 MHz might be chosen, using capacitors of 22.7 pF.

When driving an IF *bandpass filter* (BPF), proper attention must be paid to providing the optimal source and load terminations so as to achieve the specified filter response. The AD831's wideband highly-linear output amplifier helps in this connection. Figure 5 indicates how its low-impedance (voltage source) output can drive a doubly-terminated band-pass filter. The 6 dB loss of conversion gain so incurred can be made up by the inclusion of a feedback network (the two 49.9Ω resistors) which increases the gain of the amplifier by 6 dB (X2). Higher gains can be achieved, using different resistor ratios, but with concomitant reduction in the bandwidth of this amplifier. Note also that the Johnson noise of these gain-setting resistors, as well as that of the BPF terminating resistors, is ultimately reflected back to the mixer's input; thus they should be as small as possible, consistent with the permissible loading on the amplifier's output.

pled, we will have a simple and convenient example for simulating the impact of nonsinusoidal steady state on the dynamic range of a system (Figure 4a).

If we choose a 50 Ω source, 50 Ω load and 1000pF for AC coupling, we have produced a 100nsec time constant ($\tau = rc$). Suppose that the fundamental frequencies are at 100MHz and 110MHz. The beat frequency would be 10MHz, having a period of 100nsec (intentionally chosen to be equal to the time constant).

When we start a two tone simulation in the time domain, we are really driving the circuit with a unit step multiplied by each of the two tones. Thus, we are not able to start the simulation at time=0 in sinusoidal steady state.

This observation is consistent with the behavior of coupling capacitors. At $t=0+$, the voltage across the coupling capacitor remains zero, such that no apparent phase shift is observed initially. Once sinusoidal steady state has occurred, the phase shift of the two tones across the coupling capacitor has been established and remains stable. The response of the system can be expressed as

$$V_r(t) = Ke^{-\frac{t}{\tau c}} u(t) + (A \sin(\omega_1 t + \phi_1) + B \sin(\omega_2 t + \phi_2)) u(t)$$

Let us assign $A = B = 1$ for convenience. This forces K to become a relative number. The impedance of the capacitor at 100MHz and 110MHz is given below.

$$|Z_{c1}| = \frac{1}{2\pi f_1 C} = 1.59 \Omega$$

$$|Z_{c2}| = \frac{1}{2\pi f_2 C} = 1.45 \Omega$$

We can then calculate the steady state phase angles.

$$\phi_1 = \text{atan}\left(\frac{|Z_{c1}|}{R_1 + R_2}\right) = 0.91^\circ$$

$$\phi_2 = \text{atan}\left(\frac{|Z_{c2}|}{R_1 + R_2}\right) = 0.83^\circ$$

K is determined by using the steady state phase angles at $t=0+$.

$$V(0) = 0 = Ke^0 + \sin(0 + 0.91^\circ) + \sin(0 + 0.83^\circ)$$

$$K = 30mV/V = -30.5dB$$

The first four beats of the voltage drop across the capacitor in the circuit of Figure 4a in response to 1V amplitude tones is shown in Figure 3.

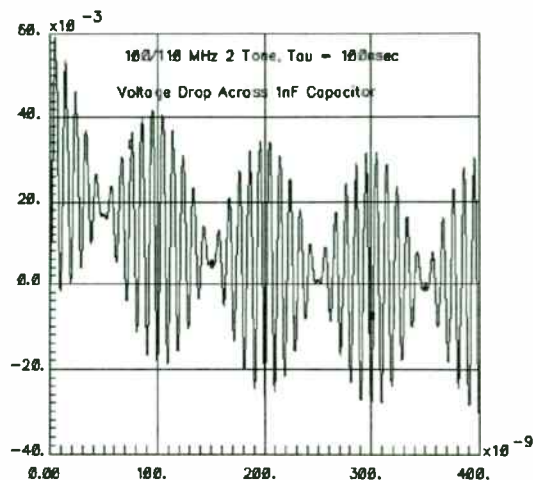


FIGURE 3. The first 4 beats of the time domain voltage across the capacitor in Figure 4a.

Notice how we have no voltage drop at $t=0+$, and that the envelope has a 100nsec time constant, with an initial value of about 30mV, as calculated.

If the capacitor voltage envelope is allowed to settle one time constant before we perform an FFT of the time domain results, the time domain instability decreases by e . This is down to 36.8% or -8.69 dB of initial value.

Suppose that we run a two tone time domain simulation for two beats, or 200nsec using the circuit in Figure 4a. Also, suppose that we allow the circuit 100nsec (one time constant) to settle, and attempt to obtain sinusoidal steady state. Then we perform an FFT of the results from 100nsec to 200nsec. At 100nsec, or one time constant, the impact of the transient response has decreased to 0.368K or 1.1% of the signal amplitude. But at 200nsec, the ending time of the FFT, the transient has decreased to 0.135K or 0.4% of the signal amplitude. Thus, we have 0.368K-0.135K = 0.7% of instability in our simulation. This would lead us to expect to see no worse than $20\log(0.011-0.004) = -43dB$ of dynamic range in our simulation due to the transient effect.

Figure 4a shows the frequency spectrum if we simply wait one time constant for settling (which might be considered a easy error to make). Of course, the transient in the time domain produces broadband spurs, so that no single frequency has the entire 43dB of error. We obtain only 60dB of dynamic range in this simple circuit. This would be considered unacceptable by most designers. Figures 4c and 4d indicate the tremendous improvement in dynamic range if we wait to 5 or 25 time constants

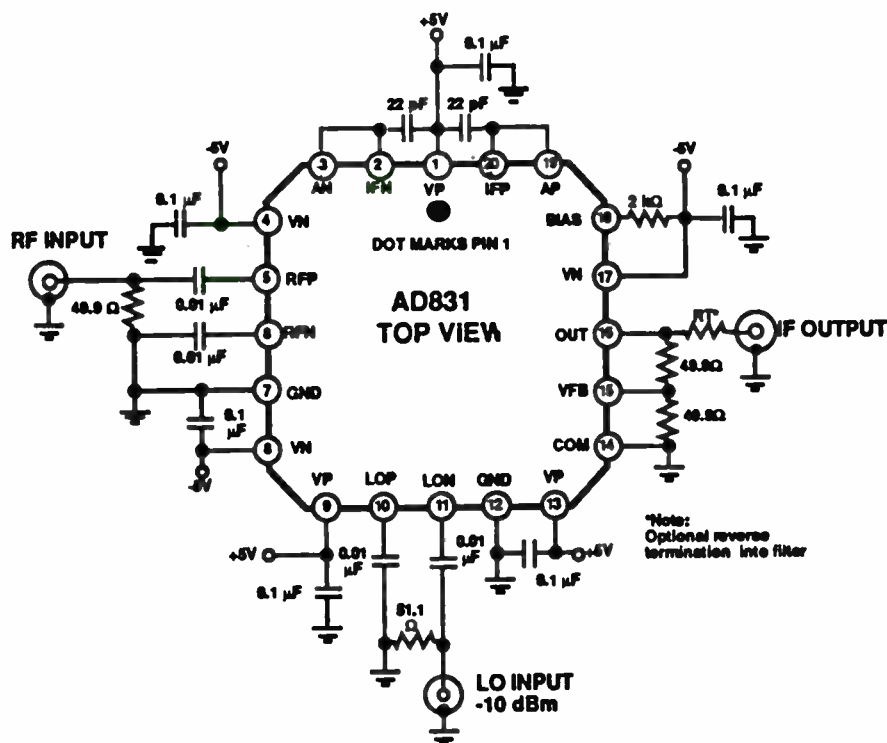


Figure 5. A Typical Down-conversion Mixer using the AD831

IF Amplifiers

IF amplifiers provide almost all of the gain in a superheterodyne receiver, and also allow this gain to be varied for AGC purposes. A well-designed IF amplifier will add a minimum of noise and distortion to the signal. An AGC range of 60 to 90 dB is usually required. While numerous circuit topologies are used, the focus here will be on the *variable-gain* requirement; the gain is assumed to be controlled by an AGC *voltage*.

A popular approach to the design of a voltage-controlled amplifier is to use the reliable exponential relationship between collector current and base-emitter voltage in a bipolar junction transistor, through which means it is possible to achieve a gain-control range of several decades. A widely-used circuit topology¹² is shown in Figure 6.

The RF signal voltage V_Y is first converted to a complementary pair of currents, which are here denoted as $(1+Y)I_Y$ and $(1-Y)I_Y$, by a voltage-to-current (V/I) converter formed

¹² W. R. Davis and J. E. Solomon, "A High Performance Monolithic IF Amplifier Incorporating Electronic Gain Control," IEEE Journal of Solid State Circuits, December, 1968. (Reprinted in "Analog Integrated Circuits," Alan Grebene, Ed., IEEE Press, New York, 1978)

before doing the FFT. Of course, the ultimate solution to this problem is to eliminate the capacitor entirely with either a wire or a battery.

starts or forcing the circuit time constants to be much larger than the period of the FFT (beat period).

The improvements resulting from using bigger capacitors are shown in Figure 5. Making the capacitor considerably larger (1000X and 10000X respectively) can dramatically reduce spurs related to transients in the time domain.

Another way to avoid these problems is to use a Harmonic Balance simulation. Harmonic Balance can be particularly effective because it will not have “noise” spurs in the results due to transients in the time domain.

The danger of only using Harmonic Balance techniques is that time domain transients, as a result of signal modulation, may produce undesirable spurs in the real circuit that are not simulated. A design may seem noisy, because the coupling circuitry interferes with the modulation of the signal. As a result, the expected system dynamic range may not be obtained.

Consider a simple case of the implicit unit step function (as discussed previously) being replaced by a pulse train. While this pulse train would be typically much slower than the signal which it is modulating, a problem might be lurking. If this modulation pulse train is close to $1/\tau$ for some important system time constant, this signal would become distorted. The spurs that we saw in the earlier example would be observed as repeating and causing the signal to appear to have poor dynamic range.

We do not recommend finishing an RF design without a check with a time domain simulator like SPICE to verify

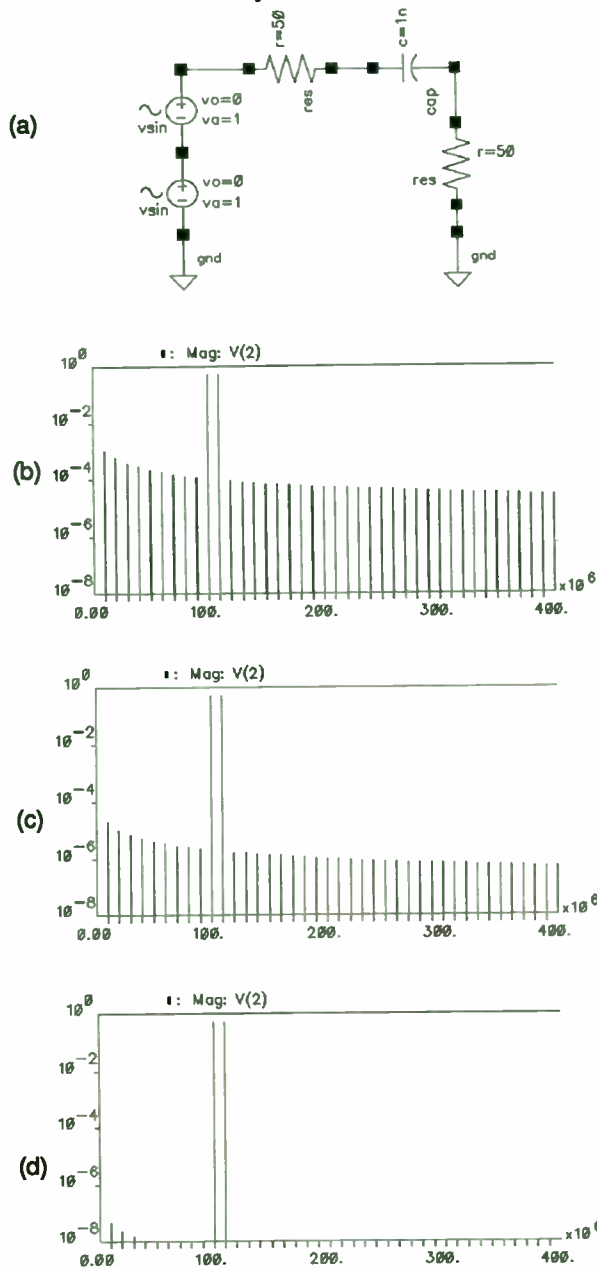


FIGURE 4. A simple two-tone circuit (a), the frequency spectrum across the load resistor, where the FFT samplings were started after 1τ (b), 10τ (c), 100τ (d).

A simple alternative to a battery or a short is a larger capacitor. The trick here is that the capacitor needs to be much larger, such that $rc \gg T_{FFT}$. This approach may seem entirely the opposite of what we have just advocated. But the real goal is to minimize transient effects. This is accomplished by either choosing the starting time of the FFT to be much larger than the circuit time con-

by Q1, Q2 and R_Y . The “modulation index” Y has a *maximum* range of ± 1 ; in practice, it will have an upper value of about 0.75, in order to minimize distortion due to the nonlinear V_{BE} of the transistors. To a good approximation, $Y = V_Y/I_Y R_Y$ (when $I_Y R_Y$ is very much greater than the thermal voltage kT/q).

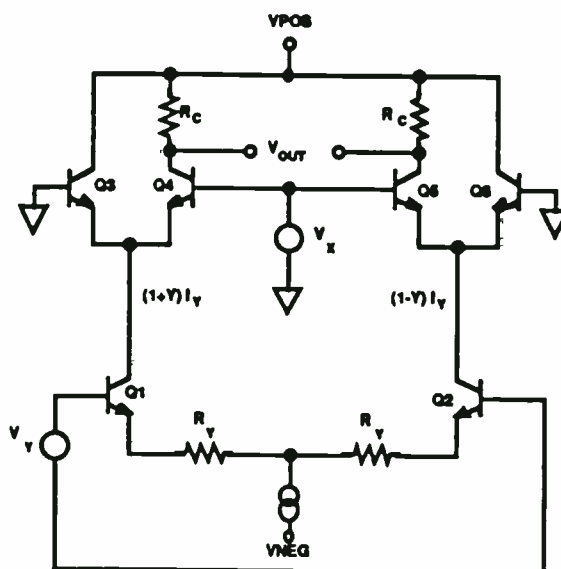


Figure 6. The Controlled Cascode Cell.

The signal-plus-bias currents are then applied to a “current-fork”, Q3 through Q6, that steers some fraction, $0 \leq X \leq 1$, of the signal currents to the output load resistors, and dumps the remainder to the positive supply. These transistors also act as a cascode stage, which extends the frequency range of the amplifier; because of this feature, we will refer to this cell as a “controlled cascode”.

The parameter X is determined by the gain-control voltage V_X . It is readily shown that

$$X = \frac{\exp(V_X/V_T)}{1 + \exp(V_X/V_T)} \quad \text{Eq. (6)}$$

where V_T is the thermal voltage kT/q , which is 25.85 mV at $T = 300$ K (about 27°C). At this temperature, X is 0.99 when $V_X = 120$ mV and 0.01 when $V_X = -118$ mV. If the system gain is normalized to 0 dB when $X = 1$, the loss is 6 dB for $V_X = 0$.

that transients in the time domain are not causing problems.

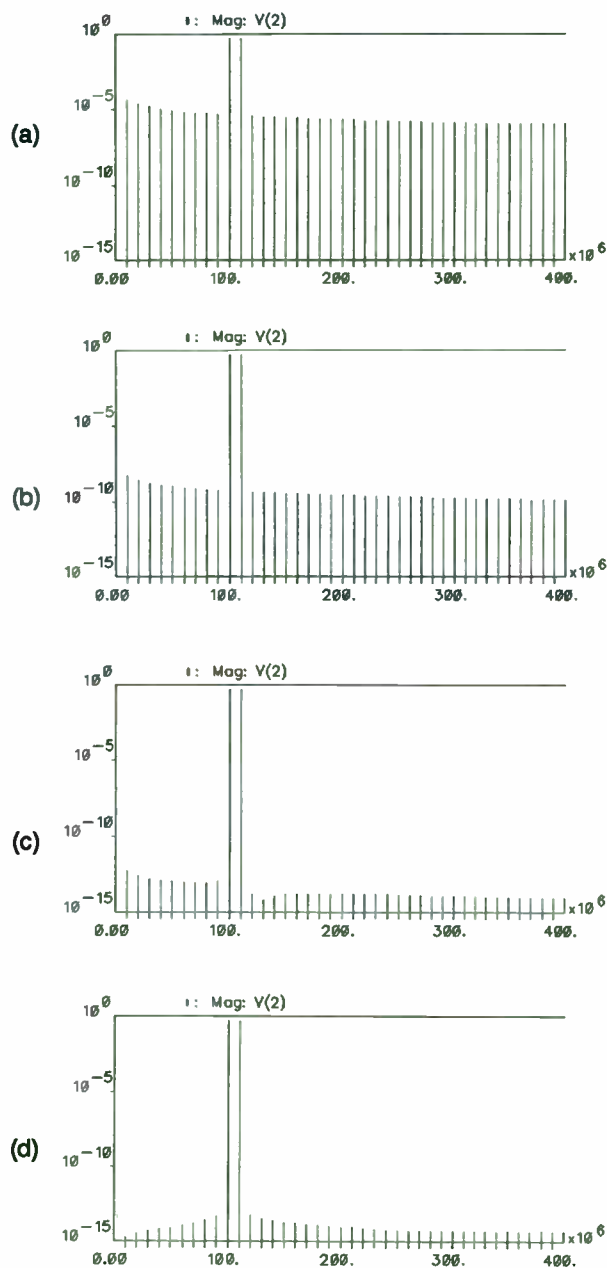


FIGURE 5. The spectrum of the voltage across the load resistor in the circuit shown in Figure 4a with the coupling capacitor set to 10n(a), 1u (b), 100u (c), and shorted (d).

V. Methods for Accurate and Efficient Simulation of P_{ip3} Using SPICE

Even when steady state is reached, the typical method of SPICE transient analysis followed by an FFT of the results to observe the nonlinearity in the frequency domain is an inaccurate (noisy) method. The major source of inaccuracy (low dynamic range) stems from the

interpolation error. Since FFT is a post processing of the transient results, generally, the simulation time steps and the FFT sampling steps are not synchronized. An interpolation between two adjacent simulation points is required to determine the value of the time domain waveform at an FFT sampling point (Figure 4).

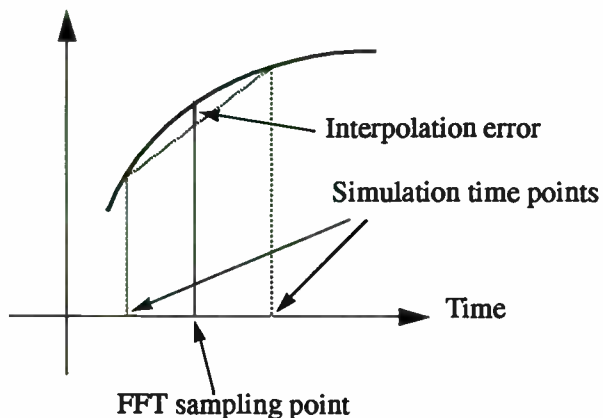


FIGURE 6. FFT Interpolation Error

Unfortunately, in typical SPICE type simulators, the user can not force the internal time points to land on specific locations.

In order to eliminate the interpolation error, the FFT sampling steps need to be predicted before the transient simulation is performed. The simulator, then, must be forced to step onto the sampling points. In the large signal AC analysis section of FIRST (Fastrack's Integrated RF Simulation Tools [5]), the following algorithm is used to eliminate the interpolation error.

- 1- Determine the frequency of the input sources.
- 2- Determine the Beat frequency, f_b . It can be shown that the beat frequency is the largest common divisor of the input frequencies.
- 3- Determine the starting point in time for the FFT sampling, t_{init} . This is the point (user specified) at which we assume that the circuit has reached satisfactory steady state.
- 4- Determine the end point for the FFT sampling, t_{end} . Where

$$t_{end} = t_{init} + \frac{1}{f_b}$$

- 5- Determine the largest non-negligible frequency content of the desired signal, f_{max} . This is the frequency at which the spectrum of the desired signal effectively dies out. Even though exact knowledge of this frequency is not required, it plays an important role in eliminating aliasing.

Figure 7 shows the decibel value of the current gain of the cascode as a function of V_X at three temperatures.

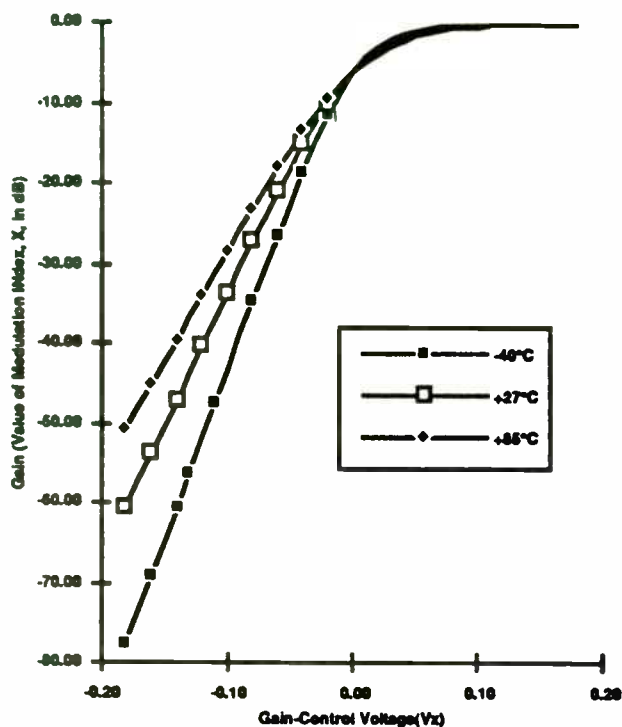


Figure 7. Decibel Gain of the Controlled Cascode

Several potential problems are immediately apparent from this graph. First, this circuit is really a voltage-controlled *attenuator*, rather than a voltage-controlled amplifier. Consequently, when this circuit is followed by a high gain stage to recover the lost signal, the noise performance at minimum attenuation may be disappointing. We will return to this in a moment.

Second, the circuit's control function is not "linear in decibels"; it approaches this condition only for very high attenuation values. Third, the attenuation is a strong function of temperature; this, and the nonlinear control function, may not matter too much in closed-loop AGC systems, but both would be troublesome in "swept-gain" VCA applications, or in feed-forward AGC systems. The temperature-sensitivity can be addressed using special resistors to form an attenuator between the actual gain-control voltage and the base nodes, where the required form is proportional to absolute temperature (PTAT).

6- Determine the number of FFT sampling points, N_{fft} .
Where

$$N_{fft} \geq \frac{2f_{max}}{f_b}, \quad N_{fft} = 2^n, \text{ and } n = \text{integer}$$

See Appendix A for proof.

7- Determine the FFT sampling points, t_i . Where

$$t_i = t_{init} + \frac{i}{f_b N_{fft}} \quad i = 0, \dots, (N_{fft} - 1)$$

8- Run the simulator and force it to step onto the FFT sampling points.

9- Perform an FFT of the time domain results from t_{init} to t_{end} using N_{fft} sampling points.

As an example, the above method was used on the circuit shown in Figure 4a. The simulator took 1029 time steps. The frequency spectrum is shown in Figure 7.

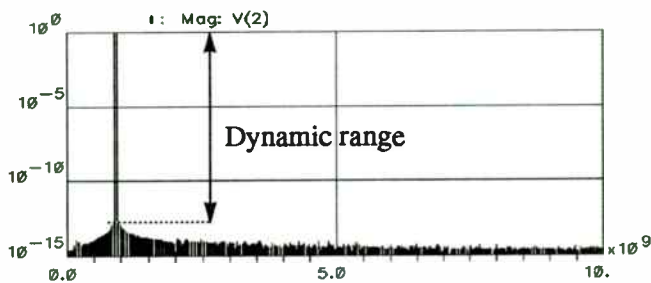


FIGURE 7. FFT results with Interpolation error eliminated

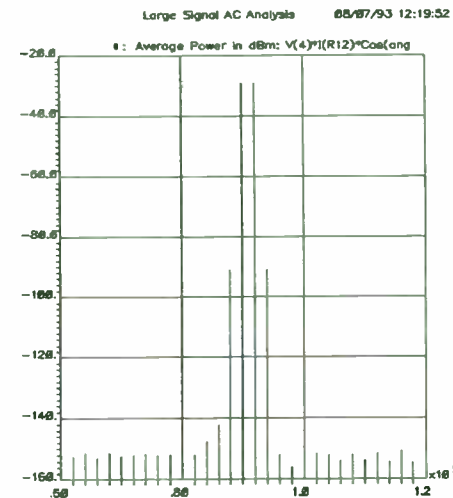
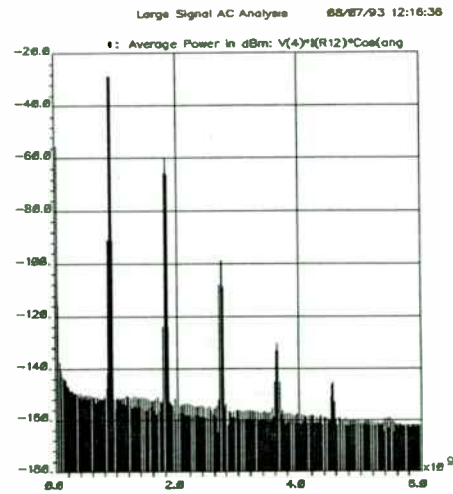


FIGURE 8. The entire frequency spectrum (a) and the spectrum around the fundamental frequencies

Even though the internal time points for the simulation were approximately 5 times less than the original attempt, the dynamic range of the FFT jumped from 80dB to over 260dB

As another example, an LNA (4 transistors) with 900 Meg and 920 Meg input signals was simulated with FIRST to determine P_{ip3} . Figure 8 shows the frequency spectrum of the output with a 7 mV amplitude for the input signals. Next, the input signal levels were varied to generate the output power plots. Figure 9 shows the power plots with and without the asymptotes.

From Figure 9, we can infer that P_{ip3} is about 2dBm. Notice how the output fundamental begins to compress at about -8dB (down 10dB as expected). Even the third order product's power curve is a straight line over 30dB of input signal dynamic range. This demonstrates sufficient dynamic range in the simulation to get consistent and useful results.

V. Practical Example of Estimation, Simulation, and Actual Measurements on a Mixer

A single balanced mixer was designed and fabricated with Harris Semiconductor's UHF-1 process. UHF-1 is an 8 GHz, silicon bipolar integrated circuit process. The power budget allowed 5mA for the bias current, and 5

Apart from these obvious weaknesses, this cell has additional, more subtle, problems. First, notice that the lower end of the input dynamic range is fundamentally limited by the Johnson noise of R_Y . Now, if this resistor is reduced to the point where acceptable noise performance is achieved, the upper end of the dynamic range will also be reduced, due to the onset of distortion, and eventually clipping, unless very large values of bias current I_Y are used to extend the input voltage range (which, as we've seen, is roughly $I_Y R_Y$).

For example, suppose we wish to achieve a short-circuited input noise spectral density of $1.5 \text{ nV}/\sqrt{\text{Hz}}$ at 300 K (which corresponds to $15 \text{ } \mu\text{V}$ RMS, or -83.5 dBm , in a 100MHz bandwidth). Then R_Y can be no more than $149 \text{ } \Omega$. But this assumes that Q1 and Q2 have no ohmic resistances; in practice, their base resistances ($r_{bb'}$) must be subtracted from R_Y to maintain the desired total noise resistance. Even well-optimized monolithic transistors may have $r_{bb'}$ values of $25 \text{ } \Omega$, typically requiring R_Y to be no more than $100 \text{ } \Omega$.

Now postulate that a maximum input of 1 V RMS must be handled with a total harmonic distortion of less than -60 dBc . (At moderate frequencies the distortion will be third-order, but there will be increasing odd- and even-order components at high frequencies.) To meet this last requirement when $R_Y = 100 \text{ } \Omega$, it can be shown that the two currents I_Y must each be at least 23 mA ; using typical $\pm 5\text{V}$ supplies, this would correspond to an expenditure of almost half a watt in just the voltage-to-current converter!

As if that were not bad enough, we have yet to include the noise due to the controlled cascode part of this circuit. This is negligible only when this cell provides a maximum voltage gain (of $2R_C/R_Y$ when $X = 1$) that is much greater than unity. Let the noise at the input (due to $2r_{bb'} + R_Y$) be E_a , and that in the load circuit (at the very best, due to $2R_C$ alone) be E_b . The total noise at the output, E_{no} , for the maximum gain condition, where noise performance is critical, is

$$E_{no} = \{ (2R_C/R_Y)^2 E_a^2 + E_b^2 \}^{0.5} \quad \text{Eq. (7)}$$

Referred to the input, this is equivalent to a noise of

$$E_{ni} = \frac{\{ (2R_C/R_Y)^2 E_a^2 + E_b^2 \}^{0.5}}{2R_C/R_Y} \quad \text{Eq. (8)}$$

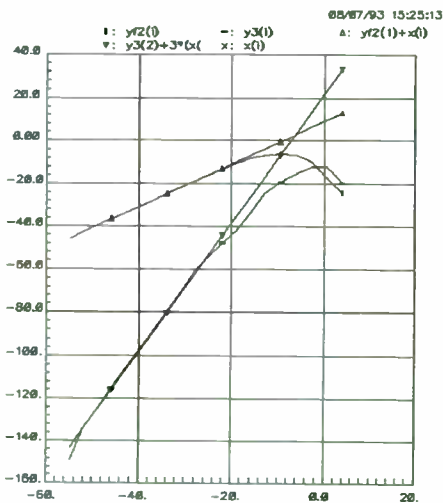
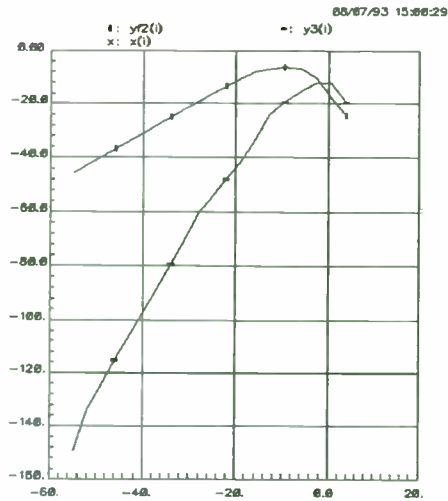


FIGURE 9. The power plots for the LNA (a) and the power plots with the superimposed asymptotes

Volts for the power supply. The part is operated in a 50 Ω environment at about 900MHz.

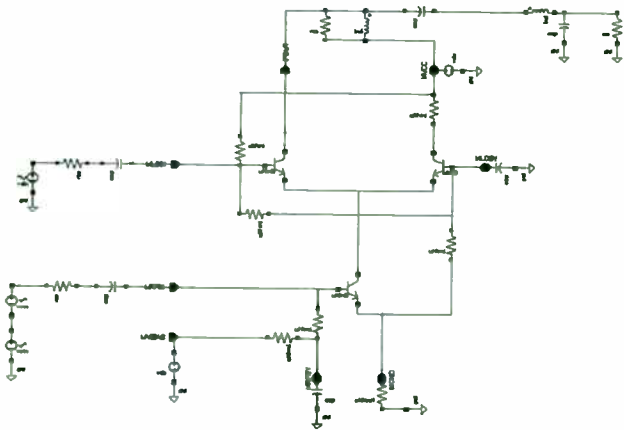


FIGURE 10. A simplified schematic of a UHF-1 single balanced mixer.

Several steps are required to estimate the P_{ip3o} of this mixer. Notice that the nominal collector current of the common emitter RF device within the mixer is 5mA. Two resistors are connected to the LO collector. One serves as a source and the other as a load, such that both are in parallel. However, the external load is a 50 Ω resistor which is reactively transformed to appear as 1K Ω to the mixer. The mixer output source resistor is 1K Ω (Figure 10).

The nominal zero to peak current allowed to the external load appears like 2.5mA into 1K Ω (as described in extension #1). However, the single side band mixing process reduces this by a factor of $\sqrt{2}$, leaving 1.77mA available.

$$P_{avail} = \frac{I_{nom}^2 R_L}{2} = \frac{(1.77mA)^2 (1K\Omega)}{2} = 1.57mW$$

$$P_{avail} = 2.0dBm$$

$$P_{ip3o} = 8 \rightarrow 12dBm$$

Experimental results indicate P_{ip3o} is +5 to +7dBm (depending on the package). Since conversion gain is +8dB, P_{ip3i} is -3 to -1dBm. Simulation results using FIRST for 40mv, 50mV, and 63mv signal amplitudes are tabulated below. Notice that the estimate is optimistic, while the simulation is more accurate.

Amplitude	40mV	50mV	63mV
P_{f1}	-20.45	-18.50	-16.50
$P_{2f_2-f_1}$	-76.31	-71.18	-65.10
P_{ip3o}	7.48	7.84	7.80

VI. Conclusions

P_{ip3} is a popular metric used by RF designers to specify the third order intermodulation products. Several rules of thumb, based on system level considerations are used to approximate P_{ip3} . However, simulation can be more accurate, and give a clearer indication of how subtle changes in a circuit impact P_{ip3} . The decaying transient response of a system and the interpolation error can cause the FFT results to appear noisy (picket fence effect). Neglecting these decaying transients (as in Harmonic Balance) may cause inaccuracy in predicting the dynamic range of the circuit. A methodology was presented to eliminate the interpolation error and thus significantly improve the dynamic range of the FFT. It was shown that by proper treatment of decaying time constants and the

Noting that $E_a = S_{\Omega}(2r_{bb'} + R_Y)^{0.5}$ and $E_b = S_{\Omega}(2R_C)^{0.5}$, where S_{Ω} is the ohm-normalized noise-spectral density and setting $r_{bb'}=0$ for simplicity (and also to show the fundamental limitations more clearly) we can write

$$E_{ni} = S_{\Omega} R_Y^{0.5} (1 + R_Y/2R_C)^{0.5} \quad \text{Eq. (9)}$$

The first part of this expression is simply the Johnson noise of R_Y . E_{ni} is increased in direct proportion to the second factor, requiring that $2R_C$ be much greater than R_Y . When $R_C = 2 R_Y$, for example, the noise is increased by about 12 % or 1 dB. In our example, therefore, we might decide to use $R_C = 400 \Omega$. But this raises a practical problem: if a value of $I_Y = 23 \text{ mA}$ were used to maintain acceptable distortion levels, the maximum voltage drop across the load resistors R_C would need to be nearly 15 V at full gain and full signal, requiring an inordinately high supply voltage. That problem can be addressed by using a more "classical" reactive load (such as a parallel-tuned LC circuit, or a more complex LC filter) having a low DC resistance. However, modern receivers make extensive use of ceramic resonators which do not provide this DC path, necessitating the inclusion of RF chokes as loads.

Further noise and distortion is generated by the base resistances and capacitances of the cascode transistors. Optimization of these transistors is difficult, since the use of large devices to lower $r_{bb'}$, noise only results in higher capacitances. At low gains, HF signal feedthrough occurs via the parasitic T-network formed by the $C_{JE} - r_{bb'} - C_{JC}$ of these transistors, causing aberrations in the AC response.

Thus, in numerous ways this type of VCA cell fails to meet the exacting requirements of many modern IF systems, although it remains appealing where some concessions to noise, distortion and gain-accuracy can be made. It is a simple cell for use in embedded applications, and provides the highest possible bandwidth for a given process technology. Variable-gain amplifiers built along these lines are available for use up to about 1 GHz.

interpolation error, P_{ip3} can be reliably measured by SPICE based time domain simulation followed by an FFT of the results.

VII. References

- [1] G. Gonzalez, Microwave Transistor Analysis and Design, Printice-Hall, Inc., New Jersey, 1984.
- [2] R. S. Carson, High Frequency Amplifiers, Second Edition, John Wiley & Sons, New York, 1982.
- [3] P. R. Gray and R. G. Meyer, Analysis and Design of Analog Integrated Circuits, Second Edition, John Wiley & Sons, New York, 1984.
- [4] L. W. Nagel, "SPICE2, A Computer Program to Simulate Semiconductor Circuits", Technical Report ERL-M520, UC Berkeley, May 1975.
- [5] M. C. Chian, S. S. Majors, and A. G. Whittaker, "Embedding RF Design Tools in an IC Design System", the proceedings of RF Expo East, 1993.

The X-AMP Concept

Two new dual-channel voltage-controlled amplifiers, the AD600 and AD602, have recently been introduced by Analog Devices. They differ radically from the circuit just discussed. The input signal is applied to a passive seven-section R-2R resistive ladder network, providing from 0 dB to 42.14 dB (7 X 6.021 dB) of attenuation at the various taps. Using a proprietary technique, these taps can be continuously interpolated, and the variably-attenuated voltage is applied to a *fixed-gain amplifier* that uses negative feedback to enhance gain accuracy and linearity. The 42.14 dB range of the attenuator is centered to provide a nominal 40 dB gain range with 1.07 dB of over-range at each end. The term "X-AMP", coined to apply to this architecture, is a reference to the exponential gain function which it inherently provides, that is, the gain control is "linear-in-dB". Figure 8 is a simplified schematic of an X-AMP.

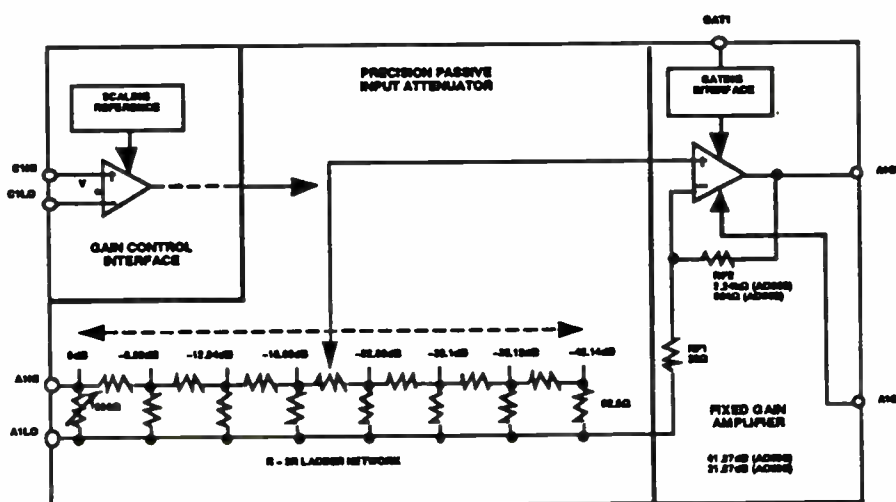


Figure 8. Simplified Schematic of an X-AMP

The X-AMP provides the unusual combination of low noise (1.4 nV/ $\sqrt{\text{Hz}}$), good signal-handling capabilities (1 V RMS at the input, 2 V RMS at the output), a constant 3 dB bandwidth of DC to 35 MHz, constant phase and group-delay characteristics, low distortion (-60 dBc to 10 MHz) and low power consumption (125 mW maximum per channel). One disadvantage in some applications is the low input resistance of 100 Ω , but this is laser-trimmed to be within $\pm 2\%$, which simplifies interfacing in many cases.

Low Cost Phase Noise Measurement Technique

Jim H. Walworth
 Tampa Microwave Lab, Inc.
 12160 Race Track Road
 Tampa, Florida 33626-3111
 (813) 855-2251

Phase noise is one of the most important specifications of an oscillator and often one of the most difficult to measure. Unfortunately it can also be one of the most expensive test set configurations an oscillator manufacturer must invest in. Many times the only equipment a small company may have is a spectrum analyzer. Usually the phase noise of a good phase locked oscillator (PLO) will be lower than the measurement capability of the spectrum analyzer. This paper suggest several techniques of measuring phase noise, not necessarily covered previously in the literature.

- | | | |
|-----|--------------------|-----------|
| 2. | HP11729C + HP8662A | > \$71.5K |
| 3. | HP11729B + SR770 | < \$13K |
| 3a. | HP11729C + SR770 | < \$13K |
| 4. | SR770 | < \$ 8K |
| | (SR550) | < \$ 6K |

This paper will offer four basic methods of measuring phase noise all with different price tags.

1. Fully automated phase noise test set such as the HP3047.
2. Measurement with the HP11729 Carrier Noise Test Set.
3. User modified (used) HP11729B test set Phase detector method
- 3a. Discriminator Method
4. Utilizing a PLL itself to measure it's phase noise with only a low cost low frequency analyzer.

The relative price tags of the above approaches are listed below. They are approximate. Number 3 has the greatest amount of uncertainty in the price since it assumes the availability of used equipment in the same order of magnitude found by the author.

RELATIVE PRICES OF THE FOUR TECHNIQUES.

- | | |
|-------------------|----------|
| 1. HP3047A SYSTEM | > \$110K |
|-------------------|----------|

Method 1. Fully automated phase noise test set. (Figure 1)

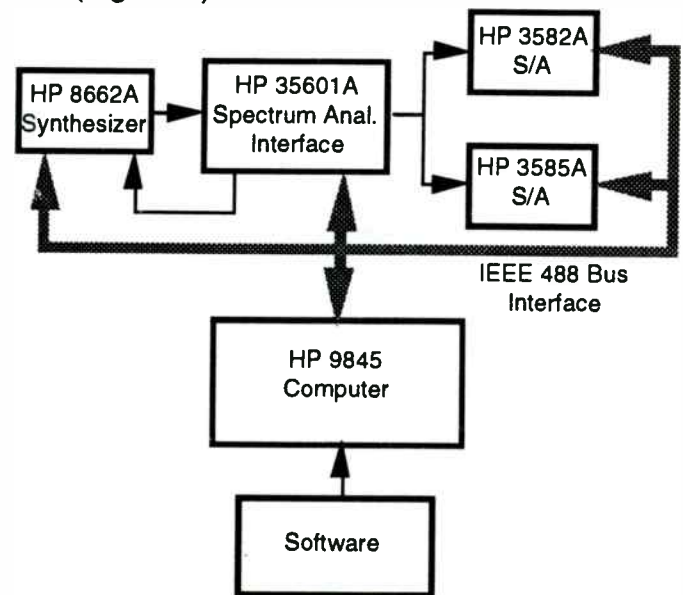


Figure 1. HP 3047 System [1], [2]

The largest advantage to this technique is the automatic calibration and compensation. All instrumentation is connected via IEE488 buss to collect error correction data, and measurement data. This is by far the best phase noise measurement system. It is also the most expensive.

Method 2. Manually calibrated and operated phase noise test set. Figure 2. shows the block diagram of a manually calibrated / operated test set up, consisting of the HP11729C Carrier Noise test set, the

The two channels of the AD600 and AD602 are independent, and may be cascaded for a gain range of up to 80 dB in one package. Separate high-impedance, differential gain-control interfaces are provided; the gain is precisely calibrated to 32 dB/Volt (31.25 mV/dB). In the AD600 the gain for each section is 0 dB for $V_G = -625$ mV, 20 dB for zero V_G , and 40 dB for +625 mV. When V_G exceeds these values, the minimum gain becomes -1.07 dB and the maximum is 41.07 dB. The AD602 is similar, except that each VCA provides a gain¹³ of -11.07 dB to 31.07 dB.

Thus, for the AD600, the gain of each amplifier is

$$G_{dB} = 32 \cdot V_G + 20 \quad \text{Eq. (10a)}$$

while for the AD602 it is

$$G_{dB} = 32 \cdot V_G + 10 \quad \text{Eq. (10b)}$$

A new product, the AD603, is a *single-channel X-AMP* in an eight-pin format. It is optimized for IF applications, providing a basic gain range of -11.07 dB to 31.07 dB from DC through 70 MHz. Using a simple pin-strap (Figure 9) the gain range becomes +8.93 dB to +51.07 dB, with a -3 dB bandwidth of about 7 MHz. Using one external resistor, any gain range in between these extremes can be provided, with pro-rated bandwidth. The gain-scaling is slightly different, requiring 25 mV/dB, that is, exactly 1V for a 40 dB gain-change; the control interface remains fully-differential, has an input impedance of about 50 M Ω and provides a somewhat larger common-mode range, and lower bias currents, than the AD600/2.

¹³ The importance of the rather precisely-specified limits values for the gains will later be understood in connection with the various gain-sequencing schemes used in practical applications to be presented.

HP8662A synthesizer, a low frequency spectrum analyzer, and a microwave spectrum analyzer.

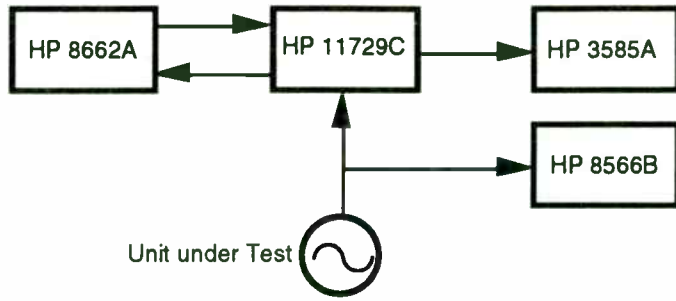


Figure 2. HP 11729C System

The block diagram of the HP11729B carrier level test set is shown in Figure 3. This test set has the basic components to make measurements in either the phase detector method or the discriminator technique. Both

techniques are described in the HP Product Note 11729B-1

Method 3. HP 11729B phase noise test set and a low frequency spectrum analyzer.

This system can be used to measure phase noise without the synthesizer for specialized applications. The diagram in Figure 4 shows the HP11729B with one slight modification to allow the injection of a microwave VCO. (instead of the synthesizer) to mix with the unit under test (U.U.T.). The modification is not a difficult one since it only requires the removal of connectors inside the unit and the addition of another connector to the front or rear panel. We chose to remove the "AUX" connector on the front panel and replace it with an SMA panel mount bulkhead.

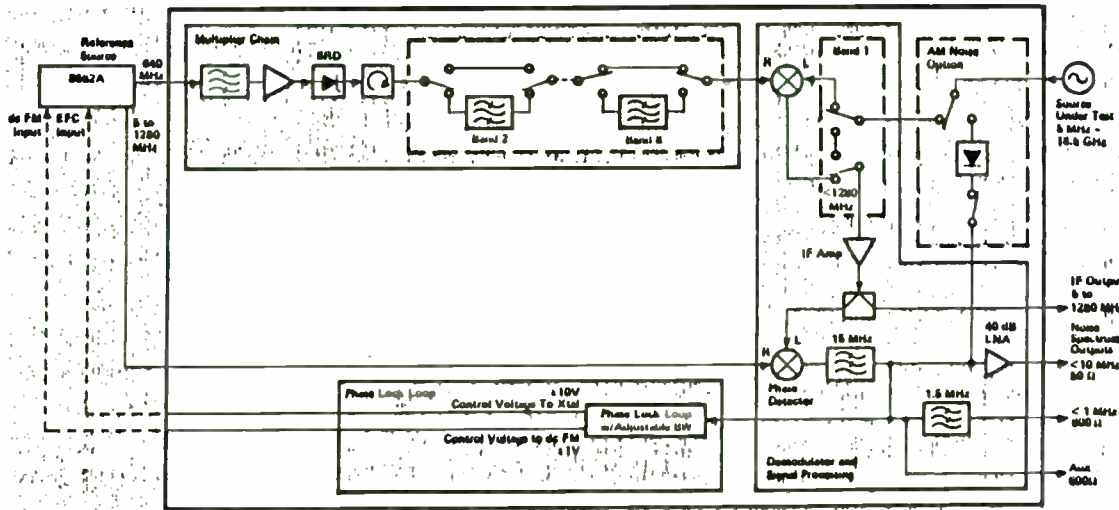


Figure 3. 11729B Block Diagram [1]

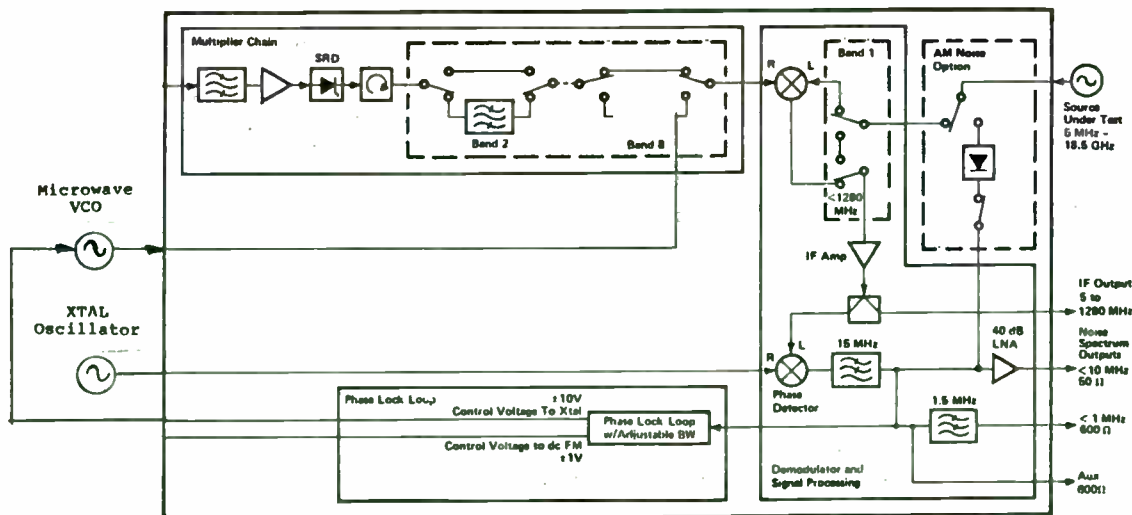


Figure 4. Modified 11729B Block Diagram [1]

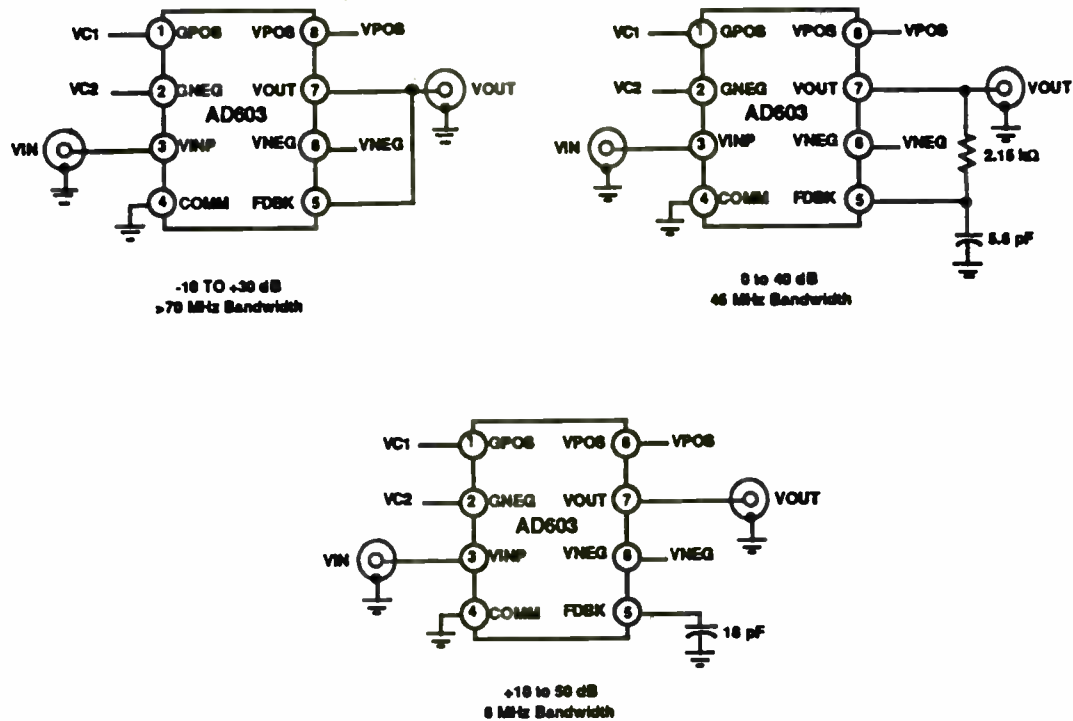


Figure 9. Pin-strapping to Set the AD603 Gain

(The capacitors are optional and serve to extend the bandwidth)

The two sections of an AD600 or AD602 or two AD603s can optionally be operated in *parallel*, to achieve an input noise spectral density of 1 nV/ $\sqrt{\text{Hz}}$ with no compromise in other aspects of performance.

60 dB AGC System with Optimal Signal-to-Noise Ratio

By way of illustration, we show how to use the AD600 in a 10.7MHz IF application.

Recall that each section provides a gain range of about -1 dB to +41 dB with independent control. These two sections can be cascaded to provide a maximum gain of 82 dB (2*41 dB), as shown in Figure 10, but the inclusion of a doubly-terminated, lossy BPF lowers this by approximately 20 dB, as indicated on the figure, to 62 dB. The minimum gain is therefore -22 dB (that is, 2*(-1 dB) - 20 dB).

The disadvantage to this technique is the fact that you must now have a low noise VCO as good as or better than the VCO inside the source under test. This also increases the uncertainty of the measurement accuracy since the contribution of the VCO isn't exactly known. It is a good idea to use a VCO that is either identical in design to the VCO inside the U.U.T. or one with known better phase noise.

The frequency of the crystal oscillator, and the offset frequency, is not critical but must be greater than 15 MHz in order to prevent saturation of the 40 db LNA inside the 11729. If you are so inclined, the 11729 can be further modified to add another filter of lower cutoff frequency in front of the LNA, thereby allowing a lower offset frequency.

Since the crystal oscillator is of much lower phase noise than the source under test, the phase noise it contributes is not very significant. Calibration and measurement of this configuration is now the same as that described in the product note "HP11729B-1" with the exception that you must add 3 dB to the noise for the effect of second VCO.

3a.) Frequency discriminator method with the HP11729.

The HP11729C with the built in 640 MHz oscillator can be utilized in the discriminator mode by following the procedure described in PN11729C-2 [2]. An alternative to purchasing the

current model of the 11729 is to purchase a used HP11729B and buy a good low noise 640 MHz source. A low cost approach to obtain the 640 MHz source is to purchase a low phase noise 160 MHz crystal oscillator and build the circuit in Figure 5 utilizing low cost doublers, amplifiers and a filter.

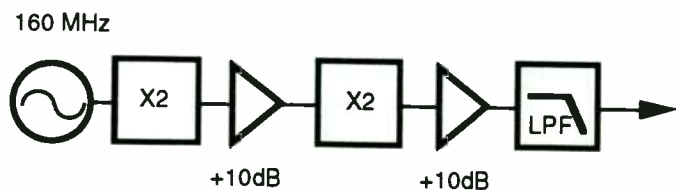


Figure 5. Low Noise 640 MHz Source

The discriminator method is accurate but can require a rather long delay line in order to obtain the required sensitivity. The HP product note PN11729C-2 [2] has a detailed discussion of the delay line discriminator.

Note that the 11729 makes it's measurement by looking at the noise outside the loop bandwidth. The loop is calibrated by unlocking and offsetting one source to produce a beat while attenuating the U.U.T. by 40 db to prevent saturation. Also the loop bandwidth correction factor is determined by injecting a source and recording the loop transfer characteristics. These are described in PN 11729B-1 [1].

Method 4. Using P.L.L. to Measure it's own phase noise. Compare the basic phase detector of diagram Fig. 6 to the diagram of a sampling P.L.L. Fig. 7.

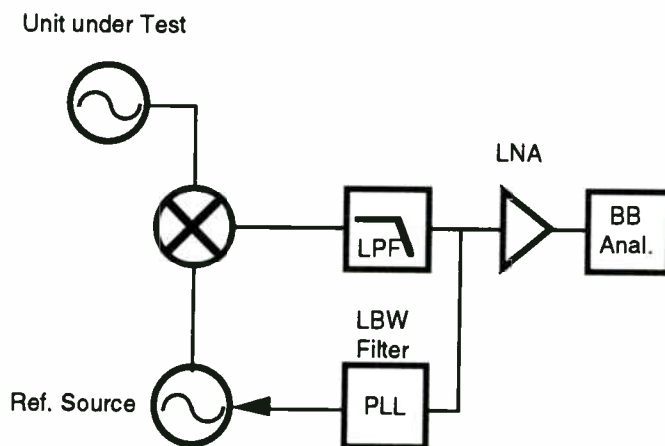


Figure 6. Phase Detector Technique

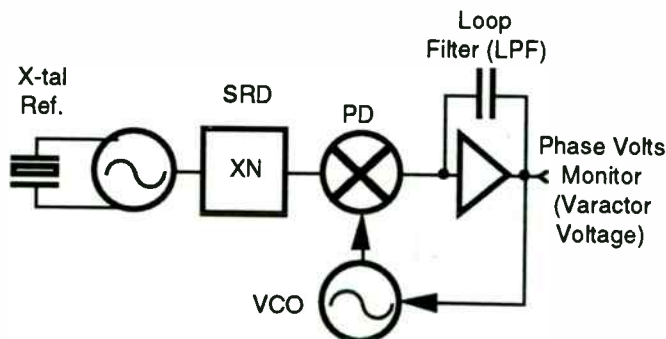


Figure 7. Sampling P.L.L. Diagram

This amplifier system includes a simple one-transistor detector, which also provides a means to integrate the AGC error signal¹⁴. However, this may be omitted and gain control effected by DSP if desired. In either case, the fact that the gain control voltage is "linear-in-dB" means that the AGC voltage bears an exact correspondence to the decibel level at the input, that is, it provides an accurately-calibrated RSSI (Received Signal Strength Indication) function.

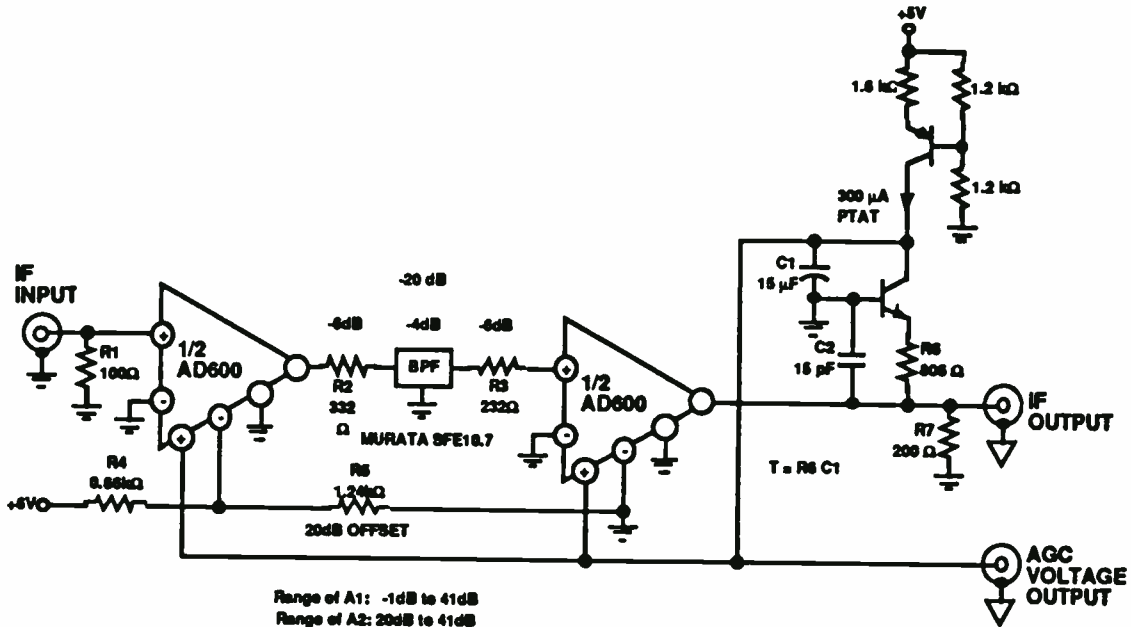


Figure 10. 60 dB AGC Amplifier

It is not necessary to provide any nonlinear shaping of the control signal because the gain of each X-AMP section remains accurate (at its minimum or maximum value) even when the control input is overdriven. The only care needed is in providing the correct amount of offset between the two sections to use the full gain range possible in each half of the AD600. In this system, A2 compensates for the 20-dB loss due to the bandpass filter and termination resistors, which leaves only half of its range, while A1 provides the full 42 dB. R4 and R5 provide this gain-control offset between the two amplifier sections, ensuring smooth transitions between the gain segments of each section.

The input impedance of this system is optionally padded to 50 Ω by the addition of R1 in shunt with the 100 Ω input resistance of the AD600. The output can drive 2V RMS into a final load of 200 Ω. For illustrative purposes, a 10.7 MHz ceramic filter (Murata SFE10.7) that requires 330 Ω terminations at both source and load is used.

¹⁴ The operation of this detector is explained at length in the AD600/2 data-sheet.

Notice the distinct similarity in the functional block diagrams. This leads to the proposed technique of using the P.L.L. to measure its own phase noise. Most P.L.L.'s have a test monitor point available after the loop filter to monitor the VCO voltage. This test point is very similar to the point used to measure phase noise in the test set except that it is inside the loop bandwidth instead of outside the loop bandwidth. This implies that it should be possible to monitor the noise at this test point with a baseband spectrum analyzer and determine the phase noise of the P.L.L. If the measurements are made within the loop bandwidth, the noise on this test point is the composite phase noise of the entire P.L.L.

This technique with no further correction is quite valuable for checking relative phase noise in a production environment. It is possible to simply clip lead a good F.F.T. analyzer to the PV test point of a P.L.L. and compare relative phase noise of several units. There are, of course, two basic assumptions; 1) the loop bandwidths are the same or sufficiently wide that the bandwidth doesn't affect the measurement, 2) the VCO constants are the same. The VCO constant can be determined by varying the reference oscillator enough to give $\pm 0.5V$ or less on the VCO curve, while observing the Δf on the output. This small delta measurement should be made about the nominal operating point.

$$K_v = \Delta f / \Delta V \text{ (MHz/V)}$$

As long as the measurement frequency, f_m , is within the loop bandwidth, the phase noise can be calculated from the measured voltage and the VCO constant K_v . The absolute level of the noise voltage within the loop at the VCO input must be measured with a low frequency spectrum analyzer or wave analyzer. The Stanford Research SR550 is a F.F.T. analyzer that can measure the spectral noise density at an economical price. Wave analyzers such as the HP3581C series are also low cost methods of measuring the rms voltage at a specified frequency, f_m , away from the carrier.

Knowing the VCO constant, K_v , and having measured the rms voltage, V_{rms} , at an offset frequency, f_m , in a resolution bandwidth, BW_{res} , the rms F.M. deviation can be calculated from:

$$\Delta f = V_{rms} * K_v * \sqrt{1\text{Hz}/BW_{res}} \text{ [Hz]} \quad (1)$$

Next the relative level of the FM carrier sideband ratio is calculated from the conventional FM theory. Obviously the voltage modulating the VCO is of a sufficiently low level to make the modulation index magnitude much less than 1, ($M \ll 1$). Therefore, the carrier to sidebands is defined by equation (2)

$$\frac{P_{sb}}{P_c} = \frac{\text{Power density in the sideband}}{\text{Power of Carrier}} \quad (2)$$

(This is also the definition of phase noise, $\mathcal{L}(f)$.)

$$\mathcal{L}(f_m) = \frac{P_{sb}}{P_c} = 20 \text{ Log } 10 \left[\frac{\Delta f}{\sqrt{2} * (f_m)} \right] \quad [3]$$

Where Δf = rms deviation in Hz
 f_m = Noise modulation frequency in Hz.

With the measured voltage and modulation frequency, calculate Δf using equation (1) and using Δf and f_m , calculate $\mathcal{L}(f_m)$ using equation (2).

Example:

A 13 GHz PLO was tested by varying the reference frequency above and below the operating point. The VCO constant was measured as 0.935 MHz/volt.

The low frequency analyzer was connected to the VCO test point and the rms voltage measured at 10KHz as $393\eta V/\sqrt{\text{Hz}}$.

From (1)

$$\Delta f = 0.393 * 10^{-6} V * 0.935 * 10^6 \frac{\text{Hz}}{V} = 0.367 \text{ Hz}$$

An interesting aspect of this amplifier is the behavior of the complete AGC loop under rapidly-changing input levels. Using a relatively small value for C1 the response time can be fast enough to allow the use of the AGC voltage as a signal output; for some modulation modes, the exponential nature of the transfer function is tolerable. Figure 11 shows the AGC output in response to different input levels, when the 10.7 MHz signal is modulated to a depth of 50 % by a 10 kHz square-wave. The constant 6 dB difference between the maximum and minimum signal levels results in a constant 188 mV ($6 \text{ dB} * 31.25 \text{ mV/dB}$) variation on the AGC line.

Figure 11. AGC Response (see text)

From (2)

$$L(10\text{KHz}) = 20 \log_{10} \left(\frac{0.367}{\sqrt{2 \times 10^4}} \right) = -91.7 \text{ dbc/Hz}$$

Compare this to the HP 8566B analyzer reading of -61.6 dB in 1 KHz or -91.6 dBc / Hz (Reference Figure 9). Remember that this technique is valid only if the measurement is within the loop bandwidth. If it is not, the noise of the VCO outside the loop bandwidth will not be present as an error voltage within the loop.

Figure 8 is a direct plot from the SR770 F.F.T. analyzer in the Power Spectral Density (PSD) mode [4]. This mode selection automatically computes the resolution bandwidth with respect to 1 Hz. Note that this display is not a normal spectral amplitude display. It is a display of the rms frequency deviation versus modulation frequency.

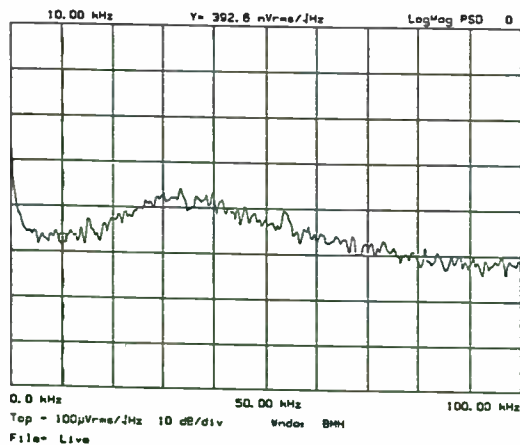


Figure 8. SR770 Spectral Density Display

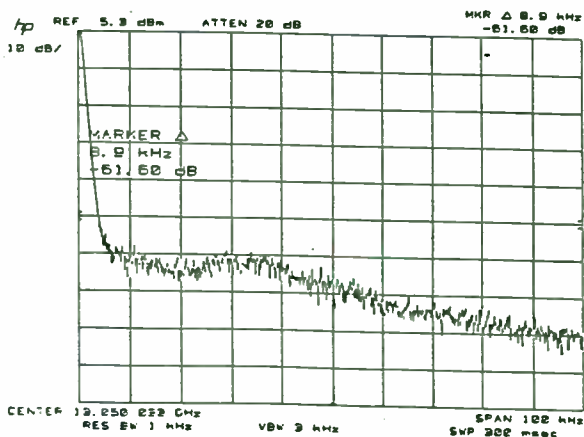


Figure 9. Hp 8566B Spectrum Display

This data doesn't become phase noise spectral information until equation 2 is applied to the data. One nice feature of the SR series analyzers is that it has a built in floppy disk on which the display information can be written in IBM ASCII format. This data can then be processed with a PC and appropriate software.

For comparative purposes, Figure 9 is a direct plot from a HP8566B spectrum analyzer with the carrier offset to the left and total span equal that of the SR 770. Several frequency points have been analyzed from Figure 9 and compared to Figure 10. This data indicates that the 10 KHz point is within the loop bandwidth of the P.L.L. and correlates well. The 50 KHz point is approximately 3 db off and the 100 KHz point 6 db off. This indicates that the measurements at these points are outside the loop bandwidth and must be ignored or compensated for.

Compensating for loop bandwidth effects require that the P.L.L. have an injection point that will allow measurement of the loop response to an outside stimulus.

If the P.L.L. manufacturer will cooperate with the purchaser, an additional loop injection test point can be provided to allow insertion of a test signal for measurement of the loop attenuation outside the loop bandwidth. Figure 10. shows a block diagram of the required loop with additional test point.

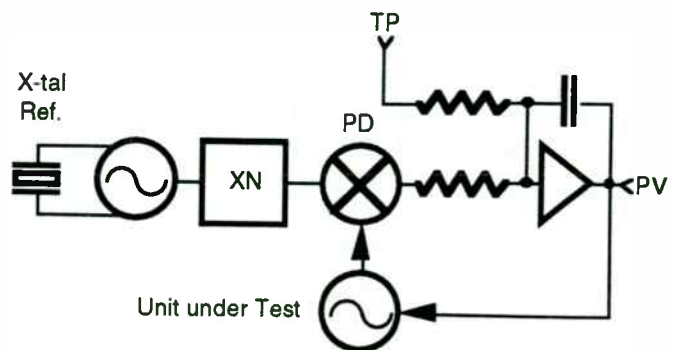


Figure 10. Modified PLO

A Log-Limiting IF Amplifier

Systems that use phase- or frequency-modulation often require an IF amplifier that provides an *amplitude-limiting* response. In many cases, the overall phase-shift in this amplifier must be very stable with fluctuations in the signal level. Some digital-mobile radio standards also require accurate signal measurement (Received Signal Strength Indication, or RSSI) in order to control transmitter power levels at both the mobile and fixed stations, thus ensuring the use of the minimum power to maintain reliable communications. This function is appropriately provided by a *logarithmic amplifier*.

The Analog Devices' AD606 was developed for such applications. It is a complete monolithic nine-stage logarithmic amplifier having a dynamic range of over 80 dB (from -75 dBm to at least $+5$ dBm) and providing a limiting output with a gain of 100 dB. It is usable to 70 MHz and consumes only 65 mW from a single 5 V supply. It may be rapidly powered-up or down (to about 100 μ A) by a CMOS-compatible logic input.

Figure 12 shows a typical application of the AD606. The nominal slope at the low-impedance RSSI output is 37.5 mV/dB up to 15 MHz; it drops to 35 mV/dB at 45 MHz. Optional adjustments R1 and R2 allow accurate calibration of the slope and intercept. The hard-limited output is 200 mV (pk-pk) minimum across the typical 200 Ω load resistor (R3 in Figure 12). The phase at this output is maintained to within $\pm 3^\circ$ over the 80 dB range at 10.7 MHz.

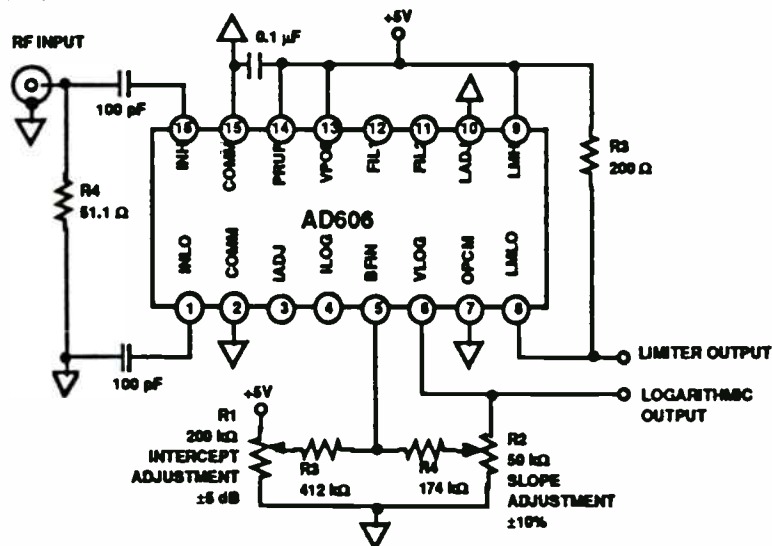


Figure 12. The AD606 80-dB Log/Limiting IF Amplifier

Utilization of this test point will be in the same manner as described in PN 11729B-1 page 19 [1]. One obvious difference will be that the curve will have the opposite characteristic from Figure 4.14 in PN11729B-1 [1].

In conclusion, three conventional and one new method of phase noise analysis have been presented. The conventional methods require expensive equipment but yield accurate results. The newly proposed method takes advantage of the fact that the phase noise of a loop is present within the loop in a measurable form. The low cost aspect of the equipment required for measurement takes advantage of powerful processor technology applied in an affordable F.F.T. analyzer.

The author has utilized this technique for several years for relative comparison of production oscillators. Only recently has the technique been applied to an absolute phase noise measurement tool. It is hoped that others will conduct further research and analysis to improve the accuracy of the technique.

References

- [1] Hewlet Packard Product Note 11729B-1 "Phase Noise Characteristics of Microwave Oscillators", Phase Detector Method, March 1984
- [2] Hewlet Packard Product Note 11729C-2 "Phase Noise Characteristics of Microwave Oscillators", Frequency Discriminator Method, March 1984
- [3] Sheilds, Robert B. , "Review of the Specification and Measurement of Short-Term Stability", The Microwave Journal, June 1969, pp49-55
- [4] Stanford Research Systems "Operating Manual and Programming Reference for SR770 FFT Network Analyzer" ©1992

A 250-MHz Voltage-out Analog Multiplier

Analog multipliers are useful in a variety of signal-processing applications. They may, for example, be used as voltage-controlled amplifiers, exhibiting a *linear* gain-control function, where the signal level and the required control range are both moderate. In the past, these have usually been limited to two types: (1) “analog computing” multipliers, with low to moderate bandwidths (1 MHz for the industry-standard AD534, or 10 MHz for the AD734, which may also be used as an analog divider with a 60-dB gain range) and operating at high signal levels (± 10 V full-scale) and requiring ± 15 -V supplies, or (2) very high bandwidth multipliers such as the popular AD834, having open-collector outputs.

The AD835 is an advanced analog multiplier which is fabricated using a very fast dielectrically-isolated complementary-bipolar process, providing four-quadrant operation from X- and Y-inputs of nominally ± 1 V and a voltage output capable of driving loads as small as 25Ω . In its basic mode of application its 3 dB bandwidth is 250 MHz. This multiplier has much lower noise than the AD534 or AD734, making it attractive in signal-processing applications as a gain-control element.

The function provided is, in its most complete form

$$W = \frac{(X_1 - X_2)(Y_1 - Y_2)}{1V} + Z \quad \text{Eq. (11a)}$$

where W, X, Y and Z are all voltages. The concept of this multiplier can be more readily appreciated by setting $X = X_1 - X_2$, $Y = Y_1 - Y_2$ and $Z = 0$, when we can write

$$W = XY \quad \text{Eq. (11b)}$$

provided it is understood that all signals are expressed in *Volts*.

The AD835 is packaged in an 8-pin format, and in spite of its high bandwidth is very versatile and easy to use. A useful feature of the AD835 is the capability to add another signal to the output using the variable “Z” in Eq. (11a), a voltage applied to pin 4. We will here show three applications of the use of this feature: a wideband voltage-controlled amplifier, an AM modulator and a frequency-doubler. Of course, the AD835 may also be used as a square-law detector (with its X- and Y-inputs connected in parallel), useful to well over 250 MHz, since this is only the bandwidth limitation of the *output* amplifier.

EXTERNALLY-INDUCED TRANSMITTER INTERMODULATION: MEASUREMENT AND CONTROL

Ernie Franke
E-Systems, ECI Division
P.O. Box 12248 MS 28
St. Petersburg, FL 33733

RF power amplifiers used for AM, FM, and TV broadcasting and for mobile, portable and base station radio transmitters are designed for maximum efficiency and output power, and not linearity. Intermodulation products can be generated in the final stages of power amplifier as a result of the mixing of the carrier frequency with one or more external signals coupled back through the transmitting antenna. Industry uses several terms such as reverse intermod, back intermod, and antenna-induced intermod to describe this externally-induced transmitter intermodulation. The level of these intermod products may be characterized in the laboratory, by injecting a known swept-frequency signal level into the output port of the power amplifier, and then used for radio system interference analysis. Although straight forward in concept, the measurement procedure and the interpretation of the results of intermod testing often cause considerable misunderstanding.

With the advent of wideband transistor power amplifiers and the need to operate at crowded repeater sites, especially with frequency-agile synthesizers, the characterization of broadband, externally-induced intermod performance becomes more important. Transistor amplifiers provide a wideband match allowing spread spectrum, fast tuning, and frequency hopping operation. This is required for mobiles operating in military tactical or cellular mobile telephone environments. Vacuum tubes have intermod performances similar to transistors, but tube power amplifiers typically operate in narrowband, cavity or high-Q output circuits which offer rejection both to the incoming interfering signal and to the generated intermod product.

This article describes how to examine externally-induced intermod performance using a wideband technique for characterization of modern power amplifiers. Variables such as supply voltage, transistor operating point, etc. are examined for effects on intermod performance. Methods of improving intermod performance through circuit design and through the use of external devices are also investigated. With this insight into the intermod process, the confusing measurements in the field or in the lab may be better understood and the intermod performance improved.

INTERMOD INTERFERENCE

Intermodulation (intermod) products can be generated in the final amplifier stages of radio transmitters that are in close proximity with other transmitters, receiver front-ends or mixers in proximity with several strong signals, common antenna feed systems, and rusty or corroded metallic structures that are exposed to high RF fields. A nonlinear amplitude response in the transmitter output power amplifier, an overdriven receiver front-end, an oxidized antenna or a corroded cable in a multiple-transmitter location can all give rise to intermod interference which masks desired weaker signals at the receiver. Although receiver and metallic intermod may be

present in such an environment, the major source of interference is due to externally-induced transmitter intermod, and will thus be the thrust of this article.

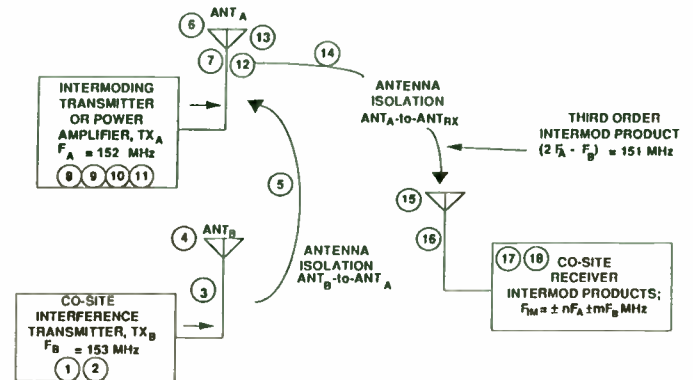


FIGURE 1 Co-site transmitter intermod interference is caused by mixing action in the output stage of an RF power Amplifier. Circled numbers represent gains and losses from the intermod budget below.

RF Budget for computing externally-induced transmitter intermod interface

TABLE 1

Location	Equipment	Frequency	Description	Level
1	Co-Site TX B	F _B	Co-Site Interfering Power	+50 dBm (100 Watts)
2	Co-Site TX B	F _B	Output Filter Cavity Loss	-1 dB
3	Co-Site TX B	F _B	Transmission Line Loss	-2 dB
4	ANT B	F _B	Antenna Gain Toward TX A	+3 dB
5	TX B-to-TX A	F _B	Space Loss from ANT B to ANT A	-2 dB
6	ANT A	F _B	Antenna Gain in Direction of TX B	+5 dB
7	TX A	F _B	Transmission Line Loss	-15 dB
8	TX A	F _B	Output Filter Cavity Loss	-1 dB
9	TX A	F _B	Externally-Induced Interference Power into TX A Power Amplifier	+20 dBm (0.1 W)
10	TX A	F _B -to-(2F _A - F _B)	Third-Order Intermod Performance of Power Amplifier	-20 dB
11	TX A	2F _A - F _B	Output Filter Loss (2F _A -F _B) = F _B	-1 dB
12	TX A	2F _A - F _B	Transmission Line Loss (2F _A -F _B) = F _B	-2 dB
13	ANT A	2F _A - F _B	Antenna Gain in Direction of Co-Site RX	+6 dB
14	ANT A-to-ANT RX	2F _A - F _B	Space Loss	-90 dB
15	ANT RX	2F _A - F _B	Antenna Gain Toward TX A	+7 dB
16	Co-Site RX	2F _A - F _B	Transmission Line Loss	-2 dB
17	Co-Site RX	2F _A - F _B	Input Filter Cavity Loss	-1 dB
18	Co-Site RX	2F _A - F _B	Interfering Signal Input at RX	-83 dBm (16 μV)

Intermod interference generated in a transmitter output stage typically occurs at sites where transmitter antennas are located in close proximity to each other and mutual coupling exists between these antennas, Figure 1. The power radiated from a co-located interference transmitter (TX_B) may be coupled into the antenna of the transmitter in use (TX_A). It must be emphasized that both the transmitter under inspection (TX_A) and the interference station (TX_B) are both operating properly and if either were operated alone they would not generate intermod products. Many installations which share the same mast often bundle transmission lines together in a trough, where the signal from one transmitter couples through the

A Wideband Voltage-Controlled Amplifier

Figure 13 shows the AD835 configured to provide a gain of nominally 0 to 12 dB. (In fact, this range extends from well under -12 dB to about +14 dB). R1 and R2 set the gain to be nominally X4. The attendant bandwidth reduction that comes with this increased gain can be partially offset by the addition of the peaking capacitor C1. Although this circuit shows the use of dual supplies, the AD835 can operate from a single 9-V supply.

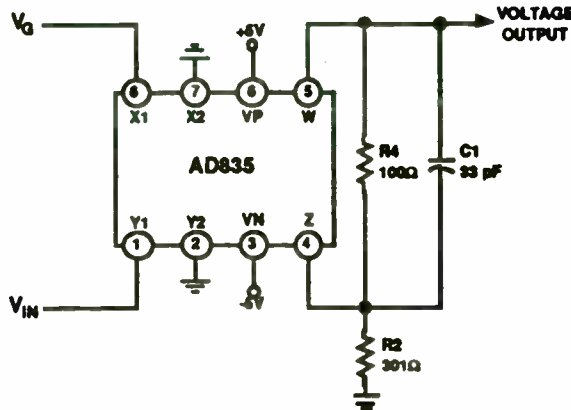


Figure 13. Voltage-Controlled 50 MHz Amplifier using the AD835

The AC response of this amplifier for gains of 0 dB ($V_G=0.25V$), 6 dB ($V_G=0.5V$) and 12 dB ($V_G=1V$) is shown in Figure 14. The phase may be inverted by the sign of V_G .

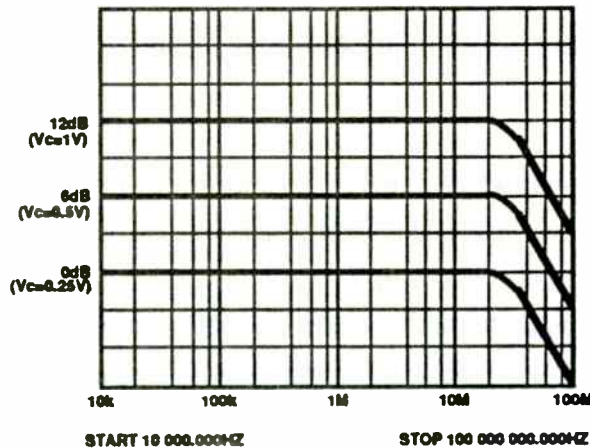


Figure 14. AC Response of VCA

braided coaxial cable into the output port of another transmitter. This results in interfering signals entering the final amplifier stage of the intermodulating transmitter or power amplifier. Since most transmitters operate in either the Class C, D or E mode for maximum efficiency, the power amplifiers are non-linear and hence act as mixers. The desired carrier signal frequency (F_A) mixes with the interfering signal (F_B) to produce intermod products (F_{IM}), which are then re-radiated via the transmitter antenna (ANT_A), just as is the desired signal, and are received as interference signals by nearby receivers.

INTERMODULATION PRODUCT FREQUENCIES

Let's begin by defining externally-induced transmitter intermodulation distortion. It is simply the mixing of frequencies in the final transmitter stage to generate new frequencies, which are then radiated from the transmitting antenna. This is different from the intermod distortion performance of a linear power amplifier used for single sideband or digital data service where two-tone test signals are injected at the input of the power amplifier stage. If two signals are present in a non-linear device, such as in the output stage of a power amplifier, mixing will occur, creating additional spurious signals according to the simple sum and difference mixing formula:

$$F_{IM} = \pm nF_A \pm mF_B$$

where; F_{IM} = frequency of the intermod product

F_A = frequency of the intermodulating transmitter

F_B = frequency of the co-site interference signal

$n, m = 1, 2, 3 \dots$ integers

If more than two frequencies are involved, the number of combinations rises rapidly. The order of the intermod product is equal to the sum of the integers n plus m . The most important intermod products are those that are closest to the carrier frequency with low integers, because they are both the strongest and the most difficult to filter. The third-order products ($2F_A - F_B$ and $2F_B - F_A$) and the fifth-order products ($3F_A - 2F_B$ and $3F_B - 2F_A$) are shown in Figure 2. The amplitude of each product is shown relative to the output signal carrier level (dBc). The third-order intermod performance is simply the difference between the co-site interfering signal level and the largest 3rd order product. The intermod products are spaced at the difference frequency ($F_B - F_A$).

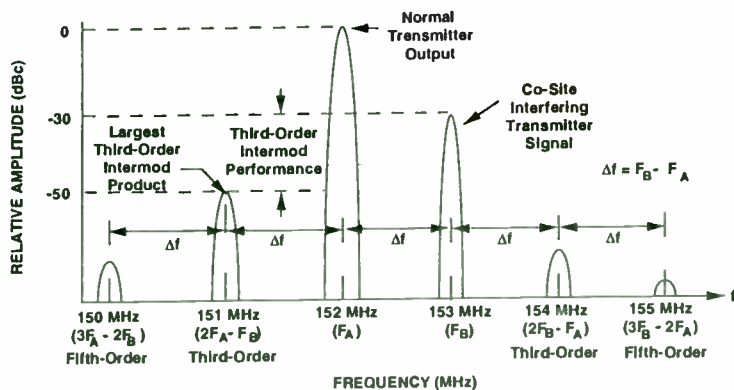


FIGURE 2 A nearby interfering transmitter signal F_B mixes in the non-linear output stage of a power amplifier with the second harmonic $2F_A$ of the operating frequency to form a strong third-order intermodulation product at $2F_A - F_B$.

In a typical transmitter output circuit, as shown in Figure 3, a co-site interfering signal (F_B) is coupled into the antenna from a nearby transmitter and beats with the second harmonic of the operating frequency ($2F_A$) in the collector or drain circuit. The third-order, sum intermod product ($2F_A + F_B$) is blocked from the antenna by the lowpass filter (LPF), normally present in a transmitter to reduce harmonic energy. The third-order, difference intermod product ($2F_A - F_B$) however will readily pass through the LPF and be radiated by the antenna. If the interference frequency is close to the operating frequency, even a high-Q cavity filter will not reflect the interfering frequency or filter the intermod product.

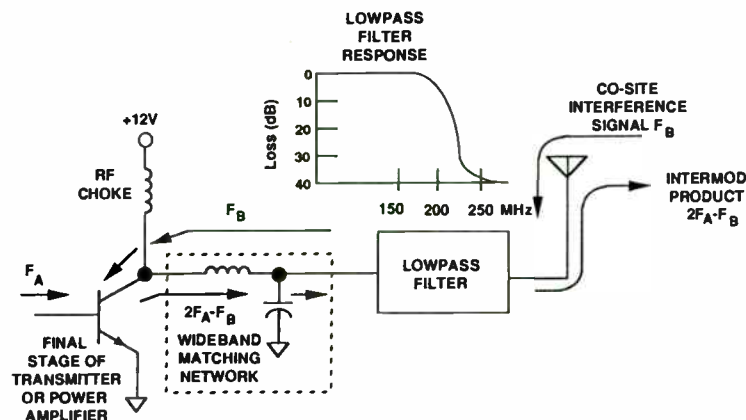


FIGURE 3 The third-order intermod product ($2F_A - F_B$) easily passes through the output lowpass filter if F_A and F_B are reasonably close to the same frequency.

INTERMODULATION PRODUCT POWER LEVEL

Intermodulation products are not only frequency related, but amplitude related as well. Because the second harmonic power varies 2 dB for each 1 dB change in output power, the intermodulation signal power for the ($2F_A - F_B$) third-order intermod product also varies 2 dB for each 1 dB of variation in normal transmitter output power. The intermod product power however varies directly dB for dB with the incoming interference signal power for this product. The signal level of the weaker ($2F_B - F_A$) intermod product however varies 2 dB for each 1 dB of variation in interference power. This power relationship is helpful for discerning the exact intermod culprit. This power relationship is shown in Figure 2 for close-in products, where the interfering signal is injected 30 dB below the normal transmitter output and the resultant intermod product is 20 dB below this interfering signal level. Class C power amplifiers typically display a third-order, externally-induced intermod performance between 15 and 30 dB. Higher-order intermod products will drop 15 dB for each successive odd higher order. The 5th order products are typically 15 dB lower than the third-order products and the seventh-order products are approximately 30 dB down from the third.

CO-SITE INTERMOD BUDGET

A typical co-site environment involving a 100 watt transmitter (TX_B) coupled into a transmitter (TX_A) creates a third-order intermod product ($2F_A - F_B$), as itemized in Table I. Because the interfering transmitter frequency (F_B) is very close to the desired operating transmitter frequency, the transmission line

An Amplitude Modulator

Figure 15 shows a simple modulator. The carrier is applied both to the Y-input and the Z-input, while the modulating signal is applied to the X-input. For zero modulation, there is no product term, so the carrier input is simply replicated at unity gain by the voltage-follower action from the Z-input. For $X = +1$ V, the RF output is doubled, while for $X = -1$ V it is fully suppressed. That is, an input of $X = \pm 1$ V corresponds to a modulation index of 100 %. Carrier and modulation frequencies can be up to 300 MHz, that is, somewhat beyond the nominal 3-dB bandwidth.

Of course, a suppressed-carrier modulator can be implemented by omitting the feedforward to the Z-input.

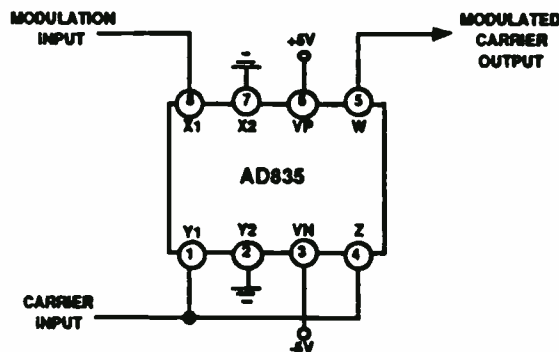


Figure 15. Simple Amplitude Modulator using the AD835

Frequency-Doubler

Finally, Figure 16 shows a frequency-doubler which provides a relatively constant output over a moderately-wide frequency range, determined by the CR product of C1 and R1. The voltage applied to the X- and Y-inputs are exactly in quadrature at a frequency $f=1/2\pi C_1 R_1$ and their amplitudes are equal. At higher frequencies, the X-input becomes smaller while the Y-input increases in amplitude; the opposite happens at lower frequencies. The result is a double-frequency output, centered on ground, whose amplitude of 1 V for a 1 V input varies by only 0.5 % over a frequency range of ± 10 %. Because there is no “squared” DC component at the output, sudden changes in the input amplitude do not cause a “bounce” in the DC level.

losses and filter losses at each site will be approximately the same for the desired operating, interfering and intermod frequencies. The antenna gain at each frequency will however not necessarily be the same because of directionality. It is interesting to note that the desired output power level of the transmitter under question (TX_A), which generates the intermod products, does not enter into the equation. The transmitter power level is always assumed to be much larger than the co-site coupled interference power level, and simply acts as a pump for generating mixer intermod products.

The resultant intermod product signal level of -83 dBm at the input to a nearby sensitive receiver will most likely overpower the desired signal. To minimize receiver interference, the amplitude of the intermod product needs to be on the order of the noise figure of the receiver. Thus even -20 or -30 dB of intermod performance at the output stage of a transmitter itself is inadequate for receiver interference protection. Control of intermod interference takes the combined effort of power amplifier design, band-pass and band-reject filtering, antenna separation, circulators, and frequency planning to effectively control intermod interference.

TRACKING DOWN ON-SITE INTERMOD INTERFERENCE

The first step in any intermodulation analysis is to write out a table of all frequencies present at a site and then compute the intermod products. Next it is essential to determine whether the intermod product originates at the transmitter, receiver or a combination of both. A variable RF attenuator placed at the receiver input permits observation of any overloading effects. An intermod product, which is produced due to receiver overload, will drop drastically as soon as the signal causing the overload is attenuated below the overload point. If the intermod product drops at the same rate as the introduced attenuation, then the receiver is not the cause and each co-site transmitter must be investigated. If the intermod product drops by twice the attenuator setting, the problem is in the receiver and the troublesome product is second-order. Third-order products in the receiver drop 3 dB for each 1 dB change in front-end attenuation.

Transmitter intermod is most easily identified by turning off suspected transmitters, changing antennas, changing operating frequencies, or operating transmitters into dummy loads. If only the interfering power is decreased by 10 dB, the ($2F_A - F_B$) internal product will reduce by 10 dB, while the other third-order ($2F_B - F_A$) product will drop by 20 dB. This reduction in signal level should be reasonably close (± 3 dB) to this predicted value. If two FM voices are heard simultaneously at normal levels, it is probably second-order intermod. If the voice on the intermoding transmitter channel sounds loud and distorted, the intermod is likely to be third-order ($2F_A - F_B$), or possibly fifth-order intermod. The deviation of the carrier signal F_A is multiplied, whereas the deviation of interference signal F_B remains constant.

MEASUREMENT SET-UP

Externally-induced intermod performance is best described, not by a third-order intercept point as is done for small-signal linear amplifiers, but by a third-order intermodulation

distortion (IMD) measurement using a carrier injected into the power amplifier output port. The performance is always stated for the third-order ($2F_A - F_B$) product, because it is the largest product. The device under test can be a single transistor in a fixture containing input/output matching, an amplifier module, or an entire high-power transmitter.

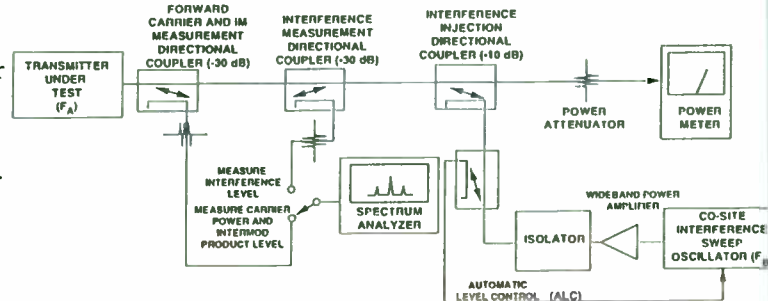


FIGURE 4 A continuous curve of intermod performance, including close-in measurements, may be made using the wideband test set-up.

A wideband equipment arrangement [1] for measuring the externally-induced intermod performance of transmitter (TX_A), Figure 4, shows a directional coupler for measuring both the forward carrier power at the operating frequency (F_A) and the intermod product levels. Two more directional couplers are added to inject the level of the co-site transmitter power at the interference frequency (F_B) and to display the actual injected value on the spectrum analyzer. The broadband co-site interference signal is injected using a broadband isolator to avoid intermoding in the sweep power amplifier.

The wideband intermod test set-up is used to plot the intermod performance as a continuous function of frequency separation on both sides of the carrier frequency. The spectrum analyzer is configured for a maximum hold display, while the interfering frequency is only swept on one side of the carrier. Because the third-order ($2F_A - F_B$) internal product, which shows up on the opposite side of the carrier from the injected signal, is the strongest intermod product, it is always the resultant intermod performance curve recorded by the peak hold display function. A plot is performed before the interference signal is swept on the other side of the carrier and then plotted again. By selectively lifting the plotter pen, a plot of only intermod performance is obtained. The resultant display of a typical 150 watt, push-pull UHF power amplifier yields a clear picture of third-order intermod performance, Figure 5, especially for close-in products. The horizontal axis shows the injection frequency relative to the output carrier while the vertical axis shows worse-case third-order intermod energy. The externally-injected interfering frequency is always on the opposite side of the carrier from the intermod energy.

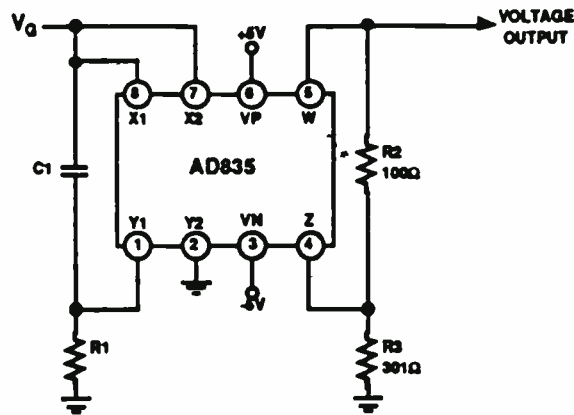


Figure 16. Broadband "Zero-Bounce" Frequency-Doubler

Summary

While there is a clear progression toward highly-integrated ASICs for modern high-volume communications applications, many of the key challenges remain in the area of high-performance analog-signal manipulation using moderate scales of integration. By focusing on some of the key challenges in this area, Analog Devices has been able to achieve some major performance advances. Thus, the AD831 the first monolithic mixer to provide a third-order intercept of +30 dBm with a noise figure of 12 dB and to include a high-bandwidth low-noise output amplifier affording high conversion gains; the X-Amp concept, embodied in the AD600, AD602, and AD603, provides a unique combination of low noise, low power, wide bandwidth and low distortion, with the added benefit of exactly-calibrated "linear-in-dB" gain control; the AD606 is the first monolithic nine-stage log-amp to be offered, and operates at only 65 mW from a single 5-V supply; the AD835 four-quadrant analog multiplier uses an advanced IC technology to provide a 250 MHz bandwidth in a voltage-output format. These, and a broad range of high-speed amplifiers and A/D converters, as well as a growing catalog of DSP products, provide a wide variety of solutions to the designer of state-of-the-art communications systems.

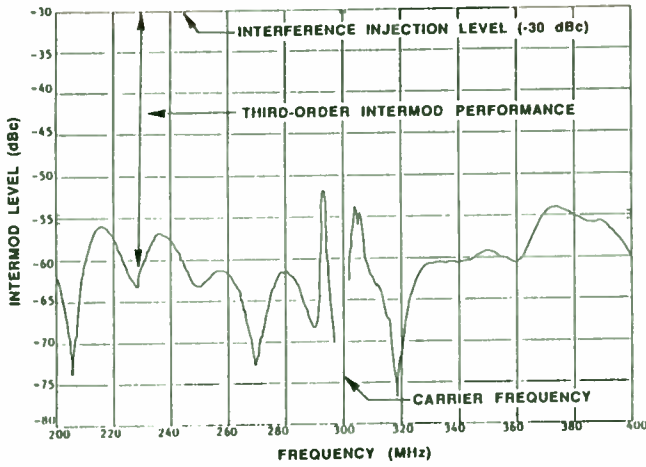


Figure 5 By sweeping the injected interference frequency, a clear picture of close-in, third-order intermod performance is produced. In this case it varies between 25 and 40 dB.

If the interference is so close to the carrier that a bandpass filter cannot provide the required selectivity, a ferrite isolator must be used. An isolator is a circulator with the third port terminated. The circulator, Figure 6, is a device which uses the interesting gyromagnetic behavior of ferrite. A transmission line is sandwiched between two ferrite discs inside a static magnetic bias. The 3-port circulator has the property that RF incident at port 1 emerges at port 2, a wave incident on port 2 emerges at port 3 and a wave incident at port 3 emerges at port 1 in a cyclic or circulating manner. An interference signal coupled into the antenna will be shunted to the circulator termination. Approximately 20 to 30 dB of reverse isolation is achieved for each circulator section added.

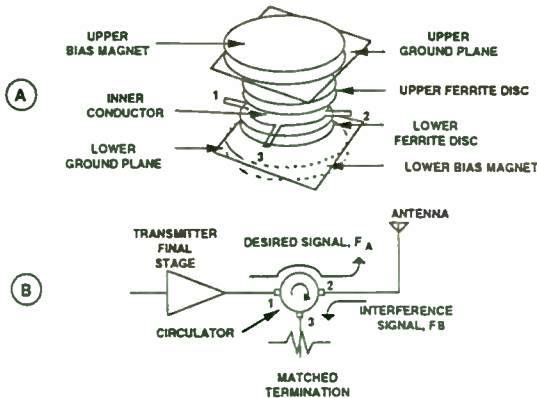


FIGURE 6 Interaction between the magnetic field of the RF signal and the magnetically biased ferrite produces a tendency for the signal to follow a circulating path.

CLOSER EXAMINATION OF INTERMOD GENERATION

The intermod products present at the output circuit of a power amplifier are dependent on several items; the level of injected interference signal, power amplifier output return loss, amplifier linearity, operating frequency, spectral proximity of the interfering signal, reverse isolation of the final stage, bias circuitry, supply voltage, and power combining techniques.

Third-order intermod performance improves for example, Figure 7, as the RF output power level is decreased or as the power supply voltage is increased. The intermod performance

consistently improved by 10 dB for each 5 Vdc increase in power supply voltage. The varactor effect of an RF voltage modulating the output capacitance becomes a smaller part compared to the steady state component. It also improves as the required output power is backed off from the design value, which is 70 watts for the example shown. At lower power, the third-order intermod power varies 2 dB for each 1 dB change in output power level. At higher power levels the intermod performance degrades 3 to 5 dB for each 1 dB change in power. Typically the final stage in an FM transmitter is operated in class C very close to its saturated power level for maximum efficiency. Distortion due to saturation may be decreased if the size of the output transistor is increased or if the output power is turned down, usually with a slight sacrifice in efficiency.

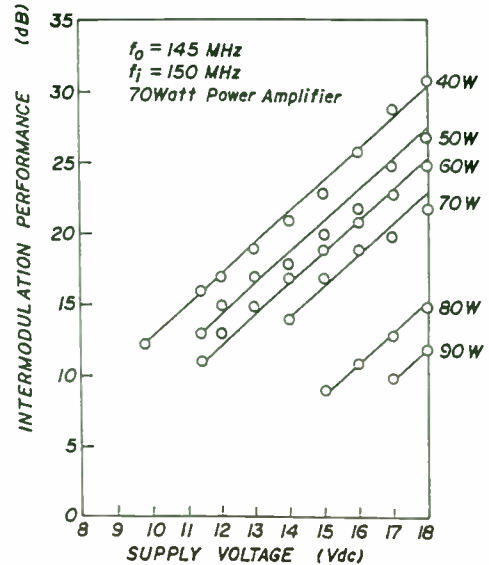


Figure 7 Third order intermod performance improves as the power level is decreased or as the power supply voltage is increased.

Measured externally-induced intermod performance may also be partially composed of forward intermod products. The collector-to-base or drain-to-gate capacitance is typically large enough and the base or gate impedance levels are high enough that reverse transmission values of -10 to -20 dB are common. Thus the interfering signal appears at the input to the final stage and mixes in the same manner as in forward intermodulation measurements for linear power amplifiers. Signals reflected off interstage filters, several stages before the final output stage, have been observed to affect third-order intermod performance, as shown in Figure 8.

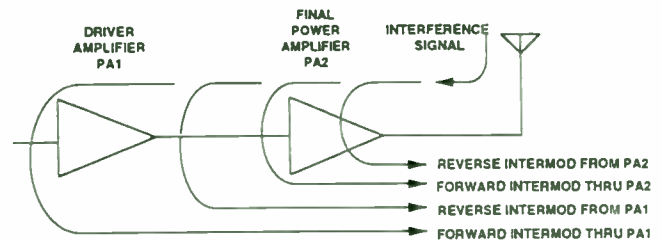


FIGURE 8 The intermod performance of a power amplifier is a composite of the forward and reverse intermod of the driver and final amplifiers.

Digital Signal Processing in Wireless Communications Focus on Digital Transmitters

Daniel A. Ash
Senior Field Applications Engineer
Analog Devices - Campbell, CA
(408)879-3037

ABSTRACT

In communication systems, modern transmitter and receiver designs use digital signal processing (DSP) microprocessors. DSPs can compute complex mathematical expressions over ten times faster than a conventional microprocessor of similar complexity. In a receiver, DSPs are used to demodulate signals from IF to baseband. In a transmitter, a DSPs are used to modulate the baseband signal to IF and to precondition the outgoing signal before it is attenuated by the channel. If the baseband signal is data instead of voice, a DSP can be used to decode the complex analog signal that represents the data to binary information. DSP based transmitters can be used to encode digital information. A DSP's reprogrammability makes possible a modem that employs different encoding and decoding schemes. DSPs can improve noise performance of a transceiver using digital filters and automatic gain control. The same circuit can be used to transmit and receive either sampled voice or data. This paper surveys the use of DSPs in radio transmitters.

INTRODUCTION

Digital signal processors are used extensively in telecommunication systems for cancelling echos, detecting tones, conferencing multiple voice channels, and compressing sampled voice data. DSPs are commonly used in central office (CO) switches, private branch exchanges (PBX), and voice mail. The advantage of DSP is reconfigurability since it executes programs from RAM.

The DSPs discussed in this paper are general purpose and fully programmable. They execute instructions from memory as the CPU in a personal computer does. By downloading a different program to the DSP, the system's function can be altered. Another advantage of a digital signal processor over analog components is the ability to process multiple channels through a single signal path. For example, one DSP can detect touch tones on 30 telephone lines simultaneously.

Some available DSPs are designed to perform a single function such a modulation/demodulation, modem signal decoding, or digital filtering. These components perform one function with higher throughput than a general purpose DSPs and are often required in high bandwidth digital radios where multiple channels of information or voice are multiplexed in a single band. These components are necessary in high speed radio modems (100Kbits/second). These components are typically more expensive than a general purpose DSP.

DSP PERFORMANCE

A DSP has performance limitations. The limit is the number of instructions that can be completed between samples. A DSP that executes instructions at 16MHz and uses an A/D converter (ADC)

The intermod performance or turn-around loss of a power amplifier is related to the level of the interfering signal, frequency spacing between the transmitter carrier frequency and interfering frequency, the bandwidth of the transmitter, and the value of loading. It is not only a function of the power amplifier output circuit bandwidth, but also of the input circuit. An experimental arrangement for measuring reverse isolation is shown in Figure 9.

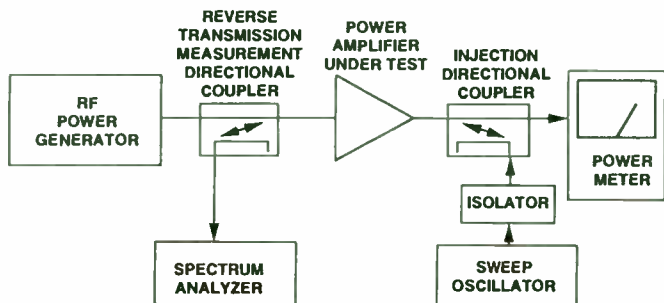


FIGURE 9 The reverse isolation of power amplifier may be measured under actual operating conditions by injecting a sweep signal into the output port and monitoring the input.

POWER AMPLIFIER INTERMOD IMPROVEMENT

Bias network impedance can also influence intermod performance. Beat notes between the operating frequency and the interfering frequency can be formed both at the output and at the input of a power amplifier. These low frequency difference frequencies can then modulate the operating frequency and appear on the spectrum analyzer in the same manner as third-order intermod products. Solid-state amplifiers typically have a much higher gain at low frequencies, as seen in Figure 10 for a typical VHF bipolar transistor. The power gain expression contains a $1/f^2$ term indicating that the power gain decreases at 6 dB per octave with increasing frequency. This figure displays the upper bound of available gain for a common emitter transistor whose input and output are matched. The unity gain intercept frequency, f_T , is a projected point due to the effect of package parasitics coming into effect as the intercept is approached. This slope approaches the low-frequency beta (H_{fe}) at f_B .

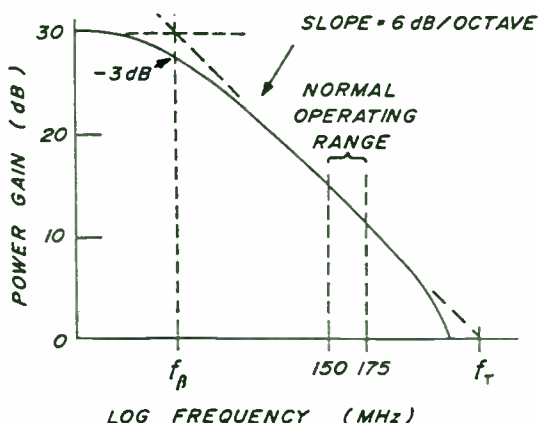


FIGURE 10 Solid state amplifier have excess low-frequency gain and thus enhance close-in mixing product.

The techniques of using feedback and shunting networks [2] may be used to decrease this low-frequency gain and improve power amplifier stability. The first method of employing a network to provide feedback is shown in the negative feedback circuit of Figure 11A. The capacitor is used to block the collector supply voltage from reaching the base. The series inductor and the resistor are used to provide 6 dB/octave of negative feedback to offset the effect of the in transistor gain slope.

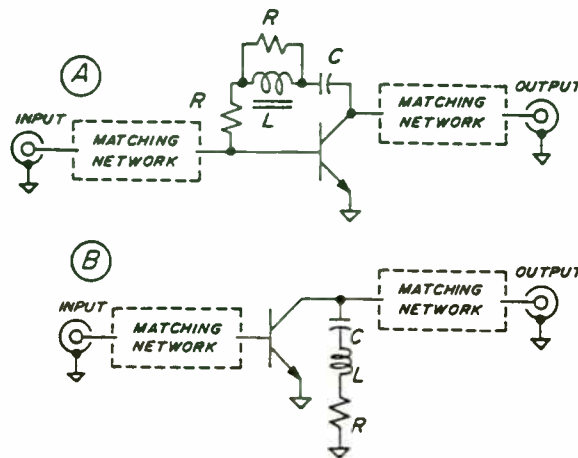


FIGURE 11 The large low-frequency gain may be controlled through A.) negative feedback or B.) shunt loading.

Low frequency gain may be controlled and stability improved by negative feedback but the intermod performance is typically degraded, as shown in the single-sided intermod sweep of Figure 12 for a 150 watt, UHF power amplifier. The second method of low-frequency gain reduction involves collector loading, as illustrated in Figure 11B, where an RLC circuit has been attached to the collector. The circuit is transparent at the operating frequency due to the inductor. At low frequencies the inductive reactance decreases such that the loading resistor appears directly across the collector. The capacitor is added solely to block the dc supply voltage.

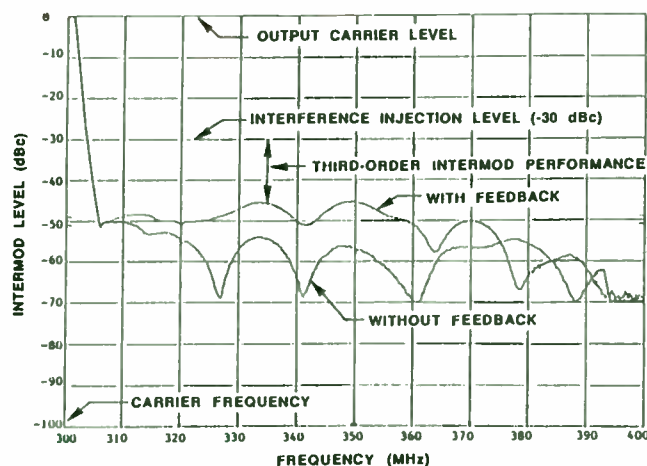


FIGURE 12 The third-order intermod performance is degraded when low-frequency feedback is added to improve stability.

that samples at 8KHz can process 2000 instructions (16MHz/8KHz) every sample interval. If there are 10 input channels, the processor must divide the 2000 instructions into 200 for each channel. System performance is dependent the processor's instruction rate, the ADC sample rate and the number of channels to be processed. The fastest DSPs available have 20MHz-40MHz instruction rates.

In real-time imaging applications, pixels arrive at a 10MHz sample rate minimum. A 40MHz DSP would only have four instructions (40MHz/10MHz) per pixel. Four instructions are hardly enough programming steps to enhance an image or to recognize an object on the production line.

In the case of radio communications, the baseband signal has a bandwidth of 4KHz-25KHz depending on the nature of the information. High fidelity audio uses over 20KHz per stereo channel. "Toll quality" voice is limited less than 4KHz of bandwidth. V.32 modems encode 9600bits/second data onto an analog signal using less than 4.8KHz bandwidth. DSPs are used in consumer audio products, telecommunication systems, and high speed modems.

RADIO TRANSMITTER

Figure 1 is a radio transmitter design that incorporates a DSP. The DSP generates the baseband signal. If the baseband signal is voice, an ADC is required for the microphone input. A CODEC circuit combines a voice band (300Hz-3700Hz) ADC, an antialiasing filter, voice band DAC, and DAC reconstruction filter in a single integrated circuit. The DSP used in this example is the ADSP-2115 from Analog Devices, a 16-bit DSP. The voice CODEC is the Analog Devices AD28msp01, a device that includes a 16-bit ADC. The DSP interfaces to the CODEC over a serial port. If the baseband signal is binary information, the data originates from a host microprocessor. The DSP's second serial port can interface to the host.

Voice is usually sampled at 8KHz. The sampled voice is modulated to an intermediate frequency (IF). In an analog transmitter, the baseband signal is modulated to IF by being multiplied or mixed with a sine wave at the intermediate frequency. The same applies for a digital transmitter, but the multiplication occurs in software. The baseband signal is multiplied by a digital sine wave stored in DSP memory. The multiplier output product is written to a DAC (Analog Devices DAC-16). The DSP is performing two tasks. One task is processing incoming voice at an 8KHz input sample rate. The other task is writing 456KHz modulated voice to the DAC at a 1.824MHz rate (4 times 456KHz). The DSP can divide its master clock to generate the master and sample clocks for the CODEC's ADC, but the 1.824MHz clock is best handled by a separate oscillator to avoid jitter noise caused by the DSP's master clock. Jitter caused by the DSP's master clock has a negligible effect on 8KHz voice band ADC.

The CODEC's ADC sample rate is 8KHz. The signal may be processed at baseband, but must be interpolated or upsampled to 1.824MHz for modulation. The DSP is used to perform the interpolation function (Figure 2). The interpolation factor between 8KHz and 1.824MHz is 228. The simplest interpolation is linear interpolation where the 227 interpolated samples are calculated by finding the values on a straight line between two 8KHz samples. Linear interpolation will introduce distortion since it approximates the original signal. Another option is to perform an interpolation filter using finite impulse response (FIR) or feedforward filters. The interpolation

An alternate method of increasing stability is achieved by low-frequency, shunt-loading of the base and collector as shown in Figure 13. The base bias current return circuit consists of two chokes, L1, which is a small inductor in the range of 100 nanohenries chosen to function as a choke at the lowest operating frequency and L2, which presents a high impedance down to very low frequencies. At normal operating frequencies, the base is effectively isolated by inductor L1 from resistor R1, forming a low Q arrangement. The Q of the network is given as $Q = 2\pi f L1/R1$ which is low. The resistor R1 is chosen to be 10 to 20 ohms. At lower frequencies, where the power gain is much greater, the shunting effect of R1 increases due to the lower inductive reactance of L1. The larger value inductor L2, consisting of a few turns of wire through a powered-iron bead, is a low ohmic dc path across R1, providing a dc bias for the base and a high impedance at low frequencies. Thus the base is effectively resistively loaded by R1 at low frequencies, where the power gain is greatest.

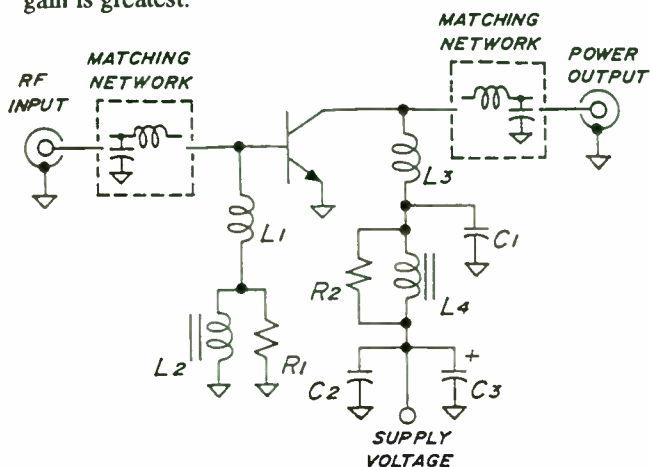


FIGURE 13 Low frequency loading techniques applied to the base and collector feed networks.

The collector feed network accomplishes a similar feat by resistively loading the collector at frequencies below the operating band. Within the frequency range of normal operation the small inductor L3 and the small shunt capacitor C1 act as an L-network to transform the resistance of R2 to a high value so that it will not load the collector. At the operating frequency, the powered-iron loaded inductor L4 appears as an open, while the capacitor C2 acts as a very low impedance. Below the normal operating range the input impedance to the network looks resistive asymptotically approaching the value of R2, typically 10 to 20 ohms. The wattage of this loading resistance need only be 1/2 or 1 watt because it is designed to absorb less than 1/4 watt of signal power at the operating frequency. The bypass capacitors, C2 and C3, placed at the supply voltage consist of a disc ceramic for bypassing at RF and an electrolytic for bypassing at audio frequencies. The resultant intermod performance improvement with base and collector low-frequency, resistive-loading is shown in Figure 14.

As the output power from a VHF or UHF solid-state transmitter is increased beyond approximately 50 to 75 watts, where the power handling capacity of a single device is exceeded, the output stage must combine the power from two

transistor packages to achieve power levels up to the 100 to 150 watt level. If the output stage uses a push-pull arrangement, it will display better third-order intermod performance because second harmonic energy is decreased.

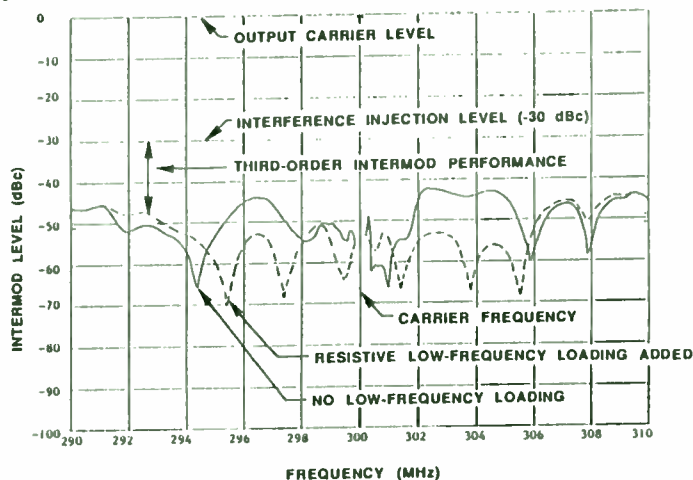


FIGURE 14 The third-order intermod performance is improved with resistive low-frequency loading techniques added to the base and collector feed networks.

In push-pull operation the even harmonic (second, fourth, etc.) distortion is balanced out. There are also several circuit techniques that may be applied to the output stage of the amplifier which will improve performance of a transmitter. These techniques include operating the final push-pull, using 90° hybrid combiners [3], and using larger output devices.

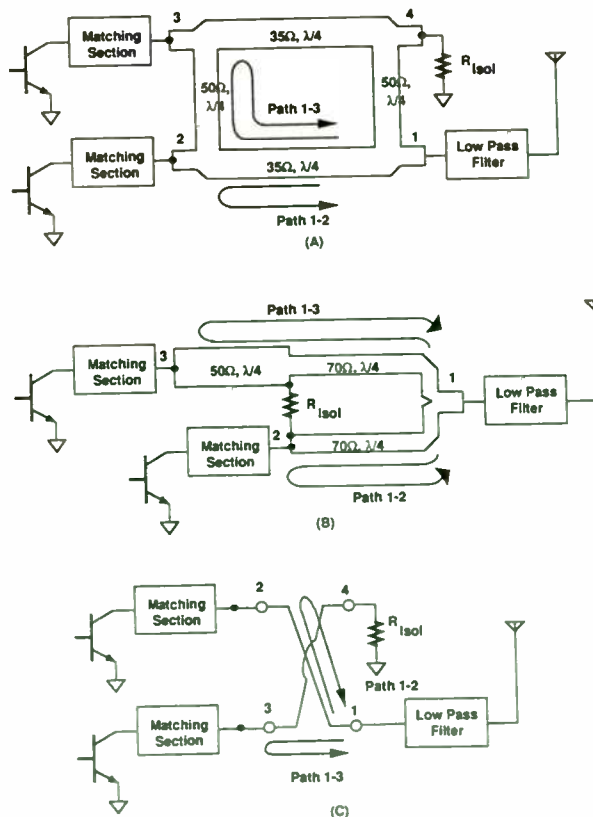


FIGURE 15 (A) Branch line coupler (B) staggered Wilkinson combiner and the (C) coupled - stripline coupler reduce externally-induced intermod generation.

filter generates 228 samples from each 8KHz sample. Interpolation filters with a large interpolation factors are typically performed in stages. In this example (Figure 2), the original 8KHz signal is interpolated by 4 to 32KHz. In the next interpolation stage, the 32KHz signal is interpolated by 3 to 96KHz. In the last stage, the 96KHz signal is interpolated by 19 to 1.824MHz. Interpolating in stages does not require any less performance from the DSP, but does reduce the number of filter coefficients stored in memory and improves distortion.

The digital IF sine wave in RAM is actually four values. A full 456KHz sine wave is a 360 degree cycle. To represent this signal at a four times sample rate (1.824MHz), means to divide the signal into four 90 degree phases, thus represent the sine wave with four values (0,1,0,-1) in memory. Every 1.824MHz interrupt will require a multiply of one of these values times the interpolated voice sample. After the multiply, the product is written to the DAC. The DAC output goes through a simple analog reconstruction filter. The remaining processing required to modulate to RF is accomplished using analog components.

MODULATION SCHEMES

In the above example, the baseband signal is modulated by the sinusoidal signal, creating a double sideband - suppressed carrier (DSB-SC) signal. As shown in Figure 3a, there is not any energy at the IF frequency, only at the two sidebands. In software, if a DC component is added to the baseband signal before multiplying by the IF sine wave, energy will be present at the carrier frequency (Figure 3b). This is amplitude modulation (AM). The sum of the DC component, a programmed constant, and the ADC sample from the CODEC should limited to 16-bits or overflow occurs. The ADC sample must be arithmetically attenuated by the DSP before it is added to the DC component.

The other modulation technique worth mentioning is single-sideband (SSB). Referring to Figure 3a, the baseband signal is replicated by the IF mixer on both sides of the IF frequency. A single-sideband transmitter requires that only one of the two sidebands is transmitted. DSPs can be used to filter one sideband simplifying the RF section.

DATA ENCODING

Radios are used to transmit binary data. In the case of digitized voice, the data rate is 64Kbits/second or more. Using linear predictive coding (LPC) speech data compression algorithms, the data rate can be compressed to 4Kbits/second. LPC algorithms require a DSP to perform mathematical analysis on short time intervals of incoming voice samples. The DSP reduces the sampled voice into speech coefficients that define the pitch and model the vocal tract of the speaker. These coefficients, when received, are used to synthesize the original speech. LPC algorithms are used to reduce transmitted data in the next generation digital cellular systems in North America, Japan, Europe, and Australia.

In telemetry systems, binary information (ones and zeros) are transmitted as samples of 16-bit magnitude (Figure 4a) at four times (4X) the data rate. If the binary data rate is 2400 bits/second, the output sample rate is 9600Hz. When this signal is transmitted it suffers degradation due in part to harmonics caused by the sharp transitions between one and zero samples. These

The use of several 90° hybrid combiners is shown in Figure 15. The cancellation is strictly a property of the circuit configuration and is independent of the transistor linearity. For each type of combiner the round-trip in path 1-3 is half-wave greater than that of path 1-2. Thus the intermod product created at each collector arrives at the summing (port 1) 180° out-of-phase with each other and thus will cancel out. Maximum cancellation will occur at the center frequency and will fall off as the transmission lines are no longer quarter-wavelength at the operating frequency. The coupled-stripline quadrature hybrid however maintains a 90° relationship for nearly an octave bandwidth. Under practical conditions, where the two amplifiers are fairly well matched, a 10 to 30 dB improvement in third-order intermod performance can be expected.

REFERENCES

- 1.) E. A. Franke, "Test Setup Gauges Externally - Induced Transmitter IM", Microwaves and RE, April 1993, pp. 95 - 98.
- 2.) E. A. Franke and A. E. Noorani, "Improving the Stability of the Mobile Radio Power Amplifier", Proc. of the 33rd IEEE Vehicular Technology Conference, Toronto Canada, May 24-27, 1983, pp. 228-234.
- 3.) E.A. Franke and A. E. Noorani, "Wilkinson Hybrid with Quarter-Wave Offset", RF Design, November/December 1981, pp. 32 - 38.

harmonics increase the bandwidth of the signal and the likelihood of bit errors. The DSP typically applies a low pass or pulse shaping FIR filter to the signal before transmission (Figure 4b).

If the data is redundant, the resulting signal's spectrum is limited to a narrow band making it more susceptible to narrow band noise and making error recovery more difficult. The data can first be scrambled using a binary polynomial. This process will make the bit pattern more random thus increasing its bandwidth. The receiver can unscramble the pattern as long as it uses the same polynomial in its decoder. Since a DSP is a microprocessor, it is well suited for such encoding. If a higher data rate is required, using the above described scheme, more bandwidth and a higher output sample rate is required.

Another possibility is to encode the signal using quadrature amplitude modulation (QAM). QAM maps two, three, or four bit symbols onto a complex signal constellation (Figure 5). Each symbol is represented on this signal map as a complex number. This complex number is applied to the system shown in Figure 6. The real and imaginary components are both applied to separate pulse shaping filters. Both filters have identical response. The filtered real component is multiplied by the cosine wave of frequency greater than one half the bandwidth of the symbol rate. The filtered imaginary component is multiplied by a sine wave of frequency greater than one half the bandwidth of the symbol rate. Both products are summed. The resulting signal has bandwidth less than if the data was not encoded and is easier to recover on the receiver.

One example is V.32 modems. Although the V.32 specification was created for wired systems, it encodes 9600 bit/second data into 5-bit symbols at 2400 symbols/sec. The symbol picks up an extra bit for noise immunity, error correction, and error detection. The resulting signal uses less than 4.8KHz bandwidth when modulated onto a 2400Hz subcarrier. The motivation of the V.32 standard was to allow higher data rates on the bandlimited (5KHz-10KHz) telephone system. Using less bandwidth also applies in radio communications. Less bandwidth per channel allows more channels to be allocated in a frequency band. Since a radio channel is not bandlimited as is a telephone line, higher data rates are possible.

In a radio transmitter that broadcasts data, the DSP encodes data, upsamples the baseband signal to the IF sample rate, and modulates the baseband signal to IF. The only limitation is the number of DSP instruction cycles available to accomplish the task.

CONCLUSION

DSPs are currently being used in wireless telephone systems (both private and public), AM radio transceivers, and in wireless data communications systems. A DSP can be used to perform multiple functions that typically require many discrete analog components. In most cases a DSP is more cost effective than a discrete analog approach. This is most true when the system has different modes of operation (modulation schemes, voice/data input). The RF section of the system will continue to be handled by discrete analog components including amplifiers, frequency generators (PLL or DDS), and narrowband filters. As DSPs execute instructions at faster rates and the costs of DSPs, ADCs, and DACs decrease, DSP will more prevalent in communications equipment.

A 3 GHz 50 Ohm Probe for PCB Measurements

Joel Dunsmore
Hewlett-Packard

Robert Kornowski
Motorola

Chuck Tygard
Everett-Charles Tech.

Introduction:

With the trend to commercial use of RF and microwave circuits, and the large increase in the communication segment, the use of PC boards as RF circuits demands non-traditional techniques to provide accurate yet automated measurements of these circuits. Manufacturing environments require high through-put measurements, and improving quality standards demand finer limits on measured parameters. An RF probe designed by Motorola and cooperatively developed with Everett Charles Technologies can be combined with high performance Vector Network Analyzers (VNAs) to support these requirements in automated measurements such as gain, return loss, output power and output match.

RF systems often use PC boards as interconnects between more complex modules, such as frequency converters, filters or amplifiers. These components may need to be pre-tested before assembly, and built-up subassemblies need to be measured before final assembly. Also, the RF match of a sub_assembly may be measured at the "socket" to ensure it is good before an expensive module is added. For example, the match of a tuning section may be measured before a power amplifier transistor is soldered in place. The problem of making the connection for the measurement, especially in an automated board test environment, requires improvements in probes and error correction in the measurement instrument.

PC Board RF Measurements:

Requirements for measurements of RF characteristics on PC board assemblies vary with the type of measurement. The predominant error to overcome is the match or return loss of the probe-to-board interface. For gain and power measurements, this mismatch may have only small effects, but for return loss or impedance measurements, the mismatch of the probe-to-board interface may be greater than the return loss of the component on the board. This mismatch adds directly to the directivity, source match, and frequency response of the test system.

Even if the test system performance is better than the match being measured significant errors in the measurement may occur. For example, figure 1 (a) shows a test circuit consisting of a 50 ohm resistor in series with a 50 ohm line, measured with a system having an interface to the test circuit of 19 dB return loss. Ideally, the test circuit has 100 ohms input impedance (about 9.5 dB return loss), and a voltage loss of 0.5 (about -4 dB insertion loss). Figure 1 (b) shows the measurement of the system interface having 19 dB return loss at 3 GHz. Figure 1 (c) shows the return loss of the test circuit without the degradation of the test system interface

The combination measurement of gain and return loss are shown, with and without the error of the measurement probe in Figures 1 (c) and 1 (d). The gain is in error by about .2 dB (theoretical worst case is .3 dB), but the match is in error by about 3.7 dB (theoretical worst case is 3.8 dB). Clearly, measurements of return loss depend very heavily on the match of the measurement system.

REFERENCES

- [1] R. Groshong and S. Ruscak, "Undersampling Techniques Simplify Digital Radio", Electronic Design, May 23, 1991, Penton Publishing
- [2] R. Groshong and S. Ruscak, "Exploit Digital Advantages In An SSB Receiver", Electronic Design, June 13, 1991, Penton Publishing
- [3] "DSP Tutorial, Modulation, Fourier Series, and Sampling Theory", Spread Spectrum Scene, October 1992, El Granada, CA: RF/Spread Spectrum, (415)726-6849
- [4] R. Higgins, "Digital Signal Processing in VLSI", Analog Devices Technical Reference Books, Englewood Cliffs, NJ, Prentice Hall, 1990
- [5] R. Crochiere and L. Rabiner, "Multirate Digital Signal Processing", Englewood Cliffs, NJ: Prentice Hall, 1983
- [6] L. Couch II, "Digital and Analog Communication Systems", New York, NY: Macmillan, 1993
- [7] "The American Radio Relay League Handbook, 1993", Newington, CT: American Radio Relay League, 1992
- [8] Analog Devices, "ADSP-2100 Family Applications Handbook, Volume 4", Norwood, MA: Analog Devices, 1990
- [9] Analog Devices, "ADSP-2100 Family User's Manual", Englewood Cliffs, NJ: Prentice Hall, 1993

There are several factors which make RF PC Board contacts difficult. Most test equipment will be connected using coaxial cables, terminated in common connectors such as SMA, SMB, type N, or BNC. It is difficult to make a good, low impedance ground connection to the PC board. Also, it is difficult to maintain a constant impedance on the RF signal line with respect to ground. Adding solder-on connectors to PC boards is expensive, and does not solve the automated test problem. Additionally, most non-solder probing techniques suffer from errors introduced by probe placement uncertainties. Even a good probe, probing a well controlled line structure will make a poor measurement if it is not exactly placed.

A New Kind of Probe - The K-50:

A new probe developed for automated testing at Motorola is well suited for RF PC board testing, shown in figure 2. It consists of an SMA connector which maintains constant impedance until terminated in a spring-loaded contact assembly. The grounds for the probe are brought down from very near the center contact with two additional spring-loaded contacts. The crown of the contact is designed to provide a small air space, more nearly maintaining a constant 50 ohms impedance to a footprint on the PC board. It is clear that this probe solves several of the problems mentioned above.

The grounding scheme of this probe has been found to provide a low impedance and be resonance free up to 3 GHz. The spring probes ensure positive contact even if not perfectly aligned either vertically or laterally. The symmetric, transmission line nature of the probe tip design provides for constant impedance, with good match beyond 3 GHz. Finally the rugged design combined with removable spring contacts provides ease of maintenance and reliability necessary for high volume automated testing. This probe demonstrates the first non-solder RF connector compatible with automated board testing equipment.

Enhancing the Probe with Vector Network Analyzers:

The vector network analyzer (VNA) can be used to make many of the necessary measurements for testing RF PC boards. It is ideally suited for gain, power and match measurements, as well as power

gain compression, harmonic distortion, impedance vs. frequency and impedance vs. distance. A key to success when using VNAs is in properly correcting for errors due to mismatch in the instrument or connections to the circuit. The process of removing systematic errors is sometimes referred to as calibration, and involves the measurement of precisely known standards to determine these systematic errors.

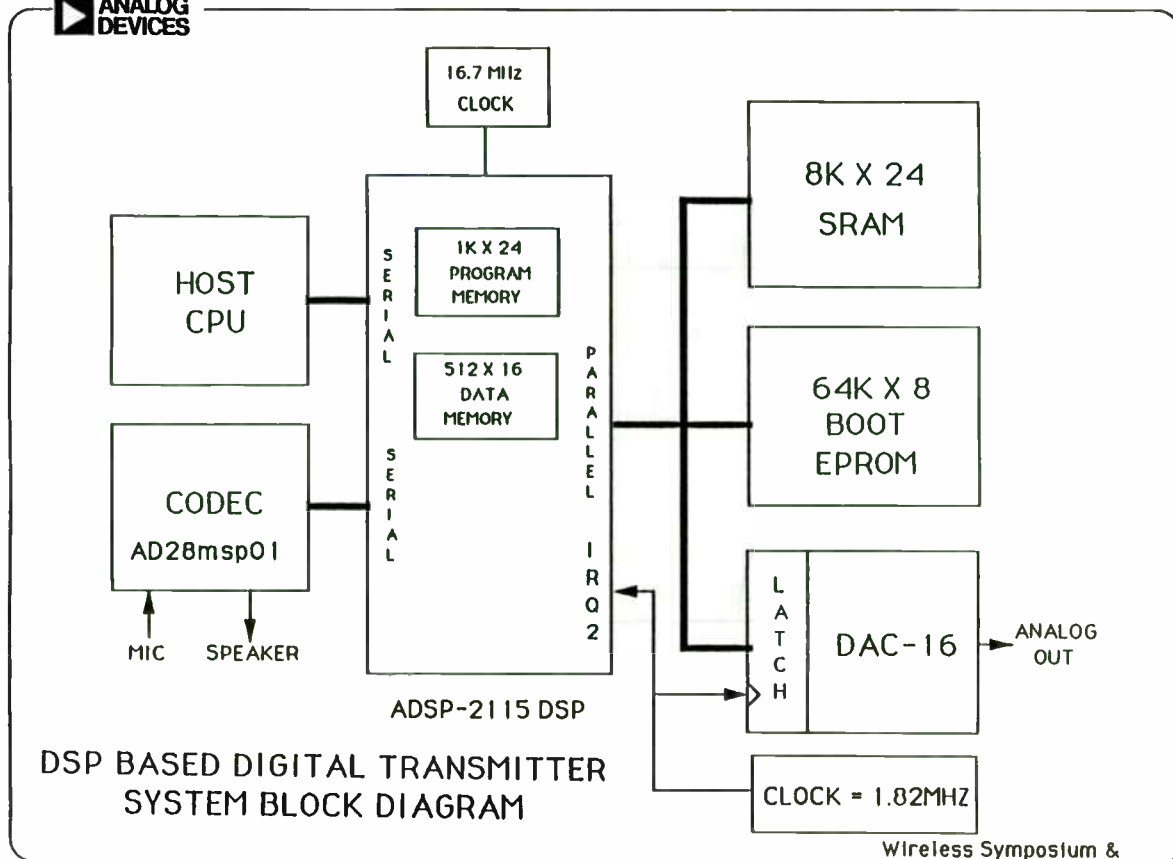
With normal calibration techniques, the errors must be stable, and cannot be corrected if they change from measurement to measurement. When using the probe, the connection repeatability error due to probe placement changes cannot be corrected in the normal fashion. However with a technique known as time domain gating, the effect of these non-repeatable errors can be removed from the measurement. This is especially useful in measurements of match or return loss where the PC board device has a match as good as or better than the uncorrected performance of the probe.

Probe Details:

The mechanical construction of the probe affords both good RF performance and rugged, reliable testing life. The key to this is combining the precision spring contacts used in high volume PC board testing with the good RF performance of the SMA connector.

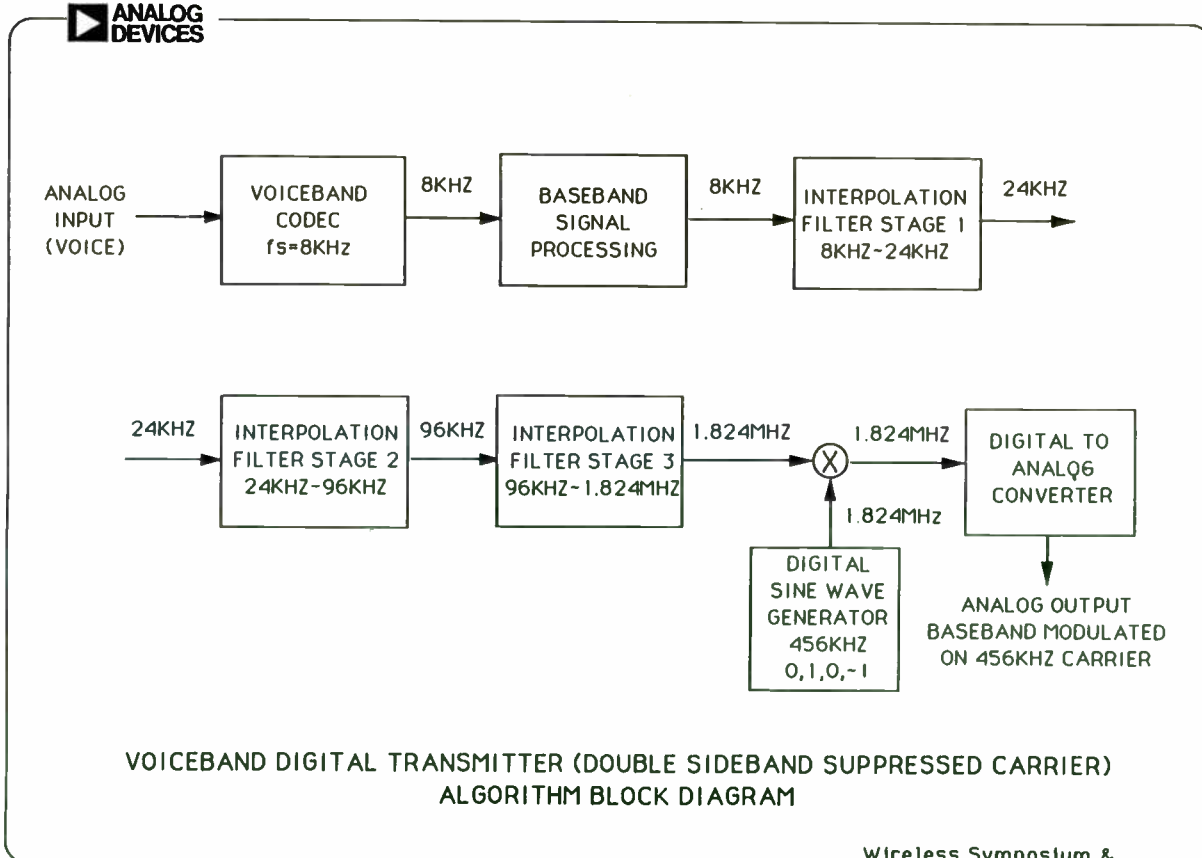
Figure 3 shows some of the mechanical details of the probe, including the replaceable spring loaded contacts.

The electrical performance of the probe can be described by its measurement of a low return loss load, Figure 4. This measurement was made by calibrating at the SMA connection, and measuring the probe and PC board load. When properly matched to a PC board trace, the probe can maintain a 26 dB return loss to 1 GHz, and a 20 dB return loss to 3 GHz. For calibration purposes, the probe has an open circuit capacitance of 0.4 pF, and a compressed short circuit length of about 6 mm. Here, compression means placing the probe on a piece of bare PC board material, and fully compressing the spring contacts. The short circuit length of the probe results in 36 picoseconds delay. Figure 4 (a) shows a Smith Chart, from which we can obtain the parasitic capacitance of the probe. Figure 4 (b)



Wireless Symposium & Exhibition January, 1993

FIGURE 1



Wireless Symposium & Exhibition January, 1993

FIGURE 2

shows the magnitude of the return loss in dB, with markers placed at 1 and 3 GHz.

To obtain best results with the probe, the PC trace must be properly configured to accept the probe. This should pose no problem in new designs, as the probe configuration is common to many devices now supplied to the RF market. The probe pad is shown in Figure 2; it is important that the PC trace "tail" is controlled, as it appears as an open circuit stub on the line.

Use with a VNA:

To use the probe with a VNA, it is first necessary to perform some type of error correction. For gain or power, it is only necessary to provide some source of RF at a known level to an SMA to PC board adapter. Placing the probe on the PC board, and performing a trace normalization (sometimes called a "thru cal") will correct for any gain slope or frequency response in the probe, connecting cables, or network analyzer. If the mismatch of the connecting cables and network analyzer is large, a small value attenuator can be added between the probe and the cables.

Error correction is much more important in measurements of return loss, input match, or impedance. The simplest form of correction is a standard open/short/load calibration in SMA (known as 3.5 mm for precision standard), adding the probe after calibration. Here, any mismatch in the probe interface is ignored. This will correct for any mismatch in the network analyzer and cabling to the probe. Since the probe has very good RF performance, this may be sufficient for many measurement needs.

In some cases, such as using the probe to characterize the impedance of PC board components, e.g. modeling active or passive components, a better calibration is needed to provide the correct phase reference. This can be obtained by starting with the normal calibration, then resetting the phase reference by shorting the probe, and adding electrical delay (also called electrical port extension) until a 180 degree phase trace is obtained.

Alternatively, a calibration "kit" can be made consisting of a PC board open (bare PC board), a PC board short, and a PC board load. Placing the probe on the three standards, as called for in the

calibration routine, will correct for systematic errors to the quality of the standards. In general, the quality of the load element determines the quality of the measurement.

Finally, it is possible to use two probes with some VNAs to perform a calibration called "Thru-Line-Reflect" or TRL. This calibration uses the impedance of the line as a reference standard, and is most often used in automated wafer probing. This calibration properly calibrates the measurement for transmission and reflection.

All of the previous error correction methods depend upon the systematic errors being repeatable, and the standards being exceptionally good. It may be difficult to obtain a very good load standard for use on a PC board, and the mismatch in the probe may mask the measurement using the port extension technique. Further, placement errors in the probe with respect to the line can cause non-repeatable errors. Fortunately, the VNA has a mode which can be used to reduce the effect of these errors, namely, time domain transforms and gating.

In a VNA, the time domain transform is used to create a display of reflections as a function of time (or distance) down a transmission line. This is accomplished by using the inverse Fourier transform. The display may be configured to show the impedance as a function of distance down the line. The time domain transform can show the reflection from the probe-to-line connection, reflections from mismatches on the PC board line, and the reflection from the termination of the line, such as some active device.

The gating function of the time domain transforms allows one to eliminate the response from the measured data. In effect, the time response data is changed to show no reflection outside the gated region. Setting the gates properly can give the result of eliminating the reflection due to the probe connection, leaving only reflections from mismatches on the PC board. In this way, even relatively large mismatches caused by mispositioning the probe can be removed from a measurement, to give a truer picture of the return loss, match, or impedance of a device on a PC board. The capabilities and applications of time domain transforms are discussed more fully in the next section.

Double Sideband Suppressed Carrier

FIGURE 3a



Amplitude Modulated

FIGURE 3b

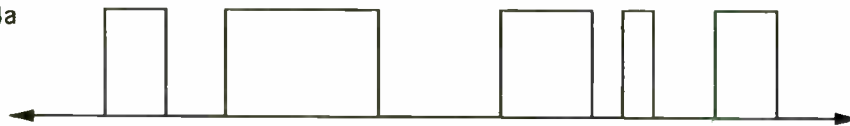


MODULATION TECHNIQUES

Wireless Symposium & Exhibition January, 1993

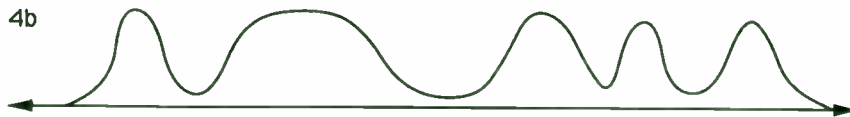
Telemetry Signal Without Pulse Shaping Filter

FIGURE 4a



Telemetry Signal With Pulse Shaping Filter

FIGURE 4b



PULSE SHAPE FILTERING BINARY SIGNALS

Wireless Symposium & Exhibition January, 1993

Time Domain Transforms:

The time domain transform is most useful used in the same manner as a traditional analog time domain reflectometer (TDR) and will be referred interchangeably with TDR in the remainder of this discussion. The TDR transform must be performed as a step response in the low pass mode to correspond directly to the analog TDR. In this mode, information about the phase of the reflections is retained, and the response shown is reflection coefficient vs. time (or distance). The distance down the line relates to the time by the propagation constant of the transmission line. The impedance of the line corresponds with the reflection coefficient; for a 50 ohm reference impedance, each percent reflection represents about 1 ohm change from 50 ohms. The exact equation is $Z=Z_0*((p+1)/(p-1))$, a 0.05 reflection corresponds to 55.26 ohms, -0.1 corresponds to 40.81 ohms.

The TDR is very useful for identifying the impedance of sections of line, or for identifying the causes of mismatch in transmission line systems consisting of various types of lines and connectors. Without going in depth into the transform, the limitations of range (or length) and resolution depend upon the lowest frequency and the bandwidth used in the frequency response measurement. The low pass mode requires that the frequencies used be harmonically related (i.e., evenly spaced), the minimum frequency is then set by the maximum frequency and the number of points chosen ($F_{min}=F_{max}/(points-1)$). The VNA will automatically adjust both the start and stop frequency to fulfill the last equation with the constraint of 1 Hz resolution on the start and stop frequency.

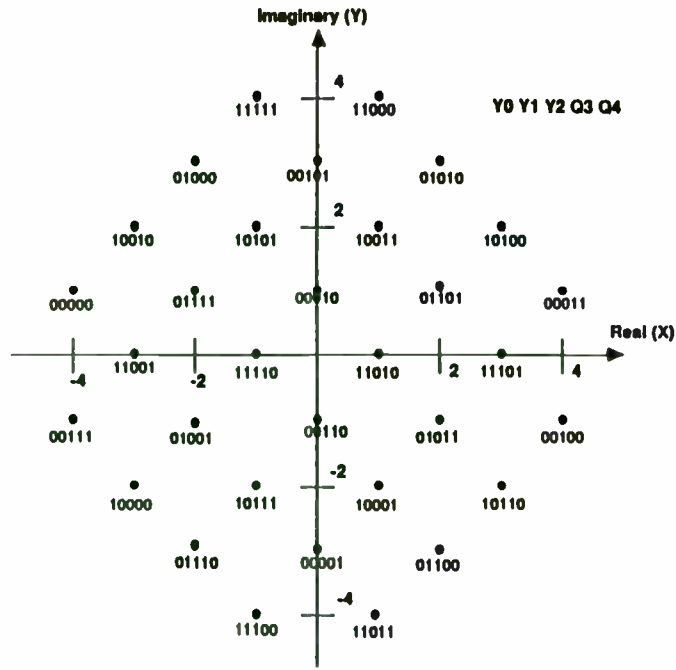
The TDR capability is ideally suited to make the RF probe most useful in investigating RF PC boards. Often, the impedance of lines on PC boards cannot be easily calculated, due to uncertainty in the board material or thickness, PC trace width changes with etching, and surrounding elements of the PC board and package. In these cases, the TDR is the easiest method for determining the characteristics of the PC board transmission line structures. The RF probe allows easy probing of various portions of a PC board. A limitation of the TDR is that it cannot resolve parallel transmission paths, so that the probe cannot be placed in the middle of a line, but must be

placed at the end of a PC trace. Even so, the probe is useful in testing in the middle of circuits if some element, such as a coupling capacitor, can be removed to eliminate a second transmission path.

Figure 5 demonstrates the usefulness of the TDR by measuring the response of the RF probe when measuring a load on a 50 ohm line. This measurement was made on a 20 GHz network analyzer; the high bandwidth allows finer resolution in the time domain. The markers are placed at significant physical attributes: Marker 1 is set at the SMA connection of the probe. Marker 2 is set at the beginning of the spring contact exiting the probe. The flat trace between these two markers indicates a well matched line through the probe. Marker 3 is set at the peak of the TDR trace. This represents the impedance of the short length coplanar structure defined by the tip of the probe. The impedance of this section is about 57 ohms. Marker 4 represents the contact to the PC board and marker 5 shows the excess capacitance of the contact pad. In the next section, techniques are described which can remove these discontinuities of the probe from the return loss measurements being made down the line.

The TDR transform's usefulness is not limited to displaying impedance vs. distance, but can be used to enhance the frequency response measurements such as impedance or input match. As indicated earlier, a function known as gating may be used to remove known, unwanted reflections leaving only the unknown reflections from the test device. The gating may be applied with the analyzer in frequency response mode, as well as TDR mode. This gives the effect of an inverse transform on the gated TDR response to display the frequency response of the remaining reflections in the TDR trace. This is a very powerful tool for investigating PC board circuits even if it is difficult to make repeatable connections to the PC board.

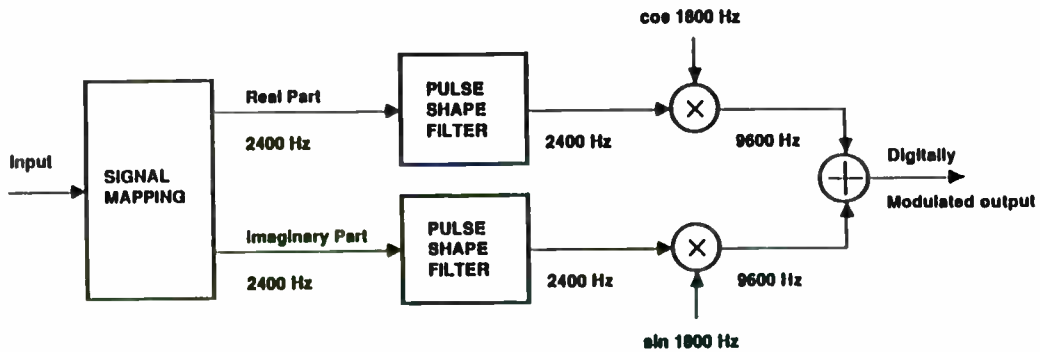
However, as with all powerful tools, the quality of the results depends greatly on the setup and implementation of the TDR and gating functions. The TDR response and the gating effects are limited by the effective rise time of the system. This is set by the maximum frequency used in the VNA, and by another term known as the windowing factor. In short, the windowing factor determines the smoothness with which the endpoints of the frequency re-



V.32 MODEM SIGNAL CONSTELLATION

FIGURE 5

Wireless Symposium & Exhibition January, 1993



MODEM SIGNAL MAPPING AND QUADRATURE AMPLITUDE MODULATION

FIGURE 6

Wireless Symposium & Exhibition January, 1993

sponse data are set to zero. Clearly, outside the frequency range of the VNA, the data is exactly zero. If the data in the transform is truncated, there will be "sidelobes" which appear as severe ringing on the TDR trace. Windowing has an effect of smoothly low pass filtering the data, which removes much of the ringing. Unfortunately, this has an effect similar to reducing the bandwidth, so the resolution will suffer. In viewing TDR responses, lowering the windowing rise time can aid in identifying and locating transitions in impedance, while increasing the windowing time can aid in smoothing the data to see the impedance value of different segments of the transmission line.

With gating, one must be aware that "looking through" a transition by gating it out results in a gated frequency response that is different from the true response, and generally has a lower reflection value (higher return loss) than actual. This change can be explained by understanding that each transition reflects some energy, so that farther reflections have less than 100 percent of the forward power available. When a large transition is gated out, the remaining reflections are not changed, thus some of the forward energy is effectively removed. For example, if a transition with a 0.1 reflection (10%, or 20 dB return loss, or SWR=1.21) is gated out, the remaining reflections are relative to .9, or will be 10% low. This would result in the return loss being about 0.92 dB low. Thus, it is very important that the RF probe used in conjunction with PC board testing have good performance to ensure accurate results after applying TDR gating enhancements.

Measurement Examples:

Figure 6 demonstrates the affect of gating on improving a measurement made with the probe. Figure 6A shows two measurements made with slightly different probe placements (approximately 1 mm). One measurement was made placing the probe to get the least ripple, the second was made by offsetting the probe slightly. The calibration for this measurement used an open/short/load cal with the cal kit modified to reflect the probe's parasitics as described earlier. The device under test (DUT) is a 25 ohm resistor at the end of a 43 mm long 50 ohm impedance line. The theoretical return loss should be about 9.5 dB plus about .3 dB/GHz due to line loss. The measurements differ by 2 dB up to 2

GHz, and by 3 dB to 3 GHz. The ripples become very large above 3 GHz, the error at 4.8 GHz is about 10 dB. Figure 6B shows the response when the portion of the TDR trace representing the probe tip is "gated out." The differences in the responses are less than 0.5 dB to 2 GHz, and less than .8 dB to 3 GHz. This represents a four times improvement in the repeatability of the measurement, with respect to probe placement, provided by the gating function. The response is much improved about 3 GHz as well.

Of course, it is most important that the measurement be correct, not just repeatable between probe placements. To attempt to provide some comparison, an identical DUT was constructed, but with a soldered-on planar SMA connector used as a launch. A TDR response of the launch enabled it to be tweaked to better than 40 dB to 3 GHz. A measurement of the DUT shows it to closely follow the ideal of about 10 dB return loss. Figure 7 shows a comparison of measurements of the 25 ohm resistor made with the soldered-on on connector and a similar DUT measured with the 3 GHz probe, with gating used to remove the probe transition. The results are remarkable in that the response is nearly identical up to 1 GHz. The results diverge by less than 0.7 dB up to 3 GHz. The fact that the gated response is somewhat lower in return loss is expected, and the 0.7 drop at 3 GHz represents 8% reduction in return loss. This is consistent with a 8% reflection for the probe transition or 22 dB return loss for that transition, which is what was measured for the probe back in Figure 4.

Finally, a calibration for a two port measurement using the TRL technique was performed on an HP 8720 Vector Network Analyzer. The calibration standards used were mating two probes directly for a "thru," using a short for the "reflect," and using line approximately 15 mm long for the "line." In this calibration technique, the exact length of line is not important. The impedance of the line sets the reference for reflection measurements. Figure 8 shows measurements of the 25 ohm DUT from figure 7, and a load at the end of a line. Here, gating was applied to remove the probe placement discontinuity. The results demonstrates very good measurements past 3 GHz. The line length chosen for the cal provides a calibration range of about 500 MHz to

Lumped and Distributed Circuits for Wireless Communications

Session Chairperson: Mark McDonald, *Wireless Communications, National Semiconductor (Santa Clara, CA)*

Key Topics In Radio System Design, John G. Freed, Teletec Corp. (Raleigh, NC).....49

A 2-GHz BiCMOS Low-Noise Amplifier and Mixer, Dave Bien, National Semiconductor, Wireless Communications Group (Santa Clara, CA)56

High-Efficiency Crystal Oscillator at High Frequencies, Sheng H. Lee and Alvin K. Wong, Philips Semiconductors (Sunnyvale, CA).....62

A 2.2-GHz, PLL Frequency Synthesizer, Thom Luich, Thai Nguyen, Craig Davis, David Byrd, Eric Lindgren, Rob Rodriguez, Maggie Speers, and Eli Miller, National Semiconductor (Santa Clara, CA).....68

A 3-V Analog Audio-Processing Chipset for Battery-Operated Systems, Omar Saleh and Saeed Navid, Philips Semiconductors (Sunnyvale, CA).....72

4 GHz. The measurement of the 25 ohm DUT agrees remarkably well with the the earlier measurements in figure 7, especially considering two entirely different calibration techniques were used. A 10 dB return loss DUT makes a good test case as both return loss and source match affect the measurement.

Real World Applications for the K-50 probe.

Measurement is the basis of evaluation. In the realm of modern high frequency design, characterization measurements enable the reduction of theory to practice and the verification of theory from practice. In manufacturing, measurement enables ongoing control and optimization of product and process. Historically, the greatest obstacle to performing useful high frequency measurements has been accomplishing the needed connection between the measuring instrumentation and the device to be measured. The K-50 was developed to provide a universal means by which precision high frequency connections can be accomplished. The following actual situations exemplify the utility and capability of the K-50 in addressing the historical obstacles to accomplishing SIX SIGMA capable designs and manufacturability.

Using The K-50 To Perform Impedance Profile Measurements.

The essential reference circuit for a transistor is the supplier's line-fixture (production line test fixture). Transistor performance is specified in this circuit environment and compliance to specification can only be assured when the transistor is operated in an equivalent circuit environment. Prior to the development of the network analyzer and the K-50, circuit equivalency determinations were performed utilizing blind cut and try correlation methods, often with disastrous results. Figure 9 shows the actual Smith Chart Signature of a test circuit with an input matching network that is inversely correlated with respect to its line-fixture. That is, the measurement of transistor performance in an amplifier module test circuit does not correlate with the same measurement of the transistor in a line-fixture at the transistor manufacturing site.

A Smith Chart Signature is the visualizable function that is created when impedance profile information is plotted as a locus of points on a Smith Chart. The

H.P. 8753 Network Analyzer measurement speed and Smith Chart display capability in conjunction with the universal connectivity of the K-50 Probe can be used to advantage by supporting the creation of equivalent circuits through real time tuning. In addition, the needed high frequency connections were typically soldered onto the linefixture commonly resulting in permanent performance degradation.

With the advent of the network analyzer having the ability to measure and display amplitude and phase data taken at numerous frequencies, and with the K-50's ability to provide nondestructive precision temporary high frequency circuit connections, the first absolute circuit equivalency determinations were successfully conducted. The equivalency referred to herein, means that the transistor views the application circuit and line-fixture circuit as having the same input and output matching network impedance profiles (the small signal impedance profile measurement methodology is depicted in Figure 10). An Impedance Profile is the tabular listing of measured impedance versus frequency values representing the transistor's view (measured with the transistor removed from the circuit) of its input and output matching networks taken with the normal circuit input and output ports terminated in 50 Ohms.

This measurement methodology was subsequently evolved into an R.F. design methodology and was first applied to problem solve an R.F. power amplifier circuit that was exhibiting substantial batch performance variation. Whereas all previous attempts to understand and resolve this amplifier performance problem had met with failure, the new design methodology readily revealed the problem. The amplifier had a rotated input matching network impedance profile relative to that of the transistor line-fixture (shown in Figure 11). Even laser tuning could not accommodate transistors that required an input matching network impedance profile that deviated from the intersection of the profiles shown in Figure 11 to any significant extent. For proper performance, the test fixture and the amplifier module should provide the same impedance profile, then the transistor manufacturer's testing will ensure all amplifier modules will meet specifications.

Key Topics in Radio System Design

John G. Freed
Teletec Corporation

I. INTRODUCTION

A radio system designer faces many challenges in the design of an RF communications system. Two of the key issues affecting the quality, and ultimately the financial success of a wireless system, are reliable coverage and freedom from interference. The subscriber is the first to notice substandard performance in these areas. Proper planning from the beginning can avoid a disaster.

II. PLANNING THE COVERAGE AREA

In the design of the system, the engineer must balance the subscriber unit to base site and base site to subscriber unit ranges. When planning the system, the engineer must consider the propagation unique to the frequency and terrain, the transmitter power output, receiver sensitivity, and antenna gain. Much study of propagation has been done [1] and will not be treated in any depth here since the designer has little control over it.

The system engineer has control over base station and subscriber unit transmitter power, receiver sensitivity, and antenna gain. In planning the system coverage, the designer needs to consider the desired communication range and then refer to one of the various references on propagation to determine the amount of attenuation that must be overcome to provide the grade of service necessary for the system. Roughly speaking, the number obtained covers the free space path loss, fading, shadowing caused by buildings and trees, and an additional factor for grade of service. Once the link loss is known the system engineer can specify the power output, receiver sensitivity, and antenna gain required to make up this loss.

The base station is generally not a problem because it is powered from the commercial power mains and situated where a gain antenna can be used. This is contrasted to the subscriber unit which must be battery operated and physically small which puts severe restrictions on transmitter power and antenna gain. With these limitations in mind, the system design can proceed. The system gain available to cover the link loss is found by comparing the EIRP, or effective isotropic radiated power available from the transmitting end of the link to the effective receiver sensitivity at the receiving end of the link. The EIRP is found by multiplying the transmitter power output in watts by the

Next the fledgling R.F. design methodology was applied to the development of a new R.F. power amplifier circuit. The amplifier input matching network design was determined based on the measured impedance profile of the corresponding transistor line-fixture (refer to Figure 12 for the input matching network impedance profiles, the output matching network impedance profile was known from previous design work and is not shown in this example). As a test of the design methodology, 50 transistors were selected for optimum performance in the supplier's line-fixture and sent to the customer. At the customer site a test fixture was made by tuning the impedance profiles of the input and output matching networks to be the same as those of the line-fixture (this tuning was performed in real time using the H.P. 8753 Network Analyzer in the Smith Chart display mode of operation). When the 50 transistors were measured in the customer's real time correlated test fixture, all 50 yielded identical measured performance. When 100 of the new amplifier circuits were fabricated in the customer's factory, all 100 passed their test specifications with substantial margin. Supported by this design methodology, the design task was completed in six weeks as opposed to prior efforts that required six months and did not accomplish defect free manufacturability. With the need to substantially reduce design cycle time in order to remain competitive, this design methodology establishes an essential capability.

Whereas R.F. designers once attempted to produce the needed circuit equivalency by making line-fixtures and application circuits physically similar, practical network analyzer real time impedance profile measurement capability has allowed physically dissimilar circuits to become explicit equivalents of each other through tuning (a transistor line-fixture is shown in Figure 13 and its equivalent application circuit is shown in Figure 14). This is the basis of SIX SIGMA R.F. performance compliance by design.

The K-50 In Support Of WORLD CLASS Manufacturing Capability.

The K-50 is especially well suited to manufacturing applications where its precision, consistency, reliability and ability to effect a highly repeatable universal high frequency connection are considered valuable attributes. The K-50 is totally automatable

and is highly utilized in the manufacture of connectorless, high circuit density, high frequency products that employ surface mount component technology. Its universal open tip architecture does not require a special contact target thus promoting usage as a common connection device across product lines throughout a factory. For example, Motorola utilizes the K-50 to manufacture:

- > Portable Cellular Telephones (refer to Figures 15 through 17),

- > Mobile Cellular Telephones,

- > Cordless Telephones,

In these applications the K-50 has enabled:

- > total manufacturing automation,

- > the establishment of common fixtures for multiple products,

- > the building of multiple products on the same production line,

- > the elimination of fixture change-over down time,

- > the elimination of ongoing fixture correlation as required by tuned R.F. connection schemes,

- > production personnel to maintain their fixtures by performing pin changing,

- > and award winning measurement consistency.

A typical automated test application of the K-50 involves operating it at 90% of full mechanical compression and terminating its SMA connector in a 6 dB coaxial attenuator. By way of example, when operated in this manner 900 MHz. 12 dB SINAD measured at a -115 dBm signal level will typically exhibit only 0.2 dB variation.

The K-50 As A Design And Manufacturing Tool.

Perhaps the most important aspect of the K-50 is its applicability as a common measurement tool in support of Design For Manufacturability. When employed as a common measurement tool, Research, Development, Factory, and Field Service personnel can all perform and exchange measurement data in a directly comparable format. With Hewlett-Packard supporting error corrected measurement, design calculations can be directly related to measured values performed by any of the technical functions

transmitting antenna gain expressed as an algebraic ratio with an isotropic antenna assumed to have a gain of one. Usually it is easier to express the transmitter power in dBm, decibels above one milliwatt, and add the antenna gain in dBi, or decibels above an isotropic antenna. As an example, suppose a transmitter has an output of 1 watt (+30 dBm) and is connected to an antenna with a gain of 2 (+3 dBi). The EIRP is then given by

$$\text{EIRP} = 1 \text{ watt} \times 2 = 2 \text{ watts}$$

or in the more commonly used logarithmic terms,

$$\text{EIRP} = +30 \text{ dBm} + 3 \text{ dB} = +33 \text{ dBm}$$

Sensitivity of a receiver is the amount of input signal that must be applied to the receiver input to produce a specified signal-to-noise ratio (or bit-error-rate) at the output. The effective sensitivity at the receiving end of the link is found by dividing the receiver sensitivity in microvolts by the receiving antenna gain expressed as an algebraic ratio. Once again, it is usually easier to perform this calculation with numbers expressed as decibels. In this case, the effective receiver sensitivity is the receiver sensitivity in dBm minus the antenna gain in dBi. For example, suppose a receiver has a sensitivity of -116 dBm and is connected directly (no transmission line loss) to an antenna with a gain of 2 dBi. The effective receiver sensitivity is

$$\text{Sens}_{\text{eff}} = -116 \text{ dBm} - 2 \text{ dB} = -118 \text{ dBm}$$

Once the EIRP and effective receiver sensitivity are known, the system gain is found as the difference between the EIRP and the effective receiver sensitivity. With the values from above, the system gain is found as

$$\text{System Gain} = +33 \text{ dBm} - (-118 \text{ dBm}) = 151 \text{ dB}$$

Next the calculation is repeated in the opposite direction. The receiving end of the link is now the transmitting end and vice versa. The goal of the system planner is to have these two numbers for system gain as close to equal as possible. Suppose that the base station to subscriber unit system gain is 170 dB and the subscriber unit to base station system gain is 160 dB. Under these conditions the subscriber unit can hear the base station at a greater distance than the base station can hear the subscriber unit. To the customer this problem would be apparent as areas where the subscriber unit could hear the base station but be unable to initiate calls.

Shown in Fig. 1 is a good example of system gain planning. An example of bad planning is shown in Fig. 2. To correct the situation in Fig. 2, the system designer might want to reduce the base station power, reduce the base station antenna gain, increase the subscriber unit receiver sensitivity, increase the

or groups within a corporation. The application possibilities and potential benefits are virtually limitless.

Motorola has elected to contribute the K-50 technology for the common benefit of the electronics industry (digital technology included). The K-50 could have accomplished only a limited usefulness if held back proprietarily, but if openly shared to provide the industry with a common basis for performing high frequency measurements has the potential to be profoundly beneficial. Unique to this type of invention, it is not possible for one party to derive a substantial benefit to the exclusion of others. For the SIX SIGMA capable design methodology to succeed, an industry majority must accept and use the K-50 tool. Your participation and contributions are, therefore, needed for the common good of our industry. With your support we can all be on the road to SIX SIGMA capable high frequency designs.

Conclusions:

In this paper we have presented a new concept for probing RF circuits without the use of solder on connectors. The K-50 probe has demonstrated usefulness in both the development and manufacturing arenas. It provides a high performance contact to RF circuits, and enables careful characterization of PC Board components in a simple and economical manner. Additionally, the probe is ideally suited for automated board test applications where reliable RF measurements are needed. The calibration and time domain capabilities of Vector Network Analyzers enable very accurate measurements to be obtained even considering difficulties such as probe placement and contact repeatability.

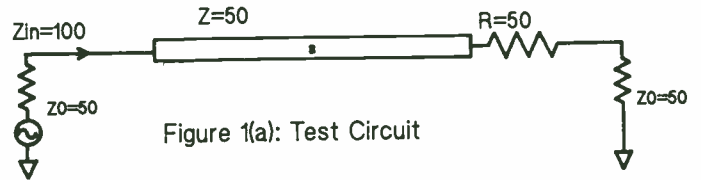


Figure 1(a): Test Circuit

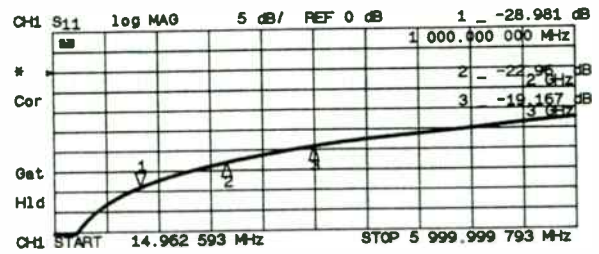


Figure 1(b): Return Loss of Test System Interface

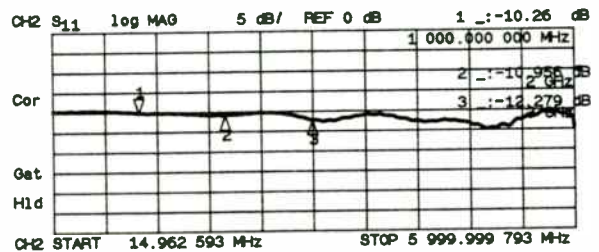


Figure 1(c): Return Loss of Test Circuit by Itself

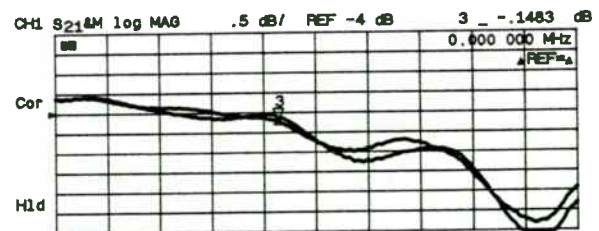


Figure 1(d): Gain Variation Due to Interface

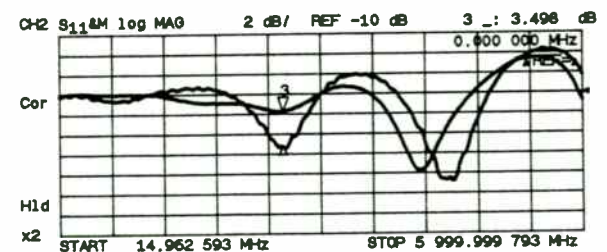
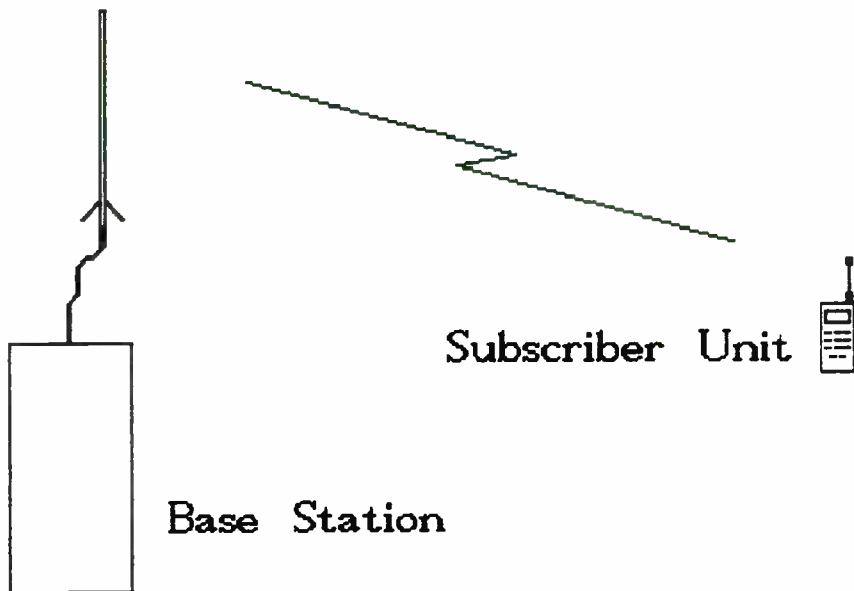


Figure 1(e): Variation in Match Measurement Due to Interface

subscriber unit antenna gain, or probably some combination of these.



Antenna Gain	+6 dBi
TX Power	+30 dBm
RX Sensitivity	-119 dBm

Antenna Gain	+6 dBi
TX Power	+27 dBm
RX Sensitivity	-116 dBm

Base to Subscriber Unit

TX Power	+30 dBm
TX Antenna Gain	+6 dBi
TX EIRP	+36 dBm

RX Antenna Gain	0 dBi
RX Sensitivity	-116 dBm
RX Sens	-116 dBm

eff	
System Gain	152 dB

Subscriber Unit to Base

TX Power	+27 dBm
TX Antenna Gain	0 dBi
TX EIRP	+27 dBm

RX Antenna Gain	+6 dBi
RX Sensitivity	-119 dBm
RX Sens	-125 dBm

eff	
System Gain	152 dB

Fig. 1

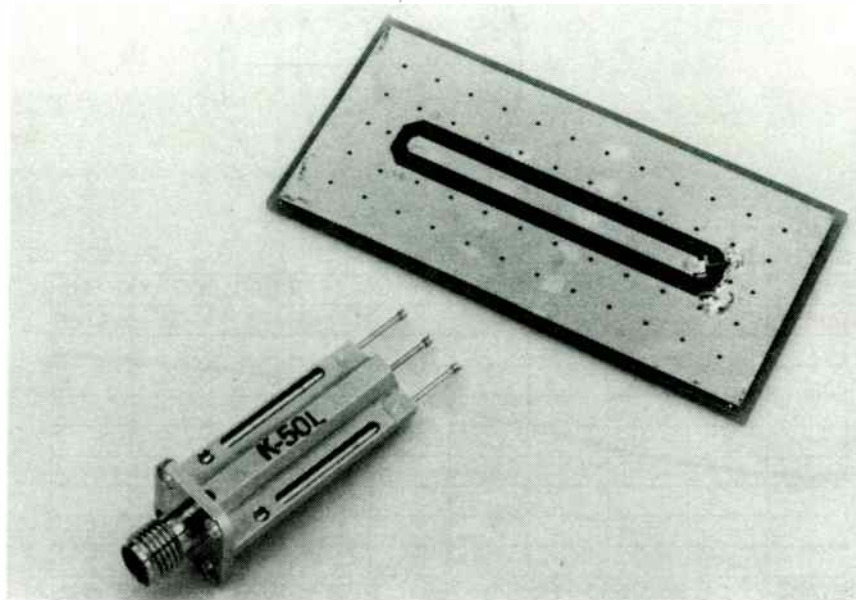


Figure 2: The K-50 Probe and Test PC Board



Broadband 50 Ohm Coaxial Test and Measurement Probe

Model Number: K-50L

Dimensions in inches (millimeters)

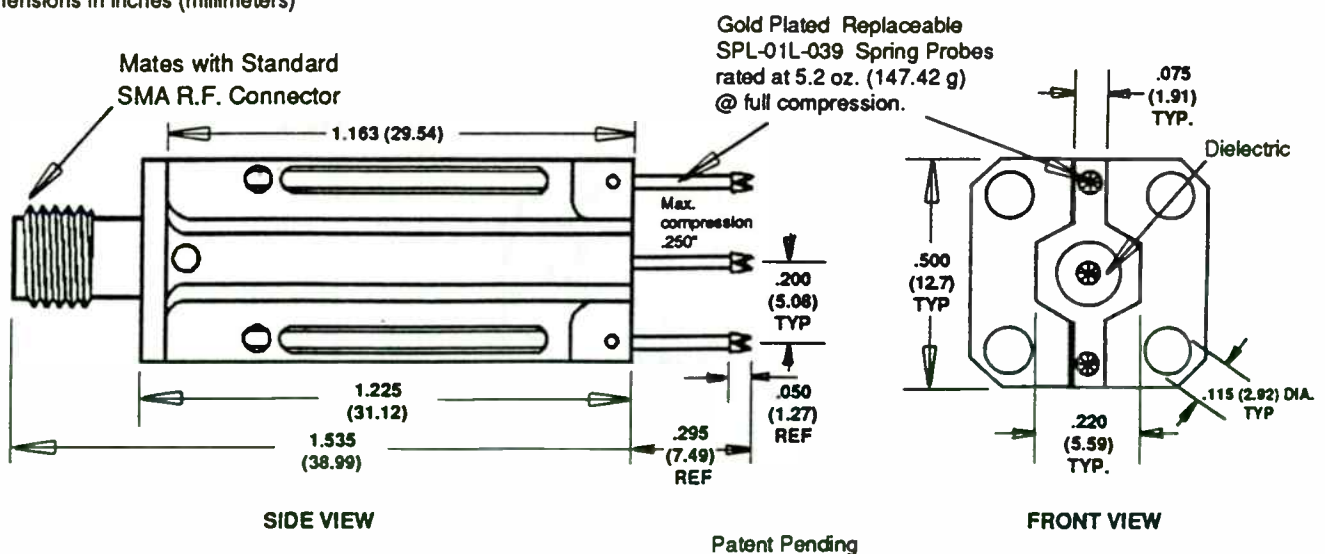
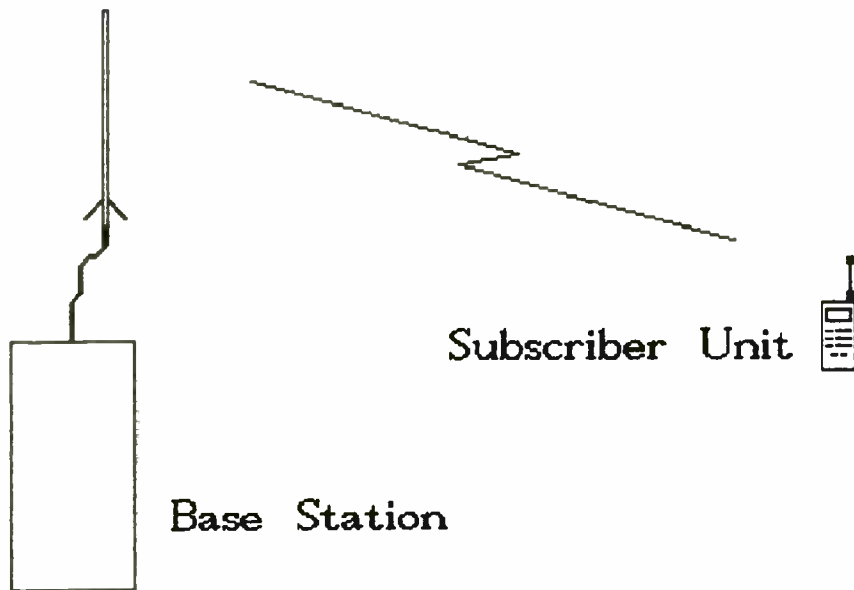


Figure 3: Mechanical Details of the K-50 Probe



Antenna Gain +10 dBi
 TX Power +37 dBm
 RX Sensitivity -120 dBm

Antenna Gain 0 dBi
 TX Power +27 dBm
 RX Sensitivity -116 dBm

Base to Subscriber Unit

TX Power +37 dBm
 TX Antenna Gain +10 dBi
 TX EIRP +47 dBm

RX Antenna Gain 0 dBi
 RX Sensitivity -116 dBm
 RX Sens -116 dBm

eff
 System Gain 163 dB

Subscriber Unit to Base

TX Power +27 dBm
 TX Antenna Gain 0 dBi
 TX EIRP +27 dBm

Rx Antenna Gain +10 dBi
 RX Sensitivity -119 dBm
 RX Sens -129 dBm

eff
 System Gain 156 dB

Fig. 2

III. REDUCING THE EFFECTS OF INTERFERENCE

Interference rejection is required to protect users of a channel from undesired signals that appear on channel, i.e., other users, interference sources appearing on adjacent channels, and interference such as intermodulation and spurious responses that arise from nonlinearities internal to the equipment.

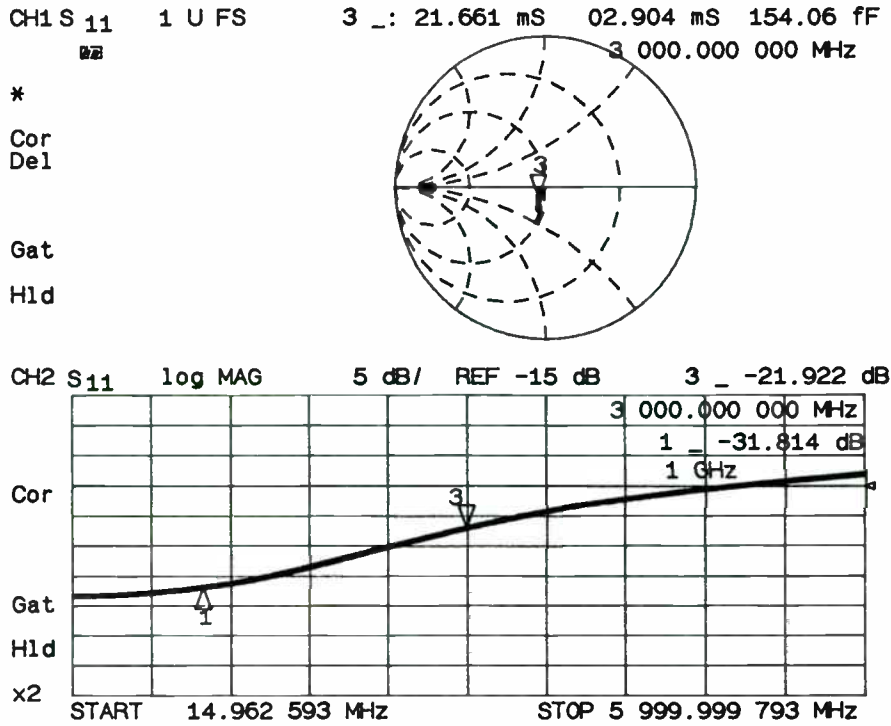


FIGURE 4: The Smith Chart shows the probe impedance, with 0.15 pF cap.
 The rectangular plot is the return loss of the probe in dB.

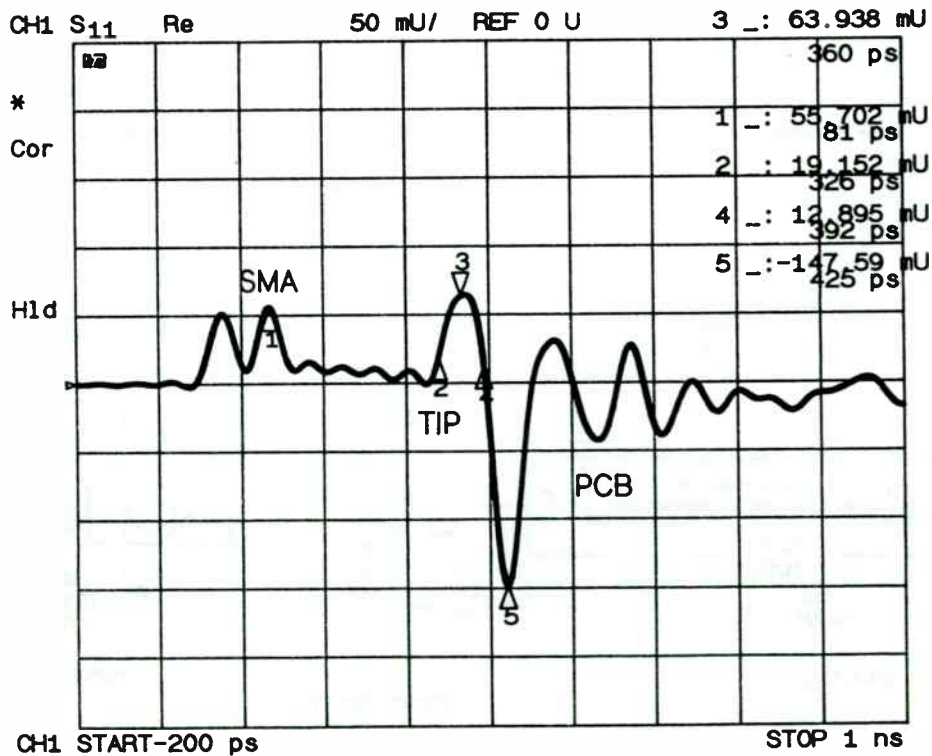


Figure 5: TDR response of the K-50 Probe

A. CO-CHANNEL INTERFERENCE

The problem of interference from other users on the same frequency can be reduced by allowing sufficient distance between areas where frequencies are reused. The coverage area of each base station should be studied thoroughly and enough separation margin should be designed in to allow for interference-free reuse of the channels. Another factor to consider is the co-channel rejection of the receiver. The co-channel rejection capability of a receiver is a measure of the receiver's ability to receive a desired on-channel signal at a certain level with a minimal specified degradation in output signal-to-noise ratio (or bit-error-rate) in the presence of an undesired signal on the same channel [2]. Co-channel rejection is usually specified as the difference in decibels between the two signals with a low number being desirable. Unfortunately, the system designer is not entirely free to specify this. It is largely a function of the type of detector used to demodulate the received signal. However, it is important to keep the concept in mind and if the choice is possible, specify units with low co-channel specification.

B. ADJACENT CHANNEL INTERFERENCE

Interference sources that appear on adjacent channels can manifest themselves in one of two ways. If a receiver is receiving a signal on one frequency and a signal appears on another frequency the selectivity of the receiver rejects the undesired signal. A typical subscriber unit might have selectivity of 70 dB. As long as any off-frequency signal is less than 70 dB above the sensitivity point of the receiver there is no problem. The receiver can not reject unwanted signals more than 70 dB above sensitivity and these signals appear at the detector along with the desired signal and create interference. To counter this, the system engineer might want to specify a high selectivity specification for the unit. Unfortunately it may not be feasible from a cost standpoint to specify selectivity any higher than absolutely necessary.

C. SPURIOUS AND INTERMODULATION INTERFERENCE

The second way that off-channel signals can create interference is by mixing in the nonlinear stages of the unit. Any nonlinear component can be represented by an infinite power series relating the output to the input [3]. For simplicity, if two undesired signals are applied to a nonlinear circuit, the output will be of the form

$$f_{\text{spurious}} = Mf_1 \pm Nf_2$$

where M and N are integers. Any response created in this manner is a spurious response. The most severe product is the third

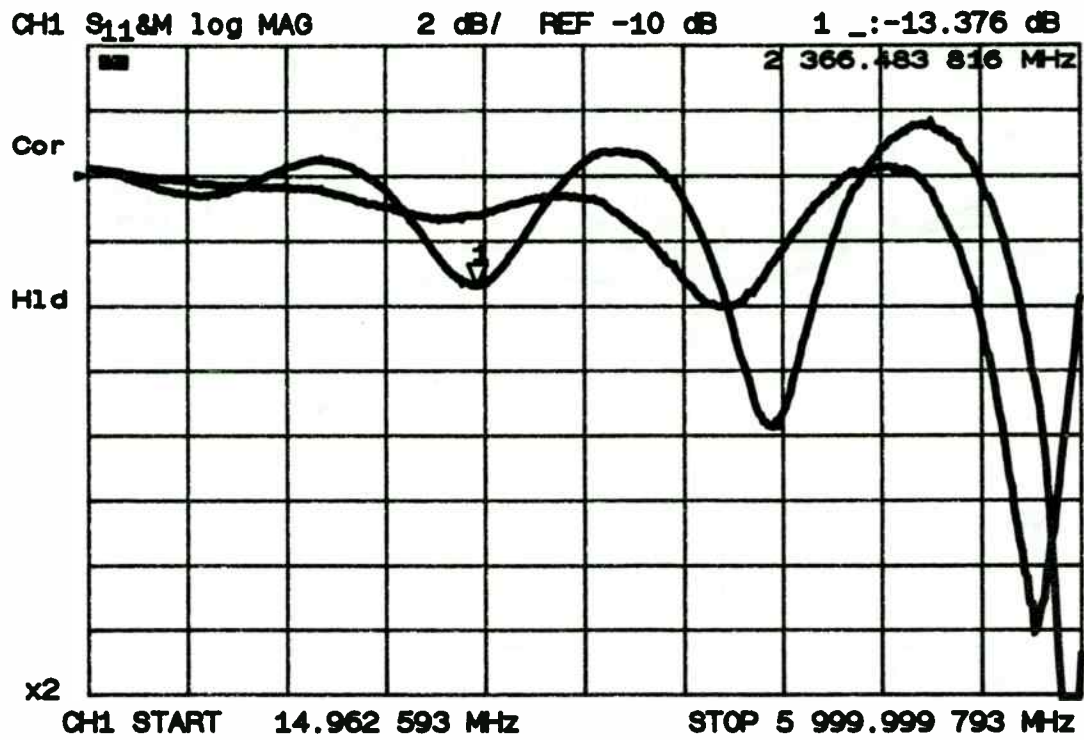


Figure 6A: Return Loss with two different probe positions.

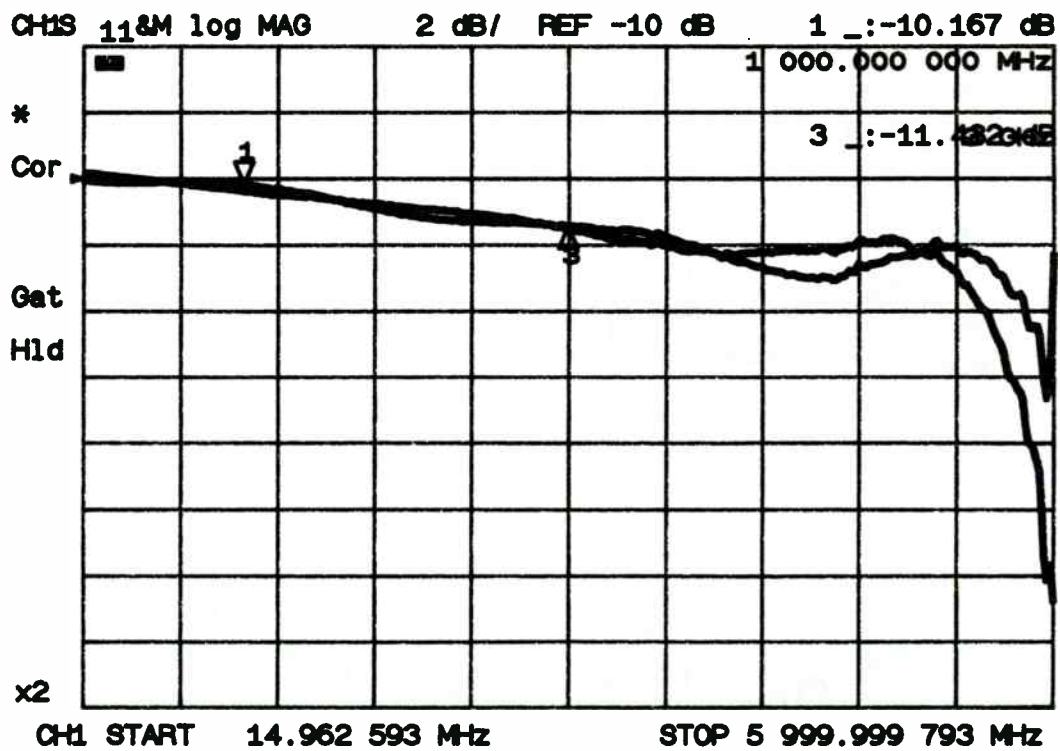


Figure 6B: Same measurement with TDR gating applied to the frequency response

order intermodulation product which occurs when $M = 2$ and $N = 1$ or when $M = 1$ and $N = 2$. In a channelized system third order intermodulation causes undesired signals at one and two channel spacings away from the desired signal to mix and produce an interfering output on the desired frequency. In fact, the undesired signals can lie at any integral multiple of one and two channel spacings from the desired signal. Fig. 3 shows two signals being applied to a nonlinear circuit and the output containing the two signals and the undesired third order products. When one of the undesired products falls on the operating channel of the radio, it interferes with the desired communication and the radio is said to suffer from IM distortion.

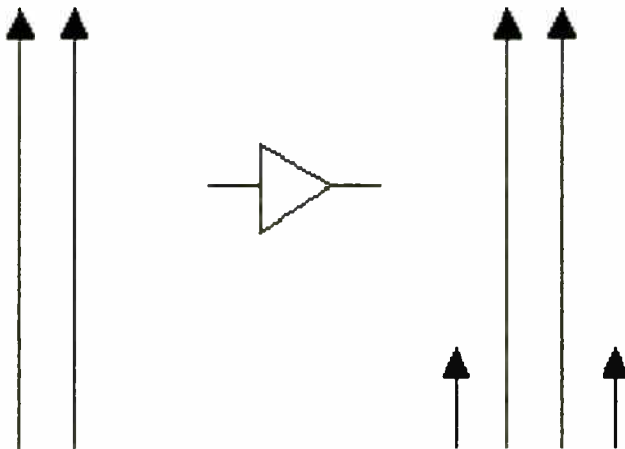


Fig. 3

This is another area where the obvious solution to specify better performance is not as simple as it seems. The system engineer needs to keep in mind the tradeoffs that occur when trying to make the system less susceptible to third order intermodulation distortion. Providing a higher level of rejection to this interference almost always requires that the active circuits in the equipment be capable of handling larger signals. This means higher operating voltage and current. While this isn't too severe a problem in a base station, it is a serious problem in a lightweight battery powered subscriber unit. Where does the designer make the tradeoff between interference rejection and

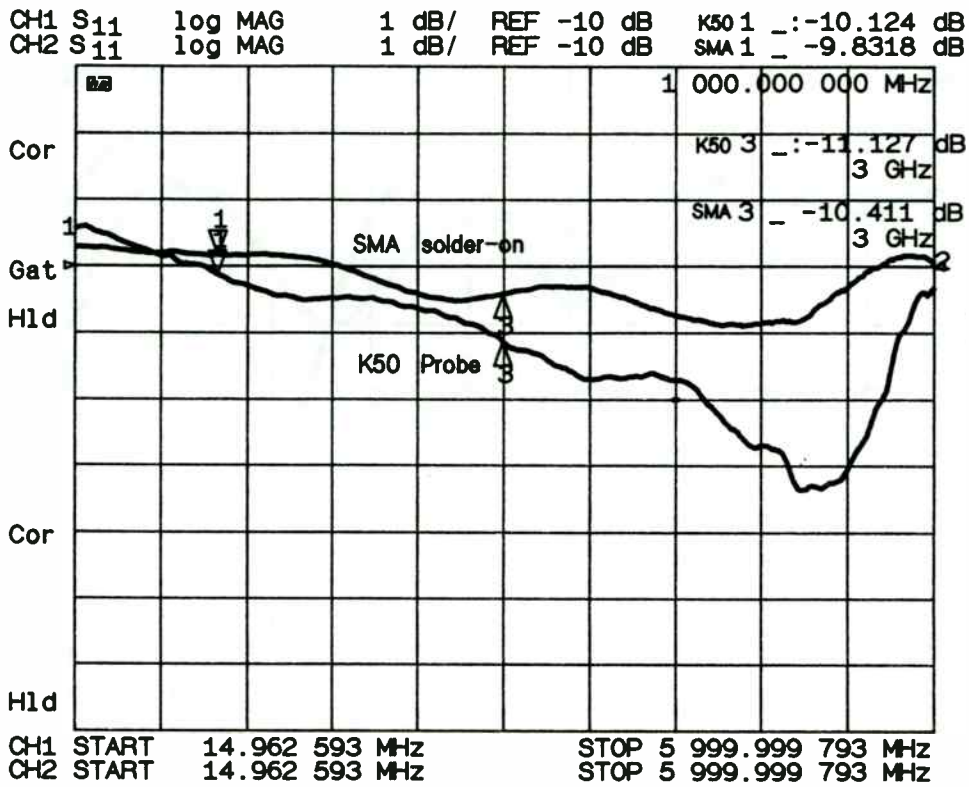


Figure 7: Comparison of SMA connection with K50 Probe (and gating).

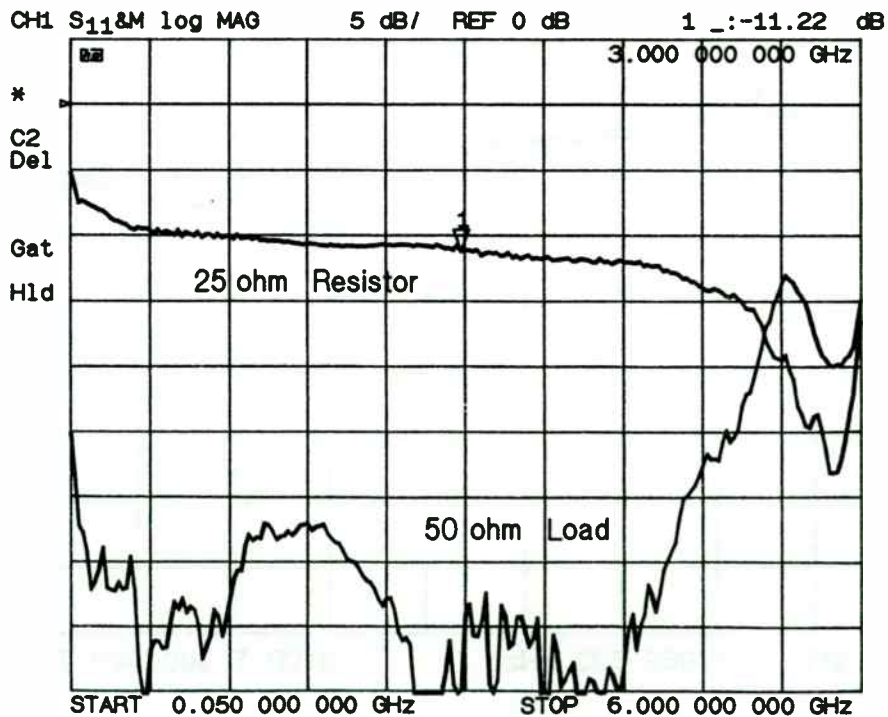


Figure 8: Measurement of a 25 ohm resistor, and a 50 ohm load with a TRL calibration of the probe, and TDR gating

battery lifetime? Minimizing spurious responses while conserving operating current requires creative design.

IV. CONCLUSION

The design of a wireless communications system is a complicated undertaking. Good coverage and freedom from interference are two of the major items that must be addressed if the system is to be successful. This paper has attempted to present a brief look at the key points to be considered when planning a system to ensure balanced coverage and to minimize interference. By keeping these points in mind, the system planner will have a better chance of getting the system right the first time.

V. REFERENCES

- [1]. W. C. Y. Lee, *Mobile Communications Design Fundamentals*. Indianapolis, IN: Howard W. Sams and Co., 1986, pp. 49-95.
- [2]. EIA/TIA Specification Number TR45.3, Project Number 2216, March 1991, p. 24.
- [3]. Franz McVay, "Don't Guess the Spurious Level," *Electronic Design*, February 1, 1967.

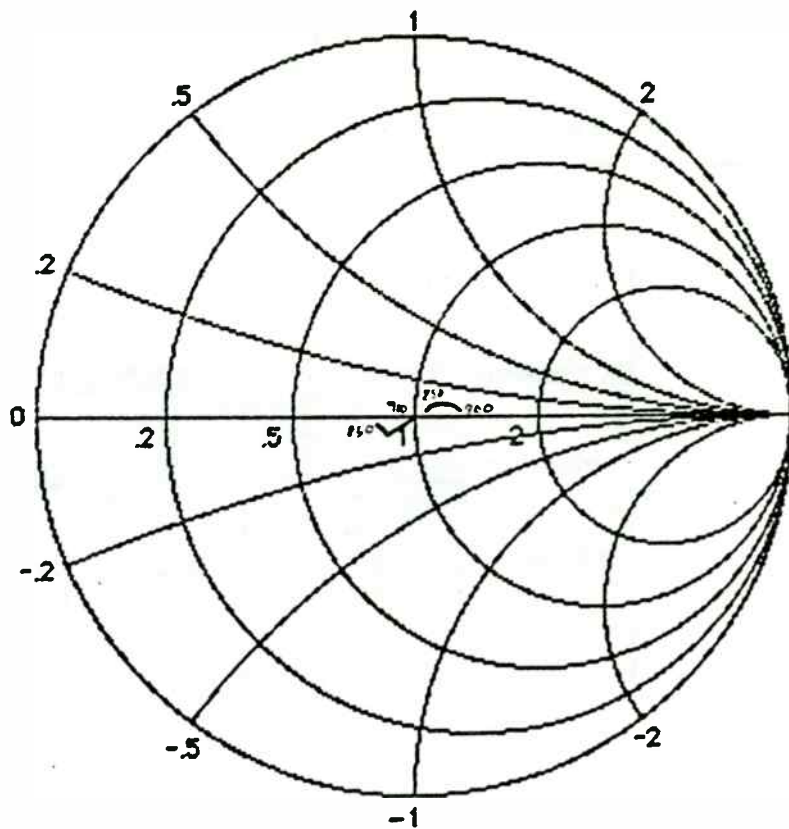


**Figure 9: Smith Chart Signatures –
Test Circuit and Line-Fixture**

A 2 GHz BiCMOS Low-Noise Amplifier and Mixer

David Bien

National Semiconductor

Wireless Communications Group

Abstract

A low-noise amplifier and mixer IC has been designed for wireless communication applications operating at frequencies up to 2 GHz. The integrated device is fabricated in a BiCMOS process with bipolar device f_T 's of 15 GHz and 0.8 μm CMOS channel lengths. The amplifier provides 16.4 dB of gain with a 2.8 dB noise figure at 1 GHz. The Gilbert-cell mixer operates with 3.9 dB of conversion gain and a 3rd-order output intercept point of 1 dBm. Total supply current for the LNA and mixer is 16.9 mA, and less than 1 μA in power-down mode.

I. INTRODUCTION

Virtually all wireless receivers include amplification and frequency conversion stages. Small form-factor battery-operated personal communications devices will continue to depend on low-power active circuits with increasing levels of integration. This paper describes a silicon integrated circuit that includes a low-noise amplifier (LNA) and a mixer. The IC provides a power-down function to help reduce current consumption in low duty cycle applications. The circuit operates with input frequencies up to 2 GHz, and can provide IF output frequencies up to 1 GHz. Signal inputs and outputs are matched to 50 Ohms over the range of operation, and circuit performance is compatible with current communications standards such as DECT [1]. Previous monolithic silicon devices that combine LNA and mixer functions on a single die do not cover this frequency range.

II. PROCESS DESCRIPTION

The LNA/ mixer IC is fabricated in a single-poly, oxide-isolated BiCMOS process [2] which is suitable for high-frequency mixed analog and digital circuits. Active device cross-sections are shown in Fig. 1. Minimum CMOS drawn gate length is 0.8 μm and bipolar NPN devices have 15 GHz f_T . Typical device parameters are given in Table 1. Also, the process includes low-parasitic capacitance polysilicon resistors and area-efficient capacitors. The completed die uses two metal interconnect layers. A photograph of the die is shown in Fig. 2.

III. LOW-NOISE AMPLIFIER

A. Circuit design

Fig. 3 shows the LNA schematic diagram. Shunt feedback lowers the input impedance of the common-emitter stage to create a nominal 50-Ohm input match without causing severe noise figure degradation [3]. In designing the LNA, the goal was an acceptable compromise among the various performance requirements, as a strong interdependency exists between several performance parameters. To achieve noise figure requirements, Q_1 must be scaled so as to have a low base resistance, since the r_b of Q_1 is the largest single noise source in the amplifier. A large input device, however, operates at low current density and has increased parasitic capacitances so that the

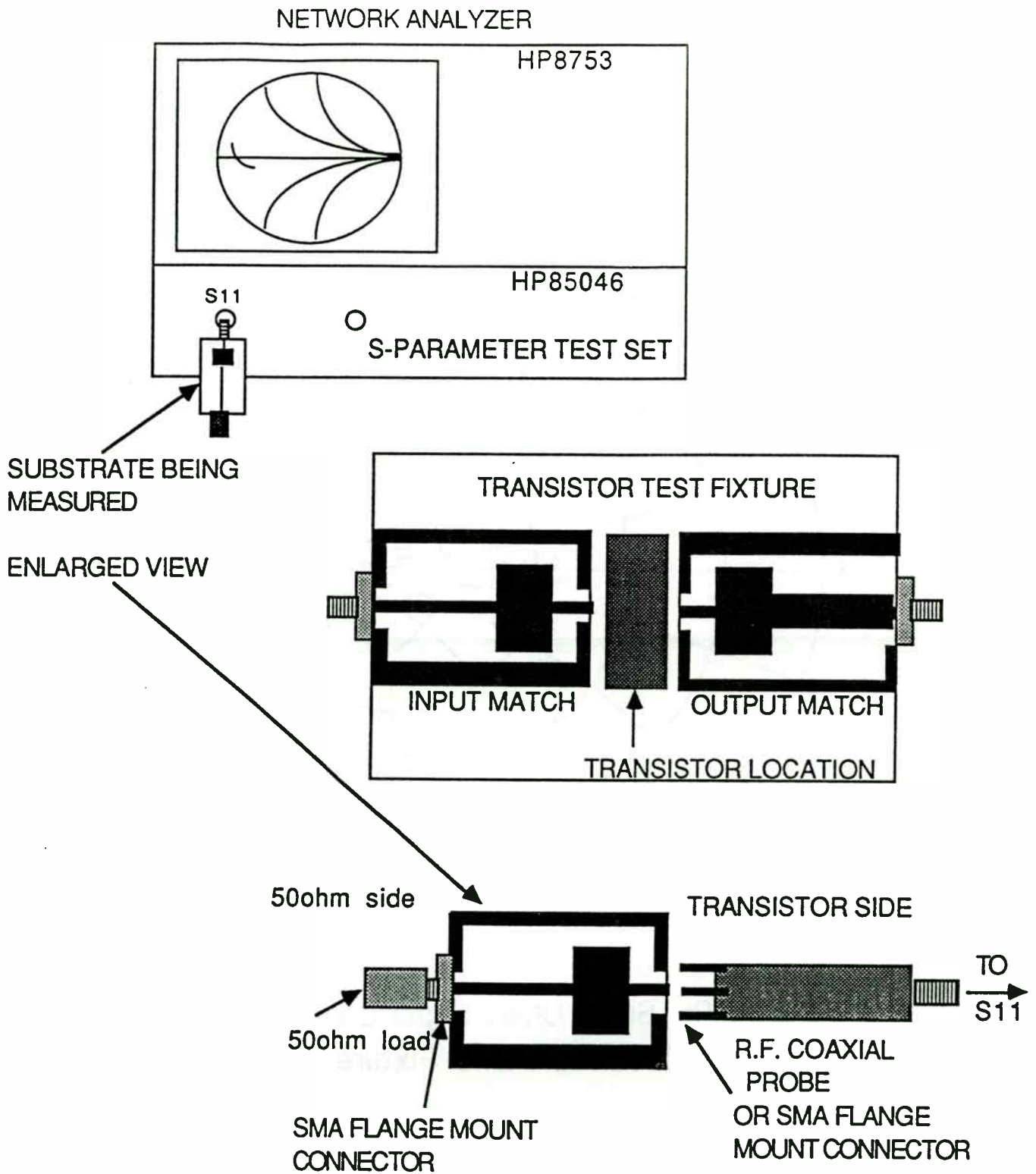


Figure 10: Impedance Profile Measurement Methodology

f_T	15 GHz
C_{jeb}	3.3 fF
C_{jec}	2.9 fF
β	90 A/A
$L_{off}(\text{MOS})$	0.6 μm
V_{TN}	0.75 V
V_{TP}	0.95 V

Table 1. Typical Device Parameters

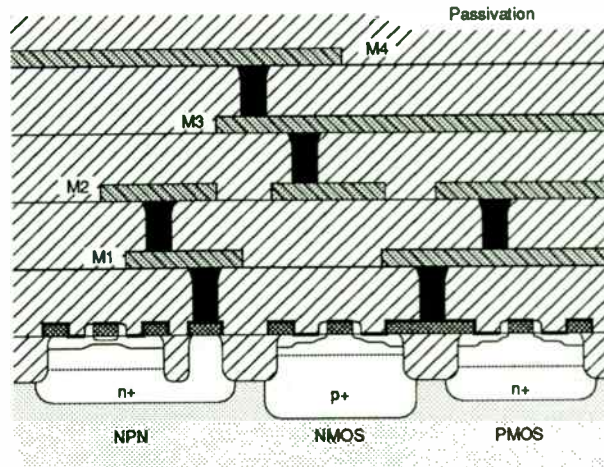


Fig. 1 - NPN and CMOS device cross-sections

speed of the device is sub-optimal. For these reasons, a large input device is in direct conflict with gain-bandwidth and input VSWR requirements. Supply current requirements add another dimension to the design compromise, as bias levels will affect all of the performance parameters mentioned here, in addition to directly determining maximum signal levels and related linearity parameters such as P_{1dB} and OIP_3 .

A simple but effective power-down feature is implemented through the use of a large PMOS switch, M_1 . During operation the switch is closed to provide bias to the amplifier. In power-down mode, the switch is open and the supply current drawn by the amplifier is determined by the leakage current of the switch, which is well below $1\mu\text{A}$. Typical turn-off and turn-on recovery times are in the range of 100ns, and are determined primarily by the size of the external coupling capacitors, which experience some charging and discharging as the amplifier is cycled through power-down.

Fig. 2. Die Photograph

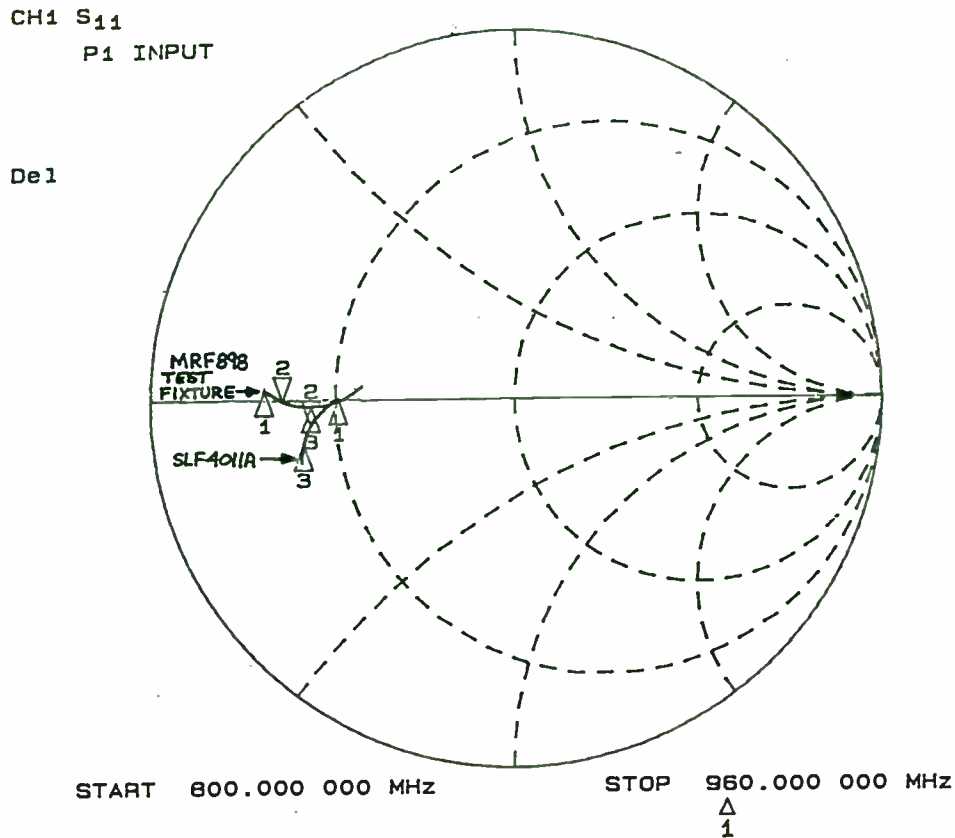


Figure 11(a): Impedance Profiles Relative to Line Fixture

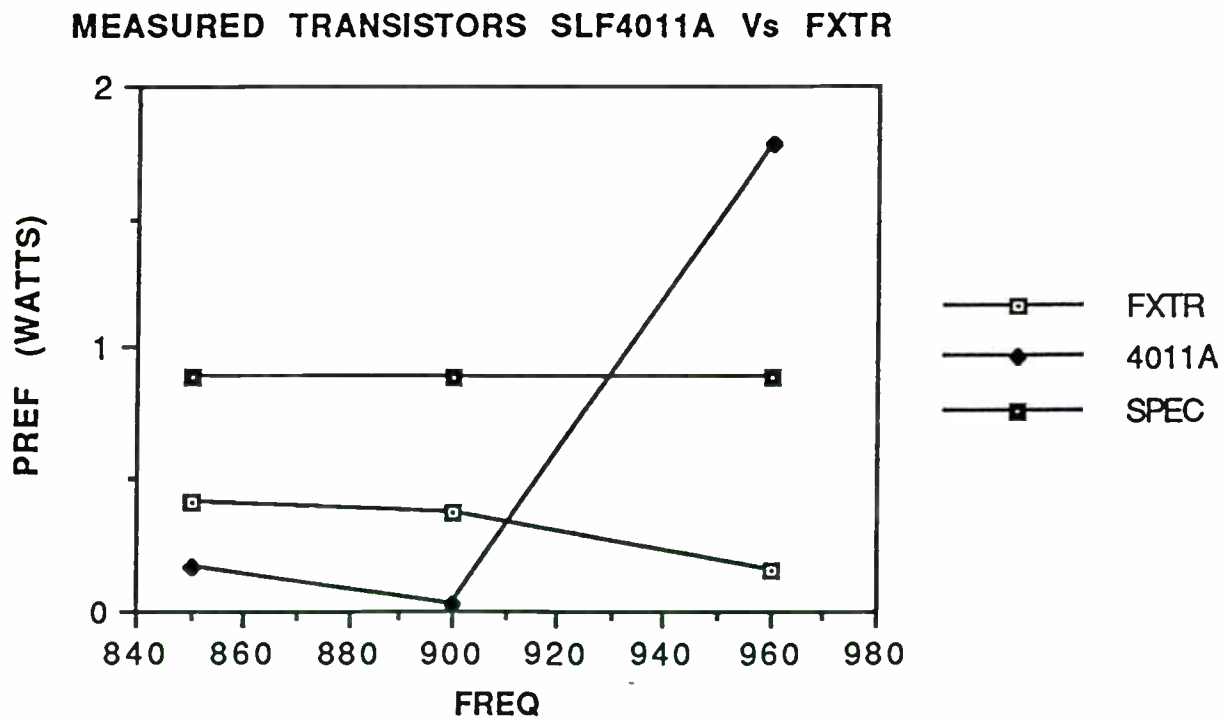


Figure 11(b): Test Results Showing Out of Spec. Performance

Supply Vcc	5	V
Icc, on	7.9	mA
Icc, off	< 1	uA
Max. Input Freq.	2	GHz
Gain, 1GHz	16.4	dB
P1dB Out, 1GHz	-7.4	dBm
OIP3, 1GHz	3.3	dBm
Noise Figure, 1GHz	2.8	dB
Inp. Return Loss	12.1	dB
Out. Return Loss	13.6	dB

Table 2. LNA Characteristics

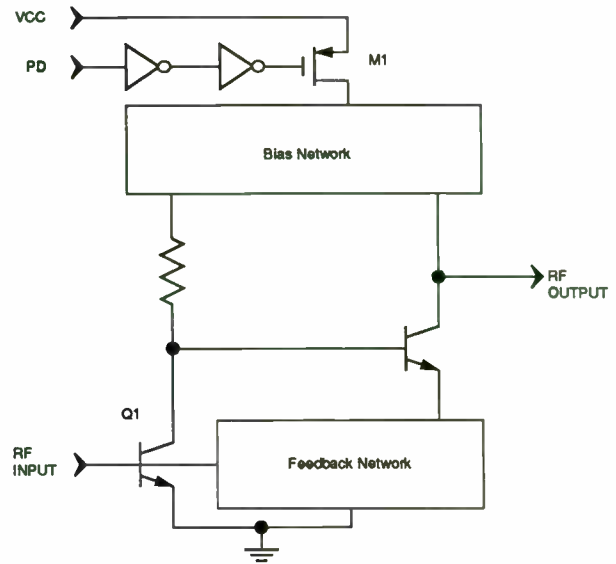
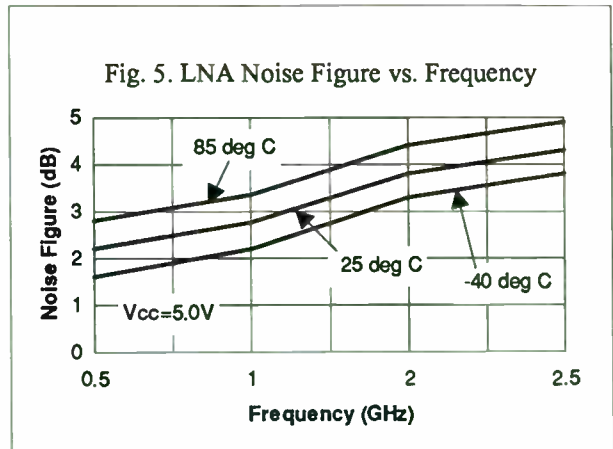
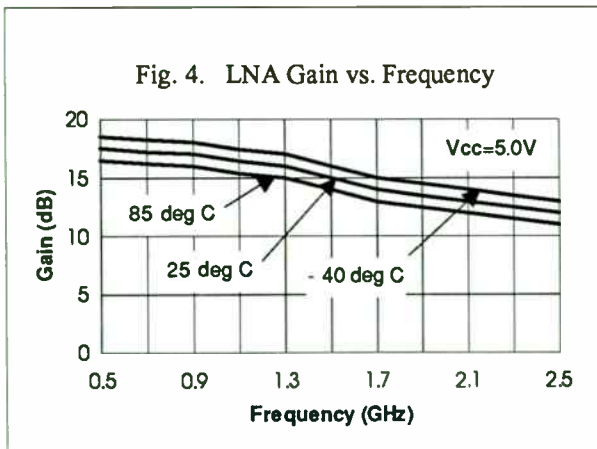


Fig. 3. LNA Schematic

B. Measured Results

Table 2 presents a summary of measured performance parameters for the LNA [4]. Amplifier supply current is 7.9 mA with a 5.0 Volt supply. Fig. 4 shows gain of the amplifier versus frequency, and illustrates the broadband behavior of the device. The amplifier provides usable gain beyond 2 GHz, and at DECT frequencies (1.9 GHz), the amplifier gain is 13.5 dB. Fig. 5 shows noise figure versus frequency. As transistor gain drops with increasing frequency, noise figure gradually increases. Noise figure is 3.8 dB at 1.9 GHz.



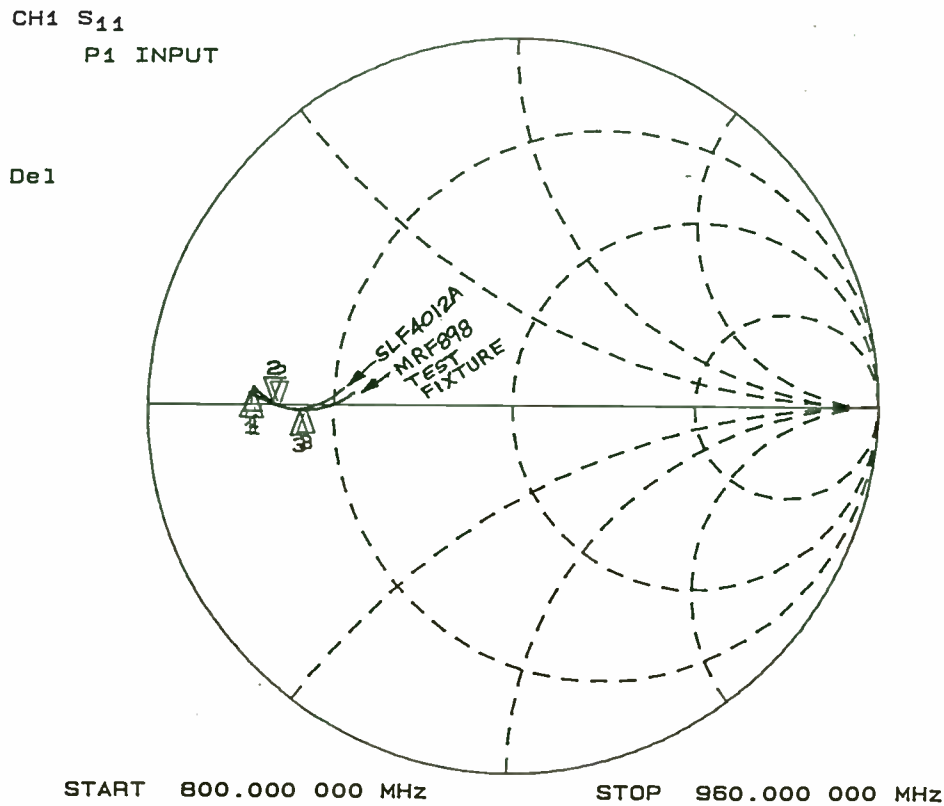


Figure 12(a): Impedance Profiles – New Methodology Design

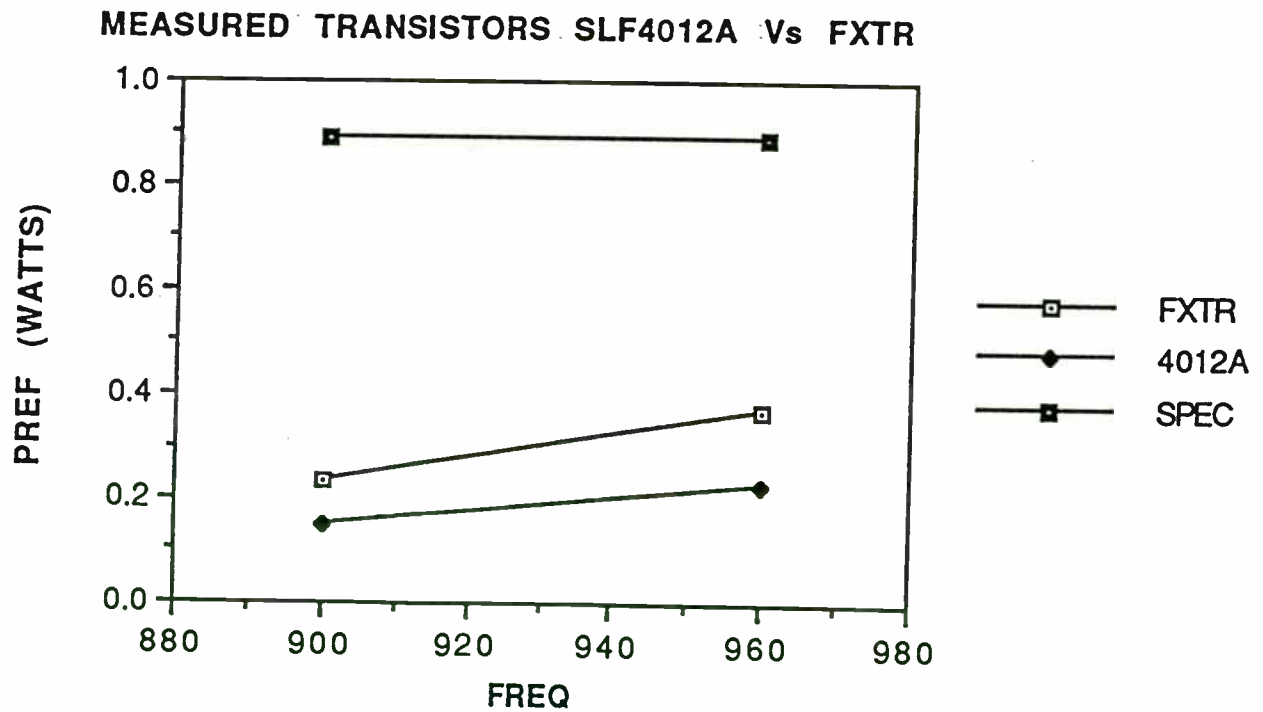


Figure 12(b): Test Results Showing Margin on Spec'd. Perf.

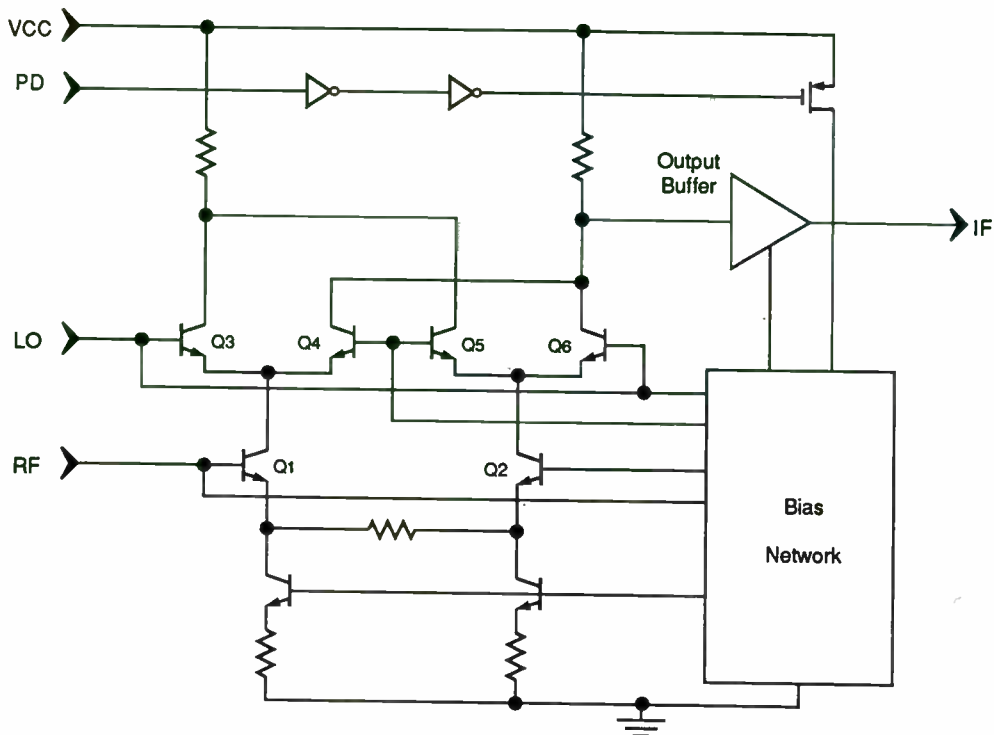


Fig. 6. Mixer Schematic

IV. MIXER

A. Circuit design

Fig. 6 shows the schematic of the mixer circuit. The mixer is based on a Gilbert cell. Although a circuit of this type inherently operates in a differential manner, the circuit has been configured with single-ended inputs and outputs since this is the most convenient mode of operation for most applications. Single-ended I/O's avoid the use of balun devices which may add significant cost to the receiver, and help simplify circuit board layout by reducing the number of signal-carrying traces that must be routed. Transistors Q_1 - Q_6 compose the Gilbert cell and an output buffer matches the multiplier output to the $50\ \Omega$ load. Other transistors provide biasing. Broadband input terminations for the RF and LO inputs are accomplished by means of on-chip terminating resistors and on-chip DC blocking capacitors. The inputs are effectively matched to $50\ \Omega$ at frequencies above 100 MHz. The IF output impedance is determined by the output impedance of the output buffer, which is approximately $50\ \Omega$ up to frequencies in excess of 1 GHz.

Power-down for the mixer is again accomplished through the use of MOS switches. During power-down the switches disable all biasing and supply current is limited to device leakage currents, which are well below $1\ \mu\text{A}$. As for the LNA, typical turn-off and turn-on recovery times are 100-200 ns, and are dependent on external blocking capacitor values.

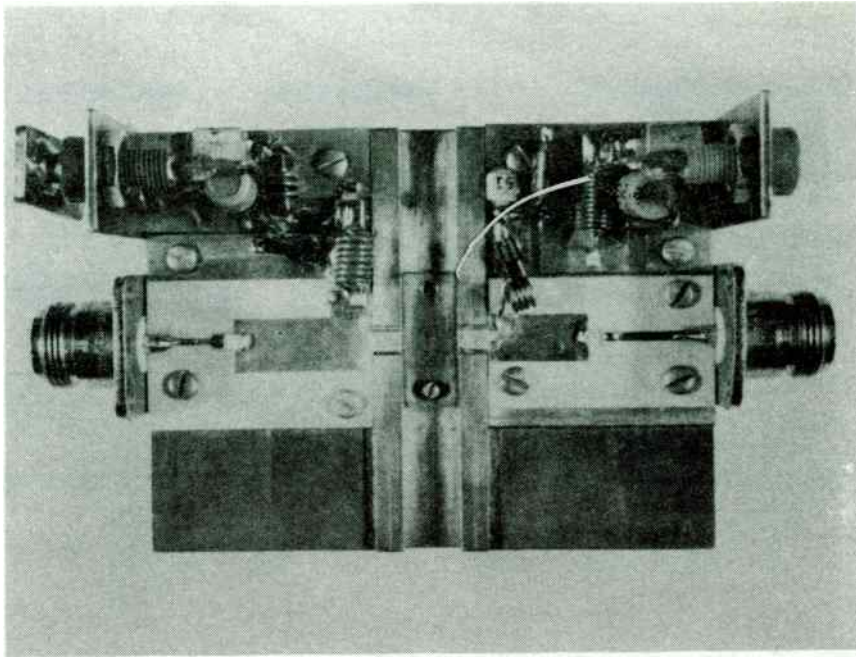


Figure 13: Transistor Line Fixture

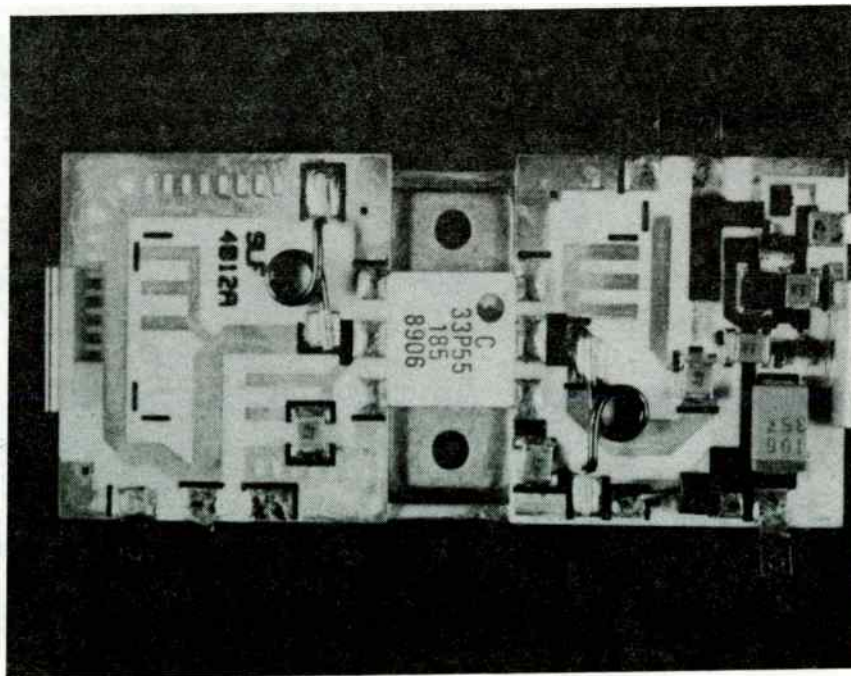


Figure 14: Application Circuit

Supply Vcc	5	V
Icc, on	9	mA
Icc, off	< 1	uA
Max. Input Freq.	2	GHz
Conversion Gain, 1GHz RF, 110 MHz IF	3.9	dB
P1dB Output, 110MHz IF	- 8.2	dBm
OIP3, 110MHz IF	0.9	dBm
Noise Figure (SSB), 1.9GHz	21	dB
LO to RF isolation, 1GHz	33	dB
LO to IF isolation, 1GHz	28	dB
RF Return Loss, 1GHz	22.9	dB
LO Return Loss, 1GHz	25	dB
IF Return Loss, 1GHz	15.4	dB

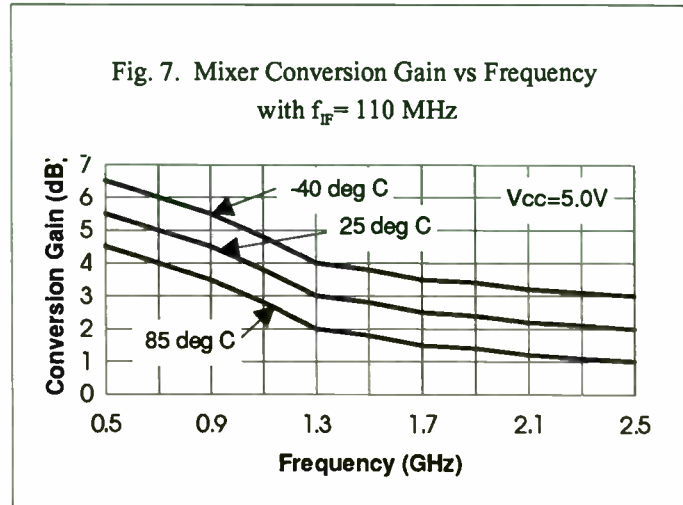


Table 3. Mixer Characteristics

B. Measured Results

Table 3 summarizes measured performance parameters for the mixer. Supply current for the mixer is 9.0 mA with a 5.0 V supply. As shown in Fig. 7, the mixer provides conversion gain up to and beyond 2 GHz. Conversion gain is 2.3 dB at 1.9 GHz.

V. CONCLUSION

A single-chip BiCMOS low-noise amplifier and mixer has been described. The IC has been designed for ease-of-use in a variety of applications at frequencies up to 2 GHz. Fabricated in an advanced BiCMOS process, the circuit takes advantage of bipolar device performance in critical signal paths, and makes use of CMOS devices to create convenient biasing and power-down features.

VI. ACKNOWLEDGMENTS

Andy Dao and Don Ferris provided characterization data for the IC. Also, the Wireless applications and design staff contributed through helpful suggestions and discussions. All contributions are gratefully acknowledged.

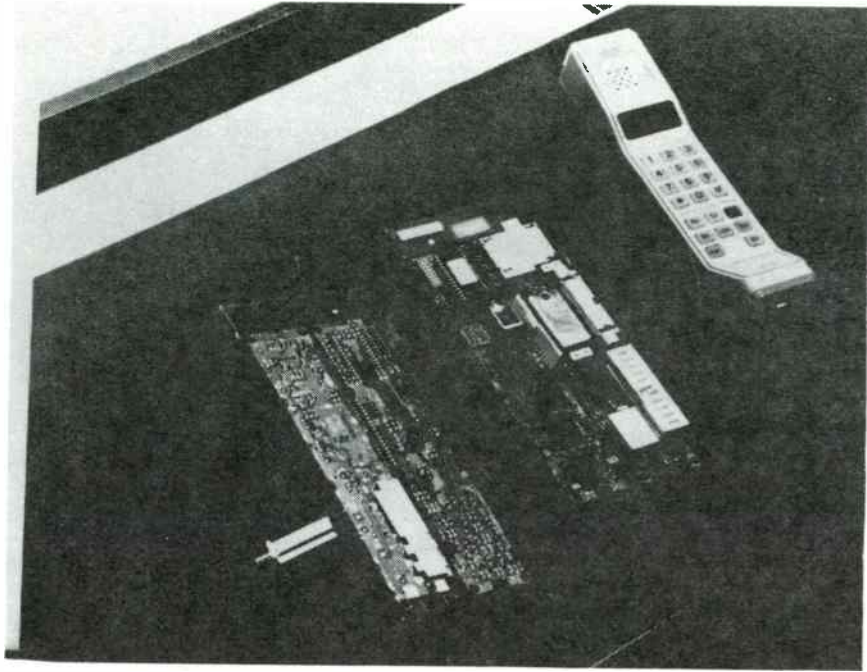


Figure 15: A K-50 Probe with A Cellular Telephone Board

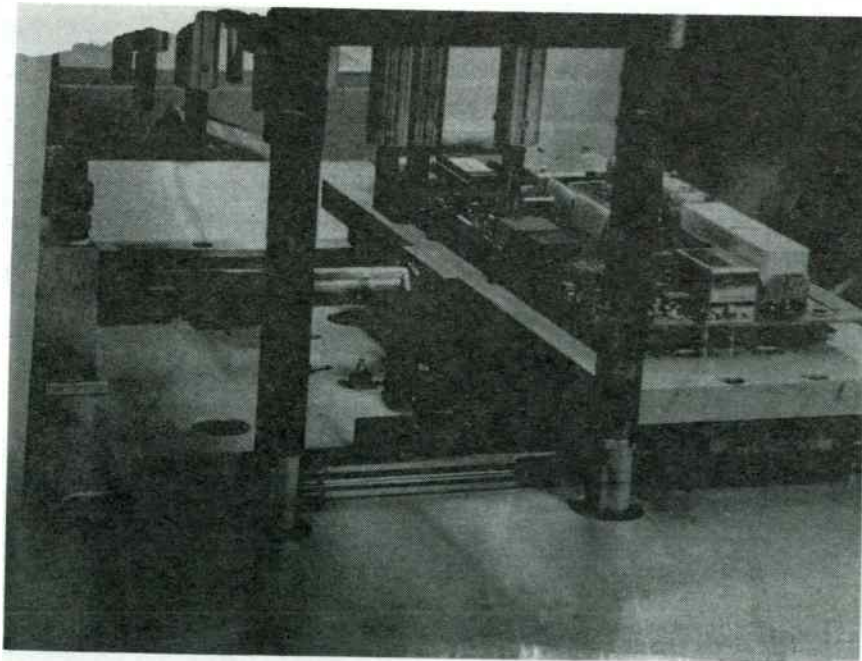


Figure 16: The K-50 Probe in an Automated Board Tester

VII. REFERENCES

- [1] ETSI, European Telecommunications Standard ETS 300 175-1: "Digital European Cordless Telecommunications (DECT) Common Interface Part 2: Physical Layer".
- [2] A. Iranmanesh, V. Ilderem, M. Biswal, B. Bastani, "A 0.8 μ m Advanced Single-Poly BiCMOS Technology for High-Density and High-Performance Applications", *IEEE J. Solid-State Circuits* (1991) 422-426.
- [3] I. Kipnis, J. F. Kukielka, I. Wholey, and C. P. Snapp, "Silicon bipolar fixed and variable gain amplifier MMIC's for microwave and lightwave applications up to 6 GHz", *IEEE MTT-S Dig.* (1989) 109-112.
- [4] LMX2215 data sheet, National Semiconductor, to be published.

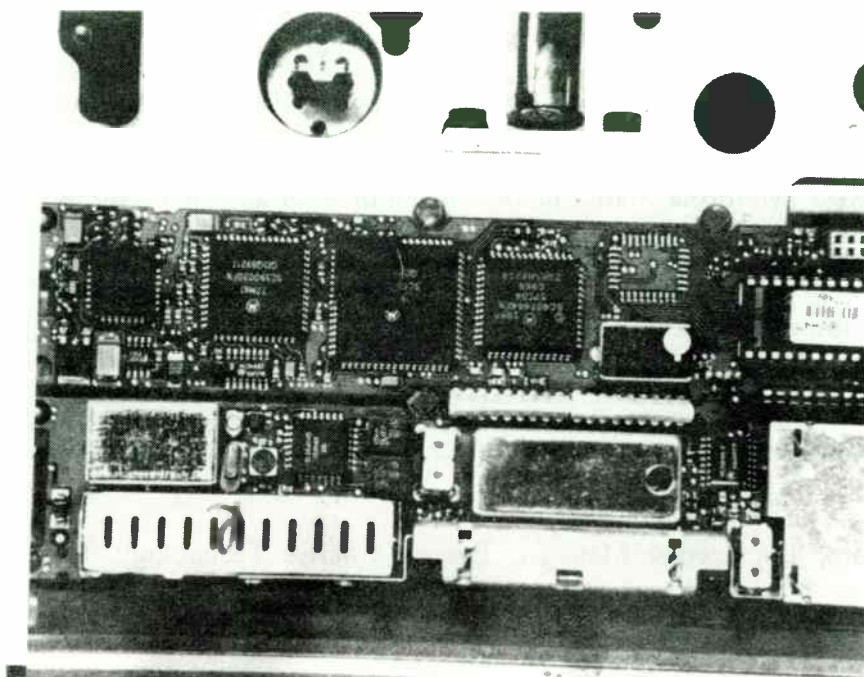


Figure 17: A K-50 Probe in an Automated Test Fixture

High Efficiency Crystal Oscillator at High Frequencies

Sheng H. Lee and Alvin K. Wong, Philips Semiconductors

Abstract — For the new 900 MHz wireless market, designers are required to implement a much higher front IF frequency. As a result, a new type of high frequency crystal oscillator has been created. This new circuit overcomes the heavy bias and difficult tuning problems associated with the conventional Colpitts crystal oscillator at frequencies above 60 MHz. The result is an oscillator with minimum bias current and flexible tuning capability.

I. INTRODUCTION

In the past, while there were many proposals made to modify the basic Colpitts crystal oscillator circuit to extend its usable frequency range above 60 MHz, none of them has ever addressed the issue of how to accomplish the goal with minimum current draw. This is of paramount importance when one considers the ever shrinking hardware as well as battery sizes. Therefore, the original Colpitts oscillator model was revisited to determine the factors that cease the oscillation at high frequencies, and develop an elegant solution to counter the negative force. The result is a 95.55 MHz crystal oscillator using a scant 0.2 mA current, yet generating 300 mV_{RMS} signal at the mixer load. The active device is from the NE605 receiver IC, which has a compatible built-in LO stage with the same bias current. In the discussions below, the design steps and their associated equations are listed, but the mathematical derivations are not included.

II. CIRCUIT ANALYSIS

A. Universal Circuit Model

Any linearized, time-invariant circuit can be reduced to a parallel L/C/R circuit if the bandwidth of interest is small and, depending on the value of R, the time-domain waveform will vary significantly, which is shown in Fig. 1.

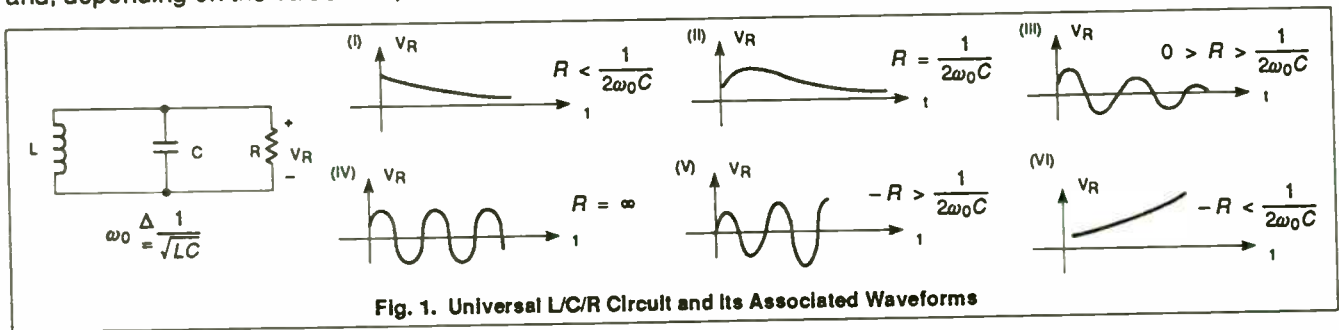


Fig. 1. Universal L/C/R Circuit and Its Associated Waveforms

It is obvious that only negative resistance can meet the start-up condition of oscillation. This is possible because the negative resistance is generated by the device that has an amplitude-dependent gain, so regardless of whether the amplitude builds up from Fig. 1, category (V) or (VI), it would wind up with category (IV) in equilibrium.

B. Basic Oscillator Model

A typical L/C type Colpitts oscillator using Philips Semiconductors NE605 and its simplified AC schematic diagram is shown in Fig. 2.

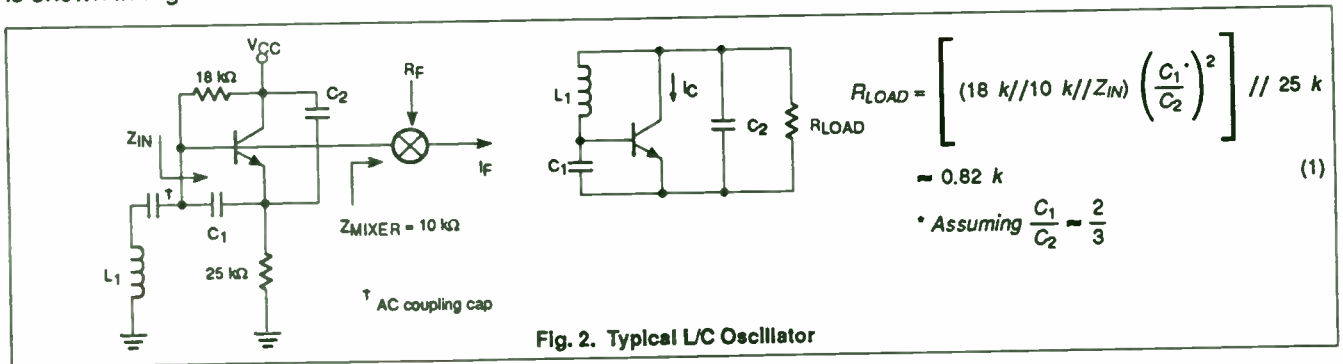


Fig. 2. Typical L/C Oscillator

Typically the device has a default bias current of 0.2 mA and an estimated AC current gain of 20 at 95.55 MHz, with a resultant input impedance (Z_{IN}) of 2.6 k Ω for the device. Therefore, we can assume that

Contributors:

Joel Dunsmore - Figures 1,2,4-8

Bob Kornowski - Figures 13-17

Jim Long - Figure 9

Miles Tusa - Figures 10-12

Chuck Tygard - Figure 3

Acknowledgments:

Joel Dunsmore, R&D Development Engineer, Hewlett-Packard, Microwave Instruments Division.

Bob Kornowski, Motorola Staff Engineer/Inventor - Originator of the K-50 Probe, the SIX SIGMA High Frequency Design Methodology, and the "QUALITY through INVENTION" Continuous Quality Improvement Culture.

Jim Long, Motorola Principle Staff Engineer - An early investigator and proponent of using the network analyzer as a problem solving tool.

Miles Tusa, Motorola Lead Engineer - Miles was the first to apply the SIX SIGMA High Frequency Design Methodology, involving Impedance Profiles and Smith Chart Signatures, to develop a new radio product.

Chuck Tygard, Engineering Manager, Everett Charles Technology, Contact Products Division.

$$Z_N \gg \frac{1}{\omega C_1}$$

$$(18k//10k) \gg \omega L_1$$

without losing the generality, the circuit can be further reduced to new equivalent circuit in Fig. 3.

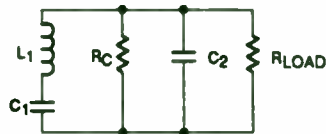


Fig. 3. Equivalent Circuit for L/C Oscillator

where the device output impedance is given by

$$R_C = \frac{\Delta V_{C2}}{i_C} = \frac{-C_1}{G_m C_2} \quad (4)$$

and the transconductance at room temperature is defined as

$$G_m = \frac{I_{DC}}{26} \quad (5)$$

where I_{DC} is in [mA] and G_m is in [S].

Comparing this circuit to that from Fig. 1, we conclude the condition for oscillation:

$$\frac{C_1}{G_m C_2} < R_{LOAD} \quad (6)$$

and, by default, the frequency of oscillation is

$$\omega_0 L_1 = \frac{1}{\omega_0 C_1} + \frac{1}{\omega_0 C_2} \quad (7)$$

In general designers can choose the condition of

$$\frac{C_1}{G_m C_2} \ll R_{LOAD} \quad (8)$$

if the maximum output power is preferred over the minimum distortion. The same circuit can also be viewed from a different angle using the phasor diagram as shown in Fig. 4, which clearly demonstrates the creation of negative resistance from the device due to the out-of-phase condition between V_{C1} and V_{C2} .

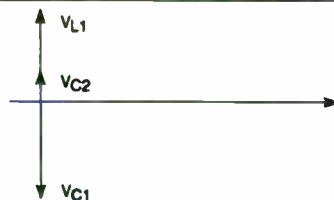


Fig. 4. Phasor Diagram for L/C Oscillator

C. Crystal Oscillator Model

So far an ideal oscillator model has been discussed and the only limitation on the frequency of oscillation is the G_m factor from the device. This is why 20 GHz oscillator, using the transistor as the active device, is feasible when high quality L/C components (or their equivalents) are used. But this is no longer true when the crystal is substituted for the inductor regardless of the frequency performance of the device. In order to fully understand the impact of the crystal, the previous simplified model will be extended by adding a resistor in series with the inductor L_1 as shown in Fig. 5 and its associated phasor diagram in Fig. 6.

Low Cost RF Tuner System for JDC Load Pull and SSPA Design

Christos Tsironis and Dominique Dubouil
Focus Microwaves Inc.
277 Lakeshore Road
Pointe-Claire, Quebec
Canada H9S 4L2

Summary

Focus Microwaves presents a Load Pull and Noise Measurement and Design System, conceived for the Basic Needs of RF Design and Test Engineers:

-Accuracy, -Low Cost, -Focus on Key Applications in Power and Low Noise and -Design Capability for Power Amplifier stages.

The new system includes all hard and software components required to configure a Test and Design Workstation based on a 80-386 or -486 IBM-PC and most commonly used GPIB equipment.

Introduction

The important market of Personal Communications (PCN) in the low microwave and RF area of 800 to 3000 MHz requires:

- New low cost, reliable and state of the art active devices (FETs, MOSFETs, bipolar transistors...)
- Efficient designs to minimize the requirements to the devices for given system performance and
- Sophisticated test methods to detect problems early in the Design Cycle.

It became common knowledge, meanwhile, that automatic load pull and noise measurement systems provide great help in understanding the devices and speed up the test and design process.

Some of the new amplifier designs are based on data generated by those computer controlled tuner systems, mostly for low noise applications, but progressively also for high power.

Still there is some time to go, before those systems develop their full potential and become as reliable, understandable and User friendly as most Users would like to have. Nevertheless the potential is there and spreading those systems in as many labs as possible will help their evolution.

Price has always been a factor keeping computerized tuner systems out of most labs. At 60 to 90,000 \$ most

managers require a thorough justification to approve, but this last one only comes with broad use. So we have a kind of self-blockade of the cycle.

We have developed the **Microwave Tuner System (MTS)** with a close look to the core needs of the RF Design and Test Engineers in the Product Development and Production teams:

- **Accuracy:** The MTS tuners cover the frequency range of 800 MHz to 3 GHz and provide state of the art 50 dB RF-impedance resetability (± 0.003 reflection factor units).
- **Low Cost:** The MTS costs about 1/3 of other (more sophisticated) computerized tuner systems.
- **Key Applications:** The MTS measures all important RF quantities; ie. Power, Gain, Efficiency, Intermod as well as 4 Noise parameters.
- **Design:** The MTS permits to transfer ISO Power contours to a Network Simulator and optimize High Power Amplifier stages.

The MTS Components and Capabilities

The MTS includes the following components:

- Two computerized tuners, model MTS-308 in SMA, GPC-7 or N-connector configuration
 - One PC insertable tuner controller
 - GPIB interface
 - Setup, test fixture and tuner calibration software
 - Measurement software
 - ISO contour generation graphics software
 - RF power amplifier design software (optional)
 - Preselectable GPIB drivers for over 50 popular instruments (network analyzers, power meters, spectrum analyzers, dc bias controllers, signal sources, frequency counters and noise analyzers).
- Figure 1 shows a typical setup for Load Pull and Noise Measurement.

The MTS permits the following operations:

- **Calibration** of the tuners, the setup components

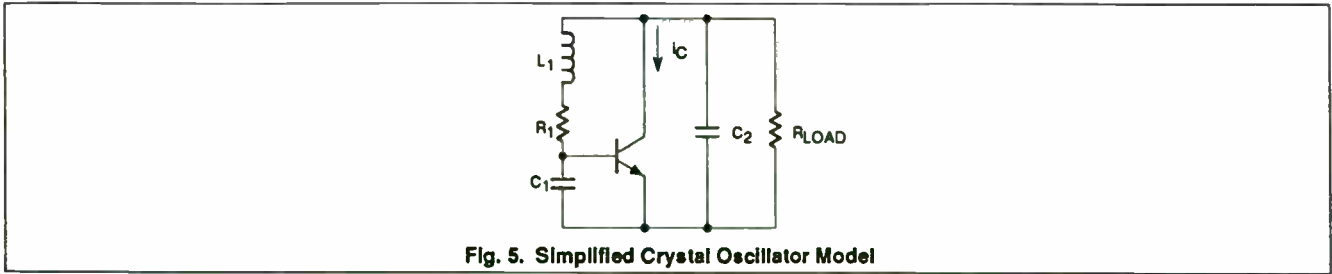


Fig. 5. Simplified Crystal Oscillator Model

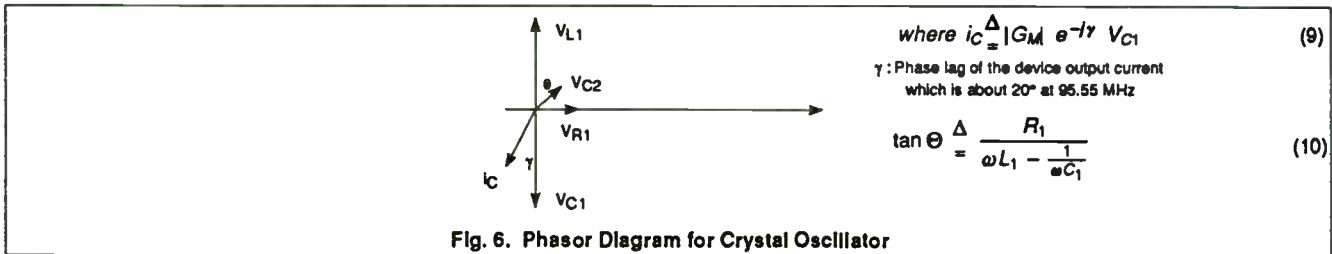


Fig. 6. Phasor Diagram for Crystal Oscillator

Judging from the relative phase relationship between V_{C2} and i_C , we know the device output admittance is complex and both its real and imaginary parts are negative if $\gamma < \theta$. The equivalent circuit and the governing equations are shown in Fig. 7.

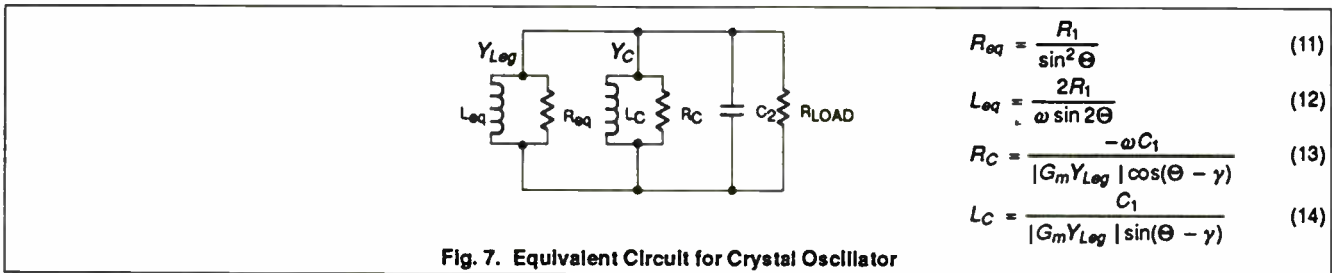


Fig. 7. Equivalent Circuit for Crystal Oscillator

D. Advanced Crystal Oscillator Model

Since part of the precious power is being converted to the inductance instead of the much needed negative resistance, the ability for the device to oscillate is diminished due to the conservation of energy. Therefore, an inductor L_2 is added in the base of the device to realign V_{C2} and i_C out of phase. The new schematic diagram, the associated phasor, its equivalent circuit as well as key design equations are shown in Figs 8, 9 and 10, respectively.

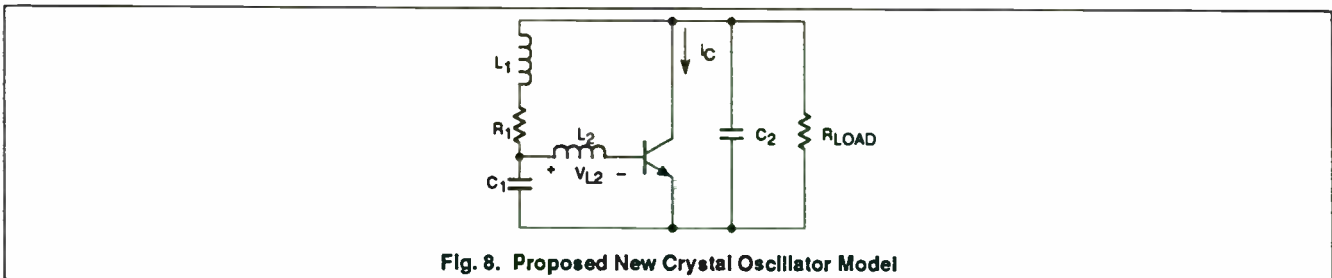


Fig. 8. Proposed New Crystal Oscillator Model

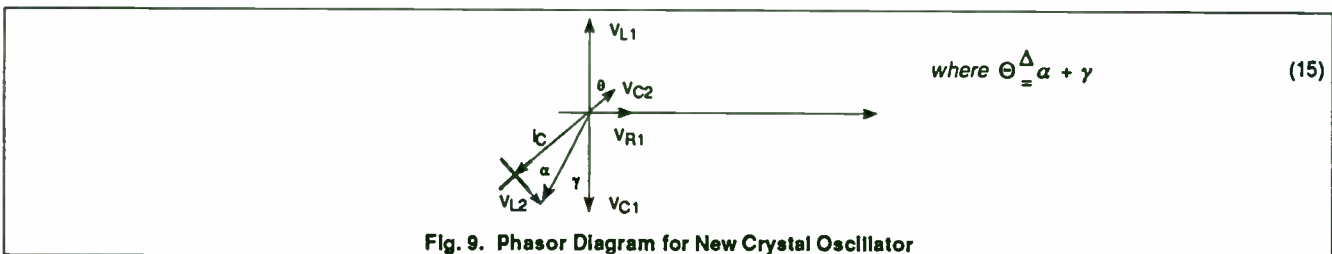


Fig. 9. Phasor Diagram for New Crystal Oscillator

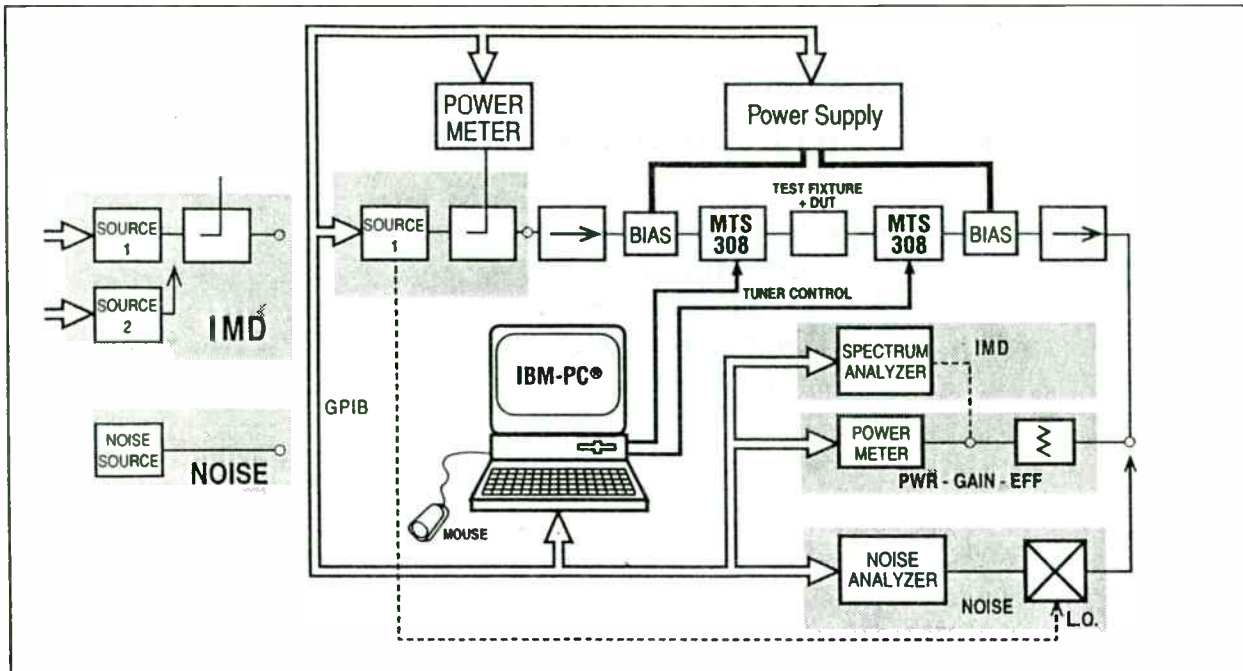


Figure 1. The MTS Load Pull and Noise Measurement setup

and test fixture using any of the available network analyzers. In particular the test fixture is characterized using generic TRL formulas, which are valid for any kind of fixture.

- **De-Embedding** to any reference plane selected by the User.
- **Mouse tuning** to any point on the Smith Chart (not only calibration points).
- **Measurements at selected Smith Chart areas**, in order to avoid oscillations.
- **Classical Load/Source Pull** of Power, Gain, Intermod and Efficiency. Further options include JDC (Japanese Digital Communication) or adjacent channel leakage tests, high order intermod and oscillator load pull tests.
- **Automatic search for best performance** in power, gain, efficiency both at the source and load side of the device.
- **Saturation measurements** of power, gain and efficiency.
- **Automatic search for optimum Noise match** and **4 Noise parameters**

MTS-308 Tuners

Figure 2 shows the MTS-308 tuners with SMA connectors. The MTS-308 are mechanical tuners using a parallel slotted airline as transmission media and a metallic RF probe to generate controllable reflection. When the probe is withdrawn the tuner behaves like a transmission line, thus avoiding parasitic oscillations. When the probe is inserted the tuner has always a low pass behaviour below ≈ 700 MHz, with the same

effect. It is obvious that among all types of variable tuners the slotted line type ones are the best compromise for parasitic oscillations.

The probe is moved using two stepper motors and a rugged translation mechanism. Most of the MTS-308 parts are 'of the shelf' articles and thus permitted low manufacturing cost and high reliability. Size and weight of the MTS-308 have been optimized to permit (manual) operation down to 750 MHz and up to 4.2 GHz (optional). The reduced weight permits to position MTS-308 tuners on wafer probe stations very easily and without any implications due to vibrations.

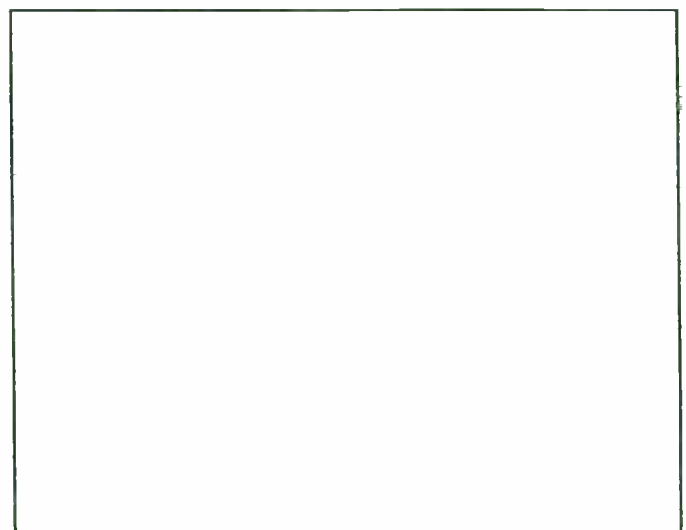
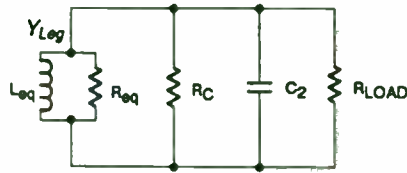


Figure 2. The MTS-308 tuners with SMA connectors



$$R_C = \frac{-R_1 \omega C_1}{|G_M| \sin \theta \cos \alpha} \quad (16)$$

$$\tan \alpha = \frac{\omega L_2}{Z_{IN}} \quad (17)$$

Fig. 10. Equivalent Circuit and Design Equations

One very important aspect of the results from Eq. (16) is that when ω increases, R_C decreases in value. Since θ is a function of ω , it also influences the R_C value, although to a lesser degree. This explains why a 100 MHz crystal oscillator is more difficult to build than a 1 GHz L/C type oscillator. In general, R_{LOAD} is much greater than R_{eq} , when the crystal is in place, so the condition for oscillation can be derived from Eq. (11) and Eq. (16), and is as follows:

$$\frac{|G_M|}{\omega_0 C_1} > \frac{\sin \theta}{\cos \alpha} \quad (18)$$

And the frequency of oscillation becomes

$$\omega_0 L_{eq} \Delta = \frac{1}{\omega_0 C_2} \quad (19)$$

III. EXAMPLE FOR LOW-POWER CRYSTAL OSCILLATOR AT 95.5 MHZ

Now we will show how to apply the theory to build a 95.55 MHz crystal oscillator. First, a model for the crystal is presented in Fig. 11.

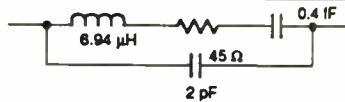


Fig. 11. 95.545 MHz Crystal Model

Eq. (12) and Eq. (19) can thus be combined to give

$$C_2 = \frac{\sin 2\theta}{2\omega_0 R_1} \leq \frac{1}{2\omega_0 R_1} = 18.5 \text{ pF} \quad (20)$$

A standard value of 15 pF is chosen for C_2 , which results in 27° for θ . After substituting values for α and θ in Eq. (18), the upper bound for C_1 is as follows:

$$C_1 < \frac{|G_M| \cos \alpha}{\omega_0 \sin \theta} \approx 28 \text{ pF} \quad (21)$$

In the meantime, Eq. (1) and Eq. (8) give a loose lower bound of

$$C_1 \gg \frac{C_2}{1800|G_M|} = 1 \text{ pF} \quad (22)$$

versus another loose lower bound from Eq. (2) for C_1

$$C_1 \gg \frac{1}{Z_{IN}\omega} = 0.64 \text{ pF} \quad (23)$$

The final value for C_1 is selected to be 10 pF after considering the constraints from Eq. (21), Eq. (22) and Eq. (23). Furthermore, since the crystal operates at the higher overtone mode, it is necessary to suppress the lower order oscillations by substituting parallel L/C for C_2 . As for the value of L_2 , 537 nH is required based on Eq. (17), however only the standard value of 560 nH will be used for the final circuit.

The MTS-308 Specifications

A key advantage of the MTS tuners is that they can handle practically unlimited RF power, either in CW or pulsed form. Because of the wideband behaviour pulsed operation is not a problem. Also fine tuning to millions of impedance states is a key benefit. The MTS-308 specifications are listed in Table 1. Figure 3 shows the MTS-308 tuning capability.

- Frequency range: 800 to 3000 MHz (4200 MHz optional).
- VSWR min: 1.12:1 (SMA), 1.06:1 (GPC-7).
- VSWR max: 10:1 min (SMA), 12:1 min (GPC-7), Typical 15:1.
- Tuning Resolution: 0.18° per step at 3 GHz.
- Insertion Loss: 0.4 dB (SMA), 0.15 dB (GPC-7).
- RF Resetability: > 50 dB.
- Total size: 300 x 150 x 175 [mm] or 11.8 x 5.9 x 6.9 [inches].
- Weight: 4.1 kg.
- Tuning Speed: 360° tuning in 1000/f[MHz] x 15 seconds.
- DC power requirements: 12V, 3A max (provided by PC controller).
- Humidity, Temperature: normal laboratory conditions.
- Vibrations: The MTS-308 units are not sensitive to moderate shocks and vibrations both from operation and accuracy points of view.
- Validity of calibration data: 1 to 3 months of normal operation.
- Calibrated points (Load Pull): 181.

Table 1. MTS-308 Specifications

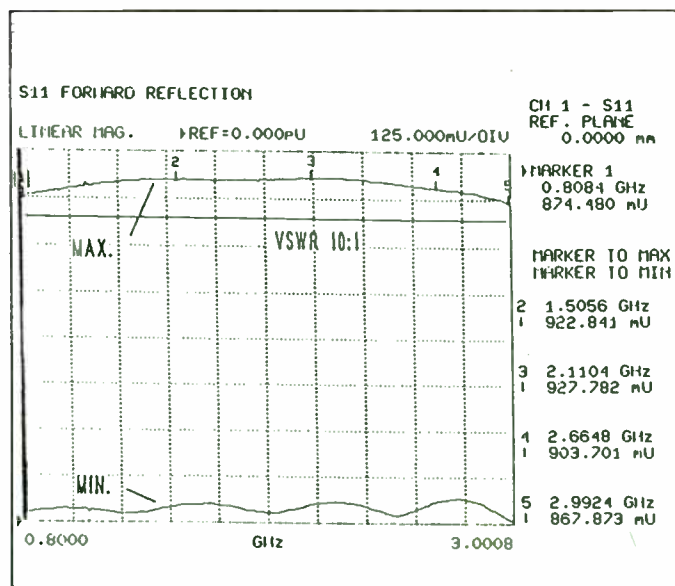


Figure 3. MTS-308 tuning capability

Table 2 shows S-parameter dispersion when the tuner is moved 10 times to the same set of positions.

RF-Resetability over 10 Cycles (0.001->60dB, 0.0001->80dB)								
TUNER MTS#02, Frequency = 0.800 GHz								
Point	S11	S11*	S12	S12*	S21	S22	S22*	
1:	-0.0014,	0.02	0.0007,	0.06	0.0006,	0.06	-0.0013,	0.11
2:	0.0006,	-0.04	-0.0004,	-0.04	-0.0004,	-0.04	0.0005,	-0.03
3:	0.0019,	-0.17	-0.0017,	-0.12	-0.0017,	-0.13	0.0020,	-0.06
4:	-0.0018,	0.14	0.0015,	0.12	0.0015,	0.12	-0.0020,	0.08
5:	-0.0007,	0.04	0.0005,	0.05	0.0005,	0.06	-0.0007,	0.06
6:	0.0001,	-0.03	-0.0001,	-0.01	-0.0001,	-0.01	0.0001,	0.01
7:	0.0006,	-0.03	-0.0005,	-0.03	-0.0005,	-0.03	0.0005,	-0.03
8:	-0.0005,	0.03	0.0008,	0.04	0.0008,	0.05	-0.0005,	0.05
9:	-0.0003,	0.04	0.0004,	0.04	0.0004,	0.04	-0.0003,	0.03
10:	-0.0016,	0.10	0.0017,	0.11	0.0018,	0.11	-0.0014,	0.12
11:	0.0010,	-0.08	-0.0016,	-0.10	-0.0015,	-0.11	0.0012,	-0.12
12:	-0.0020,	0.06	0.0020,	0.11	0.0020,	0.11	-0.0017,	0.16
STD.DEV= 0.0012, 0.08 0.0012, 0.08 0.0012, 0.08 0.0012, 0.08								
'S' parameters of above Points ...								
1:	0.390,	138.1	0.897,	56.8	0.898,	56.7	0.383,	157.6
2:	0.586,	41.0	0.777,	48.1	0.777,	48.0	0.593,	-124.2
3:	0.620,	-40.8	0.755,	48.3	0.755,	48.3	0.625,	-42.9
4:	0.607,	-85.1	0.767,	48.6	0.767,	48.6	0.607,	2.1
5:	0.574,	-123.9	0.790,	49.2	0.790,	49.2	0.575,	42.7
6:	0.519,	166.0	0.822,	49.9	0.823,	49.8	0.529,	115.3
7:	0.715,	152.9	0.652,	38.4	0.653,	38.3	0.731,	104.6
8:	0.772,	-106.2	0.600,	38.2	0.601,	38.2	0.776,	2.4
9:	0.782,	-51.2	0.590,	38.4	0.590,	38.4	0.787,	-52.4
10:	0.770,	-7.8	0.601,	38.4	0.601,	38.4	0.777,	-95.5
11:	0.780,	66.1	0.582,	34.2	0.582,	34.1	0.777,	-176.9
12:	0.737,	113.5	0.639,	37.1	0.640,	36.9	0.724,	141.6

Table 2. RF resetability

The MTS Operation

The MTS operation consists of 3 steps: **1.-Calibration, 2.-Measurement and 3.-Data Processing.** In case of **Amplifier Design** this is then a 4th step.

Calibration

All passive components of the Load Pull (or Noise) measurement system have to be pre-characterized (calibrated) using an automatic network analyzer. This includes the tuners (once every couple of months), isolators, bias tees, cables, attenuators and test fixture (calibration only once).

Test fixture calibration consists of using TRL standards to generate S-parameters of both fixture's halves using MTS's software. All calibration data are saved on harddisk files and are reusable at any time or transferrable to another computer. This allows maximum flexibility and mobility of the system.

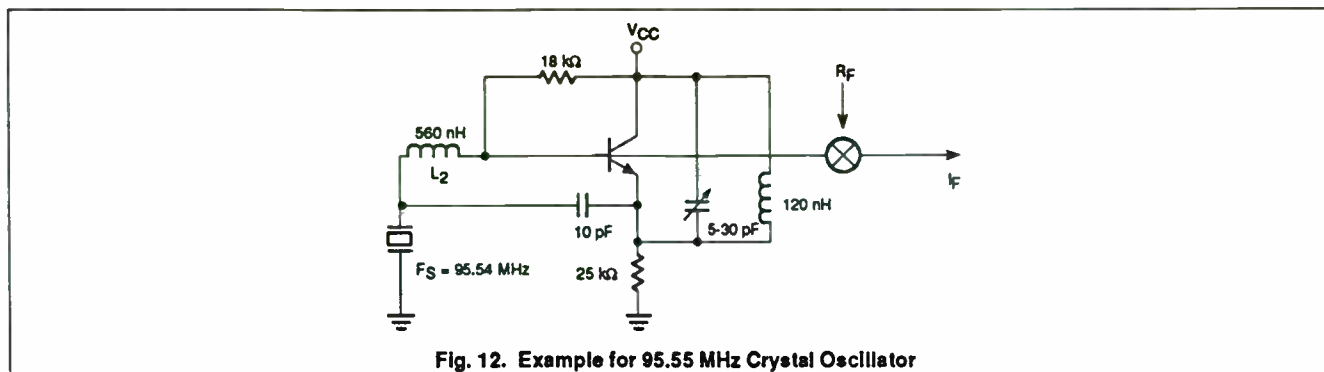
Measurement

Once the DUT is inserted in the test fixture, the MTS software controls bias and signal source power and frequency to perform a multitude of automatic or manual measurements.

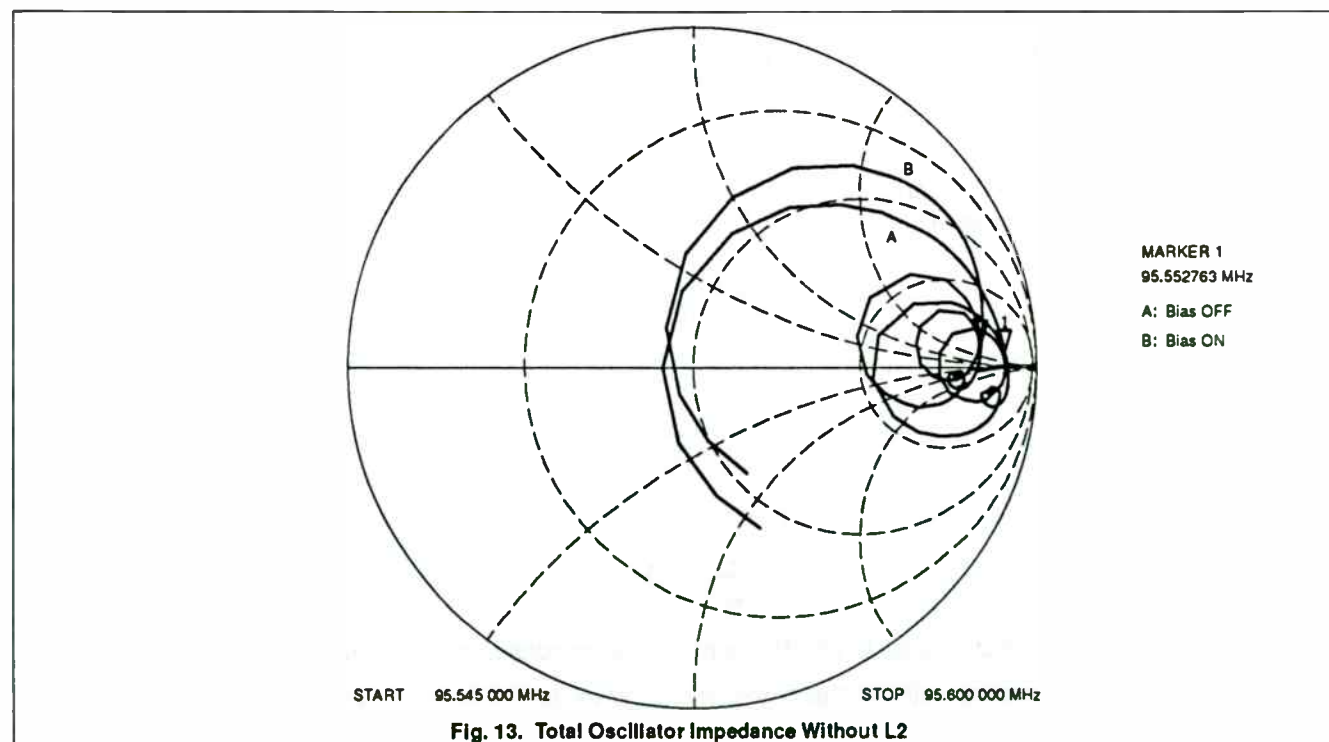
The **Setup** data are loaded automatically and the User has the choice of different reference planes to perform the measurement.

This makes it easy to evaluate the effect of different test fixtures on the device's performance or either study the effect of different device packages.

The final finished part using the Philips Semiconductors NE605 as the active device is shown in Fig. 12, which operates at a scant 0.2 mA current by default.



As confirmation, the same oscillator is tested with and without the added inductor L2 while the DC power is turned on and off. In Fig. 13 we can see that the effect of Y_C is quite inductive and almost pushes the trace along the constant conductance circle and only generates 70 mV_{RMS} at the emitter after the alignment. The output voltage can be increased to 220 mV_{RMS}, however, if the bias current is raised from 0.2 mA to 1 mA. On the other hand, in Fig. 14 the trace was pushed along the real axis to the negative resistance region and reaches 220 mV_{RMS} at the emitter after the alignment. The base voltage is about 300 mV_{RMS} in this case, which is consistent with the values of C_1 , $\cos \alpha$ and C_2 . Moreover, the tuning sensitivity in Fig. 13 is so high that only a narrow range of capacitance for C_2 can make the circuit oscillate, while the circuit from Fig. 14 is so flexible that the output voltage only changes gracefully if the capacitance for C_2 is varied over a broad range. This is fully expected because if the circuit oscillates, the frequency is always close to F_S for a crystal oscillator. So the value of L_{eq} in Eq. (10) must be self-adjusted to nullify L_C from Eq. (12), which can be out of the range if L_C and C_2 already resonate much above F_S . In another experiment, the value of C_1 was increased gradually and the oscillation stopped when C_1 exceeded the limit, 28 pF, set by Eq. (21).



The tuners are **moved manually** either using the PC's cursors or by direct tuning with the mouse and phase and amplitude corrected measurements are made via the GPIB connected and preselected instruments. The results of manual measurements are saved on ASCII (printable) files on the harddisk.

In **automatic measurements** the User can preselect a number of key settings and parameters and to perform either automatic search for an optimum (minimum Noise Figure or maximum Power for example). Or he can scan the complete Smith Chart with the tuners and generate binary Load Pull Data files which are used by the graphics software to generate ISO Contours (of Power, Gain, Efficiency or Intermod).

In case of **risk of oscillations** the User has the option to generate an **Impedance Pattern** on the Smith Chart using mouse tuning, save it on a harddisk file, and measure only along the points of this pattern. This pattern can be retrieved voluntarily, modified and resaved. Since the points are saved in Impedance (and not in tuner position) from this pattern file will generate the same impedance setup at all frequencies, independently of the actual calibration. This is important and deliberates the User from the worry to know before the tuner calibration which points he will need to measure later on.

Many power (and low noise) transistors have **very low input impedance** in the order of 1 to 2 Ω . Whereas the optimum noise reflection factor can be computed from measurements in other areas of the Smith Chart (due to the linearity of noise behaviour), in the case of power load (or source) pull the device has to be really presented the required impedance in order to show its behaviour. If a variable tuner generates such low impedances, ie. almost a short circuit, then the overall measurement accuracy will be unacceptable, this including the calibration accuracy of the automatic network analyzer.

The simplest and safest way around this measurement problem is the use of microstrip transformers. The simplest transformers are $\lambda/4$ sections of microstrip line which permit load impedances down to 0.5 Ω very easily. The bandwidth is reduced indeed, but this can be cured by using multisectional transformers. Frequency ratios of as much as 3:1 can be covered using 4 sections. It is important to realize that even the smallest transformed impedance is not exactly the same as the Z_{in} the tuner will find it in the area any how. Using an ordinary single section microstrip transforming network we were able to generate

impedances as low as 0.7 Ω using the MTS-308 (figure 4) with very good measurement accuracy.

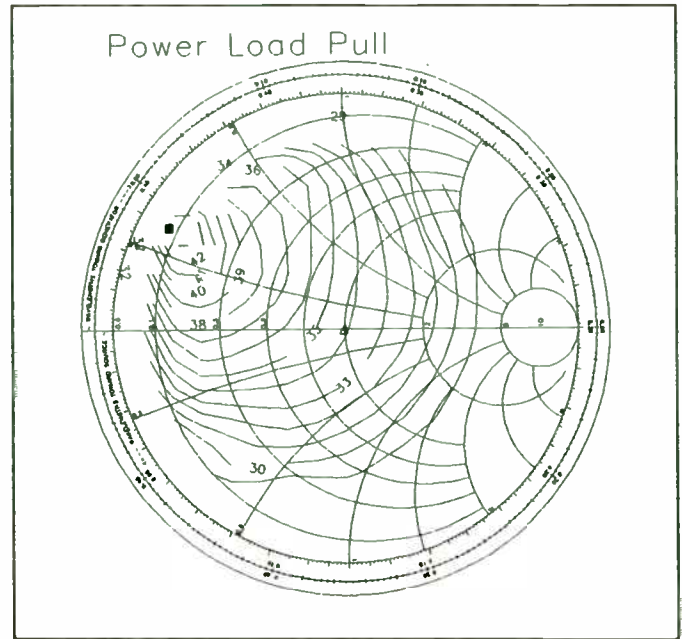


Figure 4. Load Pull using $\lambda/4$ transformers, $\Gamma_{opt} \approx 0.9$

Data Processing

The load pull files and the saturation (power transfer) files generated by the MTS software can be processed to plots:

- The load pull data files to ISO Power, Gain, Efficiency or Intermod contours (figures 5,6)
- The power transfer files to XY-plots (figure 7)

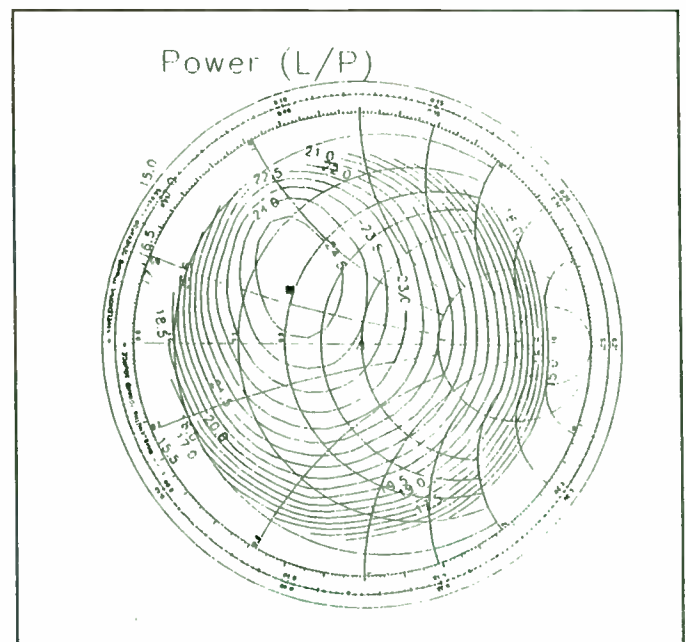
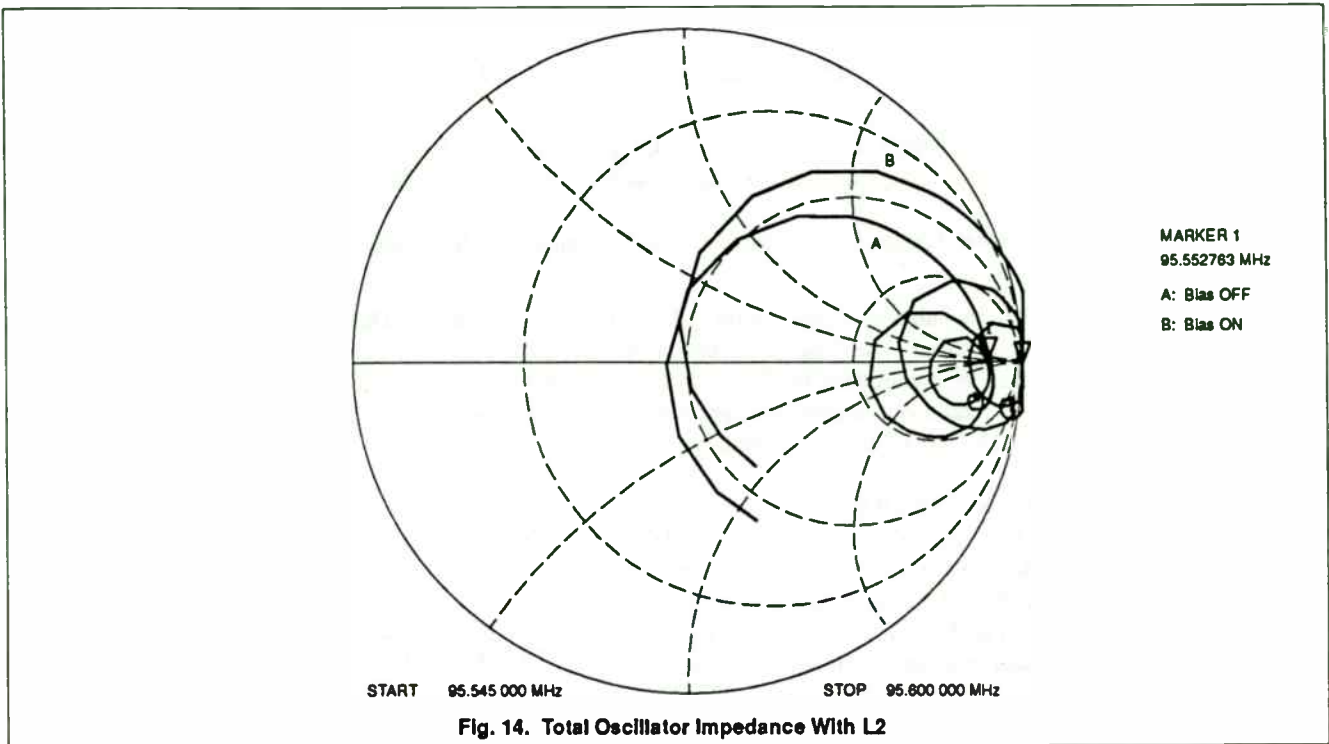


Figure 5. Load Pull in 50 Ω system, $\Gamma_{opt} \approx 0.56$



IV. CONCLUSIONS

In conclusion, an elegant solution is proposed by inserting an inductor in the base of the device for the classic Colpitts oscillator. This extends the margin for oscillation at frequencies above 60 MHz without resorting to the customary solution of increasing the bias current. The result is an oscillator which easily achieves strong output power, at the same time affording 80% current savings. This leads to longer battery life and lower production cost for the portable set.

V. ACKNOWLEDGEMENTS

The authors are grateful to Dr. Saeed Navid and Will Dresser for their enthusiastic technical input and support.

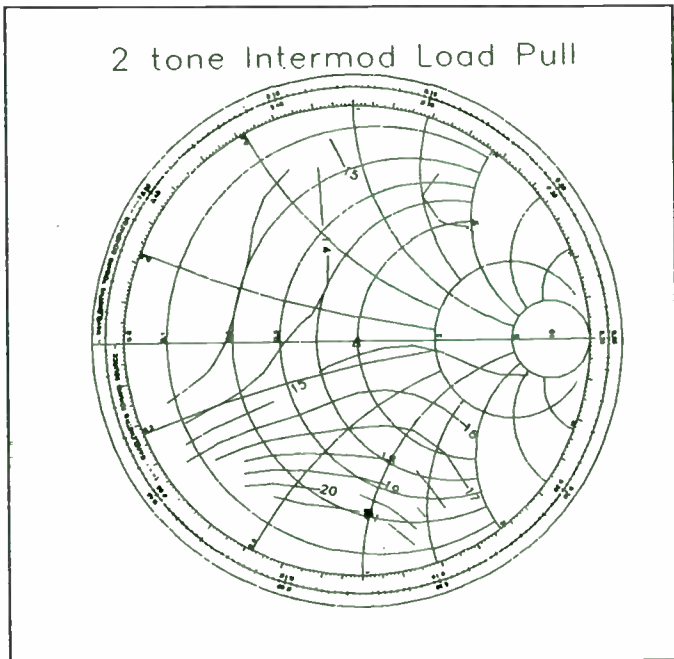


Figure 6. Intermod Load Pull

JDC spectral performance and higher order Intermod data can also be processed to ISO contours. Using these plots the Design Engineer can synthesize a matching network that will generate the required performance. Overlapping different graphs, measured under the same conditions will also permit to make the best compromise in design between conflicting requirements.

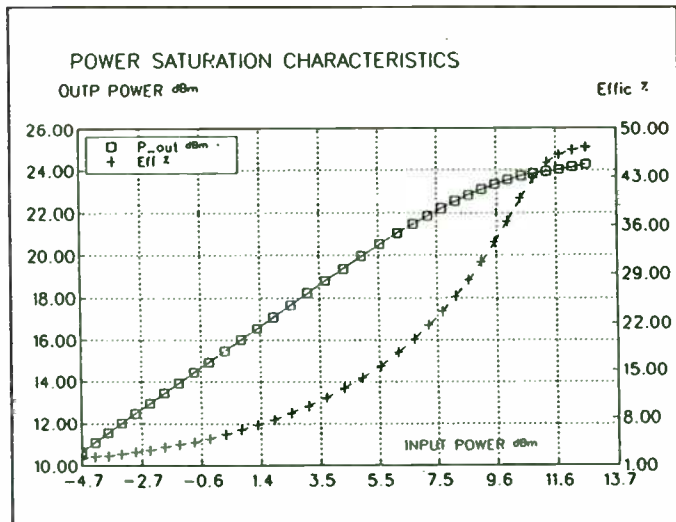


Figure 7. Power Transfer (Saturation)

JDC or Adjacent-Channel Leakage Load Pull

This test method has been developed in conjunction with our customers in the Digital Cellular Telecommunications business. It permits to optimize the performance of transceivers by measuring the

ratio of the carrier-wave power integral to the integral of the power leaked within the upper (or lower) adjacent-channel bandwidth (figure 8).

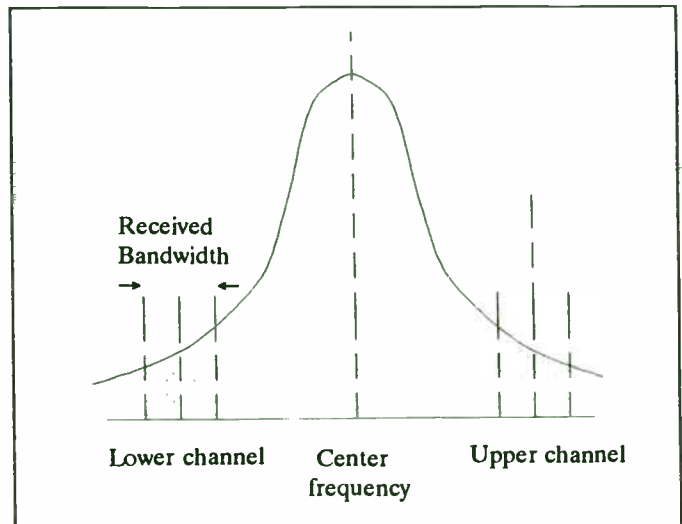


Figure 8. Adjacent channel leakage measurement

The MTS includes two types of measurement methods for this test:

- **Auto:** The MTS uses 'built in' software routines in the spectrum analyzers themselves, like the Advantest R3271 or Anritsu MS2602A and processes the final results as delivered by the analyzer. The only parameter settable by the MTS software in this case is the center frequency. The analyzer measures automatically the adjacent-channel power at preset conditions, in general at 50 and 100 kHz below and above the carrier.
- **Custom:** The MTS uses any type of spectrum analyzer, even those who do not support the JDC test method, and a MTS custom software that permits to set markers, sample the channel power at distinct windows and integrate signal power in order to generate equivalent results. In this case the User has control over the following parameters of the measurement procedure

JDC Test Parameter	Default Value
- Center frequency	Tuner Frequency
- Sideband 1 Offset	50 kHz
- Sideband 2 Offset	100 kHz
- Frequency Step between Samples	1 kHz
- Number of Samples (per sideband)	5
- Averaging Factor	2
- Settling Sweeps (before sample)	1

Table 3. Measurement Parameter settings for JDC Load Pull Test

A 2.2 GHz PLL Frequency Synthesizer

Thom Luich, Thai Nguyen, Craig Davis, David Byrd,
Eric Lindgren, Rob Rodriguez, Maggie Speers and Eli Miller

National Semiconductor, Santa Clara, California, U.S.A., 95052-8090

Abstract - A 2.2 GHz monolithic integrated circuit PLL frequency synthesizer for DECT cordless, PCN, WPABX, and WLAN applications is described. The low power circuit operates at 2.7v and 12mA with standby currents of less than 100 μ A. The chip features a selectable 64/65 or 128/129 dual-modulus prescaler, an internally regulated charge pump with tristate capability, and a microcontroller compatible serial data interface. The circuit is fabricated on a 0.8 μ m BiCMOS process with 15 GHz ft bipolar transistors.

I. INTRODUCTION

PLL frequency synthesizers are used prevalently today as electronic tuners in radios, TVs, and phone systems. These synthesizers, as shown in Fig. 1, take a stable reference signal (crystal oscillator) and in conjunction with an external Voltage Controlled Oscillator (VCO) generate local oscillator (L.O.) signals using phase locked loop techniques [1]. The integrated synthesizer being reported in this paper is particularly well suited for battery applications at 2 GHz because of its low phase noise, low power, and low spurious attributes. Though not the lowest power solution to date at this frequency [2], this device represents a higher level of integration and performance than previously available.

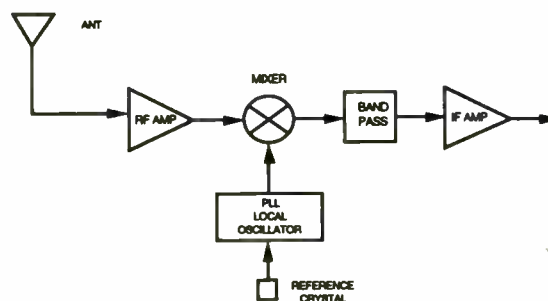


Fig. 1: System Diagram

II. PROCESS DESCRIPTION

This device was fabricated using National Semiconductor's ABIC IV (BiCMOS) process. This process features a 15 GHz ft, .8 μ feature sizes, and tungsten plug contacts and resistors. The design utilizes two of the process's four available metal layers and one silicided poly layer. A profile of the process is shown in Fig. 2. The minimum MOS gate and NPN emitter sizes are 1.2 x .8 μ m and 1.6 x .8 μ m respectively. The metal pitch is 2.5 μ m and the 1 μ m contacts and vias may be concentrically stacked.

III. CIRCUIT DESCRIPTION

A simplified block diagram of the PLL synthesizer is shown in Fig. 3. It is comprised of a 14 bit reference frequency (R) divider, an 18 bit dual modulus high frequency (N) divider, a serial control register for loading the two counters, and a phase comparator / charge pump block. An external VCO is also used in conjunction with the synthesizer blocks to close the feedback loop.

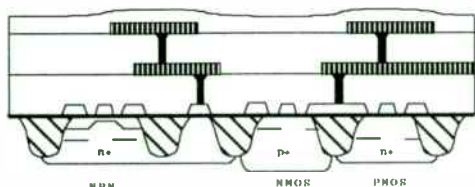


Fig. 2: Process Profile

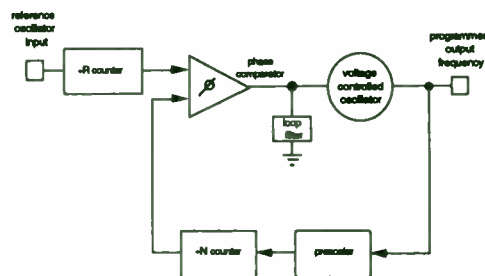


Fig. 3: Synthesizer Logic Diagram

Figure 9 shows an example of JDC contour tests made using the MTS custom test software and an HP-8562 spectrum analyzer.

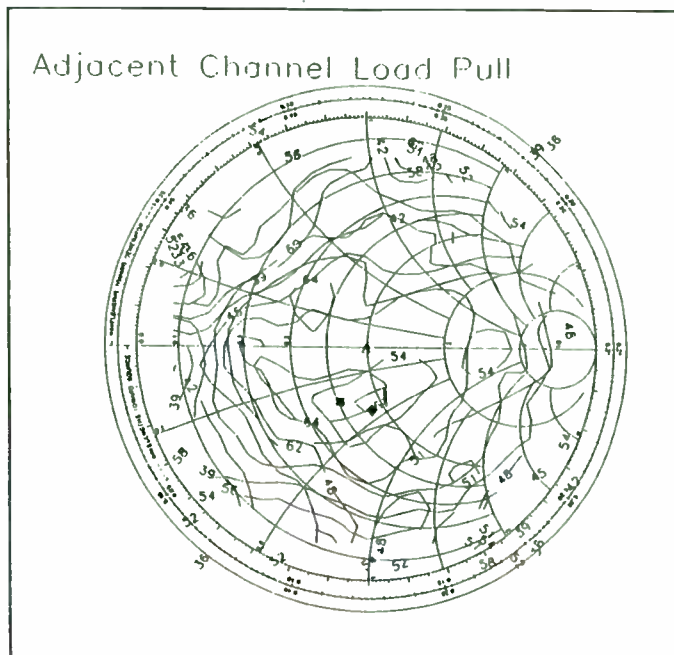


Figure 9. ISO contours of Adjacent channel leakage at 50 and 100 kHz sidebands

RF Power Amplifier Design

The MTS provides (as an option) a method to generate ISO power or Efficiency contour data compatible with Focus Microwave's network simulator **rf-PADS**, which can rapidly and accurately optimize high power and wideband amplifier stages, using power contour data only.

For this approach the User does not need to know more about the transistor than the external measurement conditions and have access to a set of small signal S-parameters, which are used to estimate only output-to-input feedback. All other optimization values, such as large signal input impedance and output power are generated directly by **numerical interpolation of power data**, measured using the MTS hard and software at rated power level. Figure 10 shows the principle of operation of **rf-PADS**.

The impedance conditions at the input are very important and they are an integral part of the data. This is also one of the main difficulties encountered by Engineers who try to design (approximately) power amplifiers using S-parameters.

In order to execute **rf-PADS**, only requires:

- the external program RF-PADS.EXE
- the Data Conversion program CNTDAT.EXE which generates ISO-power or ISO-efficiency files

from premeasured Load Pull data files.

No other hardware or software components are required to use this option of MTS.

Rf-PADS includes lossy microstrip transmission line models, together with basic circuit elements such as capacitors, inductors and resistors. For the frequencies covered by MTS these elements are sufficient to design single stage power amplifiers.

Rf-PADS uses familiar .CKT type nodal network description as most other simulators. Due to the direct processing of measured data and second order interpolation techniques **rf-PADS** delivers **excellent accuracies** for even **saturated amplifier** stages.

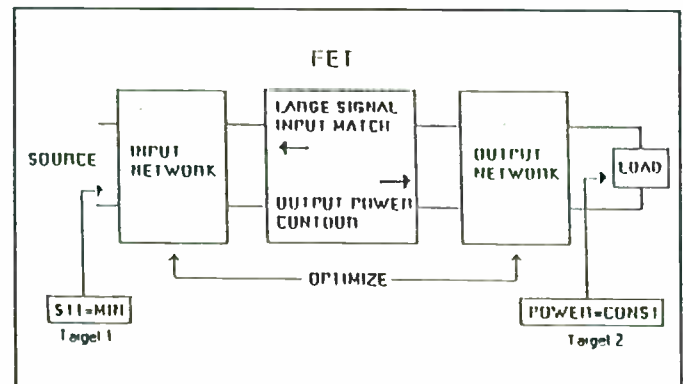


Figure 10. Principle of operation of **rf-PADS**

Power Amplifier Design procedure:

Rf-PADS uses a window type interface including a file editor.

- Step 1: Measure Load Pull data in a frequency range at prematched input conditions.
- Step 2: Convert the load pull data to **rf-PADS** contour files.
- Step 3: Generate a nodal description of a possible input and output matching network and set target performance.
- Step 4: Load the contour data into the circuit file and optimize the network parameters.

Due to direct data processing matching networks for constant output power and optimum input reflection can in general be found within minutes, using a normal -386 or -486 PC.

Figures 11-12 and table 4 show some results of high power amplifier designs together with the obtained design accuracy.

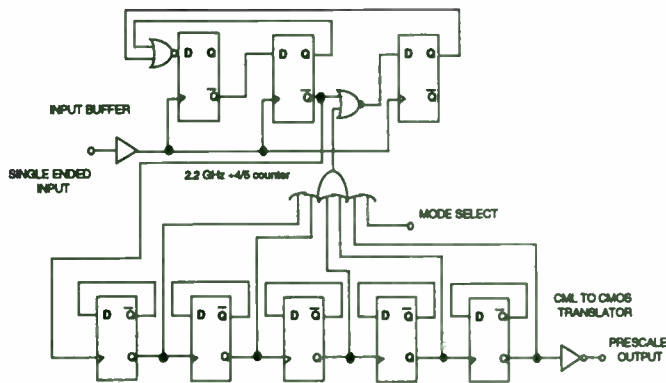


Fig. 4: Prescaler Frontend

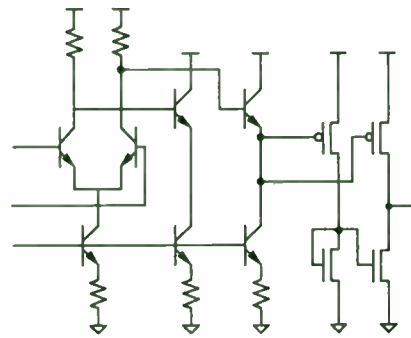


Fig. 5: CML to CMOS Translator

Device operation is attained by first dividing the frequency of a reference signal down to the desired tuning resolution of the system. This tuning resolution is usually some divisible fraction of the spacing between radio channels. The phase comparator drives the frequency of the external VCO in the direction which when divided down by the N counter equals the stepping resolution established by the R counter. The phase comparator accomplishes this by detecting the arrival of phase edges from the two counters and issuing a correction signal to the VCO which is proportional to the difference in their phases. When the phase and frequencies of the two counters outputs' agree, the frequency of the VCO will be the selected N modulus multiple of the tuning resolution.

The R counter is implemented entirely in CMOS and is composed of ripple toggle flip flops drawing less than .5mA at 30MHz. The dual modulus N counter is implemented using a selectable bipolar 64/65 or 128/129 prescaler followed by 18 CMOS counter bits [3]. The frontend of the CML prescaler, shown in Fig. 4, consists of a 4/5 divider block followed by 5 toggle CML flip flops and a CML to CMOS translator (Fig. 5). Ninety-five percent of the device's 12 mA typical current budget is consumed in the prescaler as shown in Fig. 6. The current in this block is held constant over its 2.7v to 5.5v range by a bandgap voltage regulator. The 2.2 GHz input buffer provides a sensitivity range of -15 to +6 dBm. The attributes of the bipolar transistors utilized in the frontend are listed in Fig. 7. The device geometries shown in Fig. 8 have emitter areas of 2.56 square microns and are double base stripped.

Block	(μ A)
Bandgap	300
CML Toggles	150
Translator	200
OR gate	200
Input Bias	150
4/5 Counter	5300
Input Buffer	4300
CMOS logic	500
Total	12000 μA

Fig. 6: Current Distribution

Parameter	Value
f_T (150 μ A)	15 GHz
emitter area	0.8 x 1.6 μ m
Ccs	12 fF
Cbe	5.3 fF
Cbc	10 fF
re	100 Ω

Fig. 7: Device Attributes

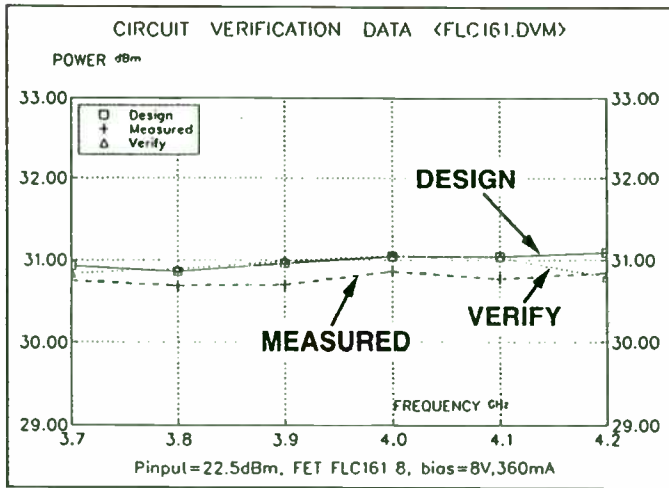


Figure 11. Comparison: Design - Measurement, Courtesy of CNET

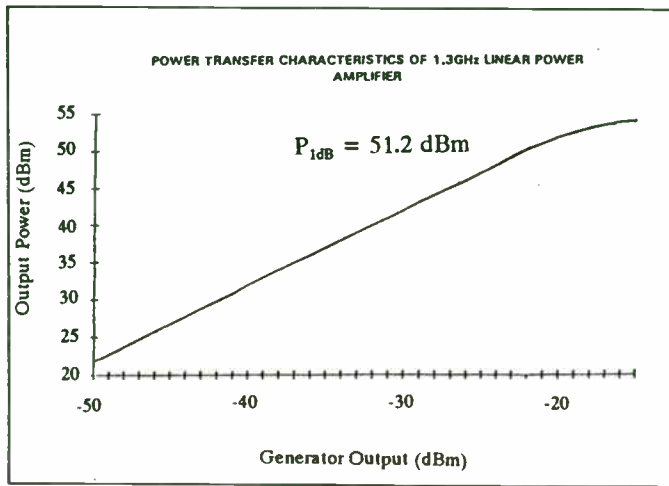


Figure 12. Pout(Pin) of High Power amplifier, Courtesy of ITS Electronics

Performance of 3.7 - 4.2 GHz Power Amplifier
FET FLC161WF (Fujitsu) Bias 8V, 360 mA
Input power 22.5dBm

GHz	Output Power dBm		Deviation dB	Gain dB	
	Design	Measure		Design	Measure
3.7	30.93	30.83	0.10	8.43	8.33
3.8	30.86	30.83	0.03	8.36	8.33
3.9	30.96	30.81	0.15	8.46	8.31
4.0	31.04	30.84	0.20	8.54	8.34
4.1	31.04	30.87	0.17	8.54	8.37
4.2	31.09	30.94	0.15	8.59	8.44

Table 4. Comparison: Design - Measurement

Conclusion

The Microwave Tuner System (MTS) of Focus Microwaves has been designed to respond to the key requirements of Test and Design Engineers in the PCN (Cellular Telecommunications) sector around 800 MHz to 3 GHz (optional to 4.2GHz).

These cover

- Accuracy (≈ 50 dB)
- Low Cost (1/3 of other systems)
- Versatility (Power - Intermod - Noise; auto and manual)
- Design Capability (0.2 dB accurate using power contours)

all integrated in an easy to calibrate and operate measurement and design workstation that can be setup around an IBM-PC and most popular GPIB instruments.

Acknowledgements

Many of the results and the measuring techniques used in the MTS software have been suggested or provided by our customers. We very much appreciate their support and contribution.



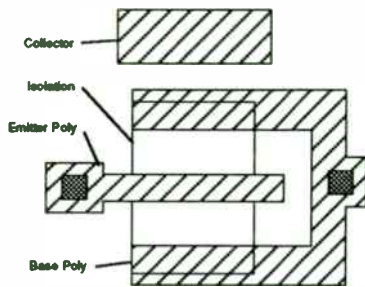


Fig. 8: Bipolar Geometry

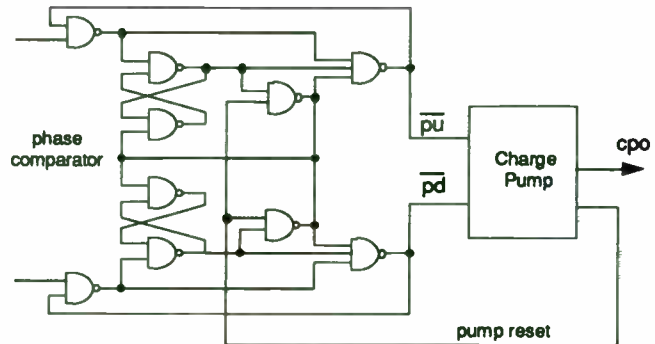


Fig. 9: Phase Comparator Reset Logic

The type-4 digital phase comparator /charge pump block incorporates two features which contribute to its low phase noise and spurious characteristics [4,5]. The first is a deadband elimination circuit, shown in Fig. 9, which ensures that a charge pump dead zone cannot occur near zero phase offset [6]. This technique guarantees that the charge pump generators have in fact responded to the phase comparator before allowing the phase comparator reset logic to activate. Phase comparator deadband is one of the primary sources of jitter in phase locked loops of this type.

The second charge pump feature minimizes reference frequency spurs. Similarity in the current generating structures for the pump up and down circuits ensure that the magnitudes of the pump up and down current sources and the turn on and off times are matched. This matching minimizes the momentary pump up or down excursions on the charge pump line which contribute to VCO FMing at the reference rate. The deadband elimination circuitry inherently also ensures that reference frequency sideband spurs are minimized. The charge pump feedback signals allow the generators on only long enough to eliminate potential deadband yet not contribute any excess active pump time. Excess pump time adds directly to the up or down excursions on the charge pump line by the amount the absolute magnitudes of the current generators differ.

IV. DIE DESCRIPTION

The die is composed of approximately 35% bipolar and 65% CMOS devices. The die photograph of Fig. 10 shows the three major functional blocks from left to right; the counters, the phase comparator / charge pump, and the prescaler. Three separate power supply buses were utilized in the design to minimize noise and jitter. The input and output buffers and ESD clamps were contained to one power bus, the CMOS logic to a second bus, and the prescaler block to the third. These precautions also helped to ensure that the VCO input sensitivity was not degraded by either output buffer or internal CMOS rail to rail logic switching spikes.

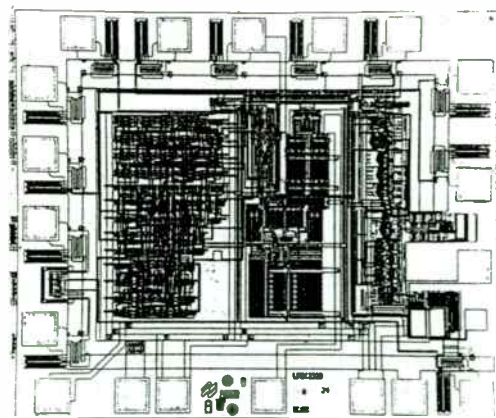


Fig. 10: Die Photograph

Noise Figure and Gain Measurement on High Speed

Bipolar Junction Transistors

Wayne Jung

Tektronix Component Corporation, P.O. Box 500, M/S 59-355, Beaverton, OR 97077

Paul Van Halen

Portland State University, P.O. Box 751, EE Department, Portland, OR 97207

INTRODUCTION

It is a fact that no electronic system is completely free of random noise. Small voltage fluctuations due to noise are always occurring in electronic circuits because electrons are discrete and are constantly moving in time. The term "noise" originated with the study of high-gain audio-frequency amplifiers. When a fluctuating voltage or current generated in a device is amplified by an audio-frequency amplifier and the amplified signal is fed into a loudspeaker, the loudspeaker produces a hissing sound, hence the name noise. This descriptive term, noise, now refers to any spontaneous fluctuation in a system, regardless of whether an audible sound is produced.

Noise obscures low level electrical signals, therefore it can be a limiting factor on component and system performance. In a spectrum analyzer, for example, noise limits the sensitivity of the instrument--that is, the lowest-amplitude signal that the analyzer can detect and display. In a radar system, noise can obscure returns from a target, and limit the effective range of the radar. In digital communications, excessive noise can cause a high Bit-Error-Rate, resulting in the transmission and reception of false information.

This analysis studies the noise and gain characteristics of the basic component in an amplifier block, the transistor, in the microwave frequency range. After identifying the noise sources in the transistor, the effect of each noise source on the performance of the device is discussed. This study will provide spot noise figure and gain data for two high speed silicon bipolar transistors manufactured on two processes from Tektronix Microelectronic (SHPi and GST-1). SHPi is Tektronix' latest generation Super-High frequency bipolar processes. The f_T of the transistor of interest (N16) of this process is measured to be close to 9GHz under the condition: $I_C = 9mA$ and $V_{CE} = 4V$. GST-1 (Giga-Speed Si-Bipolar Technology) is a high speed self-aligned double-polysilicon process. GST-1 is designed for the purpose of building high density, high performance circuits. The f_T for the G14V102, an N16 equivalent in the GST-1 process, is in the proximity of 12GHz with $I_C = 25mA$ and $V_{CE} = 4V$.

BASIC CONCEPTS

The measurement techniques used at microwave frequencies are different compared with low frequency methods. At lower frequencies, the properties of a circuit or system are determined by measuring voltages and currents. This approach is not applicable to microwave circuits since oftentimes these quantities are not uniquely defined. As a result, most microwave experimentation involves the accurate measurement of impedance and power rather than voltage and current.

S-PARAMETERS

Introduction

Linear networks can be completely characterized by parameters measured at the network terminals without regard to the contents of the network. Once the parameters of a network have been determined, its behavior in any external environment can be predicted, again without regard to the specific contents of the network.

A two-port device can be described by a number of parameter sets. Hybrid, admittance, and impedance parameters sets are often used at low frequency analysis. Moving to higher frequencies, some problems arise:

1. Equipment is not readily available to measure total voltage and total current at the ports of the network. The voltage measured will not be the same as the voltage at the ports of the network if the length of the transmission line is comparable with the wavelength of the test signal.
2. Active devices, such as transistors, very often will not be short or open circuit stable.
3. Parasitics in active devices may cause unwanted oscillations.

Some other sets of parameters are necessary to overcome these problems. Hence, dissipating (resistive) loads are used in measurements to minimize parasitic oscillations. In addition, the concept of traveling waves rather than total voltages and currents is used to describe the networks. Voltage, current, and

V. SYSTEM MEASUREMENTS

Phase noise measurements were taken of the 3 volt system at 1890 MHz with a 1.728 MHz reference frequency. The loop filter parameters were selected to be appropriate for DECT (Digital European Cordless Telecommunications) type systems with a lock time target of 80 μ secs. A -77dBc/Hz phase noise measurement at 10KHz (-120dBc/Hz at 1MHz) is shown in Fig. 11. The phase noise performance degraded approximately 7 db at +85 degrees C.

The reference frequency spurs are apparent in Fig. 12 down -68dB from the 1890 MHz carrier. (a 2nd order loop filter was used with a 12 KHz cutoff frequency.) A small degradation in reference spurs was observed as the supply voltage was increased.

A power dissipation curve is shown in Fig. 13. The internal bandgap regulator controls the variation in current to .9 mA over the -40 to +85 degrees C range (at 3v) and limits the variation over the 2.7v to 5.5v supply range at any given temperature to .8 mA.

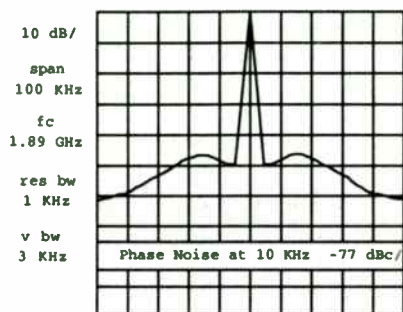


Fig. 11: Phase Noise

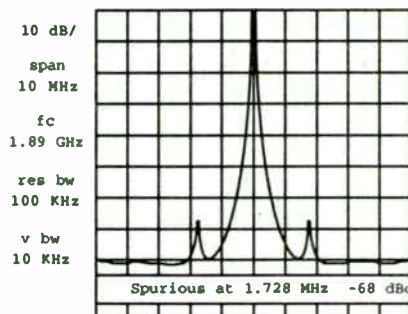


Fig. 12: Spurious

VI. CONCLUSIONS

A fully integrated silicon BiCMOS PLL frequency synthesizer function has been accomplished with performance characteristics suitable for DECT 2.2 GHz, low power, 3 volt cordless applications. The device exhibits phase noise of -77dBc/Hz at 10KHz from 1890 MHz, with the reference frequency spurs down -68dBc at 1.728MHz. In addition, an input sensitivity of less than -15 dBm was attained at 2.2 GHz while consuming less than 35mW of power.

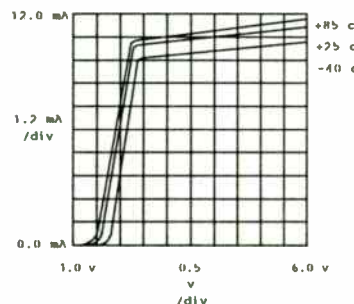


Fig. 13: Icc vs. Vcc

REFERENCES

- [1] John Hatchett, "Adding to PLL Chips' Functions Speeds RF Synthesizer Design", Electronics, pp. 148-154, Oct. 9, 1980.
- [2] Moriaki Mizuno..., "A 3 mW 1.0 GHz Silicon ECL Dual Modulus Prescaler IC", IEEE Journal of Solid-State Circuits, vol. 27, No. 12, pp. 1794-1798, Dec. 1992.
- [3] Floyd M. Gardner, "Phaselock Techniques" Wiley & Sons Inc., p. 78, 1966.
- [4] Dr. Roland E. Best, "Phase-Locked Loops, Theory, Design, & Applications" McGraw-Hill Inc., pp. 7-14, 1984.
- [5] Mark O'Leary, "Practical approach Augurs PLL noise in RF synthesizers", Microwaves & RF, pp. 185-194, Sept. 1987.
- [6] D. Byrd, G. Tietz, C. Davis, "Guaranteed Zero Deadband Phase Comparator / Charge Pump with Minimized Phase Offset", U.S. patent #4,814,726 1989.

power can be considered to be in the form of waves traveling in both directions along a transmission line (Fig. 1). A portion of the waves incident on the load will be reflected if the load impedance Z_l is not equal to the characteristic impedance of the transmission line Z_o . This is analogous to the concept of maximum power transfer. A source will deliver maximum power to a load (no reflection from the load) if the load impedance is equal to the source impedance.

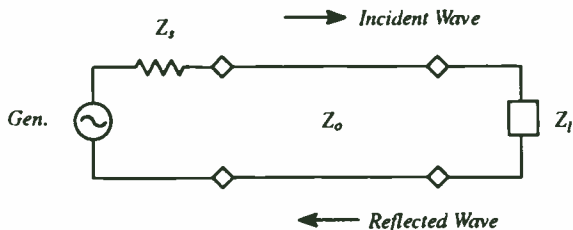


Figure 1. Traveling waves.

Reflection Coefficients

The reflection coefficient Eq. (1) is a mathematical representation of the reflected voltage wave with respect to the incident voltage wave at a specified port of a circuit.

$$\Gamma = \frac{\text{Reflected Wave}}{\text{Incident Wave}} \quad (1)$$

Eq. (2) defines the load reflection coefficient in terms of the load impedance referenced to the characteristic impedance of the transmission line.

$$\Gamma_l = \frac{Z_l - Z_o}{Z_l + Z_o} \quad (2)$$

And similarly the source reflection coefficient is

$$\Gamma_s = \frac{Z_s - Z_o}{Z_s + Z_o} \quad (3)$$

It is well known that maximum power transfer occurs when the impedance of the source matches the impedance of the load. For $\Gamma = 0$, maximum power transfer occurs, and Γ equals unity when there is no power transfer since then all the incident power is reflected back.

S-parameters

For a two-port network shown in Fig. 2, the following new variables are defined [1]:

$$\begin{aligned} a_1 &= \frac{E_{i1}}{\sqrt{Z_o}} & a_2 &= \frac{E_{i2}}{\sqrt{Z_o}} \\ b_1 &= \frac{E_{r1}}{\sqrt{Z_o}} & b_2 &= \frac{E_{r2}}{\sqrt{Z_o}} \end{aligned}$$

where E_i and E_r are the incident voltage wave and reflected voltage wave respectively. Notice that the square of the magnitude of these new variables has the dimension of power.

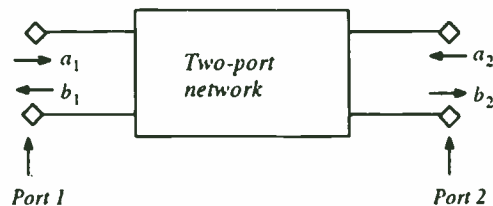


Figure 2. Incident and reflected waves in a two-port network.

By measuring incident and reflected power from a two-port network, we avoid the primary problem in microwave measurement, which is the voltage variation along the transmission line between the device under test and the test equipment. A new set of parameters relate these four waves in the following fashion:

$$\begin{aligned} b_1 &= S_{11}a_1 + S_{12}a_2 \\ b_2 &= S_{21}a_1 + S_{22}a_2 \end{aligned}$$

where

$$\begin{aligned} S_{11} &= \left. \frac{b_1}{a_1} \right|_{a_2=0} && \text{input reflection coefficient with the output matched} \\ S_{21} &= \left. \frac{b_2}{a_1} \right|_{a_2=0} && \text{forward transmission coefficient with the output matched} \\ S_{22} &= \left. \frac{b_2}{a_2} \right|_{a_1=0} && \text{output reflection coefficient with the input matched} \\ S_{12} &= \left. \frac{b_1}{a_2} \right|_{a_1=0} && \text{reverse transmission coefficient with the input matched} \end{aligned}$$

This set of new parameters is called "scattering parameters," since they relate those waves scattered or reflected from the network to those waves incident upon the network. These scattering parameters are commonly referred to as s-parameters.

Although s-parameters completely characterize a linear network, sources and loads need to be attached before the network can be used. The new input reflection coefficient Γ_{in} and the new output reflection coefficient Γ_{out} take the form [2]:

$$\Gamma_{in} = S_{11} + \frac{S_{12}S_{21}\Gamma_l}{1 - S_{22}\Gamma_l} \quad (4)$$

and

$$\Gamma_{out} = S_{22} + \frac{S_{12}S_{21}\Gamma_s}{1 - S_{11}\Gamma_s} \quad (5)$$

The second terms in the above equations show the interaction between the two ports. If S_{12} is equal to zero, the two-port network is called unilateral because whatever happens to one port does not affect the other port.

For a bilateral linear two-port network, the input reflection coefficient is not just function of S_{11} . It is a function of Γ_l as well. Therefore, the effect of the load must be considered when

A 3 VOLT ANALOG AUDIO PROCESSING CHIP SET FOR BATTERY OPERATED SYSTEMS

Omar Saleh and Saeed Navid, Philips Semiconductors

Abstract — An analog audio processing chip set which implements companding and audio filtering in two ICs has been developed. In order to maximize performance the compandor chip is designed in bipolar technology and the audio filtering is implemented in CMOS. The ICs use 3V supply, draw low current, and are packaged in 20-pin SSOP (Shrink Small Outline Package) which make them attractive for portable battery operated systems.

I. INTRODUCTION

The recent trend in the electronics manufacturing industry is to produce low power, high performance technologies to support the design and development of personal information and communication terminals. Particularly in the Electronic Data Processing and Telecom markets these technologies have produced low power, highly integrated, and small packaged ICs which have been used to design numerous transportable, and hand-held systems with an ever smaller size and light weight.

Analog audio processing is one of the major building blocks for a number of wired and wireless telecommunication systems. The performance of the audio block, its size, and its power consumption are critical to the success of the final product. This article introduces a 2-chip analog audio processing subsystem consisting of Companding (Compressor/Expander), and audio filtering. This chip set is low power, highly integrated, and can be used in cellular and cordless telephones.

II. FEATURES AND FUNCTIONALITY

The criteria for processing audio signals depend largely on the medium in which they are transponded. Typically the medium provides a limited dynamic range channel which is less than that needed by the audio signal to be transmitted and received without loss in fidelity. In FM systems, such as cellular, this dynamic range translates to a maximum deviation from center frequency (± 12 kHz for Cellular) before the carrier spills over to the adjacent channels. Also, the transmission medium introduces noise that is proportional to the square of the audio frequency, which is summed to the signal, and eventually heard by the receiving party. To meet these criteria we need key audio processing functions as follows: (1) Allow a wide dynamic range signal to be transmitted through a restricted dynamic range channel (30 kHz for cellular), (2) treat high frequency noise by maintaining a good signal to noise ratio (S/N), (3) maintain voice quality in the presence of noise and distortion, and (4) restrict the signal level from increasing beyond a certain limit to prevent over modulation. This has been achieved with the introduction of companding, pre-/de-emphasis filtering, noise cancellation, and limiting circuitry, respectively.

This audio processing chip set, termed APROC2, implements these key functions in two ICs, the SA5752 for companding and noise cancellation, and the SA5753 for pre-/de-emphasis filtering and limiting. The audio functions have been partitioned between two chips in order to maximize performance, yet maintain enough features in each chip to be utilized individually in the system. Together the SA5752 and SA5753 make up a complete analog audio processing sub-system, from microphone input to modulating signal output, and from a demodulated signal input to audio signal output. In the transmit path, a voice signal produced by a microphone enters at the low noise programmable preamplifier, is band pass filtered, compressed to fit the channel's dynamic range, emphasized to maintain a good S/N for higher audio tones, and then limited and low pass filtered to produce an audio band signal suitable for FM modulation over the cellular network.

In the receive path the demodulated signal enters at the input of the audio band pass filter, and goes through the reverse process, i.e. de-emphasis and expansion. The resultant audio signal feeds an external audio amplifier (e.g. TDA7050) that drives a speaker or an earpiece. Fig. 1. shows the signal path inside APROC2 and the key functions that contribute to improving the S/N ratio and sensitivity of the system. The shaded blocks represent signal processing inside the SA5753.

an input match circuit is built to match the signal source. Also, Γ_{out} is a function of the s-parameters and Γ_{in} , and this should be kept in mind when an output matching network is built to have all the power delivered to the load.

Smith Chart

The Smith chart (Fig. 3) is a design and analysis tool that can provide insight into the impedance and reflection characteristics of a circuit. The chart is a graphical representation that provides a transformation between the complex reflection coefficient in a polar format to the real and imaginary parts of the impedance, Eq. (2) and Eq. (3). The chart has the property of being able to graphically display the entire range of real and imaginary values of input impedances of a network. Therefore, on a Smith chart a point simultaneously represents three different things. Depending on the coordinate system used as a reference, they are: reflection coefficient, impedance, and admittance. Impedance matching circuits can be easily and quickly designed using the Smith chart.

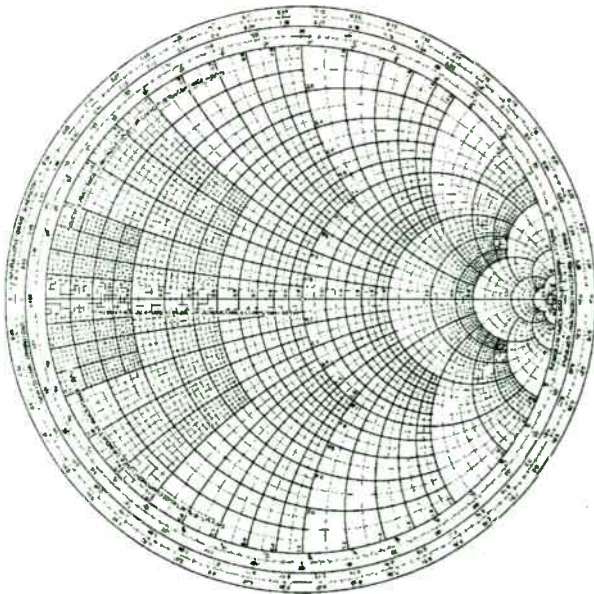


Figure 3. The Smith chart.

NOISE FIGURE

To compare the performance of high frequency devices, an important figure of merit is the noise factor/figure, which is a measure of how the thermal noise and the shot noise generated in semiconductors degrade the signal-to-noise ratio. The noise factor F of the network is defined as the ratio of the available signal-to-noise ratio at the signal generator terminals to the available signal-to-noise ratio at its output terminals.

$$F = \frac{S_i/N_i}{S_o/N_o} \quad (6)$$

The current definition for noise factor applies whether it is linear or logarithmic. The term "noise factor (F)" is used when referring to the ratio in linear terms. The term "noise figure (NF)" is used when referring to the ratio in logarithmic terms.

$$NF = 10 \log_{10} F \quad (7)$$

From the definition in Eq. (6) the ideal noise factor is unity or noise figure is 0dB, where there is no degradation in signal-to-noise ratio after the signal passes through the network.

Noise figure is a parameter that applies both to components and systems. The overall system performance can be predicted from the noise figure of the components that go into it. For a number of networks in cascade, as shown in Fig. 4, the system spot noise factor is given in terms of the component spot noise factors (F_i) and available gain (G_i) by

$$F = F_1 + \frac{F_2 - 1}{G_1} + \frac{F_3 - 1}{G_1 G_2} + \dots \quad (8)$$

From Eq. (8), the significance of the first stage gain and noise factor are evident. The first stage in the chain has the most significant contribution to the total noise factor of the chain. The total noise factor of the system is at least equal to the noise factor of the first stage. If the first stage gain is significantly large, then the noise contributions from the succeeding stages will be small.



Figure 4. Noise figure of network in cascade.

AVAILABLE POWER GAIN

A signal generator with an internal impedance R , ohms and output voltage V , volts can deliver $\frac{V^2 R_l}{(R_s + R_l)^2}$ watts into a

resistance of R_l ohms. This power is maximum and equal to $\frac{V_s^2}{4R_s}$ when the output circuit is matched to the generator impedance, that is when $R_l = R_s$. Therefore, $\frac{V_s^2}{4R_s}$ is called the available power of the generator, and it is, by definition, independent of the impedance of the circuit to which it is connected. The output power is smaller than the available power when R_l is not equal to R_s , since there is a mismatch loss. In amplifier input circuits a mismatch condition may be beneficial due to the fact that it may decrease the output noise more than the output signal. It is the presence of such mismatch conditions in amplifier input circuits that makes it desirable to use the term available power.

The symbol S_g will be used for the available signal power at the output terminals of the signal generator shown in Fig. 5. The

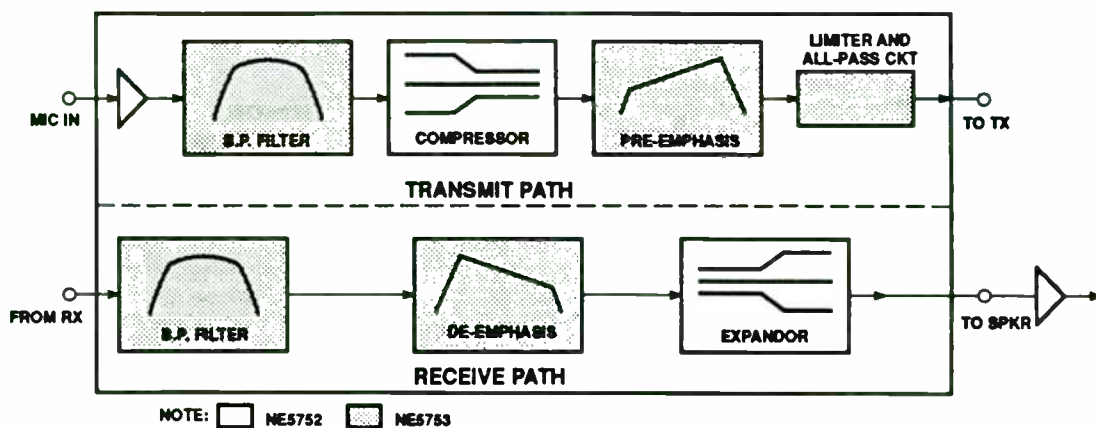


Figure 1. Key Functions of the SA5752 and SA5753 that Contribute to Improving the S/N Ratio and Sensitivity of the System.

A. Companding Chip

In the Tx path there is a 2:1 input to output compression translating to 1 dB of change in output level for every 2 dB change in input. In the Rx path, the expander circuit performs the inverse of the compressor, i.e., input to output expansion is 1:2. The compandor's 0 dB or unity gain level is fixed at 77.5 mV_{RMS}. Two other features are present inside the SA5752: a low-noise preamplifier with variable gain setting (up to 40 dB), and an adjustable threshold noise canceller with VOX (Voice Operated Transmission) circuit providing programmable attack and decay time constants. The pre-amp gain can be set by an external resistor to produce the system's 0 dB level (77.5 mV_{RMS}) from the output signal of a variety of microphones. In the absence of an audio signal (no speech into microphone) or when the audio signal drops below a set threshold, the noise cancellation circuit reduces the overall gain by 10 dB. When the audio signal resumes, the gain is increased back to the normal level. In the meantime the VOX control signal can be used to disable or enable the transmit power amplifier (PA) consistent with the variation in the gain. SA5752 has a power down pin which is typically controlled by the SA5753. During power down mode all internal capacitors remain fully charged to achieve minimum power up time.

B. Audio Filtering Chip

The SA5753 IC contains 6 dB/octave pre-emphasis and de-emphasis filters, 4th order receive and transmit band pass filters (300 - 3000 Hz), a 5th order (3000 Hz) transmit low pass splatter filter, and a soft limiter circuit guaranteeing a maximum carrier frequency deviation of 12 kHz. Additional features have been integrated into the SA5753 as a result of an optimal architectural division, making the SA5753 very attractive for cellular radio applications. These include a DTMF generator, and programmable gain blocks for volume control and on-chip trimming. A two-wire serial bus interface (I²C) links the SA5753 to the system's master control block. I²C is used to program the DTMF generator, set the volume level, program the deviation attenuators so that no manual trimming is necessary, and to power down the device. The SA5753 also has features which distinguish it from its predecessor the SA5751: a transmit and receive mute functions with programmable polarities, on-chip summing amplifier combining the audio, DTMF, and DATA coming from an external data processor (also SAT, ST tones), and a default mode whereby the device is configured to operate and meet the EAMPS standard without any external control.

III. CHOICE OF TECHNOLOGY

The compandor chip is developed with bipolar technology to make use of the large dynamic range of the exponential relationship between V_{BE} and I_C in BJT devices. This device is manufactured using Philips Semiconductors' low power oxide isolated process (HS3).

The filter chip, on the other hand, is developed with CMOS technology, using switch capacitor design techniques because of the availability of high quality capacitors in MOS integrated circuits. Switch capacitor techniques are widely used in audio frequency filter design where the resistors are replaced by capacitors and digital switches in order to eliminate the requirement of integrating large values of resistors (which can be in the M Ω) to meet the long time-constant of audio filters. This results in a small die size, and mitigates the stringent accuracy and stability requirement of integrating resistors and capacitors because neither the fabricated values nor the temperature induced variation of the

symbol S will be used for the available signal power at the output terminals of the two-port network.

The gain of the network is defined as the ratio of the available signal power at the output terminals of the network to the available signal power at the output terminals of the signal generator. Hence

$$G_A = \frac{\text{power available from the network}}{\text{power available from the source}} = \frac{S}{S_g} \quad (9)$$

Note that while the gain is independent of the impedance which the output circuit presents to the network, it does depend on the impedance of the signal generator.

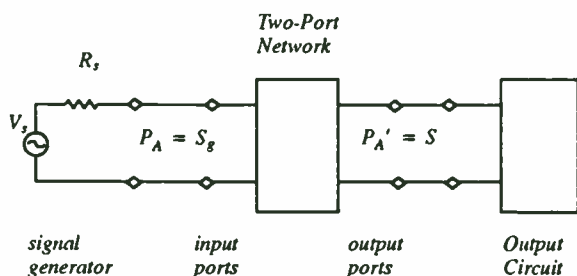


Figure 5. Available power gain of a two-port network.

NOISE FIGURE MEASUREMENT

NOISE IN BIPOLAR TRANSISTOR

The noise sources in a bipolar junction transistor are categorized into four major types:

1. Flicker noise;
2. Burst noise;
3. Shot noise;
4. Thermal noise.

Flicker Noise

Flicker noise is caused by traps associated with contamination and crystal defects in the emitter-base depletion layer. It is associated with a flow of direct current and displays a spectral density of the form [3]:

$$\bar{i}^2 = \frac{K_F I^{A_F}}{f} \Delta f \quad (10)$$

where K_F is a constant for a particular device, A_F is a constant between 0.5 and 2, and Δf is the bandwidth in Hertz. This expression shows that the noise spectral density has a $(1/f)$ frequency dependence, therefore, it is also called $1/f$ noise. Since flicker noise is most significant at low frequencies, it is not discussed here.

Burst Noise

It has been found experimentally that the low frequency noise spectrums of some bipolar transistors show a different frequency dependence than flicker noise. This could be the result of the existence of burst noise. It is caused by the imperfection in the crystal structure. The power spectrum of such signal is given by [4]:

$$\bar{i}^2 = \frac{K_B I}{1 + \left(\frac{\pi f}{2k}\right)^2} \Delta f \quad (11)$$

where K_B is a technological dependent constant for a particular device, and k is the mean repetition rate of the signal. This noise is insignificant at microwave frequencies because it is inversely proportional to f^2 , and it will not be addressed further.

Shot Noise

Shot noise is due to generation and recombination in the pn junction and injection of carriers across the potential barriers, therefore it is present in all semiconductor diodes and bipolar transistors. Each carrier crosses the junction in a purely random fashion. Thus the current I , which appears to be a steady current, is, in fact, composed of a large number of random independent current pulses. The fluctuation in I is termed shot noise and is generally specified in terms of its mean-square variation about the average value I_D and it is represented by [3]:

$$\bar{i}^2 = 2qI_D \Delta f \quad (12)$$

where q is the electronic charge ($1.6 \times 10^{-19} \text{C}$). Eq. (12) shows that the noise spectral density is independent of frequency. In a transistor, there are two such noise sources. They are the shot noise in the emitter-base junction (i_b) and in the collector-base junction (i_c).

Thermal Noise

Thermal noise is due to the random thermal motion of electrons in a resistor, and it is unaffected by the presence or absence of direct current, since typical electron drift velocities in a conductor are much less than electron thermal velocities. As the name indicates, thermal noise is related to absolute temperature T .

In a resistor R , thermal noise can be represented by a series voltage generator \bar{v}^2 . It is represented by [3]:

$$\bar{v}^2 = 4kTR \Delta f \quad (13)$$

where k is Boltzmann's constant ($1.38 \times 10^{-23} \text{J/K}$), and T is temperature in Kelvin. Like shot noise, thermal noise is also independent of frequency. Thermal noise is a fundamental physical phenomenon and is present in any linear passive resistor.

R and C elements track each other. SA5753 is manufactured using Philips Semiconductors' low power high density BICMOS process, known as QUBIC.

IV. A System Solution

APROC2 is particularly suited for analog cellular telephones because it meets the EAMPS and ETACS cellular standards. Fig. 2 shows a complete EAMPS/ETACS system block diagram of which the APROC2 is an integral part. The system controller communicates to APROC2 via a two-wire Inter-IC bus called I²C bus.

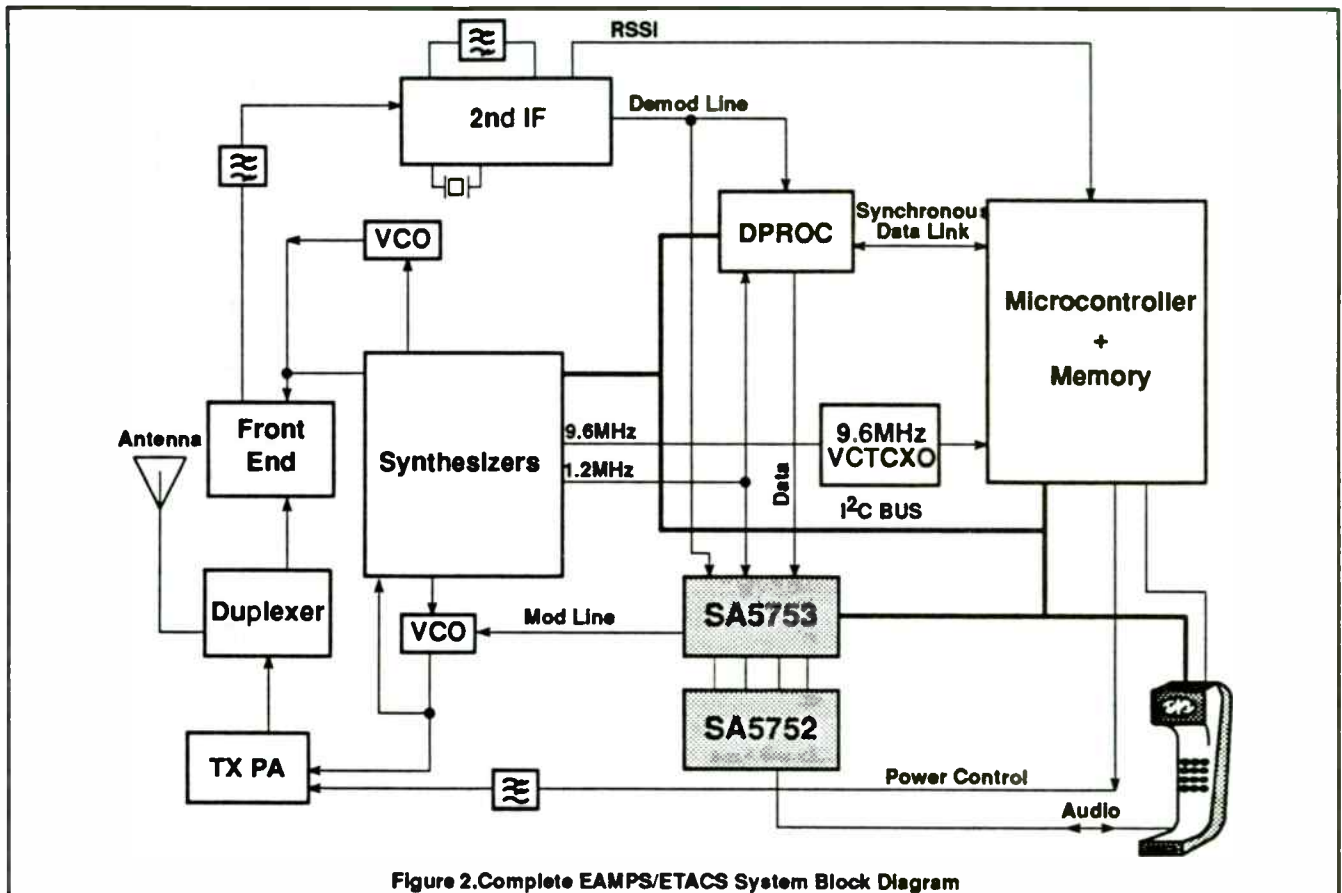


Figure 2. Complete EAMPS/ETACS System Block Diagram

This I²C control bus is a powerful means for networking between the ICs of a system. Typically the system controller acts as the bus master while the remainder of the ICs act as slaves. In systems like cellular telephones the I²C bus traffic generates digital switching noise which may couple into the synthesizer block and introduce phase noise. For this reason it is recommended that minimal I²C traffic should be maintained during conversation. With this in mind, the SA5753 has been designed to include an index addressing mode into its configuration registers bank so that only the necessary registers are addressed and modified for any change in the configuration. This will minimize I²C access and reduce digital switching which can cause noise and higher current consumption. Another system feature is the availability of the default mode which allows the use of this chip set in audio processing applications where there is no microcontroller or I²C bus available. Both SA5752 and SA5753 can operate with a supply ranging from 2.7 to 5.5 V. Current consumption is rated at 2.0mA and 2.7mA at 2.7V; 200μA and 600 μA in standby mode for SA5752 and SA5753, respectively. They are smaller than their predecessors the SA5750 and SA5751 (APROC1), while the SA5753 has extra programmable attenuators, an extra on-chip summing amp, and has more I²C control registers than the SA5751. APROC2 is packaged in two 20-pin SSOP packages (Shrink Small Outline Package) with dimensions (6.2x6.4 mm). When placed side by side, the two ICs interface directly with a small number of DC blocking caps, indicating a high degree of functional integration. Fig. 3 shows an application diagram of the APROC2. With its low power and small physical area, APROC2 is ideal for portable, battery powered applications.

Equivalent Circuit

Fig. 6 is the full small-signal equivalent circuit, including noise sources for the bipolar transistor at high frequency [3]. Three noise sources are evident from the figure. They are thermal noise from the series input resistance (r_b) and shot noise due to the base and collector currents (I_b , I_c), and their values are:

$$\overline{v_b^2} = 4kTr_b\Delta f \quad (14)$$

$$\overline{i_b^2} = 2qI_b\Delta f \quad (15)$$

$$\overline{i_c^2} = 2qI_c\Delta f \quad (16)$$

The resistors r_π and r_o in Fig. 6 are equivalent circuit elements, not physical resistors, and they do not produce any thermal noise.

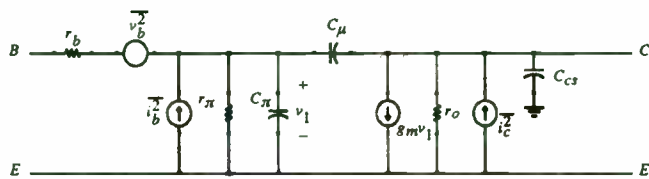


Figure 6. Bipolar transistor small-signal equivalent circuit with noise sources.

Neither thermal noise nor shot noise is frequency dependent, and both exhibit uniform noise output through the entire useful frequency range of the transistor. The internal gain of the transistor does vary with frequency, however, and it falls off as frequency increases. As a result the noise figure begins to rise when the reduction in gain becomes appreciable. Since the power gain falls inversely as frequency squared, the noise figure rises as frequency squared, or 6dB per octave [5]. Fig. 7 graphically shows the noise figure of a N16 transistor with $V_{BE} = 0.8V$, $V_{CE} = 4V$, and $R_s = 50\Omega$ in common emitter configuration.

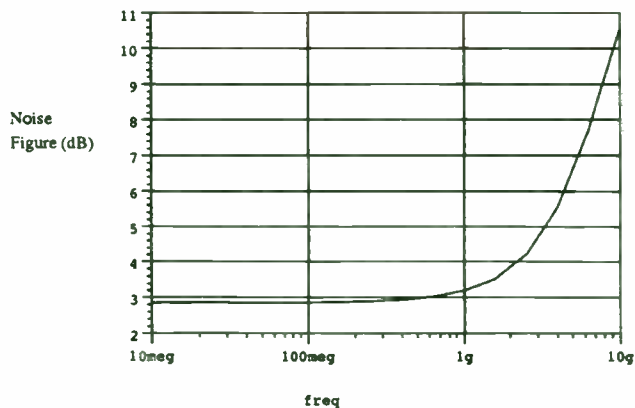


Figure 7. Noise figure vs. frequency for N16.

DETERMINATION OF NOISE PARAMETERS

Definition

As defined in 1960 by the Institute of Radio Engineers Subcommittee on Noise [6], the noise figure depends upon the internal structure of the transducer and upon its input termination, but not upon its output termination. Thus, the noise performance of a transducer is meaningfully characterized by its noise figure only if the input termination is specified. The noise factor F of any linear transducer, at a given operating point and input frequency, varies with the admittance Y_s of its input termination in the following manner [7]:

$$F = F_o + \frac{R_n}{G_s} |Y_s - Y_o|^2 \quad (17)$$

where G_s is the real part of Y_s , and the parameters F_o , Y_o and R_n characterize the noise properties of the transducer and are independent of its input termination. Thus the noise performance of a transducer can be meaningfully characterized for all input terminations through specification of the parameters F_o , Y_o and R_n .

The "optimum noise factor" F_o at the given transducer operating point and frequency, is the lowest noise factor that can be obtained through adjustment of the source admittance Y_s . The "optimum source admittance" Y_o is that particular value of source admittance Y_s which results in optimum noise factor F_o . The parameter R_n is positive and has the dimensions of a resistance. It is called the equivalent noise resistance. This parameter appears as the coefficient of the $|Y_s - Y_o|^2$ term in the general expression for F and, therefore, characterizes the rapidity with which F increases above F_o as Y_s departs from Y_o .

The parameters F_o , Y_o and R_n can be calculated if the noise theory of the transducer is known or, alternatively, can be determined empirically from noise measurements.

Two methods of computer-aided determination of noise parameters have been reported in the literature.

One of them, Kokyczka et al [8], can be thought of as an automatic version of the graphic procedure suggested by the Institute of Radio Engineers [6], which required tedious and time-consuming adjustment of some input termination admittances with constant real part and of some other with constant imaginary part.

The other one, Lane [9], is an application of the least-squares method, which reduces the determination of noise parameters to the solution of a four linear equation system, obtained as fit of noise figures measured for different source admittances.

Noise Parameters Computation

Ten sets of data for the N16 and the G14V102 are obtained with different source and are tabulated in table I and will be used to calculate the noise parameters of the devices.

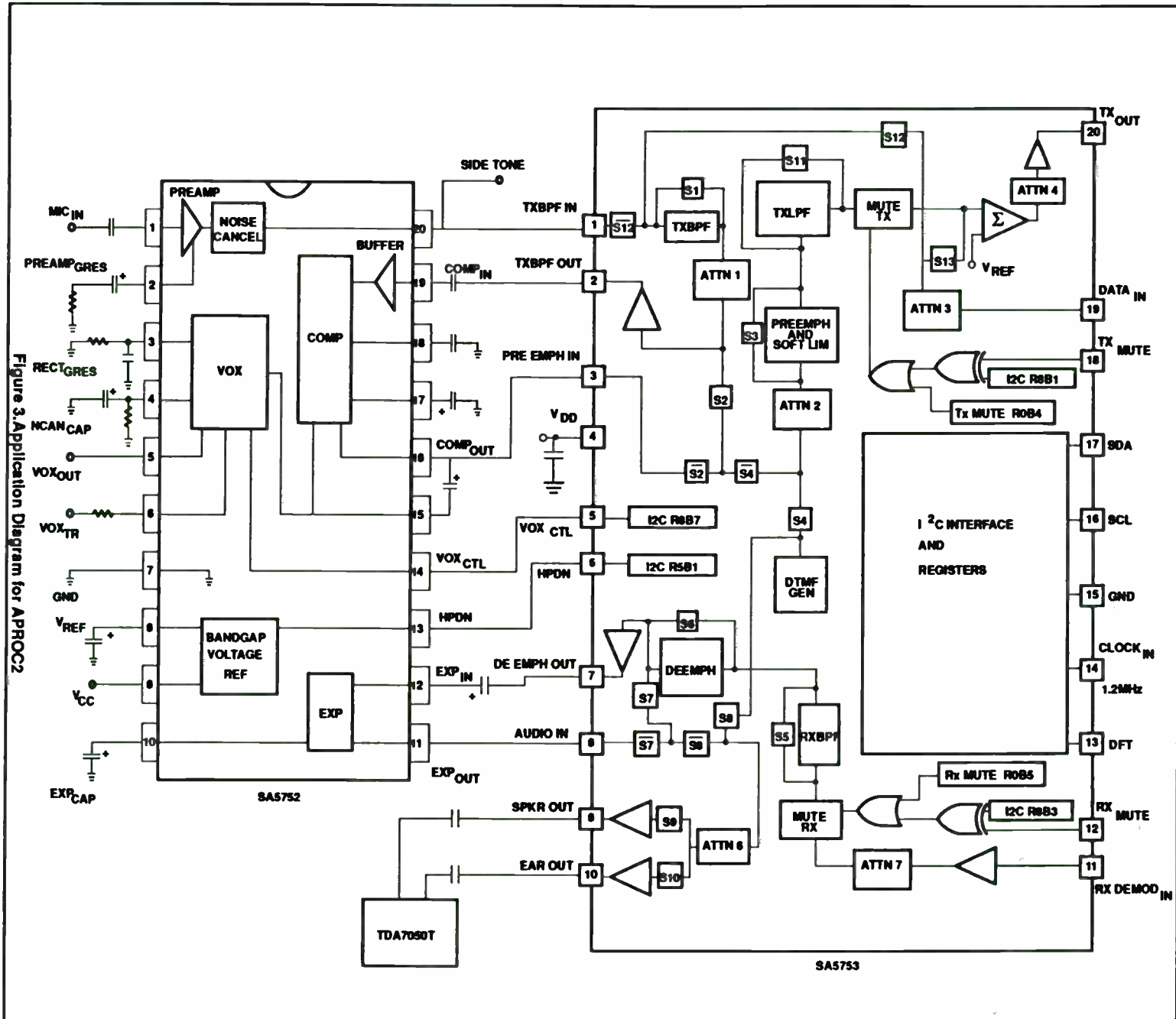


TABLE I

NOISE FIGURE MEASURED AT VARIOUS SOURCE IMPEDANCES WITH $V_{BE}=0.8V$, $V_{CE}=4V$ AT $F=1GHZ$

G_s mmhos	B_s mmhos	NF dB	
		N16	G14V102
6.33	-2.26	2.258	2.724
17.8	6.24	3.316	2.675
24.9	6.64	3.783	2.830
18.4	24.1	5.514	4.192
7.14	-7.14	2.702	2.697
13.5	-18.9	4.446	3.205
44.9	-28.1	5.751	3.948
14.2	-1.02	2.714	2.365
15.7	-3.92	2.861	2.362
22.8	-7.12	3.509	2.585

After the noise figure data for different source impedances are obtained, the minimum noise figure, the optimum source resistance, and the equivalent noise resistance can be determined. Eq. (17) is rewritten to eliminate the magnitude sign:

$$F = F_o + \frac{R_n}{G_s} [(G_s - G_o) + j(B_s - B_o)]^2 \quad (18)$$

In order to use a readily available subroutine for solving simultaneous equation solution, Eq. (18) is transformed to a form that is linear with respect to four new parameters A, B, C, and D [11].

$$F = A + BG_s + \frac{C + BB_s^2 + DB_s}{G_s} \quad (19)$$

where

$$F_o = A + \sqrt{4BC - D^2} \quad (20)$$

$$R_n = B \quad (21)$$

$$G_o = \frac{\sqrt{4BC - D^2}}{2B} \quad (22)$$

$$B_o = \frac{-D}{2B} \quad (23)$$

In principle, four measurements of noise factor from different source admittances will determine the four real numbers (F_o , R_n , G_o , and B_o). Eq. (18) becomes overdetermined if more than four measurements are taken, but by minimizing the square of error as expressed in Eq. (24), more than four measurements can be used to find those parameters which give the best least squares fit to Eq. (18). It has been shown that only slight variations of noise parameters occur versus redundancy if the number of data sets processed is greater than 7 [10]. A least-squares fit of the ten sets of noise figure data noise from table I to Eq. (19) is sought: therefore, the following error

criterion is established [9]:

$$\epsilon = \frac{1}{2} \sum_{i=1}^n W_i \left[A + B \left(G_i + \frac{B_i^2}{G_i} \right) + \frac{C}{G_i} + \frac{DB_i}{G_i} - F_i \right]^2 \quad (24)$$

where W_i is the weighting factor to be used if certain data are known to be less reliable than the average.

Base on the noise figure data in table I, the noise parameters for the N16 and G14V102 transistors are obtained.

TABLE II

NOISE PARAMETERS OF N16 AND G14V102 TRANSISTORS WITH $V_{BE}=0.8V$, $V_{CE}=4V$ AT $F=1GHZ$

	Fo dB	Rn ohms	Go mmhos	Bo mmhos
N16	2.25	42.67	6.31	-1.66
G14V102	2.34	21.32	13.12	-3.43

NOISE FIGURE CIRCLES

To plot noise figures on a Smith chart, Y_s and Y_o are expressed in terms of reflection coefficients Γ_s and Γ_o , and Eq. (17) becomes:

$$F = F_o + \frac{4R_n |\Gamma_s - \Gamma_o|^2}{(1 - |\Gamma_s|^2) |1 + \Gamma_o|^2} \quad (25)$$

This equation can be used to seek Γ_s for a given noise figure. To determine a family of noise figure circles, an intermediate noise figure parameter, N_i is defined [1].

$$N_i = \frac{|\Gamma_s - \Gamma_o|^2}{1 - |\Gamma_s|^2} \quad (26)$$

Eq. (26) is then transformed to:

$$\left| \Gamma_s - \frac{\Gamma_o}{1 + N_i} \right|^2 = \frac{N_i^2 + N_i (1 - |\Gamma_o|^2)}{(1 + N_i)^2} \quad (27)$$

Eq. (27) is recognized as a family of circles with N_i as a parameter. The center and radius of the circle can be found from:

$$C_{F_i} = \frac{\Gamma_o}{1 + N_i} \quad (28)$$

and

$$R_{F_i} = \frac{1}{1 + N_i} \sqrt{N_i^2 + N_i (1 - |\Gamma_o|^2)} \quad (29)$$

Eq. (26), Eq. (28), and Eq. (29) show that when $F_i = F_o$, then

V. CONCLUSION

We have introduced a system solution consisting of an analog audio processing chip set suitable for EAMPS/ETACS. It is made up of a compandor chip and an audio filter chip. This chip set has significant improvements over its predecessor (APROC1) in functionality and real estate (20-pin SSOP vs 24 and 28-pin SOL for SA5750 and SA5751, respectively). Its integrated functions, low power consumption, and small size make it attractive for a variety of portable, battery operated audio systems.

$N_i = 0$, $C_{F_o} = \Gamma_o$, and $R_{F_o} = 0$. That is, the center of the F_o circle is located at Γ_o with zero radius. From Eq. (28), the centers of the other noise figure circles are located along the Γ_o vector.

A set of constant noise figure circles for the N16 is shown in Fig. 8. This plot gives information about the noise figure of the device for different source impedances at 1GHz. A F_i dB noise figure circle on the plot specifies the values of source impedance at which the device will produce a noise figure of F_i . This set of curves show that the minimum noise figure, $F_o = 2.25dB$ is obtained when $\Gamma_s = \Gamma_o = 0.52 \angle 10.6^\circ$, and at point A, $\Gamma_s = 0.31 \angle 80^\circ$ produces $F_i = 3.25dB$. One point of interest is on the center of the Smith chart, which corresponds to a source impedance of 50Ω . The noise figure at this point is what we can have if the device is put into a 50Ω environment without any tuning circuitry at the input ports.

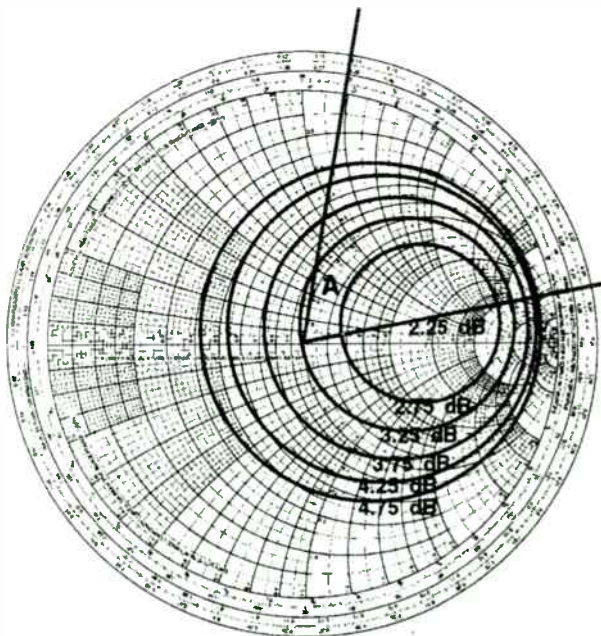


Figure 8. Constant noise figure circles for N16 with $V_{BE} = 0.8V$, $V_{CE} = 4V$ at $f=1GHz$.

COMPARISON

From the data obtained, the equivalent noise resistance (R_n) of the G14V102 is smaller than the one of the N16. This is verified by wider spacing of noise figure circles of the G14V102 as compare to the ones of the N16 (Fig. 9 vs. Fig. 10). The lower of R_n will result in reduced sensitivity of the noise figure to changes in source impedance. Therefore, a circuit designer can have more freedom on choosing source impedances for better power gain and/or better input matching for a given noise figure.

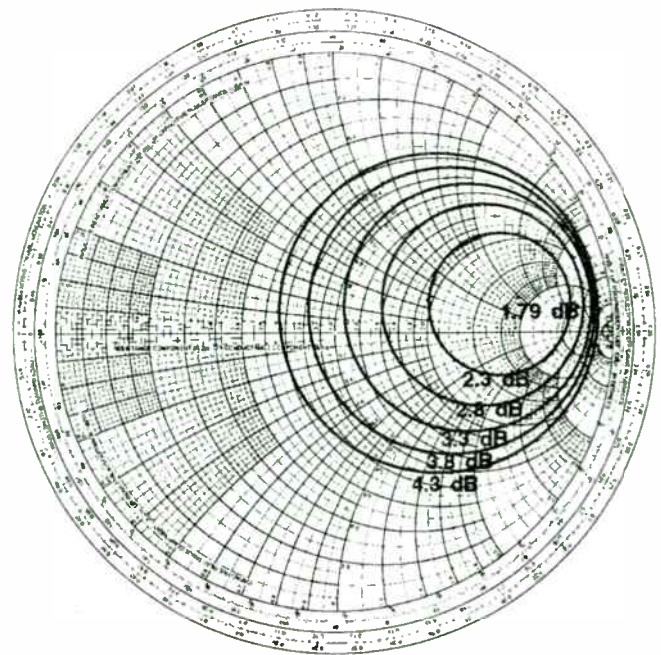


Figure 9. Constant noise figure circles for N16 with $V_{BE}=0.76V$, $V_{CE}=4V$ at $f=900MHz$.

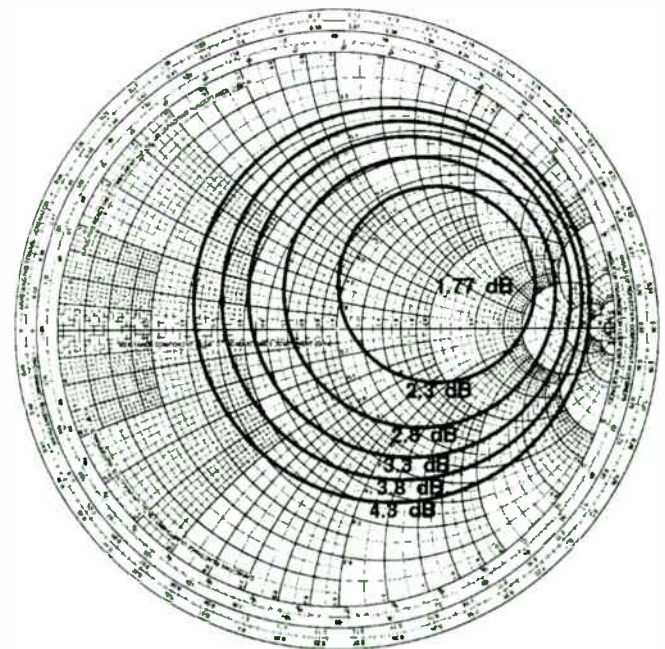


Figure 10. Constant noise figure circles for G14V102 with $V_{BE}=0.76V$, $V_{CE}=4V$ at $f=900MHz$.

Automotive Electronics Systems and Measurements

Session Chairperson: Jack Browne,
Microwaves & RF (Hasbrouck Heights, NJ)

Coaxial Vector Network Analysis Through 67 GHz: Addressing
Millimeter-Wave Commercial Applications, **Todd Antes**, Wiltron
Co. (Morgan Hill, CA).....**78**

Monolithic Components for 77-GHz Automotive Collision-
Avoidance Radars, **Lamberto Raffaelli**, Alpha Industries
(Woburn, MA).....**86**

110-GHz Wafer Probe Enables Cost-Effective Millimeter-Wave
Circuit Applications, **Edward M. Godshalk**, Cascade Microtech,
Inc. (Beaverton, OR).....**92**

Device Characterization with an Integrated On-Wafer Thermal
Probing System, **Dan d’Almeida**, Cascade Microtech, Inc.
(Beaverton, OR) and **Robert Anholt**, Gateway Modeling
(Minneapolis, MN).....**103**

GAIN MEASUREMENT

GAIN AND STABILITY

Stability Criteria

As the operating frequency of the transistor is being pushed upward, the transistor is more prone to unwanted oscillation due to parasitic elements. The necessary conditions for stability of a two-port device like bipolar transistors, had been studied by Kurokawa[12], Bodway[13], and Woods[14]. In terms of s-parameters, they are:

$$|\Delta| = |S_{11}S_{22} - S_{12}S_{21}| < 1 \quad (30)$$

and

$$K = \frac{1 - |S_{11}|^2 - |S_{22}|^2 + |\Delta|^2}{2|S_{12}S_{21}|} > 1 \quad (31)$$

Two-port devices that meets the above criteria are unconditionally stable for any positive source and load impedance.

Stability Circles

To maximize the gain, we must conjugately match the input and the output. For unconditionally stable two-ports networks there is no unwanted oscillation to worry about. But for those networks which cannot meet the above stability criteria, we will have to look at what might happen to the network in terms of stability--will the amplifier oscillate with certain values of impedance used in the matching process?

In a two-port network, oscillations are possible when either the input or output port presents a negative resistance, since noise generated in the adjoining network enters the port, the negative resistance generates more noise rather than dissipating the incident noise, and some of this generated noise combines with the incoming noise to input more noise. Negative resistances correspond to the points outside the Smith chart, which imply either $|\Gamma_{in}| > 1$ or $|\Gamma_{out}| > 1$. Therefore, we have the boundary for the input and output stability circles defined:

$$|\Gamma_{in}| = \left| S_{11} + \frac{S_{12}S_{21}\Gamma_l}{1 - S_{22}\Gamma_l} \right| = 1 \quad (32)$$

and

$$|\Gamma_{out}| = \left| S_{22} + \frac{S_{12}S_{21}\Gamma_s}{1 - S_{11}\Gamma_s} \right| = 1 \quad (33)$$

Solving for the values of Γ_l and Γ_s in Eq. (32) and Eq. (33) shows that the solutions for Γ_l and Γ_s lie on circles [2]. The radius and center of the input stability circles are:

$$r_s = \left| \frac{S_{12}S_{21}}{|S_{11}|^2 - |\Delta|^2} \right| \quad (34)$$

$$C_s = \frac{(S_{11} - \Delta S_{22}^*)^*}{|S_{11}|^2 - |\Delta|^2} \quad (35)$$

and the radius and center of the output stability circles are:

$$r_l = \left| \frac{S_{12}S_{21}}{|S_{22}|^2 - |\Delta|^2} \right| \quad (36)$$

$$C_l = \frac{(S_{22} - \Delta S_{11}^*)^*}{|S_{22}|^2 - |\Delta|^2} \quad (37)$$

where

$$\Delta = S_{11}S_{22} - S_{12}S_{21} \quad (38)$$

Having measured the s-parameters of a two-port device at one frequency, Eq. (34) to Eq. (37) can be evaluated, and plotted on a Smith chart. Fig. 11 illustrates the graphical construction of the stability circles where $|\Gamma_{in}| = 1$. On one side of the stability circles boundary, in the Γ_l plane, we will have $|\Gamma_{in}| < 1$ and on the other side $|\Gamma_{in}| > 1$.

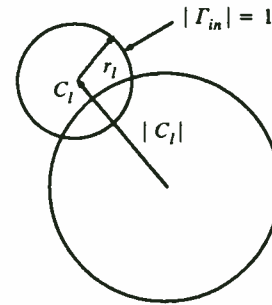


Figure 11. Stability circles construction on a Smith chart.

To determine which area represents the stable operating condition, we make $\Gamma_l = 0$, which is to terminate the output port with a 50Ω load through a 50Ω transmission line. This represents the point at the center of the Smith chart. Under these conditions,

$$|\Gamma_{in}| = |S_{11}| \quad (39)$$

For N16, the magnitude of S_{11} measured is less than unity, therefore, the center of the Smith chart represents a stable operating point. That is, the shade area on Fig. 12 represents $|\Gamma_{in}| < 1$. The same procedure applies for finding the output stability region.

When the input and output stability circles lie completely outside the Smith chart the network is called unconditionally stable for all Γ_s and Γ_l . This comes from the fact that no matter what positive termination is put at the input or output of the network $|\Gamma_{in}|$ and $|\Gamma_{out}|$ will be always less than unity.

Gain Circles

S-parameters can be used to predict the available power gain of a transistor for any input termination Γ_s . This available gain is

Coaxial Vector Network Analysis Through 67 GHz: Addressing Millimeter-Wave Commercial Applications

by
Todd Antes
Wiltron Company

I. Introduction

Nature provides several "bands of opportunity" in the microwave frequency spectrum that may be exploited by modern communication systems. These frequency bands are characterized by unique transmission phenomena such as high or low atmospheric attenuation. Depending on the application, these characteristics influence fundamental design criteria - frequency, bandwidth, power, size - of a communication system.

One millimeter-wave frequency band used by many existing and emerging systems is the oxygen absorption band at and around 60 GHz. At 62.5 GHz, the free space signal absorption coefficient peaks at nearly 20 dB per kilometer at sea level (Figure 1) - providing a form of natural isolation. Antennas at these frequencies also provide extremely narrow beam widths and high gain in a fraction of the size of lower frequency microwave antennas. These transmission properties support efficient point-to-point communications and reduce the potential for signal interference. Hence, for systems that demand localized, secure, non-interfering communication, this frequency band is one obvious choice.

As communication systems move to millimeter-wave frequencies, development engineers will require measurement instrumentation to characterize both system-level and component performance - at actual operating frequencies. Manufacturing engineers will also require efficient and economical instrumentation to make complex measurements on potentially high volume products. Modern vector network analyzers (VNA) provide complex (real and imaginary) scattering parameter and non-ratioed parameter measurement capability in frequency, time, and frequency with time gate domains. VNAs offer powerful insight into the transmission and reflection properties of millimeter-wave communication systems.

II. Commercial Applications

Secure military communications (satellite-satellite, man-tank, submarine-submarine) make up most of the communication systems operating in the 60+ GHz millimeter-wave absorption band. However, the natural advantages of this frequency band also lend themselves to several emerging commercial (non-military) applications.

Automotive Anticollision Radar

Automobile manufacturers are making significant investments in supplemental safety and control systems that operate at millimeter-wave frequencies - i.e. forward-looking collision avoidance/automatic braking radar, rear-looking blind zone/backup radar, and intelligent cruise control. These systems rely on active and passive remote sensing technology to glance the surrounding environment and warn the driver of an impending collision. In order to be effective in a variety of driving environments, these radar systems must overcome several basic problems related to signal propagation and interference.

Millimeter-wave automotive radar has inherent advantages over alternate implementations. First, millimeter-wave radar is able to "see through" bad weather conditions such as fog, rain and snow. Whereas, other radar systems, such as infrared, rely on a clear line of sight. Second, signal interference can be minimized by taking advantage of the high atmospheric absorption

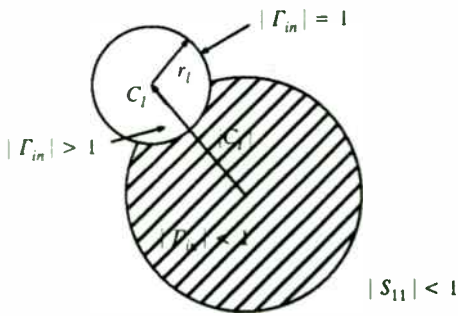


Figure 12. Stability region for Γ_s .

that gain achieved when a transistor is driven from some source reflection Γ_s , while terminated with a load impedance equal to Γ_{out} (matched output). The available power gain in terms of reflection coefficients is [1]:

$$G_A = \frac{(1 - |\Gamma_s|^2)}{|1 - S_{11}\Gamma_s|^2} |S_{21}|^2 \frac{1}{(1 - |\Gamma_{out}|^2)} \quad (40)$$

where

$$\Gamma_{out} = S_{22} + \frac{S_{12}S_{21}\Gamma_s}{1 - S_{11}\Gamma_s} \quad (41)$$

Because G_A is a function of the source reflection coefficient, constant available power gain circles can be plotted on a Smith chart together with the constant noise figure circles, and the trade-off result between gain and noise figure can be analyzed.

For a given gain G_A , the radius R_a and the center C_a of the circle can be calculated using the relations [2]

$$g_a = \frac{G_A}{|S_{21}|^2} \quad (42)$$

$$C_1 = S_{11} - \Delta S_{22}^* \quad (43)$$

$$R_a = \frac{\sqrt{1 - 2K |S_{12}S_{21}| g_a + |S_{12}S_{21}|^2 g_a^2}}{|1 + g_a(|S_{11}|^2 - |\Delta|^2)|} \quad (44)$$

and

$$C_a = \frac{g_a C_1^*}{1 + g_a(|S_{11}|^2 - |\Delta|^2)} \quad (45)$$

For a given G_A , the constant available power gain circle can be plotted. All Γ_s on this circle produce the gain G_A .

COMPARISON

Gain circles, stability circles, and noise figure circles for the N16 and the G14V102 are plotted in Fig. 13 and Fig. 14. Under the conditions $V_{BE} = 0.76V$, $V_{CE} = 4V$ at $f = 900MHz$, these two transistors can provide similar power gains. Looking

at these figures, one can see that a N16 will provide a gain of 16dB and a noise figure of 3.5dB with 50Ω source impedance, while a G14V102 will provide about the same gain but with a superior noise figure of 2.4dB.

CONCLUSION

Noise is created by many physical processes which cannot be avoided. Living with noise means we must be able to measure and predict it. The noise sources in a bipolar transistor have been identified. At microwave frequencies they are thermal noise due to base resistance and shot noise from the base and collector currents. The base resistance consists of two parts. The external base resistance, R_{b_i} , is the resistance of the path between the base contact and the edge of the emitter diffusion. The active base resistance, R_{b_a} , is that resistance between the edge of the emitter and the site within the base region at which the current is actually flowing. R_{b_i} can be reduced by decreasing the separation between the base and the emitter. This method is straightforward, but it is technology-limited. While the effect of current crowding in the base at high current level will reduce the effect of R_{b_a} , but more shot noise will be generated by the higher current.

The technique of measuring noise parameters (F_o , R_n , G_o , and B_o) of a bipolar transistor has been presented. This same measurement technique can also be employed to measure the noise parameters of a general two-port network. Power gain information is obtained through s-parameter manipulation. The noise figure and available power gain data are plotted on Smith Chart to give a clear view of how a particular device will perform in various source impedances.

near 60 GHz. Once radar systems are placed into a large number of automobiles, mutual interference will adversely affect system performance. So, it is important that transmitted signals not travel much beyond a defined sensing radius where they might interfere with another vehicle's radar.

Traffic Control Systems

Traffic congestion is a common problem in urban areas around the world. Several proposed traffic control systems aim to regulate and smooth traffic flow. In Europe, projects like PROMETHEUS will transmit information regarding route guidance, road pricing, and road condition, etc. between road and vehicle. Other proposed systems include toll booths with automatic debiting systems that will recognize passing vehicles. As in other automotive applications, the 60 GHz band offers the advantages of limited range, low interference in a potentially high-multipath environment, and the ability to travel through bad weather with little distortion.

Millimeter-Wave Radio Links

Millimeter-wave links provide a cost effective and secure form of localized communication. Signals travel between rooftop antennas rather than across underground coaxial or fiber optic cable. In comparison, installation of a wireless millimeter wave system is faster and costs far less than a system requiring routing of coax or fiber optic cable. Millimeter-wave components and systems also provide significant size and performance advantages. A 60 GHz (1 ft. diameter) parabolic antenna provides the same gain and much narrower beam width at a fraction of the size of an equivalent 10 GHz microwave antenna (6 ft. diameter). The narrow beam width is well-suited for secure point-to-point communications as signal power occupies a much smaller area. Today, millimeter-wave power device technology can support the required transmission signal levels at a reasonable cost.

Radio Local Area Networks

Millimeter-wave communication within buildings eliminates the need for cables that connect computers and workstations to a Local Area Network (LAN). Radio LANs provide freedom of movement for individual network nodes as they are no longer "tied" to a coaxial or fiber optic connection. In manufacturing, a mobile robot can perform tasks at various locations in the facility while maintaining constant communication with a central controller. In office environments, computers can be easily moved from desktop to meeting rooms or other locations in the building. Indoor millimeter-wave LANs naturally provide localized, and thus, secure communication. Transmissions within a building do not travel well through walls or outside the building.

III. Measurement of Millimeter-Wave Communication Systems

Fundamental S-Parameter Measurements

The traditional use for VNAs is measuring the fundamental S-parameters of two-port devices. VNA technology has evolved to better address these measurements by incorporating sophisticated error-correction, automatic signal reversing, and broadband frequency coverage. Today, VNAs are available that provide single connection frequency coverage from 40 MHz to 67 GHz in coax and 33 GHz to 110 GHz in waveguide bands. A variety of calibration techniques address different media types: coaxial, waveguide, microstrip, etc. Non-ratioed signal measurements of multi-port and/or frequency conversion devices (i.e. mixers, converters, etc.) are now accommodated with dual source control capability and specialized test set configurations.

Device Modeling and Model Verification

With the advent of powerful workstation computers and software, device modeling and simulation has become an important step in the product development process. Device performance can now be simulated and evaluated before investing in fabrication. In the past, VNAs were used to

REFERENCE

- [1] "S-parameter Design," Hewlett-Packard Application Note 154, Mar. 1990.
- [2] Guillermo Gonzalez, *Microwave Transistor Amplifiers*, Prentice-Hall, New Jersey, 1984.
- [3] P. R. Gray and R. G. Meyer, *Analysis and Design of Analog Integrated Circuits*, 2nd ed., John Wiley & Sons, New York, 1984.
- [4] Z. Y. Chang and M. C. Willy, *Low-Noise Wide-Band Amplifiers in Bipolar and CMOS Technologies*, Kluwer Academic Publishers, Norwell, MA, 1991.
- [5] Harry F. Cooke, "Transistor Noise Figure," *Solid State Design*, pp. 37–42, Feb. 1963.
- [6] H. A. Haus *et al.*, "IRE Standards on Methods of Measuring Noise in Linear Twoports, 1959," *Proc. IRE*, vol. 48, pp. 60–68, Jan. 1960.
- [7] H. A. Haus *et al.*, "Representation of Noise in Linear Twoports," *Proc. IRE*, vol. 48, pp. 69–74, Jan. 1960.
- [8] W. Kokyczka, A. Leupp, and M. J. O. Strutt, "Computer-aided determination of two-port noise parameters (CADON)," *Proc. IEEE*, vol. 58, pp. 1850–1851, Nov. 1970.
- [9] Richard Q. Lane, "The Determination of Device Noise Parameters," *Proc. IEEE*, vol. 57, pp. 1461–1462, Aug. 1969.
- [10] G. Garuso and M. Sannino, "Computer-Aided Determination of Microwave Two-port Noise Parameters," *IEEE Transactions on Microwave Theory and Techniques*, vol. 26, pp. 639–642, Sept. 1978.
- [11] H. Fukui, "The Noise Performance of Microwave Transistors," *IEEE Transactions on Electron Devices*, vol. 13, pp. 329–341, Mar. 1966.
- [12] K. Kurokawa, "Power Waves and the Scattering Matrix," *IEEE Transactions on Microwave Theory and Techniques*, vol. 13, pp. 194–202, Mar. 1965.
- [13] G. E. Bodway, "Two Port Power Flow Analysis Using Generalized Scattering Parameters," *Microwave Journal*, May 1967.
- [14] D. Woods, "Reappraisal of the Unconditional Stability Criteria for Active 2-Port Networks in Terms of S Parameters," *IEEE Transactions on Circuits and Systems*, Feb. 1976.
- [15] Ronald W. Kruse, "Microwave Design Using Standard Spice," *Microwave Journal*, pp. 164–171, Nov. 1988.

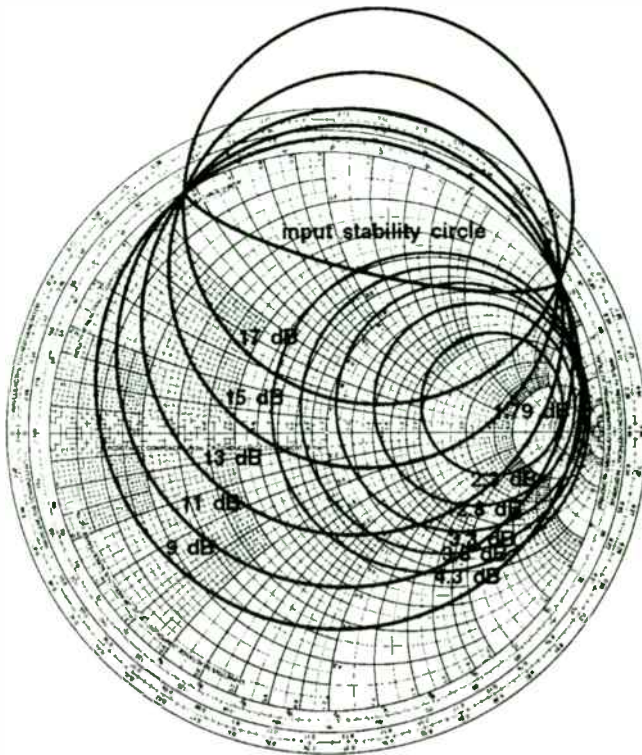


Figure 13. Gain and noise figure circles for N16 at $f=900\text{MHz}$.

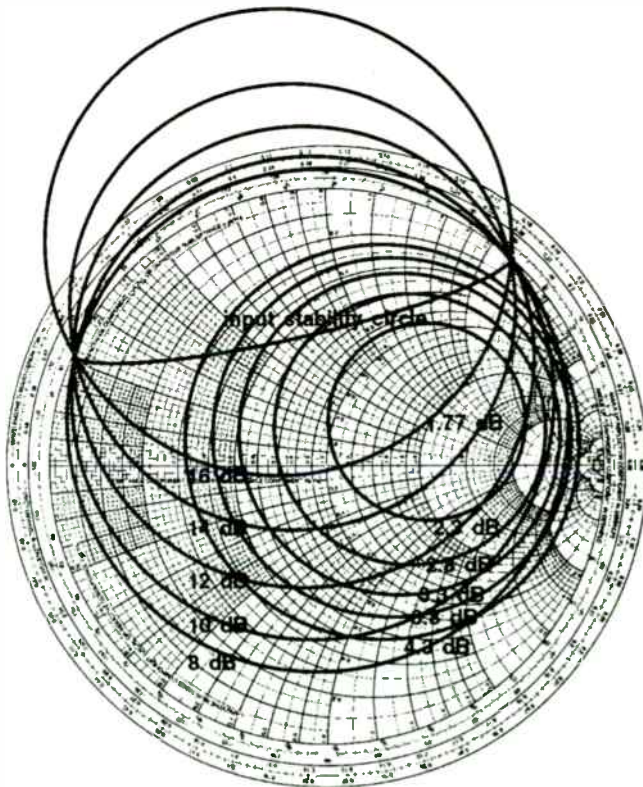


Figure 14. Gain and noise figure circles for G14V102 at $f=900\text{MHz}$.

measure the S-parameters of a device at microwave frequencies (typically <40 GHz). These measurements were then used to develop mathematical models of device performance. Once a model was established that correlated with measured data, one could extrapolate performance to higher frequencies. Unfortunately, such extrapolation usually surpassed one's ability to measure and verify actual performance. Modern VNAs address this fundamental problem with millimeter-wave frequency coverage. Now, design engineers can develop models to higher frequencies and verify these extrapolations through 67 GHz (coax) and/or 110 GHz (waveguide).

Antenna Measurements

Characterization of an antenna involves measuring its reflection and radiation characteristics. Typical measurements include match, gain, radiation pattern, bandwidth, and polarization. A VNA can measure all of these parameters at a single (CW) or multiple millimeter-wave frequencies. Long distance antenna ranges can be accommodated by remoting the system signal source up to five miles from the test set receiver and mainframe.

Transmission Time Domain Measurements

In both automotive and radio LAN applications, the presence of multipath signals and interference must be taken into account. Using the time domain transmission (S21) measurement capabilities of the VNA, one can measure the relative amplitude and phase angle of short- and long-range multipath signals. This measurement is very similar to radar cross section (RCS) measurements that measure the reflections or "signatures" of surrounding objects.

An example illustrates the basic measurement concepts. The setting consists of two metal plate reflectors of different sizes, placed at different distances from the transmit/receive antenna (Figure 2). In this case, the transmit and receive antenna are located at the same position. However, a separate receive antenna could be located some distance away from the transmit antenna. Measurements are made from 60 to 65 GHz with 501 frequency data points - providing approximately 30 meters of unaliased range.

The VNA system is calibrated by first placing a short across the antenna and performing a transmission frequency response calibration. The short is then removed, and the antenna is aligned with the targets. Figure 3 shows the time domain transmission (S21) characteristics over 0 to 8 meters from the antenna reference plane (marker values are "round-trip" - twice the actual linear distance(s) between objects). Marker 1 is placed on the antenna leakage signal. Marker 2 is placed on the response of the first object (4"x12" metal plate). Marker 3 is placed on the response from the second object (24" x 48" metal plate).

The VNA's time gating capability allows one to isolate the response from the first object (Figure 4). Linear Magnitude graph type is chosen prior to gating to provide a "sharper" display of each discontinuity. Once the time gate is activated, one may return to the frequency gated by time (FGT) domain and view the relative amplitude and phase angle response of the object versus frequency (Figure 5).

In a real world application, the two metal plates could be replaced with automobiles in a radar simulation or file cabinets and desks in an office LAN environment. In any case, it is clear that this measurement technique, traditionally used in military applications (i.e. RCS), can be adapted to conceptually similar commercial applications. Time Domain gating allows one to identify and analyze troublesome multipath and reflected responses.

Summary

Commercial systems are being specified to operate in the oxygen absorption band at and around 60 GHz. This millimeter-wave "band of opportunity" provides high free space signal absorption, a natural form of isolation, for secure and localized communications. Automotive anticollision radar,

THE CURRENT-FEEDBACK OP AMP A HIGH-SPEED BUILDING BLOCK

Anthony D. Wang
Burr-Brown Corporation
6730 South Tucson Boulevard
Tucson, AZ 85706-7087

Although current-feedback amplifiers (CFAs) have been in use for quite some time, there is a reluctance to view them in the same light as voltage-feedback amplifiers (VFAs). For instance, the gain-bandwidth curve of VFAs has a parallel in a transimpedance-bandwidth curve for CFAs. This parameter can be used to determine the closed-loop behavior of the CFA in the same way that GBW can for the VFA. Not all the fault is with the users - the amplifier manufacturers have not standardized the CFA characterization as they have done with VFAs. This paper describes the CFA and its behavior in an intuitive manner.

HISTORICAL PERSPECTIVE

The term "operational amplifier", or "op amp" in typical engineering shorthand, has generally been associated with the transistorized voltage-feedback amplifier. It is becoming more acceptable now to include the current-feedback amplifier in the same category.

Interestingly enough, the basic architecture for the CFA might have predated the VFA although it was not until the 1980's that the CFA was itself repopularized by Comlinear Corporation. To appreciate the evolution of the beast, it helps to look back to some early discrete transistor circuits.

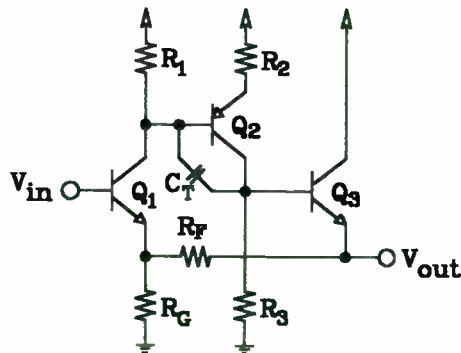


Fig. 1: Three transistor amplifier

The three transistor amplifier of figure 1 is arranged in a series-shunt configuration. However, in order to analyze the amplifier, the circuit is rearranged as shown below in figure 2.

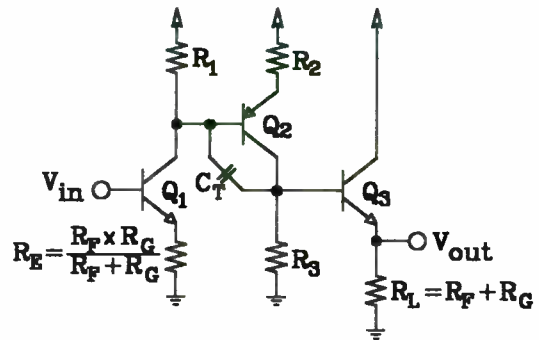


Fig. 2: Amplifier redrawn for analysis

The feedback network shows up in two places - a series network at the output and a parallel network at the emitter of the input transistor. This allows for open-loop analysis while keeping the effects of loading intact.

The loading of the output by the feedback network is generally not a problem. However, the gain of the first transistor stage is dependent on the values of the resistors in the feedback network. Thus the open-loop response will change with closed-loop gain, which could make frequency compensation an iterative chore.

Adding another transistor to buffer the input stage transistor from the feedback network can circumvent this difficulty. The discrete transistor circuit of figure 3 illustrates that this modification is the first step towards a voltage feedback amplifier.

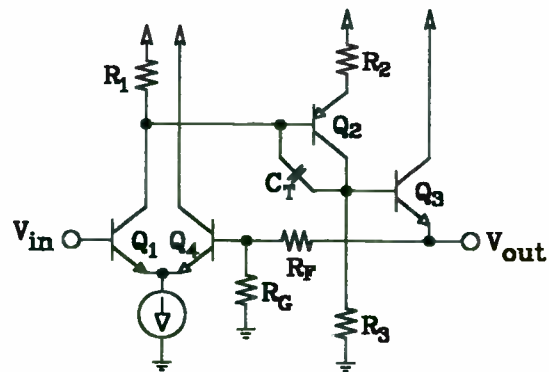


Fig. 3: Adding a buffer transistor

The added transistor presents a high impedance input to the feedback network. It also features the benefits of

traffic control systems, radio links, and local area networks are a few of the emerging millimeter-wave commercial applications.

The Vector Network Analyzer is one measurement tool that may be used by engineers to develop and test millimeter-wave communication components and systems. Broadband coaxial frequency coverage to 67 GHz and in waveguide bands to 110 GHz supports fundamental S-parameter measurement, on-wafer device characterization, antenna measurement, and gated time domain measurement capabilities.

References

1. Briere, P., Perea, E., de Saint Leger, O., "System and technology aspects of future digital cellular phones in Europe", GaAs IC Symposium, October 1991, Monterey, Tech. Digest 33-36.
2. Detlefsen, J., Rozmann, M., Troll, T., Zeilinger, "System aspects and design of an automotive collision warning PN code radar using wavefront reconstruction", MTT-S Conf. 1992, Albuquerque, Symp. Digest 625-628.
3. Goel, J., Tan, K.L., Stones, D.I., Chan, R.W., Streit, D.C., Peratoner, S., Schellenberg, J., "60 GHz power amplifier using PHEMT", MTT-S Conf. 1992, Albuquerque, Symp. Digest 587-589.
4. Haese, N., Benlamlah, M., Cailleu, D., Rolland, P.A., "Low-cost design of a quasi-optical front-end for on board mm-wave pulse radar", MTT-S Conf. 1992, Albuquerque, Symp. Digest 621-623
5. Kotaki, M., Takimoto, Y., Akutsu, E., Fujita, Y., Fukuhara, H., Takahashi, T., "Development of millimeter wave automotive sensing technology in Japan", Invited Paper, MTT-S Conf. 1992, Albuquerque, Symp. Digest 709-712.
6. Li, Z.W., Menzel, W., "A 61 GHz doppler radar using inverted strip dielectric waveguide", MTT-S Conf. 1992, Albuquerque, Symp. Digest 629-632.
7. Meinel, H., "Applications of microwaves and millimeterwaves for vehicle communications and control in Europe", MTT-S Conf. 1992, Albuquerque, Symp. Digest 609-612.
8. Meinel, H.; Jackson, P., "Progress in the commercial applications of microwaves: a review", Microwave Engineering Europe, November 1992, pp. 23-31.
9. Meinel, H., "Millimetre-wave commercial applications and technologies", Microwave Engineering Europe, November 1991, pp. 9-20.
10. Ogawa, H., Polifko, D., "Fiber optic millimeter-wave subcarrier transmission links for personal radio communication systems", MTT-S Conf. 1992, Albuquerque, Symp. Digest 555-558.

a balanced input, such as low offset voltage and equal input bias currents.

Of greater significance is the fact that the dynamic emitter resistance of the added transistor is substituted for the parallel resistance of the feedback network in figure 2. The first stage gain, and consequently the open-loop gain, is no longer dependent on the feedback network. The process of frequency compensation has one less degree of freedom to be concerned with.

These two circuits illustrate the basic distinctions between current-feedback and voltage-feedback amplifiers. In both cases, the feedback network is connected to an inverting input node. In figure 1, the emitter presents a low impedance input while in figure 3 the base presents a high impedance input.

Needless to say, the three transistor amplifier of figure 1 can be considered the forbear for the CFA as it is known today. Figure 4 shows the amplifier connected to a mirror-image of itself, whose transistors have been converted to the opposite polarity type. Once the input transistors are buffered by emitter followers, the basic current-feedback architecture emerges.

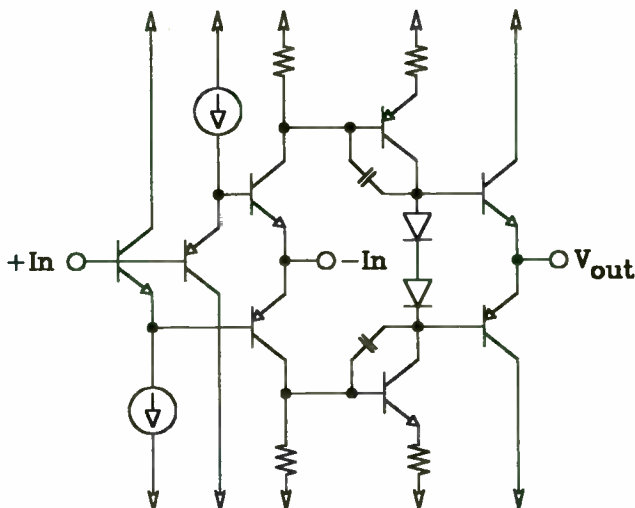


Fig. 4: Basic CFA topology

ANALYZING THE CFA

The study of the differential input, voltage-feedback amplifier is simplified with a technique known as "half-circuit analysis". This technique, illustrated in figure 5, recognizes that the symmetry of the circuit presents a shortcut whereby only half the signal path needs to be considered. The NPN current mirror, which provides double-ended to single-ended conversion, still maintains balance in the circuit because the second stage output voltage is determined by the current that flows into the high impedance presented by the collectors.

Inspection of figure 4 shows that the axis of symmetry for the CFA is centered horizontally. Therefore, the half-

circuit used for analysis is the same circuit as presented in figure 1, ignoring the input emitter follower. However, as pointed out previously, the feedback network is closely intertwined with the analysis. Therefore, the circuit of figure 2 can be used for the analysis. The compensation capacitor, C_T , can be the intrinsic base-collector capacitor of Q2 or an extrinsic capacitor.

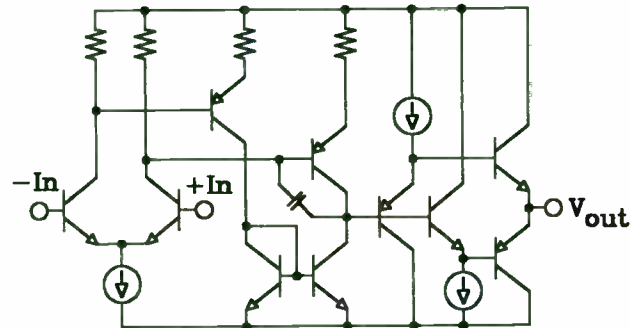


Fig. 5a: Basic VFA topology

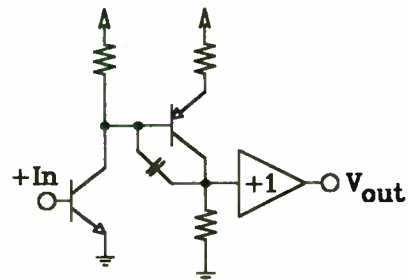


Fig. 5b: VFA half-circuit

The only real difference between figure 5b and figure 2 is the presence of the parallel combination of the feedback network resistors in the emitter of the CFA's input transistor. The analysis is very straightforward and the dc gain can be determined by inspection.

$$A_{Vdc} = \frac{R_1 \cdot R_3}{R_E \cdot R_2}$$

The open-loop pole can be approximated quite accurately as the interaction of the resistor, R_1 , with the Miller multiplied capacitor, C_T .

$$\omega_p \cong \frac{1}{R_1 \left(\frac{R_3}{R_2} \cdot C_T \right)}$$

This analysis presumes that the dynamic emitter resistance of Q1, r_{e1} , can be neglected ($R_E \gg r_{e1}$) and that R_2 includes r_{e2} .

It would be convenient at this point to define the transresistance as:

$$R_T = \frac{R_1 \cdot R_3}{R_2}$$

11. Readout: "Fibre, mm and microwave comms blend together", Microwave Engineering Europe. June/July 1992, pg. 21.
12. Rembold, B., "Communication systems at millimeter waves", 22nd EuMC 1992, Espoo, Conf. Proceedings, Vol. 1, pp. 53-72.
13. Saito, T., Okubo, N., Kawasaki, Y., Isaji, O., Suzuki, H., "An FM-CW radar module with front-end switching heterodyne receiver", MTT-S Conf. 1992, Albuquerque, Symp. Digest 713-716.
14. Takimoto, Y.; Kotaki, M., "Automotive anticollision radar", Applied Microwave, Fall 1992, pp. 70-82.
15. Williams, D.A., "Millimetre wave radars for automotive applications", MTT-S Conf. 1992, Albuquerque, Symp. Digest 721-724.

Note that the transresistance has the dimensions of ohms and is determined solely by elements internal to, the amplifier. The previous equations can be rewritten more simply.

$$A_{Vdc} = \frac{R_T}{R_E} \text{ and } \omega_p = \frac{1}{R_T \cdot C_T}$$

Now the open-loop gain can be completely described by:

$$A_V = \frac{R_T}{R_E} \cdot \frac{1}{1 + j\omega R_T C_T}$$

In order to arrive at this equation, it was assumed that the feedback network was known. This is the crux of the issue - the open-loop **voltage** gain of a CFA requires knowledge of the feedback network.

Removing R_E , the feedback network term, from the equation for open-loop voltage gain yields a more general expression that describes the amplifier's open-loop performance in terms of its intrinsic characteristics. This equation would have units of ohms and would be better identified as a complex impedance, or transimpedance, Z_T :

$$Z_T = \frac{R_T}{1 + j\omega R_T C_T}$$

This is the true measure of performance for CFAs. It is now obvious why the amplifier is known as "current-feedback." The output voltage is responsive to a **current** at the low impedance inverting input node (the emitter of Q1) that interacts with the open-loop transimpedance, Z_T .

Furthermore, the open-loop response of the amplifier is completely described by the dc transresistance, R_T , and the compensation capacitor, C_T , which is called the transcapacitance. R_T is analogous to A_{OL} , the open-loop voltage gain of a VFA, and interacts with C_T to form the open-loop pole. This is graphically depicted in figure 6.

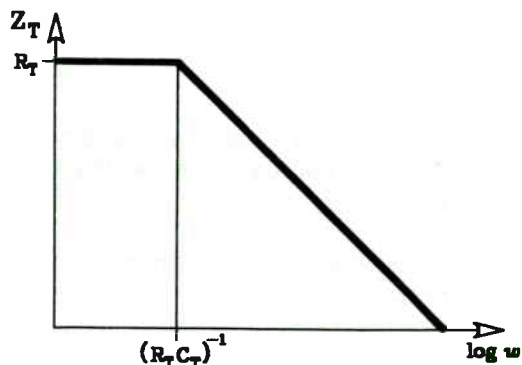


Fig. 6: Open-loop transimpedance

The ordinate axis has the dimension of ohms and is scaled logarithmically.

Having described the CFA with just two components suggests a simplified version of the half-circuit used for analysis. Figure 7 shows a convenient model that has all the essentials necessary for quick hand calculations. The inverting buffer preserves the sense of the signal as it is amplified by the Q2 stage in Figure 2.

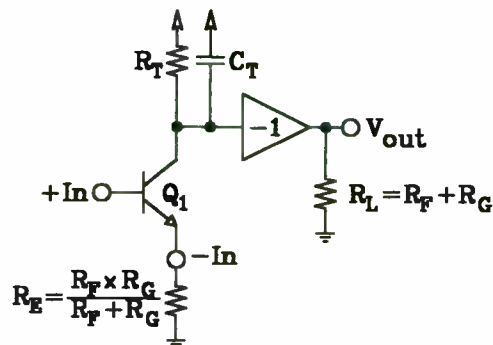


Fig. 7: CFA model for ac analysis

Comparisons with voltage-feedback amplifiers will inevitably be made when determining which op amp to use for an application. Presumably the closed-loop gain is known, which means that a feedback network can be established. Therefore, the open-loop voltage gain can be calculated for the CFA and a fair comparison with any VFA can be established.

Note that the analysis described here is based on a fairly simple current-feedback topology. Although the design of integrated circuit CFAs has become more sophisticated, the open-loop transimpedance approach (Z_T) is still valid.

CLOSED-LOOP PERFORMANCE

The closed-loop response of the CFA can be described by using classical analysis:

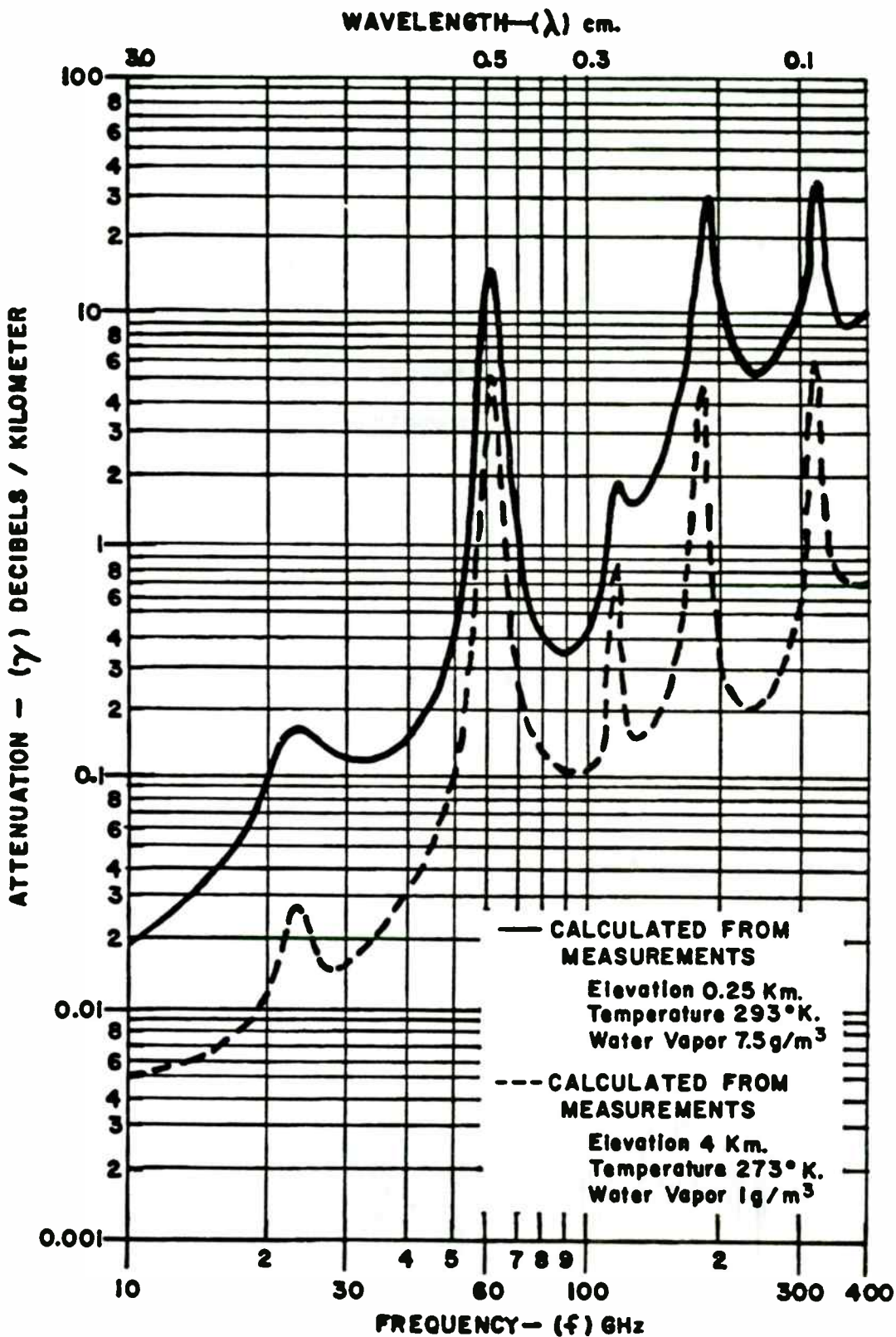
$$A_{CL} = \frac{A_V}{1 + A_V \cdot \beta} \text{ where } \beta = \frac{R_G}{R_F + R_G}$$

Substituting for A_V yields the following expression:

$$A_{CL} = \frac{\frac{R_T}{R_E} \cdot \frac{1}{1 + j\omega R_T C_T}}{1 + \frac{R_T}{R_E} \cdot \frac{1}{1 + j\omega R_T C_T} \cdot \frac{R_G}{R_F + R_G}} = \frac{\text{Open-loop gain}}{\text{Loop gain}}$$

The loop gain, of course, limits the accuracy of the closed-loop gain. Note that $R_T \gg R_F$ (typically $R_T > 100K$ and $R_F < 5K$), therefore the equation can be easily simplified to:

Figure 1. Atmospheric Attenuation



CALCULATED COMBINED WATER VAPOR AND OXYGEN ATTENUATION

$$A_{CL} = \frac{R_F + R_G}{R_F} \cdot \frac{1}{1 + j\omega R_F C_T}$$

The dc value of closed-loop gain is set by the feedback network while the closed-loop pole is determined by the interaction of the transcapacitance with the feedback resistor. This latter term is what gives the CFA its much touted characteristic of gain-independent bandwidth.

A closer look at the unsimplified equation for the closed-loop gain helps to clarify this property. The dc portion of open-loop gain in the numerator is modified by the parallel combination of the feedback network, which changes with desired closed-loop gain. As long as R_F is kept constant, the loop gain expression in the denominator does not vary, nor do any of the frequency dependent terms.

Figure 8 illustrates graphically that the open-loop gain curve slides vertically to keep the closed-loop intercept frequency constant.

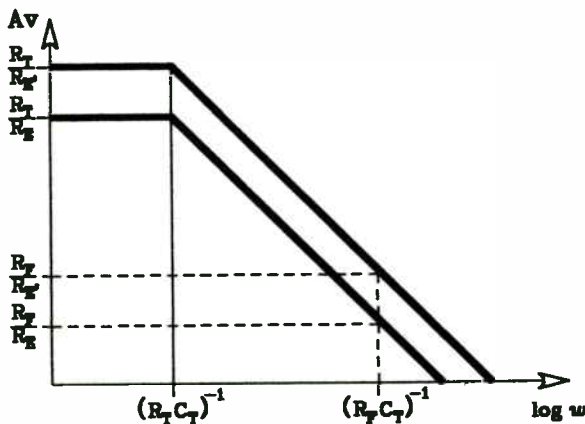


Fig. 8: Variation of open-loop gain

The closed-loop gain expressions have been expressed as a ratio of the feedback resistor to the equivalent feedback network. This can be verified algebraically as:

$$\frac{R_F}{R_E} = \frac{R_F}{\left(\frac{R_F \cdot R_G}{R_F + R_G} \right)} = \frac{R_F + R_G}{R_G}$$

Thus, the open-loop gain varies directly with the closed-loop gain for changes in R_E as long as R_F is kept constant.

NONIDEAL CONSIDERATIONS

The assumption that the r_e of Q1 can be neglected has limits. For ease of analysis, figure 6 has been redrawn to include it as an input resistance, R_{in} (figure 9). Note that R_{in} is internal to the CFA terminals.

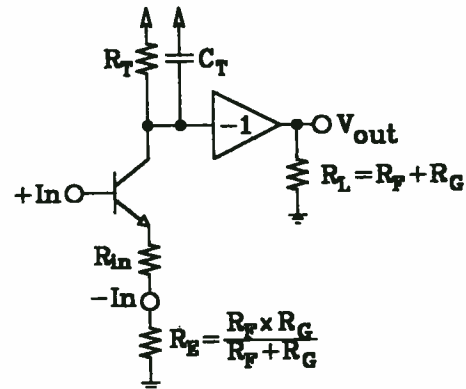


Fig. 9: CFA model modified for R_{in}

The open-loop gain equation can be modified by inspection while a new closed-loop gain equation can again be derived using the classical approach.

$$A_V = \frac{R_T}{R_E + R_{in}} \cdot \frac{1}{1 + j\omega R_T C_T}$$

$$A_{CL} = \frac{R_F + R_G}{R_G} \cdot \frac{1}{1 + j\omega \left(R_F + \frac{R_{in}}{\beta} \right) C_T}$$

R_{in} decreases the open-loop gain but not its corner frequency. On the other hand, R_{in} does not affect the dc closed-loop gain but does modify the intercept frequency. In practice, R_{in} includes more than just the dynamic emitter resistance - it also includes bulk resistances that are in series with the inverting input, as well as parasitic resistances external to the amplifier. Obviously, R_{in} should be as low as possible to get the maximum benefit from a CFA.

The modified equations lead to some practical generalizations when using CFAs. The first is that the open-loop gain has a theoretical maximum and this can be conveniently estimated as:

$$A_{V(max)} \cong \frac{R_T}{R_{in}} \cdot \frac{1}{1 + j\omega R_T C_T}$$

This is an ideal value that can never be realized since any feedback network will automatically reduce the open-loop gain. However, it is useful for estimating a CFA's merits against a particular VFA.

The second generalization is that the closed-loop bandwidth will become gain-bandwidth limited when

$$\frac{R_{in}}{\beta} \geq R_F \Leftrightarrow R_{in} \geq R_E$$

Figure 2. Example measurement setup

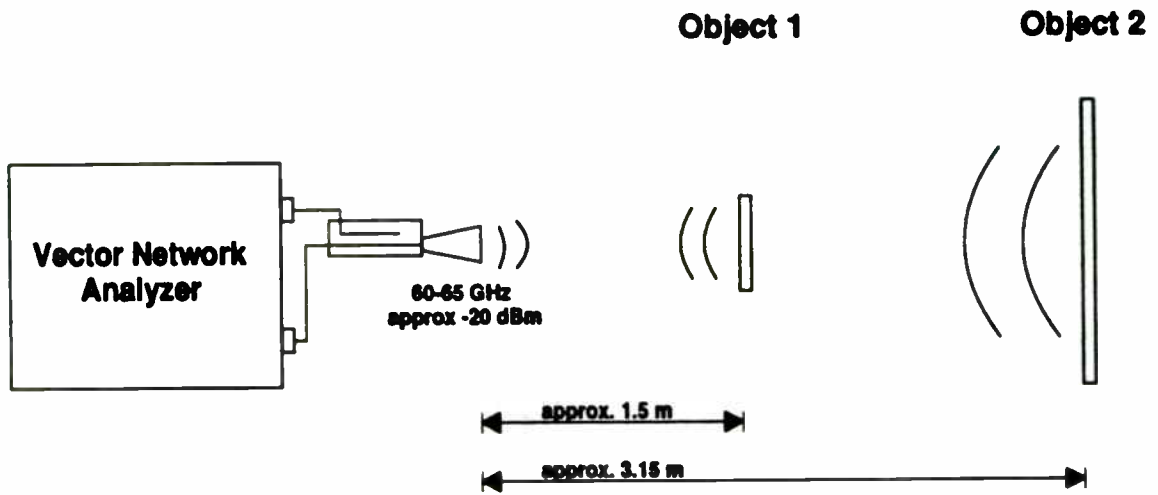
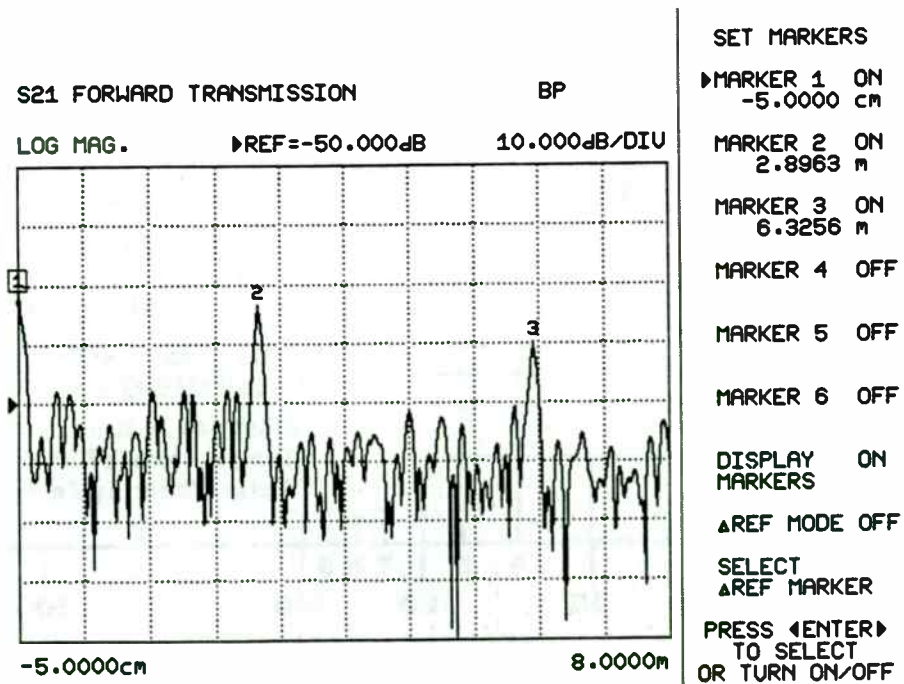


Figure 3. Time Domain response of Objects 1 and 2



The latter expression makes use of the fact that the feedback factor, β , is a function of the feedback network resistors.

Once this limit has been reached, the CFA can be associated with a gain-bandwidth product, GBW.

$$GBW = \frac{1}{R_{in} C_T}$$

The graph in figure 10 shows an asymptotic approach to estimating a CFA's closed loop response.

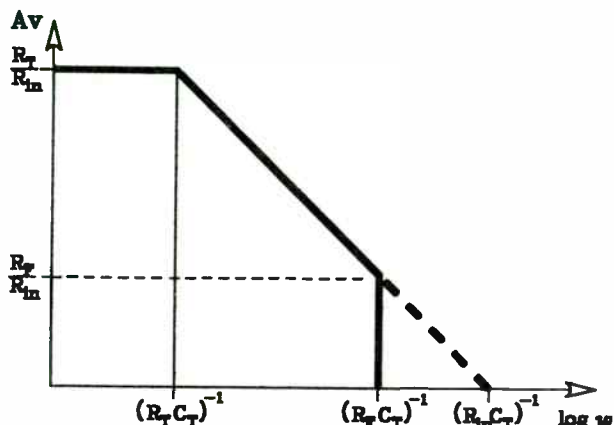


Fig. 10: CFA closed-loop performance

To be technically accurate, it should be pointed out that the inverting input is characterized by an impedance, Z_{in} , which does vary with frequency. Fortunately, the resistive portion, R_{in} , dominates over most of the CFA's useful bandwidth. At high frequency, the inverting input impedance increases, which only further degrades the closed-loop performance, although the extent of the increase is generally well under an order of magnitude.

FREQUENCY COMPENSATION

The analysis so far has centered on the gain versus frequency performance without taking into account any phase shift considerations. Excess phase plagues the CFA just as it does the VFA. The open-loop transimpedance curve of figure 6 depicts a single-pole response which would have only 90° of phase shift. Parasitic poles introduce additional phase shift to the open-loop phase response. Figure 11 displays the more complete open-loop transfer curves - both magnitude and phase.

Since the feedback network sets the open-loop gain for the CFA, it also sets the phase margin, Φ_M . This is the crucial factor that actually determines the selection of the feedback network resistors.

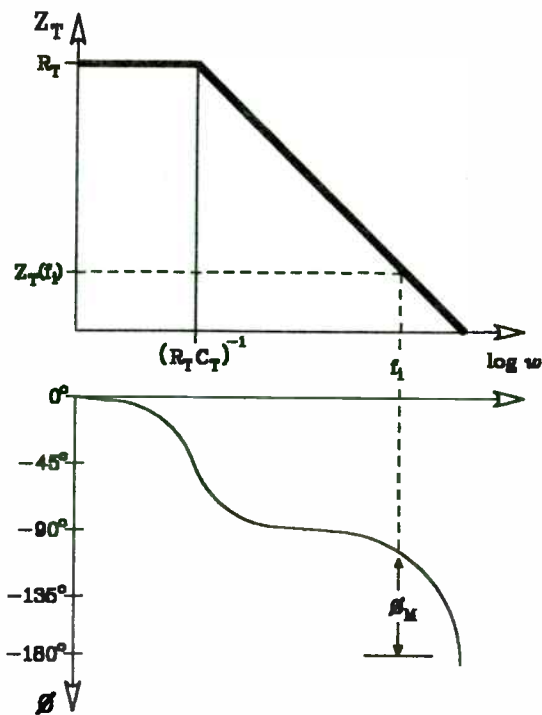


Fig. 11: CFA open-loop transfer curves

The significance of phase margin would benefit from a brief review of its properties. Phase margin, in a strictly literal sense, is measured at that frequency, f_u , where an amplifier's open-loop voltage gain has fallen to unity. It is the difference between the open-loop phase shift and -180° , where the amplifier would lose negative feedback and become unstable.

$$\Phi_M = \Phi(f_u) - (-180^\circ)$$

The concept of phase margin is best illustrated by plotting unity gain frequency response curves as phase margin is varied (figure 12).

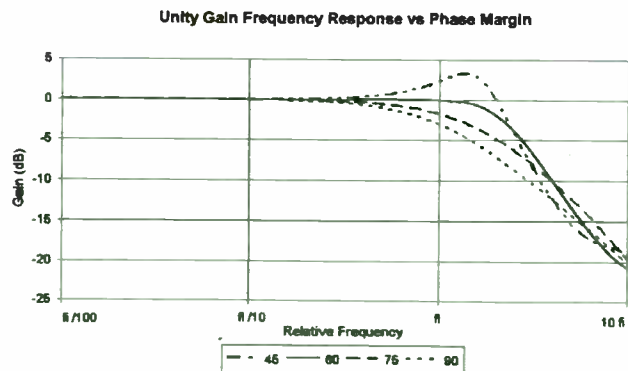


Fig. 12: Phase margin's effect on frequency response

As the plot shows, the optimum value for phase margin is 60° . This gives the desirable combination of broad bandwidth with flat frequency response. Note that an amplifier with 90° of phase margin, which implies a lack

Figure 4. Time Domain gate applied to isolate the response of Object 1

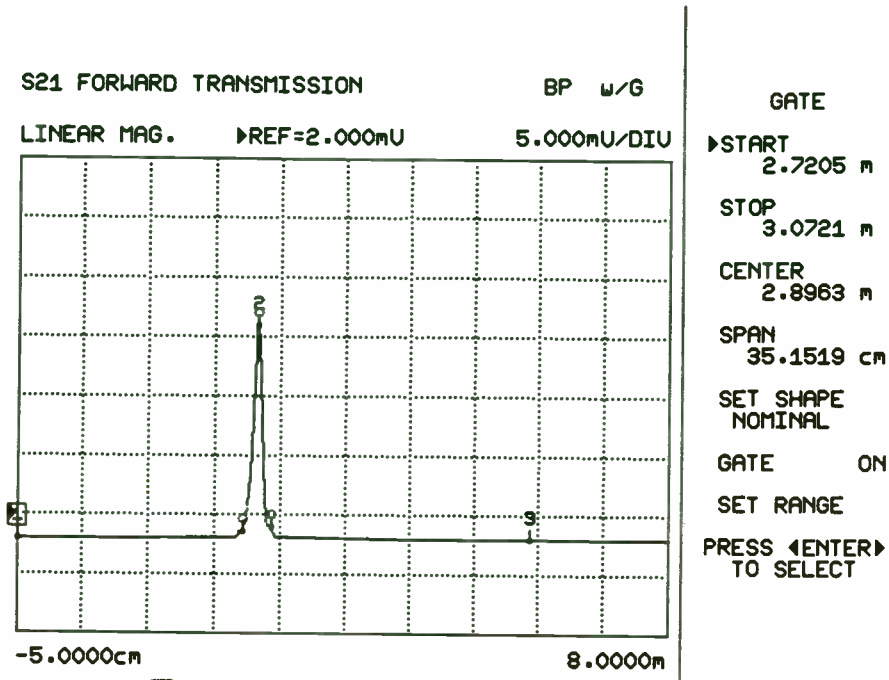
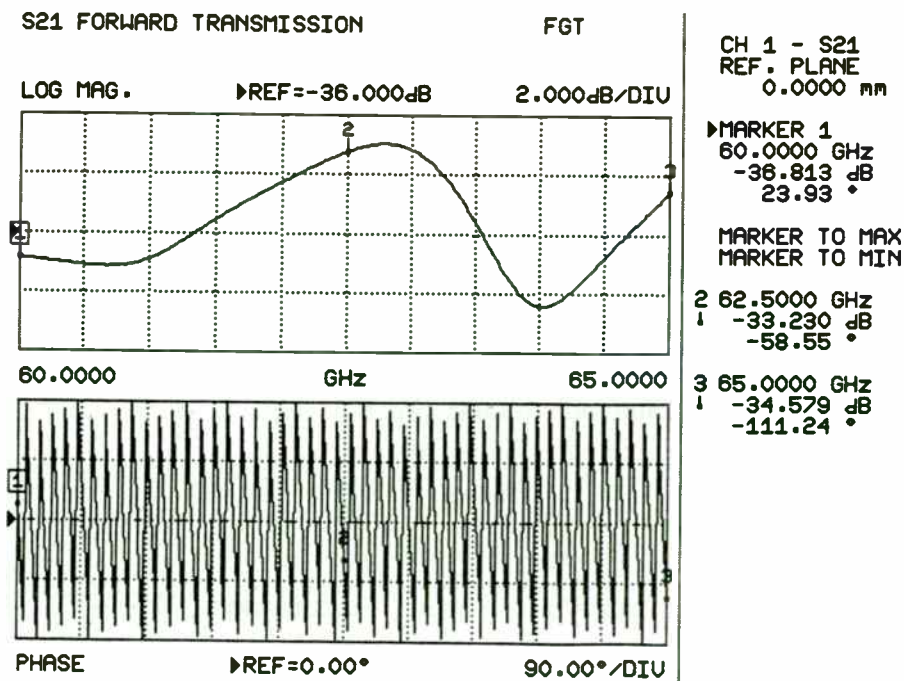


Figure 5. Response of Object 1 in the Frequency Gated by Time Domain



of excess phase, has a -3dB bandwidth less than half of the optimum response.

A more general way of looking at this is to make the observation that the closed-loop response can be extended if the open-loop phase has fallen 120° at f_i , the frequency where the asymptote for closed-loop gain intersects the open-loop gain curve.

In VFAs, the phase margin is set by design and the user does not change it. There are a few amplifiers which allow access to the high impedance node to tailor compensation, but these are in the minority. In general, VFAs break out into two categories - compensated and decompensated.

The compensated amplifiers allow operation at unity gain but at the expense of bandwidth in higher gains. Decompensated, or undercompensated, amplifiers must be operated in gains greater than unity but have a higher gain-bandwidth product. In either case, the phase margin is predetermined.

As noted previously, phase margin for the CFA is set by the user via the feedback network. However, rather than use phase margin as the design criterion, higher performance can be attained by making use of the general observations regarding phase shift and bandwidth. In other words, guarantee that the open-loop phase has fallen 120° at f_i .

The mechanics are rather straightforward because, as illustrated in Figure 8, varying the feedback network causes a simple vertical translation of the open-loop gain curve. The open-loop pole does not move and so the attendant open-loop phase shift is unaffected. The excess phase shift is also insensitive to the feedback network change. Thus, selection of a desired phase shift automatically sets the intercept frequency.

Once the intercept frequency, f_i , is determined, so is the magnitude of transimpedance, $Z_T(f_i)$. This is depicted graphically in figure 11 by following the dashed lines up from the open-loop phase curve to the intersection with the open-loop transimpedance curve.

To realize the benefit of the -120° phase shift, the feedback network has to be selected so that the open-loop gain equals the closed-loop gain at f_i . A convenient way to visualize this problem is to concentrate on the essentials of the model in figure 9.

The CFA model can be simplified further by ignoring the inverting buffer and focusing on that portion of the circuit which provides gain. In figure 13 the CFA model has been reduced to an elementary transistor amplifier. The gain for this circuit is

$$|A_V| = \frac{|Z_T(f_i)|}{R_E + R_{in}}$$

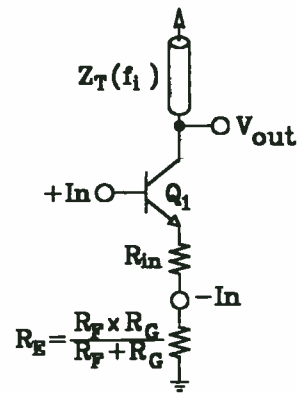


Fig. 13: Elementary amplifier

The goal, therefore, is to select the necessary feedback network so that A_V equals the desired closed-loop gain. Since Z_T has previously been defined as a complex impedance, direct substitution yields a closed form solution.

$$\frac{R_F + R_G}{R_G} = \frac{|Z_T(f_i)|}{R_{in} + R_E} = \frac{\left| \frac{R_T}{1 + j2\pi f_i R_T C_T} \right|}{R_{in} + R_E}$$

which can be reduced to a less bulky equation:

$$R_F \cong \frac{1}{2\pi f_i C_T} - \frac{R_{in}}{\beta}$$

Not surprisingly, this expression conforms to the plot of CFA closed-loop performance (figure 10). For low gains, the R_{in} term is negligible and R_F is set by f_i . As closed-loop gain increases and R_{in}/β can no longer be neglected, R_F should be adjusted according to the equation to maintain optimum performance. When R_F approaches zero, the CFA is becoming gain-bandwidth limited and the intercept frequency must be lowered.

MODEL REPRESENTATION

The single transistor model of figure 9 is a satisfactory vehicle to provide intuitive insight. It is by no means an accurate representation of the CFA but offers a good visual aid for the user.

A more generally accepted model for the CFA is depicted in figure 14. This model is a very faithful rendition of the CFA from a block diagram standpoint. It can accurately account for the bipolar input and output swings that are possible with the CFA's complementary symmetry.

MONOLITHIC COMPONENTS FOR 77 GHz AUTOMOTIVE COLLISION AVOIDANCE RADARS

Lamberto Raffaelli*

ABSTRACT

This paper will examine design methodology and test results of monolithic components specifically designed for a 77 GHz collision avoidance radar. In addition cost-trade-offs between a fundamental 0.15 micron pseudomorphic HEMT based approach and a multiplied 0.25 micron power MESFET based solution will be discussed.

INTRODUCTION

Automotive Collision Avoidance Systems include a Sensor capable of detecting the presence of obstacles in front of the vehicle, a signal processor to identify those obstacles that pose a real threat to the driver and a display to present the data to the driver.

The optimum sensor for automotive applications should satisfy high antenna directivity and small volume requirements; in addition the system should be fully operational during adverse weather conditions such as dense fog or rain. The sensor needs also to offer high reliability and low unit production cost.

Millimeter-wave radars provide significant advantages as compared to alternative technologies (such as laser-based systems) and successfully meet most of the requirements with cost being the only challenge. These systems have been mainly developed for low volume military applications based on waveguide and/or hybrid components. These technologies being labor intensive, do not lend themselves to low production cost. In addition at Millimeter-wave frequencies, integrated circuit bond wires, particularly in areas subject to high VSWR will hinder performance and repeatability.

In order to reduce production cost, automotive radars need to rely on GaAs Monolithic Components. Alpha Industries has been developing Monolithic Technology at Millimeter-wave frequencies for the last ten years, mainly for defense contracts such as SADARM, Longbow, SDI, and MIMIC.

The technology already developed find a unique opportunity to be inserted in collision avoidance production programs with projected costs, as already demonstrated for military customers at similar frequencies, fully compliant with automotive radar program requirements.

.

*Alpha Industries, Inc., 20 Sylvan Road, Woburn, Massachusetts, U.S.A.

Comparing it to figure 4, it is readily apparent that the unity gain buffer at the input is an accurate portrayal of the input stage between the input pins. The finite input resistance, R_{in} , is included for completeness.

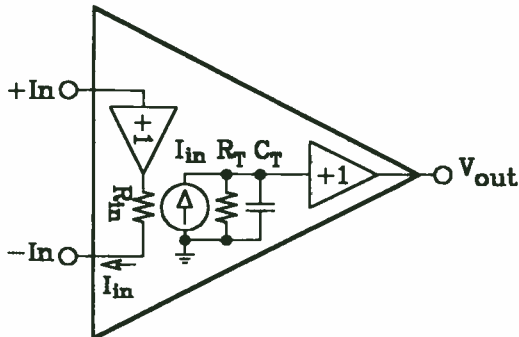


Fig. 14: Block diagram CFA model

The current-controlled current source translates the current from the inverting input to the open-loop transimpedance, again composed of R_T and C_T . The unity-gain buffer provides a low impedance source to the external load.

Either of the models is sufficient to appreciate the CFA and its performance features. Figure 9 bears a strong resemblance to the ancestral antecedent of the CFA while the latter is more readily adaptable to generating a SPICE macromodel.

Other properties of the CFA are apparent when studying these models. The slew rate is limited by the current available to charge the transcapacitance. Decreasing $(R_{in}+R_E)$ will certainly benefit slew performance. Minimizing C_T will increase slew rate as well as the small-signal performance.

Potential for trouble exists when parasitic capacitance is present at the inverting input. This parasitic capacitance can be the result of poor layout techniques, inappropriate use of a socket or even the wrong package. If C_P is the lumped parasitic capacitor, the open-loop gain will become:

$$A_V = \frac{R_T}{R_E + R_{in}} \cdot \frac{1 + j\omega R_E C_P}{(1 + j\omega R_T C_T) \left(1 + j\omega \frac{R_E \cdot R_{in}}{R_E + R_{in}} C_P \right)}$$

This expression has added a zero and a pole to the transfer function. The zero will always occur before the pole and can be the source of trouble in some cases. If instability arises because of C_P , move the **closed-loop** pole to a lower frequency by adjusting the feedback network.

To model excess phase, the addition of a delay line can be more expedient than trying to add multiple poles and

zeroes to the open-loop transimpedance. The modified transfer function is still quite compact.

$$Z_T = \frac{R_T}{1 + j\omega R_T C_T} \cdot e^{-j\omega T_D}$$

The exponential adds phase shift without affecting magnitude. A reasonable technique is to use the phase shift at the highest intercept frequency the circuit is expected to encounter.

$$T_D = \frac{1}{2\pi f_i \cdot \frac{\Phi(f_i) - 90^\circ}{360^\circ}}$$

Subtracting 90° from the open-loop phase is, of course, to remove the phase shift due to the open-loop pole.

DATA SHEET SPECIFICATIONS

The open-loop transimpedance terms, R_T and C_T , and the input resistance, R_{in} , have already been identified as necessary features to describe a CFA. Additionally, the open-loop transimpedance and phase versus frequency curves should be provided as well.

The block diagram presentation of figure 14 suggests the other specifications that should not be overlooked. The presence of a buffer between the noninverting and inverting inputs of the CFA guarantees that the input characteristics will not match. This is the main difference between the VFA and the CFA data sheets.

The VFA data sheet typically specifies the power supply and common-mode rejection for the offset voltage only. The input bias currents are also subject to disturbances from these sources but good VFA design encourages matching impedances at the inputs to mask the effects.

The CFA does not have the privilege of bias current match, so the same effects that are specified for the offset voltage need to be measured for the two input nodes. In particular, the inverting input, which is the true signal input is often the biggest source of error. It is not uncommon to see a CFA constrained to operate in an inverting gain configuration to circumvent common-mode effects.

It is not very common practice to specify power supply rejection for each supply separately but, for the CFA, it is essential. The complementary devices, NPN and PNP, should not be expected to match each other closely and usually the PNPs are the weaker. PSR measured with tracking supplies typically tend to partially cancel the errors. Real world applications usually rely on independent positive and negative voltage regulators.

MONOLITHIC TRANSCEIVER

In Europe the allocated frequency band for Collision Avoidance Radars is 76 to 77 GHz. The system architecture has different options available: the source could use either a fundamental or a multiplied approach, the modulation technique could take advantage of either FMCW or pulsed techniques; we could also use two separate receiving and transmitting antennas or combine the two functions in one.

In order to cover most system requirements, Alpha Industries is developing the following Monolithic Chips:

- * VCO (38 GHz or fundamental)
- * Driver Amplifier
- * Doubler
- * Down Converter
- * 77 GHz Pin Switch

38 GHz VCO Chip

The 38 GHz VCO MMIC Chip is shown in Fig.1. The design uses a 0.25 x 400 micron power MESFET in common source configuration and two double mesa integrated varactors (1), one for frequency tuning and one for temperature compensation. The drain of the power MESFET is connected to the output through a coupler that transforms the impedance and decouples the oscillator. The double mesa varactor technology was specifically designed to reduce the diode series resistance and improve the Q of the resonator, therefore resulting in lower VCO phase noise as compared to a planar varactor process. Typical performance is as follows:

* Frequency	38-38.5 GHz
* Pout	+10 dBm
* Tuning BW	600 MHz
* Temp. Stability	Less than 1 MHz/°C
* Phase Noise	-100 dBc/Hz @ 1 MHz offset

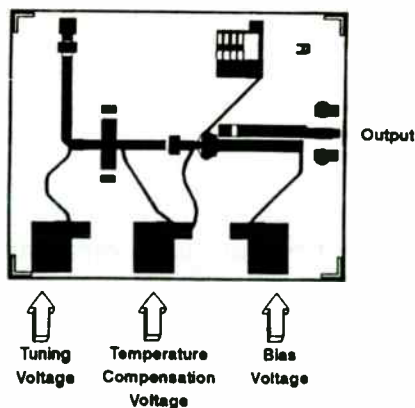


Fig. 1
38.5 GHz VCO Chip

The table below is for a medium performance CFA and exemplifies the amount of detail that should be provided.

INPUT OFFSET VOLTAGE

Initial	5	mV
vs Temperature	8	$\mu\text{V}/^\circ\text{C}$
vs Common-mode	60	dB
vs Supply (tracking)	85	dB
vs Supply (non-tracking)	60	dB

+INPUT BIAS CURRENT

Initial	5	μA
vs Temperature	30	$\text{nA}/^\circ\text{C}$
vs Common-mode	200	nAV
vs Supply (tracking)	50	nAV
vs Supply (non-tracking)	150	nAV

-INPUT BIAS CURRENT

Initial	25	μA
vs Temperature	300	$\text{nA}/^\circ\text{C}$
vs Common-mode	200	nAV
vs Supply (tracking)	300	nAV
vs Supply (non-tracking)	1500	nAV

INPUT IMPEDANCE

+Input	5M//2	Ω/pF
-Input	30//2	Ω/pF

OPEN-LOOP TRANSIMPEDANCE

Transresistance	440	$\text{k}\Omega$
Transcapacitance	1.8	pF

OUTPUT CHARACTERISTICS

Voltage	12	V
Current	150	mA
Output resistance, open-loop	70	Ω

(Source: BB OPA603 data sheet)

SPICE SIMULATION

The combination of declining hardware costs with increasing computing horsepower has made circuit simulation a required part of the design cycle. This has forced the op amp vendor to supply the macromodels for his product offering.

These simulation tools have been offered in varying degrees of complexity, from the simple Boyle model to simplified circuit models, which utilize full transistor models in the signal path. There has been a growing consensus that this latter approach is necessary for the high bandwidth amplifiers.

There can be no doubt that having these models available helps to fill in the gaps from incomplete data sheets. Although the models may not necessarily be configured for worst case process extremes, there may be some performance peculiarities that can be discovered through their use. The pitfall to be aware of is that even the simplified circuit models generally idealize the biasing circuitry, which may mask some second order PSR and CMR effects.

Figure 15 shows two alternative simulation schemes. In figure 15a, the CFA is driven open-loop to measure the open-loop transimpedance and input resistance. This requires two separate simulations. The first uses a voltage-controlled current source to find the dc value of inverting input current to servo the output to zero. The second pass is the ac simulation to actually measure the transimpedance.

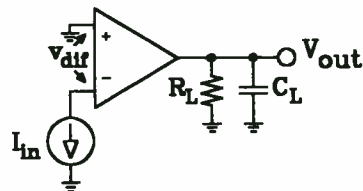


Fig. 15a: Open-loop simulation

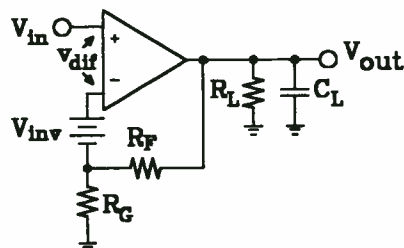


Fig. 15b: In circuit measurement

Figure 15b uses a zero volt battery to measure the inverting input current while the op amp is in a closed-loop configuration. This measures an effective transimpedance that includes the common-mode effect.

The circuit of figure 15a was simulated with the following listing:

```
* CURRENT-FEEDBACK OPEN-LOOP SIMULATION *
* file: CFA-OL.CIR
**** Simulation Commands ****
.options noecho nomod numdgt=8
.op
.ac dec 20 10 200meg
.probe
**** Library Files ****
.lib bb-updat.lib
**** Circuit Listing ****
vp 7 0 15
vm 4 0 -15
*ginv 2 0 6 0 -1
inv 2 0 dc -38.3pa ac 1
x603 0 2 7 4 6 opa603
rl 6 0 100k
.end
```

Figure 16a is the plot of input resistance as measured by dividing the ac voltage by the ac current. Note that for the useful frequency range of the amplifier (roughly 100MHz), R_{in} varies less than 10Ω . The open-loop transimpedance is displayed in figure 16b. Here the magnitude has fallen from a dc value of $790\text{k}\Omega$ to $1.5\text{k}\Omega$ at 51.6MHz , which is where the open-loop phase has fallen to -120° .

DRIVER AMPLIFIER CHIP

GAMMA¹ Monolithics has already developed and tested power amplifiers in Ka-band based on our standard 0.25 micron power MESFET process. Output power exceeding 3 watts has been achieved using basic cells which combine four standard 400 micron power MESFET devices. Test data for one of these cells is reported in Fig. 2. By using an amplified source in Ka-Band multiplied up to 77 GHz, we can very easily achieve the power levels (10-20 dBm) required for a collision avoidance system.

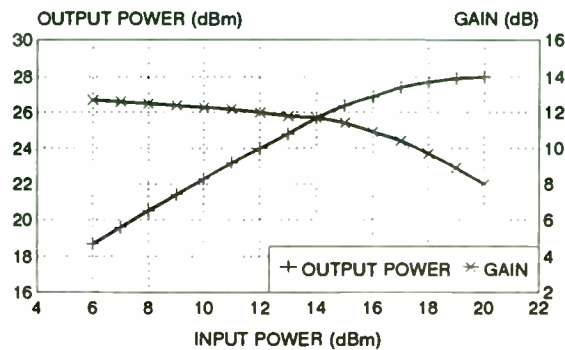


Fig. 2
Gain and Power Output
of a 400 mW Power Amplifier

38.5 to 77 GHz DOUBLER

Multipliers in W-Band could utilize either FET or Varactor Monolithic Technology(2). A Varactor-based doubler is preferred because of better conversion efficiency and superior bias and temperature stability. In addition, our VCO design integrates two high Q double mesa varactors with power MESFET material; therefore further monolithic integration of the varactor function with either the VCO or the power amplifier is an available option. A simulation of the monolithic doubler yielded better than 8 dB conversion loss at 77 GHz.

DOWNCONVERTER

A 60 GHz subharmonic mixer has been already fabricated and tested for a space communication program.

The use of a 30 GHz LO signal reduces the power required at the fundamental frequency without compromising the noise figure performance by more than approximately 1 dB as compared to a fundamental down-converter.

The mixer chip used two anti-parallel Schottky diodes to produce a virtual Lo signal at 60 GHz. The diode exhibits a series resistance of 6 ohms and a capacitance of 0.035 pF, allowing efficient frequency conversion at 60 GHz. Conversion loss is typically 6-7 dB across a 10% bandwidth. It is felt that this conversion loss can be improved by 1-2 dB by optimizing the diode structure to produce lower series resistance and capacitance. The mixer, due to the self-biased nature of the subharmonic configuration, requires as little as +6 dBm LO drive.

¹ GAMMA Monolithics is a partnership between Alpha Industries, Woburn, Massachusetts, and Martin Marietta, Baltimore, Maryland.

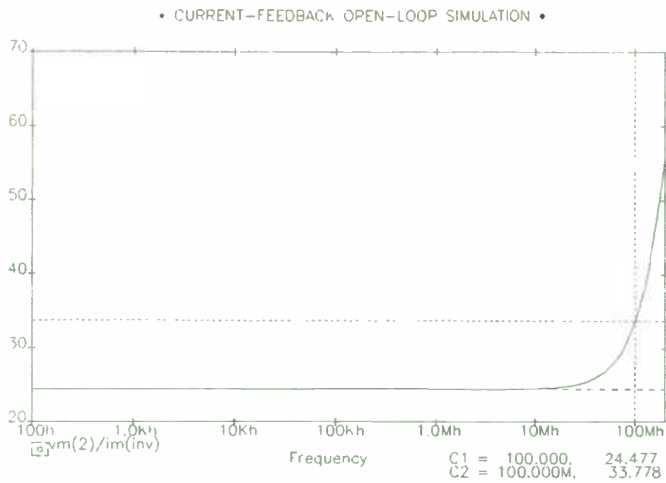


Fig. 16a: Measuring the inverting input impedance

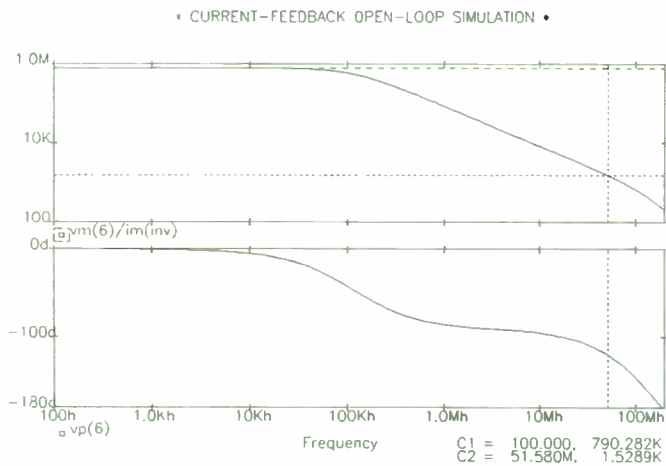


Fig. 16b: Measuring open-loop transimpedance

The circuit of figure 15b was simulated with the following listing:

```

* CURRENT-FEEDBACK CLOSED-LOOP SIMULATION *
* file: CFA-CL.CIR
***** Simulation Commands *****
.options noecho nomod
.ac dec 20 1000 200meg
.probe
***** Library Files *****
.lib bb-updat.lib
***** Circuit Listing *****
vp 7 0 15
vm 4 0 -15
vin 3 0 dc 0 ac 1
x603 3 inv 7 4 6 opa603
vinv inv 2 dc 0
rf 6 2 1450
rg 2 0 1450
.end

```

The plot in figure 17 shows the intersection of the open-loop gain curve with the closed-loop gain asymptote which occurs at 45.7MHz. The open-loop phase has the value of -120° at this frequency and the broadbanding of the closed-loop gain is quite evident. Note the technique used to generate the open-loop gain curve.

The equation relies on the calculation of open-loop transimpedance (via the current in the battery) which is divided by the sum of the equivalent feedback network plus the input resistance.

$$|A_v| = \frac{|Z_T(f_i)|}{R_E + R_{in}} = \frac{vm(output)}{im(battery)}$$

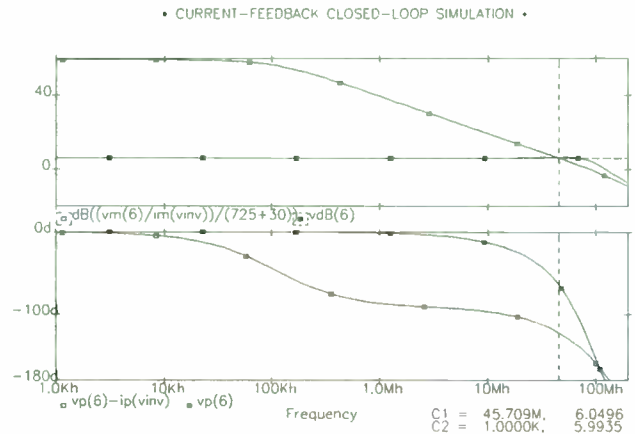


Fig. 17: Slope intercept curves for CFA circuit

MEASUREMENT CIRCUITS

If companies could just ship simulation files to their customers, life would be so easy. Sooner or later, a reality check has to be made. The following circuits have been proven to be quite reliable for measuring the CFA performance parameters.

The low impedance of the inverting input node presents a special problem for the test engineer. Conventional op amp test circuits cannot easily separate the individual parameter variations. The most logical solution is to test the CFA with a current mode test circuit.

Figure 18 shows the basic current pump topology used in the dc test circuit. It consists of an op amp, a P-channel MOSFET and a unique current reference circuit which includes two very accurate current sources and a high precision current mirror.

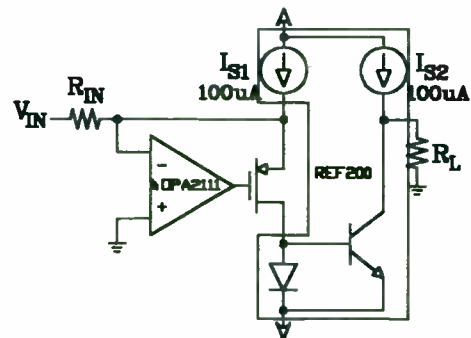


Fig. 18: Current pump topology

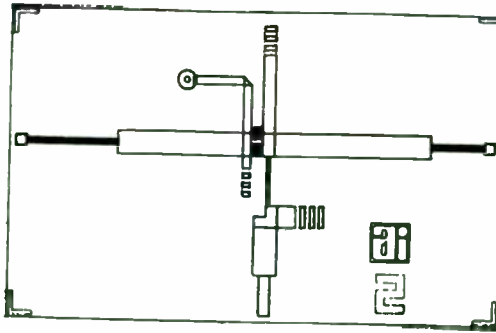
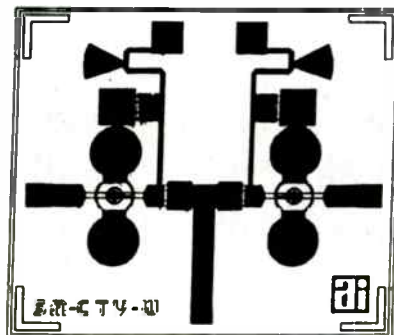


Fig. 3
77 GHz Subharmonic Mixer Chip

A simulation of a 77 GHz mixer, presently in fabrication at Alpha was performed using the same diode utilized in the V-band mixer described earlier. The simulation gave us a noise figure of 6.5 dB DSB when inserted into a balanced rat-race mixer configuration, (see Fig. 3) and 7.5 dB in a subharmonic-type down converter.

77 GHz PIN SWITCH

At 77 GHz monolithic pin-based switches are definitely offering superior performance as compared to their FET-based counterparts. Considering that in the Transceiver the power amplifier function is the major cost driver, we opted for the PIN-based solution as compared to a more integratable FET-based approach. The lay-out of a 77 GHz SPDT is represented in Fig. 4. The design yielded 25 dB of isolation and 1 dB loss at 77 GHz.



Measured
Performance
@ 77 GHz:
Insertion Loss: 1.0 dB
Isolation: 24 dB

Figure 4
77 GHz SPDT Pin Switch

MULTIPLIED VERSUS FUNDAMENTAL APPROACH

The source at 77 GHz could take advantage of either a fundamental or a multiplied approach. Let's assume an output power requirement of 100 mW and a times two multiplier conversion loss of 8 dB. (See Table 1)

The positive feature of a signal multiplied from an amplified source at 38.5 GHz is that it relies on 0.25 micron GaAs power MESFET technology that is already in production in Alpha Industries. On the other hand, assuming a monolithic varactor multiplier conversion loss of 8 dB, to generate 20 dBm at 77 GHz, would require 28 dBm of power at 38.5 GHz, which makes the driver amplifier at least twice as large and its Fet output periphery a minimum of three times as wide as compared to the buffer in W band.

The high gain of the JFET input op amp (VFA) constrains its inverting input to stay at null ground by controlling the current flowing through the MOSFET. If V_{IN} is positive, a current equal to V_{IN}/R_{IN} is shunted to the current mirror input. If V_{IN} is negative, a matching V_{IN}/R_{IN} is provided by the 100uA current source, I_{S1} , and the input to the current mirror decreases. This is an inverting current pump, a positive voltage causes the output to sink current and a negative input causes the output to source current.

The full test circuit is shown in figure 19. The input offset voltage of the DUT is measured directly by the instrumentation amplifier, A1. The RC filters minimize noise and protect the inputs of A1 from overload transients.

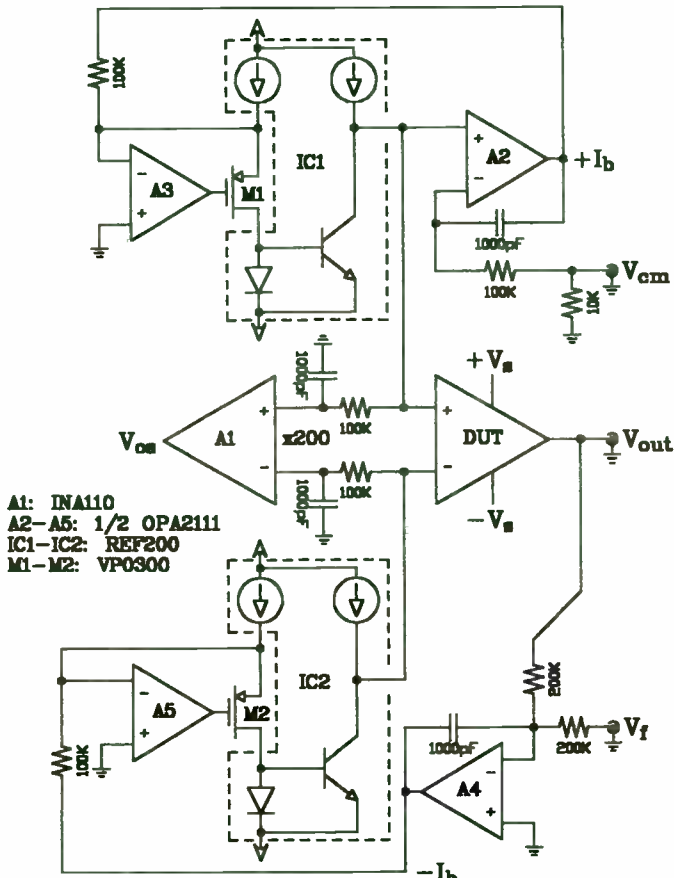


Fig. 19: Current mode CFA test circuit

Amplifier A2 maintains the common-mode bias by forcing the current pump (A3, M1, IC1) to keep the noninverting input of the DUT equal to the input, V_{CM} . The output of A2 driving the 100kΩ input resistor to the current pump is a measure of $+I_b$.

Amplifier A4 constrains the DUT output to be the negative of the input voltage, V_f , by forcing the current pump (A5, M2, IC2) to drive the low impedance inverting input. The amount of inverting current drive is reflected by the output of A4.

All dc parameters, including R_T and R_{in} , can be measured independently and directly. When adapted to a measurement card for the HP Semiconductor Analyzer, the test parameters can be displayed as slopes to determine the limits of linearity.

Figure 20 details an open-loop transimpedance test circuit which, when mated with a network analyzer, will provide the open-loop frequency response curves.

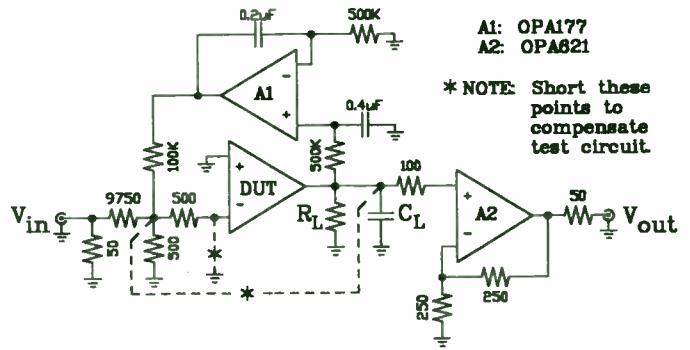


Fig. 20: Open-loop frequency response test circuit

The input ladder network divides the input by 20,000 to provide a low current level signal to the inverting input of the DUT. The 500Ω value for the input resistor dominates the small but finite input resistance of the CFA. The A1 integrator servos the output to zero by sensing the DUT output and feeding a small current back to the input. A2 buffers the DUT output and drives the 50Ω input of the network analyzer.

The only caveat is to take into account the gain and phase rolloff of A2. Automated network analyzers allow for compensation by storing an "offset" sweep which is subtracted from the actual signal sweep.

Although the network analyzer will scale the output in dB, the transimpedance can be determined by using the following equation:

$$Z_T = 500 \cdot \log^{-1} \left(\frac{\text{dB magnitude}}{20} \right)$$

The transcapacitance can be found by extrapolating the open-loop pole.

CONCLUSION

CFAs are not difficult to comprehend and work with if the basic relationships between R_T , C_T , R_{in} and open-loop phase are kept in mind. The lack of balanced input nodes require extra care be taken with applications requiring dc accuracy. Simulation is a wonderful tool for the early design stages but only actual measurements will grant peace of mind.

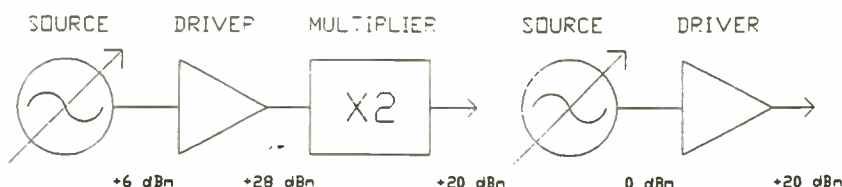
At 77 GHz the device required is based on a 0.15 micron Pseudomorphic HEMT. This technology, although demonstrated, is not as mature from a manufacturing point of view.

On the positive side, it will deliver a monolithic chip with half the size or less. In terms of yields, at 77 GHz the shorter gate length and the more complex material structure could be balanced off by the reduced gate periphery.

Assuming 4" wafers and 30% chip sort yields, a 1995 cost projection derives a chip cost of \$45 for the multiplied source. At 77 GHz, with the same overall yield, the chip cost is down to \$22.50.

MULTIPLIED
(38.5 GHz x 2)

FUNDAMENTAL
(77 GHz)



6 dBm 28 dBm 20 dBm 0 dBm 20 dBm

FET REQUIRED

Type Power Mesfet
Gate Length 0.25 Micron
Gain 8 dB (at 38.5 GHz)
Power Density 300 mW/mm (at 38.5 GHz)

Pseudomorphic
0.15 Micron
7 dB at (77 GHz)
150 mW/mm (77 GHz)
Under Development

TECHNOLOGY STATUS

Mature

DRIVER AMPLIFIER

Number Stages 3
Fet Output Periphery 2.1 mm.
SOURCE FET PERIPHERY 400 Micron

3
0.666 mm.
200 Micron

REAL ESTATE

VCO	4 mm ² (actual)	2 mm ² (projected)
Multiplier	1 mm ² (projected)	N/A
Overall Size	18 mm ²	9 mm ²
Wafer Cost/mm (assuming 4" wafer)	\$2.50 (30% yield)	\$2.50 (30% yield) \$5 (15% yield)
Overall Cost (1995 projection)	\$45	\$22.50 \$45

Table 1
Source Alternatives

The SLAM: A New Ultra-linear Power FET Module Concept for HF Applications.

Adrian I. Cogan
Lee B. Max (*)
Al Rosenzweig

MicroWave Technology, Inc
4268 Solar Way
Fremont, CA 9453

Introduction

This paper describes the application of a new family of low cost silicon FET linear Class-A HF power gain blocks. *

These gain blocks, called 'SST Linear Amplifier Modules', or 'SLAMs' use a high frequency power FET; the 'Solid State Triode™', or 'SST™'. The SLAM modules are self-biased, and exhibit excellent linearity and thermal stability. With these modules, Class A broadband amplifiers covering the frequency range of DC through 100 MHz can be easily constructed with power outputs ranging from 10 Watts to 200 Watts or more.

SLAMs can easily be power combined to deliver hundreds of watts of linear HF power. Several 10 W through 200 W class-A power amplifiers, operating from 2 MHz through 32 MHz and 10 MHz through 100 MHz are described. The actual construction of the SLAM circuits is also described.

Inside the SLAM: The SST and Self-biased SST Operation.

The active element in the SLAM building block is a high frequency Silicon FET chip called the Solid State Triode, or SST. The SST name comes from the device's I-V characteristics which are similar to those of a vacuum tube triode (Figure 1).

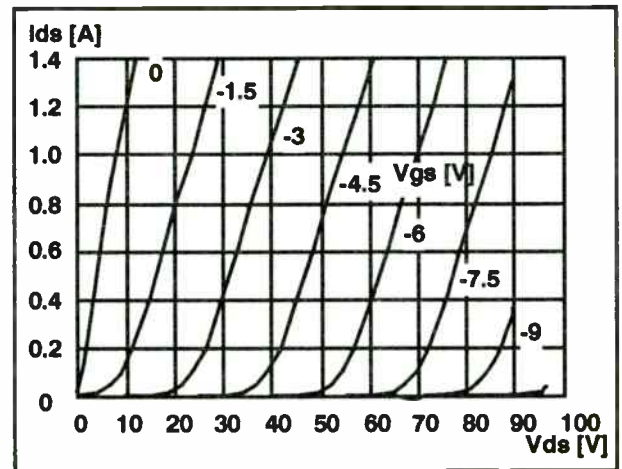


Figure 1: SST I-V Characteristics.

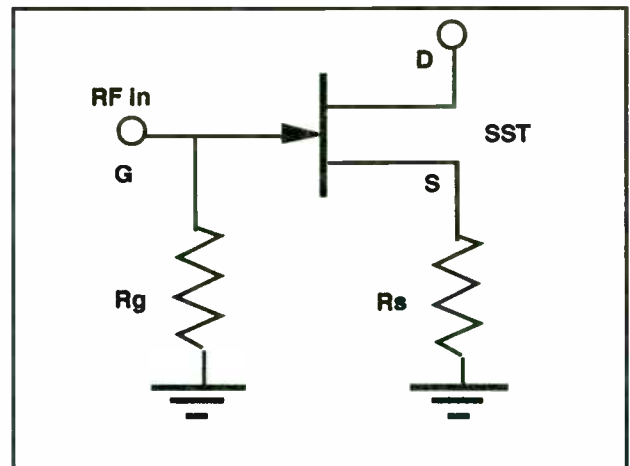


Figure 2. SLAM Internal Biasing Circuit.

The SST is a Junction FET and requires the same gate and drain bias polarity as a GaAs MESFET or a vacuum triode. Such a bias polarity (positive V_{ds} and negative V_{gs}) allows one to set the SST operating point by using the self-biasing circuit of Figure 2.

* Mr. Max is an independent consultant

CONCLUSIONS

It is true that 30% yields in W band have yet to be proven, but it is also true that 30 % yields in Ka-Band is today, based on recent experience, a conservative projection for the foreseeable future. The GaAs technology is progressing very fast when we consider that only a few years ago the 1 micron MESFET was the only process in production. The automotive sensor business is offering GaAs monolithic circuits an unprecedented opportunity to be inserted in large volume programs. To be successful in this market the engineers have to focus on how to bring the required processes, from wafer fabrication to assembly and test, in a real low cost manufacturing environment.

References

1. McDermott, M.G. et al, "Integration of High-Q GaAs Varactor Diodes and .25 μm GaAs MESFET's for Multifunction Millimeter-Wave Monolithic Circuti Applications", IEEE Trans. on MTT, vol. 38, no. 9, Sept. 1990, pp. 1183-1190.
2. Lamberto Raffaelli and Earle Stewart "Millimeter-wave Monolithic Components for Automotive Applications", Microwave Journal, Vol. 35, no. 2, February 1992.

The voltage drop produced by the source current across the source resistor sets the SST operating point by supplying the gate voltage through the gate-to-ground resistor. This biasing scheme will set a Class A operating point and, if the source resistor is not bypassed with a low reactance capacitor, the resulting negative feedback will improve the circuit linearity. Added advantages are flatter frequency response, higher input impedance, and improved stability. The resulting I-V characteristics of a self-biased SST are shown in Figure 3. Notice the current saturation trend, despite the SST triode-like characteristics.

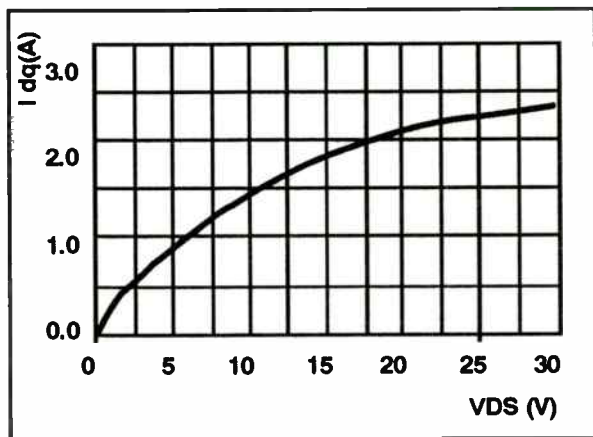


Figure 3. SLAM0111: Bias Current vs. Vds.

The SST exhibits excellent linear performance, as illustrated in Figure 4, where a 50 W SST third-order intermodulation product ('IMD3') is compared to similar power MOSFETs and bipolar transistors. This data was taken at 215 MHz without the self-biasing feature.

The self-biasing circuit improves the SST linearity even further.

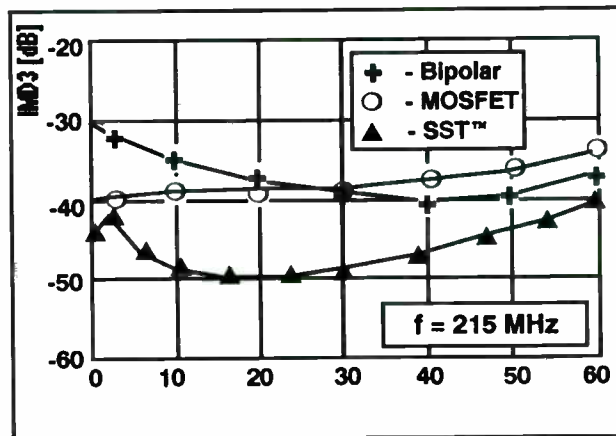


Figure 4. Typical Class AB Two Tones IMD3: 50 W BJT, MOSFET, and SST

By assembling the SST chip and the gate and source resistors inside a conventional RF transistor package, the result is a SST Linear Amplifier Module, or a 'SLAM'. The SLAM uses only a single power supply and performance remains constant over a wide range of supply voltage.

Presently, MWT supplies three power SLAMs: a single-ended unit, the SLAM-0133 rated for 10 W; and two push-pull SLAMs, the SLAM-0111, rated for 25 W, and the SLAM-0122, rated for 50 W. All three devices are designed to operate from DC through 32 MHz. SLAMs are supplied assembled in industry standard single-ended or push-pull packages (Figure 5).

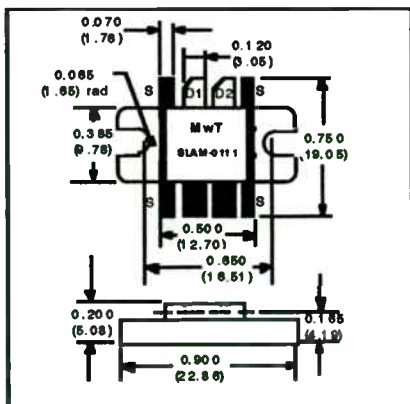
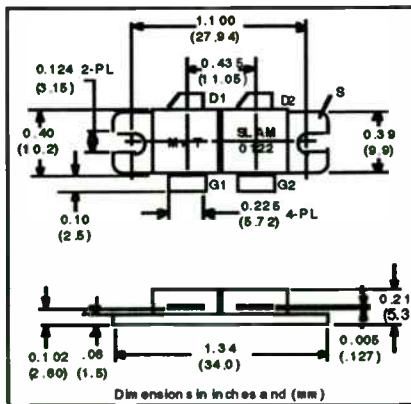
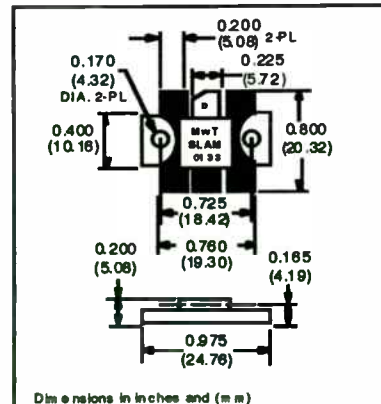


Figure 5. SLAM Packages. SLAM-0111



SLAM-0122



SLAM-0133

110-GHz Wafer Probe Enables Cost-Effective Millimeter-Wave Circuit Applications

Edward M. Godshalk
Cascade Microtech Inc.
Beaverton, Oregon

I. Introduction

Millimeter wave monolithic integrated circuit (MIMIC) technology has matured to a high degree under such programs as the DARPA MIMIC effort. The original intent was to develop cost-effective millimeter wave frequency (i.e., >30 GHz) circuits for such applications as radar front ends for missile seekers and aircraft systems. With the declining military market there has been a strong push to commercialize this technology for application such as automotive collision avoidance radar and local area communication networks (LAN).

For any of these applications, wafer probes are required for characterization and testing of the circuits while they are still in wafer form. The circuits must be tested at the wafer level, since inserting defective devices into systems typically raises the cost of using MIMICs to an unrealistic level. The cutting edge for many applications of MIMICs is in the 50 to 110 GHz region. For this reason, DARPA has funded the development of wafer probes for use in the V-band (50 to 75 GHz) [Navy Phase III MIMIC] and W-band (75 to 110 GHz) [Army Phase III MIMIC] frequency ranges. This paper will discuss the development of these probes with emphasis on the W-band probe, since it is at the cutting edge of wafer probing technology.

A brief review of wafer probes is presented in section II. Section III and IV discuss the technical aspects of the waveguide input wafer probes and section V presents measured data for these probes and some device measurements. Conclusions are in section VI.

II. Review of Wafer Probe Technology

At frequencies below 65 GHz, the wafer probe can be linked to the chosen test equipment via a coaxial cable [1]. Figure 1 shows traditional coaxial input wafer probes. Inside the probe body there is a coax-to-coplanar waveguide (CPW) transition. The coplanar waveguide is formed by depositing a layer of gold on the lower surface of an alumina probe board and guides the signal to the probe tip. This structure is known as the probe board. At the tip of the probe board a hard metal, such as nickel, is deposited on the CPW metalization to form fingers. These fingers make contact with the device under test (DUT) on the wafer

The SLAM and SLAM Circuit Building Blocks

The values of the SLAM internal components are selected to minimize or even eliminate the need for impedance matching components when operating from a 50 Ω source and load impedance.

The SST FETs in combination with the internal self-biasing circuit provide the user with a thermally compensated circuit component. The SLAM power gain has a thermal derating factor of less than 0.01 dB/°C and the SLAM bias point is virtually constant with temperature.

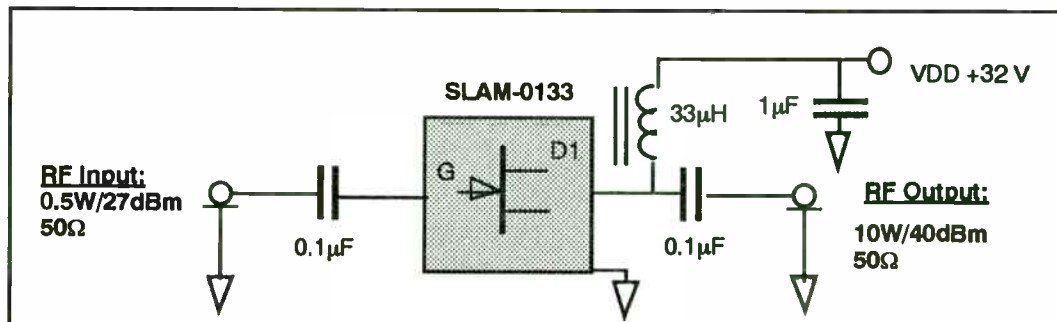


Figure 6. SLAM-0133, 2 MHz - 32 MHz Driver-Amplifier.

The simplest SLAM circuit is shown in Figure 6, where a single-ended unit is used as a 10 W HF driver. The operating bandwidth is 2 MHz to 32 MHz. Notice the simplicity of this amplifier which requires, in addition to the SLAM, only two DC-blocking capacitors and one RF choke. Figure 7 illustrates the frequency response of this amplifier.

matching components, but this will increase the circuit complexity.

The third order intermodulation products (IMD3) and the harmonic contents (f_2 , f_3) vs. the input power level for this amplifier are shown in Figures 9 and 10, respectively. The third order intercept point ('TOIP', or 'IP3') is +52 dBm, more than 10 dB above the P-1dB level.

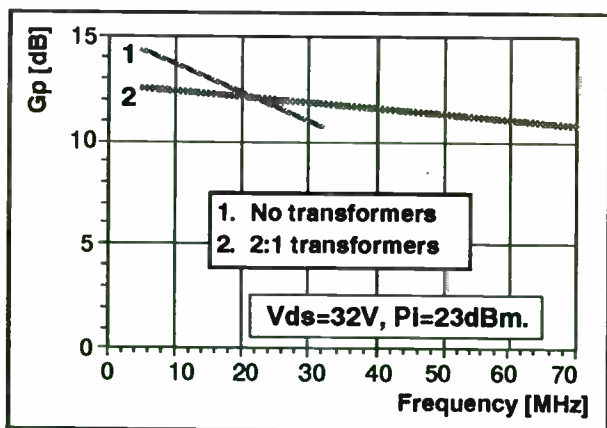


Figure 7. Typical Gp vs. Freq.

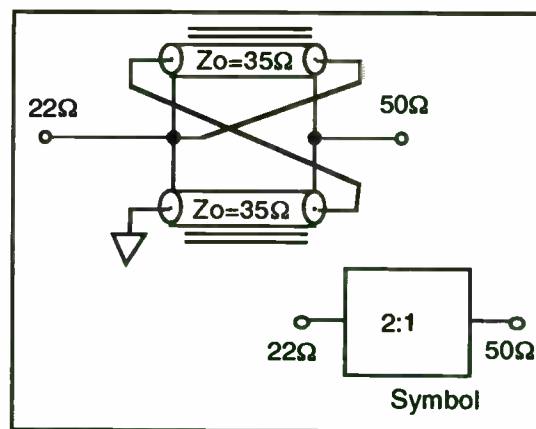


Figure 8. 2:1 Impedance Transformer.

By adding inexpensive 2:1 input and output transformers, the frequency roll-off is reduced and the bandwidth expanded. Such a transformer can be implemented using 50 Ω coaxial cables (Figure 8).

The bandwidth can be further widened to 100 MHz by using additional impedance

Figure 11 shows the input VSWR versus frequency for this simple SLAM amplifier while power gain vs. supply voltage is shown in Figure 12.

surface. Typically coplanar pads are formed at the DUT test ports to allow contact with these probe fingers.

A waveguide-to-CPW transition was required to extend the upper frequency limit of wafer probes, since commercially available coaxial cable assemblies overmode above 65 GHz [2]. Figure 2 shows an operational diagram for a waveguide input wafer probe. Rectangular waveguide enters a transition section where the dominant TE₁₀ mode of the waveguide is converted to a coplanar field pattern. The coplanar mode is then launched on a CPW probe board similar to that described above. Figure 3 shows a pair of V-band probes probing a GaAs wafer. Notice the waveguide entering the far end of each probe, and the bias cable attached to the side of the probe.

III. The Transition

Figure 4 illustrates the transition process in greater detail. The rectangular waveguide input is illustrated in (a), which supports the TE₁₀ mode as shown. Next, a ridge is gradually introduced, which forms the quasi-TEM field pattern as in (b). The ridge-trough waveguide is formed by gradually adding a trough below the ridge as shown in (c). By lowering the ridge into the trough, the electric field is split and rotated forming a coplanar field, with a characteristic impedance of 50 ohms in this case. This field pattern is similar to that found in a coplanar waveguide as illustrated in (d). The final step is to launch the coplanar mode into a 50-ohm CPW transmission line. The CPW line is inverted, as shown in (e) to bring its grounds into contact with the lower surface of the waveguide. The signal line of the CPW is attached to the ridge with a gold bond ribbon. This completes the transition process.

A test fixture was constructed to confirm the transition design. For W-band, a WR-10 rectangular waveguide was transitioned to 50-ohm ridge-trough waveguide and then back to WR-10 waveguide. Having rectangular waveguides at each port of the test fixture allowed testing with a HP-8510C waveguide test set for use at W-band. Figure 5 shows the insertion loss (S₂₁) and return loss (S₁₁) of the transition. Since the measured insertion loss is actually for two transitions (i.e. back-to-back), the appropriate scale for S₂₁ is half the measured loss to give the effective loss for a single transition. The insertion loss is less than 0.7 dB from 75 to 106.5 GHz rising to 0.8 dB at 110 GHz. The return loss is better than 15 dB over the entire band, except at two spots.

IV. The Probe Board

The CPW probe board design presented two primary challenges: low insertion loss, and low crosstalk between probes when two or more probes are in close proximity while probing some device. Insertion loss in CPW transmission lines is generally attributed to radiation loss and conductor loss when low-loss dielectric

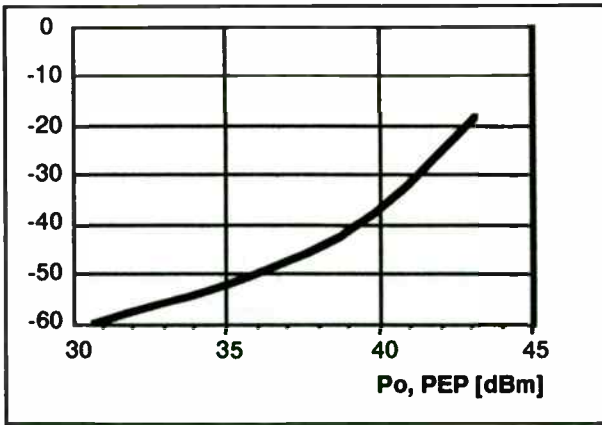


Figure 9. Typical IMD3 vs Power Output

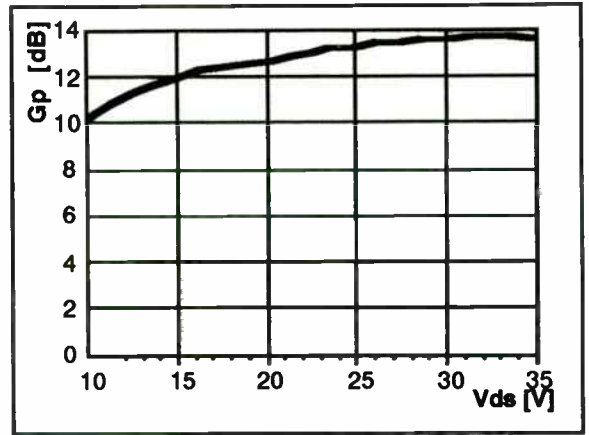


Figure 12. Typical Gp vs. Vds, f=8MHz

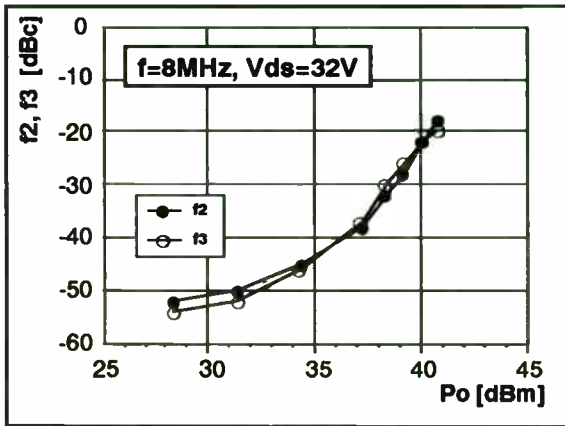


Figure 10. Typical Harmonics Content

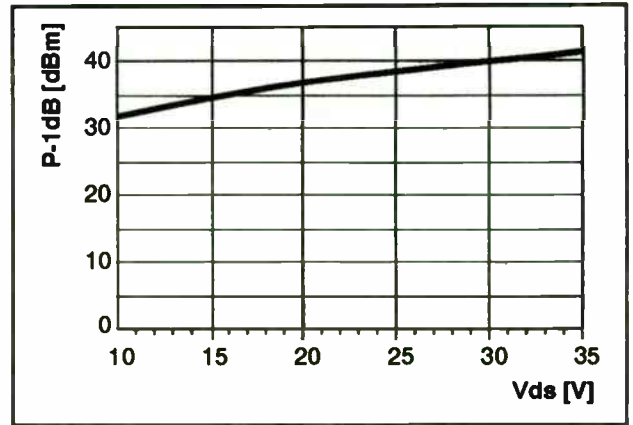


Figure 13. Typical P-1dB vs. Vds

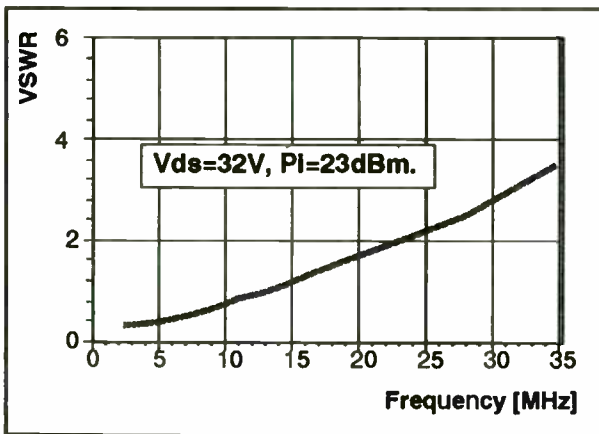


Figure 11. Typical Input VSWR vs. Frequency.

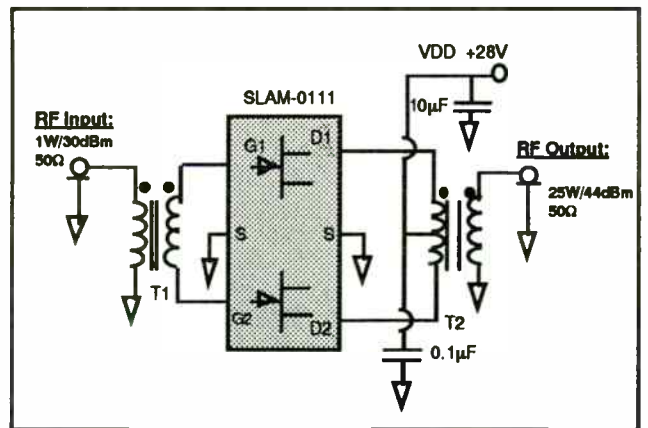


Figure 14. 2MHz - 32MHz SLAM Amplifier Circuit.

Figure 13 plots the one-dB compression point (P-1dB) dependence upon supply voltage. As shown, at the recommended operating point, the gain remains constant over a wide supply voltage variation.

A 25 W push-pull SLAM-0111 amplifier circuit is shown in Figure 14. The amplifier operates over the 2 MHz - 32 MHz HF band.

This configuration uses wire wound transformers. Notice again the simplicity of the circuit.

The wire wound 1:1 input transformer is made by winding 2 to 5 turns of #30 AWG wire on a ferrite balun core. The 1:1 output/bias transformer uses 3 turns, center tapped #26 AWG wire on a balun core. The

substrates are used. At the onset of the CPW design, radiation loss was expected to be the dominant insertion loss factor based on prior research [3]. Using a similar approach, the predicted radiation loss was computed for three CPW transmission lines on alumina, having gaps of .001, .002, and .004 inches (G in Figure 6). In each case the signal line width (W) was increased to maintain 50-ohms characteristic impedance. Figure 7 shows the results which imply that radiation loss increases with gap size.

To verify these predictions a radiation study was conducted. This consisted of measuring the insertion loss (S21) of three coplanar waveguide (CPW) transmission lines, all 1.00 inch long. The three CPW lines differ in gap and signal line dimensions (see Table 1). In each case W and G are chosen for a characteristic impedance of 50 ohms. Figure 8 shows the results which are opposite of what was predicted. The implication is that radiation loss is negligible and that the signal line width (W) dominates. It is speculated that this dominance is due to the reduction of signal line resistance with increasing width.

The tests were conducted on a .020" thick alumina substrate. This allowed scaling these 0 to 50 GHz results to those of a .010" thick substrate, with W and G half the size listed in Table 1, over the 0 to 100 GHz range. This scaling implied that no moding would take place, based on the monotonic nature of the data.

From these results the CPW probe boards were designed for primarily low conductor loss, since the radiation loss was no longer viewed as a major concern. At the probe tip the gaps and signal line width of the CPW line are reduced through a tapered region to give the required separation of the nickel fingers to match the device under test (DUT). To minimize radiation off the probe tip, this taper must maintain a constant characteristic impedance. Excess radiation can couple to another probe tip during multi-port measurements. This can perturb data, particularly where low signal levels are involved, such as S12 in FET measurements.

V. Functional Probe Data.

Figure 9 illustrates the construction techniques employed for an actual probe. The probe block is split into upper and lower halves as shown. An insulating layer is placed between the two halves to provide dc isolation. Quarter wavelength RF chokes generate a virtual ground where the waveguide interior surface is split to minimize RF losses.

The alumina probe board is captured in a pocket that is machined into the upper block. The probe board is oriented such that the metalized ground-signal-ground lines are facing down, since this is the surface that must contact the wafer. A bond ribbon joins the signal line (shown by a dashed line) to the ridge

above figures correspond to a core with a $\mu = 2000$. The actual number of turns is determined by the ferrite actual μ and the desired amplifier bandwidth. This SLAM amplifier operates at a 25 W nominal output power and exhibits a TOIP of +55 dBm. Figure 15 shows the IMD3 data at five frequencies, while P-1dB and power gain vs. supply voltage is plotted in Figure 16.

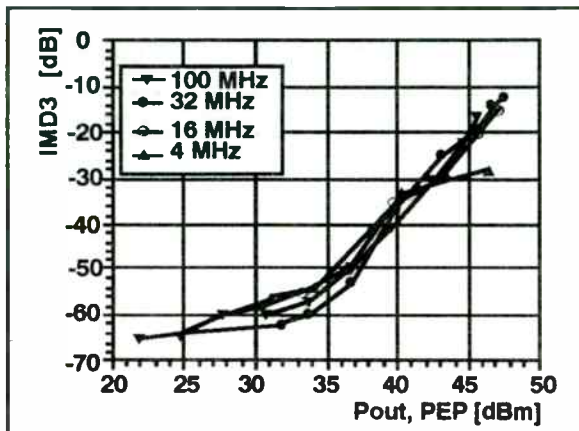


Figure 15. 25W SLAM:0111 IMD3 vs. f. Vds = 28 V.

Again, notice the reduced sensitivity to the supply voltage when operating this amplifier at the recommended voltage. One can broaden the operating bandwidth of this amplifier to 1 MHz through 100 MHz by using the circuit of Figure 17. The maximum linear output power will, however, be reduced to 20 W at the high frequency end of the band.

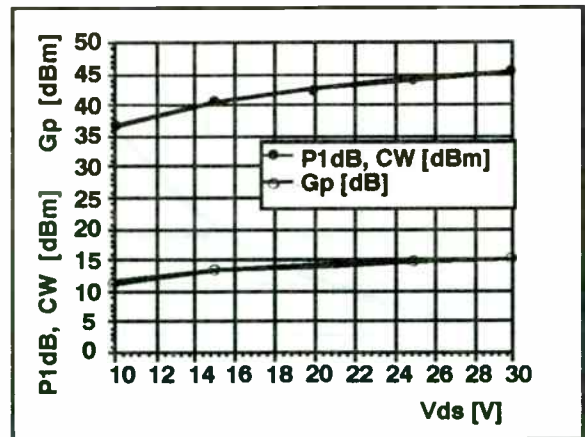


Figure 16. 25W SLAM: P-1dB, Gp @ 16 MHz.

The wire wound transformers are replaced by coaxial baluns and a coaxial biasing transformer has been added between the two drain terminals.

The input transformer can be implemented by winding three to eight turns of RG-174U, 50 Ω coaxial cable over a ferrite toroid core with a $\mu \geq 100$. The bias transformer uses 4 turns of the same 50 Ω coax and ferrite core type. The frequency response of this SLAM amplifier is shown in Figure 18.

One advantage of the SLAM concept is its modularity. By using a small number of impedance transformers, power splitters, and bias transformers, one can power-combine SLAMs to almost any practical power level. Several such 'modular' SLAM amplifiers will be described below.

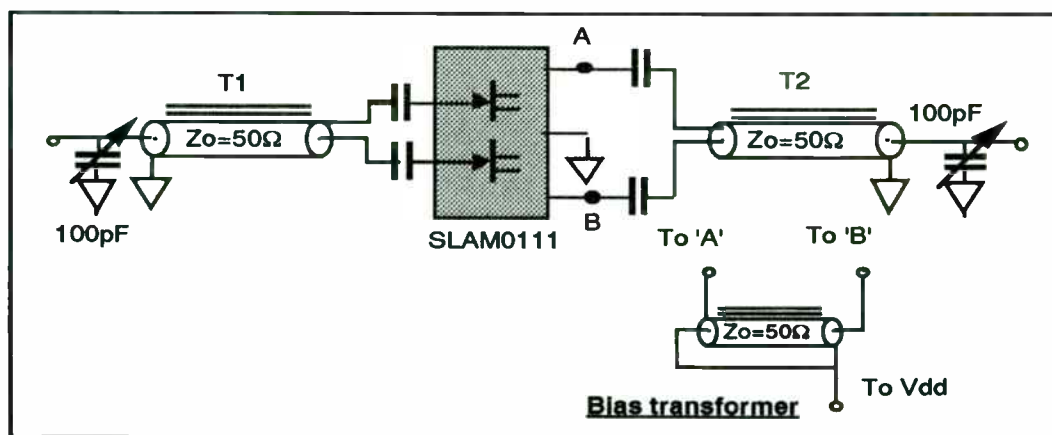


Figure 17. 20W, 1MHz - 100MHz SLAM0111 Amplifier.

Two coaxial baluns and one 2:1 transformer (Figure 8) can be combined in the configuration shown in Figure 19, to yield a

two-way power splitter/combiner with $Z_{in} = Z_{out} = 50 \Omega$. As it will be shown below, this

after the probe is situated in the upper block. When the lower block is joined to the upper block the probe board is clamped into place. This clamping also brings the ground metalization of the probe board into electrical contact with the lower block. The end result is that the signal line and ground lines are electrically isolated and may be biased by applying a voltage to the upper and lower block halves respectively. In the event of probe board breakage, the two halves may be separated and a new probe board installed.

The performance of actual V-band and W-band wafer probes are shown in Figures 10 and 11, respectively. The insertion loss (S21) is typically 3 ± 1 db for both probes, with a worst case of 4 db and 4.2 dB for each respectively. Two reflection coefficients are shown for each probe: S11 and S22. These are the reflection coefficients at the rectangular waveguide input port and at the tip of the alumina probe board, respectively.

With a pair of V-band probes, a pseudomorphic MODFET was tested, using a setup similar to that shown in Figure 2. Figure 12 shows the S21 data for this device. The device has S21=1 at 58.5 GHz. Passive devices such as capacitively couple filters have also been characterized, even when their insertion loss exceeded 30 db. At this time, no devices have been made available for testing with the W-band probes, but similar performance is expected.

VI. Conclusions

Under the Phase III MIMIC program, waveguide input wafer probes were successfully developed covering 50 to 110 GHz in two bands. These probes are required to allow MIMICs to be fully tested and characterized at the wafer level. This testing is essential if MIMICs are to be financially feasible for insertion into both military and commercial systems.

VII. References

- [1] K.E. Jones, E. W. Strid, and K. R. Gleason, "mm-Wave Wafer Probes Span 0 to 50 GHz," *Microwave J.*, Apr. 1987.
- [2] E.M. Godshalk, "A V-Band Wafer Probe Using Ridge-Trough Waveguide," *IEEE Trans. Microwave Theory Tech.*, vol.T-39, pp. 2218-2228, Dec. 1991.
- [3] M. Riazat, R. Majidi-Ahy, and I.J. Feng, "Propagation Modes and Dispersion Characteristics of Coplanar Waveguides," *IEEE Trans. Microwave Theory Tech.*, vol. MTT-38, pp. 245-251, March 1990.

combiner is used to assemble 50 W and 100 W push-pull SLAM amplifiers.

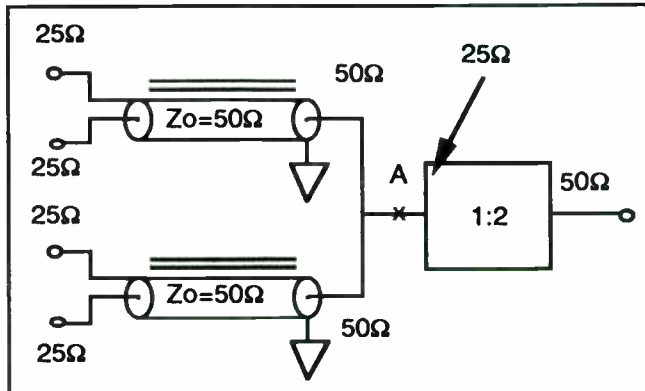


Figure 19. 4:1 Power Splitter/Combiner with (optional) improved isolation.

Another useful coaxial cable power combiner with $Z_{in} = Z_{out} = 50 \Omega$ is the four-way unit shown in Figure 20. Such combiners are used to assemble 100 W and 200 W power SLAM amplifiers.

An isolation transformer, such as the one illustrated in Figure 21, can be inserted at the point marked 'A' in the Figure 19 two-way combiner. This option will provide improved load isolation for the high power SLAM amplifiers.

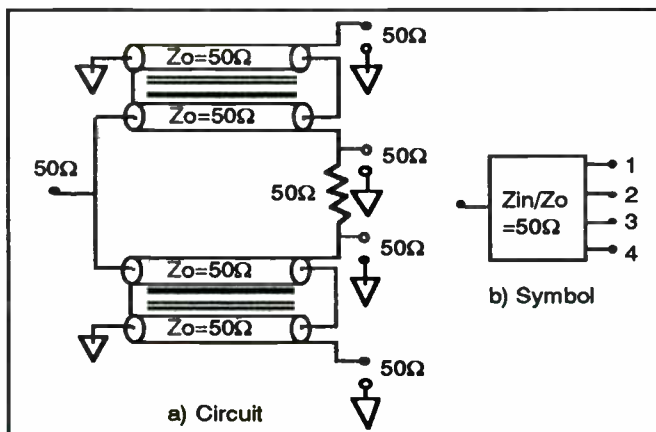


Figure 20. 50Ω/50Ω, 1:4 Power Splitter/Combiner.

Class A Linear. Power Amplifiers.

Using the impedance transformers and splitter/combiners described above, individual SLAM packages can be combined to achieve higher power levels over the HF frequency range.

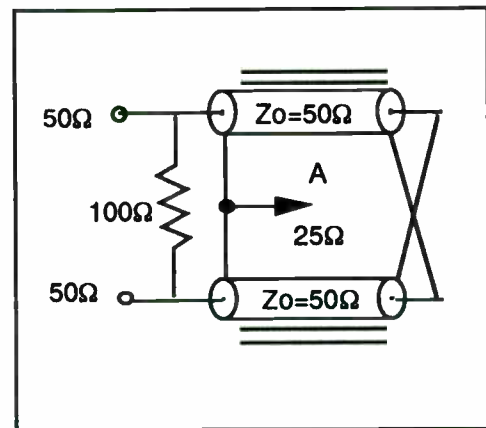


Figure 21. Isolation Transformer.

One simple combination was shown in Figure 17 where two coaxial cable baluns and one coaxial cable bias transformer are used to assemble a push-pull amplifier. The bias transformer is connected between the points marked 'A' and 'B', which represent the SST drains.

Over the 2 MHz - 32 MHz frequency range, the amplifier will yield 25 W of linear power if the SLAM-0111 is used, and 50 W with the SLAM-0122. The recommended bias voltages are 28 V for the SLAM-0111 and SLAM-0133, and 40 V for the SLAM-0122.

By combining two of the above SLAM-0111 amplifiers with two 50 Ω coaxial baluns, one will achieve 10 MHz through 100 MHz operation, with a 40 W output power (Figure 22). The inner baluns use 25 Ω coaxial cable and the same number of turn as the outer ones.

Biasing transformers are not illustrated, but they must be connected to the SLAM drains as in the Figure 16 example.

The frequency response of the SLAM-0111 version of this amplifier, which has a broadband gain of 12 dB, is shown in Figure 23.

The 2:1 transformers and 50 Ω coaxial baluns can be used as in Figure 24 to build 50 W SLAM-0111, or 100 W SLAM-0122 amplifiers. Two bias transformers will supply DC power to each of the two SLAM drain pairs. This amplifier operates over the 2 MHz - 32 MHz HF range.

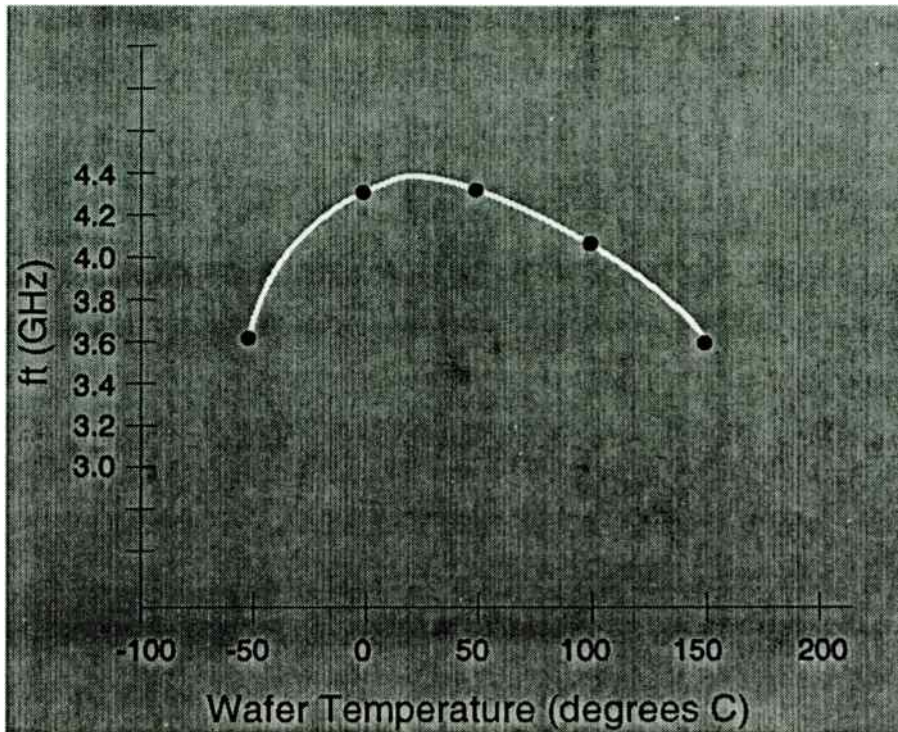


Figure 1. Typical f_t Temperature dependence of a 2x3 micron bipolar transistor ($I_c = 10$ mA).

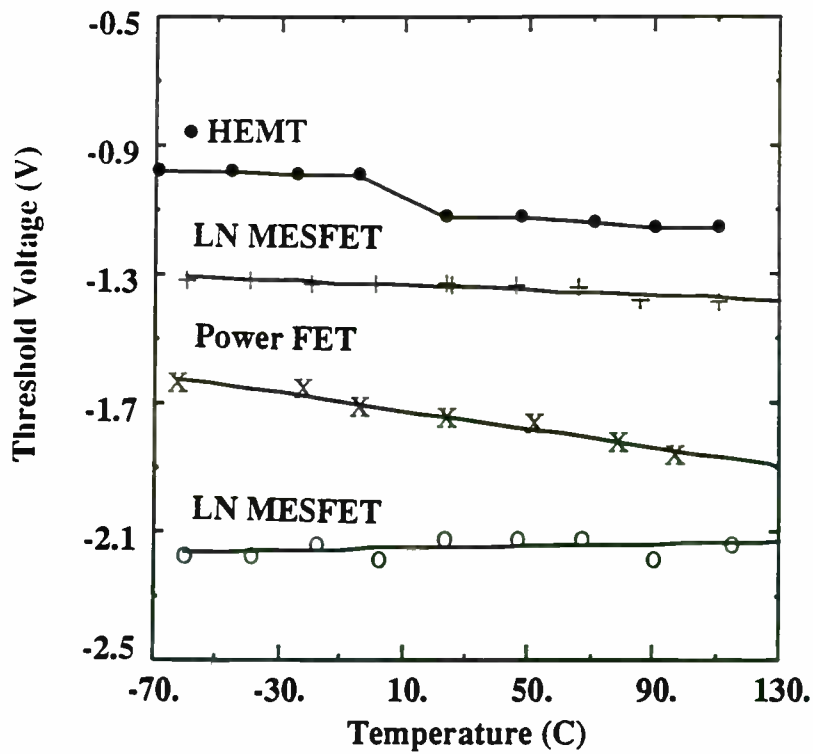


Figure 2. Differences in MESFETs and HEMT threshold voltages versus temperature

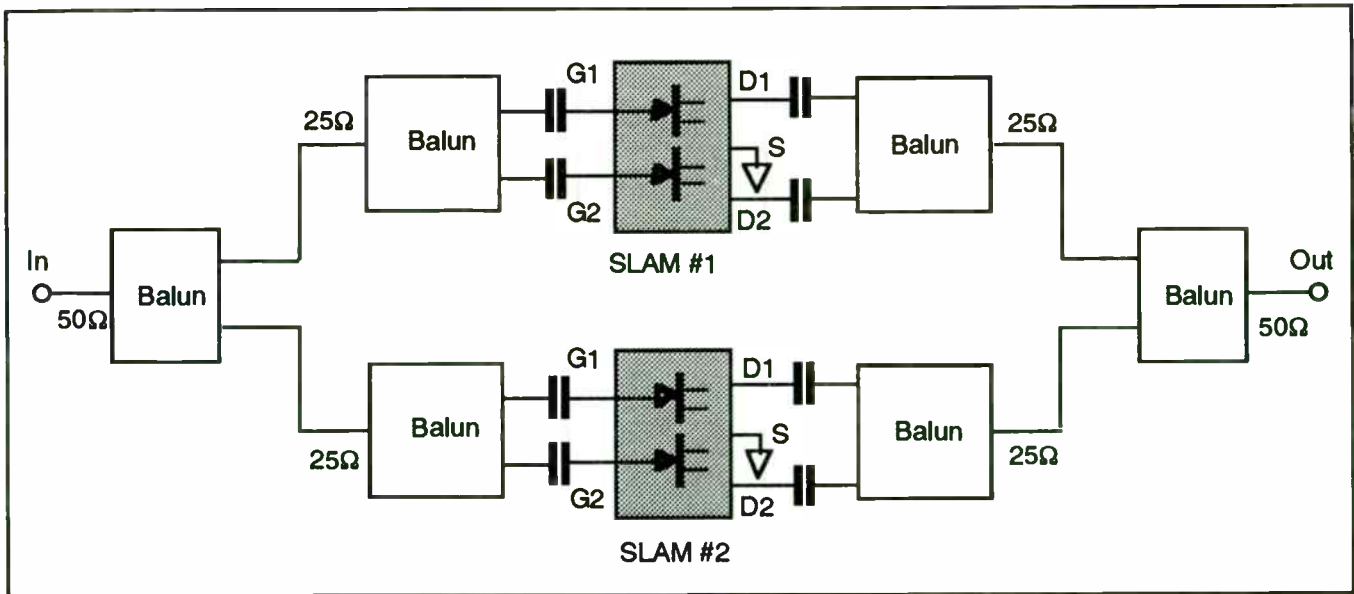


Figure 22. 40W, 10MHz - 100MHz, SLAM0111 or 75W 1MHz - 50MHz, SLAM0122 Amplifier.

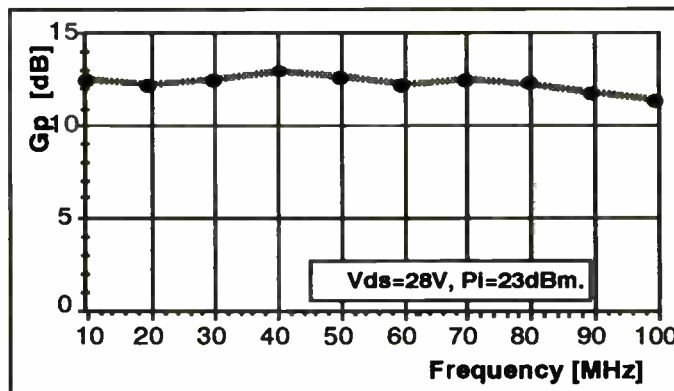


Figure 23. Broadband 50W 2xSLAM0111 Amplifier: Typical Gp vs. Frequency.

By using the coaxial transformer in Figures 19 and 21, improved isolation can be achieved

One can use four SLAMs as shown in the example in Figure 25, and implement 200 W SLAM-0122, or 100 W SLAM-0111 HF amplifiers. The four-to-one power combiners of Figure 20 are used in this example.

Conclusions

Linear, Class A, HF amplifiers with power outputs of from 10 W to over 200 W can be fabricated with far fewer circuit elements using internally matched, self-biased gain blocks that employ Solid-State Triode

JFETs. Only simple transformers are required for combining push-pull elements or to combine several SLAMs into higher power amplifiers.

Acknowledgements.

The authors acknowledge the critical contribution made at MwT by N. Thornton and P. Pacada, and the support and guidance provided by M. Omori.

Bibliography

A. Cogan, "SST for Microwave Applications", RF Expo East Proceedings, October 1989, Atlantic City, NJ.

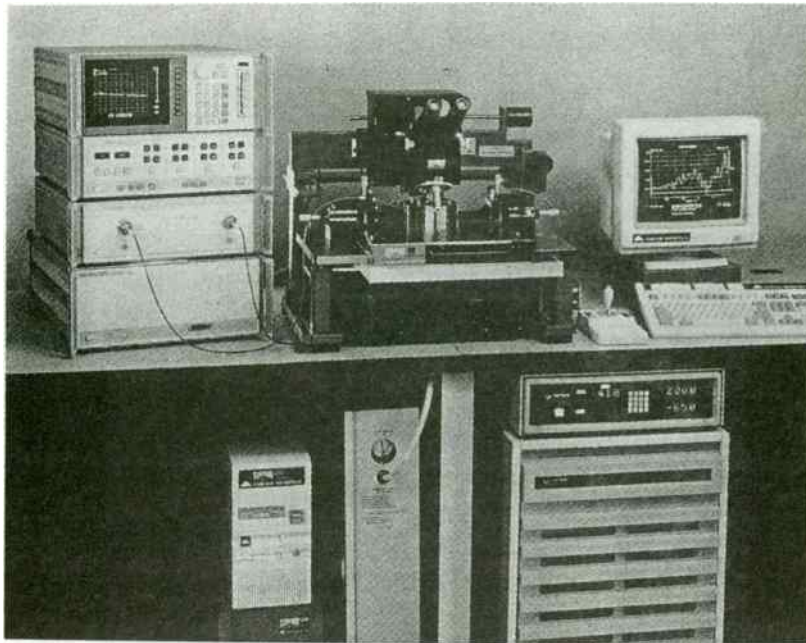


Figure 3. The Summit 10600 Thermal Probing System shown with an HP 8510 Network Analyzer.

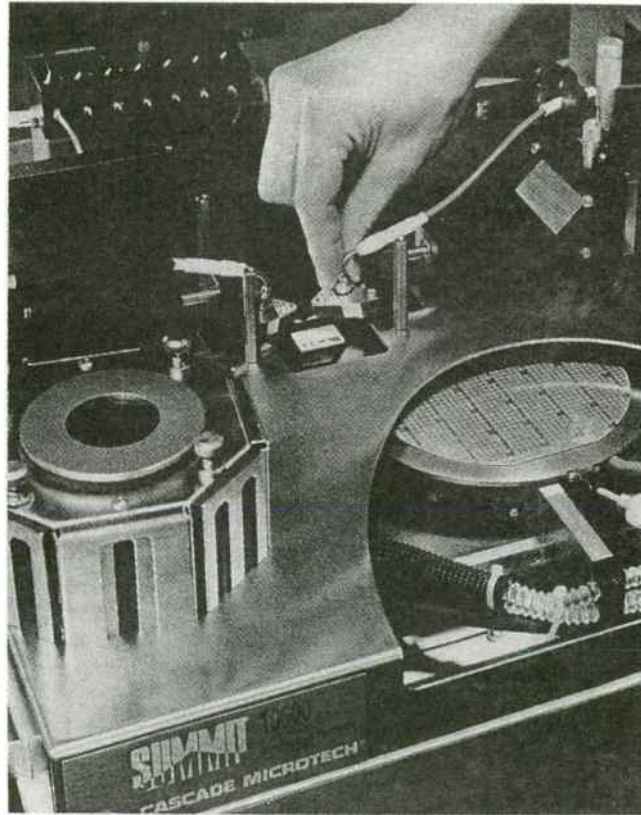


Figure 4. Close-up of the small volume Summit MicroChamber™ and thermal chuck assembly.

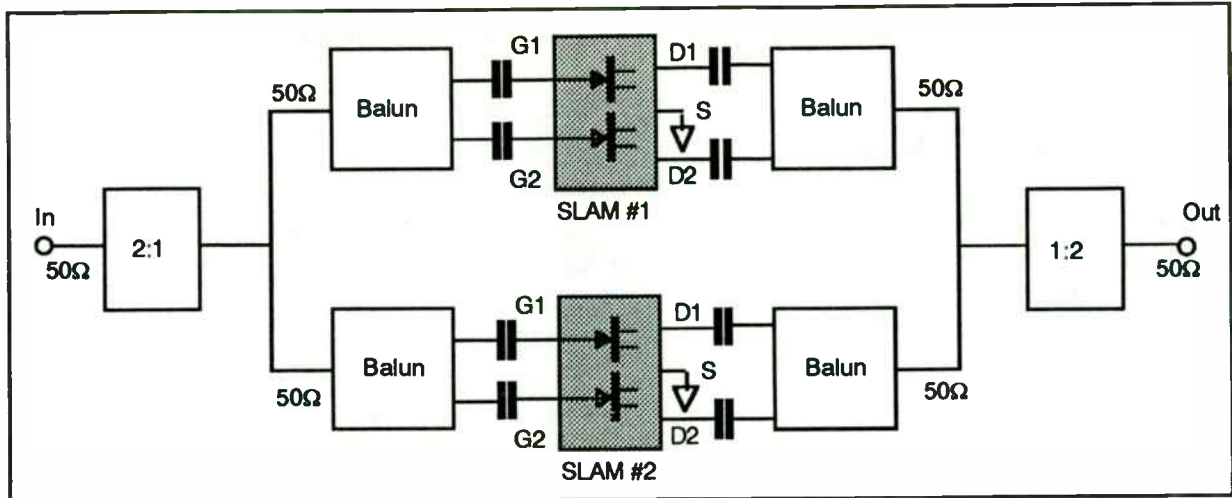


Figure 24. 50W (SLAM0111) or 100W (SLAM0122). 2MHz - 32MHz Amplifier.

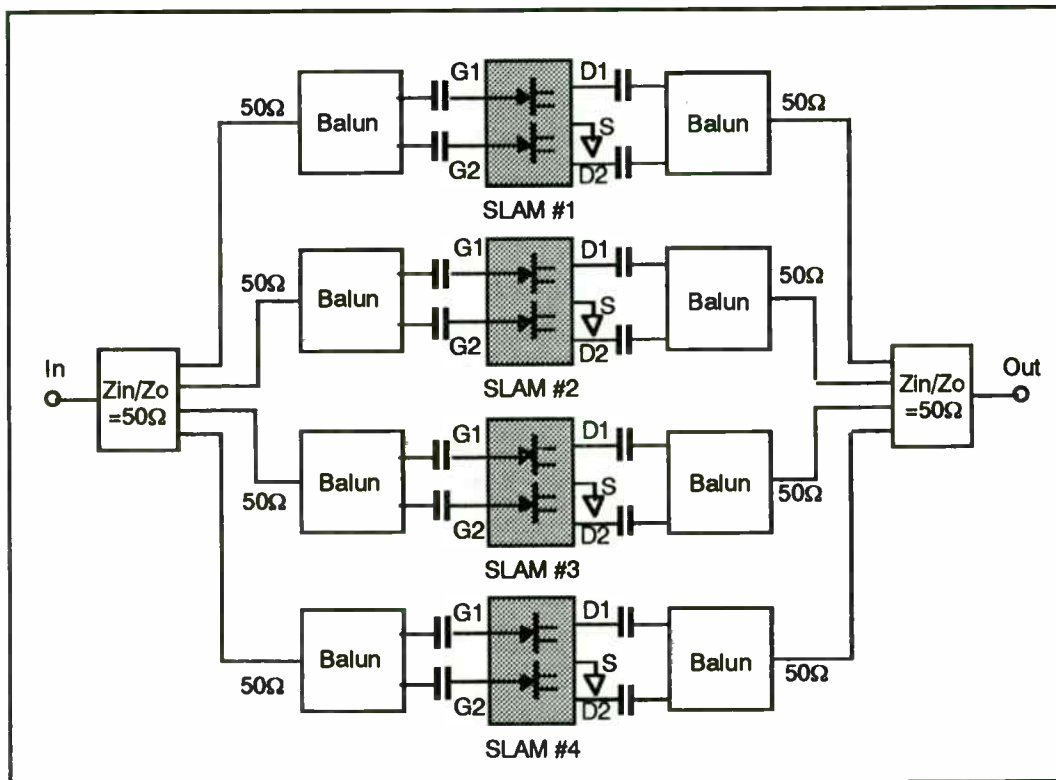


Figure 25. 2MHz - 32MHz. 100W SLAM0111 or 200W SLAM0122 Amplifier.

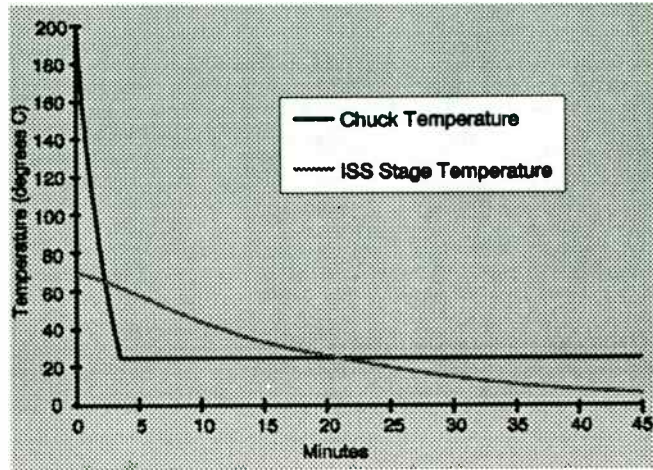
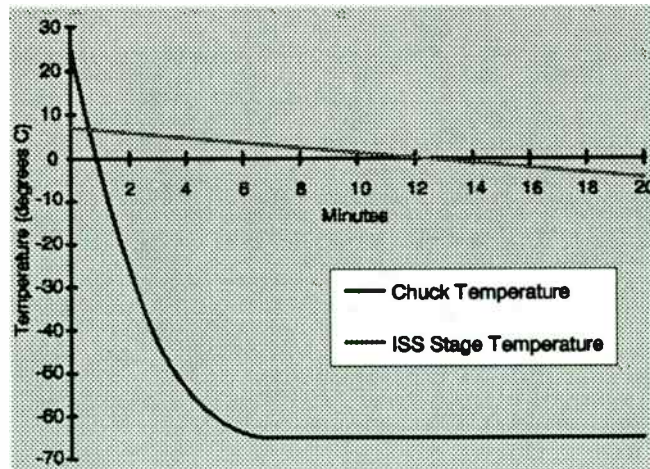


Figure 5. Temperature excursions of wafer stage and ISS stage over time.



Tradeoffs in Practical Design of Class-E High-Efficiency RF Power Amplifiers

Nathan O. Sokal, President
Laszlo Drimusz, Project Engineer

Design Automation, Inc.
4 Tyler Road
Lexington, MA 02173-2404
U.S.A.

TEL. +1 (617) 862-8998
FAX +1 (617) 862-3769
E-mail 73507.247@compuserve.com

Prof. István Novák

Department of Microwave Communications
Technical University of Budapest
P. O. Box 91
H-1502 Budapest
HUNGARY

TEL. and FAX +36 1 181-2968

E-mail t-novak@nov.mht.bme.hu

SUMMARY

A Class E RF power amplifier would have 100% efficiency at any output power and any frequency if it could use *ideal components*: transistors with zero conduction resistance, output capacitance, and turn-on and turn-off switching times; and inductors and capacitors with infinite quality factors (zero parasitic losses).

Real transistors have nonzero conduction resistance, output capacitance, and switching times, and the output capacitance has only finite Q . *Real inductors and capacitors* have parasitic resistance (finite Q) which causes power loss. At a given frequency and output power, the efficiency of an amplifier can be optimized by making a design which deviates slightly from the published nominal design (transistor voltage and time derivative of voltage both zero when the transistor is turned on). In a circuit using real (lossy) components, any deviation from the nominal design will *increase* some components of power loss and will *decrease* others. The efficiency can be optimized by exchanging increases of *some* components of power loss for *larger decreases* of *other* components of power loss, until the *total* power loss (at a specified output power) is minimized. The paper includes equations for all important components of power loss in a nominally tuned Class E circuit. A complete set of analytical expressions does not exist for circuits with *off-nominal tuning* (and probably never will exist), but a circuit simulator can calculate all of the power losses numerically for a specific set of circuit parameters.

The paper explains how efficiency varies with each circuit parameter, and gives transistor figures of merit which quantify transistor power losses in terms of combinations of transistor parameters. With that background established, the paper discusses the practical tradeoffs in optimizing a design which uses nonideal (real) components. For example:

- Reducing the output power reduces transistor-conduction power loss, but can increase output-capacitance discharge power loss, depending on frequency and transistor output capacitance.
- Efficiency can be traded against the flatness of the curve of output power *vs.* frequency across a specified frequency band.

Table A.

When reading taken	Room temperature Cal stability value (dB)	At-temperature Cal stability value (dB)
After room temp. cal	-55	n/a
After 125 deg. cal	-32	-50
After 125 device measurement	-20	-40
After 50 deg. cal and measurement	-36	-55
After -60 deg. cal and measurement	-25	-36
Return to room temp	-35	n/a

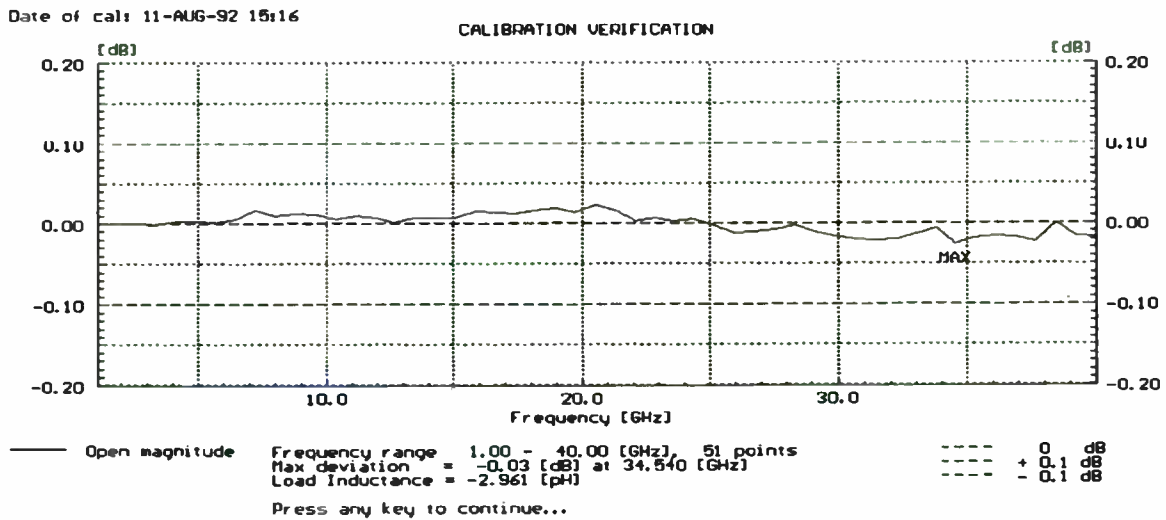


Figure 6. Plot of calibration stability on the Summit Thermal Probing System.

- Output-capacitance discharge power loss can be traded against transistor conduction power loss, at high frequencies where the transistor output capacitance is larger than the capacitance desired at that place in the circuit.
- Increasing the transistor input drive reduces the power loss in the output stage, but increases the dc power consumption of the driver chain (principally the last driver stage). The optimum choice of input drive minimizes the sum of [power dissipation in output stage + power consumption of driver chain].

The optimum tradeoff is specific to each specific design, for its specific set of values of output power, frequency, amplifier bandwidth, and circuit-component loss parameters. For each such specific set of parameters, there is a *best tradeoff* among the different power losses which yields the *lowest total power loss* for a given output power, *i.e.*, the best possible efficiency at that value of output power. For example, if the transistor to be used has *high conduction resistance* and operates at a relatively *low frequency*, the optimum tradeoff will be towards exchanging a *small* increase of capacitance-discharge power loss (proportional to the [low] operating frequency) for a *larger* decrease of conduction power loss (proportional to the [high] conduction resistance).

Analytical equations do not yet exist (and probably never will exist) for the best-tradeoff off-nominal design, but the best design can be found *numerically* by an optimizer computer program which calls repeatedly on a circuit simulator for answers to "what if?" questions, starting from an initial rough design obtained by using a *qualitative understanding* of the circuit operation and tradeoffs. The HEPA-PLUS computer program yields an optimized design in less than a minute on a 33-MHz 486 IBM-compatible PC. The authors' experience has been that

- performance predicted by the HEPA-PLUS circuit simulator program always agrees well with laboratory measurements, and
- in contests between the HEPA-PLUS optimizer program and the authors' expert design capabilities, *the optimizer program always wins*. One of the authors slaves for two hours on a manual optimization, using the HEPA simulator program to answer "what if?" questions. The resulting "best" design is given to the HEPA-PLUS optimizer program to use as a starting point. In less than a minute, the optimizer program always improves the authors' "best" design by 3 to 6 percentage points.

The paper gives numerical examples of practical tradeoffs, including the predicted performance of an optimized wide-band Class E amplifier which maintains >80% efficiency and ± 1 dB variation of output power, across a 1.7:1 frequency band. For that amplifier, the paper shows graphs of output power and efficiency vs. frequency, for the amplifier "before" and "after" optimization. The differences are striking.

For another example of optimizing a Class E amplifier design, including experimental results, see the companion paper at this conference, "Class-E power amplifier delivers 24 W at 27 MHz at 89-92% efficiency, using one transistor costing \$0.85," Nathan O. Sokal and Ka-Lon Chu.

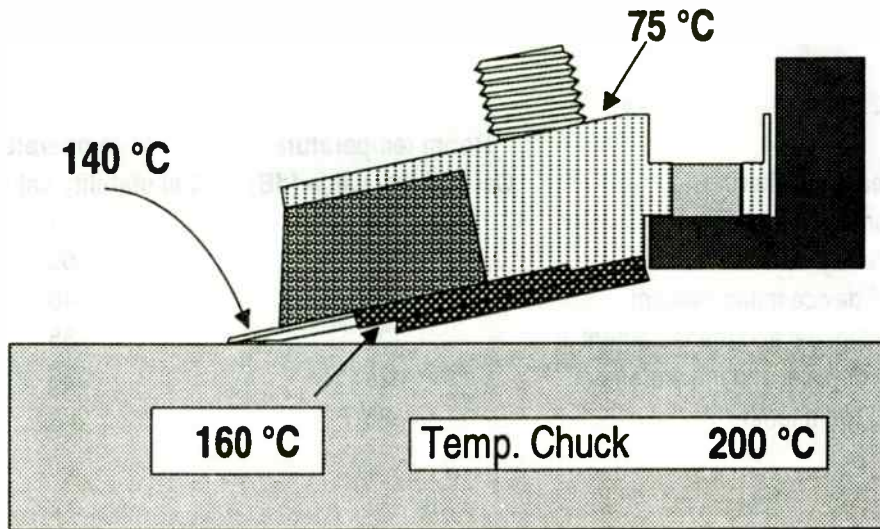


Figure 7. Temperature readings across a WPH probe when the chuck is at 200° C.

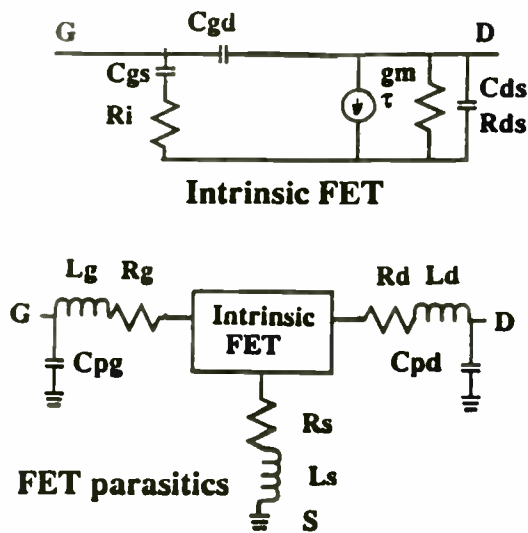


Figure 8. FET equivalent circuit.

BACKGROUND - 1

- Switching-mode RF power amplifiers (Class D and E) can approach 100% efficiency at the design frequency.
- Harmonic content and variations of Pout and efficiency with operating frequency are functions of designer-chosen parameters.
- Power losses are caused by non-ideal parameters of transistors, inductors, and capacitors; can be quantified.

RFW3A020

BACKGROUND - 2

- Design parameters can be chosen to obtain "best" tradeoff.
- Class E retains high efficiency to higher frequencies than does Class D.
- Remainder of this presentation will be about tradeoffs in design of Class E power amplifier.
- Similar tradeoffs can be made in design of Class D amplifier.

RFW3A025

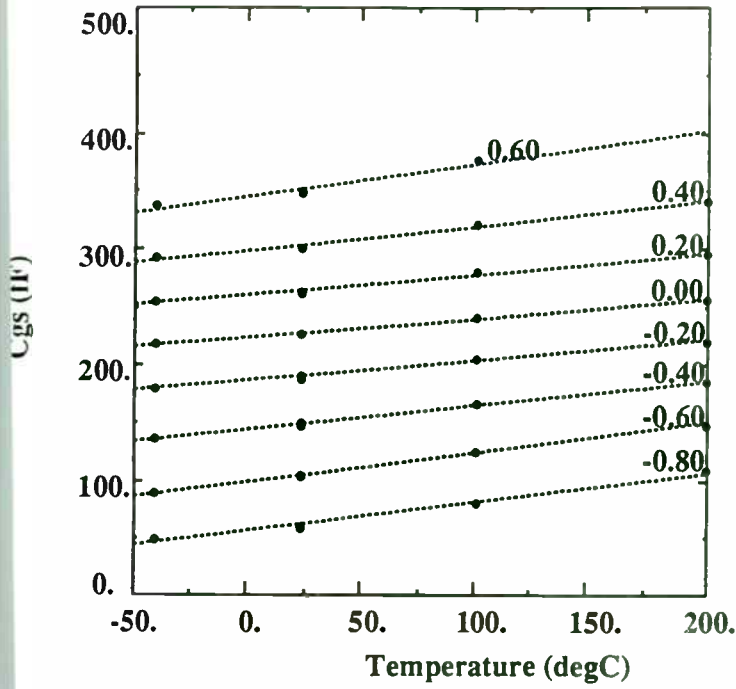


Figure 9. Temperature dependence of gm at various gate voltages.

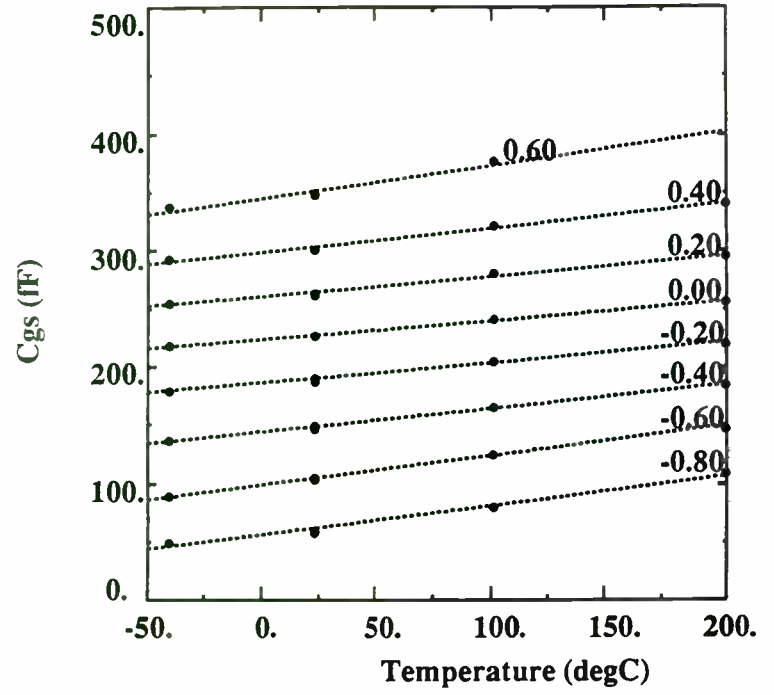


Figure 10. Temperature dependence of Cgs at various gate voltages.

Temperature Coefficients and Percent Differences for Cray MESFETs					
Parameter	B(RT)	B(T)	Δ (RT)	Δ (200)	Δ (-40)
gm (Idss)	-1.09(-3)	-1.16(-3)	0.8%	-0.2%	-0.4%
Cgs (Idss)	0.91	0.74	0.45	2.6	-0.74
Cgd(Idss)	-0.22	-0.11	-1.4	-2.0	0.47
Rds(Idss)	0.2	0.7	-1.0	-7.3	2.2
τ (Idss)	1.7	2.1	-0.04	-4.0	2.9
Ri(Idss)	2.4	1.6	-2.5	6.4	-6.2
f_t (Idss)	-1.69	-1.62	0.66	1.9	0.6
$g_m / C_{gs} + C_{gd}$	-1.65	-1.64	0.45	1.0	0.25
Rs	1.44	1.52	0	-1.3	0
Rd	2.03	1.87	0.3	0.23	-2.0
Rg	5.2	4.2	0.6	2.3	-12.6
Ld	1.2	0.43	1.1	19	-2.
Lg	2.6	1.4	-2.2	11	-9.
Cpg	2.4	1.15	-1.9	14	-6.3
Cpd	2.2	1.23	1.0	9.4	-2.0
Cgd,pin	0.44	0.51	-0.7	-1.3	0
Idss	0.8				
δV_p	-1.57mV/°C				

Table B

BACKGROUND - 3

Typical Results of Tradeoffs

- Single-frequency design: Get good design from nominal design equations. Get about 3-5% higher efficiency from applying tradeoffs.
- Wide-band design, up to 1.7:1 f_{max}/f_{min} : Flatness of power and efficiency vs. frequency improved by an order of magnitude over a nominal single-frequency design. No design theory yet exists for a wide-band design; automatic optimizer does excellent job.

RFW3A027

APPROACH - 1

- V and I waveforms are easy way to define and understand high-efficiency operating condition. Examine how design choices affect waveforms and performance parameters.
- Explicit mathematical relationships among performance parameters and component parameters for circuit with nominal waveforms.
- Going slightly off-nominal increases some components of P loss, but decreases others. If decrease > increase, circuit efficiency is higher.

RFE3A030

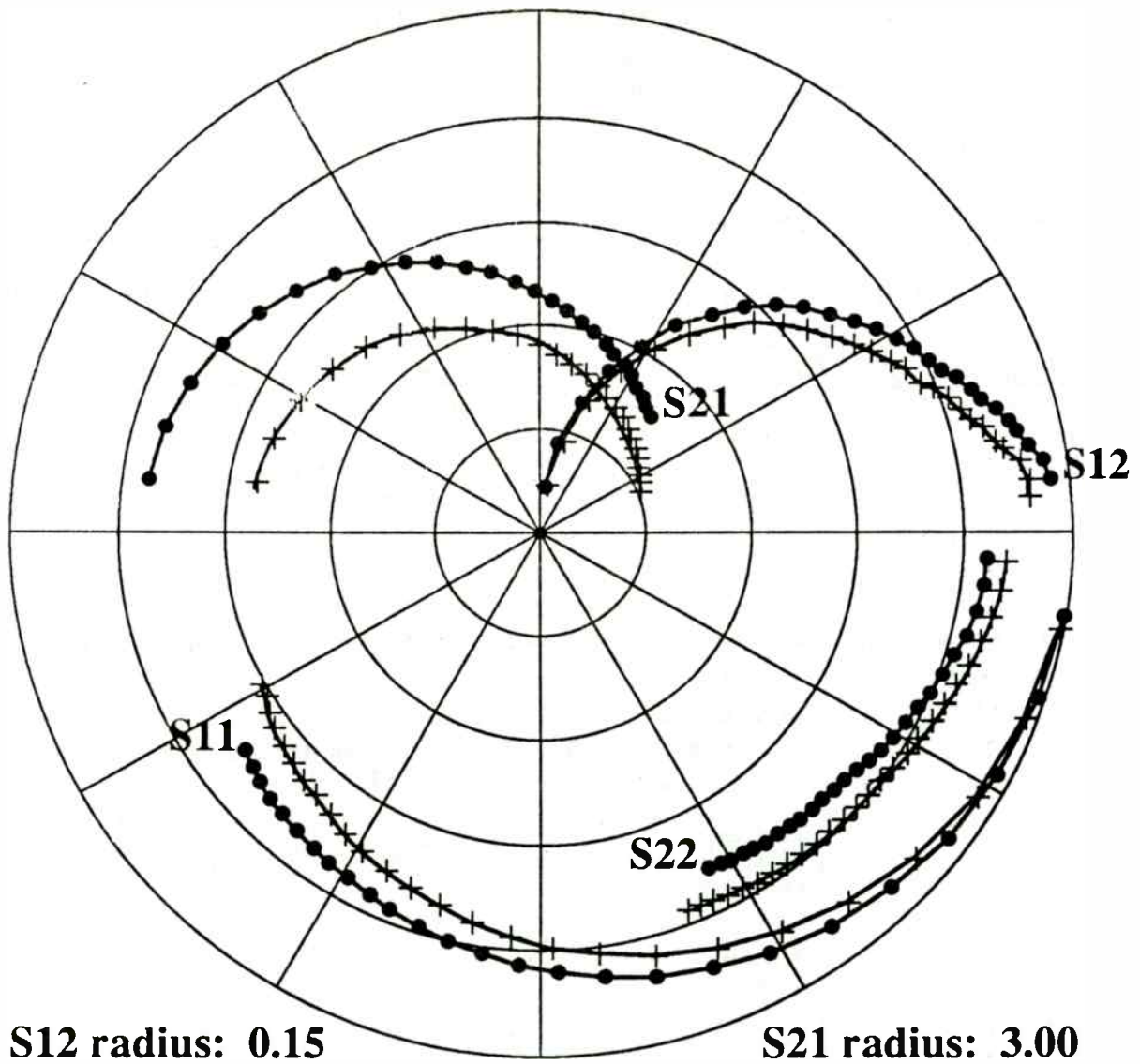


Figure 11. S-parameters at I_{dss} at -40° (\bullet) and 200° ($+$)

APPROACH - 2

- Equations show directions of tradeoffs for nominal-tuned circuit. HELPS BUILD UNDERSTANDING of tradeoffs. Extrapolate to off-nominal circuit for qualitative answers.
- For quantitative answers: (a) Tradeoffs change with frequency and with combinations of parasitic-loss parameters. (b) No equations exist for off-nominal operation. Computer analyses or lab experiments are only ways to get quantitative answers.

RFW3040

APPROACH - 3

- Good software tool gives same answers as careful lab tests, but much faster, and gives other information not observable in lab. Aids engineer's understanding.
- Manual method: Identify circuit evaluation parameters; define required performance; vary circuit parameters to achieve required performance with many different sets of circuit parameters; choose "best" set. Better: Use computer method below.
- Define "best" and then find it; use computer.

RFE3A050

Device Characterization with an Integrated On-Wafer Thermal Probing System

Dan d'Almeida
Cascade Microtech, Inc., 14255 SW Brigadoon Ct., Beaverton, OR 97005

Robert Anholt
Gateway Modeling, 1604 East River Terrace, Minneapolis, MN 55414

Background

Most wireless IC applications require operation at temperatures that fluctuate widely from the ambient temperature used in the test environment. As wireless applications become more technically demanding and are driven toward higher yields, accurate device models based on temperature-dependent RF equivalent circuits become critical. Several large semiconductor companies are now actively monitoring or controlling chuck temperature in production for commercial applications.

Wireless applications across the world subject communications systems to extremes ranging from the bitter chill of an Alaskan winter to the scalding heat of an Ecuadorian summer. Customers demand performance in these wide ranging thermal environments requiring survival of ICs in both storage and operating conditions. Characterizing the performance of these ICs over temperature is most economically accomplished at the wafer level.

Historically, high-frequency on-wafer measurements over temperature have been prohibitively expensive and inefficient. Previous test setups have involved a collection of probe station, Plexiglas dry box, probes, and cables. These setups take weeks to install and debug since the components are autonomously designed. Since a dry box encapsulates the entire probe station, these systems also provide poor throughput due to the large volume that must be purged to avoid frost at low temperatures. Also, the issues of on-wafer calibration accuracy and stability caused by temperature-related probe and cable drift have been erroneously ignored.

Temperature-dependent device models

In order for ICs or communication systems to perform effectively over temperature, accurate, temperature-dependent device models must be generated. Both silicon- and GaAs-based devices are being designed into wireless systems. Measurements of silicon bipolar devices at Cascade Microtech show that f_t as a function of temperature can be non-linear (Figure 1). To accurately characterize f_t at any temperature, parasitic pad capacitance must be determined and removed. Cascade's algorithm first measures and stores a "dummy device," consisting of only the pads and interconnects. Subsequent measurements are calculated by subtracting the "dummy" from actual device data to obtain a correct f_t . Interestingly, competing physical factors contribute to

PERFORMANCE PARAMETERS

with Defined Ranges of Load,
DC Supply Voltage, & Frequency

- Output power
- Harmonic content
- Variation of P_{out} across frequency range
- Variation of efficiency across frequency range
- Freedom from parasitic oscillation (many possible causes; sometimes several exist at the same time).

RFE3A060

EVALUATION FACTORS - 1

- Efficiency of entire amplifier chain ($P_{out}/total$ DC Pin)
- Variation of amplifier efficiency and harmonic content across frequency band.
- Reliability (V, I and P-dissipation stresses on power transistor)
- Product manufacturing cost (e.g., can trade efficiency or stresses for cost).
- Size and weight

RFW3A070

a curvilinear f_t response versus temperature for a single bias point. The bias point could be adjusted to find the optimal f_t at any given temperature. A thorough evaluation for a GaAs MESFET is presented¹ to understand several potential temperature dependent physical factors including:

- the materials factors (energy gap, N_c , N_v , dielectric constant)
- the electron saturated velocities and mobilities
- the contact resistance
- the Schottky-barrier height and the surface potential
- trap-related phenomena.

In summary, for the devices measured, the temperature coefficients suggest a stronger dependence of the electron velocity and a weaker dependence of the electron mobility on temperature than previously thought. The most dominant factor where these GaAs MESFET performance data is concerned is the reduction of the electron velocity with temperature. This causes f_t values and thus gain values to decrease significantly with temperature, even for devices biased at a constant current. HEMT devices also exhibit much stronger shifts in threshold voltage near 0° C than MESFETs, indicating trapping effects and making derivation of linear temperature coefficients impossible (Figure 2). Thus, temperature stable circuit designs with HEMT technology is more difficult.

Measurement setup and algorithms

High-frequency measurements were made at -40, 23, 100 and 200° C with the Cascade Microtech Summit Thermal Probing System (Figure 3) and microwave probes. The 23° C measurement was repeated at the end of the sequence to verify that the device and system was stable. Transitions to sub-zero temperatures were expedient since the Summit uses a MicroChamber™ environment (Figure 4) enclosing only 7.0 liters, to allow purging in a matter of minutes instead of hours required with traditional Plexiglas dry boxes that surround an entire probe station. At each temperature, the system was recalibrated using LRRM calibrations with automatic load inductance correction². This load inductance compensates for the micron-level misplacement of the probes on the standards to obtain the correct reference reactance. Two sets of measurements were taken over a series of bias conditions using the room temperature calibration and an at-temperature calibration. The at-temperature calibration was performed about fifteen minutes after making a chuck temperature change, roughly three times the thermal time constant of the probes and cables.

Calibrations were performed by contacting a separate ISS, or impedance standard substrate, located on a separate thermally-isolated stage. When the

¹R. Anholt and S. Swirhun, "Experimental Investigation of the Temperature Dependence of GaAs FET Equivalent Circuits," IEEE Transactions on Electron Devices, Sept. 1992.

²A. Davidson, K. Jones, E. Strid, "LRM and LRRM Calibrations with Automatic Determination of Load Inductance," ARFTG Digest, Winter 1990.

EVALUATION FACTORS - 2

- Design cost and schedule (good design tool helps produce better design and save labor cost and schedule time).
- Evaluate potential designs by weighted sum of evaluation factors.

RFW3A080

BRIEF REVIEW OF CLASS E

- Before discussing tradeoffs, review
 - circuit operating principles
 - high-efficiency waveforms
 - nominal design procedure
- Problem in all switching-mode power circuits: switching power dissipation is proportional to frequency.
- Turn-on dissipation if load is C; turn-off dissipation if load is L; both if load is R.

RFE3A090

main chuck is at -65°C , the calibration chucks stabilize at -5°C (Figure 5). The calibration substrates, consisting of shorts, thru, and loads are relatively insensitive to temperature. The element most affected by temperature is the 50-ohm resistor, exhibiting a TCR of $-100\text{ ppm}/^{\circ}\text{C}$. Therefore, worst-case deviations of the resistor for a -65 to 200°C wafer chuck excursion adds only a 0.7% error.

The microwave probes are constructed to withstand the large thermal excursions, especially high heat. Even after prolonged exposure, Figure 6 shows that the most temperature-sensitive component of the probe, the coaxial connector, is comfortably below its rated specification of 85°C . The air flow purge minimizes the thermal coupling between chuck and probes and cables. RF cables tend to exhibit significant phase changes with temperature so recalibration is generally recommended for temperature excursions of greater than 25°C .

The Cascade Microtech Thermal Probing System offers sophisticated software algorithms for fast and easy network analyzer calibrations at-temperature. To get a good comparison, the probes were left in contact with the device while the different calibration sets were recalled. This removes the unwanted effect of measurement errors caused by varying probe placement, which is the leading cause of poor on-wafer high-frequency measurement repeatability. After each measurement run, a calibration stability reading was taken to understand quantitatively the changes from continued temperature settling of probes and cables (Table A). This test requires a measurement of an open so no probe placement issues are raised. Generally, Cascade Microtech recommends recalibrating whenever the cal stability gets worse than -40 dB or 1% (Figure 7). To further reduce probe placement errors when measuring multiple devices on a wafer, a look-up table can be created by the Summit station to store x-y stage correction values which compensate die-to-die movements for wafer expansion effects as a function of temperature.

Effects of system calibration on FET temperature-dependent equivalent circuits

The device used in the experiment was a $2 \times 75 \times 0.8$ micron MESFET. The layout is a symmetric multi-finger, ground-signal-ground arrangement with active fingers pointing in the direction of the gate-drain probe axis. Figure 8 shows the equivalent circuit for this device. Previous investigations used only a single room temperature calibration, which may have lead to erroneous derived temperature coefficients, especially for capacitances which may be susceptible to changes in transmission line lengths with temperature. About 8 gate biases were measured at $V_{ds} = 2\text{V}$, then 3 cold-FET and one pinched-FET measurement was made at $V_{ds} = 0\text{V}$.

The direct extraction technique^{3,4} was employed involving three cold-FET measurements ($V_g = 0.8, 1.0$ and 1.2V) to derive the source, drain, and gate

³R. Anholt and S. Swirhun, "The measurement and analysis of GaAs MESFET parasitic capacitances," IEEE MTT vol. 39, pp. 1243-1246, July 1991.

SOLUTION ("CLASS E" PRINCIPLE)

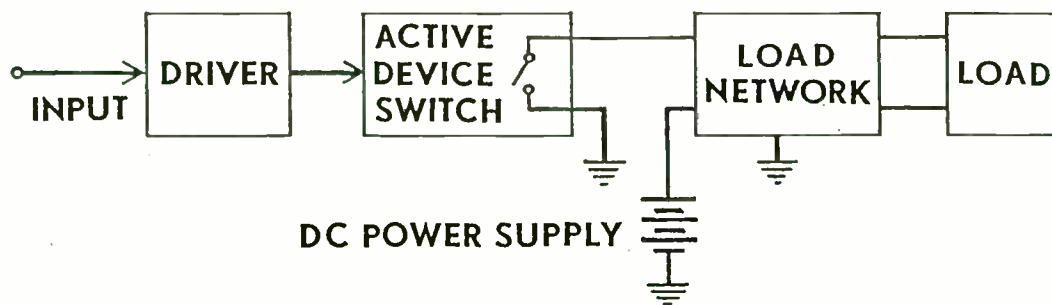
1. Switching power dissipation is $i(t) \cdot v(t)$.
2. Current and voltage each must rise and fall, but they don't have to do it *at the same time!*
3. Time-displace voltage and current transitions; never have high i and high v simultaneously.
4. Don't discharge charged shunt C through switch ($[CV^2]f/2$).

Result: High efficiency and low stress *even if switching times are considerable fractions of waveform period.*

Idealized waveforms on next slide.

RF91W032

POWER-AMPLIFIER BLOCK DIAGRAM



RF91W036

resistances and inductances. At high temperatures, however, the alpha-method gave inconsistent ratios of the channel to source resistance, forcing the value to be fixed at the room-temperature measurement. The pinched-FET measurement ($V_g = -4.0$ V, three volts below pinchoff) was used to estimate pad capacitances, as no dummy-FET or width-dependent capacitance data was available for this layout. The difference between C_{gs} and C_{gd} for the pinched FET is approximately equal to the gate-pad capacitance C_{pg} , and C_{ds} is equal to the sum of the drain-pad capacitance, C_{pd} , and the active-FET drain-source capacitance. The part due to C_{pd} was estimated at room temperature and the ratio of C_{pd} to the total pinched-FET value of C_{ds} was kept constant for other temperatures. Empirically, the best value of C_{pd} gives the best hot-FET S_{12} fits. Also, the resulting value of C_{pd} and C_{pg} are approximately equal given the symmetric layout. The resulting direct-extracted equivalent circuit parameters generally had less than 3% variations from 1 to 26 GHz.

Figures 9 and 10 show typical temperature dependent equivalent circuit parameters for g_m and C_{gs} at various gate voltages ($V_{ds} = 2$ V). The data is quite consistent and easily fits to

$$P(V_g, V_{ds}, T) = P(V_g, V_{ds}, T_0)(1 + B(T - T_0))$$

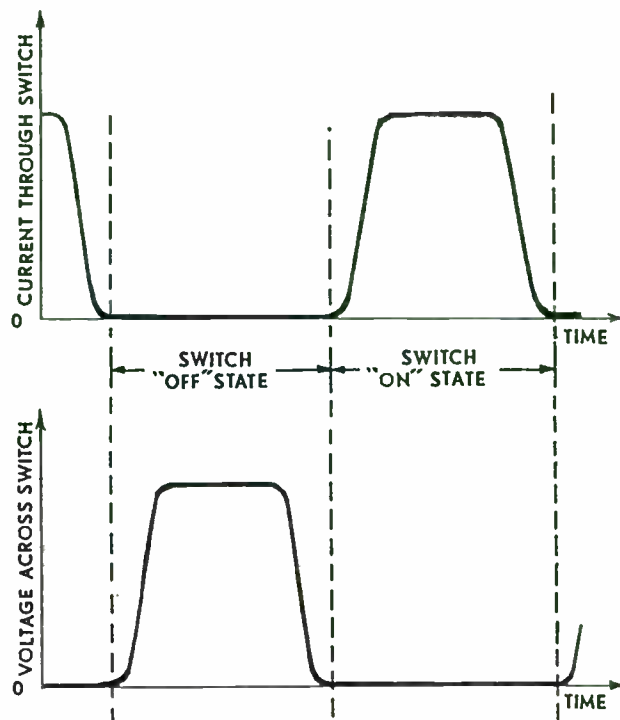
where $T_0 = 0^\circ$ C and B varies with gate and drain voltages. This FET exhibited a very steep threshold-voltage shift with temperature, and as a result the I_{ds} and g_m values tended to have negative temperature slopes at high V_g (due to reduced electron saturated velocity at high temperature), whereas they show a positive slope at low V_g due to the lower threshold voltage.

Table B summarizes the resulting temperature coefficients B . For each parameter, $B(RT)$ was derived using S -parameters measured with the original room-temperature calibration. $B(T)$ was obtained by using the at-temperature calibration. The largest differences in the B coefficients are in the pad capacitances C_{pg} and C_{pd} as well as in the inductances L_d , L_g , and L_s . L_s is not shown since its value is nearly zero. We believe the differences in B values for R_{ds} , τ , and R_i are secondarily due to pad capacitance deviations since empirical studies show that these parameters are very dependent on what is assumed for these inductances and capacitances.

Differences in the B coefficients are generally due to very small differences in the extracted equivalent circuit parameters. To test their significance, a comparison to the relative change Δ in each parameter due to using the room-temp or at-temp calibration at 200° and -40° C was performed. The S -parameters are shown in Figure 11. S -parameters for room-temp measurements done at the start and end of the session was provided in $\Delta(RT)$ for system stability information. If the difference in parameters at 200° or -40° C is not much larger than $\Delta(RT)$, the differences in B coefficients are insignificant. For example, C_{gs} was measured at 223.8 and 224.8 fF in the room-temp measurements, so $\Delta = 0.45\%$. At 200° C, C_{gs} was extracted at 253.6 and 260.1

⁴R. Anholt and S. Swirhun, "Equivalent-circuit parameter extraction for cold GaAs MESFETs," IEEE MTT vol. 39, pp. 1247-1252, July 1991.

IDEALIZED WAVEFORMS



LOAD-NETWORK PROPERTIES - 1

- Excited at input terminals by periodic switch.
- Manufacture time-displaced V and I waveforms at network input terminals.
- Deliver sine-wave current to load at network output terminals.
- Bring network input voltage to zero at switch turn-on time, with zero slope.

yielding a $\Delta=2.6\%$ so we conclude that the difference of 9.1 and $7.3 \times 10^{-4}/^\circ\text{C}$ in B for C_{gs} is significant. However, the differences in the f_t values and the pinched-FET value of C_{gd} are not.

Conclusions

A turnkey thermal probe station can minimize the setup and debug time needed to gather over temperature S-parameter data for equivalent circuit extractions and RF circuit designs. Simple software-aided routines and ergonomic controls make it feasible to gather data over a wide range of temperature settings to capture non-linear effects such as the V_t of a GaAs HEMT or the f_t of a silicon bipolar device. One-button calibrations at each measurement temperature yield more accurate FET equivalent circuit temperature coefficients, especially for the parasitic pad capacitances and inductances.

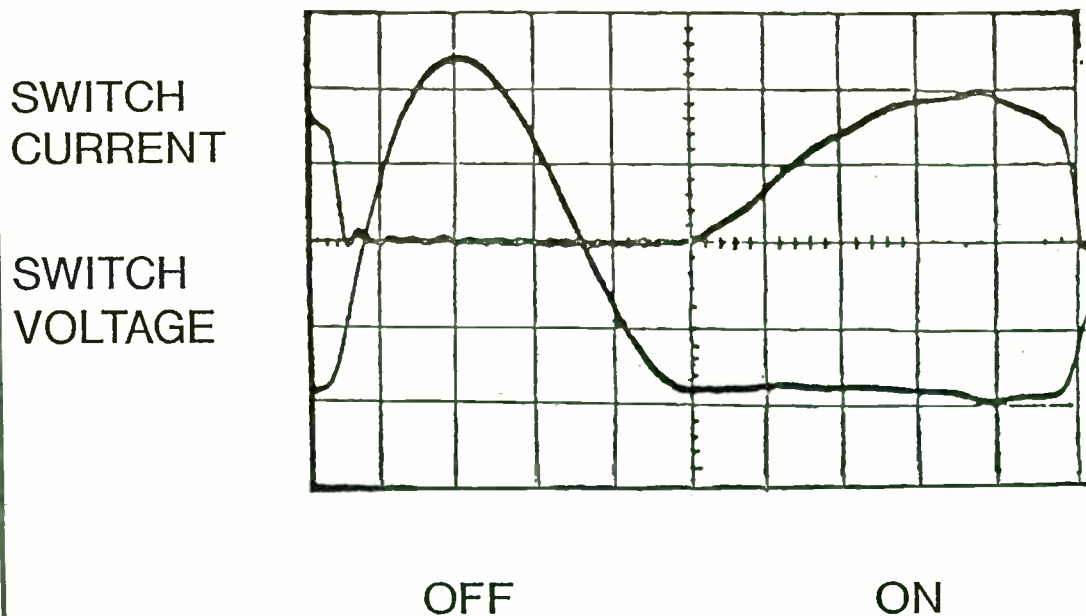
Acknowledgements: The authors would like to thank Tom Myers at Cascade Microtech for providing helpful test software modifications.

LOAD-NETWORK PROPERTIES - 2

- Load network contains any combination of L_s , C_s , transmission lines, magnetic cores, and wire which causes waveform requirements to be met.
- Switching-mode Class F_2 and F_3 are a subset of Class E.
- NEXT SLIDE: Waveforms in published low-order Class E circuit

RF91W040

Low-Order Class-E Amplifier Waveforms



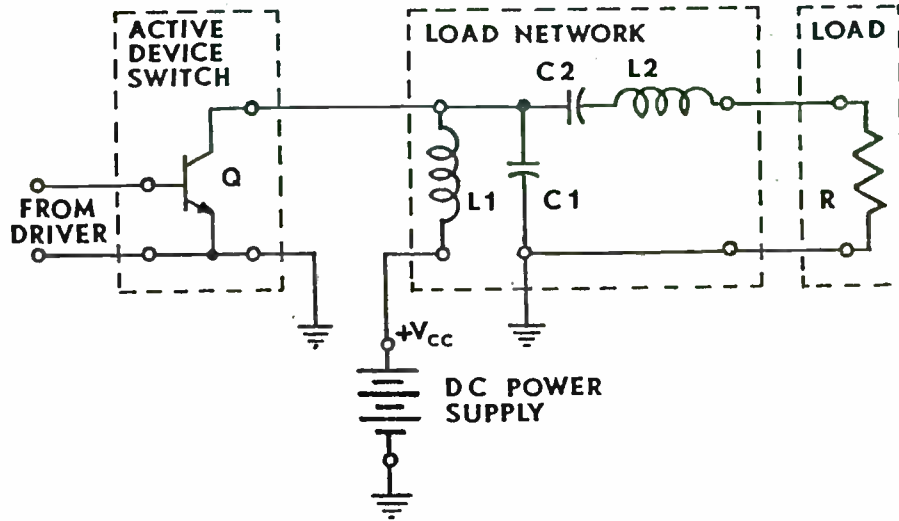
RF1B0200

Integrated-Circuit Technologies for Wireless Applications

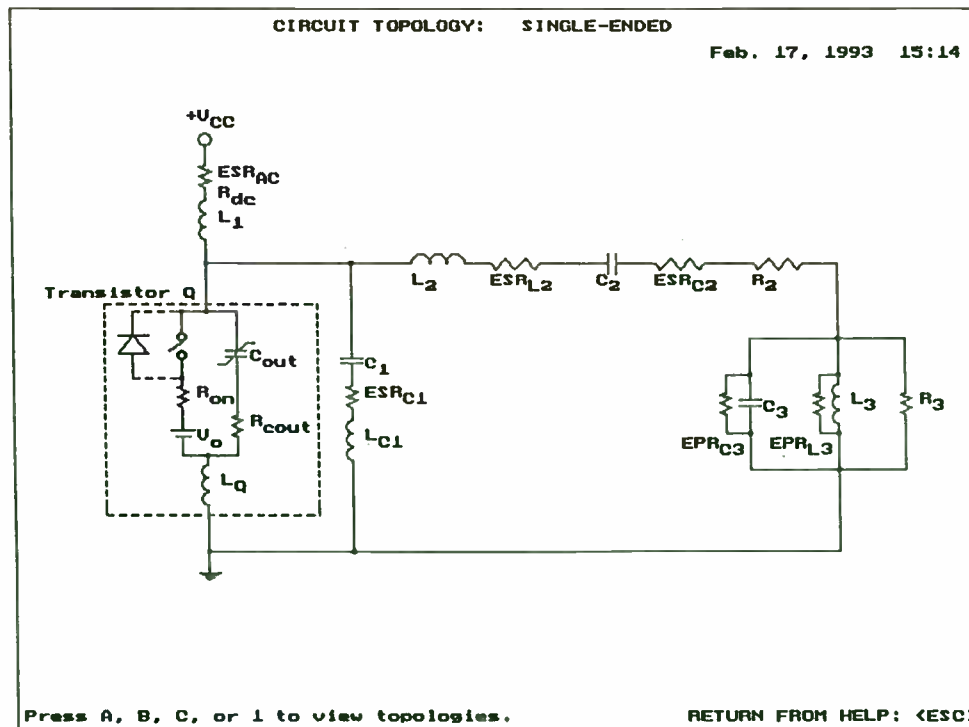
**Session Chairperson: Dan Millicker, Hewlett-Packard Co.,
Communications Components Division (Newark, CA)**

- Direct Versus Dual Conversion Quadrature (Vector) Modulation,
**Mark Rehorst, Hewlett-Packard Co., Communications
Components Division (Newark, CA)**.....109
- Silicon Bipolar RF Integrated Circuits for Cellular Radio and
Wireless Applications, **Nhat Nguyen, James N. Wholey, and
Madhu Avasarala, Hewlett-Packard Co., Communications
Components Division (Newark, CA)**.....117
- A Silicon Bipolar Mixed-Signal RFIC Array for Wireless
Applications, **Bob Koupal, Keith Carter, and Kevin Negus,
Hewlett-Packard Co., Communications Components Division
(Newark, CA)**.....132
- Wireless Applications for GaAs Technology, **Michael Frank,
Henrik Morkner, and Craig Hutchinson, Hewlett-Packard Co.,
Communications Components Division
(Newark, CA)**.....143
- Low-Cost, High-Performance Receiver for Wireless Applications,
**Brian Kirk, California Eastern Laboratories, Inc.
(Santa Clara, CA)**.....154

Low-Order Class-E Amplifier Schematic



RF1B0190





HEWLETT PACKARD

Direct vs. Dual Conversion Quadrature (vector) Modulation

Mark Rehorst
Communications Components Division
Applications Engineering

39201 Cherry St.
Newark, Ca. 94560
Phone: 510-505-5548

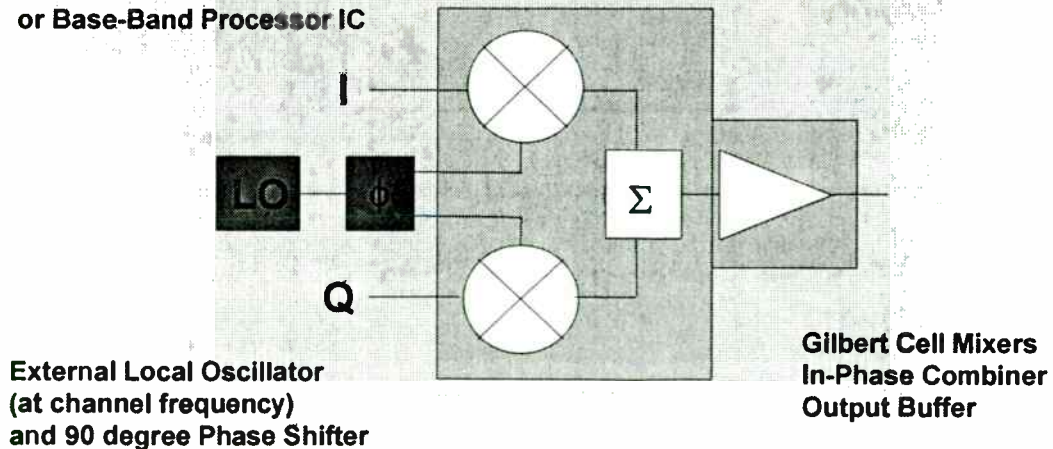
Communications Components Division



Direct Conversion (HPMX-2001)

I and Q signals
come from DSP circuits
or Base-Band Processor IC

Output at Channel Frequency



Communications Components Division

FWS1712.DRW #1



NOMINAL DESIGN EQUATIONS

$$1. V_{CE(pk)} < BV_{CEV}$$

$$2. V_{CC} = f(V_{CE(pk)})$$

$$3. R = f(P, V_{CC})$$

$$4. Q_L \geq 1.7879, \text{ free choice}$$

$$5. L2 = Q_L / 2\pi f$$

$$6. C2 = f(R, f, Q_L)$$

$$7. L1 \geq \dots$$

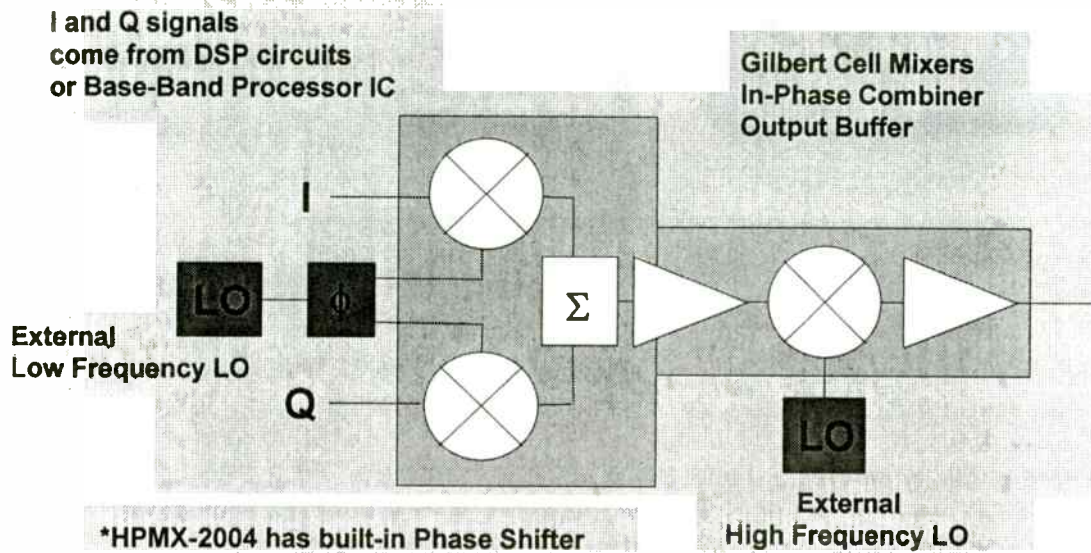
$$8. C1 = f(R, f, Q_L, L1)$$

TRADEOFFS - 1

- Efficiency vs. output power for a given transistor and frequency: $P_{loss}/P_{out} \sim P_{out}$.
- Less P_{out} increases efficiency, but increases transistor cost/watt output.
- Efficiency vs. frequency for a given P_{out} : switching losses and C losses \sim frequency (conduction loss does not); first tradeoff multiplier factor increases with frequency.
- Reduce R_{on} with larger transistor. Improves efficiency but increases cost.

RFW3A120

Dual Conversion (HPMX-2002, HPMX-2004)



Communications Components Division
FR8712.DRW 82



Direct Conversion

(+)
Simple
Low DC Power
Low Cost

(-)
Filters
Shielding

Dual Conversion

(+)
Cheap Filters
Better Isolation

(-)
More Filters
More Complex
DC Power?

Communications Components Division
FR8712.DRW 82



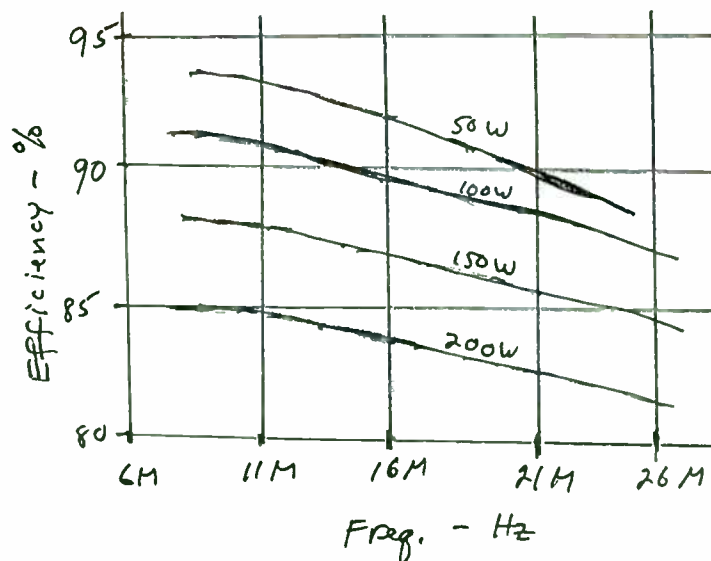
TRADEOFFS - 2

- Limit on larger transistor: When all of C_1 is provided by C_{out} (depends on freq.). Four possible strategies re too-large C_{out} ; sacrifice of eff'y depends on R_{on} , Q_L1 , and frequency; different combinations --> different "best" choice.
- Result: Tradeoff factors are functions of frequency. "Best" strategy in one frequency region may not be best in another region.
- Results of preceding tradeoffs: graph on next slide.

RFW3A130

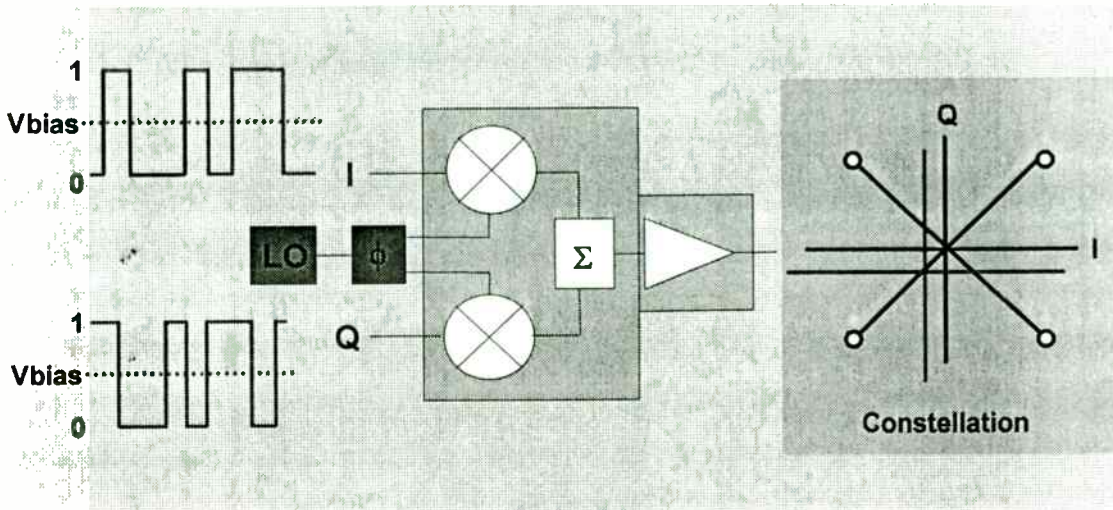
TRADEOFFS - 3

Efficiency vs. Power and Frequency



RFW3A140

LO Leakage

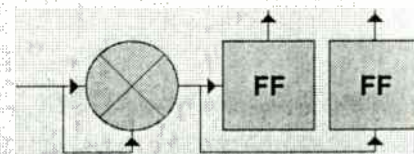


Adjusting Vbias at I and Q shifts the I and Q axes onto the "ideal" axes.

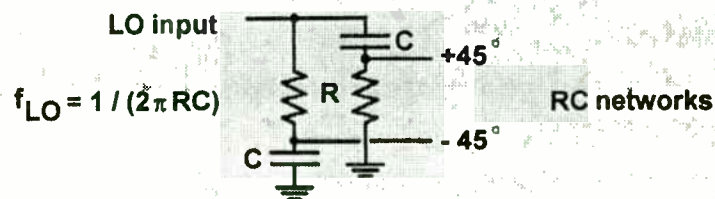
Phase Shifters



Hybrids (Murata, Shoshin)

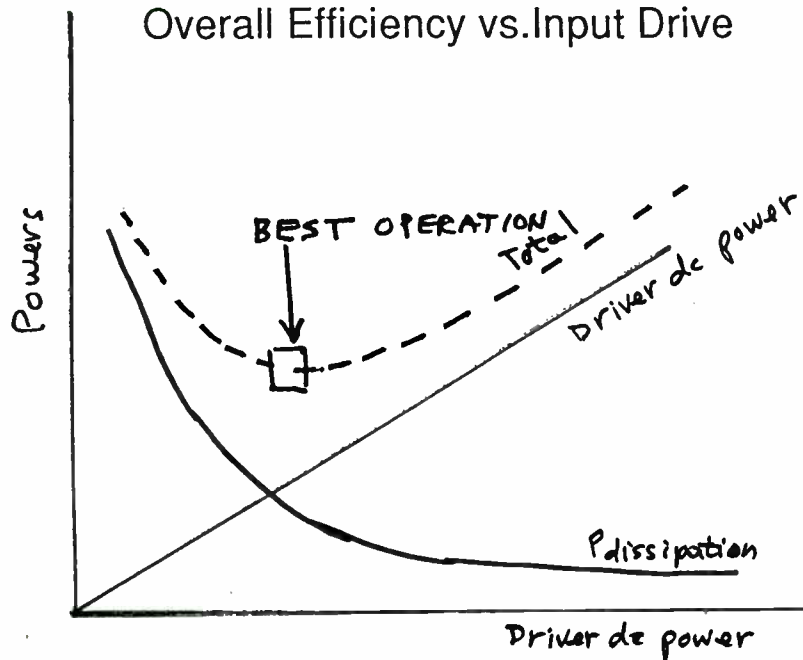


Active "Digital" Phase Shifter
(HPMX-2004 uses this technique)



TRADEOFFS - 4

Overall Efficiency vs. Input Drive



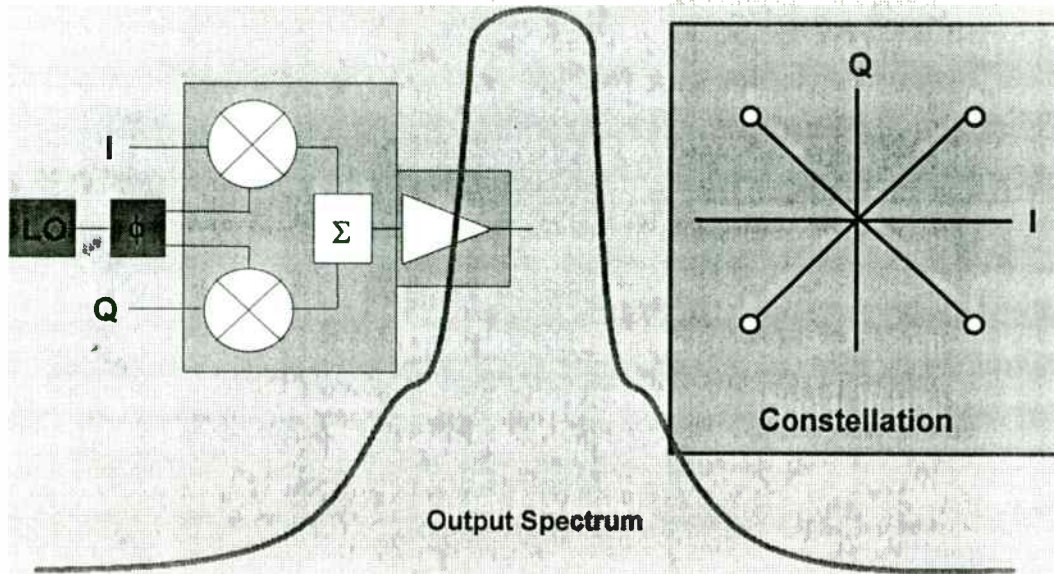
RFW3A150

TRADEOFFS - 5

- Efficiency vs. deviation from nominal waveforms if $C_{out} > \text{needed at } f: i^2(R_{on})$ vs. $C_{out}(dV)^2f/2$
- Efficiency vs. required bandwidth = f_{max}/f_{min} , harmonic content, and post-filter cost, size, and weight: BW, harmonic content, & needed post-filter $\sim 1/QL$, but $P_{loss}/P_{out} \sim QL/Qu$ of L and C. Power-loss penalty depends on Qu (if high Qu , little penalty for high QL).
- Best wide-band design doesn't have exactly nominal waveforms at ANY frequency in band.

RFW3A160

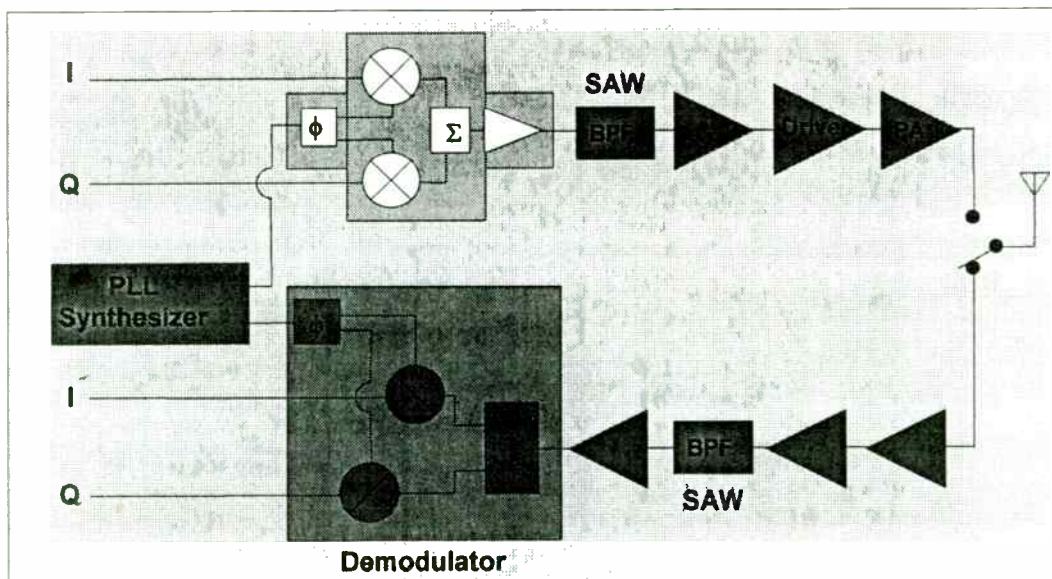
Direct Conversion



Communications Components Division
FR3713.DRW 04



Direct Conversion



Communications Components Division
NEXT12.DRW #2



Power loss with nominal waveforms
Power output

$$R_{ou}: \approx 1.37 \frac{R_{ou}}{R}$$

$$R_{c1}: \approx 0.2 \frac{R_{c1}}{R}$$

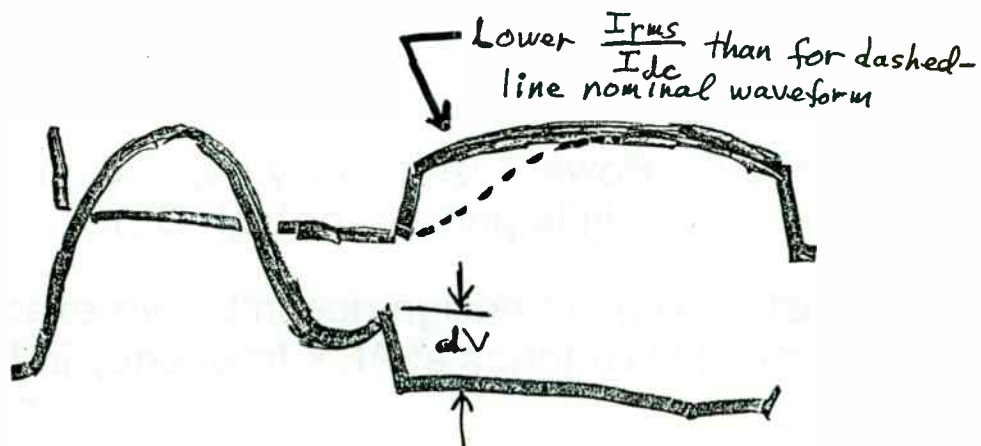
$$C1 \& L2: \approx Q_L \left(\frac{1}{Q_{UC2}} + \frac{1}{Q_{UL2}} \right)$$

$$Q_u \text{ of } L1: \approx \left(\frac{1}{Q_{UL1}} \right)$$

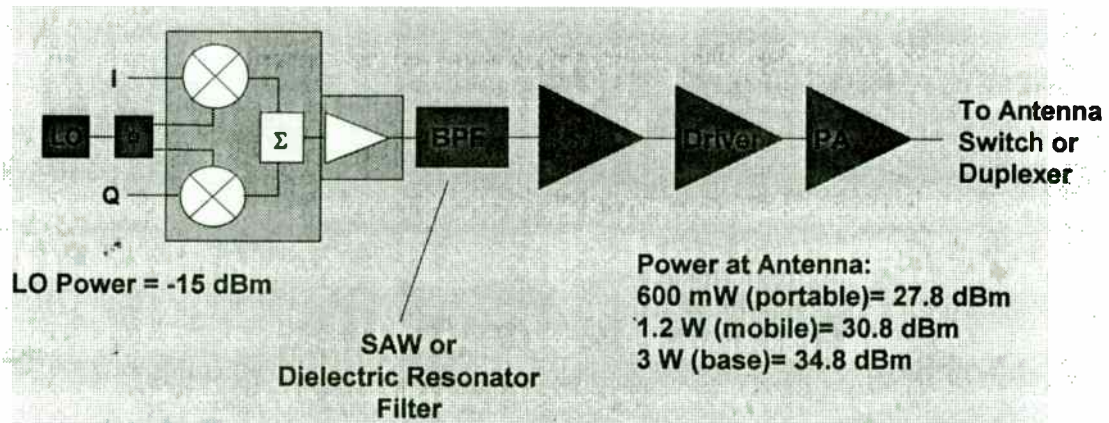
$$R_{dc} \text{ of } L1: R_{dc} \left(\frac{P_{out}}{V_{cc}^2 \eta^2} \right) \quad \left[\eta \text{ includes effects of all sources of } P_{loss} \right]$$

RFW3A162

TRADEOFF IF HIGH R_{ou} AND NOT HIGH $\frac{1}{2} C1 (dV)^2 f$

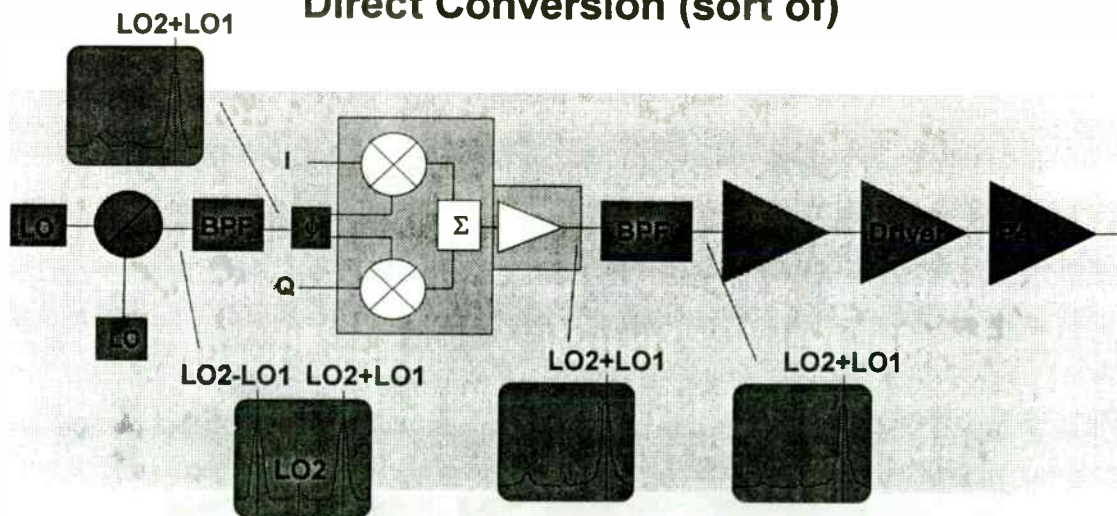


Direct Conversion Transmitter



Problem: Output signal leaks back into LO causing spurs and jitter
Solution: Metal shields over LO and modulator with careful bypassing of all leads going in and out of shields

Direct Conversion (sort of)



Problem: Shielding is impractical, reverse isolation too low...
Solution: Use mixer and filter at input of modulator to allow use of a different LO frequency

TRADEOFFS - 6

MOSFET dV/dt CAPABILITY

- Load $R <$ nominal causes drain to swing negative. Then MOSFET substrate diode can conduct.
- High dV/dt during diode turnoff after conduction can cause second breakdown of parasitic NPN (less likely as vendors improve products).
- International Rectifier guarantees 3.5 - 5.5 V/ns capability for HEXFET III products.

RFW3A170

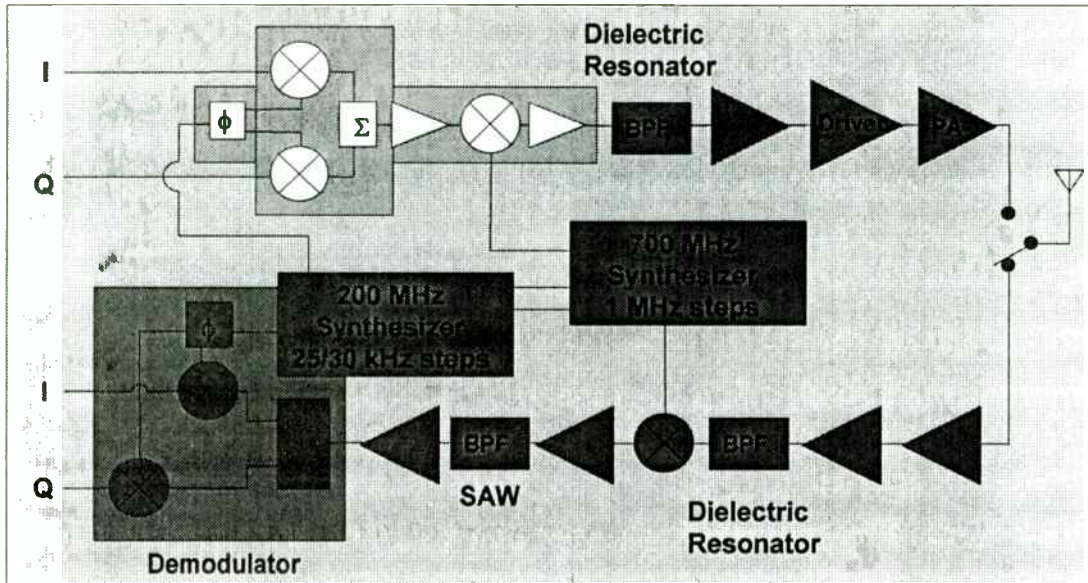
TRADEOFFS - 6 (cont.)

MOSFET dV/dt Capability

- Evaluate capability of your vendor's MOSFETs at your highest frequency and V_{cc} . If a danger, impose limit on lowest load R .
- This phenomenon does not apply to GaAs MESFETs.
- BJT: next slide.

RFW3A180

Dual Conversion

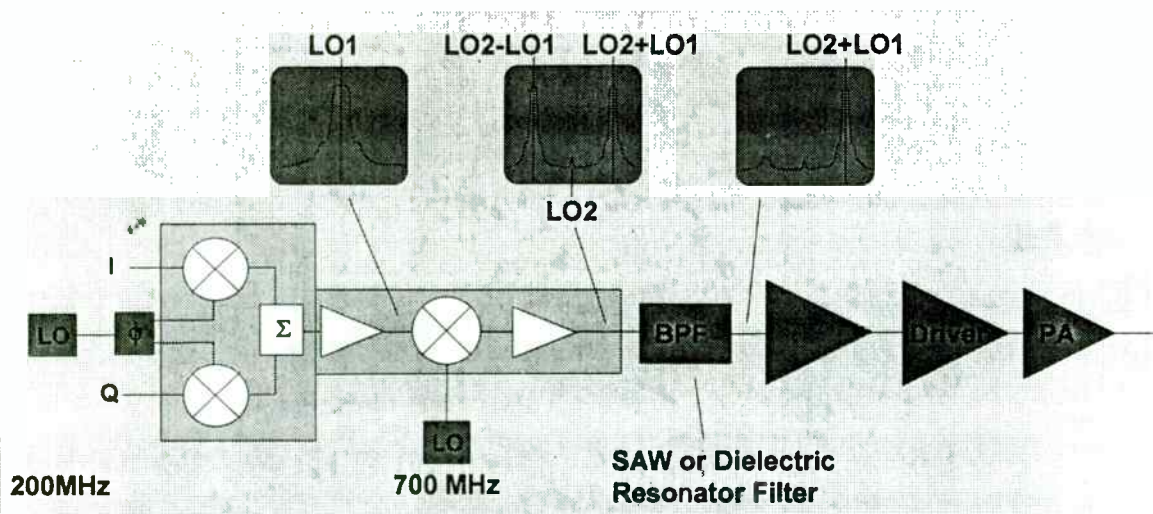


Communications Components Division

NEXT12.DRW #1

HEWLETT
PACKARD

Dual Conversion (HPMX-2002, HPMX-2004)



Communications Components Division

FR5712.DRW #12

HEWLETT
PACKARD

TRADEOFFS - 7

BJT Negative Collector

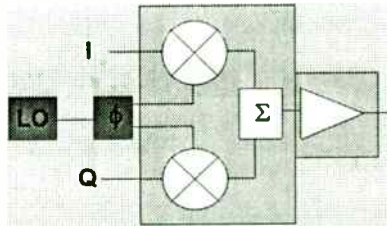
- BJT collector swing negative below "off" base voltage will turn E-B "on" when intended to be "off" --> possible parasitic oscillation.
- Impose limit on low end of range of load R, or connect inverse-diode clamp across C-E.

RFW3A190

BASE OR GATE DRIVER CIRCUIT

- Similar set of tradeoffs for base or gate driver, but influence on overall amplifier performance is smaller by factor of power gain in output stage, e.g., factor of 10.
- Base or gate driver must provide good drive to output stage to ensure good efficiency in output stage. Inadequate drive yields inferior efficiency and can result in parasitic oscillation.

Direct Conversion

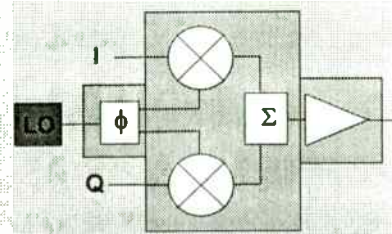


HPMX-2001

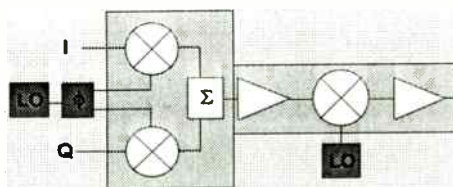
P_{out} = -9.5 dBm (900 MHz)
I_d = 20 mA
LO: DC - 2000 MHz

HPMX-200C (coming soon)

P_{out} = +4 dBm (900 MHz)
I_d = 39 mA
LO: 800 - 1000 MHz

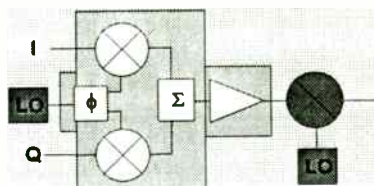
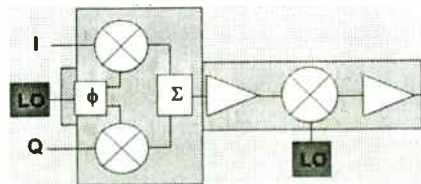


Dual Conversion



HPMX-2002
P_{out} = -11 dBm (800 MHz)
I_d = 12.2 mA
LO1: 40 - 300 MHz
LO2: 250 - 2000 MHz
Output: 250 - 2000 MHz

HPMX-2004
P_{out} = -13 dBm (800 MHz)
I_d = 30 mA
LO1: 40 - 240 MHz
LO2: 250 - 2250 MHz
Output: 250 - 2000 MHz



HPMX-200E (coming soon)
P_{out} = -4.5 dBm (100 MHz)
I_d = 16 mA
LO: 45 - 200 MHz

HOW TO MAKE QUANTITATIVE TRADEOFFS

- Evaluate candidate transistors: HEPA transistor-evaluation module.
- Starting-point design from which to optimize tradeoffs: HEPA preliminary-design module.
- Evaluate the design: HEPA simulation/analysis module (100-1000 times faster than SPICE).
- Automatically optimize the design according to criteria for your specific application: HEPA optimizer (can optimize at up to 16 frequencies in a band, with same or different weighting at each frequency).

RFW3A210

EXAMPLE

- For example of tradeoffs in designing a Class E power amplifier, see paper on 27-MHz PA at this conference. Result: efficiency improved from about 83% to about 90%.
- Computer helped answer many questions about what would be best to do.
- Computer analysis showed that experienced designer's first approach was wrong, and gave a better alternative. Lab tests proved that the computer program was correct.

RFE3A220

Direct vs. Dual Conversion

Direct Conversion:

Simple Circuit
- Requires shielding
Low DC Power
- Not much different from dual conversion
Low Cost
- Requires SAW filter
- Requires high resolution synthesizer

Filter
- only one required
Shielding
- low cost, no DC power

Dual Conversion:

Cheap Filters
- may require more of them
Better Isolation
- more complex circuit

More filters
- relatively cheap
More complex
- synthesizer produces at least two signals anyway
DC power
- only for mixer- synthesizer runs anyway

Choose your Headache!

Class-E Power Amplifier Delivers 24 W at 27 MHz, at 89-92% Efficiency, Using One Transistor Costing \$0.85

Nathan O. Sokal, President and Ka-Lon Chu, Senior Engineer
Design Automation, Inc.
4 Tyler Road
Lexington, MA 02173-2404

Tel. +1 (617) 862-8998
Fax +1 (617) 862-3769
E-mail 73507.247@compuserve.com

SUMMARY

Switching-mode RF power amplifiers (e.g., Class E and voltage-switching Class D) provide significantly higher efficiency than that of Class B and Class C amplifiers. A Class E power amplifier uses a single power transistor, in contrast with the Class D, which uses two or four transistors in a half-bridge or full-bridge topology. (Two 180°-phased Class E circuits can be combined in push-pull if desired, at double the output power of a single circuit.) In all types of switching-mode power amplifiers, (a) the transistors are driven to act as switches at the operating frequency, to minimize the power dissipated while the transistors are conducting current, and (b) the drain or collector efficiency is ideally 100% at low frequencies.

In principle and in practice, the decrease of efficiency with increasing frequency is lower for the Class E amplifier than for the Class D. The penalty for this higher efficiency at high frequency is that the output power per transistor for a given [(peak voltage)*(peak current)] stress is lower for the Class E circuit than for the Class D, by a factor of about 1.5. On the other hand, the Class E circuit avoids the Class-D input-drive difficulties of (a) a large common-mode voltage at the input port of the upper transistor, equal to the full output-voltage swing, and (b) tight tolerance requirements on the relative timing of the switching of the two transistors (with only a single transistor, the Class E circuit has no requirement at all for relative timing between two transistors).

A quasi-complementary half-bridge (two power transistors) voltage-switching Class D power amplifier was reported by F. H. Raab and D. J. Rupp at RF Expo East '92 and in *RF Design*, Sept. 1992. This paper reports on a single-transistor Class E power amplifier.

The Class E amplifier delivered 24 W at 27 MHz, at 89-92% drain efficiency, using a single International Rectifier or Harris Semiconductor IRF520 MOSFET (TO-220 plastic package; price U.S.\$0.85 at 100 quantity). This range of efficiency was measured for thirteen amplifiers using transistors from two vendors and three date codes. Circuit simulations established that the best efficiency would be obtained by using one IRF520 transistor, rather than one larger transistor or two IRF520 in parallel.

The presentation includes circuit details and waveform photographs, for the output stage.

Silicon Bipolar RF Integrated Circuits for Cellular Radio and Wireless Applications

Nhat M. Nguyen, James N. Wholey, and Madhu Avasarala

Communications Components Division
Hewlett Packard Company
Newark, California 94560

I. Introduction

The current development of digital cellular radio systems with high spectral efficiency places significant demands on the associated r.f. components. This includes high levels of r.f. performance with low noise, high power, and adequate suppression of undesired signals. These requirements are combined with desired operation at low voltage and current to prolong battery life, and a high level of integration to reduce the overall system size and cost.

A typical radio system is illustrated in Fig. 1. RF components on the transmit section include a quadrature modulator to up convert DSP (digital signal processing) data. This is followed by a driver and output amplifier capable of power control. The receive side includes a low noise amplifier (LNA), a down-converting mixer, and appropriate phase-locked loop circuitry. This paper will discuss the quadrature modulator, the driver amplifier, and the LNA and down-converting mixer circuits for use in the 800 MHz to 960 MHz communication bands.

The ISOSAT-II silicon bipolar IC technology used to fabricate these circuits is illustrated in Fig. 2. Bipolar devices feature a transition frequency f_T of 10 to 20 GHz, and a maximum frequency of oscillation f_{max} of 25 GHz. A thick field oxide and a low resistance gold metallization system are used to achieve low parasitics for interconnections and polysilicon resistors. This structure also provides for high-Q capacitive and inductive elements [1]. The use of LC elements for reactive tuning can significantly improve the overall performance of these circuits.

II. Quadrature Modulator

As digital modulation techniques are incorporated into wireless communications to increase system capacity, the quadrature modulator becomes an increasingly important component. Ideally, its basic function is to provide a one-to-one correspondence between the input voltage at the in-phase (I) and quadrature-phase (Q) ports and the amplitude and phase of the output signal.

SWITCHING-MODE RF POWER AMPLIFIERS Class D and E

- Class D: pairs of switches, tightly coupled
Class E: single switch
Both types: can combine two in push-pull
- Efficiency is ideally 100% at low switching frequencies.
- Efficiency decreases with increasing frequency; less so for Class E.
Authors' opinion: crossover at a few MHz;
specific value depends on the application.

RFW3B010

CLASS D AND E AMPLIFIERS

- Tradeoff for higher efficiency of Class E at high frequency: factor of 1.5 lower value of $(P_{out} \text{ per transistor}) / (V_{pk} * I_{pk})$
- However, Class E avoids Class D input-drive difficulties, namely
 - a. large common-mode RF voltage on upper-transistor drive port (the full V_{cc})
 - b. tight tolerance requirement on relative timing of switching of the two transistors.These difficulties become more formidable with increasing frequency. Quit about 10 MHz.

RFW3B020

Two fundamental methods are commonly used to achieve this modulation: a direct modulation of the r.f. signal (approximately 900 MHz) and a two-stage up-conversion process involving the modulation of an i.f. signal (approximately 100 MHz) followed by an up-conversion to the r.f. band. Two ICs were developed to perform the quadrature modulation required by these systems.

The basic functional diagram for both the 100-MHz and 900-MHz quadrature modulators is shown in Fig. 3 [2]. A carrier frequency ω_c is applied to an RC-based phase shifter that generates two signals in quadrature, $\sin(\omega_c t)$ and $\cos(\omega_c t)$. These signals are then applied to the LO sections of two Gilbert-cell based double-balanced mixers that are driven by appropriate I-Q representations of digital data. The outputs of the two mixers are then summed and amplified.

Single-ended high-frequency outputs are desirable since they eliminate the need for output combining circuitry such as baluns. The amplifier topology in both quadrature modulators is designed to provide single-ended operation. In the case of the 900-MHz version, the output is matched internally to a 50- Ω impedance using a shunt-L series-C network. The on-chip matching not only provides the user with an ac-coupled 50- Ω output line, but also improves the power efficiency by eliminating losses associated with matching a high-impedance node external to the IC.

A variety of measurements can be used to characterize the performance of a quadrature modulator. Many are based on the correspondence between the input plane (I-Q modulating voltage) and the output plane (r.f. amplitude and phase). Figure 4 depicts the basic mapping function. The input axes I and Q are the voltages of the I and Q modulation ports above their reference voltage. The output is ideally proportional to

$$I \cdot \sin(\omega_c t) + Q \cdot \cos(\omega_c t). \quad (1)$$

Mapping of a variety of inputs is investigated. For the 900-MHz quadrature modulator they are:

- 1) a high power output versus frequency with $I = Q = 1.25$ V (above a reference level of 2.5 V) (point A, Fig. 4);
- 2) a leakage output power versus frequency with $I = Q = 0$ V (at the reference level) (point B, Fig. 4);
- 3) a sequence of points to determine the amplitude and phase mapping uniformity of the modulator (points C, Fig. 4).

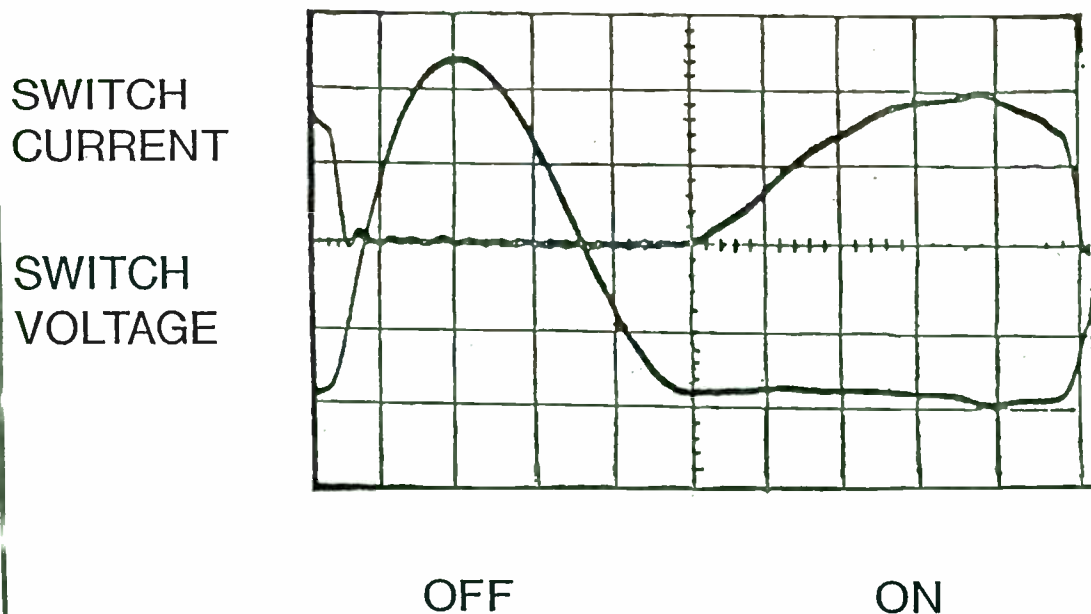
Additionally, a low-frequency modulating signal ω_m can be applied to the I-Q ports with the following spectral results:

CHARACTERISTICS OF CLASS E

- Transistor operates in switching mode; each transition time up to 15% of the RF period.
- Switch turn-off voltage is low, giving low loss during slow turn-off.
- Switch turn-on current is low, giving low loss during slow turn-on.
- Allowing slow turn-on and turn-off makes Class E work well at high frequencies, up to 15% of $1/(\text{turn-off transition time})$.

RFW3B040

Low-Order Class-E Amplifier Waveforms



RF1B0200

- 4) a single sideband up-conversion spectrum obtained from

$$I = 1.25 V \cdot \sin(\omega_m t), Q = 1.25 V \cdot \cos(\omega_m t); \quad (2)$$

- 5) a double sideband up-conversion spectrum obtained from

$$I = 1.25 V \cdot \cos(\omega_m t), Q = 1.25 V \cdot \cos(\omega_m t). \quad (3)$$

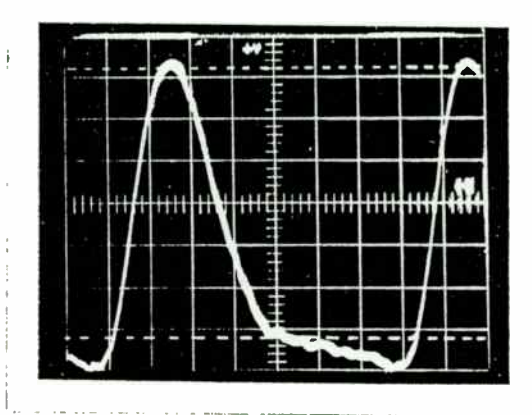
Figures 5 through 9 show the results of these tests for the 900-MHz quadrature modulator. The high power sweep (Fig. 5) corresponds approximately to a 0.5-dB gain compression level. The optimum power at 900 MHz, as well as the low output VSWR, result from the reactive output impedance matching used. Figure 6 shows the LO leakage versus frequency. This parameter is highly sensitive to internal device-to-device variations and can be improved by 10 to 20 dB by individually applying small offset voltages to the I and Q ports. Gain and phase mapping errors are shown in Fig. 7. A sequence of relative output amplitudes and phases are obtained from S_{21} measurements as the input I-Q vector traces a circle of 1.25-V magnitude. Ideally, the magnitude of S_{21} should remain constant and the phase of S_{21} should track the phase of the input I-Q vector. Deviations from the average magnitude and phase are shown versus input angle of the I-Q vector. Applying low-frequency quadrature inputs results in a single sideband up-conversion spectrum shown in Fig. 8. In addition to the desired sideband, the LO leakages and image suppression are also visible. Caution must be used in evaluating non-linear products from this spectrum since the signal, if passed through a limiting amplifier, would further suppress unwanted tones. Figure 9 shows a measurement of third-order distortion products. Here a two-tone output of a quadrature modulator is obtained from dual in-phase I and Q inputs. The third order products are at 35 dB below the fundamental tones of 0 dBm while the device is biased at 5 V and 37 mA.

III. Driver Amplifier

The driver amplifier receives a signal from either an up-converting mixer or a direct quadrature modulator and amplifies it to an output level of about 200 mW. Since the driver amplifier must consume a large amount of current in order to deliver the required output power level, heat dissipation must be carefully considered. The desirable characteristics of a driver amplifier are thus small size, low cost, good power efficiency, and ease of use in circuit board design. In many of the emerging digital cellular communication systems there is also a need for output power control over a wide range.

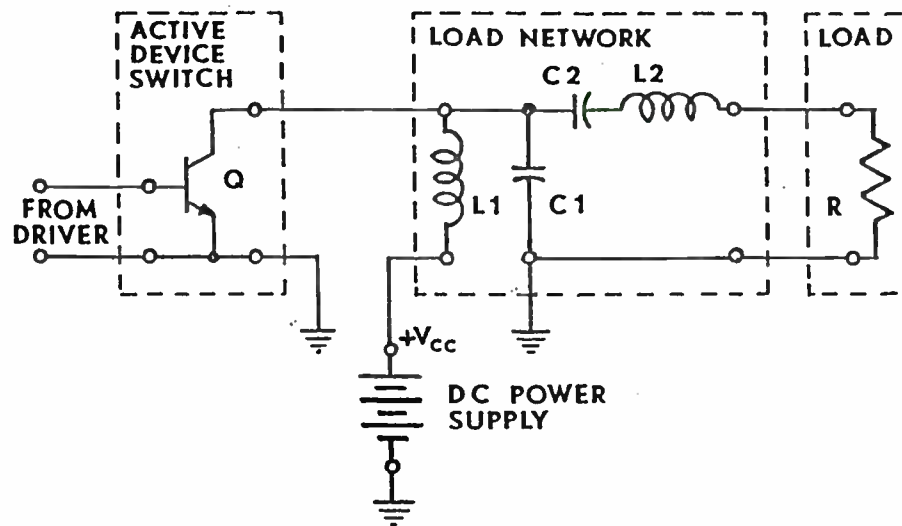
27-MHZ CLASS E AMPLIFIER

Drain-voltage waveform



RFW3B055

Low-Order Class-E Amplifier Schematic



RF1B0190

A driver amplifier for use in the 800 MHz to 960 MHz communication bands was developed to meet the above objectives. It is housed in a low-cost and compact S0-8 narrow body surface mount plastic package with improved heat dissipation capability. The topology of Fig. 10 was chosen for broad band operation, stability, and high efficiency. The amplifier consists of 3 gain stages, each contributing about 10 dB of small-signal gain. The first stage is a CE-CC configuration driving a CE second stage through a coupling capacitor for optimum voltage swing. These two stages have on-chip resistive loads to set proper bias level and to provide the appropriate gain. Additionally, interstage reactive matching is used to achieve maximum power efficiency. The final stage is a CE configuration with an open collector and is matched to 50Ω externally with a shunt-L series-C network for best performance. At 900 MHz, a shunt inductor of 10 nH and a capacitor of 10 pF were used. The inductor is thus small enough to be printed on a PC board.

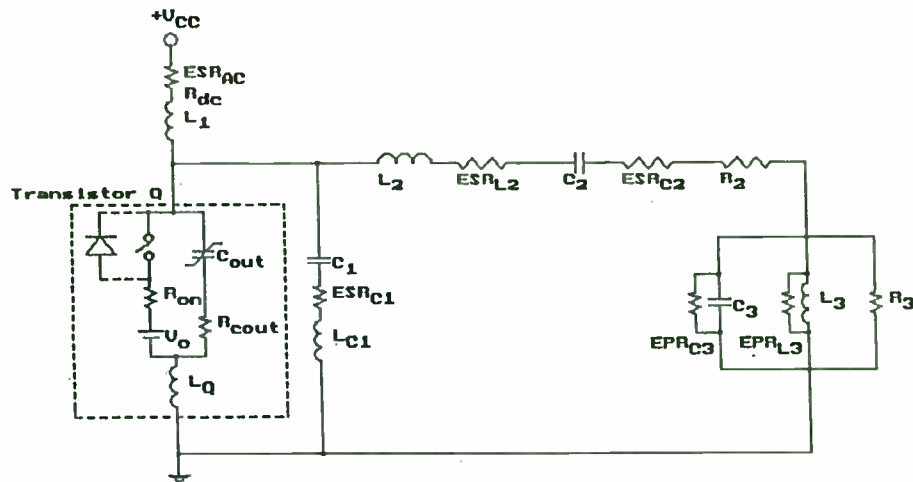
The driver amplifier has an on-chip biasing circuit to stabilize the amplifier gain for temperature and process variations. With $V_{CC1} = 4.5 \text{ V}$, $V_{CC2} = 6 \text{ V}$, and $V_{control} = 2.2 \text{ V}$ (which results in a total bias current of 180 mA), the amplifier achieves a measured small-signal gain of 32 dB, an output 1-dB compression point of 22.5 dBm, a third-order intercept point of 30 dBm, and a noise figure of 9.5 dB. The input return loss is 12 dB. Figure 11 shows the measured output power and small-signal gain versus frequency.

The output power can be varied over a 50-dB range with a control bias signal of 0 to 2.5 V on the second and third stages. The measured output power as a function of control voltage and frequency is shown in Fig. 12.

IV. Integrated LNA and Mixer

A family of combined low noise amplifier and mixer circuits has been developed for use in the 900-MHz cellular or 1900-MHz PCN and DECT applications. These circuits which are intended to operate as the front end for communication systems, achieve low noise performance, wide dynamic range with acceptable impedance matching over the voltage range of 3 V to 5 V.

The basic LNA topology as shown in Fig. 13 is a two-stage non-feedback circuit with reactive matching at both the input and output, and the two stages are coupled via an on-chip capacitor for optimum voltage swing. The first stage is optimized for a low noise figure and $50\text{-}\Omega$ input impedance matching. The second stage uses emitter degeneration to set the overall gain and functions as a class-A output stage. The output impedance is matched externally to 50Ω with a shunt-L series-C network. The LNA achieves required electrical specs through the use of user-supplied off-chip tuning elements. The input impedance and noise figure of the circuit are



Press A, B, C, or 1 to view topologies.

RETURN FROM HELP: <ESC>

RF-GENERATOR REQUIREMENTS

(Master oscillator/power amplifier)

- Frequency: 27.12 MHz
- Output power: 20 W minimum with 24 Vdc from battery pack; change power by changing taps on battery pack.
- Overall efficiency: >80%
- Low product cost: use low-cost plastic-packaged transistor.

RFW3B070

approximated by

$$Z_i \approx \left[r_{b1} + \omega_T L_{g1} \right] + j\omega \left[L_{g1} - \frac{1}{\omega^2 C_{\pi 1}} \right], \quad (4)$$

$$\begin{aligned} NF &= 1 + \frac{r_{b1}}{R_S} + \frac{g_{m1}}{2R_S |\beta(j\omega)|^2} \left[\left(r_{b1} + R_S \right)^2 + \omega^2 \left[L_{g1} - \frac{1}{\omega^2 C_{\pi 1}} \right]^2 \right] \\ &= 1 + \frac{r_{b1}}{R_S} + \frac{1}{2g_{m1}R_S} \left[1 + \omega^2 C_{\pi 1}^2 \left(r_{b1} + R_S \right)^2 \right] \end{aligned} \quad (5)$$

where ω_T is the transition frequency, R_S is the source resistance, and L_{g1} is the effective inductance at the emitter of Q_1 . It is apparent from (4) and (5) that a proper input device size and a careful board layout are necessary to ensure a low noise figure and 50- Ω input impedance matching.

The basic mixer topology as shown in Fig. 14 is a double-balanced active mixer for good isolation and low LO leakages. Again, through the use of LC reactive elements, the mixer achieves a lower noise figure than previously reported Gilbert-cell active mixers for the same input linearity [3]. It also achieves narrow-band matching at the RF port with simple LC matching elements. The single-ended conversion gain of the circuit is approximated by

$$G_C \approx \frac{1}{2} \left[\frac{g_{m5}}{1 + g_{m5} (R_E / 2)} \right] \left[\frac{a_1}{2} \right] R_{Leff} \sqrt{\frac{R_S}{R_L}} \quad (6)$$

where

$$\lim_{V_{LO} \rightarrow \infty} \left[\frac{a_1}{2} \right] = \frac{2}{\pi} = -3.9 \text{ dB}$$

is due to the LO switching action. R_S is the source resistance, R_L is the load resistance, R_{Leff} is the effective output impedance, and R_E is the emitter degeneration. As a test vehicle, a separate mixer/IF circuit using the topology of Fig. 14 was implemented on the HP BCA-02 transistor array. The circuit uses a single supply of 3 V and draws a bias current of 11 mA for the mixer and 7 mA for the IF amplifier. With an RF frequency of 1900 MHz and an LO frequency of 1800 MHz, the mixer/IF circuit achieves a measured conversion gain of 13 dB and a noise figure of 11 dB. Figure 15 shows the conversion gain versus RF frequency for a constant IF frequency of 100 MHz. Also shown is the input return loss at the RF port. The conversion gain as a function of RF frequency for a constant LO frequency of 1800 MHz is shown in Fig. 16.

TRANSISTOR CHOICE - 1

- MOSFET instead of BJT
 - a. effects of unspecified parasitic parameters are less important
 - b. potential efficiency is higher
 - c. easier to drive input
 - d. easier to understand (fewer arcane effects)
 - e. less problem if accidental overstress
- Required voltage rating: $3.5 \times 24 \text{ Vdc} \times \text{safety factor} = 100 \text{ V}$
- Low-cost, in plastic package: International Rectifier IRF510 series (multiple sources)

RFW3B080

TRANSISTOR CHOICE - 2

Which 100-V transistor?

- Two IRF510 or 520 in parallel to halve the parasitic lead inductances (expect problem)
- IRF530
- IRF540 is too large (suitable for 200 W).
- Compare computer-predicted results (HEPA program) and choose best tradeoff.
- Tradeoff is lower R_{on} (less conduction loss) vs. higher C_{out} (more turn-on loss).

RFW3B090

Each LNA/mixer circuit has an on-chip bandgap reference to stabilize the LNA gain to less than ± 0.5 dB over the -40° and $+85^\circ$ temperature range and to maintain the overall circuit operation as the power supply is lowered to 3 V. A power-down function is incorporated into the circuit by disabling the bandgap reference with a control voltage. The circuit is housed in a low-cost 16-lead surface mount plastic package. Simulation results at 900 MHz (two versions) and 1900 MHz for a single power supply of 5 V are shown below. As the supply voltage reduces to 3 V, the LNA's S_{21} is about 2.5 dB lower and its NF is about 0.3 dB higher. The mixer characteristics remain almost unchanged.

LNA @ 5 V and 27°C			
Frequency (MHz)	900	900	1900
I_{cc} (mA)	7.6	5.5	7.6
S_{11} (dB)	-19	-19	-8
S_{22} (dB)	-17	-16	-16
S_{21} (dB)	16.1	15.3	13.9
NF (dB)	2.1	2.2	3.4
Input $P_{-1 dB}$ (dBm)	-16	-19.5	-16
Input IP_3 (dBm)	-5.6	-10.5	-7.0
Mixer @ 5 V and 27°C			
I_{cc} (mA)	5.5	4.6	5.5
RF S_{11} (dB)	-16	-16	-23
G_C (dB)	8.5	8.3	6.3
NF (dB)	10	10	10
Input $P_{-1 dB}$ (dBm)	-10	< -10	-10
Input IP_3 (dBm)	4.0	3.0	0

TRANSISTOR CHOICE - 3

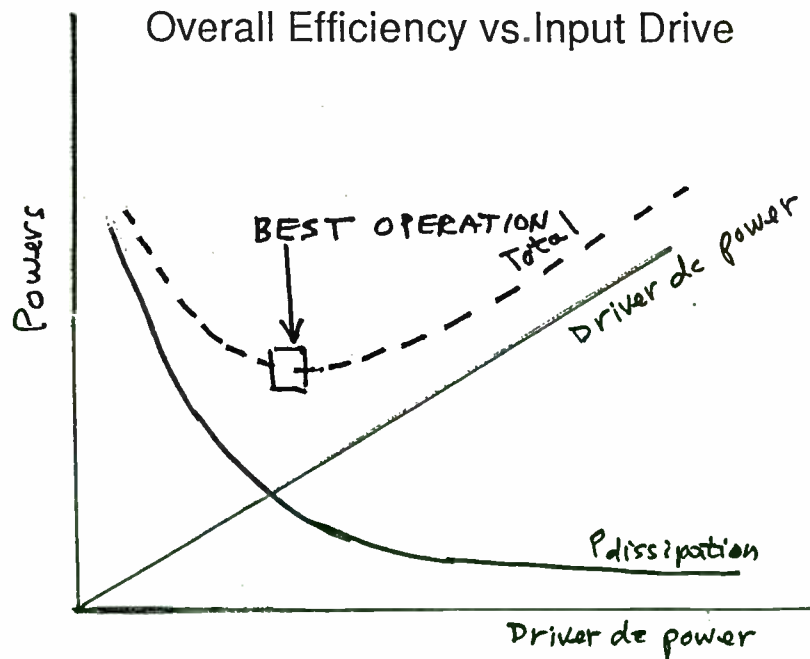
Comparison Results

- Computer optimization gives best efficiency with two IRF520 in parallel.
- Experimental results: Effects of parasitic inductance much less than feared, due to careful low-L PC layout.
- But driver stage has heavy load of doubled inputs of output stage; uses more driver P.
- Try single IRF520 to trade slightly higher loss in output stage for less driver power.

RFW3B100

TRADEOFFS - 4

Overall Efficiency vs. Input Drive



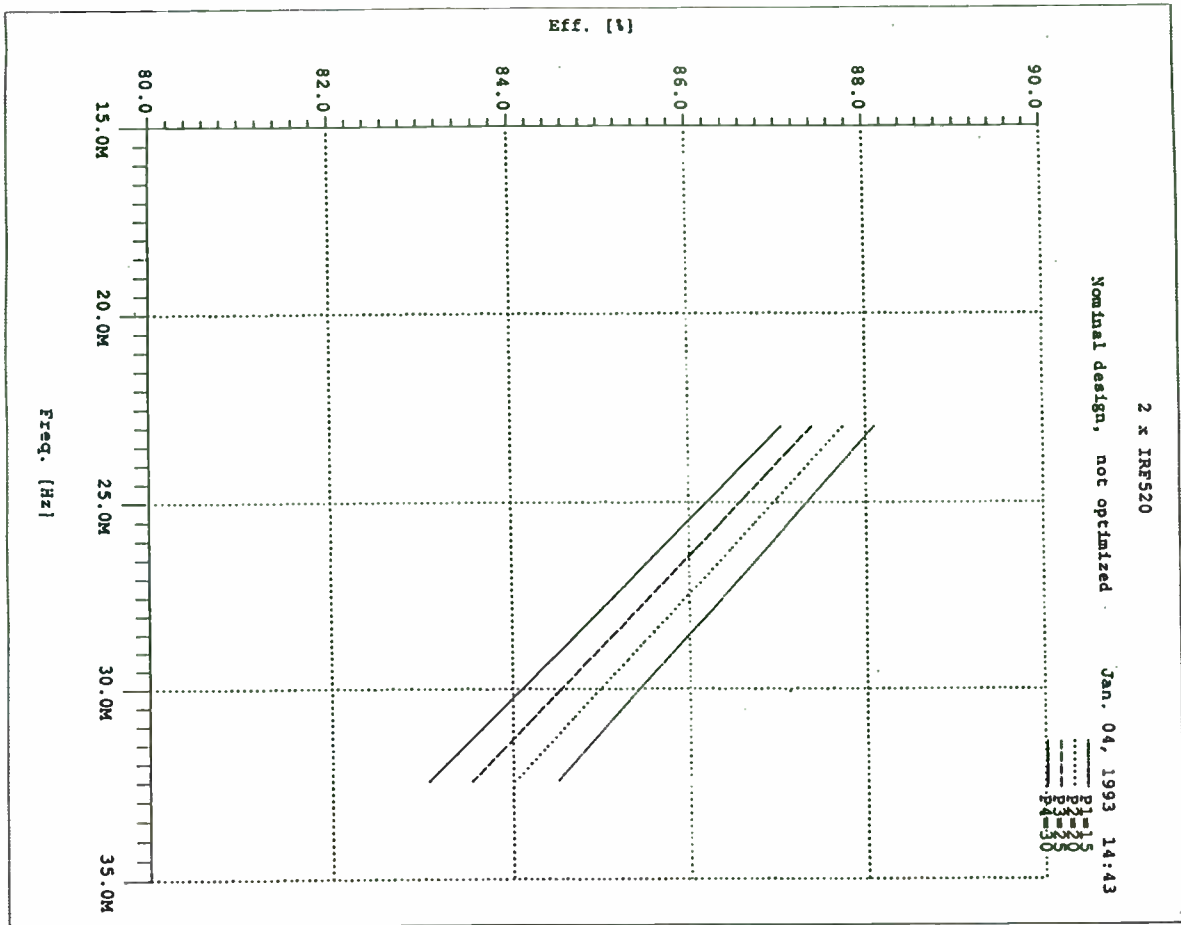
RFW3A150
B102

V. Conclusion

A variety of high-performance integrated circuits appropriate for wireless communications has been demonstrated. High level of performance is achieved using the ISOSAT-II silicon bipolar process. In addition to transistor devices with excellent performance at microwave frequencies, incorporation of high-Q inductive and capacitive elements have allowed the circuits to be further optimized in the frequency band of interest. These techniques result in components with low noise, good power efficiency, and high level of integration.

References

- [1] N. M. Nguyen and R. G. Meyer, "Si IC-Compatible Inductors and LC Passive Filters," *IEEE J. Solid-State Circuits*, vol. SC-25, no. 4, pp. 1028-1031, August 1990.
- [2] E. A. Lee and D. G. Messerschmitt, *Digital Communication*, Kluwer Academic Publishers, Boston, 1988.
- [3] J. Wholey, I. Kipnis, and C. Snapp "Silicon Bipolar Double Balanced Active Mixer MMICs for RF and Microwave Applications up to 6 GHz," in *IEEE MTT-S Digest of Technical Papers*, pp. 133-137, May 1989.



```

High-Efficiency Power Amplifier PLUS (HEPA II+/WB) Jan. 04, 1993 16:51
1 x IRF520
ENTER CIRCUIT PARAMETERS and/or TITLE

Common-Source TRANSISTOR with diode          LOAD without filter
Frequency (f).....[Hz]: 2.712E+07           Load location, R3 or R2? R3
Duty ratio (D).....: 0.5                     Load resistance..[ohms]: 50
"on" resistance...[ohms]: 0.25               R3/Rload.....: 1
Vo[V]:0          Lq [H]: 6E-09              L3.....[henries]: 1E-05
Transition times: turn-on,turn-off [s]      Qv:10000      at freq: 2.694E+07
on:3.5E-09      off: 3.5E-09              C3.....[farads]: 2.3509E-10
Cout.....[farads]: 1.3E-10                Qv:200       at freq: 2.694E+07
Cout series resis.[ohms]: 0.625

LOAD NETWORK, Single-ended
DC supply (Vcc)..[voits]: 24.              C2.....[farads]: 2.5E-09
L1.....[henries]: 3E-06                    Qv:200       at freq: 2.694E+07
Qv: 50      at freq: 2.694E+07
Rdc.....[ohms]: 0.051469                   Network loaded 0 or L2? L2
C1.....[farads]: 1.4683E-11                L2.....[henries]: 2.053E-07
Qv: 200    at freq: 2.694E+07              Qv:200       at freq: 2.694E+07
Lc1.....[henries]: 0                       Network loaded 0.....: 3.2176
) ENTRY: ALPHANUM.  COMPUTE: (PgDn)  MAIN MEMJ: (ESC);
  
```

SELECTING PARAMETER...

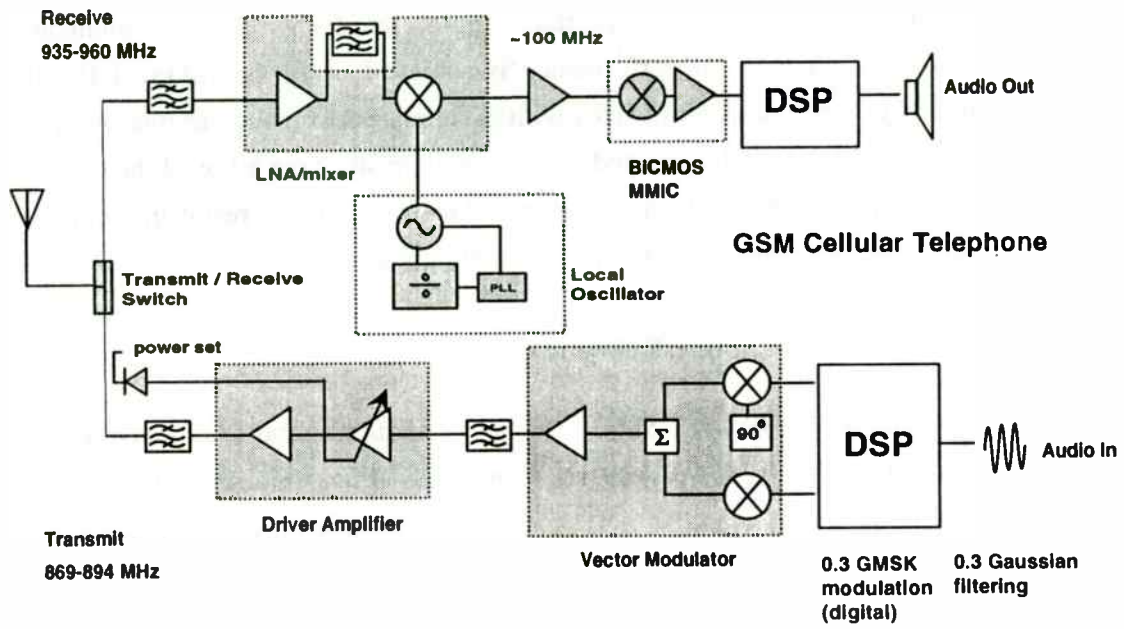


Figure 1 Typical Architecture of a Cellular Radio Handset

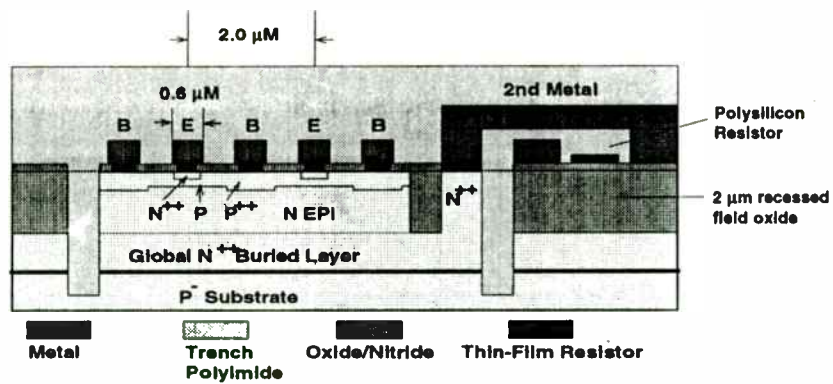


Figure 2 ISOSAT™ Process Silicon MMIC Structure


```

High-Efficiency Power Amplifier PLUS (HEPA II+/WB) Jan. 04, 1993 16:51
1 x IRF520
EFFICIENCY, POWERS, and STRESSES
Single-ended
Collector/drain efficiency.....[Pout/Pin] 89.897%
Collector/drain inefficiency...[(Pin-Pout)/Pin] 10.103%
Overall efficiency.....[Pout/(Pin+Pid)] 82.101%
DC power input (Pin).....[watts] 26.326
Input-drive power (Pid).....[watts] 2.5
Power output (Pout).....[watts] 23.667
Power loss in L1.....[watts] 0.088116
Power loss in L2.....[watts] 0.41123
Power loss in C2.....[watts] 0.027872
Resistive power loss of transistor & C1 [watts] 1.1856
Turn-off power loss of transistor.....[watts] 0.64045
Turn-on power loss of transistor.....[watts] 0.070132
Power loss in L3.....[watts] 6.8523E-05
Power loss in C3.....[watts] 0.23622

Output voltage, current (at Rload) [V.A]: 34.4 0.68799
Transistor peak voltages....[volts]: normal 79.559 inverse None
Transistor peak currents..[amperes]: normal 6.5714 inverse None
'DISPLAY RESULTS' MENU: (ESC)

```

DISPLAYING COMPUTED POWERS...

TRANSISTOR CHOICE - 4

Experimental Results

- Output stage drain efficiencies of one or two IRF520 were as predicted by HEPA program.
- Final design: one IRF520 for 24 W RF output.
- Single IRF520 had slightly lower drain efficiency, but power saved in driver stage more than made up for the slightly higher drain power loss.
- Fifteen assemblies with IR and Harris transistors had drain efficiencies of 89 to 92%.

RFW3B110

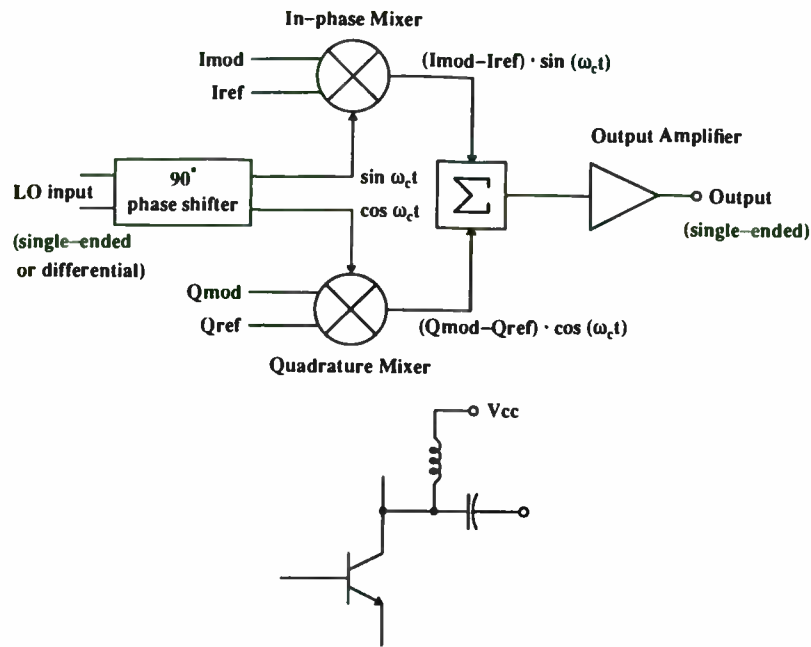
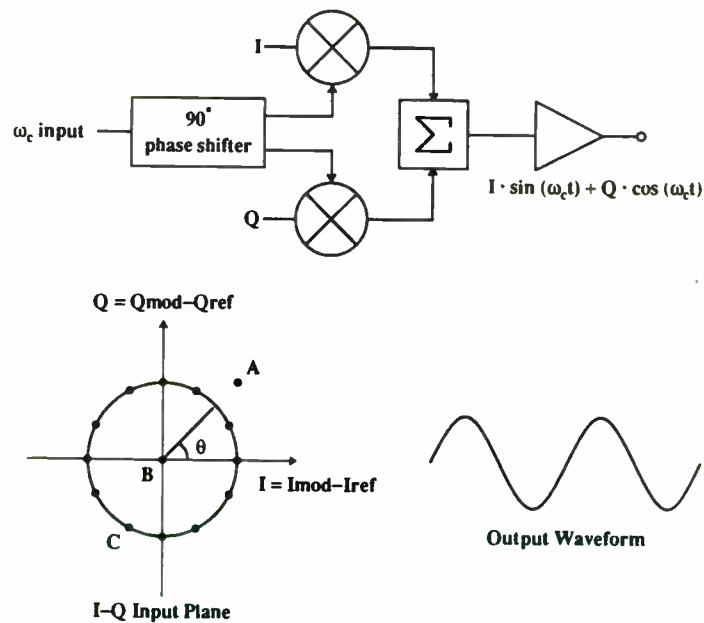
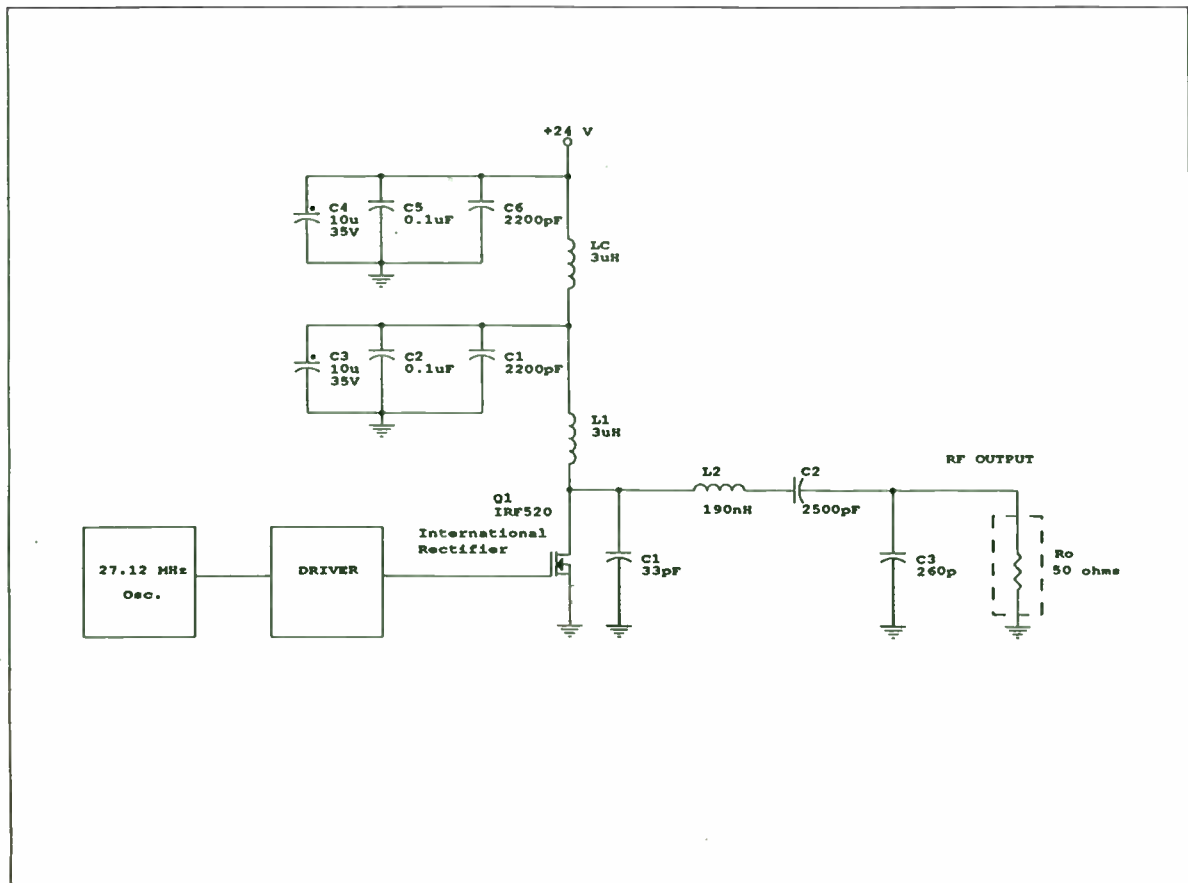


Figure 3: Functional Diagram and Simplified r.f. Output Stage of the Quadrature Modulator



	Ideal case	Measured case
Amplitude:	$-\sqrt{I^2 + Q^2}$	$-\text{Mag}(S_{21})$
Phase:	$-\tan^{-1}(Q/I)$	$-\text{Angle}(S_{21})$

Figure 4: Mapping Function of the Quadrature Modulator



EXPERIMENTAL RESULTS

Using One IRF520, 24 W, 27.12 MHz

- Measured drain efficiency = 89 to 92%.
(HEPA computer program predicted 90%.)
- Overall efficiency = 84%, including dc power to crystal oscillator and driver chain.

RFW3B120

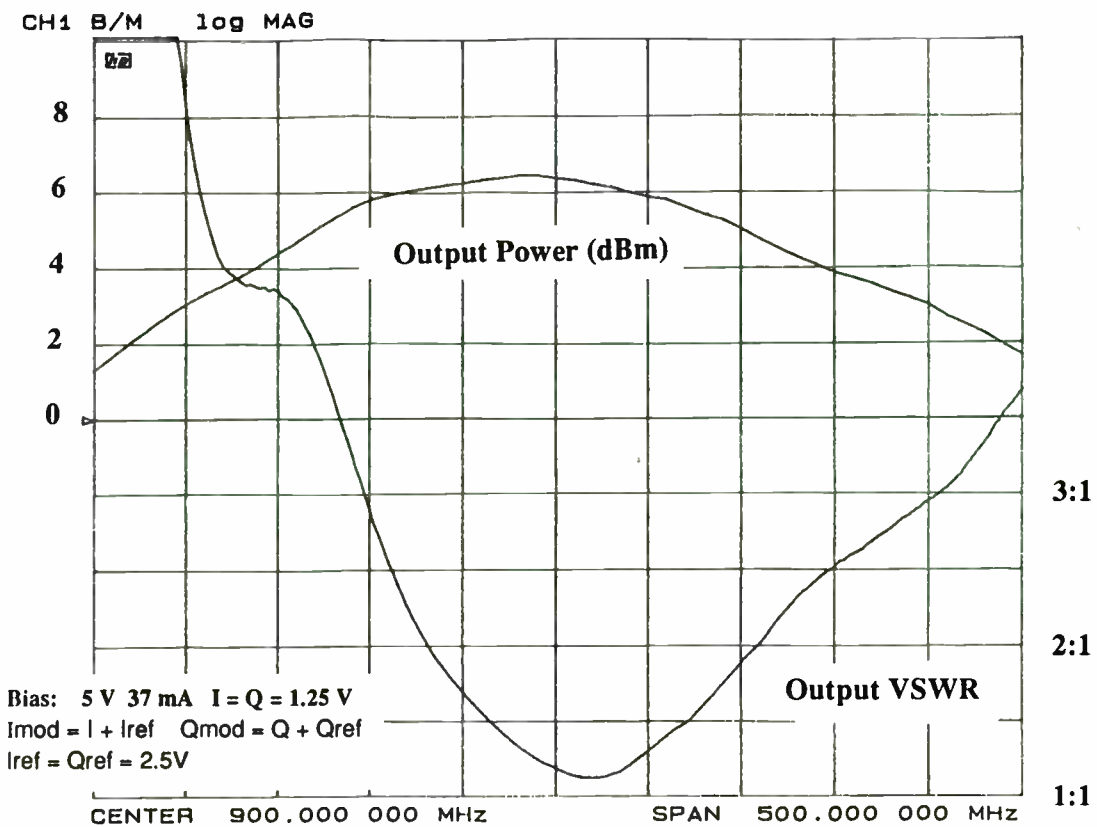


Figure 5: Output Power and Output VSWR vs Frequency

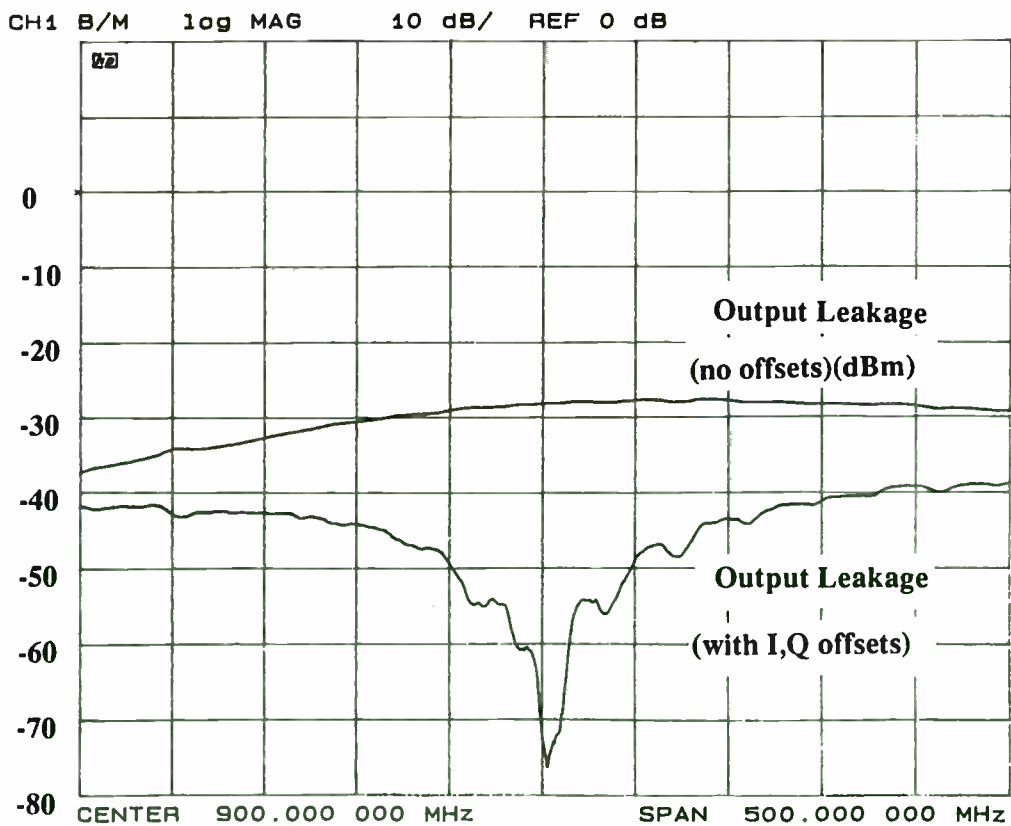


Figure 6: Output Leakage with and without Offsets

A UHF/L-Band FET Module **for** **Pulsed Power Avionics Applications.**

Frank Sulak, Ken Sooknanan,
Toru Nakamura, Al Rosenzweig,
Adrian I. Cogan

MicroWave Technology, Inc.
4268 Solar Way
Fremont, CA 94538

Summary

A large number of applications exist for pulsed solid-state power in the frequency range between 800 MHz and 1300 MHz. These include modern avionics systems, such as distance measurement equipment (DME), air-traffic control transponders, identification friend or foe (IFF), and secure communications systems such as the Joint Tactical Information and Distribution System (JTIDS). These systems, as well as air traffic control radars, are being designed to communicate more and more information in digital format or with sophisticated pulse trains requiring that the power amplifiers reproduce the modulation accurately while occupying less volume and using less DC power.

This paper describes a new technology used in the design and fabrication of very small size pulsed operation, high power, broadband and narrow band amplifier modules for avionics applications. These Compact Amplifier Modules (CAMs) exhibit high peak power (50 W through 250 W) in a very small size and operate broadband, from 800 MHz through 1250 MHz.

The CAMs use power silicon FETs called Solid State Triodes™ (SSTs). The main design aspects related to such high power pulse SST circuits operating at L-band frequencies are discussed, and practical CAM fabrication issues are addressed.

In high pulse power avionics applications, the SST CAMs have unique performance advantages over bipolar transistors. CAMs exhibit wide dynamic range of gain control, wide dynamic range for linear gain, excellent thermal stability, and have very short pulse rise and fall times.

CAM applications and performance figures are presented and discussed in the last section of the paper. While the SST CAMs were developed for avionics applications, the technology can be used for other areas where tens and hundreds of watts of pulsed RF power are required over narrow band or broadband frequencies ranging from 500 MHz through 1300 MHz.

Introduction: The SST.

In recent years, power Bipolar Junction Transistors (BJTs) have seen their virtual monopoly in RF applications challenged first by MOSFETs and recently, by Solid State Triodes (SSTs). While at RF and VHF frequencies MOSFET use keeps increasing at the expense of BJTs, the BJT domination at UHF frequencies and into L-band has continued. The SST, has now demonstrated performance levels superior to BJTs and MOSFETs.

SSTs are depletion-mode silicon junction FETs which exhibit unsaturated, triode-like I-V characteristics, similar to those of a vacuum

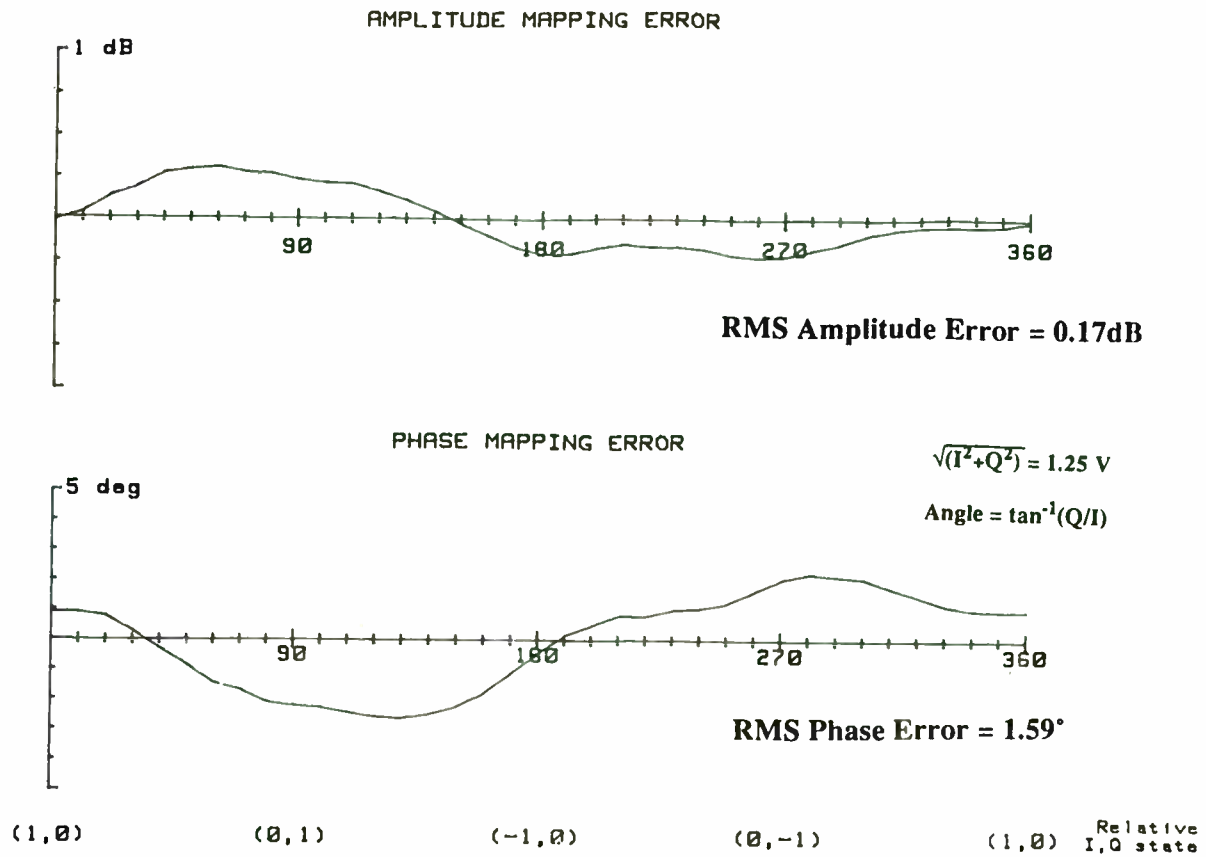


Figure 7: Amplitude and Phase Mapping Error vs IQ input angle

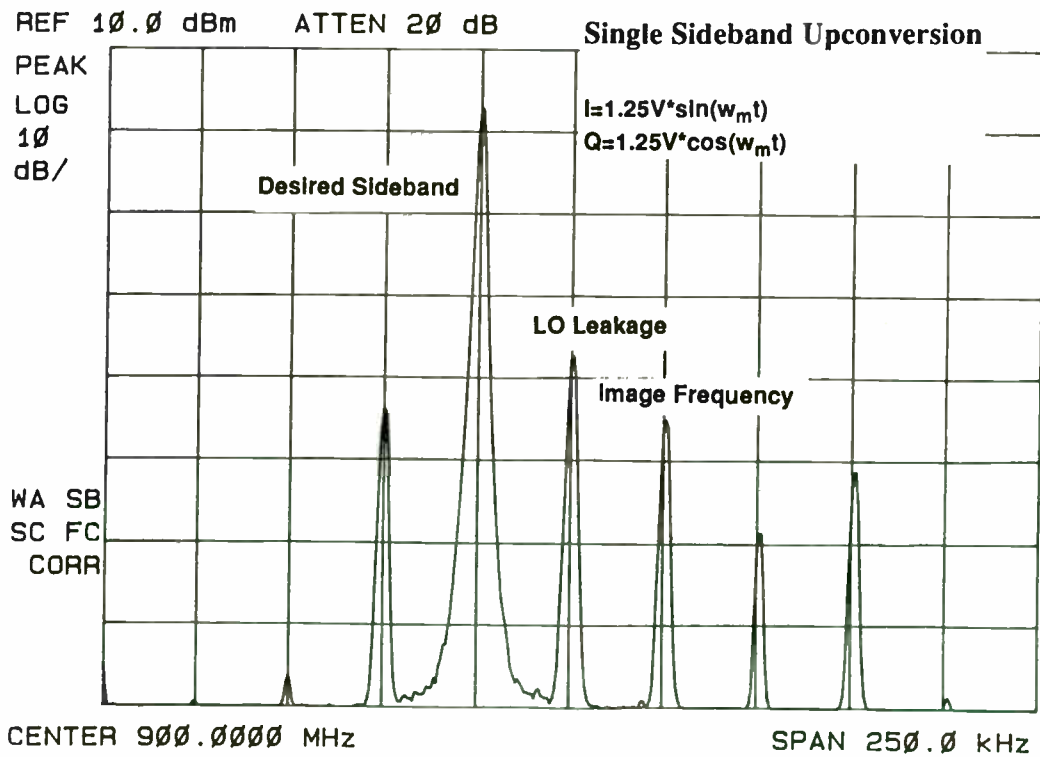


Figure 8: Single Sideband Upconversion, 25kHz quadrature inputs

triode (Figure 1). The SST requires bias conditions similar to a vacuum tube or a GaAs MESFET: negative gate voltage and positive drain voltage.

As with any other RF transistor, the SST electrical performance, and parameters such as power gain, efficiency, output power, etc. , are dependent on the operating point.

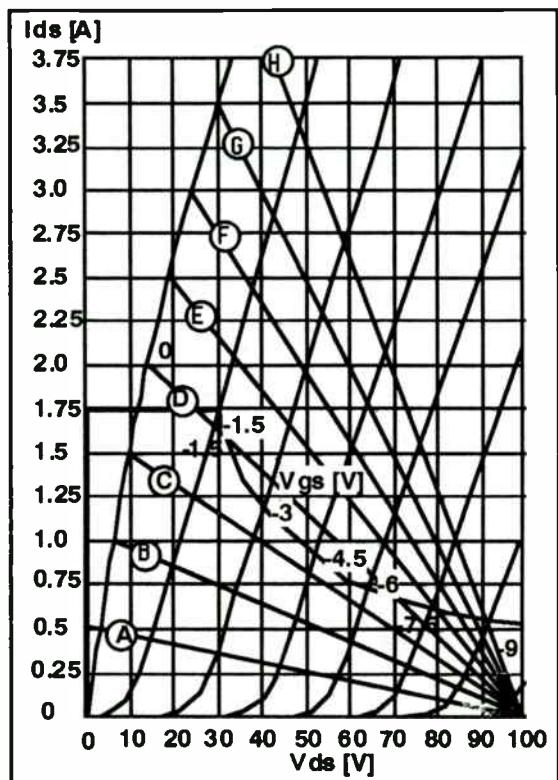


Figure 1. SST I-V Characteristics.

The maximum power available from a given transistor active area remains constant and is limited by thermal dissipation and is bounded by a maximum (breakdown) voltage and current. The resulting safe operating area (SOA) widens as one moves from CW into pulse operating conditions. The shorter the pulse and the lower the pulse duty factor, the wider the device SOA. Ultimately, a maximum allowed current density and the junction breakdown voltage define a rectangular SOA for BJTs and MOSFETs.

For the BJT, exceeding the maximum specified current will result in a significant decrease in current gain, while for the MOSFET, attempts to further increase the drain current by increasing the gate voltage

will result in gain compression and, if V_{gs} is further increased, the gate oxide will rupture.

Unlike the BJT and the MOSFET, the SST pulsed SOA extends beyond the shaded CW SOA boundary in Figure 1. As a consequence, in selecting the load impedance for maximum output power, one can access a wider region of the I-V characteristics. As shown in this figure, the SST transconductance keeps increasing with the operating current. One consequence of this unusual operating behavior is that higher pulsed power levels can be achieved from the same silicon active area when comparing SSTs to BJTs or to MOSFETs. The pulsed power to CW power ratios of better than 6 dB are routinely measured with present SSTs.

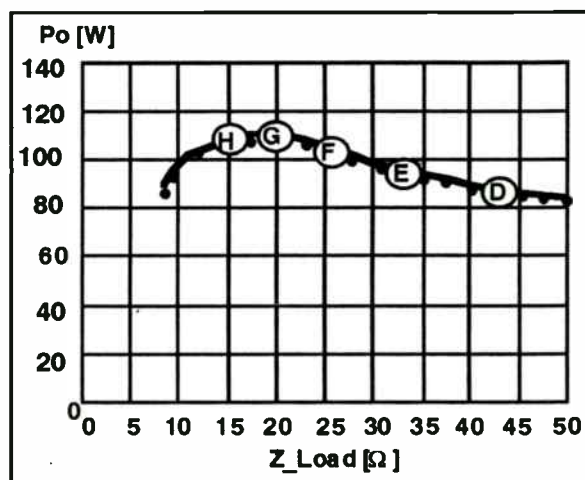


Figure 2. Pout vs. Load Impedance.

Several load impedance values are marked in Figures 1 and 2. The calculated dependence of the maximum available output power on the load impedance is plotted in Figure 2. This illustrates the relatively slow P_o vs. Z_L dependence. This is another SST advantage since in the case of BJTs and MOSFETs the maximum power load impedance is always selected to run from the 'knee' of the collector or drain current to the off-current maximum voltage point.

MWT has performed extensive SST testing under RF pulse operating conditions at frequencies ranging from 500 MHz through 1300 MHz. It should be noted that, to date, no power MOSFETs compete with BJTs and

Double Sideband Upconversion

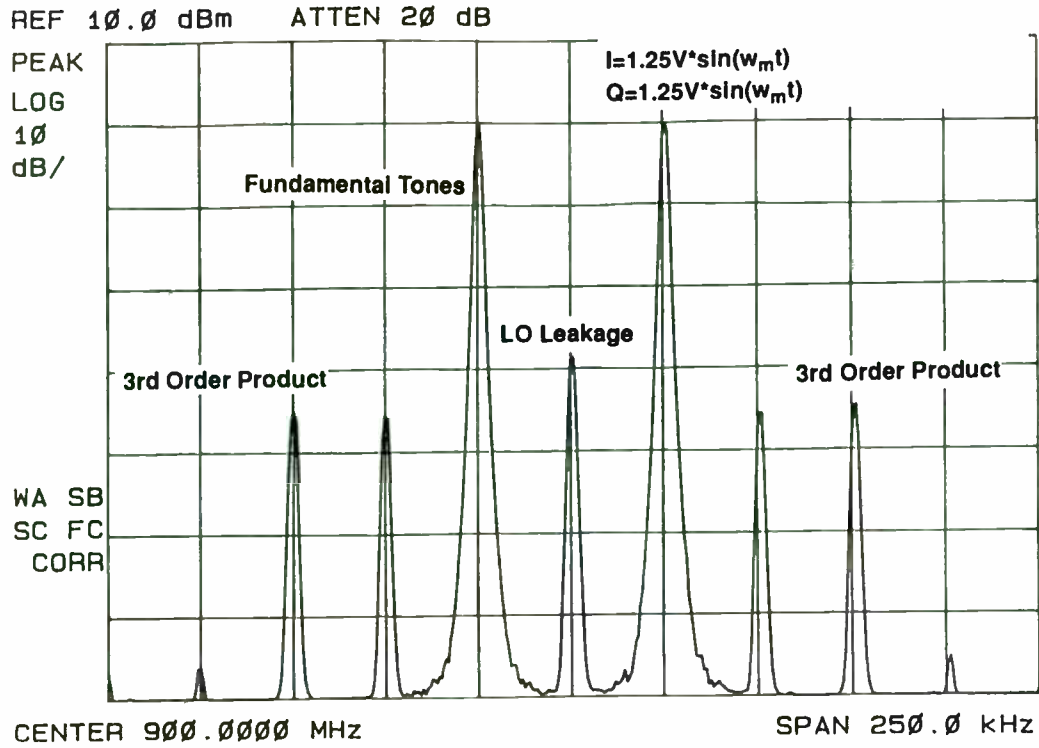


Figure 9: Double Sideband Upconversion, 25kHz in-phase Inputs

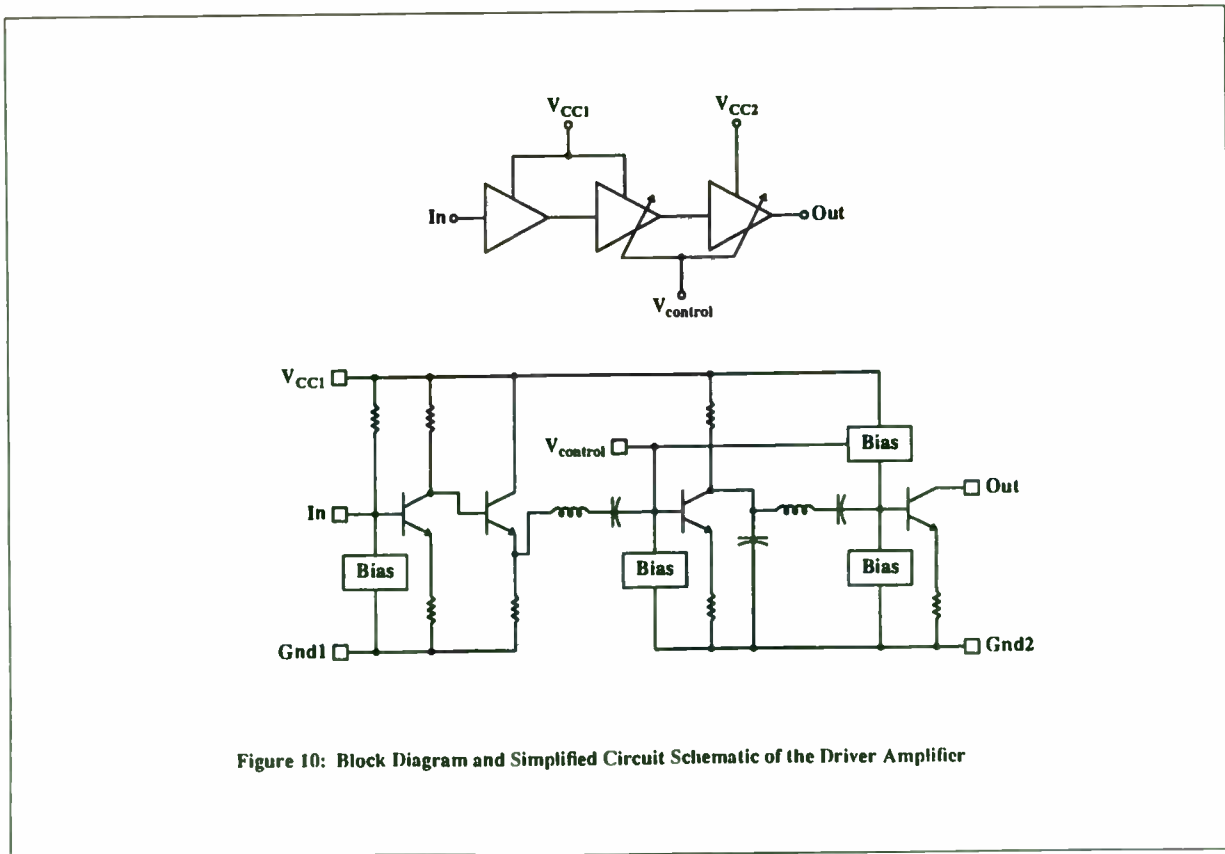


Figure 10: Block Diagram and Simplified Circuit Schematic of the Driver Amplifier

SSTs for this type of applications. Some of the most relevant SST advantages for pulsed applications are as follows:

- The SST can switch RF pulses with rise and fall times of less than 10 ns. By comparison, BJTs usually switch in tens of nanoseconds.
- The SST excellent linearity allows for the RF pulse spectral response to be better preserved or to be easier shaped to desired specifications. In present BJT applications, the pulse spectral response is tailored by modulating the transistor collector voltage at high current levels, a very difficult task to implement. By contrast, in a SST CAM power control requirements are easily met in a low current, high impedance environment.
- The SST has a wide dynamic range of linear gain control, typically more than 10 dB. This feature provides previously unachievable control levels in avionics high power RF applications presently relying on PIN diode or mechanical switches. On-Off RF power ratios of better than 40 dB can easily be achieved.
- The SST is thermally stable as the drain current will decrease slightly with an increase in temperature. It also has no power drift after turn-on and its power derating coefficient is approximately 0.01 dB/°C. One consequence is that simpler thermal compensation circuitry is required. SSTs operation was tested at junction temperatures ranging from liquid helium (3°K) through 300°C. Both the BJT and the MOSFETs cease to operate at such low temperatures.
- The SSTs are extremely rugged transistors, withstanding VSWR figures in excess of 20:1. This ruggedness is due mainly to the SST JFET structure, which has fewer parasitic components when compared to BJTs and MOSFETs and does not have very thin junctions or thin gate oxides, which are easily degraded by over-voltage, over-current, or high operating temperatures.

- The SST is its inherently radiation hard. Due to the simplicity of its structure, when irradiated, the SST does not exhibit a current gain decrease such as with the BJT, or threshold voltage shifts, such as with the MOSFET. SSTs are superior in both total dose and radiation bursts environments. While this is not directly an electrical circuit advantage, it will promote SST use in applications which require the electronics to operate under harsh ionizing radiation conditions.

Compact RF Power Amplifier Modules.

Conventional high power pulsed RF amplifiers use discrete transistor packages mounted on external heat sinks, with softboard printed circuits, and mostly lumped discrete passive components. While this is a convenient and well proven approach, it does not make maximum use of the transistor capabilities. These amplifiers are also relatively bulky.

Microwave Technology (MwT) has developed a hybrid circuit technology suitable for the fabrication of high power, compact RF amplifier modules. Based on its present thin film hybrid IC technology, the new circuit modules eliminate the need for discrete RF power packages and present the user with a very convenient $Z_{in} = Z_{out} = 50 \Omega$ solution.

These modules have the internal matching elements fabricated in the immediate vicinity of the SST chip. Near chip matching increases circuit efficiency by reducing loss associated with power combining and broad-banding and also improves system reliability. Costs are usually reduced, when compared to the present single device unit cost and circuit fabrication costs for discrete L-band power transistor amplifiers.

The first step in implementing these compact SST power amplifiers is the Aluminum Nitride Carrier Assembly (ANCA). An ANCA consists of a high thermal conductivity rectangular ceramic pill with metallized "via" grounding holes, on top of which thin film distributed

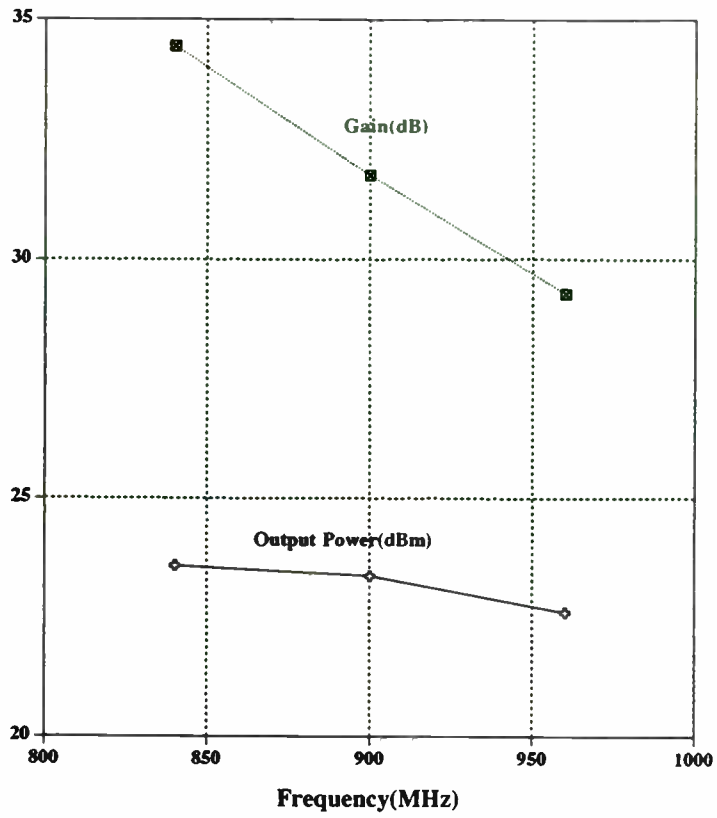


Figure 11 Output Power & Gain vs Frequency

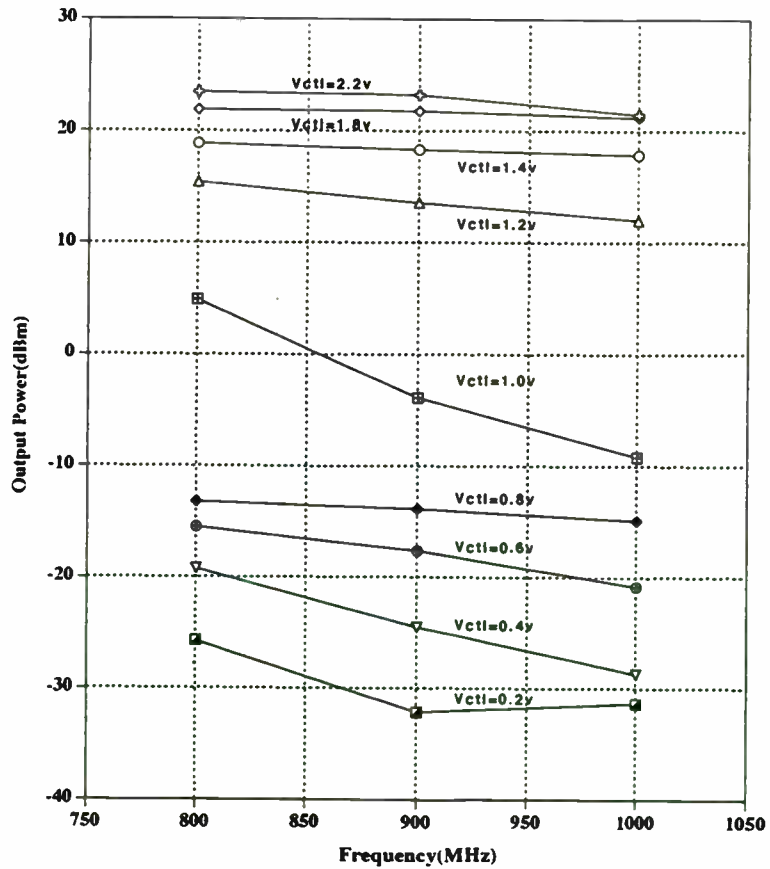


Figure 12 Output Power vs Frequency & Vcontrol

impedance matching element circuitry is deposited and patterned.

A single-ended ANCA and its equivalent circuit are shown in Figure 3.a. As shown, the first output impedance matching step uses a shunt inductor decoupled through a low reactance capacitor. Low-pass LC sections are used on the SST input side and are easily recognized in the figure. As shown, the first matching elements are placed in close proximity to the SST chip, thus reducing parasitic component contribution and the loss due to the high circulating currents in the shunt L.

Additional input and output matching sections are used to achieve the desired output power over the specified bandwidth. These distributed element circuits are fabricated on low loss alumina, also using thin film processing technology.

circuits and RF bypassing elements inside a small size housing, one ends up with a Compact Amplifier Module (CAM), such as the one illustrated in Figure 4. These less than 2" long CAMs deliver 150 W of peak power at 1000 MHz with over 30 % bandwidths.

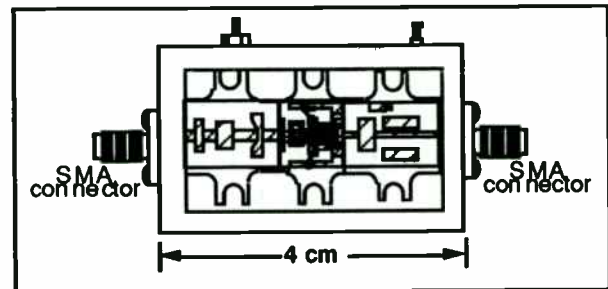
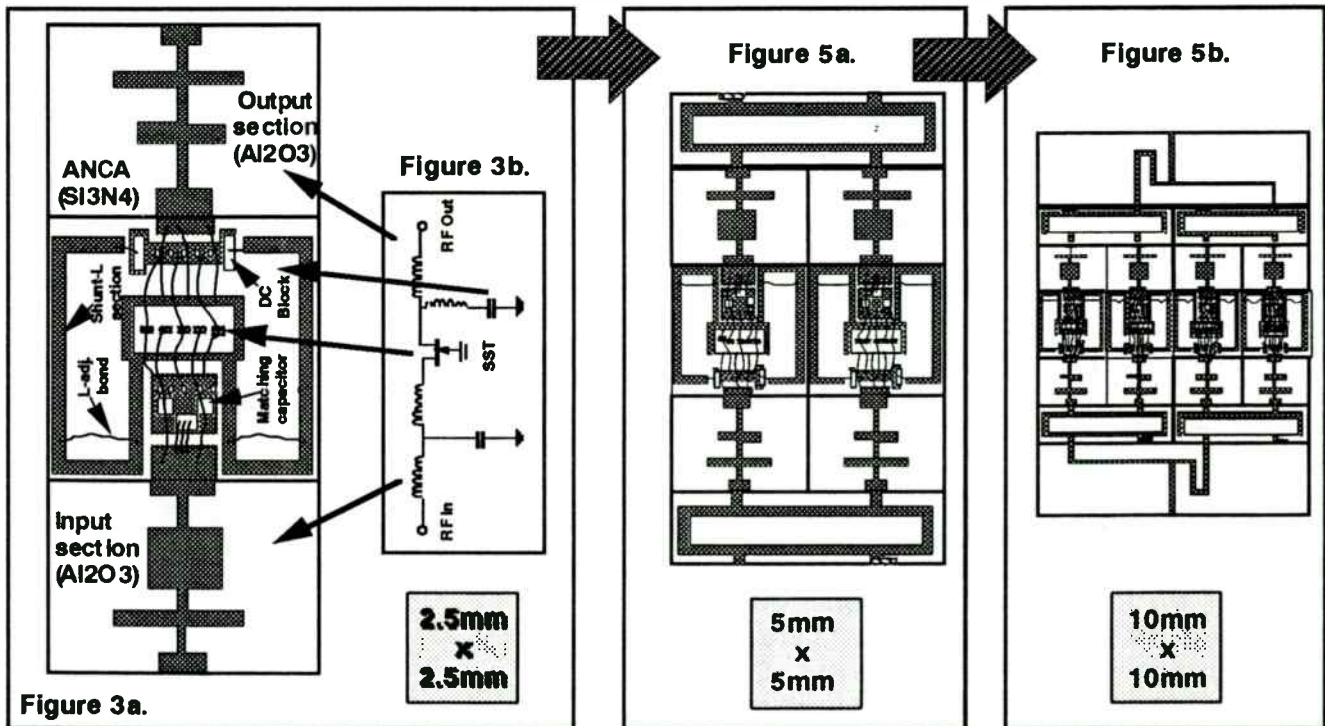


Figure 4. 100W CAM.

Two ANCAs and their matching circuits are power combined into a higher power CAM using Wilkinson or 90° hybrid couplers, as illustrated in Figure 5.a. Further combining will yield Power Amplifier Modules (PAMs) capable to deliver 300 W - 500 W of peak RF



CAM Components: ANCA + Input and Output Matching Sections

200W CAM Layout.

400W PAM Layout.

When an ANCA and its corresponding input and output matching circuits are assembled together with the appropriate DC biasing

power (Figure 5.b.). The PAM operating frequency can be centered at any frequency

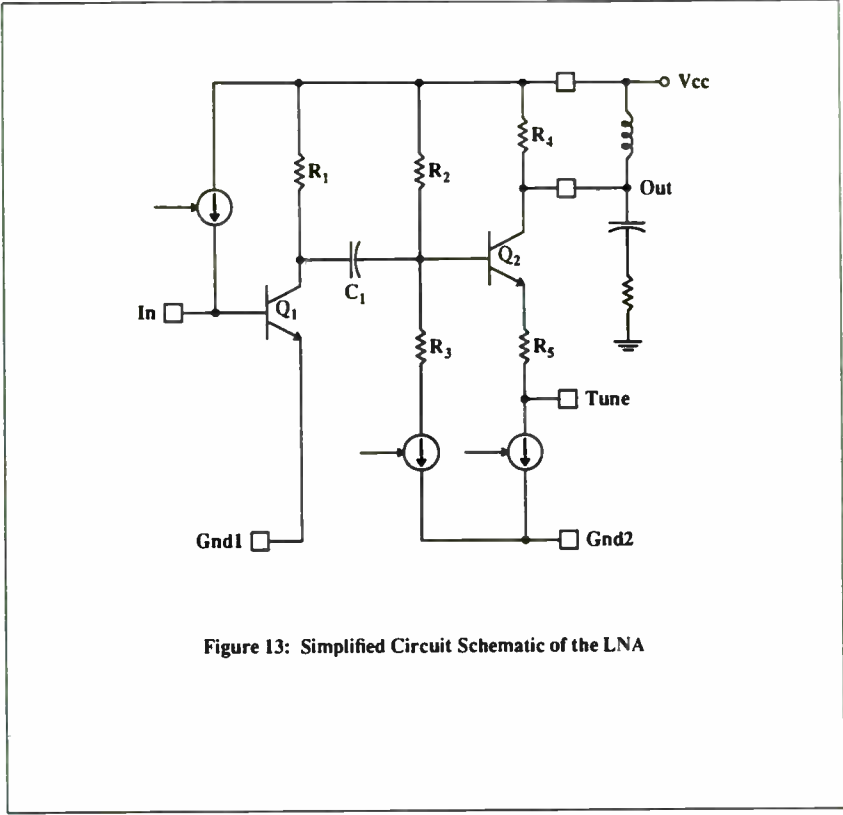


Figure 13: Simplified Circuit Schematic of the LNA

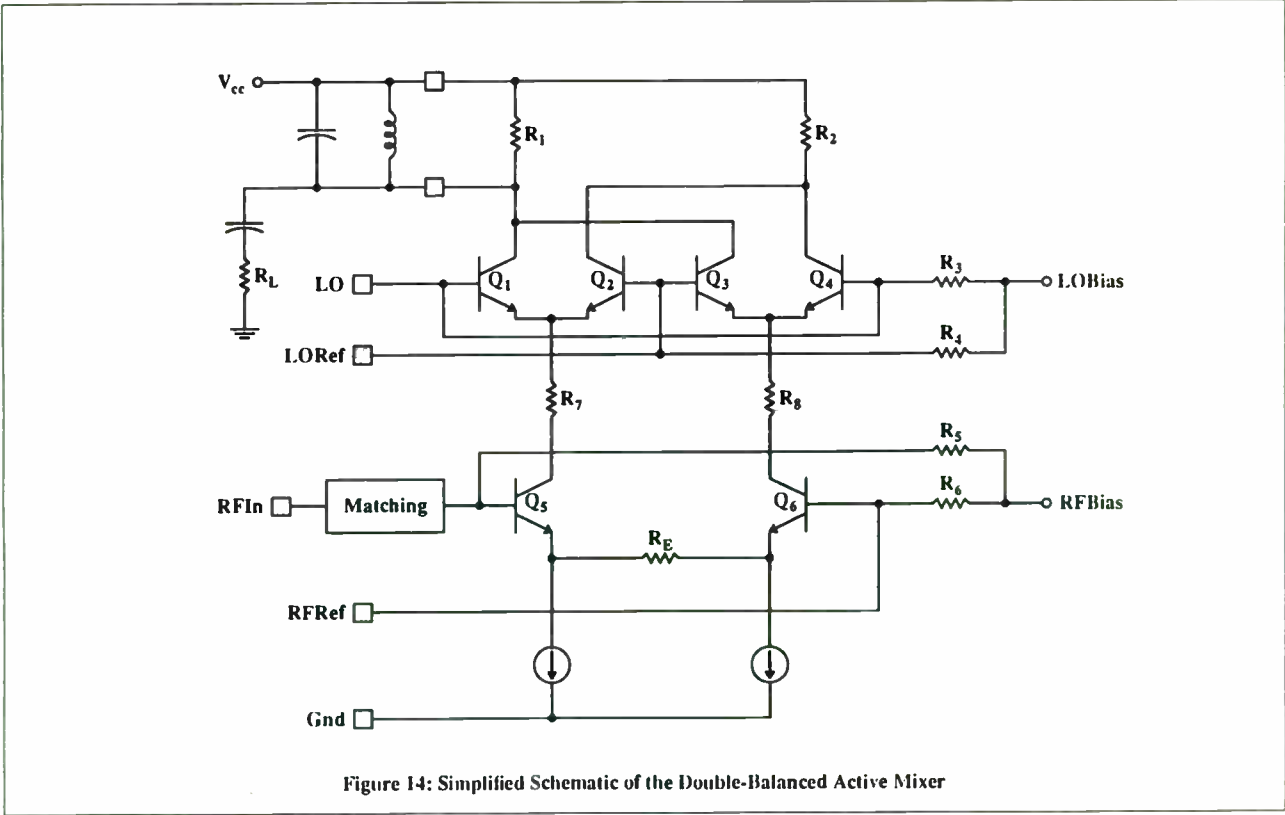


Figure 14: Simplified Schematic of the Double-Balanced Active Mixer

in the 800 MHz through 1000 MHz with a bandwidth that can exceed 30%.

The CAM design, fabrication and characterization work proceeds by addressing one matching section at a time, and moving from the SST die plane toward the module outputs, and begins with the output shunt-L section.

In order to facilitate the design of the ANCA and CAM matching circuits, RF characterization proceeded in two steps: a) before connecting the matching elements (active SST die deembedding) and b) with shunt matching elements connected. As shown in Figure 3., bonding wires are used to tune the ANCA section of the matching circuit.

ANCA and CAM device characterization was carried out over the 500 MHz - 1300 MHz frequency range. Relying on test data acquired during the above evaluation steps, single and then two stage input matching elements were added and their contribution characterized. 'On board' DC feed circuit elements were also included, and designed to provide the best pulsed mode operation characteristics.

Presently, CAMs are fabricated with the ANCAs and the matching circuits mounted inside nickel plated aluminum or OFHC copper housings, which are hermetically sealed. SMA and DC feedthrough connectors allow for RF, DC power and control signals to be fed to the amplifier (Figure 4).

SST Biasing Considerations.

As mentioned, the SST is a depletion mode JFET. When the source is DC ground and the drain is positively biased, the device requires negative gate voltage to be turned off. In order to preserve the SST performance into the 1400 MHz frequency range, the device has to be operated common-gate. Common-gate, the SST exhibits an extremely low feedback capacitance (C_{ds}), of approximately 0.1 pF/W, assuring a virtual separation between the SST input and output sections.

Figure 6 shows the SST biasing circuit used for pulsed RF operation. The circuit provides a DC pulse input and an independent adjustment of the device quiescent current. Between the RF pulses, the SST is turned off by adjusting the gate voltage to the appropriate value of V_{gs} . During the RF pulse, the NPN transistor is turned on, thus setting the gate voltage to a less negative value with respect to the source.

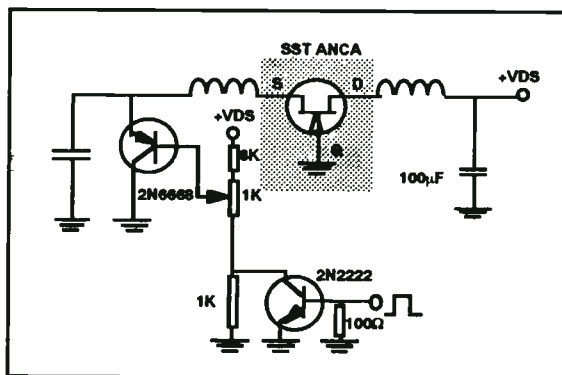


Figure 6. CAM Internal Biasing Circuit.

This circuit allows one to set the SST operating point for class A, B or C operation for the duration of the RF pulse. The same circuit can be used for CW RF operation if the NPN transistor is eliminated or kept on.

Pulsed Power Avionics Applications.

Some of the most commonly known applications in avionics equipment utilize the 800 to 1400 MHz frequency band and fall into the following categories:

- 960 to 1220 MHz - DME & JTIDS
- 1030 & 1090 MHz - IFF
- 1200 to 1400 MHz - Radar

These systems operate in a pulse modulated RF signal mode and information is carried in the pulse characteristics. Distance information is derived from signal travel time while additional information resides in the pulse coding.

DME and IFF systems basically have been operating in narrow pulse, low duty cycle modes (<10 μ s and < 10%). JTIDS requires

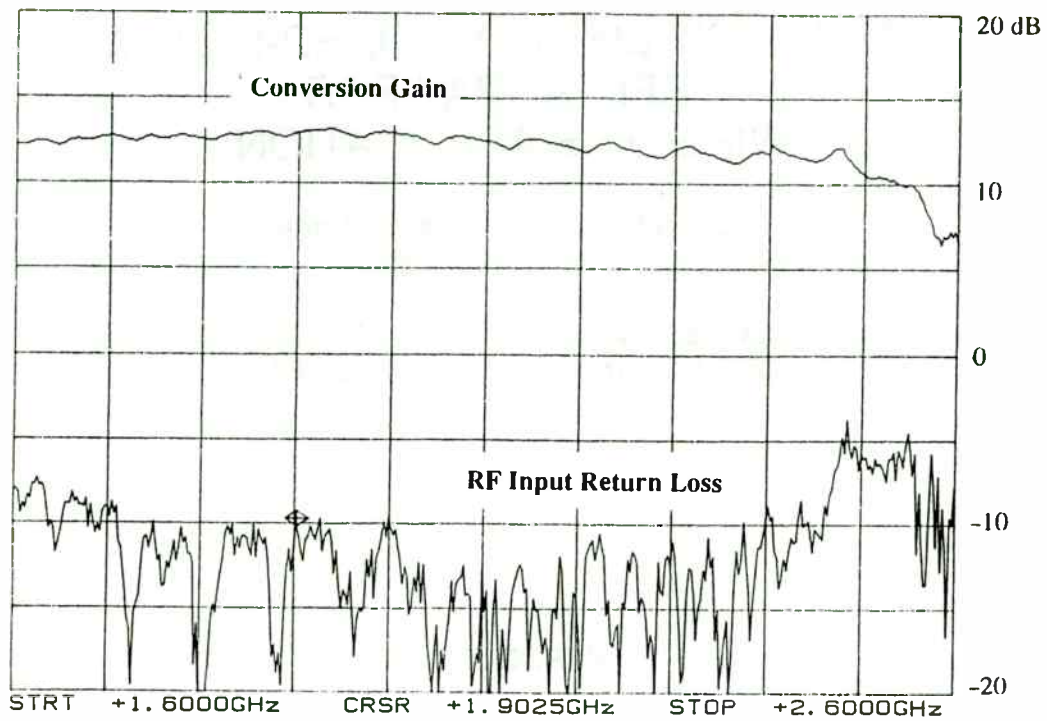


Figure 15: Conversion Gain and RF Input Return Loss vs RF Frequency

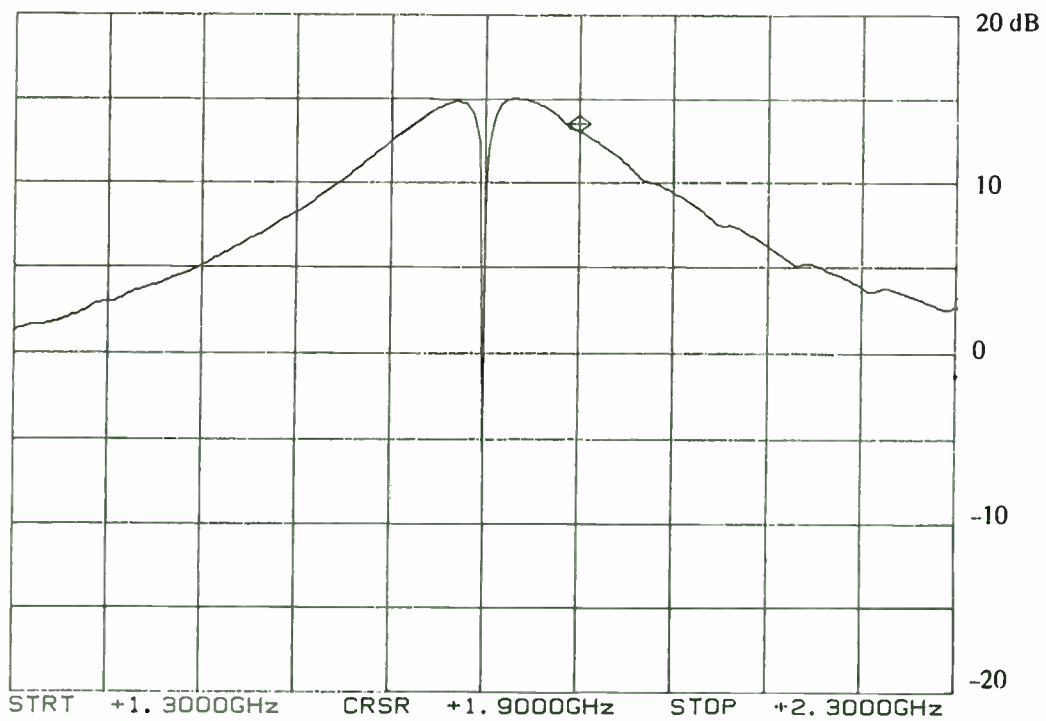


Figure 16: Conversion Gain vs RF Frequency for a fixed LO of 1800 MHz

high duty capability for some given time intervals while some of the radar systems operate with fairly long pulses.

Linear pulse envelope modulation characteristics are of primary interest for DME operation while other applications require fast rise and fall time capability. The compact amplifier modules can satisfy all of these requirements.

Experimental Performance Figures.

Most of the MwT Pulsed RF CAM work is done at the JTIDS, DME, and IFF frequency ranges. Typical experimental results are presented below. The module RF performance is evaluated using the computer controlled test setup of Figure 7. RF output power, power gain and efficiency are determined over various pulse and biasing conditions and over a wide temperature.

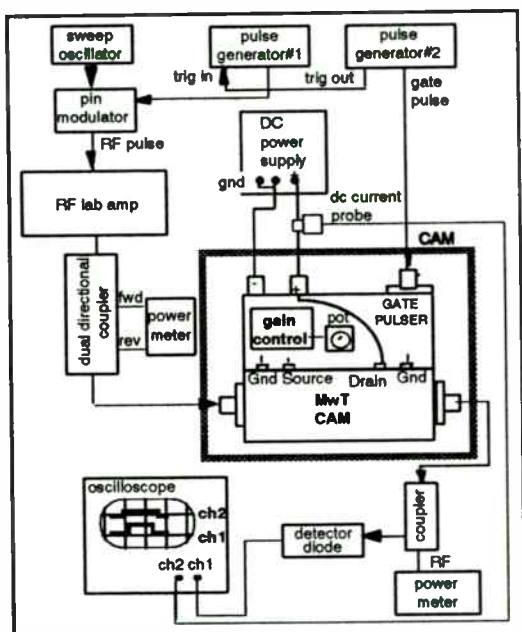


Figure 7. CAM Test Setup.

The equipment shown is linked by the GPIB bus and controlled by an IBM compatible PC. The system is capable of both pulsed and CW measurements. Pin vs. Pout at any frequency in the 500 MHz to 1300 MHz band can be measured to obtain linear gain, one-dB gain compression, and saturated power output. CAM frequency response vs. gain, Pout, return

loss, and efficiency can be quickly measured on this automated test station. All data generated can be saved in non-volatile memory for future use.

Calibration of the system is also automated. The coupling factors of the input dual-directional coupler, any insertion loss of the connectors, and the attenuation of the load are all measured vs. frequency and stored in a calibration file. This data is then used to correct the raw measurement data.

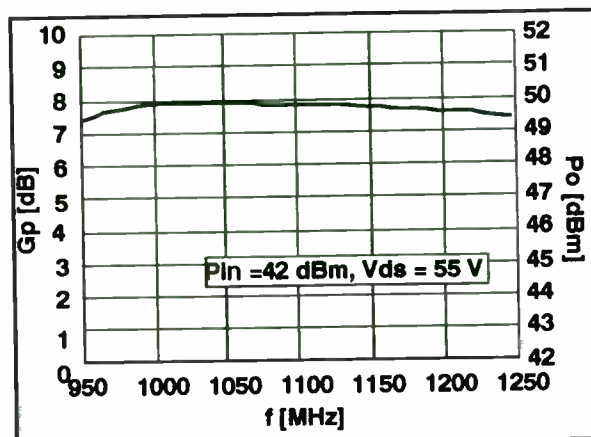


Figure 8. 100 W CAM: Gp vs. frequency.

Figure 8 shows the frequency dependence of an JTIDS CAM rated for 85 W. This CAM has a power gain of $7.5 \text{ dB} \pm 0.5 \text{ dB}$ across the 960 MHz - 1220 MHz frequency band. The output power dependence versus the input power (Figure 9) for the same CAM illustrates the wide linear power dynamic range of approximately 50 dB.

Data taken on a 65 W broadband CAM, tested over the 800 MHz through 1100 MHz frequency range (Figure 10), demonstrates a module efficiency of 40 % across the whole bandwidth. As shown, this CAM has a nearly flat power gain of 8 dB.

Typical CAM power gain vs. output power data for a 50 W CAM is plotted in Figure 11. The figure also contains input return loss data. As shown, when the input power increases and the SST moves from class A and into class AB and then B operation, the device power dissipation is reduced as efficiency increases. This change, combined with the fact that the module was designed for best

A SILICON-BIPOLAR, MIXED-SIGNAL RFIC ARRAY FOR WIRELESS APPLICATIONS

By Robert A. Koupal, Keith Carter
and Kevin J. Negus

Communications Components Division, Hewlett-Packard Co.
39201 Cherry Street, Newark, CA 94560

INTRODUCTION

Consumer markets such as the Cellular Telephone (AMPS, GSM, JDC and NADC), Global Positioning System (GPS), Cordless Telephone (DECT, CT-2 and PHP), Personal Communications Network (PCN) and Wireless LAN have passed their developmental stages and are poised for rapid expansion in the near future. All these markets require reliable, low-cost components that can be repeatably manufactured in large volumes. Early receivers and transmitters were constructed from discrete components and required significant labor costs for assembly and performance optimization. The current trend is toward lower cost, smaller size, less manual circuit tuning, lower power consumption and increased reliability through the use of Integrated Circuits which reduce component count. Several single function ICs are presently available such as low noise amplifiers, matched 50Ω gain blocks, prescalers and Gilbert cell mixers. The next step in size reduction is to incorporate these RF functions into a single, complex, multifunction, high density IC.

To address some of the varying needs of these consumer markets, Hewlett-Packard Co. has developed a mixed signal array Receiver-on-Chip (ROC) which is fabricated on a mature silicon bipolar IC process. This chip has been optimized to generate a variety of transmit/receive circuits utilizing frequency plans ranging from 800MHz to 2500MHz with supply voltages ranging from 3V to 5V. The low power consumption and small size make this an ideal technology for battery operated, hand-held applications. In today's competitive and rapidly changing market place, it is imperative that new product development cycles be minimized. Since the ROC array requires only three mask layers (metal 1, via, metal 2) for customization to a specific application, the fabrication time can be reduced from months to weeks. Furthermore, the close coupling of design and layout through parameterized standard cells greatly reduces the design time associated with complex RFICs. The chip is packaged in a low cost, industry standard 32 lead plastic quad flat pack and test costs are minimized through the use of automated test.

match at the higher power levels, induces a small increase in the voltage gain as the CAM approaches power saturation.

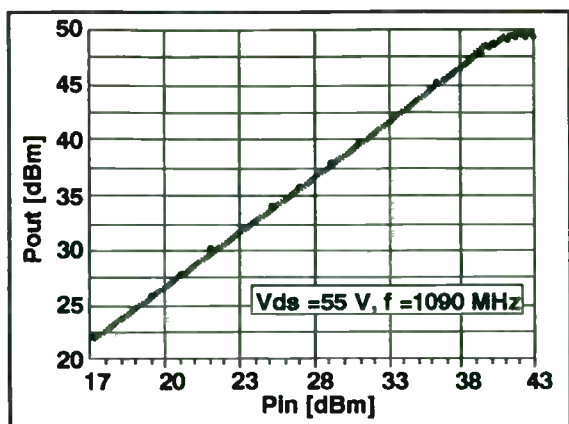


Figure 9. IFF CAM: Pout vs. Pin.

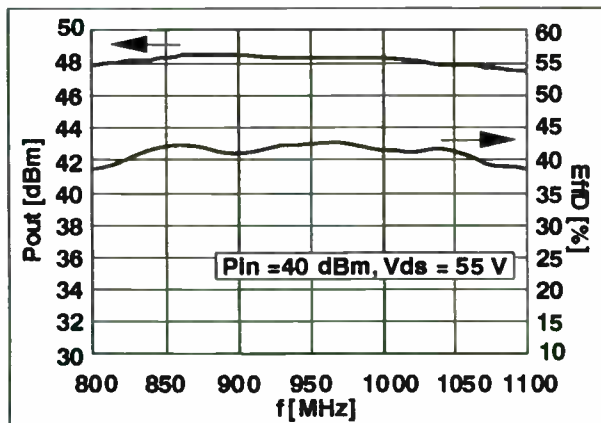


Figure 10. Roadband 65 W CAM. Pout & Eff_D vs. frequency

As mentioned previously, one of the SST CAM unique characteristics is the gain control capability. This feature is illustrated in Figure 12, where the gain/attenuation data of a 75 W CAM is plotted as a function of the SST gate DC voltage. As the 1100 MHz input RF signal is kept at a constant power level of 39 dBm, the CAM power transfer factor changes from approximately 10 dB down to -20 dB. This 30 dB change is accomplished by a 8 V swing in Vgs. Additional gain control data is shown in Figure 13, where output power is plotted as a function of Vgs at various input power levels.

The SST dynamic range of gain control illustrated here significantly exceeds bipolar transistor performance for these types of applications. State of the art BJT JTIDS pulse

power amplifiers have to rely on complicated, bulky, and expensive electronic switches to rapidly modulate the output power. The MOSFET, like the BJT, has a narrower gain control dynamic range than the SST. No

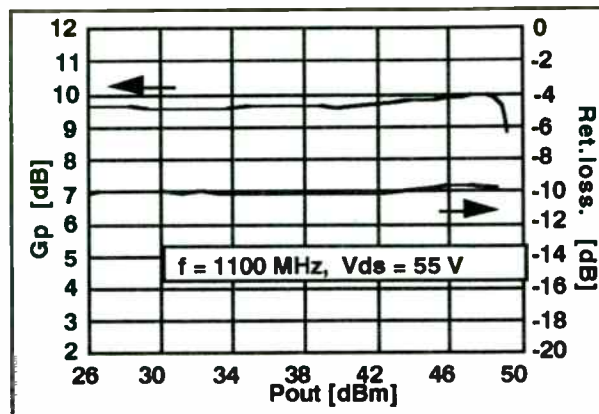


Figure 11. 50 W CAM: Gp & Input Return loss vs. Pout.

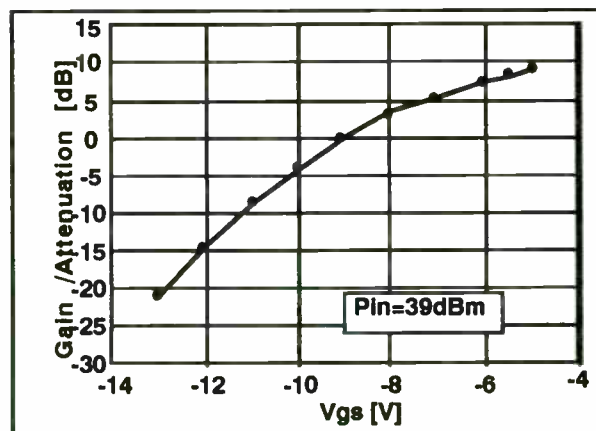


Figure 12. 75 W CAM: Power Gain/Attenuation vs. Vgs.

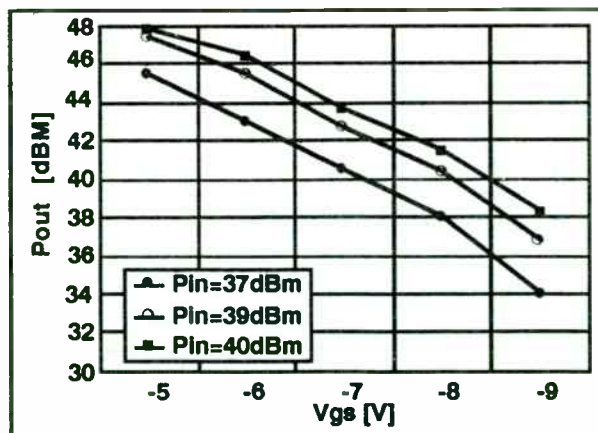


Figure 13. JTIDS CAM: Pout. vs. Vgs
f = 1050 MHz, Vds = 55 V.

ISOSAT-II PROCESS

Hewlett-Packard Co.'s ISOSAT-II silicon bipolar IC process combines the advantages of proven military grade reliability with the stable, low cost manufacturability required for high volume consumer markets. Many features in the process, such as gold metallization, can meet or exceed the rigid and exacting requirements of a military Space grade qualification. Despite this high reliability level, ISOSAT-II is focused squarely on the delivery of high volume large scale integration (LSI) density ICs for consumer products.

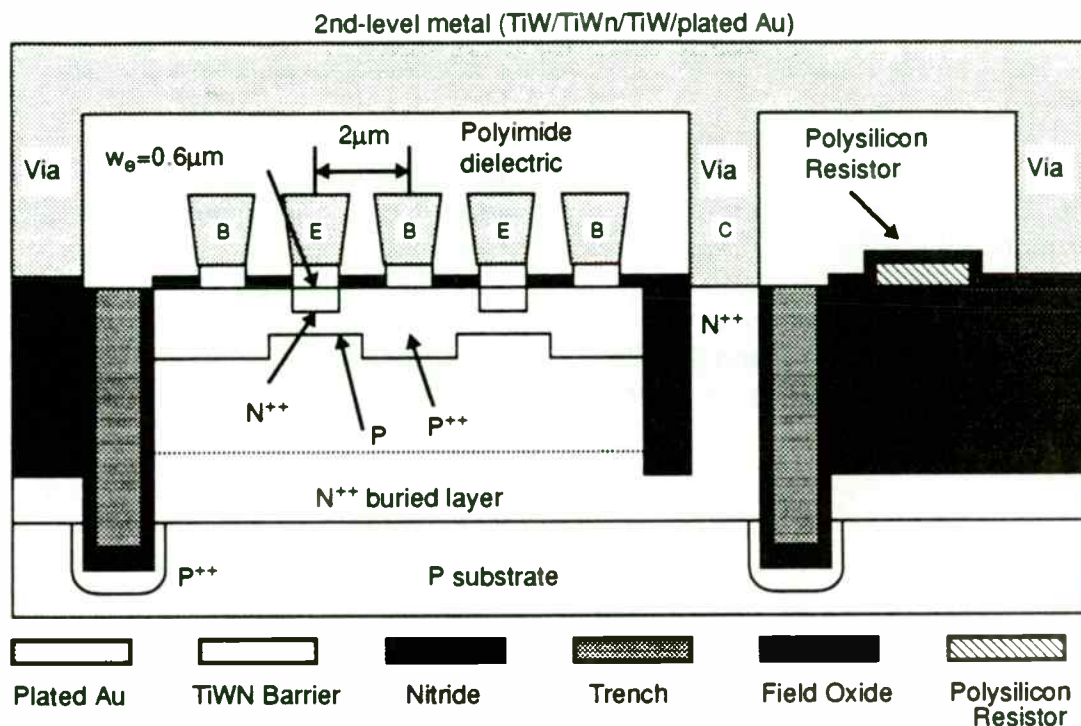


Figure 1: The ISOSAT-II silicon bipolar IC process which yields transistors with an f_T of 14GHz and an f_{max} of >20GHz

The ISOSAT-II process features an npn transistor with gold-metallized $0.6\mu\text{m}$ wide interdigitated emitters on a $2.0\mu\text{m}$ emitter to base pitch. An $8.0\mu\text{m}$ deep trench isolates the transistor from adjacent devices. These npns with $f_T = 14\text{GHz}$ and $f_{max} > 20\text{GHz}$, can easily be scaled for low power consumption or high output power drives. Undoped polysilicon resistors are deposited on a $2.0\mu\text{m}$ thick field oxide which minimizes parasitic capacitance to the substrate for resistors and metal interconnects or bondpads. The thin-film

MOSFETs are known to be commercially available for comparison in this application.

In addition to varying the V_{gs} , one can also use the SST drain voltage to modify the CAM output power. Knowing the output power dependence upon the drain voltage helps one also define the power supply regulation requirements. Figure 14 shows the output power dependence upon V_{ds} for a 200 W power CAM, tested at 800 MHz.

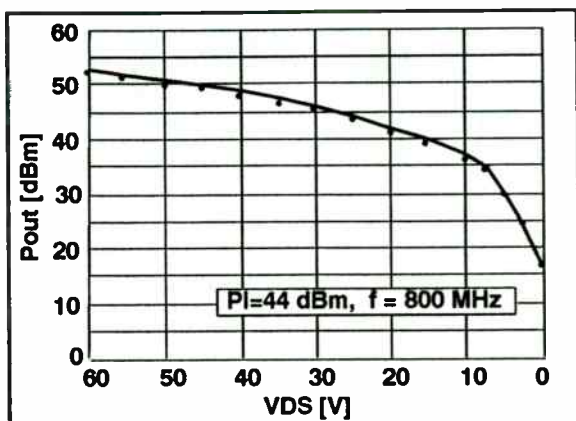


Figure 14. 100W CAM: Pout vs. Vds.

The 200 W CAM was fabricated by combining two 100 W CAMs using Wilkinson combiners. The basic CAM layout was shown in Figure 4. Figure 15 plots the output power and return loss data versus frequency for this CAM. Although the data was taken over the 700 MHz through 1200 MHz frequency range, this CAM was initially fabricated for 850 MHz - 1050 MHz operation.

Most of the CAM data illustrated so far is for modules set for class A operation. Data for a class B 100 W CAM tested at 800 MHz is shown in Figure 16. Notice the increase in efficiency as a consequence of the change in the SST operating point.

Another CAM characteristic mentioned above is the excellent pulse spectral response. A typical frequency domain pulse response for a 75 W CAM is shown in Figure 17. One can see the good symmetry of the $\sin(x)/x$ power spectrum lobes which confirms the low level of phase modulation generated by the SST during the pulse. To achieve similar results using BJTs, sophisticated pulse shaping

circuitry operating at high currents would have been required.

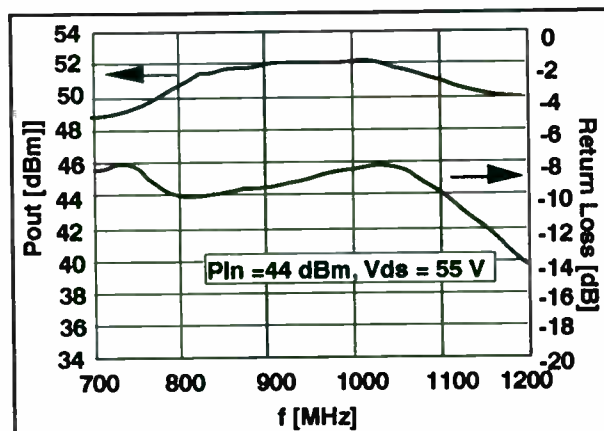


Figure 15. Wilkinson Combined Broadband 200 W CAM. Pout & Eff D vs. frequency.

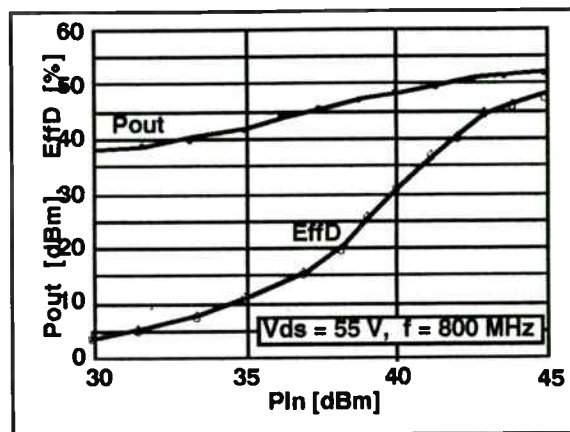


Figure 16. 100W CAM: Pout & Efficiency vs. Pin.

As a thermally stable device, the SST power capabilities show reduced sensitivity to temperature variations. Figure 18 contains peak output power data vs. the package flange temperature for an SST tested at 750 MHz and with a V_{ds} of 55 V. The power derating factor resulting from this figure is 0.01 dB/°C.

The following list illustrates the power the MWT pulsed power SST CAM capabilities:

- Frequency: 960 MHz - 1215 MHz or 1030/1090 MHz (add 0.5dB)
- Pout: 50 W, 8.5 dB
size: 1.75" x .75" x .25"

resistors are then implanted to produce either high or low sheet resistance values and a designer can select resistors ranging from a few Ohms to hundreds of kOhms. Two levels of metal interconnects are formed using gold metallization for low electromigration and a thick, low parasitic polyimide layer as the inter-metal dielectric. The combination of thick field oxide and low sheet resistance of gold metallization produces spiral inductors with performance comparable to those of GaAs processes up to 5GHz. A cross-section of the ISOSAT-II process is shown in Figure 1.

Other components such as Schottky diodes with $f_c=100\text{GHz}$, zener diodes, MIS capacitors and lateral pnp transistors allow designers additional flexibility in circuit design without adding significantly to the complexity or cost of the basic 10 mask process. Note that these diodes and the lateral pnps were not included on this mixed-signal array. The performance of passive elements in ISOSAT-II in the 800-2500MHz range is characterized by typical values of $Q>10$ for inductors up to 10nH and $Q>25$ for capacitors up to 20pF. These passive elements with high Q values and excellent repeatability allow ISOSAT-II designers to optimize circuits for significantly increased efficiencies within specific narrow bands.

Future process enhancements will include fully walled emitters and self align base contacts. The process will yield $0.4\mu\text{m}$ emitter widths with $0.8\mu\text{m}$ emitter to base pitch using conventional stepper lithography. Unlike many bipolar processes using polysilicon emitters, this process will produce completely inter-digitated devices with superior noise and power characteristics. Current development efforts are targeted toward achieving npn transistors with 30GHz f_t and 60GHz f_{max} without sacrificing the performance of passive elements or degrading the manufacturability of the current process.

ROC ARRAY

Wireless markets demand a variety of frequency plans, functionality and supply voltages. The ROC-01 mixed signal array was developed to be flexible enough to meet as many of these requirements as possible. It was originally developed for integrating receiver functions in L-band satellite systems such as GPS, GLONASS, Inmarsat and Iridium. The array can also be employed in applications such as 900MHz spread-spectrum transceivers and cellular telephones, 1900MHz European and Japanese cordless telephone systems, and 2500MHz wireless LANs. Array technology allows designers to produce chips to meet these diverse needs with relatively short development times. With the array approach, new RFIC development times are often reduced from several months to several weeks. The ROC-01 array combines high speed analog function blocks and ECL digital logic blocks to create a versatile mixed signal IC.

- Pout: 5 W, 8.5 dB
size: 1.75" x .75" x .25"
- Pout: 100 W, 8 dB
size: 1.75" x .75" x .25"
- Pout: 150 W, 7.5 dB
Wilkinson combined
size: 2.5" x 1.5" x .35"
- Pout: 200 W, 7 dB
Wilkinson combined
size: 2.5" x 1.5" x .35"

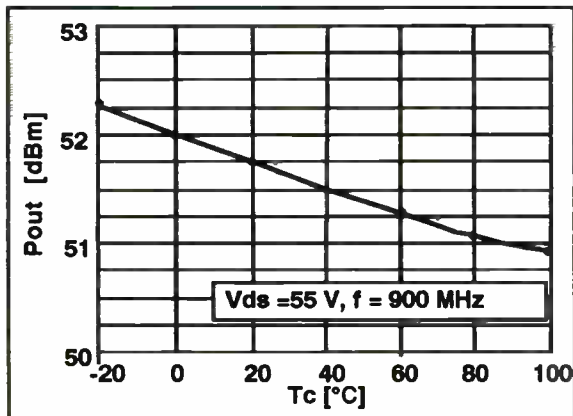


Figure 18. Power SST: Pout vs. Temperature.

Conclusions.

The development of hybrid circuits using the Solid State Triode is leading to a new capability for the designers of pulsed RF systems operating in the 800 to 1300 MHz region. Using Compact Amplifier Modules power amplifiers can be reduced in size and complexity. The internally matched CAMs can be easily combined to achieve almost any practical power level. The need for pulse conditioning and the use of special high power attenuators for power control can be eliminated saving precious real-estate in airborne and mobile systems.

Development of the SST CAM is continuing. Improved geometry SST chips and other biasing approaches will result in higher power and improved efficiency. New processing technology will increase the device cut-off frequency boasting the gain at lower

frequencies and extending practical operation to near 2 GHz, further expanding the applications for the CAMs in radar, while CW operation at power levels of 10 W to 25 W can be applied to wireless digital communications systems.

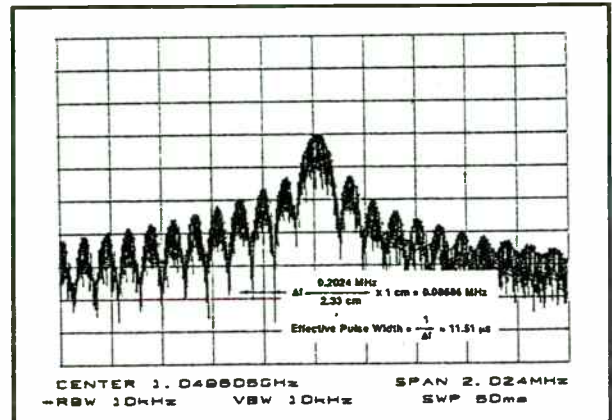


Figure 17. RF Pulse Spectral Response.

Acknowledgements.

The SST and CAM work was supported in part by the Naval Air Warfare Center, Warminster, PA and by the Wright Laboratory, Dayton, OH.

The authors also acknowledge the critical contribution made at MwT by N. Thornton and P. Pacada, and the support and guidance provided by M. Omori.

Bibliography

- A. Cogan, "SST for Microwave Applications", RF Expo East Proceedings, October 1989, Atlantic City, NJ.
- S. McIntyre, "Demystifying New Generation Silicon Power FETs.", Microwave Journal, April, 1984.
- H.O. Grandberg, "Building Push-Pull Multioctave VHF Power Amplifiers.", Microwaves & RF, Nov., 1987.
- M. Abdollahian et. al. "Design and Performance of a Broad-band, High Voltage SIT Power Amplifier." RF Expo, East. Oct. 1991, Orlando, FL.

Cell Type	# on Chip	Max.Freq	Comments
LNA	1	2GHz	900 and 1600 MHz versions
RFAMP	1	2.5GHz	Reduces noise figure of mixers
MIXER	3	4GHz	Upconverter to 2 GHz
IFAMP	4	3GHz	Interfaces to 50-1000 Ω
VAR GAIN AMP	1	2GHz	30dB gain control range
OSCILLATOR	2	4GHz	Uses external resonator
DIG LOGIC	39	4GHz	Standard differential ECL gates
CMOS/TTL IN	4	500MHz	Can be AC-coupled
CMOS/TTL OUT	4	200MHz	Can drive 10pF at 50MHz
BANDGAP REF	5	N/A	Temp. comp. options for flat gain/current

Table 1: Major Parameterized-cells available on the ROC-01 array

The array is 1.8mm x 1.8mm (72mil x 72 mil) and has 32 bond pads. Within the body of the array are many parameterized layout cells placed in predetermined locations. Cells include mixers and amplifiers sufficient to produce three down or upconversion stages. Also included are various RF and IF amplifiers, bandgap voltage references, about 40 digital logic and buffer cells, and a negative resistance cell for creating an oscillator (see Figure 2 and Table 1).

CELL PARAMETERIZATION EXAMPLE

Parameterization of schematic and layout cells allows the designer to tailor the performance of the cell in fixed increments to trade off speed for power consumption in a digital cell or gain, linearity and noise figure versus power consumption in an analog cell. By merely changing the layout cell's parameter value, the wiring internal to the cell is automatically redrawn giving the mask designer a powerful tool for quickly creating a customized LSI layout. A corresponding parameter on the schematic cell multiplies resistors within the schematic by fixed increments to generate a new subcircuit for simulation. Figure 3 illustrates a parameterized mixer cell for the ROC-01 array in three different views. The designer usually interacts with the symbolic representation where discrete changes in the cell parameters are made by editing a list within the CAE system. These parameter changes then automatically update the schematic using the rules shown in the schematic view of Figure 3. Within the same CAE system the layout representation of the mixer cell is also automatically re-generated by the same list of parameters to ensure complete

FREQUENCY SYNTHESIZER STRATEGIES FOR WIRELESS

Bar-Giora Goldberg, MSEE
Henry Eisenson
Sciteq Electronics, Inc.

PURPOSE

This presentation illustrated some of the challenges posed by emerging wireless/PCN/PCS industries (hereafter "wireless"), particularly as they apply to a key subsystem: the frequency synthesizer. Wireless creates a spectrum of opportunity and technical challenge, as well as risk, and since the frequency synthesizer is one of the most difficult developments in any analog system this document will seek to present some potential strategies for meeting those requirements.

Optimistically, the authors have written to two audiences. The first includes design and system engineers, who may be very competent at designing the RF systems of five years ago but with the advent of wireless are encountering new arrays of challenges based on economic, production engineering, and performance factors. The second target audience includes program managers and company executives, who may have limited technical knowledge yet must listen to the engineer's explanations as to why the strategies of yesterday simply don't work in this new technical and marketing environment.

DEFINITIONS

One of the problems facing many designers of systems and subsystems for the wireless businesses is a lack of structure. Operating bands, modulation schemes, protocols, power limitations, and – surprisingly – even applications, are all poorly defined. Firms developing systems and making investments in this new market, and particularly those who are aggressively working to establish a position early in the evolution of the industry, are very much at risk because of the lack of structure, protocols, spectrum allocations, and – of course – definitions. It is beyond the scope of this paper to attempt to generate such a set of data, however, so this statement is presented only as a warning to those investing money and engineering, and a plea to those involved in the establishment and standardization of protocols and definitions.

Regarding frequency synthesizers, for the purpose of this document historical definitions apply. Though they will not be listed in this paper, they correspond with those appearing in many publications.

INTRODUCTION

Radio systems are tuned by generating a frequency reference, and the quality of that reference determines the performance of the radio circuit. Accuracy is critical; both transmitters and receivers must be at the same frequency for communication to occur. When the energy of the signal appears only at the desired frequency, phase noise is considered perfect, and as that energy spreads to nearby frequency, phase noise is described as less perfect. A good reference generates no discrete uncommanded signals (spurs). Together, accuracy, phase noise and spurious signals define the performance of a reference.

By far, the best way to tune a radio or any RF system is with a crystal, and when multiple frequencies are necessary, multiple crystals and a switch can be used. Eventually, however, it becomes first impractical and then impossible to use complex arrays of crystals, as shown in Figure 1.

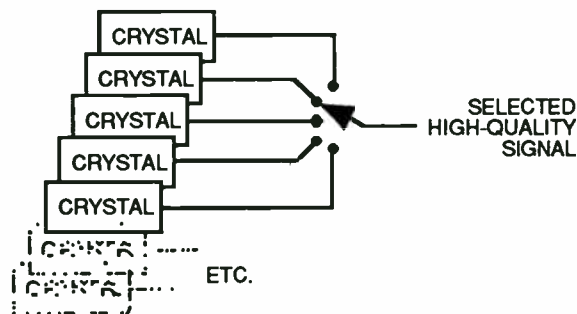


Figure 1

A "frequency synthesizer" is a device or circuit that synthesizes a new frequency based upon an original one (reference), retaining the stability, accuracy, and spectral purity of the reference though at a new point in the spectrum. It can generate one frequency (beyond that of the crystal reference) or multiple frequencies, as selected by a control mechanism (Figure 2).

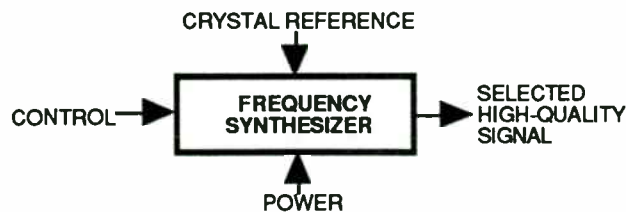


Figure 2

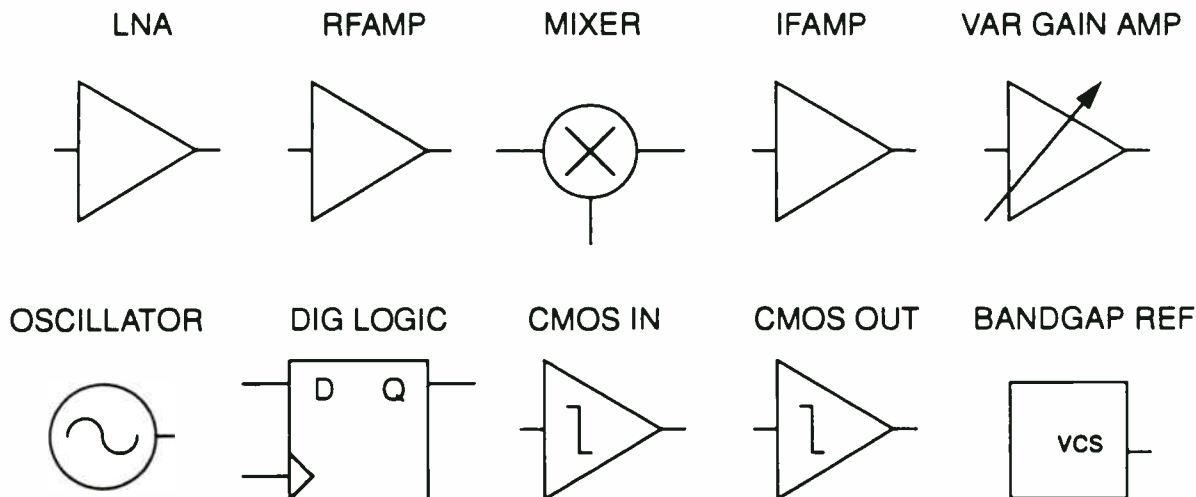


Figure 2: Cell types available on the ROC-01 Array

correspondence between design and layout. This ROC array design methodology is currently based on the Cadence Analog Artist software with significant extensions and modifications developed by Hewlett-Packard, Co. design engineers.

Table 2 summarizes a simple simulation example to illustrate the diversity of choices available within a given parameterized cell on the array. In this case the mixer cell of Figure 3 is simulated for different values of CS,LR,ER and EF with SE=1 (forces single-ended output and removes bias on unused output) and CR=0 (removes low-pass filtering capacitor completely). All simulations are performed with -10dBm of LO input power at VCC=5V and T=25°C. The RF, LO and IF ports are all resistively (wideband) matched to 50Ω. Different input/output impedances have also been used to advantage in ROC array designs. The supply current results in Table 2 include an LO buffer cell from the ROC array which is used to drive the LO quad of the Gilbert cell mixer.

The first case in Table 2 shows the cell as might be used for a handheld satellite receiver downconverter with emphasis on low current and high conversion gain. In the second and third rows of Table 2, a more "general-purpose" downconverter arrangement is compared for operation in both the 900 and 2500 MHz spread-spectrum bands. The additional supply current for the 2500MHz case is used for more LO drive. Note that for downconverters with very low IF frequencies (especially second downconverters), the parameter CR is often set to 100-400 so that the undesired RF+LO product is low-pass filtered to significantly improve the linearity of the output stage. The final row of Table 2 illustrates an upconverter realized with the same ROC array parameterized cell. In this

Like shoreline, spectrum is limited and precious, and the synthesizer (among other factors) determines how efficiently spectrum is used and how many channels can be compressed into any given operating band. Frequency synthesis is always a challenge, and the characteristics of the synthesizer have long defined the performance of the system that employs it.

Though there are as many synthesizer designs as there are designers, only three synthesizer techniques can be described as fundamental; all others are variations or combinations of one or more of them.

DIRECT-ANALOG

This (mix/filter/divide) is the oldest frequency synthesis method. The first time an engineer amplified a reference sufficiently to saturate a diode and used a filter to pick out a new frequency derived from the original, direct-analog was born. Today, many direct-analog techniques exist for multiplying, dividing, adding and subtracting an array of references, all locked to a common reference, to produce new frequencies.

This process supports very high spectral purity, since there is no correction circuit's "seeking" (that corrupts phase noise in a PLL), and careful planning can achieve frequency manipulation that avoids spurious signals. An important advantage of this technique is fast switching. The major drawback of direct-analog is the cost of the array of references required to cover the desired frequency range, plus the cost of one echelon of mix/filter/divide circuitry for each decade of resolution (step size) required.

Nevertheless, the finest synthesizer performance achieved by the industry employs direct-analog techniques, and appears in the Comstron FS-5000. Expensive, but there is no better method for generating a fast-switching, high spectral purity, broad bandwidth signal. Obviously, while this may be interesting to the designer of a simulator or radar system, the direct-analog approach is of little interest to a designer of wireless systems.

DDS

In one sense, the only true "synthesizer" is a DIRECT-DIGITAL SYNTHESIZER (DDS), since it literally constructs the waveform from the ground up (synthesizes the frequency) rather than combining or controlling existing oscillators.

A "vanilla" DDS appears in Figure 3, which also shows the signals generated by each circuit element.

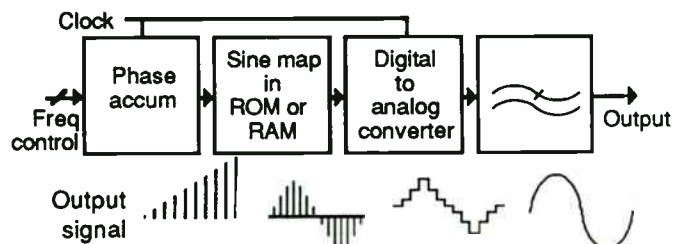


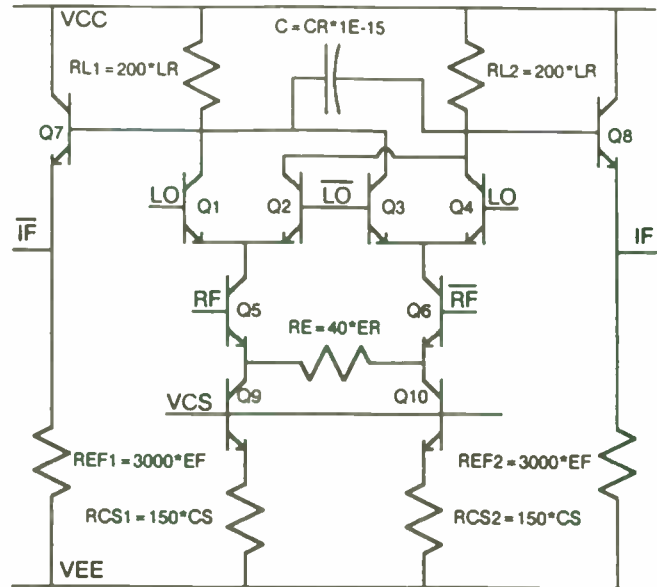
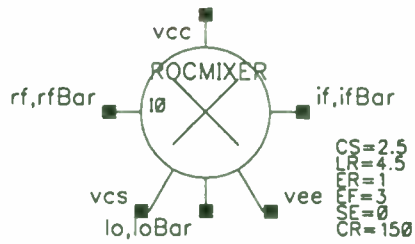
Figure 3

Though each of the blocks can be broken into many smaller ones (even down to the transistor level), the arrangement shown permits understanding of the means by which a DDS constructs a waveform.

The PHASE ACCUMULATOR correlates the clock with a control word, defining a "ramp" from 0° to 360° within some time period, and therefore the output frequency. A MEMORY maps the phase data in that ramp to a series of digital amplitude words, and a digital-to-analog converter DAC converts those digital data to an analog sinusoid (or any waveform stored in memory). That process must comply with sampled data rules, and therefore any frequency to be produced must be sampled *at least* twice each 360° (cycle), and the highest frequency that can be digitally generated is exactly one half the clock rate – though filter realities make the available output closer to 45%.

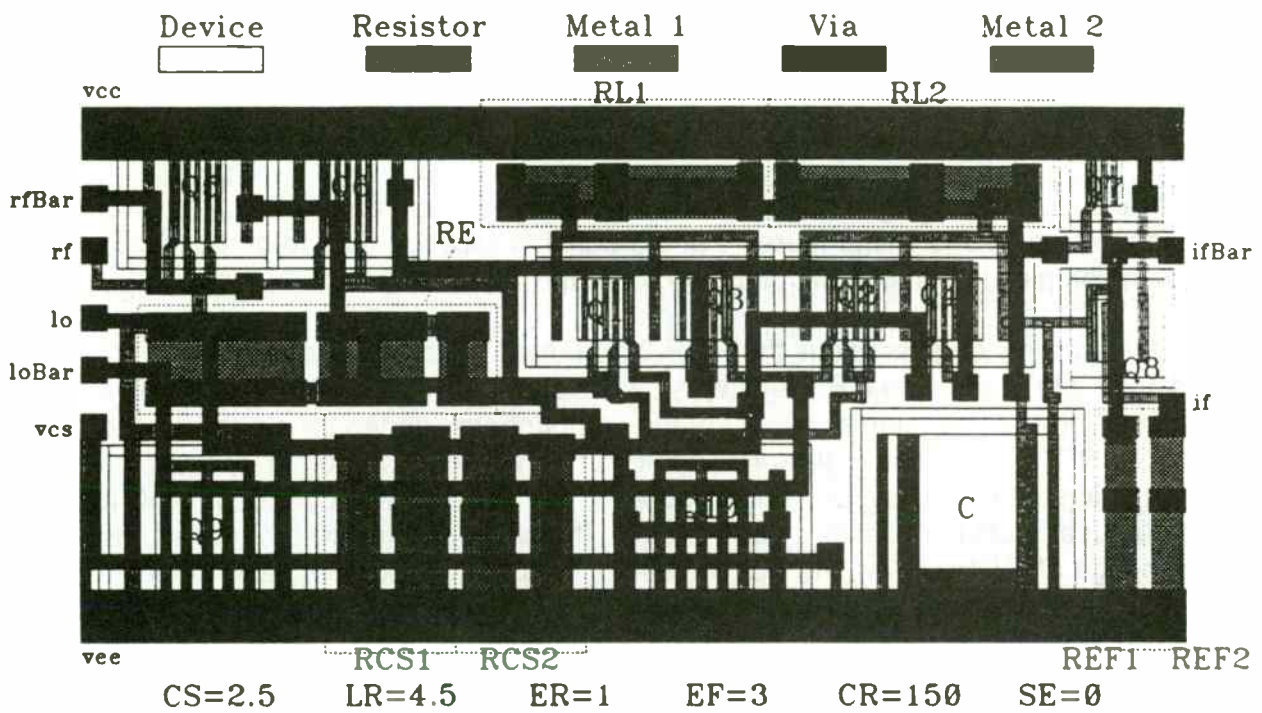
The DDS is also a supreme modulator. Digital shifting of frequency supports FM and toggling between two frequencies supports MSK/FSK; in fact, the DDS is a theoretically perfect FSK modulator. By placing an adder between the accumulator and the memory, the output can be shifted in time (phase), and a multiplier between the memory and the DAC permits scaling of the output, and therefore amplitude control. Both phase and amplitude modulation is therefore possible with a DDS, and with digital precision not possible with analog circuitry. Finally, SSB implemented using DDSs approaches theoretical perfection.

The advantages of the DDS include inexpensive high resolution (fine step size), fast switching speed, excellent phase noise, and while the signal is in the digital domain it can be manipulated/modulated with exceptional accuracy. The disadvantages include the fundamental limit of bandwidth (maximum frequency output is less than one half the clock rate, and logic has limits), and discrete spurious signals at a higher level than with other techniques. Nevertheless, in only twenty years the DDS has grown from an engineering novelty to a serious design tool. There are many DDS products on the market today, and they're generally divided into two categories



(a) Symbolic Level

(b) Schematic Level



(c) Layout Level

Figure 3: Three views of a parameterized cell showing corresponding parameters of the symbol, schematic and layout views.

based upon a combination of price and performance. The "commodity DDS," typically in CMOS and from Analog Devices, Harris, Qualcomm, and Stanford Telecommunications, is characterized by low price, performance that is most often exploited as part of a much more complex synthesizer, and a high level of integration. Such DDS products often offer waveform manipulation capabilities, modulation, and other features sought by the wireless designer, but do not operate in the frequency ranges of most wireless systems.

High performance DDS products are often executed using very fast silicon or gallium arsenide logic so they can be clocked at a much higher rate than the commodity-level products. These DDS products cover a band much broader than that of the commodity DDSs. Expanded bandwidth requires higher clock rates, and therefore faster logic and more critical manufacturing and testing processes, hence higher prices. Even the fastest of the high performance DDSs operate only at about 400MHz, and that plus their relatively higher prices make the DDS unsuited to the needs of wireless systems.

While there are many specifications and architectures that differentiate one DDS from another, in general, a DDS can be characterized by a combination of bandwidth and spurious signals. By that simple standard, the state of today's DDS art will not meet the needs of wireless. The DDS should not be ignored by the wireless system designer, however, because as will be seen there are techniques by which the performance of the DDS can be translated to the frequency ranges of interest.

PLL

The PHASE LOCKED LOOP (PLL) is the single most commonly used synthesis technique, and is unquestionably the most flexible and adaptable. Perhaps more than ninety-nine percent of all synthesizers use one variant or another of the PLL. It appears in countless automobile radios and television sets, yet variants of the same architecture are used in exotic satellite transponders.



Figure 4

In Figure 4, a free-running oscillator generates a signal, the frequency of which varies (drifts) over time, according to circuit anomalies, temperature, etc.

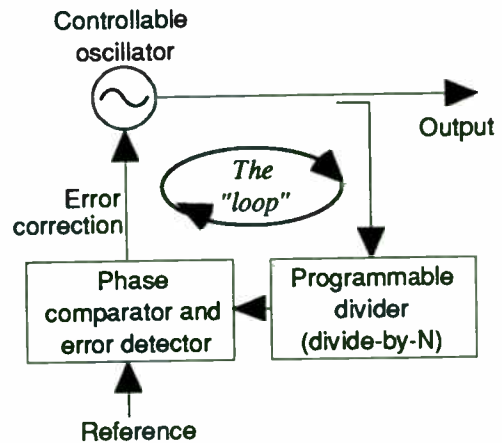


Figure 5

Figure 5 adds feedback and a phase detector, a correction mechanism that completes a loop to lock the output to some reference (thus "phase locked loop" or PLL), in accordance with some numeric ratio set by the frequency control command.

The PLL does not synthesize a waveform; rather, it controls the oscillator to the desired output frequency by dividing the output of the oscillator by some number, and then comparing the result with a reference. When errors are detected, they produce correction signals that return the oscillator to the correct operating frequency. For that reason, the system is always "seeking perfection," and the effectiveness of that seeking process determines the performance of the synthesizer. As that seeking occurs, the greater the deviation from the commanded frequency the worse the purity of the output signal. Such deviations are called "phase noise."

The advantages of PLL are low cost and excellent spurious suppression. The major disadvantage is that *both* fine steps *and* good phase noise can be achieved only in expensive implementations. In fact, the primary deficiency of PLL is that inverse relationship between step size and phase noise, because as step size decreases, division ratios in the system must increase, and the higher the division ratio the worse the phase noise within the loop bandwidth (close to the carrier). There is another drawback to PLL: switching speed. While the direct approach (DDS and direct analog) can be very fast, the PLL is slow because there is a certain electrical inertia involved before the system settles at a new frequency. The finer the required steps (the higher the division ratio) the longer it takes a typical PLL design to reach a new commanded frequency.

CS	LR	ER	EF	I _{cc} (mA)	P _{1dB} (dBm)	Gain (dB)	Test Conditions
4.5	6	0	1.5	2.8	-17	10.5	RF=1575MHz, LO=1400MHz
2.5	3.5	2.5	0.4	6.9	-8	3.2	RF=2450MHz, LO=2200MHz
2.5	3.5	2.5	0.4	6.4	-7	6.5	RF=900MHz, LO=1000MHz
1	1	2.5	.25	12.4	-9	-3.5	RF=100MHz, LO=1000MHz

Table 2: Parameterized cell example demonstrating the changes in the performance of a Gilbert cell mixer as parameter values are varied.

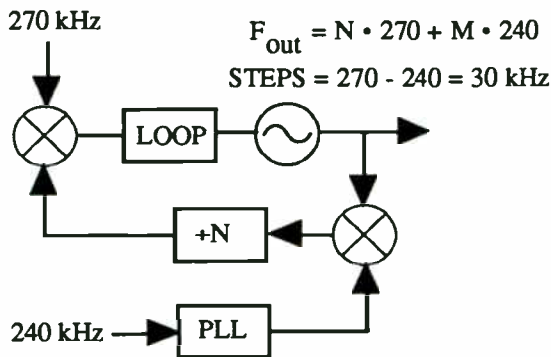
case the conversion gain is not very meaningful and in most cases, a higher impedance low frequency RF input would be preferable. The P_{1dB} of Table 2 in this case is for each of the two LO-RF and LO+RF output tones generated by the upconverter.

ROC ARRAY EXAMPLES

Several successful designs have already been implemented on the ROC array. Two design examples shown in Figures 4 and 5 will be discussed here to demonstrate the level of complexity that can be integrated onto the array.

The first application example is the RGP-03 product which has successfully been designed into production GPS receivers by Navstar, Ltd. This design incorporates two stages of downconversion and most of the components needed for a phase-locked loop onto the ROC array. (see Figure 4). The first LNA, which is the dominant component in determining the overall system noise figure, is intentionally left external to the IC to allow the end user maximum flexibility and choice. The chip operates off a nominal power supply voltage of 5V. However, through the use of temperature compensated bandgap references, the power supply can vary from 4.5V to 5.5V over a temperature range of -50°C to +100°C with little variation in overall gain (see Figure 6). An excellent correlation between measured and simulated results is also observed. Both down converters consist of an input amplifier followed by a Gilbert cell mixer with an emitter follower output. The two converters are separately optimized using the parameters discussed in the previous section to provide low noise and reasonable linearity to the first stage and high gain for minimum current in the second stage. Both converters are nominally matched at the input and output to 50Ω. The first stage provides 15dB of conversion gain with a 13dB noise figure. Isolation between ports is very good with an LO to IF leakage of typically less than -50dBm. An on-chip negative-resistance cell is combined with an external varactor/resonator to generate the first LO frequency of 1280MHz. That LO signal is then

Phase noise can be reduced by using two PLLs wherein a primary loop generates the required operating band but in coarse frequency steps, therefore with low division ratios and acceptable phase noise. A second loop, also doing coarse steps, is combined with the first to generate fine steps (a difference). See Figure 6.



TYPICAL TWO-LOOP SYNTHESIZER

Figure 6

Switching speed can be improved by generating a tuning signal to the VCO early in the change process. That's usually done by generating a digital change word, and converting it to an analog voltage applied to pre-tune the VCO. This approach can increase speed, but it also increases circuitry, cost, power dissipation, etc.

Another approach is to simply use two PLLs, with a switch to select between them. Assuming only that the system "knows" the next frequency, it can tune PLL-2 to that frequency while PLL-1 dwells at the prior frequency. When the time comes to change, a digital command switches to PLL-2. This obviously requires two PLLs, with twice the power, etc.

As can be seen, the PLL is a very useful technique, but a conventional single PLL cannot achieve aggressive combinations of fine steps, fast switching, and good phase noise.

COMBINATION DESIGNS

Many systems combine two or more of the basic techniques, and this approach is constantly being explored for wireless applications. To cover a limited band in fine steps, above the range of a DDS, the output of a DDS can be mixed with an LO and a filter used to select the desired sideband. In direct-analog systems, a PLL might be used to generate some of the required references. PLLs are often successfully combined with DDS to achieve fine

frequency steps with reasonable phase noise. Ever more inventive combination designs appear every year, and some include elements of all three building blocks: PLL, DDS, and direct analog.

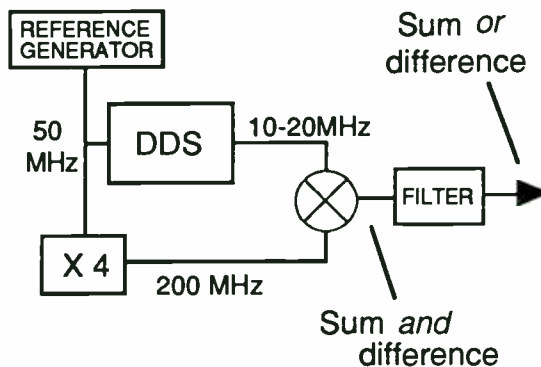
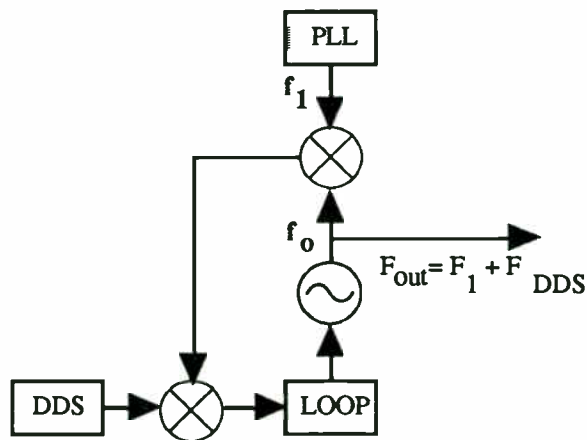


Figure 7

When a system concept dictates operation over a relatively narrow band but at a higher center frequency, a DDS can be upconverted to that range so as to exploit the DDS' fine steps, modulation capabilities, and fast switching. An example of such an architecture appears in Figure 7. In the example shown, 10 MHz of the DDS' output is translated or upconverted to the 200 MHz range. Obviously, the same architecture can be used to achieve a wide variety of goals, limited by DDS bandwidth and the physics of the filter.

It is sometimes useful to upconvert the DDS with a PLL, and, again, there are many ways to accomplish this. One mechanism (developed in 1984) uses a DDS as a reference to the phase detector of the PLL, though multiplication seriously degrades spurious performance.



TYPICAL DDS+PLL SYNTHESIZER

Figure 8

Another (also from that period) uses a DDS, a PLL, plus a combining loop. A typical DDS+PLL

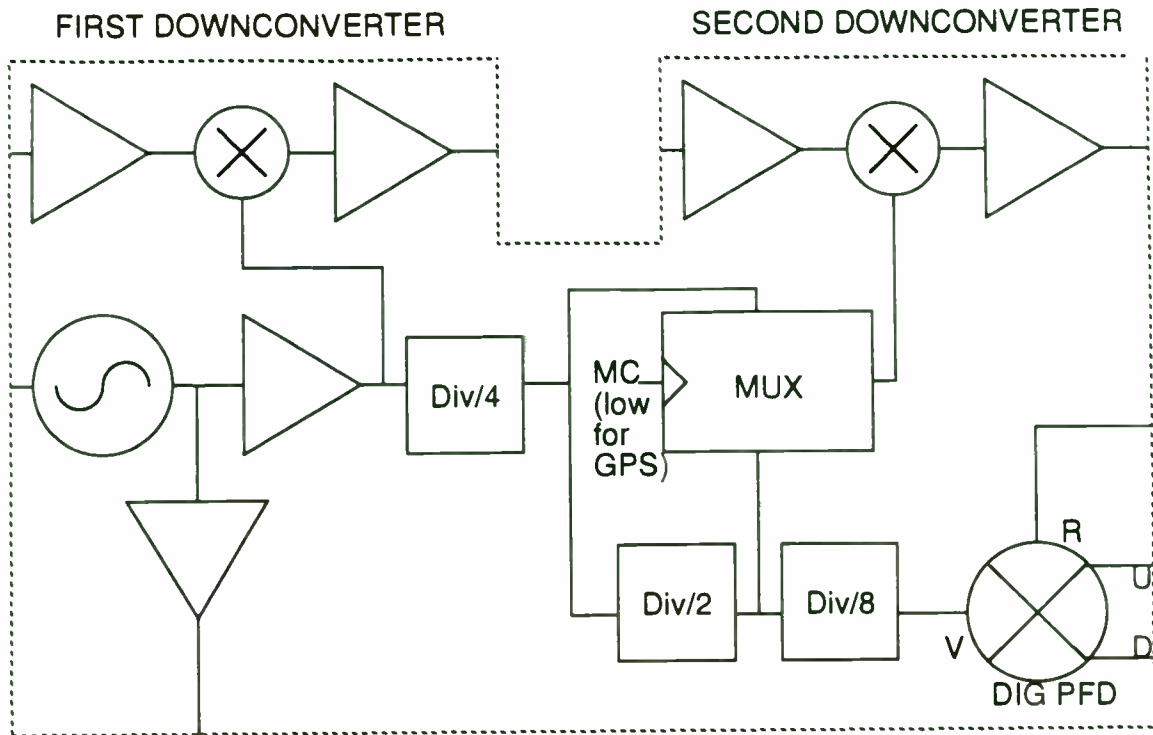


FIGURE 4: Block diagram of the RGP-03 GPS receiver IC with dual downconversion.

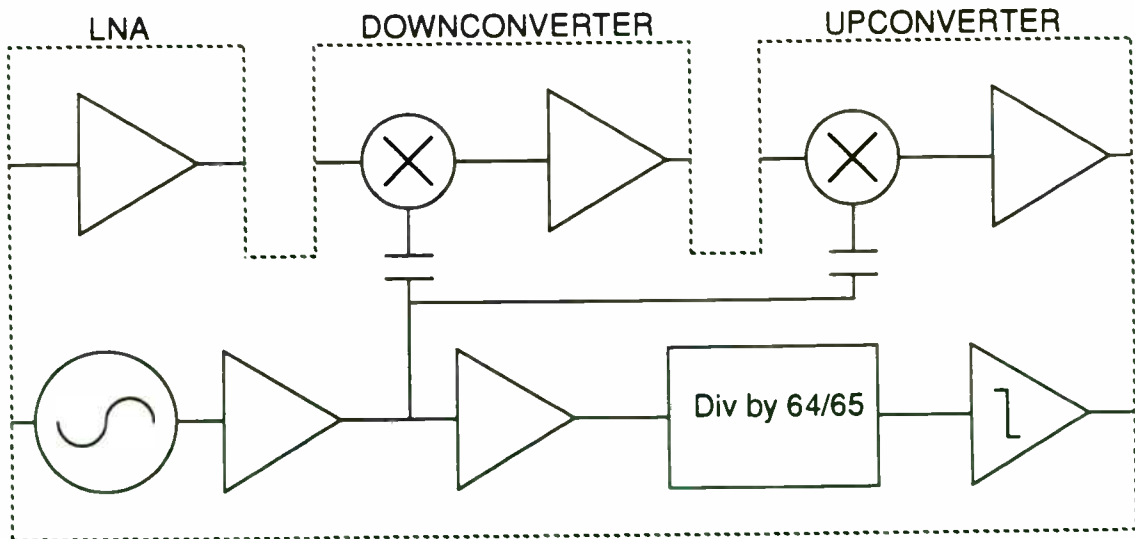


FIGURE 5: Block diagram of an R&D prototype 900MHz transceiver IC.

approach is shown in Figure 8. These techniques are useful, but involve cost and power compromises.

There are other interesting PLL mechanisms, which will be discussed as the needs of the emerging wireless market are analyzed.

GENERAL REQUIREMENTS OF WIRELESS SYSTEMS

The wireless industry will be filled with cell or base stations, of which each interacts wirelessly with dozens, hundreds, or even thousands of portable stations. The consumer purchases the wireless portable but the price of the cell/base radio is usually buried in service charges by the network owner. Also, because power, cost, and size are less important in immobile cell/base radios, this paper addresses only the requirements of portable systems.

It also considers only frequency-agile systems. The synthesizer for a typical wireless system (for instance a TDMA-based wireless PBX) will operate near 900 MHz with steps under 50 kHz, spectral purity that supports digital modulation, and power dissipation that ensures reasonable battery life. CDMA-based designs can trade frequency agility for complex coding circuitry, but TDMA, N-AMPS, AMPS, GSM, and most other cellular/PCS/PCN wireless systems require channel selection, hence agility.

Throughout wireless, once the basic function is accomplished price becomes paramount. Few engineers are experienced in designing products for the volumes involved in the wireless market. When millions of units will be made, savings of a few cents on each can have a profound effect upon the profitability of the enterprise. There is a spectrum of companies addressing every emerging opportunity in wireless, hence competition is fierce and will only grow tougher as the industry evolves. The relationship between price and performance, therefore, determines corporate success and failure.

Required performance is established by marketers who determine what the end user needs and wants, and what limits are acceptable. Once that information is collected and integrated, it is the engineer's task to achieve that performance at the lowest possible price. The most general assumption is that parts count will affect price, particularly when assembly effort is considered, and therefore the simplest (or more highly integrated) product will probably be lowest in cost and most competitive.

In wireless, reliability and durability are only barely behind price in relative importance. Historically, our industry has defined quality as either "military" or "commercial," and the assumption was that "military quality" produced the highest reliability. There are two reasons why production methodologies that define "military" quality won't work for wireless. Military quality standards require training programs, a wall full of diplomas, constant inspections, intensive testing, and reams of documentation. Like the ubiquitous pager, wireless products are measured only by the simplest standard of all; they must work nearly forever.

Generally, in the electronics industry, parts count and reliability are inversely related, and the more parts the more opportunities for manufacturing defects, so the simplest (or more highly integrated) product will be the most reliable.

Size is an issue because wireless system developers are driven toward exceptional portability, and small size always complicates RF/analog design problems, involves higher levels of integration, and generally raises the cost of engineering the final product.

Some system architects have described requirements that include rapid settling. GSM (the European standard), for instance, establishes timing standards that dictate a fast switching solution. Designers of PBX and security systems have also asked for fast switching. A generic wireless synthesizer solution must, therefore, include the ability to switch at rapid rates. By extension, that seems to demand either multiple synthesizers with a selector and supporting software, or some implementation of a direct design.

"Wireless" implies exactly that, so not only is the communication by radio rather than coaxial cable, there are no extension cords and portable elements of the system run on batteries. Power consumption determines battery life, and one of the major engineering challenges of the wireless industry is efficiency of power utilization.

Marketing defines the needs of the end user and ensures that the product will have salable competitive advantages. The engineering group must develop a product that first attains those goals, but also costs little to make and works forever.

The needs of the wireless industry, in general, can best be met by simple, highly integrated, physically small, low-power designs. That is true in general, and it is especially valid for the frequency synthesizer engine that drives the system.

divided to provide the second LO of 320MHz. The second LO is further divided to 20MHz as an input to a digital phase frequency detector which provides a differential offset voltage to an external loop filter which is proportional to the amount of phase offset (see transfer curve in Figure 7). Key characteristics of the RGP-03 are summarized in Table 3. Note also that the second LO drive can be user configured to either 1/4 or 1/8 of the first LO as shown in Figure 4. This RFIC is not narrow-band tuned and with some creativity in frequency planning, it can be used for many applications within the 800-2500MHz range.

Another design which has been successfully prototyped is a 900MHz spread spectrum transceiver IC. The downconverter of Figure 5 used a 10nH on-chip ISOSAT-II inductor to improve the noise performance at 900MHz by 4dB for a given current draw and linearity. The upconverter had a P_{1dB} of nearly 0dBm per tone at 900MHz with broadband output matching straight into 50Ω. The input impedance of the upconverter is intentionally high to allow operation as a BPSK modulator. The divide by 64/65 prescaler provided a TTL compatible output for input frequencies up to approximately 1.6 GHz.

Parameter	Measured Value
First Stage Conversion Gain (RF to IF1)	15 dB
Second Stage Conversion Gain (IF1 to IF2)	33 dB
Noise Figure of First Downconverter	13 dB
Third-Order Intercept Point of First Downconverter	+5 dBm
VSWR (in band) of all RF and IF Ports	< 2:1
Phase Frequency Detector Output	.2 V/rad
LO Leakage at IF1 Output	-50 dBm
LO/4 Leakage at IF1 Output	-70 dBm
LO/64 Leakage at IF2 Output	-60 dBm
Supply Current at Vcc=5V	60 mA

Table 3: Measured performance of the packaged RGP-03 GPS receiver IC for RF=1575MHz, LO=1280MHz and 50Ω impedances on all RF and IF ports.

FREQUENCY SYNTHESIS FOR WIRELESS

The frequency synthesizer subsystem of a wireless product does exactly the same job as a synthesizer does for any RF system. It is the system's tuning mechanism, and its performance determines the product's compliance with many marketing-driven requirements. Channel spacing determines step size, and in a PLL that establishes a mathematical relationship between operating band and division ratios that also dictates phase noise performance. Spurious signals can fool the system, lack of reliability can kill it, and excess cost makes everything else insignificant. This is valid for all RF systems and subsystems, including the synthesizer.

We've learned that the frequency synthesizer "menu" offers many alternatives from which the system designer can select, and we've also covered some of the needs of marketable wireless systems. Perhaps one valid method for identifying the best approach for wireless is to eliminate those techniques that will not work. The problem would be solved if a wireless portable end-user would pay for – and carry around – a Comstron FS-5000, or if the industry knew how to clock a cheap DDS at 2 GHz and still get good spurious suppression from the result. For reasons of cost, bandwidth, size, or spectral purity, therefore, pure-direct (analog or digital) synthesizers do not work for wireless.

What about a DDS upconverted using mix/filter circuitry – in other words, one of the "combination" designs? One advantage is the ability of the DDS to generate a modulated signal derived from digital manipulation of the waveform, and a second advantage is switching speed. At first glance, this approach looks inviting, but what are the disadvantages?

Make the estimate. Assume that the system demands 10 MHz bandwidth at a final operating frequency near 900 MHz. If reasonable filters are to be used, then there must be either two upconversions or substantial bandwidth in baseband. Two upconversions are expensive, since two good LOs must be generated and that greatly increases complexity.

For a single upconversion the required baseband coverage might be 50 MHz, which implies a clock rate for the logic near 110 MHz. Consider Figure 9, which illustrates the limitations imposed by filter issues.

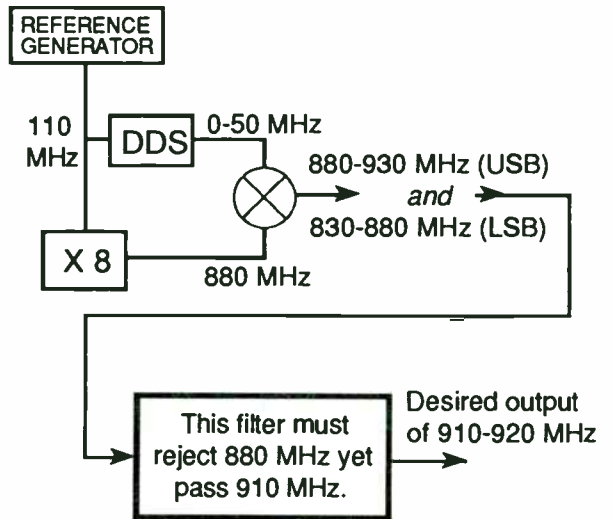


Figure 9

Depending upon the required suppression of the undesired sideband, the filter requirements shown are not impossible to meet. They are, however, difficult, very expensive, labor intensive, and impractical for inexpensive portable equipment.

Power is another issue that probably disqualifies the DDS. Even an advanced-technology, fractional-micron CMOS, fully integrated DDS will occupy a die of about 100 x 100 mils, and assuming a clock rate of 100 MHz the most optimistic dissipation estimate is 0.5W. Wireless portables will probably use a tenth of that for the entire design, hence the likely disqualification of DDSs using today's technology.

For these reasons, neither two conversions nor a 100 MHz DDS clock rate are practical. The designer must look beyond the direct approach. That leaves indirect, or PLL, which works for nearly all RF applications throughout the electronics industry.

In today's wireless, synthesizers are almost all PLL and use either one or two loops. Both have been implemented with very high levels of integration, and single chip PLL ASICs are available at \$5 or less, with operation from 6-15 mA. These devices include all functions and require only an external VCO plus a few discrete devices for the loop filter.

The single loop iteration of such a design is simple, economical, reliable, and small, but it does not meet the requirements of digital modulation techniques.

For many years, a broad variety of simple single loop synthesizers have used inexpensive PLL chips by Fujitsu, Plessey, Motorola, etc. to meet the requirement of early wireless, including FM/analog

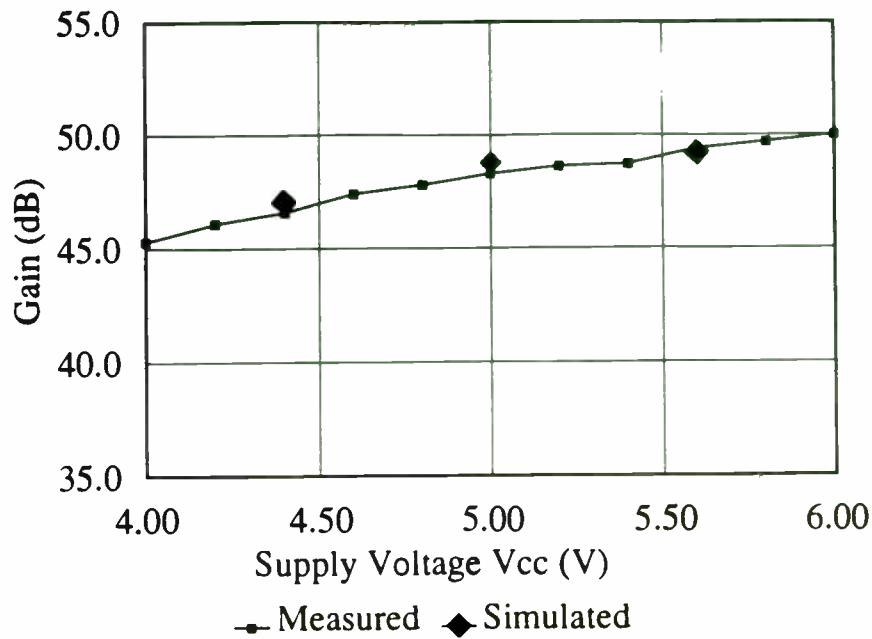


Figure 6a: Conversion gain of the RGP-03 versus supply voltage (VCC)

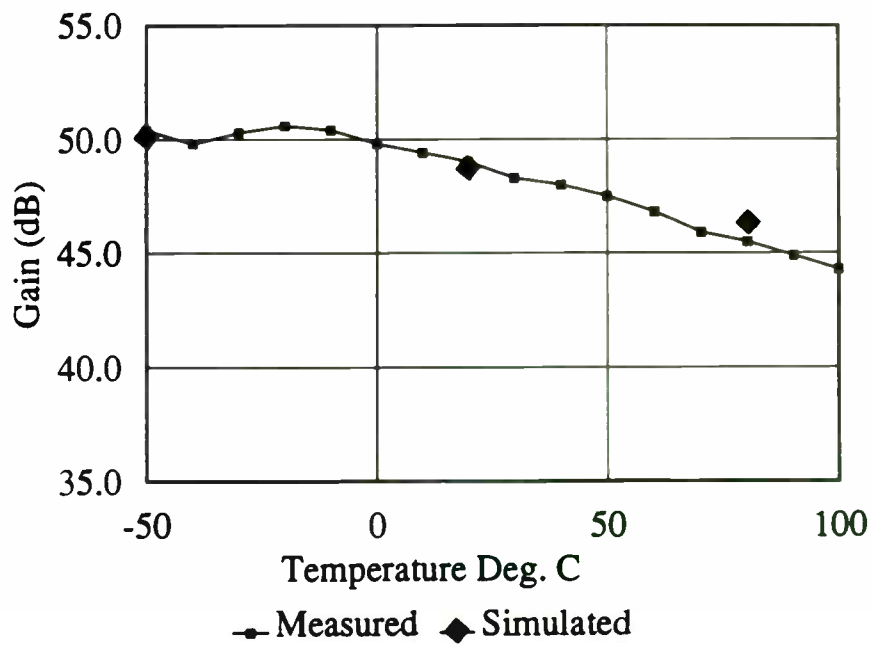


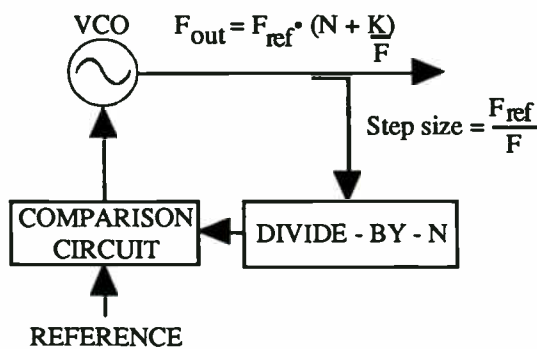
Figure 6b: Conversion gain of the RGP-03 versus temperature

cellular. Close channel spacing of agile wireless requires fine tuning steps and therefore high division ratios, yet digital modulation demands phase noise better than conventional PLL architectures can achieve.

Designers have therefore used two loops to achieve the combination of phase noise and step size needed by digital modulation schemes, which means two synthesizers with two VCOs, etc., and all the baggage a double circuit implies. The two-loop solution therefore implies higher power, complexity, cost, and likelihood of failure – everything the successful wireless system designer was directed to avoid. Nevertheless, state of the PLL art for wireless has been two loops, which achieve the required phase noise. In some systems, the requirement is for two such assemblies with a switch, to support fast switching. That's four loops, with four VCOs and associated circuitry; it's expensive, large, power hungry, and in general is an array of compromises.

FRACTIONAL N

There's a relatively little-known derivative of PLL that can address many such requirements with only one loop; it's called fractional n . Though mysterious to many engineers, it is not a true innovation because some fractional designs have been used for years. Fractional n synthesis can best be understood by examining the conventional block diagram for a PLL, but with one twist. The divide-by- N circuit appears where it always has, but additional circuitry changes the *value* of N from an integer to some fraction. Consider the impact, as suggested by Figure 10.



Conventional PLL: N is an integer
 Fractional: N can be a fraction

Figure 10

N is programmable, of course, to define the relationship between the output and the reference. Suppose the requirement is to operate at about 1 GHz in 30 kHz steps. In conventional PLL designs, the

output (1000 MHz) is divided by 33,000 to reach a value that can be compared to the reference (30 kHz), and that division imposes a phase noise degradation of $20 \log N$, or 90 dB. That degradation can be cut by 20 dB with a good fractional design, and there are several ways to achieve the desired result. Fractional division can be used to *increase* the reference by an order of magnitude, or to *reduce* the division ratios, and in any case the effect is to reduce the division ratio for a given combination of output frequency and step size, thus improving phase noise.

Fractional at first appears to be an aspirin for all forms of PLL headaches, but that hasn't been the case. Conventional implementations of fractional require major increases in circuitry, and that implies increased power dissipation, parts count, complexity, labor costs, and therefore overall costs – again, all the things the designer was told to avoid.

Naturally, fractional division generates a new periodicity within the divide-by- N circuitry, and therefore introduces spurious signals. For the above example, if the reference goes from 30 to 300 kHz, for 30 kHz steps there will be 30kHz/60/90...etc. spurs in addition to the 300 kHz spurs. Those spurs are at the frequency of the new periodicity or its harmonics, but in either case they can produce a major degradation of spurious suppression. In a way, fractional has been largely ignored because those who have experimented with it consider the improvement in phase noise to be virtually a trade off for spurs.

Yet another problem with fractional is that the fractionality of conventional circuits is fixed, hence a given design has little flexibility and new applications imply new designs. For these and allied reasons, fractional n synthesis has been largely ignored. This situation is about to change, as market factors drive engineering to examine every alternative.

An important derivative of fractional is Sciteq's Arithmetically Locked Loop (ALL), which combines aggressive digital signal processing (DSP) with fractional to overcome all of the disadvantages outlined above. ALL is a simple – and patented – design that increases overall gate count (compared, for instance, to the Fujitsu or Plessey PLL chips) by about 3%, so complexity is not an obstacle. The effect of the new periodicity is minimized, hence spurious signal level is also not an obstacle. Finally, fractionality is programmable, making one design suitable to a spectrum of applications.

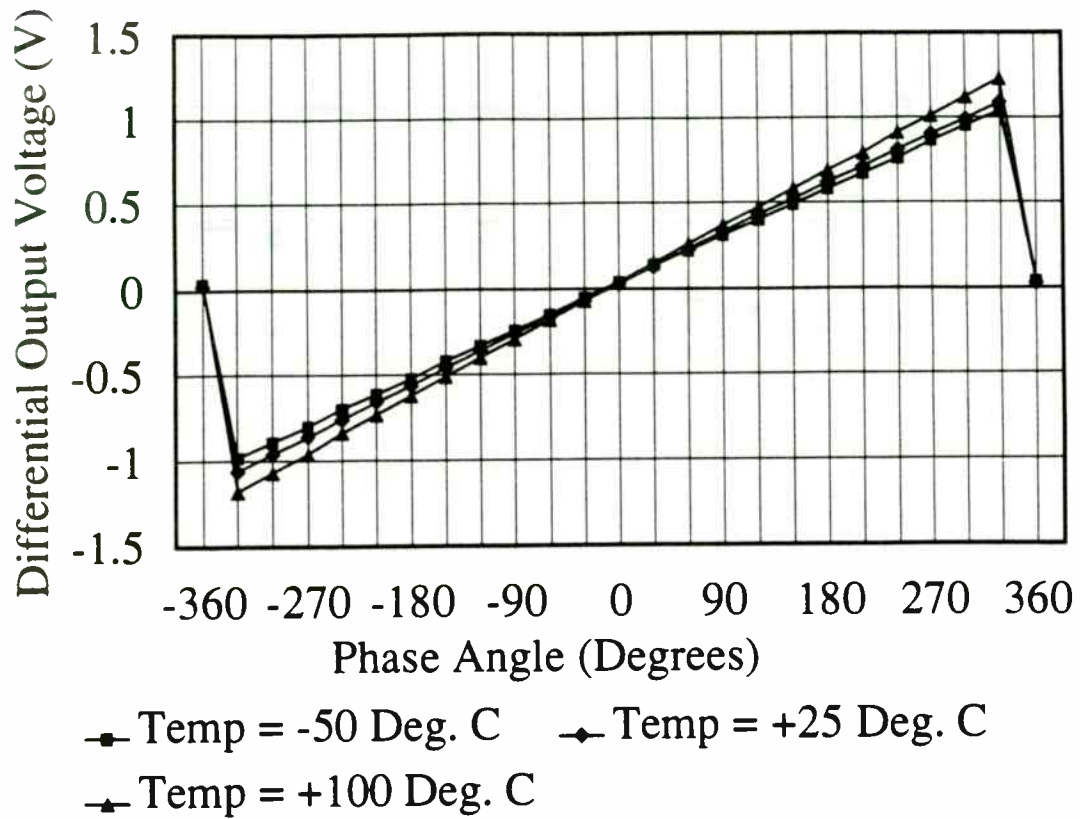


Figure 7: Transfer characteristics for the output of the phase-frequency detector on the RGP-03.

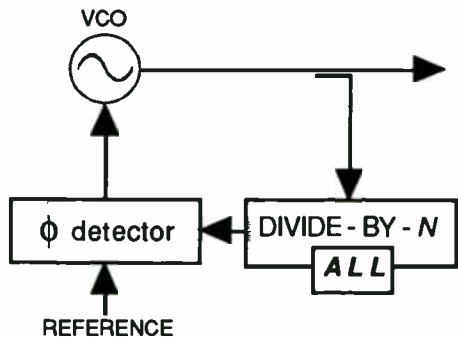


Figure 11

Adding ALL to a synthesizer design is simple, as implied by Figure 11. There is no change to the existing design except for I/Os in the divider circuit; the ALL block adds simple DSP that does the actual job of managing the division process and reducing the required ratios. In most cases, ALL will add approximately 3% more gates to non-ALL circuitry.

ALL APPLICATIONS IN WIRELESS

The ALL can operate over all wireless segments of the spectrum up to C-band. Comparisons are best made by examining any of the standard single-chip

solutions (Fujitsu, National Semiconductor, Plessey, etc.) and adding about 3% in gate count and power while reducing close-in phase noise by about 20 dB.

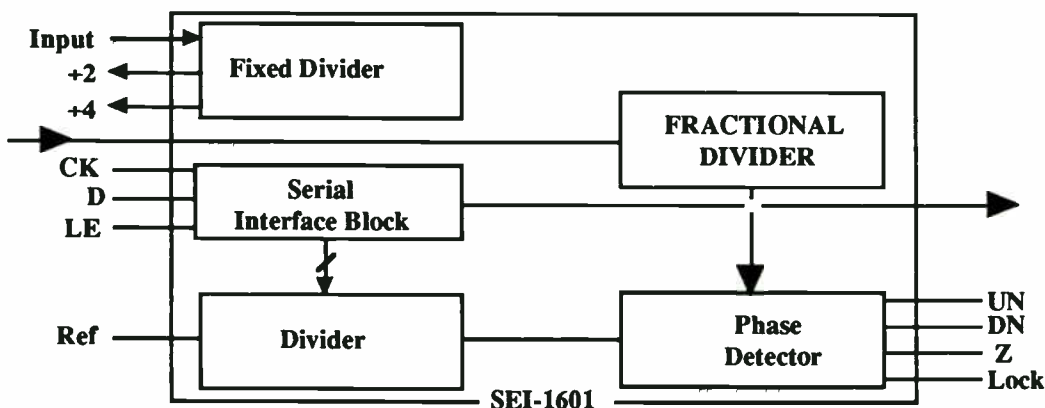
That performance level support digital modulation scenarios with a single loop solution. Even close-in, phase noise is competitive with levels ordinarily achieved using two loop designs.

Frequency switching is faster than conventional PLL designs, even without pretuning, since the reference frequency can be much higher for a given step size.

ALL has been in full production for two years, executed with discrete components to build modular synthesizer products. Potential ALL users can today support system development using prototypes built with discrete devices, in the expectation that a fully integrated solution will be available late 1993.

Many technologists who have evaluated ALL believe that some derivative will appear in most successful cellular and other wireless products that require frequency agility. Developers of such systems should contact Sciteq.

Arithmetically Locked Loop as a 2.5 GHz monolithic synthesizer:



- 20 dB phase noise improvement over other single loop designs
- Integrated +16/17 dual modulus
- 2.5 GHz front end

Wireless Applications for GaAs Technology

Michael Frank, Henrik Morkner, Craig Hutchinson
Hewlett Packard, Newark, California

Introduction

The applications of Gallium Arsenide to the wireless marketplace are now becoming too large to ignore. As the military markets are winding down, commercial opportunities are crying for attention. These opportunities are very different from the traditional military opportunities, with much greater cost and volume pressures, but with equivalent performance requirements. And there are hidden costs in the transition, as low volume, high skill production lines are replaced with the high volume, automated lines required for cost efficiencies.

In this paper we will discuss three different GaAs Integrated Circuits and some of their applications. The first is an IC which provides the transmitter and receiver front end for a half duplex transceiver. The second device is a power FET for a hand held cellular telephone. The third IC we will discuss is a C band low cost, low noise, low power gain block.

Half Duplex Transmitter / Receiver IC

The emergence of the 1.9 GHz PCN market has intensified the friendly rivalry between Silicon and GaAs MMIC designers. In reality, if the system is partitioned correctly there are sufficient opportunities for both technologies. Half duplex systems such as DECT, PHP, CT2 etc., can utilize a partition that plays well to the strengths of GaAs. This partition, shown in figure 1, includes the input low noise amplifier, the output power amplifier, and the SPDT switch between them, all on a GaAs MMIC.

The switching function would be difficult to realize with silicon IC technology. While 2 GHz low noise amplifiers are of course possible with silicon technology, the improved noise figure performance of GaAs provides the designer with a little more margin. And finally, at low bias voltages (3-5 volts) the efficiencies of a GaAs based power amplifier exceed that which can be obtained using silicon devices. In order to compete with silicon in price the GaAs MMIC die size will have to be minimized. As

Time Division Multiple Access (TDMA) Transmitters: Characterizing Power, Timing, and Modulation Accuracy

Helen Chen
Hewlett Packard Corporation
Microwave Instrument Division
1400 Fountain Grove Parkway
Santa Rosa, CA 95403

This paper explores the test requirements of digital RF communication transmitters, presenting practical measurement techniques that reduce system development time and installation costs. Practical spectrum analyzer measurements for TDMA carriers are described, including power, timing, and modulation accuracy tests. Examples from the NADC, PDC, GSM, and CT-2 systems are presented.

The new digital TDMA communication systems present diverse and complex test and measurement issues. Each digital RF system has a unique set of measures for transmission that ensure high quality signals. This paper relates some of the quality metrics to characteristics of the TDMA signal under test. We examine the spectrum analyzer as a powerful, flexible solution to TDMA transmitter measurement challenges. Many digital TDMA transmitter tests can be done with new, expanded spectrum analyzer measurement capabilities. We describe practical spectrum analyzer measurement techniques for TDMA carriers, including carrier power, carrier-off power, adjacent channel power, spurious emissions, and TDMA burst timing. A new digital RF demodulation capability is examined for extracting digital modulation metrics such as error vector magnitude and I/Q offset. Measurement optimization and performance limits are described, and examples from the North American Digital Cellular (NADC) system are shown. We also consider other digital RF formats, including GSM, DCS-1800, PDC, CT-2, and DECT.

Key TDMA Measurement Challenges

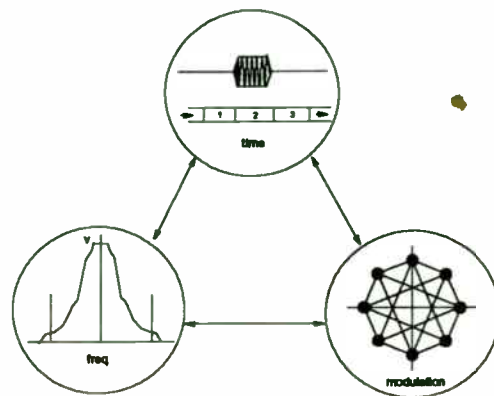


Figure 1: Digital TDMA Signals

Digital RF communication systems have complex, many layered signals. Performance requirements must be met in three domains: the time domain, the frequency domain, and the modulation domain. A time division multiple access (TDMA) channel structure increases carrying capacity by placing multiple users on the same carrier frequency, each user transmitting in turn on the carrier. The user's turn, or time slot, must be precisely placed in time to avoid overlaying users in adjacent time slots. The transmission must comply with a strict time and power mask. In the North American Digital Cellular (NADC) system a mobile time slot is 6.67 ms long.

In the frequency domain, each channel is restricted to a narrow bandwidth, and therefore requires high spectral efficiency. Spectral interference in adjacent channels has many causes, such as poor power control or problems with digital modulation. The NADC channel bandwidth is 30 kHz. Adjacent channel power and spurious emissions are carefully specified in system standard documents.

The quality of digital modulation must also be assured. Clear, error-free transmission is essential to voice and data

much as possible, the large passive components should be realized off chip. To further reduce cost plastic surface mount packaging is essential.

The MMIC was fabricated using Hewlett Packard's MMICB process. The process features MESFETs with .5 μm gate lengths and an Ft of approximately 25 GHz. This MESFET uses an MBE active layer with a low temperature buffer. Proton isolation is used to separate active regions. Passive components available to the designer include: silicon nitride thin film capacitors (.43 pF/sq. μm), n-layer bulk resistors (340 ohms/sq.), and tantalum nitride thin film resistors (22 ohms/sq.). The process features true two level metal interconnects. The second level metal is plated to 2 μm to reduce resistive losses in transmission lines and spiral inductors. While backside via holes are also available in this process, they were not used in this design in order to reduce die cost. All ground connections are made with bond wires.

The schematic of the low noise amplifier portion of the chip is shown in figure 2. The input match is realized by using the package's lead inductance. The output requires a shunt inductor and blocking capacitor to supply bias and transform the impedance to 50 ohms. A tradeoff exists between supply current and ease of match. At 2 GHz larger FETs (around 1 mm) require much simpler matching circuits due to the larger input capacitance. However, the supply current required to keep the FET in the high Gm region (40 to 50 mA) is excessive for many system requirements. Smaller FETs would require less current but would need 3 to 4 element matching circuits to transform their high input impedance to 50 ohms. Furthermore, a small device would impact the dynamic range of the system by limiting the amount of incident power. The LNA presented here represents a compromise utilizing a 500 μm FET biased at 15 to 20 mA. At this bias, the LNA has a linear output power (P1dB) of greater than +10dBm, and an Output Third Order Intercept Point (IP3) greater than +20dBm. The current can be reduced for applications which do not require the high IP3 performance.

The schematic of the SPDT switch is shown in figure 3. Since this application is for a half duplex system, the receive chain is powered down when transmitting and the transmit side is powered down while receiving. The purpose of the switch therefore is to minimize the loading that the unpowered amplifier has on the other. Such a system allows the designer to tradeoff switch isolation for lower loss and higher linearity. To accomplish this the shunt stages typical to FET switches were removed. The linearity is increased because without these shunt FETs the switch can float on the RF signal. Therefore, a much larger signal level is required to override the gate bias, the principle cause of distortion. The capacitors included on chip tune out the package lead inductance.

quality. Digital modulation metrics are tailored to each modulation format. In the European Global System for Mobile Communication (GSM), the global phase of the Gaussian minimum phase shift keyed (GMSK) modulated carrier must be less than 5 degrees RMS. In the NADC system, the $\pi/4$ shifted differentially encoded quadrature phase shift keyed ($\pi/4$ DQPSK) modulated carrier must have an error vector magnitude less than 12.5 percent RMS.

The complex signals of a digital TDMA system are required to support high capacity, high performance service at a low cost. In addition, digital TDMA is a new technology with rapidly changing system structure and modulation formats. Digital TDMA systems are proliferating worldwide. Pacific Digital Cellular (PDC), European Global System for Mobile Communication (GSM), and North American Digital Cellular (NADC) are spreading rapidly, an evolving to fit their markets. Assuring the quality and the low cost operability of these systems requires flexible, low cost test equipment tailored to the new digital TDMA performance metrics.

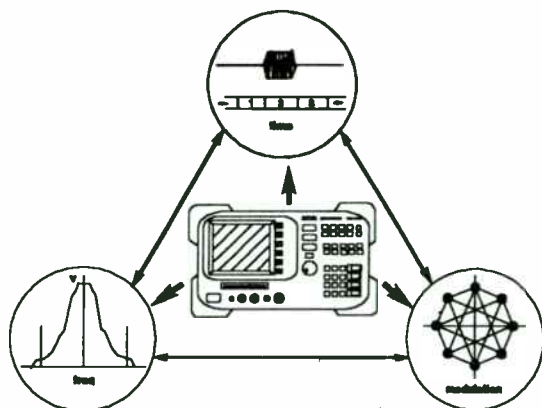


Figure 2: Low Cost, Flexible Tools

A spectrum analyzer can be a low cost platform for test solutions for digital TDMA systems. The Hewlett-Packard 8590 E-series spectrum analyzer can be adapted to make many digital communication system measurements. The architecture supports upgrades to new formats in the future. An expanding set of custom options adapt the analyzer for time, frequency, and modulation domain measurement. On a spectrum analyzer platform, digital RF tests can be done over the full frequency range (9 kHz-26 GHz) and signal sensitivity of the instrument.

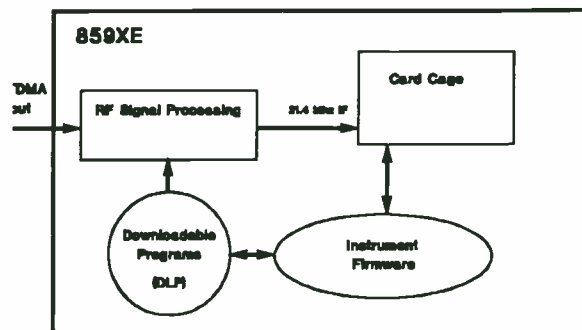


Figure 3: 8590E-Series Flexible Architecture

The HP 8590 E-series spectrum analyzers have a unique, flexible architecture that allows new measurement capabilities to be added quickly to the instrument. See Figure 3 . A traditional RF signal processing chain downconverts the carrier, and filters it through resolution bandwidth filters for subsequent power detection. The HP 8590 E-series instruments add an option card cage to the RF chain. This allows optional hardware to be connected to the signal processing, including extensions for precise time domain and modulation measurements.

The spectrum analyzer not only has flexible hardware, but also has adaptable software, in the form of downloadable programs (DLPs) on memory cards. (Downloadable programs are also called measurement personalities.) New measurement algorithms can be driven from code loaded from memory cards into the spectrum analyzer's memory. Spectrum analyzer hardware setup, trace manipulation, and test limits can be automated with a DLP. By changing the DLP loaded in the instrument, a GSM analyzer can be reconfigured easily into an NADC analyzer.

The key parts in adapting the spectrum analyzer will be highlighted as we describe practical measurement techniques.

Finally, the schematic of the power amplifier is shown in figure 4. Only the FET resides on chip and the input and output matching circuits were chosen to incorporate the package lead inductance.

Refer to the photograph of the die shown in figure 1. The LNA occupies the lower left hand corner of the chip. The SPDT switch occupies the right side of the chip. The 3 mm FET used in the power amplifier is found in the upper left hand corner. The chip size is 800 um by 900 um (31.5 mils X 35.5 mils). This device was designed for a 16 lead plastic package. Seven of the sixteen leads are connected to the die attach paddle, and thus to ground. This configuration minimizes the package's ground inductance and provides the thermal dissipation needed for the power amplifier. Packaged units were soldered to test circuit boards (figure 5) and each circuit function was tested separately. At 2 GHz the board's loss was measured at 0.5 dB. This loss is included in the measured responses that follow.

Figure 6 shows the response of the low noise amplifier. The amplifier is biased at 3 volts. The wide bandwidth allows the LNA to absorb large variations in process parameters as well as component values. Figure 7 shows the measured noise figure of the LNA. Again the response is flat from 1 to 3 GHz. And the LNA has an output one dB compression point (P1dB) of +10 dBm.

Figure 8 shows the measured response of the SPDT switch. Through Loss and Return Loss of both the on and off states are shown. An output third order intercept point (IP3) of 50 dBm was measured with -5 volts applied to the gate.

Finally, figure 9 shows the measured small signal response of the power amplifier. With a 5 volt supply the power amplifier produces an output P1dB of 26.5 dBm and a power added efficiency (PAE) of 40%. At 3 volts the output P1dB is 23.5 dBm and the PAE is 34%.

Table 1 is a summary of all the specifications for this T/R IC.

Cellular Telephone Power Amplifier Device

Modern cellular Telephony is currently undergoing a revolution. North America Europe and Japan are changing to digital transmission. Because of this transition, some new phones (NADC) must be able to move seamlessly from a digital environment to an analog environment, each of which has its own set of specifications. The current generation phones are very small, requiring great packing density of the circuitry. Because weight is an important feature, batteries must be small, and consequently the circuit must be very efficient. The phones range cannot suffer, however. This puts very

Catching Time Conflicts

We will first describe measurement techniques using a spectrum analyzer to catch time conflicts in a TDMA system.

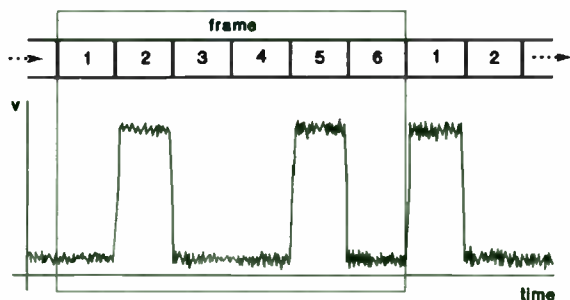
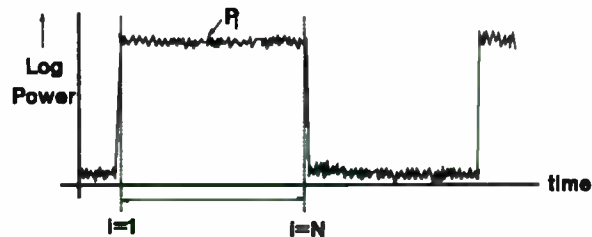


Figure 4: Burst Amplitude Modulation for TDMA

A time division multiple access (TDMA) system requires transmissions to be pulse-amplitude-modulated, or burst. Several users are time-multiplexed onto the same carrier to increase spectral efficiency. As shown in Figure 4, time on a carrier frequency is divided into a stream of frames. Each frame contains a fixed number of time slots. The time slot sequence repeats as the frames are transmitted. In the NADC system, a 40 ms frame had six 6.67 ms time slots. A user may transmit a packet, or burst, of modulated carrier only when his time slot appears in a frame.

In a TDMA burst carrier, good transmission power versus time characteristics are critical to avoid interference with adjacent channels in the time domain and in the frequency domain. Four key areas of concern are carrier power, carrier off power, time position of the burst, and burst shape. Measuring these parameters is a good way of exposing potential interference problems.



$$P_{\text{mean}} = 10 \times \log \left[\frac{1}{N} \times \sum_{i=1}^N 10^{\frac{P_i}{10}} \right]$$

Figure 5: Carrier Power

where:

- P_{mean} = mean carrier power during on part of burst (dBm)
- P_i = power level at sample point i of the waveform (dBm)
- n = number of sample points in the "on" part of the burst

Carrier power is defined to be the mean power transmitted during the active, or "on," portion of the burst. Testing the carrier power in the "on" portion of the burst ensures that burst power is sufficient for clear reception.

With a spectrum analyzer, the measurement is made with the instrument fixed tuned to a single frequency, yielding a power versus time trace on screen. The resolution bandwidth and video bandwidth in the RF signal processing chain are set wider than the channel bandwidth to avoid distorting the pulse shape. The trace data is averaged for the "on" portion of the burst.

Since the trace is defined on a logarithmic power scale, a true power average can be obtained only by performing an anti-log transformation to linear units prior to averaging the data. In general, the mean of log powers is not equal to the log of the mean power. In the equation above, each sample of trace data in the "on" portion of the burst (P_i) is anti-logged and summed. An average value is calculated using this linear unit sum. The mean power is then returned to the logarithmic scale for display as P_{mean} . For modulation formats with significant amplitude modulation, such as $\pi/4$ DQPSK, true power averaging is essential to accurately finding the mean carrier power.

stringent requirements on that device which takes the bulk of the battery power, the power amplifier. To maximize talk time, the device must show better than 45% efficiency at 936 MHz, at 600mW in the analog mode. To minimize adjacent channel spillover, the device must exhibit a third order intercept point of 39dBm for the digital mode, all at a bias of 6V. Since this is a very high volume application, the average sale price must be very aggressive.

The device reported on here is a 10mm GaAs FET. The gate length is 0.9 micron. The epitaxial layer is grown using Hewlett Packard's proprietary vapor phase epi process, providing a very uniform structure. The transition from the semi insulating substrate to the semi conducting epi must be very sharp to support the efficiencies necessary. The device utilizes a wrap around ground, providing a very low impedance path to the bottom of the package. Table 2 contains a summary of the device performance.

Why use GaAs instead of Silicon? GaAs is generally more expensive than Silicon, at least at the current manufacturing volumes. The frequency is quite low for traditional GaAs, but Silicon has inherent limitations. Because the gain is lower, a Silicon power amplifier may require three stages (compared to two for a GaAs power amplifier with the same gain), adversely affecting the efficiency of the power amplifier. In Silicon devices the collector is at the bottom of the chip, so the output and thermal ground are the same node. This complicates the circuit board layout. GaAs FETs have both the signal and thermal grounds at the source, which is connected directly to amplifier ground. This means that a negative supply is required.

Packaging is critical to the performance and cost of this device. The package must present low thermal and electrical impedance at the common node, low losses at the signal terminals, and be inexpensive. Shown in figure 10 is an example of a low cost, high performance transistor package suitable for a multi watt power transistor. This proprietary package consists of a ceramic puck with a hole in the middle, brazed to a metal lead frame. The FET to thus die attached directly to the lead frame. This package concept can be used to build a hermetic device for high reliability applications.

The requirements for this amplifier are not trivial. The combination of linearity and efficiency is especially challenging. To achieve this performance, the device must exhibit a linear G_m Vs V_{gs} relationship down to about 15% of I_{dss} . This puts severe requirements on the material, forcing the transition from the semi insulating bulk to the semiconducting channel to be tremendously sharp. Figure 11 shows an example of a device exhibiting the critical DC characteristics. At the required current, the G_m must still be close to the value at saturation.

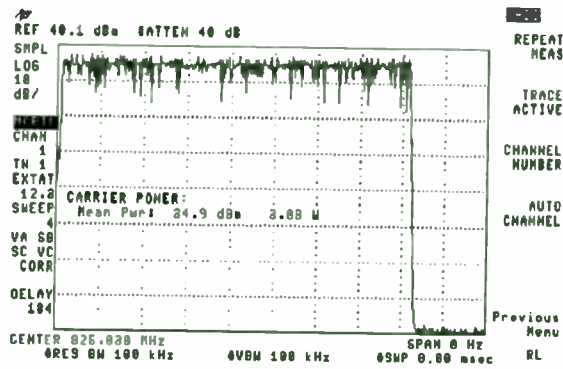


Figure 6: NADC Carrier Power

Here is an example of carrier power measured for a burst NADC-TDMA carrier. The HP 85718A NADC-TDMA downloadable program automates spectrum analyzer setup and power calculations.

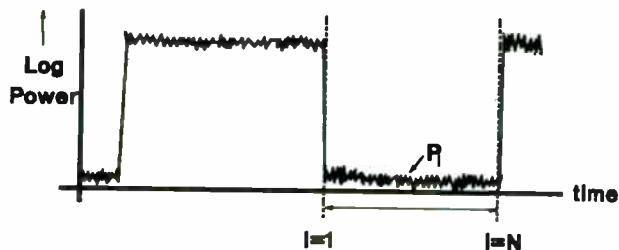


Figure 7: Carrier Off Power

Carrier off power is defined similarly to carrier power. Carrier off power is the mean transmitter power during the part of the frame where the transmitter is inactive or "off." In Figure 7, the inactive portion of the burst is in samples $i=1$ to N . The power in "off" portion of the burst must be low to avoid obscuring a burst in the other time slots.

The spectrum analyzer is again used in a mode fixed tuned to the carrier frequency. For better noise rejection and improved sensitivity, a narrower resolution bandwidth and video bandwidth are used to measure the low level "off" signal. The trace data is averaged for the "off" portion of the signal shown on screen.

The narrow video bandwidth averages the "off" power of the carrier, so that a stable power level can be read.

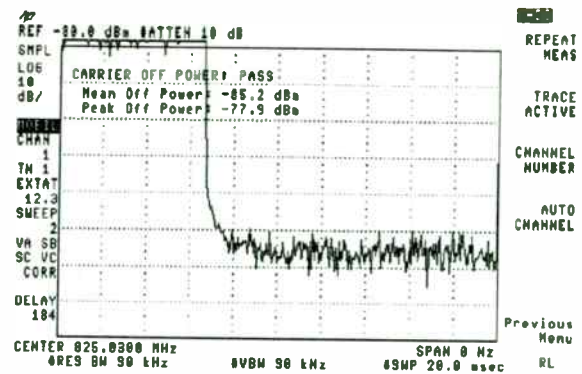


Figure 8: NADC Carrier Off Power

Here is an example of an NADC-TDMA carrier off power measurement, part of the HP 85718A NADC downloadable personality.

Note the 30 kHz resolution bandwidth used in carrier off power compared to the 100 kHz resolution bandwidth used in the carrier power measurement example. The results are compared to limits specified in the NADC standard document, IS-55. A "PASS" or "FAIL" indicator is displayed.

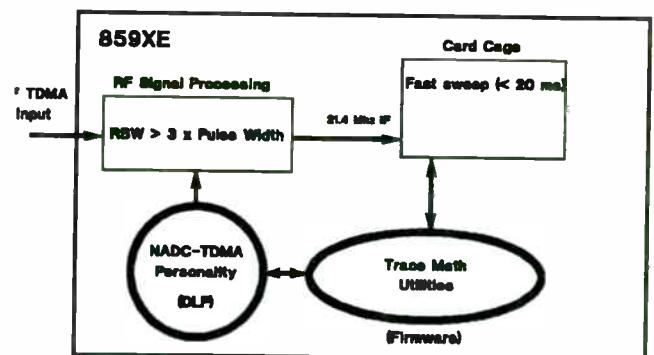


Figure 9: Carrier Power Measurement Tool

The HP 8590 E-series spectrum analyzer supports the tailored trace manipulation needed for true power averaging. The HP 85718A NADC-TDMA downloadable program automates a measurement customized for NADC test limits.

The FET must be able to handle the power at all portions of the cycle. Saturated performance must be more than 3 dBm higher than the nominal output power. In practice, this means the saturated output power must be +31.5 dBm (in production) for a +28 dBm amplifier. A consequence of the linear operation requirements of the radio system, this is essentially an out of band emission specification.

To maximize the efficiency of a power device, one must match the output for maximum power transfer, short circuit all the even harmonics, and open circuit the odd harmonics. Unfortunately, this scheme causes the harmonics to mix with the fundamental, causing excessive intermodulation. For high linearity, the wave form must be as close to a sine wave as possible. This means that the harmonics must be power matched as well, so that the energy is not available to mix with the fundamental. Due to the out of band emission requirements, these harmonics cannot be present at the antenna. A diplexer can be used to terminate the harmonics separately. This results in a rather less than optimally efficient amplifier (65% PAE is a typical specification for analog systems), but the compromise is necessary to achieve the required linearity. Figure 12 shows the circuit schematic. Figure 13 is a photograph of the device. Figure 14 illustrates the two tone response of one of these FETs.

C Band Low Cost, Low Power LNA

There are numerous commercial bands from 1.5 to 8 GHz, some mature, many emerging. These bands include 1.5 GHz (GPS), 1.9 GHz (PCN), 2.1 GHz (MMDS), 2.4 GHz & 5.7 GHz (ISM), 3.7 to 4.2 GHz (Satellite/TVRO), C-Band (Aviation), and the full 1.5 to 8 GHz band (Instrumentation). A MMIC LNA has been designed to help those system designers involved at these frequencies. It includes integrated bias and impedance matching, eliminating most of the 10 to 15 components required to implement a comparable discrete design. A low cost surface mount package is utilized to maintain performance without significant degradation. This MMIC is a functional marriage of military technology (PHEMT) and a commercial application (low manufacturing cost / high yield).

This MMIC uses state-of-the-art 0.15u gate PHEMT devices, self-biasing current sources, source follower interstage, resistive feedback, and on-chip matching to make a unique low noise amplifier. The die area is small (0.40 mm sq.) and is compatible with surface mount packages. DC power requirements are low, consuming only 15mA from a single +7V supply.

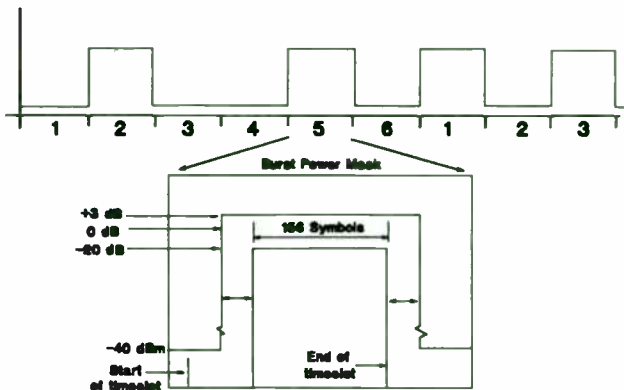


Figure 10: TDMA Burst Position in Time

Many standards define time domain masks for the position and shape of a TDMA burst., such as the one in Figure 10. Bursts should be verified to be in the assigned time slot. Transmission power must be maintained in a narrow window during the "on" part of the burst. The ramp-up and ramp-down times do not extend into adjacent time slots. Examining burst ramp shape can expose not only problems due to infringement on adjacent time slots, but also interference due to excess spectral splatter of burst power transitions.

To make the time position and shape measurements, the spectrum analyzer must be able to find and focus on any desired time slot. The transmission is then shown on screen and compared with the power and time limits specified in the standards.

The HP 8590 E-series spectrum analyzers use an adjustable delayed trigger to focus the spectrum analyzer measurement sweep on the desired pulse. The coordination of this measurement is shown in Figure 11. At the top of the timing diagram, an RF burst is the input to the spectrum analyzer. Additionally, a TTL trigger input is required, usually synchronous with the frame rate of the TDMA RF signal. This input trigger is processed through hardware on the Option 105 time gate card, which provides a user adjustable delay of the input trigger signal. Using the time gate, the trigger output is positioned to be just before the time slot of interest. The delayed trigger is connected to the external trigger of the spectrum analyzer, initiating a sweep at the rising edge of the delayed trigger at the time gate trigger output. The spectrum analyzer sweep time is adjusted to capture the time interval of interest. In Figure 11, the timing diagram shows the capture of the rising edge of the burst.

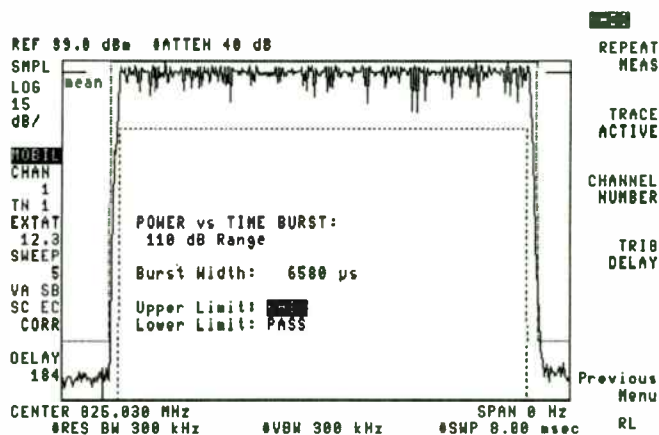


Figure 12: NADC Full Timeslot

The figure above shows a power versus time measurement executed on an NADC burst in time slot 1. This burst is barely within specification. Spectrum analyzer setup, measurement, and result display are completely automated in the HP 85718A NADC-TDMA personality.

Although spectrum analyzers are high dynamic range instruments, the signal range requirements for some TDMA system are a challenge. For example, the NADC-TDMA IS-55 standard specifies a -60 dBm burst "off" level. For this limit, a 3-watt mobile phone requires 95 dB of measurement range. The downloadable software can extend the on-screen calibrated dynamic range. Notice in Figure 12 that the screen displays 110 dB of range on

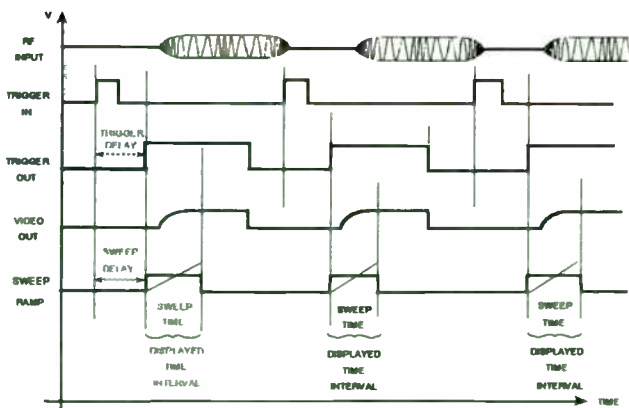


Figure 11: Delayed Sweep Trigger Timing

This monolithic low noise MMIC amplifier employs Hewlett-Packard's advanced PHEMT (Pseudomorphic High Electron Mobility Transistor) process, which yields 0.25 dB noise figure at 4.0 GHz. The devices are built using MBE (Molecular Beam Epitaxy) material growth techniques. The gates are defined using electron-beam lithography. Typical lengths range from 0.12 to 0.17 microns. A mushroom shaped gate is used in order to reduce gate parasitic resistance by increasing the gate's cross sectional area.

Figure 15 presents a schematic of the PHEMT MMIC LNA, and a photograph of the device assembled into a surface mount package. The MMIC LNA consists of two primary FET gain stages, one source follower stage, three current sources, two feedback networks, and two source capacitors. Each 12 dB gain stage consists of a PHEMT FET biased at 25% of I_{dss} with the use of a current source. The source follower also consists of FET at 25% of I_{dss} bias with a current source. The use of active current sources on each stage allows for a robust design tolerant of natural variation in the fabrication process. The source follower provides impedance transformation for an internal feedback point. This interstage-to-input resistive feedback is used to improve stability and VSWR, with minimum degradation of the noise figure. A second capacitor and resistor network provide feedback on the last stage to improve the output match, stability, and gain flatness. Source capacitors allow for a single DC supply, and provide high pass filtering. The die size is small, approximately 0.59 mm (23 mils) by 0.68mm (27 mils).

Figure 16 illustrates typical performance, derived from more than 200 parts. In a 50Ω system, typical gain is 21 dB, noise figure is 1.9 dB, input VSWR is 3.0:1, output VSWR is 2.0:1, and output power at one dB compression is greater than 7 dBm. A simple external input match (series inductance of .1 to 2 nH) produces the minimum noise figure of 1.5dB, gain greater than 22 dB, and VSWR below 1.5:1. If output power is not critical, a 5 volt supply can be used with minimum degradation of the other specifications. As all stages share current, the MMIC consumes typically only 15mA, 1/3 less than any published, comparable devices. Table 3 shows measured performance for this MMIC. This MMIC LNA compares favorably in noise figure, gain, low current, match, wide bandwidth, and price with any advertised or published products presently available.

an analyzer that normally has an 80 dB log display. The personality controls the spectrum to analyzer take two sweeps: one optimized to measure the active portion of the burst, the second optimized to measure the inactive portion of the burst. The two sweeps are time matched, and pasted together. They can be displayed as one trace, showing 110 dB of display range.

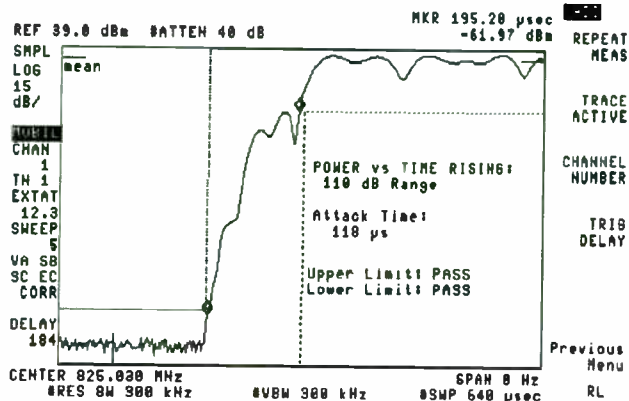


Figure 13: NADC Burst Rising Edge

In this example, the spectrum analyzer delayed trigger and sweep time have been adjusted to focus on the rising edge of an NADC burst. The time selection adjustments are automated in a DLP. A fast digitizer in the card cage is needed to extend spectrum analyzer sweep times to sweeps faster than 20 ms.

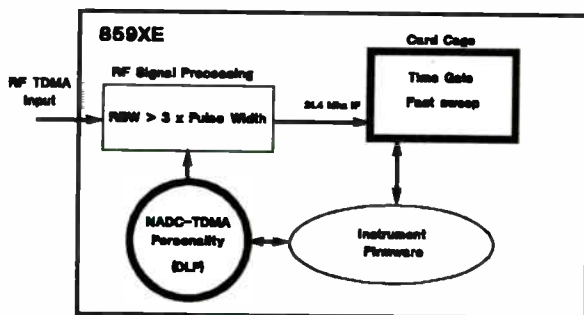


Figure 14: Burst Position Measurement Tool

The key additions to the HP 8590 series spectrum analyzer for digital TDMA time domain measurements include card cage hardware and downloadable software. The time gate and fast digitizer are needed to find and focus on the time intervals of interest. Adjustments are simple, if driven from the specialized DLPs.

Detecting Sources of Frequency Interference

In addition to time domain conflicts, frequency domain interference must be detected in a digital communication system. Both interference close to a carrier transmission and distant spurious should be kept at low levels.

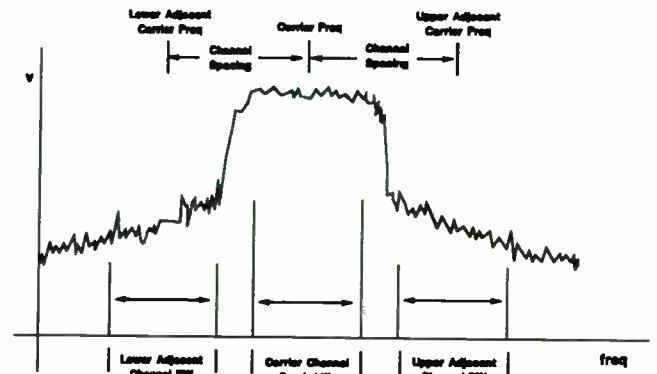


Figure 15: Adjacent Channel Power

Adjacent channel power (ACP) is a measure of the amount of leakage power spilled into adjacent channels. Usually, ACP is specified as a ratio to the total carrier power, but some standards specify absolute power levels. The total power in the lower adjacent channel or in the upper adjacent channel is compared to the total carrier power. In a mobile communication network, the interference from the adjacent channel must be kept very low. Users on one channel should be able to communicate without interference from another channel. High adjacent channel power can degrade communication quality or increase the interference rejection required in the mobile station for good overall performance.

In a spectrum analyzer, adjacent channel power measurement begins with obtaining a frequency domain trace of the spectrum, centered about the carrier channel of interest. The analyzer sample detector is used to accurately detect the power of the digitally modulated signal. The instrument resolution bandwidth is set to be much narrower than the channel bandwidth to yield a more accurate integration of power over the adjacent channel bandwidth. The video bandwidth should be at least ten times larger than the resolution bandwidth to remove any video averaging of the trace sample points. Video averaging can lead to errors as great as 2.51 dB in the sampled power reading.

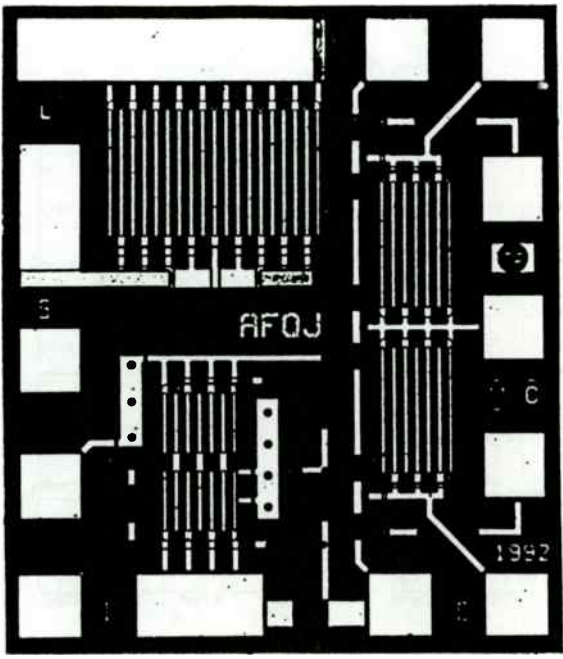


Figure 1: T/R Chip Photograph

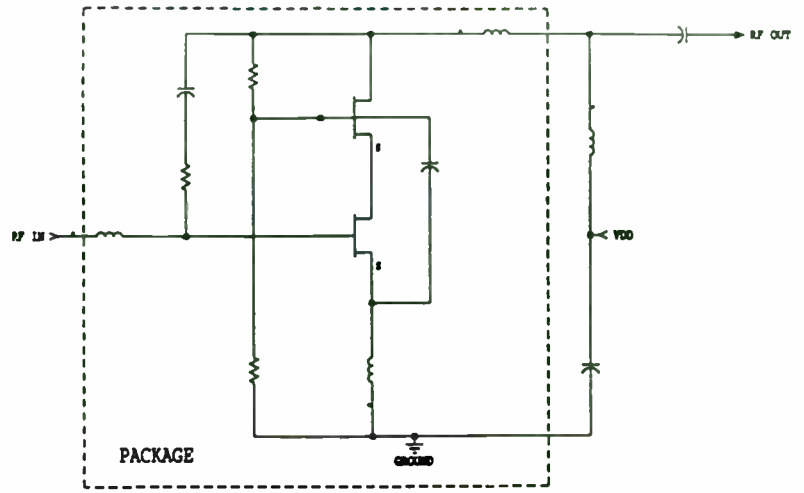


Figure 2: Low Noise Amplifier Section

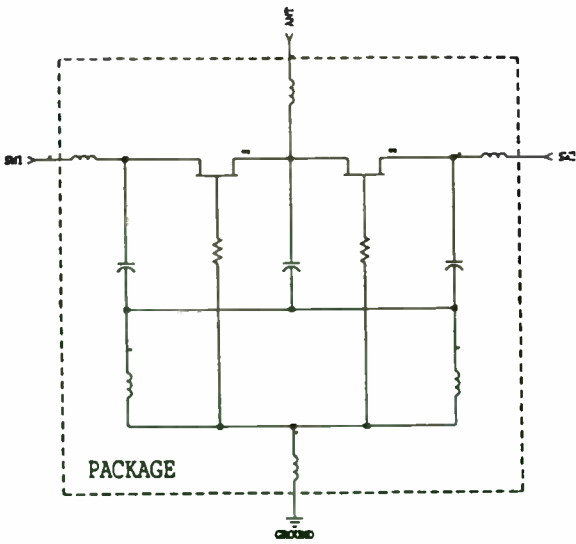


Figure 3: Switch Section

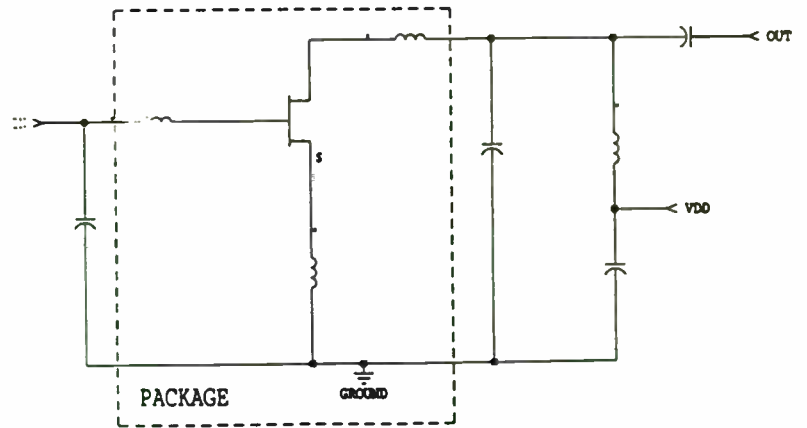
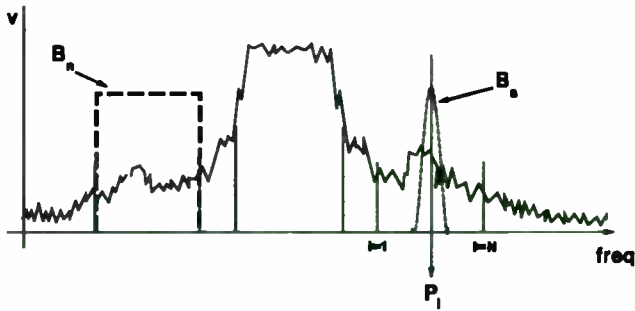


Figure 4: Power Amplifier with Off Chip Matching



$$P_{ACP} = \frac{B_s}{B_n} \times \frac{1}{N} \times \sum_{i=1}^N P_i$$

Figure 16: Continuous Carrier ACP

where:

- P_{acp} = RMS-like power in the specified integration bandwidth (watts)
- P_i = power level at sample i of the spectrum analyzer trace (watts)
- B_s = specified integration bandwidth for adjacent channel (Hz)
- B_n = effective noise bandwidth of spectrum analyzer (Hz) 1.13 x resolution bandwidth of spectrum analyzer
- N = number of sample points in specified bandwidth

For an analog communications system or a continuous (non-burst) digital carrier, the ACP calculation is made after obtaining a frequency domain trace of the spectrum. Adjacent channel power is calculated in the spectrum analyzer using an integration method. The leakage power in the adjacent channel is computed with the power integration equation shown in Figure 16, above. The trace sample points (P_i) within the adjacent channel integration bandwidth are averaged in linear units (watts). The adjacent channel integration bandwidth is sometimes called the specified bandwidth. A scaling factor, B_s/B_n, is applied to compensate for the shape of the spectrum analyzer signal processing filters, the resolution bandwidths.

The power at each trace sample point is detected after filtering by the spectrum analyzer resolution bandwidth. The HP 8590 series resolution bandwidth is a four-pole synchronously tuned filter. This filter captures more power under its flared skirts than a straight-sided, rectangular filter of the same 3 dB bandwidth. The power measured by the spectrum analyzer must be corrected for the excess

power caught under the skirt of the synchronously tuned filter. The factor B_s/B_n multiplies the average power in the adjacent channel by the number of effective noise bandwidths in the specified bandwidth. A rectangular filter correction factor is usually required, but NADC-TDMA standard IS-55 and IS-56 specify the application of a Nyquist square-root raised cosine filter prior to performing the integration. The HP 85718A NADC personality software applies the Nyquist correction.

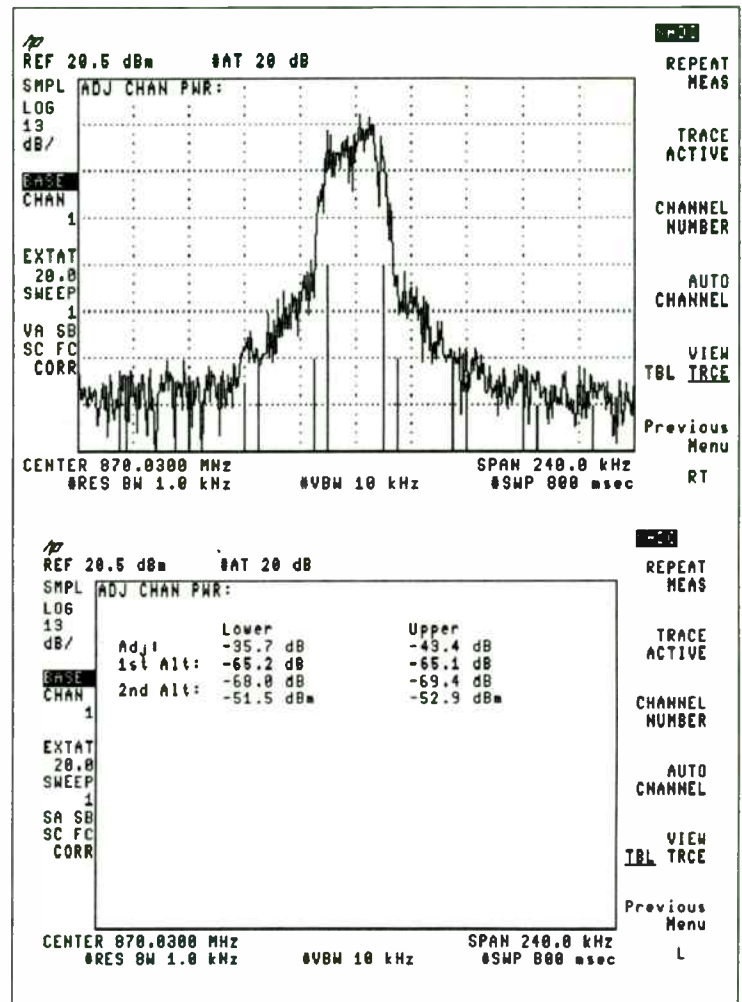


Figure 17: ACP Continuous Carrier

The top HP 8593E spectrum analyzer screen shows the spectrum of an NADC transmitter at 870.03 MHz. The carrier channel and adjacent channels are marked by vertical lines at the lower edge of the screen. The bottom spectrum analyzer screen shows the table of adjacent channel powers resulting from the NADC-TDMA personality ACP test.

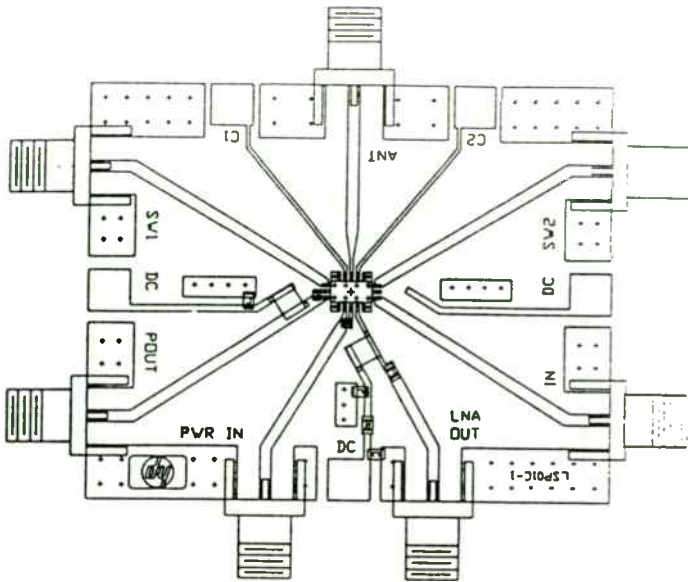


Figure 5: Test Board

CH1: A -M REF = 9.55 dB 5.0 dB/ REF = .00 dB
 CH2: B -M REF = 10.74 dB 5.0 dB/ REF = .00 dB

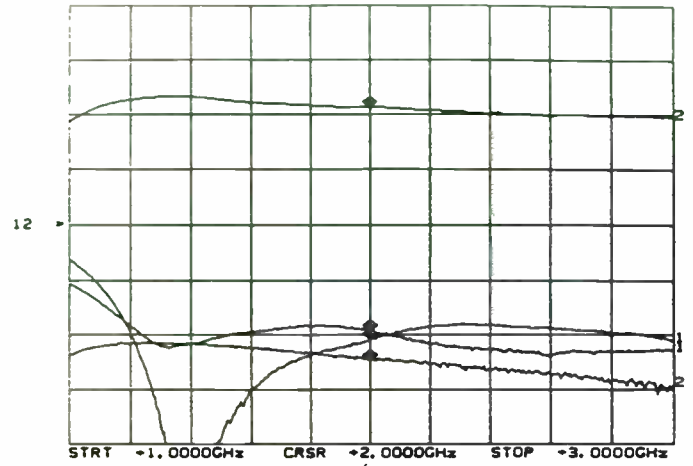


Figure 6: Gain, Isolation, and Return Loss of LNA

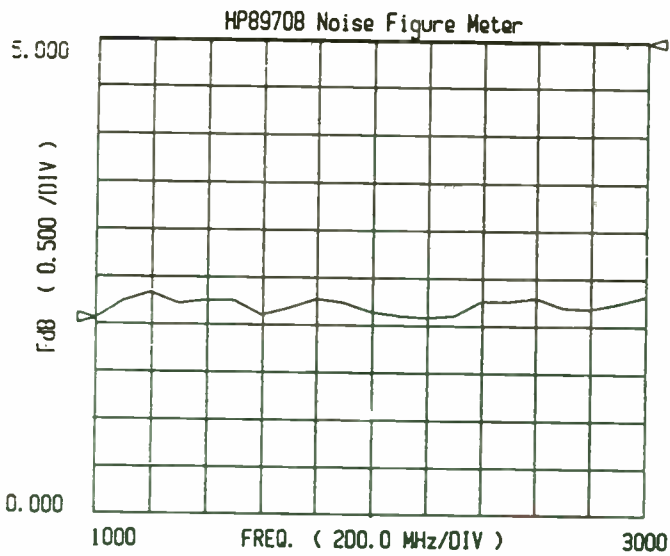


Figure 7: Noise Figure of LNA

CH1: A -M REF = 17.26 dB 5.0 dB/ REF = .00 dB
 CH2: B -M REF = 1.27 dB 5.0 dB/ REF = .00 dB

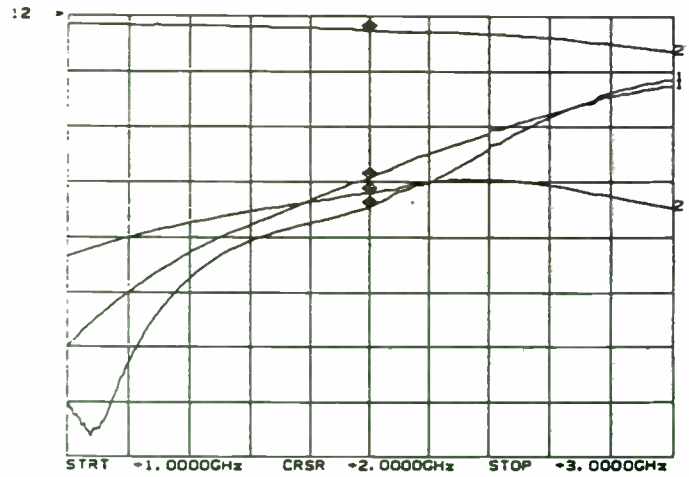


Figure 8: Gain, Isolation, and Return Loss of Switch

Measuring adjacent channel power on burst TDMA signals is more complex than in the continuous carrier case. Burst amplitude modulated carriers produce transient spectra whose power adds to that of the digital modulation. These transient spectra often obscure the lower level digital modulation spectra, making burst adjacent channel power tests difficult. Abrupt power transitions create more transient spectra than slower, more gentle burst ramps. Digital TDMA communication systems usually require slow burst ramps to avoid increasing the adjacent channel power due to transient spectral splatter. An unusually high adjacent channel power may indicate a burst shaping problem.

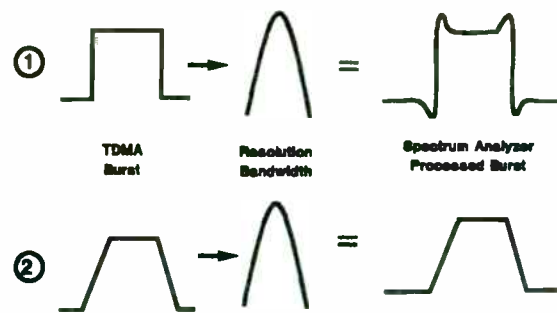


Figure 19: TDMA Burst Interaction with Spectrum Analyzer Resolution Bandwidth

Transient spectra may be formed within the spectrum analyzer. As the TDMA burst passes through the resolution bandwidth filter during a spectrum analyzer sweep, the pulse shape will become distorted at the edges, particularly at frequencies near the beginning and the end of the spectrum analyzer sweep. This distortion is a natural consequence of the way a traditional spectrum analyzer measures the spectrum. As the spectrum analyzer steps through the frequencies in the sweep, the burst is convolved through the impulse response of the filter at each sample point. The convolution of the burst with an off-center-tuned resolution bandwidth filter produces peaks at the edges of the pulse. The distortion peaks, or "ears," are recorded by the analyzer peak detector, so a trace sample point reflects the peak power of the "ears" rather than the true stable power of the burst. See example 1 in Figure 19. A burst with a slow ramp will suffer less distortion, yielding less peaking of the power readings of each sample. See example 2 in Figure 19.

Separating the adjacent channel power due to stable, digital modulation and the ACP due to transient spectra induced by the pulse in the spectrum analyzer is essential to correctly assessing the interference due to spectral spillover in adjacent channels. Note that the spectrum analyzer distortion peaks are positioned near the edges of the burst. A true reading of the power level of the burst is possible away from the edges of the burst.

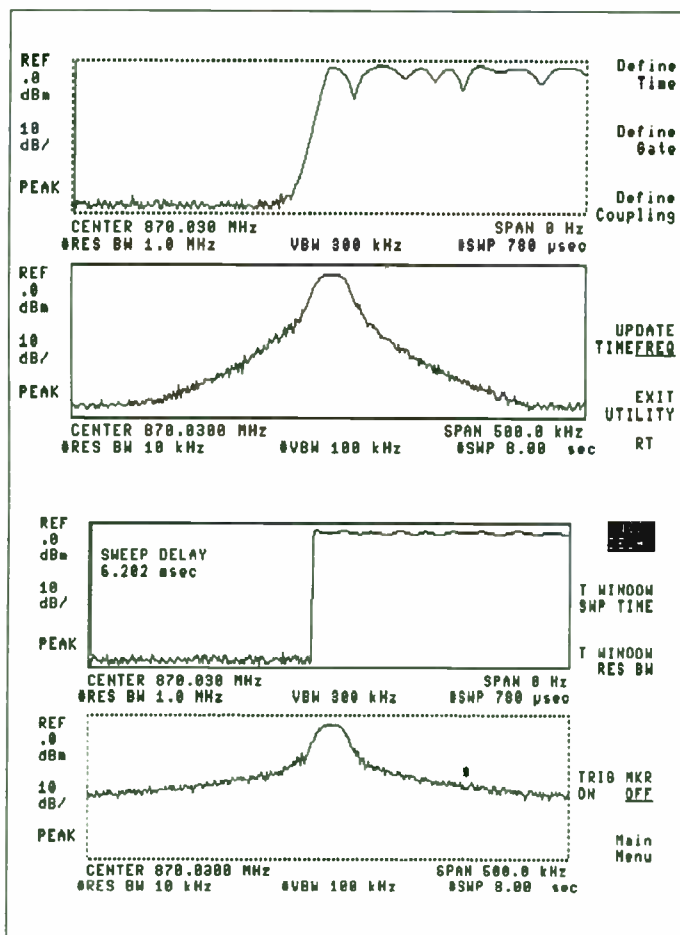


Figure 18: Transient Spectra

The pictures in Figure 18 show transient levels detected in a spectrum analyzer from a slow burst ramp and from an abrupt ramp. Note that a large portion of the spectral splatter displayed is formed within the spectrum analyzer itself.

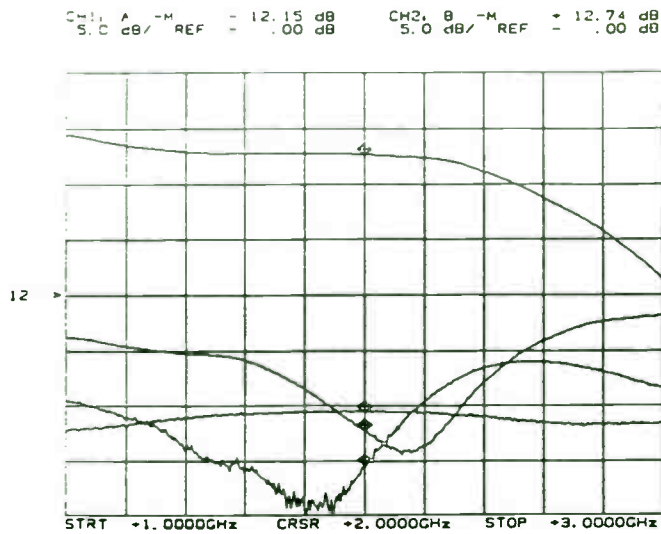


Table 1 Half Duplex T/R IC

	Parameter	Specification
LNA	Frequency	1 to 2 GHz
	Noise Figure	2.0dB
	Gain	12dB
	Return Loss	14dB
	P1dB	10dBm
Switch	Power Supply	5V/20mA
	Insertion Loss	1.3dB
	Return Loss	15dB
	Isolation	18dB
	IP3	50dBm
PA	Power Supply	-5V
	Gain	13dB
	P1dB	26dBm
	PAE	40%

Figure 9: Small Signal Response of Power Amplifier

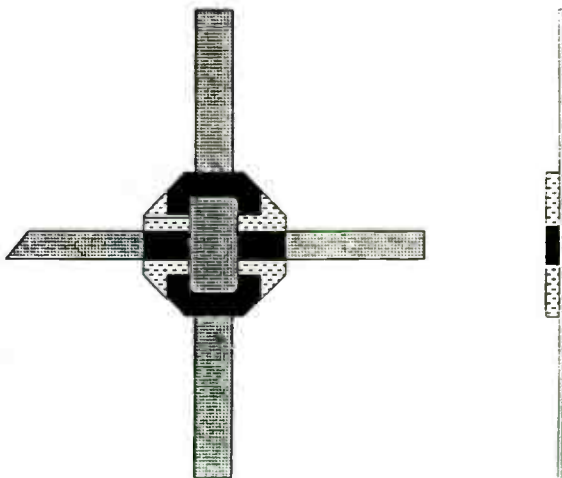


Table 2 Cellular Telephone Power FET

Parameter	Specification
Frequency	830 to 842 MHz
Gain	14dB
Analog PAE	45%
Pout	+28dBm
IMD 3	-26dBc
IMD 5	-36dBc
IMD 7	-40dBc
Power Supply	6V

Figure 10: Cellular Power FET Package

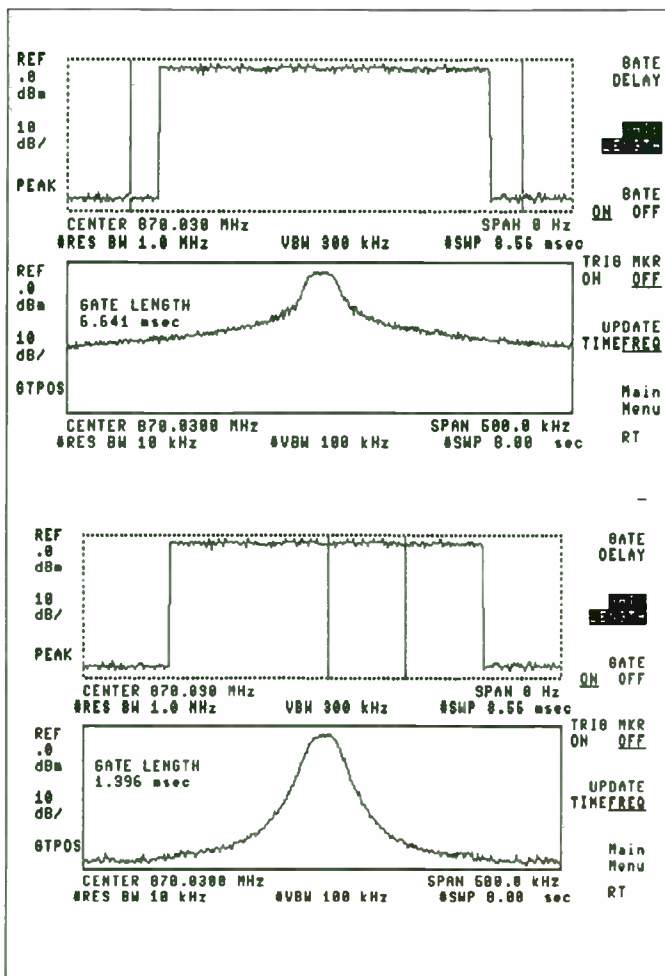


Figure 20: Time Gate Focus on a Stable Portion of the Burst

In the HP 8590 series spectrum analyzers, card cage Option 105 permits the analyzer measurement to be time-limited, or gated, to include only the amplitude-stable portion of the burst. Every point in the trace reflects two samples only from the undistorted part of the burst, removing the undesired effects of spectrum analyzer measurement.

The Option 105 time gate adds a switch in the signal processing path of the analyzer. When the switch is closed, the signal passes through to the peak detector and sampler. When the switch is open, no signal is passed to the sampler. The time position of the switch closure, or gate, is easily adjusted from the front panel, using a gate positioning utility.

The spectrum analyzer screens shown in Figure 20 display both the time domain and the frequency domain effects of the time gate. In the pair of spectrum analyzer screens on the top, above, the time gate was positioned to include samples from the entire burst, including the distortion peaks. Using vertical bars, the time gate position is shown in the upper half-screen in time domain.

Since the time gate allows samples of the power in the "ears," the peak detector records a high transient level, including that of the "ears." In the lower left, the frequency domain trace shows these high transient spectra. In the pair of spectrum analyzer screens on the bottom, above, the time gate was positioned to direct samples to the amplitude-stable portion of the burst only. The upper time domain picture in the upper right shows the time gate position near the center of the burst. The lower frequency domain half-screen shows the channel spectrum without the effects of spectrum analyzer transients.

In addition to positioning the time gate, a complete spectrum analyzer setup for a burst adjacent channel power measurement includes a few more optimizations. The sweep time must be long enough to catch at least one burst per trace sample value. This means the sweep time should be set greater than the number of trace values times the burst repetition interval. The HP 8590 instruments have 400 trace values per sweep. The peak detector is used to catch and hold the power of the "on" time of the burst. As in the continuous carrier ACP case, a narrow resolution bandwidth is chosen. Dynamic range is often extended through a downloadable program.

Figure 21, on the next page, is a burst adjacent channel power measurement on a Pacific Digital Cellular (PDC) signal. (Note that PDC was formerly known as JDC, Japan Digital Cellular) The screen on the top shows two traces: the higher level trace with time gating distortion peaks; the lower level trace using the time gate to remove distortion peaks. The HP 85720A JDC measurements personality displays a table of ACP values calculated from the two traces, separating ACP due to modulation from ACP due to transient spectra.

Note that the correct integration equation for transient spectra is calculated with an impulsive noise power integration equation. A total power is sometimes calculated by adding the ACP due to modulation to the ACP due to transients. The total is a result of adding two peak powers with different time characteristics, and should not be considered an RMS adjacent channel power.

Ids & gm vs. Vgs
M161 1542-1

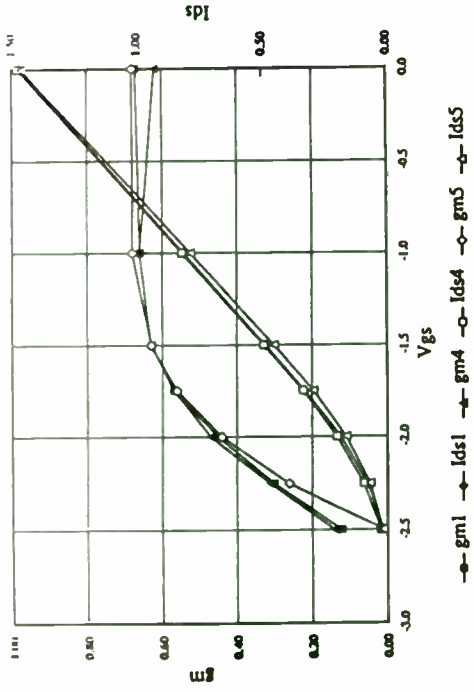


Figure 11: Gm & Ids vs Vgs for Cellular Power FET

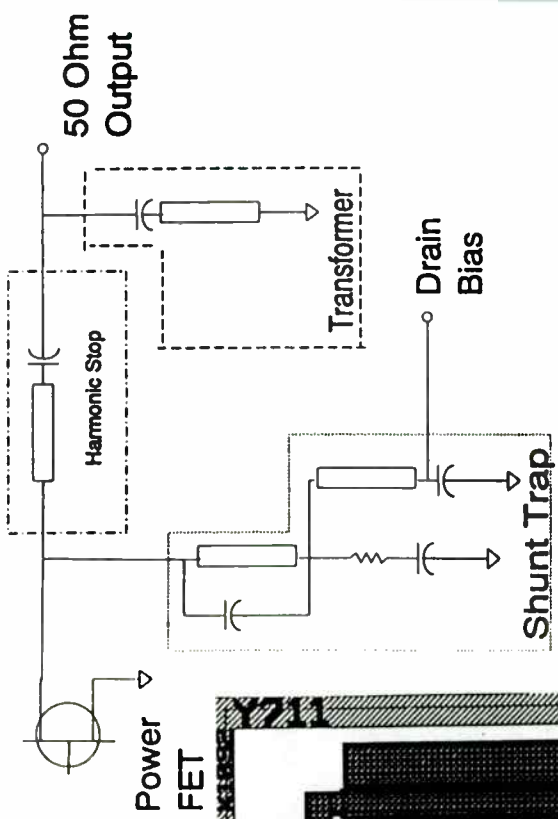


Figure 12: Diplexed Output Circuit

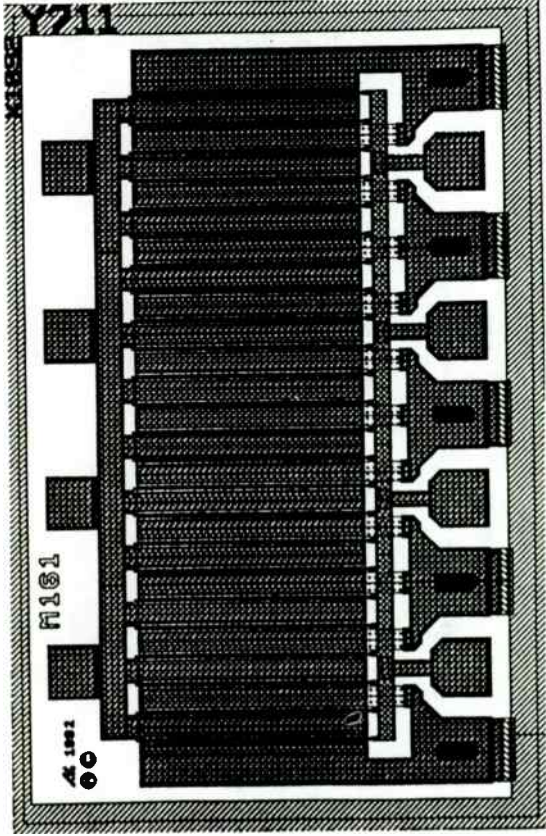


Figure 13: Cellular Power FET

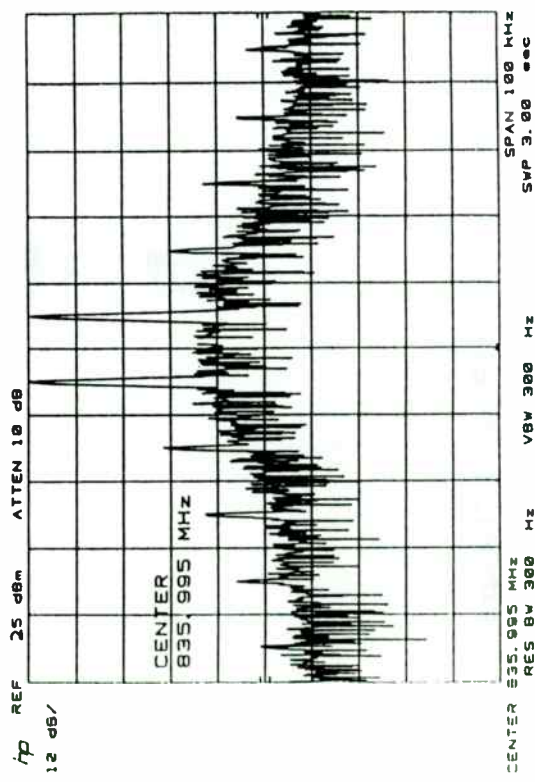


Figure 14: Intermod Performance of Cellular Power FET

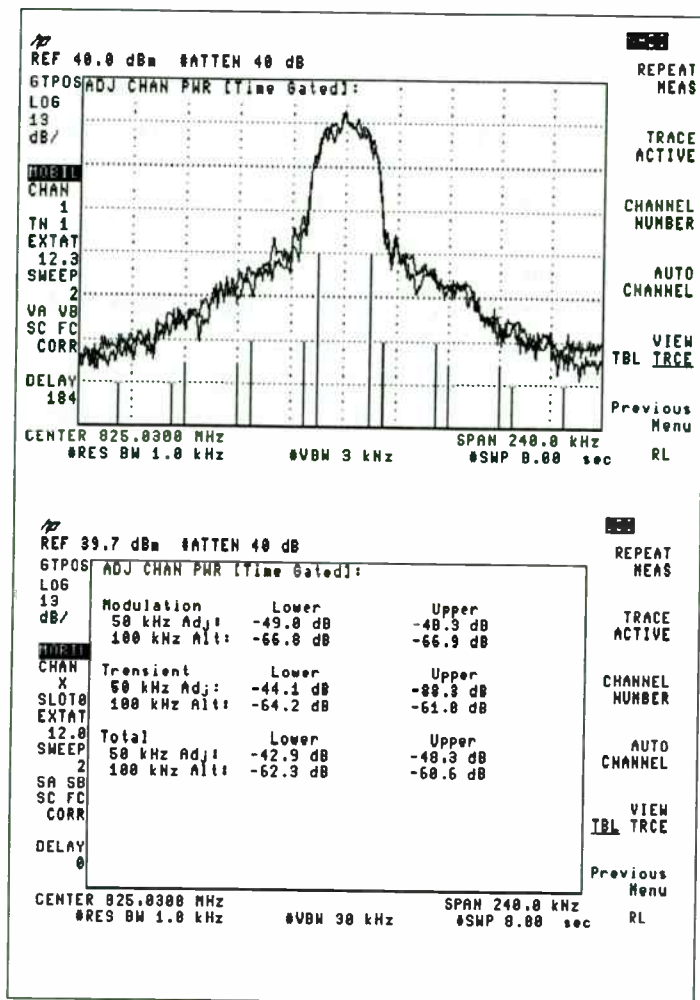


Figure 21: Burst Carrier ACP Test

Both continuous carrier ACP and the intricate burst carrier ACP measurements can be obtained by simple option additions to the HP 8590 series spectrum analyzers. In the card cage, fast sweep and time gate enable ACP in hardware. Specialized ACP tests can be obtained by loading the HP 85718A NADC or HP 85720A JDC personalities. A general adjacent channel power is available as a standard measurement from the spectrum analyzer front panel.

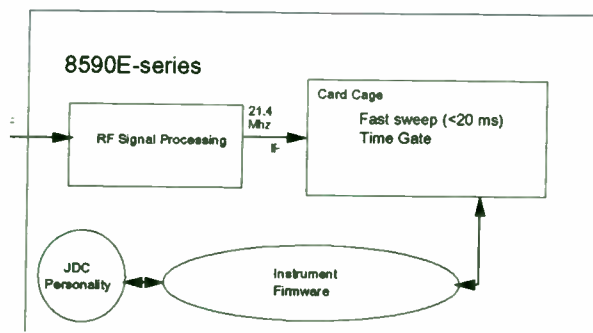


Figure 22: ACP Test Solution

Spurious interference far away from the digital RF transmission frequencies is as important to system performance as adjacent channel interference. Spur searching is a traditional spectrum analyzer measurement, one which the instrument is optimized to perform automatically.

However, there is an important point that is often overlooked. The normal spectrum analyzer auto-sweep time will ensure that continuous spurious signals have the correct amplitude, but burst spurious may be underrepresented or even missed. A spur search for burst spurious signals requires a slower sweep time as given by the equation above. For example, NADC and PDC have a pulse repetition interval of 20 ms. For a resolution bandwidth of 1 MHz, the sweep time must be at least 20 s

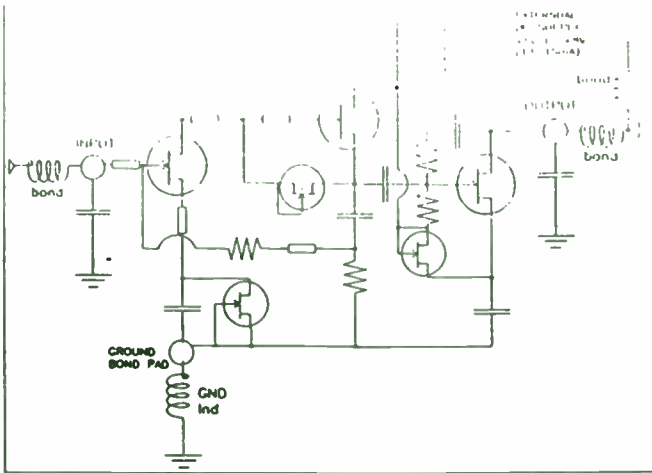
To avoid missing spurs during analyzer sweep:
 Set spectrum analyzer:

$$\text{Sweep time} \geq \text{PRI} \times \frac{\text{Span}}{\text{Resolution Bandwidth}}$$

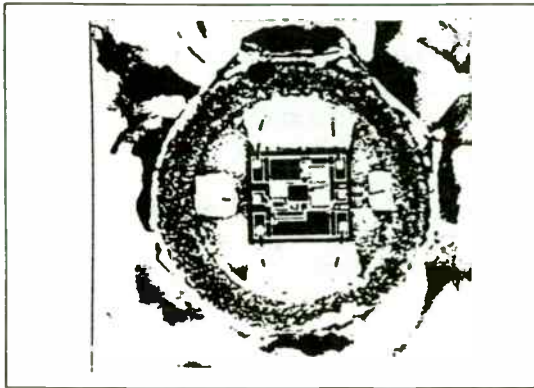
for a 1 GHz sweep.

where:

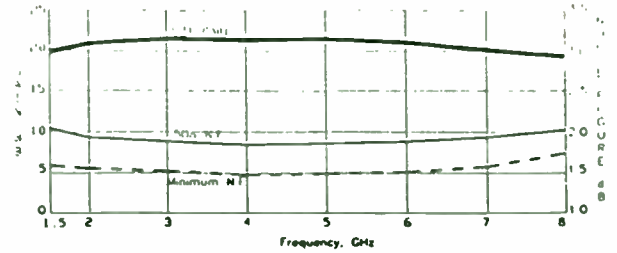
- sweep time = spectrum analyzer sweep time (sec)
- span = the frequency range of the analyzer sweep
- resolution bandwidth = the measurement bandwidth of the analyzer (Hz)
- pulse repetition = time span between bursts (sec)
- interval (PRI)



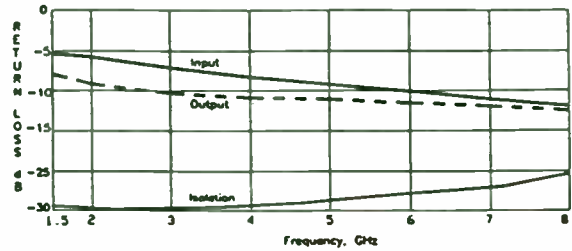
The Hewlett-Packard PHEMT MMIC 3 stage LNA schematic.



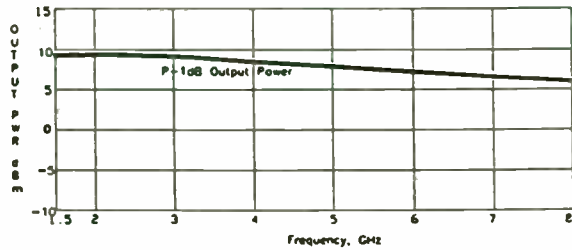
The MMIC LNA Chip in a standard 70 mil surface mount package.



Measured gain and noise figure of the MMIC LNA. Minimum noise figure is obtained for narrow bands with the addition of a .1-2 nH input series inductance.



Measured typical input return loss, output return loss, and isolation of the MMIC LNA. All data measured in a 50 Ohm system. An input match (series inductance) typically improves the input return loss by 10 dB.



Measured typical power output of the MMIC LNA at one dB compression. V_{ds} is +7.0 V for power measurements.

Figure 15: PHEMT MMIC LNA

Figure 16: PHEMT LNA Performance

Electrical Specifications, $T_a=25$ C

Symbol	Parameters and Test Conditions: $V_d=7.0V$, $Z_0=50$	Units	Min.	Typ.	Max.	
Gp	Power Gain (S21[-2])	f=1.5 GHz	dB	20.0	19.0	
		f=4.0 GHz				22.0
		f=6.0 GHz				18.0
		f=8.0 GHz				15.0
NF	50 Ohm Noise Figure	f=1.5 GHz	dB	2.1	2.1	
		f=4.0 GHz				1.9
		f=6.0 GHz				2.0
		f=8.0 GHz				2.1
P1dB	Output Power @1dB Gain Comp.	f=4.0 GHz	dBm	8.0		
IL	Input Return Loss	f=1.5 GHz	dB	-5.0	-5.0	
		f=4.0 GHz				-7.5
		f=6.0 GHz				-10
		f=8.0 GHz				-10
OL	Output Return Loss	f=1.5 GHz	dB	-7.0	-9.0	
		f=4.0 GHz				-12
		f=6.0 GHz				-16
		f=8.0 GHz				-20
Id	Device Current		mA	15.0	20.0	

Table 3: LNA MMIC

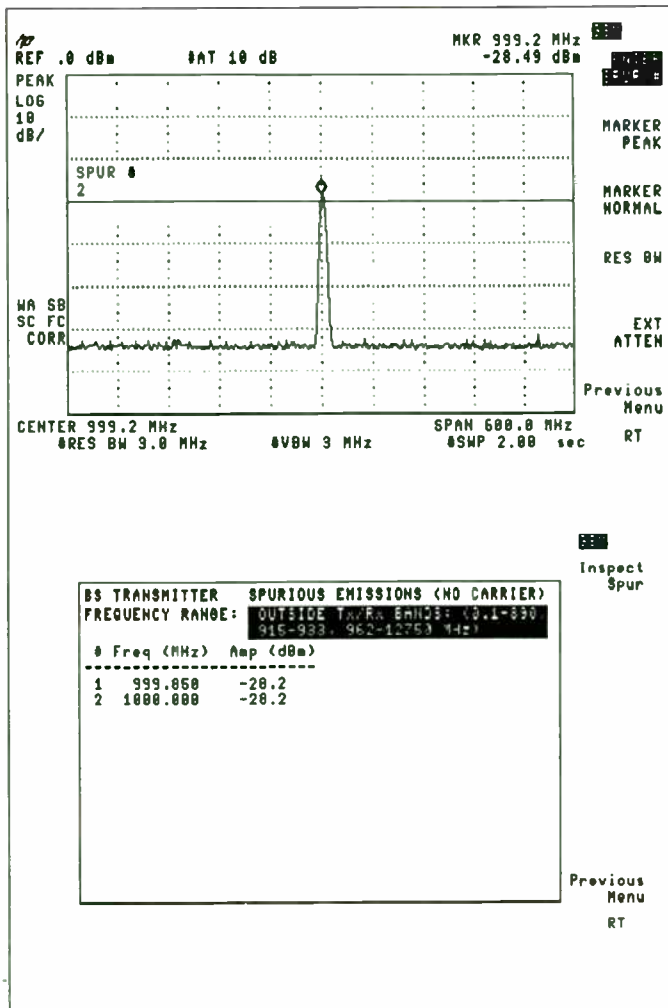


Figure 23: GSM Spurious Emissions Test

Figure 23 shows a spurious emission test performed on the HP 8590 series spectrum analyzer as defined by the GSM standard documents 11.10 and 11.20. The HP 85715A GSM measurement personality performs the complete spur search and highlights in a table any spurs that fail the GSM spec. The user may then examine each spur in the table using a spur inspection utility in the DLP, as shown in the picture on the right.

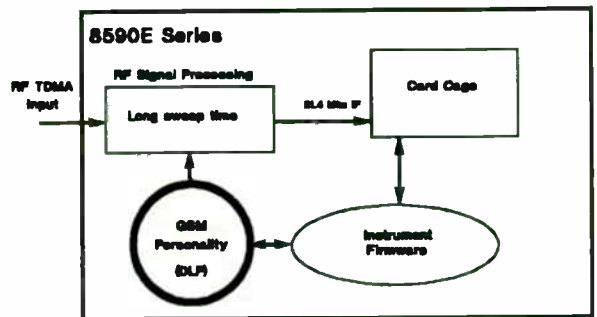


Figure 24: Spurious Emissions Test Solution

The GSM personality is needed to perform a spurious test in the spectrum analyzer. Tailored spur searches for other formats are also available.

Assessing the Quality of Digital Modulation

The last area of digital TDMA communication system test we will examine is assessment of the quality of digital modulation. High quality voice and data transmission rely on accurate digital modulation.

A few simple analog-like modulation quality metrics can be determined independent of the exact digital modulation structure. Two of these are peak frequency deviation and mean frequency error, metrics used in the CT-2 cordless telephone standard. CT-2 employs approximately Gaussian filtered binary phase shift keying (BPSK) to transmit 72 Kbits per second.

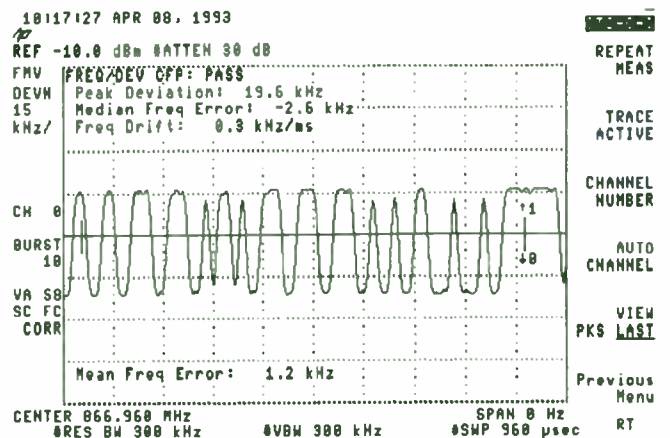


Figure 25: CT-2 Frequency Deviation

LOW COST, HIGH PERFORMANCE RECEIVER FOR WIRELESS APPLICATIONS

By Brian M. Kirk
Applications Engineer: California Eastern Labs

Introduction: With the increase in commercial applications of microwave and radio frequency (RF) equipment, designers have placed a greater demand on consistent performance and low price. The receiver front end described in this paper utilizes low-cost, off-the-shelf technology from NEC/California Eastern Labs to produce a circuit which can be used in many commercial designs.

The starting point for this circuit was the uPC2721GR MMIC down converter. This device includes a mixer with an internal local oscillator (LO) and an intermediate frequency (IF) buffer amplifier on a single MMIC chip. The internal LO is tuned using an external varactor diode. The uPC2721GR also allows the option of using an external oscillator.

In order to achieve an improved noise figure for the circuit, a low noise amplifier (LNA) was added at the RF input to the down converter. The LNA was designed using a discrete low noise GaAs MESFET (NE76038) with a matching structure made using discrete components. The NE76038 is fabricated using ion implantation techniques to improve RF and DC performance, and features a recessed 0.3 micron gate and triple epitaxial technology. Typical noise figures of 1.8 dB can be obtained at 12 GHz, with 7.5 dB associated gain, even in the low cost plastic "38" package. The device is also available in ceramic packages and in chip form.

A low-pass filter was placed after the down-converter to reduce the LO and RF power at the output, and an MMIC buffer amplifier (uPC2710T) was included at the end of the chain to increase the overall system gain. The uPC2710T features 33 dB typical gain up to 1500 MHz in an inexpensive six-pin minimold plastic package. A block diagram of the entire system is shown in Figure 1.

Both the MMIC parts used in this design are manufactured using the NESAT III MMIC process developed by NEC. The process features include:

- * a low-energy, boron-ion base implant which reduces base transit times
- * a 0.6- μ m emitter line width which results in low base resistance and low parasitic capacitances.
- * an arsenic ion-implanted buried layer and thin epitaxial layer to reduce collector resistance.
- * arsenic ion-implanted poly-silicon resistors on a thick SiO₂ layer to reduce parasitic capacitances of the on-chip resistors.
- * PtSi/Ti/Pt/Au metalization and reactive ion etching to permit reliable production of 1- μ m electrode lines and gaps.
- * a silicon nitride passivation layer for scratch and contamination protection.

The peak frequency deviation in the CT-2 signal is measured using a simple FM detector. The screen in Figure 25 shows the demodulated FM on the CT-2 carrier. The HP 85717A CT-2 personality reads out the peak frequency deviation on screen and calculates the median frequency error.

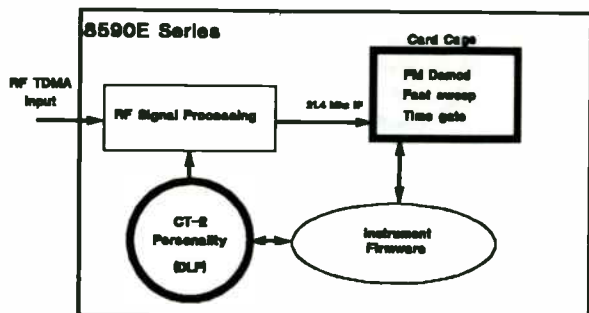


Figure 26: CT-2 Modulation Metrics

With the addition of the FM demodulator, a fast sweep option, and the time gate, the CT-2 spectrum analyzer system hardware is complete. The CT-2 personality provides convenient automatic tests and compares results to CT-2/CAI standard limits.

Most digital modulation metrics do depend on the modulation format, and sometimes even on the exact bit sequence being sent. The two most common digital modulation forms for the larger communications systems are $\pi/4$ DQPSK and GMSK. $\pi/4$ DQPSK is used in the NADC, PDC, and PHP standards. GMSK is the modulation for GSM, DECT, and in a simplified form in CT-2. For $\pi/4$ DQPSK, the key quality metrics are RMS and peak error vector magnitude (EVM), carrier frequency error, and I/Q origin offset. For GMSK, the measures include global phase error and carrier frequency error. In each case, we would like to measure these metrics on any time slot, directly from the RF carrier.

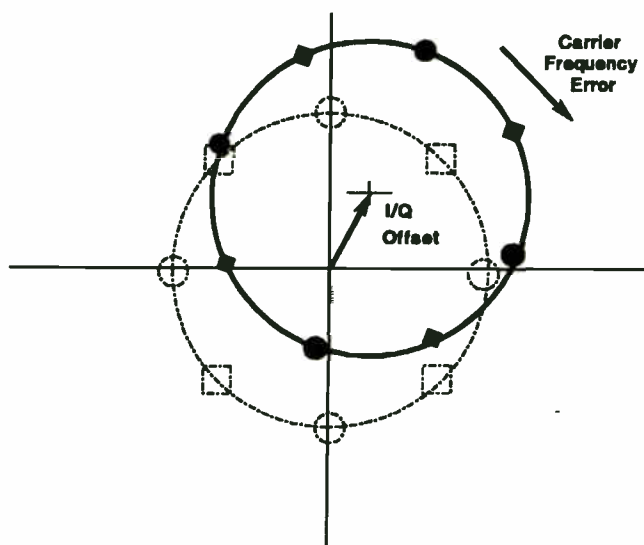


Figure 27: NADC Modulation Metrics

The remaining portion of this section will concentrate on measuring the $\pi/4$ DQPSK form of digital modulation in the NADC-TDMA cellular communication system. Figure 27 shows the decision states of an NADC modulation constellation. A perfectly modulated NADC carrier has a baseband I/Q constellation with eight states, divided into two groups. At each decision point the differential phase and the amplitude of the modulation lands exactly on one of the eight states, after compensation with a root-Nyquist filter. A decision point is the point in time at which the constellation state, or symbol, can be read. An ideal constellation is shown with dotted lines above.

The solid lines show a decision point in a transmission with some I/Q offset and frequency error. A real transmission may have a baseband constellation with some inphase (I) and quadrature (Q) channel imbalance, or DC component. The constellation will be shifted away from the origin, where I and Q are zero. This is I/Q offset. Frequency error is exhibited by a slow rotation of the eight transmitted states about the constellation center. This represents a linear phase gain as time increases.

These process features result in reliable and reproducible silicon MMIC's with cutoff frequencies (f_T) approaching 20 GHz.

Target Specifications: The design goal for this circuit was to produce a low-noise, high-gain receiver front-end. Operating frequency was to be 1800 MHz at the RF input, with a 1700 MHz LO resulting in a 100 MHz IF at the output. A further design goal was that the active parts used should be low cost: less than \$10 (based on 10K piece quantities). The design specs were as follows:

<u>Parameter</u>	<u>LN Amp*</u>	<u>Mixer</u>	<u>Filter</u>	<u>IF Amp*</u>	<u>Overall</u>
Gain (dB)	14	20	-6	32	60
Noise Fig (dB)	1	11	6	3.5	2.5
Sat Power (dBm)	2	5	-	13	13
Inp Ret Loss (dB)	10	-	15	6	10
Out Ret Loss (dB)	8	-	15	12	12
Cost (\$ @ 10K pc)**	\$2.10	\$2.00	-	\$1.70	\$5.70

* LNA specs at 1800 MHz, IF Amp specs at 100 MHz

** Cost of active parts only

Design Approach: Since the MMIC portions of this circuit are fixed in their performance, the design focused on the low noise amplifier. The NE76038 GaAs FET was chosen for its low noise figure, high reliability and low cost. The device was modeled using CAD (Touchstone) and the matching structure was optimized for a 100 MHz bandwidth centered at 1800 MHz. Discrete tuning elements were used with the goal of minimizing noise figure, while maintaining reasonable gain and return loss. The predicted circuit performance was 1.02 dB noise figure with 15.7 dB gain at 1800 MHz. Input and output return loss were predicted to be -9.9 dB and -8.3 dB respectively.

A test circuit for the low noise amplifier was assembled and tested separately from the other components of the receiver. This was done so that the tuning elements could be optimized for minimum noise figure. The test circuit layout with the initial and final values of the tuning elements is shown in Figure 2. 1800 MHz test results obtained from the final circuit were:

Small Signal Gain: 15.2 dB	Noise Figure: 0.6 dB
Input Return Loss: 5.2 dB	Output Return Loss: 3.5 dB

The next stage of the design was to test the low noise amplifier breadboard with the other components of the system. To accomplish this, separate test fixtures were built for each of the components in the chain. Test results on circuits for the downconverter and the IF buffer amplifier were:

<u>Down-Converter: uPC2721GR</u>	<u>IF Amp: uPC2710T</u>
RF=1800 MHz, LO=1700 MHz	Small Signal Gain: 33.5 dB
IF= 100 MHz	Input Return Loss: 9.8 dB
Conversion Gain: 19.5 dB	Output Return Loss: 14.0 dB

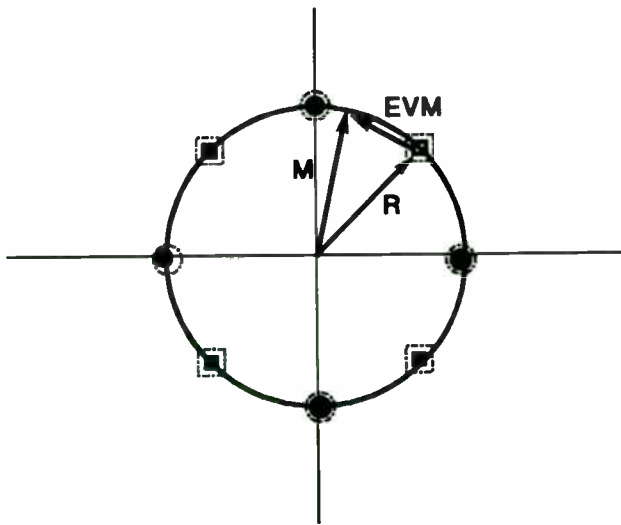


Figure 28: NADC EVM

Error vector magnitude (EVM) is the distance from the ideal state to the measured transmitted state after I/Q offset and frequency error are removed. Amplitude droop, or rolloff, in a burst transmission is also factored out of the EVM. EVM is usually calculated as an RMS value across the symbols in the time slot. The peak EVM achieved at an individual time slot may also be important. A large EVM will cause a symbol to be incorrectly detected, introducing bit errors into the data stream. Voice quality will be degraded.

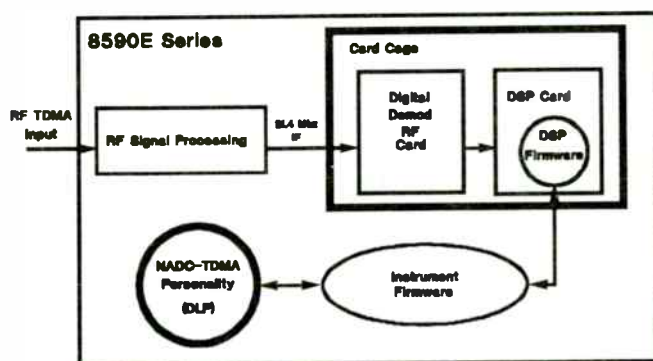


Figure 29: 8590E Digital RF Demodulation System

A new digital RF demodulation capability (digital demod) can be added to the HP 8590 E-series spectrum analyzers for measuring NADC quality. This feature uses digital signal processing to demodulate the digital demodulation. The hardware that must be added to the spectrum analyzer consists of two card cage cards: an RF downconversion

card and a digital signal processing card (DSP). The modulated carrier at the input to the spectrum analyzer is downconverted to the spectrum analyzer IF frequency, 21.4 MHz. The RF downconversion card translates the spectrum analyzer IF to 213 kHz for sampling by a fast ADC. The DSP card receives these samples and processes them using a Motorola 56000 DSP chip dedicated to digital modulation measurements.

The digital signal processing algorithms are contained in DSP firmware on the DSP card. This compact firmware is optimized for fast digital signal processing, taking advantage of the parallel processing available on the 56000 DSP chip. The DSP firmware communicates through the spectrum analyzer firmware. Measurements tailored to NADC are driven through a new NADC personality (the HP 85718B), which provides the user interface to the digital demod system. The NADC personality controls the digital demod system, displays the metrics, and compares the results to NADC specification limits.

The HP 8590 E-series NADC digital demodulator system implements a coherent demodulation for NADC pi/4 DQPSK. The downconverted carrier frequency is recovered from the received signal. The reconstructed carrier frequency is used to downconvert the IF samples to baseband. A root-Nyquist filter is applied to corrected baseband samples to compensate for the transmitter root-Nyquist filter. The measurement algorithm complies with NADC-TDMA standards IS-54, IS-55, and IS-56. A minimum error vector magnitude is calculated after removing frequency error, phase offset, amplitude droop, I/Q origin offset, and amplitude scale mismatch.

To begin an NADC digital demod measurement, the spectrum analyzer is optimized to maximize the accuracy of the results. The spectrum analyzer is tuned to a single fixed frequency (zero span) using the most accurate downconversion tuning (counter lock resolution 1 Hz). Several sweeps are taken to stabilize the downconversion tuning. A wide resolution bandwidth is chosen to minimize phase distortion and amplitude ripple. The NADC measurement resolution bandwidth is 1 MHz. Last, the signal level is set to read 2 dB below the top of screen. This signal level maximizes the dynamic range available to the fixed point 56000 DSP processor for accurate calculation.

The signal is then sampled at 1.458 MHz, 60 times the NADC symbol rate of 24.3 KHz. The sample record sent to the digital demod DSP card can be up to half a frame in length, or 3.33 ms.

The low pass filter test circuit was adjusted to reduce the LO and RF power level at the output to 10 dB below the IF signal level. At this time it became apparent that even though the filter had been designed to be somewhat lossy, the oscillator power being reflected back into the mixer of the uPC2721GR was causing an unacceptable level of spurious signals. A 3 dB pad was inserted between the filter and the mixer of the uPC2721GR, and this minimized the spur problem. The small signal gain of this line-up was 59.8 dB - close enough to the design goal to go to a final layout.

Final Layout: The final circuit layout is shown in Figure 3. The pad between the mixer and the filter was increased to 6 dB in the final design to further improve the spur performance at the output. The circuit was etched on Duroid 5880 substrate. Outside dimensions are 1.8 by 1.25 inches. The gain and noise figure performance of the final circuit versus input frequency are shown in Figure 4. In addition, the following data was taken:

Input Return Loss (1800 MHz): 6.0 dB
Output Return Loss (100 MHz): 14.2 dB
Power (1 dB compressed gain): 11.2 dBm

Conclusion: The drive to reduce costs for commercial RF and microwave products does not mean that performance must be sacrificed. Low-cost, off-the-shelf discrete and MMIC parts from NEC/California Eastern Labs can be used to provide reliable circuits which deliver top shelf performance for commercial applications.

Acknowledgements: Many thanks to Huy Tran for his efforts in the fabrication, assembly, tuning and testing of the circuits described in this article.

For further information please contact Brian M. Kirk, Applications Engineer at California Eastern Labs, (408) 988-3500.

Digital signal processing of the sample record begins with synchronizing the time of the sample record to the desired time slot. Next, a sample record focused on the desired time slot is taken, sampling synchronously with the symbol rate of 24.3 kHz. The sample record is processed to detect the bit sequence transmitted in the time slot. Provided the detected bit sequence has no errors, a perfect reference signal can be generated. The reference signal is the ideal baseband modulation trajectory for the exact bit sequence that was transmitted. The reference signal is time matched with the decision points of the measured samples. The reference signal is subtracted from the measured samples. The difference is the residual error in the real transmitted signal. The residual error is processed to separate magnitude and phase error components, such as carrier frequency error and error vector magnitude.

Note that a complete error vector magnitude measurement may be made off-the-air from the transmitted carrier. The measurement is automatically focused on the desired time slot.

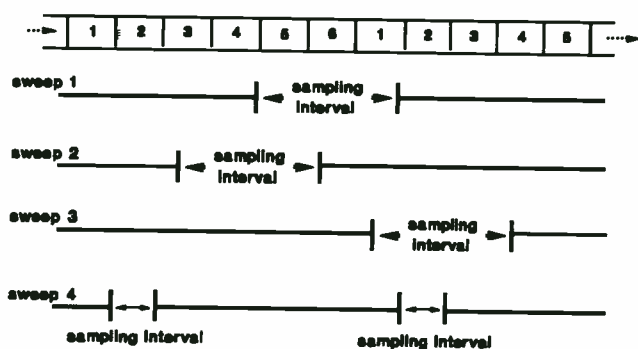


Figure 30: Synchronizing the Measurement

Let us examine the measurement process in more detail, starting with the synchronization of the measurement interval to a user-specified time slot.

A sampling trigger signal is generated on the digital demod cards at the NADC frame rate, 40 ms. The sampling trigger is sometimes called a frame trigger. This trigger frequency is locked to the 10 MHz frequency reference of the spectrum analyzer. The sampling trigger rate is not exactly synchronous to the transmitted frame rate. If, however, the transmitted frame rate is close to nominal, the rate of drift of the sample window relative to the stream of time slots is very slow.

Initially, the NADC digital demod trigger places the sample window at a random offset relative to the desired timeslot, as in sweep 1, 2, and 3 pictured in Figure 30. Remember that sampling intervals occur at the frame rate. To synchronize the sample window, the sample trigger must be offset to place the beginning of the sample window just before the desired time slot. The time slot length is then shortened to the appropriate length. Sampling sweep 4 has been synchronized to time slot 2, focusing the sample window on time slot 2.

The synchronization process requires the digital demod system to find the desired sync word in a stream of transmitted time slots. The sample window is set to capture the longest record of transmitted bits, half a frame or three NADC time slots. A long sample record is taken, and the transmitted bits are detected. The DSP processor then matches a specified sync sequence to the detected bits and determines the time position of the best match. In the NADC system, this requires correlating the 28 bit long sync word with over one thousand detected bits.

Note that if the desired sync sequence is not found in the first half-frame, the sample trigger is repositioned to capture the other half-frame in the sample window. A complete frame is searched to find the sync word.

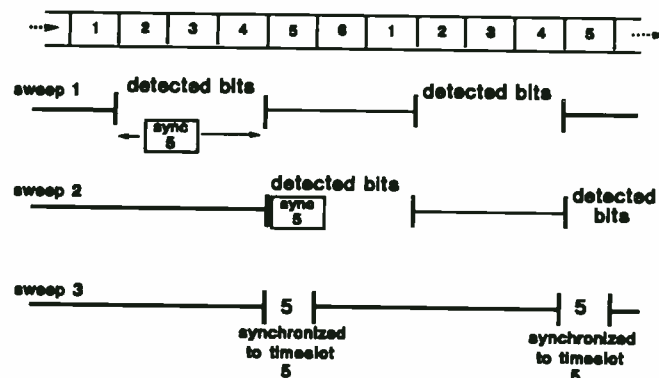


Figure 31: Frame Acquisition

In Figure 31, the digital demod system is synchronizing to NADC sync word five. The sync word is not found in the first half-frame examined. The next half-frame contains the sync sequence near the beginning of the sample record. Knowing the original position of the sampling trigger and the time position of the desired sync sequence in the sample record, the DSP processor can easily determine the time offset to reposition the sample window. The sampling trigger is offset in time from its position in sweep two, placing the sample window at time slot five. The

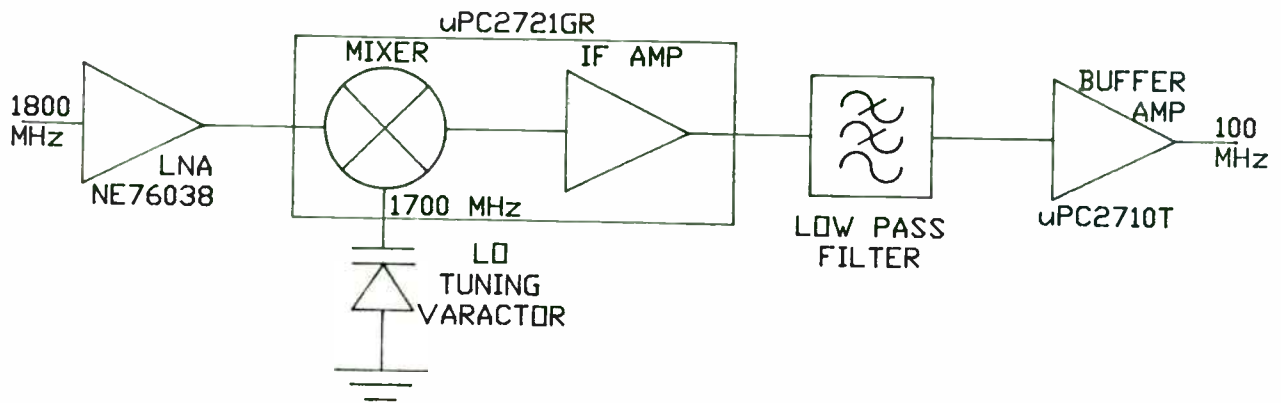


Figure 1: Block Diagram

- PART LIST:**
- 1 100 pF CHIP CAPACITOR
 - 2 0.9 pF CHIP CAPACITOR
 - 3 L1: \varnothing 0.095, \varnothing 0.020, 2T (INCH)
 - 4 NE76031
 - 5 20 pF CHIP CAPACITOR
 - 6 L2: 0.6 nH MICROSTRIP LINE--- 0.1 LENGTH AND 0.01 WIDTH.
 - 7 220 nH CHIP INDUCTOR
 - 8 10000 pF CHIP CAPACITOR

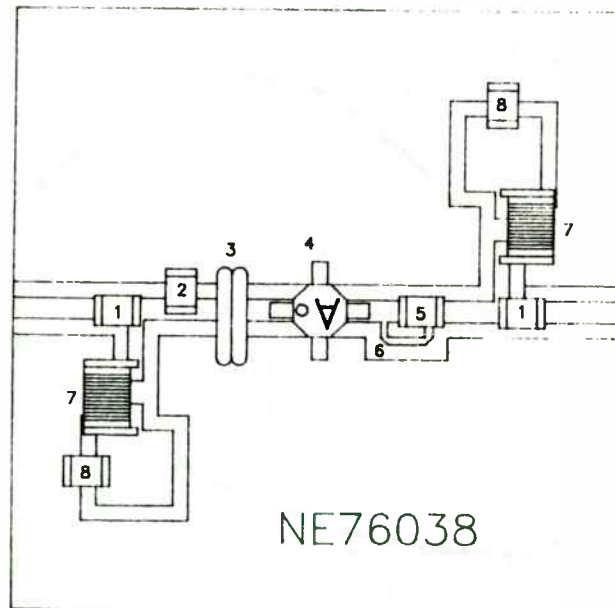


Figure 2: NE76038 LNA

sample window is shortened for metric measurement on time slot five.

Since the sampling trigger may not be locked to the frame clock of the communication system, the position of the sampling trigger can slowly drift away from time slot five over time. The NADC digital demod system will track this position drift at every measurement. If the drift exceeds a target window, the sampling trigger is automatically repositioned.

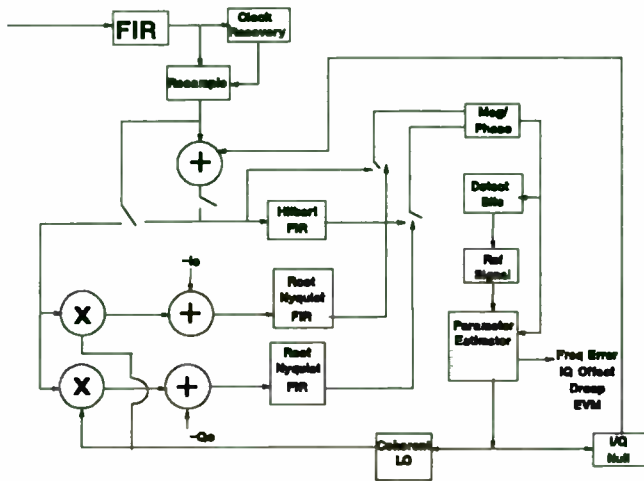


Figure 32: NADC Coherent Demodulation

The synchronized sample record is fed into the NADC coherent demodulation algorithm. A simple block diagram of the algorithm is in Figure 32. The samples are digitally downconverted to baseband in two passes. The first pass uses an initial guess at the correct downconversion frequency. The symbol clock is recovered, and samples are repositioned in time to place one sample per symbol at a decision point. Remember that the decision point is the point in time at which the magnitude and phase of the modulation are at a constellation state where the symbol may be read. In pass 1, the quadrature component is extracted using a Hilbert FIR filter, and sample magnitude and phase are calculated.

Bits are detected from the differential phase of the samples at the decision point. A reference signal is generated. Correction parameters for frequency error, phase offset, amplitude scaling and droop, and I/Q offset are extracted from the difference between the reference signal and the measured samples.

In pass 2, inphase and quadrature coherent local oscillators are generated from the pass 1 corrections to downconvert the measured samples to baseband. The

coherent local oscillators are adjusted to remove frequency error, phase offset, amplitude scaling droop, and I/Q offset from the sampled signal. Root-Nyquist filtering is applied to compensate for the transmitter root-Nyquist filter. The magnitude and phase are recalculated. Bits are re-detected and compared to results in pass 1. A new reference signal is created, and residual correction parameters are found. A final correction is applied to the sample record to remove residual traces of frequency error, phase offset, amplitude scaling and droop, and I/Q offset. The RMS and peak EVM are extracted from the final corrected signal and the pass 2 reference signal.

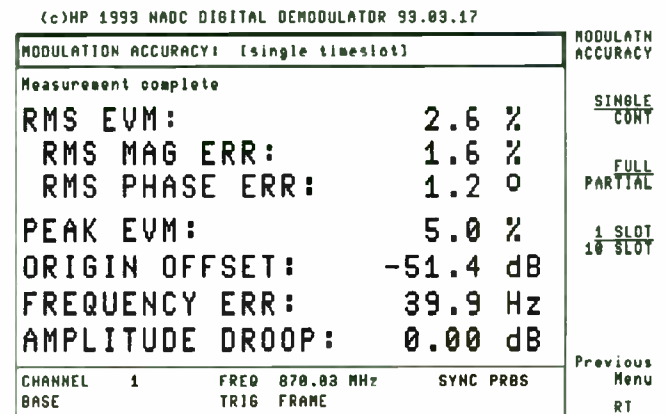


Figure 33: NADC Modulation Metrics

Figure 33 shows some sample output from the NADC digital demodulation system. A summary of metrics is available. RMS error vector magnitude is shown with the magnitude and phase error components. Peak EVM in the time slot is also shown. Carrier frequency error, I/Q offset, and amplitude droop are displayed. Although the initial setup time for this measurement is about 15 seconds, the update rate can be 0.5 to 2 seconds, depending on the exact measurement mode selected. This permits fast feedback on the performance of the NADC-TDMA system.

A baseband modulation pattern diagram displays the modulation trajectory as it travels between symbol states. An example of a pattern diagram is in Figure 34. This is the fully corrected trajectory, reflecting only EVM errors. The corresponding EVM value is shown, so that the user can correlate EVM performance with the appearance of the constellation and trajectory pattern. Gross EVM errors at a single symbol are seen in the pattern diagram. A constellation diagram, showing only the samples at decision points, is also available.

PART LIST:

- 1 100 pF CHIP CAPACITOR
- 2 0.9 pF CHIP CAPACITOR
- 3 L1: #0.085, #0.020, 2T
- 4 NE76038
- 5 20 pF CHIP CAPACITOR
- 6 L2: 0.8 nH MICROSTRIP LINE--- 0.100 LENGTH AND 0.010 WIDTH
- 7 220 nH CHIP INDUCTOR
- 8 10000 pF CHIP CAPACITOR
- 9 22 pF CHIP CAPACITOR
- 10 UPC2721
- 11 0.5 pF CHIP CAPACITOR
- 12 2 pF CHIP CAPACITOR
- 13 47000 Ohm CHIP RESISTOR
- 14 SY168 VARACTOR DIODE
- 15 50 Ohm CHIP RESISTOR
- 16 270 Ohm CHIP RESISTOR
- 17 L3: #2.0mm, #0.3mm, 10T
- 18 1000 pF CHIP CAPACITOR
- 19 220 Ohm CHIP RESISTOR
- 20 50 Ohm CHIP RESISTOR
- 21 33 Ohm CHIP RESISTOR
- 22 14 pF CHIP CAPACITOR
- 23 L4: #4.0mm, #0.4mm, 3T
- 24 18 pF CHIP CAPACITOR
- 25 UPC2710TE3 PACKAGE
- 26 1.0 uH CHIP INDUCTOR

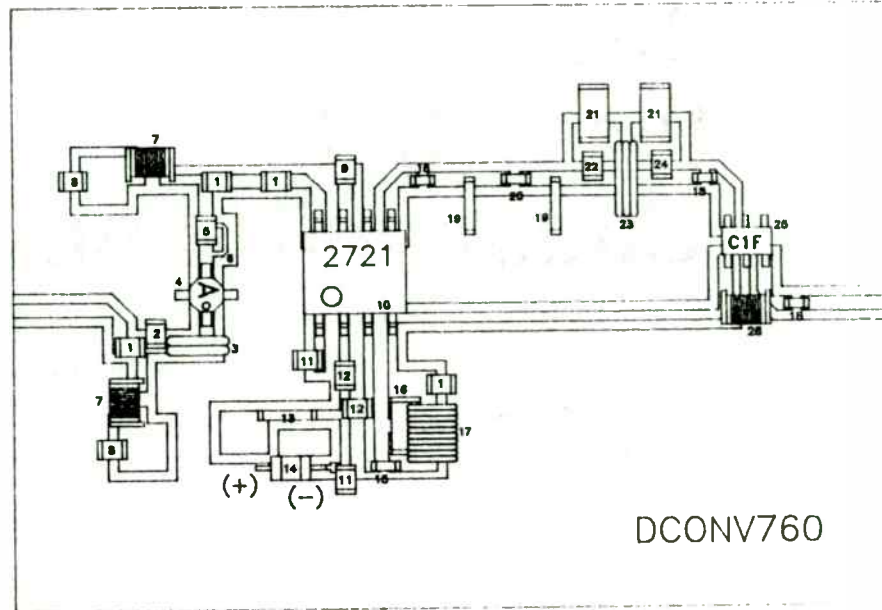


Figure 3: Overall Down-Converter Layout

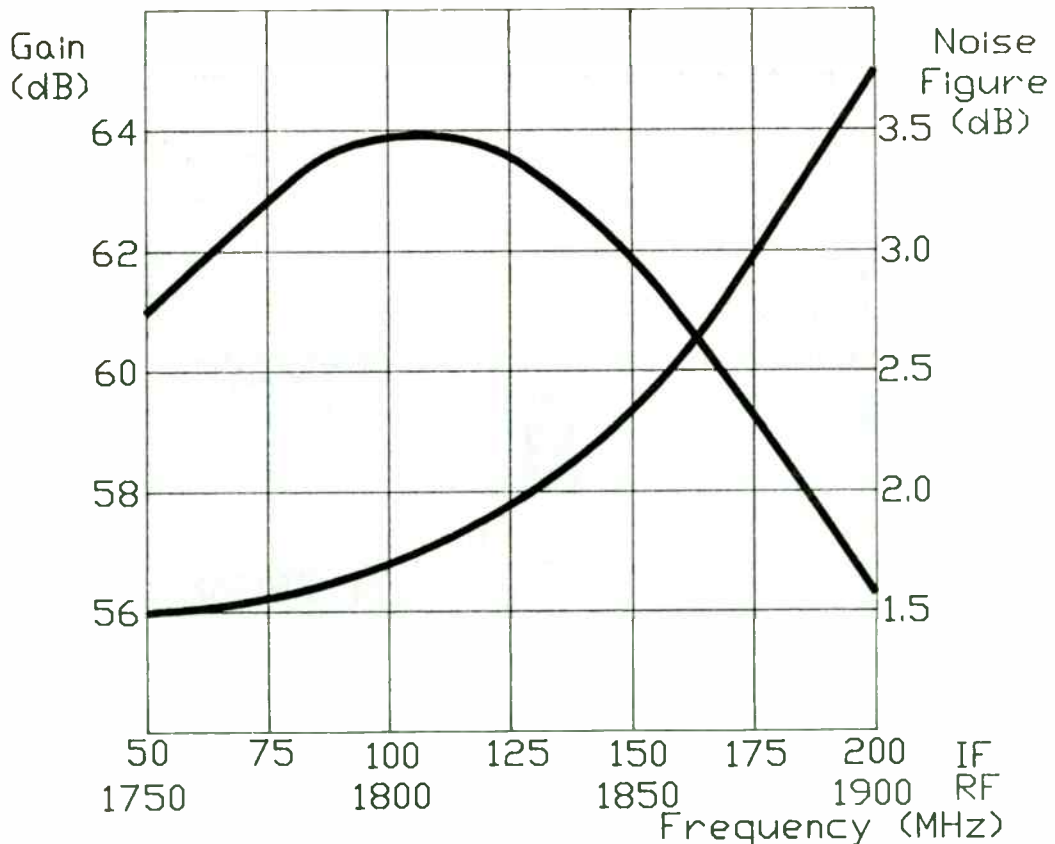


Figure 4: Gain & Noise Figure
(Local Oscillator: 1700 MHz)

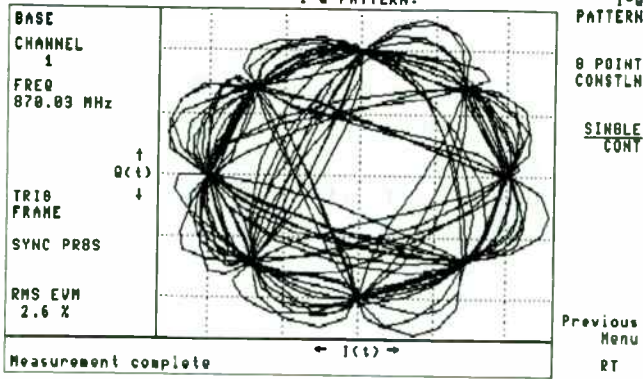


Figure 34: NADC I/Q Pattern Diagram

	Digital Demod System Specs	NADC System Performance Limits
EVM Accuracy: Max EVM Floor Typ EVM Floor	+1.7 % ± 1.3 %	12.5 %
Freq Accuracy: • freq ref accuracy x carrier ± 40 Hz typ	± 18 Hz ± 40 Hz typ	± 200 Hz offset (mobile) .25 ppm base station
I/Q Origin Offset Accuracy	.5 dB origin offset for offsets > -40 dB	-20 dBc max (mobile)

Figure 36: Digital Demod System Specs

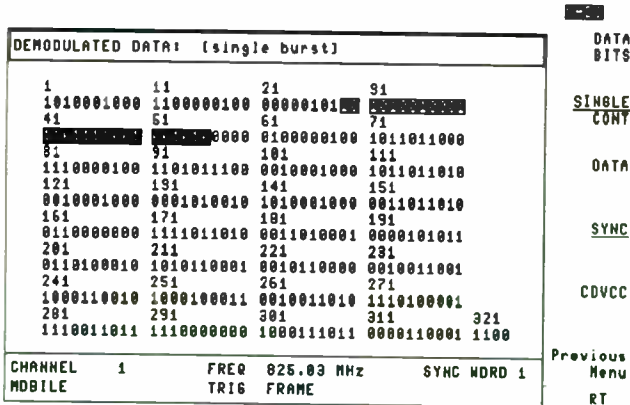


Figure 35: Detected Bits

The detected bits of the time slot can be displayed. Transmitted data, the sync word, or the color code may be highlighted. This screen shows a burst sent from a NADC mobile phone in test mode in time slot 1. Sync sequence 1 is highlighted.

Compare the accuracy of the HP 8590 E-series NADC digital demod measurements to NADC system limits. An EVM accuracy is specified in two parts: a maximum EVM floor and a positive/negative measurement repeatability. The maximum EVM floor specifies the smallest RMS EVM that the spectrum analyzer can measure. The maximum EVM floor also defines the maximum positive offset added to the true RMS EVM of the signal by the spectrum analyzer. The measurement repeatability specifies the range of displayed values that are possible while measuring a stable EVM source. For example, if the on-screen RMS EVM reading is 6%, the actual RMS EVM may be as low as 4.3% and not larger than 6%, due to the maximum EVM floor of 1.7%. The next measurement could have an on-screen reading as high as 7.5% or as low as 4.5%, due to the measurement repeatability of +1.5%. If measurements are averaged, the measurement repeatability will average to zero.

The frequency accuracy specification separates the frequency error due to spectrum analyzer downconversion and the digital signal processing limitations from the error due to the accuracy of the frequency reference. This allows users to ascertain the frequency error with an external reference. The basic frequency accuracy of the digital demod is +-18 Hz, plus the frequency reference error at the carrier frequency. For example, PDC users may want to use a rubidium frequency standard to improve the total frequency error accuracy. With the option 004 HP 8590 high-stability reference, the typical frequency accuracy will be +-40 Hz, immediately after calibration of the frequency reference.

Technologies for Cellular Communications

Session Chairperson: Keith Kaczmarek, NEXTEL Communications, Inc. (Fleet Call) (Lafayette, CA)

Power Products for Cellular Telephone Handsets, **William Mueller**, Hewlett-Packard Co., Communications Components Division (Newark, CA).....**160**

Cellular and PCS TDMA Transmitter Testing with a Spectrum Analyzer, **Larry Nutting**, Hewlett-Packard Co., Microwave Instruments Division (Santa Rosa, CA).....**172**

Error-Free Mobile Data Communications: Principles and Protocols, **Parviz Yegani**, IBM Networking Systems (Research Triangle Park, NC).....**179**

GaAs MESFET Direct Quadrature Modulator Integrated Circuit for Wireless Communications Systems, **Chris Fisher**, RF Micro Devices, Inc. (Greensboro, NC).....**200**

System Aspects and RF Component Design for European Mobile Communication System, **Dr. Ing. Vinod Kumar**,* Alcatel Radiotelephone (Colombes, France).....**205**

**Paper presented by Eric Botharel, Alcatel Radiotelephone (Colombes, France)*

The I/Q origin offset can be measured to an accuracy of 0.5 dB down to a floor of -40 dBc.

EVM measurement error comes from both hardware and firmware limitations. The digital signal processing algorithms have an accuracy defined by the filters and algorithms used and by the limits of the fixed point 56000 DSP processor. For example, the ripple of the FIR filters contributes to error in calculating the magnitude component of the EVM. The spectrum analyzer also has some amplitude ripple across the NADC signal bandwidth. The spectrum analyzer frequency accuracy adds to phase and frequency measurement errors. Carrier frequency error accuracy is dominated by the accuracy of the frequency standard. Spectrum analyzer frequency stability is the main limitation of the EVM measurement accuracy. The phase noise of the downconversion adds directly to the EVM measured. The maximum EVM floor value is derived from the RMS phase noise level. The measurement repeatability is derived from the standard deviation of the phase noise distribution.

Conclusions

We have seen that the spectrum analyzer provides a platform for time domain, frequency domain, and modulation domain testing of digital RF communications

Measurement Personalities	Hardware Options
86715A GSM Measurements	004 Precision Freq Reference
86717A CT2-CAI Measurements	010 Tracking Generator
86718A NADC-TDMA Measurements	101 Fast Time Domain Sweep
86720A JDC Measurements	105 Time Gate
86718B NADC with Digital Demod Measurements	110 CT2 Demodulator
86719B Digital Radio Measurements	151 + 161 Digital Demod for NADC
	060 Improved Amplitude Accuracy for NADC/JDC

Figure 37: Options Used in Examples

systems. The analyzer may easily be configured to accommodate solutions tailored to many current formats, including GSM, DCS-1800, CT-2, DECT, NADC, and PDC. The spectrum analyzer platform also accommodates future upgrades to expand capabilities to new formats.

Figure 37 is a summary list of the hardware and software solutions that have been presented.

References

1. R. Birgenheier, "Measuring the Modulation Accuracy of pi/4 DQPSK Signals for Digital Cellular Transmitters," Hewlett-Packard Journal, April 1991, pp 73-82.
2. H. Chen, "Time-Selective Spectrum Analysis (TSSA): A powerful tool for analyzing TDMA communication signals," Hewlett-Packard RF & Microwave Measurement Symposium, Signal Analysis Division, 1992.
3. EIA/TIA IS-54, "Cellular System Dual Mode Mobile Station-Base Station Compatibility Standard," Telecommunication Industry Association, April 1992.
4. EIA/TIA IS-55, "Recommended Minimum Performance Standards for 800 MHz Dual Mode Mobile Stations," Telecommunications Industry Association, December 1991:
5. EIA/TIA IS-56 "Recommended Minimum Performance Standards fo 800 Mhz Base Stations Supporting Dual Mode Mobile Stations," Telecommunication Industry Association, March 1991.
6. J. Gorin, "Make Adjacent-Channel Power Measurements," Microwaves and RF, May 1992, pp 137-143.

Power Products for Cellular Telephone Handsets

William Mueller
Hewlett Packard Communications Components Division



Power Products for Cellular Telephone Handsets

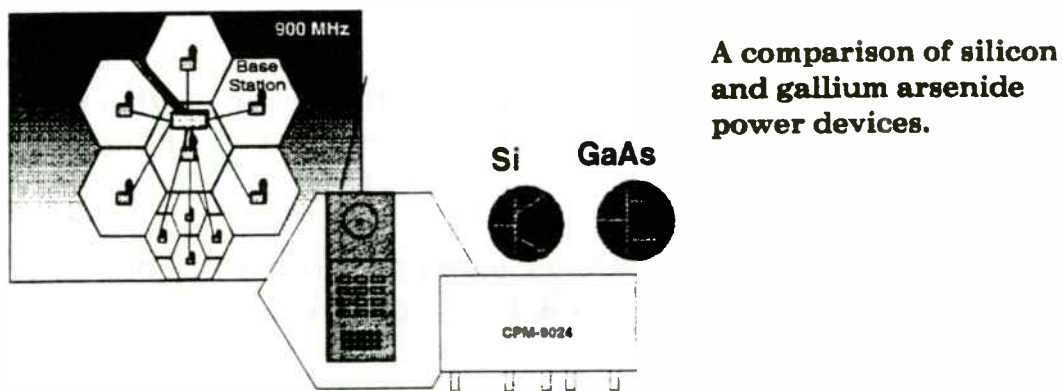


Figure 1. Power Products for Cellular Telephone Handsets.

This paper compares Gallium Arsenide Field Effect Transistor and Silicon Bipolar Junction Transistor options for the output device in 900 MHz cellular telephone handsets.

7. D. Hoover, "An Instrument for Testing North American Digital Cellular Radios," *Hewlett-Packard Journal*, April 1991, pp 65-72.
8. I-ETS 300 131 "Radio Equipment and Systems (RES); Common air interface specification to be used for interworking between cordless telephone apparatus in the frequency band 864.1 MHz to 868.1 MHz, including public access services." European Telecommunications Standard Institute, France, April 1991.
9. MPT 1375 "Common Air Interface Specification," Department of Trade and Industry, London, May 1989.
10. L. Nutting, "Cellular and PCS TDMA Transmitter Testing with a Spectrum Analyzer," *Hewlett Packard RF and Microwave Measurement Symposium, Signal Analysis Division*, 1992.
11. RCR STD-27A "Japan Digital Cellular Telecommunication System Standard," Research and Development Center for Radio Systems, Japan, January 1992.

Cellular Handset Block Diagram

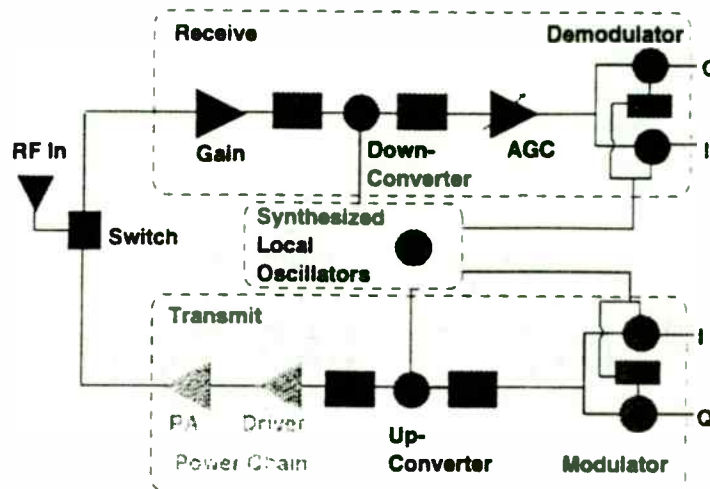


Figure 2. Cellular Handset Block Diagram

The block diagram shows a generalized architecture for a cellular handset. The products we are concerned with in this paper are the Power Amplifier and its' Driver. They are represented by the last two "triangles" in the transmit chain. The task of the power chain is to increase the magnitude of the modulated signal to the desired level for broadcast. The architecture shown is generalized, and many variations are possible, especially in the area of the modulator and up-converter.

Practical Applications of a Low Cost Low Noise GaAs PHEMT MMIC for Commercial Markets

by

A. Ward

Hewlett-Packard CMCD Applications Department
Richardson, TX.

and

H. Morkner

Hewlett-Packard CMCD R&D Division
Newark, Ca.

ABSTRACT

A high performance low cost surface mount ceramic packaged GaAs MMIC for the 1.5 to 8 GHz frequency range is described. The MMIC uses .15 μ gate PHEMT devices, self biasing current sources, source follower interstage, resistive feedback and internal impedance matching to produce a state-of-the-art amplifier. Using a minimum of external components, the MMIC provides a nominal 20 dB gain from 1.5 to 8 GHz, a 2 dB noise figure and a nominal power output of +5 dBm from a single dc power supply. With a simple series inductor, the noise figure can be lowered to 1.6 dB over a smaller bandwidth. Working circuits for various commercial applications are presented along with actual test results.

INTRODUCTION

A GaAs monolithic microwave integrated circuit low noise amplifier has been designed for use in the numerous commercial applications in the 1.5 to 8 GHz frequency range¹. Typical markets include GPS at 1.5 GHz, PCN at 1.9 GHz, MMDS at 2.1 GHz, ITFS at 2.5 GHz, ISM at 2.4 GHz and 5.8 GHz, TVRO at 4 GHz and

instrumentation in the 1.5 to 8 GHz frequency range.

The MMIC includes internal impedance matching and integrated biasing allowing simplified low noise amplifier design eliminating the numerous components normally required for a discrete low noise amplifier design. The MMIC delivers an F_{min} within a dB of a typical discrete design in a fraction of the space. The MMIC is available in a low cost ceramic package and is now available as the Hewlett-Packard MGA-86576.

The performance of the MMIC as a low noise amplifier will be described. Other special applications such as a variable gain amplifier and active mixer will also be addressed.

DESIGN

The schematic diagram shown in Figure 1 is a lumped element representation of the MMIC. The MMIC consists of two gain stages, an interstage source follower stage, three current sources, two resistive feedback networks, several bias resistors and bypass capacitors. The current sources insure that each PHEMT stage is biased at 25% of I_{dss} . Process variations effect both

Cellular Handset Power Requirements





 AMPS	 ADC	 JDC	 GSM
Analog	Digital ($\pi/4$ DPQSK)	Digital ($\pi/4$ DPQSK)	Digital (0.3 GMSK)
824-849 MHz 0.6W no IM spec	824-849 MHz 0.6W IM3<-26 IM5<-35 IM7<-40	810-826 MHz 1477-1489 MHz 1501-1513 MHz 0.6W linearity equivalent to ADC	890-915 MHz 3.5W peak (577 μ sec 10%) no IM spec

Figure 3. Cellular Handset Power Requirements.

Cellular can be divided into three major segments, with differing requirements for the handset power transistor.

North American Cellular consists of both an installed analog system (AMPS) and a developing digital system ADC (American Digital Cellular). At present the digital portion contains many factions, including NAMPS, CDMA users, ETDMA users, and others. North American cellular systems use a handset broadcast frequency range of 824 to 849 MHz.

AMPS requires +28 dBm (0.63 Watts) of CW output power, but places no linearity or intermodulation constraints on the power amplifier. The output transistor is usually expected to provide a power added efficiency in the 45% range.

ADC in general uses $\pi/4$ QPSK modulation, and has a linearity requirement that translates into an intermodulation specification on the output part of -26 dBC on the third order products, -35 dBC on the fifth order products, and -40 dBC on the seventh order products, all relative to two +25 dBm output signals. System operation is essentially pulsed.

JDC (Japan Digital Cellular) is the new Japanese digital system. JDC uses $\pi/4$ QPSK modulation. Handset broadcast frequencies are 810 to 826 MHz for the 800 MHz system, and 1477 -1489 MHz and 1501 - 1513 MHz for the 1500 MHz system (metropolitan Tokyo and Osaka; also called MCA or Multi-Channel Access). The linearity and power requirements are essentially the same as for ADC use. In general, the same power transistors can be used to meet both JDC and ADC requirements.

GSM (Group Speciale Mobile) is the new European system, replacing many previous non-compatible analog systems that were similar to AMPS, NMT, etc. GSM uses 0.3 GMSK modulation. The output requirement is for 3.5 watts of peak output power with a 577 μ sec, 10% duty cycle pulse. This system does not have the linearity requirement of ADC or JDC. GSM uses a handset broadcast frequency range of 890 to 915 MHz.

the FET and current source simultaneously resulting in a constant device I_{dss} producing devices with very repeatable RF performance. .

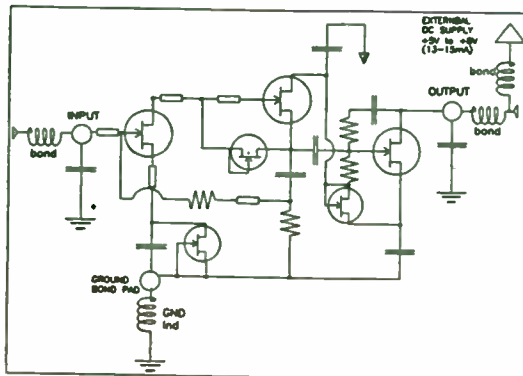


Figure 1. MMIC Schematic Diagram

An advantage of the PHEMT process is the inherent low knee voltages which allow the FET stages to be connected in series to share the device current. This results in a low current MMIC that operates from a supply voltage of only 5 volts.

PERFORMANCE: MMIC VS FET

The MMIC offers several advantages over a discrete FET design. The primary advantage of the MMIC is in the bias configuration. Whereas a typical discrete FET amplifier design may use active biasing to set the bias point, the MMIC requires only a simple RF choke to feed in bias from a 5 volt power supply. This minimizes the board space required to bias the device by eliminating 10 to 15 components. The internal current sources in the MMIC keep the device current bias in a fairly narrow window which results in very repeatable RF performance.

A second advantage of the MMIC is that the input is partially matched to 50Ω making the MMIC easier to match than the generally high impedances associated with the unmatched FET. As an example at 4 GHz, the S_{11} of the MMIC is less than 0.5 while Γ_{opt} is less than 0.4. Typically, the S_{11} and Γ_{opt} of the unmatched FET are much higher at 4 GHz. The lower

input impedance generally means it is easier to achieve a wide bandwidth with a low tolerance matching structure. Even with no input matching, the 50Ω noise figure is about 2 dB. With a small amount of inductance in the input network, it is possible to achieve device noise figure as low as 1.6 dB.

A third advantage of the MMIC is that its gain is equivalent to a two stage FET amplifier. This has additional advantages in the form of decreased component count and decreased board space required.

The disadvantage is its inherently higher noise figure. The MMIC noise figure is generally about 1 dB higher than the typical low noise PHEMT device. This is due to the resistive loading and feedback inherent to the design. For most applications, this may not be a problem. The nominal 2 dB noise figure does make the MMIC an ideal first stage for most applications and an ideal second stage device in a very low noise amplifier.

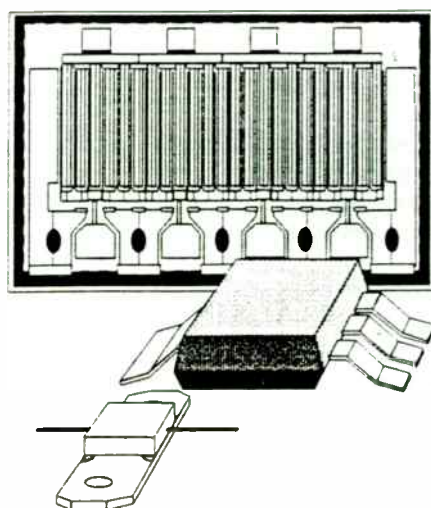
APPLICATION

BIAS DECOUPLING NETWORKS

Biasing the device simply requires the use of an RF choke to supply 5 volts to the output terminal. The RF choke at microwave frequencies can be in the form of a high impedance microstripline properly bypassed at the power supply end. The optimum length would be a quarterwave at the desired frequency of operation but as the results show one nominal length does provide good operation from 2 to at least 6 GHz. The use of lumped inductors is not desired since they do tend to radiate and cause undesired feedback.

Low loss capacitors are used to couple the RF in and out of the device. The dc blocking capacitors should provide a low impedance over the desired operating bandwidth without adding excessive series inductance. Although there is no voltage present at the input of the device, it is suggested that a dc blocking capacitor be used especially if the device is preceded with another amplifier device. A suggested value of blocking capacitor for use in the 1.5 to 6 GHz frequency range is 27 pF.

GaAs Device Performance



7.2 mm gate width
0.7 nominal gate length

die size: 41 x 29 mils

material optimized for linearity:
low g_m , medium breakdown,
low current density

	Pout	Gp	IM3	IM5	IM7	Vds	Vgs	Id
ADC:	2x+25	10dB	-27	-35	-43	6V	-2 V	210 mA

Figure 4. GaAs Device Performance

One technology option for the output transistor is a Gallium Arsenide MESFET. GaAs is touted for superior mobility, operation at low voltages, and high linearity. Let's examine the performance offered by a typical device.

Gate length: 0.7 μm nominal

Gate width: 7.2 mm

The device has been optimized for linearity by targeting for low g_m , medium breakdown voltages, and low current density. These features derive both from the processing and the physical layout (finger length, spacing).

Packaging is a major concern, as source inductance from package parasitics significantly degrades performance. The desired package is something like a SOT-223: plastic, surface mount, low cost. However the SOT-223 package has very large parasitic inductances, and gives an unrealistically poor view of the GaAs FET performance. Additionally, it can limit the power dissipation of the assembled device due to poor heat conduction. The GaAs FETs measured for this paper were mounted in a 100 mil flange package which, in addition to having minimal source inductance, also provides excellent heat sinking. Although this package is too costly for commercial applications, it allowed us to examine the capabilities of the die unencumbered by package limitations. We felt this approach to be valid, as present market use is commonly in hybrid power modules which may make use of low parasitic carriers rather than packages.

Typical performance capability of one cell in 100 mil flange:

Pout	Gain	IM3	IM5	IM7	Vds	Ids	η_{add}
[dBm]	[dB]	[dBC]	[dBC]	[dBC]	[V]	[mA]	[%]
2x+25	14	27	35	43	6	210	48

NOISE MATCH

The device's 50Ω noise figure is approximately 2 dB. Decreasing the noise figure at 4 GHz, as an example, requires that a matching network transform 50Ω to Gamma Opt of the device. (Gamma Opt is the device reflection coefficient required for the device to produce its minimum noise figure) At 4 GHz, the Gamma Opt is .38 @ 51 degrees. A Smith Chart exercise suggests a series inductance of about 2 nH and a shunt capacitance less than 0.2 pF to transform 50Ω to Gamma Opt. The best way to implement this matching circuit would be to raise the input lead of the device and make it into a loop. The shunt capacitance required is so low that it can be overlooked and still achieve good results. The matching network will lower the noise figure about 0.5 dB at 4 GHz.

PRINTED CIRCUIT BOARD MATERIALS

Most commercial applications dictate the need to use inexpensive epoxy glass materials such as FR-4 or G-10. Unfortunately the losses of the this type of material can become excessive above 2 GHz. A 0.5 inch long 50 Ω microstripline along with a 27 pF blocking capacitor and two SMA end launch connectors has a measured 0.35 dB loss at 4 GHz and 1.25 dB loss at 6 GHz! We can generally tolerate the loss as a gain loss but not as an increase in device noise figure.

A second concern would be the thickness of the material. In a typical microstripline topology, the common leads of the MMIC must be attached to the bottom ground plane with the use of plated through holes. The inductance associated with these plated through holes adds series inductance which can cause gain peaking and potential instability. The MMIC has been designed to accommodate dielectric board thicknesses of 0.040 inch or less without adversely effecting MMIC operation.

ACTUAL CIRCUITS AND MEASURED PERFORMANCE

GAIN AND NOISE FIGURE PERFORMANCE

The schematic diagram of the demonstration amplifier is shown in Figure 2. The amplifier consists of 50 Ω microstripline and dc block capacitors and a bias decoupling line. The resistor in series with the bias decoupling line can be adjusted depending on the available supply voltage. It is suggested that a minimum of 10Ω be used to de-Q the bias decoupling line.

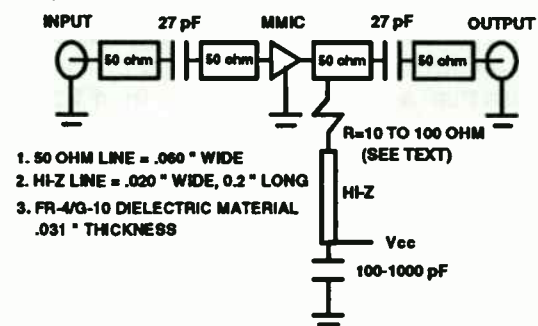


Figure 2 Schematic Diagram of MMIC demonstration amplifier

The gain performance of the MMIC as measured in a demonstration amplifier built using G-10 dielectric material is shown in Figure 3. The gain is shown for device voltages of 5, 6, 7, and 10 volts.

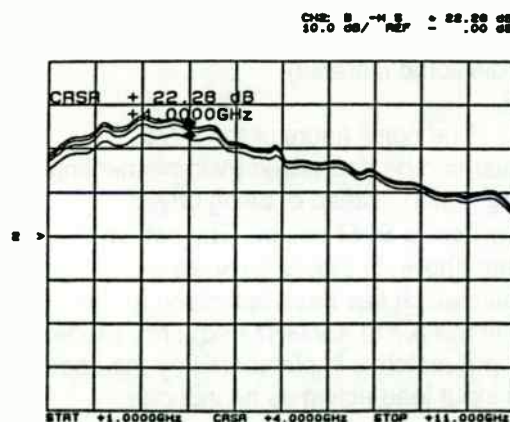
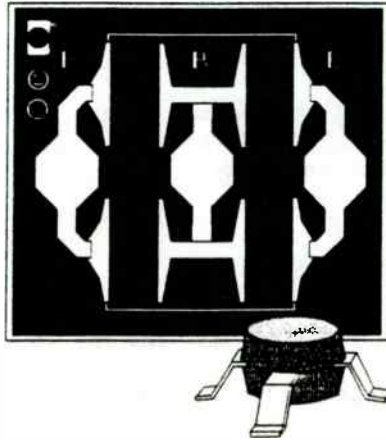


Figure 3. Gain vs. frequency for G-10 demonstration amplifier

The extraordinary band width of this amplifier makes it usable anywhere in the 1 to 10 GHz frequency range. The gain peaks

Silicon Bipolar Power Transistor



Silicon power cell:

19 x 24 mils
 3.4 micron E-E pitch
 160 fingers
 40 microns long

$f_t = 10$ GHz
 $f_{max} = 23$ GHz

	Pout	Gp	IM3	IM5	IM7	Vce	Ic
ADC:	2x+25	10dB	-27	-37	-43	6V	270 mA

Figure 5. Silicon Bipolar Power Transistor

A second option for the output transistor is a Silicon bipolar junction transistor (BJT). Silicon is touted for low cost and repeatability. High frequency silicon cells are less common than GaAs devices, but can perform nearly as well. A typical silicon power cell has the following features.

3.4 micron emitter to emitter pitch
 160 fingers each 40 microns long

The device is optimized for high f_t through material and diffusion, and laid out for best thermal distribution - note the four active areas to distribute the power dissipation.

The silicon die is smaller than the GaAs FET shown previously, and is used as a building block. A single cell can work as a driver device; producing an output power of several hundred milliwatts. For pulsed operation a single cell can be mounted in an 85 mil plastic surface mount package with low parasitic inductance. For higher power output, three cells are combined in parallel on a low parasitic ceramic carrier. Data in this paper is most often for the three-cell carrier configuration.

Typical performance capability of 3 cells on a carrier:

Pout	Gain	IM3	IM5	IM7	Vds	Ids	η_{add}
[dBm]	[dB]	[dBC]	[dBC]	[dBC]	[V]	[mA]	[%]
2x+25	10	27	37	43	6	270	35

between 3 and 4 GHz with about 22 dB gain at a device voltage, V_{dd} , of 5 volts. Increasing, V_{dd} , to 7 volts increases the gain at 3 GHz to 26 dB. The noise figure of the device was optimized for lowest noise in the 2 to 6 GHz frequency range. Actual untuned noise figure at 2.3 and 4 GHz including board losses is 2.5 dB. Subtracting the 0.35 dB loss for the input microstripline plus dc blocking capacitor suggests an untuned device noise figure of 2.15 dB at 4 GHz.

For applications that require a lower noise figure, the use of a low loss material such as DuroidTM or Taconics TLY-5 is highly recommended. Measured noise figure of a demonstration board using Duroid 5880 is shown in Table I. The amplifier exhibits less than a 2.54 dB noise figure from 1.3 to 5.8 GHz. The low noise performance of this device makes it suitable for low noise amplification in the 2.4 and 5.8 GHz spread spectrum bands. Noise figure at 900 MHz increases to 2.97 dB while noise figure at 10.5 GHz is still a respectable 3.34 dB.

FREQ(GHz)	Noise Figure(dB)
0.9	2.97
1.3	2.46
1.6	2.27
2.3	2.10
4.0	2.04
5.8	2.54
10.4	3.34

Table I Noise Figure vs. frequency (Duroid 5880 dielectric material)

The noise figure of the MMIC amplifier can be decreased by implementing a noise match instead of being driven directly from a 50 Ω source. The schematic diagram shown in Figure 4 shows an amplifier which has been optimized for low noise in the 3.7 to 4.2 GHz frequency range. The input match is implemented by the use of the input lead acting as an inductor.

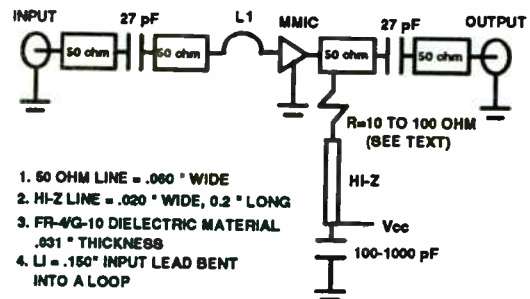


Figure 4 Noise Matched MMIC amplifier (G-10 dielectric material)

The performance of the circuit shown in Figure 4 is shown in Table II.

FREQ(GHz)	GAIN (dB)	N.F.dB)
3.7	24.0	1.92
3.8	24.0	1.92
3.9	23.7	1.89
4.0	24.0	1.89
4.1	23.9	1.90
4.2	23.3	1.86

Table II Gain and Noise Figure for MMIC amplifier with noise match (G-10 dielectric material)

Subtracting the 0.35 dB loss of the G-10 dielectric material suggests an actual noise figure of 1.55 dB for the device. To achieve within a 0.1 dB of this noise figure in an actual board will require the use of one of the lower loss materials discussed earlier.

POWER OUTPUT PERFORMANCE

Although primarily designed for low noise and broad band stable gain, the MGA-86576 provides moderate power output considering its low bias point. At a V_{dd} of 6 volts, the device provides a measured output 1 dB gain compression point, P1dB, of +5 dBm at 4 GHz. At a higher V_{dd} of 7 volts, P1dB increases slightly to +5.5 dBm. The measured two-tone third order intercept point, IP3, as referenced to the output is +16 dBm. Increasing the V_{dd} to 7 volts increases IP3 to +17 dBm.

Operating Voltage

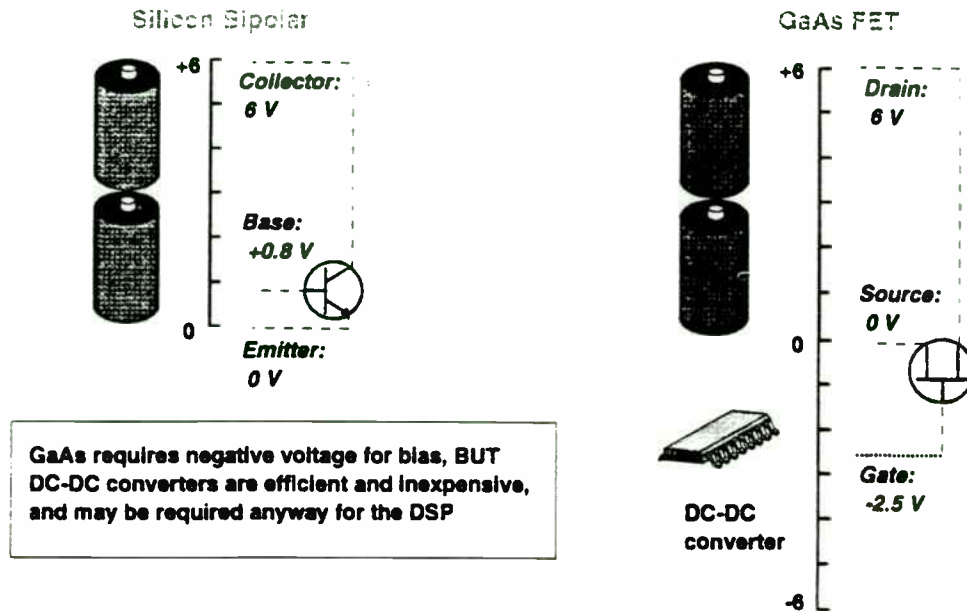


Figure 6. Operating Voltage

Cellular handsets run from batteries. Present phones have 6 V available, with a trend to lower voltage (3V) in the future. The output transistor must be able to operate from this kind of voltage source.

GaAs has the reputation for being the better power provider at low V_{ds} values. Significant power can be obtained with V_{ds} as low as 1 to 2 volts. However for a depletion mode GaAs FET, the gate must be at a lower potential than the source for operation. This adds the need for a negative power supply rail, typically on the order of -2 V. The availability of highly efficient, inexpensive DC-DC converters keeps the need for a second supply line from being a problem in most cases.

Silicon reputedly requires a high V_{ce} for power. This is somewhat misleading: most Si transistors on the market have not been optimized for operation at low voltages. With proper targeting, good gain and power can be obtained at voltages in the 3 to 5 V range, and no negative supply is needed.

Both technologies can work now from a 6 volt battery; both can be target to work in the future from a 3 volt supply. If the need for a DC-DC converter is discounted, there is no clear "low voltage advantage" to either technology.

OTHER PROPERTIES

Although specifically designed for use as a low noise amplifier, the MMIC also works well as a variable gain amplifier and an active mixer. The following section discusses the MMIC in these two applications and presents actual but not guaranteed performance data.

VARIABLE GAIN AMPLIFIER

An added benefit of the MGA-86576 is its ability to operate as a variable gain amplifier. By simply adding a 7.5 K ohm chip resistor and an additional bias decoupling line appropriately bypassed, an additional positive or negative voltage can be injected into the input terminal of the device for manual gain control. The device can only withstand a small voltage at this port.

Figure 5 shows the decrease in gain in 5 dB steps as the input voltage is increased to a maximum of +.430 volts. Figure 6 shows the decrease in gain in 5 dB steps as the input voltage is increased to -.762 volts. With a slight negative voltage applied to the input terminal of -.093 volts, the gain actually increases about 2.7 dB before decreasing with increased negative voltage. The graphs also indicate that the gain reduction versus frequency is fairly constant over a very wide bandwidth.

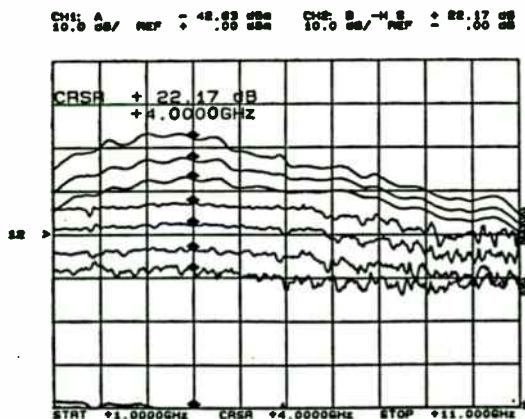


Figure 5 Variable gain operation with positive control voltage

CH1: 0 dB/REF ± 22.55 dB
10.0 dB/REF ± 22.00 dB

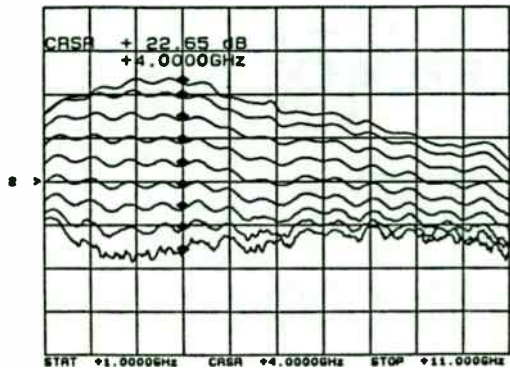


Figure 6. Variable gain operation with negative control voltage

Using a negative control voltage as opposed to a positive voltage for gain control actually is better if lower noise figure at reduced gain is desired. As an example at 4 GHz, when using a negative voltage to decrease the gain by 15 dB, the noise figure increases to 3.9 dB. Using a positive voltage to decrease the gain by 15 dB increases the noise figure to 9.9 dB.

12 GHz ACTIVE MIXER

The MMIC was also tested as an active downconverter for use in DBS applications at 12 GHz. A schematic diagram is shown in Figure 7. The circuit is etched on low cost G-10 dielectric material. The MMIC was configured as a drain or output pumped mixer by injecting a +11 dBm 10.8 GHz local oscillator signal into the output port. The input port is used as the RF port while the IF is coupled out the output port. Quarterwave microstriplines are used at the output port to achieve LO to IF isolation. The mixer achieved a SSB noise figure between 11 and 12 dB and a conversion gain between 1.5 and 2.5 dB over the entire 11750 to 12250 MHz frequency range. The noise figure performance can be improved by several dB by using lower loss material. Considerably better performance is possible at the lower frequencies where dielectric losses are lower and the basic noise figure of the device is a couple of dB lower.

Efficiency

Theoretical Limits for Current and Power

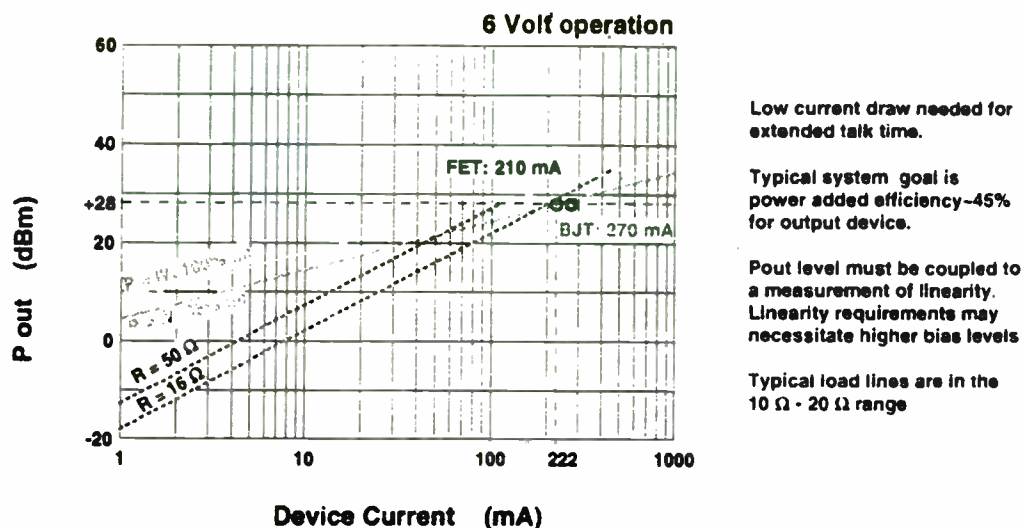


Figure 7. Efficiency: Theoretical Limits for Current and Power

One of the primary selling features of handsets is talk time. This translates into a need for the lowest achievable current draw from the power stage, which is the "current hog" of the phone. With the assumption that the voltage is fixed by the battery selection, efficiency becomes the measuring stick for device performance.

However power is the product of voltage and current. So when the voltage is fixed by battery selection and the power is fixed by radio specification, a minimum current results from $P = IV$. It is unrealistic to expect 100% efficiency, so it is also informative to look at curves for Pout vs. Device Current for an expected efficiency of 45% (a typical target for the cellular handset output device).

Load line also affects efficiency, since $P = I^2 R$. The design of the output match must set R low enough that the desired efficiency can be reached. For most devices, the output load line will be between 10 and 20 ohms. The FET circuit used a 16 Ω load line; the bipolar circuit used a 12 Ω load line.

From these curves we can see that the target current draw is in the low 200's of mA for the required +28 dBm of output power.

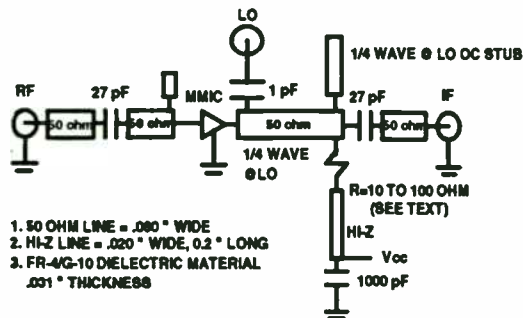


Figure 7. MMIC DBS downconverter (G-10 dielectric material)

The measured LO to IF isolation is 17 dB while the measured LO to RF isolation is 23 dB. The LO to IF isolation is obtained by the use of simple quarterwave microstriplines in the output network while the S12 of the device contributes to the LO to RF isolation of the mixer.

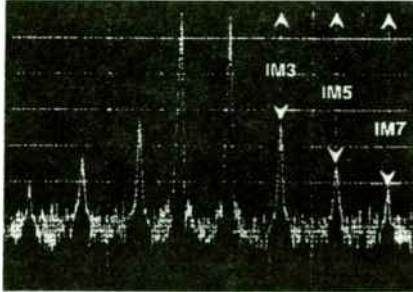
CONCLUSIONS

GaAs PHEMT technology is revolutionizing the implementation of low cost high performance low noise amplifier designs for commercial applications. Surface mount packaged MMICs are achieving noise figures and gains that rival discrete amplifier designs.

REFERENCES

1. H. Morkner, M. Frank, D. Millicker, "A High Performance 1.5 dB Low Noise GaAsPHEMT MMIC Amplifier for low cost 1.5 - 8 GHz commercial applications"; 1993 IEEE MONOLITHIC CIRCUITS SYMPOSIUM, PG13

Load Line



Loadline = 16 Ω
 Harmonics (2nd and 3rd) terminated in 16 Ω

Pout	IM3	IM5	IM7	Vds	Vgs	Id
2x+25	-27	-35	-43	6V	-2 V	210 mA

Loadline = 16 Ω
 Harmonics (2nd and 3rd) reflected

Pout	IM3	IM5	IM7	Vds	Vgs	Id
2x+25	-24	-35	-38	6V	-2 V	240 mA

Output Power depends on linearity, which is a function of loadline at the fundamental and harmonics

Figure 8 Load Line

Linearity isn't as simple as just the bias. The load line must be set to allow the output voltage to swing without "clipping" or distorting. The loadline is set by some resistance, derived from voltage swing for desired power, modified by some reactance, set by the device parasitics (typically output capacitance and bond wire lengths). As parasitics are similar for GaAs and Si, the load lines (i.e. the output impedance to match to) are also similar, so neither technology has a significant advantage in impedance matching requirements.

Termination of the harmonic will additionally effect efficiency and intermodulation levels. If the harmonics are reflected, efficiency will be maximized. If the harmonics are terminated, lowest distortion will result. It turns out that from a system point of view optimum performance is in the "harmonics terminated" case. The attached data compares the same device in a circuit which reflects the harmonics with one that terminates them. The termination selected was 16 Ω , the same load line presented at the fundamental. This circuit technique works with both Si and GaAs.

HIGHLY INTEGRATED GaAs MMIC RF FRONT END FOR PCMCIA PCS APPLICATIONS

J. Mondal, S. Geske, T. Kotsch, A. Landrie, G. Dietz, E. Bogus, J. Blubaugh, S. Moghe

Northrop Corporation
Electronics Systems Division Rolling Meadows Site (ESD-RMS)
600 Hicks Road
Rolling Meadows, IL 60008

Abstract

A fully integrated GaAs Microwave Monolithic Integrated Circuits (MMIC) transceiver chip for use on Personal Computer Memory Card International Association (PCMCIA) card in wireless modem and Local Area Network (LAN) applications is described. The chip is small in size (100x150mil²) and exhibits good performance after the first fabrication pass. An ongoing activity to further improve the electrical performance, reduce the size of the chip and develop a low cost composite package using multilayer ceramic microwave integrated circuits (MCMIC) is also outlined. A proposed system-specification and -architecture is presented.

1. Introduction

This paper describes the design, fabrication, and performance of a highly integrated GaAs MMIC radio frequency (RF) front-end. Designed specifically for wireless modem and LAN

applications, the front-end achieves the performance and small size necessary to contain all RF and digital hardware on a single PCMCIA card. Such cards are increasingly used to expand the capabilities of notebook and palm-size computers.

The RF front-end employs a highly integrated transceiver chip. The GaAs Integrated Circuit (IC) includes an upconverter, a medium-power output amplifier, a transmit/receive switch, a low-noise input amplifier, and a downconverter. A Voltage Controlled Oscillator (VCO) is also included on the PCS transceiver chip to supply an LO signal to both the upconverter and the downconverter. The chip is designed to operate from 800 to 1800 MHz.

The Personal Communication System (PCS) transceiver IC described exhibits good performance after first-pass fabrication. The front-end utilizes the MMIC on a MCMIC substrate. This approach should significantly reduce the size of the front end. MCMIC will include a synthesizer IC for the transceiver LO, as well as biasing and filtering components not included on the transceiver chip.

2. Applications

The transceiver MMIC demonstrates the highly integrated GaAs MMIC subsystem development capabilities of the Advanced Microwave Technology group at Northrop Electronic Systems Division (Rolling Meadows, IL). The technology under development is suitable for a variety of commercial applications, including PCS and Intelligent Vehicular Highway Systems (IVHS), and also for military Electronic Warfare (EW) systems.

The great demand for portable phones during recent years is expected to continue, as more wireless modem and LAN products are offered to the public. One such wireless data communication device, that is being developed at ESD-RMS, is illustrated in Figure 2-1.

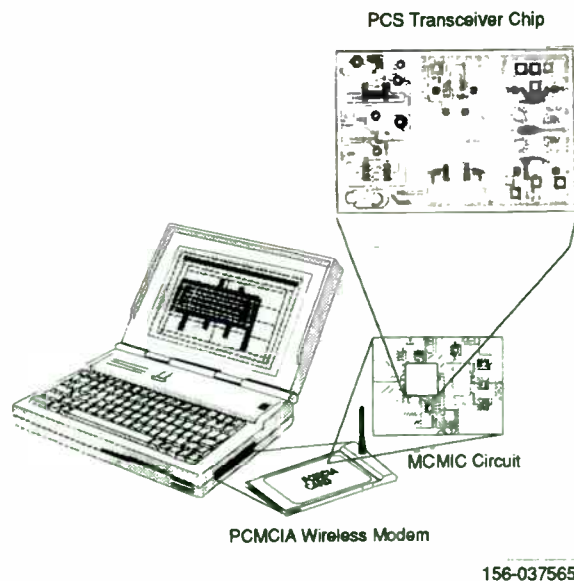


Figure 2-1. Wireless data communications using highly integrated PCS MMIC chip.

Efficiency

Collector / Drain Efficiency:

$$\eta_c = \frac{P_{out RF}}{V_c \cdot I_c}$$

Si Bipolar Transistor

$$\frac{0.63 \text{ W}}{6\text{V} \cdot 270 \text{ mA}} = 39\%$$

GaAs HBT

$$\frac{0.63 \text{ W}}{6\text{V} \cdot 210 \text{ mA}} = 50\%$$

Power Added Efficiency:

$$\eta_{add} = \frac{P_{out RF} - P_{in RF}}{V_c \cdot I_c}$$

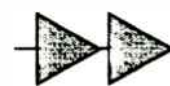
$$\frac{0.63 \text{ W} - .06\text{W}}{6\text{V} \cdot 270 \text{ mA}} = 35\%$$

$$\frac{0.63 \text{ W} - .02\text{W}}{6\text{V} \cdot 210 \text{ mA}} = 48\%$$

System:



20mA 60mA 270mA
10dB 10dB 10dB
350 mA / 30 dB



60mA 210mA
14dB 14dB
270 mA / 28 dB

Figure 9. Efficiency

Efficiency should be evaluated using η_{add} (power added efficiency) in preference to η_c (collector - or drain - efficiency) as η_{add} takes into account the reduction in current that will result with the use of a high gain driver stage. Efficiency is tied to some output power level, which for digital phones is a function of the linearity needed. For a quotation of efficiency to be meaningful, the linearity as well as the power level must be clearly specified. The goal of the designer is to expend minimum current to get sufficiently low intermodulation distortion at the necessary output level and still maintain reasonable gain.

Collector / drain efficiencies are similar for Si and GaAs; however the present higher gain of GaAs gives this technology an edge in power added efficiency.

Bias point.

Biasing enters the picture to set the linearity associated with the output power. Very high efficiencies (>65%) are possible for self biased or "Class C" amplifiers, however these amplifiers have poor dynamic range and high distortion. Class C amplifiers can meet the requirements of analog AMPS, but not of any of the digital cellular schemes. Linear performance is achieved by biasing the device fully on (class A - no current shift with applied RF), but class A has a theoretical maximal efficiency of 50% and realistic performance in the 30% range. Most handsets actually allow the current to pull somewhat with drive (Class AB operation). In this mode it is important to select a quiescent (no drive) bias point that results in the lowest intermodulation. Often there is a distinct "nulling" phenomena that occurs with class AB bias. Typical efficiencies in handsets are in the 45% range.

Si obtains a class AB bias by applying a slight positive voltage across the emitter base. GaAs requires a partial (but not full) pinching off of the gate. Thus GaAs needs more complicated circuitry in that a negative supply voltage must be provided. The alternative of a source resistor to allow the Gate to be more negative is usually impractical in a power stage because of the high dissipation requirement that results from the significant amount of current flowing. A bypassed source resistor also provides more parasitic source inductance than does a grounded source configuration.

Thus Si has a slight edge over GaAs in ease of use for biasing.

3. GaAs MMIC PCS Chip

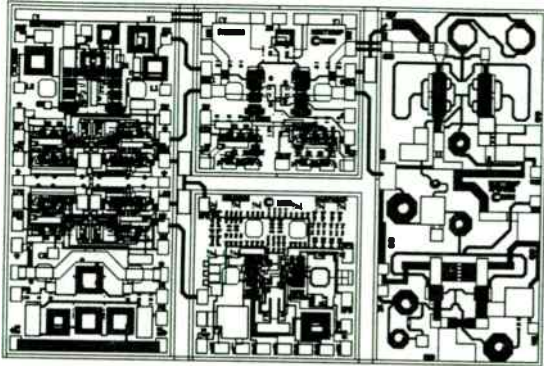


Figure 3-1. Transceiver MMIC with all RF functions for wireless LAN/modem.

The transceiver MMIC (Figure 3-1) is a fully integrated chip on a GaAs-substrate. It measures $100 \times 150 \text{ mil}^2$. The chip is designed to cover the bandwidth 0.8-1.8 GHz. It has all the essential RF functional blocks (Figure 3-2) for a transmit/receive (T/R) RF front end in wireless modem/LAN and cellular applications. In this section the functional blocks will be discussed, and measured data will be presented for individual blocks. The measured data were taken after the first pass fabrication of the chip. The chip is being slightly redesigned to accommodate additional functions and to reduce the size by 33%. The final chip size will be $100 \times 100 \text{ mil}^2$. The main advantages of a higher level of integration are smaller size, lower cost, high reliability and ease of assembly.

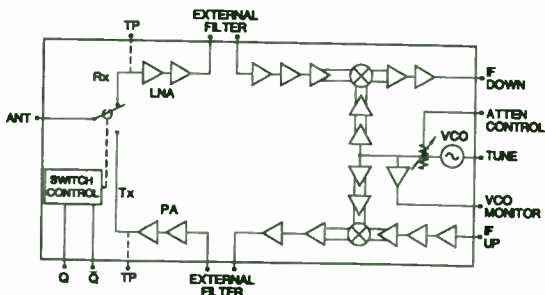


Figure 3-2. Essential RF functional blocks on transceiver chip.

The receive path of the transceiver chip (Figures 3-1 and 3-2) consists of two stages of low noise amplification, followed by an external

filter (optional), a differential down converter and two stages of intermediate frequency (IF) amplification. The transmit path has three stages of IF amplification followed by differential up-conversion and two stages of power amplification. The transmit/receive (T/R) switch at the output routes transmit and receive signals to and from the antenna, respectively.

The individual building blocks of the integrated PCS chip have been characterized and the performance data are shown below. The whole PCS chip is being mounted in a package for full characterization as an integrated chip.

Description and Performance of Individual MMIC in the Transceiver Chip

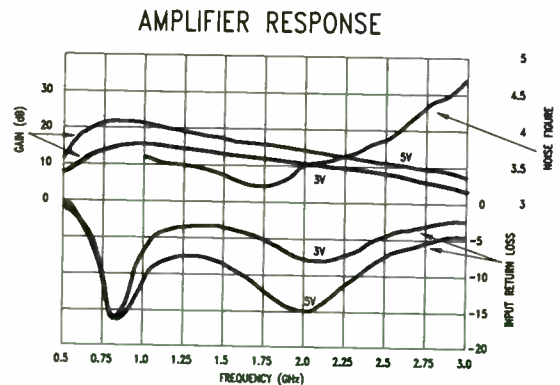


Figure 3-3. Gain, Noise Figure and Return loss of the LNA in the transceiver chip.

Low Noise Amplifier (LNA): The LNA has two stages of amplification and is designed to operate from 0.8 to 2.4 GHz. It operates from a single positive supply (3-5V) with low power dissipation (30-50 mW). The active devices are enhancement metal semiconductor field effect transistors (MESFETs). Resistive biasing is used and it decreases the size of the chip at a slight cost of dissipated power and reduced efficiency. In the receive path, the total current drawn from the supply by the LNA is 10-12 mA. The MESFETs, after the resistive drop in the drain bias circuits operate very close to the knee voltage of the I-V curves. The measured performance of the LNA is shown in Figure 3-3. The performance is shown at both $V_D=3V$ and $5V$. At $V_D=5V$, the amplifier shows a gain of 20 dB from 0.8 to 1.25 GHz and it rolls off to 12 dB at 2.6 GHz. At $V_D=3V$, the gain is between 10 and 15 dB over most of the 0.8-2.4GHz band.

Thermals

Die Configuration

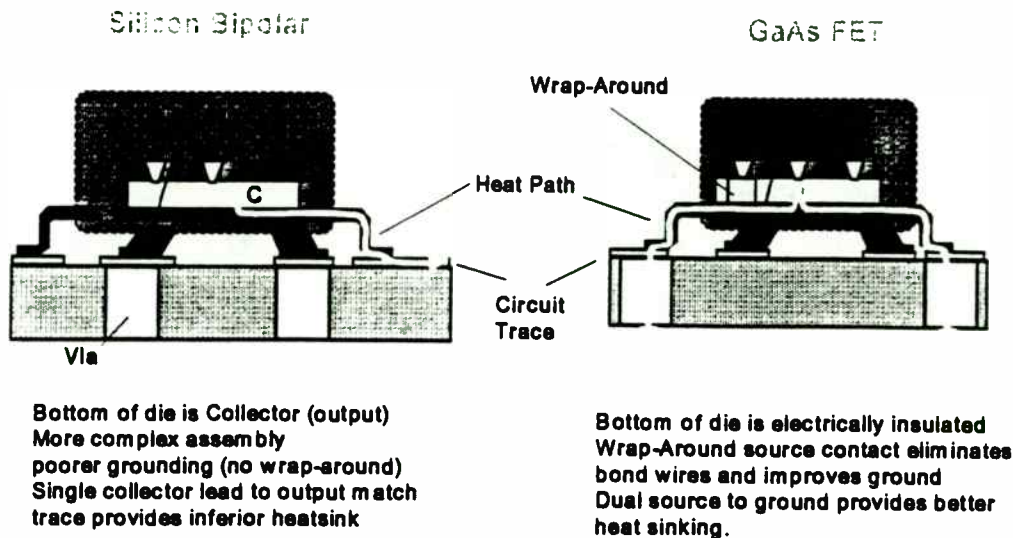


Figure 10. Thermals (Die Configuration)

The reliability of semiconductor devices ultimately reduces to the junction (or channel) temperatures at which they operate. From a purely theoretical point of view, GaAs usually allows channel temperatures as high as 175°C , whereas Si allows junction temperatures up to 200°C . This apparent edge to Si is largely negated by packaging: most cellular output devices are placed in plastic packages to keep costs low, and the plastic typically reduces maximum operating temperature for either technology to 150°C .

GaAs has a layout advantage over Si for heat sinking. The backside of a GaAs FET is electrically isolated from the FET, and so may be die attached to the "common" or ground metalization of the device package. Common leads provide the best heat sinking for several reasons. First, most high frequency packages used multiple ground leads to keep parasitic inductance small. This also provides multiple heat flow paths for improved thermal conductivity. Second, common leads attach to the ground plane, which is typically the largest heat mass and thus the best heatsink in the system.

In contrast, the backside of a Si BJT is the collector, or output terminal. The collector must attach to the output circuit, a much poorer heatsink than the ground plane as its' shape (both electrical and mechanical) is determined by loadline requirements.

Thus GaAs has an advantage in thermal performance. However, proper design for current density typically keeps MTTFs for both devices in excess of 10^6 hours. (MTTF or Mean Time To Failure is the time at which 50% of the devices have failed in a reliability test, and is an accepted reliability measure of a non-repairable device such as a semiconductor.) Thus reliability is not an issue for either technology. The fact that digital cellular effectively uses pulsed operation also removes much of the thermal load from handset parts.

The noise figure is less than 3.5 dB over this same 0.8-2.4 GHz bandwidth. The chip is redesigned for the second iteration to deliver a gain of 20 dB at $V_D=5V$ and a noise figure of 3 dB from 0.8 to 2.4 GHz.

Down-, Up-Converter: The converter MMICs form a part of a bigger section in the transceiver chip that also has the LNA and a 90° splitter. The 90° splitter is not being used on this iteration. The splitter will be added on the second iteration to provide I-Q outputs.

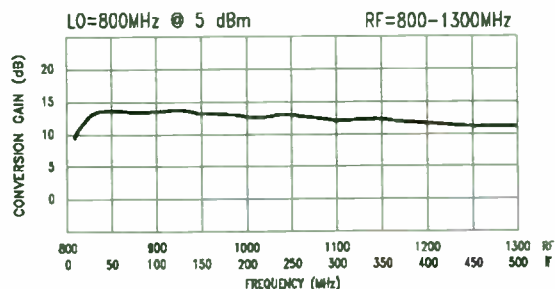


Figure 3-4. Performance of the down-converter in the transceiver chip.

The RF is first amplified by a two stage amplifier and then split by a differential amplifier for feeding to a MESFET-quad mixer. The LO is also split and amplified by a two stage differential amplifier and then fed to the gates of the FET-quad mixer. The IF from the FET-quad mixer is combined and amplified through a differential amplifier to provide single ended output.

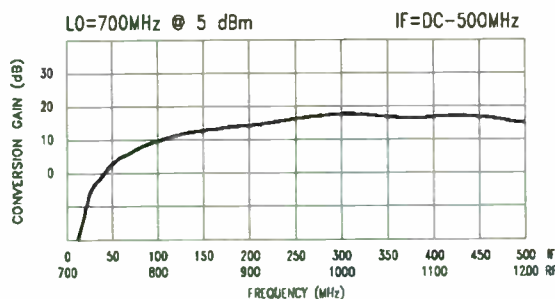


Figure 3-5. Performance of the up-converter in the transceiver chip.

The dc power consumption of the converter is approximately 100 mW for a 5V drain supply. Figure 3-4 shows the down conversion gain with the LO fixed and RF varied. Up to 1300 MHz, the conversion gain is 11-12 dB. Figure 3-5 similarly shows the up-conversion performance. The up-converter is a mirror image of the down-converter

along the X-axis. The up-conversion performance degrades at lower IF (less than 100 MHz). Above 100 MHz IF, the up-conversion gain is more than 10 dB.

In the second iteration, the up-conversion gain is being increased to more than 10 dB for an IF down to 30 MHz, by increasing the coupling capacitor between IF amplifier stages.

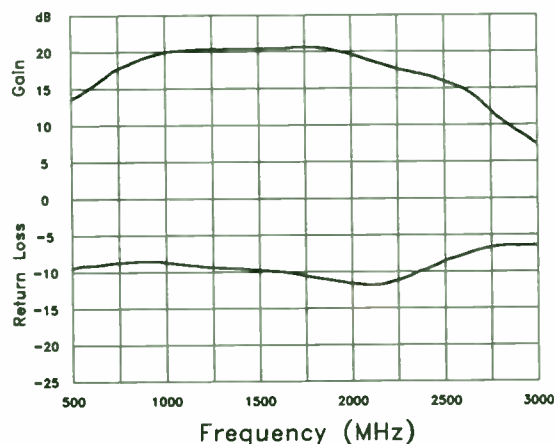


Figure 3-6. Small signal response of the power amplifier in the transceiver chip.

Power Amplifier: The power amplifier in the transmit path is designed to deliver 25-27 dBm of power at 1-3 dB compression points with 18-20 dB of gain over 0.8-1.8 GHz. It uses off-chip coils and capacitors for dc-biasing. The off-chip bias components are necessary to handle the total current (350-450 mA). The on-chip coils have low Qs and dissipate a fair amount of dc-power, thus degrading the efficiency. The MMIC occupies $50 \times 100 \text{ mil}^2$. The MMIC does not utilize via holes, the ground is provided by a number of bond wires that connect the ground pads (distributed around the chip) to the carrier plate. The MMIC requires a negative gate supply. A self-biasing scheme can be adopted by connecting a resistor and by-pass capacitor to the ground pad. The self-biasing scheme requires a single bias supply at a cost of degraded efficiency. Figure 3-6 shows the small signal response of the power amplifier. The amplifier shows 17-20 dB gain from 0.8 to 2.0 GHz. Figure 3-7 shows the power output and power added efficiency over frequency. The output power at 1 dB compression is more than 25 dBm from 0.8 to 2.0 GHz. The output power is 25-27 dBm for 1-3 dB compression or expansion. The associated power added

Device Cost

	GaAs FET	Silicon Bipolar
Cost of Processing a Wafer Lot	\$ \$	\$
Die Size - Parts per Wafer	\$	\$
Process Consistency	\$ \$	\$
Capacity - Market Price	\$	\$
Overall	\$ \$	\$

Figure 11. Device Cost

Cellular telephones are consumer products. This puts extreme price pressure on all components. The output device probably needs to sell for <\$5 at present, with this number decreasing in the future.

Silicon is less expensive to process, sometimes only costing 1/2 as much as Gallium Arsenide. Silicon and GaAs can achieve roughly equivalent power densities, so number of chips/wafer should be similar (assuming the same size wafer). Silicon material is typically more consistent than GaAs, and the process more mature, so the expectation is that silicon based products will be more repeatable, have narrower distributions of performance and hence higher yields. The repeatability also leads to better modeling and improved simulation for design, which may translate into fewer design iterations and faster time-to-market.

However, it's a tough market place, and at present there are an overabundance of GaAs FABs all seeking to defray costs by manufacturing something. Consequently, the market price of GaAs products may not necessarily reflect the manufacturing costs. If GaAs manufacturers are actually operating at a loss, then the present situation may prove unstable and not be indicative of long term pricing. None-the-less, although silicon should perhaps have a big plus in lower cost, in fact it may not in today's market place.

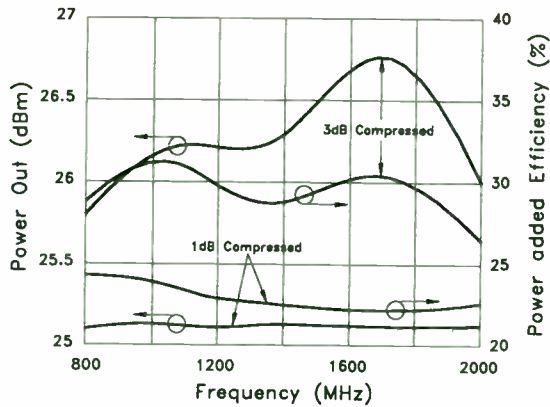


Figure 3-7. Power output and power added efficiency of the power amplifier @ P_{1dB} and @ P_{3dB} in the transceiver chip.

efficiencies are between 22 and 30% over the 0.8-2.0 GHz bandwidth. The power output in the second iteration design is being increased to 27 dBm (at 1dB compression point) over the 0.8-2.0 GHz bandwidth.

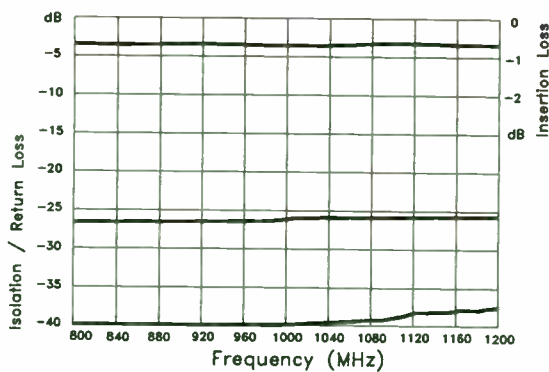


Figure 3-8. Insertion loss, return loss and isolation of T/R switch in the transceiver chip.

Transmit/Receive (T/R) Switch: The T/R switch is a single-pole double-throw (SPDT) type. It routes the signal between the antenna and receiver or transmitter. Its measured performance is shown in Figure 3-8. The switch has an insertion loss of less than 1dB, input output return loss of better than -20dB and an isolation better than 35 dB up to 1.2 GHz. The switch has a 1dB compression point of 24 dBm. In the second iteration, the switch power handling is being increased to 25 dBm and the isolation is being improved to 45 dB.

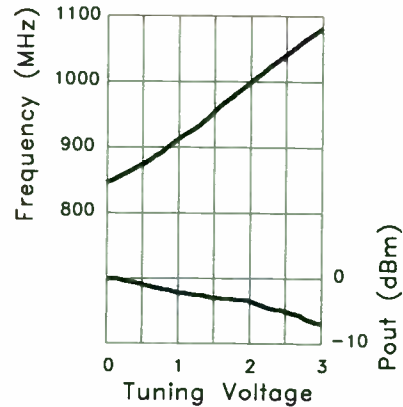


Figure 3-9. Frequency tunability and power output of VCO in the PCS MMIC.

Voltage-Controlled Oscillator (VCO): The on-chip VCO provides the LO for both receive and transmit paths. Tuning is achieved by an off-chip varactor, the capacitance of which is changed by a tuning voltage. The VCO chip also incorporates a buffer amplifier that follows the oscillator. There is an on-chip attenuator (optional) between the oscillator and the buffer amplifier to control the output power. The oscillator and buffer amplifier are designed to draw a total dc current of 18-22 mA from a 3-5V supply. Figure 3-9 presents the measured VCO performance over 0-3V tuning voltage. Total tunability is 840 MHz to 1085 MHz. The power out is 0 to -8 dBm. A redesign of the VCO for the second iteration is underway to increase the power to 6 dBm and tunability from 0.8 to 2.0 GHz range.

Integrated PCS MMIC: The PCS chip is being put in a package as shown in Figure 3-10. The overall system performance as an integrated PCS chip is being evaluated.

4. Example System Architecture

The application for this design is in a PCMCIA card. The product would be housed in a PCMCIA card that plugs into an ExCA compatible port on a portable notebook or handheld computer. There are significant advantages in implementing a wireless data product in a small package. Unrestricted portability is the prime drive of PCMCIA based wireless products. However, along with the smaller package comes the requirement for reduced power consumption. Recent developments in MMIC and MIC

Summary

Si



1. Silicon power devices cost less to produce than GaAs power devices. The materials costs are lower, and the yields typically higher due to better product consistency. This advantage is at present largely negated by the current glut of GaAs fab capacity.

GaAs



1. The gain of GaAs FETs is presently higher than that of Si BJTs. This results in fewer stages of amplification (simpler / smaller design) and lower system current drain (longer talk time).
2. The semi-insulating nature of the GaAs substrate and the physical layout of a depletion mode MESFET allow for die attach on the common lead. This results in both better heatsinking (lower operating temperatures) and lower common lead inductance (improved gain).

Figure 12 Summary

Examining the two technologies, we see that on most issues both silicon and GaAs can provide equally acceptable solutions.

Silicon's greatest strengths are its consistency and lower manufacturing costs. At present these may not be meaningful because of the over-abundance of GaAs suppliers and their willingness to take business at small margins. It remains to be seen if this situation is stable.

GaAs's greatest strengths are higher gain and a superior physical configuration. The gain advantage may disappear with future generations of bipolars. A advantage of a superior configuration is likely to exist for some time.

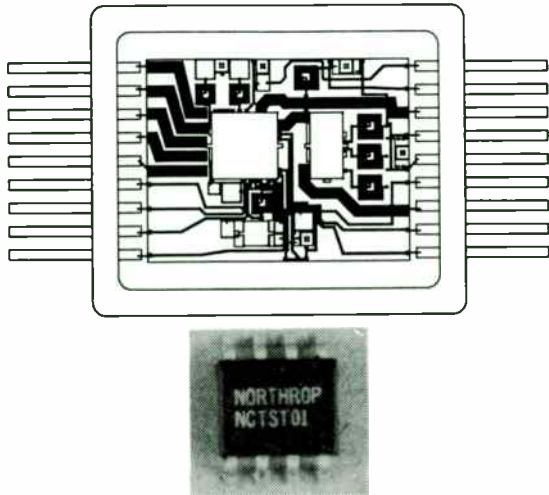


Figure 3-10. The plastic package in which the transceiver MMIC is being inserted along with the multilayer ceramic interfacial circuit.

technologies in the defense industry provide an opportunity to address these requirements.

A proposed modem (Figure 4-1) product would consist of several key functional blocks: 1) PCMCIA interface, 2) digital modem function, 3) spread-spectrum function, 4) RF functional block, and 5) antenna system.

In general, the computer architectures that this wireless modem product will be used with must adhere to the PCMCIA 2.0 standards as well as ExCA interface format compatibility. Most computer manufacturers have adopted these formats as standards for their current and next generation products. The physical form of the module follows along the lines of a Type II extended PCMCIA card. This allows sufficient room to implement the interface, processing, and RF components as well as the antenna system. Due to various host computer physical housing designs, a non-shielded area in the housing for antenna applications cannot be guaranteed. Thus, a small portion of the PCMCIA card may extend out of the host housing.

The system design provides peer-to-peer wireless communications. Such a local wireless network can be used for warehouse inventory-taking, cooperative learning in classrooms, and pen- and notepad-based applications. A peer-to-peer system would consist of two portable computers and two wireless modems. The physical nature of the system is such that its operation would be transparent to the user. Application software and system specific drivers

can be easily written to interface with the modem protocols and to provide various specific functions.

PCMCIA Interface: The PCMCIA interface would consist of a 68-pin PCMCIA connector, RAM and ROM, and an interface adapter for communicating card specific functions and configurations to the host computer. The function of the interface follows the card interface structure (CIS) as defined in the PCMCIA 2.0 standard.

Modem Function: The modem function would provide for a maximum of 19.2 Kbps data rates and will interface with the host computer through the PCMCIA interface adapter function.

Spread Spectrum Function: The wireless modem would be required to meet FCC part 15 in the 902-928 MHz ISM band for spread-spectrum operation. The spread-spectrum function would be addressed using a PN code generator and matched filter receiver with correlator/accumulator functions. These functions are implemented using the latest in digital signal processing technologies.

RF Function: The RF functional block uses advanced GaAs MMIC device technology as well as advanced MCMIC substrate technology. At the heart of the RF block is the Northrop PCS transceiver chip described earlier. It provides the majority of the RF functions in a 100x100 mil² area. These functions include the LNA, downconverter, VCO, upconverter, and .25 watt power amplifier, all operating at a nominal 3-5 volts.

GaAs MMIC provides an enabling technology for high levels of RF subsystem integration. MMICs simplify design and manufacturing for OEMs by reducing package size and weight, reducing parts inventory, and minimizing dependence on skilled technicians all while offering high levels of performance.

Recent technology advances have led to the development of MCMICs which can implement traditional lumped element components in a highly integrated, very dense package. Resistors, capacitors, inductors, and transmission lines are laid out on a ceramic substrate as-off chip circuitry for the GaAs MMIC transceiver chip. The MCMIC circuit provides for a higher level of integration when designed with Northrop MMIC

Cellular and PCS TDMA Transmitter Testing with a Spectrum Analyzer

Larry Nutting

Hewlett-Packard
Microwave Instruments Division
1400 Fountain Grove Parkway
Santa Rosa, CA 95403

ABSTRACT: New technology has provided spectrum analyzers with specialized measurement capabilities for testing time-division multiple-access (TDMA) carriers. Time-domain and time-gated functions, along with built-in and downloaded measurement routines, simplify testing of burst carriers for the new mobile-communication digital formats.

Practical spectrum analyzer measurement techniques are described for these tests: carrier power, carrier-off power, adjacent channel power, spurious emissions, burst timing, and frequency deviation. While most examples are for the North American Digital Cellular TDMA (IS-54) system, the information presented also applies to other formats such as GSM, DCS 1800, JDC, CT2, and DECT.

Introduction

The spectrum analyzer is recognized as a valuable tool for making RF performance measurements on analog mobile communication systems. It has found use for both in-channel and out-of-channel transmitter measurements. The spectrum analyzer can also be an extremely useful tool for measuring and troubleshooting the base and mobile stations of the new digital mobile communication systems that employ TDMA (Time Division Multiple Access) or TDD (Time Division Duplex). The TDMA and TDD systems have burst carriers rather than the continuous carriers of analog systems. This poses new challenges for test equipment. In the last few years new capability has been added to some spectrum analyzers to provide sophisticated measurements on burst carriers.

Spectrum Analyzer Requirements for Burst Carriers

New spectrum analyzer hardware is required for measurements made on burst carriers. Traditionally, the spectrum analyzer has been used primarily for making measurements in the frequency domain. But for communication systems using TDMA or TDD, time domain measurements are also important. Adding a fast digitizer allows zero-span measurements to be made with sweep times as fast as 20 μ s. Delayed sweep trigger capability allows the displayed waveform to be expanded about an arbitrary point in time. Limit lines for time domain waveforms provide internal comparison between the waveform and a specified limit mask. An important development is time-gated spectrum analysis, which adds a gated-video capability to frequency domain measurements. This technique allows the transient spectral power to be excluded, revealing the spectrum due to modulation and noise.

The spectrum analyzer setup and computation for these digital burst carrier systems are more complex than for the analog systems. Built-in functions or application specific downloadable software allow these complex measurements to be made quickly and accurately by the user. One-button measurements can be provided that automatically measure the signal level, adjust the input attenuation and reference level of the spectrum analyzer, establish the spectrum analyzer settings, perform computations, and display graphical and numerical results. The measurement sets are similar for the different digital cellular and

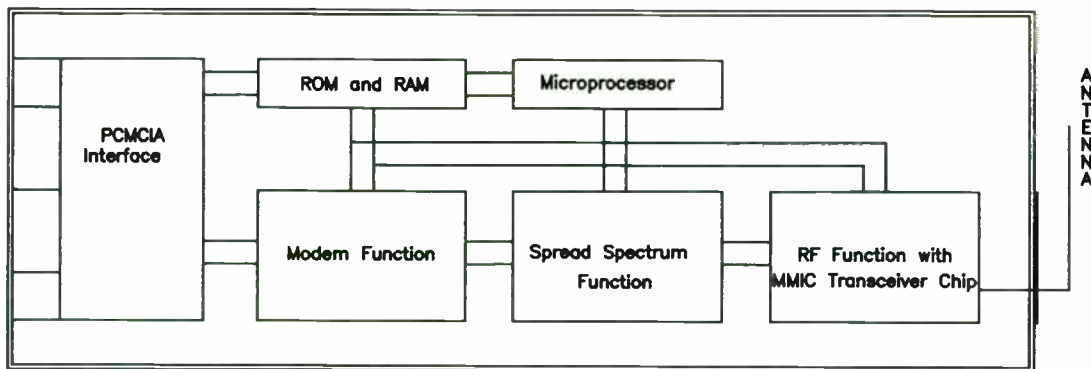


Figure 4-1. Proposed wireless modem PCMCIA card with transceiver chip.

devices.

Due to the high level of integration of the Northrop PCS transceiver MMIC, the RF layout is significantly simplified. All required components can be integrated on the MCMIC substrate as shown early in Figure 3-10. Inductors are realized with planar technology using airbridges and passivated underpasses. Capacitors can be realized with either Metal Insulator Metal (MIM) technology or interdigitated designs. This design uses all MIM capacitors. It should be noted that the MCMIC technology can be used to create a hierarchy where increased levels of integration are made possible by adding more MMIC devices to the design.

Antenna: The internal antenna provides unobstructed working space and easy portability. The design of internal antenna would take into account the PCMCIA card housing in the computer. Other external antennas would not guarantee unobstructed working space, because the location of the external antenna would change as that of PCMCIA card changes on the computer housing.

Modem Specifications: The wireless modem is designed to operate in the 902-928 MHz ISM band at a maximum data transfer rate of 19.2 Kbps. The RF design will adhere to the FCC Part 15 rules for spread spectrum operation with power levels under 1 watt. It would use a bi-phase shift-keyed modulation scheme and incorporate a PN code generator for spectrum spreading providing at least 20 dB of processing gain. The RF spectrum will occupy a 2 MHz bandwidth with a maximum of 13 separate

channels. The modem design will meet PCMCIA 2.0 standards and be ExCA compatible.

900 MHz Wireless Modem Specifications

Frequency Band	902-928 MHz
Maximum Data Transfer Rate:	19.2 Kbps
Power Level:	1 Watt max
Modulation Type:	BPSK
Access Type:	Peer-to-Peer
Module Function:	Wireless Modem
RF Bandwidth:	2 MHz
Number of Channels:	13
Processing Gain:	20 dB

5. Conclusion

A plan and development activities for a highly integrated MMIC transceiver chip for use in a PCMCIA card are presented here. The MMIC chip under development can address other PCS applications including, wireless LAN and cellular phones. The goal is to lower the cost with high volume production and inexpensive packaging. The complete package would use three technologies – plastic, MCMIC and MMIC. The MCMIC technology contains the necessary bias circuits and the interfacing circuit between MMIC and the leads. The projected cost for the complete packaged transceiver is \$30 - \$40 each by the end of 1995 in volumes of 10,000 or more.

Acknowledgement

The authors are glad to acknowledge the help from Mr. Bob Anderson and Mr. Len Baran for manuscript preparations, Mr. Khoi Vu for providing measured data and Mr. Ron Langietti for useful suggestions.

Carrier Off Power

The carrier off power is the transmitter power during that part of the frame when the carrier is off. A spectrum analyzer also makes this measurement in zero span. Very low levels are specified for the carrier off power to insure that one radio does not interfere with another. For improved sensitivity, a narrower spectrum analyzer resolution bandwidth is often chosen for this measurement than for the carrier power measurement. A video trigger is usually used. Fig. 3 shows a carrier off power measurement on a NADC-TDMA carrier.

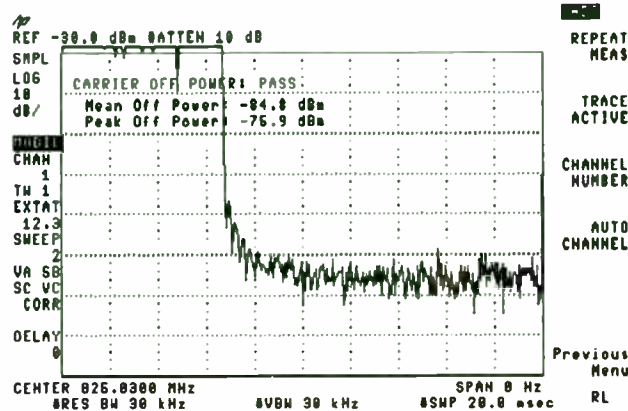


Fig. 3 Carrier off power measurement example for a burst NADC-TDMA carrier

Burst Timing Ramp-up and Ramp-down

The various standards define time domain masks; an example is given in Fig. 4. A minimum power must be maintained for the on part of the burst. To avoid interference it is important that the ramp-up and ramp-down times do not extend into adjacent time slots. The time domain masks do not specify a minimum limit for the ramp-up and ramp-down times. However, the faster these transitions, the greater will be the spectrum broadening (splatter) into the adjacent channels. The adjacent channel power limits allow very little spectrum broadening from ramping, so in practice nearly all of the allotted time is used for the ramp-up and ramp-down of the burst. The standards generally specify relative limits, but certain segments are sometimes specified at absolute power values.

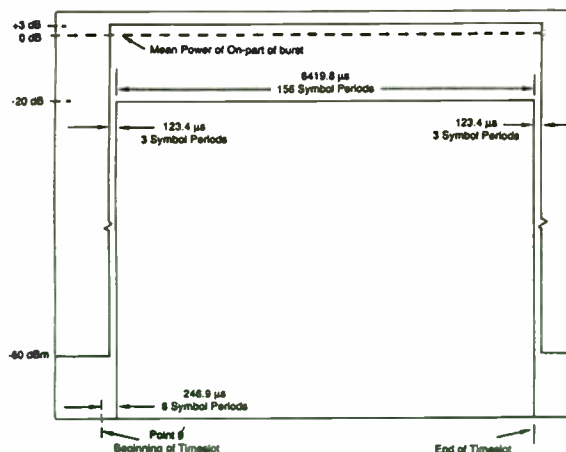


Fig. 4 Burst power mask for NADC as defined in EIA/TIA IS-55

Spectrum analyzers are high dynamic range instruments, but even they are challenged by the requirements for some TDMA systems. For example, the NADC-TDMA IS-55 standard specifies a -60 dBm off level, which for a 3 watt mobile requires a 95 dB measurement range. By the use of downloadable software routines, it is possible to get as much as 110 dB of on-screen calibrated dynamic range for this measurement, even from an analyzer that normally has an 80 dB log display.

LOW-POWER TRANSMITTER DESIGN USING SAW DEVICES

Earl E. Clark
RF Monolithics, Inc.
4441 Sigma Road
Dallas, Texas 75244

Surface-Acoustic-Wave-(SAW) resonator low-power transmitters have been in widespread use since the early 1980s. They are found in a wide variety of applications such as automotive keyless entry, door and gate openers, wireless alarm sensors, medical alert pendants, bar code readers, and many other applications in the wireless remote control, security, and data transmission area. There are many constraints that impact the transmitter configuration: range, data rate, battery life, size, and emissions requirements. The inter-relationship of these constraints must be understood so that an optimal transmitter is designed. This paper will focus on the different types of SAW-resonator low-power transmitters and their performance characteristics.

There are many benefits to using SAW resonators in low-power transmitters. They provide outstanding performance when compared to traditional LC stabilized transmitters, frequency synthesizers, or multiplied bulk crystal transmitters. The SAW resonator-based oscillator, used in low-power transmitters, is a very stable, fundamental mode frequency source at UHF. Properly designed SAW oscillators are relatively insensitive to changing load impedance and have good temperature stability. They are very rugged and, being hermetically sealed in TO-39 package, have excellent aging characteristics. Being a fundamental mode devices means the circuit complexity is greatly reduced. This has a direct impact on overall transmitter size. SAW devices simplify product design and manufacturing by removing costly alignment steps. These properties give SAW resonator-based oscillators a very low cost/performance ratio.

In order to gain the maximum benefit from using a SAW device in the transmitter it is important to take advantage of the SAW device's characteristics when designing a new system. Due to their fundamental mode of operation and high degree of temperature stability, SAW devices can be used to stabilize the frequency of both the receiver and the transmitter. Therefore, receiver bandwidths can be reduced, increasing sensitivity and decreasing susceptibility to interfering signals. Due to the explosion of wireless applications, the finite amount of spectrum allocated to low-power applications is becoming more and more crowded. The use of SAW devices, whether resonators for frequency stability, or filters for rejection of out-of-band

signals, is a very cost effective way to decrease the required system bandwidth.

Using SAW devices in a system reduces the circuit complexity. This means that systems can be made smaller without sacrificing the performance advantages of more complex systems. Additionally, a less complicated circuit results in a lower power requirement, conserving precious battery resources. SAW devices make it possible to have a simple, low-power system, with no production alignment, and performance characteristics that rival much more complex systems.

SAW resonators are fabricated by depositing a thin film of metal, typically aluminum, onto a highly polished quartz substrate. The frequency, Q, and insertion loss are a function of the geometric pattern that is etched into the metal. Figure 1 shows a drawing of the different parts of a resonator.

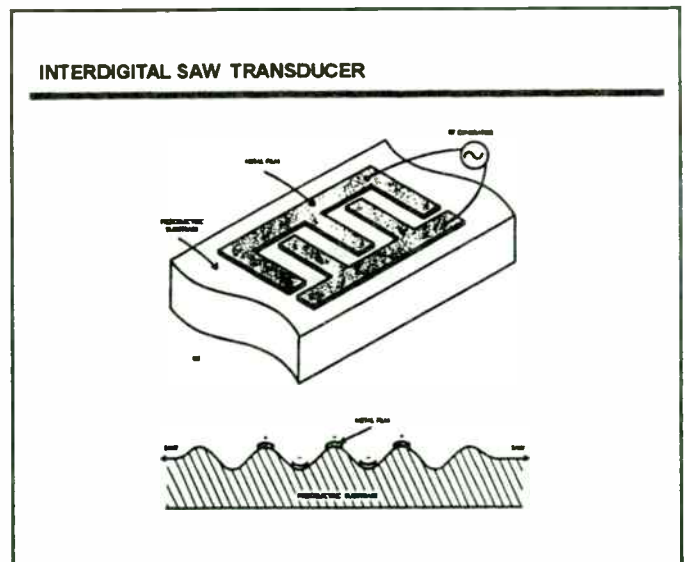


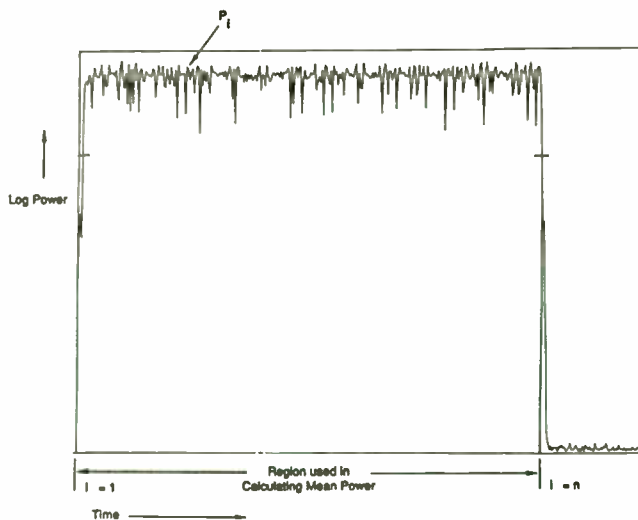
Figure 1: SAW Resonators

SAWs can be fabricated on many types of piezoelectric substrates. There are Lithium Niobate and Lithium Tantalate used for wide band SAW filters, and ST cut Quartz used for narrow band SAW filters and resonators. Of these, quartz is the most temperature stable. Figure 2 shows the relative temperature stability of the three materials.

PCS systems such as GSM (Groupe Speciale Mobile), DCS 1800 (Digital Communications System 1800 MHz), NADC-TDMA (North American Digital Cellular, IS-54), JDC (Japan Digital Cellular), CT2 (Cordless Telephone 2nd generation), PHP (Personal Handi-Phone) and DECT (Digital European Cordless Telecommunications). But, the standards for each of these have unique measurement methods, terminology, and limits. Separate software specifically tailored for each format offers convenience and confidence to the user. Additional confidence is provided when the manufacturer specifies the range and accuracy for each one button measurement.

Carrier Power

The carrier power is specified to be the mean power during the on part of the burst. With a spectrum analyzer, the measurement is made in zero-span (fixed tuned) mode with a log amplitude display. The analyzer's resolution bandwidth is set to be greater than the channel bandwidth, and the video bandwidth is set to be equal or greater than the resolution bandwidth. A video trigger is usually used, but an external trigger is also possible. The trace data is then averaged for the on part of the burst. For modulation formats with a significant amplitude variation, such as $\pi/4$ DQPSK (differential quadrature phase shift keying), it is important that a true power average be performed. Using the video average function or a reduced video bandwidth will provide averaging of the trace, but it will be the average of the log of the power. Obtaining the mean power requires that the trace data be anti-logged prior to averaging the data numerically (Fig. 1). An actual measurement of carrier power on a NADC-TDMA carrier is shown in Fig. 2.



$$P_{\text{mean}} = 10 \times \log \left[\frac{1}{n} \times \sum_{i=1}^n 10^{P_i/10} \right]$$

where:

- P_{mean} = Mean carrier power during on part of burst (dBm)
- P_i = Power level at sample point i of the waveform (dBm)
- n = Number of sample points in the on-part of the burst

Fig. 1 Carrier power definition and equation

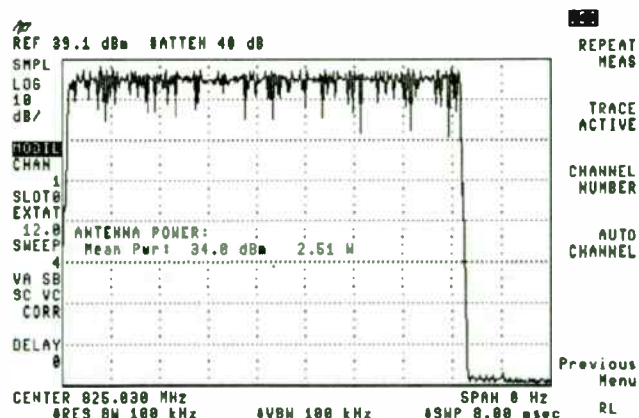


Fig. 2 Carrier power measurement example for a burst NADC-TDMA carrier

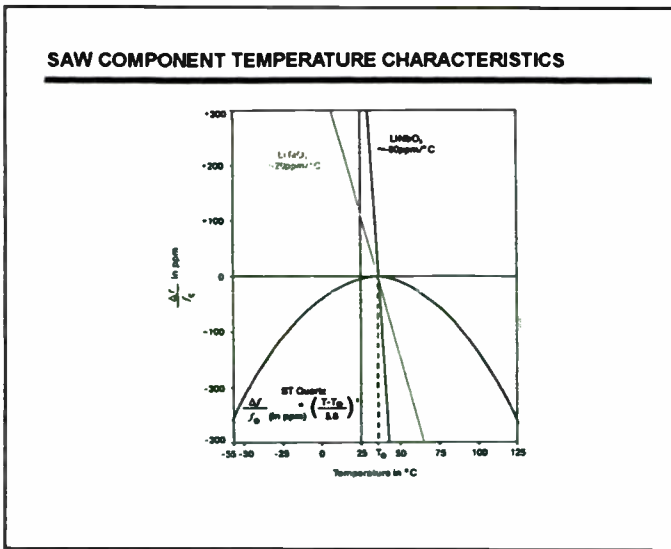


Figure 2: Temperature Characteristics

The frequency of the SAW resonator and oscillator exhibits the parabolic dependence described by the equation in the figure. For a typical transmitter, designed to operate from -40C to +85C, the change in center frequency would be approximately 125 PPM. This is at the minimum when the SAW resonator has its turnover temperature centered in the operating temperature range. The turnover temperature is defined where the frequency is at the maximum value and is set by the design of the SAW device.

SAW resonators can be modeled by an equivalent circuit using lumped elements. Figures 3 and 4 show the equivalent circuit for two commonly used SAW resonators in low-power transmitters. Figure 3 is the equivalent circuit for a two-port resonator. This model is valid near the center frequency of the SAW resonator. The phase shift through this device can be set to either 0 or 180 degrees. The equivalent circuit for the more popular one-port resonator is shown in Figure 4.

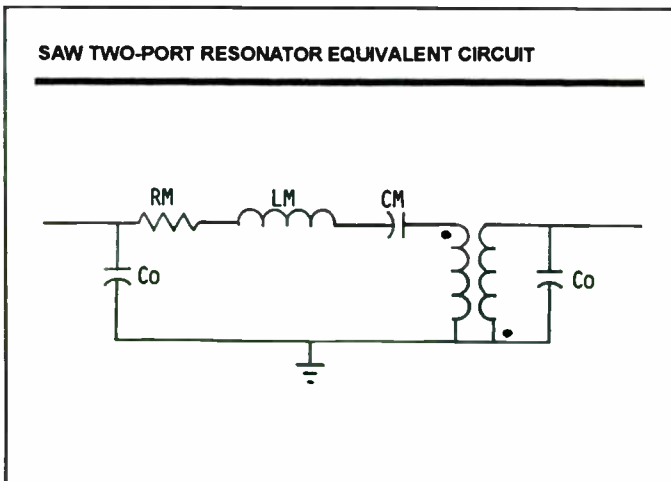


Figure 3: Two-port Equivalent Circuit

These one-port resonators are used as the frequency determining element in a Colpitts oscillator. This topology is

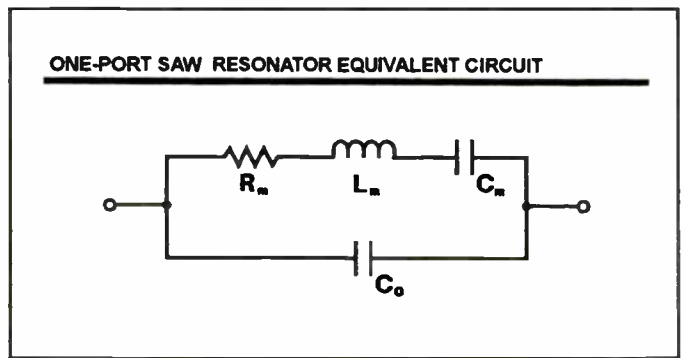


Figure 4: One-port Equivalent Circuit

the most popular found in low-power transmitters. Figure 5 shows the reactance versus frequency of a single-port SAW resonator. This plot can be used to determine the frequency of oscillation when the circuit is tuned properly. The frequency of oscillation will be at the low reactance point near the real axis. The exact frequency will depend on the circuit tuning.

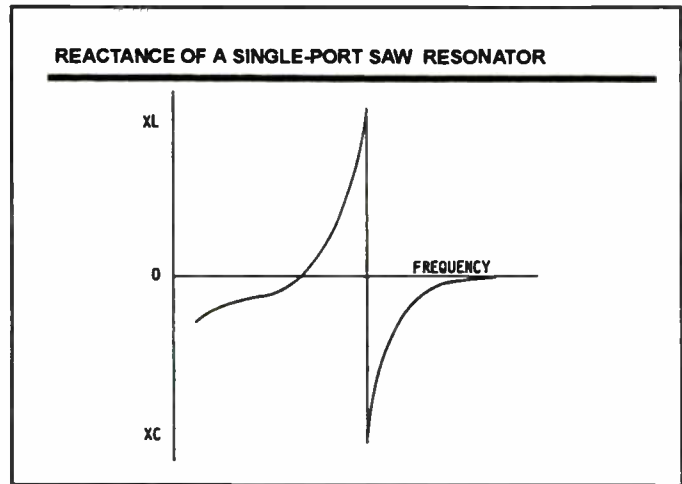


Figure 5: Reactance versus Frequency

Figure 6 shows the schematic diagram of the first generation SAW transmitter. The circuit uses the Colpitts oscill-

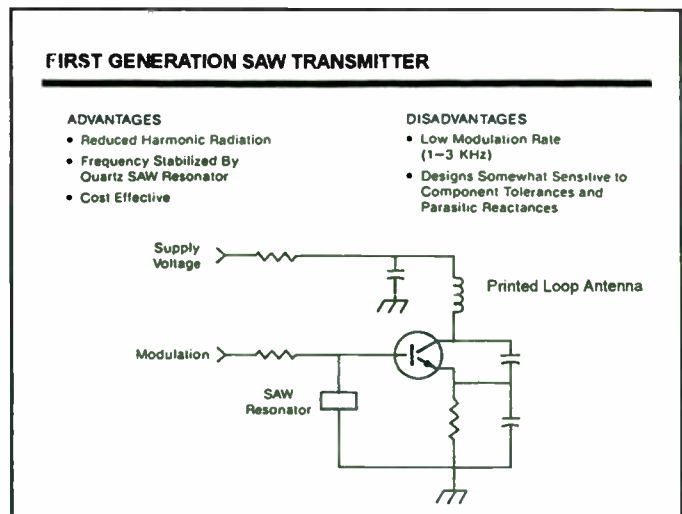


Figure 6: First Generation SAW Transmitter

A fast digitizer and delayed sweep trigger capability are required to make these burst timing measurements. An external trigger signal is needed to trigger the delayed sweep. One way to obtain this trigger is to use a burst carrier trigger device that envelope detects the rising edge of the RF burst and converts it into a TTL signal. Fig. 5 shows a power versus time measurement over the entire burst and Fig. 6 shows a measurement for the ramp-up part of a burst.

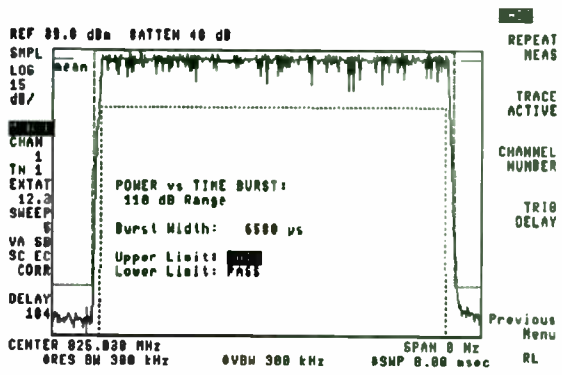


Fig. 5 Burst measurement example for a NADC-TDMA carrier

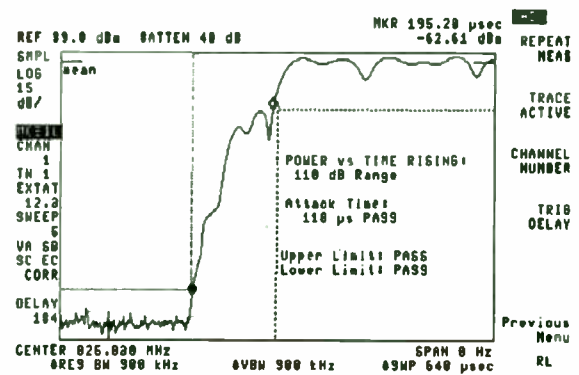
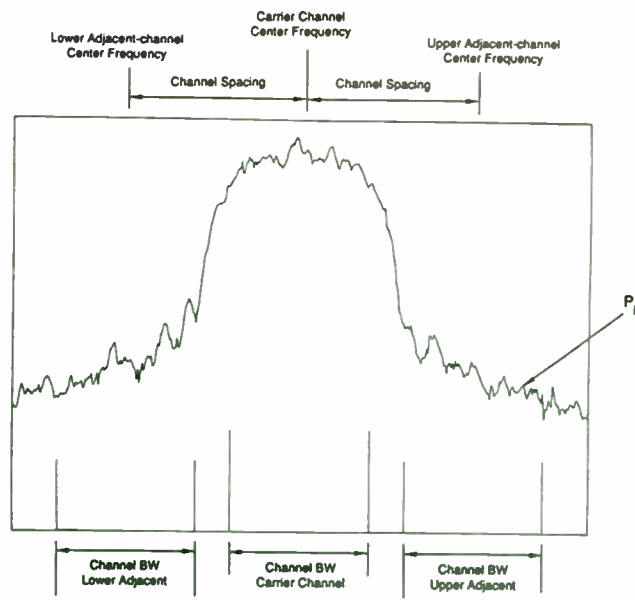


Fig. 6 Ramp-up measurement example for a NADC-TDMA carrier

Adjacent Channel Power (ACP)

Adjacent channel power is a measure of the amount of leakage power that is present in the adjacent channels. It is usually specified as a ratio to the total carrier power, but sometimes it is specified as an absolute power. It is measured with a spectrum analyzer using an integration method. For analog or continuous (non-burst) digital carriers, the measurement is made by obtaining a frequency domain trace of the spectrum using a sample detector. The analyzer's resolution bandwidth is set to be much narrower than the channel bandwidth. The video bandwidth should be at least ten times the resolution bandwidth to give power detection. The leakage power contained in the adjacent channel is computed with the power integration equation (Fig. 7). This equation averages the power contained in the all the trace elements within the adjacent channel integration bandwidth (sometimes called the specified bandwidth); and it applies a scaling factor based upon the ratio of the power (noise) bandwidth to the integration bandwidth.



$$P = (B_s/B_n) \times (1/n) \times \sum_{i=1}^n P_i$$

where:

- P = RMS-like power in the specified integration bandwidth (watts)
- P_i = Power level at sample point i of the spectrum (watts)
- B_s = Specified integration bandwidth for adjacent channel (Hz)
- B_n = Effective noise bandwidth of spectrum analyzer (Hz)
- B_n = 1.13 x BW_{3dB} (for 4-pole synchronously tuned RBW filter)
- n = Number of sample points in the specified bandwidth

Fig. 7 ACP definition and power integration equation

LOW POWER SYSTEM REGULATIONS

COUNTRY	REGULATION	FREQUENCY LIMITS (MHz)	FUNDAMENTAL POWER	2nd HARMONIC	3rd HARMONIC	GREATER THAN 3rd
UNITED KINGDOM	DTI MPT1340	417.9 - 418.1	250 uW	4 nW	1 uW	1 uW
GERMANY	FTZ 17 TR 2100	433.05 - 434.79	25 mW	1 nW	30 nW	30 nW
FRANCE	CNET PAA1542	224.6 - 224.8	5 mW	250 nW	4 nW	250 nW
NETHERLANDS	PTT	433.052 - 434.797	50 uW	4 nW	1 uW	1 uW
JAPAN	MPT	303.675-303.975	500 uV/m	35 uV/m	35 uV/m	35 uV/m
U.S.	FCC PART 15	260 - 470	3750-12500 uV/m	375-1250 uV/m	375-1250 uV/m	375-1250 uV/m

Figure 7: Regulations

lator topology. The printed loop antenna is used as the tuning inductor with the feedback accomplished with the collector to emitter capacitor. The feedback should be set so that the gain of the circuit is not so great as to cause oscillation at frequencies other than the SAW frequency, or so small that the oscillator does not modulate properly.

There are several advantages to this circuit such as no production tuning, minimum parts count, and the ability to be designed so that the harmonic emissions meet the FCC Part 15 specification. This results in a very cost effective, high-performance transmitter.

This generation of transmitter has proven to be both popular and reliable for applications that fall under FCC Part 15. There are some limitations, however, to this design. Due to the high Q of the resonator, the data rate is limited to a maximum of about 3 kHz. The transmitter frequency can also be sensitive to component tolerances and parasitic reactance. An additional problem encountered is trying to use this circuit topology for a transmitter that will be subject to the European emissions regulations. These regulations are much more stringent in the allowable level of the harmonic than the FCC Part 15. The chart shown in Figure 7 highlights the important differences in the various regulations.

The series-fed antenna, typically a trace on the circuit board, does not provide enough frequency selectivity for the transmitter to meet the more stringent regulations. There are some design tools that can help such as using a lower frequency transistor, which further reduces the maximum data rate, or using a trap at the second harmonic which typically calls for an alignment step in manufacturing. Both of these options set further constraints on the transmitter design.

In order to comply with the European regulations, specifically DTI MPT1340, RFM developed the MB1005. (This circuit is shown schematically in Figure 8.)

Like its predecessor, it also uses a Colpitts oscillator; but in order to reduce the harmonic emissions to the required level, two modifications have to be made. First, the fundamental output power is reduced so that the required rejection of the second harmonic is not as great. Second, the addition of two adjustments is necessary. One adjustment is needed to set the oscillator on frequency and the other is needed to tune the antenna. This design makes use of a tapped antenna, which has a higher impedance allowing the Q of the tuned antenna circuit to be made higher. This reduction of fundamental power and use of a higher impedance antenna is typical of most of the transmitter designs used in the European market.

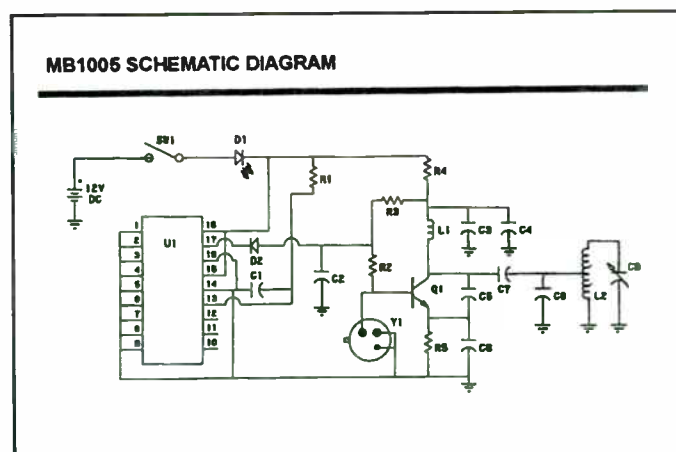


Figure 8: MB1005

However, even this design was not capable of meeting the German FTZ 17 TR2100 emissions requirements. A further reduction in output power would be required for this design to pass the more stringent second harmonic specification. This would obviously have a great impact on the system range.

The need for greater power, reduced harmonic levels, and no adjustments gave rise to a new design approach for low-

The ACP measurement is much more complex for burst carriers. To acquire a frequency domain spectrum trace without “drop-outs” requires the use of a peak detector rather than a sample detector. In addition, the sweep time must be slow enough so that at least one burst will occur for each trace element point. For example, the NADC and JDC systems have one burst every 20 ms, which, with a 400 point trace, requires an 8 second sweep.

The spectrum of a burst carrier also contains a transient component due to the burst ramping, in addition to the usual modulation and noise component. The correct integration equation for the ramping component is different than the equation for the modulation and noise component. The modulation and noise result is calculated with the power integration equation, whereas the transient component result is calculated with an impulsive noise power integration equation.

A very effective and practical way to separate the spectrum due to modulation and noise from the total spectrum, which also contains the transient spectrum, is with time-gated spectrum analysis (Fig. 8). This gated-video approach requires an external trigger signal. The gated-video is typically set so that the gate is on during the 50% to 90% part of the burst. If the gate is turned on too early, the IF filters will not have settled sufficiently and a residual transient will affect the spectrum. With correctly set gating, the resulting spectrum is the same as would be obtained if the transmitter had a continuous carrier. The adjacent channel power due to modulation can then be calculated by using the power integration equation. The adjacent channel power due to transients can be obtained by using the impulsive noise integration equation on the difference between the total spectrum and the modulation and noise spectrum. A total is sometimes calculated by adding the ACP due to modulation to the ACP due to transients. This total results from adding two peak powers with different time characteristics, so it should not be considered an RMS adjacent channel power (Fig 9).

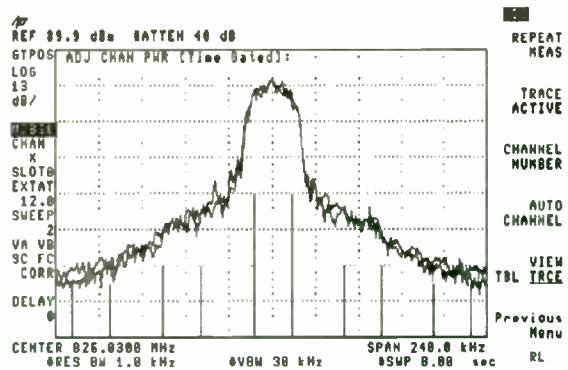


Fig. 8 ACP measurement example for a JDC-TDMA carrier showing separation of modulation spectrum from total spectrum by using time-gated spectrum analysis

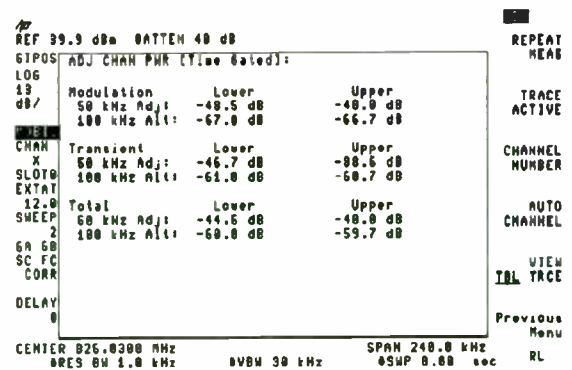


Fig. 9 ACP numerical results example for a JDC-TDMA carrier

The method of measurement for ACP varies in many details for the different digital mobile communication systems. Some systems specify only lower and upper adjacent channels, others specify additional channels (sometimes called alternate channels). A rectangular integration bandwidth is usually specified or assumed, but IS-55 and IS-56 specify the application of a Nyquist square-root-raised cosine filter prior to performing the integration. For the new digital cellular phone and cordless phones the ACP limits in the adjacent channel are rather loose, so the phase noise performance of the spectrum analyzer is not an important issue. However, spectrum analyzer dynamic range needs to be considered for measurements in the alternate channels. With downloadable software, the on-screen calibrated dynamic range can be extended beyond the capability of the unaided spectrum analyzer. The display in Fig 8 shows a dynamic range of over 100 dB (the log scale is 13 dB per division).

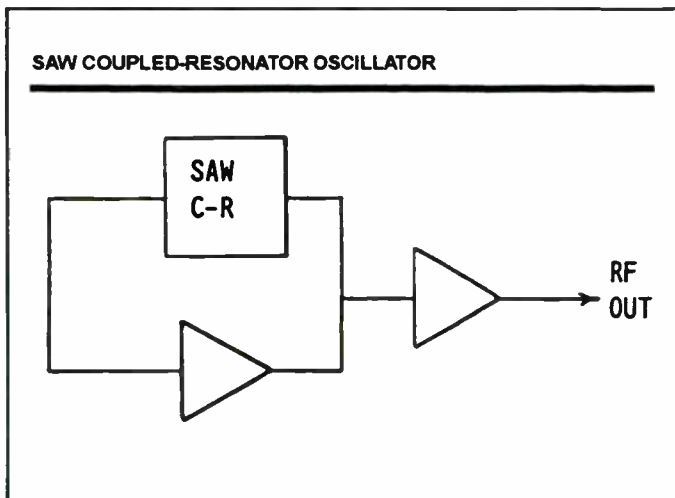


Figure 9: Pierce Block

power transmitters. This design uses a Pierce oscillator configuration which is shown in the block diagram of Figure 9.

In order to implement this circuit, RFM developed a SAW coupled resonator. The coupled resonator is a two-pole SAW resonator with a frequency response similar to that shown in Figure 10. This is contrasted with Figure 11 which shows the response of a standard resonator at the same frequency. Perhaps the most important difference between the two devices is the amount of phase shift across the 3 dB bandwidth. The standard resonator having a single-pole has only 90 degrees of phase shift while the two-pole coupled resonator has 180 degrees.

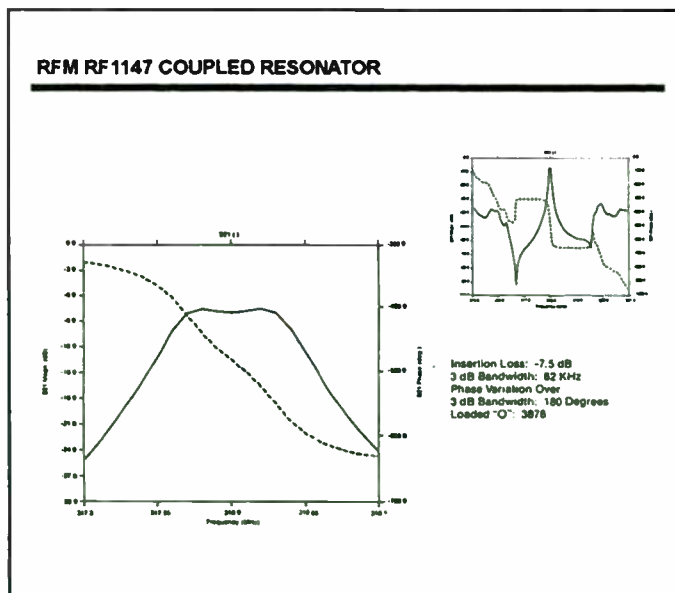


Figure 10: Coupled-resonator

Referring to the block diagram in Figure 9, the requirement for oscillation is that the gain around the loop be at least unity with a phase shift of 0 degrees, 360 degrees, or an integer multiple of 360.

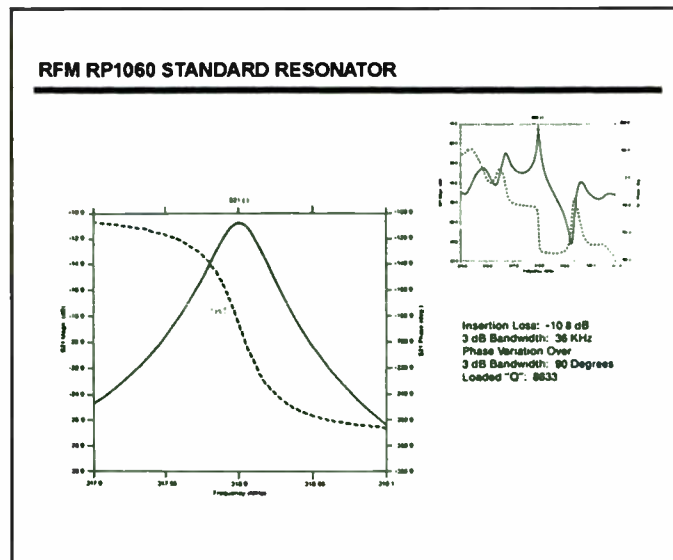


Figure 11: Two-port Resonator

The importance of the extra 90 degrees of phase shift across the SAW coupled-resonator bandwidth can be illustrated with the following example:

The phase shift through a normal transistor amplifier at UHF frequencies is approximately 240 degrees. In order for this circuit to meet the phase requirement, the phase shift provided by the feedback element must be either +120 or -240 degrees. The normal single-pole resonator has either 0 or 180 degrees of phase shift at the center frequency with a +/-45 degree phase shift across the 3 dB bandwidth. A quick calculation shows that the phase criteria would not be met within the 3 db bandwidth of the resonator.

The coupled resonator, on the other hand, has a similar absolute phase at the center frequency, but has a +/-90 degree phase shift across the 3 dB bandwidth. Using a coupled resonator and a properly designed amplifier, it is possible to guarantee the oscillator frequency to be within the 3 dB bandwidth of the SAW. The benefit of this topology is that it requires no tuning and is relatively insensitive to stray reactance. In contrast, if a single-port resonator were used it would be necessary to introduce an added phase-shift circuit to the oscillator loop in order to obtain the required phase shift.

Based on this approach, RFM then designed its first integrated circuit transmitter called the Microtransmitter (MX). A block diagram of the MX is shown in Figure 12. This circuit is designed for FCC Part 15 applications and is capable of full compliance with all current and proposed FCC Part 15 regulations.

A buffer amplifier is used so that the oscillator frequency is insensitive to changes in load parameters. The buffer amplifier also allows for a much higher modulation rate than would be possible if the oscillator were to be directly

Spurious Emissions

Both in-band and out-of-band spurious emissions, including intermodulation spurious, are measured in much the same way for TDMA and TDD systems as for analog mobile communication systems. However, there is an important point that is often overlooked. The normal spectrum analyzer auto sweep-time will ensure that continuous spurious signals have the correct amplitude, but burst spurious may be under-represented or even missed. A spur search for burst spurious signals requires a slower sweep time as given by:

$$ST \geq PRI \times \text{Span}/\text{RBW}$$

where:

- ST = Sweep Time of spectrum analyzer (sec)
- PRI = Pulse Repetition Interval of burst (sec)
- Span = Frequency span of spectrum analyzer (Hz)
- RBW = Resolution Bandwidth of spectrum analyzer (Hz)

For example, NADC and JDC have PRI= 20 ms. Then for RBW = 1 MHz, the sweep time must be at least 20 s/GHz.

Modulation Accuracy

By using a hardware analog FM demodulator circuit in conjunction with an external trigger signal, it is possible to obtain traces of the frequency deviation versus time for a burst FM carrier. The trace data can then be used to compute the peak frequency deviation and mean frequency error (Fig 10). This technique is useful on burst BPSK modulated carriers, such as those used in the CT2 system. The modulation and frequency analysis for $\pi/4$ DQPSK and GMSK modulations requires DSP (digital signal processing) techniques. This capability could be provided in a spectrum analyzer through the use of DSP processing hardware and downloadable software.

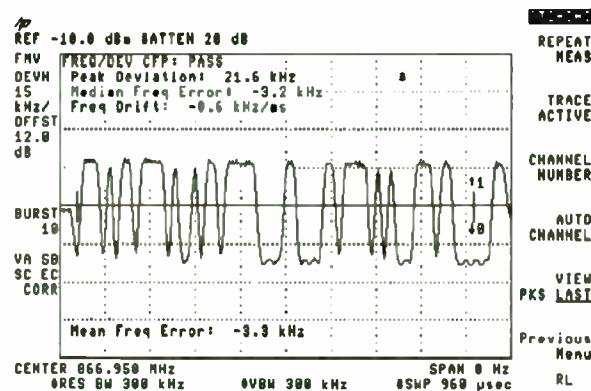


Fig. 10 FM deviation measurement example for a burst CT2 TDD carrier

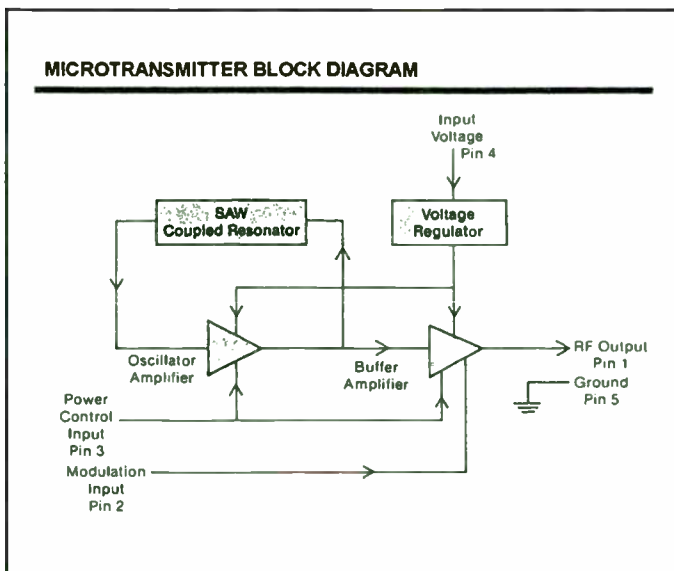


Figure 12: MX Block Diagram

DESIGN GOAL PERFORMANCE AND MEASURED PERFORMANCE OF MICROTRANSMITTER AT 318 MHz		
Specification	Design Goal	Typical Measured Performance
1. Output Frequency	318.000 MHz +/- 250 KHz	318.000 MHz +/- 100 KHz
2. RF Output Power (50Ω Load)	≥ +7 dBm	+12 dBm
3. Power Output Variation over a Supply Voltage Range 6.0 to 10.0 V _{oc}	+/-1 dB	+/-1 dB
4. Modulation Depth (On/Off Ratio)	35 dB Min	>50 dB
5. Modulation Rate Capability	<50 KHz	<50 KHz
6. Modulation Rise or Fall Time	<1 μsec	<1 μsec
7. Radiated Harmonics when used with RFM Specified Antenna	-20 dBc	-20 dBc
8. Output Power Control Adjustment Range	15 dB	10 dB
9. Power Supply Current Drain at 10 V _{oc} and Maximum Power	<25 mA	<20 mA
10. Power Supply Current Drain at 10 V _{oc} and Power Control Resistor Grounded	<1 μA	<10 μA

Figure 13: MX Performance

modulated. The design goals and actual performance are shown in Figure 13.

A transmitter based on the MX is capable of putting out the maximum amount of power allowed and still meeting the emissions specification under FCC Part 15. It also is capable of a high data rate, up to 50 kHz, and requires no production tuning. The disadvantages of this product are its power consumption, which limits its battery powered applications, and its relatively high harmonic levels, which make it difficult to use in European applications.

The MB1003 demonstration transmitter was developed to show that a European design could be accomplished with the Microtransmitter. Although it requires an adjustment to center the antenna circuit, it reduces the number of adjustments from two, on the MB1005, to one. The schematic representation of this circuit is shown in Figure 14.

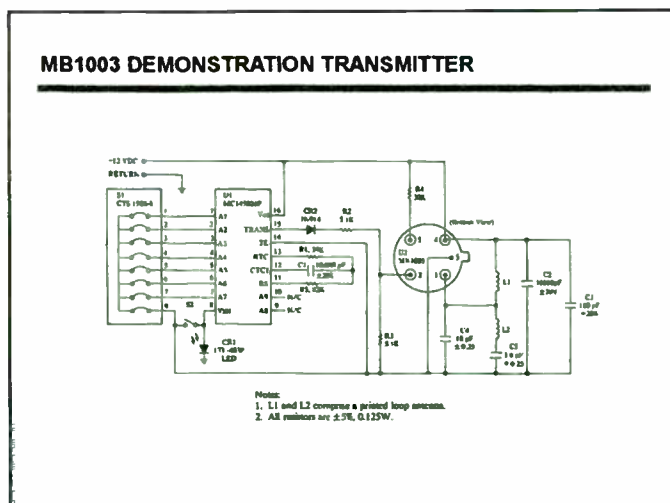


Figure 14: MB1003 Schematic

In order to more effectively address the unique emissions requirements of the European market as well as US markets that require a high degree of miniaturization, RFM has developed the third generation of transmitter components: the HX series. This series is a fully functional RF building block that engineers, who may have little RF background, can incorporate into a transmitter design with little effort.

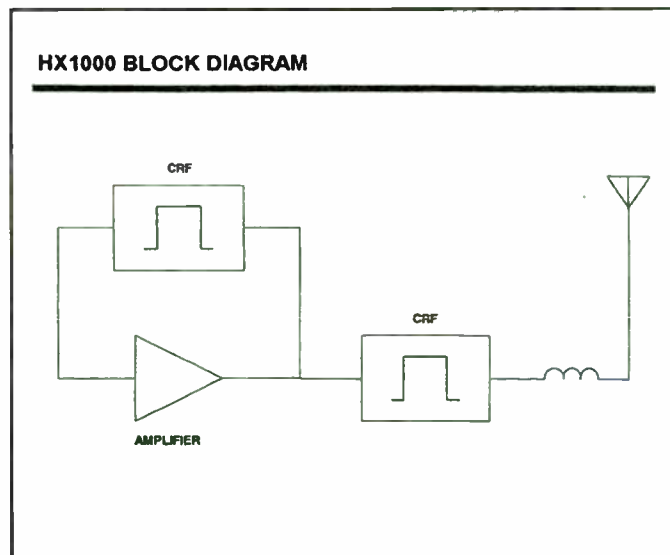


Figure 15: HX Block Diagram

The HX is a hybrid transmitter that is packaged in a hermetically sealed surface mount package. The block diagram of the HX is shown in Figure 15. The oscillator topology is a Pierce configuration using a SAW coupled resonator as the feedback element. Like the Microtransmitter the HX transmitter is also very insensitive to changing load conditions and parasitic reactance.

Advances in SAW technology at RFM have led to coupled resonator designs that have 3-5 dB of insertion loss, untuned, in a 50 Ohm test fixture, at frequencies as high as 930 MHz. This new SAW technology has greatly simplified the oscillator circuit. The result being a very

Conclusion

Spectrum analyzers with the right hardware features are especially well suited for measuring the burst carriers of the new digital TDMA or TDD mobile communication systems. Fast digitized sweeps, delayed sweep trigger, and time-gated spectrum analysis (gated-video) are available on the Hewlett-Packard HP 8591 and HP 8560E families of portable spectrum analyzers. In addition there are a number of mobile communication downloadable software products for use on the HP 8591 spectrum analyzer family. Downloadable measurement personalities are currently available for the GSM, DCS 1800 (PCN), NADC, JDC, and CT2 formats. These offer automated one-button measurements that follow the method of measurements, terminology, and limits of the applicable standards document. Powerful measurement solutions are provided by the combination of a full-function general purpose spectrum analyzer and downloadable software tailored for specific mobile communication systems. With the current hardware and downloadable software, most digital transmitter parametric measurements can be made with a spectrum analyzer. It is expected that additional measurements for digital mobile communication systems will be added to spectrum analyzers in the future. While this paper has dealt with measurements on TDMA systems, with appropriate downloadable software, spectrum analyzers could also provide a similar set of useful measurements for CDMA systems.

References

1. J. Gorin, "Make Adjacent-Channel Power Measurements," *Microwaves & RF*, May 1992, pp 137-143
2. H. Chen, "Time-Selective Spectrum Analysis (TSSA): A powerful tool for analyzing TDMA communication signals," Hewlett-Packard RF & Microwave Measurement Symposium, Signal Analysis Division, 1992.
3. EIA/TIA IS-54 "Cellular System Dual Mode Mobile Station - Base Station Compatibility Standard," Telecommunication Industry Association, Apr 1992.
4. EIA/TIA IS-55 "Recommended Minimum Performance Standards for 800 MHz Dual Mode Mobile Stations," Telecommunication Industry Association, Dec 1991.
5. EIA/TIA IS-56 "Recommended Minimum Performance Standards for 800 MHz Base Stations Supporting Dual Mode Mobile Stations", Telecommunication Industry Association, Mar 1991.
6. RCR STD-27A "Japan Digital Cellular Telecommunication System Standard," Research and Development Center for Radio Systems, Japan, Jan 1992.
7. MPT 1375 "Common Air Interface Specification," Department of Trade and Industry, London, May 1989.
8. I-ETS 300 131 "Radio Equipment and Systems (RES); Common air interface specification to be used for interworking between cordless telephone apparatus in the frequency band 864,1 MHz to 868,1 MHz, including public access services." European Telecommunications Standard Institute, France, Apr 1991.

cost effective transmitter building block. This advanced low-loss coupled resonator has also been used as the output filter. With this new SAW coupled resonator, the fundamental output power can be high and still provide the necessary harmonic rejection. It was necessary to have a low-loss filter so that the transmitter power could be made as high as possible with a minimum amount of current, thus enhancing battery life.

MB1007 AM KEYHEAD TRANSMITTER (Performance Parameters)				
Characteristics	Minimum	Typical	Maximum	Units
Operating Frequency	433.72	433.92	434.12	MHz
RF Output Power	25	50		µW
Spurious Emissions	FTZ 17TR2100 Compliant			
Power Supply	2.7	3	3.3	Volts
Operating Current		7	10	mA Peak
Operating Temperature	-30		+85	C
Data Rate		1		KHz
Oscillator Turn On Time			100	µs
Oscillator Turn Off Time			100	µs

Figure 16: HX Performance

Figure 16 shows the specifications of the HX1000: the hybrid transmitter designed for the German market. This module, when properly used, will meet the German FTZ 17 TR2100 emissions specification. This is evidenced by the MB1007 demonstration unit whose data is shown in Figure 17.

MB1007 TRANSMITTER PERFORMANCE vs REGULATION (Handheld Measurements)					
Harmonic	Freq (MHz)	Power Measured (dBm)	Power Measured (Watts)	FTZ Spec (Watts)	DTI Spec (Watts)
Fund.	433.92	-12	63E-6	25E-3	250E-6
2nd	867.84	-60	1E-9	1E-9	4E-9
3rd	1301.76	-65	0.3E-9	30E-9	1E-6
4th	1735.68	-62	0.6E-9	30E-9	1E-6
5th	2169.70	-46	25E-9	30E-9	1E-6
6th	2603.52	-49	13E-9	30E-9	1E-6
7th	3037.44	-47	20E-9	30E-9	1E-6
8th	3471.36	-48	16E-9	30E-9	1E-6

Figure 17: MB1007 Performance

The HX series of hybrid transmitters are designed to operate on a 3 volt Lithium battery. This greatly reduces the size of the transmitter. The MB1007 demonstration transmitter is configured on the head of an ignition key and uses the key stem as the antenna. In addition to the HX1000 at 433.92 MHz, an HX has been designed for all the other major low-power frequencies.

Conclusion

SAW resonator transmitters have been around for many years. The differing governmental regulations have given rise to the need for the various transmitter topologies. In the US, the harmonic emission requirement is only 20 dBc. This leads to a simple low-cost design. The major changes in these transmitters has been the replacement of the LC frequency determining elements with the SAW resonator. The surface mount revolution is currently causing changes in transmitter design. SAW resonators in surface mount packages are now available.

The European regulations, with more stringent harmonic requirements, create the need for a different transmitter design. These harmonic requirements generally cause the transmitter power to be low or have an elaborate filter. New advances in SAW technology at RFM have led to RF modules that allow for both a high fundamental power level, and sufficient harmonic rejection to meet the appropriate regulation.

Acknowledgment

The author wishes to thank Christina McFarland for her help in putting this paper together.

ERROR FREE MOBILE DATA COMMUNICATIONS: PRINCIPLES AND PROTOCOLS

Parviz Yegani
IBM
D81A/060
P.O. Box 12195
Research Triangle Park, NC 27709
YEGANI@ralvm11.vnet.ibm.com
Tel: (919) 254-3474
Fax: (919) 543-7575

Abstract - The potential growth of wireless data communications over digital cellular and cell digital packet data presents new challenges to those engineers who are or will be involved in design and development of such systems. This paper describes protocols for error-free data transmission over communications links in these cellular systems. Efficient ARQ-based protocols are introduced to achieve high transmission throughput in multipath fading environments that these cellular channels encounter. In order to further reduce severe multipath fading and signal shadowing effects and to achieve robust data transmission auxiliary error protection techniques such as forward error correction (FEC) and diversity reception together with ARQ scheme must be employed. These schemes are incorporated into radio link protocols so called ARQ/FEC/DIV RLPs which are designed to support reliable data transmission across a radio link having a cellular frame architecture. These protocols can be used , for example, to provide error-free facsimile signal transmission and async data services in mobile radio environments.¹ The throughput performance of ARQ/FEC/DIV protocols as a function of fading parameters for different communication channels are investigated.

¹ Async Data and Group 3 Fax services are currently being standardized by EIA/TIA.

FILTER COMPARATOR NETWORK FOR BEAM POSITION MONITORING

Michael Ferrand and Mark McWhorter
Vernitron Corporation
Lorch Electronics Division
2801 72nd St. N. St. Petersburg, FL 33710

Lorch Electronics has completed development and is currently manufacturing a Filter / Comparator network has been developed for Argonne National Laboratory for use in their Advanced Photon Source. This passive device operates in close proximity to the accelerator ring and provides boresight accuracy measurements to aid in the alignment of the beam.

The Filter / Comparator is the front end of a Beam Position Monitor, and is installed in close proximity to the particle accelerator ring. The device is connected by short phase matched cables to four capacitive "buttons" inserted on the perimeter of the ring which produce a very sharp voltage spike each time a particle "bunch" passes by. See Figure 1. The signal is an impulse 30 to 60 picoseconds wide, with an amplitude of 0.2 to 200 Volts. These signals must be stretched to about 100 nanoseconds in order to allow processing.

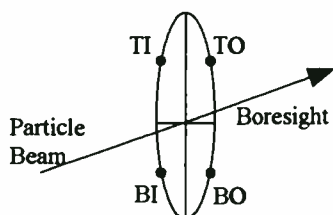


Figure 1 - Boresight

The purpose of the Filter / Comparator is to stretch and compare the signals from the four buttons in the time domain, such that the Sum and the Differences of the X and Y axis of those signals are provided with a high degree of accuracy.

The stretching is performed by matched sets of Gaussian response filters. The arithmetic summing / differencing is performed by the Hybrid Matrix. Additional Test / Trigger circuitry for timing is realized using Directional Couplers and a 4-way Power Splitter.

The beam position within the ring is related by the amplitude of the device outputs. Time domain distortion of the amplitude in terms of overshoot and ringing may create a measurement error.

The Filter / Comparator is comprised of the following matched components:

- 4-Input Attenuators, 6 dB, Broadband
- 4-Directional Couplers, 10 dB, Broadband
- 1-Power Divider, 4-Way, Broadband
- 3-Bandpass Filters, 352 MHz.
- 4-Lowpass Filters, 400 MHz.
- 4-180° Hybrids, Broadband
- 4-Amplitude / Phase Trim Circuits (as required)

Figure 2 provides a block diagram of the Filter / Comparator. The four inputs are labeled TI (Top In), TO (Top Out), BI (Bottom In) and BO (Bottom Out).

The individual components that comprise the Filter / Comparator are described below.

INPUT ATTENUATORS

The input attenuators reduce the signal by 6 dB at the input. Their primary function is to avoid the development of large standing waves caused by the reflections between the buttons and the

I INTRODUCTION

Error control is an area of increasing importance in data communications. The problem of providing reliable data communications over a mobile radio channel using error control techniques has received considerable attention recently [1 – 9], [20 – 30]. There are two main classes of channel coding techniques which are commonly used to improve the performance of a mobile communications system: ARQ schemes and forward error correction schemes (FEC). Error detection combined with retransmission on request, known as automatic RQ (ARQ) is a basic channel coding technique which have been used over three decades as a means of obtaining reliability in digital data transmission primarily for wireline channels [10 – 19], [31 – 35]. However, mobile digital communications systems are generally affected by noise and channel impairments such as multipath fading and Doppler effects as well as interference that degrade the reliability of the received information. In order to reduce severe multipath fading and signal shadowing effects and to achieve robust data transmission auxiliary error protection techniques such as forward error correction (FEC) and diversity reception together with ARQ scheme has been proposed. When FEC is used in conjunction with an ARQ protocol, it is called hybrid error control or *hybrid ARQ*. Hybrid ARQ schemes potentially offer better performance if appropriate ARQ and FEC schemes are properly combined. Either block or convolutional codes may be used for FEC. There has been a large number of variations on the basic ARQ theme which are detailed in [13] and references therein. These schemes are incorporated into radio link protocols so called ARQ/FEC/DIV RLPs which are designed to support reliable data transmission across a radio link having a cellular frame architecture. These protocols can be used, for example, to provide error-free facsimile signal transmission and async data services in mobile radio environments. The throughput performance of ARQ/FEC/DIV protocols as a function of fading parameters for different communication channels are investigated.

Figure 1 shows a reference model of the Interim Standard (IS-54) data channel set-up for a digital cellular system [22]. The terminal (TE2) is assumed to generate a stream of user's (raw) data in data blocks format. The mobile modem (MT2) is responsible for providing a reliable, connection-oriented, data delivery service by encoding the incoming data stream with a proposed FEC and to maintain a book-keeping service on data blocks delivered across U_m interface by using a proposed ARQ scheme. A diversity technique must be used to further improve the perform-

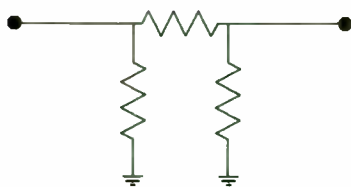


Figure 3 - 'Pi' Pad

TEST / TRIGGER CIRCUIT - 10 dB DIRECTIONAL COUPLERS / POWER SPLITTER

The couplers combine the reflected signals from the filters, and create a trigger for timing purposes. They also allow the injection of four test signals into the system. The coupled port on BO will have a 6 dB pad added to create a predetermined offset, negative for Dx and positive for Dy. The path from the 4-way power divider input to each coupler output is matched in amplitude and phase. The couplers are comprised of lumped elements to allow for adjustment in matching amplitude and phase.

BANDPASS FILTERS

The Filter / Comparator contains three bandpass filters whose purpose is to provide a Gaussian shaped 100 nanosecond wide modulated pulse from the input impulse passing through the lowpass filters and hybrid matrix. The filters must be matched in amplitude, phase and delay. So that the filters were matched well beyond their 3 dB points a 12 dB "Transitional Gaussian" filter was used. The individual filter specifications were as follows:

- Center Frequency: 351.93 MHz
- 3 dB Bandwidth: 10 MHz
- Number of Poles: 3
- Sidelobe Rejection: 60 dB. min.
- Amplitude Matching: ± 0.05 dB
- Phase Matching: $\pm 0.5^\circ$
- Insertion Loss: 4 dB max.

With the exception of the matching requirements, the filter fell into the realm of a "catalog standard". The filter was realized as a mutually-coupled circuit which provides excellent insertion loss and ease of alignment. The filter schematic is shown below in Figure 4.

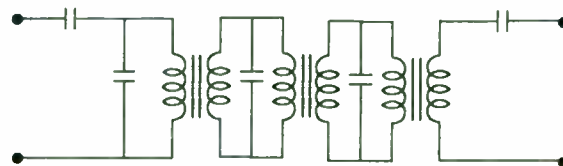


Figure 4 - Bandpass Filter

180 DEGREE HYBRID BUTLER MATRIX

The Filter Comparator uses four 180° Hybrids to linearly process the outputs of the filters in the time domain. The hybrid matrix produces three output signals:

$$\text{SUM} = \text{TI} + \text{TO} + \text{BI} + \text{BO}$$

$$\text{DY} = \text{TI} + \text{TO} - \text{BI} - \text{BO}$$

$$\text{DX} = \text{TO} + \text{BO} - \text{TI} - \text{BI}$$

The 180 degree hybrids are constructed using twisted pair ferrite miniature transformers and have a usable bandwidth from 10 to 500 MHz. In order to meet the key specification of cancellation ratio (-45 dB @ Dx and Dy outputs with inputs at boresight), we tuned the hybrids to less than one degree phase error and 0.15 dB amplitude error between all four ports at the critical frequency of 351.93 MHz. Sets of four phase / amplitude matched hybrids are required to create the matrix. The fourth output of the matrix is terminated internally into 50 Ohms. We manufactured the hybrids were manufactured on a PC mountable header. A schematic of the 180° hybrids is shown in Figure 5.

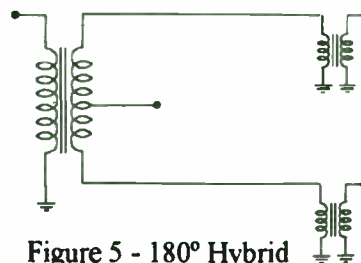


Figure 5 - 180° Hybrid

ance of the system across the link. EIA/TIA² standard committee has formed a task force which is currently investigating appropriate radio link protocols for mobile data services [38]. There are two types of Fax/Data services: *transparent* and *nontransparent*. In a transparent service the fax quality or data bit error rate is affected by the condition of the channel. Data throughput and fax transmit time in this case is constant. However, in a nontransparent service both data error rate and quality of fax remains the same under different channel conditions. But transmit delay for fax and throughput for data services are affected by the level of channel impairments. This group is planning to develop performance metrics which can be used to quantify the degree of improvement gained by using RLPs for various mobile data services and applications [22].

This paper is organized as follows. In section II an overview of ARQ protocols is given. Section III provide an insight into the FEC schemes. Hybrid ARQ schemes are presented in section IV. Section V discusses the use of diversity reception for cellular channels. Throughput performance of RLPs are outlined in section VI. Finally, the conclusions are given in section VII.

II ARQ PROTOCOLS

ARQ schemes are widely used in data communications systems for error control because they are simple and provide high system reliability [13]. For example, they are used extensively in packet-switched data networks and computer communications networks where they are mostly combined with adaptive routing techniques. In such a network if a packet hit a bad or noisy link, then this packet can be repeated and most likely it will be routed on a good link. An error control strategy is characterized by its complexity, the undetected bit error probability, and the throughput. There are three main protocols used in ARQ schemes: stop-and-wait (SW), the go-back-N (GBN), and selective repeat (SR). The SW protocols are easy to implement which is their main advantage. However, these protocols are inherently inefficient due to the idle time spent waiting for the receiver to acknowledge each transmission. The GBN schemes are more efficient since codewords are transmitted continuously one after another. These protocols have been studied previously [3,4,13,15,16]. The results show that at low error rates their performance is satisfactory particularly when the round-trip delay is small. However, for situations where the error rates are high and/or round-trip delays are large (for example, in satellite communications) their performance may deteriorate very rapidly. The

² EIA/TIA stands for Electronics Industries Association/ Telecommunications Industry Association.

LOWPASS FILTER

The lowpass filters are required to reject the high frequency components of the input impulse to the Trigger output, and allow the desired frequency of 351.93 MHz to pass for processing into the hybrid matrix. They are realized as a 3 pole lumped element Chebyshev design. The series inductor is tuned during the final alignment process to optimize the cancellation ratio.

AMPLITUDE / PHASE TRIMMERS

In order to achieve the 45 dB cancellation ratio, we must compensate for manufacturing and component tolerances. An adjustment is provided by the lowpass filter's series inductor. Additional capacitive tuning between hybrids of the Butler matrix is also required. In order to phase and amplitude match all three outputs, it is necessary to use "select at test" shunt chip resistors and capacitors at each filter output.

MECHANICAL CONFIGURATION

The components are mounted on a PC board inserted into a machined aluminium housing. Because of the necessity of maintaining equal phase lengths / delays between channels, all the RF traces on the board are the same length. The PC board is manufactured from FR-4.

The system application is in close proximity to the accelerator ring. The Filter / Comparator is designed to withstand a high gamma radiation environment of up to 50 Krads/year, which precludes the use of radiation sensitive materials within the unit. Teflon[®] could not be used, therefore the connector dielectric is made of Rexolite. The epoxy to secure the components is also certified to withstand this type of environment.

The finished unit is 6 x 6 x 2 inches. SMA-female connectors are used for the TI, TO, BI, BO inputs and TNC female connectors are used for the Sum, Dx, Dy and Test/Trigger

THEORETICAL DATA

The customer required exhaustive computerized analysis to show the effects of component tolerances. We presented design data and analysis to the customer in December of 1992. The report contained well over one hundred pages of test data and drawings and showed the effects of component tolerance on the cancellation ratio. Data on individual components including the coupler, pads, filters, hybrids and the power splitter were also provided.

The customer required data to show performance in both the time and frequency domains. For analysis in the time domain we used iSpice by Intusoft. For the frequency domain, we used Touchstone[®] by EEsof was used.

In addition to analyzing the individual components, we performed a complete systems analysis in the time and frequency domain.

ACTUAL DATA

The key performance criteria of the device is cancellation ratio. Return loss and insertion loss / phases are also measured on each unit.

Cancellation ratio is defined at boresight in the ring, where all four input signals have identical amplitude and time of arrival at the device inputs. Under this condition, each device must be painstakingly tuned to achieve the desired -45 dB ratio of Sum to Dx (or Dy) output.

Tests were carried out using both methods until it could be proven that correlation existed between Time and Frequency Domain measurement techniques. Production testing was then performed using the HP-8753C network analyzer with the Time Domain Option. The units are tuned in the frequency domain while simultaneously viewing both D-output ports. Final data is taken using the Time Domain option.

Figure 6 shows the smooth Gaussian shape of the Sum output, which is the sum of all 4 inputs.

most efficient of the ARQ protocols are the SR schemes. The transmitter in an SR scheme repeats only those blocks which are in error. There is an overhead due to the retransmissions of the blocks which is traded for higher reliability. The degree of overhead will vary greatly depending on how noisy the channel is. This scheme can be implemented only with large buffers at the receiver which make them less attractive for most of the communications applications. In order to enhance protocol efficiency there are numerous modifications of these three basic schemes which have appeared in the technical literature [12 – 17].

Most of the work in the area of ARQ error control has been done using block codes [31 – 32]. However, convolutional codes have a number of features that make them attractive for use in systems with repeat request. A number of ARQ schemes with convolutional codes have been proposed. Sequential decoding of convolutional codes appears to be the most promising method of ARQ error control [16, 34 – 35]. Drukarev et al. [16] analyzed two sequential decoding algorithms for memoryless channels with noiseless feedback. It was shown that the memory requirement for these algorithms when ARQ error control is used are less stringent than those for FEC error control. FEC error control is discussed next.

III FORWARD ERROR CONTROL

Forward error control (FEC) strategies are used in data transmission systems to achieve higher throughputs. In an FEC error-control system, an error correcting code (block or convolutional) is used for correcting transmission errors. Since no retransmission is required in an FEC error-control system, no feedback channel is needed. The overhead with an FEC scheme is always fixed and the throughput of the system is constant and is equal to the rate of the code used by the system. Compare this with bit-oriented protocols like SDLC and HDLC [17] in which the size of the data blocks (frames) are variable, therefore, the overhead due to cyclic redundancy check (CRC) varies from less than one percent in lengthy frames, to as much as 10 percent with relatively short frames [18]. The main drawback of FEC scheme is that it is not easy to obtain high system reliability with a moderate code length. Furthermore, the error probability of FEC systems is higher than those of ARQ systems. This is mainly due to the error-detecting capabilities of a code which exceeds its error-correcting capabilities in ARQ systems [16]. This is true when block codes and convolutional codes with Viterbi decoding is used. However, by using sequential decoding it is possible to achieve both lower error probability and higher throughput in FEC systems. Because of these reasons ARQ schemes are often preferred to FEC schemes.

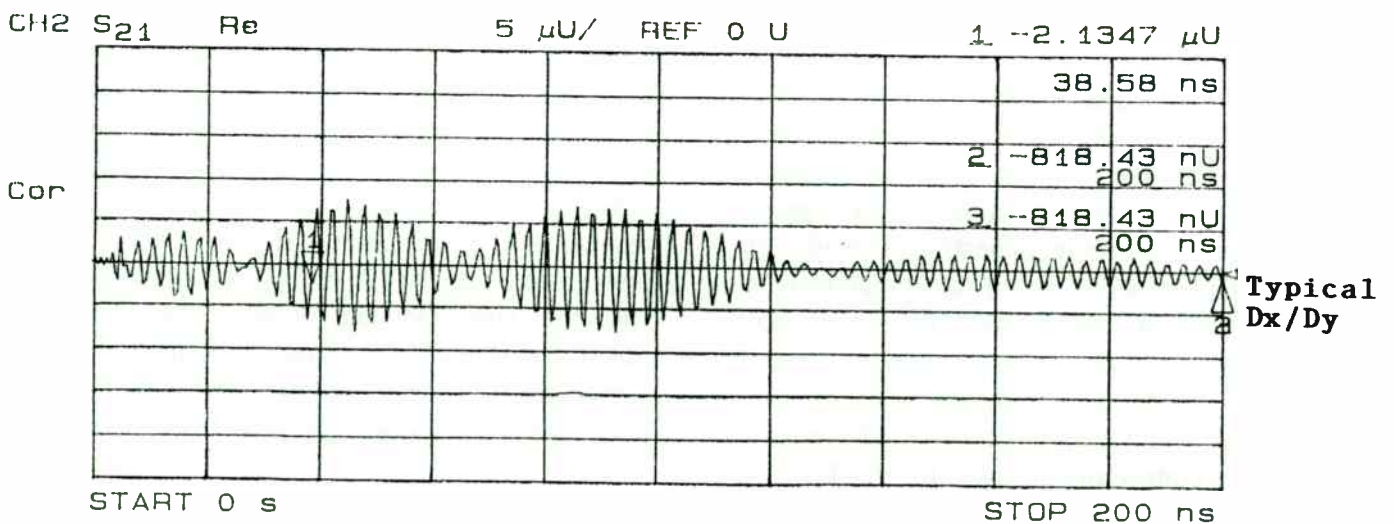
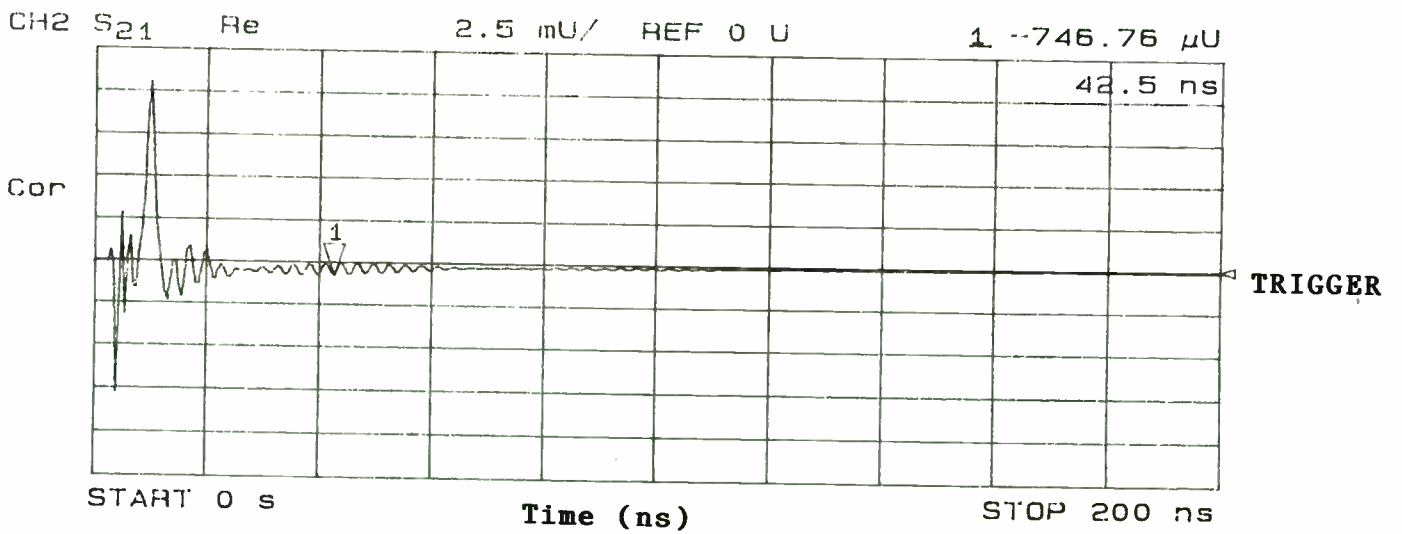
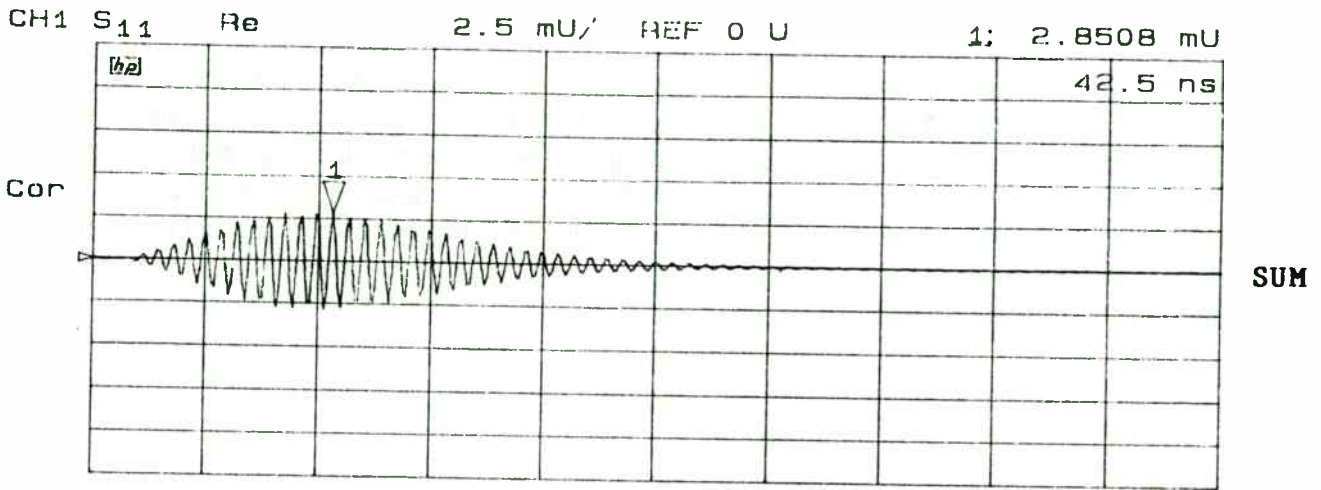


FIGURE 6

There are certain applications when there is no return channel, necessary for ARQ operations, for example in data storage systems, or when the time involved in retransmission adds an intolerable delay to error correction then FEC is the only viable solution. This is why FEC (in the form of Trellis coding [36]) has been included as an integral part of the CCITT's new dial-up high-speed modem specifications. Trellis coded modulation allows more data to be transmitted over a channel with limited bandwidth. The block error rate performance of a TCM modulator used in a high speed modem is shown in Fig. 2 [19]. As it is seen from this figure the performance improvement of TCM is 3 dB more than with a QAM scheme. Unfortunately Trellis coding alone is not very effective against deep fades and interference bursts. It is mostly used for voice grade channels with Gaussian noise in which the overwhelming majority of errors usually affect only a single bit. It is also difficult to use Trellis for very high-speed applications ($\geq 20\text{Mbps}$). This is mainly due to the difficulty of implementing decoders and demodulators at such speeds. An appropriate coding strategy for these applications is to use low-redundancy block codes with simpler modulations or concatenated with Trellis codes.

More recently, FEC has been used to improve the performance of mobile radio communications systems [21, 25, 27 – 30]. For example, TCM and multiple TCM (MTCM) has been used and demonstrated improved performance at data rates of practical interest [29]. In [30] a combined TCM and type-I hybrid ARQ (HARQ) protocol is used to enhance system performance over slowly fading channels. It is shown that the TCM-HARQ and MTCM-HARQ protocols provide excellent reliability performance at the expense of some reduction in throughput at nominal signal-to-noise ratio over such channels. One disadvantage of an FEC system is that decoding FEC is normally more complex than encoding and it is mostly often done by the Viterbi algorithm [11]. With convolutional codes if the decoder makes a mistake in the history of the data stream (due to either fading or burst interference) error will propagate making these codes less attractive for error control in wireless data communications. Besides, the decoder of convolutional codes must know the boundaries of each sub block. Figure 3 illustrates the features of two commonly used FEC codes in practice [18]. It is seen that user data typically suffers a longer delay in block coding than with convolutional schemes. The error detection and correction capabilities of these schemes are different. As the figure indicates block coding seems to be the best technique for handling long error bursts.

It also shows the typical Dx (or Dy) output at -45 dB or more and the narrow pulse signal, used for timing at the next stage of the Beam Position Monitor.

Measured into a fifty ohm system, the Filter Comparator has typically 13 dB of insertion loss, and phase balance between outputs of ± 3 degrees with various input conditions applied. Return losses are typically 16 dB.

Lorch is currently producing five hundred units in support of the Argonne Advanced Photon Source.

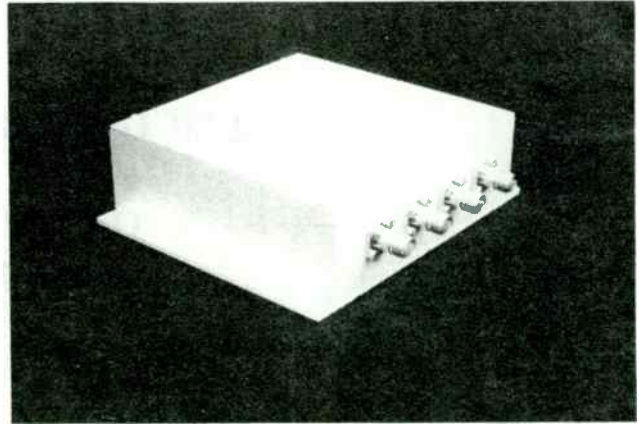


Figure 7. Filter/Comparator

This work was carried out under a U.S. Department of Energy contract through Argonne National Laboratories. The authors would like to acknowledge the design effort and help of Manny Kahana of Argonne National Laboratories and Tho Van Nyugen for his bench work and support.

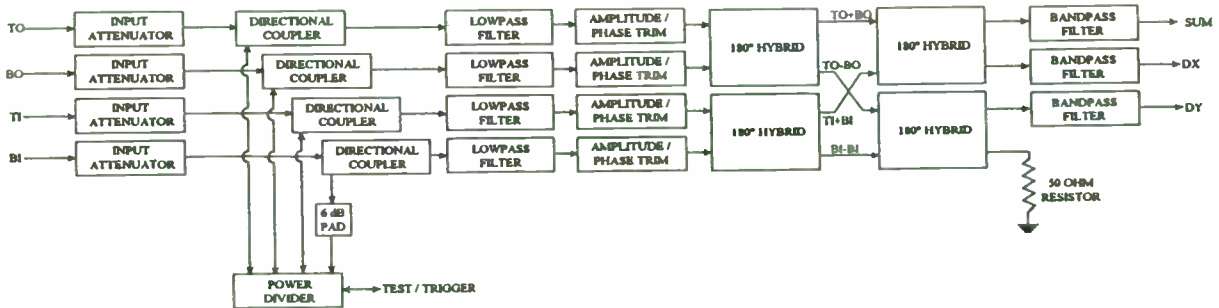


Figure 2
BLOCK DIAGRAM, FILTER COMPARATOR UNIT

IV HYBRID ARQ ERROR CONTROL

The most important advantage of ARQ is that the quality of the received data is predictable; the greatest disadvantage is that throughput depends on the channel condition. However, in a system employing FEC data is delivered with a constant throughput and a quality depending on the noise characteristics of the channel. From the above statement it is obvious that one should use a combination of FEC and ARQ, known as *hybrid ARQ*, in order to take advantage of the fact that these two schemes behave in a complementary fashion. The combined scheme can fundamentally change system performance provided that they are matched to the channel conditions and user requirements. In other words, FEC increases the system throughput by reducing the frequency of retransmission and correcting the error patterns which occur frequently. However, when a less-frequent error pattern occurs and is detected, the receiver requests a retransmission rather than passing the unreliably decoded message to the user. This increases the system reliability. Therefore, by properly combining FEC and ARQ the overall system throughput will be higher than that of a system with ARQ alone and the reliability will be higher than that of a pure FEC system. Hybrid ARQ schemes can be classified into two categories, namely *type-I* and *type-II* schemes [33]. These schemes are discussed next.

Type 1 ARQ is the one commonly used in practice. It is best suited for communications systems in which a fairly constant level of noise and interference is anticipated on the channel. In a type-I hybrid ARQ the data and error correcting parity bits are encoded with an FEC code. The bits added by the error correction code are called error correction parity bits to distinguish them from the error detection parity bits [14]. In this system channel errors are corrected and FEC decoder outputs an estimate of data and the error detection parity bits. The error detection decoder accepts the data if it is error free. However, if an error is detected a request for retransmission is sent to the source by the ARQ protocol.

Type I FEC/ARQ has a major disadvantage when used to control errors in less noisy or perfect channels. That is when the channel bit error rate is low the transmission is smooth and no (or little) error correction is needed. As a result the extra parity-check bits included in each transmission is wasted and, therefore, reduces the throughput. On the other hand, when the channel is very noisy, the designed error correcting capability may become inadequate. Therefore, for a channel with a nonstationary bit error rate it is desirable to have an adaptive hybrid ARQ scheme. This has led to the design of type-II ARQ. The most common form of type-II ARQ is ARQ/FEC scheme in which the system behaves like a pure ARQ when the channel

Digital Temperature Compensation of Oscillators Using a Mixed Mode ASIC

Steven Fry
muRata ERiE North America
1900 West College Avenue
State College, Pa. 16801

Abstract

This paper will describe the design, construction, calibration and operation of digitally compensated crystal oscillators, making use of a custom Application Specific Integrated Circuit developed specifically for the purpose. This IC is fabricated in a "Triple Technology" process. This allows the integration of all of the digital functions, supporting analog blocks and an Electrically Erasable PROM in a single +5 V device. A true "single chip" DCXO is therefore made possible.

Also described will be a novel compensation scheme which allows autonomous calibration, requiring no interface to an external test computer in order to acquire the unique set of compensation data for each oscillator.

Introduction

Digital frequency vs. temperature compensation has been a reality since the early days of the integrated circuit. Even then, these schemes achieved quite respectable performance with some capable of achieving compensation less than the magnitude of typical quartz crystal thermal hysteresis. (1)

These original devices tended to be bulky and complicated to assemble and were therefore large and expensive. As the available integrated circuits began to improve and with the aid of hybrid construction techniques, the oscillator sizes began to shrink, but the costs remained relatively high. (2)

With the advent of Large Scale mixed mode integration, it is now feasible to design a true "single chip" DCXO allowing dramatic size and cost reductions.

Digital Compensation Basics

The block diagram of a fundamental digital compensation system is shown in Figure 1. A temperature sensor which is in close thermal contact with the crystal senses the instantaneous crystal temperature. This analog signal is then properly scaled to match the end points of the operating temperature range to the zero and full scale limits of the A/D converter. Almost any type of A/D may be used since conversion speed is not an issue. In some cases, a temperature to frequency converter using a crystal may be used.

is in good condition. The data in this scheme is sent without FEC and only error detection parity-bits is attached to it. If data is delivered with no error, then a new block of data (if any) is sent. If an error is detected, source will send an error correcting code along with the error detecting code, to recover the erroneous data. If these codes are received correctly the receiver will use them to correct errors and the process ends. If the receiver detects errors in these codes, it will still try to recover data and if succeeds the process is terminated. Otherwise, the data or code are retransmitted and the process begins again until the data is properly delivered.

V DIVERSITY TECHNIQUES

As mentioned earlier (fast) multipath fading severely degrades the performance of a mobile data transmission system. One of the most effective techniques to cope with this problem is the use of diversity reception. Various diversity techniques have been proposed for digital mobile radio systems. This includes *Branch Construction Methods, Combining Methods*. Branch diversity can be constructed using the following methods [39]:

- Space Diversity
- Angle Diversity
- Polarization Diversity
- Frequency Diversity
- Time Diversity

Among these techniques space diversity is the one which is widely used. This comprises a single transmitting antenna and a number of receiving antennas. By adjusting the spacing between receiving antennas it is possible to uncorrelate signals received from each branch. Similar techniques are applied to angle and polarization diversity. For frequency and time diversity the required frequency and time spacing are determined from the characteristics of the time-delay spread and the maximum Doppler frequency. An advantage of these techniques is that only one receiving antenna is required to implement them. Combining methods are classified into three different categories:

- Maximal-Ratio Combining
- Equal-Gain Combining
- Selection Method

The output of the A/D then becomes the address which is applied to a non-volatile ROM which contains the required compensation data at each temperature increment. This memory is typically a low-powered CMOS device.

The contents of the addressed memory location are then applied to the D/A converter which produces the compensating voltage which is fed back to the voltage control port on the crystal oscillator to compensate the frequency. This type of "brute force" look-up table technique has been used successfully by a number of manufacturers, but the assembly is still relatively complicated and a coarse compensation network is sometimes necessary to reduce the frequency excursion of the crystal to a lower level.

The ultimate achievable accuracy of the system is determined by several factors: (3) (4)

- 1.) The total temperature range to be covered.
($T = T_{max} - T_{min}$)
- 2.) The maximum peak-to-peak frequency excursion of the crystal.
($F = F_{max} - F_{min}$)(PPM)
- 3.) The maximum slope of the crystal's frequency vs. temperature characteristic.
($S = \text{PPM/Deg. C}$)
- 4.) The number of bits of resolution of the temperature measurement as determined by the A/D.
($N_t = \# \text{ of A/D bits}$)
- 5.) The smallest increment of frequency adjustment as determined by the D/A.
($N_v = \# \text{ of D/A bits}$)

The smallest delta F achievable can then be calculated by:

$$dF = (S/2)(T/2^{N_t}) + (F/2)(1/2^{N_v})$$

One additional factor which must be taken into account is that this formula assumes that 100% of the A/D and D/A range will be used. It is

more practical to expect that an average of 70% will be usable without spending a large amount of test time on the initial set-up, therefore:

$$dF = (S/2)(T/(0.7)(2^{N_t})) + (F/2)(1/(0.7)(2^{N_v}))$$

The typical calibration procedure for this type of DCXO would require that the PROM be replaced with an interface cable which would be connected to a test computer. As the Unit Under Test is then put through a temp. run, the computer reads the A/D and exercises the D/A to determine the required data. A curve-fit is then performed and the entire data table is burned into the PROM. (5) This procedure is fairly straight forward, but designing a system to compensate multiple units can be quite complicated. It would therefore be desirable if some on board intelligence could be added to the oscillator to simplify the data acquisition for calibration. Several companies have taken this approach by adding a micro-computer to the oscillator, but the procedure still requires interactive communication with the host computer and assorted instruments. It was therefore a goal of the project undertaken by muRata to produce an oscillator which was "self compensating".

ASIC Configuration

With the goals of producing a single-chip DCXO that was cost effective and required a minimum amount of testing time and test hardware, the necessary block diagram was designed. After some refinements to match the configuration to the chip vendor's processes and cell library, the system was breadboarded using similar packaged kit parts. The circuit was controlled with an emulator which also served as the software development tool. After finalizing the hardware configuration and the system software for the internal ROM, the chips were produced by Sierra Semiconductor.

Digital Section

All of the chip operations are controlled by a COP880 series 8-Bit microcomputer cell. The memory available consists of: 128 Bytes of RAM

Maximal-ratio combining achieves the best performance improvement compared with the other methods, but it is the most difficult one to implement. Selection method is more suitable for mobile radio application due to its simple implementation. One attractive way to implement this technique is by switching diversity branches periodically. Performance improvements achieved by diversity techniques has been extensively researched (refer to [39]). These techniques combined with ARQ and FEC error control are used to design radio links for digital mobile radio systems.

In the next section an overview of some of the most recent work on throughput performance for different radio link protocols are presented and their performance are compared.

VI THROUGHPUT PERFORMANCE

The throughput of an RLP scheme depends on several parameters [9]:

- block length of data and acknowledgement
- signal-to-noise-ratio of forward and reverse channels
- signalling rates
- FEC code rate
- ARQ strategy
- environment of mobile terminal
- velocity of mobile terminal
- type of diversity

The throughput performance of a plain (also called type-0) ARQ is heavily dependent on the channel conditions (see Fig. 4). As the Figure indicates the throughput of the system decreases drastically when the bit error rate of the channel approaches some moderate values (between 10^{-3} and 10^{-2}) The other major disadvantage of using type-0 ARQ is its vulnerability to periodic (but not bursty) interferences. For mobile communications where channel is subject to short bursts of interference ARQ type 0 proves to be an effective error control mechanism. A throughput comparison of hybrid ARQ is shown in Fig. 5. It is noticed that a type-I hybrid ARQ system has lower throughput than its corresponding ARQ system when the channel error rate is low. However, when the channel error rate is

for temporary program storage; 4 KBytes of mask programmed ROM which contains the firmware to execute the self-calibration and normal operational modes and 256 Bytes of EEPROM into which the uCPU loads the compensation data as it is acquired. A charge pump is included so that write operations to this non-volatile memory are completely transparent. Analog cells are used to implement the power-on-reset and low voltage detect functions which ensure reliable operation of the uCPU under any power supply conditions.

The clock for the digital section is derived from the external crystal which is prescaled by an on-chip divider. This divider is adjustable by the uCPU from /5 to /127. The desirable clock frequency to the uCPU is around 620 KHz so that a wide range of external crystal frequencies may be used directly.

A serial address/data bus allows communication with an external computer or test fixture to load the application specific program constants, to run diagnostics or to examine the data tables after calibration. Using this bus, the uCPU can also execute from an external ROM so that the chip operations maybe customized for certain lower volume applications without changing the on-chip mask ROM and fabricating new wafers.

Also included in the digital section is a power-down timer. The uCPU may load this register with a specific delay time and then put itself into a "Halt" mode. Program execution is then suspended until the timer period has elapsed and the uCPU is re-started. This halt period is dynamically adjusted by the uCPU as it monitors the rate at which the temperature is changing. When the temperature is stable, the compensation data output only needs to be updated periodically and the "sleep" mode may extend to greater than 2 minutes to conserve power and reduce the noise generated. An external signal may be asserted to completely inhibit the uCPU from running if so desired.

Several general purpose digital I/O pins are available for monitoring program status, accurate

signal timing, or any digital I/O function as defined by the program. A programmable pulse counter is also available which may be used for synthesis of accurate low frequency signals.

Analog Section

The measurement of the crystal temperature is implemented with 12-Bits of accuracy by a dual slope integrating A/D converter. This type of A/D was chosen for the most efficient use of die area, low power consumption and capability of achieving the needed accuracy. This configuration does require two external capacitors and a resistor but good performance has been achieved with small, low cost components. The integration cycles are controlled and switched by the uCPU which also counts clock cycles to perform the conversion. Although the conversion time is typically 130 mSec, speed is of little concern here since the parameter being measured has a relatively slow rate of change.

The temperature of the ASIC die is indicated by an on-chip temp. sensor. If closer thermal contact with the crystal is necessary, an analog switch is set so that the voltage from an external temp. sensor is applied to the A/D amplifier. This amplifier must be a low noise device since the equivalent bit size referred to the input may be less than 10 uV.

The temp sensors typically produce a voltage of 300 mV at +25 C and change at +1 mV/Deg. C. The A/D's zero and full scale points are then scaled to match the endpoints of the desired operating temperature range by having the uCPU load the gain and offset registers with the proper binary value. The zero range is therefore settable from about -55 to +10 C and the full scale from +30 to +100 C without any external component change.

The output voltage which controls the oscillator frequency is produced by a 10-Bit charge integration D/A converter. The output is buffered and scaled to give an output range of 0 to +4.1 V.

high type-I hybrid ARQ has a higher throughput as compared to a pure ARQ system. This is mainly due to the error-correction capability which reduces the retransmission frequency.

There has been numerous publications on throughput performance of ARQ schemes combined with FEC and diversity which has appeared in the literature over the past few years. Some of these research results pertaining to throughput of RLPs are discussed next.

Jalali et al. [1] studied the performance of data protocols for their proposed in-building CT2Plus wireless system. Their result on performance comparison of different R-S codes, GBN ARQ for a Time Division Duplex (TDD) system is shown in Fig. 6. A buffer at the receiver is used to queue the user data during poor channel conditions, therefore, preventing data from being lost. A higher throughput is obtained by emptying the buffer via using fast code rates in this system. A frequency non-selective Rayleigh fading channel using Jake's model [37] was used to evaluate the performance. The simulation results show that a coding gain of 2.8 dB was achieved at 80% throughput by FEC of 2/3 rate using (63,48;3) and (63,44;3) R-S codes. This gain reduces to 2.0 dB when no antenna diversity is used. This indicates that the use of diversity improves the performance of a radio link. For a Frequency Division Duplex (FDD) system performance reported in [1] show similar results. This study recommends the use of type-I hybrid ARQ schemes with the Reed-Solomon code (63,44;3) and the GB7 ARQ protocol for the proposed CT2Plus system.

A similar study for fax transmission over a Rayleigh fading channel for Japanese Digital Cellular (JDC) system was performed by Ito et al. [2]. A buffer at the receiver is used to keep track of the sequence number of the incorrect received data frames. These frames are repeated until they are received with no error. Differentially coherent QPSK with post detection selection diversity reception was used in the simulation experiments. As shown in Figure 7 the throughput efficiency of the WORM-ARQ protocol is 4 times of that of Rej-based HDLC protocol. Benelli proposed a new GBN protocol and its performance for a mobile communications channel was studied [3]. In this protocol also a buffer at the receiver was proposed. The results reported in this paper show that by introducing a memory at the receiver the throughput of an ARQ may be kept to acceptable values even for poor channel conditions where FEC techniques become unreliable.

An application of frequency diversity (in the form frequency hopping) combined with FEC is discussed in a paper by Parviz Yegani and C. McGillem. This paper pro-

Other analog functions included on the chip are: a 4.1 Vdc voltage reference and several gain stages for use as the crystal oscillator and buffer. A phase detector, reference counter and various analog switches are available to be used in the calibration mode.

This circuitry is integrated on a single die with dimensions of 5.77x7.20 mm (0.227x0.283 ") in a 1.5 micron process. The parts are presently packaged in a 28 pin PLCC although plans are underway to design a hybrid layout to use the ASIC in die form for further miniaturization.

Oscillator Calibration/Data Acquisition

In order to minimize the amount of testing time required and reduce the cost of building a test system, a unique calibration configuration was designed. An applied reference frequency is used to phase lock the crystal oscillator at its nominal frequency. The operation of the self-compensating procedure is described as follows:

1.) The initial set-up variables are loaded into the EEPROM through the serial data bus. These variables customize the internal program operation for the intended application by setting the clock frequency, loading the A/D gain and offset registers and adjusting the system timing.

2.) The unit to be calibrated is placed into a temperature chamber and the temperature is increased to the highest operating temp. After a stabilization period, a reference frequency from a synthesizer is applied to the unit. The uCPU is then initialized. The first task performed by the ROM program upon initialization is to interrogate the reference detection counter to determine if the reference signal is present. If so, it indicates to the program that a calibration run is being started.

In order to begin the calibration procedure, the uCPU places the phase locked loop section into the calibration configuration by asserting the calibrate mode select signal which closes an analog

switch, closing the phase locked loop and phase locking the crystal oscillator to be compensated to the reference. It is, of course, necessary to have the center frequency and voltage tuning range of the crystal oscillator properly adjusted. A passive loop filter is connected between two external pins. As the ambient temperature subsequently changes, the tuning voltage will be adjusted by the loop to maintain phase lock as the crystal frequency tries to drift. Since the same voltage will be required to keep the oscillator at nominal frequency after the reference is removed, it can be digitized to determine what compensation data value is required.

When the calibration configuration is set, a switch is opened removing the negative feedback from the D/A amplifier so that it now functions as a high gain comparator instead of a unity gain buffer. Another switch is closed so that the uCPU may read the state of the comparator output from the D/A amp.

3.) After detecting the reference and setting the calibrate mode, the uCPU begins measuring the crystal temperature with the A/D converter. When the temperature has stabilized to within 1 Bit (approximately 0.04 Deg. C) over a period of time, a data point measurement is initiated. By controlling the D/A converter and using its buffer amp as a comparator, a successive approximation A/D conversion of the oscillator control voltage is performed. This determines to the nearest D/A bit what data will be required to achieve nominal frequency at this specific temperature when the reference is not present. This 10-Bit DAC frequency data and the corresponding 12-Bit temperature measurement define the x-y coordinates of a data point which is packed into a 3-Byte block and written into the EEPROM.

4.) The temperature is then lowered by the predetermined temperature increment and allowed to restabilize. Once again when the uCPU determines that the temperature has stabilized to within 1-Bit, a data point measurement is triggered and subsequently stored in the next sequential group of EEPROM locations.

poses a Frequency-Hopped, M-ary, Frequency-Shift-Keyed (FH-MFSK), Spread-Spectrum Communication System operating over the Factory Radio Channel [40]. The performance of the system for Rayleigh, Rician, and logNormal multipath fading for factory environments was investigated. The statistics of these channels, based on recent channel modeling studies [41], were used to evaluate the performance of the FH-MFSK system. Frequency hopping spread spectrum (FH-SS) which has a longer chip interval offers some advantages over DS-SS for mobile users in heavy multipath channels. There are cases where the rms delay spread of the channel is small and the signal components are not resolvable for reasonable chip durations. For example, in a typical factory environment with an rms delay of about 200 ns using FH-MFSK offers promise of reducing the serious fading that occurs in the channel. The FH-MFSK system block diagram is shown in Fig. 8. In the transmitter data modulation (MFSK) and frequency hopping modulation (FH) have been implemented in a two-step modulation process. MFSK modulation provides the multiple-access capability to the system while the FH modulation protects the system against multipath losses. The MFSK modulator produces an M-ary signal based on the simultaneous dictates of the PN code and the data. In this system FEC is introduced by a simple repeat code where each data symbol is transmitted N times, every time via different MFSK tones. Since every single tone is hopped independently, the different replica of each symbol passing through the channel experience different transmission losses. The results reported show that with the proposed system a much higher throughput can be obtained under the specified conditions than is possible with previously proposed systems.

VII CONCLUSIONS

This paper presented protocols for error-free data transmission over radio communications links in digital cellular systems. Efficient ARQ-based protocols were introduced to achieve high transmission throughput in multipath fading environments that these cellular channels encounter. A combination of forward error correction and diversity reception with ARQ scheme was incorporated into the link protocol so called ARQ/FEC/DIV RLPs. Various RLPs have been designed and used to support reliable data transmission across a radio link having a cellular frame architecture. It was shown that these protocols are efficient and can support standard data services including facsimile signal transmission and async data services in mobile radio environments. Finally, the throughput performance of ARQ/FEC/DIV protocols

5.) Step 4 is then repeated until reaching the lower limit of the operating temperature range. After the last data point has been acquired and stored, the chamber temperature is brought back up to room temperature. The uCPU senses this change, signifying the end of the calibration procedure. The data and status registers are then checked for any error flags which may have been set during calibration. A square wave signal is then output on one of the digital I/O pins, the frequency of which signifies the status of the run and the validity of the data.

6.) The reference frequency is then removed. This is sensed by the uCPU causing the program to branch to the normal frequency compensating mode of operation. The test system may then immediately begin a frequency verification run to determine the accuracy of the data.

Operational Mode

When the uCPU is initialized and the reference frequency is not present, the program immediately branches to the operate mode. It first of all makes sure that the configuration switches are set to the proper state, breaking the phase locked loop path and configuring the D/A amplifier as a unity gain buffer.

The program immediately measures the present temperature with the A/D. It then indexes through the data table looking for a stored temperature point close to the present temp. If a stored data point does not match the present temp. exactly, then the addresses above and below the present one are read into RAM along with their corresponding DAC data. A linear interpolation is then performed to determine the DAC voltage slope and to calculate the new DAC data required for the present temperature.

The typical temperature increment between the stored data points is 2 Deg. C. With about 40 bytes of the 256 byte EEPROM space used for storing set-up variables, this allows space for 72 data points to be stored. This would allow for a temperature span as wide as 144 Deg. C. with two degree steps. It has been shown that a look-up

table with interpolation is capable of matching the crystal curve almost as well as a seventh order curve fit. (6) The linear interpolation was therefore chosen since it was much simpler and efficient to implement in machine code.

When the program is initialized, the uCPU continuously measures the temperature, interpolates the data and updates the DAC. If the A/D data shows little or no temperature change between readings, a number will be loaded into the standby timer register and the uCPU execution will be halted for some period of time. If the temperature is stable enough that there is still no significant delta, the standby time will be increased even further and eventually may extend for more than two minutes. This sleep time minimizes the DC power consumption and also shortens the amount of time that the uCPU will be generating digital noise.

When it is detected that the temperature is beginning to change, the standby time will be progressively shortened in order to track the temperature as closely as possible. By controlling the sleep mode duration, sampling interval, and the number of ADC samples per update cycle, a dynamic balance is maintained between the ability to track rapid temperature variations and the average power consumption.

Performance Results

Since most of the required components have been included in the ASIC chip design, only a crystal, a varactor diode and a few passive components are needed to implement a complete Digitally Compensated Crystal Oscillator. (See Figure 4)

After the initial calibration run has been completed, the data table may be read out of the EEPROM and examined if so desired. A graph of a typical table is shown in Figure 5. Since the compensation voltage is applied to the cathode of the varactor diode, a positive frequency vs. voltage transfer function results so that the data in

as a function of fading parameters for different communication channels was investigated.

REFERENCES

- [1] A. Jalali et al., "Performance of data protocols for in-building wireless systems," ICUPC '92, pp. 407-411, Dallas, 1992.
- [2] S. Ito et al., "Facsimile signal transmission using WORM-ARQ in TDMA cellular system," Proc. IEEE VTC '92, pp. 247-250, 1992.
- [3] G. Benelli, "A go-back-N protocol for mobile communications," IEEE Trans. Veh. Technol., vol. 40, no. 4, pp. 714-720, Nov. 1991.
- [4] J. C. Chaung, "Comparison of two ARQ protocols in a Rayleigh fading channel," IEEE Trans. Veh. Technol., vol. 39, no. 4, pp. 368-373, Nov. 1990.
- [5] L. F. Chang and P. T. Porter, "Data services in a TDMA portable radio system," Proc. IEEE Globecom '90, pp. 480-484, 1990.
- [6] N. R. Sollenberger et al., "Architecture and implementation of an efficient and robust TDMA frame structure for digital portable communications," Proc. IEEE VTC '89, pp. 169-174, 1989.
- [7] S. Ito et al., "Facsimile signal transmission in digital mobile radio," Proc. IEEE VTC '88, pp. 83-88, 1988.
- [8] Y. Furuya et al., "High speed digital mobile facsimile with effective error protection," Proc. IEEE VTC '87, pp. 32-37, 1987.
- [9] E. Lutz, "Simulation of FEC/ARQ data transmission using stored land mobile satellite channels," Proc. IEEE VTC '86, pp. 109-115, 1986.
- [10] D.-L. Lu and J.-F. Chang, "Analysis of ARQ protocols via signal flow graphs," IEEE Trans. Commun., vol. COM-37, no. 3, pp. 245-251, March 1989.
- [11] N. Seshadri and C.-E. W. Sundberg, "Generalized Viterbi algorithm for error detection with convolutional codes," Proc. IEEE Globecom '89, pp. 1534-1537, 1989.
- [12] P. T. Brady, "Performance evaluation of multireject, selective reject, and other protocol enhancements," IEEE Trans. Commun., vol. COM-35, no. 6, pp. 659-666, June 1987.
- [13] S. Lin et al., "Automatic-repeat-request error-control schemes," IEEE Commun. Magazine, vol. 22, no. 12, pp. 5-17, Dec. 1984.
- [14] R. A. Comroe and D. J. Costello, JR., "ARQ schemes for data transmissions in mobile radio systems," IEEE J. Selected Area on Commun., vol. SAC-2, no. 4, pp. 472-481, July 1984.
- [15] E. R. Berlekamp et al., "The Application of Error Control to Communications," IEEE Communications Magazine, Vol. 25, No. 4, pp. 143-152, April 1987.

the table appears to be the inverse of the normal "AT" cut crystal curve.

Given a typical extended temperature range application of -40 to +85 Deg. C with a crystal peak-to-peak frequency deviation of 27 PPM, the maximum slope would be at the cold end of the crystal curve at about 1 PPM/Deg. C. Since the ASIC gives an A/D resolution of 12-Bits and a D/A resolution of 10-Bits, equation 2 on Figure 3 may then be used to calculate the best achievable stability in this application. Putting these numbers into the equation gives a temperature error term of 0.022 PPM and a voltage error term of 0.019 PPM which are summed together to give a total error of 0.041 PPM. Although this level may be achieved with great care, experience has shown that a factor of X2 to X3 should be added to allow for non-linearities and component anomalies which typically show up in production.

Figure 6 shows the frequency vs. temperature performance of this compensated oscillator on a scale of 0.05 PPM per division. This oscillator achieved a deviation of +/- 0.07 PPM compared to the predicted achievable value of 0.041 PPM.

Due to the small physical size of this system, it is inevitable that the CMOS uCPU and other digital circuitry will cause some degree of clock noise to appear on the oscillator signal. The chip however, was designed to segregate and minimize this feedthrough. The close to the carrier spurious signals are typically down -90 to -100 dBc and may be eliminated completely if the update inhibit line is asserted during critical periods. The oscillator board layouts have also been optimized to reduce the higher frequency clock feedthrough. Figure 8 shows a typical spectrum analyzer display of a 12 MHz oscillator with all clock noise close to -80 dBc.

Future Developments

As this project moves into production and the basic DCXO application begins to mature, work will continue on adding advanced functions.

One area which is being evaluated is the possible implementation of long term aging correction to offset the drift of the crystal by changing the firmware to include a predetermined extrapolation algorithm.

This same chip may also be used for direct frequency compensation of DRO's, SAW's and other high frequency oscillators. It will also be possible to implement indirect frequency compensation using high-Q "SC" cut crystals for even better stability.

The variety of useful functions on the chip may be designed in various configurations by re-writing the firmware to perform accurate timing and counting, digital I/O, frequency synthesis, and various phase locking functions, possibly for integration with the end user's system.

Conclusion

This paper has described a practical ASIC which has been developed specifically as a single chip solution for temperature compensation of oscillator frequency. This versatile device should make possible many new applications such as re-compensation in the end user's equipment and remote frequency adjustment.

Acknowledgments

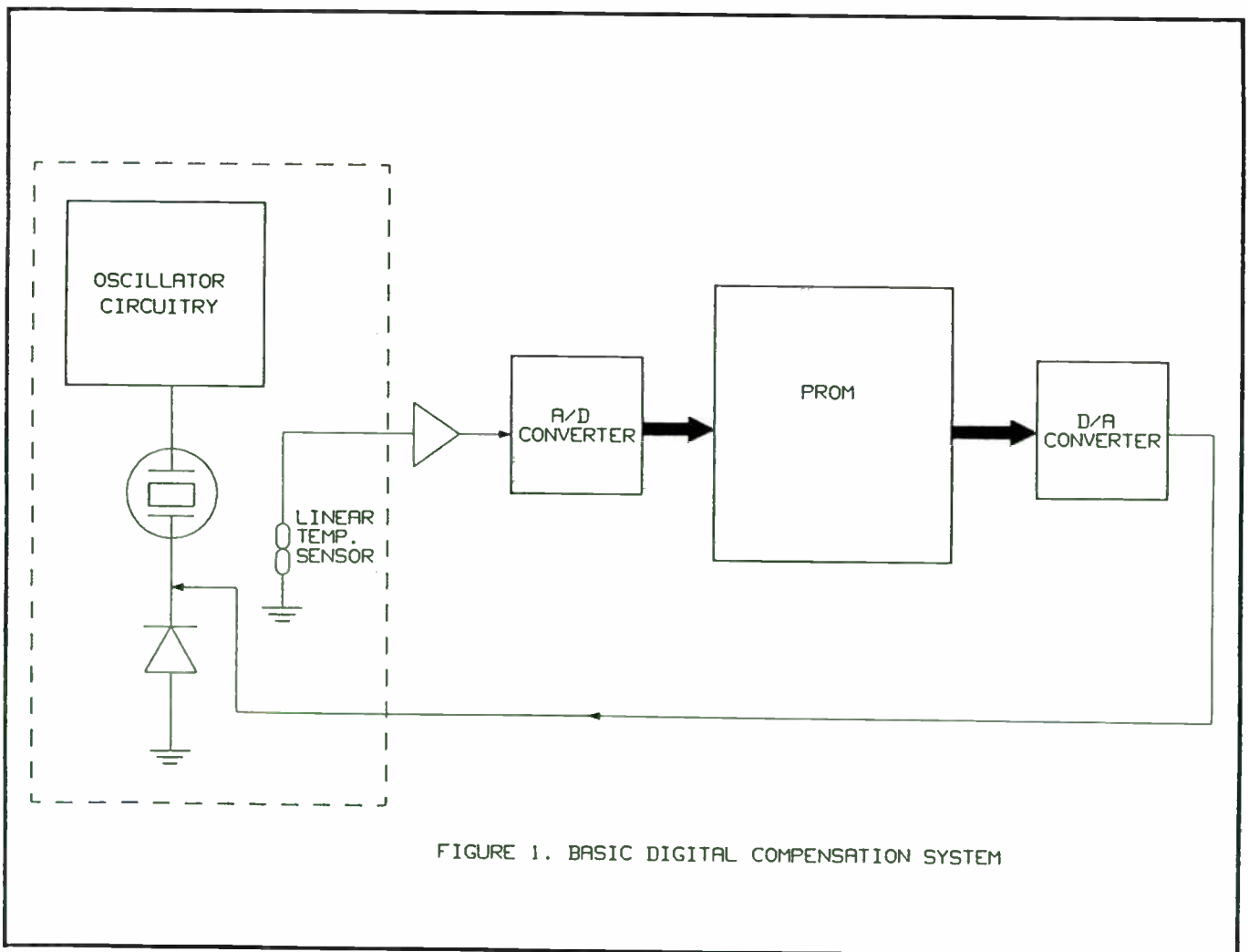
Several people deserve recognition for their work on this project; without their help, it would have been very difficult to pull this thing together:

- >> Bob Antes, for writing thousands of lines of machine code and not missing a bit.
- >> Tom Everingham, for the patience and perseverance to make things work like they're supposed to.
- >> The Design Engineers at Sierra Semiconductor who proved that it could all fit on one chip.
- >> The management of muRata who gave us the resources and the opportunity to make it happen.

- [16] A. Drukarev and D. J. Costello, "Hybrid ARQ error control using sequential decoding," *IEEE Trans. Inform. Theory*, IT-29, no. 4, pp. 521-535, July 1983.
- [17] W. Bux et al., "Balanced HDLC procedures: A performance analysis," *IEEE Trans. Commun.*, vol. COM-28, no. 11, pp. 1889-1898, Nov. 1980.
- [18] E. E. Mier "The ABC's of FEC", *Data Communications Magazine*, pp. 64-70, May 1984.
- [19] John Payton and Shahid Qureshi, "Trellis encoding: What it is and how it affects data transmission," *Data Communications Magazine*, pp. 143-152, May 1985.
- [20] S. B. Wicker, "High-Reliability Data Transfer Over the Land Mobile Radio Channel Using Interleaved Hybrid-ARQ Error Control," *IEEE Trans. Veh. Technol.*, vol. 39, no. 1, pp. 48-55, Feb. 1990.
- [21] ----, "Reed-Solomon Error Control Coding for Rayleigh Fading Channels with Feedback," *IEEE Trans. Veh. Technol.*, vol. 41, no. 2, pp. 124-133, May 1992.
- [22] A. D. Sacuta, "Performance metrics for radio link protocols supporting async data type I and fax type I services," An Intrim Report by TR 45.3.4, July 1992.
- [23] Li Fung Chang and N. R. Sollenberg, "Performance of a TDMA Portable Radio System Using a Block Code for Burst Synchronization and Error Detection," *Proc. IEEE Globecom '89*, pp. 1371-1376, 1989.
- [24] A. M. Bigloo, Q. Wang and V. K. Bhargava , "A Robust Rate-Adaptive Hybrid ARQ Scheme and Frequency Hopping for Multiple-Access Communications Systems," *Proc. IEEE Globecom '92*, pp. 889-893, 1992.
- [25] S. Periyalwar , "Multiple Trellis Coded for the Mobile Radio Channel," *Proc. IEEE Globecom '92*, pp. 894-898, Orlando, FL, Dec. 1992.
- [26] L. F. Chang and S. Ariyavisitakul, "Performance of Convolutional Codes with Interleaving in the Interference Limited Rayleigh fading Channels," *Proc. IEEE VTC '91*, pp. 812-816, May 1991.
- [27] G. Femenias and R. Agusti , "Switched Diversity Trellis Coded 8-DPSK for Mobile radio Applicxations," *Proc. IEEE VTC '90*, pp. 476-481, May 1990.
- [28] N. Seshadri and C.-E. W. Sunberg, "Multi-level Block Coded Modulations for the Rayleigh Fading Channel," *Proc. IEEE Globecom '91*, pp. 47-50, Dec. 1991.
- [29] D. Divsalar and M. K. Simon, "The Design of Trellis Coded MPSK for Fading channels: Set partitioning for Optimum Code Design," *IEEE Trans. Commun.*, vol. COM-36, pp. 1013-1021, Sept. 1988.
- [30] L. K. Rasmussen and S. B. Wicker, "A Performance Analysis of Trellis Coded Hybrid-ARQ Protocols in a Fading Environment," *Proc. IEEE Globecom '92*, pp. 899-904, Orlando, FL, Dec. 1992.
- [31] R. J. Benice and A. H. Frey, "Comparing of error control techniques," *IEEE Trans. Commun. Technol.*, vol. COM-12, pp. 146-154, 1964.
- [32] ----, "An analysis of retransmission systems ," *IEEE Trans. Commun. Technol.*, vol. COM-12, pp. 135-145, 1964.

References:

- (1) G.E. Buroker, M.E. Frerking, "A Digitally Compensated TCXO", Proceedings of the 27th Annual Symposium on Frequency Control, June 1973, pp. 191-198
- (2) G.B. Pollard, "A Digitally Compensated Hybrid Crystal Oscillator" Proceedings of the 36th Annual Symposium on Frequency Control, June 1982, pp. 474-485
- (3) Marvin E. Frerking, "The Application of Microprocessors to Communications Equipment Design", Proceedings of the 33rd Annual Symposium on Frequency Control, May 1979, pp. 431-435
- (4) Marvin E. Frerking, "Crystal Oscillator Design and Temperature Compensation", Van Nostrand Reinhold Co., New York, 1978, p. 155
- (5) Steven Fry, "Digital Temperature Compensation for Oscillators", RF Design, February 1989, pp. 116-119
- (6) A.M. Renard, K. Barnhill, "Digital Temperature Compensation of Crystal Oscillators", Proceedings of the 35th Annual Symposium on Frequency Control, May 1981, pp. 455-457



- [33] S. Lin and D. Costello, Jr., *Error Control Coding: Fundamentals and Applications*. Englewood Cliffs, NJ: Prentice-Hall, 1983.
- [34] A. Drukarev, "Error control using sequential decoding with repeat request," Ph.D. dissertation, Illinois Institute of Technology, Chicago, IL, May 1981.
- [35] A. Drukarev and D. J. Costello, Jr., "A comparison of blocks and convolutional codes in ARQ error control schemes," *IEEE Trans. Commun.*, vol. COM-30, pp. 2449-2455, Nov. 1982.
- [36] G. Ungerboeck, "Channel Coding with Multilevel Phase Signals," *IEEE Inform. Theory*, vol. 28, Jan. 1982, pp. 55-67.
- [37] W. C. Jakes, *Microwave Mobile Communications*, Wiley, 1974.
- [38] Draft Standard Document, TR45.3 Committee, Cellular Service Description, Async Data / Fax services.
- [39] Kamilo Feher, *Advanced Digital Communications*, Prentice-Hall, 1987.
- [40] Parviz Yegani and Clare D. McGillem, "FH-MFSK Multiple Access Communications System Performance in The Factory Environments," *IEEE Trans. Veh. Technol.*, to appear.
- [41] Parviz Yegani and Clare D. McGillem, *IEEE Trans. Commun.*, vol. 39, No. 10, Oct. 1991, pp. 1445-1454.

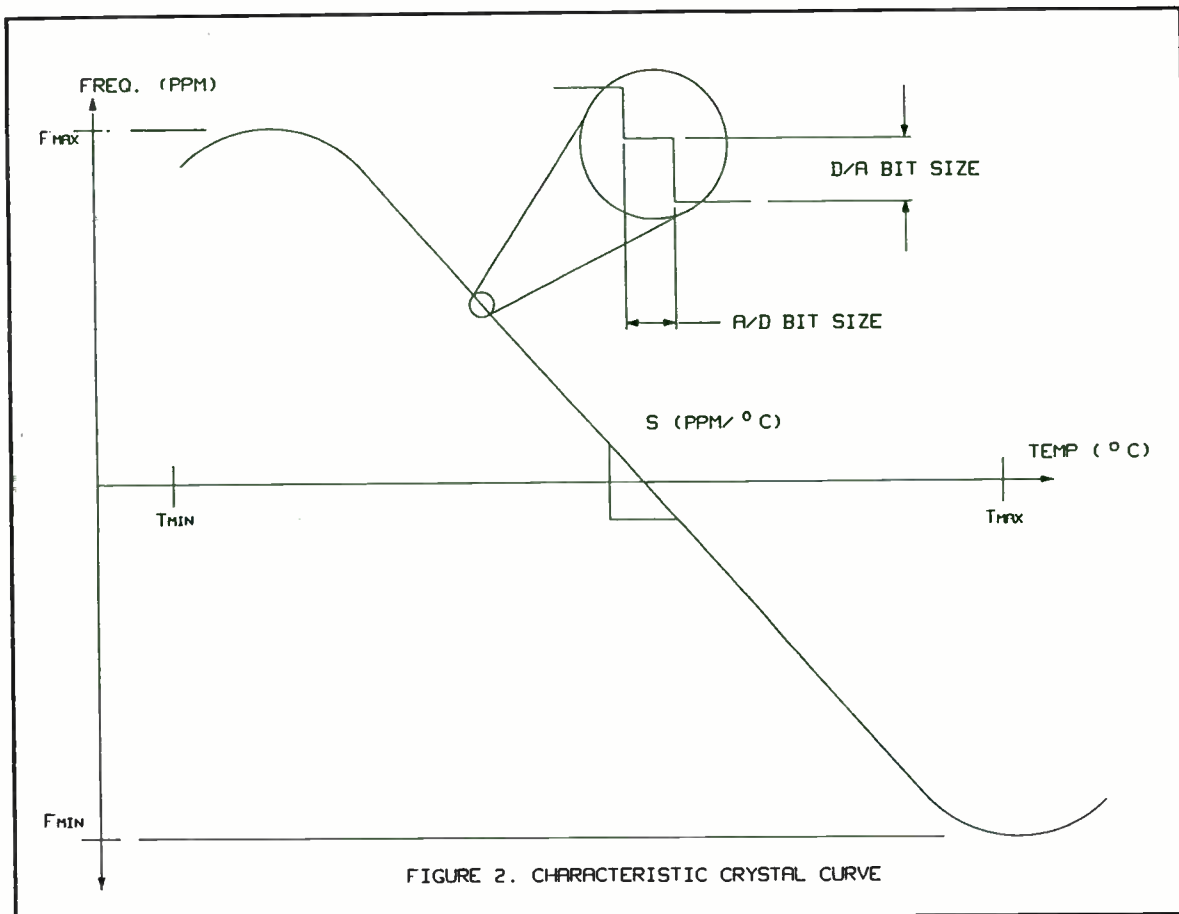


FIGURE 2. CHARACTERISTIC CRYSTAL CURVE

$$\Delta f = \left(\frac{S}{2}\right) \left(\frac{T}{2^{N_d}}\right) + \left(\frac{F}{2}\right) \left(\frac{1}{2^{N_a}}\right)$$

WHERE: $T = T_{MAX} - T_{MIN}$ (°C)
 $F = F_{MAX} - F_{MIN}$ (PPM)
 $S = \text{MAX. SLOPE OF CRYSTAL}$ (PPM/°C)
 $N_d = \# \text{ OF A/D BITS}$
 $N_a = \# \text{ OF D/A BITS}$

ALLOWING FOR MANUFACTURING TOLERANCES:

$$\Delta f = \left(\frac{S}{2}\right) \left(\frac{T}{0.7 \cdot 2^{N_d}}\right) + \left(\frac{F}{2}\right) \left(\frac{1}{0.7 \cdot 2^{N_a}}\right)$$

FIGURE 3.
 MAXIMUM ACHIEVABLE FREQUENCY STABILITY
 OF DIGITAL COMPENSATION SYSTEMS

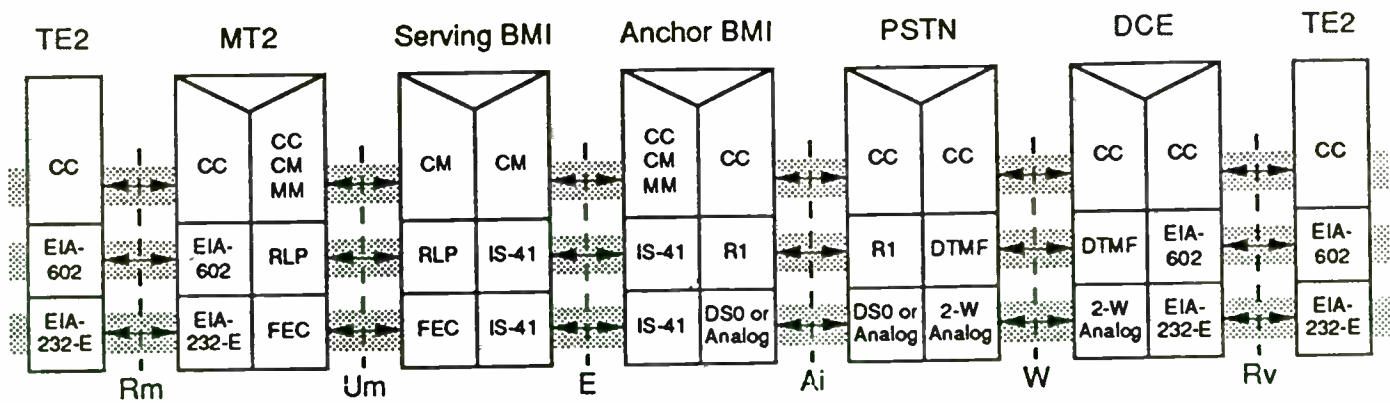


Figure 1. A reference model for a cellular network.

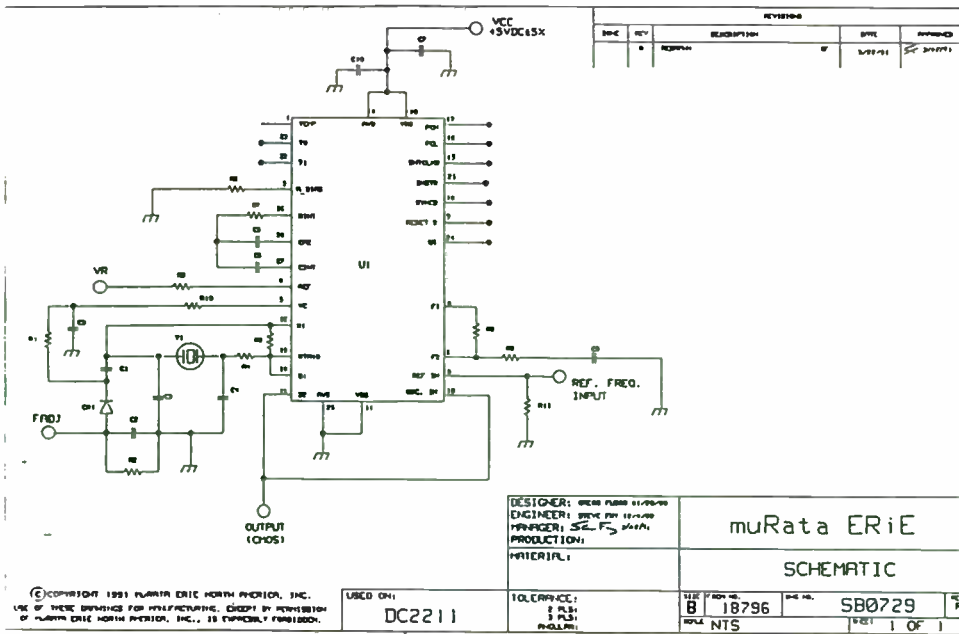


Fig. 4

DAC vs. Temperature
27 AUG 1992 (#1)

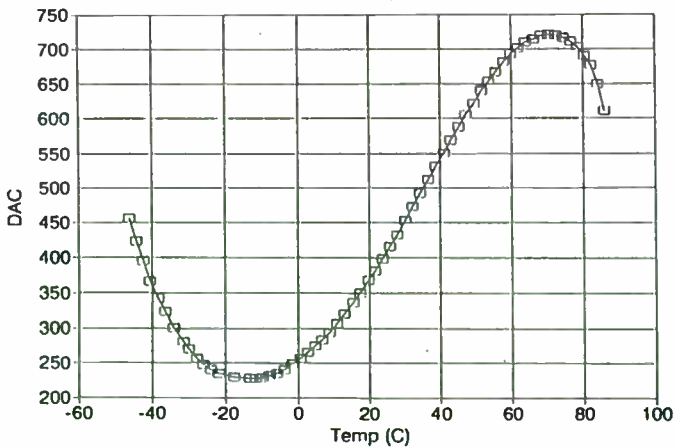


Fig. 5

Frequency vs. Temperature
27 AUG 1992 (#1)

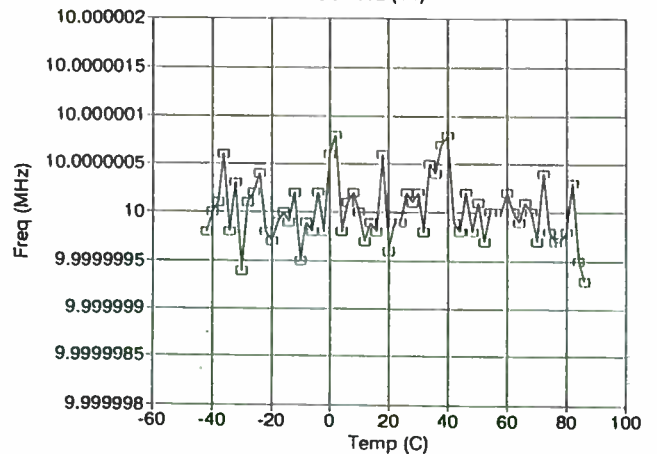


Fig. 6

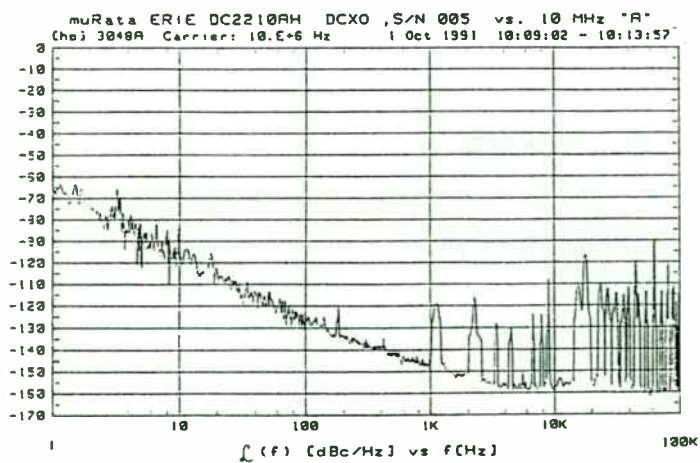


Fig. 7

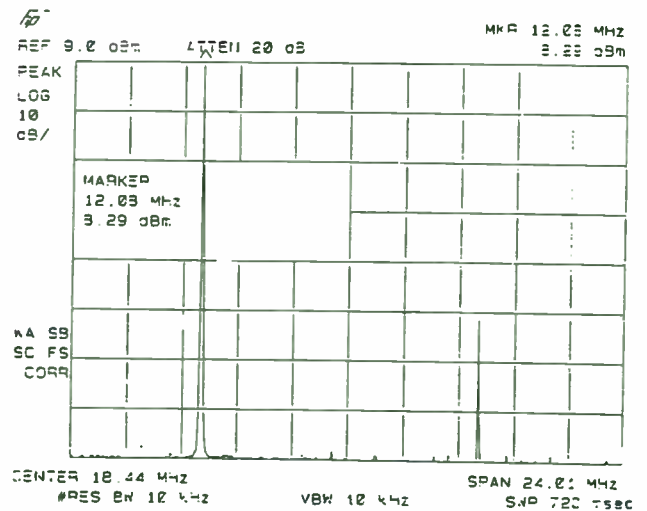


Fig. 8

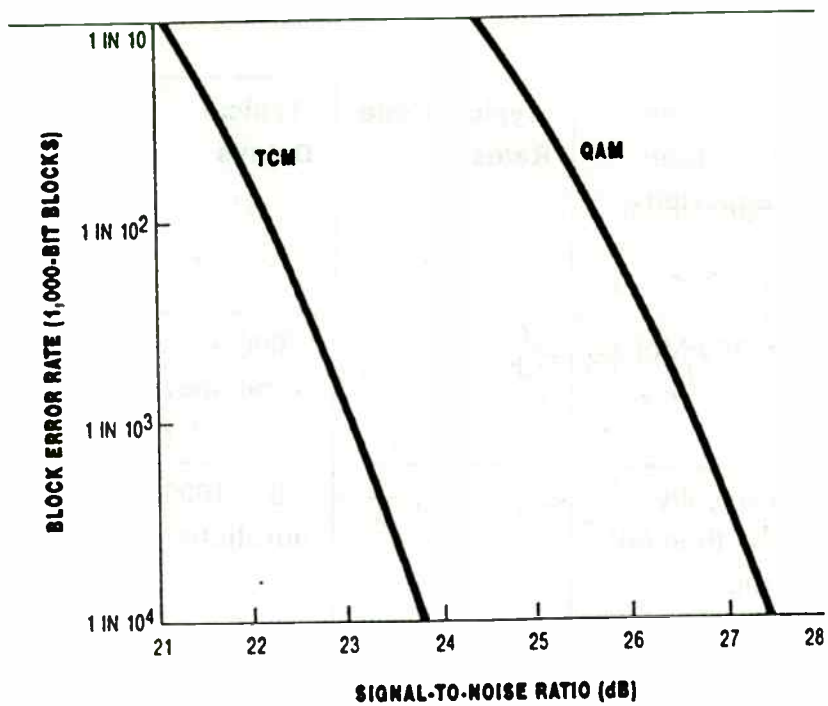


Figure 2. BER performance of TCM vs QAM.

A Synthesizer Design Program with Detailed Noise Analysis

Terry Hock
National Center for Atmospheric Research
Boulder, CO 80301

Abstract

There are several factors which determine or limit the phase noise of a synthesizer. The total phase noise of the synthesizer is determined by several noise sources in the loop such as the reference oscillator, voltage controlled oscillator (VCO), phase detector and operational amplifier (op amp) loop filter. Typically the op amp noise is considered a second or third order effect when a good low noise op amp is used, but in reality the op amp may be the limiting noise factor in a synthesizer. This program will analyze synthesizer taking into account all the noise sources in a synthesizer. The program will analyze and design the loop filter and calculate the loop steady state responses. All results are in both table and graphic form. It will also compute the reference spur levels for a digital phase/frequency detector with a differential output and provide the option to add an active low pass filter to reduce the spur level. The program was written to simplify the design of synthesizers using commercial synthesizer integrated circuits (IC). It operates on a DOS machine and requires a minimum of VGA graphics.

Overview

When designing a synthesizer, there are several performance criteria that must be considered: phase noise, switching speed, reference spur levels, etc. Usually optimizing one parameter gives less than adequate performance in another area. The performance of a single loop synthesizer is typically a compromise of all design goals.

In the past when designing synthesizers, I have used several design tools: spread sheets, small basic programs and spice simulators to analyze and design a synthesizer. This program was developed to combine all synthesizer design criteria into one easy to use program. A single program allows all aspects of a synthesizer design to be completed in a minimal amount of time. One parameter can be varied while the effect is observed in all performance areas of the synthesizer. Also in the past,

an adequate model for the phase noise of the synthesizer was lacking in my design tools.

The program calculates the noise contribution from the individual stages and the total phase noise of the synthesizer. The loop bandwidth can easily be changed while observing the phase noise; this allows for easy optimization of the phase noise. The program displays the integrated phase jitter providing an aid in choosing the loop bandwidth for lowest overall phase noise. The loop filter model incorporates the performance of a real op amp for the calculations of op amp filter noise, reference spurs levels and steady state loop responses. The Johnson noise of the resistors is also incorporated into the op amp noise calculation.

All calculations use linear control theory in the frequency domain for both the steady state responses and phase noise calculations. A wideband synthesizer (loop bandwidth greater than 20% of the reference frequency) analyzed with linear analysis will introduce errors. A better approach would be to use discrete time analysis or Z-transforms for analysis. However, if wide loop bandwidths are desirable for fast switching speeds, the reference spurs may be at undesirable high levels when using a standard digital phase/frequency detector in a low cost synthesizer IC. To improve the accuracy of the calculations, the user has the option of adding a delay term to the steady state loop calculations. There have been considerable discussions in past issues of RF Design as to what the delay value should be [1]. The value of this delay term is dependent upon the type of phase detector (digital phase/frequency, sample & hold) used in the synthesizer and location of the first pole. There is not a clear consensus of what the sampling delay should be for all cases, so it's value is left to the user to choose.

Currently the program does not calculate the switching speed of the synthesizer, but uses a simple approximation for a rough estimate of the switching speed. Dan Gavin has demonstrated how a spice simulator can be used to estimate the switching speed

Type	Maximum Data Rates Supported	Typical Code Rates	Typical Delays	Length of Error Bursts Corrected without Inter-leaving
Block (e.g. Reed-Solomon)	> 100 Mbps	$\frac{7}{8}$, $\frac{15}{16}$	2000 + bit durations	100 bits
Convolutional (e.g. Viterbi, Sequential)	Typically less than 50 Mbps	$\frac{1}{2}$, $\frac{3}{4}$, $\frac{7}{8}$	30 – 1000 bit durations	Typically less than 20 bits

Figure 3. Two commonly used FEC Schemes.

incorporating all delay terms for accurate switching speed analysis [2].

Phase Noise

When designing a synthesizer for lowest phase noise, optimum placement of the synthesizer loop bandwidth is critical. Typically only the VCO noise and phase detector noise floor are considered in determining the final phase noise of the synthesizer. Usually the phase noise inside the loop bandwidth is approximated by equation 1.

$$\text{phase noise} = 20 \log(N) + \text{phase det. noise floor} \quad (1)$$

N is the total division ratio of the VCO frequency to the reference frequency and the phase detector noise floor might be -155 dBc. The phase detector noise floor varies with the type of technology used such as CMOS, ECL and GaAs. CMOS has the lowest noise floor of the three. The loop bandwidth would be chosen where the noise floor from equation (1) intersects the phase noise of the VCO for optimum phase noise performance. This simplified analysis is shown in figure 1. As a quick evaluation of where to place the loop bandwidth, this procedure is quite valid. However this method excludes the true loop behavior or closed loop response and error loop response as they modify the VCO phase noise and the phase detector noise floor.

A more detailed analysis is required to predict the actual value of the phase noise in the synthesizer. As the architect of the synthesizer changes from large values of N to high VCO phase noise, this simple model will have significant errors in predicting the phase noise. A block diagram of all the noise sources that contribute to the phase noise is shown in figure 2. The op amp noise source is typically neglected when high quality low noise op amps are used in the loop filter integrator circuit. Yet in certain cases the op amp will be the major contributor to the phase noise, even when very low noise op amps are used, this is typically the case when a VCO with a high tuning sensitivity of 25 MHz/v or greater and phase detectors with low gain (1v/rad or less) are used.

Program Description

The program has four major sections: Design, Analysis, VCO phase noise and Synthesizer phase noise. The program assumes the user is familiar with designing synthesizers. Figure 3 is a schematic showing the circuit topology which the program evaluates. The synthesizer is a type II fifth order including the VCO bandwidth as

a pole and first pole in a op amp. If an active filter is used to reduce the reference spurs, the synthesizer is a type II seventh order control system.

Design

The synthesizer design routine prompts the user for the common parameters in designing a synthesizer such as VCO tuning sensitivity (or gain), phase detector gain, reference frequency, loop bandwidth, etc. The component values of the loop filter are calculated based on the equations from reference [3]. The program allows the user to easily change the component values for practical sizes in the loop filter without having to re-enter the initial design data. The new values are immediately updated on the screen. The program will next compute the value of the reference spurs at the VCO output. The spur calculation is only valid for a digital phase/frequency detector when using the differential phase detector outputs. This type of phase detector is used in the spur calculation since it has lower spur levels than a single ended output from a digital phase/frequency detector when the loop filter is an op amp integrator. The program then provides the option to add a 2-pole active low pass filter to reduce the spur level. The program prompts for bandwidth and damping coefficient of the filter. The filter component values are easily changed for practical values.

The design routine will also compute the steady state responses of the synthesizer both in table and graphic form. The steady state responses computed are closed loop gain, open loop gain, error loop gain and phase margin. The open loop gain and phase margin are the most critical parameters for evaluating the loop stability. The phase margin at 0 dB open loop gain frequency should typically be 40 to 60 degrees for a well behaved loop.

Usually, a synthesizer is designed to operate at several different frequencies. In a single loop synthesizer the output frequency may vary 25% or more, which requires changing the divider value thus the loop gain varies. The loop should be evaluated at several operating conditions for stability and bandwidth. Typically the tuning sensitivity of the VCO changes at different control voltages. This variation in the VCO gain must also be considered in a design. Both the tuning sensitivity and divider values can be evaluated quickly by entering either K or F followed by new values. The output frequency is changed in lieu of changing the actual divider ratio. The loop switching speed is also calculated based on a simple approximation of $t = 4/\text{loop BW}$.

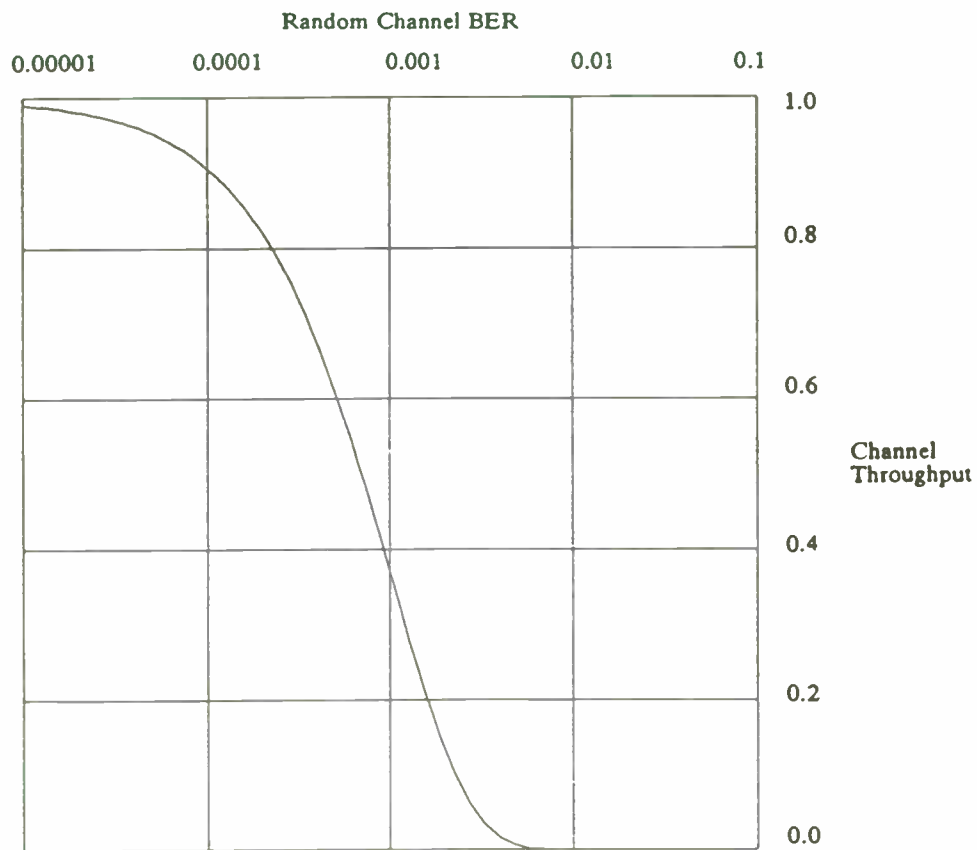


Figure 4. ARQ Throughput for 1000-Bit Blocks.

Analysis

The synthesizer analysis routine is very similar to the design routine except actual component values of the loop integrator and active low pass filter are entered. The steady state responses of the loop are calculated along with reference spur level. The steady state responses, open, closed and error loop are calculated in table and graphic form. The switching speed is not calculated since the analysis routine does not directly compute the loop bandwidth. The analysis routine is very valuable for analyzing current designs and to evaluate component sensitivity in the loop filter versus performance variations. The output frequency and the VCO gain can both be easily changed for different operating frequencies and VCO gain variations.

VCO Phase Noise

The VCO routine uses Leeson's equation for calculating the phase noise of an oscillator [4]. The two dominant parameters that set the phase noise are the loaded Q of the resonator and the operating frequency or the ratio of operating frequency to Q. The output power and flicker frequency are also required in the VCO phase noise calculation. The varacter diode is also a major noise source in a voltage controlled oscillator. The varacter diode has an effective thermal noise resistance. This resistance generates a noise voltage given by Nyquist's equation which modulates the varacter diode. This noise source typically dominates the phase noise of the VCO in wide frequency tuning oscillators.

The VCO routine prompts the user for operating frequency, loaded resonator Q, output power, flicker frequency, effective noise resistance of varacter diode and tuning sensitivity. The VCO phase noise analysis separately calculates the phase noise due to the varacter diode, Leeson's equation and the total phase noise. The performance of the VCO is easily evaluated showing which factors dominated the VCO phase noise. The results are in table and graphic form.

The resonator Q and tuning sensitivity can easily be changed in 5% increments up or down. This feature is useful for adjusting the phase noise performance to match that of a commercial VCO that may be used in the synthesizer design. When the Q and tuning sensitivity are changed, the results are updated real time on the screen. **The phase noise from this routine will be used in the synthesizer phase noise calculations.** When designing VCO's this routine is very useful for estimating the phase noise performance of an oscillator.

Synthesizer Phase Noise

The synthesizer phase noise routine is the most useful feature of the program. It computes the individual phase noise terms of each noise source in the loop and simultaneously displays the level of the reference spur, switching speed and integrated phase jitter. All design parameters are displayed on one screen while the user can easily change the loop bandwidth while observing the phase noise, spur level, switching speed, etc. The output frequency and VCO tuning sensitivity can also be changed to account for the different operating conditions as the synthesizer is set to different frequencies.

The synthesizer phase noise calculation uses data from either the Design of Analysis routine for the loop filter and data from the VCO phase noise routine. Phase noise is computed for the op amp filter, reference oscillator, VCO, phase detector and the sum of these noise sources. The op amp noise model also includes the active low pass filter if it is chosen in either the analysis or design routines. The model includes the thermal noise of all the resistors in the filters. The phase jitter is also computed by integrating the total phase noise from 100 Hz to 1 MHz. The phase jitter is useful when adjusting the loop bandwidth for lowest phase noise.

The loop bandwidth, tuning sensitivity and output frequency can all be easily changed in either the table or graphic display of the synthesizer phase noise. When a change is made, all data is updated automatically on the screen. When the loop bandwidth is changed, the feedback capacitor is held constant so all resistor values change. This is very important when the loop bandwidth is reduced as all the resistor values will increase in thus increasing the op amp noise level. The loop bandwidth is not an option for changing its value when using data from the analysis routine. The phase noise plot has five parameters plotted simultaneously, so when a parameter like VCO gain is changed several times the graph becomes cumbersome to evaluate. A redraw feature is available that will update the display with the last data set by simply pressing R.

Miscellaneous Features

The program also has a help file for operating the program, but it is assumed that the user is familiar with synthesizer design. There are also a few common parameters such as sampling delay and resistance tolerance that seldom require changing; they are entered in a special utility routine. The resistance tolerance is

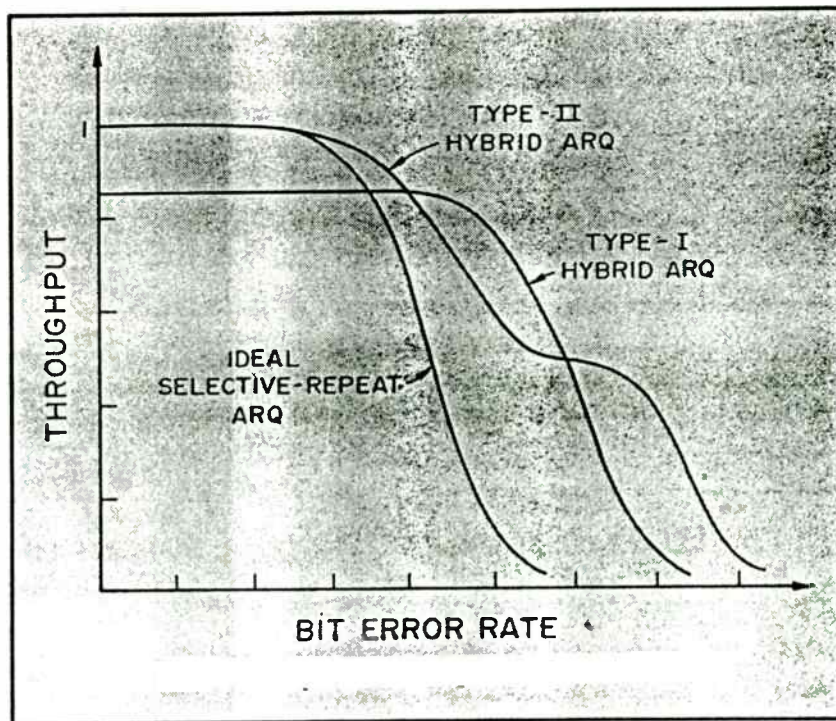


Figure 5. Comparison of hybrid ARQ schemes.

required for the spur calculation. The spur calculation computes the common mode rejection of the op amp integrator from the op amp data and resistor values. The op amp data is in a separate ASCII file that contains the individual parameters for each op amp. This ASCII data file can easily be changed with any text editor to add, delete, or modify the op amp data file. The read.me file provides the format for the ASCII op amp data file. A second ASCII data file is required which stores all synthesizer data parameters as the default values when the program is terminated. These parameters will then be recalled when the program is run again. The op amp and PLL data files must reside in the same directory when the program is executed for proper operation.

General Operation

The program is designed to be very easy to use and operate with a minimal number of key strokes. At each prompt there will be a question which will ask for a value, such as phase detector gain, or a single letter for an option. At the end of a prompt, a number will be in brackets which is the default value. By simply pressing return, the program accepts the default value. When only one parameter has to be changed, this feature quickly allows one to go through the input parameters without having to retype in every value. An option selection will have different letters in brackets; pressing the letter will execute that command.

Printing

The results on the screen can easily be dumped to a printer using the PrintScreen key. A printed hard copy of the graphs can also be dumped to a printer by running the DOS utility GRAPHICS.COM prior to running the program. To dump the graphs to a printer, simply press [Shift] and [Print Screen] simultaneously. If a Laser printer is being used, be sure to add the appropriate extension to the graphics command given in a DOS manual.

Phase Noise Model

Several assumptions are made in the computation of the phase noise. The steady state equations used for the analysis and design routine are used for the phase noise calculations in modifying the appropriate noise source in the loop. The Z-transforms would be the better choice for improved accuracy in wide loop bandwidth designed synthesizers. However for small loop bandwidths relative to the reference frequency, using linear equations provides excellent results.

The most unique feature of the program is that it incorporates all noise contributions from the loop's integrator and active low pass filter. In designing low phase noise synthesizers the op amp noise can limit the phase noise performance.

A block diagram of the noise sources considered in this program are shown in figure 4. The noise sources $E1(s)$ and $E2(s)$ are lumped together into the op amp noise source when displayed on the screen. $E1(s)$ represents the output noise of the integrator circuit including the thermal noise of all the resistors. $E2(s)$ represents the output noise of the active low pass filter including the thermal noise of the resistors. The noise from the low pass filter is only considered if selected in the design or analysis routines. Since most synthesizers use CMOS technology, the final frequency division of the VCO is with CMOS technology. CMOS has the lowest phase noise of all technologies available. Therefore the frequency divider phase noise was omitted from the analysis. However, the reference oscillator noise floor and divider noise are equivalent in the system equations. The phase noise of the reference oscillator is based upon Leeson's equation with a very high Q representative of a crystal oscillator. The reference oscillator usually dominates the total phase noise below 100 Hz in designs with high divider values.

An accurate model of the phase detector noise floor is not available for the various types of technologies and types of phase detectors so a constant value is entered by the user. Even though the phase noise density of the phase detector is not constant versus frequency, the noise floor will dominate the total phase noise typically at only one frequency range. The value entered should correlate to this frequency region.

The noise model of the loop filter accounts for the internal noise generated by the op amps (input noise current density and input noise voltage density) and the thermal noise of the resistors. Figure 4 shows the noise sources considered in the filter noise model used by the program. Only the Johnson or thermal noise of the resistors is considered. Contact or popcorn noise in the resistor is not considered, as this noise is very dependent on the type of resistor used and is not well defined. Metal film resistors are a good choice in the integrator filter for low noise since they have minimal contact noise. The output noise of each filter stage is computed for the calculation of the phase noise. The flicker frequency noise of the op amps, typically DC to 100 Hz is not considered in the calculation of the op amp noise. In many cases the data sheets for op amps do not provide complete noise information to consider the low

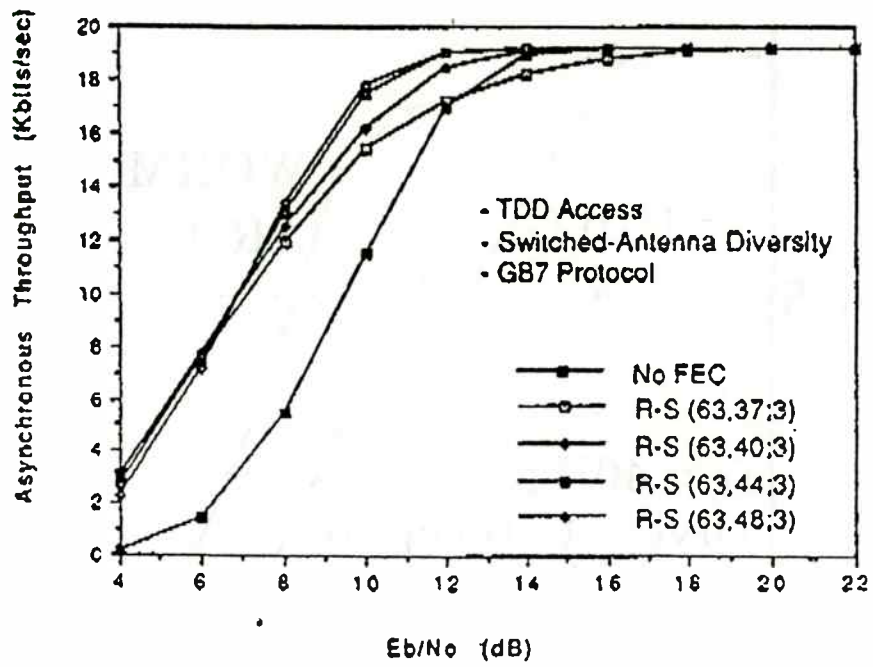


Figure 6. Comparison of different ARQ/FEC/DIV protocols.

frequency flicker noise. Therefore this noise source is not considered in the model. The phase noise of the synthesizer is typically dominated by the reference oscillator at these low frequencies, as a result the addition of the flicker noise in the op amp would add little more accuracy in the calculations.

The op amp noise is minimized by keeping the input resistors of the integrator circuit small. The input noise current is effectively magnified by the size of the input resistors. Also the Johnson noise from the input resistors can become excessive if the resistors are large. If the low pass active filter is implemented, it does contribute noise to the overall loop filter and is added to the op amp noise display.

The program requests a VCO bandwidth which is used in the steady state analysis and synthesizer phase noise calculations. This is an additional pole in the loop. The VCO bandwidth in the analysis is represented as a single RC low pass filter. The VCO bandwidth can be either the actual bandwidth of the VCO or an RC low pass filter located at the input of the VCO. This additional pole filters the noise generated in the op amp circuits which can improve the phase noise performance when op amp noise is high.

Example

It is very easy to evaluate which is the dominating noise source at a given offset frequency from the carrier in a synthesizer with this program. In loops with high division values, the phase noise inside the loop bandwidth is typically dominated by the phase detector noise floor and the loop filter (op amp noise). If a VCO with poor phase noise is used, it still will contribute significant noise inside the loop bandwidth as there is not enough loop gain to reduce the VCO noise. The phase noise is dominated again by the op amp noise and VCO noise outside the loop bandwidth. It becomes clear that for low phase detector gains and large VCO tuning sensitivities the loop filter is a major noise contribution to the overall performance.

The op amp noise can be minimized by using a VCO which has a lower tuning sensitivity or a phase detector with higher gain. A sample and hold phase detector with high gain of 10 v/rad or more may significantly improve the overall phase noise by minimizing the op amp noise. A second approach would be to use a phase detector whose output is a current driver that does not require an op amp yet is still a type II control system [5].

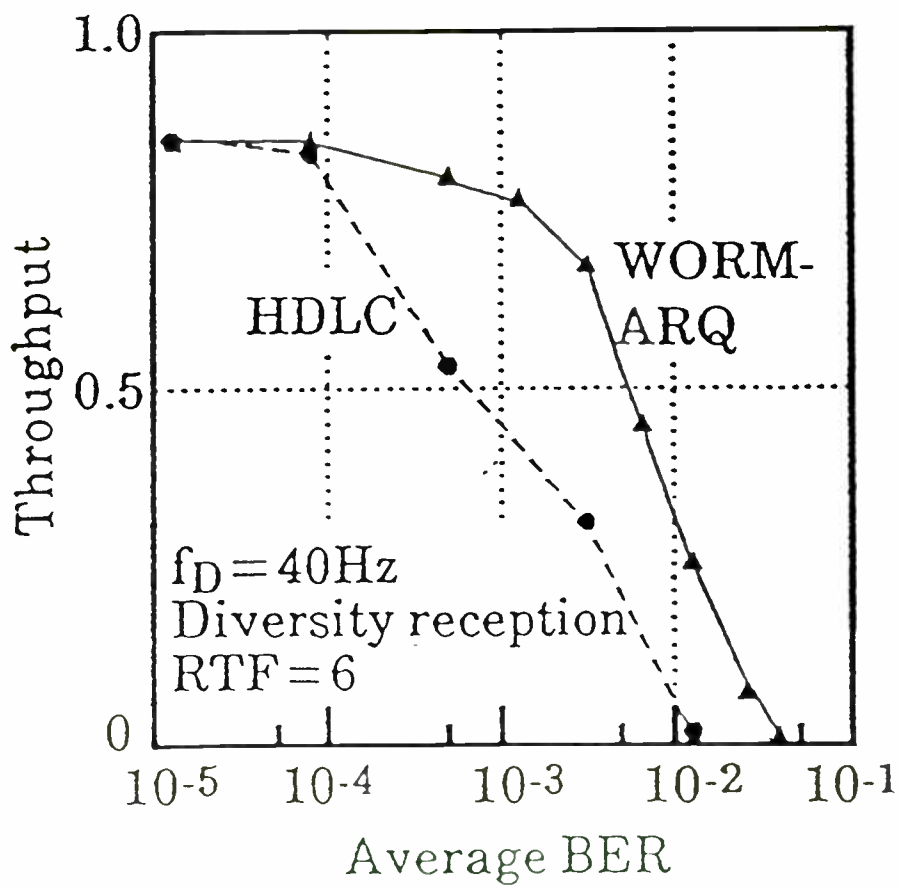
A synthesizer operating at 1280 MHz with a reference frequency of 250 kHz was designed and analyzed using this program. The main design goal was for low phase noise using a commercial VCO, good sideband reference suppression greater than 60 dB, and switching speeds less than 5 msec. Figure 5 is a plot of the measured phase noise of the synthesizer and figure 6 is a plot of the calculated data from the program. Note the small noise peak at an offset of 3 kHz in the measured data, this agrees with the predicted from the program. The noise peak may be mistaken for a marginally stable loop with a low damping coefficient but the frequency step response shows that the loop is well behaved. There is quite good agreement between measured data and calculated data. The measured switching speed for a 200 MHz change is shown in figure 7. The simple switching speed approximation in the program does give a good first order approximation when compared to measured results.

Conclusion

It is very easy to evaluate which component in a synthesizer is the dominating noise source at a given offset frequency from the carrier with this program. The engineer can quickly evaluate several different synthesizer architectures for best performance without having to prototype a synthesizer. In today's competitive market, an accurate synthesizer model is extremely valuable in minimizing development time of a new synthesizer. The program has been shown to have good agreement with measured data of an actual synthesizer. I would especially like to thank Mitch Randall and Tom Thompson for their valuable feedback in evaluating the program as it was developed.

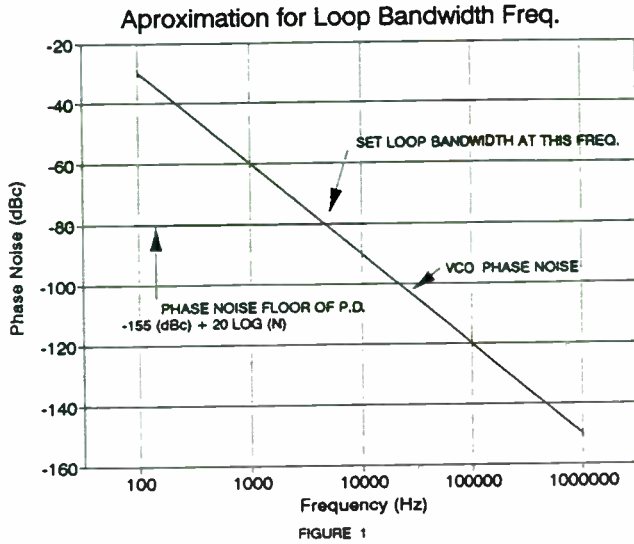
References

1. Egan, William, Sampling Delay - Is It Real?, RF Design, Cardiff Publishing, February 1991.
2. Gavin, Dan T., Phase Locked Loop Synthesizer Switching Speed Optimization and Measurement Techniques, RF EXPO Proceedings West 1989, Santa Clara, CA pp. 355-372.
3. Przedpelski, Andrzej B., PLL Primer Part III, RF Design, Cardiff Publishing, July/August 1983.
4. Robins, W. P., PHASE NOISE IN SIGNAL SOURCES THEORY AND APPLICATIONS, Peter Peregrinus Ltd., 1982.
5. Beam, William C. and Rezin, Phillip J., Design



f_D = Doppler Frequency
 RTF = the number of frames transmitted during the round-trip delay

Figure 7. Throughput Comparison between WORM-ARQ and HDLC protocols.



$$\text{REF OSC PHASE NOISE} = \frac{K_{pd} K_{vco} F_1(s) F_2(s) F_3(s)}{1 + \frac{K_{vco} K_{pd} F_1(s) F_2(s) F_3(s)}{s N}} \cdot \theta_{Ref}(s)$$

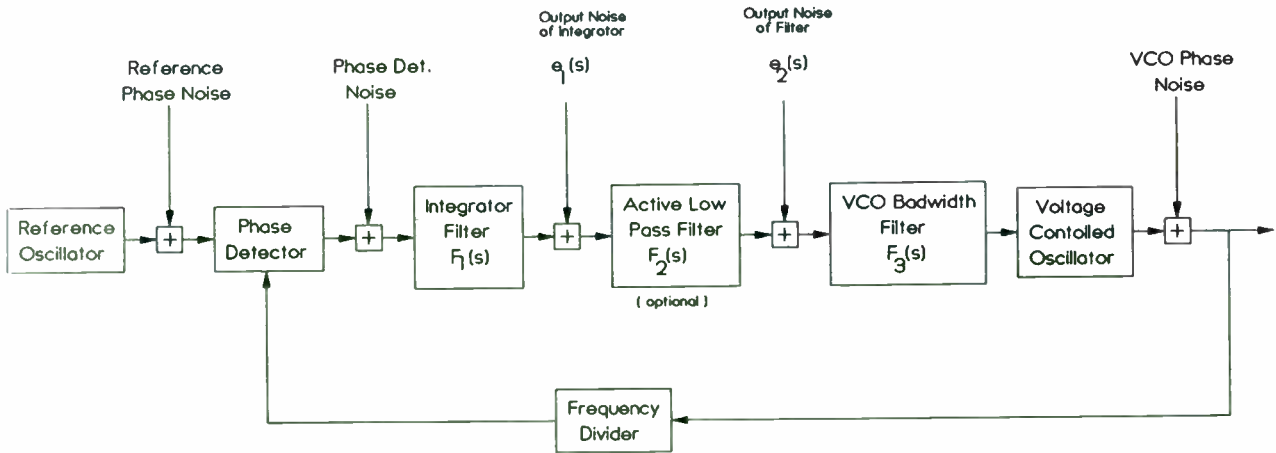
$$\text{PHASE DET. PHASE NOISE} = \frac{K_{vco} F_1(s) F_2(s) F_3(s)}{1 + \frac{K_{vco} K_{pd} F_1(s) F_2(s) F_3(s)}{s N}} \cdot \theta_{PD}(s)$$

$$\text{VCO PHASE NOISE} = \frac{1}{1 + \frac{K_{vco} K_{pd} F_1(s) F_2(s) F_3(s)}{s N}} \cdot \theta_{VCO}(s)$$

$$\text{OP-AMP INTEGRATOR NOISE} = \frac{K_{vco} F_2(s) F_3(s)}{1 + \frac{K_{vco} K_{pd} F_1(s) F_2(s) F_3(s)}{s N}} \cdot E_1(s)$$

$$\text{OP-AMP LOW PASS FILTER NOISE} = \frac{K_{vco} F_3(s)}{1 + \frac{K_{vco} K_{pd} F_1(s) F_2(s) F_3(s)}{s N}} \cdot E_2(s)$$

FIGURE 2A



Noise Sources in Synthesizer Figure 2

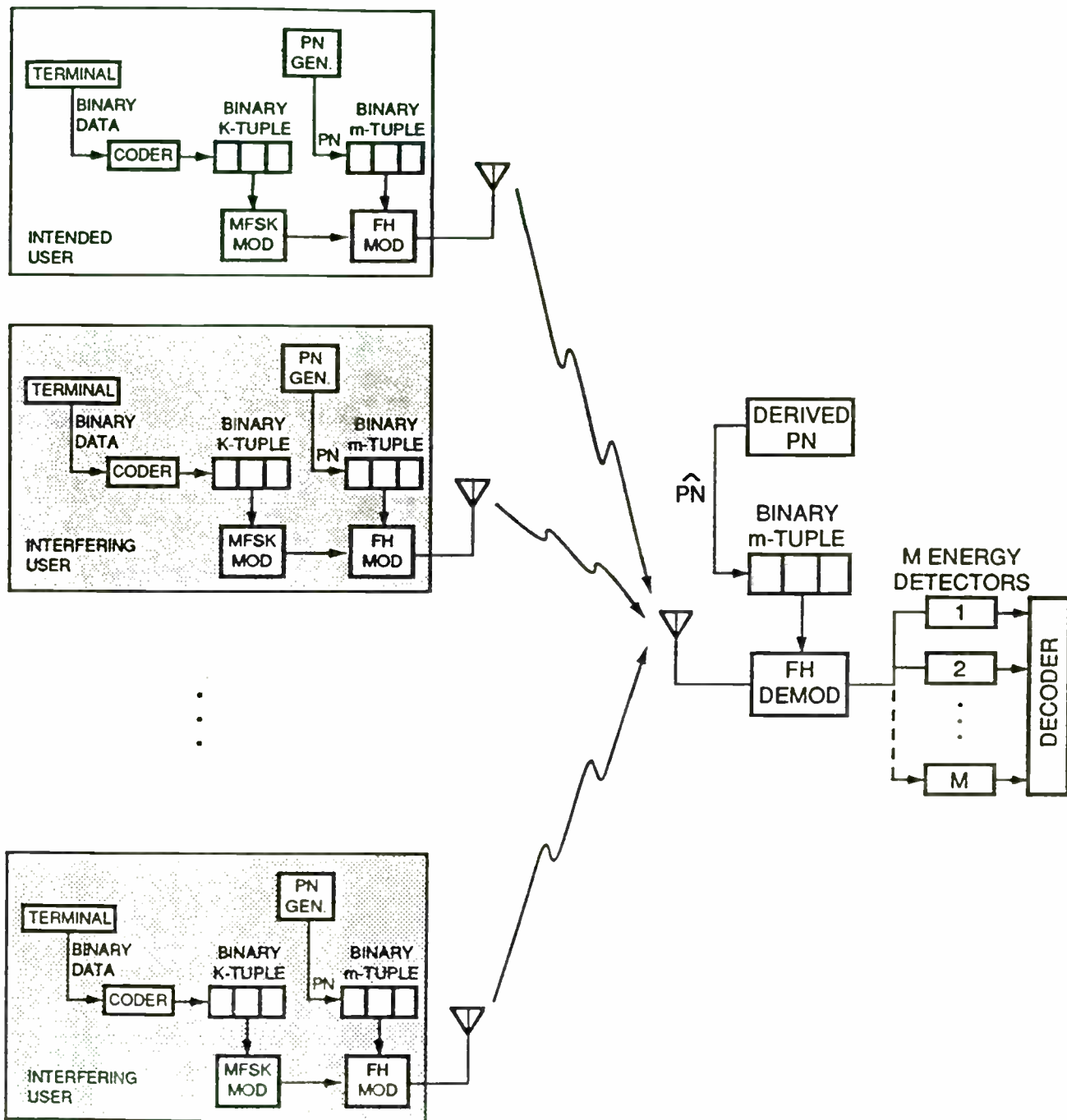


Figure 8. Block Diagram of the FH-MFSK system.

SYNTHESIZER TOPOLOGY

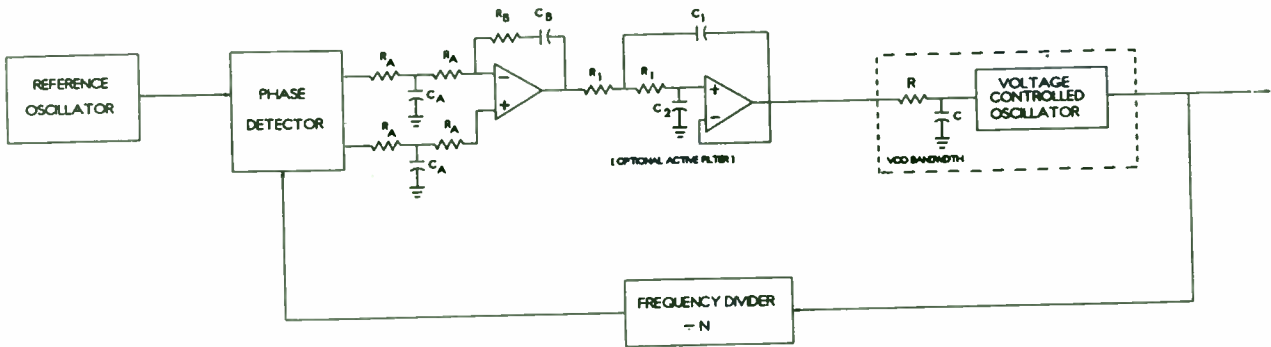


FIGURE 3

LOOP FILTER NOISE MODEL

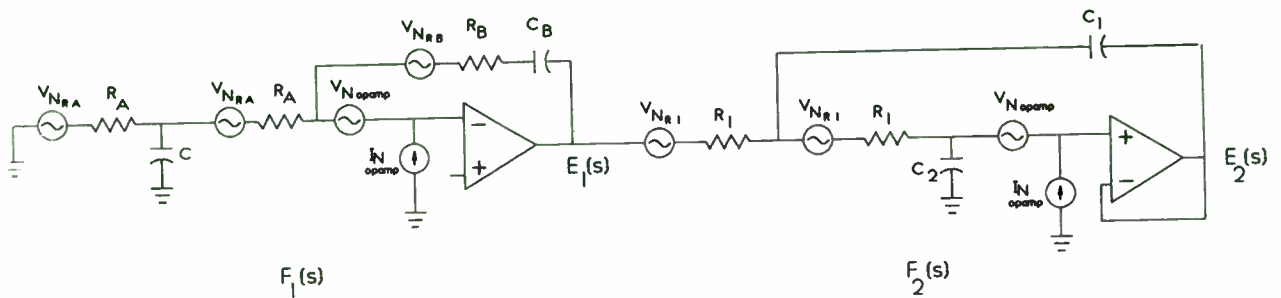


FIGURE 4

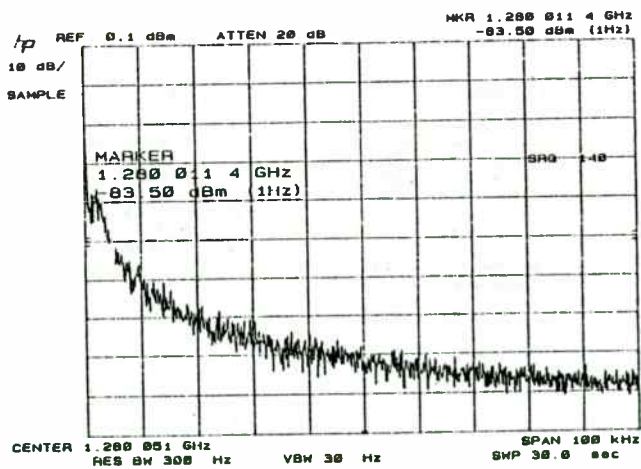


FIGURE 5A MEASURED PHASE NOISE AT 50 MHz OFFSET OF 1280 MHz SYNTHESIZER

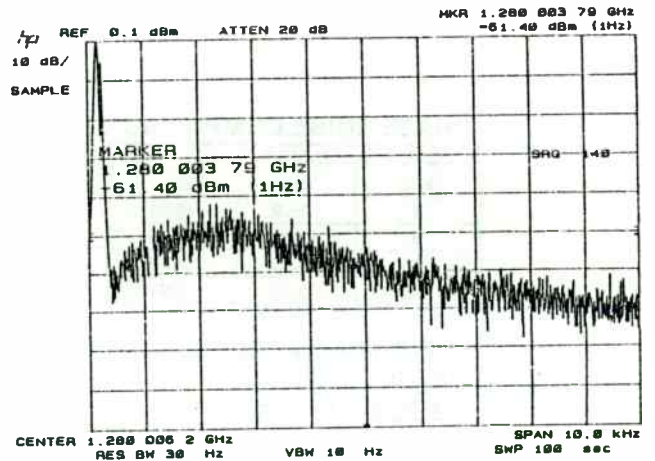


FIGURE 5B MEASURED PHASE NOISE AT 3 MHz OFFSET OF 1280 MHz SYNTHESIZER

GaAs MESFET DIRECT QUADRATURE MODULATOR INTEGRATED CIRCUIT FOR WIRELESS COMMUNICATION SYSTEMS

Chris Fisher

RF Micro Devices, Inc.
7341-D W. Friendly Ave.
Greensboro, NC 27410

Abstract

An RF quadrature modulator integrated circuit utilizing GaAs MESFET process technology has been developed for wireless communication systems operating between 700 and 1000 MHz. The IC is packaged in a plastic SOIC package which makes it suitable for low cost, high volume consumer oriented products. The device consists of two input differential amplifiers, two limiting input LO amplifiers, two double balanced mixers, a hybrid phase splitter, a combining amplifier and an output RF amplifier which will drive a 50 Ω load at -3 dBm (typical). The device also contains a phase adjust pin to allow for optimum phase balance between the in-phase (I) and quadrature (Q) channels. The device is powered by a single +5 V supply. This modulator can be used for any type of vector based modulation.

Introduction

Current communication architectures that have been proposed and implemented for wireless communication systems utilize vector based modulation schemes. Inherent in these architectures are RF transmitter functions that require the baseband vector to be modulated onto an RF carrier. It is the conversion of this baseband vector to an RF transmit frequency via a GaAs MESFET integrated circuit that this device and paper addresses.

The baseband vector is a complex signal comprising an in-phase and quadrature component. These components are always 90° out of phase with respect to each other. It is the amplitude of each component which uniquely identifies each transmit vector. Given the fact that the phase of the transmit vector is changing with respect to time as information is sent, and the fact that the LO source has singular phase, it is necessary to modulate each component

Frequency (Hz)	FILTER (dBc)	UCD (dBc)	REF (dBc)	Phase Det. (dBc)	Total (dBc)
10.0	-80.1	-84.3	-64.7	-80.0	-64.4
17.0	-80.1	-81.8	-69.6	-80.0	-68.7
31.6	-80.1	-79.3	-74.4	-80.0	-71.8
56.2	-80.1	-76.8	-79.0	-80.0	-72.9
100.0	-80.0	-74.3	-83.4	-80.0	-72.2
177.0	-79.0	-71.8	-87.3	-80.7	-70.6
316.2	-79.1	-69.5	-90.6	-80.5	-68.7
562.3	-77.7	-67.3	-92.9	-79.9	-66.7
1000.0	-75.6	-65.6	-93.9	-78.0	-65.0
1770.3	-73.4	-64.0	-94.8	-77.4	-64.1
3162.3	-73.5	-66.6	-95.6	-70.1	-65.6
5623.4	-80.6	-75.1	-104.3	-86.2	-73.0
10000.0	-89.0	-84.0	-116.1	-97.6	-83.4
17702.0	-90.0	-92.9	-120.9	-110.2	-91.0
31622.0	-100.1	-100.1	-142.0	-124.0	-99.5
56234.1	-117.0	-106.9	-157.4	-130.5	-106.5
100000.0	-127.7	-113.3	-172.3	-153.4	-113.1
177027.9	-137.7	-119.3	-187.3	-160.4	-119.2
316227.0	-147.7	-125.0	-202.6	-183.7	-125.0
562341.3	-157.7	-130.5	-210.4	-199.5	-130.5
1000000.0	-167.7	-135.0	-235.2	-216.2	-135.0

Input Parameters:

Output Frequency: 1200 MHz
 Reference Frequency: 250 kHz
 Phase Detector Gain: .796 V/rads
 UCD Gain: 23 MHz/V
 Total division N: 5120
 UCD Bandwidth: 8 kHz
 Op Amp: LT1012
 Resistance Tolerance: 5 %
 Ra: 2.43 kohms
 Rb: 3.74 kohms
 Ca: 12 nF
 Cb: 47 nF

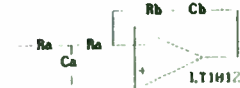


FIGURE 6A CALCULATED PHASE NOISE RESULTS.

FIGURE 6B PARAMETERS USED FOR CALCULATION OF 1200 MHz SYNTHESIZER PHASE NOISE.

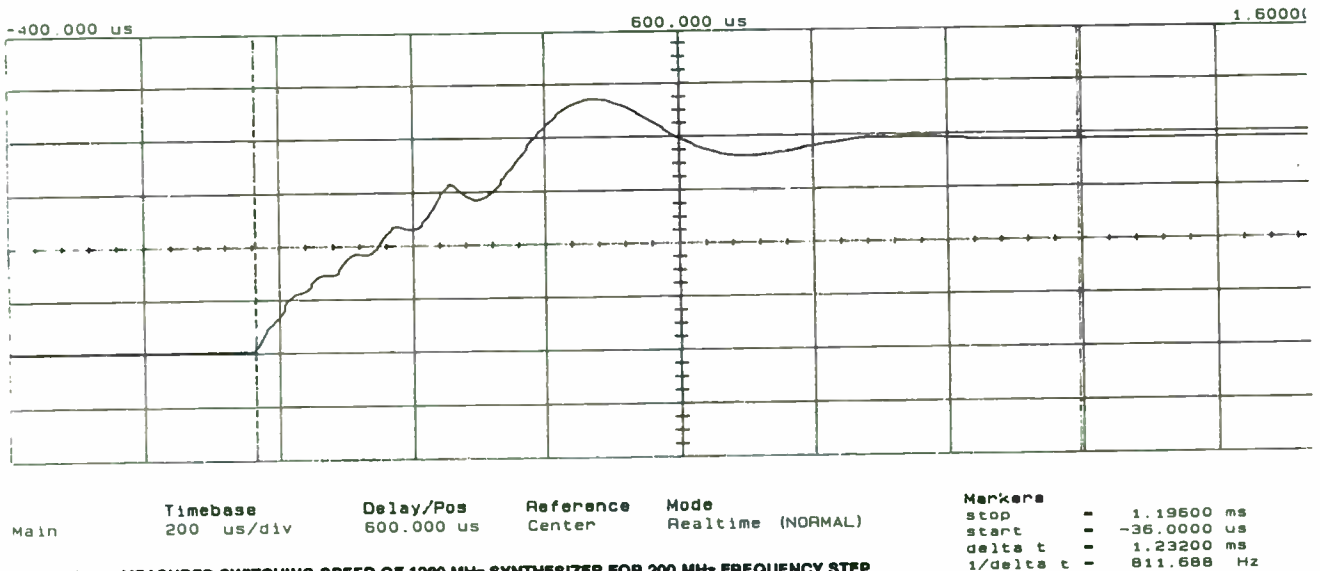


FIGURE 8 MEASURED SWITCHING SPEED OF 1200 MHz SYNTHESIZER FOR 200 MHz FREQUENCY STEP.

PHASE NOISE COMPARISON

FREQUENCY kHz	MEASURED dBc	CALCULATE dBc
1	-86.9	-85.0
3	-81.4	-85.6
10	-83.5	-83.4
50	-106	-106.0

SWITCHING SPEED

MEASURED	1.2 msec
CALCULATE	1.54 msec

FIGURE 7

Input Parameters:

Output Frequency: 400 MHz
 Reference Frequency: 50 kHz
 Phase Detector Gain: .796 V/rads
 UCD Gain: 5 MHz/V
 Total division N: 8000
 UCD Bandwidth: 15 kHz
 Op Amp: LF156
 Resistance Tolerance: 5 %
 Loop Bandwidth: 1.3 kHz
 Phase Margin: 50 deg.
 Low Pass BW 3dB: 18 kHz
 Low Pass Damping: .5

Calculated Filter Parameters

Ra = 18.878 k ohms
 Rb = 57.828 k ohms
 Ca = 7.11 nF
 Cb = 6.890 nF
 R1 = 5.684 k ohms
 C1 = 5.680 nF
 C2 = 1.400 nF

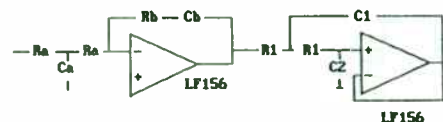


FIGURE 9 DISPLAY OF INPUT DESIGN SCREEN.

independent of the other and then add the two signals to obtain the transmit vector at an upconverted RF frequency. In the process of mixing, it is necessary to first phase shift the quadrature channel LO by 90° so that there is phase matching with respect to the quadrature component. This function is implemented via a hybrid phase splitter and is included on the chip. No external components are necessary to implement this function. It is also desirable to reduce the amplitude of the carrier and the undesired image which is obtained in the process of upconverting. This too is accommodated within the device by virtue of its basic architecture. GaAs MESFET process technology is used to obtain a relatively high level of gain and to implement the hybrid phase splitter with a high degree of accuracy.

Device Architecture

The architecture of the device is shown in figure #1.

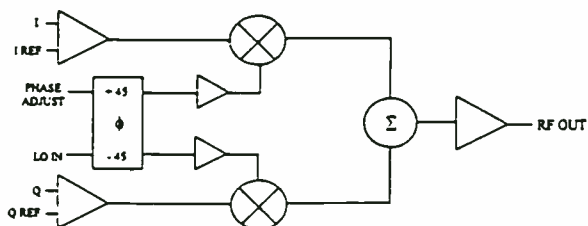


Figure # 1: Basic Quadrature Modulator Architecture

I, Q & LO Input Considerations and Resultant Performance

The I and Q inputs are differential inputs. They are loaded with approximately 3000Ω . Typically these inputs are produced by baseband D/A converters and are DC coupled. They can be AC coupled as well, however. Because the

device is a single power supply device, an artificial ground or reference has to be connected to the reference inputs. Since the input amplifiers are differential, their output is the difference between the two inputs. The driving source usually provides the reference voltage which is 2.5 V DC for this device. The input signal must be equal to the reference input for each amplifier ($I=Q=2.5 \text{ V DC}$) for the mixer to be in its balanced state (no output) whereas an output is obtained for any non-zero sinusoidal inputs on either the I or Q channel. The maximum input condition for the I and Q channel is +5 V (2.5 V DC plus 2.5 V AC zero to peak).

DC offsets in the I and Q channel inputs can cause reduced carrier suppression. The offsets may originate in the digital signal source, D/A converters, the interconnects, or in the device itself. The design of the system must account for these errors when a high degree of carrier suppression is required. In testing, we have found that unadjusted I and Q inputs will provide about 25 dB of carrier suppression. Induced I and Q DC offsets on the order of 10 to 20 mV have produced carrier suppression levels of 40 dB.

The LO input is a low VSWR match to a 50Ω line provided that an external terminating resistor of about 56Ω is used. The DC component of the LO signal must be near zero volts so a coupling capacitor should be used if any DC is present in the LO driver. The devices LO limiting amplifiers normalize the LO signal being applied to the mixers. In order to maintain good normalization, the input signal should be at least -6 dBm. Optimal performance

FREQUENCY (Hz)	OPEN LOOP GAIN Gain (dB)	OPEN LOOP GAIN Angle (deg)	CLOSED LOOP Gain (dB)	ERROR LOOP Gain (dB)	59.8 kHz REFERENCE SPUR ANALYSIS
10.0	74.6	1.2	78.1	-74.6	
17.0	64.6	2.1	78.1	-64.6	Spur level with only Op-Amp
31.6	54.6	3.7	78.1	-54.6	Integrator (Ra,Rb,Ca,Cb).
56.2	44.7	6.5	78.1	-44.6	INITIAL LEVEL: -44.2 dbc
100.0	34.8	11.3	78.2	-34.7	
177.0	25.3	19.2	78.5	-24.9	
316.2	16.6	38.2	79.2	-15.4	Attenuation Phase
562.3	9.1	48.7	80.3	-6.8	@ 59.8kHz @ 1.3kHz
1000.0	2.8	44.4	81.2	0.3	(dB) (deg)
1770.3	-3.1	36.4	79.3	4.4	UCD BW: 18.8 -5.8
3162.3	-9.4	13.7	72.0	3.4	ACTIVE LFF: 27.8 -7.5
5623.4	-16.8	-28.1	62.5	1.2	TOTAL 38.6 -12.5
10000.0	-27.7	-183.8	50.3	-0.1	
17702.8	-48.4	-178.9	29.6	-0.0	Final Reference Spur Level:
31622.8	-72.4	141.0	5.6	-0.0	-82.8 dbc @ 59.8 kHz
56234.1	-97.1	118.5	-19.0	-0.0	
100000.0	-122.0	105.3	-43.9	-0.0	
177027.9	-146.9	97.2	-68.9	0.0	
316227.8	-171.9	91.6	-93.9	0.0	
562341.3	-196.9	86.5	-118.9	0.0	Approximate switching speed:
1000000.0	-222.1	80.4	-144.0	0.0	3.00 nsec

FIGURE 10 DISPLAY OF STEADY STATE RESPONSES, SPUR AND SWITCHING SPEED CALCULATION.

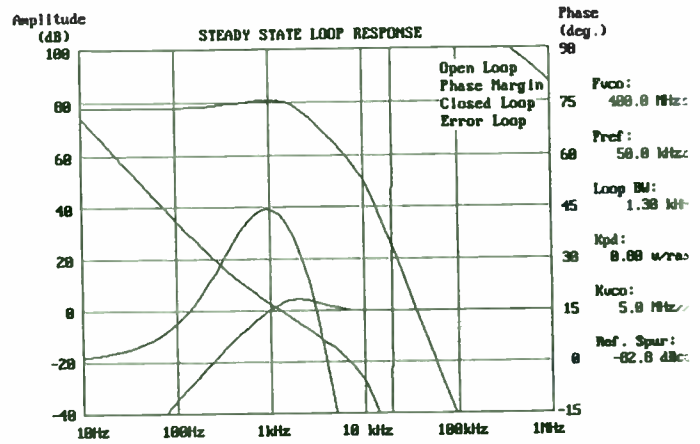


FIGURE 11 GRAPH OF STEADY STATE RESPONSES.

Frequency (Hz)	Loaded Q (dBc)	Varac. Diode (dBc)	TOTAL (dBc)	Input Parameters:
10	-19.5	-49.9	-19.5	UCD Frequency: 480 MHz
18	-27.0	-54.9	-27.0	UCD loaded Q: 6.0
32	-34.5	-59.9	-34.5	Power output: 18 dBm
56	-42.0	-64.9	-42.0	Flicker frequency: 5000 Hz
100	-49.5	-69.9	-49.4	UCD tuning sensitivity: 5.0 MHz/v
178	-56.9	-74.9	-56.8	Varactor noise resistance: 10.0 kohms
316	-64.3	-79.9	-64.2	RMS phase jitter: 100 Hz to 1 MHz: 1.965 deg.
562	-71.6	-84.9	-71.4	Press:
1000	-78.8	-89.9	-78.4	[1] increase Q
1770	-85.7	-94.9	-85.2	[2] decrease Q
3162	-92.4	-99.9	-91.7	[3] increase Kuc0
5623	-98.8	-104.9	-97.8	[4] decrease Kuc0
10000	-104.8	-109.9	-103.6	
17703	-110.5	-114.9	-109.1	
31623	-115.9	-119.9	-114.4	
56234	-121.2	-124.9	-119.6	
100000	-126.3	-129.9	-124.7	
177028	-131.4	-134.9	-129.8	
316228	-136.5	-139.9	-134.8	
562341	-141.5	-144.9	-139.8	
1000000	-146.5	-149.9	-144.9	

FIGURE 12 DISPLAY OF VCO PERFORMANCE.

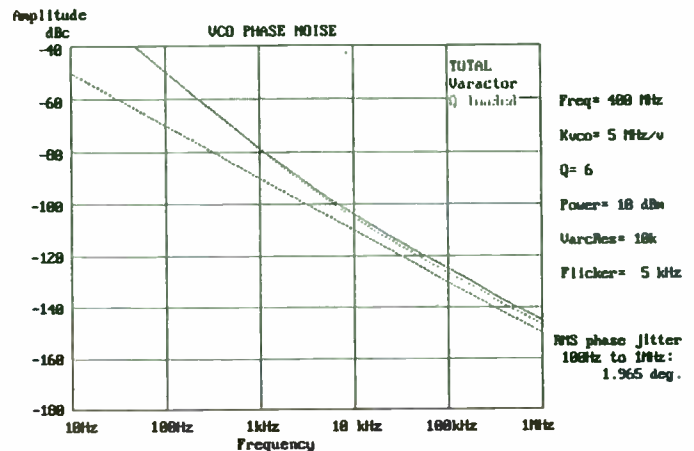


FIGURE 13 GRAPH OF VCO PERFORMANCE.

Frequency (Hz)	FILTER (dBc)	UCD (dBc)	REF (dBc)	Phase Det. (dBc)	Total (dBc)	Parameters
10.0	-78.9	-94.1	-68.8	-76.9	-68.7	Fuc0: 480.00 MHz
17.0	-78.8	-91.6	-65.7	-76.9	-65.2	Pref: 50.00 kHz
31.6	-78.7	-89.1	-78.5	-76.9	-69.1	Kuc0: 5.0 MHz/v
56.2	-78.5	-86.6	-75.1	-76.9	-71.7	Kpd: 0.796 w/rad
100.0	-78.1	-84.1	-79.4	-76.8	-72.8	Loop Bandwidth, Fo: 1.3 kHz
177.0	-77.1	-81.7	-83.1	-76.5	-78.2	Phase jitter over 100 Hz to 1 MHz: 1.322 deg.
316.2	-75.5	-79.6	-85.9	-75.8	-71.7	
562.3	-73.5	-78.2	-87.6	-74.7	-78.2	
1000.0	-71.8	-78.1	-88.9	-73.8	-69.1	
1770.3	-72.6	-80.8	-92.3	-75.7	-78.4	
3162.3	-77.8	-88.3	-100.5	-83.0	-76.3	
5623.4	-83.0	-96.6	-110.7	-92.5	-83.1	
10000.0	-91.0	-103.7	-123.2	-104.7	-90.6	
17702.8	-105.6	-109.1	-144.0	-125.4	-104.0	
31622.8	-121.2	-114.4	-168.2	-149.4	-113.6	
56234.1	-134.6	-119.6	-192.9	-174.8	-119.5	
100000.0	-146.1	-124.7	-217.8	-198.9	-124.7	
177027.9	-156.7	-129.8	-242.8	-223.9	-129.8	
316227.8	-166.9	-134.8	-267.8	-248.9	-134.8	
562341.3	-176.9	-139.8	-292.8	-273.9	-139.8	
1000000.0	-186.9	-144.9	-317.9	-299.0	-144.9	

FIGURE 14 DISPLAY OF SYNTHESIZER PHASE NOISE.

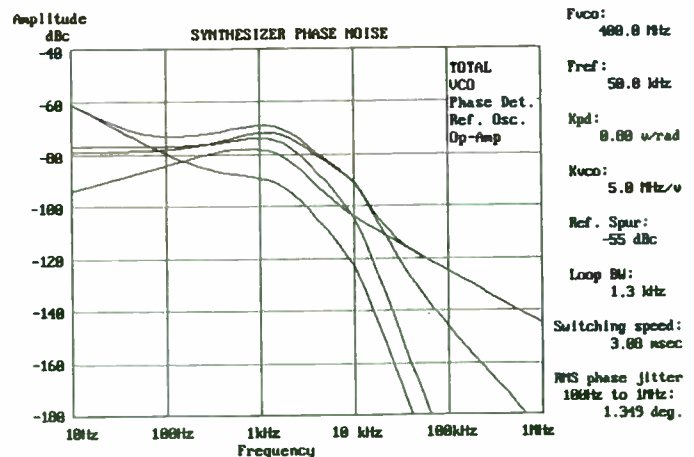


FIGURE 15 GRAPH OF SYNTHESIZER PHASE NOISE.

will be achieved at a level of around 0 dBm. No more than +6 dBm of LO input power should be used. The RF output vs. LO drive level is displayed in figure #2.

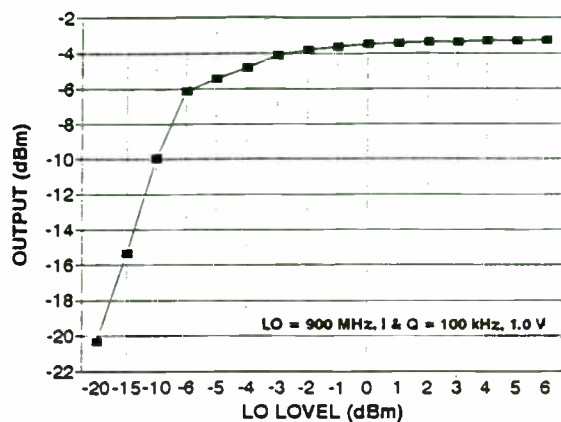


Figure #2: RF Output vs. LO Level

The device is optimized for use at frequencies of 700 MHz to 1 GHz. The unit may be used up to 1.2 GHz provided that a lower output RF amplitude can be tolerated. The curve of figure #3 shows the amplitude response of the unit vs. frequency. At frequencies below 700 MHz, the output RF amplitude remains constant but the internal phase and amplitude tracking errors between the I and Q channels become progressively worse. The curves of figure #4 and #5 show amplitude and phase error, respectively, vs. LO frequency.

Symmetry

Quadrature operation of the device requires that the phase balance between the I and Q channels be optimally 90°. By viewing figure #5, one can see that the phase error of the device is a function of LO frequency. This error can be compensated by using the "phase adjust" function of the device. This function has the net effect of moving the curve of

figure #5 to the right horizontally. This movement causes the zero phase error point to cross at different frequencies. This is done by adding a DC voltage on the phase adjust pin. Typically, for no phase correction, the pin is left floating and is not used. To compensate for phase error, one should connect a 10 kΩ potentiometer to the pin and tie it to the +5 V source. The value of resistance and thus voltage drop can be varied until the optimum sideband suppression is obtained and thus phase matching is achieved. Once this level is obtained a fixed resistor can be used to avoid tuning requirements. Remember that phase error is also a function of frequency and does vary on a device by device basis so some level of phase error will have to be tolerated. Typically a level of 25 dB sideband suppression can be achieved at 900 MHz. A level of 40 dB can be achieved by using the phase adjust mechanism.

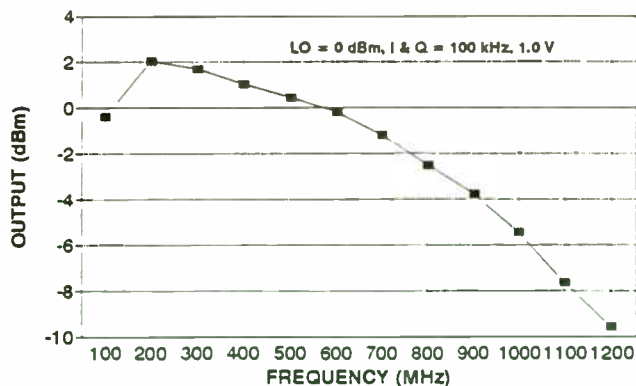


Figure #3: RF Output vs. Frequency

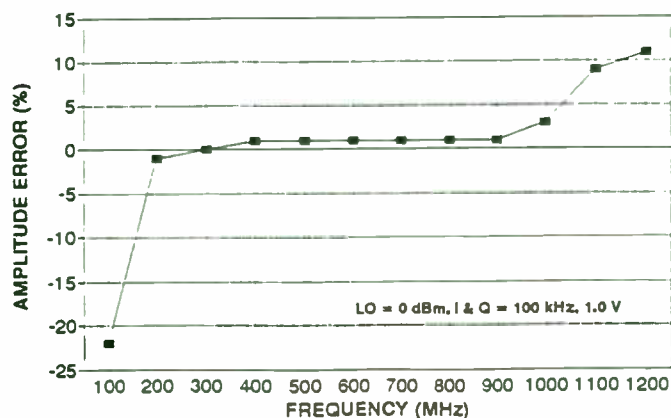


Figure #4: Amplitude Error vs. Freq.

PLL Settling Time: Phase vs Frequency

Donald E. Phillips
Rockwell International
400 Collins Road
Cedar Rapids, IA 52498

Frequency synthesizers for frequency hopping systems need to tune rapidly to permit efficient transmission of data during each hop period. The tuning speed is usually specified by either frequency or phase settling time. The purpose of this paper is to show that the phase settling characteristics correspond to system performance better than the frequency settling characteristics. A simulation will be used to clarify this paradoxical relationship intuitively, followed by a mathematical analysis.

There is a performance loss in a frequency hopping FSK system where each hop period is degraded by the time used to tune the synthesizer to each new frequency. For systems that are not phase-coherent (where the phase of each hop is independent of the phase of other hops) the signal during each hop is integrated over the hop period to obtain the best signal to noise ratio. Various techniques are used such as matched filters, FFT or other digital filters, etc. The following simulation uses a high-Q filter to integrate the signal over the first part of a hop where the synthesizer settling occurs. The results will be compared to an analysis using pure integration.

Simulation

The simulation circuit of figure 1 consists of a variable frequency source driving the two inputs to identical band-pass filters. These inputs are 90 degrees apart in phase. The filters are series resonant circuits L, C, and R. The output

voltages across the resistors are squared and summed to indicate the power out of the filter. One circuit would give the same result but with a more uneven power output and a poorer plot.

This band-pass filter (BPF) is normalized to a 1 rad/sec resonance. Since $R = 1$ ohm, the filter Q is set by the L and C values. For this example, a Q of 50 resulted in $C = 1 / Q = 0.02$, and $L = Q = 50$.

The four state-variables are the inductor currents and capacitor voltages, which are found by a differential equation solver. Two solutions were found, one which started on the desired frequency (1 rad/sec) centered in the pass-band at $t = 0$. The other started with a considerably higher input frequency of 5 rad/sec and settled to the desired frequency at an exponential rate simulating a phase-locked loop.

Since the filter $Q = 50$, the bandwidth is 0.02, or from 0.99 to 1.01 rad/sec. The frequency change compared to one side of the passband is $(5 - 1) / 0.01 = 400$.

The phase-locked loop bandwidth is 0.2 rad/sec, a time-constant t of 5 seconds. A first-order loop equation is used since higher order loops end up with the same settling pattern. The early part of the transient consists of many phase oscillations from which no useful output is obtained. The phase error eventually reaches a value of zero, arbitrarily assigned as the final phase value.

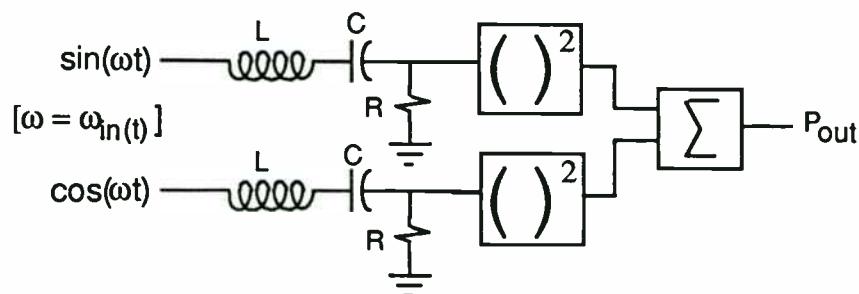


Fig. 1 - Simulation Model

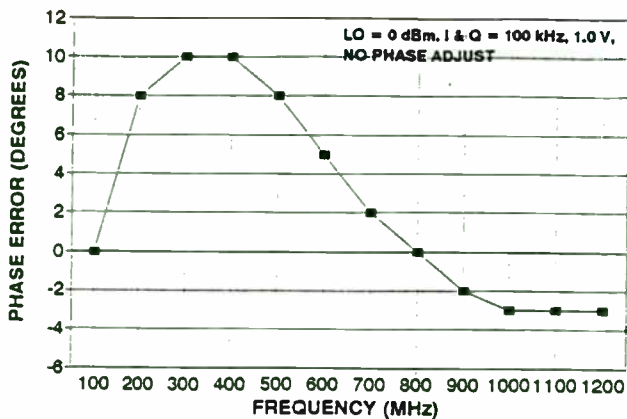


Figure #5: Phase Error vs. Frequency

RF Output

The output spectrum of the device is rich in harmonics, particularly the third harmonic. Thus, a low pass or band pass harmonic filter is generally used between the device's output and the final power amplifier stage (or antenna when the output level is sufficient). A plot of SSB output level vs. peak I & Q amplitude is shown in figure #6. This operation is all within the linear range. As you can see a peak output of +2.5 dBm is attainable. The output IM3 level varies with respect to SSB output level, but a level of -40 dB suppression is typical for this unit at -3 dBm RF output under two tone conditions at 900 MHz.

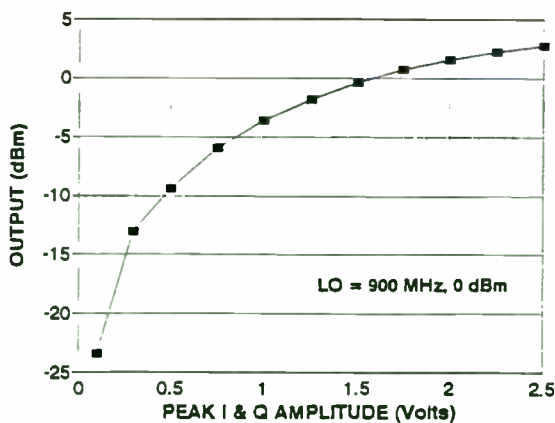


Figure #6: SSB Output vs. Peak Input

Power Management

The device typically consumes 28 mA of supply current, 35 mA maximum. This is satisfactory for the power budgets that have been established for most wireless applications. Given the fact that power should be conserved when possible, a power down function has been incorporated in the device. This is a pin that should be tied within 1 V of ground to be inactive and all the way to Vdd to be active. This pin is typically driven with an unloaded CMOS gate. When the power down function is enabled, the device typically consumes approximately 200 μ A. This function is particularly useful for TDMA type applications where the transmitter duty cycle is less than 50%.

Connections

The device has been designed to be as integrated as possible. However, a minimal amount of external componentry is required. The LO input and RF output are UHF frequencies and need to be connected on the PCB with microstrip lines. Also, as much power supply bypassing as feasible is provided on the chip, however, it is preferable to have some bypassing externally. This is accomplished via a single 0.1 μ F capacitor from Vdd to ground on the supply input pins.

Conclusion

An RF quadrature modulator has been successfully implemented in a GaAs MESFET process technology and packaged in a low cost plastic package.

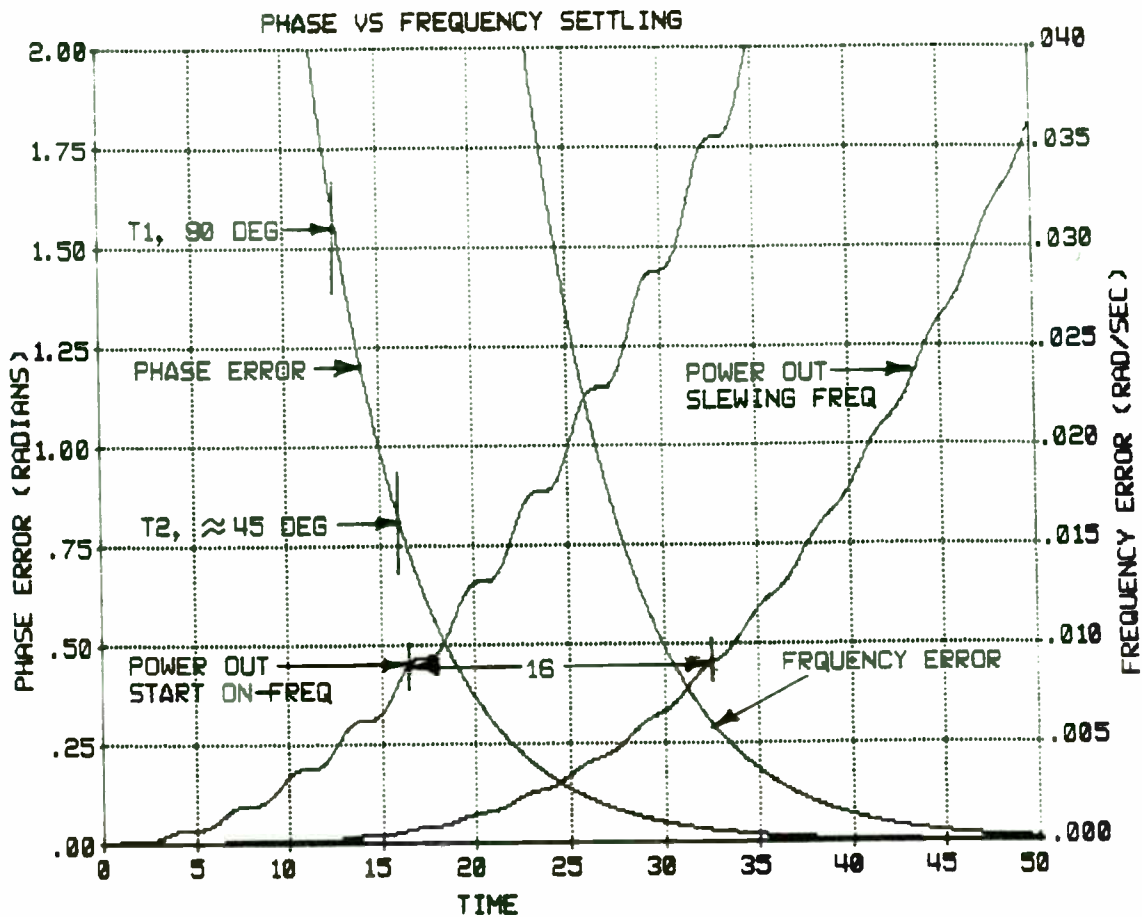


Fig. 2 - Simulation Results

The plot in figure 2 is from 0 to 50 time units (seconds in this case). The rising line marked "power out, start on-freq" is the filter output power build-up from a sudden application of the correct frequency and stable phase, as the high-Q filter integrates the input signal. This is the filter response with an input of zero settling time.

The next rising line marked "power out, slewing freq" is delayed because of the input settling time. The delay is almost uniform over time, as these output levels illustrate:

Times(sec)	Delay(sec)
12.5	27.5
17.5	33
25	42

This indicates that the total hopping period has lost about 16 time units of performance under these settling conditions. Now let us compare this delay with the frequency and phase settling characteristics.

The phase error has settled to within 90 degrees at $t_1 = 13$ sec. At $t_2 = 16$ sec. the phase error is about 45 degrees, which corresponds to a system performance loss

of 16 seconds delay of signal reception. Note that the time t_2 is 3 sec. later than t_1 . This will be checked in the analysis section.

The frequency error is shown according to the right-hand scale. Starting at an error of 4 rad/sec, it finally reaches the passband of .01 rad/sec in 30 sec. or almost twice as long as the beginning of signal reception!

Comments on the Simulation Results

This simulation illustrates the following very important points:

- (a) By far the largest contributor to performance loss is the time (t_1) spent *before* the incoming phase comes to within 90 degrees from its final settling value.
- (b) A small additional time (from t_1 to t_2) is spent just after the phase reaches its final 90 degrees, until the equivalent time of full system performance.
- (c) The frequency error ω_e is the loop bandwidth times the phase error θ_e : Note that faster tuning (wider

This device operates from 700 MHz to 1000 MHz and is applicable to most wireless applications within that frequency range. The device will produce an output level of +2 dBm maximum and can maintain a high degree of phase accuracy. Sideband suppression, carrier suppression and IM3 performance (-40 dB or better with adjustments) has been shown to be excellent and well within the bounds of most system requirements. Further, a minimum amount of peripheral components is necessary to make this device operate and overall performance is significantly higher than an equivalent architecture implemented in bipolar silicon.

Acknowledgments

The author would like to thank Bill Pratt, the principal designer of this device, and Kellie Chong, whose persistence in test and evaluation made the contents of this paper possible.

bandwidth) loops have higher frequency errors for the same phase error. The basic first-order equations are:

$$\text{eq(1)} \theta_{e(t)} = \frac{\Delta\omega}{\omega_n} e^{-\omega_n t}, \quad \text{eq(2)} \omega_{e(t)} = \Delta\omega e^{-\omega_n t}$$

where $\Delta\omega$ = frequency step and ω_n = pll bandwidth.

Higher order loops have more complex expressions but the final phase settling is similar. At time t_2 , the instantaneous frequency error is the loop bandwidth times the phase error, or $0.2 * 0.785 = 0.157$ rad/sec. This is over 15 times the filter upper band edge of 0.01 (above the band center of 1)! This is a subtle point because it is somewhat of a brain-teaser that even though the incoming instantaneous frequency may be much different from the steady-state-bandwidth of the receiving system, the filter does in fact derive useful energy from the incoming signal!

(d) One explanation for this paradox is that the transient (as opposed to steady state) frequency response of filters increases towards infinity as the applied transient time decreases from 1/bandwidth to zero.

(e) Another way of looking at this is that the faster a frequency changes, the wider its spectrum becomes due to the FM sidebands. The sidebands are already driving the filter even though the "carrier" ("instantaneous frequency") is not "there" yet.

(f) Still another intuition is that the filter is driven by phase. During the earlier part of settling the phase is rotating completely around the circle (because the frequency difference produces a beat note) and so the net effect is zero. The filter output starts rising when the periods of the incoming signal are approximately equal so that they continue to be in phase with the previously established filter ringing. The instantaneous frequency is the derivative of phase, so if the phase is settling rapidly the frequency is still outside the passband! In this sense a filter acts like a phase detector.

Settling Specifications

It is desirable, in terms of overall loss, for a frequency hopping system to have a phase characteristic such that the incoming and reference phases come to within 90 degrees as fast as possible. The time spent later on in matching the two frequencies is not nearly as important for minimizing total system loss.

A frequency hopping system should be specified in terms of overall performance loss given a hopping rate and related parameters. The commonly used specification which requires the receiver to be within a certain frequency offset of the desired frequency is not a good one, because it can be met with many different combinations of design parameters each of which combinations results in a different performance loss for the overall system!

Simultaneous phase and frequency settling specifications are not advisable because they effectively specify the phase-locked loop bandwidth, which may very likely interfere with obtaining the best tradeoffs between tuning speed, noise, and spurious levels, as well as cost, size, power, etc.

Measurement of "Instantaneous" Frequency

The concept of instantaneous frequency is hazy and should be approached with caution. It seems wise to reserve the word frequency for steady state conditions, unless very special precautions are taken. Measurement of the instantaneous frequency in a fast hopping system can be very difficult, which can lead to traps for the unwary. For example, if the synthesizer "slewing" frequency is gated at very short intervals to a narrow band filter, such as a spectrum analyzer with a 10 Hz bandwidth, it can appear to be within the 10 Hz band when the filter is simply ringing because of the sudden gating impulse, even when 100 kHz away!

Instantaneous frequency has also been measured by the slope of the phase error. A synthesizer phase error is easily measured by mixing with the desired reference frequency and observing the beat note on an oscilloscope. The reference phase is adjusted until the phase error crosses the zero center line at the specified settling time. From a measured small $\Delta\phi$ ($\ll 1$ radian) and corresponding Δt , the frequency = $\Delta\phi/\Delta t$. For small frequency errors this can be a very difficult measurement, even buried in the noise, which led to the suspicion that it may not have been a good system parameter.

Analysis

Various methods of analysis of system performance loss have been used, all of which have given approximately the same results. An analysis by Caloyannides [ref. 1] used integration of $(\sin x) / x$ terms which is difficult mathematically.

SYSTEM ASPECTS & RF COMPONENT DESIGN FOR EUROPEAN MOBILE COMMUNICATION SYSTEMS

by
Dr. Ing. Vinod Kumar,
Alcatel Radiotelephone,
32, Avenue Kleber,
92707 Colombes.
France.

ABSTRACT: This article offers a brief outline of radio interface specifications and functioning of various mobile communication systems recently standardised or still in process of standardisation in Europe. After a short introduction concerning the deployment of these systems, technical analysis based on typical values of their radio parameters is presented. Specifications of RF components and/or sub-assemblies for both Rx (receiver) and Tx (transmitter) chains are discussed. Only active circuits elements for both mobile subscriber (MS) and cell site (BS) equipments are considered. Comparison between radio parameters for various systems rather than detailed design calculations are stressed upon. Paragraph II gives details of frame structure for TDMA systems and Para III describes how specific system features are to be considered to determine the RF specifications. Details of system features and Rx and Tx parameters are given in Tables I, II and III respectively.

I. INTRODUCTION :

The field of mobile communications has been attracting lot of attention during last few years. In Europe, a variety of wireless systems have already been standardised by European Telecommunication Standards Institute (ETSI). Some others are approaching final standardisation. A relatively big set of radio communication systems, each suitable for a particular service application, are known to exist. Some of these are :

- **GSM** : Pan-European Cellular (Mobile) Communication System earlier known as "Group Special Mobile" is now called the - Global System for Mobile Communications. A more accurate name is GSM-900.

- **DCS-1800** : It is the Digital Cellular Communication System operating at 1800 MHz. Adopted by the U.K Personal Communication Networks (PCN) operators, this is derived from GSM-900 with adaption of radio parameters to suit micro-cellular systems. At times it is simply called PCN.

An analysis by Schoenike [ref 2] used a simpler method which gives approximately the same results. The model is an integrated output of an orthogonal synchronous detector, whose equation for the output voltage is eq(3):

$$E_o = K \sqrt{\left[\int_0^T \cos\theta_1(t) \cos\theta_2(t) dt \right]^2 + \left[\int_0^T \cos\theta_1(t) \sin\theta_2(t) dt \right]^2}$$

Trigonometric substitution results in sum and difference terms. The sum terms can be eliminated because it is assumed that there are many phase oscillations over the period T, so a very close approximation is eq(4):

$$E_o = \frac{K}{2} \sqrt{\left[\int_0^T \cos[\theta_1(t) - \theta_2(t)] dt \right]^2 + \left[\int_0^T \sin[\theta_1(t) - \theta_2(t)] dt \right]^2}$$

By a proper choice of $\theta_2(t)$, the sine integral can be made zero. Then

$$\text{eq(5)} \quad E_o = K_1 \int_0^T \cos[\theta_1(t) - \theta_2(t)] dt$$

To evaluate this integral, θ_2 is set equal to the final angle at which θ_1 eventually stabilizes. Also, the period between samples of θ_1 must not exceed π , so the numerical integration should not begin until the phase difference between adjacent samples is less than π . This effectively sets the integral to zero up to the first usable sample, because the positive and negative half-cycles up to this point tend to cancel each other.

A phase-locked loop phase settling characteristic (as previously defined) is substituted for the phase difference in eq. 5. The integration result is divided by the total time T to find the actual voltage to ideal voltage ratio. This loss ratio is now:

$$\text{eq(6)} \quad \text{Loss} = \frac{t_{\pi/2}}{T} + \int_{t_{\pi/2}}^T \cos\left(\frac{\Delta\omega}{\omega_n} e^{-\omega_n t}\right)^2 dt$$

$$\text{eq(7)} \quad \text{Loss} = \frac{t_{\pi/2}}{T} - \frac{\Delta\omega^2}{2\omega_n^2} \int_{t_{\pi/2}}^T \left(e^{-2\omega_n t}\right) dt$$

$$\text{eq(8)} \quad \text{Loss} = \frac{t_{\pi/2}}{T} + \frac{1}{4\omega_n T} \left(\frac{\Delta\omega}{\omega_n} e^{-\omega_n t_{\pi/2}}\right)^2$$

$$\text{eq(9)} \quad \text{Loss} = \frac{t_{\pi/2}}{T} + \frac{\pi^2}{16\omega_n T} \approx \frac{t_{\pi/2}}{T} + \frac{0.6}{\omega_n T}$$

The loss is in two parts:

(1) the time from the start of frequency switching ($t = 0$) until the final 90 degrees from the final phase, and

(2) an additional time related to the loop bandwidth. This is commonly a much smaller time, such that the equivalent phase for a "settled" condition may approximate 1 radian.

The previous simulation had no specified T, so the actual settling times will be found by multiplying eq. 9 by T, resulting in the time t_1 plus the time interval $t_2 - t_1$, or t_{add} , the additional settling time after the 90 degree point:

$$\text{eq(10)} \quad t_{add} = \frac{0.6}{\omega_n} \text{ sec.} = \frac{0.6}{0.2} = 3 \text{ sec.}$$

which agrees with the simulation.

Conclusion

The frequency synthesizer phase settling characteristics were found to be a critical factor in the performance of frequency hopping systems with FSK type of modulation with integration over each hop period. When the synthesizer settles in an exponential manner (such as with PLLs), the effective system performance starts after two time intervals have elapsed. The first is from the start of frequency change to the last time that the phase error (relative to final settled phase) is 90 degrees. An additional small time interval is 0.6τ ($1 / \text{PLL bw}$). Typically this results in a settling time until the phase error is approximately 45 degrees.

Other conditions can also affect the system performance, but frequency error has no direct effect. In some cases specifying frequency settling may lower system performance or compromise the synthesizer design, because of the many parameter trade-offs in PLL design.

References

- 1 Caloyannides, Michael. A., *An Analytic Evaluation of Synthesizer-Switching Performance Loss*, Rockwell International Working Paper, 1981.
- 2 Schoenike, Edgar. O., *Synchronous Detection of a Slewing Signal Frequency*, unpublished paper, 1976.

- **DECT** : Digital European Cordless Telecommunication System has been standardised by ETSI for wireless office communications.
- **TFTS** : Terrestrial flight Telephone System is to be applied for ground to air communications for commercial telecommunications services in civilian aircrafts.
- **TETRA** : Trans European Trunked Radio System is in the process of standardisation by ETSI for Special/Private Mobile Radio (SMR/PMR) applications.
- **DSRR** : Digital Short Range Radio system has been standardised for voice and data transmission applications using low power radio transmission.

All these systems are suitable for full duplex digitised speech transmission and special provisions have been made in TETRA & DSRR for simplex and semi-duplex operation. Various services based on digital data transmission have also been designed in each of these systems. GSM-900, DCS-1800 and TFTS are deployable for multi-operator, wide area public networks. DECT is used mainly for special (private) network applications.

Two more systems namely European Radio Message Service (ERMES) and CT2 (second generation Cordless Telephone) have been standardised and widely deployed during the previous years. However these systems are not discussed any further in this paper.

Different Technical Committees or Radio Equipment and Systems groups in ETSI carry out this standardisation work. Radio Interfaces of standardised systems are detailed in series 05 of ETSI recommendations. Recs. 05.04 and 05.05 for each specific system are of major importance for Rx and Tx designs. Parameter values in Table I, Table II and Table III, are based on information from the recommendations.

II. TDMA FRAME AND SLOT STRUCTURES

GSM-900 and DCS-1800

$$1 \text{ bit} = 48/13 = 3.69 \mu\text{s}$$

$$1 \text{ time slot} = 156.25 \text{ bits} = 577 \text{ ms (including interburst guard time of 8.25 bits)}$$

$$1 \text{ frame} = 8 \text{ time slots}$$

$$26 \text{ multiframe} = 26 \text{ frames}$$

$$51 \text{ multiframe} = 51 \text{ frames}$$

- . Each active MS transmits traffic information during one TS per frame in normal functioning.
- . Traffic and associated signalling are transmitted modulo 26 -multiframe and 51 multiframe is used for dedicated and common channel signalling.
- . Shorter bursts for random access are also used.

Linear Frequency Modulation — Theory and Practice

Bar-Giora Goldberg, MSEE
Henry Eisenson
SCITEQ Electronics, Inc.

Introduction

Linear frequency modulation (FM), or a "chirp," is a swept frequency change over some bandwidth. An ideal chirp has a perfectly constant rate of change (time vs. frequency), and is generated by a means that makes it perfectly reproducible. Stimulated by emerging radar requirements to distribute energy across a range of frequencies, early LFM signals were generated with analog devices such as a voltage controlled oscillator (VCO) or (later) by surface acoustic wave (SAW) resonator.

This paper will address chirp signals in general, and present one aggressive all-digital mechanism for generating them with a combination of linearity and operating bandwidth not previously achieved.

History

In the late 40's and early 50's, as pulse radar technology grew out of its infancy, a problem became visible. Radar range depends on $\frac{E}{N_0}$, where E is the pulse energy, $E = P \cdot T$, (P is the received power proportional to the transmit power, T is the pulse duration) and N_0 is the receiver noise density, and resolution depends on the signal bandwidth. These two values are related diagonally, as improving E makes it necessary to increase T and an increase in T increases the pulse bandwidth and therefore resolution.. One solution was to modulate the pulse, making pulse bandwidth dependent upon the modulating waveform rather than pulse length of (approximately) $\frac{1}{T}$. Linear FM (LFM) was developed and adopted long ago, and it remains useful today in many radar applications. Relatively recently, the utility of LFM in non-radar applications has been recognized and explored, and chirp is now important in communication, semiconductor process control, sonar, seekers, range measurement, simulation, test equipment and other system categories. VCO solutions have analog accuracy, and problems with linearity and repeatability. Those effects are lessened with SAW devices, but SAW is neither programmable nor deterministic.

In 1989, Sciteq began work on an all-digital technique to generate LFM, using direct-digital

synthesis (DDS) technology. A DDS consists of an accumulator stage to correlate the clock with a control word to produce a phase word, a memory to map phase information to amplitude, and a digital-to-analog converter (DAC) to produce the analog waveform. The problem was that architectures selected for typical accumulators included a great deal of latency partly due to pipelining (to conserve power), which meant that a new frequency could not be loaded until the previous one had propagated through the logic. The resulting delay was acceptable for audio/sonar frequencies, but not at microwave. In addition, some means had to be developed to change the frequency control word to the accumulator at a rate commensurate with the desired output ramp. These deficiencies mandated development of new DDS integrated circuitry that would provide a cost-effective approach to an idealized chirp signal.

The goal therefore was to develop a fully digital, programmable, chirp generator to enable the digital of F_{start} , slope, and phase modulation — all fully synthesized. The solution must provide total parameter control, with digitally deterministic repeatability.

By 1990, necessary digital and data conversion components had already been developed, or were being developed, either by Sciteq or other agencies (Sandia National Laboratories, for one), and for the first time it appeared possible to produce the industry's first wideband digital chirp synthesizer. Accordingly, Army Research Laboratory (then Harry Diamond Labs, in Adelphi, MD), let a Small Business Innovative Research (SBIR) Phase I contract to Sciteq to determine the practicality of meeting theoretical goals for the Army's next-generation battlefield surveillance radars. Specifically, the ARL group working on Synthetic Aperture Radar believed that a digital signal generation solution was important to future program objectives. Sciteq's interface for this program, and sponsor, was and remains Barry Scheiner, of ARL.

Phase I defined a practical path to the desired goal, leading to a Phase II contract award. Most SBIR projects are considered high risk, but this development was successful and prototypes have been delivered to the Army and to other agencies interested in evaluating ideal linear FM signals.

DECT:

1 bit = $1/1.152 \mu\text{s}$

1 time slot = 480 bits (this includes an inter burst guard time equivalent to 60 bits)

1 frame = (12+12) time slots = 10 ms

1 multiframe = 16 frames

- . A normal voice only MS transmits once every frame.
- . Signalling information is carried in the header portion of each burst, both in forward and reverse links.
- . Shorter bursts are also defined.

TFTS:

1 bit = $1/44.2 \text{ ms}$.

1 time slot = 208 bits = 4.706 ms.

1 frame = 17 time slots = 80 ms

1 Superframe = 20 frames = 1.6 ms.

- . A total guard time of 5 bits is included in the time slot duration. An equivalent of 2.5 bits is provided at each end of the burst.
- . Each active voice channel occupies four out of 17 time slots in a frame.
- . Shorter time slots have been defined for specific functions.

TETRA:

1 bit = $1/36 \text{ ms}$

1 time slot = 510 bits = 14.167 ms

1 frame = 4 time slots = 56.66 ms

1 multiframe = 18 frames = 1.02 ms

1 hyperframe = 12 multiframe = 12.24 ms.

- . Interslot guard time is included in the above time slot duration. Its exact position in the burst is to be determined.
- . Shorter time slots (or sub slots) are also defined.
- . Numbering of time slots on reverse link is derived from forward link numbering with a shift.

The nature of the SBIR program permits the contractor to retain control over the new technology, and to productize the results where possible, hence the availability of Sciteq's direct-digital chirp synthesizer (DDCS) to the industry. That product, designated the DCP-1, is a DDCS that produces linear FM signals over a band of more than 230 MHz, with linearity approaching an ideal level previously defined only by mathematics and never actually observed.

Waveform Properties

A substantial amount of theoretical work was done to calculate the properties of LFM signals, i.e., power spectrum, auto-correlation, etc., and the characteristics of a theoretically perfect LFM signal were defined. A general description of such a signal is given by:

$$s(t) = A \cdot \sin(\alpha t + \frac{\beta}{2} t^2 + \phi_0)$$

If the signal bandwidth is designated as W, then the product, $W \cdot T = TB$, becomes the time bandwidth product in radar applications or processing gain in spread spectrum communication. For $W \cdot T = TB \gg 1$, the power spectrum is flat and the signal energy is distributed almost equally across the bandwidth, W. Signal auto-correlation is given by:

$$R(\tau) = \left(\frac{\sin X}{X} \right)^2 \text{ where } X = \pi \cdot \tau \cdot W = \pi \cdot \tau \cdot \frac{TB}{T}$$

It can be shown that the signal auto-correlation has relatively high sidelobes with the worst case of -13.5 dB (approximately $20 \cdot \log \left(\frac{\sin X}{X} \right)$ for $X = 1.5 \cdot \pi$). This parameter can be improved by adding the complexity of either amplitude modulation or phase modulation (pulse weighting).

Applications

LFM is used for fuzing, altimetry, ranging, pulse Doppler radars, synthetic aperture imaging radars and more. The better the linearity of the LFM signal the better the performance of the system, but even the chirps generated by analog circuitry were better than non-chirped operation. With the advent of DDCS technology, with its inherent deterministic linearity, imaging resolution of SAR and performance of other chirp-dependent systems were substantially improved. For those same reasons, LFM provides advantages to range measurement systems, for altimeters, flight control and similar applications.

Compressive receivers are used to scan the spectrum, and unlike typical spectrum analyzers, which sweep the spectrum and find signals that are within the analyzer bandwidth during the time of the sweep only, these receivers see ALL signals that occur within the sweep time. In this respect, a compressive receiver operates like a real time DFT analyzer. An ideal compressive receiver depends upon a linear and fast chirp over the desired band of reception.

In semiconductor production, wafer perfection is a critical issue that influences yield, and therefore has serious economic impact. Surface anomalies and contamination are usually detected using a laser beam, which is reflected off the wafer surface and scatter characteristics evaluated to determine surface characteristics, resulting in a map of the wafer showing imperfections, contamination, and therefore usable dice. In most such applications, the wafer is moved mechanically in one dimension, and the laser is modulated by a Bragg cell driven by a linear FM signal (produced from an expensively-compensated VCO). The linearity of the FM signal is one of the factors that determines resolution of the system along the appropriate axis, and also affects the "guard" area around imperfections that are detected (because of inherent error). The more accurate the signal (the more controllable the laser position) the smaller the guard area and the higher the yield.

Digital LFM Synthesis

Evolution of digital technology has allowed certain Direct Digital Synthesizer (DDS) implementations to operate at sufficient speed to produce output bandwidths sufficient for the above described applications.

The use of DDS disciplines brings with it cardinal improvements in the waveform features such as:

- The signal is synthesized and therefore every pulse is identical to the previous one.
- The chirp linearity approaches the limits of measurement.
- Phase manipulation is digitally accurate and is available at almost no additional cost.
- Control of parameters such as start frequency, stop frequency, chirp rate, on/off, etc. are completely and inherently deterministic and accurate.

III.1 TIME DIVISION MULTIPLE ACCESS (TDMA), CONSTANT ENVELOPE MODULATION and POWER AMPLIFIER DESIGN

Table I shows that all the considered systems, except DSRR, use TDMA. Also most of these (four out of six) use constant envelope modulation of GMSK type. The two remaining systems namely TETS and TETRA intend to use $\pi/4$ shifted differential quadrature phase shift keying ($\pi/4$ - DQPSK). This is designed to minimize the modulated signal form factor.

Such modulations (GMSK and $\pi/4$ - DQPSK) facilitate the use of linearised power amplifiers for Tx signal amplification : Intermodulation noise and spectral distortion specifications for GSM, DCS and TETS being very stringent , the power amplifiers need to be operated with a certain (sometimes high) back-off. This back-off is minimised if signal form factor is reduced.

However, Transmitter attack and Tx release time for GSM/DCS are rather fast and not so easily achievable without use of good linear amplifiers.

Moreover, once the initial switching transient at Tx output is absorbed, the power level for GSM/DCS Tx has to stay within ± 1 dB of the normal transmit power. Similar constraints for DECT, DSRR are also applicable. The respective values are listed in Table II.

III.2 TRANSMITTED CARRIER STABILITY, POWER IN ADJACENT CHANNELS & PILOT SOURCE SELECTION.

Most of the digital radio systems require that both timing signals and carrier frequencies be derived from one common pilot source. Its stability has to be calculated for worst case condition which can be different for different systems.

A typical DECT network shall use one carrier per base station where as GSM, DCS and TETS will require multi-carrier BS's. In such a case accurate receive-transmit timing for different carriers (rather than the carrier frequency stability itself) imposes the worst case requirement on pilot source.

In this context, it is really interesting to analyse the influence of doppler shift experienced by the radio signal in different systems. In DECT/DSRR indoor networks the relative Rx/Tx velocity is rather small (typically 3 Km/h). Whereas in TETS high relative Rx/Tx velocities can induce a doppler shift of a few KHz on radio signal. Such a carrier shift coupled with any initial carrier inaccuracy could mean that the signal energy in the adjacent channel is increased much beyond acceptable limits. Signals in GSM-900 and DCS-1800 networks shall experience doppler shifts in range of a few hundred hertz in worst case.

The output of the digital process is represented as:

$$s(n \cdot t_0) = \sin \left(\frac{\beta (n \cdot t_0)^2}{2} + \alpha(n \cdot t_0) + \phi_0 \right)$$

The general structure is that of a dual accumulator. Since an accumulator is a discrete integrator and the requirement is to generate a quadratic function, two accumulators are used. The output of the first accumulator is the instantaneous frequency and the frequency adder allows the setting of a start frequency. The F output allows the monitoring of the instantaneous frequency. The input of the first accumulator is therefore β in the equation and the frequency input is α . The output of the second accumulator is the signal's phase and therefore can be phase modulated by another adder. This input is equivalent to the term, ϕ_0 , in the equation.

Such structure can be implemented in CMOS at low clock frequencies, and in high speed ECL and GaAs technologies up to 1000 MHz, though the nature of a DDS limits output to less than half the clock.

In the existing design, the chirp chip and phase adder (implemented in one device) are followed by a SINE ROM, a DAC (digital to analog converter), and a low pass filter. Because of the nature of the output spectrum from a DDS $\left(\frac{\sin x}{x} \right)$ and the group delay of the filter, amplitude and group delay equalization is included to improve the result.

Practical Implementation: the DCP-1

The Sciteq model DCP-1 is a direct-digital chirp synthesizer (DDCS) that is clocked at 500 MHz and therefore generates output frequencies from DC to 230 MHz (limited by Nyquist and the low pass filter characteristics). The basic chirp generation function is achieved by three devices, a double-accumulator, a memory, and a digital-to-analog converter.

In the double accumulator, both accumulators are 24 bits in size, thus yielding a minimum step size of ~29.8 Hz at a clock rate of 500 MHz. The frequency and phase accumulator functions are integrated into one device, developed by a Sandia National Laboratories program under the leadership of Bruce Walker. The part includes not only the specified accumulation functions, but also 12-bits of phase control and a time-equalized 8-bit frequency output that supports system timing. The memory device uses a patent-pending algorithm (Sciteq's) to map the phase output of the accumulator to digitally-defined amplitudes, also at a 500 MHz rate or better. The digital output of the memory is considered near-perfect, with digital error

supporting a spurious response better than 70 dB below the carrier, so it is the digital-to-analog converter (DAC) that limits the spectral purity of the system. Initial DCP-1s used a 12-bit GaAs part developed by a consortium including GE, Sciteq, Motorola, and Hughes, and typical spurs are at the -45 dBc level.

In the LFM mode, the DCP-1 updates frequency at a 500 MHz rate, which means that a new frequency is synthesized every two nanoseconds. The slowest chirp rate is ~15 kHz/ μ sec (~30 Hz times 500, since there are 500 steps in each microsecond). For a full band sweep, this would take approximately 13.4 msec (230,000,000 \div 29.8 \cdot 2 nsec = 15.4 msec). Faster sweeps are possible, limited by acceptable resolution (as an extreme, at 230 MHz resolution it's one full chirp – a single step in two nanoseconds). A chirp rate of 10 MHz/ μ sec is practical if it is desired to cover a 50 MHz bandwidth in 5 μ sec (5 μ sec \div 2 nsec for the number of steps gives a required resolution of 20 kHz).

The synthesizer is controlled by loading two registers — start frequency and chirp rate (or step size). When the chirp begins, the step size will be added to the start frequency every 2 nsec. At any point during the chirp it is possible to change the chirp rate to produce different time:frequency relationships. A negative value in the chirp rate register (2's complement) will produce a sweep starting at a higher frequency and moving lower, thus supporting complete manipulation of all output parameters.

In addition, 12 bits of phase control permit compensation of the response during the sweep to reduce side lobes. This may be updated at a rate limited only by speed limitations of TTL logic. Phase control adds another dimension of flexibility by permitting the control of phase from pulse to pulse, which permits accurate matching of signals.

Applications and Experimental Results to Date

The DCP-1 is now used by a variety of systems, including (upconverted/multiplied) two millimeter-wave seeker programs, four synthetic aperture radar systems, two electronic warfare programs, and (in baseband) at least one wafer process control system.

So far, system developers have reported favorable results. Spurious signal level was initially a concern (as is the case in most DDS applications), but one unpredicted result of experimentation is that discrete spurious signals seem to be integrated into the general output, and have little result on overall system performance.

Table II presents the figures on Tx output carrier stability of the BS. Generally an MS adjusts the frequency of its transmitted carrier in synchronisation with the received BS carrier. For example, a DECT-BS carrier can stay within +/- 50 KHz of an absolute reference and a MS has to stay within +/- 50 KHz w.r.t the recovered carrier or w.r.t an absolute reference.

Since TETRA should permit a co-ordinated use of available radio channels between different systems in trunked mode, good carrier stability and low adjacent channel power (-60 dBc) are prime requirements. Also, disturbance to existing analog PMR/SMR networks have to be kept to a minimum.

Some other considerations for pilot source accuracy are detailed in coming paragraphs.

III.3 FREQUENCY HOPPING, DUPLEX METHOD and SPEED of Rx-Tx SYNTHESIZER

GSM/DCS implement slow frequency hopping (SFH) to improve radio link performance. In such a case, each MS should have the capacity to operate (Rx & Tx) on a different radio channel every TDMA frame. Moreover MS reception and Transmission use two frequencies 45 MHz apart.

In addition the MS is supposed to perform measurements on set-up channels of surrounding BS per TDMA frame. Hence its synthesizer has to be tuned to at least three different frequencies per frame of 4.6 ms. Synthesizer settling speeds of about 500 μ s are usually considered. The frequency accuracy to which the synthesizer has to settle is very stringent in view of a total 50 Hz carrier frequency error on the transmitted burst. Total range of frequencies over which a synthesizer may have to place its 200 KHz mode channel is 70 Mhz for GSM-900 and about 200 Mhz for DCS 1800.

A typical DECT network would employ only one radio channel per BS. Also Rx and Tx during a call are performed on one same frequency in TDD mode. However for radio control functions both MS and BS may be required to switch operation to other radio channels for interference calculations. Any receiver trying to perform its normal reception and interference calculation in two consecutive time slots may require to shift frequency of its local oscillator in less than the 60 bit guard period provided after each time slot. However, the DECT standard does accommodate much higher carrier frequency error than the GSM or DCS. Ref Table II and Table III.

Linearity is within quantization levels, therefore for broadband chirps the errors are smaller than conventional measurement techniques can detect. Initially, repeatability was evaluated by delaying the output of the DCP-1 and then comparing that signal with the original; the result was measured on an HP 3561A FFT and found to be virtually perfect. Linearity testing was conducted using the Racal-Dana 2351 Time Interval Analyzer, and the HP 5373A Modulation Domain Analyzer.

The results include both time vs. frequency data and a histogram displaying frequency distribution, and again support the contention that the linearity is perfect within the limit of granularity.

SUMMARY

Several niches in the RF industry can benefit from linear FM signals. Such waveforms have been generated using various analog means, with results that improve system performance despite the ambiguities of the analog design, and engineers in these niches seek to generate signals with improved linearity and predictability. Sciteq, sponsored by the U. S. Army and in cooperation with Sandia National Laboratory, has developed a linear FM generator that synthesizes a new frequency each two nanoseconds. Based upon direct-digital synthesis, the new technology creates opportunities for optimization of synthetic aperture radar, altimetry, ranging, seeker, and even process control systems.

III.4 Tx-Rx SYNCHRONISATION, INTER-SLOT GUARD PERIOD and RECEIVER SETTling TIME

As seen from Table I, DSRR & DECT would experience small Tx-Rx separation in comparison to the one for GSM-900, TETS and TETRA. DCS-1800 falls in some intermediate range. Moreover, greater the Tx-Rx separation greater is the multipath time dispersion in a Rayleigh channel like for GSM 900/DCS 1800 and TETRA. Signal in TETS shall be affected by proportionately smaller multipath time dispersion as TETS channel behaves similar to a land mobile communication channel only during aircraft take off and landing.

MS generally is synchronised to BS timing in GSM / DCS, TETS & TETRA. Once the MS burst transmission is time aligned to compensate for the radio propagation delay due to large BS-MS separation, MS maintains its timing within +/- 1 bit with respect to BS timing. By taking into account different parameters like Tx attack time, MS-BS timing mis-alignment, multipath timing dispersion on the received signal it can be concluded that only a small part of the total interburst guard period is available for receiver settling (e.g less than 10 μ s for GSM 900).

Moreover, a BS receiver for any of the GSM, DCS, TETRA or TETS may receive two consecutive signal bursts with wide amplitude differences. Such a situation is more probable in a system implementing slow frequency hopping without a perfect MS power control in a GSM/DCS network. Total received signal dynamic range of about 90dB has to be considered for an Rx design based on the worst case values.

DECT networks would mostly operate without any MS-BS time alignment. An interburst guard period of about 50 μ s is useful to accommodate all the timing inaccuracies and the small cell time delay dispersion too.

III.5 DISCONTINUOUS TRANSMISSION (DTx), Tx POWER CONTROL and SYNTHESIZER FREQUENCY PULLING :

In call, dynamic transmit power control is applied in large cell systems like GSM / DCS, TETS and TETRA. Transmitting just the required amount of power helps to reduce radio interference and the MS can save on battery consumption. In addition possibility of speech interpolation based discontinuous transmission is also available in most of the systems. The BS Tx must be designed to ensure the required carrier frequency stability (< 100 Hz for DCS) for all power levels. This carrier stability might be slightly affected by the variation in power supply current.

Burst to burst Tx power (over 30 dB dynamic range) and frequency changes have to be considered for the design of frequency hopping transmitters for GSM & DCS. TETRA & TETS have to accommodate even larger power variations and DECT does not implement dynamic power control. A typical GSM/DCS MS has to implement rather slow (Tx active during one burst per frame) power variations i.e +/- 2 dB from one frame to next.

RF ACTIVE DEVICE MODELING FOR CAD, A COMING NECESSITY

Gary Roberts
Hewlett Packard Company
Santa Rosa Systems Division
1400 Fountaingrove Parkway, Santa Rosa Ca, 95403

INTRODUCTION

As the world electronics industry has reoriented to focus on commercial and consumer electronics, products in the RF frequency range have become extremely important. Further, the competitiveness in these markets demands that reduced cost and time to market become primary goals in product development.

Accomplishing these goals requires the ability to consistently simulate the performance of circuits before they are built. Key to achieving a single design cycle, and the associated cost/time reduction, is the availability of accurate, up-to-date device models.

In the past, the importance of accurate models in achieving a single design cycle has been recognized. However, actual statistics illustrating the importance are rare. Figure 1 shows data from a world-class foundry for 36 MMIC product designs completed over a ten year period. Each design experienced a number of iterations, and the reasons for each iteration have been analyzed and plotted. The lack of adequate models was the largest contributor to added iterations, accounting for over 30% of the total. The breakout of data for the last two years indicates it is still the major cause (40%).

MODELS AS A COMMON LANGUAGE

Achieving a single design cycle requires the total engineering efforts of the device designer, the fabrication engineer, and the circuit designer, each working individually and in combination. In today's environment, device models have come to serve as indispensable tools to aid the success of each engineer as well as to provide a common language that facilitates the summing of their efforts. For example, the circuit designer now has a broad range of CAD tools available, yet it is accurate device models which allow these tools to be used to their maximum extent. Circuit performance may now be optimized with select model parameters, and specification of circuit needs is communicated with model parameter values, thereby providing targets for device/technology development. These same model parameters then provide both targets and quantitative measures for the fab engineer

to monitor and control the key process steps that assure product consistency.

WHAT IS A MODEL?

To achieve its ideal, a device model should provide a representation of the electrical performance of the device which can then be used either for circuit simulation or as a detailed measure of transistor performance. However, there is not yet one "universal" transistor model type which ideally suits all purposes. Accordingly today, models are divided into three broad categories: physical models, empirical models, and data-based models (Figure 2). Each has its advantages and disadvantages.

Physical models derive device performance from a two-dimensional analysis of the electron dynamics in the device structure (ref1). Electrical performance is obtained from a detailed solution of Poisson's equation while evoking current continuity, and energy and momentum conservation. Performance is provided in terms of device geometry, doping concentrations, and material constants. This class of models is particularly useful in directly relating device physics, geometry, and fabrication details to device performance. Thus it provides the best insight into how to design and fabricate a better device.

Physical models, however, often must be simplified to provide reasonable circuit simulation times. In doing so, they lose varying amounts of accuracy. Recent work to overcome this deficiency for GaAs FET and HEMT devices has shown promise(ref1). However, their usefulness to circuit designers is still limited because they still require knowledge of fabrication details which are not always available, or are considered to be proprietary by component vendors.

Empirical models are the most widely used today for circuit simulation. They represent the best compromise for use by both the device and circuit designers. Examples of this class of models are the industry standard Gummel-Poon model for BJT devices (ref2), and the SPICE MOS models for MOSII and III(ref3) and BSIM (ref4). Here the device is represented by an equivalent circuit schematic whose form and components are derived from both device physics and

III.6 Tx SPURIOUS EMISSIONS & Rx SPURIOUS REJECTION FOR CO-SITING OF DIFFERENT SYSTEMS :

Three out of the six systems discussed above operate in the frequency range 1670 to 1900 MHz. A separation (in operating frequency) between co-sited networks of these systems has to be respected to avoid mutual interference. This is determined on the basis of interference calculations.

Important Tx parameters for these calculations are :

- transmitted power at frequencies offset from the wanted signal.
- intermodulation products created by a multi channel BS (especially in case of GSM/DCS and TFTS) after the transmitter output.

N.B suitable margins to account for the multiplicity of channels on a given BS site have to be considered on top of single Tx specs. of spurious emissions and intermodulation product generation.

Important Rx parameters for those calculations are :

- Rx sensitivity with respect to thermal noise, co-channel interference adjacent channel interference and in band and out of band signals.
- Rx desensitisation performance. The receiver ability to detect a weak wanted signal in presence of a very strong unwanted signal (offset in frequency w.r.t wanted channel) is considered here.

Receiver selectivity in terms of image frequency rejection and local oscillator noise directly influence this performance. Reverse mixing due to local oscillator re-injection has to be controlled too. A typical GSM-900 receiver may need -150 dBc/Hz of phase noise at 600 KHz from the wanted carrier frequency.

IV. CONCLUSION: The above system description and analysis shows that interdependence between various apparently different looking parameters. A comparison between parameters values for GSM-900 and DECT shows that components for wide area applications in public mobile networks are required to meet much more stringent specifications than those used in private networks for on-site and indoor applications. Cositing and coexistence of various systems can impose specific requirements for RF equipment design.

V. REFERENCES: 1. ETSI-SMG Recs. of Series 05. GSM and DCS Radio Interface.

2. ETSI-RES3. DECT Common Interface Part 2. Physical Layer.

3. ETSI-RES7. Digital Short Range Radio (DSRR). Interim Standard.

4. E. Fernandez et al. Le TFTS Alcatel 9810. Un Système Européen de Communication Sol-Air. Commutation et Transmission.

empirical equations. Device nonlinear behavior is modeled with parameterized empirical equations that are functions of the various control voltages. Parameter values are "extracted" by curve-fitting simulated results to measured data. Model accuracy depends on the accuracy of the measured data, the fitting process, and the complexity of the empirical functions. Often, the equations that describe a particular schematic component are intentionally made simple to facilitate model use in circuit simulators. This simplification bounds model accuracy and limits the voltage or current ranges and the circuit applications for which a particular model may accurately apply.

Data-based models are the newest form of nonlinear device model. They have been created specifically to address the need for higher accuracy in circuit simulation. For this class of models, the measured data itself is used to generate nonlinear model functions. HP's Root Models for FETs (ref5), diodes (ref6) and MOS devices are examples. Because the model is explicitly constructed from the measured data (S-parameters vs bias) it is technology and process independent. This class of model provides the highest level of overall accuracy for use in circuit design, but is not useful in providing insight into how to design and manufacture higher performance devices.

HOW IS A MODEL OBTAINED?

Because empirical models represent a good compromise for use in both circuit design and device development/fabrication, it is informative to review the key steps involved in obtaining a parameter set for a typical SPICE model. For our example let's use the Gummel-Poon (GP) model for a silicon BJT (ref2)

The schematic equivalent circuit derived by Gummel and Poon for an NPN BJT is shown in Figure 3a. It was obtained from a consideration of the device physics and geometry. The model DC node currents, I_B and I_C , were obtained by summing the contributions of current flowing through each of the diode and current sources (Figure 3b). Values for the empirical model parameters (such as the diode ideality factors n_F and n_R) are empirically determined in the modeling process by adjusting their values until the simulated currents agree with the measured currents over specified ranges of voltage. Through the use of select DC and RF measurement sequences and techniques, and appropriate test hardware and test and modeling software, complete BJT SPICE parameter sets (Figure 4) can now be obtained in as little as two hours (ref7).

Once the SPICE model parameter set is obtained, device S-parameters can then be simulated over a wide range of bias conditions from near cutoff, through the active region, to near saturation (Figure 5). The parameter set may then be set up as a device model file in a model library, ready for use by the circuit simulation software. Thus, through the

use of fast efficient modeling methods and systems, it is now possible to build and maintain model libraries in support of CAD circuit simulation tools.

WHERE, THEN, DO MODELS COME FROM?

For the circuit designer today, device modeling information to support CAD tools is available from three major sources: model libraries, a model extraction service, or a modeling group/system set up in support of the circuit design. Since information from the latter two sources ultimately ends up in some kind of custom library made by combining custom and commercial model data, the information in such a library may take many forms and vintages.

The information found in commercial libraries provided by CAD vendors is in two tiers. The first tier consists of S-parameters data at a fixed bias, the same data typically available from data sheets or data books. CAE software companies have simply repackaged it into a form more directly usable within their simulation software. The data is available on a broad range of devices, but its usability is limited to small-signal applications at the same bias at which the initial data was taken. The second tier is represented by complete sets of extracted model data. This data exists for many fewer devices, but the data is much more usable in that it can be used to simulate device operation for a wide range of nonlinear circuit applications over a wide range of bias conditions. It thereby provides the circuit designer more flexibility in optimizing circuit performance.

Recently, CAD vendors have also begun to include device layout data (when available) in addition to the electrical data. This facilitates circuit layout as well as the simulation of circuit electrical performance.

Model data contributed from commercial libraries has both pros and cons. On the one hand, it is relatively inexpensive, while on the other it is most often encrypted in the CAD vendor's code and not available for inspection. In this form its accuracy or age is difficult to assess. Commercial libraries usually contain only the most popular commercial devices and do not include custom devices or models sometimes desired and used by designers. Even for standard devices, the designer may not have control over how the data was generated (e.g. bias points), or what device model may have been used to fit the data.

A parameter extraction service is an excellent alternative to supplement the information contained in a commercial library. Here the designer may pay the service to have a specified device (or devices) modeled by an experienced modeler. The fees charged are typically economical for a small number of devices; the designer may often specify a preferred model type; and the service provides a means to obtain models for custom or newly-developed devices that have not yet found their way into existing libraries. These

TABLE I SYSTEM CHARACTERISTICS

	GSM 900	DCS 1800	DECT	TFTS	TETRA	DSRR
FREQUENCY BAND in MHz						
REVERSE LINK (MS Tx)	865 - 890	1710 - 1785	Both MS & BS 1881.792 to	1800 - 1805	450 Mhz	933 - 935
FORWARD LINK (BS Tx)	910 - 935	1805 - 1880	1897.344	1670 - 1675	Range	888 - 890
MULTIPLE ACCESS SCHEME	TDMA	TDMA	TDMA	TDMA	TDMA	See Note 1 FDMA
FRAME TO FRAME FREQ. HOP.	YES	YES	POSSIBLE	?	POSSIBLE	NO
DUPLEXING TECHNIQUE	FDD	FDD	TDD	FDD	FDD	FDD
DUPLEX SEPARATION	45 MHz	45 MHz	5 m Sec.	130 MHz	N. AV	45 MHz
RADIO CHANNEL SPACING	200 KHz	200 KHz	1728 KHz	30.30 KHz	25 KHz	25 KHz
TOTAL NO. OF RADIO CHANNELS	124	373	10	164	N. AV.	79
RADIO CHANNEL BIT RATE	270.83 Kb/S	270.83 Kb/S	1152 Kb/S	44.2 Kb/S	36 Kb/S	See Note (2)
MAX. No. OF CALLS PER R.F CHANNEL	8	8	12	4	4	1
MODULATION	GMSK	GMSK	GFSK	$\pi / 4$ - DQPSK	$\pi / 4$ - DQPSK	GMSK
B.W x SYMBOL DURATION	0.3	0.3	0.5			0.25 and 0.45 See Note(3)
MAX Tx-Rx DISTANCE	35 KM	8 KM	100 M	280 KM	40 KM	5 KM

(1) Both single frequency and double frequency of functioning is possible in DSRR. Channels from these two frequency bands are used in case of double frequency operation.

(2) Depends upon used channel coding and it is different for speech or data transmission.

(3) BT = 0.25 is used for 16 Kb/s speech transmission and BT = 0.45 for data transmission at 4 kb/s.

services should not, however, be viewed as a primary method to obtain a custom library. When a large number of devices are to be modeled, the service may become prohibitively expensive. Also, long lead times may be experienced depending on the backlog at the service. These delays are additive to the circuit design cycle, and increase the time to market.

As the quantity of devices modeled becomes large, or as competition grows, there is a point at which companies are finding it economically or competitively advantageous to establish their own in-house modeling capabilities. These functional areas may be set up in support of a variety of needs: those of in-house circuit designers, those of component vendors who supply model data along with their components, and those of in-house device design and manufacturing. With this alternative, the designer may exercise more control over the modeling process, can obtain models on a timely and periodic basis, and can quickly obtain models for new or custom devices. More companies are realizing that ready access to and use of this model information represents a competitive weapon that can be used to differentiate them from the competition.

While there is a larger initial cost to the establishment of such an internal modeling capability, represented by the purchase of the hardware and modeling software and the establishment of the engineering expertise, even more rewards are to be reaped in the potential reduction of design cycles and time to market.

MODELS (AND LIBRARIES) ARE TIME-PERISHABLE

In today's dynamic business and technical climate, the advantages gained from a custom device library are not long-lived unless the information is continuously reviewed and updated. Both standard and custom devices must be characterized, models generated, and information archived. However, this alone does not assure that the model data, once created will continue to be useful. For data to remain useful, it must represent what can currently be manufactured. But because device technology is continually evolving, and fabrication processes are time-varying, there is a continued requirement for new models to be developed and model data to be periodically reverified. Models and data that reside in libraries must be viewed as time perishable.

To illustrate this point, Figure 6 plots the normalized value of the gate capacitance, C_{gs} , for a GaAs MESFET device extracted using a simple FET model. The data represents measurements from over 1300 FETs from 56 different wafers that were fabricated using the same foundry process over a period of eleven months. The distribution of C_{gs} values from FETs on each wafer are represented by each box and its outlying points. The slow time variations of C_{gs} are due to slow changes in the overall fab process. The

abrupt changes were due to an intentional change in one portion of the process to retarget the capacitance. The C_{gs} data illustrates that, once created, device model data needs to be reverified with a frequency that relates to the dynamics of the technology and/or the fabrication process stability.

LET THE DESIGNER BEWARE

Library model data should, therefore, be used with caution. The designer would be wise to question its age and accuracy before use. Not all the data that exists in CAD libraries, or that is available from component vendors' data sheets, may be adequate to support the full capabilities of CAD software tools. As we have seen before, some of the data may be in a limited form, (DC and small-signal S-parameters only). Also, some may be out-of-date (no longer representing what is manufactured), or some may be inaccurate (having been taken with less-controlled methods in years past). The use of this data may provide "first pass" circuit designs, but may also necessitate further design cycles to adjust the circuit performance to acceptable levels.

Accordingly, designers are increasing requests to component vendors (both captive and commercial) to supply more accurate, up-to-date model data, and to do so on a more regular and ongoing basis. In defense of these same vendors, many are now establishing or upgrading modeling capabilities using systems like that shown in Figure 7. These systems typically consist of a suite of hardware and test and modeling software. The systems interface to the device in a variety of ways, with probes for die in wafer form, and fixtures for die in chip or packaged form. Older versions of these systems have been put together using hardware from a variety of commercial sources, and modeling software which is either commercial or (in most cases) "home grown".

For those that are upgrading or establishing new modeling facilities, complete modeling systems like the HP system in Figure 8 are now available. These systems provide a variety of test hardware combinations, and also include test/modeling software, documented modeling techniques (instrument cal, device biasing, probing and fixturing), and total system support for both the hardware and the modeling software.

CONCLUSIONS

Component vendors are realizing the benefits of these systems in the form of added component sales because designers prefer parts that are supplied with accurate, updated model data. Indeed, these same vendors now view the supplying of this data as a competitive weapon. In the future, it will become an absolute necessity as more of their competitors are able to supply reliable component models.

TABLE II :Tx CHARACTERISTICS

	GSM 900	DCS-1800	DECT	TFTS	TETRA	DSRR
MAXIMUM OUTPUT POWER (dBm)						
BS	55	43	24	46	N. Av.	36
MS	43	30	24	40	40	36
Tx POWER vs TIME IN A BURST (dB)	+/- 1	+/- 1	+/- 1	+/- 1	N. Av.	+/- 1.5
Tx ATTACK TIME (μs or ms)	10 (18)	10 (18)	< 10	6 (10)	N. Av.	25 ms
Tx RELEASE TIME (μs or ms)	10 (18)	10 (18)	< 10	6 (10)	N. Av.	5 to 25 ms
See NOTE (1) Below.						
TRANSMITTED CARRIER FREQUENCY ACCURACY (Hz or KHz)	50 Hz	50 Hz	+/- 50 KHz	80 Hz	N. Av.	2.5 KHz
Tx POWER IN ADJ. CHANNEL (dBc)	- 50	- 50	- 60	- 50	- 60	- 50
INTRA BTS Tx INTERMODULATION ATTENUATION at 400 KHz (dB)	70	70	54	N. Av.	N. Av.	40 to 70
MAXIMUM Tx DUTY CYCLE (percent)						
BS	100	100	50	100	100	100
MS	12.5	12.5	50	25	25	100

213

N.AV = not available
N. AP = not applicable

- NOTES (1). The figures in brackets include the transient duration.
 (2) Different bandwidths for power measurements are specified in different cases.
 (3) This table gives a subset of all the parameters specified in the Recs.

While this greatly benefits the circuit designer, not all sources of desired components will be able to supply data in as timely a manner as may be required to meet future time-to-market goals. For this reason, design groups are still choosing to establish their own modeling capabilities in direct support of their design efforts, using these capabilities to create their own custom libraries of component models. The benefits are added performance, reduced product cost, and reduced time-to-market, all competitive weapons in an increasingly competitive electronics market place.

REFERENCES:

- 1) Snowden, C.M., MESFET Modeling, Compound Semiconductor Device Modeling, Springer-Verlag, London, 1993, pp 26-55.
- 2) Gummel, H.K., and Poon, H.C., "An Integrated Charge Control Model of Bipolar Transistors", Bell System Technical Journal, 49, 1970, pp 827-852.
- 3) Vladimirescu, A., and Liu, S., "The Simulation of MOS Integrated Circuits Using SPICE2", Electronics Research Laboratory Rept. No. M80/7, University of California, Berkeley, 1980.
- 4) Sheu, B.J., Scharfetter, D.L., and Poon, H.C., "Compact Short Channel IGFET Model (CSIM), Electronics Research Laboratory Rept. No. M84/20, University of California, Berkeley, 1984.
- 5) Root, D.E., "A Measurement-Based FET Model Improves CAE Accuracy", Microwave Journal, September 1991, pp 126-136.
- 6) Root, D.E, Pirola, M., Fan, S., and Cognata, A., "A Measurement-Based Large Signal Diode Model, Automated Data Acquisition System, and Verification with On-Wafer Power and Harmonic Measurements", IEEE MTT-S International Microwave Symposium Technical Digest, 1993, pp 261-264.
- 7) Dunn, M., "Device Model and Techniques for Fast, Efficient Nonlinear Parameter Extraction of BJT Devices", Asia-Pacific Microwave Conference Technical Digest, 1993 (to be published).

REASONS FOR DESIGN ITERATIONS

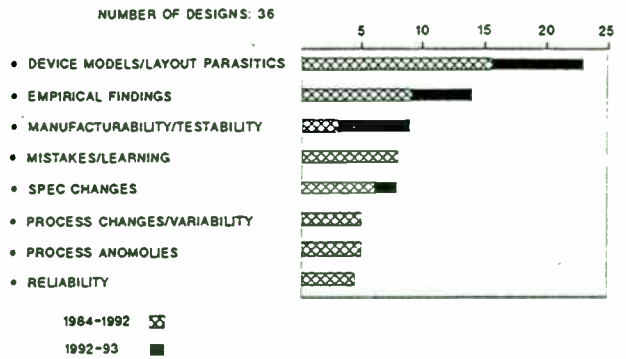


Figure 1. Design iterations

MODEL HP HEWLETT PACKARD

MODELS

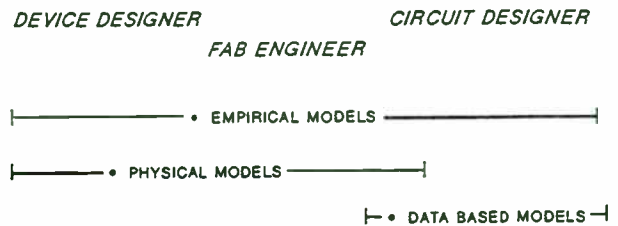


Figure 2. Model types

MODEL HP HEWLETT PACKARD

NPN GUMMEL-POON MODEL SCHEMATIC

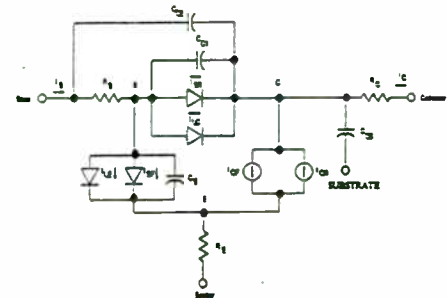


Figure 3a. BJT model schematic

MODEL HP HEWLETT PACKARD

NPN GUMMEL-POON MODEL EQUATIONS

$$I_C = \frac{I_{CF}}{Q_b} \left(\frac{V_{CE}}{e^{V_{CE}/V_T} - 1} - \frac{I_{CR}}{e^{V_{CE}/V_T} - 1} \right) - \frac{I_{BR}}{\beta_R} \left(\frac{V_{CE}}{e^{V_{CE}/V_T} - 1} \right) - I_{SC} \left(\frac{V_{CE}}{e^{V_{CE}/V_T} - 1} \right)$$

$$I_B = \frac{I_{BF}}{\beta_F} \left(\frac{V_{BE}}{e^{V_{BE}/V_T} - 1} \right) + I_{SE} \left(\frac{V_{BE}}{e^{V_{BE}/V_T} - 1} \right) + \frac{I_{BR}}{\beta_R} \left(\frac{V_{BE}}{e^{V_{BE}/V_T} - 1} \right) + I_{SC} \left(\frac{V_{BE}}{e^{V_{BE}/V_T} - 1} \right)$$

$$\text{where } Q_b = \frac{1}{1 - \frac{V_{BE}}{V_{AP}} - \frac{V_{CE}}{V_{AS}}}, \quad 1 + \frac{1}{2} \left[\frac{I_{CF}}{I_{SE}} \left(\frac{V_{BE}}{e^{V_{BE}/V_T} - 1} \right) + \frac{I_{BR}}{I_{SE}} \left(\frac{V_{BE}}{e^{V_{BE}/V_T} - 1} \right) \right] \quad \text{and } V_T = \frac{kT}{q}$$

Figure 3b. BJT model equations

MODEL HP HEWLETT PACKARD

TABLE III :Rx CHARACTERISTICS

	GSM 900	DCS-1800	DECT	TFTS	TETRA	DSRR
Rx SENSIVITY (in dBm)						
BS	- 104	- 104	- 83	- 122	- 106	> - 100
MS	- 102	- 100	- 83	- 112 (see note 1)	- 104	
Rx NOISE BANDWIDTH (KHz)	200	200	800	30	20	10 or 18
Rx SELECTIVITY BETWEEN ADJACENT CHANNELS (dB)	- 9 see note 2	- 9 see note 2	- 18 see note 2	N.AV	N.AV	- 50
DIVERSITY RECEPTION (BS)	USEFUL	POSSIBLE	RECOMMENDED	USEFUL	USEFUL	N.AP
MAXIMUM Rx DUTY CYCLE (in %)						
BS	100	100	100	100	100	100
MS	25	25	16 or 100	50	25	100
Rx TIMING SYNC. ACCURACY						
MS	+/- 1 bit	+/- 1 bit	+/- 2 bits	N.AV	N.AV	N.AP
BS	REFERENCE	REFERENCE	REFERENCE			

N.AV = not available

N.AP = not applicable

Note (1) = Power level expressed in dBW/m² on the antenna

Note (2) = this expresses carrier/interference ratio for good system operation

Note (3) Different bandwidths for power measurements are specified in different cases.

Note (4) This table gives a subset of all the parameters specified in the Recs.

GUMMEL-POON PARAMETERS

SYMBOL	DESCRIPTION	SYMBOL	DESCRIPTION
IS	Transport saturation current	RBM	Minimum base resistance
NF	Forward ideality factor	RE	Emitter resistance
VAF	Forward Early voltage	RC	Collector resistance
IKF	Forward knee current	CJE	Base-emitter zero-bias capacitance
BF	Forward beta	VJE	Base-emitter built-in potential
ISE	Base-emitter saturation current	MJE	Base-emitter grading coefficient
NE	Base-emitter ideality	CJL	Base-collector zero-bias capacitance
BR	Reverse beta	VJL	Base-collector built-in potential
NR	Reverse ideality factor	MJL	Base-collector grading coefficient
VAR	Reverse Early voltage	TF	Forward transit time
IKR	Reverse knee current	XTF	Coefficient of TF bias dependence
ISC	Base-collector saturation current	ITF	Models TF dependence on IC
NC	Base-collector ideality factor	VTF	Models TF dependence on VBC
RB	Zero-bias base resistance	PTF	Excess phase of TF
IRB	Current where base resistance falls halfway to its minimum value	XCJC	Models distributed nature of base
		FC	Models transition from junction of diffusion capacitance

Figure 4. Gummel-Poon BJT parameters  HEWLETT PACKARD

MODELING RESULTS

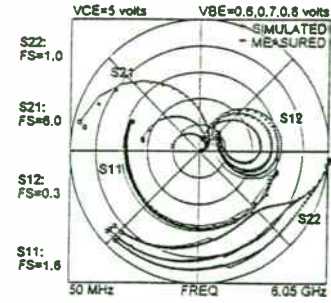


Figure 5. Verified S-parameter data at three Vbe values  HEWLETT PACKARD

EXTRACTED FET GATE CAPACITANCE C_{gs} (normalized) vs TIME

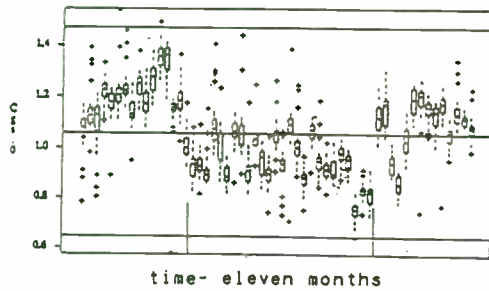


Figure 6. Modeled capacitance vs time  HEWLETT PACKARD

RF MODELING SYSTEM

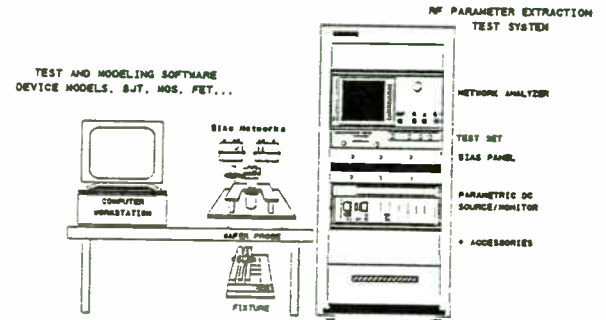
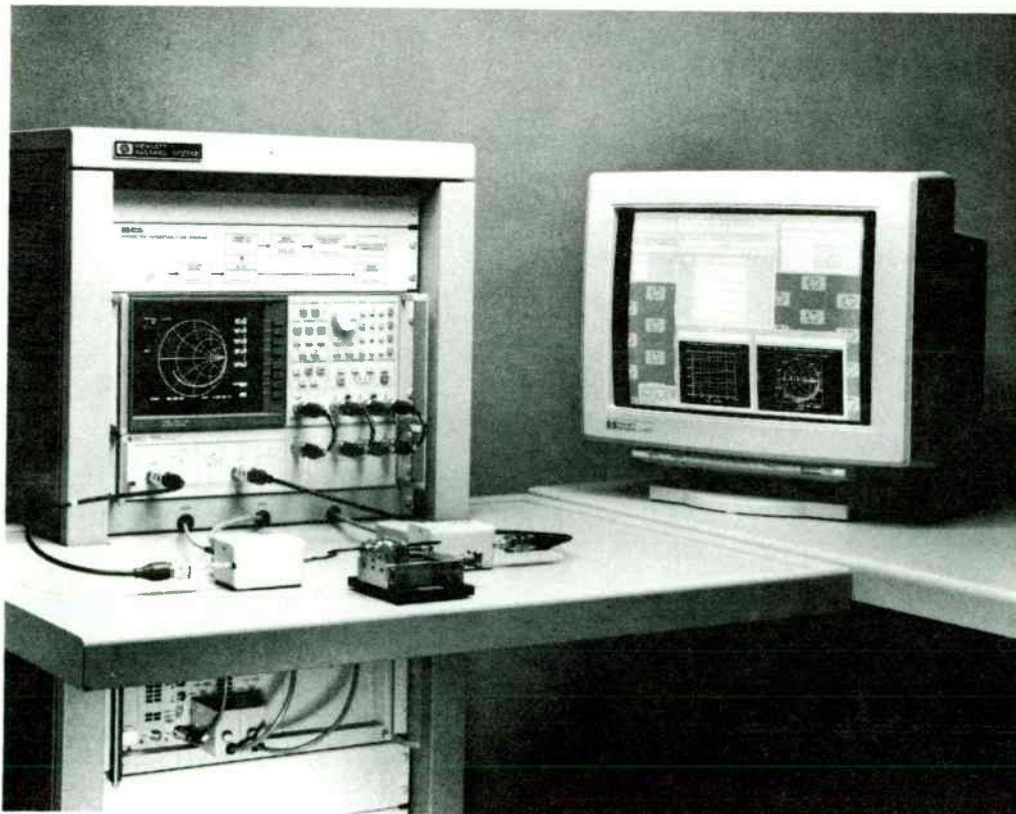


Figure 7. Typical modeling system configuration  HEWLETT PACKARD



VSAT, GPS, and DBS Technologies

Session Chairperson: Tim Shroyer, FEI Communications, Inc.
(Sunnyvale, CA)

VSAT Performance Fits Market Niche Applications, **Tim Shroyer**,
FEI Communications, Inc. (Sunnyvale, CA).....**216**

The Integration of GPS and a Wide Area Cellular Packet Data
Network, **John Lawler**, Cellular Data, Inc.
(Palo Alto, CA).....**N/A**

Environmental Effects on Mobile Satellite Communications,
Dennis A. Jiraud, Defense Systems, Inc. (McLean, VA).....**228**

Synthesizers for VSAT Applications,* **Uri Yariv**, Communication
Techniques, Inc. (Whippany, NJ).....**N/A**

A New Variable-Rate Vocoder for Wireless Communications and
Voice Storage Applications, **Steve Morley**, QUALCOMM, Inc.
(San Diego, CA)**238**

**Revised paper to appear in Microwaves & RF, August 1993.*

Regression-Based Algorithms for Inductor Modeling

Edmund (Joe) Tillo II, Ph.D.
Ford Motor Company
Electronics Division
16800 Executive Plaza Drive
Regent Court Building
Suite 321
Dearborn, Michigan 48126

This paper describes inductor models developed by using generalized linear regression. Data for these models can be obtained by using either an impedance analyzer or a Q-meter. The resulting models, while based on low-frequency data, accurately predict inductor Q and impedance versus frequency and inductor self-resonant frequency.

Introduction

This paper is written to describe the application of statistical data reduction techniques to inductor modeling. The ultimate goal of this data reduction process is to produce models for inductors that accurately estimate observed measurements. The resulting models, obtained from closed-form equations, can be used as they are, or as starting points for optimizer-generated models. The inductor model to be used in this paper is shown in Figure 1.

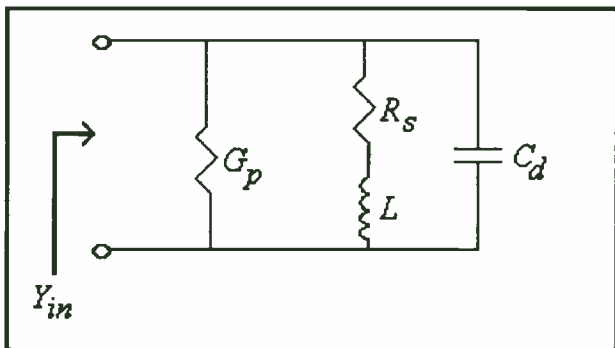


Figure 1. Four-element Inductor Model

The immediate goal of the modeling procedure is to find values for L , C_d , G_p , and R_s , based on laboratory measurements. It must be remembered that resulting models are *statistical* not *functional*. That is, since a finite-size physical structure is being modeled as a network of linear lumped elements, the models obtained are intended for use in

the frequency and power range where the inductor to be modeled is linear and physically small relative to one wavelength. This has several implications. First among these is that estimates for self-resonant frequency based on low-frequency data may not agree with measured self-resonant frequency. This may be due to changes in core permeability as a function of frequency or transmission-line effects. Thus, attempts to reconcile observed oscillatory behavior with data obtained from these methods may prove frustrating. Viewed in another light, these methods produce data on distributed capacitance that may be unobtainable by measurement of self-resonant frequency.

A second implication is that these models will not work very well if the inductor is characterized at a low magnetic flux level, and then operated in saturation.

The paper is broken into sections covering background, general assumptions, lossless models, lossy models, and laboratory results.

Background

Inductances are fundamental lossless *elements* in many circuits, including filters¹, diplexers², directional couplers³, matching networks⁴, and switch-mode power supplies⁵.

¹Kuo, F. F. *Network Analysis and Synthesis*. Second edition (New York: Wiley, 1966), pp. 397-410

²Youla, D. C., Pillai, S. U., and Winter, F. "Theory and Design of Maximally Flat Low-Pass High-Pass Reactance Ladder Diplexers." *IEEE Transactions on Circuits and Systems-I*, Vol. 39 No. 5 (May 1992): pp. 337-349

³E. J. Tillo, "Design and Optimization of Lumped-Element LCM Directional Couplers," *RF Expo East Proceedings*, September 22-24, 1992, pp. 467-479

⁴Besser, L. "Designer Tips: Reactive Transformation of Resistances." *Applied Microwave Magazine* (Winter 1993): pp. 104-110

⁵Mitchell, D. M. *DC-DC Switching Regulator Analysis* (New York: McGraw-Hill, 1988), p. 7

VSAT Performance Fits Market Niche Applications

Tim Shroyer - FEI Communications, Inc.

Historic VSAT Applications

When satellite communications systems were first developed antennas were very large. This large size or aperture was required to get enough gain to be useful in satellite communications. High earth terminal receive gain was necessary due to the low transmit power or EIRP from the satellite transponders. High earth terminal transmit gain was necessary due to the relative insensitivity (high noise figure) of the satellite transponders. As transponders became more powerful and more sensitive, smaller earth stations became possible. Thus, Very Small Aperture Terminals or "VSATs" were born.

The first satellite communications systems tended to simply be functional replacements for other terrestrial communications media. For a while multi-channel telephony was the bulk of the traffic being carried. Data communications were very limited, not because the satellite links were inadequate, but rather because computers did not have much communication capability. Most data communication was still teleprinter traffic at 75 or 100 baud using Baudot code.

It was in this environment that the first VSATs were developed. Because governments tended to tightly regulate interconnection to the public switched network these VSAT systems tended to be private. Essentially they became private telephone network bypass systems installed for users who had large enough long distance telephone bills to justify their development and installation.

There were, of course, some notable exceptions to the norm in these initial satellite systems. One of the most significant was the system developed by Equatorial, now a part of GTE Spacenet. A system was developed which took advantage of the inherent broadcast nature of satellite communications to send the same low-rate digital information to several thousand stations simultaneously. Such a system was ideal for the distribution of stock market data and news feeds to multiple affiliates. The Equatorial system design was contrary to what many in the industry believed to be the most economical. Spread spectrum techniques were used and it required higher transponder power and bandwidth than would normally be expected. Satellite capacity was sacrificed to push earth terminal prices lower and lower. Since the system served hundreds of thousands of terminals the economics proved successful.

Evolution of Systems Requirements

Things began to change as the FCC broke up the Bell system. Competition after the break-up in the U.S. meant that standards needed to be published for the

Thus, in order to build such circuits it is necessary to fabricate *components*, called inductors, that approximate the desired inductance to some degree. For this to be accomplished, it is often necessary to obtain comprehensive and accurate measurements of inductor properties, which may include more than inductance. For purposes of this paper, losses and self-resonance will also be considered and accounted for with additional elements in the inductor model. Losses and self-resonance are a consequence of physical constraints, including capacitance between winding turns and winding resistance⁶.

Several different instruments are suitable for measuring inductor properties, the two considered in this paper are the impedance analyzer and the Q -meter. With each of these instruments there is a temptation to obtain a simple inductor model by performing a measurement at a single frequency and then using the calibrated scales or displays to determine inductance without applying further data reduction techniques. These "single-frequency" methods may produce inductor models that have a great degree of inaccuracy. A brief explanation of single-frequency measurement procedures and the resulting models follows.

In the case of the impedance analyzer, a model consisting of an inductance and a single resistance can be readily obtained by merely connecting an inductor to the instrument terminals, entering a frequency value, and selecting a model for the inductor with a few keystrokes on the front panel of the instrument⁷. The available inductor models include an inductance in series with a resistance and an inductance in parallel with a conductance. A problem with this measurement technique is that the reactance of the inductor is due to both inductance and capacitance, and the resistance of the inductor is due to several frequency dependent phenomena. Thus, as the measurement frequency is varied, the inductive and resistive elements in the model also vary.

Inductor measurements are performed in a somewhat different fashion with the Q -meter. The routine procedure is to connect an inductor under test to the appropriate terminals on the Q -meter, forming a series resonant circuit with an internal oscillator and capacitor. The internal oscillator frequency is manually adjusted to a specified value f_0 , and the internal capacitor is manually adjusted to produce a resonant condition. Resonance is indicated by a peak response on a voltmeter. When the peak is found the measured inductance and Q of the inductor under test, referred to as L_{qm} and Q_m , are read directly from calibrated scales on the capacitor and voltmeter respectively. Simple two element models can then be easily generated. For the

case of the inductance with series loss, the resistor R_{sqm} , is found to be⁸:

$$R_{sqm} = \frac{\omega_0 L_{qm}}{Q_m}. \quad (1)$$

For the case of parallel loss one obtains⁹:

$$G_{pqm} = \frac{1}{Q_m \omega_0 L_{qm}}. \quad (2)$$

Where the angular frequency for both cases is defined by:

$$\omega_0 = 2\pi f_0. \quad (3)$$

When this method is followed, L_{qm} , R_{sqm} , and G_{pqm} , vary with frequency.

In addition to the inconvenience of element values that vary with frequency, both of the single-frequency measurement techniques described above for the impedance analyzer and the Q -meter have a serious shortcoming in that they do not account for the self-resonance phenomenon.

General Assumptions

For the purposes of this paper three assumptions will be made at the start. First, the network shown in Figure 1 accurately models an inductor. Second, the condition of resonance will occur when the magnitudes of the reactances of the inductance L and capacitance C_d are equal. That is, the self-resonant frequency is given by:

$$f_{sr} = \frac{1}{2\pi\sqrt{LC_d}}. \quad (4)$$

The third assumption is that the Q of an inductive circuit is defined by:

$$Q_{circuit} \equiv \frac{-\text{Im}[Y_{in}]}{\text{Re}[Y_{in}]}. \quad (5)$$

In preparation of the application of Equation (5) to the circuit shown in Figure 1, the driving point admittance is written as:

$$Y_{in} = G_p + \frac{1}{R_s + j\omega L} + j\omega C_d. \quad (6)$$

⁶Snelling, E. C. *Soft Ferrites: Properties and Applications*. Second edition (London: Butterworths, 1988), pp. 175-187

⁷Hewlett Packard, *Model 4192A LF Impedance Analyzer Operation and Service Manual* (Manual Part No. 04192-90001, March 1982), page 3-41

⁸ibid. page 3-41

⁹ibid. page 3-41

interconnection of telephone equipment. These standards were just what satellite communications systems needed for full connection. The standards permitted manufacturers to develop systems which interfaced to telephone switches (including PBXs) just like existing long distance lines. With these improved interfaces satellite communications systems expanded in usefulness. Since PBXs could be interfaced directly, VSATs could eliminate "the last mile" of connectivity which was historically contracted from the local phone company. This meant that satellite communications systems were beneficial both for wide bandwidth applications (trunked multi-channel systems such as between telephone Dial Central Offices) or for thin route applications (such as between PBXs at remote company locations). The thin route requirement was ideal for VSAT applications because the lower data rates could be handled easily by VSAT terminals.

Satellite communications voice requirements continue to evolve. High bandwidth point-to-point multi-channel voice systems are often better served by fiber optic systems today. In cases where it is difficult or impossible to install a fiber infrastructure, satellite systems continue to have substantial advantages. Satellite communication also often proves its effectiveness in handling thin route traffic where the installation of a dedicated fiber is not justified and in multi-point applications where the broadcast nature of satellite signals is optimal. Both thin route and multi-channel requirements continue to expand.

Early VSAT systems could do a pretty good job of transmitting data while the computers of the era had very limited communications capabilities. Even similar mainframe computers were often not designed to communicate among themselves effectively. When PCs became popular, communications requirements increased dramatically. Not only did users want their PCs interconnected but they wanted them to communicate with their mainframes. Several different approaches were developed for solving this problem. Many were attempted with satellite communications. One of the most common difficulties encountered was protocol incompatibility. While one computer might be able to send and receive data, it might not be able to understand data passed from a dissimilar machine. The solution had a tremendous impact on satellite communications.

Today almost all computers can communicate using the X.25 packet communications protocol. Thus, regardless of the size or type of the computer, X.25 is often a reasonable choice for a standardized communications interface. Satellite communications systems have been designed to make use of this feature. VSAT systems, using X.25 as the access protocol, can pass data between widely diverse computer systems on an international basis. While VSATs could pass data long before computers were ready for it, X.25 brings a relatively easy-to-use standard interface to both. The future holds even higher data rates with variations of existing and future protocols to meet expanding user requirements.

When this expression for Y_{in} is substituted into Equation (5) the result is:

$$Q_m = \frac{\frac{\omega L}{R_s^2 + \omega^2 L^2} - \omega C_d}{G_p + \frac{R_s}{R_s^2 + \omega^2 L^2}} \quad (7)$$

Where Q_m is the value that would be measured with either a Q -meter or impedance analyzer when the circuit is built with ideal elements. Hence, Equation (7) shows the measured value of Q for an inductor when the appropriate element values are used in the model.

When circuit losses are small, Equation (7) can be simplified by neglecting second-order loss terms:

$$Q_m = \frac{\frac{1}{\omega L} - \omega C_d}{G_p + \frac{R_s}{\omega^2 L^2}} \quad (8)$$

Equation (8) shows that the measured Q of an inductor will become lower as shunt capacitance increases. This shunt capacitance is the result of the so-called distributed capacitance of the inductor as well as any stray capacitance present at the terminals of the measuring instrument. Since it is beneficial to remove the effect of stray capacitance present due to the measuring instrument from the numerical value of Q , Equation (8) will be re-written with the capacitance C_d set equal to zero:

$$Q = \frac{\frac{1}{\omega L}}{G_p + \frac{R_s}{\omega^2 L^2}} \quad (9)$$

The quantity Q will be referred to as the Q of the inductor. The m subscript has been dropped because this quantity cannot be directly measured.

Determination of Inductance and Distributed Capacitance

The process of obtaining estimates of the numerical values of C_d and L shown in Figure 1 will now be given. The crucial assumption at this point is that the losses in the coil are small enough to neglect. First, a data set is obtained by performing measurements on an inductor at a series of n different frequencies using either an impedance analyzer or Q -meter.

Once this is done, generalized linear regression can be used to estimate the numerical values of C_d and L , and thus the self-resonant frequency of the inductor.

For the case of the impedance analyzer, the observed admittance will be considered to be a combination of an inductance and capacitance connected in parallel. The equation for the driving point admittance is:

$$\text{Im}[Y_{in}(\omega)] = \omega C_d - \frac{1}{\omega L} \quad (10)$$

This equation can be re-written in the form used in the statistics literature¹⁰:

$$Y_i = B_0 + B_1 X_{i1} \quad (11)$$

Where the input admittance is a function of the angular frequency ω ,

$$Y_i = \frac{\text{Im}[Y_{in}(\omega)]}{\omega}; \omega = \omega_i, i = 1 \dots n, \quad (12)$$

the coefficient terms are capacitance,

$$B_0 = C_d, \quad (13)$$

and reluctance,

$$B_1 = \frac{1}{L}, \quad (14)$$

and the independent variable is a function of angular frequency:

$$X_{i1} = \frac{1}{\omega^2}; \omega = \omega_i, i = 1 \dots n. \quad (15)$$

At this point, the values of C_d and L can be found by using the methods of linear regression.

Capacitance and inductance estimates can also be made based on data obtained with Q -meter measurements. In this case the equations are slightly different, but the result is the same. The initial step is to write the condition of resonance at some frequency and Q -meter capacitor setting C :

$$\omega_0 = \frac{1}{\sqrt{L(C + C_d)}} \quad (16)$$

¹⁰Neter, J., Wasserman, W., and Kutner, M. H. *Applied Linear Regression Models* (Homewood, IL: Irwin, 1989), pp. 204-209

VSAT RF Link Requirements

To see why a particular type of earth terminal is suitable for a specific service application it is important to consider the characteristics of the signals. One can then determine the quality of service which could be provided with a specific earth terminal. This permits a system designer to define overall system requirements and thus the specification requirements for the individual equipment. Satellite systems engineers consider these requirements in terms of the "satellite link equation".

The basic satellite link equation for determining downlink performance is:

$$\text{EIRP}_{\text{reqd}} = P_L + L_i - G/T_{\text{ET}} + k + 10\log(R_s) + E_b/N_o + M \quad (\text{Equation 1})$$

Where:

$\text{EIRP}_{\text{reqd}}$	= Required EIRP (or satellite Effective Isotropic Radiated Power)
P_L	= Downlink Path Loss
L_i	= Implementation Losses
G/T_{ET}	= Earth Terminal "Figure of Merit" (receive Gain divided by Noise Temperature)
k	= Boltzmann's constant
R_s	= transmitted Symbol Rate (data rate with coding, etc.)
E_b/N_o	= Required MODEM energy per bit divided by Noise density
M	= Link Margin (for rain attenuation, etc.)

We can consider an example of a Ku-Band VSAT system by inserting appropriate values and calculating the results over a nominal range. For this example we will use the following:

P_L	= 206 dB
L_i	= 2 dB
T_{ET}	= 160 K Earth Terminal Noise Temperature
k	= -228.6 dBw/Hz/K
E_b/N_o	= 8.5 dB (for BPSK, rate 1/2 k=7 coded, BER 1×10^{-5})
M	= 8 dB Link Margin

Table 1 below provides the results of this analysis. There are definitely other factors which affect link performance as well, such as transponder loading and intermodulation distortion, etc., but if the system remains within nominal linear range Equation 1 provides a reasonable prediction. It shows the required satellite EIRP at various data rates (from 2.4 to 256 KBPS) with different earth terminal antenna gain values (from 28 to 45 dB) to satisfy the desired link performance. The table illustrates that changes in any of these different values result in a change in the required EIRP value.

Equation (16) can be re-written as:

$$C = -C_d + \frac{1}{L\omega_0^2}. \quad (17)$$

Equation (17) is of the form:

$$Y_i = B_0 + B_1 X_i, \quad (18)$$

which is the form used in the statistics literature.

At this point, linear regression can be applied to Equation (17) to determine C_d and L . It should be noted that a similar technique has been applied to Q -meter data in the past. Determining C_d and L graphically from a plot of C

versus $\frac{1}{\omega_0^2}$ is known as the "negative-intercept method"¹¹.

When either of the above procedures is followed, the estimates of inductance and distributed capacitance are constant as a function of frequency, and thus the values of C_d and L can be substituted into Equation (4) to find the self-resonant frequency of the inductor.

Determination of Series Resistance and Shunt Conductance

In order to account for inductor losses it is necessary to perform a series of measurements at n different frequencies. The resulting data can be used to obtain values of resistive elements in the inductor model. The technique will now be shown.

This technique is based on the value of Q for an inductor at a series of frequencies. This value of Q may be obtained from the Q -meter or a LF Impedance Analyzer with the application of a correction technique designed to remove the effect of shunt capacitance, C_d , from the Q measurement. The correction for Q -meter data, described in the *Model 4342A Q Meter Operating and Service Manual*¹², is:

$$Q = Q_m \left(\frac{C + C_d}{C} \right). \quad (19)$$

Where, as before, C is the value indicated on the capacitance dial on the Q -meter.

The correction for the LF Impedance Analyzer data is similar, with the exception that the values used are the estimate of inductance, L , and the inductance, L_m , measured at a particular frequency:

$$Q = Q_m \left(\frac{L_m}{L} \right). \quad (20)$$

The choice of which instrument to use depends on several factors, including the Q of the inductor to be modeled. When the inductor Q is above 100, the Q -Meter can be more accurate¹³.

Equation (9), relating Q to the resistive and inductive elements for the circuit shown in Figure 1 can be re-written as:

$$\frac{1}{Q} = \frac{R_s}{\omega L} + \frac{\omega L}{R_p}. \quad (21)$$

Where:

$$R_p \equiv \frac{1}{G_p}. \quad (22)$$

Equation (21) can be re-written as:

$$\frac{\omega L}{Q} = R_s + \frac{\omega^2 L^2}{R_p}, \quad (23)$$

which is of the form:

$$Y_i = B_0 + B_1 X_{i1}. \quad (24)$$

Where Y_i is a function of the angular frequency ω ,

$$Y_i = \frac{\omega L}{Q}; \omega = \omega_i, i = 1 \dots n, \quad (25)$$

¹¹Rao, V. V. K., "The Q -Meter and Its Theory." *Proceedings of the I.R.E.*, Vol. 30 No. 11 (November 1942): pp. 502-505

¹²Hewlett Packard *Model 4342A Q Meter Operating and Service Manual* (Manual Part No. 04342-90009, August 1981), pages 3-15 to 3-16

¹³Honda, M. *The Impedance Measurement Handbook* (Hewlett Packard, 1989), pp. 5-4 to 5-7

By considering Table 1 it is relatively easy to see that a larger antenna aperture (and the resulting increase in gain) can be directly applied to reduce the required transponder EIRP. In most cases, this reduced EIRP translates into reduced space segment charges. If a small increase in EIRP results in a drastic reduction in total earth terminal cost, however, it may be worth consideration. For example, in an application with 10,000 earth terminals a modest decrease in each earth terminal's cost becomes very significant. This could easily offset a significant increase in space segment costs, as long as the capacity is available.

	EIRP dBW								
R_s KBPS	2.4	4.8	9.6	19.2	38.4	56	76.8	153.6	256
G_{ET}									
28	23.74	26.75	29.76	32.77	35.78	37.42	38.79	41.81	44.02
29	22.74	25.75	28.76	31.77	34.78	36.42	37.79	40.81	43.02
30	21.74	24.75	27.76	30.77	33.78	35.42	36.79	39.81	42.02
31	20.74	23.75	26.76	29.77	32.78	34.42	35.79	38.81	41.02
32	19.74	22.75	25.76	28.77	31.78	33.42	34.79	37.81	40.02
33	18.74	21.75	24.76	27.77	30.78	32.42	33.79	36.81	39.02
34	17.74	20.75	23.76	26.77	29.78	31.42	32.79	35.81	38.02
35	16.74	19.75	22.76	25.77	28.78	30.42	31.79	34.81	37.02
36	15.74	18.75	21.76	24.77	27.78	29.42	30.79	33.81	36.02
37	14.74	17.75	20.76	23.77	26.78	28.42	29.79	32.81	35.02
38	13.74	16.75	19.76	22.77	25.78	27.42	28.79	31.81	34.02
39	12.74	15.75	18.76	21.77	24.78	26.42	27.79	30.81	33.02
40	11.74	14.75	17.76	20.77	23.78	25.42	26.79	29.81	32.02
41	10.74	13.75	16.76	19.77	22.78	24.42	25.79	28.81	31.02
42	9.74	12.75	15.76	18.77	21.78	23.42	24.79	27.81	30.02
43	8.74	11.75	14.76	17.77	20.78	22.42	23.79	26.81	29.02
44	7.74	10.75	13.76	16.77	19.78	21.42	22.79	25.81	28.02
45	6.74	9.75	12.76	15.77	18.78	20.42	21.79	24.81	27.02

Table 1 Ku-Band Downlink Analysis Example

the coefficient terms are resistance,

$$B_0 = R_s, \quad (26)$$

and conductance,

$$B_1 = G_p, \quad (27)$$

and the independent variable is a function of angular frequency,

$$X_{ii} = \omega^2 L^2; \omega = \omega_i, i = 1 \dots n. \quad (28)$$

Linear regression can be applied to Equation (23) to obtain R_s and G_p .

Example

Consider the case of an air core inductor with a nominal inductance of 10 μ H. Data sets obtained with a Q -meter and LF Impedance Analyzer are shown in Table 1 and 2 respectively. The measurement frequencies were selected to provide convenient settings of the Q -meter capacitance dial. The entries in the "single-frequency inductance" (L_{qm}) column in Table 1 were calculated by solving Equation (16) for the inductance L with the capacitance C_d set equal to zero.

F; MHz	C; pF	Q_m	Q	L_{qm} ; uH
2.3	470	210	213	10.14
3.33	220	239	247	10.3
4.65	110	257	273	10.63
6.68	50	261	297	11.37
8.90	25	236	301	12.81

Table 1. Q -Meter Data

F; MHz	G_x ; uS	B_x ; mS	Q_m	Q	L_m ; uH
2	55	-7.821	142	143	10.18
3	47	-5.166	110	112	10.27
4	39	-3.806	98	101	10.45
6	29	-2.389	82	90	11.10
9	24	-1.374	57	73	12.87

Table 2. LF Impedance Analyzer Data

There are a few observations to make about these data sets. First, the agreement of the single-frequency inductance L_{qm} in Table 1 and measured inductance L_m in Table 2 is quite good. This is to be expected with a low-loss inductor, where

the major contribution to the impedance is due to inductive reactance. When losses are low the LF Impedance Analyzer makes an accurate estimate of the imaginary part of an unknown impedance and the Q -meter shows a sharp easy-to-locate peak near resonance. Consequently, precise measurements can be on high- Q inductors. The fact that the values of single-frequency and measured inductance vary as a function of frequency is due to the effect of shunt capacitance.

Second, note the large disagreement in inductor Q between Tables 1 and 2. No satisfactory explanation was found for this difference.

The data from Tables 1 and 2 were used to determine the elements for the model shown in Figure 1. The results are summarized in Table 3. Note that there is good agreement between inductance, capacitance, and self-resonant frequency values, but poor agreement with the resistance values. This is a consequence of the difference in measured Q values.

Element or parameter	Q -Meter	LF Imp. Ana.
L ; uH	9.9949	10.0676
C_d ; pF	6.9079	6.2441
R_s ; ohms	.6731	.8749
R_p ; k ohms	255.25	46.176
f_{sr} ; MHz	19.15	20.07

Table 3. Modeling Results

Calculated Q values are shown for the Q -meter and LF Impedance Analyzer results in Tables 4 and 5 respectively. The "model" values were obtained by substituting the estimates of element values into Equations (8) and (9) for Q_m and Q respectively. The Q -meter results show close agreement between measurement and model values, especially near the center frequency of the measurement range. The fit is not quite as good for the LF Impedance Analyzer results; this may be due to measurement error.

F; MHz	Q_m ; measured	Q_m ; from model	Q ; calc. from meas.	Q ; from model
2.3	210	188	213	191
3.33	239	240	247	248
4.65	257	273	273	289
6.68	261	271	297	307
8.90	236	231	301	294

Table 4. Q -Meter Results

If we assume the values used to be appropriate, Table 1 lets us consider the effects of equipment changes on overall system performance. Consider the use of a transponder on a satellite like GTE Spacenet's GStar 1. Such a transponder has a total EIRP of about 42 dBW, depending upon where the receive earth station is located. Since this value is greater than all those in Table 1, with small exceptions, one might assume any of the analyzed configurations could be used. This power, however, is the total available over the full transponder bandwidth. If any other signals are to be transmitted by the same transponder (which is usually the case with such narrow signals) their power usage must also be considered.

The situation is similar on the uplink side of the equation. There the satellite G/T becomes the limiting factor in absolute signal levels. This G/T value is constrained not only by the physical design of the satellite transponder components but also by such factors as antenna pattern, adjacent signal interference, and radiated earth noise.

Table 1 illustrates the downlink performance expected from a typical Ku-Band link. Similar analysis needs to be performed for the uplink side of each communications link as well. VSATs make use of the property that a relatively large antenna can be used as a hub to transmit to small antennas at the remote terminals. The large hub antenna is able to transmit a stronger signal to the remote sites and is able to provide acceptable BER performance on receive links from the small transmit antennas.

Equation 1, presented above, can also be used to determine uplink performance if the appropriate values are used. In the uplink case the EIRP becomes the earth terminal EIRP instead of the satellite EIRP and the G/T becomes the transponder G/T instead of the earth terminal G/T. Appropriate values for our Ku-Band example are:

P_L	= 207.5 dB (Uplink path loss)
L_1	= 2 dB
G/T_{SAT}	= 0 dB/K (varies greatly depending upon satellite, gain, etc.)
k	= -228.6 dBw/Hz/K
E_b/N_o	= 8.5 dB (for BPSK, rate 1/2 k=7 coded, BER 1×10^{-5})
M	= 8 dB Link Margin

Table 2 illustrates the Transmit Power, in dBW, required for the desired BER at the satellite, which is then translated to the receive earth terminal. For this analysis to be valid the receive earth terminal has a sufficiently high G/T that the E_b/N_o received at the satellite is essentially the same as at the receive terminal. This is the general case of a VSAT hub terminal. Table 2 illustrates that changing the transmit terminal antenna gain, power, and data rate are all directly related.

F; MHz	Q_m ; measured	Q_m ; from model	Q ; calc. from meas.	Q ; from model
2	142	102	143	103
3	109	112	112	114
4	97	107	101	111
6	82	86	90	95
9	57	57	73	72

Table 5. LF Impedance Analyzer Results

Conclusion

Usefulness of data obtained from Q -meter and impedance analyzer measurements on inductors can be significantly increased with the application of simple data reduction techniques.

The circuit shown in Figure 1 with statistically derived element values produces an inductor model whose elements are not a function of frequency. This model also accounts for the observed self-resonance phenomenon as well as the change of inductor Q as a function of frequency.

The Q -meter may produce more accurate data on inductor Q than the impedance analyzer does, particularly when high- Q inductors are being measured.

Acknowledgment

The author is indebted to Ms. JoAnne Casey-Roney for her assistance with statistics texts, Mr. Steve Schwinke for his insightful discussions, and Professor A. B. Macnee for his suggestion of the negative-intercept method.

	Xmtr Pwr dBW								
R _e KBPS	2.4	4.8	9.6	19.2	38.4	56	76.8	153.6	256
G _{ET}									
26	5.20	8.21	11.22	14.23	17.24	18.88	20.25	23.26	25.48
27	4.20	7.21	10.22	13.23	16.24	17.88	19.25	22.26	24.48
28	3.20	6.21	9.22	12.23	15.24	16.88	18.25	21.26	23.48
29	2.20	5.21	8.22	11.23	14.24	15.88	17.25	20.26	22.48
30	1.20	4.21	7.22	10.23	13.24	14.88	16.25	19.26	21.48
31	0.20	3.21	6.22	9.23	12.24	13.88	15.25	18.26	20.48
32	-0.80	2.21	5.22	8.23	11.24	12.88	14.25	17.26	19.48
33	-1.80	1.21	4.22	7.23	10.24	11.88	13.25	16.26	18.48
34	-2.80	0.21	3.22	6.23	9.24	10.88	12.25	15.26	17.48
35	-3.80	-0.79	2.22	5.23	8.24	9.88	11.25	14.26	16.48
36	-4.80	-1.79	1.22	4.23	7.24	8.88	10.25	13.26	15.48
37	-5.80	-2.79	0.22	3.23	6.24	7.88	9.25	12.26	14.48
38	-6.80	-3.79	-0.78	2.23	5.24	6.88	8.25	11.26	13.48
39	-7.80	-4.79	-1.78	1.23	4.24	5.88	7.25	10.26	12.48
40	-8.80	-5.79	-2.78	0.23	3.24	4.88	6.25	9.26	11.48
41	-9.80	-6.79	-3.78	-0.77	2.24	3.88	5.25	8.26	10.48
42	-10.80	-7.79	-4.78	-1.77	1.24	2.88	4.25	7.26	9.48
43	-11.80	-8.79	-5.78	-2.77	0.24	1.88	3.25	6.26	8.48
44	-12.80	-9.79	-6.78	-3.77	-0.76	0.88	2.25	5.26	7.48
45	-13.80	-10.79	-7.78	-4.77	-1.76	-0.12	1.25	4.26	6.48

Table 2 Ku-Band Uplink Analysis Example

Two of the factors which can be considered here are the effects of antenna gain and required transmit EIRP. An increase in antenna gain, resulting from the use of a larger antenna aperture, results in a lower required transmitter power. If installation space is not a problem a larger antenna reflector may be much less costly than a larger earth terminal High Power Amplifier. The VSAT system designer can trade-off such considerations in the design of the overall system.

COMPUTER AIDED DESIGN TOOLS FOR SMALL SIGNAL RF MATCHING NETWORKS

BY

Michael Rothery, Sam Richie, and Madjid A. Belkerdid

University of Central Florida
Electrical and Computer Engineering Department
Orlando, Florida 32816

ABSTRACT

This paper presents PC based computer aided design tools for small signal RF amplifiers and oscillators in the VHF and UHF bands. The development of these systems is based on the small signal S parameters and noise parameters which can supply information on stability, gain, and noise figure. The manual work generally involved in developing solutions for these types of problems can become tedious and time consuming.

The input to the CAD system consists of the operating frequency, the four small signal S parameters, the noise figure parameters, and the system resistance. The CAD system then plots the stability circles, the constant gain circles, and the constant noise figure circles on a graphical display of the Smith chart.

A user based iterative optimization routine may then be employed to complete the hardware requirements for the matching network design. This design method provides for a user friendly, interactive, fast, and inexpensive PC based design tool.

I. INTRODUCTION

This paper first demonstrates the computerized algorithm used to determine the component values of a matching network. For the given reflection coefficient on the Smith chart, an intersection of circles technique is used to determine the amount of reactance or susceptance required from each component in the matching network. Then, given the frequency of operation and the system resistance, the value of the inductor or capacitor may then be determined.

Some of the basic theory that is used by the CAD system for designing two-port small signal

amplifiers is then reviewed. The design concepts are based on the information provided by the S parameters and noise parameters of a biased active device. Used in conjunction with the Smith chart, these parameters supply the information necessary to develop the proper matching networks for the input and output ports. The matching networks determine the stability, gain, and noise figure of the small signal, two-port amplifier.

Finally, the method employed by the CAD system for the design of a negative resistance oscillator will be presented. Instead of matching the input and output ports of the active device, a resonant circuit is chosen for one port, while the other is matched under loaded conditions.

II. COMPUTERIZED SMITH CHART

A computerized Smith chart is the heart of the CAD tools. A mathematical model is first presented, followed by the Smith chart concept, and a design example.

A. Mathematical Model

The Smith chart may be used to transform a reflection coefficient, Γ , to a normalized impedance, z , following the relation [1]

$$z = \frac{1+\Gamma}{1-\Gamma} \quad (1)$$

The reflection coefficient may be expressed in polar coordinates or rectangular coordinates. In polar form, $\Gamma = m\angle\theta$, where $-180 \leq \theta \leq 180$ and for any passive reflection coefficient, $m < 1$. In rectangular form, Γ is given as $\Gamma = U + jV$, where of course $U = m\cos(\theta)$ and $V = m\sin(\theta)$.

Transceiver Characteristics

From the range of VSAT systems requirements, we observe that there are distinctly different types of systems. Our analysis of the link equations shows that the low rate systems can operate with relatively small antennas and moderate High Power Amplifiers. High rate systems require larger antennas and substantial High Power Amplifiers. Clearly, a VSAT built for the most stringent (high rate) requirements will exceed the requirements of a low rate system. If the costs of each were about the same there would be little need to worry about building one system which meets all requirements. In fact, the costs vary greatly depending upon the capabilities of the individual subsystems. This means that a prudent system designer can significantly enhance cost-effectiveness by using subsystems which meet the minimum requirements with desired margin for system expansion. This may seem fairly obvious, but it is not always the way current systems are designed.

Many of the subsystems of a VSAT need not change from one requirement to another. For example, Low Noise Amplifiers are moderately low in cost and can serve both high rate and low rate requirements equally well. Antennas are limited by the laws of physics so one must select an antenna of adequate aperture to produce the desired gain. Probably the most expensive single elements of VSATs, which can change greatly based upon system requirements, are the High Power Amplifiers and the transmitter and receiver, or transceiver.

As can be seen in Table 2 above, selection of an appropriate antenna/HPA trade can have a substantial effect. A change in antenna aperture by 1/2 provides a gain change of 6 dB, and a corresponding 6 dB HPA power requirement change. HPAs are among the most costly subsystems in a VSAT terminal so this is often an excellent trade. Due to this fact it is usually beneficial to design a VSAT system with a separate HPA so appropriate units can be installed in each VSAT to meet requirements. Too large an HPA results in undue expense. Too small causes unsatisfactory link performance.

There are other transceiver characteristics which have more subtle effects. The next most costly element in a VSAT transceiver, after the HPA, is the synthesizer. The performance-limiting specification of any VSAT synthesizer is its phase noise. High synthesizer phase noise results in poor BER performance which is especially pronounced on low rate digital signals. Different approaches can be taken to reduce this cost impact. If the synthesizer can be designed with larger step sizes its phase noise is easier to reduce-- this limits channel spacing however. In some systems it is possible to use a higher symbol rate with FEC and/or Time Division Multiple Access (TDMA) transmission to achieve the same user data rates with less phase noise effects. Similarly the system designer can consider different modulation formats which are less susceptible to the phase noise. The bottom line is: there is no single best answer. From a conceptual standpoint the easiest answer is to use the synthesizer

The normalized impedance, z , will be given in the form $z = z_R + jz_X$, where z_R and z_X represent the normalized resistance and normalized reactance components, respectively. The normalized admittance is given by $y = y_G + jy_B$, where y_G is the normalized conductance and y_B is the normalized susceptance.

Substituting $z = z_R + jz_X$ and $\Gamma = U + jV$ into (1) yields the relationship

$$z_R + jz_X = \frac{(1+U)+jV}{(1-U)-jV}$$

Separating this expression into its real and imaginary parts yields

$$z_R = \frac{1-U^2-V^2}{(1-U)^2+V^2}$$

and

$$z_X = \frac{2V}{(1-U)^2+V^2} \quad (2)$$

Given the location of Γ , the expressions for z_R and z_X respectively provide the values of the normalized resistance and normalized reactance circles in the Smith chart.

In order for the CAD system to determine the component values of a matching network, it is necessary to know the amount of reactance or susceptance needed from each component. The Smith chart naturally lends itself to this. In order to "read" the reactance or susceptance from the Smith chart, an intersection point between two circles will be calculated. The following derivation is for the value of the reactance circle at the intersection point between the normalized unit constant conductance circle ($y_G=1$) and a normalized constant resistance circle where $0 \leq z_R \leq 1$.

Assume the constant unit conductance circle is centered at the rectangular coordinates $(U_1, 0)$ with radius r_1 as shown in Figure 1. Let the point to match be selected on a constant resistance circle centered at $(U_2, 0)$ with radius r_2 .

The equations for these two circles are

$$\begin{aligned} (U - U_1)^2 + (V - 0)^2 &= r_1^2 \\ (U - U_2)^2 + (V - 0)^2 &= r_2^2 \end{aligned}$$

This system of equations may be written

$$U^2 - 2 \cdot U \cdot U_1 + U_1^2 + V^2 = r_1^2 \quad (3)$$

$$U^2 - 2 \cdot U \cdot U_2 + U_2^2 + V^2 = r_2^2 \quad (4)$$

Subtracting (4) from (3) yields

$$-2 \cdot U \cdot U_1 + 2 \cdot U \cdot U_2 + U_1^2 - U_2^2 = r_1^2 - r_2^2, \quad (5)$$

where U now represents the horizontal offset from the center of the Smith chart to where the two circles intersect.

Substituting U_{int} for U and noting that $U_1 = -.5$ and $r_1 = .5$, equation (5) may be written

$$\begin{aligned} U_{int} &= \frac{r_1^2 - r_2^2 - U_1^2 + U_2^2}{2 \cdot U_2 - 2 \cdot U_1} = \frac{.5^2 - r_2^2 - .5^2 + U_2^2}{2 \cdot U_2 + 1} \\ &= \frac{U_2^2 - r_2^2}{2 \cdot U_2 + 1} \end{aligned} \quad (6)$$

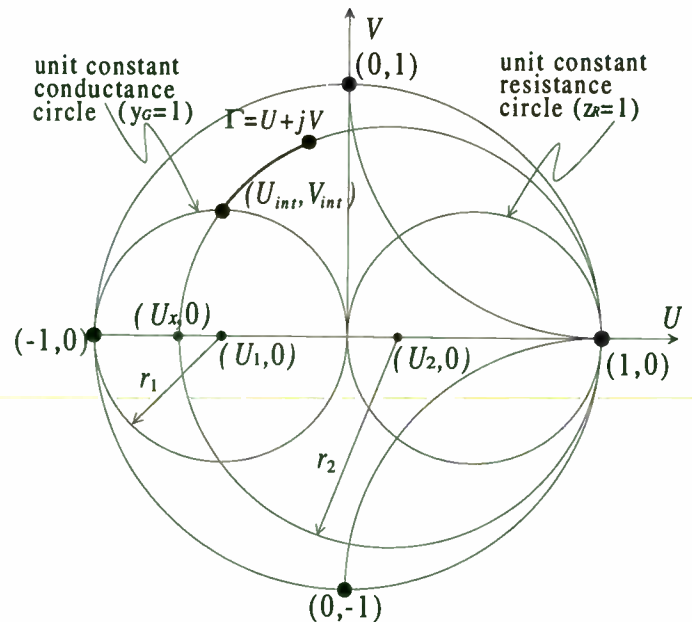


Figure 1. Intersection of constant resistance circle with unit constant conductance circle

To determine U_2 and r_2 , we first need to find the point where the resistance circle crosses the real ($V=0$) axis. Note that equation (1) may be rewritten in the form

$$\Gamma = \frac{z-1}{z+1},$$

which leads to the relationship

$$U + jV = \frac{(z_R-1)+jz_X}{(z_R+1)+jz_X}$$

with the lowest possible phase noise. From a practical standpoint, however, this can result in undue cost increases.

Another more subtle effect is Intermodulation Distortion or IMD. This often becomes a concern when more than one carrier is transmitted simultaneously. Solutions include improved transmitter design or the use of a single carrier with some type of TDMA. The cost impact of improvements in transmitter design to reduce IMD are sometimes difficult to assess. If each transmitter must be hand-tuned in production to reduce IMD its cost would be much higher than one which produces acceptable performance in automated production. The upconverter and HPA power levels are often major considerations for the desired IMD performance. Building in extra power margin for improved IMD performance can sometimes cause an unacceptable increase in costs.

Market Niche VSAT Examples

Having examined the "top level" factors in VSAT performance one can consider some typical examples of VSAT operation. While these examples will not be considered in minute detail, they illustrate the differences in requirements between various applications. VSAT performance can be adjusted to provide a cost-effective system solution in each case. While in each case there are obvious trade-offs in antenna aperture and EIRP, it is interesting to note that VSAT transceiver performance can also be considered in cost for performance trades.

Multi-Channel Telephony Example. Multi-Channel Telephony is one of the most demanding of VSAT applications. Telephony requires substantial communications throughput-- typically 32 KBPS full-period, full-duplex, for each toll-quality voice channel. "Bursty" transmission characteristics which may be acceptable with data traffic are not acceptable for voice. This means that sustained communications throughput must be maintained during the entire call. There are basically two ways to achieve this-- either transmit continuously during the call (using Frequency Division Multiplex, for example) or burst (with TDMA, for example) at such a high symbol rate that an effective 32 KBPS continuous rate is maintained. In the later case, if the symbol rate is 128 KBPS the transmitter would have to be on the air for more than 1/4 the time. The obvious trade-off there is that a higher symbol rate requires higher EIRP on both the uplink and downlink. In such a TDMA case, for example, a 4 times increase in symbol rate (a 6 dB increase) would require a 6 dB increase in EIRP for the same BER performance. In practice, TDMA systems usually use the same frequency for multiple stations so if a particular station is capable of transmitting 4 carriers, for example, and 4 such stations must be accommodated the symbol rate must be at least 16 times the basic channel data rate. A 16 times symbol rate increase (24 dB) would require a 24 dB EIRP increase. Considering Table 2, one can see that this soon becomes a substantial amount of transmitter power.

Separating this into its real and imaginary parts yields

$$U = \frac{z_R^2 - 1 + z_X^2}{(z_R + 1)^2 + z_X^2}$$

and

$$V = \frac{2z_X}{(z_R + 1)^2 + z_X^2}$$

Along the real axis, the solution for U leads to the result

$$U = \frac{z_R - 1}{z_R + 1} \quad \left| \quad z_X = 0 \right.$$

This expression may be generalized to the form

$$U_x = \frac{z_R - 1}{z_R + 1},$$

where $(U_x, 0)$ is the point where the given constant resistance circle, z_R , crosses the real axis of the Smith chart. Since all constant resistance circles also pass through the point $(U, V) = (1, 0)$, the radius, r_2 , of a given constant resistance circle may be found as half the distance between points $(1, 0)$ and $(U_x, 0)$; or

$$r_2 = \frac{1 - U_x}{2} = \frac{1 - \frac{z_R - 1}{z_R + 1}}{2} = \frac{1}{z_R + 1}. \quad (7)$$

U_2 may then be found as the relation

$$U_2 = U_x + r_2 = \frac{z_R}{z_R + 1}. \quad (8)$$

Substituting (7) and (8) into (6) gives the horizontal offset of the intersection point from the Smith chart center as a function of only z_R .

$$U_{int} = \frac{z_R - 1}{3z_R + 1}, \quad 0 \leq z_R \leq 1. \quad (9)$$

To find the vertical offset of the intersection point from the center of the Smith chart, simply substitute U_{int} for U and V_{int} for V in equation (3) and solve for V_{int} , yielding

$$V_{int} = \pm \sqrt{-U_{int}^2 - U_{int}}, \quad -1 \leq U_{int} \leq 0$$

$$= \frac{\pm 2 \sqrt{z_R - z_R^2}}{3z_R + 1}, \quad 0 \leq z_R \leq 1. \quad (10)$$

From (9) and (10), it can be seen that the intersection points $(U_{int}, \pm V_{int})$ may be obtained as functions of only the constant resistance circle, z_R .

It is then possible to directly find the value of the normalized reactance at the intersection point given any normalized resistance circle $0 \leq z_R \leq 1$. By substituting U_{int} and V_{int} for U and V in equation (2), the normalized reactance at the intersection point may be found directly as a function of z_R by

$$z_{X,int} = z_X = \pm \sqrt{z_R - z_R^2}, \quad 0 \leq z_R \leq 1 \quad (11)$$

The CAD system uses the same geometric layout for an admittance chart as it does for the impedance chart just described. Therefore, the determination of the normalized susceptance at the intersection of a constant conductance circle $0 \leq y_G \leq 1$ and the unit resistance circle can easily be shown to be

$$y_{B,int} = \pm \sqrt{y_G - y_G^2}, \quad 0 \leq y_G \leq 1 \quad (12)$$

B. Matching network design using the computerized Smith chart

The following steps outline the procedure used by the CAD system for developing four two-element matching networks for a given impedance using the Smith chart.

- 1) Assume the point is selected from the Smith chart at $\Gamma_1 = U_1 + jV_1$ and has the associated impedance $z_1 = z_{R1} + jz_{X1}$, where $z_{R1} < 1$.
- 2) Equation (11) provides the value of the normalized reactance circle at the intersection point between the constant resistance circle, z_{R1} , and the upper half of the unit constant conductance circle (i.e. the positive solution for $z_{X,int}$). This will be $z_{int} = z_{R,int} + jz_{X,int}$, where $z_{R,int} = z_{R1}$.
- 3) Calculate the admittance associated with z_{int} . This yields $y_{int} = 1/z_{int} = y_{G,int} + jy_{B,int}$, where $y_{G,int}$ will always be unity because y_{int} lies on the normalized unit constant conductance circle.
- 4) The normalized reactance needed from the series element of this matching network is given by $z_{X,int} - z_{X1}$; and the normalized susceptance needed from the shunt element is $0 - y_{B,int}$.
- 5) Repeat step 2, but use the negative solution for $z_{X,int}$. Repeat steps 3 and 4.
- 6) Let y_1 be the admittance associated with z_1 . ($y_1 = 1/z_1 = y_{G1} + jy_{B1}$, where $y_{G1} < 1$).

If FDMA is used the VSAT terminal can transmit continuously for each channel. In multi-channel telephony this means that the VSAT would have to transmit a separate signal for each channel continuously. Multiple simultaneous signals through the same transmitter require better IMD performance than a single signal but this may be advantageous in utilizing the total EIRP over a wider bandwidth.

The effect that multi-channel telephony service has on the VSAT transceiver is significant. There are at least three major performance requirements for this application:

- 1) Moderately high power HPA. Due to the relatively high user data rate (whether with a single signal or multiple) a moderately high EIRP is required. Since we are discussing a "VSAT" application relatively small antenna aperture is considered to be inherent.
- 2) Synthesizer phase noise must be relatively low if FMDA is used. High synthesizer phase noise could cause interference with adjacent carriers as well as causing demodulator BER problems.
- 3) IMD performance must be high if FDMA is used. Multiple simultaneous carriers on the uplink increase susceptibility to noise and resultant reductions in BER on the transmitted carriers.

Multi-channel telephony is one of the most demanding VSAT applications. Transceiver performance must be among the best and thus costs tend to be among the highest in any VSAT application. One of the only optimizations which can be used is the trade-off of antenna aperture to HPA power level.

Point-of-Sale Data Terminal Example. Point-of-Sale Data Terminals have become one of the largest VSAT applications. Currently there are probably more VSATs used for this application than any other. In this application "bursty" data is perfectly acceptable but since it tends to use operator-controlled transactions the response through the network or latency must be on the order of a few seconds at most. This implies that some type of TDMA or packet access may offer optimal use of the communications resources. Data rates tend to be relatively low (19.2 KBPS or so) because only a few bytes of information need be transferred in each transaction. One of the factors which makes these systems practical, however, is often the ability to transmit large blocks of computer data in "off-peak" periods. Typical applications make use of the network for credit verification during the business day and backhaul inventory control at night. This means that low data rates may be needed for the transaction processing but a dynamically higher data rate capability may be advantageous.

One of the overpowering factors in this application is that each network tends to have a large number of remote sites-- sometimes several thousand. This means that cost

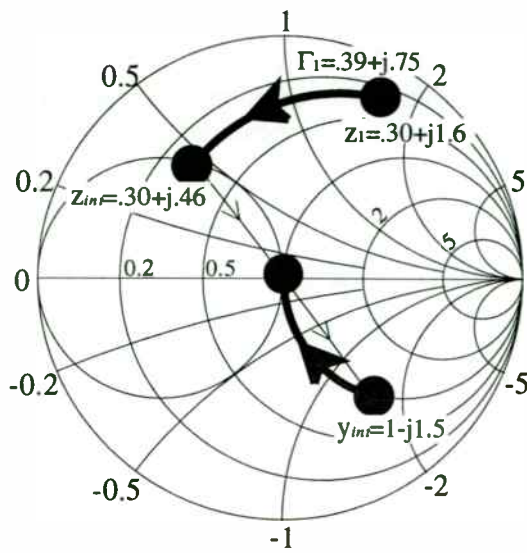


Fig. 2a

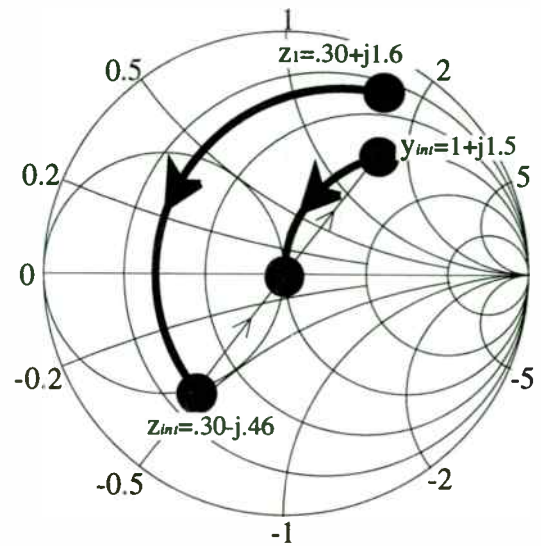


Fig. 2b

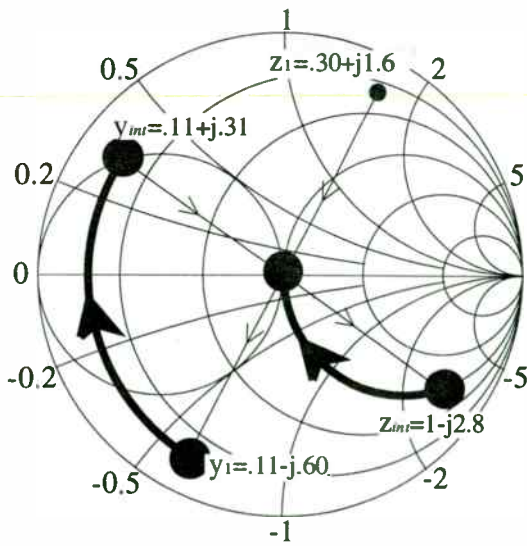


Fig. 2c

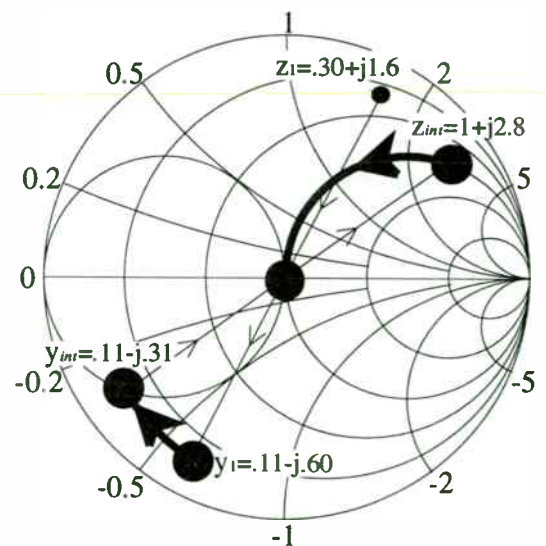


Fig. 2d

Figure 2. Methods for matching a given impedance

of each remote terminal is a significant factor! Thus, steps taken to reduce the terminal cost even slightly can have a very big effect on overall cost-effectiveness. This can translate into things like designing the system for the relatively low data rates needed for the transaction processing and simply using whatever capability results in the backhaul function. Since there is such a large number of terminals it may also be prudent to use a moderately inexpensive control mechanism and have less than optimum space segment usage while absolutely minimizing the costs of each remote terminal.

This application offers some opportunities in cost reduction over other VSAT applications. The performance requirements placed on the VSAT transceivers include:

- 1) Reduced HPA output power. Since relatively low data rates are required, a lower EIRP from each terminal is necessary. This can mean smaller antennas and/or reduced HPA power requirements. Since HPA costs are among the largest factors in VSAT transceiver design, a reduction in HPA power levels is often prudent.
- 2) Synthesizer phase noise should be relatively low. Since fairly low data rates are used synthesizer phase noise should be considered to improve BER. Also since the rate is so low, however, FEC coding or other steps could be taken to improve BER for the same power level at the expense of bandwidth. The coding trade-off could be considered to reduce costs.
- 3) IMD performance is not as critical. This application almost always requires a single carrier on the uplink so IMD susceptibility is usually negligible. A system designer can make use of this fact in specifying transceiver performance to reduce costs.

Point-of-Sale data terminals are a very widespread VSAT application. With several trade-offs available a prudent system designer can relax some specifications and tighten others to minimize system costs while still meeting performance requirements.

SCADA Terminal Example. Supervisory Control and Data Acquisition, or SCADA, is an interesting VSAT application. SCADA systems require relatively small blocks of digital data to be passed between a central control site and many remote locations. For many years this application suffered from the early VSAT data transmission problems-- the VSATs could pass the data but the computers weren't ready to communicate. Progress in data communications protocols and microprocessor systems have now positioned SCADA to become a very popular VSAT application in the next few years.

The principal requirements in SCADA systems are to pass relative low rate data of a "bursty" nature. This implies the use of some sort of TDMA or packet transmission

- 7) Using equation (12), solve for the positive solution of $y_{B,int}$ to obtain $y_{int} = y_{G,int} + jy_{B,int}$, where $y_{G,int} = y_{G1}$.
- 8) Calculate the impedance of y_{int} to obtain $z_{int} = 1/y_{int} = z_{R,int} + jz_{X,int}$, where $z_{R,int} = 1$.
- 9) The susceptance needed from the shunt element will be $y_{B,int} - y_{B1}$; and the reactance needed from the series element is $0 - z_{X,int}$.
- 10) Repeat step 7, but use the negative solution for $y_{B,int}$. Repeat steps 8 and 9.

It should be noted that if a point to be matched is selected from the impedance Smith chart within the unit constant conductance circle ($y_{G1} > 1$), only steps 1 through 5 may be used for developing a two-element matching network. On the other hand, if the point is selected within the unit constant resistance circle ($z_{R1} > 1$), then only steps 6 through 10 apply.

C. Design example

An example implementation of the design procedure outlined above is described in the following steps and graphically depicted in Figure 2.

- 1) Assume the point selected is at the position $\Gamma_1 = U_1 + jV_1 = .39 + j.75$ as shown in Figure 2a. Using equation (1), the associated impedance is found to be $z_1 = z_{R1} + jz_{X1} = 0.30 + j1.6$.
- 2) Equation (11) determines the reactance at the intersection point between the unit constant conductance circle and the constant resistance circle, $z_{R1} = 0.30$; this yields the point $z_{int} = z_{R,int} + jz_{X,int} = 0.30 + j.46$.
- 3) The admittance associated with z_{int} is $y_{int} = 1/z_{int} = y_{G,int} + jy_{B,int} = 1.0 - j1.5$.
- 4) A series element with reactance $j(z_{X,int} - z_{X1}) = j(0.46 - 1.6) = -j1.14$, and a shunt element with susceptance $j(0 - (-1.5)) = +j1.5$ are required for the matching network.
- 5) Using the negative solution for equation (11) provides the following information: (see Fig. 2b)
 $z_{int} = .30 - j.46$; $y_{int} = 1.0 + j1.5$.
 series element: $-j2.06$ reactance.
 shunt element: $-j1.5$ susceptance.
- 6) $y_1 = 1/z_1 = .11 - j.60$. (see Fig. 2c)
- 7) Calculating $y_{B,int}$ from (12) leads to $y_{int} = .11 + j.31$.
- 8) $z_{int} = 1.0 - j2.8$.
- 9) shunt element: $j(.31 - (-.61)) = +j.91$ susceptance.
 series element: $+j2.8$ reactance
- 10) $y_{int} = .11 - j.31$; $z_{int} = 1.0 + j2.8$. (see Fig. 2d)
 shunt element: $(j(-.31 - (-.60))) = +j.29$ susceptance.
 series element: $-j2.8$ reactance.

Given the amount of reactance or susceptance needed, the value of the necessary component may then be calculated. The capacitive reactance, x_c , and the inductive reactance, x_L , are provided by the impedance chart. The capacitive reactance is given by

$$jx_c = \frac{1}{jR_0(2\pi f_0 C)},$$

where, R_0 = system resistance,
 f_0 = frequency of operation,
 and C = capacitor value.

The capacitor value is then easily shown to be

$$C = \frac{1}{R_0(2\pi f_0 x_c)}, \quad x_c < 0. \quad (13)$$

Similarly, the normalized reactance of an inductor may be found by

$$jx_L = \frac{j2\pi f_0 L}{R_0}, \quad \text{where } L \text{ is the inductor value.}$$

Solving for L yields

$$L = \frac{x_L R_0}{2\pi f_0}, \quad x_L > 0. \quad (14)$$

The capacitive susceptance, b_c , and the inductive susceptance, b_L , are read from the admittance chart. The capacitor and inductor values are then given by

$$C = \frac{b_c}{R_0(2\pi f_0)}, \quad b_c > 0 \quad (15)$$

and
$$L = -\frac{R_0}{(2\pi f_0)b_L}, \quad b_L < 0. \quad (16)$$

By knowing which chart, impedance or admittance, is being "read" from, the component values for the matching network may be calculated using equations (13) through (16).

III. SMALL SIGNAL AMPLIFIER DESIGN

Some of the basic principles applied to the design of transistor amplifiers include stability, gain, and noise analysis. The method of design employed by the CAD system is based on the S parameters of the DC biased transistor circuit at the frequency of operation. The S parameters provide all the information necessary to design for the desired stability and gain. In addition,

protocol. Communications takes place between computers so latency is not as big a problem as with point-of-sale terminals. There are, however, some critical SCADA applications where response needs to be very short. These include things like remotely responding to a pipeline failure or powerline fault. A good compromise for these situations is some sort of prioritization scheme which could dynamically shorten latency when required. This is usually a matter of concern to the control system rather than for the communications system engineer.

Also, since SCADA applications tend to be very remote it may be advantageous to permit operation with low input power. Some SCADA systems have even been implemented with solar power supplies to permit unattended, excessively remote installations, away from conventional power supplies. Since data rates tend to be low and thus EIRP can be low, a low input power requirement is realistic for SCADA.

This application again offers some opportunities in cost reduction over other VSAT applications. The performance requirements placed on the VSAT transceivers in SCADA service include:

- 1) Reduced HPA output power. Since relatively low data rates are required, a lower EIRP from each terminal is necessary. This can mean smaller antennas and/or reduced HPA power requirements. Since HPA costs are among the largest factors in VSAT transceiver design, and since a lower input power requirement is also often desired, a reduction in HPA power levels is often prudent.
- 2) Synthesizer phase noise should be relatively low. Since fairly low data rates are used synthesizer phase noise should be considered to improve BER. Also since the rate is so low, however, FEC coding or other steps could be taken to improve BER for the same power level at the expense of bandwidth. The coding trade-off could be considered to reduce costs.
- 3) IMD performance is not as critical. This application always requires a single carrier on the uplink so IMD susceptibility is negligible. A system designer can make use of this fact in specifying transceiver performance to reduce costs.

SCADA terminals are a very rapidly growing VSAT application. With the many trade-offs available, a prudent system designer can optimize earth terminal design for SCADA and achieve substantial cost reductions while still meeting all operational requirements.

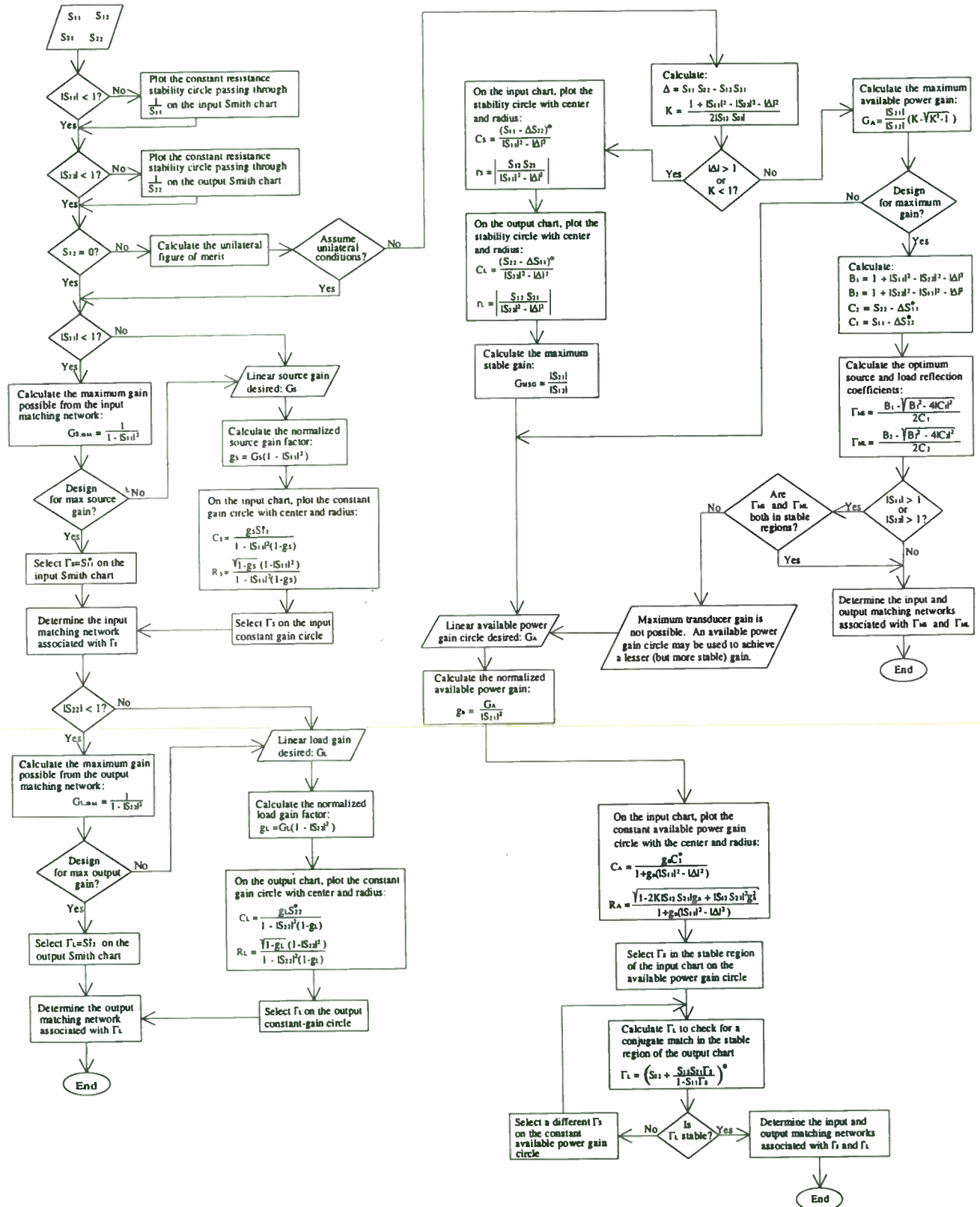


Figure 3. Flowchart for amplifier design

Summary

We have seen that VSAT systems continue to evolve as satellite transponder performance increases and as users increase their needs for VSAT services. User equipment (like PBXs and networked computer systems) now have a greater capability to make use of VSAT-delivered communications than ever before. Current VSAT systems are exceptionally flexible and capable of meeting dynamically changing market needs with sometimes minor and other times more substantial modifications.

We have also seen the quantitative effects illustrated with the satellite link equation. Analysis of the individual communications links permits the VSAT system designer to consider several alternatives to maximize performance for a given cost or minimize cost for a specified service quality. Since VSAT systems can have several thousand terminals, careful consideration of cost-reducing strategies are usually warranted. It's no longer enough simply to buy the "latest and greatest" VSATs and install them consistently. Attention must be paid to the minimum subsystem requirements necessary to provide the desired level of service. HPA power levels are but one example-- bigger isn't always better.

Some VSAT systems will consistently place a heavy burden on maximum subsystem performance-- like the multi-channel telephony example. The available industry performance limits will continue to be the ultimate limits of service quality offered by those systems. Even there, intelligent trade-offs can be made to minimize costs while meeting performance requirements. Other applications exist which can benefit greatly by designs optimized not for performance but for price. When several thousand earth stations are being installed in a single VSAT system every dollar saved becomes significant. The prudent VSAT system engineer considers this fact and examines the desired level of service carefully when specifying VSAT subsystem requirements.

Tim Shroyer is Vice President of Business Development for FEI Communications, Inc. in Sunnyvale, California. Mr. Shroyer received a BSEE degree from the University of Southern California. His experience includes over 20 years of satellite communications operation, system engineering, and program management with the U.S. Navy, the Defense Communications Agency, Stanford Telecommunications, Inc., Loral Aerospace, and FEI Communications, Inc.

given the noise parameters of the circuit, the user may factor the desired noise figure criteria into the design.

The flow chart in Figure 3 provides for the manual development of stability circles and constant gain circles under unilateral ($S_{12}=0$) and bilateral conditions.

A. Stability analysis

Referring to the single stage amplifier model of Figure 4, a requirement for a two-port network to be considered unconditionally stable at a given frequency is

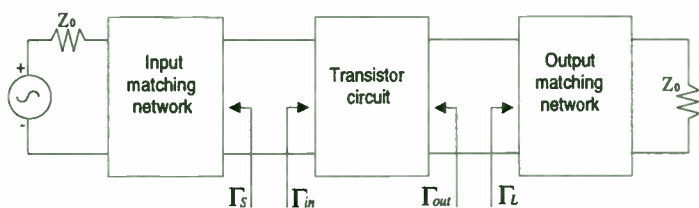


Figure 4. Two-port amplifier block diagram

for both the input and output port impedances to produce a positive real part. This requirement implies that $|\Gamma_{in}| < 1$ and $|\Gamma_{out}| < 1$, where Γ_{in} and Γ_{out} are defined as [1]

$$\Gamma_{in} = S_{11} + \frac{S_{12}S_{21}\Gamma_L}{1-S_{22}\Gamma_L} \quad (17)$$

$$\text{and } \Gamma_{out} = S_{22} + \frac{S_{12}S_{21}\Gamma_S}{1-S_{11}\Gamma_S} \quad (18)$$

Note that Γ_S and Γ_L are the source and load reflection coefficients to be selected from the Smith chart Γ -plane. Since Γ_{in} is a function of Γ_L , and Γ_{out} is a function of Γ_S , it is true that the stability of the amplifier depends upon the matching networks to be determined by the selected locations of Γ_S and Γ_L . Therefore, it is necessary to determine the loci of Γ_S which produce $|\Gamma_{out}| = 1$ and the loci of Γ_L which produce $|\Gamma_{in}| = 1$. These values may be shown to lie in circles called stability circles whose centers and radii are functions of the S parameters. There has been a wealth of previously published work [1,2] regarding the derivation of the stability circles for the Smith chart Γ_S and Γ_L planes, only the results of which are presented here. However, it is first helpful to know whether or not the development of the stability circles is even necessary. A device may be determined to be unconditionally stable without resorting to the task of calculating the location of the stability circles. First, define Δ (the determinant of the S parameter matrix) as

$$\Delta = S_{11}S_{22} - S_{12}S_{21}.$$

The necessary and sufficient requirements for unconditional stability when $|S_{11}| < 1$ and $|S_{22}| < 1$ may be shown to be [3,4]

$$K = \frac{1-|S_{11}|^2-|S_{22}|^2+|\Delta|^2}{2|S_{12}S_{21}|} > 1$$

$$\text{and } |\Delta| < 1.$$

Satisfying the above criteria indicates that the stability circles do not enter the passive region of the Smith chart Γ_S -plane or Γ_L -plane; therefore their calculation and plot is unnecessary.

However, under conditions where a device is determined to be potentially unstable (i.e. $K < 1$ or $|\Delta| > 1$), it becomes necessary to plot the input and output stability circles as follows:

In the Γ_S -plane, the *input stability circle* is centered at C_S with radius R_S , where

$$C_S = \frac{(S_{11}-\Delta S_{22}^*)^*}{|S_{11}|^2-|\Delta|^2}$$

$$\text{and } R_S = \left| \frac{S_{12}S_{21}}{|S_{11}|^2-|\Delta|^2} \right|.$$

In the Γ_L -plane, the *output stability circle* is centered at C_L with radius R_L , where

$$C_L = \frac{(S_{22}-\Delta S_{11}^*)^*}{|S_{22}|^2-|\Delta|^2}$$

$$\text{and } R_L = \left| \frac{S_{12}S_{21}}{|S_{22}|^2-|\Delta|^2} \right|.$$

In short, the input stability circle represents the boundary along which $|\Gamma_{out}| = 1$, and the output stability circle represents the boundary along which $|\Gamma_{in}| = 1$.

It is then necessary to determine which values of Γ_S (inside or outside the stability circle) are in the stable region ($|\Gamma_{out}| < 1$) of the input chart, and which values of Γ_L are within the stable region ($|\Gamma_{in}| < 1$) of the output chart. Referring to the definition for Γ_{in} above, if $\Gamma_L = 0$ (the center of the output Smith chart), then $|\Gamma_{in}|$ is simply $|S_{11}|$. Therefore, if $|S_{11}| < 1$ then $|\Gamma_{in}| < 1$ and the center of the output chart is a point in the stable region. Conversely, if $|S_{11}| > 1$ then $|\Gamma_{in}| > 1$ and the center is a point in the unstable region. Similarly, if $\Gamma_S = 0$ and $|S_{22}| < 1$ then $|\Gamma_{out}| < 1$ and the center of the input chart is in the stable region, and if $|S_{22}| > 1$ then $|\Gamma_{out}| > 1$ and the input chart center is part of the

ENVIRONMENTAL EFFECTS ON MOBILE SATELLITE COMMUNICATIONS

**DENNIS A. JIRAUD
10/14/92**

In recent years there has been much effort devoted to making land mobile communications possible using low Earth orbiting satellite systems. Satellite communications with the mobile terminal can suffer from the unpredictability of the propagation environment. In this environment, a received signal undergoes extreme variations in amplitude due to multipath fading and shadowing. Multipath signals can combine destructively to attenuate the received signal below usable levels resulting in outage times. Another effect of multipath is time delay spread, that is, multipath signals arrive in time intervals that cause a definite overlapping of symbols. This leads to intersymbol interference that in turn limits the symbol transmission rate.

Satellite communications is also limited by interference from other transmitters. Outage times occur when the sum of interfering signal powers exceeds the instantaneous signal power. In the absence of interference, outage times occur when shadowing decreases the signal-to-noise ratio below the minimum ratio required by the receiver. This suggests the need for a link margin that can be excessive to cope with multipath fading and shadowing. Unfortunately, a link margin is influenced by many factors including the type of terrain, the height and density of the vegetation, and the distribution of trees and man made structures.

Any satellite mobile communication system transmitting narrow-band signals can overcome the effects of multipath and shadowing by using a mixture of schemes. Among these schemes are adaptive equalization, adaptive symbol rate, and error-control. However, much greater resistance to multipath and interference is possible with spread spectrum wide-band signals. The most popular scheme appears to be direct-sequence code division multiple access (CDMA).

Multipath

Regardless of the radio transmission scheme, the power radiated from a satellite antenna will spread over a particular service area. It is desired that the spreading signal travel from satellite to receiver along a direct propagation path. However, as the signal spreads over the service area it will reflect off objects in the environment. This creates reflection signals that may return to the receiver along indirect propagation paths as illustrated in Figure 1. Notice that some of these paths are longer than others and with each reflection there is a corresponding loss of signal energy. Therefore, each reflection signal arrives delayed from the others and with a different power.

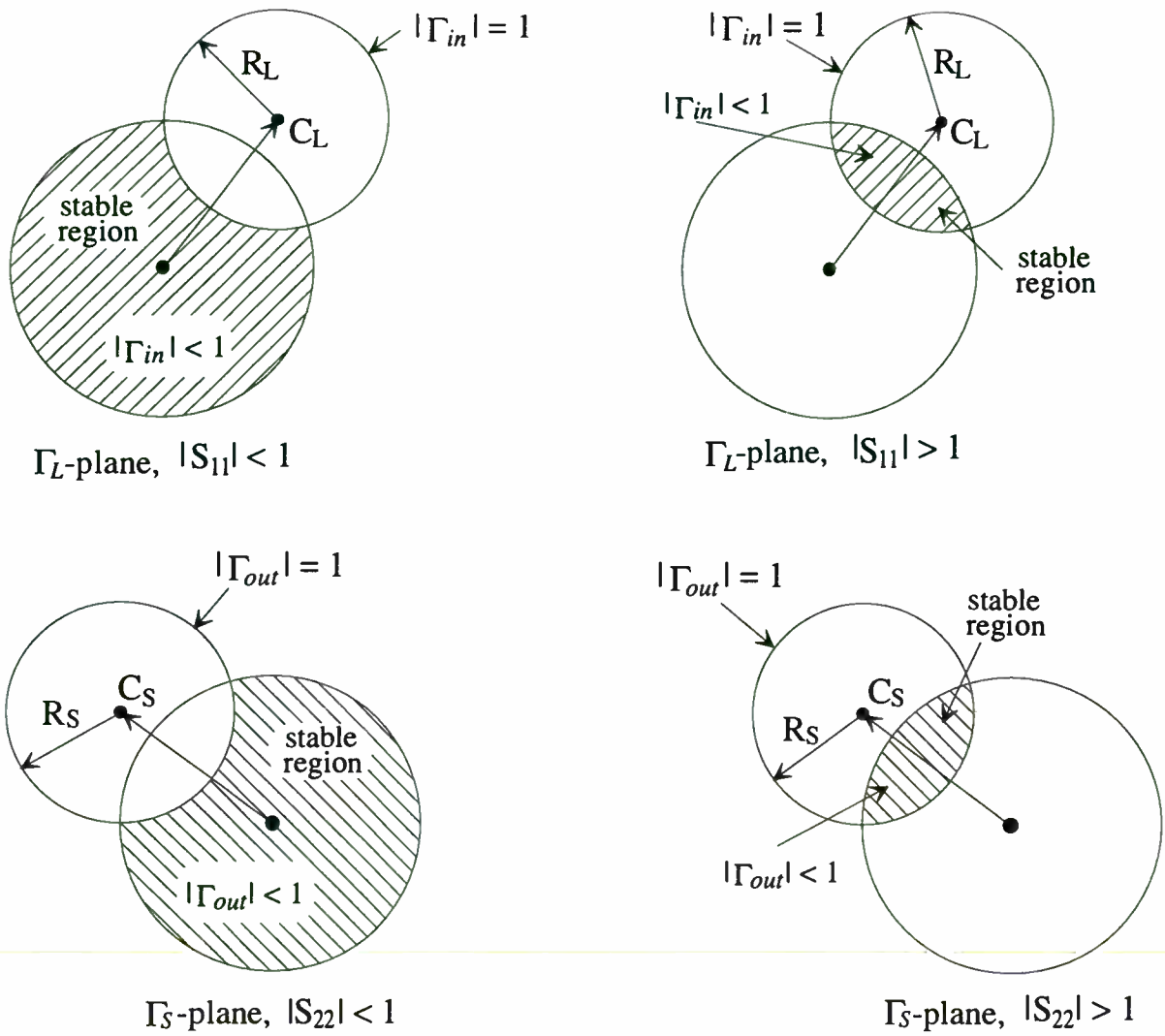


Figure 5. Stability circles for $|\Gamma_{in}|=1$ and $|\Gamma_{out}|=1$

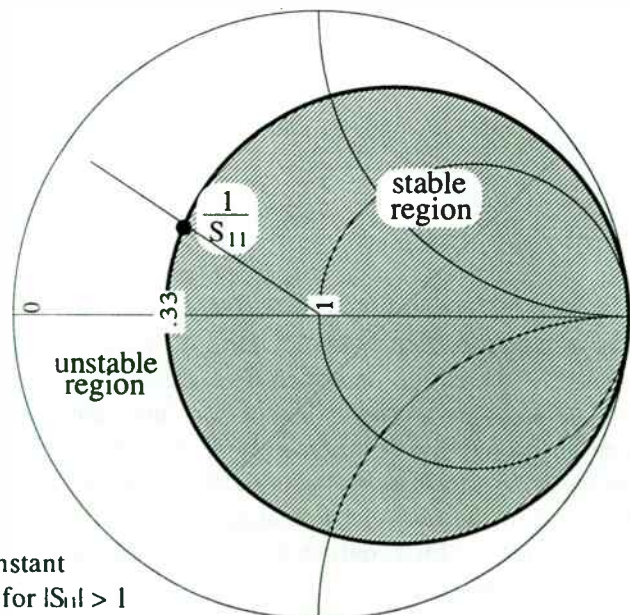


Figure 6. Example of constant resistance stability circle for $|S_{11}| > 1$

When two or more of these signals combine at the receiver, the amplitude of the resultant signal may increase or decrease. This of course, depends upon the phase and amplitude relationship of the arriving signals. Their phase relationship will depend upon the distance of each path measured in wavelengths. If the two distances differ by an integral number of wavelengths, the phase of the two signals will be in alignment, and the resultant signal will be the sum of the two signals. Should the two distances differ by an odd number of half wavelengths, the two signals will be 180 degrees out of phase and the resultant signal will be the difference between these signals. Since the location of a mobile radio is not constant, the phase relationship between the different path signals will vary with receiver location and hence the envelope of the resultant signal will vary. For this reason, the mobile radio experiences fades in signal strength that varies in depth and duration depending upon the mobile's speed and operating frequency.

Multipath also occurs when a radio wave traverses a medium with physical scatters. This medium includes tree foliage, ground vegetation, and rocky slopes. Because the tree foliage presents a discontinuous reflecting surface, a single traversing signal diffuses into a multitude of closely spaced signal paths. Upon reception, the diffused signals combine to create a resultant signal. This resultant signal undergoes amplitude and phase variations described by the Rayleigh and uniform distributions, respectively.

Since the antenna of a mobile radio is close to the ground, multipath signals resolve into three components. One is a specular component (often the ground reflection) which is coherent with the incident signal (line of sight) and the other is a noncoherent (diffuse) component that fluctuates in amplitude. The term specular refers to a nonfading signal, which usually arrives Doppler shifted from the transmitted frequency. Specular reflections arise when the incident signal bounces off the smooth surface of buildings or the ground. Should a strong specular path and many weaker path signals combine at the receiver, the resultant signal produces amplitude variations that follow a Rice-Nakagami distribution.

unstable region. These results may be described graphically as in Figure 5.

A second requirement for unconditional stability on the Smith chart is for $|S_{11}| < 1$ and $|S_{22}| < 1$. For instance, given an input reflection coefficient, S_{11} , whose magnitude is greater than unity implies that the real part of the impedance associated with S_{11} is negative and there is a potential for instability. For this reason, the real part of the source impedance, Z_S , associated with the selected source reflection coefficient, Γ_S , must provide for a total input loop resistance that is positive.

The minimum normalized resistance that Γ_S can acquire may be determined by plotting the critical point $\Gamma_{s,c} = \frac{1}{S_{11}}$. Γ_S must then be selected such that the real part of the impedance associated with Γ_S is greater than the real part of the impedance associated with $\Gamma_{s,c}$. In other words, $\text{Re}(Z_S) > \text{Re}(Z_{s,c})$. A similar argument may be followed if $|S_{22}| > 1$. The minimum normalized resistance required from Γ_L in the output chart is determined from the critical point $\Gamma_{L,c} = \frac{1}{S_{22}}$.

A short example will clarify the situation. An input reflection coefficient $S_{11} = 1.77 \angle -130$ has an associated normalized impedance $Z_{S_{11}} = -.33 - j.42$.

The critical point $\Gamma_{s,c} = \frac{1}{S_{11}} = .565 \angle 130$ is calculated and found from the Smith chart to have the associated normalized impedance $Z_{s,c} = .33 + j.42$. Therefore, the source reflection coefficient, Γ_S , must be selected such that its normalized real part is within the $+.33$ normalized constant resistance circle on the Smith chart as shown in Figure 6. In addition, it will be shown that an infinite value for the gain is calculated by selecting the reflection coefficient at the critical point.

B. Transducer Gain Analysis

The CAD system follows two separate procedures for the calculation of constant gain circles, one for the unilateral case ($S_{12} = 0$) and the second for the bilateral case. Under unilateral conditions the gain may be expressed in the form

$$G_S = \frac{1 - |\Gamma_S|^2}{|1 - S_{11}\Gamma_S|^2}$$

$$\text{and } G_L = \frac{1 - |\Gamma_L|^2}{|1 - S_{22}\Gamma_L|^2},$$

where G_S and G_L represent the gain produced by the input and output matching networks, respectively.

As stated earlier, if $|S_{11}|$ or $|S_{22}|$ is greater than unity, then by substituting $\Gamma_S = \Gamma_{s,c} = \frac{1}{S_{11}}$ or $\Gamma_L = \Gamma_{L,c} = \frac{1}{S_{22}}$ into the expressions for G_S or G_L , respectively, an infinite value for that particular gain will be calculated.

Under unilateral and unconditionally stable conditions the maximum values of G_S and G_L may be obtained by letting $\Gamma_S = S_{11}^*$ and $\Gamma_L = S_{22}^*$. The expressions may then be written

$$G_{S_{\max}} = \frac{1}{1 - |S_{11}|^2}$$

$$\text{and } G_{L_{\max}} = \frac{1}{1 - |S_{22}|^2}.$$

However, a unilateral transducer gain other than $G_{S_{\max}}$ or $G_{L_{\max}}$ may sometimes be desired. The values for which Γ_S or Γ_L produce values of $G_S < G_{S_{\max}}$ or $G_L < G_{L_{\max}}$, respectively, may be shown [1,2] to lie in circles on a Smith chart. The center and the radius of the *input constant-gain circles* for the unilateral case are given by

$$C_S = \frac{g_S S_{11}^*}{1 - |S_{11}|^2 (1 - g_S)}$$

$$\text{and } R_S = \frac{\sqrt{1 - g_S} (1 - |S_{11}|^2)}{1 - |S_{11}|^2 (1 - g_S)}.$$

where $g_S = \frac{G_S}{G_{S_{\max}}}$ is known as the normalized input gain factor with G_S as the desired gain produced by the input network.

The center and radius of the *output constant-gain circles* under unilateral conditions can be shown to be

$$C_L = \frac{g_L S_{22}^*}{1 - |S_{22}|^2 (1 - g_L)}$$

$$\text{and } R_L = \frac{\sqrt{1 - g_L} (1 - |S_{22}|^2)}{1 - |S_{22}|^2 (1 - g_L)}$$

where $g_L = \frac{G_L}{G_{L_{\max}}}$ is the normalized output gain factor with G_L as the desired gain produced by the output network.

Under bilateral conditions, the CAD system provides two options to the user for the design of a desired transducer power gain. The first is to select Γ_S

The destructive combining of multipath signals creates a communication's channel with a range of channel frequencies that undergo attenuation. This range of channel frequencies is commonly called the "coherence bandwidth." A channel exhibiting flat frequency fading has a coherence bandwidth that is greater in comparison to the bandwidth of the transmitted signal. In a flat fading channel any two identical signals transmitted on separate frequencies (within the coherence bandwidth) will arrive with their envelopes fading in unison. As the frequency separation increases, their envelopes will no longer fade in unison. Such a channel is exhibiting frequency selective fading, because the channel has a coherence bandwidth that is smaller in comparison to the bandwidth of the transmitted signal. As a result, the signal is amplitude and phase distorted, by what appears in the frequency domain to be a notch in the bandwidth of the received signal.

Mathematically the coherence bandwidth is inversely proportional to the differential delay time between the multiple signals that reach the receiver. For example, a transmitted signal traveling at 1 ns/ft along multipaths that differ by 200 feet in length will arrive 200 ns apart, causing a fading bandwidth of approximately 5 MHz. If these multipath signals destructively combine to produce a very deep fade, the mobile is likely to experience a communication outage. This is not unusual as the mobile radio often passes through random fades of varying depths. These depths vary by 10 to 40 dB below the mean level with successive minima occurring every half wavelength.

Frequency selective fading or time delay spread occurs when the difference in propagation delay on the different paths is similar to or greater than the symbol duration. If the difference is very much smaller than the symbol duration, then the multipath channel resembles a flat frequency fading channel. When multipath signals arrive in intervals comparable to the symbol duration each symbol will overlap with preceding and following symbols. In a digital system, particularly one attempting to operate at a high symbol rate, the overlapping of symbols creates intersymbol interference (ISI). A transmitted signal traveling at 1 ns/ft along multiple paths that differ by 1000 feet in length will arrive 1 us apart. If the symbol rate is 125 kilosymbols per second, the symbol duration is 8 usec. As a result, the average symbol overlap is 12.5 percent, which may be an unacceptable level of ISI. The overall effect of the energy contributed by overlapping symbols are greater bit errors. Intersymbol interference can produce error bursts even if the signal-to-noise ratio is high. Designers can lessen ISI by reducing the symbol rate or by employing adaptive equalization.

from an available power gain circle, G_A , in the stable region on the input chart, then to calculate and plot its conjugate match (i.e. $\Gamma_L = \Gamma_{out}^*$) on the output chart to determine the stability for an output matching network. If Γ_L does not provide for the proper stability, then another point may be selected on the desired available power gain circle until the appropriate stability is achieved. The second option is similar except that the first point is selected from an operating power gain circle, G_P , in the Γ_L -plane, and the conjugate match (i.e. $\Gamma_S = \Gamma_{in}^*$) is then calculated and plotted on the input chart.

If a design procedure using an available power gain circle is to be followed, the desired available power gain circle, G_A , may be shown to lie in the Γ_S -plane centered at C_A with radius R_A given by

$$C_A = \frac{g_a C_1^*}{1 + g_a (|S_{11}|^2 - |\Delta|^2)}$$

and
$$R_A = \frac{\sqrt{1 - 2K |S_{12} S_{21}| g_a + |S_{12} S_{21}|^2 g_a^2}}{1 + g_a (|S_{11}|^2 - |\Delta|^2)}$$

where
$$g_a = \frac{G_A}{|S_{21}|^2}$$

and
$$C_1 = S_{11} - \Delta S_{22}^*$$

On the other hand, if an operating power gain circle, G_P , is to be selected from the Γ_L -plane, then the center, C_P , and radius, R_P , are given by

$$C_P = \frac{g_p C_2^*}{1 + g_p (|S_{22}|^2 - |\Delta|^2)}$$

and
$$R_P = \frac{\sqrt{1 - 2K |S_{12} S_{21}| g_p + |S_{12} S_{21}|^2 g_p^2}}{1 + g_p (|S_{22}|^2 - |\Delta|^2)}$$

where
$$g_p = \frac{G_P}{|S_{21}|^2}$$

and
$$C_2 = S_{22} - \Delta S_{11}^*$$

When the S parameters of the device indicate unconditionally stable bilateral conditions, the maximum available power gain or the maximum operating power gain is obtained at the point where $R_A=0$ or $R_P=0$. Either case leads to the following expression for maximum gain [1]

$$G_{max} = \frac{|S_{21}|}{|S_{12}|} (K - \sqrt{K^2 - 1}).$$

Under potentially unstable conditions where $K < 1$, the maximum stable gain is given by

$$G_{MSG} = \frac{|S_{21}|}{|S_{21}|}.$$

G_{MSG} is the gain that can be achieved by resistively loading the transistor to make $K = 1$ and then simultaneously conjugately matching [1] the input and output ports. Any time a simultaneous conjugate match is performed, it is assumed that the active device is unconditionally stable. If $K < 1$, oscillations may occur if either of the power gains are selected such that $G_A > G_{MSG}$ or $G_P > G_{MSG}$.

C. Noise figure analysis

In addition to stability and gain, another consideration in amplifier design is its noise figure. The noise figure of a two-port amplifier may be given in the form [2]

$$F = F_{min} + \frac{4R_N}{Z_0} \frac{|\Gamma_S - \Gamma_{opt}|^2}{(1 - |\Gamma_S|^2) |1 + \Gamma_{opt}|^2},$$

where

R_N = equivalent noise resistance of the transistor.

Γ_S = source reflection coefficient on the input chart.

Γ_{opt} = optimum reflection coefficient resulting in minimum noise figure.

F_{min} = minimum noise figure of the transistor.

Z_0 = system impedance.

This expression defines a family of noise figure circles in the Γ_S -plane. To compute the center and radius of a noise figure circle, it is first necessary to calculate the noise figure parameter, N , defined as

$$N = \frac{F - F_{min}}{4R_N/Z_0} |1 + \Gamma_{opt}|^2.$$

The center, C_F , and radius, R_F , of a constant noise figure circle are then given by

$$C_F = \frac{\Gamma_{opt}}{N+1}$$

and
$$R_F = \frac{\sqrt{N(N+1 - |\Gamma_{opt}|^2)}}{N+1}.$$

Path Losses

The direct path is one in which the propagation path is free of obstacles that might absorb or reflect the incident signal's energy before it reaches the receiving antenna. As the signal travels from transmitter to receiver it will undergo path attenuation due to free-space loss and transmission losses. The distance dependent free-space loss is given by

$$L_p = 10 * \log [(Y)^2 / (4*PI*d)^2] \text{ dB}$$

Where d is the distance in meters between terminal and satellite and Y is the wavelength in meters.

For a one wavelength separation between isotropic antennas, the free space loss is 22 dB and it increases by 6 dB each time the distance doubles. Consider the 42,162 km distance a radio wave travels to or from a geostationary satellite. If the system employs a 1.6 GHz operating frequency, the free space loss is almost 190 dB, which is enormous amount of signal loss. Overcoming this loss usually requires higher power transmitters, which places a considerable strain on satellite energy resources. Also, the round trip distance creates long propagation delays (approx. 0.5 sec.) that limits voice transmission quality. On the other hand, low Earth orbiting satellites are closer (765 km), which greatly reduces the free space loss to the mobile terminal. This allows for higher signal levels, lower propagation delays (0.003 second), and lower cost, which is appealing for future satellite mobile applications.

For satellite communications at frequencies above 8 GHz, transmission losses due to rainfall and atmospheric moisture become major concerns in the link design. This is because rain and atmospheric losses increase significantly at higher frequencies and at lower elevation angles. A uniquely troublesome path-loss occurs when the propagation path is partially obstructed by tree foliage, large buildings, or tall vegetation. Within this short obstructing path distance, the signal may undergo considerable attenuation. This path attenuation is highly dependent upon the frequency and upon the absorption properties of the obstacle. For instance, the average amounts of attenuation a 900 MHz signal undergoes when traversing 4 meters of roadside trees is 2.9 dB. That is, the signal lost about half its power. We can predict the average attenuation due to foliage by [1]

$$L = [0.187 * f^{0.284} * d^{0.588}] \text{ dB.}$$

Where f is frequency in MHz and d is the length of foliage traversed by the signal in meters. Undoubtedly, variations in shadowing loss will arise because of changes in the physical surroundings. Unfortunately, these variations may require a link margin for a given service (voice, data, fax, etc.) to be excessive to cope with the shadowing losses of a particular service area (urban, rural, mountainous, etc.).

It is generally not possible to obtain a minimum noise figure and a maximum gain in the same design, this would only be possible if $\Gamma_{opt} = \Gamma_{in}^*$. Therefore, a compromise between the two may be reached by plotting both the constant gain circles and the constant noise figure circles on the input chart and selecting Γ_S to obtain an acceptable trade-off.

IV. Oscillator Design

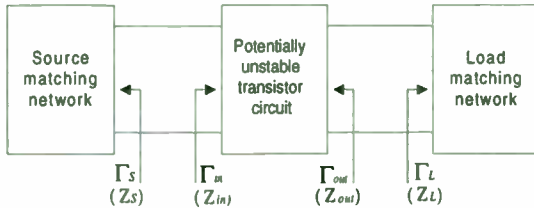


Figure 7. Two-port transistor oscillator model

The same S parameters used in the design of a two-port amplifier may be applied to the design of a two-port oscillator. One principal difference, however, is that the oscillator ports are passively terminated such that the biased transistor circuit is operating in an unstable region. This implies that the unmatched device should be potentially unstable (i.e. $K < 1$ or $|\Delta| > 1$) to function in an oscillator circuit.

To be consistent, the same reflection coefficient notation will be used for the oscillator design as for the amplifier design. Referring to the oscillator block diagram in Figure 7, further necessary conditions for oscillation can be expressed as

$$\Gamma_{in} \Gamma_S = 1 \quad (19)$$

and
$$\Gamma_{out} \Gamma_L = 1. \quad (20)$$

It can be shown [3] that if (19) is satisfied then (20) will also be satisfied, and vice versa.

If an active device is potentially unstable, the following steps will outline the procedure to meet the conditions given in equations (19) and (20).

- 1) Select Γ_S at any point in the unstable region indicated by the stability circle on the input Smith chart.
- 2) Calculate Γ_{out} as given in equation (18)
- 3) Γ_L may then be located from equation (20) as

$$\Gamma_L = \frac{1}{\Gamma_{out}}.$$

- 4) Determine the matching networks associated with Γ_S and Γ_L .

For completeness, the design for calculating Γ_S from a selected Γ_L is given.

- 1) Select Γ_L at any point in the unstable region indicated by the stability circle on the output Smith chart.

- 2) Calculate Γ_{in} as given in equation (17)

- 3) The location of Γ_S from equation (19) is

$$\Gamma_S = \frac{1}{\Gamma_{in}}.$$

- 4) Determine the matching networks associated with Γ_S and Γ_L .

V. Computer Aided Design Summary

The input to the CAD system consists of the operating frequency, the four small signal S parameters, the system resistance, and the noise figure parameters. The opening screen displays two Smith charts representing the Γ_S and Γ_L planes (i.e. the input and output charts, respectively). However, each chart may also be displayed individually in a larger scale if desired. If the S parameters indicate potential instability, the input and output stability circles will automatically be plotted.

From 'pull-down' menus the user is then able to plot constant gain circles in both the Γ_S and Γ_L planes. In addition, constant noise figure circles may be added to the Γ_S plane. A user based iterative optimization routine may then be used to design the hardware requirements for the matching network.

The optimization routine allows the user to continuously move a pointer around the computer generated image of the Smith chart. This permits selection of a position for the reflection coefficient that meets the requirements for a specified design. On this same Smith chart may be displayed the stability circle, constant gain circles, or constant noise figure circles. As the reflection coefficient is being determined, the possible networks to achieve the match for the port of interest are displayed. This method provides the user with immediate information on stability, gain, noise figure, and component values. Sample screens of the computerized Smith chart are shown in Figures 8, 9, 10, and 11.

REFERENCES

- [1] G. Gonzales, *Microwave Transistor Amplifiers Analysis and Design*, Prentice-Hall, Englewood Cliffs, NJ, 1984.
- [2] D.M. Pozar, *Microwave Engineering*, Addison-Wesley, Reading, Mass, 1990.

The result of increasing shadow loss, rain attenuation, or flat frequency fading is equivalent to decreasing the instantaneous signal-to-noise ratio. As the losses become significant, detection errors occur in clusters commonly called burst errors. In this case, burst errors occur when the symbol rate is too high for the instantaneous signal-to-noise ratio. As a result, an outage occurs because the energy per symbol is too low. Note that the bit error rate is not always equal to the symbol error rate this depends on the number of modulation levels. One way to increase the energy per symbol is to raise the transmitter power. However, this may not be possible for a hand-held radio due to its limited battery power. On the other hand, raising the up-link transmission power of a fixed base station is not a problem. It is a practical way to reduce outage times due to rainfall [2].

Also, one can raise the energy per symbol by lowering the symbol rate. Since the energy per symbol is equal to the received signal power divided by the symbol rate, we can double the energy per symbol simply by halving the symbol rate. This suggests the possibility of adaptive symbol rate schemes that operate at higher data rates when the signal-to-noise ratio is high, and at lower data rates when the signal-to-noise ratio is low. Another way to overcome shadowing losses is to employ simple error control techniques that cope with short fade durations. Often satellite systems offering packet data communications overcome the occasional shadow outage by using error detection followed by retransmission.

CDMA

To resist multipath fading and allow users to communicate simultaneously over a single channel, designers are considering spread spectrum schemes. The favored scheme uses code division multiple access (CDMA) with direct spread modulation bandwidths ranging from 1 to 20 MHz. Direct spread modulation multiplies the data sequence by a pseudo random bit sequence that spreads the information far beyond the information bandwidth. By employing unique pseudo random bit sequences many CDMA users are able to transmit on the same frequency simultaneously and each user receives its information by recognizing its unique sequence pattern.

The CDMA receiver is able to synchronize to one of the multiple signal paths. As long as the remaining signal paths are delayed by more than the chip duration from the synchronization path. The despreading process will greatly attenuate the remaining signal paths. To illustrate, consider a CDMA system using a chip rate of 5 Mc/s, the chip duration is 200 ns, and therefore multipaths that differ by 200 feet or less create overlapping chips. This would normally result in loss of synchronization unless the chip rate is increased until the differential path delay is one or more chip lengths. The remaining multipath signals are treated as uncorrelated interference signals whose signal power is reduced by the process gain of the system.

[5] M. Vai and S. Prasad, "Computer-Aided Microwave Circuit Analysis by a Computerized Numerical Smith Chart", *IEEE Microwave and Guided Wave Letters*, vol. 2, No. 7, July 1992.

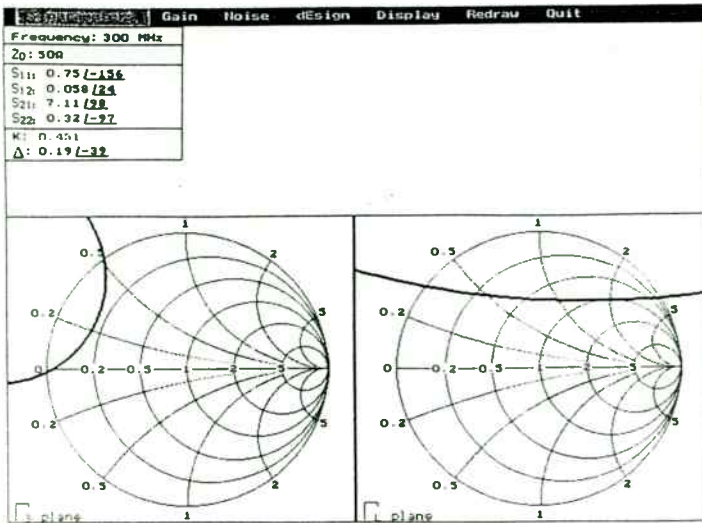


Figure 8. Stability circles

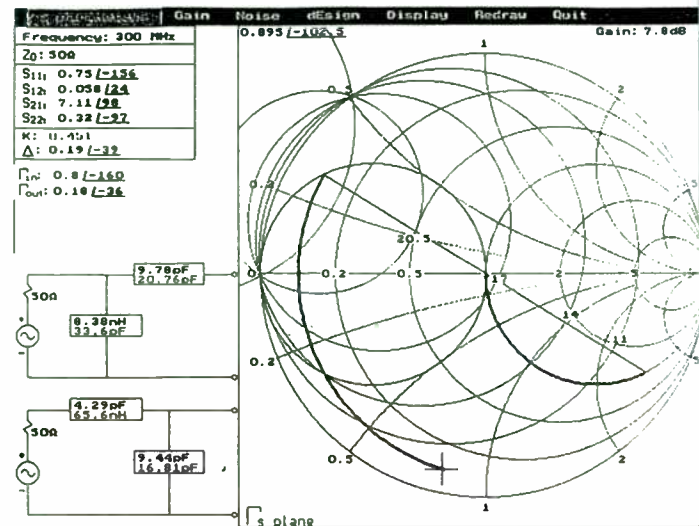


Figure 10. Input matching network menu

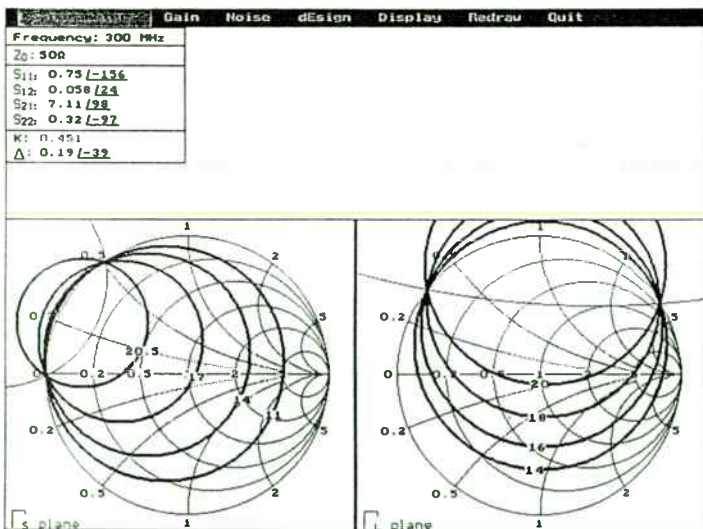


Figure 9. Constant gain circles

[3] G.D. Vendelin, *Design of Amplifiers and Oscillators by the S-parameter Method*, App. A, Wiley-Interscience, NY, 1982.

[4] D. Woods, "Reappraisal of the Unconditional Stability Criteria for Active 2-Port Networks in terms of S-parameters," *IEEE Transactions on Circuits and Systems*, February 1976.

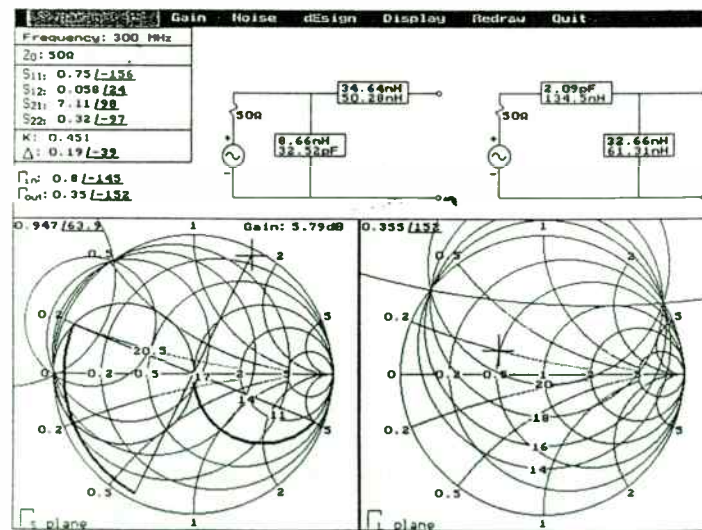


Figure 11. Input/Output matching network menu

Recent urban propagation studies report fade bandwidths of 3 to 15 MHz [3,4], those CDMA systems employing spread bandwidths that are less than the reported fade bandwidths may also expect synchronization problems during deep fades. In this case, the synchronization path is likely to drop to power levels comparable to that of the multipath signals, giving rise to Rayleigh fading. As a result, the despreading scheme decrease the total signal power considerably, creating loss of synchronization leading to an outage time.

Mobile satellite systems are developing in many directions. Besides CDMA schemes, there are the traditional radio transmission schemes. Among these schemes are frequency division multiple access (FDMA), time division multiple access (TDMA), and hybrids of these schemes. Gains in the art of low cost satellite design allow system planners to move away from expensive large geostationary satellites toward medium-sized multiple low Earth orbiting satellite systems.

DERIVATION OF THE RICE-NAKAGAMI DISTRIBUTION

What follows is the derivation of the Rice-Nakagami multipath envelope distribution. We assume the transmitted signal is unmodulated this will simplify the analysis. The direct path component is represented by

$$E_i(t) = A \cos[(\omega_c + \omega_d)t]$$

and the specular path component by

$$E_s(t) = B * \cos[(\omega_c + \omega_d)t + \theta]$$

Where ω_c is the angular carrier frequency, ω_d is the angular doppler frequency shift, and θ is some arbitrary phase.

Using the trigonometric identity

$$\cos(W + Z) = \cos W * \cos Z - \sin W * \sin Z$$

We can define $X(t)$ and $Y(t)$ as the sum of the in-phase and quadrature phase components of the direct and specular signal, respectively. Hence

$$X(t) = A * \cos(\omega_d * t) + B * \cos(\omega_d * t + \theta)$$

and

$$Y(t) = A * \sin(\omega_d * t) + B * \sin(\omega_d * t + \theta)$$

then

$$m(t) = X(t) * \cos(\omega_c * t) - Y(t) * \sin(\omega_c * t)$$

SAW RESONATOR OSCILLATOR DESIGN USING LINEAR RF SIMULATION

Alan R. Northam
RF Monolithics, Inc.
4441 Sigma Road
Dallas, Texas 75244

The RF design engineer faces two basic problems when designing a Surface Acoustic Wave (SAW) Oscillator. The first problem the designer faces is how to properly model the SAW oscillator utilizing Computer Aided Design (CAD) software. The second problem is how to model and connect the SAW resonator in an oscillator circuit. This paper discusses the four ways the SAW resonator can be connected in an oscillator, and which configuration is the most appropriate to use. This paper also demonstrates that linear RF simulation is a very close approximation to the actual oscillator performance.

There are many design topologies in which oscillators can be configured. Among the most popular topologies are the Pierce, Colpitts, and Clapp. Each of these topologies have their advantages and disadvantages. It is not the intent of this paper to go into a discussion of each of these oscillator topologies. The purpose of this paper is to illustrate the four ways of configuring a two-port SAW resonator, to present the electrical differences between them, and then to determine the proper SAW configuration to be utilized given a certain oscillator type.

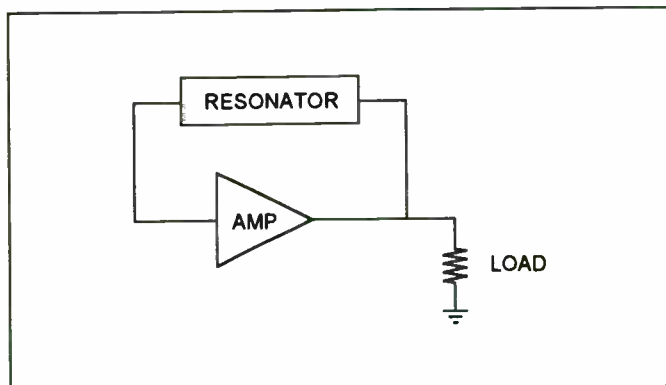


Figure 1. Pierce Oscillator

BASIC OSCILLATOR CIRCUIT

A simplified block diagram of a Pierce Oscillator is illustrated in figure 1. The basic oscillator loop consists of three basic elements: 1) An amplifier, 2) a feedback path and 3.) a load. The amplifier can be either of a discrete design, such as a transistor or FET, or it can be of a hybrid design, such as an Monolithic Microwave Integrated Circuit (MMIC). The feedback path typically contains a frequency selective network such as an LC resonant circuit, a crystal or, in the case of a

SAW oscillator, a surface acoustic wave resonator. The load can either be a resistor or a complex impedance, such as the input of a following amplifier stage.

The basic criteria for oscillation in an oscillator are that: 1) the open loop gain must be greater than the losses around the oscillator loop and 2) the phase shift around the oscillator loop must be either 0 or 360 degrees.

In a typical oscillator, the amplifier starts off in its linear gain region, but as oscillation builds up the amplifier goes into its non-linear region as it goes into compression. The amount by which the amplifier goes into compression is a function of the loss in the oscillator feedback loop. As a minimum, the loss in the feedback loop is controlled by the loss of the SAW resonator, and the loss due to splitting the RF signal coming out of the amplifier into two paths, one path being the feedback loop, and the other path going to the Load. Additional loss can be established utilizing resistive pads, mismatch loss or lower gain transistors or MMIC amplifiers.

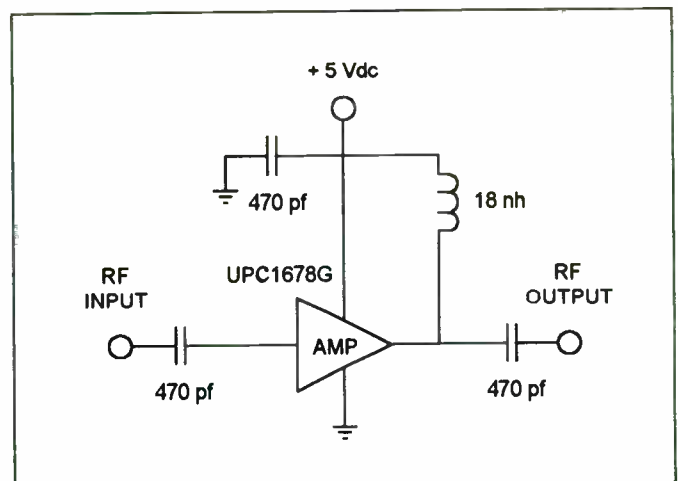


Figure 2. Amplifier Circuit

THE AMPLIFIER

The oscillator design example, as shown in figure 12, utilizes a MMIC amplifier. The amplifier circuit is shown in figure 2. The amplifier uses an NEC UPC1678G MMIC which has a fixed linear gain of 23 dB. The amplifier has a flat gain response with a 3 dB roll-off point of 1.9 GHz. The power supply voltage (Vcc) equals 5 volts dc and the bias current is 50 milliamps. The coil is used as an RF choke as well as a

Likewise, the diffused in-phase and quadrature signal components can be represented by

$$I(t) = \text{SUM} \{ A_k * \cos(\omega d * t + P_k) \} \text{ for } k=1 \text{ to } N$$

and

$$Q(t) = \text{SUM} \{ A_k * \sin(\omega d * t + P_k) \} \text{ for } k=1 \text{ to } N$$

By the central limit theorem the I(t) and Q(t) components are approximately independent Gaussian random variables, with the approximation becoming more accurate as the N gets large.

$$S(t) = I(t) * \cos(\omega c * t) - Q(t) * \sin(\omega c * t)$$

Where P_k are fixed random phases uniformly distributed from 0 to 2π and S(t) is Gaussian, and the envelope

$$R = [I(t)^2 + Q(t)^2]^{0.5}$$

has a Rayleigh distribution,

$$p_R(r) = (r / \text{var}) * \exp [- r^2 / (2 * \text{var})]$$

Define new parameters (drop the time variable)

$$x = X + I \quad \text{and} \quad y = Y + Q$$

Therefore

$$r^2 = x^2 + y^2$$

$$z = \tan^{-1} (y / x)$$

Since I and Q are Gaussian, zero mean with variance $\text{var} = Q^2$, and uncorrelated, x and y are Gaussian and independent. Thus,

$$p(x,y) = \frac{1}{2 \pi \text{var}} \exp \frac{- [(x - X)^2 + (y - Y)^2]}{2 \text{var}}$$

path to provide high dc current to the output stage of the MMIC amplifier. This coil could also be used to match the output of the MMIC to a real impedance if desired. The input and output capacitors are used to block dc. The capacitor connected between the coil and ground is used to return the RF currents in the coil to ground.

Figure 3 is a graph of the MMIC amplifier gain. The theoretical transmission gain curve was plotted utilizing the scattering parameters generated for the amplifier design utilizing a linear RF simulator. The MMIC amplifier scattering parameters used in the simulation were those typically supplied by the manufacturer. The second curve is measured amplifier gain. Notice that the measured gain curve is virtually the same as the calculated gain curve and is approximately 17 dB. The third curve is measured gain with the amplifier 6 dB into compression. It is in this compressed condition that the amplifier will operate when the oscillator loop reaches equilibrium. The compressed gain of the amplifier is approximately 17 dB (23 dB - 6 dB = 17 dB).

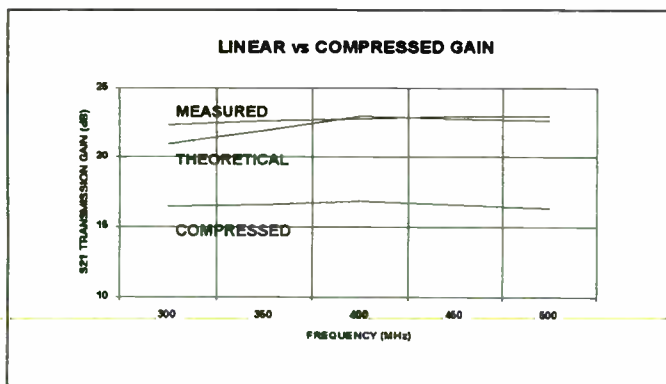


Figure 3. Amplifier Gain Response

In looking at the graph in figure 3, it is apparent that linear simulation of the amplifier is all that is needed to analyze the gain requirement of the oscillator. The designer can then easily determine the linear gain, using published scattering parameters and then offset the calculated gain by 6 dB to arrive at the compressed power gain. Using this approach to determining compressed gain can however lead to some error and the designer must determine if he or she wishes to accept that possibility. Notice, for example, that the measured linear gain and the theoretical gain deviate by about 2 dB at 300 MHz. Calculating compressed gain from the theoretical gain curve would lead to a 2 dB error or 15 dB (21 dB - 6 dB = 15 dB) versus the actual 17 dB (23 dB - 6 dB = 17 dB). The compressed gain curve in figure 3 was not generated by making such an assumption, it was generated using measured scattering parameters while maintaining the amplifier 6 dB in compression over a wide frequency range. Once these scattering parameters are measured they can then be used to design amplifiers over the entire frequency range characterized. When making these measurements it is desirable to also characterize the amplifier over a range of differing amounts of compression.

In looking at the amplifier phase plots in figure 4 notice that the difference in the calculated (theoretical) phase obtained from the published scattering parameters and the phase of the amplifier in compression is quite large: 50 degrees at the low frequency end and 30 degrees at the high frequency end of the graph. It is not possible to assume this phase offset by observation like it was in the case of the compressed amplifier gain of the MMIC. To determine the phase response of an amplifier in compression it becomes necessary to measure its phase response, or to utilize non-linear RF simulation software and an accurate model of the active device. Non-linear CAD software is expensive and in some cases is unnecessary in the design of RF circuits. Simple RF amplifier circuits involving one non-linear active device is such a case.

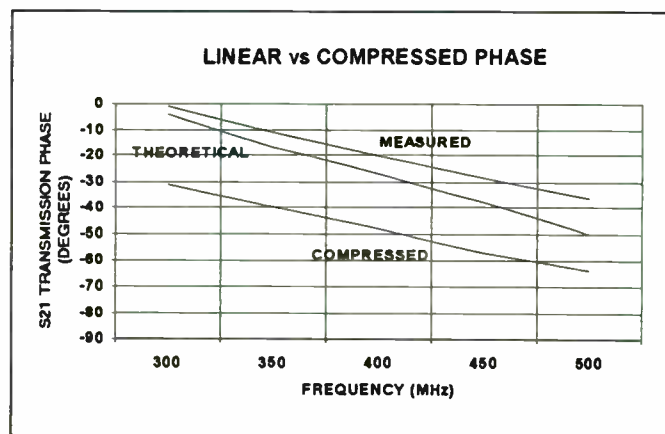


Figure 4. Amplifier Phase Response

While making phase measurements of the amplifier in compression, the designer should go ahead and measure all four scattering parameters. Once the compressed amplifier scattering parameters are measured it is then possible to determine not only the transmission gain and phase of the amplifier but also its input and output impedance. The compressed amplifier gain, phase, and matched input and output impedance, are the conditions under which the oscillator will exhibit proper loop gain and loop phase.

It is also under these conditions that the SAW resonator will be properly matched so as not to distort its passband characteristics. The amplifier's compressed input and output impedance is plotted on the graphs of figure 5 and 6 respectively.

The key to utilizing linear RF simulation involving non-linear devices is to characterize them under the conditions they will be used in the circuit. In the case of a transistor or MMIC used in an oscillator, the designer must measure its scattering parameters over, 1) the frequency range of interest, and 2) over a range of differing compression levels. These scattering parameters can then be used to design the amplifier stage used in an oscillator. The rest of the oscillator loop circuitry is easily designed using linear RF simulation as it is typically composed of linear network elements.

At baseband doppler is zeroed, therefore X is the length of the fixed coherent vector and Y is zero. From the Jacobian technique of transformation of variables, the joint probability density of the envelope and phase is given by

$$p_{x,y}(x,y) \iff p(r,z) = r * p_{x,y} (r * \cos z, r * \sin z)$$

$$p(r,z) = \frac{r}{2 \pi \text{ var}} \exp \frac{- [(r * \cos z - X)^2 + (r * \sin z)^2]}{2 \text{ var}}$$

Simplify using the trigonometric identity $[(\sin z)^2 + (\cos z)^2 = 1]$

$$p(r,z) = r / (2 * \pi * \text{ var}) * \exp \{ [-(r^2 + X^2) + (2 * r * X \cos z)] / (2 * \text{ var}) \}.$$

$$p(r,z) = \frac{r}{2 \pi \text{ var}} \exp \frac{- (r^2 + X^2 + Y^2) + (2 * r * X * \cos z)}{2 \text{ var}}$$

The probability density of the envelope is found by integrating out the phase variable

$$p(r) = \int p(r,z) dz$$

$$p(r) = \frac{r}{\text{ var}} \exp \frac{- (r^2 + X^2)}{2 \text{ var}} * \frac{1}{(2 \pi)} \int \exp [(r * X / \text{ var}) * \cos z] dz$$

We can express the integral by means of a Bessel function;

$$I_0(k) = 1 / (2 * \pi) \int \exp (k * \cos z) dz$$

$$= 1 / (2 * \pi) \int \exp (r * X / \text{ var}) * \cos z dz.$$

Where $I_0(k)$ is the modified Bessel of order zero. At last we get the Rice-Nakagami density, which describes the summation of a strong specular signal and weaker multipath signals

$$p(r) = (r / \text{ var}) * \exp [-(r^2 + X^2) / 2 * \text{ var}] * I_0 (r * X / \text{ var})$$

$$\text{for } r \geq 0 \quad \text{and} \quad 0 \leq z \leq 2 * \pi.$$

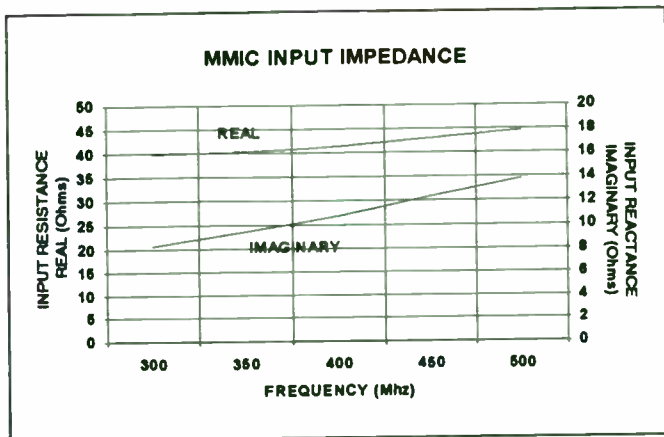


Figure 5. Compressed Amplifier Input Impedance

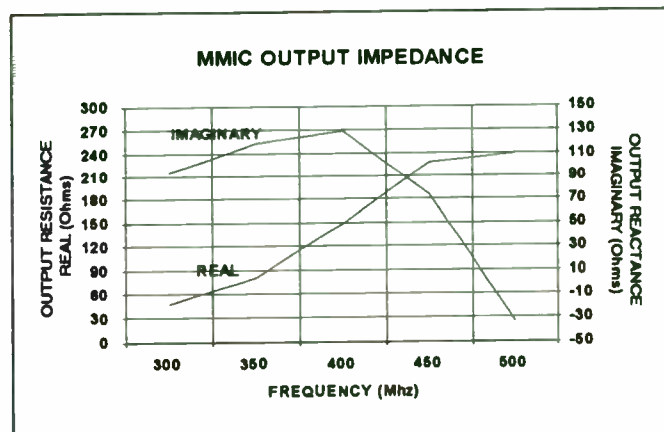


Figure 6 Compressed Amplifier Output Impedance

THE TWO-PORT SAW RESONATOR

The feedback path of the oscillator loop contains a frequency selective resonator network as shown in figure 1. In the case of a SAW oscillator this resonator is a SAW resonator. The SAW resonator is equivalent to a series LC network with a very high Q: a Q of 5000 or more is typical. The electrical model of a typical two-port SAW resonator is as shown in section (a) of figure 7.

The two-port SAW resonator can be connected in four different configurations as shown in figure 7. Section (a) of figure 7 shows the two-port SAW resonator connected such that its transmission phase is typically 180 degrees at its resonate frequency. The same two-port SAW resonator can also be connected such that its transmission phase at resonance is zero degrees. This is shown in section (b) of figure 7. The only difference between the SAW resonator having a transmission phase of zero degrees or 180 degrees is the selection of which output port terminal is grounded. From the electrical equivalent circuit shown in section (a) and (b), the proper transformer secondary winding is selected to set the transmission phase of the RF signal. The series LCR network represents the emotional inductance, capacitance, and the loss of the SAW resonator. The shunt capacitors represent the interdigital capacitance of the SAW structure. It is this capacitance that makes the SAW resonator input and

output impedance capacitive even though the series LC network is at resonance. It is also this capacitance that keeps the resonators transmission phase from being either zero degrees or 180 degrees. These interdigital capacitances are quite often tuned out by resonating them with inductors to return the SAW resonator transmission phase back to either zero or 180 degrees. Tuning out the interdigital capacitance

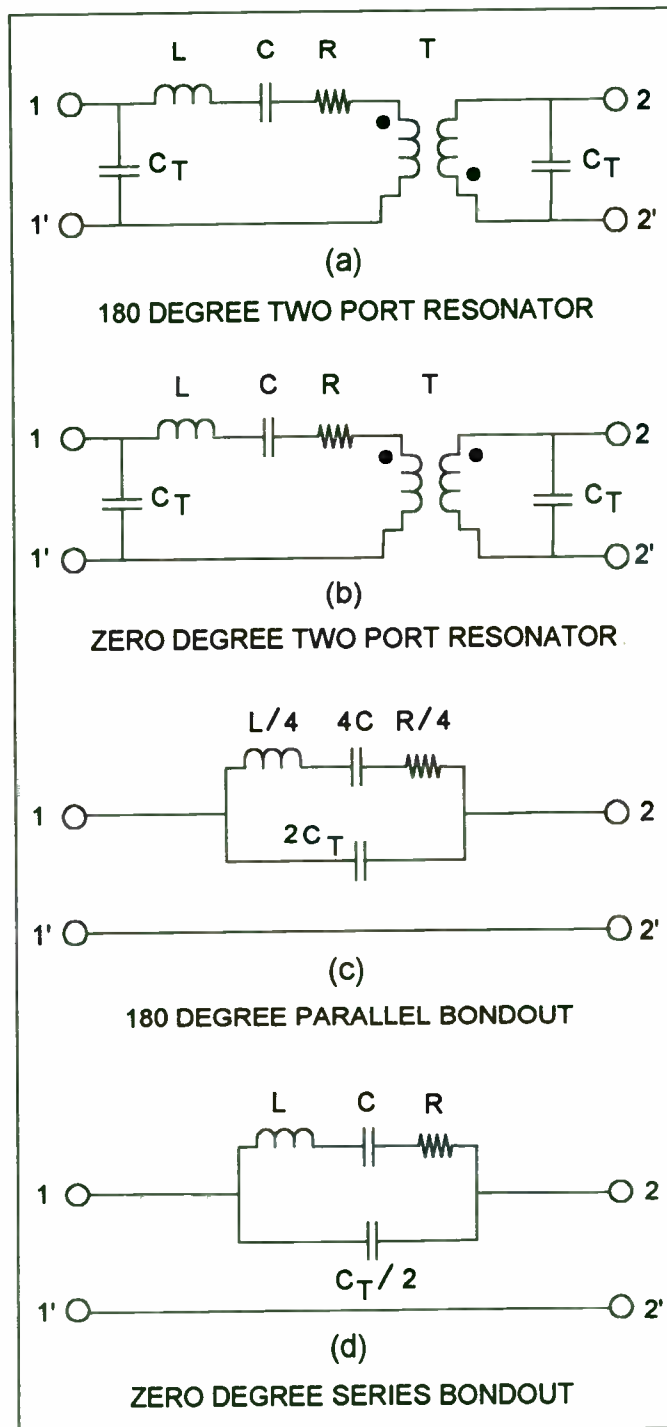


Figure 7. Two-Port SAW Resonator Equivalent Circuit

using series inductors will have the effect of reducing loss through the resonator at the expense of increasing its bandwidth, thereby decreasing its Q. Tuning out the interdigital capacitance using shunt inductors will not

We can include the contribution of additive white Gaussian noise (AWGN) to the quadrature Gaussian terms of the diffuse component together with the specular and direct component to form

$$p(r) = \frac{r}{V_n^2 + E_{rms}^2} \exp \left[\frac{-(r^2 + E_s^2)}{2(V_n^2 + E_{rms}^2)} \right] I_0 \left[\frac{E_s * r}{V_n^2 + E_{rms}^2} \right]$$

Where r is the instantaneous peak envelope voltage, V_n^2 is the variance (average power) of the AWGN, $(E_s^2)/2$ is the average power in the specular signal, and E_{rms}^2 is the average power in the in-phase or quadrature components of the diffuse multipath. The total average received signal power is $[E_{rms}^2 + (E_s^2) / 2]$.

The probability that the envelope of the received signal exceeds a defined value, s , is given by

$$P(r \geq s) = \int_s^{\infty} p(r) dr$$

If the dominate signal level $(E_s^2)/2$ drops to power levels comparable to that of the multipath signals, then Rayleigh fading occurs.

degrade the loss through the resonator nor degrade bandwidth or Q. This results in the network impedance being real at the resonant frequency and is typically in the 50 ohm region for the series tuned inductor configuration, and in the 300 ohm region for the shunt inductor configuration.

The two-port SAW resonator can also be connected as shown in section (c) of figure 7. This configuration is created by taking the 180 degree SAW resonator connected as shown in section (a) of figure 7 and folding it in half, connecting terminal 1 to terminal 2 and terminal 1' to terminal 2'. The connection of terminal 1 to terminal 2 becomes terminal 1 of section (c), and the connection of terminal 1' to terminal 2' becomes terminal 2 of section (c). The return path, terminal 1' and terminal 2' of section (c) was added. This then connects the two interdigital capacitances C_T in parallel. Note in section (c) that the interdigital capacitance C_T is now twice the value or $2C_T$. Also notice that due to the transformer action the emotional inductance and the resistive loss is divided by four, and the emotional capacitance is multiplied by four.

The two-port SAW resonator can also be connected as shown in section (d) of figure 7. This configuration is created by taking the zero degree SAW resonator connected as shown in section (b) of figure 7 and connecting the input port in series with the output port. This is accomplished by connecting terminal 1' to terminal 2. Terminal 1 of section (b) remains unchanged and becomes also terminal 1 of section (d). Terminal 2' of section (b) now becomes terminal 2 of section (d). The connection of terminal 1' to terminal 2 of section (b) is an interstage connection in section (d) and is not shown in section (d). The return path, terminal 1' and terminal 2' of section (c) was added. This then connects the two interdigital capacitances C_T in series. Note in section (d) that the interdigital capacitance C_T is now half the value or $C_T/2$. Note that, due to the transformer action, the emotional inductance, capacitance and the resistive loss are not effected.

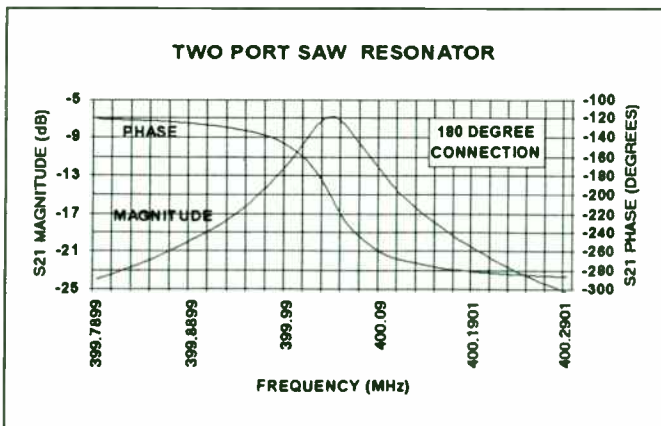


Figure 8. Two-Port Saw Resonator

The frequency and phase response of the two-port resonator connected as per section (a) of figure 7 is shown in the graph in figure 8. This graph was plotted from measured scattering parameters. Notice that the 3 dB bandwidth is approximately

60 kHz and the center frequency is 400.03 MHz. Calculating Q we find it to equal 6667 ($400.03 \text{ MHz} / 60 \text{ KHz} = 6667$). Also notice that the phase is approximately -200 degrees. Resonating out the interdigital capacitances with an inductor connected in parallel on both the input and output of the SAW resonator would bring the phase back to -180 degrees. (Series inductors will decrease Q and broaden bandwidth.) The SAW resonator has approximately 7 dB of loss and the phase change across the 3 dB bandwidth is approximately 90 degrees.

The input and output impedance's of the two-port resonator connected as per section (a) of figure 7 are shown in the graph in figure 9. This graph was plotted from measured scattering parameters. Notice that at the resonant frequency of the SAW resonator the reactance is at its minimum value and increases rapidly after passing through resonance. Also notice that the resistance of the resonator is close to 100 ohms and also increases rapidly after passing through resonance. By tuning out the interdigital capacitance of the SAW resonator with an inductor will reduce the input and output reactance to zero ohms, leaving the input and output impedance under this tuned condition real and approximately 100 ohms if series inductors are used and 300 ohms if shunt inductors are used.

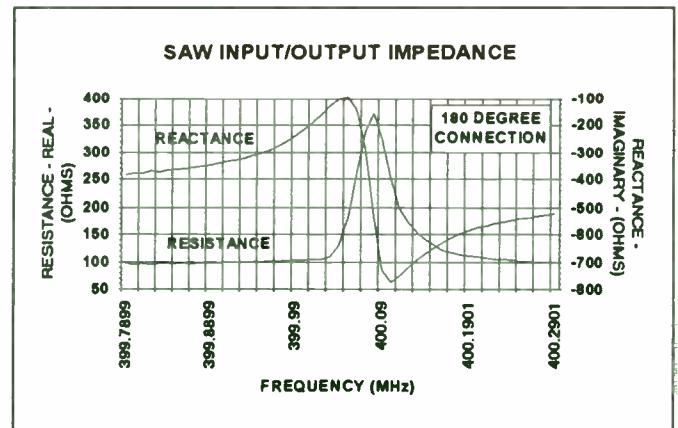


Figure 9. Two-Port Resonator Input / Output Impedance

The two-port SAW resonator connected as shown in section (b) and (d) of figure 7 yields virtually the same magnitude and phase response as shown in figure 8 and 9 and will not be discussed. The only difference is that the transmission phase is close to zero degrees at resonance for both the (b) and (d) connections provided the interdigital capacitances are tuned out. Notice that only a single inductor connected from terminal 1 to terminal 2 in section (d) of figure 7 is needed to tune out the interdigital capacitance. Tuning out the interdigital capacitance of section (d) does not effect bandwidth of loss.

When the same two-port SAW resonator is connected, as shown in section (c) of figure 7, the resonator exhibits lower loss and broader bandwidth. The lower loss is expected because its loss being divided by four, $R/4$. However the increased bandwidth may not have been expected by the

References

1. CCIR report 236-5, "Influence of Terrain Irregularities and Vegetation on Tropospheric Propagation," Vol. V, 1982.
2. N. Lay, K. Dessoucky, "A Communication Protocol for Mobile Satellite Systems Affected by Rain Attenuation," IEEE J. Select. Areas Commun., Vol. 10, No. 6, August 1992.
3. L. Milstein, D. Schilling, R. Pickholtz, et al., "On the Feasibility of a CDMA Overlay for Personal Communications Networks," IEEE J. Select. Areas Commun., Vol. 10, No. 4, May 1992.
4. D. Schilling, L. Milstein, R. Pickholtz, et al., "Field Test Experiments Using Broadband Code Division Multiple Access," IEEE Commun. Mag., pp 86-93, Nov. 1991.

Recommended Reading

1. C. Loo, "Digital Transmission Through a Land Mobile Satellite Channel," IEEE Trans. Commun., Vol. 38, No. 5, May 1990.
2. CCIR report 236-6 "Ionospheric Effects Upon Earth-Space Propagation," Vol. VI, 1986.
3. P. J. Crepeau, "Uncoded and Coded Performance of MFSK and DPSK in Nakagami Fading Channels," IEEE Trans. Commun., Vol. 40, No. 3, May 1992.

Acknowledgments:

The author would like to thank Dr. David Smith and Dr. Syed Ali at Defense Information Systems Agency, and Harvey Rubinstein at Defense Systems Inc. for their many helpful suggestions.

casual observer. Increased bandwidth occurs because the 50 ohm source and load impedance environment remained constant while the resistive loss R of the resonator was reduced by a factor of four. Had the 50 ohm source and load environment changed proportionally the bandwidth of the resonator would have remained unchanged.

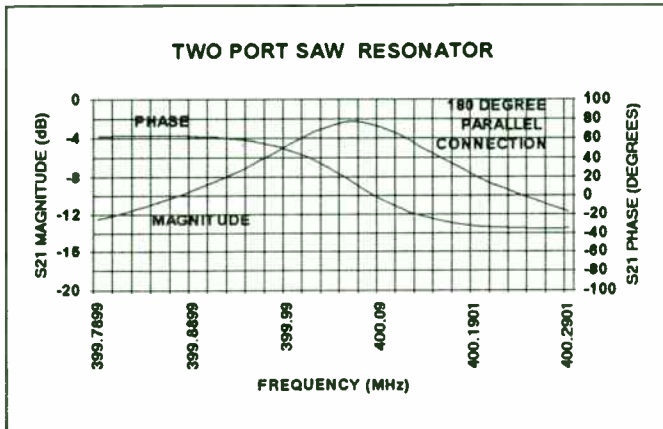


Figure 10. Two-Port SAW Resonator (Section C of Figure 7)

Figure 10 is a plot of the magnitude and phase of the two-port resonator connected as shown in section (c) of figure 7. Notice that the loss has dropped to 2 dB and the bandwidth has increased to 170 kHz. Calculating Q yields a Q of 2353. Notice that the phase slope has become more shallow while still exhibiting approximately 90 degrees across the 3 dB bandwidth.

Decreased Q equates to less stability in an oscillator. Although a Q of 2353 is still quite high and the oscillator will still appear to be quite stable, in a high stability oscillator design connection (c) of figure 7 would not be the best choice.

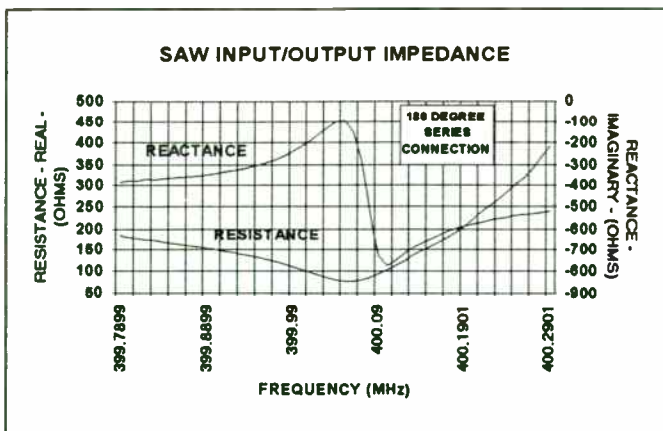


Figure 11. Two-Port SAW Resonator (Section C of Figure 7)

The input and output impedance for the Two-Port SAW Resonator connected per section (c) of figure 7 is plotted in the graph in figure 11. Notice that at resonance the real resistance is closer to 50 ohms than any of the other three connections, hence its lower loss. Notice also that the capacitive reactance curve has a similar shape to the other three connections and is again at a minimum at resonance.

From the four different ways of connecting a two port resonator, three of the configurations yield the same magnitude response, section (a), section (b), and section (d). A SAW resonator connected as in section (c) of figure 7 offers lower loss but at the cost of increased bandwidth. A SAW resonator connected as shown in section (b), section (c), and section (d) of figure 7, has a transmission phase of zero degrees at the resonant frequency and exhibits 90 degrees of phase shift across its 3 dB bandwidth. The SAW resonator connected as per section (c) exhibits a more shallow phase slope than the other two connections due to its wider bandwidth. A SAW resonator connected as shown in section (a) is the only configuration that offers -180 degrees of transmission phase at resonance.

Deciding on which SAW resonator configuration to use comes down to basically two choices: 1) A SAW resonator connected as per section (a), if the phase shift through the SAW resonator need be -180 degrees to satisfy the oscillator loop phase requirement, and 2) The SAW resonator connected as per section (d), if the phase shift through the SAW resonator need be zero degrees to satisfy loop phase requirements. The SAW resonator connected as per section (b) could be used instead of section (d) but would require two inductors to resonate out the interdigital capacitances, whereas connected as per section (d) requires only one inductor. From a printed circuit board real estate and a cost viewpoint the connection shown in section (d) of figure 7 is most likely the better choice. The configuration of section (c) would be a good choice if lower loss were required, or broader bandwidth to speed up turn-on time. Another application of the configuration of section (c) would be for voltage controlled oscillators where broader frequency tuning is required.

OSCILLATOR DESIGN EXAMPLE

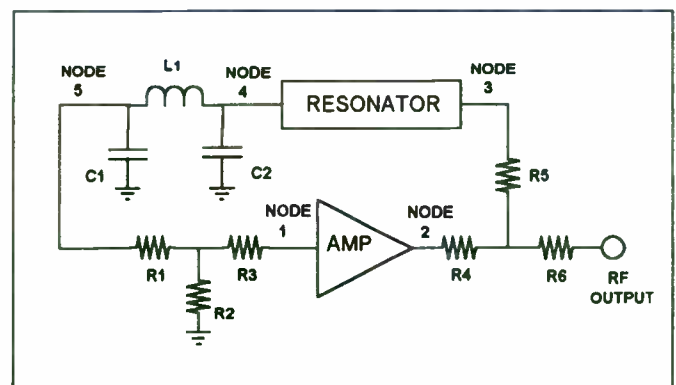


Figure 12. 400 MHz Fixed Tuned Oscillator

The oscillator design example is shown in block diagram form in figure 12. The amplifier circuit is shown in further detail in figure 2. A 6 dB resistive power splitter made up of R4, R5, and R6 is connected to the amplifier output. One output of this divider is connected to the RF output while the other output is connected to the feedback path. The resonator is a two-port SAW resonator configured for the proper

A New Variable Rate Vocoder for Wireless Communication and Voice Storage Applications

by

Steven A. Morley
Vice President

QUALCOMM Incorporated
San Diego, CA 92121 USA

Introduction

Since the invention of the telephone more than a century ago engineers have sought to increase the number of voice channels that can be transmitted over bandwidth-limited electronic media. This includes both "wired" and "wireless" transmission systems. Recently, this quest has also led designers to find more efficient methods for storing voice signals for applications such as voice mail systems.

A key aspect of efficient digital voice transmission or storage is the use of a suitable voice digitizing system that reduces the data rate required to send or store voice signals. Voice encoding systems can be either simple, low cost techniques which usually require higher encoding data rates. Alternatively, more sophisticated, higher cost, low data rate approaches may be used. This paper presents a new voice encoding algorithm that provides telephone quality voice encoding at low data rates. This system combines the latest in digital signal processing (DSP) algorithms, modern VLSI technology, and a unique feature: dynamically variable data rate determination.

This paper describes the motivations for the use of digital voice encoding along with the tradeoffs and considerations associated with the selection of an appropriate coding system. Example applications are presented which demonstrate the value of variable rate voice coding systems. Finally, a single-IC implementation of such a variable rate coding algorithm is described. This device is commercially available and is designed to provide high quality speech coding to applications requiring low cost and low power consumption, such as digital cellular and cordless phones, VSAT systems, voice storage systems, and "voice over data" modem systems.

Background

Since the 1960's, the Bell system has been slowly switching over to digital technology for the efficient transmission of wireline voice communications. Only in the past few years has this conversion of digital voice transmission been applied to commercial wireless communication systems. The transmission of

transmission phase. Notice that in this design example the SAW resonator's interdigital capacitance is not tuned out by resonating them with parallel or series inductors. The LC pi-network is used to set the loop phase to zero degrees. The resistive T-network is used to set the loop gain to 6 dB. The LC pi-network and or the resistive T-network may or may not be necessary depending upon frequency, the amplifier used, or how accurately the designer wishes to set loop gain and phase.

In low cost circuits the resistive pad used to set loop gain precisely and the phase setting LC network are compromised or left out completely. This decision may or may not cause problems to the performance of the oscillator. An oscillator designed without regard to setting loop phase properly will result in an oscillator running off the center frequency of the SAW resonator. Depending upon the amount of phase error, the oscillator loop gain can be reduced due to the oscillator running too far off the center frequency of the SAW resonator and the resonator acting like the bandpass filter that it really is. If loop gain is not set properly then the oscillator could have too much loop gain that it will oscillate off frequency due to the SAW resonator's other modes. In addition, too much loop gain can cause the amplifier to be overdriven, causing the output power to foldback.

The oscillator loop was modeled using a linear RF simulator. The compressed amplifier scattering parameters were input to an ASCII file of the proper format for the RF linear simulator used. The resistive power splitter was then modeled and cascaded to the amplifier output at node 2 in figure 12. A two-port network consisting of scattering parameters of a SAW resonator was also modeled and cascaded to the power splitter at node 3. A linear RF simulation analysis was then run from node 1 to node 4 to determine the overall gain and phase of the oscillator loop thus far. The result showed that the loop still had an excess of 5.5 dB of gain and that the phase was -261 degrees. The phase setting pi-network consisting of C1, L1 and C2, and the resistive T-pad network consisting of R1, R2 and R3 were then modeled and cascaded to the output of the SAW resonator node 4 of the open loop model of the oscillator loop. The linear RF simulator was then programmed to optimize for a loop gain of zero to 1 dB and loop phase of zero to 1 degrees. After the optimization was complete the closest standard values for R1, R2, R3, C1, C2 and L1 were chosen and a final simulation analysis performed. The result of the final simulation analysis of the oscillator loop yielded a loop gain of -0.6 dB and loop phase of 4.3 degrees. Installing the final component values in the oscillator should cause the oscillator to operate in the middle of its passband of the SAW resonator at 400.03 MHz (refer figure 8), and the amplifier should be 6 dB in compression.

The oscillator output power cannot be predicted using a linear RF simulator, so it becomes necessary to employ a different technique to make this prediction. The output power of the amplifier (refer to figure 2) is measured for different input

power levels applied. This data is then input to a computer application spreadsheet program and graphed as shown in figure 13. From the graph the designer can determine the output power of the oscillator. Alternately, the data can simply be graphed using graph paper. The amplifier output power should be characterized over several different frequencies across the frequency spectrum of interest. Once this full matrix of graphs is created the designer can interpolate between the frequencies graphed to determine output power at a specific frequency. With the computer applications spreadsheet program, the designer can input equations into the spreadsheet to do the interpolation. Once the spreadsheet is set-up, and all the equations entered, it can be used as a template for other amplifier circuits the designer wishes to characterize.

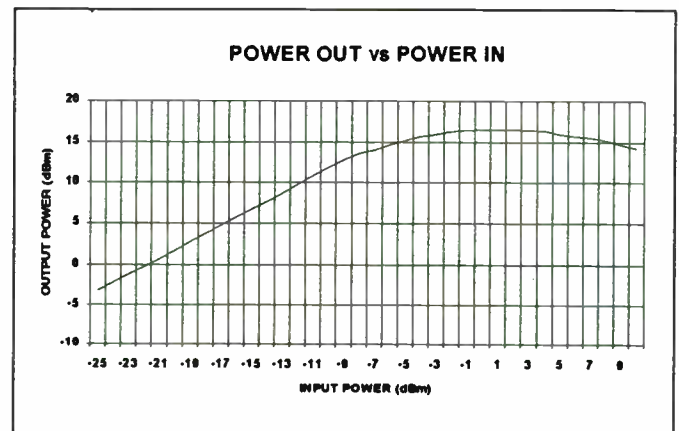


Figure 13. Amplifier Output Power vs. Input Power

From the graph of figure 13 it can be seen that the amplifier output power is at its maximum when the input power is somewhere between -3 dBm and +3 dBm, and is approximately 17 dBm. From the previous discussion of the oscillator design example, it was determined that the oscillator loop was to have a loss of 17 dB. Since the amplifier output compresses at 16 dBm the power fed back to the amplifier input will therefore be -1 dBm (17 dBm - 17 dB = 0 dBm). From the graph of figure 13, it is seen that with the input power of the amplifier at 0 dBm, the output power of the amplifier will be close to its peak at 17 dBm.

Notice that too much power applied to the input of the amplifier causes the output power to foldback thus decreasing more and more with increased input power. This is a typical phenomena of an RF amplifier being driven too hard. This phenomena is also a cause of error in predicting the output power of an amplifier when loop gain is improperly set as previously discussed.

OSCILLATOR PERFORMANCE

The oscillator design example was built using component values determined with the linear RF simulator optimizer. The oscillator's actual frequency of oscillation was 400.022 MHz, or only a 8 kHz off the center of the SAW resonator's

digitized voice signals over RF channels began with military systems. Then came satellite-based telephone systems, VSAT's and, more recently, digital cellular telephony and similar services. This extensive switchover is not yet completed, but all these systems are benefited by the inherent advantages of transmission of digital signals. These advantages include:

- 1.) The use of sophisticated channel multiplexing techniques (e.g., TDMA, FDMA, packet switching, spread spectrum technology);
- 2.) The ability to control the transmission-induced noise levels, as well as the volume of the transmitted speech through the use of digital equipment such as regenerative repeaters and forward error correction (FEC) technology;
- 3.) The ability to provide security on the voice channel through the use of digital encryption technology;
- 4.) In some cases, digitized voice transmission will actually require less channel bandwidth than the transmission of analog voice information;
- 5.) The ability to buffer and store voice information using digital storage techniques (e.g., hard disks);
- 6.) Maximal use of advanced digital signal processing (DSP) techniques combined with low cost VLSI digital integrated circuit technology.

To take maximum advantage of these characteristics of digital transmission technology, an appropriate voice coding system must be selected for a given system. Many different voice coding systems exist and provide selective features and performance to meet the requirements of any specific application. To determine the right choice for voice coding, several factors must be considered as described below.

What is "Speech Encoding"?

Speech encoding is the conversion of analog speech signals to a digital format. The goal of speech encoding is to encode and decode speech signals so that the original voice message is accurately reconstructed.

A typical "telephone quality" analog speech signal is limited to a bandwidth ranging from about 300 Hz to about 3400 Hz. For simplicity, the desired bandwidth is filtered to range from near D.C. (0 Hz) to 4 kHz. To transmit higher fidelity audio signals, such as music, higher bandwidths are required and different encoding systems are used. However, we will limit our interest to the encoding of standard speech signals with no more than a 4 kHz bandwidth.

Given a 4 kHz signal bandwidth, sampling theory states that we must sample the signal at a rate of at least twice our "bandwidth of interest"; that is, at least 8,000 samples per second. If we use a simple linear digitizing approach to our 8,000

400.03 MHz center frequency. This error is well within expectations and equates to a phase error of only 11 degrees.

phase error = frequency error * delta phase shift / bandwidth

$$11 \text{ degrees} = 8 \text{ kHz} * 90 \text{ degrees} / 65 \text{ kHz}$$

The delta phase shift term in the phase error equation refers to the change in transmission phase across the 3 dB bandwidth of the SAW resonator.

Recall that in selecting standard values, after optimizing the oscillator loop using the linear RF simulator, the final analysis showed that there would be a 4.3-degree phase error. Thus the 11 degrees of phase error determined by calculation due to the actual closed loop oscillator frequency measurement is actually only a 7 degrees from what the linear RF simulator predicted.

The oscillator output power is calculated as follows:

$$P_o = \text{Max Amplifier } P_o \text{ (dBm)} - \text{Power Splitter loss (dB)}$$

$$11 \text{ dBm} = 17 \text{ dBm} - 6 \text{ dB}$$

The oscillator performance is shown in figure 14. Notice that the output power measures to be 12 dBm and is only 1 dB different than the calculation. Some of this error is due to the accuracy of interpreting the actual amplifier output power from the graph in figure 13.

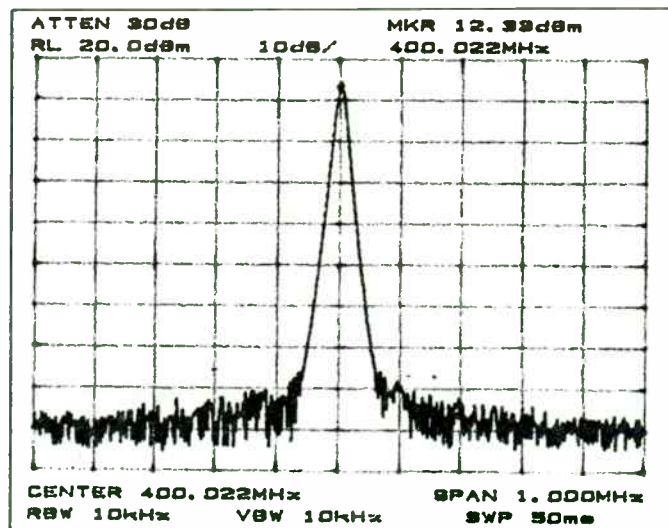


Figure 14. Actual Oscillator Performance

CONCLUSIONS

There are four different ways of connecting a SAW resonator as a two-port device. Each configuration has its advantages and disadvantages. Two of the configurations require two inductors to resonate or tune out the interdigital capacitances, while two of the configurations only require one inductor. One of the four configurations have a transmission phase of -180 degrees while the other three has an S21 transmission

phase of zero degrees. One of the configurations has reduced transmission loss but at the expense of increased bandwidth.

The SAW resonator interdigital capacitance can be tuned out by using series inductors or parallel inductors. Series inductors have the effect of reducing loss but causes bandwidth to increase, while parallel inductors do not reduce loss nor increase bandwidth.

The key to using linear RF simulation is to characterize the amplifier while in its compressed state. The designer should measure all four scattering parameters over the frequency range of interest. These scattering parameters are then used with the linear RF simulator to predict loop gain, loop phase, and input and output impedance.

Open loop linear RF simulation of the oscillator, utilizing compressed amplifier scattering parameters, accurately predicted the oscillating frequency of the oscillator. It also calculated the component values needed to meet specific performance goals, i.e. loop gain and loop phase.

Output power can also be predicted quite accurately by measuring the output power of the amplifier at various input power levels and then graphing the result. Graphs of output power versus input power should be created for various frequencies across the frequency spectrum of interest. This data can then be used to interpolate the output power expected at a particular frequency. A similar technique can also be used to predict harmonic levels.

The linear RF simulator is an appropriate tool for modeling non-linear oscillator circuits. As shown in the design example, quite accurate results can be achieved in predicting the oscillator frequency and output power. The key to its accuracy is in characterizing the amplifier over power input levels and over frequency. Once this characterization is complete the data can be used to design oscillators over a wide frequency range.

ACKNOWLEDGEMENTS

I gratefully acknowledge the efforts of Lonnie Harmon for characterizing many two-port SAW resonators and building and testing the prototype oscillator, and Christina McFarland for editing the manuscript and coordinating all the efforts necessary to make this paper possible.

REFERENCES

1. Robert J. Kansy, "Introducing the Quartz Surface Acoustic Wave Resonator," 1983 RF Monolithics Application Note No. 1 page 13.
2. Marvin E. Frerking, "Crystal Oscillator Design and Temperature Compensation," Van Nostrand Reinhold Company Inc, New York, c. 1978, page 58

sample per second signal, 12 bits are required to encode each sample to provide a full 72 dB dynamic range, which is considered adequate for normal speech signals. However, the result is a digitized transmission rate of: (8,000 samples/second x 12 bits/sample) = 96,000 bps! Assuming a transmission bandwidth efficiency of about 1 bps per Hertz of bandwidth, we see that the digitized speech would require 96 kHz of bandwidth to transmit only 4 kHz of information. This 24:1 increase in bandwidth expansion is not very efficient.

Types of Speech Encoders

So far, we have only described a basic speech "digitization" system. However, even simple speech "compression" techniques provide a much greater efficiency in our speech encoding system. A very simple compression system is called "companding". Companding takes advantage of the fact that, although the human ear can hear a wide dynamic range of signal levels, the "instantaneous" dynamic range is limited by the loudest signal input to the ear at that moment. A companding voice encoding system encodes each speech sample into a value with a limited dynamic range. However, the compander also provides a value, similar to a gain value, that determines where, within the full encoding dynamic range, that particular sample lies. Using such techniques, the required data rate for telephone quality speech signals is reduced to 64 Kbps (from 96 Kbps). Two commonly used companding techniques are called "mu-Law" and "A-Law" systems, used by the North American Bell System and the European telephone systems, respectively.

Companding is just one (simple) approach to speech encoding. Other commonly used waveform coding techniques include "adaptive delta pulse code modulation" (ADPCM), "continuously variable slope delta modulation" (CVSD), and sub-band coders. These types of waveform encoders provide good quality speech to data rates as low as 24 Kbps and can encode intelligible speech to as low as 16 Kbps.

Figure 1 shows the "universe" of speech encoding techniques. This figure illustrates the set of all signal encoders, speech encoders or otherwise, and the subset of speech specific encoders. The set of all speech encoders is further divided into "waveform encoders" and "vocoders".

Waveform coders are actually sophisticated Analog-to-Digital Converter (ADC) systems. Our previous example of the compander approach is one type of waveform coder. Waveform coders do not assume that the signal being encoded is a speech signal, but can be any type of analog signal. As a result, waveform coders are typically better at encoding non-voice signals, such as tones or music. Waveform coders also typically require simple architectures and short processing delay times. The generally simple architectures of waveform coders typically result in lower cost implementations.

However, even though waveform coders provide these advantages, the data rate required to encode speech signals to achieve good quality is typically quite a bit higher than for the alternative encoding approach, i.e., vocoding.

Embedding RF Design Tools in an IC Design System

Mojoy C. Chian, Steve S. Majors, and Alan G. Whittaker

Harris Semiconductor
Melbourne, FL 32901

Abstract -The recent introduction of IC technologies offering high frequency transistors with f_t in the vicinity of 10 GHz has opened new opportunities for higher integration of wireless communication systems. Fast silicon IC devices make possible the integration of many RF subsystems on a single die and offer a total solution to mixed frequency (low frequency and RF) and mixed signal systems. To realize this opportunity, IC design systems have to be enhanced to accommodate RF specific design tools. This paper presents a unified design environment for combined IC and RF designs. The approach taken was to enhance and modify an IC design framework, simulation engine, and data analysis tools to provide RF specific design and data representation capabilities.

I. Introduction

This decade will foster a growing and rapidly changing market segment in wireless communication products and lightwave components. The driving force behind the fast pace is the search for lower cost, smaller size, and higher performance products. However, traditional discrete based designs are unable to keep up with the pace. Discrete based designs are quickly reaching the physical limits on size, package and interconnect parasitics, and electrical performance.

RF designs are typically comprised of many individual subsystems such as low noise amplifiers, mixers, filters, and automatic gain controls. Traditionally, RF system designers have realized the individual subsystems with discrete components. With the emergence of IC processes offering transistors with an f_t around 10 GHz, silicon ASICs are offering a higher level of integration of RF designs. A system level solution, in which many RF subsystems are integrated on a single silicon die promises dramatically smaller size and in many cases higher performance.

The other major advantages of silicon ASICs over discrete designs are customizable transistors and pre-designed cell libraries. RF and low frequency microwave circuits typically require customized transistors to opti-

mize gain, minimize noise figure, and reduce distortion. Predesigned cells in an ASIC vendor's cell library can drastically reduce the overall design time of an RF system. IC foundries offering high frequency processes, variable geometry devices, predesigned cells, and a front-to-back design system will prove to be the essential ingredient for reducing the cost, size, and time-to-market for RF systems.

To realize opportunities in the new and expanding wireless market, an efficient methodology for the design of RF ASICs is needed. Reliable and accurate tools for predicting the ASIC performance before fabrication is essential, since breadboarding is not possible and refabrication is very costly. Historically, IC and RF designers have used different design goals, design methodologies, and practices [1-3]. As the boundary between IC and RF design blurs, both IC and RF designers are compelled to design in each others domain. Designers in both areas are beginning to recognize the need for a CAD system that supports the design tools of both domains. The combined system should provide a consistent design environment in which both IC and RF designers will find their familiar tools and user interface as well as the capability to easily traverse to the other environment.

This paper describes FIRST (Fastrack's Integrated RF Simulation Tools). FIRST is a set of embedded RF design tools in an IC design system aimed at the design requirements for RF designs in silicon ASICs. The following sections elaborate on the structure and capabilities of FIRST, and demonstrate its use on a production circuit.

II. System Architecture

There are two possible methodologies to combine IC and RF design systems in one environment.

Direct Integration

With direct integration of IC and RF design tools, the IC and RF design systems are merged together to form a superset system. The direct integration of the two design

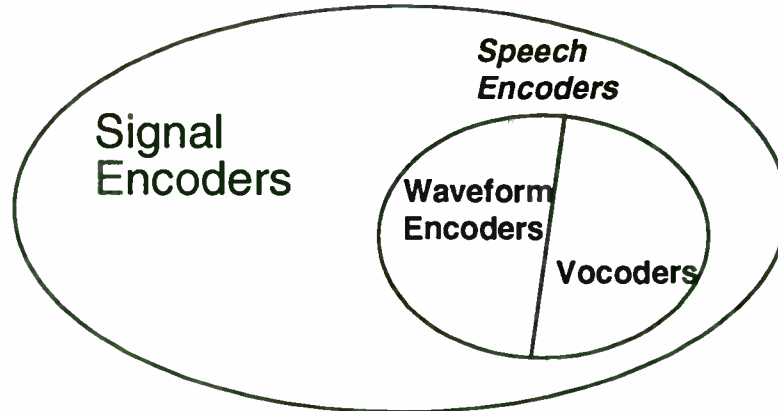


Figure 1: The Universe of Signal and Speech Encoders

Like waveform coders, vocoders convert speech signals from analog to compressed digital format and back to analog speech. However, vocoders are optimized to operate with speech signals. Vocoders assume that the signal being encoded is a human speech signal and attempt to electronically model the human speech mechanism. Because vocoding makes such assumptions about the encoded signal, the resulting data rate is typically quite a bit lower for similar quality when compared to a waveform coder system. The data rate reduction using vocoder technology can be as high as a factor of four or more when compared to a similar quality waveform coder.

Because vocoders are generally more sophisticated in their approach to speech encoding, more powerful processing is required, which results in typically more expensive implementations and longer throughput processing delays. Also, vocoders do not, in general, encode non-speech signals with the same quality as a waveform encoder. Some commonly used vocoder algorithms include "linear predictive coding" (LPC), "residual excited LPC" (RELPC), "vector sum excited LPC" (VSELPC), and "codebook excited LPC" (CELPC). Figure 2 illustrates a general comparison of data rate and speech quality for vocoder and waveform coding technology.

Selecting a Speech Encoding Technology

Given the diverse capabilities and limitations of both waveform coders and vocoders, how do designers go about selecting the right solution for their systems? There are a number of characteristics and parameters that should be included in this decision process, including:

systems may seem to be an obvious solution. Unfortunately, because of little commonality between the two systems, direct integration has proven to be impractical. The two systems typically use different frameworks, simulation engines, and data analysis routines. To further complicate the problem, the cell libraries and device models are also different. The device models (which generally are not generic Spice models) must be ported, supported and maintained in two or more different simulators. Another factor is the price. Typically IC and RF design systems are owned by different vendors, which raises the cost of the combined system.

Embedded Tool Methodology

An alternate solution is to embed RF design tools in an IC design environment. In an embedded (or native) tool methodology the capabilities of one system are replicated inside the other system utilizing the same analysis engines. IC frameworks have typically matured much more than RF frameworks and thus can better serve as the host. In this case, the IC framework, simulation engine, data analysis tools, etc. are enhanced and modified to provide RF specific design tools. In an embedded methodology, the simulation data base and cell libraries are the same, regardless of the type of application (RF or IC). Also, a single analog simulator serves as the common simulation engine. This greatly reduces the device modeling problems. It is easier to implement a new model and easier to upgrade and maintain the existing device models. There is never an issue with model consistency since there is only one simulator.

The structure of FIRST

FIRST is a set of RF design tools integrated into FASTRACK [4], based on the embedded tool methodology. FASTRACK is a complete front-to-back (schematic-to-layout) IC design system (Figure 1). cdsSpice [5], an enhanced derivative of SPICE [6], serves as the simulation engine.

The raw data for RF results is generated from internally controlled single or multiple simulations. The netlist for each simulation is automatically generated according to the particular setup requirements of that analysis (see next section). The raw simulation data (e.g. S parameters) is saved in cdsSpice memory. The user can then choose the desired RF results (e.g. stability circles). A unified post processor uses the raw simulation data, performs the required mathematical processing to generate the user requested results and displays them on an appropriate plot format (e.g. Smith chart).

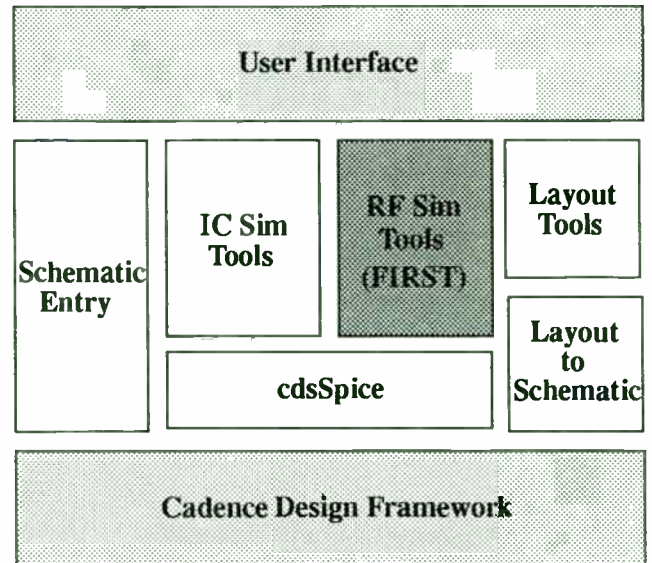


FIGURE 1. The structure of Fastrack, showing the embedded RF design tools, FIRST.

III. System Capabilities

Many RF specific design tools fundamentally use the same mathematical basis and numerical algorithms that exist in IC tools. The procedure to extract the required data can be different and it may require a special set up and a controlled environment. The user interface, analog simulation engine (cdsSpice), and the data representation routines in FASTRACK were enhanced and modified to implement FIRST. The major components of FIRST are described below.

S parameter measurement

S parameter measurement enables the designer to measure all four S parameters [7] for a single transistor or a two port network. The system establishes the proper loading and excitation (also auto biases single transistors) (Figure 2), runs multiple simulations and mathematically processes the results to determine the S parameters [8]. Once the S parameters are determined they can be printed to the screen or to a user specified file in any user specified format. They can also be plotted on Smith charts, polar, or rectangular plots. A full-function graphical environment allows the user to change plot axes, do multiple overlay plots, zoom into a specified region of the plots, etc. The S parameters are also used to generate constant power gain and stability circles, plot and print K factor, input and output VSWR, and input and output impedances.

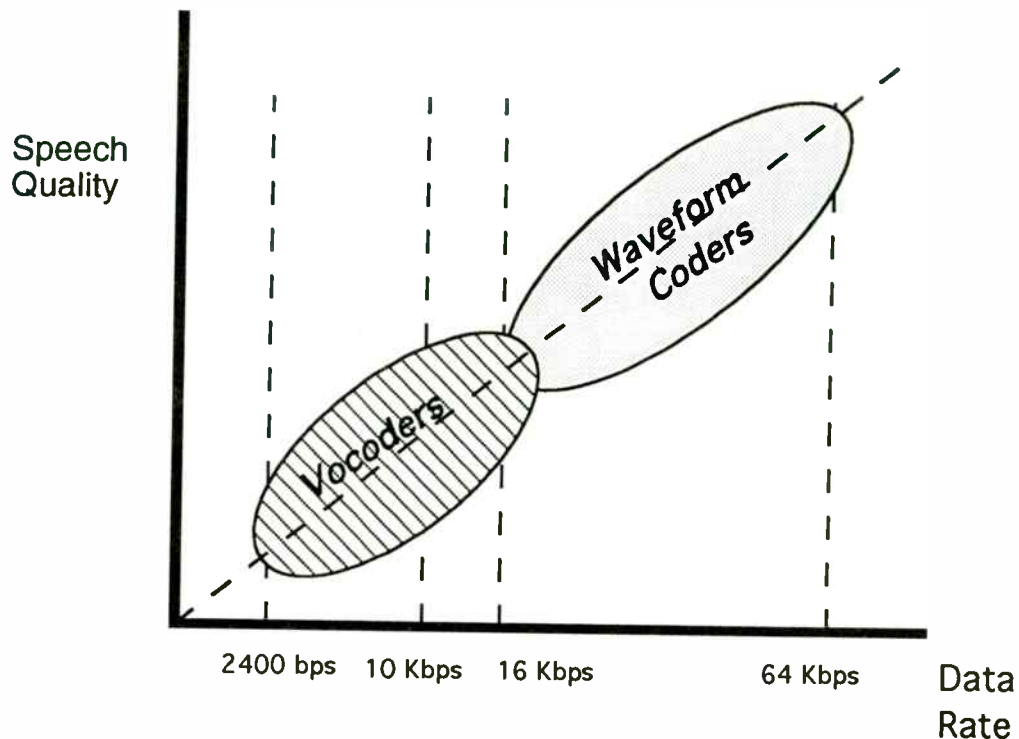
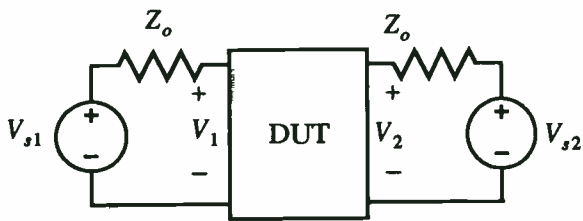


Figure 2: Speech Quality vs. Data Rate for Waveform Coders and Vocoders

- 1.) Speech Quality: Speech quality is measured in several ways, usually with subjective testing which compares the encoder being tested to some standard comparison system. "Speech quality" includes consideration of the ability of the encoding system to provide good speaker recognition, intelligibility of words, and general acceptability. Speech quality may vary for a given system between male and female voices, different languages or dialects, and performance in the presence of more complex audio signals such as multiple speakers or in the presence of background noise, such as street noise.
- 2.) Encoded Data Rate: The data rate compression factor is an important aspect of voice coding system selection. Differing system requirements dictate different level of compression. Increased speech quality with decreased encoding data rates are the two major conflicting system requirements in many systems.
- 3.) Processing Delay: The amount of time (measured in milliseconds) required for encoding and subsequent decoding of the voice signal can be an important design criteria, especially in systems where real-time two-way communications are required. In other systems, such as voice mail or broadcast voice transmission, minimizing the throughput delay is not as critical to the system overall performance. One-way processing delays of less than about 100 msec. are usually acceptable for two-way communications.



Test #1

$$\begin{aligned}
 V_{s1} &= 1 \\
 V_{s2} &= 0 \\
 S_{21} &= 2V_2 \\
 S_{11} &= 2V_1 - 1
 \end{aligned}$$

Test #2

$$\begin{aligned}
 V_{s1} &= 0 \\
 V_{s2} &= 1 \\
 S_{22} &= 2V_2 - 1 \\
 S_{12} &= 2V_1
 \end{aligned}$$

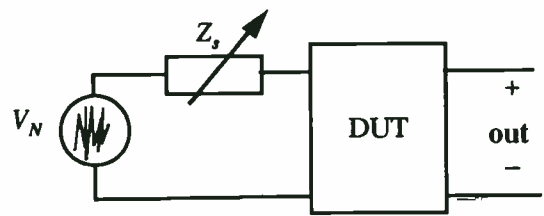
FIGURE 2. S Parameter measurement circuit.

S Parameter Modeling and Simulation

Frequently, RF designers require the capability to represent a two-port network by its S parameters in a tabular form. In the embedded RF tools, a generic macromodel provides the capability to represent the external behavior of any two-port network using an S parameter file. This file can either be generated by the S parameter measurement utility in FIRST or from a data sheet for other vendor's parts. The modeling is based on the equivalent two port Y parameters which in turn are generated from the complex tabular S parameters.

Noise parameter measurement

RF designs are frequently driven by noise specifications. Even though, IC and RF designers basically use the same noise models and AC small signal noise analysis, the interpretation of the results, the type of requested information, and the noise information processing are different. RF designers are typically interested in noise figure at a given frequency, minimum noise figure, noise resistance, and optimum reflection coefficients versus frequency. The noise parameter measurement capability in FIRST enables the designer to measure RF specific noise parameters for a single transistor or a two port network. As with S parameter measurement, the system automatically connects a bias circuit to a single transistor. The system places a noise source and an internally controlled impedance at the input of the circuit and runs 4 simulations to determine noise figure, minimum noise figure, noise resistance, and optimum reflection coefficient versus frequency [9].



$$F = 10 \log \left(\frac{S_T}{S_s} \right)$$

$$S_T = \sum_{\text{all noise components}} S_i$$

FIGURE 3. S Parameter measurement circuit. Noise figure (F) is defined as the ratio of the total available noise power at the output (S_T) to the available noise power at the output due to the input noise (S_s).

Noise figure, minimum noise figure, and noise resistance versus frequency can be plotted or printed (to the screen or a user specified file). Optimum reflection coefficient can be printed or plotted on a rectangular plot or a Smith chart. The user can also plot the constant noise circles on a Smith chart. In addition, constant noise circles can be overlaid on the constant gain or stability circles to allow for a visual design trade off between gain, stability, and noise performance of a circuit.

Large Signal AC

This analysis enables the RF designer to observe the non-linear performance of a circuit in the frequency domain. It can be used for single tone circuits to observe harmonic distortion or for multitone circuits to observe the intermodulation products. The third order intercept point is automatically calculated from the frequency spectrum. The power spectral density can be plotted (in a spectrum analyzer type bar plot) or printed (to the screen or to a file). The system determines the desired frequency spectrum by invoking an internally controlled and automated nonlinear transient analysis followed by a Fast Fourier Transform (FFT). The transient analysis and FFT are designed to internally control each other for optimum accuracy and efficiency (Figure 4).

While most time domain analysis and FFT based methods only offer about 60-80 dB of dynamic range, this new method can offer up to 260 dB of dynamic range. This methodology is totally different from Harmonic Balance, even though both methods use a combination of FFT and nonlinear transient analysis. Harmonic Balanced based simulators are more suitable for smaller circuits (less

- 4.) Ability to Process "Non-Voice" Signals: Today's telephone system is required to process more than just speech signals. The use of telephones and similar systems for transmission of data, tone signaling, and faxes requires voice coding functions in such systems to either process these non-voice signals or at least to detect their presence and provide an alternative transmission routing.
- 5.) Cost/Size/Power Requirements: In a practical world, the voice coding system must meet the tangible constraints of cost, size, and power requirements. The complexity of the processing required for a particular voice coding scheme determines the computing power requirements (usually referred to in terms of millions of instructions per second (MIPS)). More complex processing usually results in higher cost, size, and power consumption. Fortunately, the evolution in increasingly powerful DSP processors with lower cost, size, and power continues at a fast rate. As a result, very complex voice coding systems which were not practical even a few years ago are now available and cost effective.

Of all these contributing factors to the selection of a voice coding system, the most important are typically 1.) speech quality, 2.) data rate compression ratio, and 3.) cost. The particular order of importance depends on the requirements of the specific system.

When the combined requirements of good voice quality and data rates below 10 Kbps are necessary, vocoder technology is the most appropriate choice for voice coding. Modern vocoders are available in single-chip VLSI-based DSP implementations. Some of these require less than 0.5 Watts of power to operate and provide near-toll quality speech encoding at data rates of 8 Kbps or less. The price of such vocoders is still typically twice as high as the price of a comparable quality waveform coder, but the data compression ratio is also better by about a factor of about three.

Variable Rate Vocoding

If vocoder technology is appropriate for a particular system design, it is important to select a vocoder which gives maximum performance at a minimal cost. Given that the voice compression ratio is an important selection criteria, a vocoder technology which minimizes the compressed speech rate while maintaining high quality is very useful. As previously mentioned, a "vocoder" is able to compress voice with high quality results because it attempts to model the human speech tract. Therefore, the extra "knowledge" the vocoder has about human speech generation provides greater efficiency.

One characteristic of human speech is that it is not a continuous process (at least not for most people!) There are pauses between words and sentences, as well as pauses for breathing and for listening to another speaker (in the case of two-way conversations). Obviously, during such periods of silence or near-silence the data rate required to accurately portray the speech signal is not as high as during

than 10 transistors) that either take a long time to reach steady state (e.g. switching power supplies) or when the beat frequency in a multitone application is several (6 or higher) orders of magnitude smaller than the tones. While, Harmonic balanced based simulators become extremely inefficient for anything but very small circuits, large signal AC analysis in FIRST is as efficient as typical SPICE transient analysis for larger circuits.

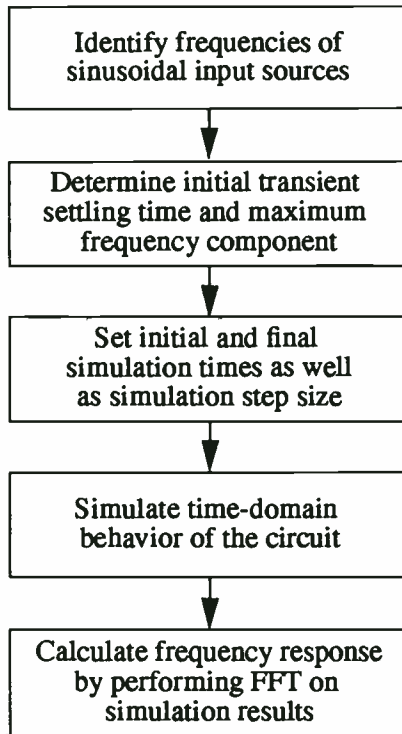


FIGURE 4. Flow of large signal AC analysis.

Small Signal Distortion

This analysis enables the designer to observe the nonlinearity and distortion for quasi-linear circuits. Quasi-linear circuits are a class of circuits that are ideally linear. In reality, they are almost linear but exhibit some undesired

nonlinearities (e.g. an LNA). Small signal distortion analysis [10, 11] exploits this nonlinearity by determining the undesired effects of each nonlinear component in the circuit on an output load. This analysis uses linear transfer functions and, consequently, it is significantly faster than FFT based analyses. At a given fundamental frequency, the frequency spectrum, comprised of the major intermodulation components, can be plotted or printed. The fundamental frequency can also be varied over a specified range, and the intermodulation components can be plotted or printed versus the fundamental frequency. The third order intercept point can also be automatically calculated.

Backend Tools

The RF specific analysis tools and data representations in FIRST provide a familiar working environment throughout the circuit design stage. Equally important, the physical design and verification tools in FASTRACK provide a smooth transition from electrical design to physical design so that the success of the silicon ASIC is not compromised by the level of understanding of the IC technology. This system offers a comprehensive set of physical design automation tools that allow the user to create a full-custom layout, while operating at a high level of abstraction.

Parameterized device libraries are the basis for the layout strategy. These device layouts are designed to fully implement the variable geometry structures that were modeled during simulation; they are not limited to discrete values. In effect the parameterized cells completely remove the numerous IC device level design rules from the layout process, without loss of freedom or functionality. This is most easily appreciated by observing the cross-sectional area of a Harris UHF-1 transistor (Figure 5). Each interface between process steps is the source of a design rule that is critical to the success of the process flow.

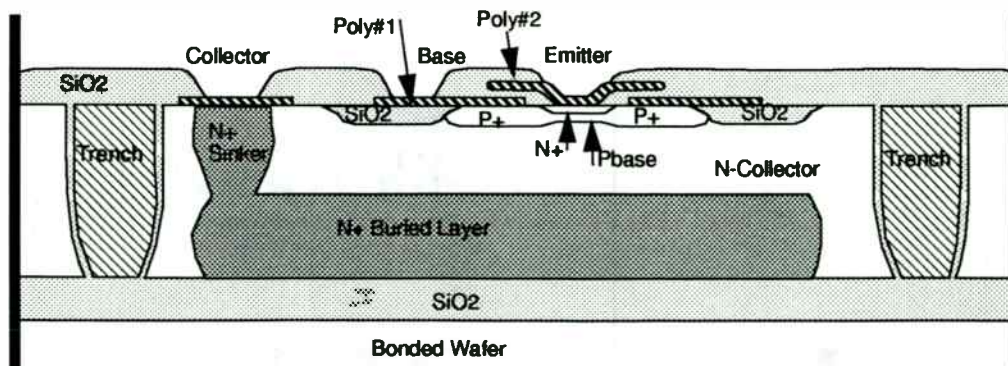


FIGURE 5. Cross-section of Harris UHF1 transistor showing numerous process interfaces that must conform to design rules

active talking periods. A vocoder that can recognize these periods and reduce the encoded data rate during these times will provide greater average data rate compression efficiencies.

Simple techniques for reducing the data rate during periods of silence involve actually stopping the transmission of encoded voice during these periods. While this technique does result in a lower average data rate for encoding, the abrupt transitions from fully encoded speech to complete silence can be very disruptive to the listener. Because such systems cannot perfectly predict the end of speech segments or the start of new segments, the beginning of new speech segments are often truncated or clipped. Also, it is quite unnatural for a listener to hear complete silence between segments of speech. In an uncompressed voice transmission system, some level of background sounds are constantly being heard even when the speaker has stopped talking. To attempt to offset this, some voice coding systems inject artificially generated "comfort noise" at the receiver when actual voice is not being encoded. However, the mismatch of the levels and characteristics of the actual background sounds (during speech) and the artificial comfort noise does not create a natural effect on the listener's ear.

A more sophisticated method for taking advantage of these periods is one that automatically adjusts the coding rate of the vocoder at a frequent rate. The coding rate is optimized for a particular short period of time. A new algorithm called "QUALCOMM Codebook Excited LPC" (QCELP) provides this type of intelligent vocoding. This algorithm, developed by QUALCOMM Incorporated of San Diego, California, is an enhanced version of the basic CELP vocoding approach.

The QCELP encoder partitions uncoded speech into frames which are 20 msec in duration. The QCELP algorithm performs a variable coding rate determination process and decides whether to encode each frame at one of several data rates, ranging from a low of 800 bps to a high of 9600 bps. During periods of silence, the QCELP encoder operates at a rate of only 800 bps. This very low data rate is useful for transmission of actual encoded background noise. Also, certain long-term voice parameters are continually updated when operating at this low rate. When speech resumes, the vocoder selects a higher rate for vocoding. The selected data rate is determined by the speech energy in each frame. As embodied in the QUALCOMM Q4400 single-chip QCELP vocoder device, the QCELP algorithm selects from one of three possible encoding rates for each frame. The sets of available rates are user selectable to be either 800/4000/8000 bps or 800/4800/9600 bps.

Using the QCELP algorithm, the average encoded rate for typical "constant talk" speech encoding is about 7,000 bps while maintaining near toll quality speech. Even greater efficiency is achieved when the vocoder is used in a two-way "full duplex" conversation mode, such as during a telephone call. In this case, during the period of time when the local party is listening to the remote speaker, the voice encoder is using only the lowest, 800 bps, coding rate. During such two-way conversations, the average transmitted voice coding rate is about 3.5 Kbps while still maintaining near toll quality.

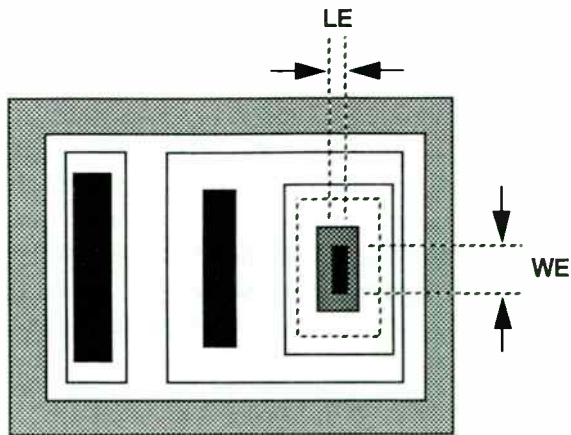


FIGURE 6. Simplified top view of Harris UHFN1 transistor showing emitter length (LE) and emitter width (WE) electrical parameters

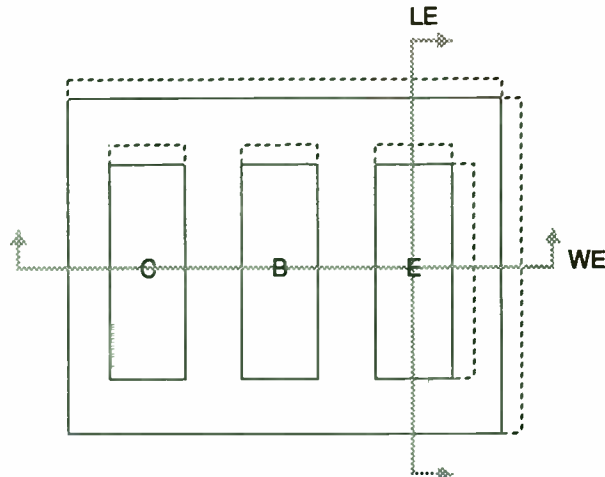


FIGURE 7. Effective parameterized cell of Harris UHFN1 transistor showing stretch lines that adjust internal geometries based on electrical parameters

The device layouts are automatically synthesized from the schematic by placing the parameterized cells relative to their schematic positions and applying the corresponding model parameters to size the geometries. In this way, the transistor in Figure 6 can be thought of as a virtual black box, as shown in Figure 7, with terminals for connecting the collector (C), base (B), and emitter (E). The device can now be thought of as having stretch lines that bisect the layout structure to adjust all of the internal geometries as a function of the electrical parameters (e.g. emitter length, emitter width, etc.). A wide range of lay-

out optimizations are also supported by simply changing device parameters; for example, parallel and serpentine resistor structures, trimmable thinfilm (as a function of trim range and trim sensitivity), and capacitor aspect ratio. This allows the user to concentrate on just the circuit level interconnections.

Verification of the completed IC layout is accomplished with a Design Rule Checking (DRC) tool to ensure that the layout conforms to all manufacturing specifications, (metal width, metal spacing, etc.), and a Layout Versus

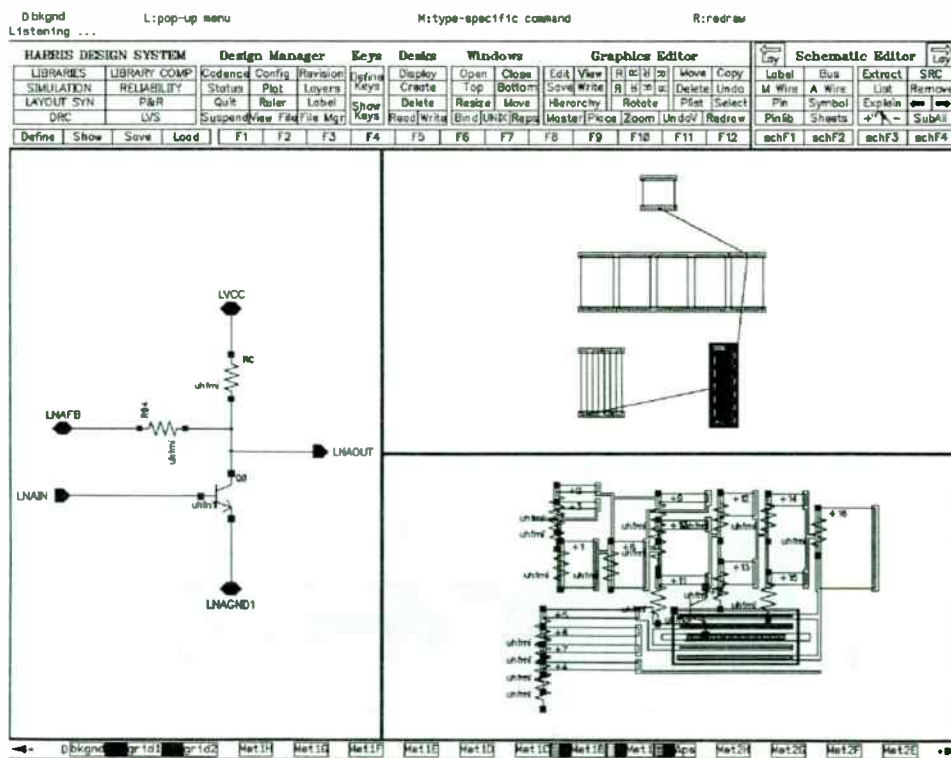


FIGURE 8. A screenshot of FASTRACK, showing the schematic, "light-lines", and the extracted schematic overlaid on the layout.

An interesting aspect of the QCELP algorithm is its ability to automatically adjust thresholds to "filter out" undesired background noise when performing speech encoding. This is due to the fact that the speech energy measurement thresholds used to determine the encoder data rate are automatically adjusted over time. In the presence of high background noise levels, such as when using a cellular phone in the presence of high levels of "street noise", the QCELP encoder automatically shifts the rate determination thresholds to a higher level. Therefore, the high background noise is encoded at lower coding rates. The effect to the listener is an attenuation in the levels of the background noise without reducing the quality or volume of the encoded speech.

As shown in Figure 3, the QCELP algorithm provides good speech quality at a low data rate. This makes the QCELP algorithm suitable for a range of practical applications.

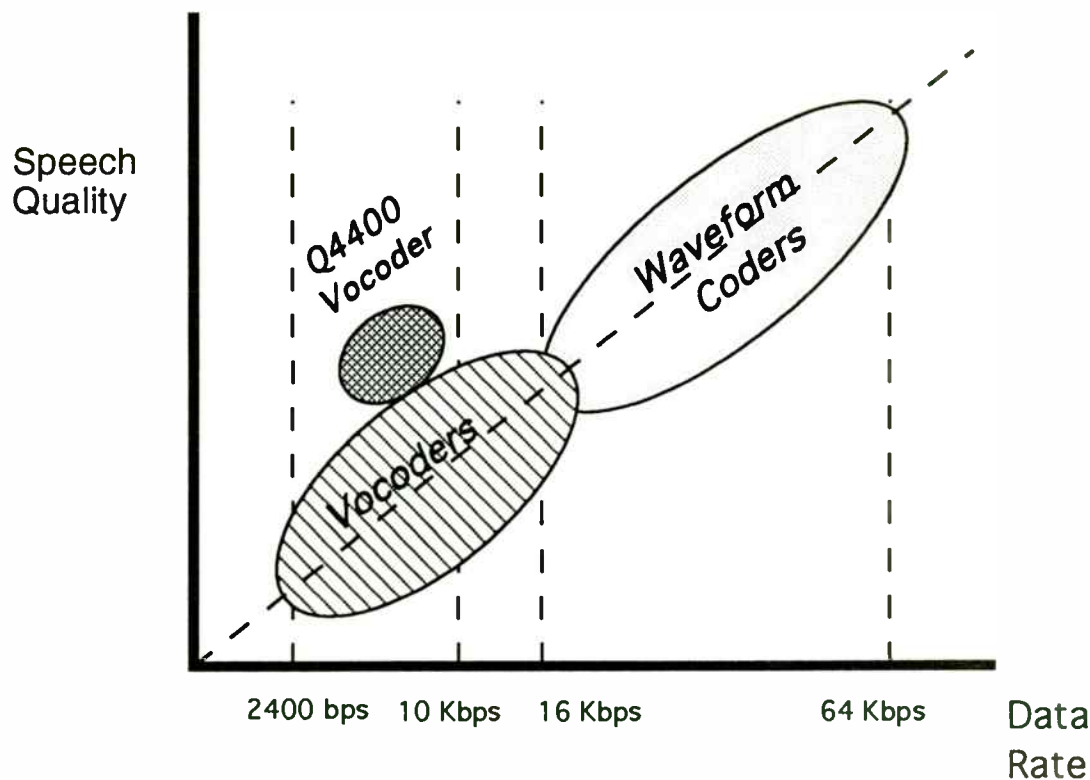


Figure 3: Q4400 Speech Quality and Data Rate Performance

The QCELP algorithm is currently under evaluation for standardization for use with the spread spectrum (CDMA) cellular phone system for the United States. Because of special inherent properties of spread spectrum communications, the decreased coding rate required for high quality cellular phone communication provide by QCELP directly increases the total call capacity of the cellular network. However, the special advantages of variable rate speech encoding are useful in a number of other system applications such as those listed in the following section.

Schematic (LVS) tool to validate the electrical functionality of the layout with respect to the schematic. DRC highlights portions of the layout (Figure 8, top) that fail to meet manufacturing guidelines and provides detailed information on how to correct the errors in terms of layout dimensions. LVS matches the connectivity between the interconnections of the devices in the schematic (Figure 8, left) and the electrically equivalent interconnections between the extracted devices in the layout (Figure 8, bottom). The layout extraction identifies the devices and the interconnections between devices by recognizing the diffused patterns and relational interactions among all of the different layout mask layers. The resulting extracted view of the layout (Figure 8, bottom) includes all of the electrical and physical attributes of the circuit in a form that can be compared with the schematic. This process requires no input from the user regarding the IC technology or the design application.

The results of the comparison between the layout and schematic describe differences in the interconnect paths (e.g. opens, shorts), the device types, and the device sizes. The layout and schematic networks are automatically reduced to minimum equivalent circuits so that, for example, a single resistor in the schematic can be represented by a complex series/parallel configuration in the layout and the two views will still match electrically. Throughout the layout and verification process, a tight correspondence is maintained between devices and interconnections in different representations. This allows “flight-lines” to be drawn in the layout showing what connections need to be made to implement the schematic design (Figure 8, top). It also provides cross-probing between all of the circuit representations after LVS.

Once the layout is verified, parasitic resistances and capacitances can be measured and back-annotated to the schematic netlist for simulation of the parasitic effects on circuit performance.

IV. Results

The low noise amplifier (LNA) shown in Figure 9 was used to demonstrate the analysis capabilities of FIRS. The LNA is part of a Harris LNA/Mixer IC designed to operate around 900 MHz.

The S parameter measurement capability of FIRS was used to determine the forward and reverse reflection parameters, S11 and S22 and plot them on a Smith chart (Figure 10).

The same analysis tool generated the data required to calculate the forward and reverse transmission parameters, S12 and S21. A polar plot of S21 is shown in Figure 11

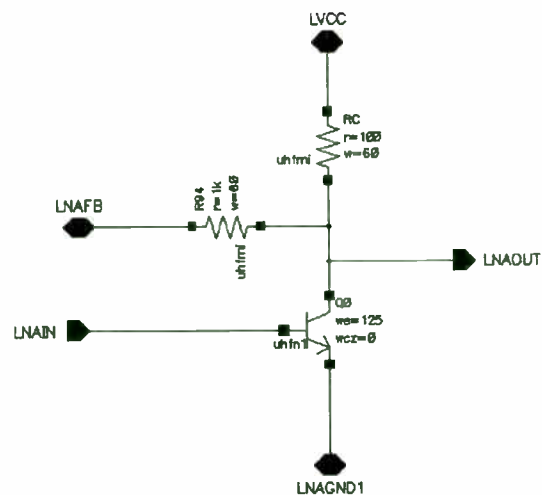


FIGURE 9. Schematic of a low noise amplifier circuit.

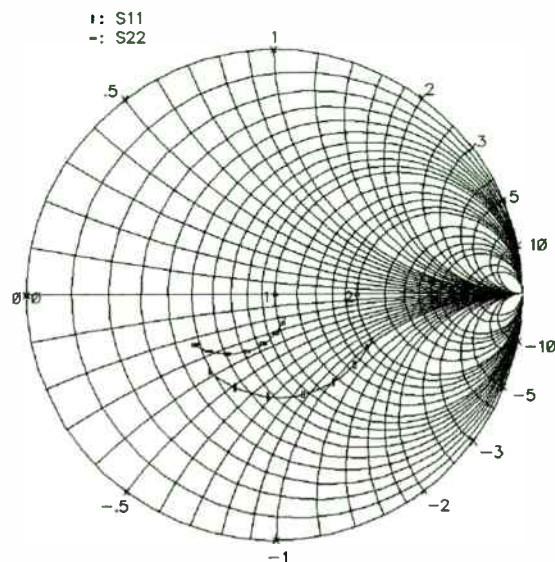


FIGURE 10. Plots of S11 and S22 on a Smith chart. The frequency varied from 100MHz to 1GHz.

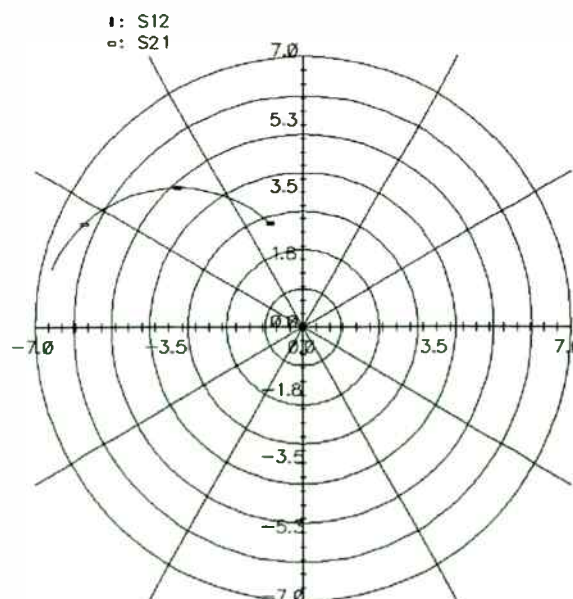


FIGURE 11. Polar plot of S21. The frequency varied from 100MHz to 1GHz.

Applications of Variable Rate Vocoding

VSAT and other SatCom Systems

A typical VSAT terminal might provide a 64 Kbps transmission data rate. If this channel is used for voice communications, a single 64 Kbps PCM voice signal may be transmitted from this station. If this same VSAT terminal uses a QCELP vocoder operating at a fixed rate of 8,000 bps it is easy to see that as many as eight voice circuits can be provided over this same channel. However, since most voice terminals are used for two-way telephone-like conversations (i.e., essentially half-duplex), the average data rate from the QCELP vocoder operating in variable-rate mode might be less than 3.5 Kbps. Even if one user is talking constantly and, therefore, requires the full data rate for vocoding, other users will probably not require full rate at any given moment. Therefore, a statistical multiplexing technique can be used resulting in the ability to carry as many as 16 voice circuits or more over the same terminal that could only handle a single PCM-encoded voice channel!

Voice Storage Systems

Voice mail and similar systems have become increasingly popular. In most voice mail systems the recorded messages are first digitized and then stored on a digital magnetic storage medium, such as a hard disk. Of course, the limit on how many minutes or hours of voice messages can be stored is determined by the size (in megabytes) of the storage media as well as the data rate of the encoded speech. Using the QCELP vocoder in variable rate mode, near toll quality speech is encoded at about 7 Kbps. This means that, for a given size hard disk, as many as nine times as many hours of speech can be recorded using QCELP-vocoded speech when compared to standard 64 Kbps speech digitizing. And, since only a few vocoder channels are actually required for even a large voice mail system, the cost for the advanced capabilities of the QCELP vocoder is minimal to the overall system.

Spread Spectrum Systems

The QCELP vocoding technique was initially developed for use in the QUALCOMM CDMA (spread spectrum) cellular telephone system. In spread spectrum systems, the limit on performance and capacity is directly related to the total number of "bits per second" being transmitted by all users at a given moment. If each user in a spread spectrum two-way voice communications system transmits only the average 3.5 Kbps data rate when using the QCELP vocoder, the total system capacity (in terms of the number of simultaneous users) is more than *double* that of the same system using a fixed rate 8 Kbps vocoder.

"Voice Over Data" Systems

An exciting new market is developing for data transmission systems that simultaneously transmit voice signals. An example of such a system is a baud-

The S parameters were then used to construct constant gain and input/output stability circles (shown in Figure 12). Note that portions of the stability circles are plotted in the upper left-hand corner of the figure. None of these analyses required the user to add any additional circuitry to the schematic and all plots were generated by FIRST. The user was not required to transfer or convert data in any way.

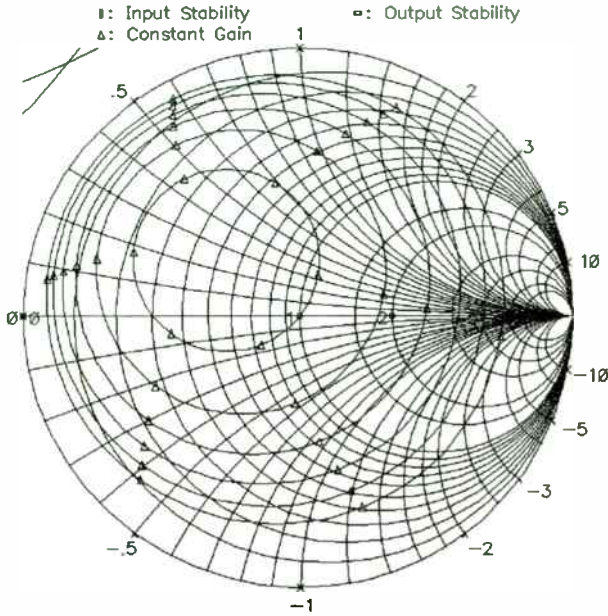


FIGURE 12. Constant gain and stability circles plotted on a Smith chart at a frequency of 1GHz. Gain circles are plotted at 1 dB intervals.

The noise analysis tool in FIRST was utilized to obtain the noise optimization parameters (minimum noise figure, optimum reflection coefficient, and noise resistance).

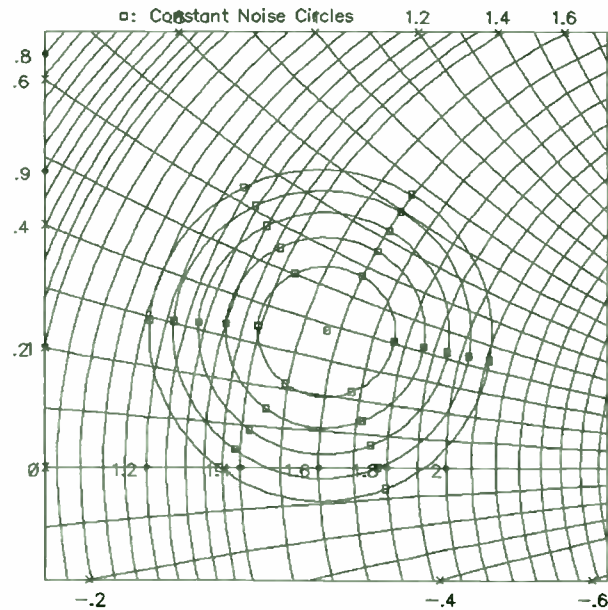


FIGURE 13. Zoomed-in view of noise circles plotted on a Smith Chart at 1GHz. Noise circles are plotted at increments of 0.5 dB.

This information was used to construct the noise circles in Figure 13. Again, all post-processing steps, test circuit insertions and graphics generation are performed transparently.

With the addition of sinusoidal input sources and an output load to the schematic the user has a choice of two forms of distortion analysis. For high accuracy at given input frequencies a large signal AC analysis can be performed (Figure 14). Note the high dynamic range of the frequency spectrum.

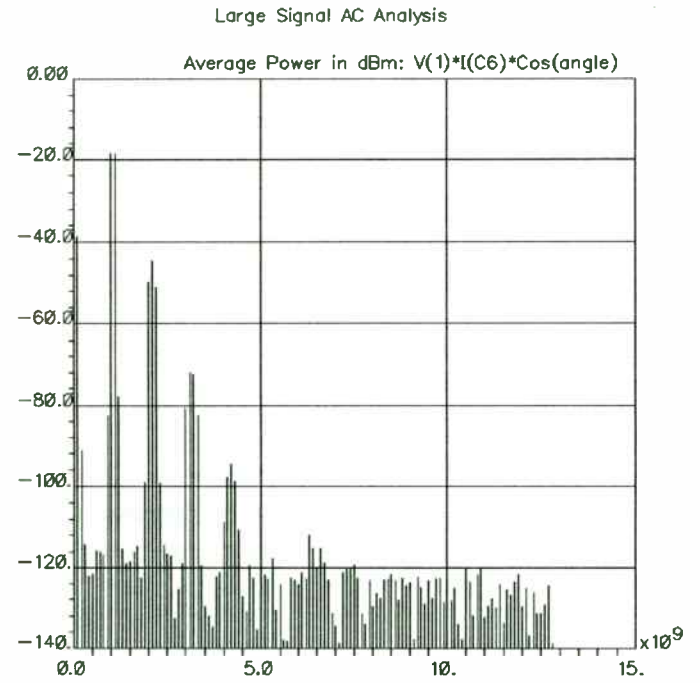


FIGURE 14. Magnitude of large-signal AC response of LNA circuit with input sources operating at 1GHz and 1.1 GHz.

Alternatively, a small signal distortion analysis can be performed when the desired information is the power of the distortion components over a range of fundamental frequencies. Figure 15 shows a plot of the output third-order intercept point as a function of the fundamental frequency. Note that both the large signal and small signal analysis show an output third order intercept point at around 10 dBm.

rate telephone modem like those found in personal computers. While uploading a file between modems, or perhaps while playing a multi-player modem game, a voice conversation can also be held between people at either end of the link. This is also useful for multi-media networks where computer information is conveyed via phone modem while a voice conversation is also being held. Videophones are examples of transmission of simultaneous voice and "data" (in this case, digitized video signals) over a telephone. In each of these cases, it is desirable that the data rate of the voice signal be minimized to allow the maximum amount of data to be transmitted. QCELP vocoding not only is very efficient in its overall data rate requirement, but also allows the channel to be used almost totally to transmit data when speech is not present. The QCELP vocoder has the ability to limit the maximum speech rate to "half-rate" (either 4000 or 4800 bps) for short periods of time to allow short data transmissions to occur without interruption or degradation in the voice quality.

The Q4400 Single-Chip QCELP Vocoder System

QUALCOMM has implemented a full-duplex QCELP vocoder in a single DSP-based integrated circuit -- the Q4400 Variable Rate Vocoder. The Q4400 implements both encoding and decoding of voice signals which have been previously digitized using a standard off-the-shelf mu-Law PCM codec device. The Q4400 uses a standard 8-bit microprocessor bus interface to output speech samples which have been encoded by the QCELP encoder and to input previously encoded speech samples to be decoded by the QCELP decoder (refer to Figure 4).

The Q4400 provides several additional functions and features that are commonly required when using a voice coding system as shown in the block diagram of Figure 5. These features include built-in diagnostics, loopback modes, mute selection, and single or dual tone generation. The Q4400 also implements a useful VOX function which acts as an echo suppression capability. This is particularly useful for operation with a speakerphone or "hands free" cellular phone.

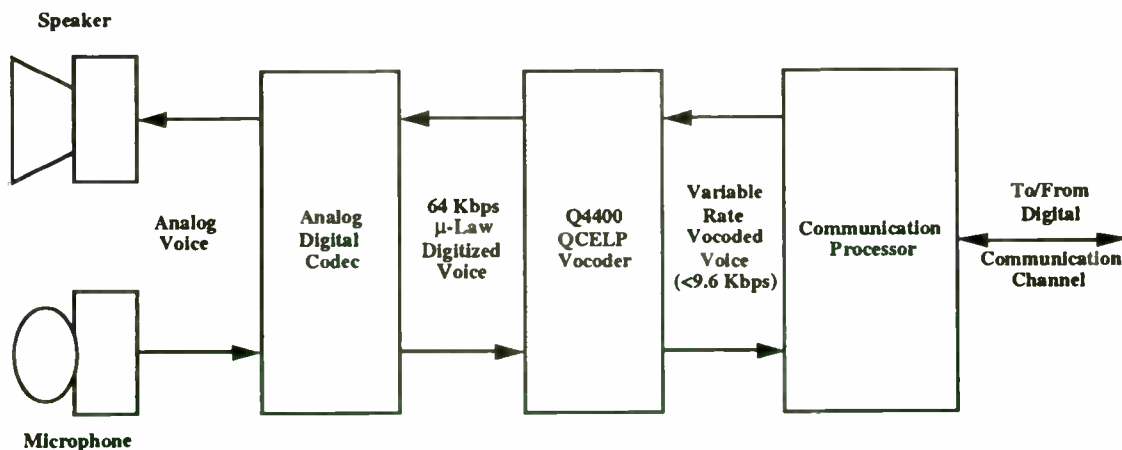


Figure 4: Q4400 Vocoder Typical Application

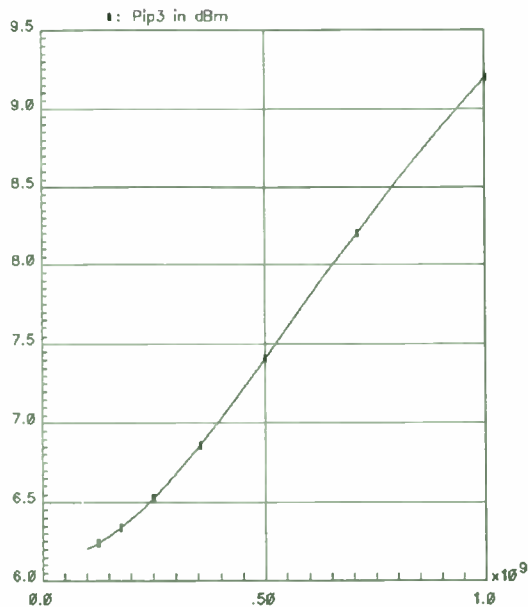


FIGURE 15. Plot of the third-order intercept point over the fundamental frequency with one input source operating at 0.9091 times the frequency of the other.

Once performance specifications were met, the layout of the LNA/Mixer was constructed using the FASTRACK layout tools described earlier (Figure 16). These tools were also used to verify the physical and electrical integrity of the layout. At this stage interconnect parasitic resistance and capacitance can be extracted and automatically back-annotated to the schematic netlist for post-layout simulations.

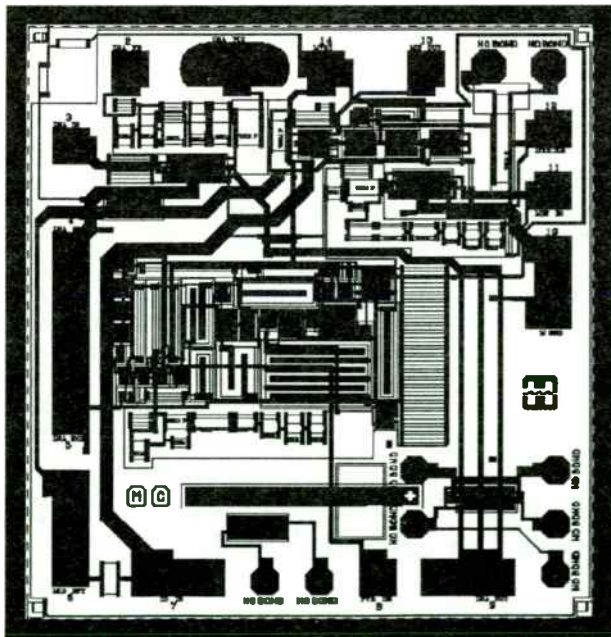


FIGURE 16. Layout of a combination LNA/Mixer circuit.

V. Conclusions

Embedding RF tools in an IC design system is an enabling factor for the transition from discrete based designs to using silicon ASICs. FIRST is a set of embedded RF design tools in Harris Fastrack's IC design system. It enables high frequency IC designers to easily traverse to the RF domain and it provides a traditional RF- design-system-like environment for RF designers. Regardless of IC or RF design, the user interface, simulation engine, and device models are the same. FIRST has been successfully used by many HSS' internal and external high frequency IC and RF designers.

VI. References

- [1] P. R. Gray and R. G. Meyer, Analysis and Design of Analog Integrated Circuits, Second Edition, John Wiley & Sons, New York, 1984.
- [2] G. Gonzalez, Microwave Transistor Analysis and Design, Prentice-Hall, Inc., New Jersey, 1984.
- [3] R. S. Carson, High Frequency Amplifiers, Second Edition, John Wiley & Sons, New York, 1982.
- [4] "Harris Fastrack Design System", Harris Semiconductor, Release 3.6, Sep. 1993.
- [5] "Cadence SPICE Reference Manual", Cadence Design Systems, Version 4.2.2, June cdsSpice
- [6] L. W. Nagel, "SPICE2, A Computer Program to Simulate Semiconductor Circuits", Technical Report ERL-M520, UC Berkeley, May 1975.
- [7] R. A. Anderson, "S-Parameter Techniques for Faster, More Accurate Network Design", Hewlett-Packard Journal, Vol. 18, No. 6, Feb. 1967.
- [8] T. B. Mills, "S-Parameters in Spice", RF Design, June, 1989.
- [9] J. Ortiz and C. Denig, "Noise Figure Analysis Using Spice", Microwave Journal, April 1992.
- [10] P. Antognetti and G. Massobrio, Semiconductor Device Modeling with Spice, McGraw-Hill Book Company, New York, 1988.
- [11] S. Chilsholm and L. Nagel, "Efficient Computer Simulation of Distortion in Electronic Circuits", IEEE Trans. Circuit Theory, 1973

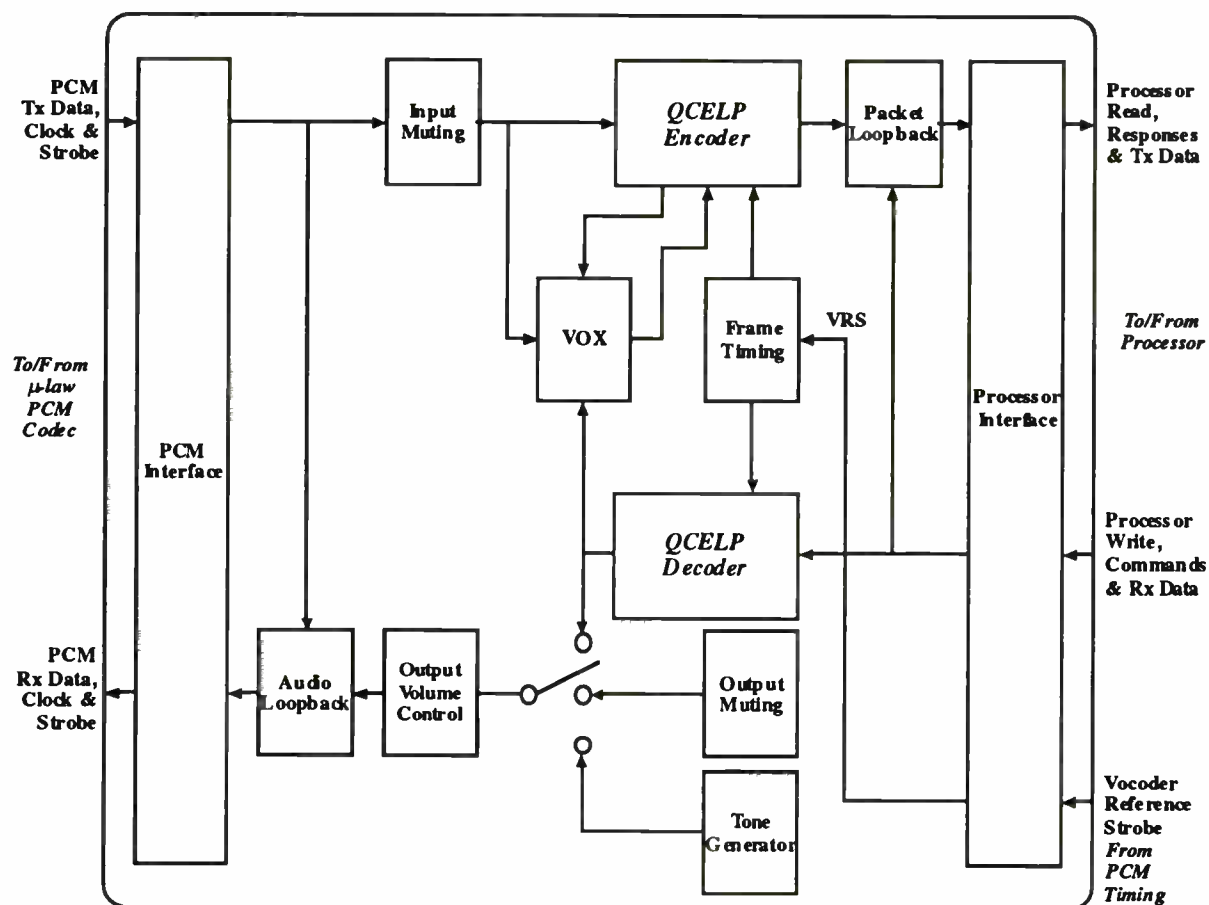


Figure 5: Q4400 Vocoder Functional Block Diagram

The encoding rate of the Q4400 is selectable to be a fixed rate of either 4000, 4800, 8000, or 9600 bps, or the automatically variable rate can be selected, using one of two data rate sets. The Q4400 decoder operates at a rate which is commanded to the decoder when a frame of data is transferred from the microprocessor controller.

The Q4400 is offered in a 100-pin PQFP package and requires less than 0.5 Watts of power from a single +5VDC supply. A 30 MHz clock signal or crystal controls the internal processing clock frequency.

Summary

As digital voice transmission and storage systems require greater speech compression rates while maintaining high speech quality, more "intelligent" vocoding algorithms must be developed. The QCELP algorithm is an excellent choice for systems that can take advantage of the unique ability to automatically determine the encoding data rate on a frequent basis. While maintaining speech

"Electromagnetic Simulation for High-Frequency Planar Circuits"

Daren McClearnon
Hewlett-Packard
1400 Fountaingrove Parkway, M/S 2US-P
Santa Rosa, CA 95403

Abstract

Electromagnetic (EM) simulation is emerging as an important way for high-frequency circuit designers to enhance the performance of their circuit-oriented simulation tools. This paper begins by identifying the role of Method of Moments (MoM) EM simulation among high-frequency simulation tools. It explores the advantages of using a multilayer planar EM simulator (based on a recent proprietary implementation of the MoM analysis technique) to supplement traditional circuit simulation tools. The planar Method of Moments approach is contrasted with a more general 3-dimensional approach using the Finite-Element Method and is shown to have significant advantages for most circuit designers.

Introduction

Electromagnetic simulation is outgrowing its reputation as an expensive, time-consuming, and exclusively academic endeavor. Electromagnetic simulation tools are now part of the standard product lines of all high-frequency CAE vendors. They have become integrated within CAE environments for schematics and artwork, enjoying better user-interface design, documentation, and support than ever before. Electromagnetic simulation is "here" today.

This is an informal discussion of today's state-of-the-art in high-frequency electromagnetic simulation. The discussion is oriented toward circuit designers and engineering managers with an eye toward the practical benefits of electromagnetics, rather than a detailed look at the underlying principles. Recently, Hewlett-Packard introduced a MoM-based simulator; it is used to illustrate current trends in the industry and electromagnetics. The simulator is called HP Momentum. It is considered a "2.5-dimensional" simulator since it assumes a planar circuit, but allows many planes to be entered and connected with vias. Specific product information is available directly from Hewlett-Packard and is not discussed here.

The Need for Greater Accuracy

Although commercial electromagnetic simulators for the high-frequency market have come a long way in the last five years, this discussion wouldn't be necessary if normal circuit simulators completely "did the job."

Circuit simulators operate within a framework of assumptions and simplifications that reflects the way electrical engineers think about circuits: in terms of schematics that show connections between components.

Schematics are abstract, symbolic; they are only related to a physical implementation to the extent that a designer includes the extra details (*i.e.* - "physical modeling"). This level of detail includes parasitics, self-resonances, microstrip transmission lines and discontinuities.

One key assumption is that each of these second-order effects is independent of everything else in the circuit. Depending on the frequency range and the physical distance between phenomena, this is more than just a valid assumption; it makes circuit simulation *feasible*. A completely interconnected circuit would be too hopelessly complex to understand or simulate in any reasonable time.

However, as frequencies and densities increase, certain weaknesses in the assumptions begin to appear. A few of the possible interactions become significant, such as coupling between adjacent traces, or non-ideality of the ground plane. This then is the justification for using some form of electromagnetic analysis: to enhance the accuracy of an ordinary circuit simulation over an extended range of topologies, materials, and frequencies.

In some situations, the electrical representation of a structure itself changes with increasing frequency, from an inductance to a high-impedance transmission line to a set of n-coupled striplines in an IC package. In other situations, circuit features begin to interact through radiation, higher-order modes, or surface waves.

E&M simulators can quantify whether a certain phenomenon is significant and allow the designer to enter the result directly into a circuit, all from within the circuit-oriented CAE environment. The established path for this information is a linear S-parameter data file vs. frequency. Like the electromagnetic solvers themselves, S-parameters make no assumptions about whether crosstalk or other phenomena are best described in terms of lumped elements, distributed elements, or fullwave formulations. The S-parameters are simply inserted into the circuit at the location of the interaction without interpretation. This means that design engineers can reliably obtain accurate answers with a minimum of sophistication in the field of electromagnetics.

Physical Phenomena Not Ordinarily Modeled in Circuit Simulators

A variety of components and phenomena that circuit simulators do not address are listed in this section. Due to time constraints, it is not possible to elaborate in detail on all the items listed below. A small sampling of real circuits is shown to illustrate the principles.

quality equivalent to a 9600 bps fixed rate vocoder, the QCELP algorithm encodes and decodes voice at an average data rate of less than 4 Kbps. The Q4400 single-chip vocoder implements the QCELP algorithm with user-selectable parameters and a variety of useful features. These attributes, along with the small size, low power requirement, and low cost of the Q4400, make this an ideal selection which meets the requirements for vocoding technology in many system applications.

Physical phenomena and structures not ordinarily modeled by circuit simulators

Phenomenon or structure	Example(s)	Illustration
Proximity, coupling and crosstalk effects	Coupled-line filters, TAB leads in a digital pkg.	Figure 5
Higher-order and evanescent mode effects	Coupled microstrip discontinuities	Figures 4,6
Nonstandard structures with no commercially implemented model	Microstrip Y-junctions, planar baluns	---
Discontinuous or optimized ground planes	Slotted ground planes, cut-outs under spiral inductors, digital package power/ground planes	Figure 3
Transitions between propagating media	Microstrip to buried layers or coplanar waveguide	---
Radiation and surface wave phenomena	Microstrip patch antennas	Figures 1, 2
Wide variety of dielectric materials/thicknesses	Models used beyond accuracy guidelines	---
Cover heights and passivation layers	Package lids, buried microstrip	---

Computer-Aided Engineering and PCN Components

Session Chairperson: Ray Pengelly, Compact Software, Paterson, NJ

Simulating Digital Radio Performance Using the HP Microwave Design System, **Kirt Kisling and John Hirsekorn**, Hewlett-Packard Co. (Santa Rosa, CA).....251

The Design of Low Power Consumption RF Circuits for Digital European Cordless Telephones Using Microwave Harmonica, **Raymond S. Pengelly**, Compact Software (Paterson, NJ).....275

An Integrated Microwave Radio Transceiver for WLAN Applications, **David A. Williams**, GEC Plessey Semiconductors (Microwave Division, Lincoln, United Kingdom).....305

GMIC Planar Mixers for Communications Applications, **Paul J. Schwab and Timothy A. Murphy**, M/A-COM, Inc. (Burlington, MA).....314

GMIC Interdigital Filters for Microwave Applications, **Holly A. LaFerrara**, M/A-COM, Inc., IC Design Center (Lowell, MA).....318

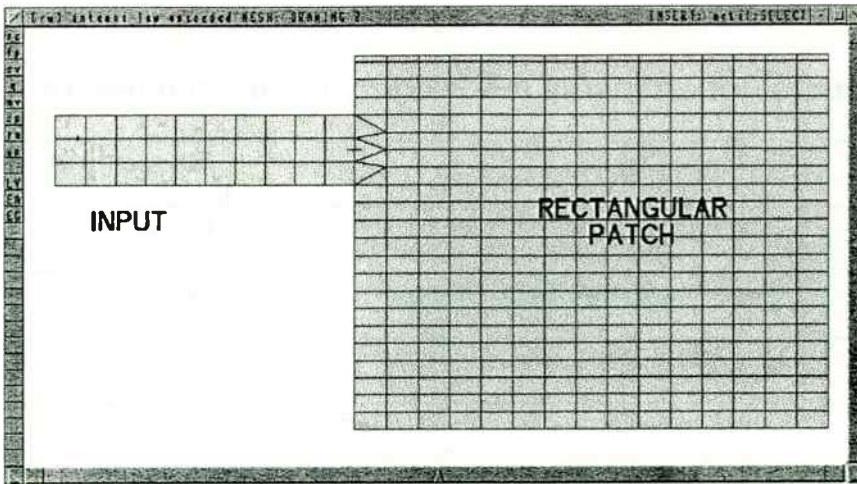
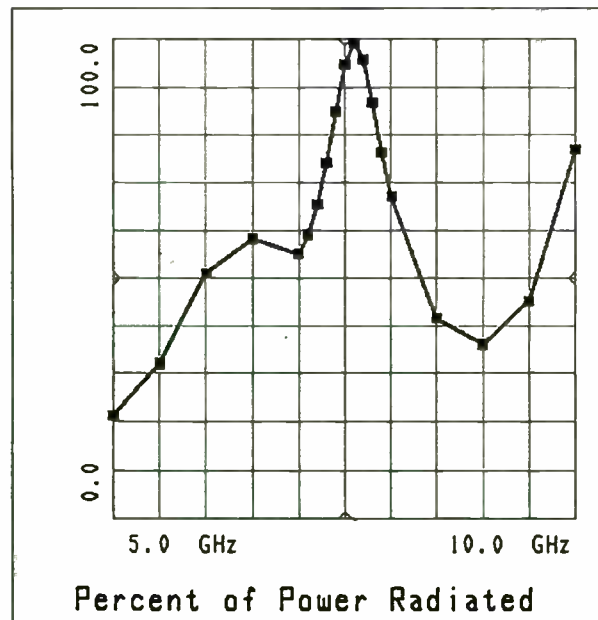
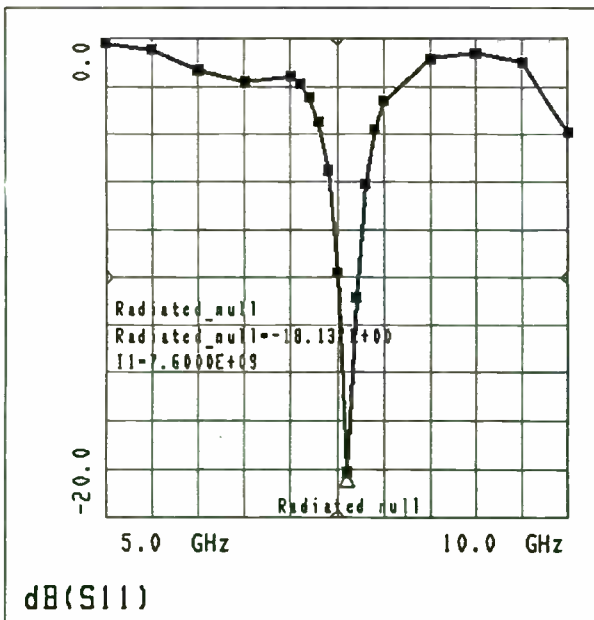


Figure 1. Rectangular microstrip patch antenna. Note that the magnitude of S_{11} varies significantly, even though the structure has only one port and the metallization is relatively lossless. This indicates that much of the energy of the system is lost to radiation. This effect is not modeled by circuit simulators.



The measurements for this example were obtained from a paper in the IEEE Transactions on Antennas and Propagation.

Shih-Chang Wu, N. Alexopoulos, O. Fordham, "Feeding Structure Contributions to Radiation by Patch Antennas with Rectangular Boundaries", IEEE Trans. on APS, vol. 40, no. 10, pp. 1245-49, October 1992.

SIMULATING DIGITAL RADIO PERFORMANCE USING THE HP MICROWAVE DESIGN SYSTEM

Kirt Kisling and John Hirsekorn
Hewlett-Packard Co.,
1400 Fountaingrove Parkway,
Santa Rosa, CA 95401;
(707) 577-2663.

AGENDA

- Digital communications basics
- Important MDS capabilities
- A Case study: DQPSK Radio
 - Transmitter performance
 - Channel distortion and correction
 - Receiver performance
- Summary



© 1991 HP

Today we will be discussing ways to simulate digital radio performance using the HP High-Frequency Design System.

First we will discuss the basics of digital communications systems, briefly discussing block diagrams, modulation formats, and common performance measurements. Next we will look at the features of the HP High-Frequency Design System that are especially important when analyzing digital systems. From there, we will discuss techniques to simulate transmitters, channel distortions, and receivers.

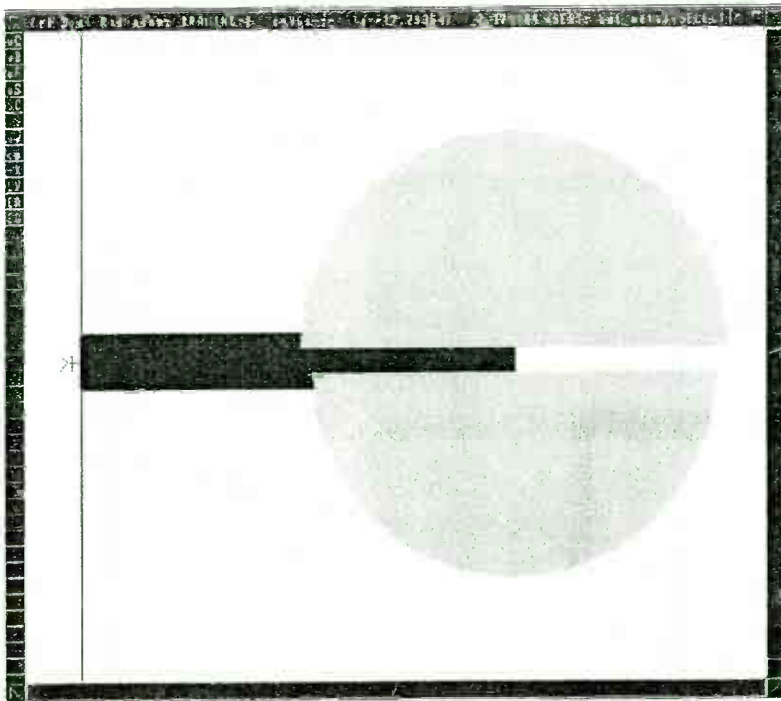
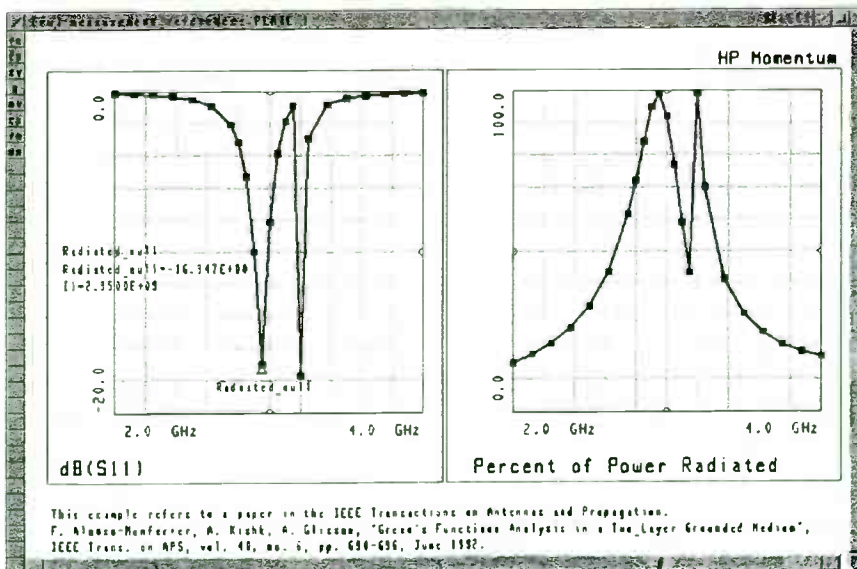
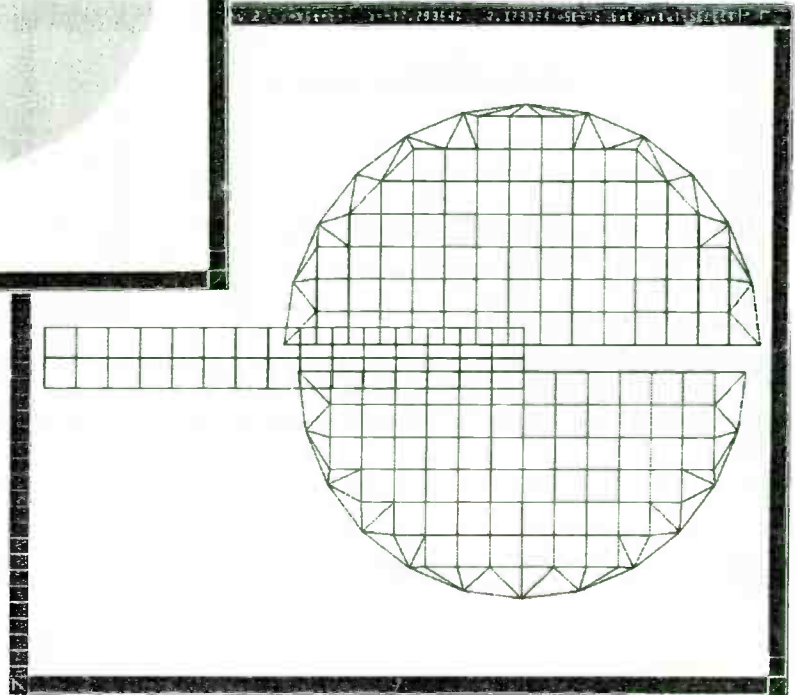


Figure 2. Bi-radial microstrip patch antenna. Two semicircular metal patches sit atop a dielectric layer that separates them from a microstrip feedline. The two radiating resonances are clearly visible in the frequency response.



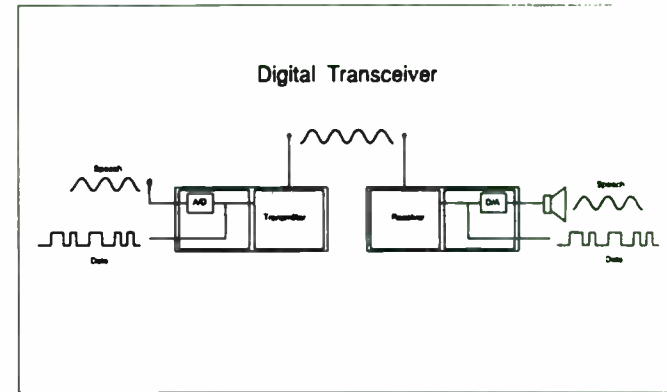
WHY THE MOVE TO DIGITAL COMMUNICATIONS

- Increased capacity for users
- More secure communications
- Additional services available
- Reduced fraud
- Common system across Europe



HEWLETT
PACKARD

DIGITAL TRANSCEIVER



HEWLETT
PACKARD

Digital modulation used in communication systems provide several benefits over analog. One of the primary benefits is the increase in capacity that can be gained by sending information in a digital format. Digital modulation also provides more secure communications than analog. With analog systems anyone with a frequency scanner can listen to a conversation. With digital systems the information is encoded and can have encryption added for even further security. Some digital modulation systems offer ISDN interconnect services. Any of the information available with an ISDN system would also be available over the communication link. So a user of a digital cellular phone would be able to transmit faxes, send/receive data files to/from his cellular phone, etc..

Another reason for the move to digital communications is to reduce the fraudulent use of cellular phones. Cellular service providers are losing millions of dollars every year to "pirated" cellular phones. These cellular phones are typically used by criminals. The calls are very hard to trace and provide good communications for the illegal operations.

Finally, a common cellular system is being implemented using digital modulation across Europe. Previously several different analog cellular systems were used by the different countries. This made it impossible for users to use their cellular phones as they crossed borders of countries. The new GSM digital cellular system will give users seamless phone coverage throughout Europe.

A digital transceiver transmits and receives voice on each end. However it converts the analog voice to data before modulating the carrier frequency. At a very basic level this can be done by using an analog to digital converter to digitize the voice, then send the data to the modulator of the transmitter. On the receiving end, the data is demodulated and run through a digital to analog converter to recover the original voice. Digital transceivers may also send and receive data directly between transmitters and receivers.

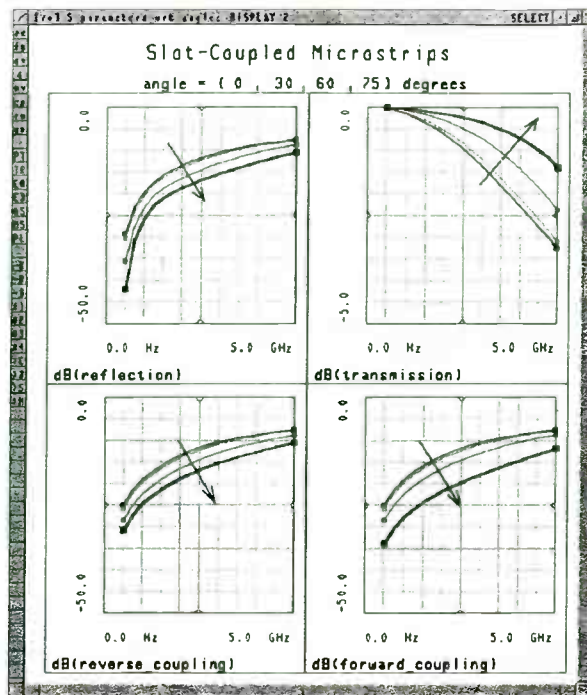
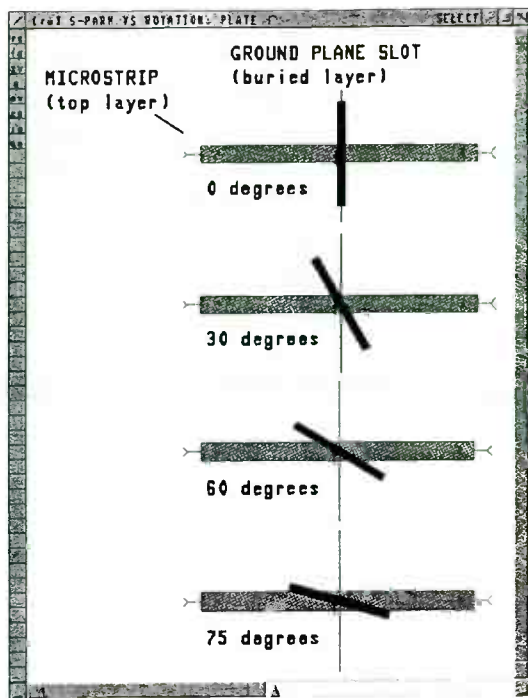


Figure 3. Slot-coupled microstrip lines. A two-layer dielectric has a ground plane sandwiched in the middle. Microstrip lines are established above and below the ground plane. They are coupled through a slot in the ground plane that has been rotated at various angles from perpendicular.

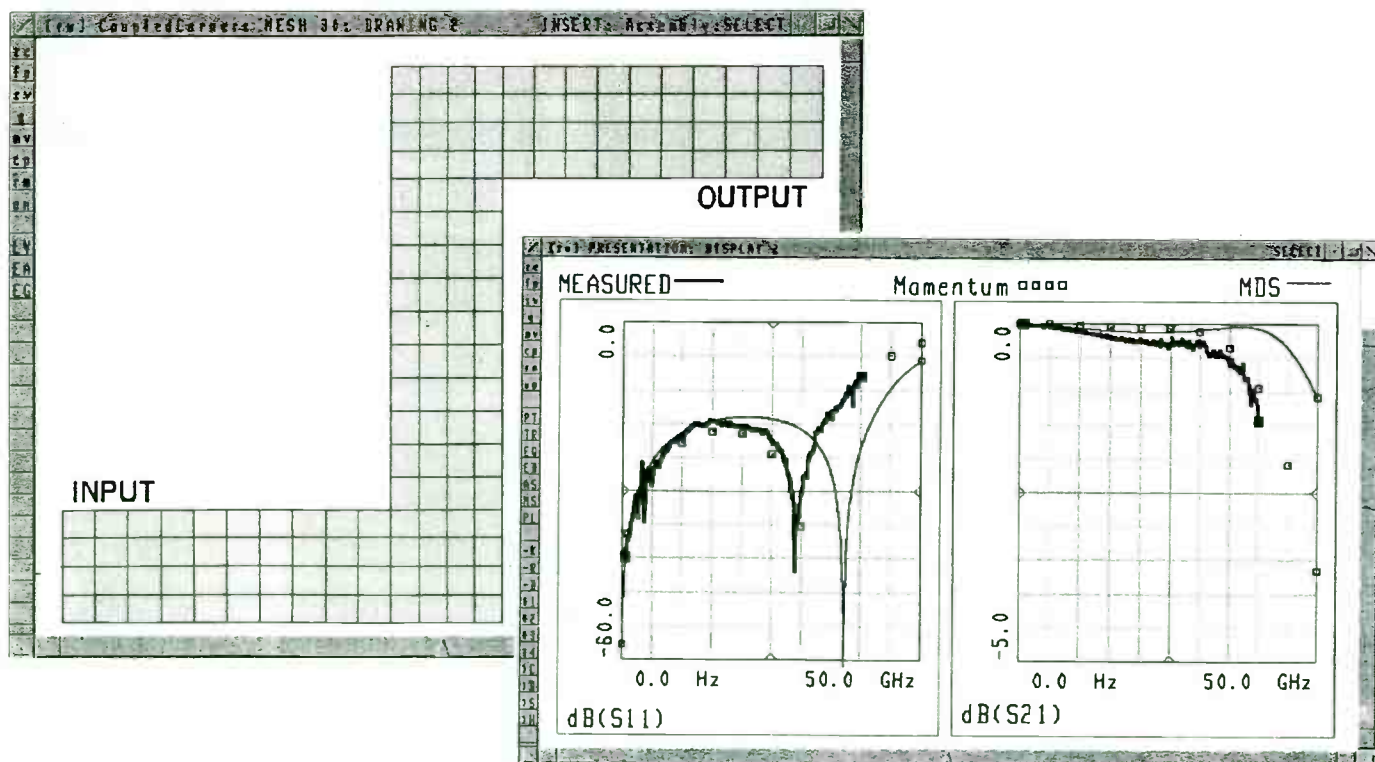
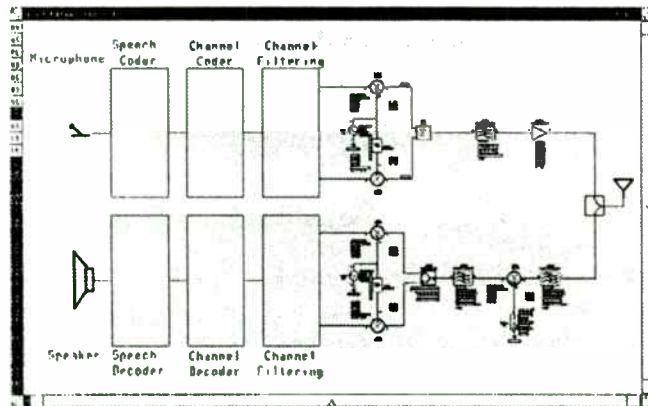


Figure 4. Coupled microstrip corner discontinuities. Even though these two simple microstrip corners are separated by a distance of several substrate-heights, they are coupled through higher-order modes excited in their vicinity. In practice, this alternate propagation path shifts a resonance down in frequency, a subtlety predicted by a MoM simulator and verified by measurements, but not modeled by a circuit simulator.

DIGITAL RADIO BLOCK DIAGRAM



HEWLETT
PACKARD

CHANNEL FILTERING

- Needed to reduce occupied bandwidth of digital modulation
- Is applied to digital data stream before input to digital modulator
- Can cause intersymbol interference

HEWLETT
PACKARD

This is a generic digital radio block diagram. As can be seen the voice or audio is input to the microphone of the transmitter. The speech then goes through a speech coder. The primary purpose of the speech coder is to convert the audio into data and minimize the number of bits needed to represent the audio. The data then goes into a channel coder. The channel coder takes the voice data and adds additional data information that will be used by the receiver to recognize and reconstruct the transmitted signal. The channel coded data is then modulated onto an RF carrier, filtered (to reduce the bandwidth required to send the information) and pulsed out in "packets". On the receiving end, the pulsed carrier is received, filtered, and downconverted to an intermediate frequency (IF) which is again filtered and then demodulated. The data out of the demodulator is sent to the channel decoder to strip off channel coding information and then sent to the speech decoder to reconstruct the original speech.

Once the digital information is channel coded, it is passed through a channel filter. Filtering allows more channels to be packed together, optimizing the use of airspace. The choice of the filter is very important, as it can easily introduce what is known as intersymbol interference. This interference degrades the performance of the radio by increasing the bit-error-rate (BER).

Figure 5. Coupled-line bandpass filter. The shape and pass band of this microstrip coupled line filter is predicted by a planar E&M simulation.

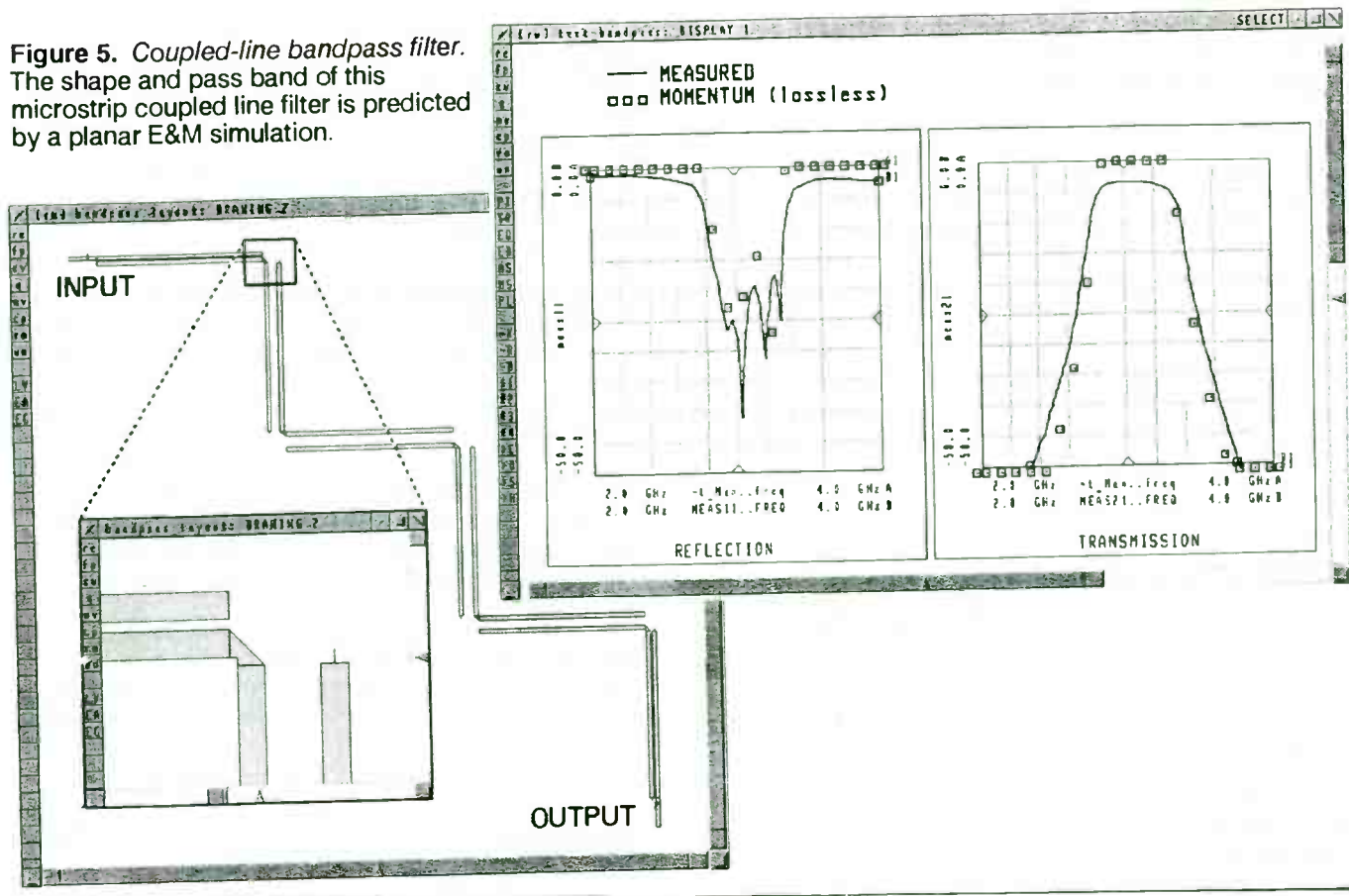
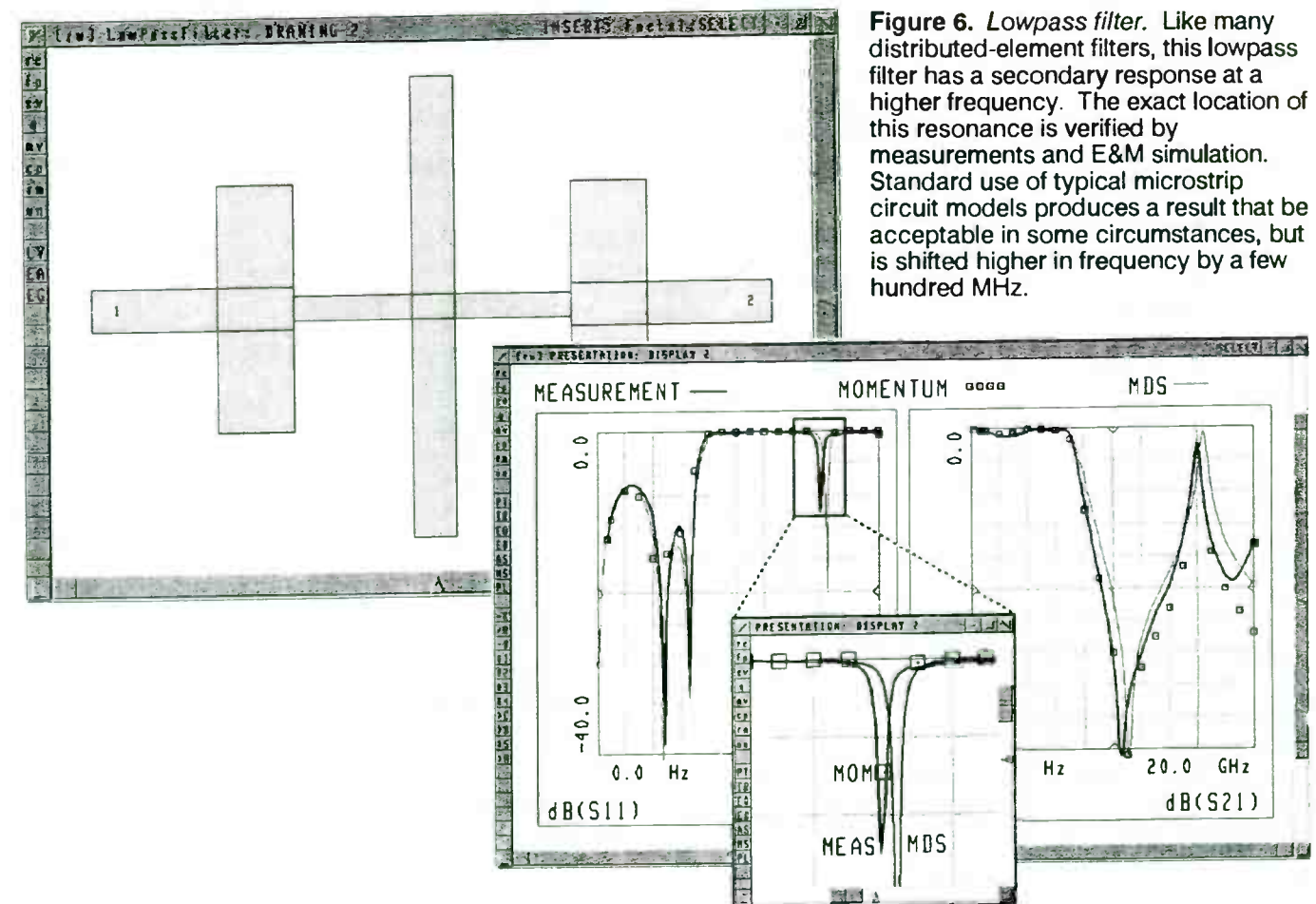


Figure 6. Lowpass filter. Like many distributed-element filters, this lowpass filter has a secondary response at a higher frequency. The exact location of this resonance is verified by measurements and E&M simulation. Standard use of typical microstrip circuit models produces a result that is acceptable in some circumstances, but is shifted higher in frequency by a few hundred MHz.



Comparison of different EM simulation methods

There are two dominant electromagnetic solution techniques in commercial use today, Method of Moments and the Finite Element Method. The basic differences between the two approaches are illustrated and summarized here using two commercially-available simulators from Hewlett-Packard. They are the 2.5-dimensional (multi-layer planar) MoM simulator (HP Momentum) and full 3-dimensional FEM simulator (HP HFSS).

3D Finite Element Method

The 3-dimensional approach is the more general of the two alternatives discussed. The working equation used by HP HFSS is an energy minimization problem shown below.

$$F(\vec{E}) = \int_{\Omega} \{(\nabla \times \vec{E})^2 + k^2 \vec{E}^2\} d\Omega + \sum_{i=1}^2 \int_{P_i} (\hat{n} \times \nabla \times \vec{E}) \cdot d\vec{S}$$

Equation 1. The HFSS energy equation

First, the volume is subdivided into a 3-dimensional mesh. The port solutions are then determined and used as "excitations" on the structure. The energy within the volume is minimized and the electric field that satisfies Maxwell's Equations is determined. The S-parameters are then calculated from the resulting field distributions.

In the equation above, the volume and the port definitions are known, leaving the electric field (E vector) as the only unknown. The problem statement makes few assumptions about the nature of the circuit and allows for complete generality.

2.5D Method of Moments

The 2.5-dimensional approach assumes that the circuit is planar, or a series of planes connected by idealized vertical currents (vias). It also assumes that the metallization has zero thickness. For circuit designers, these operating assumptions are quite reasonable. In return for these assumptions, the problem can be stated as shown in Equation 2.

$$\int_S dS' [G_m(r, r') J(r') - \nabla \cdot (G_e(r, r') \nabla' \cdot J(r'))] = -E^i(r)$$

Equation 2. the Momentum equation.

Green's Function

The above equation stands in contrast to Equation 1. $G_e()$ and $G_m()$ are known as the electric and magnetic Green's Functions. $J()$ is the current distribution throughout the system and represents the only unknown.

Since the substrate dielectrics and thicknesses are known in advance, the Green's Functions can be

calculated once and stored in a database. Although the pre-calculation of the Green's Functions may be a significant computational step, it is only required once. All subsequent simulations of any patterns of metallization on that substrate are greatly accelerated. In practice, the assumption of a planar circuit and pre-calculation of the Green's Function can reduce the overall computation time to seconds or minutes instead of minutes or hours (per frequency point).

Other Advantages of HP Momentum

HP Momentum has two additional advantages over the general 3-D FEM simulator. First, HP Momentum allows the user to choose between meshing the metal or absence of metal on a particular layer. This is useful for transmission media that use large ground planes, such as coplanar waveguide or slotline. It is also very efficient for estimating the effect of discontinuous ground planes. The 3-D FEM tool must create mesh elements in the entire volume, thus adding considerably to the size of the problem, which further impacts resource usage and solution times.

Finally, HP Momentum is an open-boundary simulator that does not require that the circuit to be placed inside a conducting metal box. This allows the simulator to account for radiation loss and surface waves correctly.

Disadvantages of Method of Moments

Like all good compromises, the efficiency of the Method of Moments technique comes at a price. First, there are large classes of electromagnetic problems that cannot be solved using a planar tool, the most common involving packaging and transitions between transmission media. Some multi-layer planar simulators have been represented as being quasi-3-D with the generous use of vias, but all commercial MoM simulators have similar limitations in this regard.

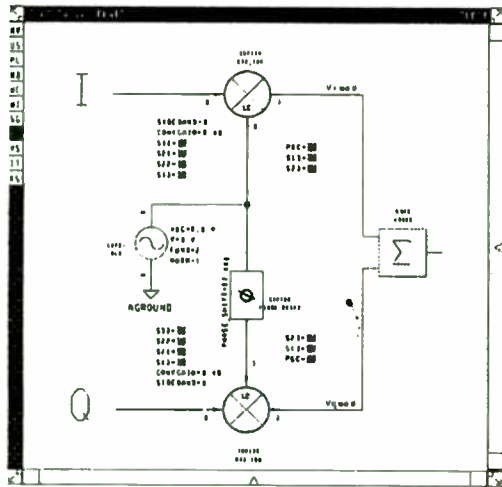
Growth of resource usage and solution times

Second, the Method of Moments formulation leaves behind a smaller, but full matrix to solve. In fact, this is a benefit for some circuits since the MoM technique tolerates a coarser mesh for comparable accuracy. However, the full matrix causes the resource usage to grow as the *square* of the number of unknowns, while the solution times grows as the *cube* as the number of unknowns. This is inescapably true of all of today's commercial MoM simulators.

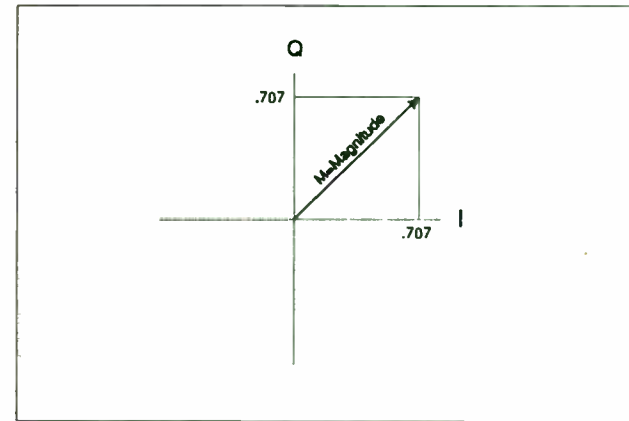
In contrast, FEM matrixes remain sparse longer and grow at slightly lower geometric rate (closer to *n-squared*). At some point, MoM can lose its efficiency advantage and take longer than a full 3-D FEM simulation. This point seems to be on the order of several thousand unknowns but is difficult to verify, since the crossover point occurs at the RAM and disk horizon of today's desktop computing capacity.

This crossover point could be reached sooner with inefficient gridding schemes. An example of an overly-conservative MoM mesh is the use of hundreds or thousands of tiny rectangles to simultaneously represent curved or angled patterns on a large pattern. A few triangular sections might be more than adequate for the situation.

MODULATION



THE I/Q PLANE



255

Once the voice information has been filtered, it is placed on a carrier through some type of modulation. Many modulation formats, such as amplitude-shift-key (ASK), frequency-shift-key (FSK), and phase-shift-key (PSK), are used in digital radios. Shown here is a basic I/Q modulator. The signal applied to the I channel controls the amplitude of the in-phase signal; the signal applied to the Q channel controls the magnitude of the quadrature signal.

A convenient way to look at modulation is to use the I/Q plane. This plane is a way to show both amplitude and phase information of the carrier. Digital modulation can use both phase and Amplitude to carry information. Let's look at a few basic types.

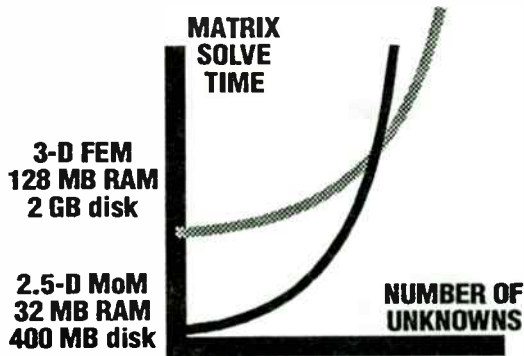


Figure 7. Matrix solve time vs. number of unknowns

Notice that in the nominal case, the 3-D FEM tool requires a dedicated "number-crunching" workstation for reasonable design capacity, while the MoM tool runs on the class of desktop workstation already used for typical CAE applications.

Conclusion

Many companies continue to invest in their own specialized electromagnetic tools in order to retain a proprietary advantage. However, as the commercial CAE vendors make each generation of these electromagnetic tools available to wider audiences, the tools are also being integrated more tightly into the mainstream CAE environments. This makes the commercial tools more accessible, convenient, and typically makes them better-documented and supported relative to in-house tools.

Having taken this brief tour of electromagnetic simulation tools, the high-frequency circuit designer should feel confident that E&M tools have matured quickly to help meet the challenges of a new era. Method of Moments simulators are of particular value to circuit designers because they provide accurate results quickly from within the CAE environment.

APPENDIX: Mechanics and Interaction with a MoM Simulator

For the benefit of designers who have never interacted with an E&M simulation tool, the mechanics and internal computations are summarized here at a high level. Principles are illustrated with screens and examples from HP Momentum, a recently introduced MoM-based simulator.

As viewed from the user's perspective, the amount of activity belies the actual complexity of events inside the software. At the very simplest level, the procedure has these steps (illustrated in figure 8):

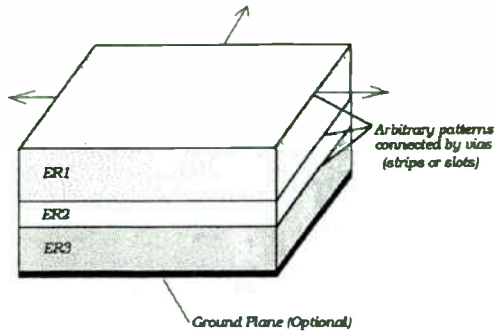
1. Define a substrate and do a pre-calculation
2. Define the planar metallization and slot patterns, resistivities, and ports
3. Simulator subdivides pattern (a "mesh" is generated)
4. Feedline analysis is performed to determine port impedances and circuit parameters.
5. Method of Moments is applied to calculate distribution of currents, from which the S-parameters are calculated.
6. Results are fed back for plotting, visualization, and re-use in subsequent circuit simulations.

The substrate definition and pre-calculation (Step 1) is done once and stored for re-use, while the software performs Steps 3 through 6 automatically. This leaves the drawing of the planar patterns (Step 2) as the only significant task for the user. In the case of HP Momentum, which is fed directly from the HP RF/Microwave Design System, this information comes directly from the schematic or layout that has already been entered for the circuit. Therefore, as much of the task as possible has been automated.

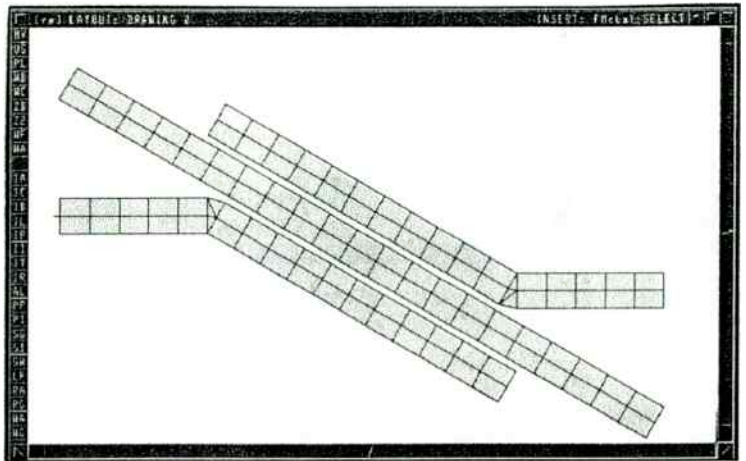
Acknowledgements:

The author wishes to thank Alex Anger, Brad Brim, Charles Plott, and Dave Wilson of Hewlett-Packard for their assistance in preparing this survey.

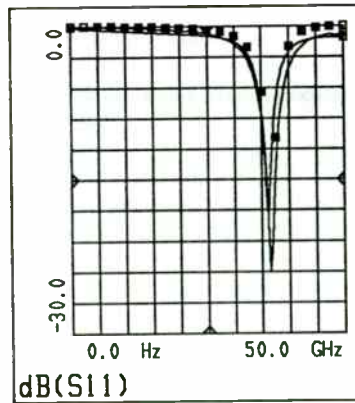
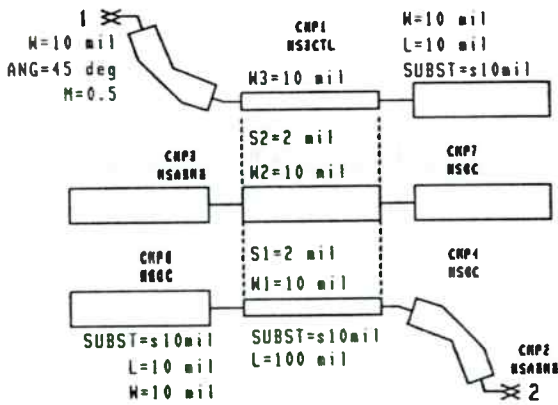
Figure 8. Steps in Using a Method of Moments Simulator



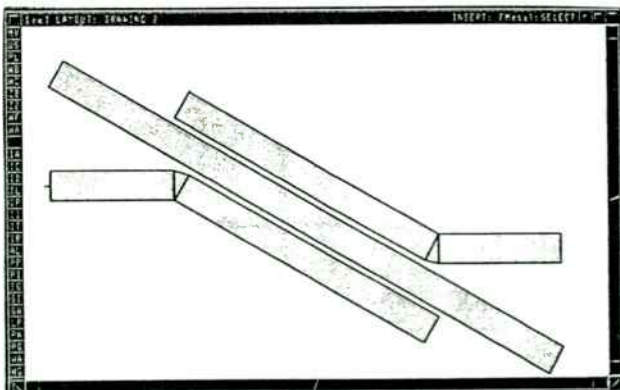
Step 1. Define the substrate and perform any precalculations.



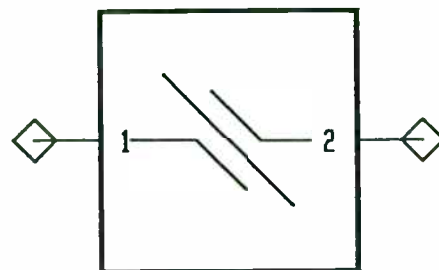
Step 3. Simulator subdivides structure into a "mesh". **Step 4 (not shown)** feedline analysis performed to determine port impedances and circuit parameters.



Step 5. Method of Moments is applied to calculate the distribution of currents, from which the S-parameters are calculated.

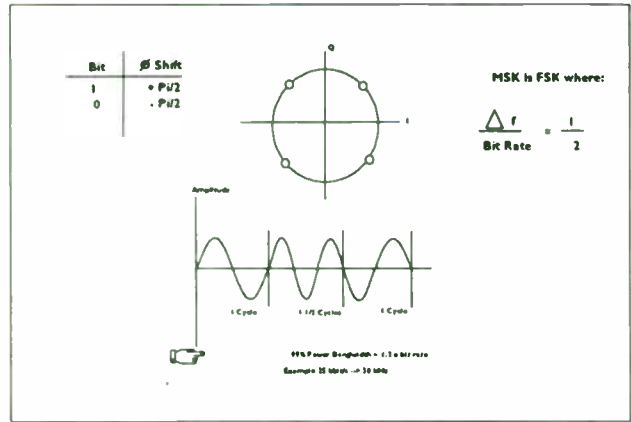


Step 2. Define the planar metallization and slot patterns and ports using schematic or graphical editors.



Step 6. Results are fed back for post-processing and re-use in circuit simulations.

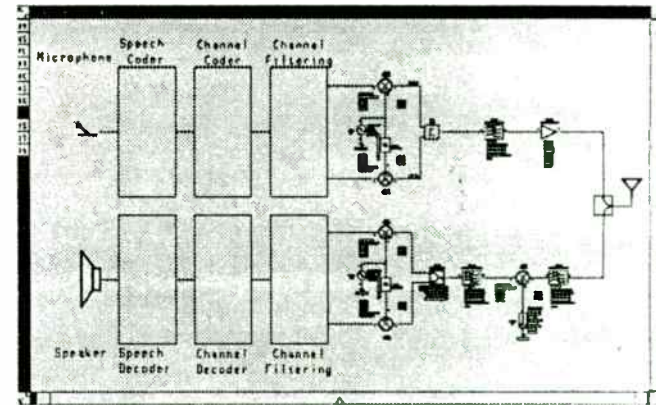
MSK MINIMUM SHIFT KEYING



HEWLETT
PACKARD

10001 00010010 000

SUMMARY: THE DIGITAL RADIO



HEWLETT
PACKARD

10001 00010010 000

Another possible digital modulation format is Frequency Shift Keying. Like BPSK, simple FSK involves shifting the carrier between two values, but uses frequency instead of phase. FSK is widely used for computer MODEMS and other digital transmission systems. For digital communications systems a popular modulation format is Minimum Shift Keying (MSK). MSK is a special form of FSK where the frequency shift is chosen to be exactly twice the data bit rate. It is called minimum shift keying because the frequency spacing between the two frequency states is the minimum spacing which allows the two frequency states to be orthogonal to each other. On the I/Q diagram, MSK appears to be a circle with a radius of one. Because the two frequency states are orthogonal, the frequency shift translates to either a +90 degree phase shift or a -90 degree phase shift (for either a one or zero data bit input to the modulator). Note on the amplitude versus time graph that MSK results in one cycle of the lower shift frequency and one and one-half cycles of the higher shift frequency. The main advantage of MSK is its spectral efficiency. As a rough rule of thumb, 99% of the power in a MSK modulated carrier will occupy a bandwidth equal to 1.2 divided by one over the bit rate. For a 25 kbits/s data stream, MSK would require 30 kHz of bandwidth. This performance is far better than other modulation formats.

That ends the brief tour of a digital radio. In summary, a signal is received from a microphone, digitized, speech encoded, channel coded, filtered, and modulated. On the receiving end, the signal is demodulated, filtered, decoded, and delivered to the speaker.

A Monolithic 915 MHz Direct Sequence Spread Spectrum Transmitter

Stephen Press
Jeff Barry
Jim Marsh
Tektronix Microelectronics
P.O. Box 500
Beaverton, Oregon 97077

The allocation of the Spread Spectrum bands has spawned a wide range of applications which demand high performance designs with economical implementations. This article describes one such design which is a 915 MHz Spread Spectrum transmitter implemented with a minimum number of parts and a low manufacturing cost. An overview of the system design will be presented, however the bulk of the discussion will concern the transmitter ASIC which is a monolithic implementation including the 915 MHz oscillator, a divide-by-eight prescaler, a pseudorandom code input buffer, an up-converting mixer, an AGC amplifier, and an output driver.

SYSTEM OVERVIEW

This design is part of a fault detection system that broadcasts a signal to a remote location, identifying the fault condition. The transmitted signal has to be successfully received at distances up to two miles. The sensitivity of the receiver requires the transmitted signal output be +20 dBm. The total transmitter design fits on a circuit board which is less than 1.5 square inches. As shown in Figure 1, there are two ASICs in the design, the bipolar ASIC described above and a CMOS ASIC. The CMOS ASIC includes a pseudo-random code generator, a crystal controlled oscillator, a phase detector, and an integrating amp. In addition to the two ASICs, the transmitter board contains a prescaler, a regulator, and various passive components.

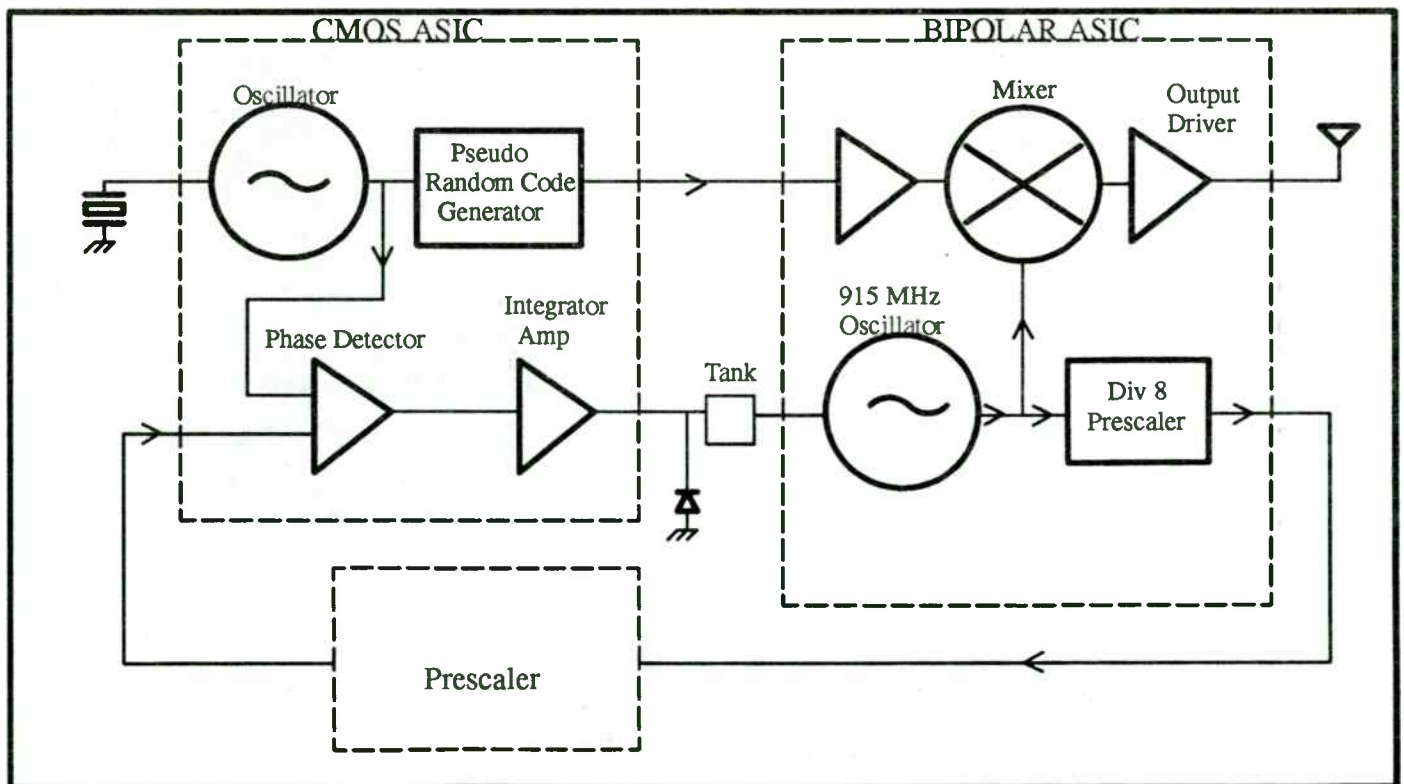


Figure 1. System Overview

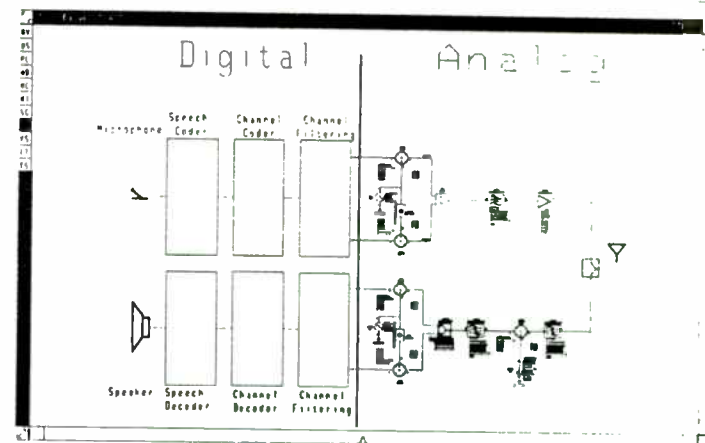
AGENDA

- Digital communications basics
- Important MDS capabilities
- A Case study: DQPSK Radio
 - Transmitter performance
 - Channel distortion and correction
 - Receiver performance
- Summary



110041024208 (Rev. 1)

DIGITAL RADIO: DIGITAL vs. ANALOG



110041024208 (Rev. 1)

Looking one more time at this block diagram, much of modern digital radios are implemented using Digital Signal Processing, or DSP, chips. The contribution of the HP High-Frequency Design System is in the analysis of the system from the output of the transmitter DSP to the input of the receiver DSP. Other simulation tools are available to analyze the DSPs.

So, the HP High-Frequency Design System takes the I and Q outputs, and analyzes the channel performance up to the I and Q inputs on the receiver.

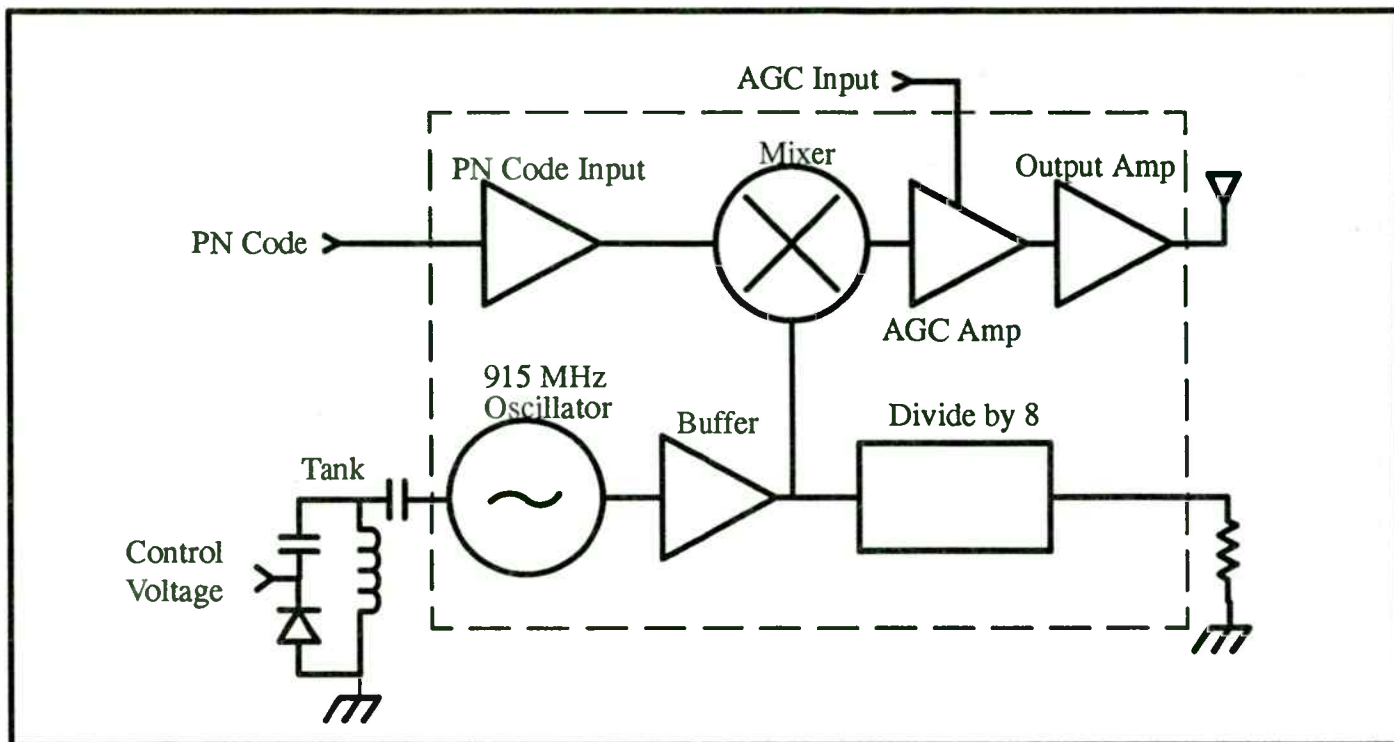


Figure 4. Transmitter ASIC

915 MHz OSCILLATOR

The negative impedance oscillator used in this circuit is single ended and resembles the Colpitts architecture. (See Figure 5.) The principal components include transistor Q7, capacitors C1 and C2, and the external tank circuit. In the tank circuit a varactor diode was used as a means of adjusting the frequency of oscillation. A parallel tank circuit was used to desensitize the oscillation frequency to bond wire inductance. In a negative impedance oscillator the real portion of impedance looking in from the tank is negative at the frequency of oscillation (and for some surrounding bandwidth). It is this negative impedance that allows the circuit to oscillate. The reflection coefficient looking into a negative impedance is more than one, which implies a continually growing oscillation at the resonant frequency of the tank. The factor limiting the amplitude of oscillation varies in different oscillator architectures. However a convenient way to view amplitude limits can be presented with a series resonant tank. In a series resonant tank there will be a parasitic resistance in the L and the C tank elements and the trace connecting the elements and the oscillator on the IC. The relationship between this resistance and the inductance and capacitance of the tank can form the main contribution to determining the Q of the circuit where;

$$Q = \frac{1}{R} * \sqrt{\frac{L}{C}}$$

During a cycle of oscillation the sinusoidal voltage variation

changes the input impedance of the oscillator from the initial impedance at the DC bias point. This is due to large signal effects on the bias point of the transistor base. When the magnitude of the negative resistance of the oscillator equals the parasitic resistance then the oscillation amplitude will grow no further.[2][3]

The oscillation at the tank is transferred to the emitter of Q7 where it is converted to a current. This current is mirrored from Q8 to Q9. Q10 is a cascode stage used to increase the bandwidth. The mirrored current is converted to a voltage across R9. This signal is buffered by Q1 and fed into the single-ended-to-differential stage (Q2, Q3). R10 biases the undriven side of the differential stage (Q3). C3 provides an AC ground at this input. The signal is amplified across the differential pair, Q2 and Q3. One draw back to differential conversion using this technique is that the DC voltage dropped across R10 forms an offset on the Q3 side of the amplifier. To minimize the offset R10 must not be too large.

The initial amplitude of the oscillation at the tank is determined by large signal phenomena. Because it is difficult to predict the exact amplitude of the oscillation at the tank, the oscillator was designed to limit at the Q2-Q3 amplifier for all temperature and process conditions. Thus the limiting conditions of this amplifier, which are predictable, control the output amplitude of the oscillator stage. Limiting at this stage does introduce harmonics, however these are reduced by the bandwidth limit of later stages and by the matching network used at the output.

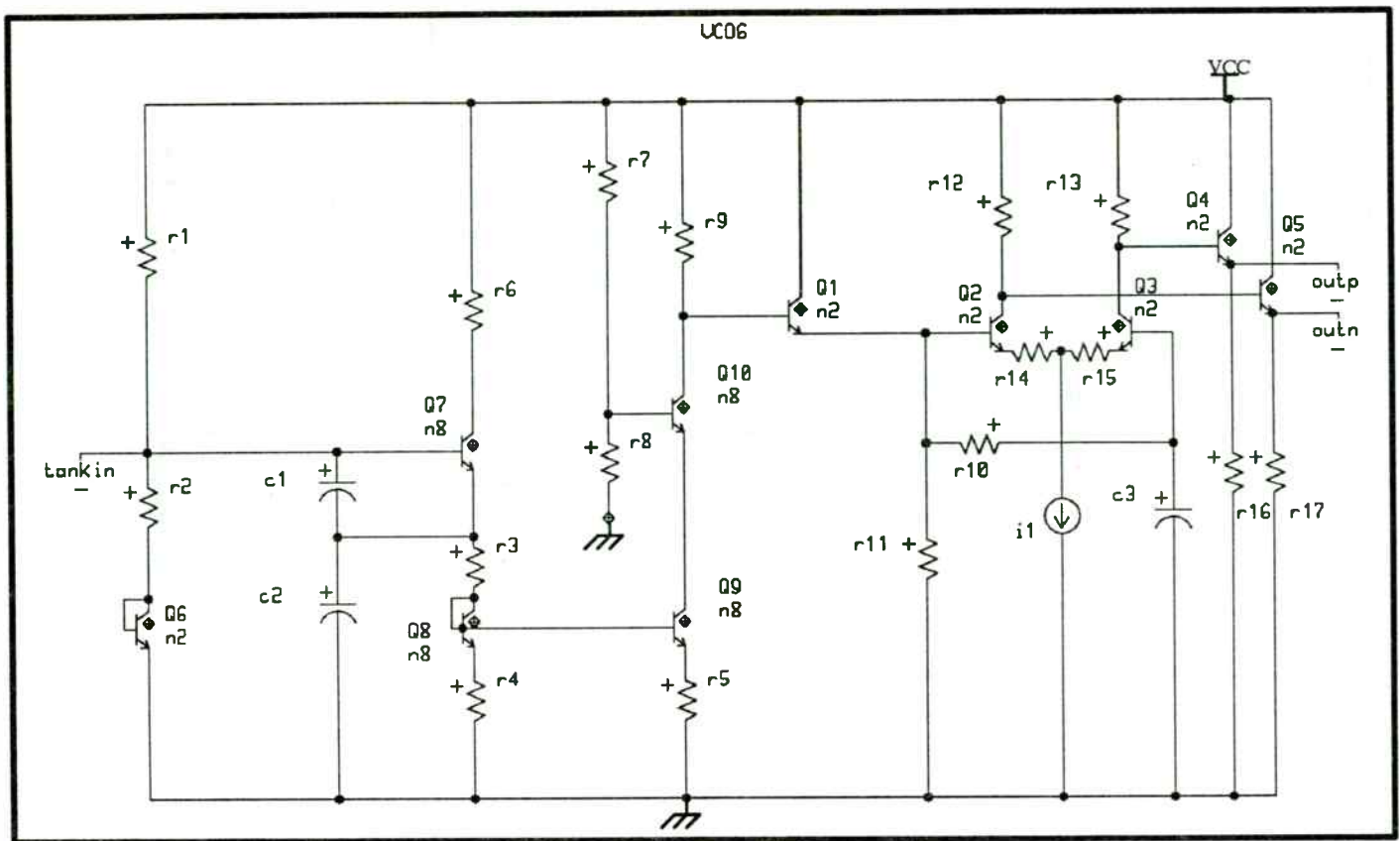


Figure 5. Simplified schematic of the VCO

THE PRESCALER

Although it would be desirable to put the complete prescaler on chip, this was not possible since this design was done on a standard array with limited numbers of devices. It is useful to have some of the prescaler on chip for two reasons. First it is an excellent buffer between the oscillator and the off chip prescaler and second, a 115 MHz signal coming off chip is handled much more easily than a 915 MHz signal.

The prescaler is a traditional ECL sequential divider using three flip-flops. Since the architecture is standard it will not be discussed further here.

PN CODE INPUT

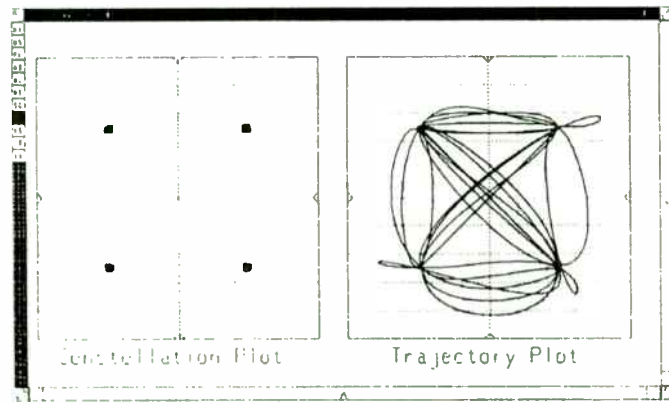
The PN Code input is designed to accept a CMOS input signal. In this particular application the code rate is about 3 megabits per second (MBPS).

THE MIXER

The mixer as shown in Figure 6 is based on the Gilbert mixer design. Normally in a mixer the lower port (Q5 and Q6) is the

RF port and the LO input is the upper port (Q2, Q3, Q7, and Q8). The amplifier formed with the lower differential pair is linearized with the addition of the emitter degeneration resistors R4 and R11. By so doing IP3 is increased and harmonics are decreased. Q5 and Q6 are large devices to lower noise on the RF port. However in a mixer which is part of a Spread Spectrum transmitter these rationales may not hold. As shown in Figure 6, the LO from the VCO is placed at the lower port and the PN code is placed at the upper port. This connection scheme is the opposite of that used in most applications. In a Spread Spectrum system the LO is phase modulated by the PN code, in particular the phase shift during a PN code transition is 180 degrees. The quicker this phase shift occurs the better defined is the information. The upper port accomplishes this task. The lower port accepts the high frequency 915 MHz LO. Because the lower port was used for the LO the bandwidth of the mixer remains relatively flat to 1 GHz. Two factors act to increase the bandwidth in the LO path through the mixer. First the transistors in the upper port, which are switching at a relatively slow rate (≈ 1.5 MHz), act as a cascode for the the transistors at the lower port. Second, by keeping the degeneration resistors (R4 and R11) at the lower port the gain is reduced to about 1.5 which also increases the bandwidth. The goal in this design was to keep the bandwidth flat past the frequency of transmission. As shown in Figure 7, simulation indicates this goal was achieved in the mixer.

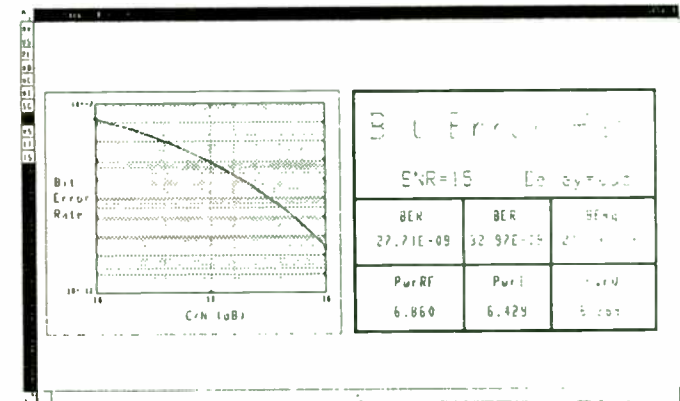
CONSTELLATION PLOT



HEWLETT
PACKARD

100041000000 700

BIT ERROR RATE



HEWLETT
PACKARD

100041000000 700

261

A constellation plot is just a plot in the I/Q plane. If the number of points displayed is equal to the number of time samples, a cluster of dots appear around each state. Ideal systems have all of the points aligned directly at the input data. The right plot is the same plot, however this time the trajectory of I versus Q is shown. This clearly illustrates how previous states affect the current state. Notice all of the different paths that are followed as the system traverses the -1,-1 to 1,1 state.

The ultimate test of radio performance is bit error rate. This is the single quantifiable measure of radio performance. Eye diagrams and constellation plots give insight into system performance, but the only real specification is how error-free are the bits at they are transmitted and received.

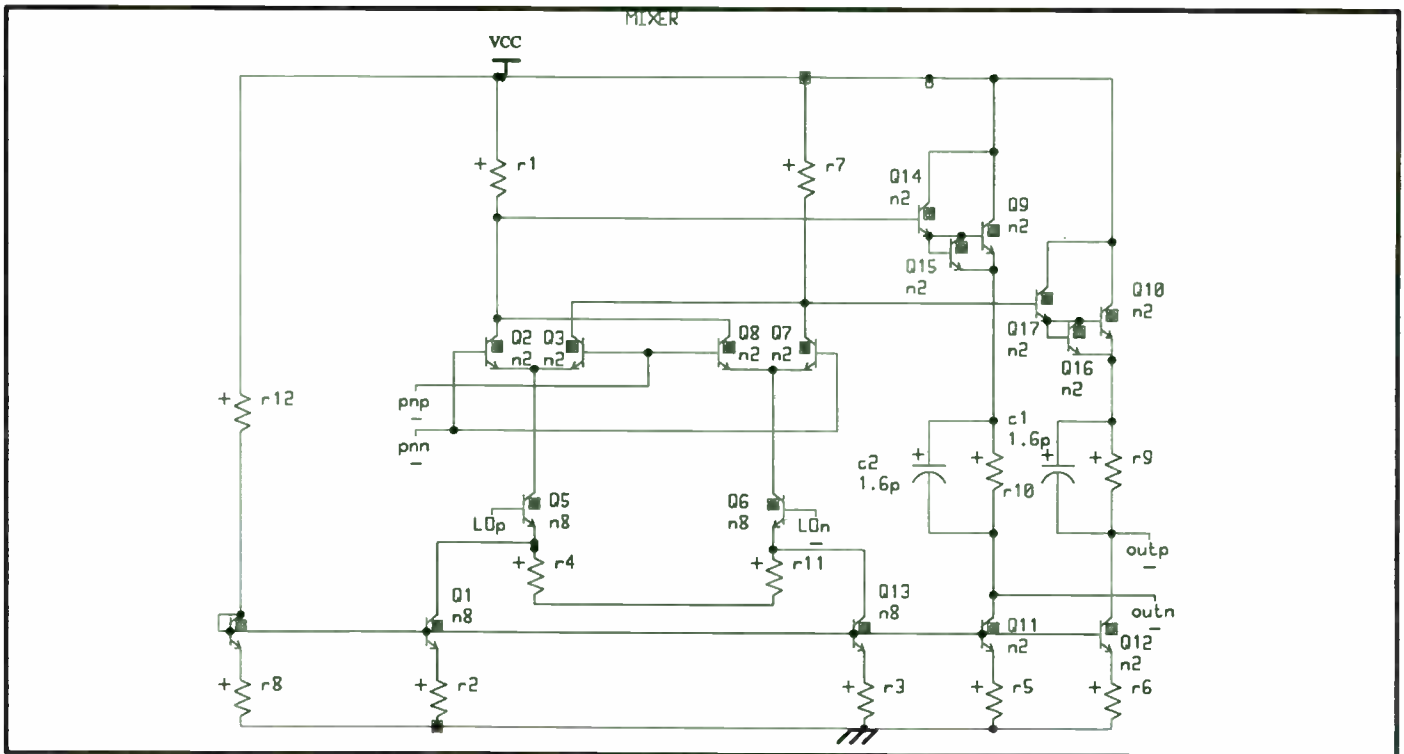


Figure 6. Simplified mixer schematic

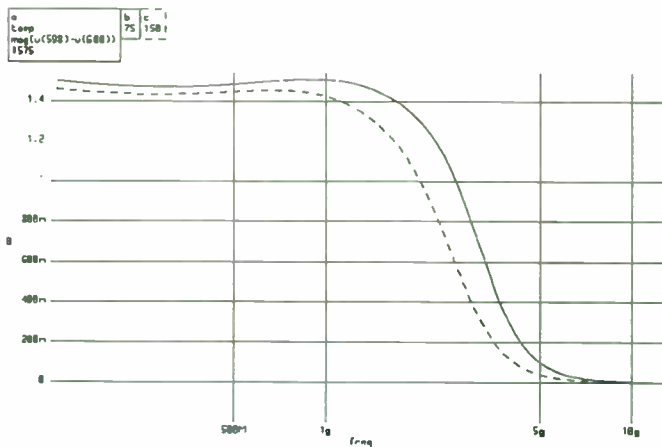


Figure 7. Mixer gain over bandwidth and temperature (simulated)

AGC AMPLIFIER

The peak to peak voltage coming out of the mixer is about 1 volt. The AGC amplifier increases this signal to about 1.8 volts. Since the circuit operates with a 5.2 volt supply and signal levels become relatively large, it is important to assure that for all

signal conditions no transistors saturate. The mixer output is level shifted through two diode drops and an additional 1 volt through R9 and R10 before being passed on to the AGC amplifier. This allows the AGC enough headroom to swing a 1.8V signal. Amplification in the AGC stage is provided by the differential pair Q1 and Q2 (see Figure 8). Gain is adjusted by varying the bias current in Q1 and Q2. This is accomplished by circuitry consisting of Q7, Q3, Q4, Q12, Q13 and associated resistors. As the applied AGC voltage at the base of Q7 is reduced from the nominal 5.2 volts, the current supplied to Q1 and Q2 is reduced which decreases the gain. The AGC gain adjustment does not have to be linear for this system but it does require 20dB of range which is achieved. (Figure 9). The purpose of the AGC is to cut back the transmitted power when the system battery power starts to fall. Since there is no requirement for a linear relationship between the AGC voltage and output power, the system described above is satisfactory.

The circuitry comprised of PLAT1, PLAT2, and Q16-Q20 keep the output common mode voltage level constant over the normal AGC voltage range. This compensation circuitry prevents the Output Amplifier stage from saturating. As the AGC voltage is reduced the common mode voltage level at R10 and R11 rise due to the reduced current supplied to Q1 and Q2. Also as the AGC voltage drops, the compensation circuitry increases the common mode voltage drop across R20 and R21 to keep the AGC amplifier output common mode voltage level constant.

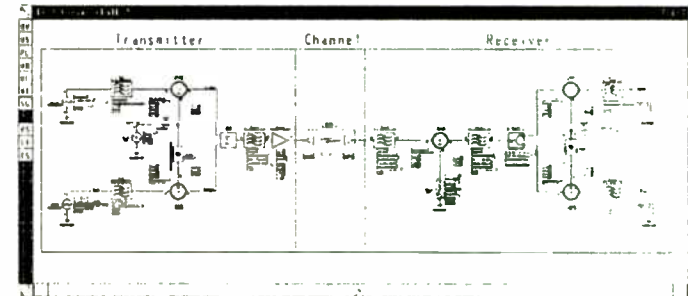
AGENDA

- Digital communications basics
- Important MDS capabilities
- A Case study: DQPSK Radio
 - Transmitter performance
 - Channel distortion and correction
 - Receiver performance
- Summary



© 1991-1992 HP

THE RADIO



Now let's look at a specific radio and analyze how different errors in the design of the system affect system performance. The analysis is separated into transmitter, channel, and receiver tests.

For our example, we have chosen this radio, a DQPSK radio. Although the raised-cosine filtering is normally done by a DSP, here we have included it so that we can more closely analyze the system. The system is stimulated by two pulse train sources of definable length. Here we have made the length of the pulse sequence equal to eight, thus accounting for filter ringing effects for the previous eight bits. The I and Q data are filtered and modulated, amplified and filtered, distorted by the channel, amplified, filtered, down converted, demodulated, and finally filtered again. The output data is sampled at the two terminating resistors.

Note that no clock regeneration circuitry is shown. Most modern radios use DSP techniques to generate clock timing, so we are assuming that the clock recovery is not part of the analog circuitry and that it has been perfectly recovered by the DSP.

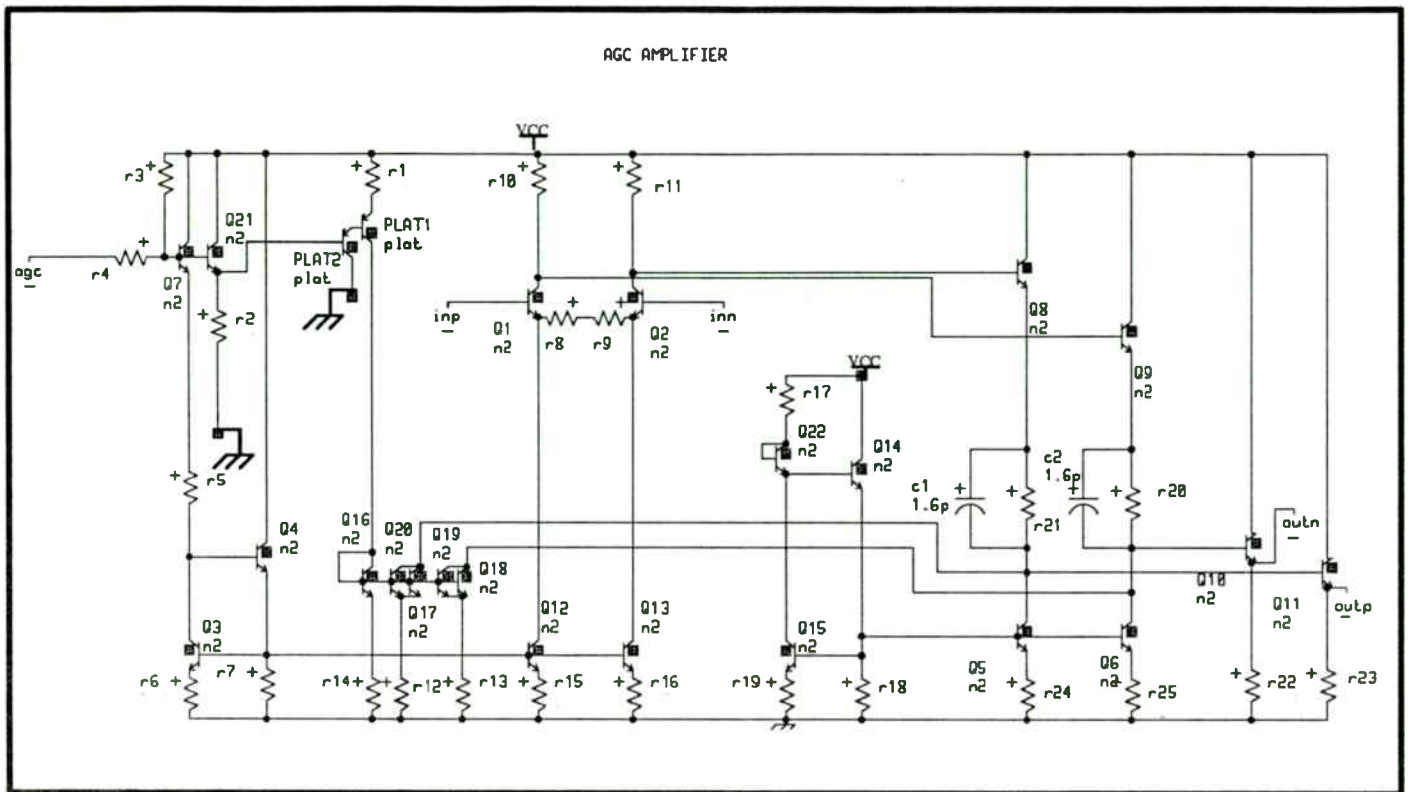


Figure 8. Simplified schematic of AGC amplifier

C11 to two emitter follower stages (Q7, Q12, Q24). These drive into the final common emitter stage consisting of Q21–23 and Q25. The output driver transfers power to a 37 ohm antenna through a matching network.

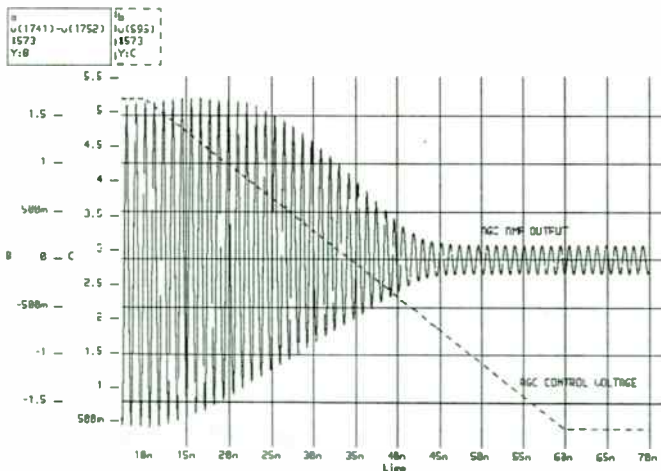


Figure 9. AGC effect on the transmitter output

RESULTS

The initial results on the bipolar ASIC have been measured in isolation from the rest of the system to separate the performance of the ASIC from the total system. As shown in the plot of Figure 11, the measured output power was 18dBm which is 2 dB below our system goal of 20dBm. Since the tests were run in isolation from the rest of the system, the oscillator was not phase locked and thus the frequency is not exactly 915 MHz. Figure 12 shows a narrow band plot of the output signal as viewed on a spectrum analyzer. The resolution bandwidth of the measurement was 1 kHz. Extrapolating from this the phase noise measured 10kHz from the fundamental is 97.2 dB down for a 1 Hz bandwidth. Also specified was the match between the transmitter output power with the PN code in either state (logic 1 or 0). This output power with PN code in logic state 1 and in logic state 0 matched to within 0.5dBm. This result achieved the required level. All results were measured with a Tektronix 2756P spectrum analyzer.

OUTPUT DRIVER

The output driver initially performs a differential to single ended conversion with the amplifier composed of Q3 and Q18 (in Figure 10). The output of this stage is AC coupled through

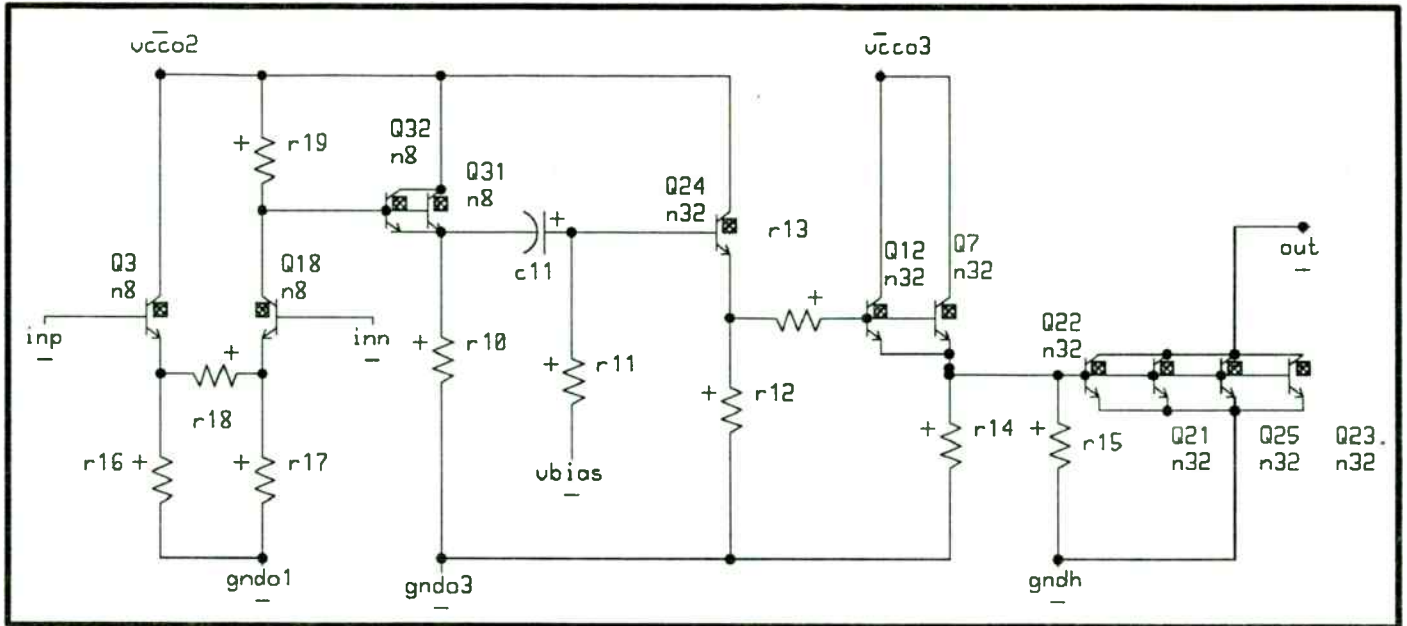


Figure 10. Simplified schematic of output driver

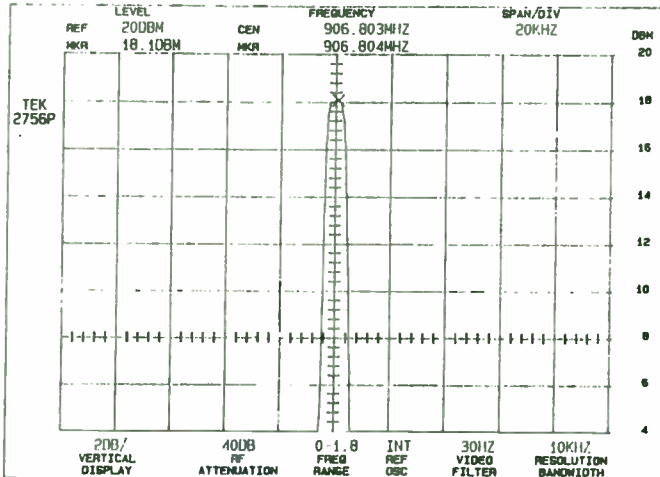


Figure 11. Transmitter output power

DISCUSSION

This design has successfully integrated five RF functions on a monolithic integrated circuit design. By so doing we have been able to make possible from a size and cost standpoint a system that would not have been possible with a discrete or multiple IC approach. With the rapidly growing use of the 915 MHz band this type of design will enable the implementation of many systems that would not otherwise be viable.

The RF ASIC met all of the system goals with the exception of transmitter output power. As discussed in the earlier section the measured output power was 2dB below the required 20dBm level. It is believed that the output stage is responsible for this problem. There are a number of reasons indicating that the fault does not lie in earlier stages. In addition, there are several possible effects in the output stage which could cause the observed problem. These will not be discussed here. Further experimentation will need to be performed to test these theories.

REFERENCES

- [1] "Quickchip 6 Integrated Circuit Design Guide", Version 1, Tektronix, Inc., June 1989
- [2] Gonzalez, Guillermo "Microwave Transistor Amplifiers, Analysis and Design", Prentice-Hall, Inc., Englewood Cliffs, N.J., 1984
- [3] Hayward, W.H. "Introduction to Radio Frequency Design", Prentice-Hall, Inc., Englewood Cliffs, N.J., 1982

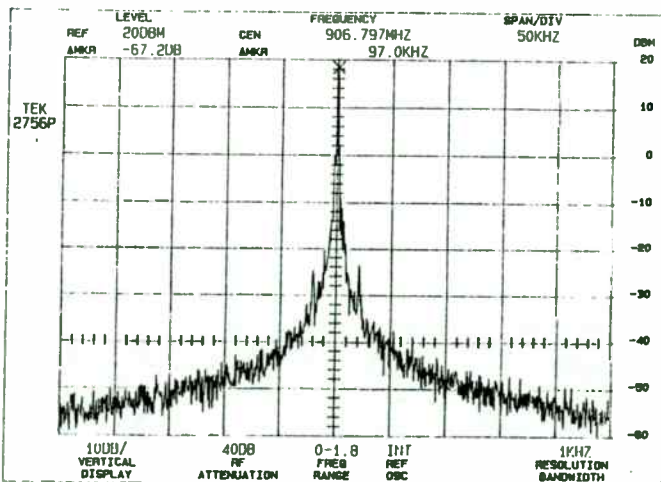


Figure 12. Phase noise at the output of the transmitter.

A Low Power RF ID Transponder

By Raymond Page
Wenzel Associates

This is the Grand Prize winner in the design category of the 1993 RF Design Awards Contest. This entry exhibited both innovative use of RF technology and an elegant implementation of that technology. The author was awarded a NOISE COM model UFX-BER noise generator for bit error rate testing.

For some time railroad companies have been wrestling with the problem of tracking rail cars. This has traditionally required manual log entry of identification numbers displayed on the cars as they pass through the switching yard. Some years ago, an effort was undertaken to use an optically scanned ID system. Dirt and optical registration problems led to its demise, forcing railroad companies to revert to the manual system. RF engineers have come up with a solution, using transponders mounted on the side of the cars which are read by interrogating transceivers positioned along the track.

Design Considerations

A practical transponder design must include minimal maintenance, a rugged low profile and low cost. The most elusive of these has been low cost. Presented here is a design which meets these requirements along with a brief discussion on the current state-of-the-art in passive RF identification transponders.

An important design constraint is that the transponder require little or no maintenance. Since no power is available from the rail car, the only conventional options are batteries or solar cells that maintain rechargeable batteries. The non-rechargeable batteries require periodic replacement, and the solar cell option would be both expensive and vulnerable to the environment. A passive design eliminates the need for batteries by rectifying energy from the interrogating RF field to power the circuitry.

The harsh environment presented to an RF device mounted on the side of a rail car is a challenging problem. Minimum clearance requirements, dirt, weather, vibration and an extremely large chunk of ferro-magnetic material near the antenna have to be considered. Additionally, the unit should be encapsu-

lated. Microstrip patch antennas have come to the rescue. They afford a low profile and can be made with an ordinary double-sided printed circuit board. The patch antenna is on the top and a ground plane is on the bottom, thereby eliminating the effects of the steel mounting surface.

A Low Cost Transponder

An unusually simple method of converting the interrogating RF field into a data-modulated signal which can be transmitted back to the reader contributes to the low manufacturing cost of this transponder design. The circuit uses only one inexpensive microwave semiconductor (a diode) and allows all parts to be mounted on an FR-4 printed circuit board with the patch antennas (Figure 1). By contrast, other approaches use expensive microwave parts, including SAW devices, oscillators, mixers, filters and amplifiers. Designs involving more RF circuitry tend to be power hungry, requiring increased RF interrogation fields.

Figure 2 shows the block diagram of the low power transponder. A 915 MHz receive antenna powers the rectifier/frequency doubler/AM modulator. It provides a rectified DC source to the MCU which returns data to be AM modulated onto the doubled frequency. An 1830 MHz antenna transmits the modulated

carrier.

A reader, incorporating an unmodulated 915 MHz interrogation transmitter with low (< -60 dBc) second harmonic distortion and an 1830 MHz AM receiver, is placed a relatively short distance away from where the transponder will pass (Figure 3). The amount of transmitted RF interrogation power needed to make the system function properly at a given distance can be estimated by equation 1:

$$P_r = P_t G_t G_r \lambda^2 / (4\pi R)^2 \quad (1)$$

Where P_r is the received power, and P_t is the transmitted power radiated by an antenna of gain G_t . G_r is the gain of the receive antenna, λ is the free space wavelength and R is the distance between transmitters. G_t and G_r are the gains over an isotropic radiator. A sufficient second harmonic return path signal will occur for any combination of power gain and distance capable of energizing the MCU.

One watt of power transmitted with an antenna gain of 31.6 (16 dB) and received with an antenna gain of 2 (3 dB) allows the transponder to function from as far as 20 feet away. This suggests that just over 1 mW is adequate to energize the transponder.

The transponder's surprisingly low

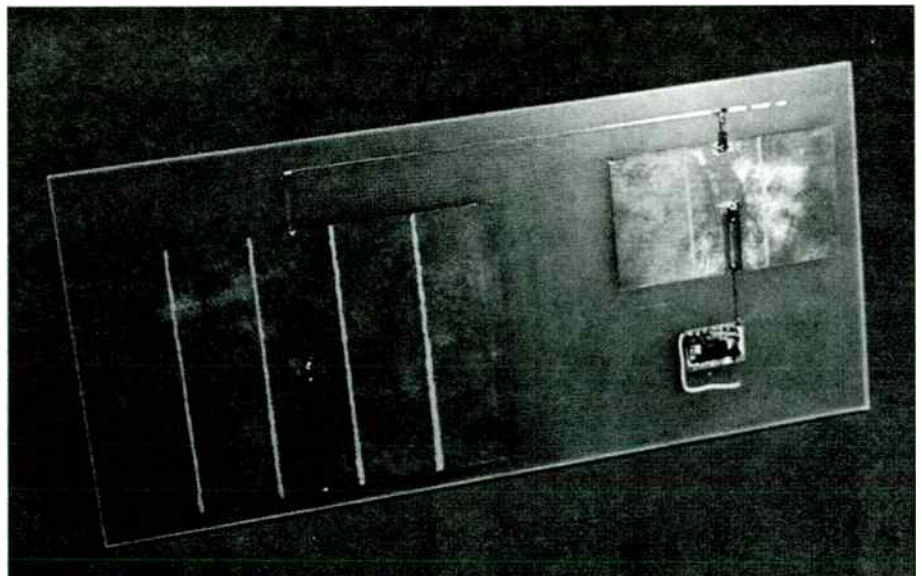


Figure 1. The complete transponder, with the 74AC00 test oscillator.

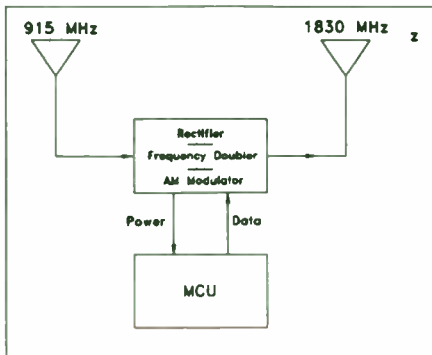


Figure 2. Block diagram of the passive transponder.

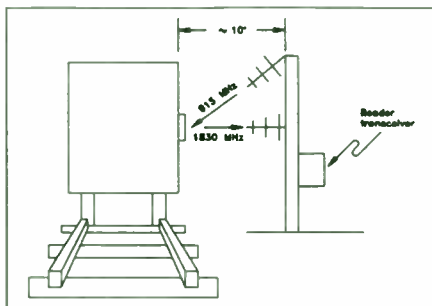


Figure 3. RF ID reader and transponder with rail car.

power requirement is due to its efficient means of rectification, frequency doubling and modulation. All of these functions are accomplished by a single microwave diode. A hybrid schematic in Figure 4 details the circuit. The 915 MHz patch antenna has two connections, a DC return path connected at the zero impedance point and a transmission line matched to the 120 ohm impedance at the edge of the antenna. The transmission line routes the signal to CR1 for rectification. A DC tap on the 1830 MHz antenna provides the power connection for the MCU. (See side bar on microstrip patch antennas.)

Careful placement of CR1 along the transmission line is crucial in creating the proper AC impedances for efficient frequency doubling. The 1830 MHz antenna becomes a 90 degree open stub at 915 MHz at the cathode of CR1, effectively giving the 915 MHz signal a low impedance trap to work against (Figure 5). Since the transmission line does not provide a similar low impedance on the anode side of CR1, a 90 degree open stub at 1830 MHz must be added.

Less than 100 uA are required to power the MCU (Figure 6). Consequently, little second harmonic is produced by

CR1, leaving plenty of modulation headroom. Increased frequency multiplication occurs when the output port of the MCU goes low providing a path to ground for rectified current via the 1 kohm resistor, R1. Varying the value of R1 controls the modulation depth. CR2 and C2 work together to maintain sufficient voltage to the MCU while the voltage at C1 is being pulled down by the modulation action.

Performance

As previously noted, the system can operate up to 20 feet away. However, performance is measured at the 10-foot separation required during normal operation (Figure 7). For test purposes, a spectrum analyzer functions as the receiver. A 74AC00 gate oscillator in Figure 4 is substituted for the MCU to simulate load and logic level conditions. The oscillator simplifies confirmation of the concept. Three kHz modulation is used for easy detection by the analyzer.

The transponder transmits data at 94 percent AM modulation. Figure 8 is the detected 3 kHz square wave. Measurements of the rectified voltage (2.7 VDC) and current (1.45 mA DC) give 3.9 mW total power which correlates nicely with the received power (5.3 mW) predicted

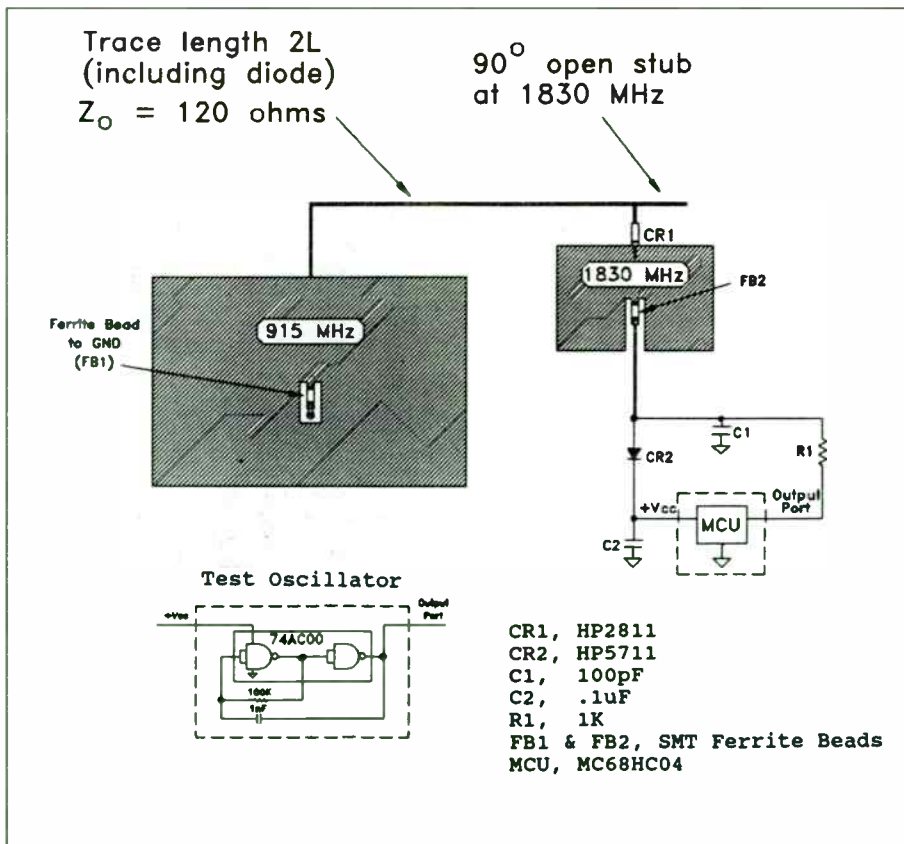


Figure 4. Hybrid schematic of transponder circuit.

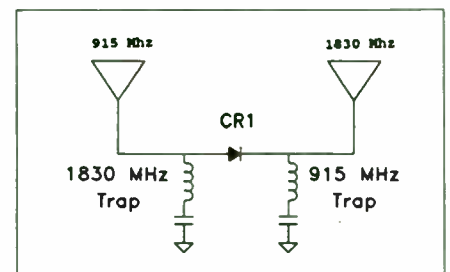


Figure 5. Equivalent AC circuit of transponder showing RF traps.

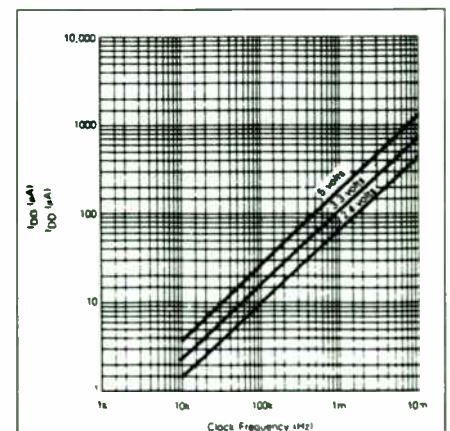


Figure 6. Current vs. clock frequency for a typical 68HC04 MCU.

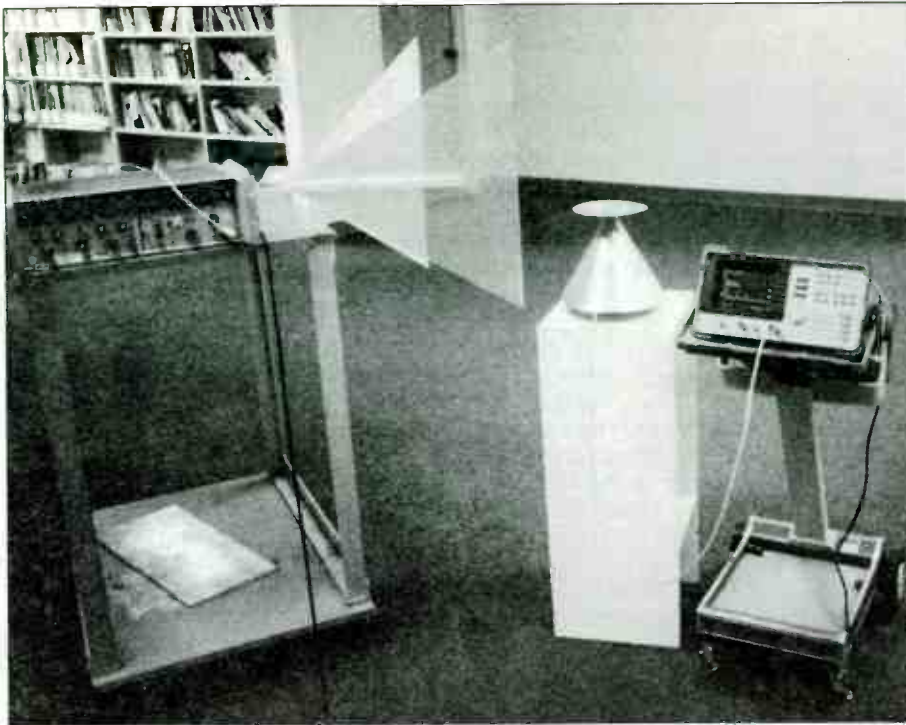


Figure 7. Test setup for transponder operating at a distance of 10 feet.

by equation 1 at a distance of 10 feet.

Improvements

Inherent compatibility with spread spectrum is provided by this design

since the returned signal frequency is derived directly from the interrogation signal. Frequency spreading is limited only by the bandwidth of the patch antennas. With the simple addition of a

Rectangular Microstrip Patch Antenna

The rectangular patch antenna is essentially a resonant microstrip with an electrical length of 1/2 the wavelength of the frequency to be transmitted or received. Microstrip patch antennas work well for applications requiring a low profile, offering a height equal to the thickness of the printed circuit board from which they are made. PTFE substrates are normally used to minimize dielectric losses which affect the efficiency of patch antennas. However, FR-4 is a cost effective alternative for low power applications at frequencies below 2 GHz.

Microstrip antennas come in all sizes and shapes. A rectangular patch is chosen for its simple geometry and linear polarization when fed from the center of an edge. The input impedance varies as a function of feed location. The edge of a 1/2 wavelength antenna has an input impedance of approximately 120 ohms which drops to zero ohms as the feed point is moved inboard to the center of the antenna. This allows easy impedance matching and provides a convenient means of DC tapping the antenna as seen in the transponder design.

For simplicity, the dimensions of the microstrip patch antennas in Figure 9 are in terms of L, which is equal to 1/2 the electrical wavelength of the receive antenna (915 MHz). L can be determined by equation 2:

$$L = 0.49(\lambda\epsilon_R) \quad (2)$$

where λ is the free-space wavelength and ϵ_R is the relative permittivity of the printed circuit board.

Bandwidth is determined by the substrate thickness and can be approximated for an SWR of less than 2 by equation 3:

$$BW = 128f^2t \quad (3)$$

BW is in MHz, f is the operating frequency in GHz, and t is the substrate thickness in inches.

Applying equations 1 and 2 to the transponder design using 0.125 inch FR-4 substrate material with an effective permittivity of 4.7 results in a value of 2.92 inches for L and a bandwidth of 13.4 MHz at 915 MHz.

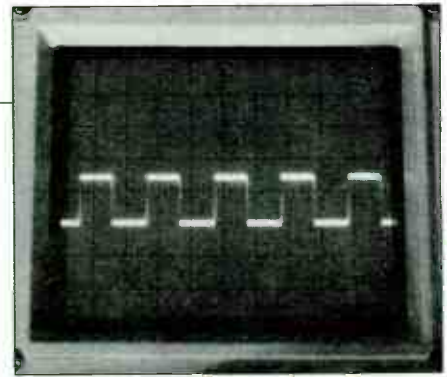


Figure 8. Detected 3 kHz square wave.

micro-power line receiver and the associated communications software, the transponder can be upgraded for two-way information applications. Size reduction can be accomplished by increasing operating frequency at the expense of costlier substrate material. Borrowing technology from missile and aircraft radar technology the transponder could be made a part of the "skin" of its host.

Summary

This paper has described the design, operation and application of a low-power RF identification transponder. The simple design is spectrum friendly, requiring

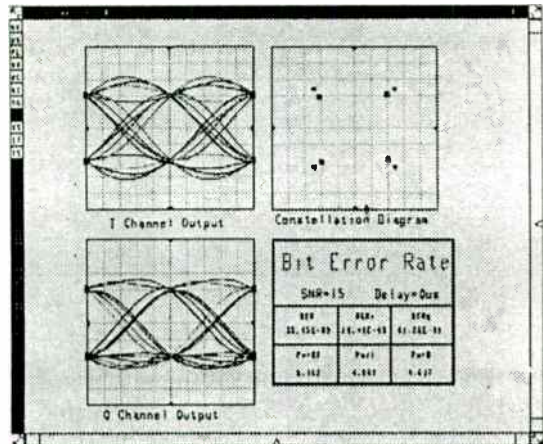
Our Design Contest Winner

Raymond Page is a design engineer for Wenzel Associates, a manufacturer of high performance crystal oscillators and frequency standards. Ray specializes in low noise designs for devices including oscillators,



phase locked frequency sources, multipliers and dividers. In addition to having fun with electronics, he enjoys outdoor sports and music. He can be reached at Wenzel Associates, 1005 La Posada Drive, Austin, Texas 78752, or by telephone at (512) 450-1400.

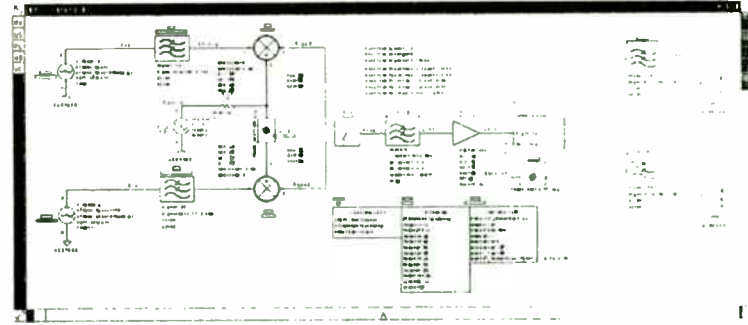
PERFORMANCE: TRANSMITTER OUTPUT FILTERING



HEWLETT
PACKARD

1989 80000000 000

COMBINED TRANSMITTER IMPERFECTIONS



HEWLETT
PACKARD

267

Looking at the eye diagrams, the effect of the output filtering is not immediately apparent--the eye shows just a little closure. The constellation diagram, however, shows clearly the effect of the filter--the filter has begun to roll off, decreasing the amplitude of the received signal. Because the roll off effects both channels, the SNR is equal for both channels, which drives the BER up by only a factor of two.

One effect that is not apparent from these diagrams is the phase shift, or delay, that is imposed on the signal. This delay has been compensated for by adjusting the phase of the clock as we saw on the previous slide. DSPs easily compensate for clock delay. Interestingly, the phase slope resulting from the filter is barely apparent. It is that phase slope that ever-so-slightly closes the eye.

Pictured here is the radio with all three distortion mechanisms in place: quadrature error, gain imbalance, and output filtering.

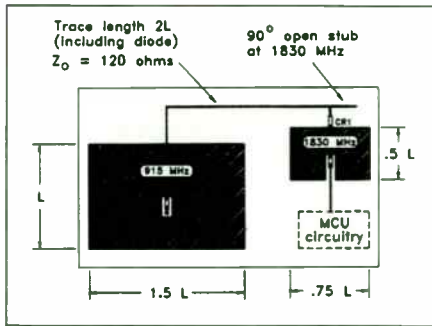


Figure 9. Dimensions for patch antennas.

minimal interrogation power and allows easy conversion to spread spectrum without modification to the transponder. Designed with one inexpensive microwave part on a single piece of FR-4 substrate, component and manufacturing costs are kept down, potentially opening up markets served exclusively by bar coding technology. Other uses include automatic tolling, inventory track-

ing and military vehicle security. **RF**

References

1. Howard W. Sams & Co., *Reference Data for Radio Engineers*, Chapter 27, Sixth Edition, 1977.
2. Robert E. Munson, "Conformal Microstrip Antennas," *Microwave Journal*, March 1988, pp. 91-109.
3. Alan Tam, "Principles of Microstrip Design," *RF Design*, June 1988, pp. 29-34.

MULTI-COMPONENT MODULE FOR HIGH SPEED PASSIVE DESIGN

Mark Brooks
Thin Film Technology
1980 Commerce Drive
N. Mankato, MN 56003

ABSTRACT

As electronics becomes evermore sophisticated in terms of advanced semiconductor devices, there will always remain a need for passive components to provide the necessary support functions. Resistors, capacitors, inductors, and transmission line components exist as a passive subset to high performance designs. Notwithstanding, advancements in the packaging of such devices must go hand in hand with the evolution of other circuit counterparts in order to realize total system improvement. In order to satisfy these requirements, a technique to allow the assembly of high performance thin film devices on ceramic into a sophisticated multilayer package has been devised, with circuit topologies limited only by the designers imagination.

Scope

This paper will outline the approach of Thin Film Technology Corporation for high speed passive component design utilizing multilayer ceramic. Construction of a high speed delay line is first presented, followed by a discussion for application of the technology to produce a Butterworth filter.

Passive Multilayer Component Module Introduction

Though not an offspring of Multi-Chip Module (MCM) technology, this Passive Multilayer Component Module (PMCM) technology parallels the MCM approach; but shines in it's processing simplicity as opposed to conventional MCM types and applications:

MCM-L: laminated board approach

MCM-C: cofired ceramic approach

MCM-D: traditional thin film approach

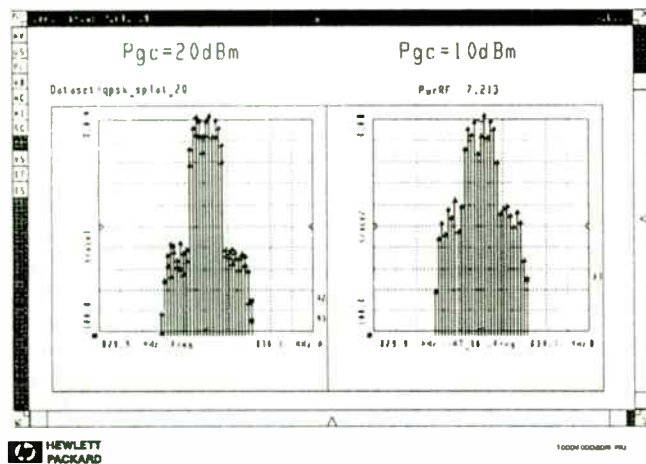
PMCM: thin film on via processed sintered ceramic

These PMCMs offer an approach that allows for substrates containing vias to be metallized by thin film processing and provide for electrical interconnect. A novel technique to select appropriate alloys and alloy thicknesses, however, is also cause for a mechanical connection between layers. By depositing different alloys at the surface sites of two adjacent vias to be connected, the prerequisite for combination into a binary alloy is created. After micron level alignment of these metallized vias to one another, sufficient heat to induce a liquidus state to the metals is provided. Subsequent diffusion of the different metals results in a different melting point alloy, one that is appreciably different than that of the initial metals. This melting point is higher than that achieved in conventional circuit board assembly production, and consequently serves to mechanically hold the interconnect intact.

The PMCM's show improvement for a variety of designs and offer advantages to other technologies by realizing flexibility

alumina reduces dependency on cofired ceramic suppliers, as vias can easily be machined in house. The ability to produce the PMCM with sintered ceramic reduces tooling costs, eliminates via location tolerance drift, and provides custom via patterns as needed substrate by substrate. Standardized fabrication of subassembly components allows for combination of multiple circuits elements into custom circuits with ease. Tape and reel packaging of individual chip subassemblies provides for pick and place assembly in a highly automated production line. Standardized input/output cover ceramics provides final form factor variations so that the same module may be packaged either as a leaded device, face down solder bump, or for wire bonding.

PERFORMANCE: TRANSMITTER BANDWIDTH



AGENDA

- Digital communications basics
- Important MDS capabilities
- A Case study: DQPSK Radio
 - Transmitter performance
 - Channel distortion and correction
 - Receiver performance
- Summary

Here we see how the spectrum expands depending on the 1-dB compression level of the output amplifier. The two plots shown have an output signal level of 7 dBm. The plot on the left shows the output spectrum from an amplifier that has a 1-dB compression point at 20 dBm. The plot on the right shows the output spectrum from an amplifier that has a 1 dB-compression point at 10 dBm. Notice the spurious spectral lines have increased by about 20 dB. These plots help the designer to decide what compression characteristic the output amplifier must have to meet the occupied bandwidth specification.

Further added benefits include high speed circuit applications, where microwave circuitry can perform due to the absence of leads and lead length for the interconnect. This dramatically reduces inductance, which is critical for high speed designs. Solder bump terminations of the PMCM vehicle realizes the shortest length possible from the circuit board trace to the device elements. Coplanar stripline termination pads further improve high frequency performance providing impedance control. With this reconstruction of multilayer ceramic technology, a viable method is available for commercial microwave applications.

CONSTRUCTION

A typical thin film sequence is used for the fabrication of the PMCM device. The fabrication of each via is accomplished by ceramic machining, with appropriate control of program and process parameters to achieve the necessary via quality.

In the first step, a sintered ceramic substrate (96% to 99% alumina oxide) is positioned to a holder, where computer control of X, Y, and Z axes is maintained in relation to the machining tool. At each via location, table movement of the Z axis may raise and lower the substrate coincident to the machining. Each via is precisely formed into the substrate. Because the substrate is machined in a sintered state, concern for the shrinkage movement that occurs when vias are processed in green state ceramic is eliminated.

Substrate thickness and composition are selected for effective via processing and cost consciousness. An important additional benefit of the via is to use a grid or nest of vias for thermal management of a particular area. Metallized blind or through vias can be fabricated to serve this purpose.

Thin film processing techniques applied in the following steps later define the metallization and features of the circuit patterns, which may include combinations of resistors, capacitors, inductors, and transmission line structures. The delay line device described contains microstrip transmission line on individual ceramic substrates, which will become of stripline design as the ceramics are stacked adjacent to one another. Of particular importance is the plating processing step, where the appropriate thicknesses of three metals is achieved. These metals fill the via conductor hole, and are then plated to a "bump" on the substrate surface. Plating thickness control is responsible for the different metals final atomic weight % ratio, which is necessary to allow for the correct binary alloy result during the assembly lamination process.

Dicing or laser scribing and breaking each substrate into individual pieces allows for tape and reel packaging of separate subassemblies. This prepares the product for pick and place processing into the correct "stack" sequence for final assembly (Figure 1).

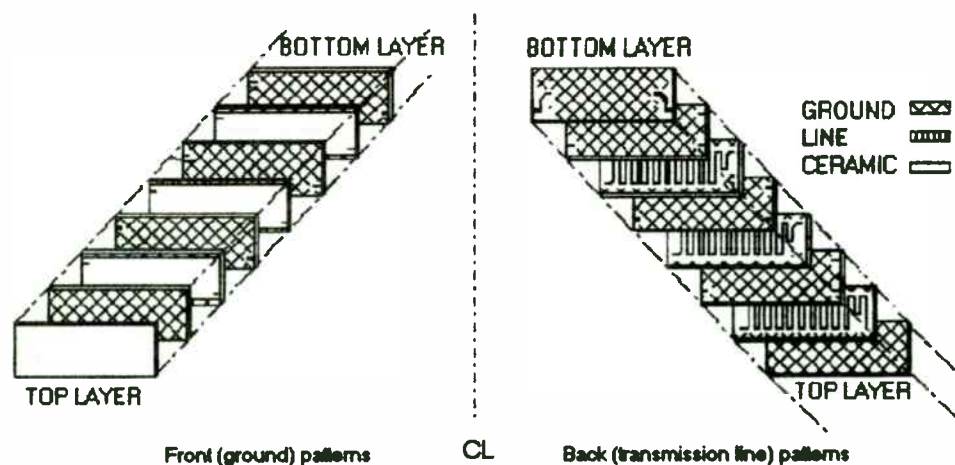
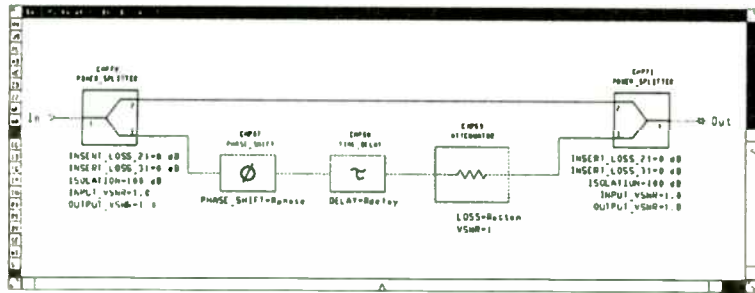


Figure 1

Assembly of the product follows in a clean room environment. Alignment of the subassemblies into lamination tooling is prerequisite for successful lamination to follow. With several "stacks" loaded into a lamination jig, proper pressure, temperature and time, and atmosphere is provided to impart a liquidus state to the plated bumps adjacent to one another. The metals then diffuse into one another, and create a substrate to substrate bond after cooling.

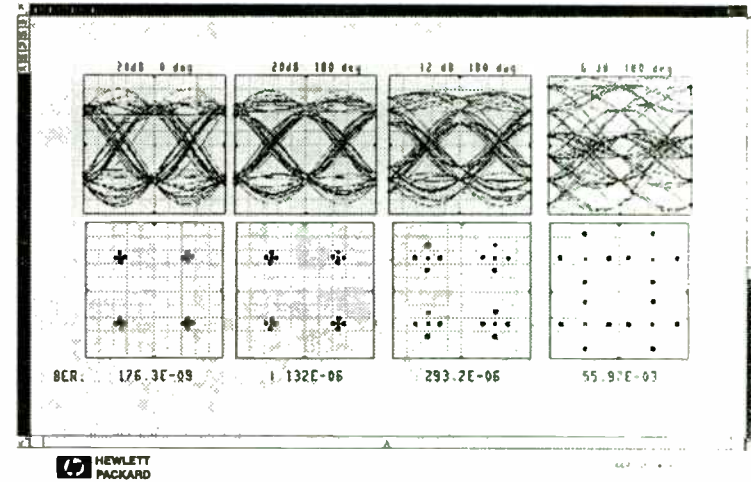
MULTI-PATH MODEL



HEWLETT
PACKARD

100011000001 PNA

EFFECTS OF CHANNEL DISTORTION



HEWLETT
PACKARD

100011000001 PNA

Now that we have looked at the transmitter, let's briefly look at how the transmit channel can add distortion to the signal. Probably the most common form of channel distortion is multi-path distortion. This diagram is a model of a transmitted signal as it follows a direct path and an indirect path from the transmitter to the receiver. The indirect path is formed as the signal reflects off of buildings, mountains, other cars, et cetera and arrives some time later at the receiver. Normally this reflected signal is attenuated from the direct path. The attenuation is modeled by the fixed attenuator. The delay can vary, but here is shown to be about one signal period. The incident phase is random; so here we will look at two cases, 0 and 180 degrees.

Shown here are the effects of varying degrees of interference. The leftmost picture shows an eye diagram, constellation plot, and the 15 dB C/N BER when the multi-path is attenuated 20 dB and there is no relative phase shift. The second column shows plots again with 20 dB attenuation, but this time 180 degrees of phase shift. Note that the relative phase has a dramatic effect on the BER, which is not immediately obvious from the eye diagram. Then we see the results with 12 dB and 6 dB attenuation. The eye closes a great deal. The constellation plot clearly shows the interfering signal as a set of points that are forming around the desired data points. If the phase were random, those points would form circles whose radius is equal to the magnitude of the multi-path signal. These diagrams show the significant effect that multi-path has on digital radio performance.

The final processes serve to package the product into a surface mount configuration and verify AC and DC performance. The gullwing form factor (Figure 2) follows traditional SMT packaging. Alternate packaging schemes include face down solder bump (flip chip) and a non-molded approach for wire bonding.

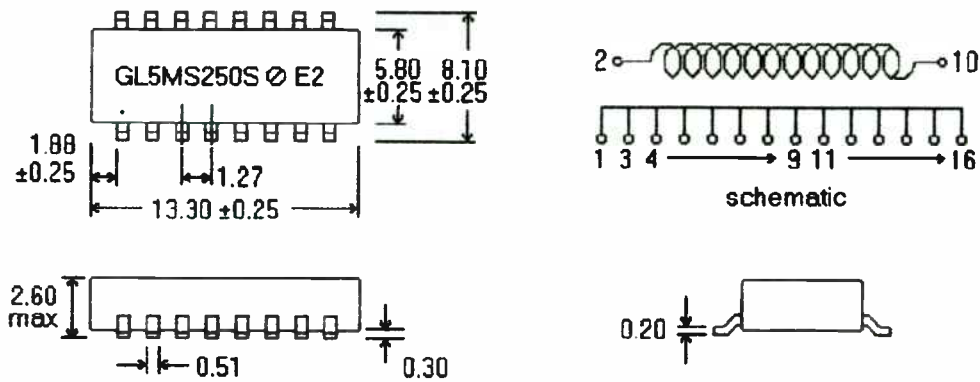
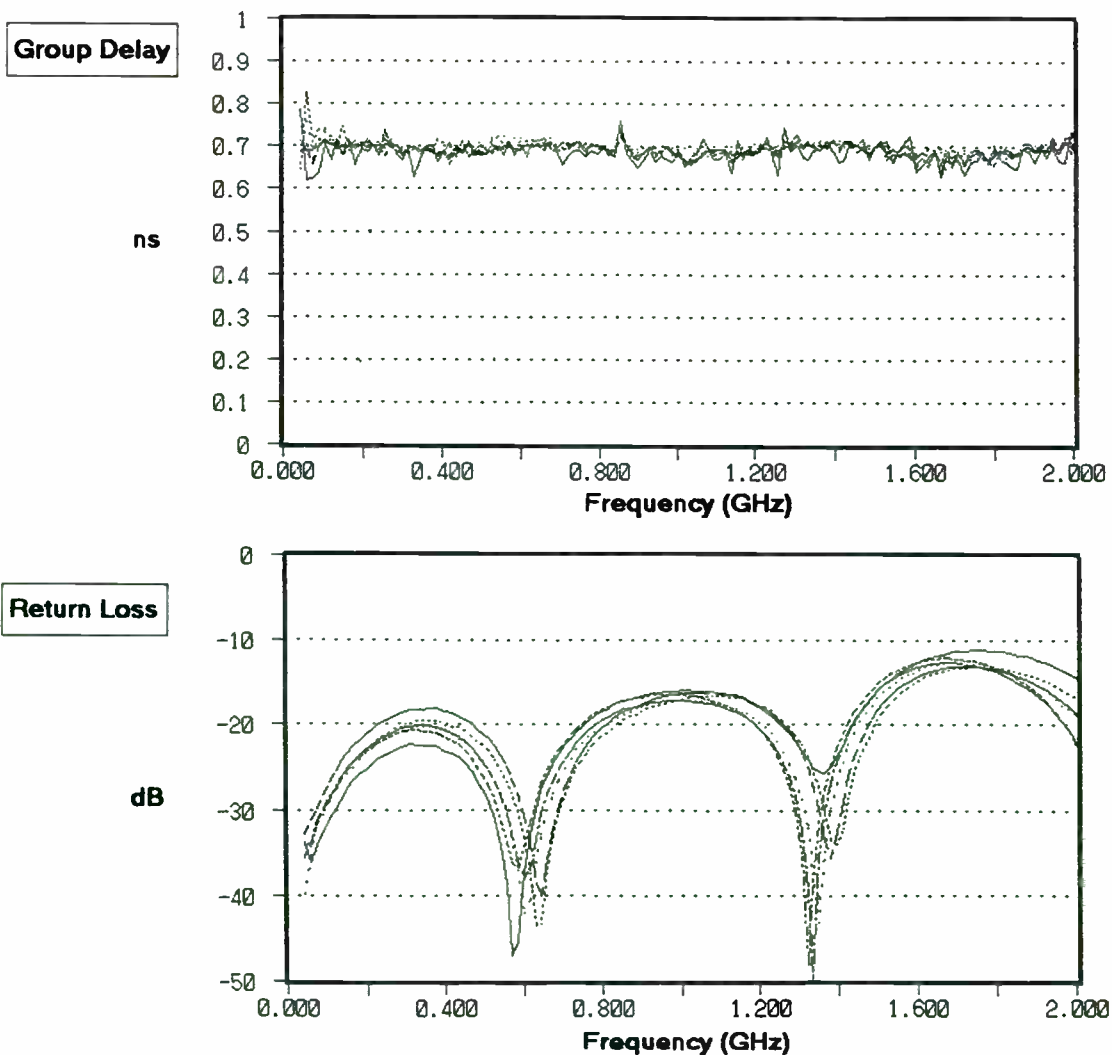


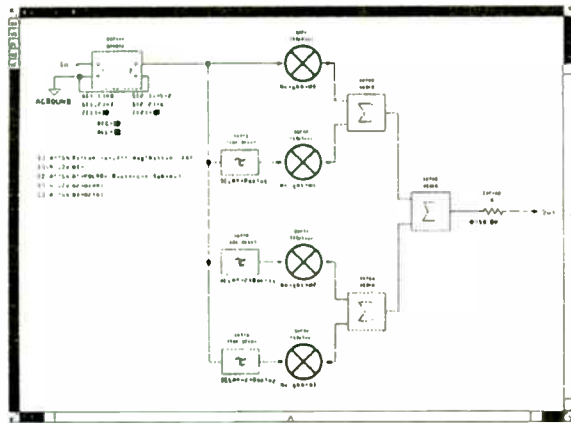
Figure 2

PERFORMANCE

Performance for a 0.5 nanosecond device can be seen as follows. Five devices were tested for group delay, return loss, insertion loss, and impedance.



CHANNEL COMPENSATION: THE FIR FILTERS



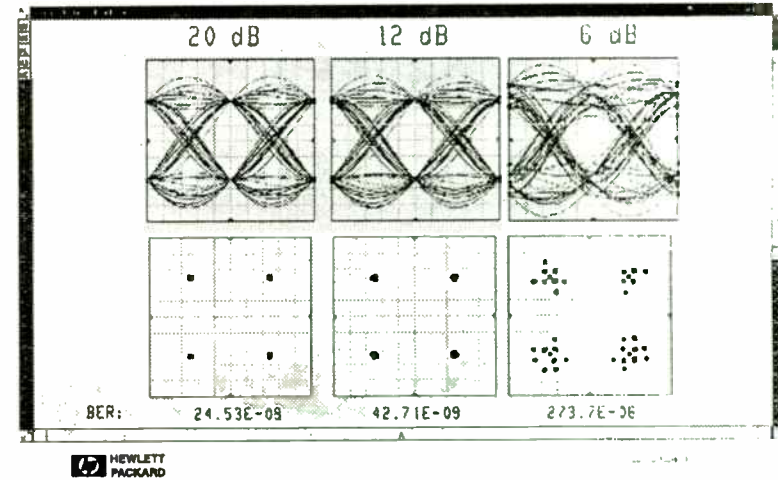
HEWLETT
PACKARD

1000000000 PIV

271

Many digital systems are able to compensate for multi-path distortion using adaptive equalizers implemented as Finite-Impulse-Response (FIR) filters. Pictured here is a simple 4 stage filter that was designed to compensate for the specific multi-path distortion shown earlier. Although we will analyze them with fixed coefficients, modern systems are able to adjust the coefficients using training bursts and adaptive techniques.

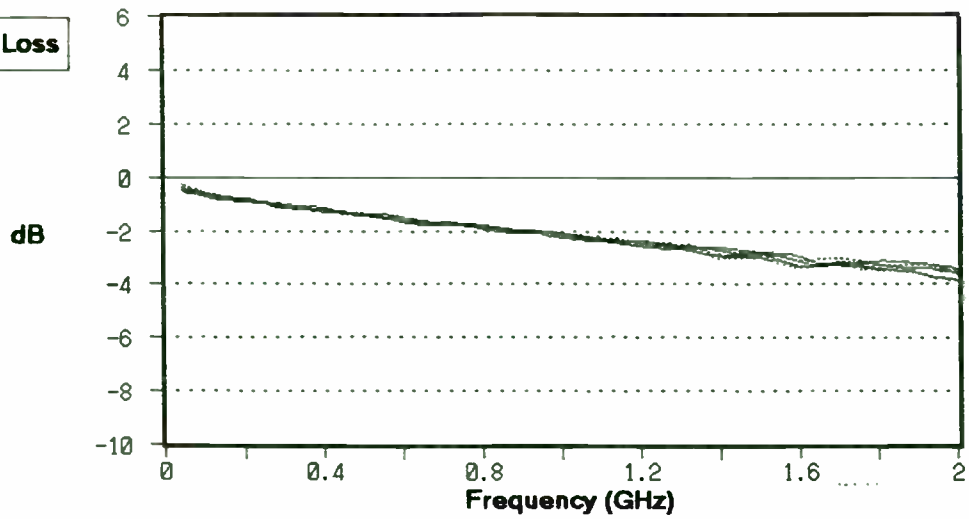
PERFORMANCE: FIR COMPENSATION



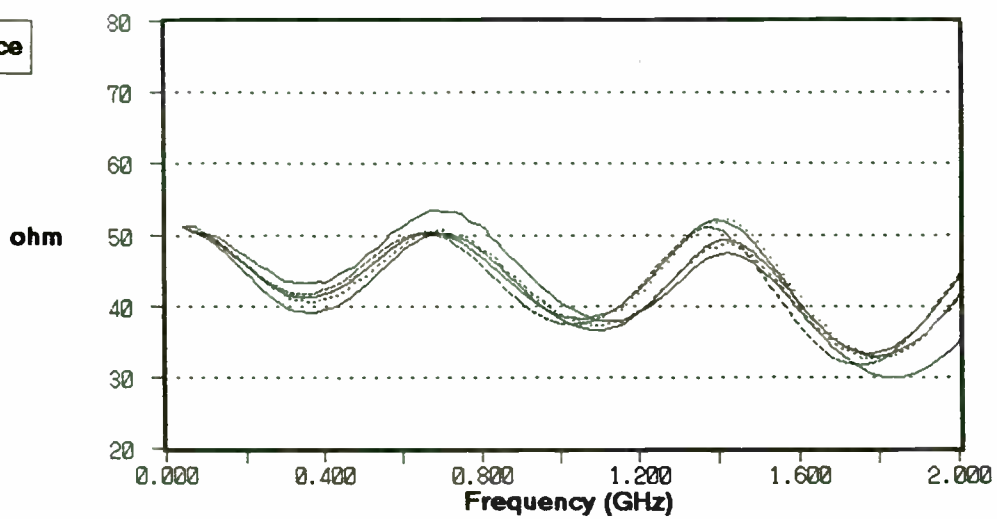
HEWLETT
PACKARD

This slide clearly shows the benefit of using FIR filters. The filter coefficients were chosen to compensate for the multi-path distortion. Normally, the coefficients are dynamically adjusted to minimize BER. In this example, we assume knowledge of the multi-path attenuation and phase. All of these plots show dramatic improvement as compared to the performance without the FIR filter. With an interfering signal that is 20 dB down, the FIR filter is able to nearly perfectly correct for the distortion. The BER is almost at the theoretical minimum. It is less able to correct for the 12 dB, and even less the 6 dB. Nonetheless, the BER with the multi-path 6 dB has been improved by five orders of magnitude. Even better performance would be obtained by using more segments in the filter.

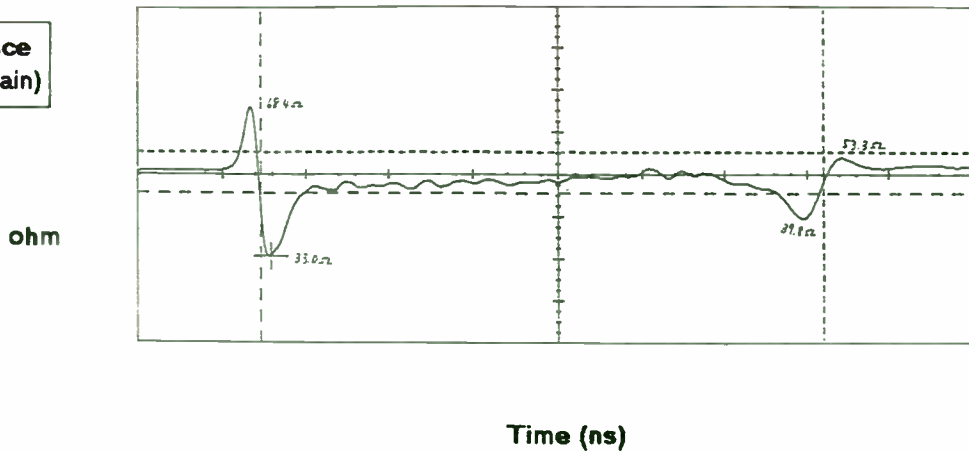
Insertion Loss



Impedance



Impedance (time domain)

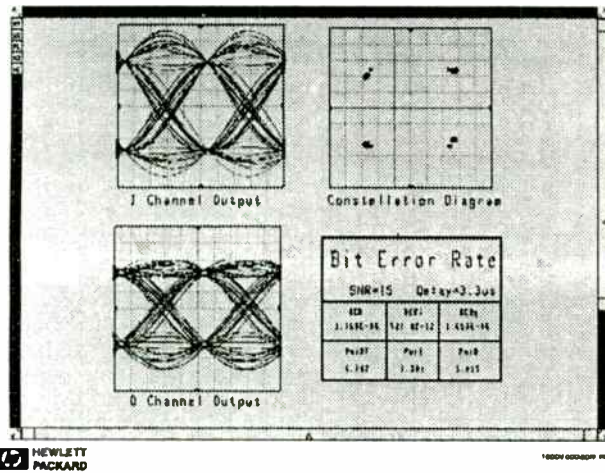


Time delay is varied by more or less microstrip and ground substrates in each stack. The above 0.5 ns device is comprised of four ceramic layers. Twelve layered stacks are common. Additional time delays make the component taller, and affect system and board design vertically, but not in terms of square surface displacement. Top and bottom ground planes provide shielding for interference.

DIRECTION

A simple Butterworth filter is made possible by the PMCM approach. Using spiral inductors with vias, and capacitors utilizing the ceramic as the dielectric, this design provides superior performance to discrete mounted SMT components. Additional products, such as sophisticated high density resistor or resistor/capacitor networks are also possible. Using multiple layers in parallel allows a current sense resistor (<2 ohms) to be fabricated. Many commercial RF products can utilize PMCM technology for cost competitive applications.

PERFORMANCE: THE IMPERFECT RECEIVER



HEWLETT
PACKARD

10000 00000000 100

273

Now let's look at the performance. Note that the eye diagram is not only distorted, it is shifted in time due to the filter delays, particularly the narrow first IF filter. The constellation plot and the bit error rates are degraded. Both used data points that were delayed by 3.3 us.

It is interesting that the I channel is nearly without distortion. The Q channel is attenuated, and the eye has collapsed significantly. The constellation plot shows the shift in quadrature and gain very clearly. The BER has degraded to 1.16×10^{-6} , 55 times worse than ideal.

SUMMARY

- Digital Radios
- MDS capabilities
- Transmitter tests
- Channel tests
- Receiver tests

HEWLETT
PACKARD

In summary, we have seen how the HP High-Frequency Design System is a complete tool for the system-level analysis of digital radios. It is able to calculate the key system performance specs for complete radios, including transmitters, channels, and receivers.

DESIGN OF A SEARCH BASED PLL

Michael F. Black
MS 3145, 8505 Forest Lane,
Texas Instruments
Dallas, TX 75266

Before a phase lock loop can lock some mechanism must move the VCO and the input signal close enough for acquisition. Different frequency ranges and circuit requirements will allow different circuit topologies to achieve proximity. Logic level loops have the advantage of simple flip flop arrangements that combine a frequency discriminator detector with a $\pm 2\pi$ linear phase detector. Self correcting detectors with frequency discriminators become much more complicated when the PLL input is a wide dynamic range analog signal or a pulsed signal. Search circuits become a simple alternative for lock acquisition with these types of phase lock loops.

Search circuits can provide either an open or closed loop action. The search circuit should sweep the VCO control voltage until lock is acquired then shut down. The lock action will normally be strong enough to overcome the search action. A closed loop sweep will sense lock and disable itself. Sweep is reinitiated with loss of lock. Gardner¹ has described a unique circuit of this type as illustrated in Figure 1. The opamp loop filter serves also as a low frequency sine wave oscillator. The feedback network from the output to the non inverting input sets the oscillator frequency. This network could be a Wien bridge or a shunt T network. Before PLL closure the oscillator output voltage sweeps the VCO. When the VCO frequency moves across the input, the phase detector provides an error voltage which slows the sweep rate and drives the loop into lock. The feedback with the phase lock loop closed is enough to overcome the positive feedback of the loop filter oscillator circuit and it stops oscillating. As simple and interesting as this circuit may seem, its applications are limited. The sine wave sweep is inefficient and the circuit elements are very critical. The loop filter design goals may have to be compromised to satisfy the additional oscillator requirements.

Figure 2 illustrates another approach to frequency sweep and search. The loop filter again does double duty. During search it acts as an integrator. A constant current input provides a voltage ramp to the VCO. With lock the current source turns off. The loop filter closes the loop and controls the VCO.

A circuit topology of Figure 2 provides a type two second order loop. This is one of the most versatile and forgiving PLL circuits for analog input requirements. Additional filtering or phase margin optimization can be gained by changing the loop filter to the third order circuit as shown in Figure 3, but for this paper the circuit of Figure 2 will be assumed.

With an ideal opamp, the PLL transfer function of the loop in Figure 2 can be described by the well documented second order equation. The parameters damping ratio and natural frequency describe the time domain and frequency domain response. The loop design parameters include the VCO gain, the phase detector gain, the frequency divide ratio, the loop bandwidth and the damping ratio. The VCO gain, K_{vco} , is the measured tuning slope in Hz/volt. With an analog phase detector such as a mixer the typical error voltage output is a cosine wave where the amplitude is proportional to the phase difference between the two inputs and the amplitude of the input signal. For a given signal level the phase detector gain, K_{pd} , in Volts/Rad is the slope of the cosine wave at the zero crossing. The slope is equal to the zero to peak output voltage. Damping ratio, δ , and natural frequency, f_n , are design goals set by the system requirements. Design nomograms illustrate the performance expected with normalized bandwidths at various damping ratios. Figures 4, 5, and 6 plot the relationship between the 3 dB bandwidth, the 0 dB bandwidth, the phase margin and selected values of damping ratio and natural frequency.

	CT-2	DCS-1800 (PCN)	DECT	Japan Digital Cordless Phone (JCT)
Geography	UK (Telepoint)	Europe	Europe	Japan
Service	1989	1992-1993	1992-1993	1991-1992
Frequency Range	864-868 MHz	1.7-1.9 GHz	1.88-1.9 GHz	1.9 GHz
Data Structure	TDD	TDMA	TDMA/TDD	TDMA/TDD
Channel per Frequency	1	8=16	12	4=8
Modulation	Two-level GFSK ± 14.4-25.2 kHz deviation	0.3 GMSK	GFSK ± 259-317 kHz deviation	π/4 DQPSK
Speech CODEC	ADPCM 32 Kbits/s	RELp-LTP 13 Kbits/s	ADPCM 32 Kbits/s	ADPCM 32 Kbits/s
Mobile Output Power	1 mW to 10 mW	250 mW to 2W	250 mW	10 mW
System Spectrum Allocation	4 MHz	75 MHz	20 MHz	20-25 MHz
Modulation Data Rate	72 Kbits/s	270.833 Kbits/s	1.152 Mbit/s	384 Kbits/s
Filter	0.5 Gaussian	0.3 Gaussian	0.5 Gaussian	√raised cosine
Channel Spacing	100 kHz	200 kHz	1.728 MHz	300 kHz
Number of Channels	40	3000 - 6000	132	
Estimated # of Subscribers year 2000				6.5-13 million
Source	MPT 1375 Common Air Interface (CAI)	prl-ETS 300 176 prETS 300 175-2	CI Spec Part 1 Rev 05.2e	

March 18, 1992

	GSM	NADC	JDC	CDMA
Geography	Europe	North America	Japan	U.S.
Service	1991	1991-1992	1991-1993	1992-1993?
Frequency Range	935-960 MHz 890-915 MHz	824-849 MHz 869-894 MHz	810-826 MHz 940-956 MHz 1429-1441 MHz 1447-1489 MHz 1453-1465 MHz 1501-1513 MHz	824-849 MHz 869-894 MHz
Data Structure	TDMA	TDMA	TDMA	CDMA
Channel per Frequency	8=16	3=6	3=6	118
Modulation	0.3 GMSK	π/4 DQPSK	π/4 DQPSK	BS/MS QPSK/OQPSK
Speech CODEC	RELp-LTP 13 Kbits/s	VSELP 8 Kbits/s	VSELP 8 Kbits/s	8550 bps
Mobile Output Power	3.7 mW to 20W	2.2 mW to 6W		2.2mW to 6W
System Spectrum Allocation	50 MHz	50 MHz	110 MHz	50 MHz
Modulation Data Rate	270.833 Kbits	48.6 Kbits	42 Kbits	1.2288 Mbits/s
Filter	0.3 Gaussian	√raised cosine	√raised cosine	
Channel Spacing	200 kHz	30 kHz	25 kHz	1.23 MHz
Number of Channels	124 frequency channels w/8 timeslots per channel (1000)	832 frequency channels w/3 users per channel (2496)	1600 frequency channels w/3 users per channel (4800)	10 channels 118 calls/channel
Estimated # of Subscribers year 2000	> 20 million			
Source	GSM Standard	IS-54	RJR Spec	Qualcom

The loop filter determines the closed loop operation of the PLL. The standard design methodology will determine the required filter values based solely on this closed loop criteria. For a typical PLL, the VCO gain, K_{vco} , and the phase detector gain, K_{pd} , will be known values. The frequency divide ratio, N , is set by system requirements. A value of $N = 1$ will be used. The damping ratio, δ , and the natural frequency f_n or 3 dB bandwidth are the design goals. The loop filter has three unknown components, R_{input} , R_{fb} and C_{fb} . With two design goals and three unknowns an infinite number of solutions results. So pick a value for C_{fb} and then determine R_{fb} and R_{input} .

$$(1) R_{fb} = \frac{\zeta}{\pi * f_n * C_{fb}}$$

$$(2) R_{input} = \frac{K_{vco} * K_{pd}}{\pi * f_n^2 * C_{fb} * N}$$

The design nomogram in Figure 4 describes the relationship between natural frequency and 3 dB bandwidth as a function of damping ratio. As an example assume a loop with a VCO that tunes at 100 MHz/volt and a phase detector that produces ± 190 mV output. For this example the system analysis indicates the damping ratio should be 2.0 and the 3 dB bandwidth 300 KHz. For these values Figure 4 shows that the natural frequency must be 71 KHz. Figures 5 and 6 indicate the 0 dB open loop bandwidth will be 284 KHz and the phase margin will be 86 degrees.

The feedback capacitor is picked to be .1 ufd. Then from equations 1 and 2, $R_{fb} = 89.9$ and $R_{input} = 6033$. Figure 7 illustrates this configuration.

As discussed earlier this circuit has no means of signal acquisition. It will only capture and lock if the VCO and input frequency are close. Figure 8 illustrates modifications that will implement a sweep function using the loop components. The switched current sources will cause the loop filter to act as an integrator before lock and produce a positive and

negative slope linear waveform. Voltage comparators limit the sweep range to levels slightly greater than required to allow the VCO to cover the desired frequency range. The basic operation is simple and the hardware is simple but the design parameters must be carefully controlled to insure initial lock and the correct closed loop performance.

During the search phase one of the current sources injects current into the loop filter opamp inverting input. The opamp is in a stable closed loop mode during search but the PLL is not locked and the loop is not closed. As the VCO sweeps across the input frequency an error voltage develops at the phase detector output. This is a cosine wave equal in frequency to the difference between the input and the VCO frequencies. When this error frequency comes within the PLL loop bandwidth, feedback will push the VCO closer to the input and lock will occur. With lock the VCO must stop sweeping. This implies that the VCO control voltage is now constant. However search current is still being injected. The rules of operation for a closed loop opamp require that the net current into the inverting node be zero. Since this search current is not being used to sweep the output voltage it must go somewhere. It is in fact sunk out from the inverting input through R_{input} . If the search current is I then a voltage equal to $I \times R_{input}$ will be measured at the phase detector output while the search current is on. If it is turned off the phase detector output will drop to zero to match the non inverting input voltage. However it is easy to pick a combination of values that create a no lock circuit. Consider the values used in the example circuit of Figure 8. If the search current were chosen to be .1 mA, at the instant of lock a voltage of $R_{input} \times I = 603$ mV must be present at the phase detector output. But from the initial design values, the phase detector is only capable of producing 190 mV. As the VCO sweeps across the input frequency, lock will not occur. A small disturbance will be observed in the VCO sweep voltage at crossover, but the sweep will not stop. So a set of design goals and equations are needed to insure both lock and correct closed loop operation after lock is achieved.

Figure 9 illustrates the design parameters for a versatile search derived loop. Several items must be determined by the system requirements and external interfaces.

**THE DESIGN OF LOW POWER
CONSUMPTION RF CIRCUITS FOR
DIGITAL EUROPEAN CORDLESS TELEPHONES
USING MICROWAVE HARMONICA**

*by Raymond S. Pengelly
Vice President
Compact Software, Inc.
New Jersey, USA*

Compact Software

Digital European Cordless Telephone

DCS 1800 System based on GSM 900

TDMA and FDMA combination

Mobile Station

Base Station

Mobile Switching Center

Using GaAs MMIC Technology

***Designs for Low Current Consumption and High
DC to RF Conversion Efficiency***

Compact Software

The standard PLL loop parameters of damping ratio and bandwidth must still be part of any design set. Next is the sweep time, T_{total} . This example allows for a different up and down time, T_{up} and T_{dn} . The characteristics of the VCO will determine the upper and lower sweep voltage, V_{vcoup} and V_{vcodn} , required. The values chosen should allow margin for tolerances to guarantee a useable lock range. The last system level design parameter is the up and down phase detector voltage levels, V_{pdup} and V_{pddn} . These are the voltage levels at the phase detector output at the moment of lock when the up or down search current is on. These voltages will be opposite in sign because of the reversal of the search current for up and down sweep. These two levels need to be carefully chosen. Correctly used they can provide a valuable amplitude discrimination action to limit the range of acceptable signals. Figures 10 and 11 illustrate typical transfer curves for a phase detector. Note that the positive and negative values are not normally the same. These graphs plot the phase detector peak voltage outputs vs the amplitude in dBm of the input. For example the system requirements might dictate that the loop should first try for lock to inputs greater than -2 dBm. Failing to lock at greater than -2 dBm the loop could then try for greater than -6 dBm. From the graph in Figure 10, -2 dBm will produce a 175 mV output and from Figure 11, -6 dBm will produce a -100 mV output. If the value of sweep current I and the loop filter input resistor R_{input} are chosen with these levels in mind then the loop can be constructed to insure no lock below these levels. These two levels define the lock threshold parameters V_{pdup} and V_{pddn} .

The system level design parameters include damping ratio, natural frequency, frequency division ratio, T_{up} , T_{dn} , V_{vcoup} , V_{vcodn} , V_{pdup} and V_{pddn} . The design constants are the Vco gain, K_{vco} , and the phase detector gain, K_{pd} . The design equations must determine R_{input} , R_{fb} , C_{fb} , I_{up} , and I_{dn} to insure both correct search and lock. Equations 3, 4 and 5 develop the ratio between I_{up} and I_{dn} .

$$(3) V_{pdup} = I_{up} * R_{input}$$

$$(4) V_{pddn} = I_{dn} * R_{input}$$

$$(5) \therefore I_{dn} = \frac{V_{pddn}}{V_{pdup}} * I_{up}$$

The ramp up time and the ramp down time can be found from the equations for a constant current source driving an integrator.

$$(6) V_{vcoup} = \frac{I_{up} * T_{up}}{C_{fb}}$$

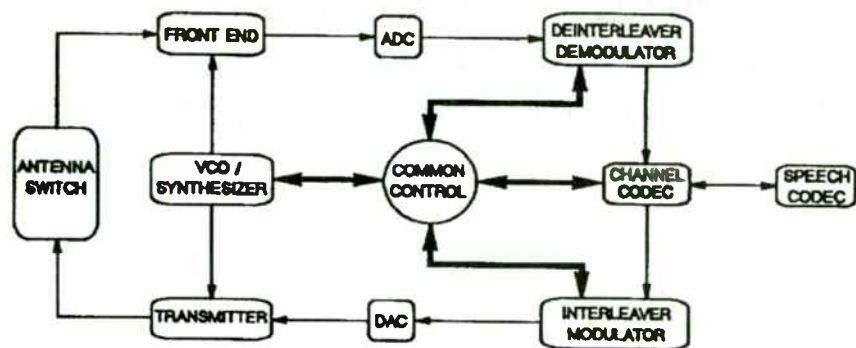
$$(7) V_{vcodn} = \frac{I_{dn} * T_{dn}}{C_{fb}}$$

$$(8) LET A = \left(\frac{V_{pddn}}{V_{pdup}} \right) * \left(\frac{V_{vcoup}}{V_{vcodn}} \right)$$

$$(9) THEN T_{up} = A * T_{dn}$$

The value of the up and down current sources and the loop filter input resistor come from rearranging equations 6 and 7 and then solving for R_{input} .

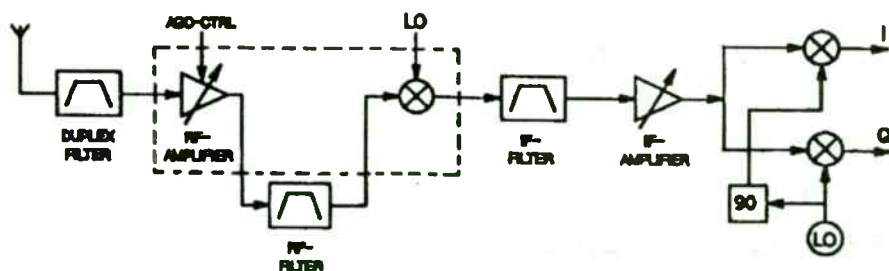
Digital European Cordless Telephone



Structure of DECT Mobile Station

Compact Software

Digital European Cordless Telephone



DECT Front End with GaAs MMIC Subsystem

Compact Software

$$(10) I_{up} = \frac{V_{vcoup} * C_{fb}}{T_{dn}}$$

$$(11) I_{dn} = \frac{V_{vcodn} * C_{fb}}{T_{dn}}$$

$$(12) R_{input} = \frac{V_{pdup}}{I_{up}}$$

$$(13) \therefore R_{input} = \frac{V_{uppd} * T_{up}}{V_{vcoup} * C_{fb}}$$

The final value required for the loop filter is the feedback resistor, Rfb. In the earlier example the three unknowns, Rfb, Rinput and Cfb had a infinite set of solutions with only the two design goals of damping and natural frequency. These are still two of the design goals but the search constraints have reduced the size of the solution set. Cfb was picked early in the search equation derivation. Rinput was derived from the threshold and sweep range values. With only Rfb left either the damping ratio must be chosen and the resultant natural frequency calculated or vice versa. Picking the damping ratio is usually the most practical choice.

To find Rfb and the natural frequency equations 1 and 2 may be rearranged.

For a PLL with a damping ratio ζ , a VCO gain K_{vco} , a phase detector gain K_{pd} , and a divide ratio N

$$(14) R_{fb} = \zeta * \sqrt{\frac{2 * N * R_{input}}{\pi * K_{vco} * K_{pd} * C_{fb}}}$$

$$(15) f_n = \sqrt{\frac{K_{vco} * K_{pd}}{2 * \pi * N * C_{fb} * R_{input}}}$$

Applying these equations to the original example will result in a fully defined search driven PLL.

For $K_{vco} = 100$ MHz/volt

$K_{pd} = .190$ V/RAD

$V_{pdup} = .175$ volt

$V_{pddn} = .100$ volt

$V_{vcoup} = 7$

$V_{vcodn} = 1$

Total search time = 50 ms

and again picking $C_{fb} = .1\mu f$

Equations 10 through 13 yield

$I_{up} = 33.0$ mA

$I_{dn} = 18.9$ mA

$T_{up} = 18.2$ mS

$T_{dn} = 31.8$ ms

$R_{input} = 5303$

Repeated iterations for values of Rfb for various damping ratios shows the effect on bandwidth and damping as listed in Table 1. Although none of the combinations of 3 dB bandwidth and damping match the design goals exactly the closest match comes with $R_{fb} = 81$.

Figure 12 illustrates the schematic of the final design. Circuit details of the window comparators and logic controls have been omitted for clarity. Figure 13 shows the loop bandwidth and Figure 14 plots the sweep voltage when the circuit is allowed to free run. Design verification of the performance comes from both SPICE simulation and actual hardware measurements.

Shutting off the search circuit is another topic that is very dependent on system requirements. The easiest circuit is shown without detail in Figure 15. This uses a retriggerable one shot that is fired each time the sweep voltage trips the high or low level of the window comparator. The one shot time out is set longer than either the up sweep or down sweep time. If the one shot is not retriggered before it times out, then the assumption is made that the loop has locked and the VCO voltage is at a constant value. When the one shot times out, the search current is turned off and the phase detector offset voltage returns to ground.

More demanding systems may require full lock verification circuits with signal injection or quadrature detectors. With these circuits only a full lock confidence check will shut down search.

Digital European Cordless Telephone

Subject:	SiBip- Technology	GaAs- Technology
Active Components	npn- Transistors	Depletion MESFETS Enhancem. MESFETS Schottky Diodes
Passive Components	Resistors (Capacitors)	Resistors Capacitors (Inductors) Lumped Elements
Maximum f_T	30 GHz	45 GHz
Minimum Noisefigure F	< 1 dB	< 3 dB
Suitability for analog	moderate	good
Suitability for digital	good	moderate
Reproducibility	good	bad
Production Efficiency	97 %	5 %
Production Costs	low	high

General Properties of Si BJT and GaAs Technologies

Compact Software

Digital European Cordless Telephone

Component	Frequency Range / GHz	Key Property	Possible Technology	Preferable Technology
LNA	1-3	low- noise	GaAs	GaAs
PRA	1-3	low- distortion	SiBip, GaAs	SiBip
HPA	1-3	power effic.	SiBip, GaAs- hybrid	SiBip hybrid
MPA	1-3	linearity	SiBip, GaAs	SiBip
VCO	2-6 (4-12)	stability, linear.	SiBip, GaAs	SiBip
PSC	2-6 (4-12)	low- power	SiBip, GaAs	SiBip
PSW	1-3	low- loss	GaAs	GaAs
RIM	1-3	uncritical	SiBip, GaAs	SiBip
TIM	1-3	low- sp. emiss.	SiBip, GaAs	SiBip
QDC	2-6 (4-12)	linearity	SiBip, GaAs	SiBip
QUC	2-6 (4-12)	gain/phase bal.	SiBip, GaAs	SiBip

Technologies for Specific RF Circuits for Mobile Communications

Compact Software

CONCLUSIONS

The conflicting PLL requirements of efficient search for lock and loop bandwidth after lock can be resolved with a versatile set of equations and design methodology. With a defined set of system requirements and component parameters a simple loop filter/sweep generator can be designed. The measured results can be expected to closely match the predicted performance.

This search system matches the component values to both the lock and search requirements. Search times and lock thresholds determine the sweep currents and the natural frequency. The selection of a feedback resistor sets the closed loop 3 dB bandwidth, the phase margin and the transient response.

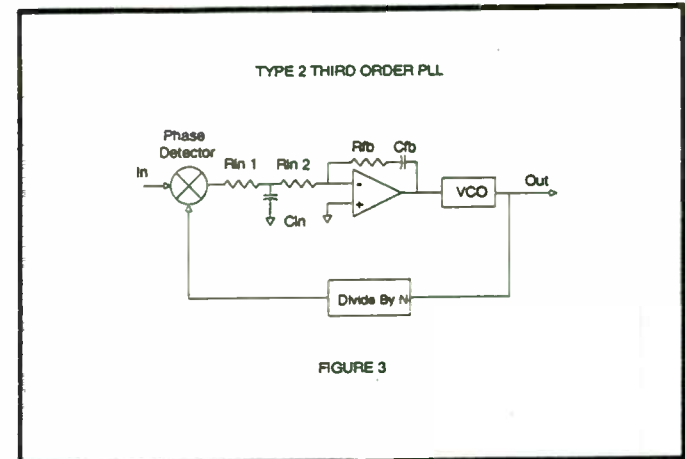
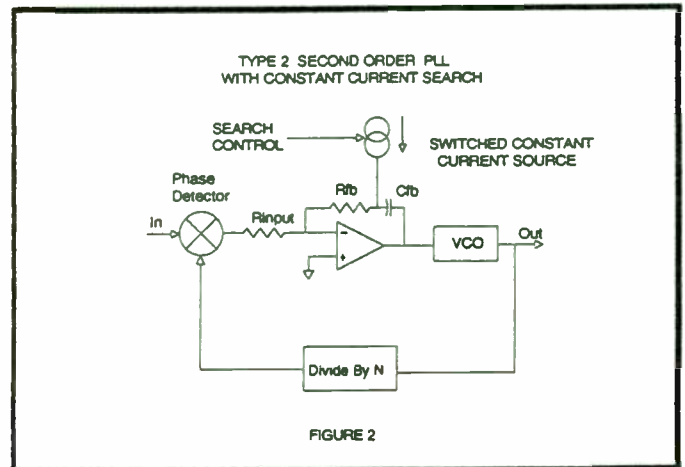
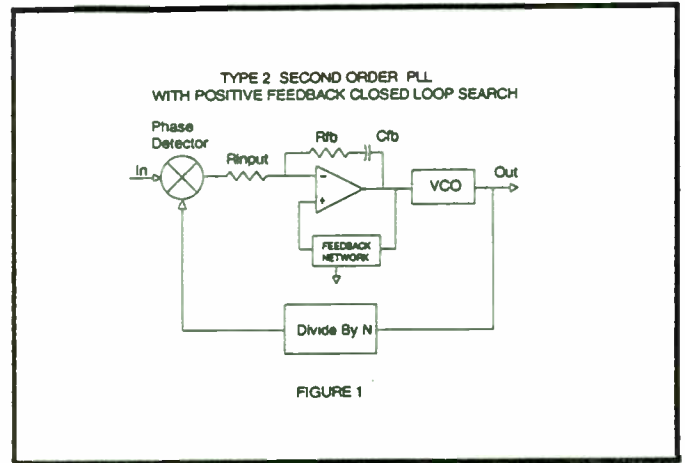
References

1. F.M. Gardner, *Phaselock Techniques*, John Wiley & Sons, New York, 1979, p82

FEEDBACK RESISTOR	DAMPING RATIO	ZERO DB BW Hz	PHASE MARGIN	THREE dB BW Hz
75.0	1.779	2.69547E+05	85.497	2.89278E+05
76.0	1.803	2.73096E+05	85.613	2.92600E+05
77.0	1.827	2.76649E+05	85.726	2.95793E+05
78.0	1.850	2.80203E+05	85.833	2.99113E+05
79.0	1.874	2.83758E+05	85.937	3.02439E+05
80.0	1.898	2.87317E+05	86.037	3.05798E+05
81.0	1.922	2.90874E+05	86.134	3.09140E+05
82.0	1.945	2.94433E+05	86.227	3.12430E+05
83.0	1.969	2.97992E+05	86.316	3.15889E+05
84.0	1.993	3.01551E+05	86.403	3.19231E+05
85.0	2.016	3.05114E+05	86.487	3.22574E+05
86.0	2.040	3.08680E+05	86.567	3.25829E+05
87.0	2.064	3.12243E+05	86.645	3.29221E+05
88.0	2.088	3.15805E+05	86.721	3.32643E+05
89.0	2.111	3.19375E+05	86.793	3.35950E+05
90.0	2.135	3.22939E+05	86.864	3.39427E+05

Table 1

Loop Parameters as a Function of Loop Filter Feedback Resistor



Simulation Requirements

Nonlinear Simulation needed for:

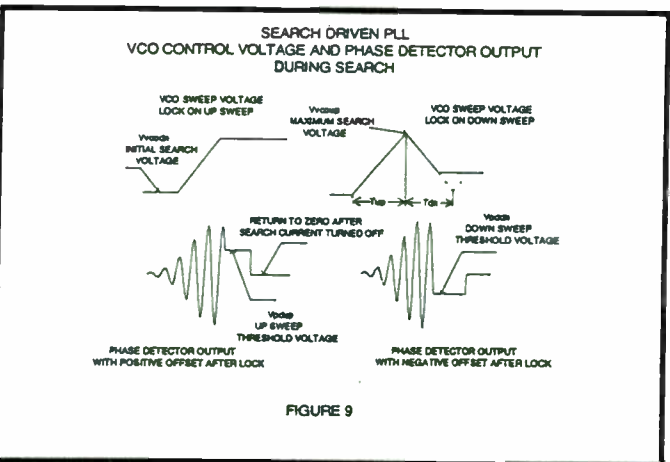
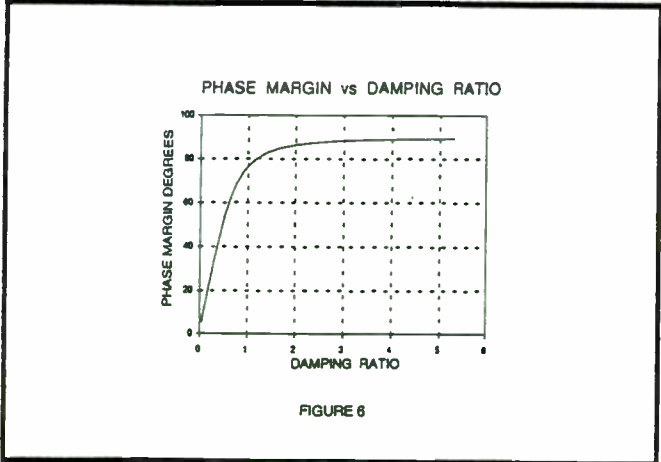
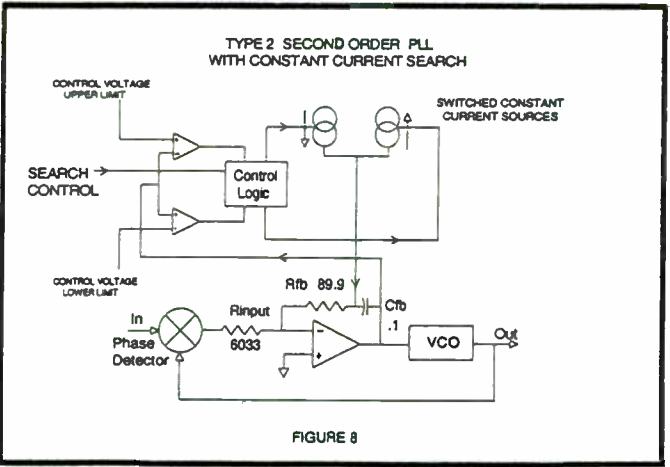
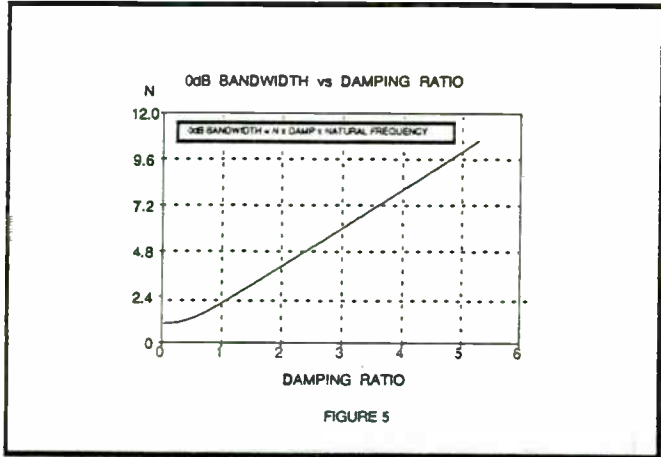
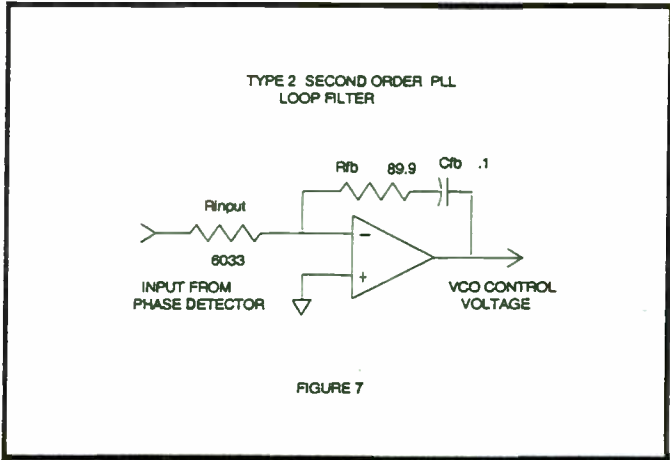
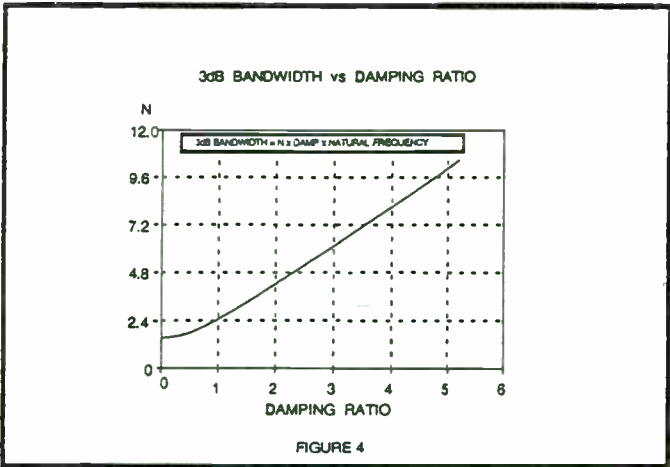
- * System Gain***
- * System Noise Figure***
- * Compression***
- * Dynamic Range***
- * Third Order Intercept Point***
- * Temperature Effects***
- * Design Trade-Offs***

Digital European Cordless Telephone

Compact Software

Microwave Harmonica is a Harmonic Balance Simulator providing:

- * Efficient and Accurate Analysis**
- * High Dynamic Range -- 140 dB**
- * Optimization**
- * Design Centering**
- * Nonlinear Noise Analysis**
- * Temperature Analysis**



Microwave Harmonica uses a variety of nonlinear models as well as transistor libraries:

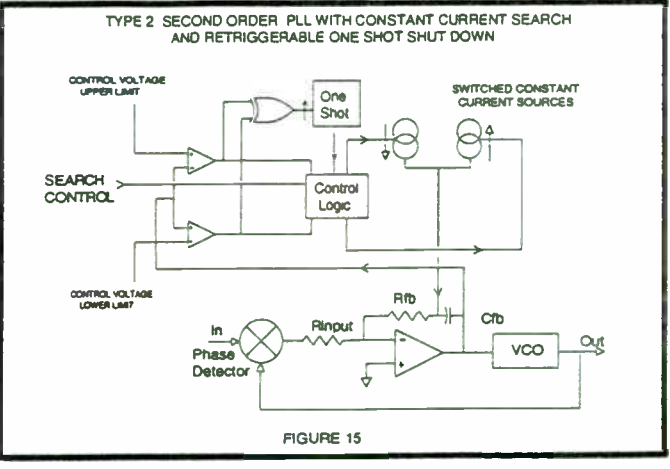
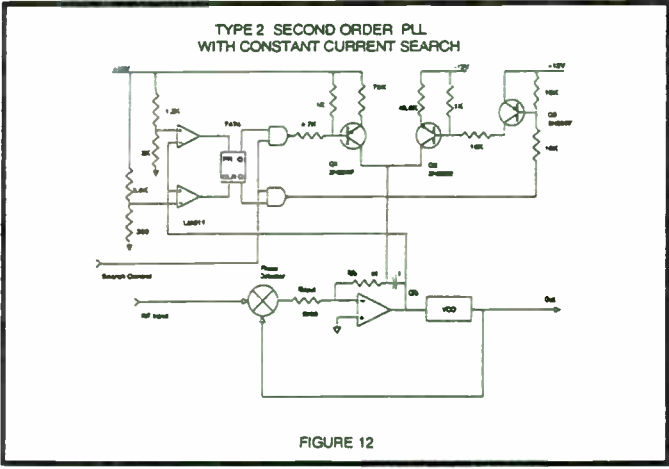
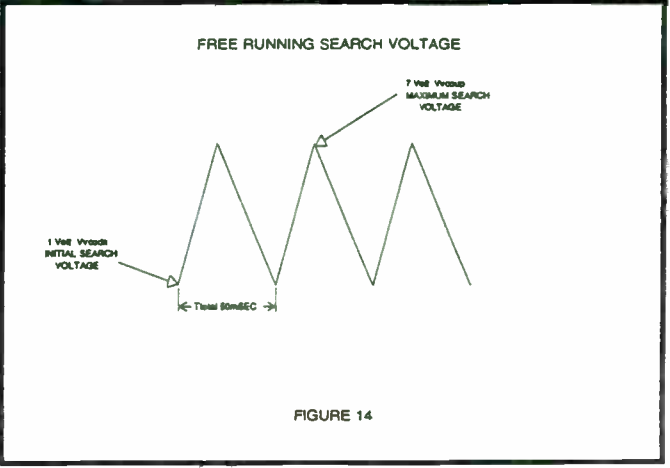
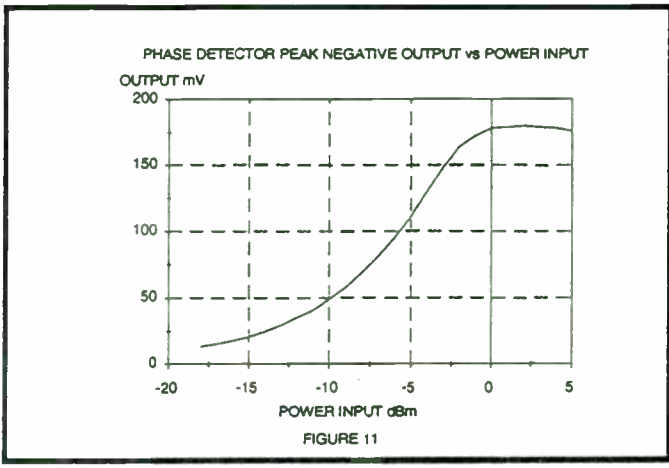
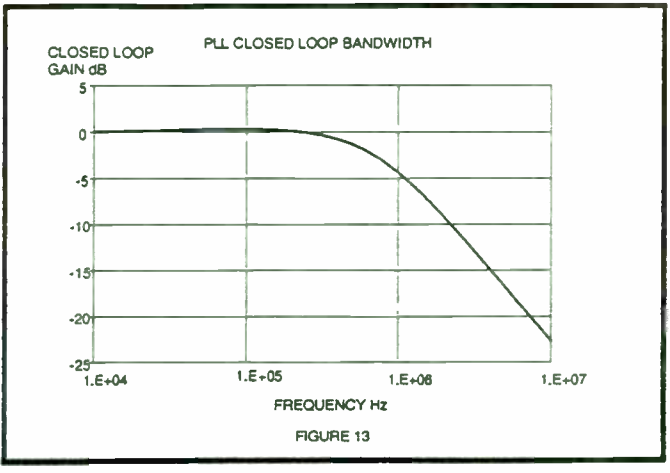
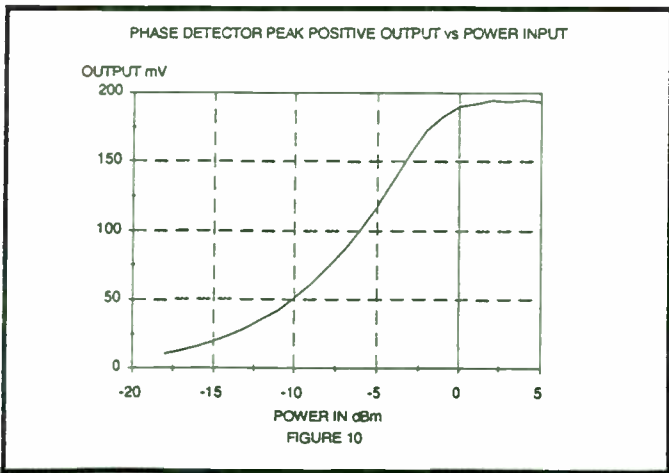
- * Models need to be accurate particularly close to pinch-off and breakdown
- * Models need to be consistent i.e.
 - Linear/Nonlinear
 - Spice syntax
 - Noise
 - Temperature Coefficients

Result of System Analysis

Stage	RF-Amplifier		Mixer		Front End	
F	4		12		23.30	
G _v	-5		15		SNR _v = 74.7	
IP _{1,2}	0		0 / 7		-4.3 / 1.8	
Stage	1	2	3	4	5	6
P _{out}	-26	-31	-34	-19	-29	-15
F	4		12		19.12	
G _v	0		10		SNR _v = 78.9	
IP _{1,2}	0		0 / 7		-4.8 / 0	
P _{out}	-26	-26	-29	-19	-29	-15
F	4		12		14.66	
G _v	5		10		SNR _v = 83	
IP _{1,2}	0		0 / 7		-9.8 / -5	
P _{out}	-26	-21	-24	-14	-24	-10
F	4		12		9.93	
G _v	12		10		SNR _v = 88.1	
IP _{1,2}	0		0 / 7		-16.8 / -12	
P _{out}	-26	-14	-17	-7	-17	-3

Digital European Cordless Telephone

Compact Software



Digital European Cordless Telephone

Mixer: RF-input impedance : 50 Ω
LO-input impedance : 50 Ω
IF-output impedance : 500 Ω
RF-frequency : 1805 - 1880 MHz
LO-frequency : 1935 - 2010 MHz
IF-frequency : 130 MHz
LO-input signal : > -10 dBm
Gain : 10 dB
Noise figure : \leq 12 dB
IP_{3,d} : > 0 dBm

Compact Software

***Low Current, Dual-Gate GaAs FET Mixer
with Active Matching for LO and RF***

Compact Software

Analysis of Transversely Coupled SAW Resonator Filters Using Coupling of Modes Technique

by

V. Narayanan and S. M. Richie
University of Central Florida
Electrical and Computer Engineering Department
Orlando, Florida 32816-2450

ABSTRACT

This paper presents the Coupling of Modes (COM) analysis technique as applied to SAW device component elements, such as the SAW reflective grating and the interdigital transducer, which are then cascaded to analyze a class of SAW resonator filters called proximity coupled or waveguide coupled resonator filters. It also presents the technique to determine the number of transverse guided modes for a particular device structure employing a simplified waveguide model. The excitation and propagation of the modes can then be solved independently for each mode with its corresponding mode velocity using a PC based CAD tool written to implement COM solutions for the various SAW components. The proximity resonator is structured to have a coupling of resonant energy between two transducers placed in close longitudinal proximity to each other with a single reflective grating on each side. The number of transverse modes in a device structure is dependent on the acoustic beamwidth of the structure and for a device with small beamwidth there can be two dominant guided modes, the velocity difference of which results in a two pole response. In addition to the discussion of the analysis of proximity coupled SAW resonators, this paper presents the responses of other SAW structures obtained using a computer model "RESCAD" developed at the University of Central Florida.

INTRODUCTION TO SAW RESONATOR FILTERS

Surface acoustic wave devices are being utilized more frequently in high performance RF applications as these devices are continually offering higher performance with

lower cost in smaller packages. A surface acoustic wave resonator is a high Q element which is used for frequency control and narrow band filter applications operating in a frequency range between 20MHz and 2GHz. The lower frequency limit is determined by the size of the device but at high frequencies fabrication tolerances and propagation losses are the limiting factors.

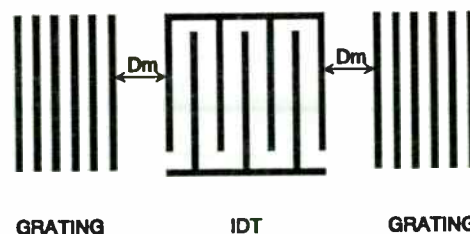


FIGURE 1 : One port resonator configuration

The commonly used resonators are the one port resonator, as shown in Figure 1, and the two port in line resonator, as shown in Figure 2. Other resonator filter structures include the acoustically coupled inline resonator filter and the proximity coupled resonator filter discussed in this paper.

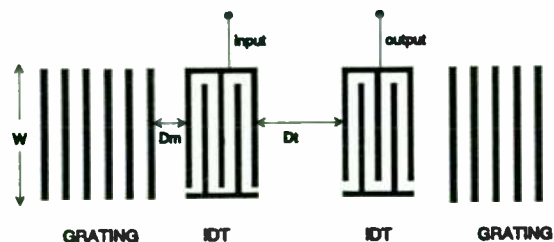


FIGURE 2 : SAW two port resonator

Quartz coupled resonator filters have provided a low cost solution for many VHF and UHF filter requirements. Over the past decade, SAW coupled resonator filters have seen a dramatic increase in their application as a key element in oscillator and RF filter circuitry because of their small size, low insertion loss and low relative cost. A typical proximity coupled resonator structure is shown in Figure 3.

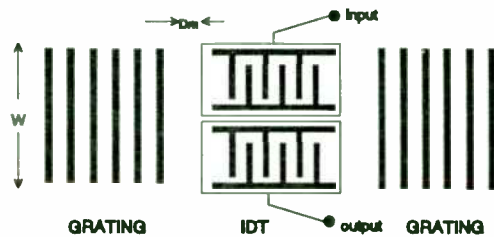


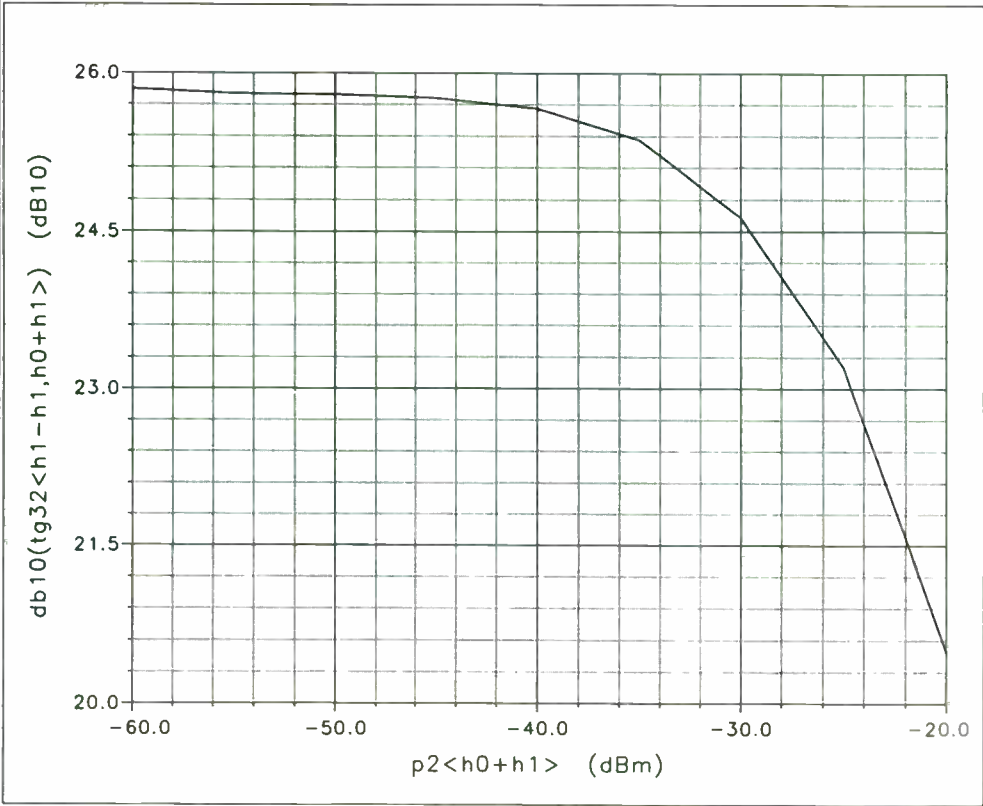
FIGURE 3: Transversely coupled SAW Resonator Structure

The proximity coupled or the guided mode resonator filter was first demonstrated in 1975 by H.F.Tiersten and R.C.Smythe [2], who described the coupling between resonators in terms of trapped energy modes of the surface wave guiding structure. The proximity of the transducers results in resonant energy in each of the two cavities being coupled together by virtue of the evanescent acoustic fields. Since that time a significant amount of SAW coupled resonator designs have been studied [1].

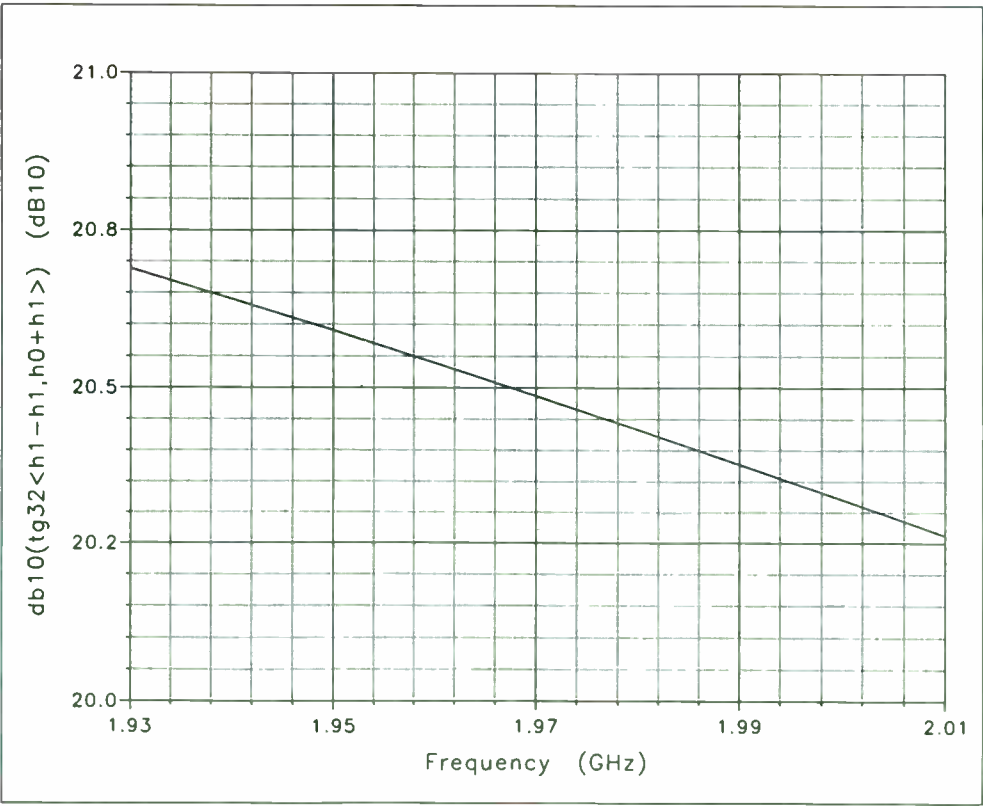
MODELING APPROACHES

Since the invention of SAW devices, a large variety of filters and resonators have been developed and used in signal processing applications. Many different device models have been derived to analyze and synthesize them. Physical effects like the excitation of different wave types, perturbations and scattering caused by different metallisation structures, wave diffraction, and other phenomena of wave propagation in the different materials have also been studied. Presently, there exists several device models which have become very popular in the analysis of SAW devices. These include the equivalent circuit model, the impulse response model, the coupling of modes model, and the waveguide model. The inline and cross field equivalent circuit model allows for the analysis of SAW devices including second order effects like that of internal reflections. These internal reflections result from the presence of the electrodes in the SAW transducer. As Rayleigh waves propagate under a SAW transducer, portions of the waves reflect from the electrodes. Analysis of SAW devices using this model requires cascading sections of

the transducers. The curved electrostatic fields in between the metal fingers near the surface are replaced by a homogeneous electrical field distribution parallel or perpendicular to the surface [3]. Each periodic section of the device is represented by an equivalent circuit and analyzing a typical device would require cascading several hundred such equivalent circuits. As a result this method of modeling can be very numerically intensive. Moreover, due to its numerical nature the equivalent circuit model is not applicable to synthesis. The impulse model is an analytic model used to analyze SAW devices which lack any internal reflections. Analysis of SAW devices using the impulse model may be done in real time. The strength of the impulse model has been in its usefulness as a synthesis tool since closed form expressions for SAW device responses are possible. The generalized impulse response is closely related to Fourier transformation of the transducer weighting function and therefore this model is called the impulse model [4]. It is also based on the Green's function analysis of wave coupling and the principle of charge superposition [5]. The coupling of modes model is considered to be a hybrid of the equivalent circuit model and the impulse model and is an analytic model which includes the effects of distributed internal reflections. This model may be thought of as a generalized impulse model which includes internal reflections in its analysis or as an analytic equivalent of the equivalent circuit model. Since closed form expressions for the responses of SAW devices may be obtained using the coupling of modes model, it is applicable to synthesis as well. With the growth of SAW technology, a great deal of attention has been given to the application of the coupling of modes (COM) theory, better known for its contribution in the analysis of microwave and optical structures. It was successfully applied to the analysis and synthesis of SAW devices with small distributed reflections by P. V. Wright and H. A. Haus in 1980 [6]. Since then it has been used for various SAW device applications. It has demonstrated its usefulness as a simpler, less cumbersome design and analysis tool. The use of the COM theory provides efficient computations and good accuracy for the analysis of SAW devices, as compared to most field theory approaches which involves greater model complexity and can be more numerically inefficient. Lastly, the waveguide model was developed for microwave and optical waveguides [7] and has long been used for the calculation of wave propagation in SAW devices. The effect of waveguiding and transverse modes in SAW resonators was discussed by O.Schwelb, E.L.Adler and G.W.Farnell in 1977. A well known principle in wave propagation is that if a region with low wave velocity is surrounded by faster regions, the wave



fetmixer
Y:db10(tg32<
db10(tg32<h1-h1,h0
dfetmix5.ckt



fetmixer
Y:db10(tg32<
db10(tg32<h1-h1,h0
dfetmix5.ckt

is confined to the slow region. The best way to achieve this is to provide a thin metallic overlay in the wave propagation path which slows the wave and provides the desired wave guiding, as shown in Figure 4.

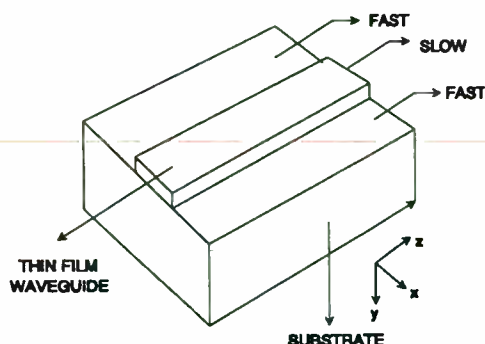


FIGURE 4 : SAW waveguide

Modes propagate with certain relative amplitudes in a waveguide. The model complexity required to account for waveguiding in the COM formalism or any other transducer model overshadows the usefulness of the model results and would be numerically cumbersome. The more prevalent approach is to account for the waveguiding independently from the SAW response model. It is best to use the waveguide model to determine the number of modes propagating in a particular device beamwidth for the analysis of a transversely coupled resonator filter. The response of each guided mode is then determined by the COM model.

ANALYSIS APPROACH

The technique used to analyze a SAW coupled resonator in this paper is based on the coupling of modes and waveguide model approach. Applying the coupling of modes formalism to a SAW structure, it is possible to calculate the required fundamental parameters from basic principles and conclude with the closed form solutions for the device response. The coupling of modes theory describes the acoustic field distribution in the resonator in terms of a forward traveling and a backward traveling wave. The coupling of modes formalism requires that the system be described by a set of N first order coupled differential equations governing the propagation of the N modes in the system. Each equation governs the propagation of a specific mode and describes how the remaining modes couple to it. In a transducer, as a Rayleigh wave propagates under the edge of an electrode, a portion of the wave reflects from the edge of the electrode. The portion of the wave that is reflected from the edge becomes part of the wave

traveling in the opposite direction. Therefore, the reflections cause coupling of waves. Each of the waves propagating under the transducer will require that first order differential equations be derived describing the wave characteristics. Using this method, each of the SAW components can be analyzed independently. In a SAW device component there are four different types of transverse guided modes. These are the symmetric and antisymmetric trigonometric and the symmetric and antisymmetric hyperbolic modes. If the width of the transducer is under a certain limit only the trigonometric modes are guided by the device structure. Consider a uniform overlap SAW transducer, which can be Fourier decomposed to a $\sin x/x$ response in the frequency domain. Symmetric and antisymmetric modes are launched in the waveguide. The waves extend partially outside the guiding region and eventually die off as shown in Figure 5.

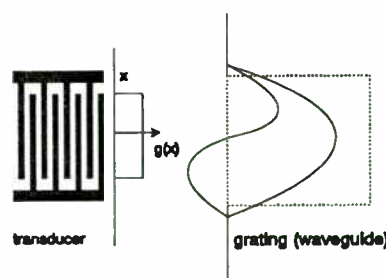
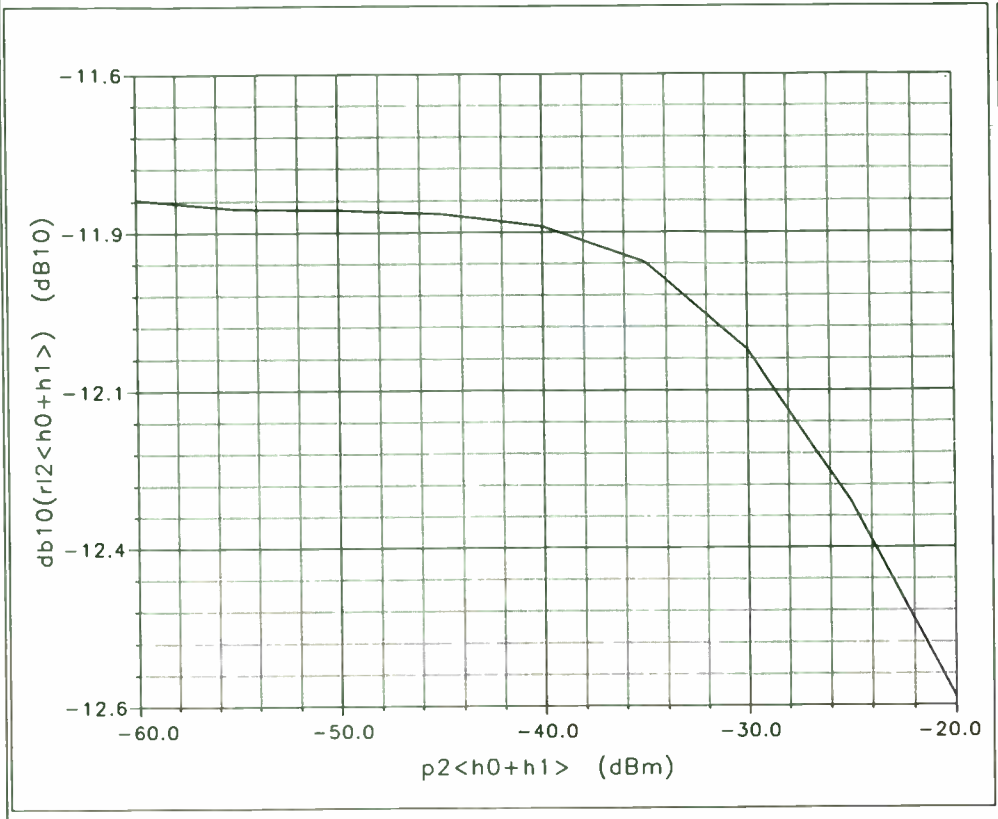


FIGURE 5

However, if another waveguide is placed next to the guiding region, the modes no longer die off and evanescent coupling results in the coupling of energy into the extended new waveguide and other modes are launched. In effect, for the analysis of proximity resonators, the two guiding regions are replaced by a single waveguide where the modes are supported.

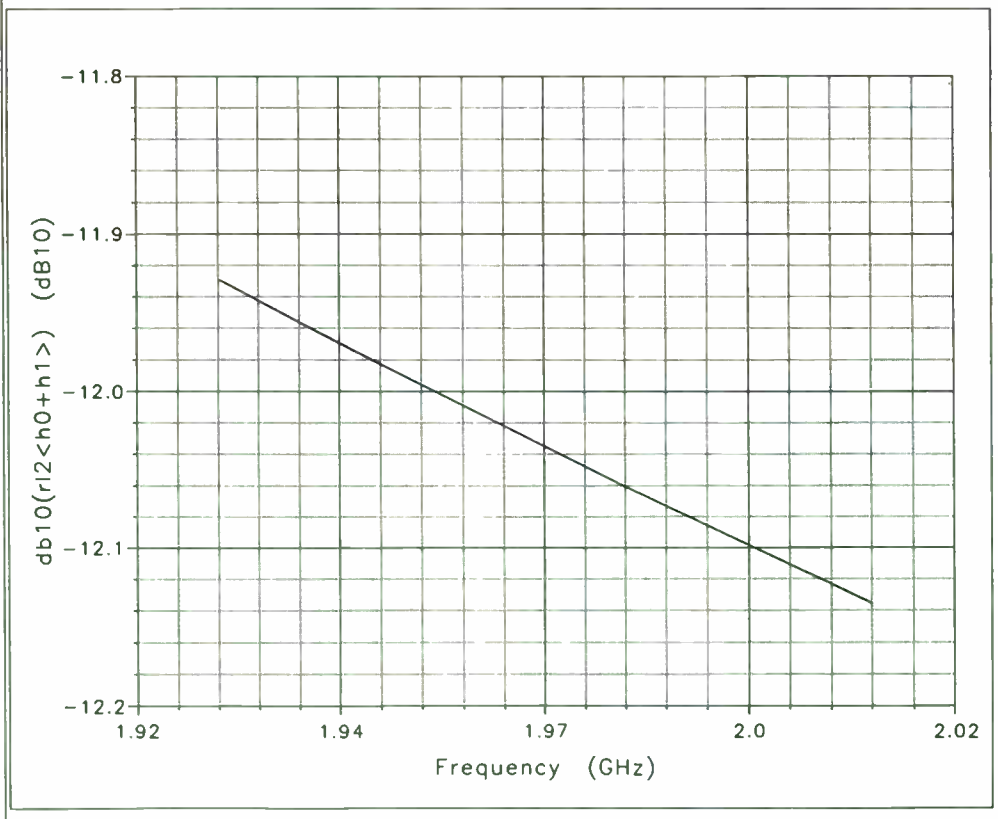
COUPLING OF MODES ANALYSIS OF A SAW REFLECTIVE GRATING

The coupling of modes formalism describes the motion of the surface acoustic wave propagating across the substrate. It is derived from equations which are actually a set of first order wave equations. One of the main motivations for using the COM approach is its simplicity of application to SAW devices. Using the COM approach a closed form analytic description of periodic structures may be obtained which is of extreme importance especially when considering the synthesis of SAW devices. The reflective grating consists of 'n'



fetmixer
 Y:db10(r12<h
 db10(r12<h0+h1>
 dfetmix5.ckt

Ave
 NY , NY 10172



fetmixer
 Y:db10(r12<h
 db10(r12<h0+h1>
 dfetmix5.ckt

periodic strips with period 'p', strip width 'a_g' and height 'H_m' as shown in Figure 6.

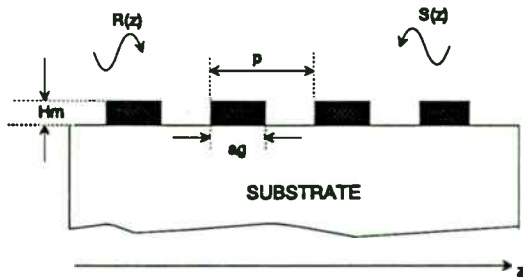


FIGURE 6 : A typical grating

A surface wave, $U(z)$, can be broken into two propagating waves, the forward traveling wave $a(z)$ and the reverse traveling wave $b(z)$. The waves have slowly varying amplitudes, $R(z)$ and $S(z)$, respectively. The forward traveling wave, $a(z)$, is assumed to be traveling in the $+z$ direction and the reverse surface acoustic wave is assumed to be traveling in the $-z$ direction. These waves are described by

$$a(z) = R(z)\exp(-jk_f z)\exp(j\omega t) \quad (1)$$

$$b(z) = S(z)\exp(+jk_f z)\exp(j\omega t) \quad (2)$$

where ' k_f ' is the wave vector of the surface wave on a surface without electrodes, and ' ω ' is the angular frequency. Let ' k_g ' be the wave number under the grating, so that

$$k_f = \frac{k_g}{2} \quad (3)$$

where,

$$k_g = \frac{2\pi}{p} \quad (4)$$

Assuming steady state time dependency, the factor $\exp(j\omega t)$ can be dropped in the analysis. An accurate description of the field distributions, e.g. displacements, would require an infinite number of "space harmonic" components, but in the COM approach only the two lowest order dominant harmonics are taken into account. The field may be written in the form of complex wave amplitudes and the local complex amplitude, $U(z)$, can be approximated by superposition of the reverse and forward waves as stated below.

$$U(z) = R(z)\exp(-j\frac{k_g}{2}z) + S(z)\exp(j\frac{k_g}{2}z) \quad (5)$$

In the absence of the grating, the following differential equations are satisfied by the waves $a(z)$ and $b(z)$,

$$\frac{da(z)}{dz} + jk_f a(z) = 0 \quad (6)$$

$$\frac{db(z)}{dz} - jk_f b(z) = 0 \quad (7)$$

If a grating is placed onto the substrate, the periodic discontinuities disturb the propagation of the wave. The wave amplitude changes along ' z ' because of the wave reflections from the grating strips and the phase velocity also changes since the free space velocity is higher than the velocity under metallized regions. The reflection mechanism therefore gives rise to coupling between the forward and the reverse waves. The strength of the coupling is determined by the form of the irregularities disturbing the propagation. Generally, a "mode" of propagation, means an infinite number of space harmonics characterizing the wave propagation. These space harmonics have different wavelengths at the same frequency and hence different phase velocities. In the COM approach, only one harmonic component is taken into account for each propagation direction. Therefore, the forward and backward waves are referred to as "modes". The presence of the grating changes the propagation constant by Δk so that

$$\frac{da}{dz} + j(k_f + \Delta k)a = jk_{21}b \quad (8)$$

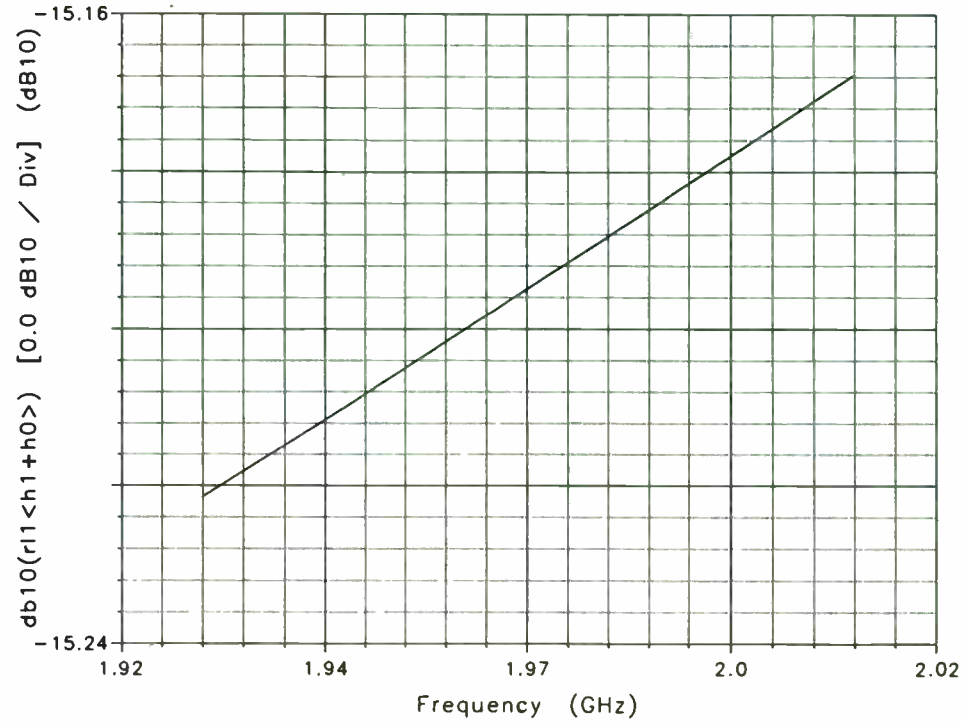
$$\frac{db}{dz} - j(k_f + \Delta k)b = jk_{12}a \quad (9)$$

The periodic perturbations leads to power exchange between modes. $R(z)$ couples to $S(z)$ and $S(z)$ couples to $R(z)$. Using the differential form of the equations and assuming the change of amplitude per period of the grating is small, the law of conservation of energy requires

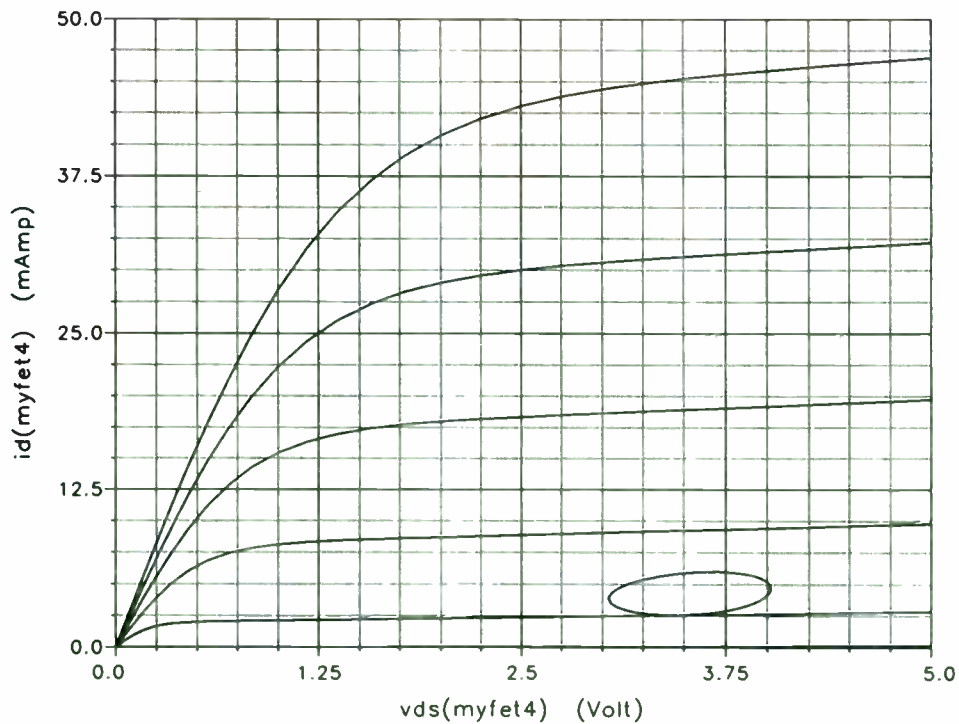
$$\frac{d}{dz}\{|R|^2 - |S|^2\} = 0 \quad (10)$$

since $R^2(z)$ and $S^2(z)$ correspond to the power carried by the "modes" $R(z)$ and $S(z)$ respectively. This condition leads to

$$k_{12} = -k_{21}^* \quad (11)$$



fetmixer
 Y:db10(r11<h
 db10(r11<h1+h0>)
 dfetmix5.ckt



fetmixer
 Y:id(myfet4)
 id(myfet4)
 Voltage = -1.904

fetmixer
 Y:id(myfet4)
 id(myfet4)
 Voltage = -1.6

fetmixer
 Y:id(myfet4)
 id(myfet4)
 Voltage = -1.2

fetmixer
 Y:id(myfet4)
 id(myfet4)
 Voltage = -0.8

fetmixer
 Y:id(myfet4)
 id(myfet4)
 Voltage = -0.4

fetmixer
 Y:id(myfet4)
 id(myfet4)
 Voltage = 0

fetmixer
 Y:id(myfet4)
 id(myfet4)
 dfetmix5.ckt

where the coefficient k_{12} is the coupling coefficient and is a periodic function of z . Generally speaking a complex Fourier series of the periodic function k_{12} of period 'p' is given by

$$k_{12} = \sum_{n=-\infty}^{\infty} K(n) \exp(jnk_g z) \quad (12)$$

Substituting, (1) and (2) into (8) and (9) gives the following equations (13) and (14)

$$\frac{dR}{dz} = -j(k_f - \frac{k_g}{2} + \Delta k)R + j \sum_{n=-\infty}^{\infty} K(n)S \exp[j(n+1)k_g z]$$

$$\frac{dS}{dz} = j(k_f - \frac{k_g}{2} + \Delta k)S - j \sum_{n=-\infty}^{\infty} K^*(n)R \exp[-j(n+1)k_g z]$$

Of all n Fourier components, only the $n=-1$ term produces coupling between the forward and backward traveling waves that is independent of z . To simplify the equation, a "wave mismatch" parameter is used, called the detuning parameter as

$$\delta = k_f - \frac{k_g}{2} + \Delta k \quad (15)$$

Using the detuning parameter and writing $K(-1)$ as just K , the COM equations can be simplified as

$$\frac{dR}{dz} = -j\delta R + jKS \quad (16)$$

$$\frac{dS}{dz} = j\delta S - jK^*R \quad (17)$$

Now, solving these equations is straightforward and given by Elachi [8] as,

$$R(z) = c_1 \exp[j(\delta - D)z] + c_2 \exp[j(\delta + D)z] \quad (18)$$

$$S(z) = c_1 \exp[-j(\delta + D)z] + c_2 \exp[-j(\delta - D)z] \quad (19)$$

where an additional frequency variable D , the propagation constant which includes the detuning effects of the reflective grating, is included and is given as

$$D(\omega) = \sqrt{\Delta^2(\omega) - K_R(\omega)K_S(\omega)} \quad (20)$$

$K_R(\omega)$ and $K_S(\omega)$ are the real and imaginary terms of the reflection (coupling) coefficient. The constant c_1 and c_2 are determined by boundary conditions. The total wave $U(z)=a(z)+b(z)$ and its derivative with respect to position must be continuous. Figure 7 shows the behavior of the forward and reverse waves at the device

boundaries. Since, the wave has to be a continuous function with respect to position, the boundary conditions are given to be

$$R(0) = 1 \quad (21)$$

$$S(L) = 0 \quad (22)$$

where L is the length of the grating and is given to be the product of the number of finger strips and the period of the grating structure, $L = np$.

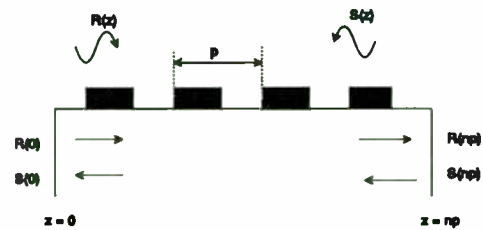


FIGURE 7 : Forward and Backward waves at the device boundaries

Solving for the coefficients c_1 and c_2 and substituting into (18) and (19) gives the amplitudes $R(z)$ and $S(z)$ to be

$$R(z) = \frac{D \cos[D(L-z)] + j\Delta \sin[D(L-z)]}{D \cos(DL) + j\Delta \sin(DL)} \quad (23)$$

$$S(z) = \frac{jK^* \sin[D(L-z)]}{D \cos(DL) + j\Delta \sin(DL)} \quad (24)$$

Figure 8, shows the relative amplitudes of the forward and backward traveling waves as a function of position z with fixed frequency.

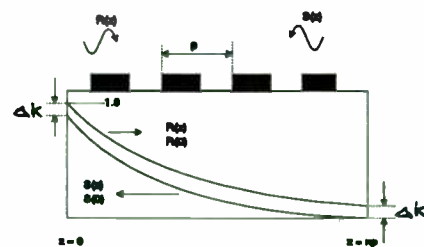
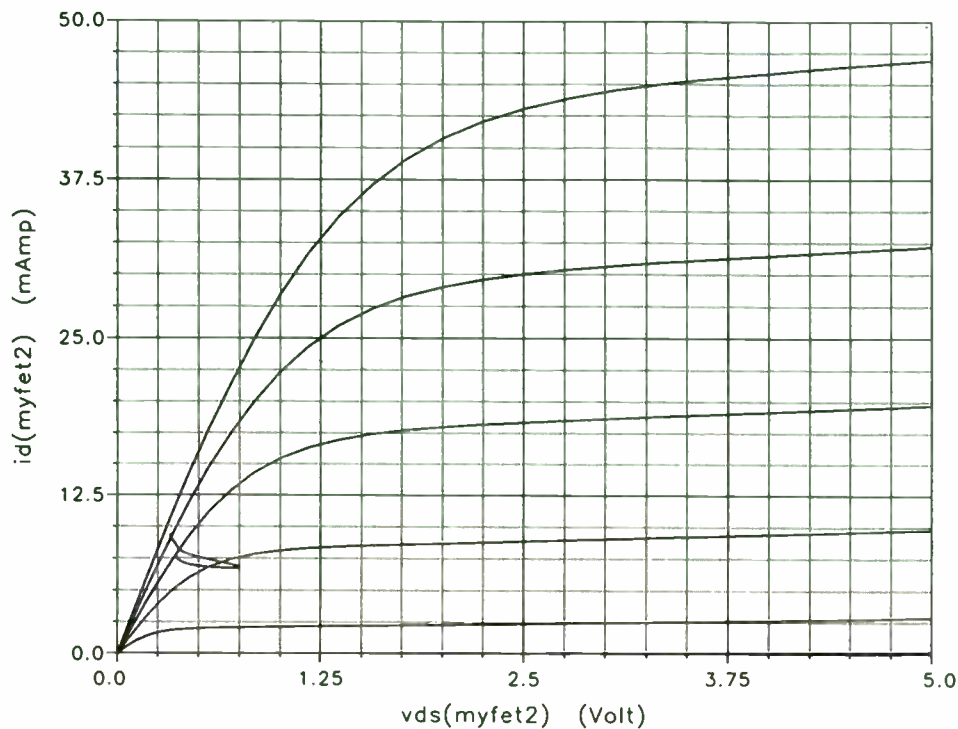
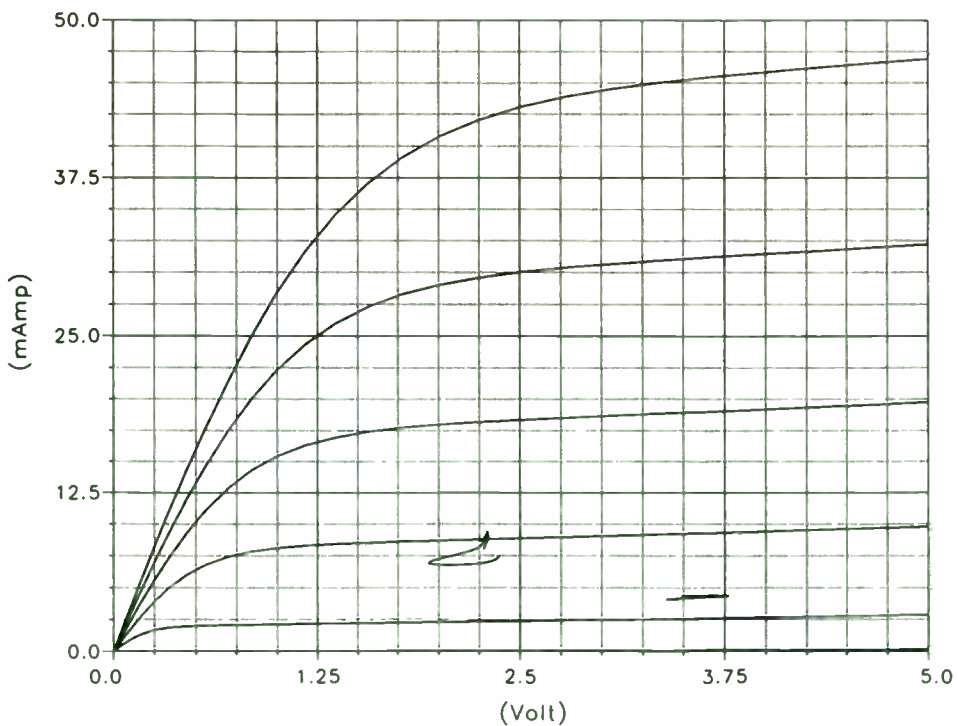


FIGURE 8 : Power coupling from incident to reflected wave

The magnitude of the incident wave $R(z)$ decays exponentially along the grating due to the reflection of power into the backward traveling wave. The amplitude $S(z)$ of the backward traveling wave builds up due to the power from the forward wave. This exponential decay behavior occurs only for a narrow band of frequencies, and only when the propagation constant D is real. Now,



- fetmixer
Y:id(myfet2)
id(myfet2)
Voltage = -1.904
- fetmixer
Y:id(myfet2)
id(myfet2)
Voltage = -1.6
- fetmixer
Y:id(myfet2)
id(myfet2)
Voltage = -1.2
- fetmixer
Y:id(myfet2)
id(myfet2)
Voltage = -0.8
- fetmixer
Y:id(myfet2)
id(myfet2)
Voltage = -0.4
- fetmixer
Y:id(myfet2)
id(myfet2)
Voltage = 0
- fetmixer
Y:id(myfet2)
id(myfet2)
dfetmix5.ckt



- fetmixer
Y:
id(myfet3)
Voltage = -1.904
- fetmixer
Y:
id(myfet3)
Voltage = -1.6
- fetmixer
Y:
id(myfet3)
Voltage = -1.2
- fetmixer
Y:
id(myfet3)
Voltage = -0.8
- fetmixer
Y:
id(myfet3)
Voltage = -0.4
- fetmixer
Y:
id(myfet3)
Voltage = 0
- fetmixer
Y:
id(myfet3)
dfetmix5.ckt

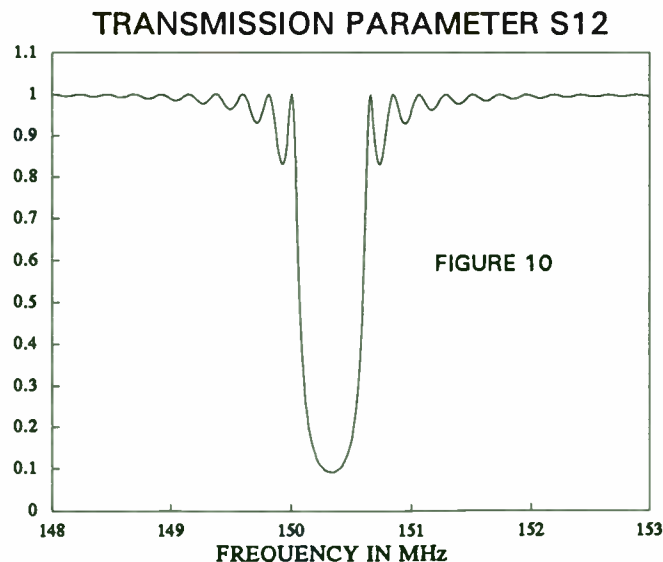
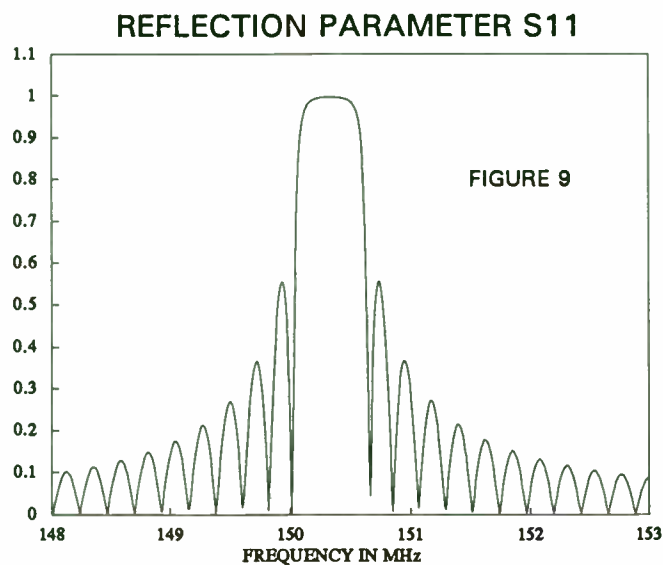
having obtained the wave equations, the scattering matrix characterization of the grating can be determined as

$$S = \begin{bmatrix} b(0) & a(np) \\ a(np) & b(0) \end{bmatrix} \quad (25)$$

Therefore, making use of the solutions for the forward and backward waves as given in (23) and (24), the expressions for the scattering parameters is obtained to be

$$S_{11} = S_{22} = \frac{jK^* \sin(DL)}{D \cos(DL) + j\Delta \sin(DL)} \quad (26)$$

$$S_{12} = S_{21} = \frac{(-1)^n D}{D \cos(DL) + j\Delta \sin(DL)} \quad (27)$$



The grating can be analyzed separately and the scattering parameters can be obtained directly using the RESCAD computer model. The solutions for a typical grating are plotted in Figures 9 and 10.

EFFECT OF METAL THICKNESS

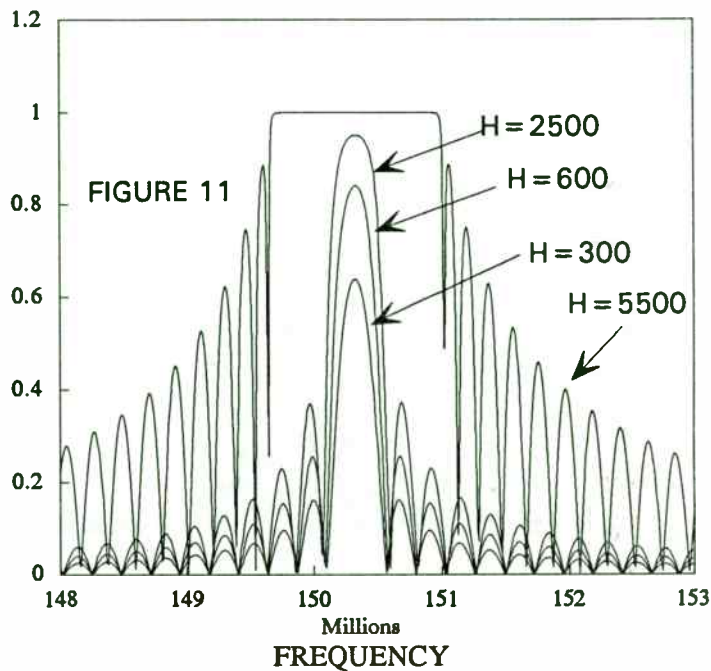
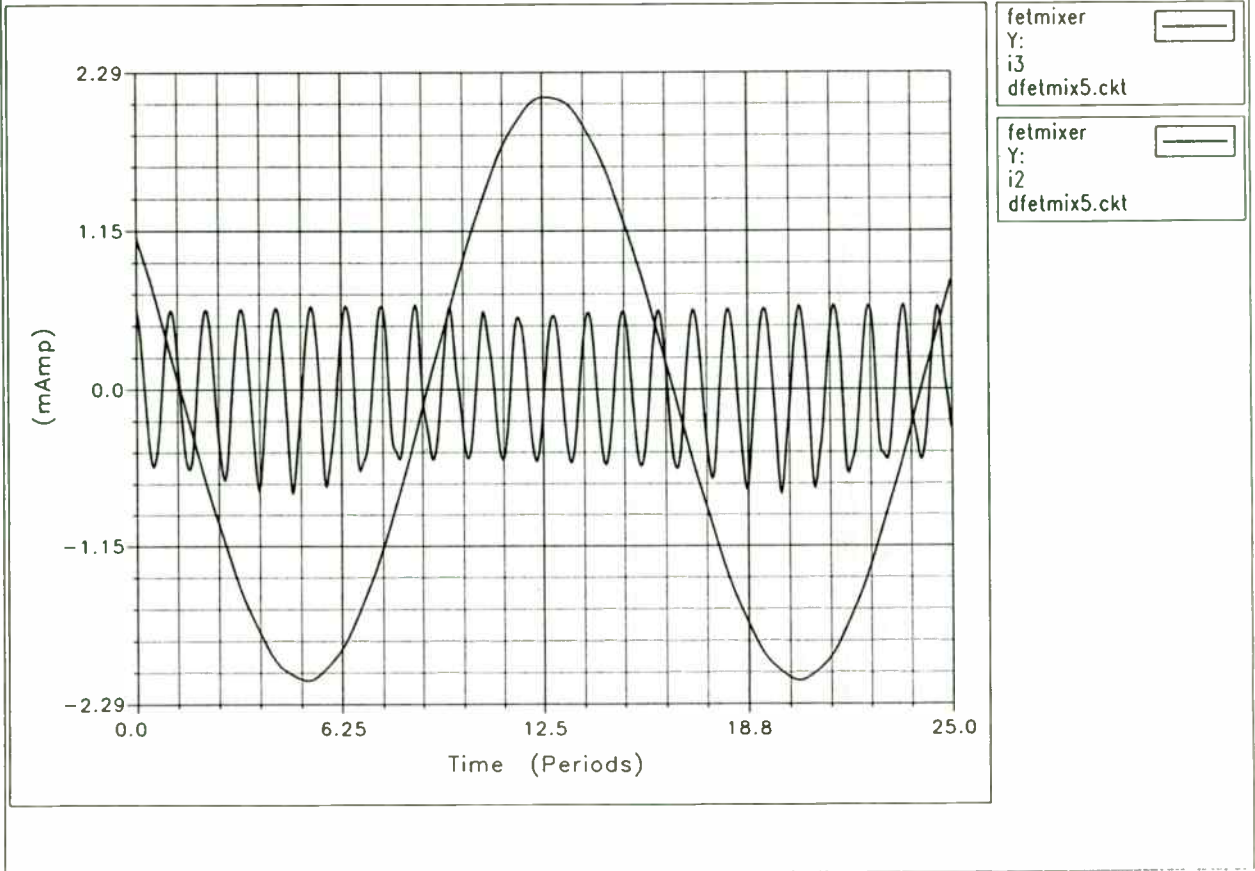


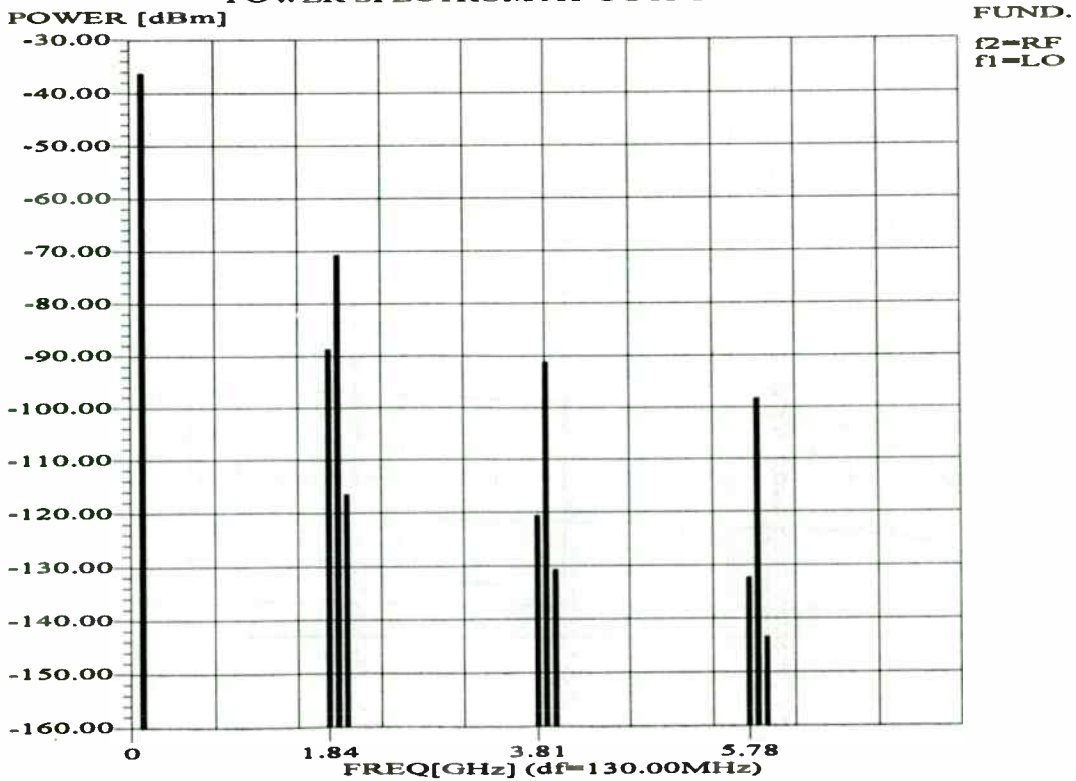
Figure 11 shows the effect of metal thickness on the grating reflection coefficient. The reflection coefficient is described by (26) where 'K' the reflection (coupling) coefficient is given by [9]

$$K = \left\{ \left[\frac{2\pi f}{v_f} \right] * \left[\frac{e_4 k^2}{2} + \frac{e_5 H_m}{L} \right] \right\} \quad (28)$$

where e_4 and e_5 are material constants for the substrate, ' k^2 ' is the acoustic coupling coefficient of the substrate material and the other notations have the usual meanings. To show the variation on the reflection coefficient with respect to metal thickness, the number of grating electrodes was held constant in Figure 11. As can be observed from Figure 11, as the metal thickness increases, the stopband for the reflector is broader and the sidelobes are higher. A broader stopband increases the number of longitudinal resonance modes. The unwanted longitudinal modes occur near the edges of the stopband, and to reduce or eliminate these modes the transmission response of the reflective grating should be centered in the reflector stopband. As the metal thickness of the reflector increases, the reflectivity also increases. Figure 12, shows the effect of the number of



09-JAN-93 MICROWAVE HARMONICA PC V5.1 (BETA2) 10:55:10
 File: DFETMIX5.CKT
 IF Output Spectrum with an RF power level of -60 dBm
 POWER SPECTRUM AT OUTPUT PORT#1



grating strips on the reflection coefficient which is done by maintaining a constant metal thickness.

EFFECT OF NUMBER OF STRIPS

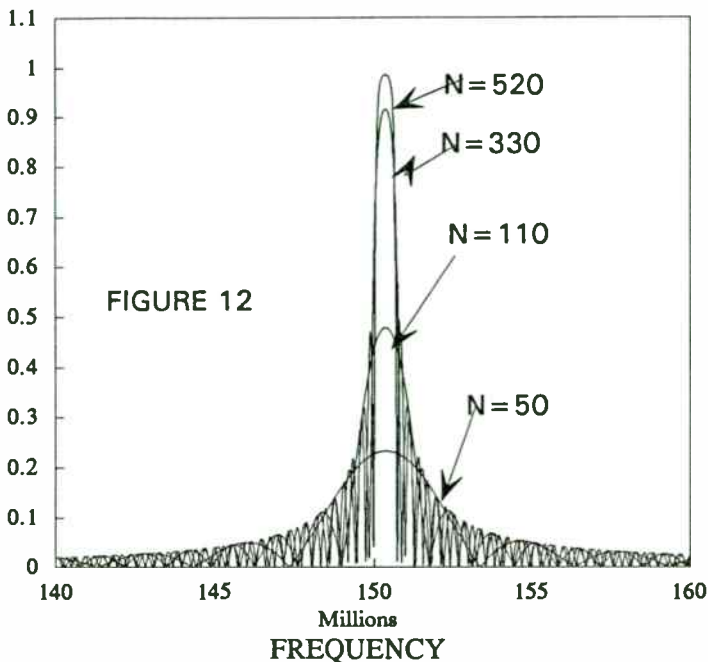


Figure 12 shows that the reflectivity increases with the number of electrodes. The passband gets narrower and the sidelobes become higher with an increase in the number of strips.

COUPLING OF MODES EQUATIONS FOR AN INTERDIGITAL TRANSDUCER

The transducer generates forward and backward propagating surface waves with complex slowly varying amplitudes, $R(z)$ and $S(z)$, that are coupled together, similar to a grating. The physical arrangement of the

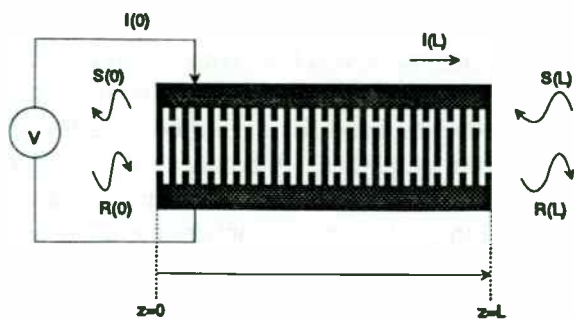


Figure 13 : IDT schematic

interdigital transducer with the forward and the reverse traveling wave is shown in Figure 13. The IDT is more

complicated because of the combinations of elementary source transduction and internal reflections. A third port, an electrical one, is added. For a transducer, the basic COM equations of the grating will have to be modified by adding a new term called the transduction term. The transduction term describes the SAW excitation of a voltage V applied to a pair of electrodes. An equation is needed to represent the current drawn by the electrical port of the interdigital transducer. Within a uniform transducer, the effects of reflection and transduction can no longer be assumed to be independent. This relationship between the transduction and reflection weighting results directly from the structure of the transducer. The transduction period is twice the period of reflection. So, in order to get the COM equations for the IDT, the grating equations are altered by adding a transduction term and by using an additional equation to describe the relationship between the current and the voltage at the electrical port. Doing so yields,

$$\frac{dR}{dz} = jKS + j\xi V - j\delta R \quad (29)$$

$$\frac{dS}{dz} = j\delta S - jK^* R - j\xi^* V \quad (30)$$

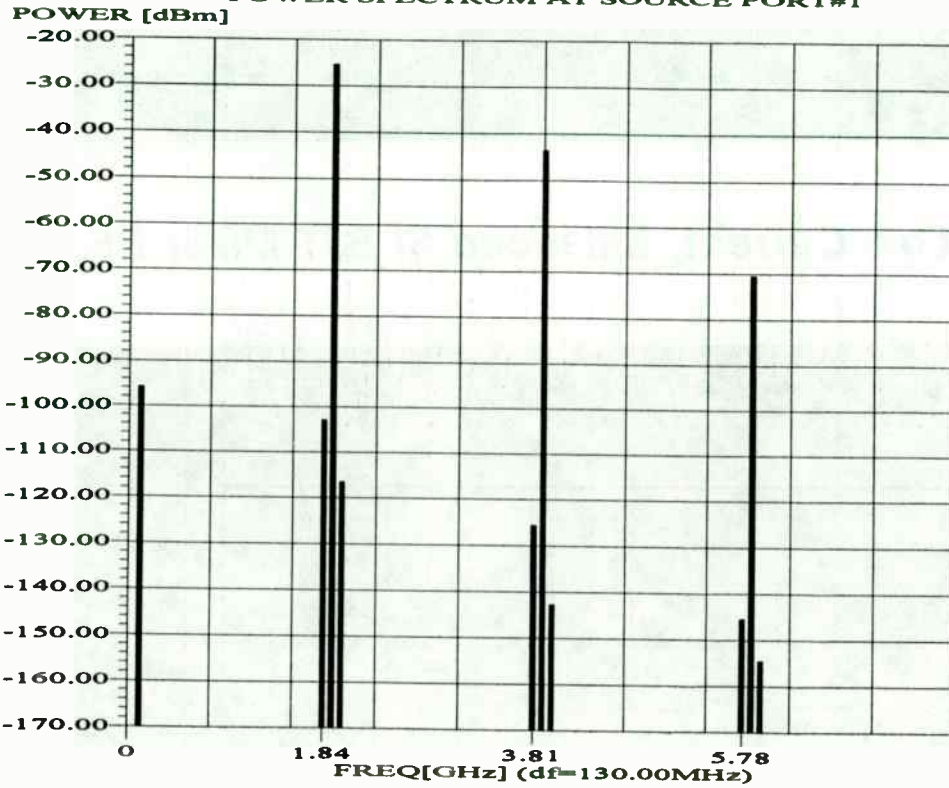
The parameter ξ is the transduction coefficient. The electrical port can be described by

$$\frac{dI}{dz} = -2\xi^* jR + 2j\xi S + j\omega CV \quad (31)$$

where C is given as $C = C_s W$. C_s is the static capacitance per finger pair and W is the IDT aperture. R and S are amplitudes of the forward and backward waves. Equations (29), (30) and (31) are first order differential equations. The P-matrix notation has been used in the literature to present the results of a coupling of modes analysis. This is a very convenient approach since the solutions to the COM equations are dependent on the elements of the P matrix. In the P-matrix representation, the acoustic ports are treated as scattering ports and the electrical port as an admittance port. Figure 14 shows the three port scattering matrix description. The scattering and admittance properties of the three port junction can be written in matrix notation as

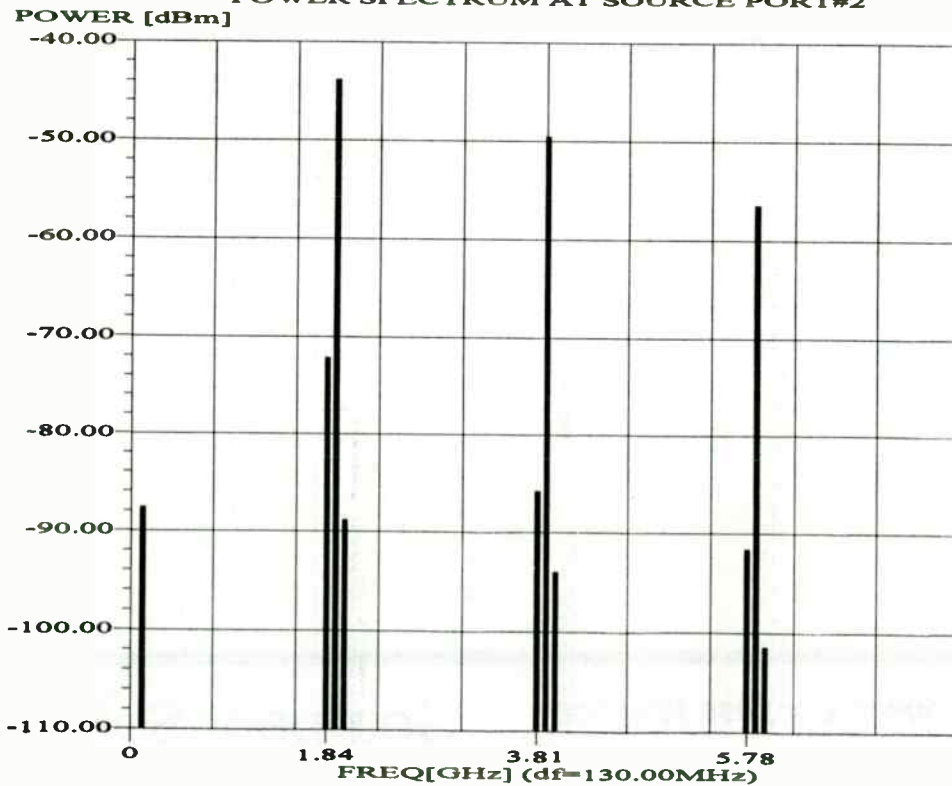
$$\begin{bmatrix} b_1 \\ b_2 \\ b_3 \end{bmatrix} = \begin{bmatrix} P_{11} & P_{12} & P_{13} \\ P_{21} & P_{22} & P_{23} \\ P_{31} & P_{32} & P_{33} \end{bmatrix} \begin{bmatrix} a_1 \\ a_2 \\ a_3 \end{bmatrix} \quad (32)$$

RF Signal coming out of LO Port of Mixer
POWER SPECTRUM AT SOURCE PORT#1



FUND.
f2=RF
f1=LO

LO Signal coming out of RF Port of Mixer
POWER SPECTRUM AT SOURCE PORT#2



FUND.
f2=RF
f1=LO

The power incident on one port is distributed to the others depending on the coupling at the ports. A set of input waves is scattered into a set of output waves.

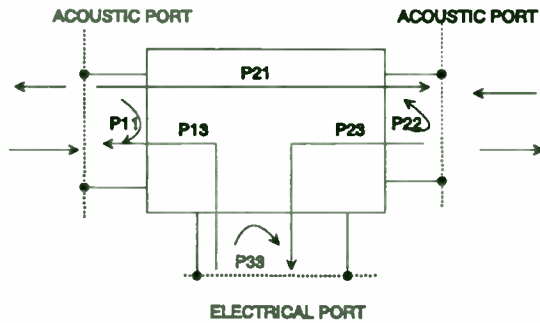


Figure 14 : P parameter description

The third port which is an electrical port is represented by the current drawn by the IDT and the terminal voltage. So equation (32) can be rewritten as

$$\begin{bmatrix} b_1 \\ b_2 \\ I_3 \end{bmatrix} = \begin{bmatrix} P_{11} & P_{12} & P_{13} \\ P_{21} & P_{22} & P_{23} \\ P_{31} & P_{32} & P_{33} \end{bmatrix} \begin{bmatrix} a_1 \\ a_2 \\ V \end{bmatrix} \quad (33)$$

The IDT admittance is characterized by the P_{33} parameter. The P-matrix for a SAW transducer must satisfy three reciprocity relationships.[10]

$$P_{21} = P_{12}; \quad P_{31} = -2P_{13}; \quad P_{32} = -2P_{23}$$

Moreover, for a SAW transducer if loseless, the P-matrix will satisfy three unique energy conservation relationships. [10]

$$Re\{P_{33}\} = |P_{13}|^2 + |P_{23}|^2 \quad (34)$$

$$|P_{11}|^2 + |P_{21}|^2 = 1 \quad (35)$$

$$|P_{22}|^2 + |P_{12}|^2 = 1 \quad (36)$$

The advantages of using this representation is that it allows easier manipulation of the parallel electrical circuit and acoustically cascaded connection for multiple transducer/grating circuits. The elements P_{11} , P_{12} , P_{21} and P_{22} are identical to the scattering parameters developed for a grating. P_{33} is the admittance of the IDT as seen at the electrical port if no incoming waves are present and

P_{13} and P_{23} are the voltage to SAW transfer elements. Applying B.P.Abbott's solutions [10] for the uniform IDT and expressing them in P-matrix form yields

$$P_{11} = S_{11} = \frac{jK^* \sin(DL)}{D \cos(DL) + j\Delta \sin(DL)} \quad (37)$$

$$P_{12} = S_{12} = \frac{(-1)^n D}{D \cos(DL) + j\Delta \sin(DL)} \quad (38)$$

$$P_{13} = jLB \left[\frac{\xi^* D \cos(\frac{DL}{2}) + j(K^* \xi + \Delta \xi^*) \sin(\frac{DL}{2})}{D \cos(DL) + j\Delta \sin(DL)} \right] \quad (39)$$

where $B = \left[\frac{\sin(DL/2)}{DL/2} \right]$

$$P_{22} = \frac{jK(-1)^{2n} \sin(DL)}{D \cos(DL) + j\Delta \sin(DL)} \quad (40)$$

$$P_{23} = jL(-1)^n B \left[\frac{\xi D \cos(\frac{DL}{2}) + j(K\xi^* + \Delta \xi) \sin(\frac{DL}{2})}{D \cos(DL) + j\Delta \sin(DL)} \right] \quad (41)$$

$$P_{33} = -j2 \frac{X}{D^3} \left[DL - \frac{D \sin(DL) + j\Delta(1 - \cos(DL))}{D \cos(DL) + j\Delta \sin(DL)} \right] - 2 \frac{Y}{D^3} \left[\frac{1 - \cos(DL)}{D \cos(DL) + j\Delta \sin(DL)} \right] + j \left[\frac{3\omega C_F L / \Delta_T}{3 + j\omega C_F R_F} \right] \quad (42)$$

where $X = K^* \xi^2 + K \xi^{*2} + 2\Delta |\xi|^2$ and

$$Y = \Delta(K \xi^{*2} + K^* \xi^2) + 2|K|^2 |\xi|^2$$

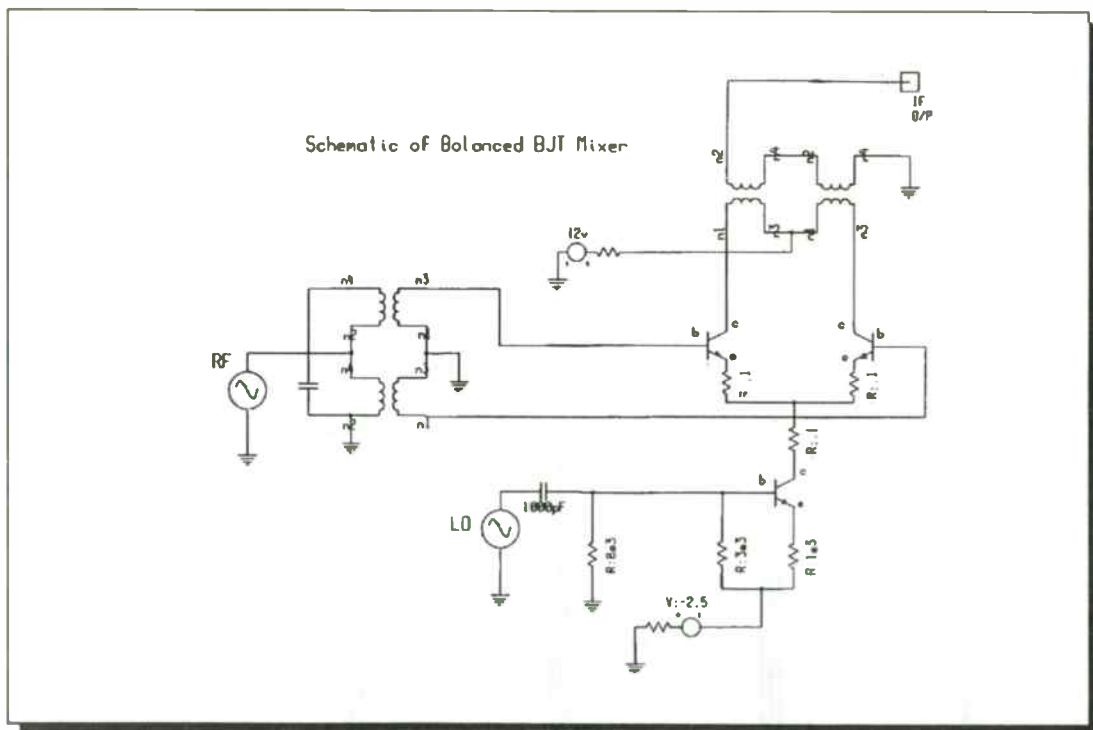
Using the reciprocity relationship for the mixed P-matrix the remaining elements can be found. Using energy conservation the acoustic conductance can be expressed in terms of the waves leaving the SAW transducer.

$$G(\omega) = Re\{P_{33}\} = |P_{13}|^2 + |P_{23}|^2 \quad (43)$$

The interdigital transducer can be analyzed separately and the P-matrix parameters can be obtained using

Low Current, Balanced Si BJT Mixer RF

Compact Software



Digital European Cordless Telephone

Compact Software

"RESCAD". The typical P parameter responses are shown in Figure 15.

COM PARAMETERS

In order to use the coupling of modes technique, the various parameters used in the COM equations will have to be determined. The detuning parameter is also the "wave mismatch" parameter and is defined in (15) where 'k_t' is the wave vector of the surface wave on a surface without electrodes and is also the undisturbed propagation constant at the Bragg frequency, so that

$$\delta = \frac{2\pi f}{v_f} - \frac{\pi}{p} + \Delta k \quad (44)$$

Δk is relatively small and can be neglected from the above equation. The reflection coefficient 'K' models the effects of the electrode strips on the surface wave, electrical loading, as well as the various mechanical loadings. A strip which is conducting, when placed on a piezoelectric substrate shorts out the tangential electric field associated with the wave. The electrical loading reduces the surface wave velocity and provides a mismatch of the gap regions and the electrode which have different wave impedances. The mechanical perturbations arise from different mechanical natures. Firstly, loading occurs due to the mass of the electrode metal which results from the difference in the mass densities of the metal strip and the piezoelectric substrate [9]. Secondly, there is loading due to elasticity of the strips. To reduce these mechanical disturbances, a metal film that has elastic properties and mass density similar to the substrate is desired for the grating strips. The reflection coefficient is given by equation (28) and is dependent on material constants. There are two coupling of modes parameters used to model transduction. These are the transduction strength and the transduction phase. The transduction process is common to all the SAW device analysis methods. There is a fundamental difference between the impulse model and the coupling of modes model in that the impulse model assumes that the reflectivity from the transducer electrodes is zero. As a result K must be zero. This effectively uncouples the two acoustic modes. Comparing the impulse model solutions for P₁₃ with the COM model solution yields

$$\xi = |k| \epsilon_s (\infty) \frac{V_F(k)}{L_t} \sqrt{\frac{\omega W \Gamma_s}{2}} \exp(j\Phi_T) \quad (45)$$

where 'k' is the wave number, ϵ_s is the electrostatic

permittivity of the substrate, Γ_s is the SAW coupling coefficient defined by Morgan [11], $V_F(k)$ is the Fourier transform of the elemental potential of the transducer structure and L_t is the transduction period. An expression for the static capacitance per finger pair, was given by Engan[12] and is computed by calculating the total charge per unit length of each electrode.

$$C_s = (\epsilon_0 + \epsilon_p) \frac{K(\xi)}{K(\sqrt{1-\xi^2})} \quad (46)$$

where ϵ_0 is the dielectric permittivity and ϵ_p is the zero stress permittivity.

TRANSVERSE MODE EQUATIONS

In order to determine the number of modes in a device structure, the dispersion relationship dependent on the transverse boundary conditions must be solved. In other words, the number of modes has to be solved by taking into account the different velocities in the different metallized regions such as the bus bars, finger region and free surface. Each mode can be viewed as a plane wave propagating at an angle to the direction along the guide, which is reflected at the waveguide boundaries, following a zig zag path [13].

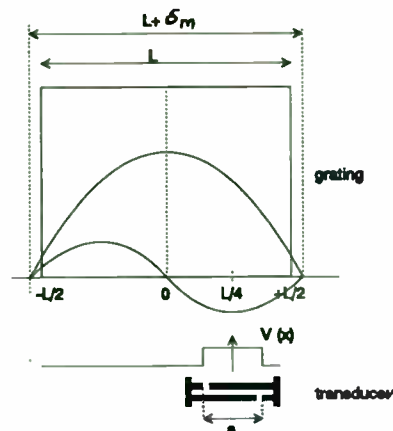
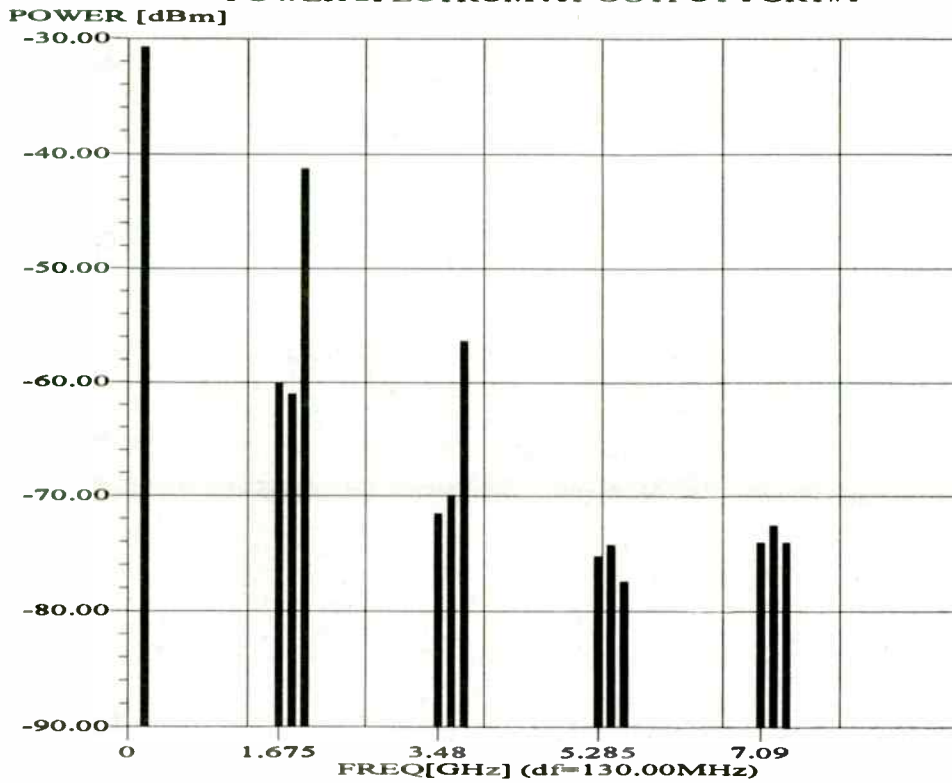


Figure 16 : Occurrence of modes

The basic equations for the mode analysis of a device structure propagating symmetric and antisymmetric modes as shown in Figure 16 is considered. The equation for the rectangular function is given as

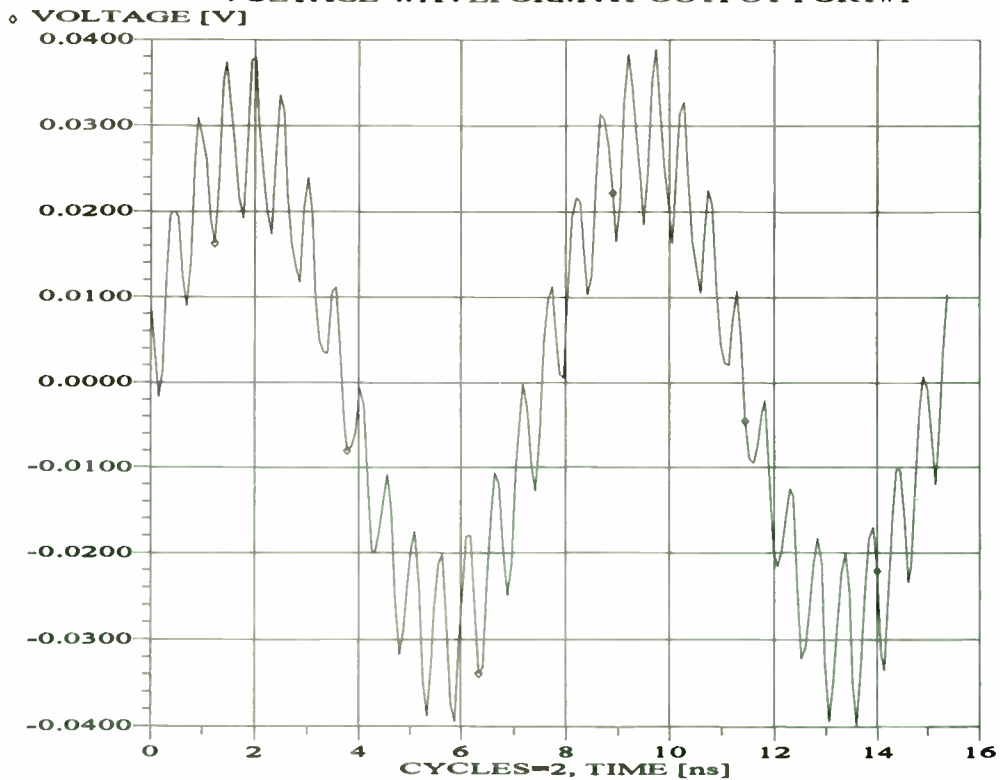
$$V(x) = A \text{rect}\left(\frac{x-L/4}{a}\right) \quad (47)$$

File: MIXTEST.CKT
IF Output from Balanced BJT Mixer
POWER SPECTRUM AT OUTPUT PORT#1

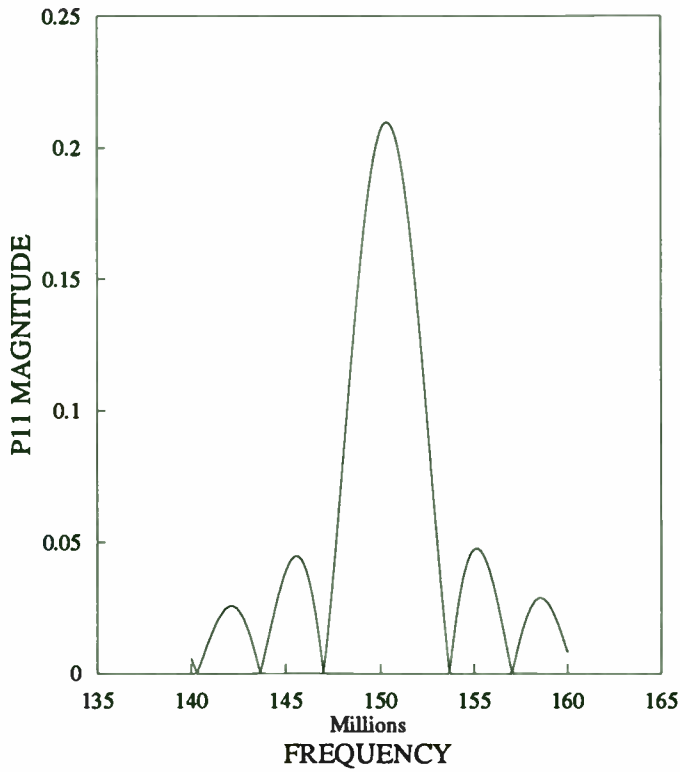


FUND.
f2=RF
f1=LO

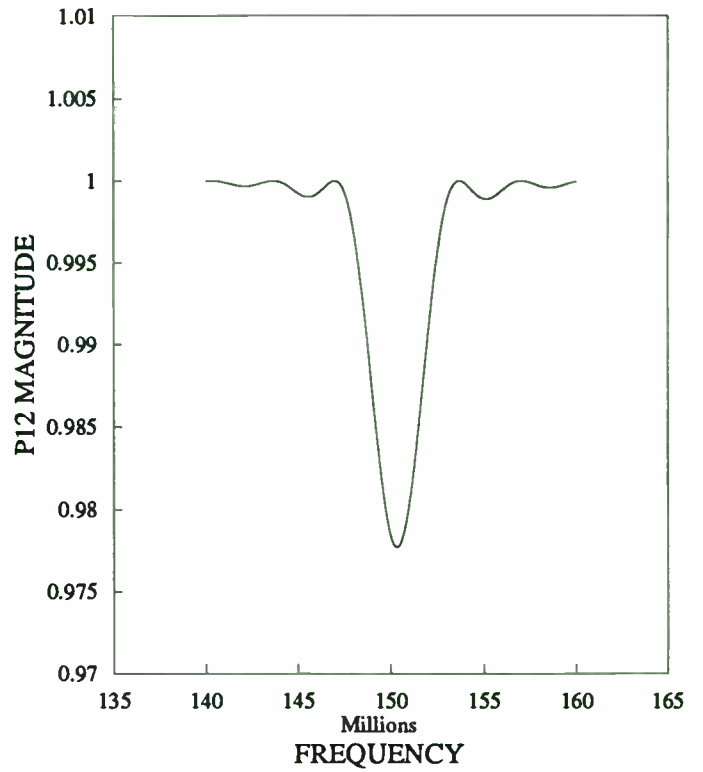
File: MIXTEST.CKT
IF Output from Balanced BJT Mixer
VOLTAGE WAVEFORM AT OUTPUT PORT#1



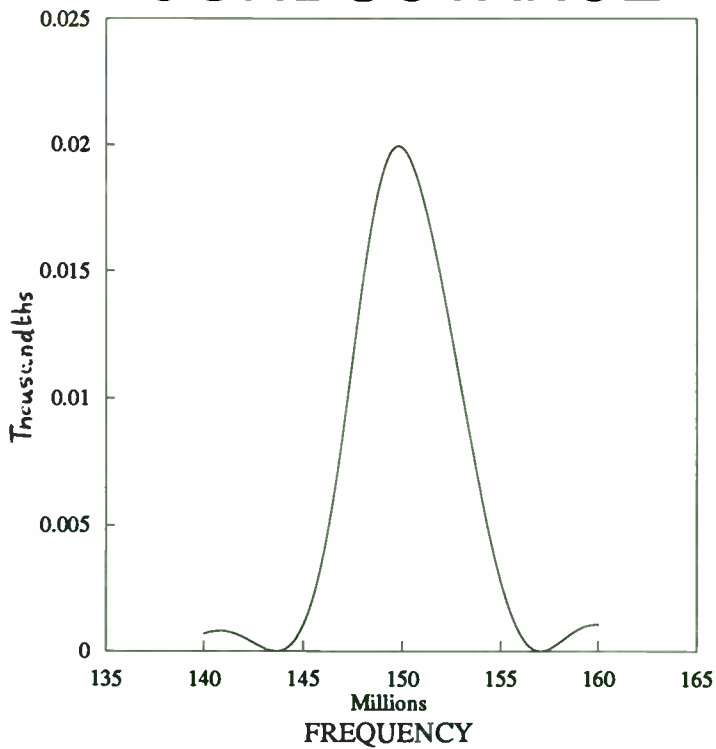
P11 PARAMETER OF IDT



P12 PARAMETER OF IDT



CONDUCTANCE



SUSCEPTANCE

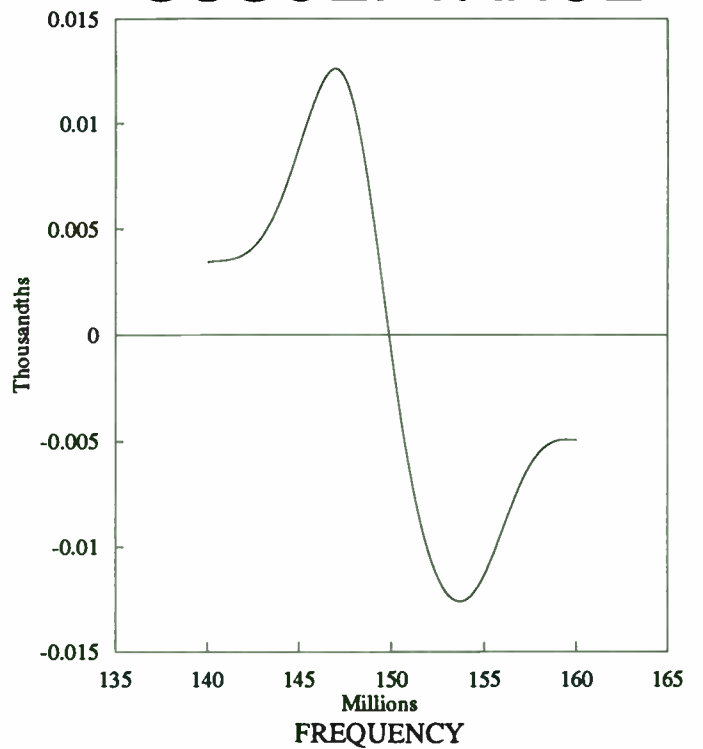
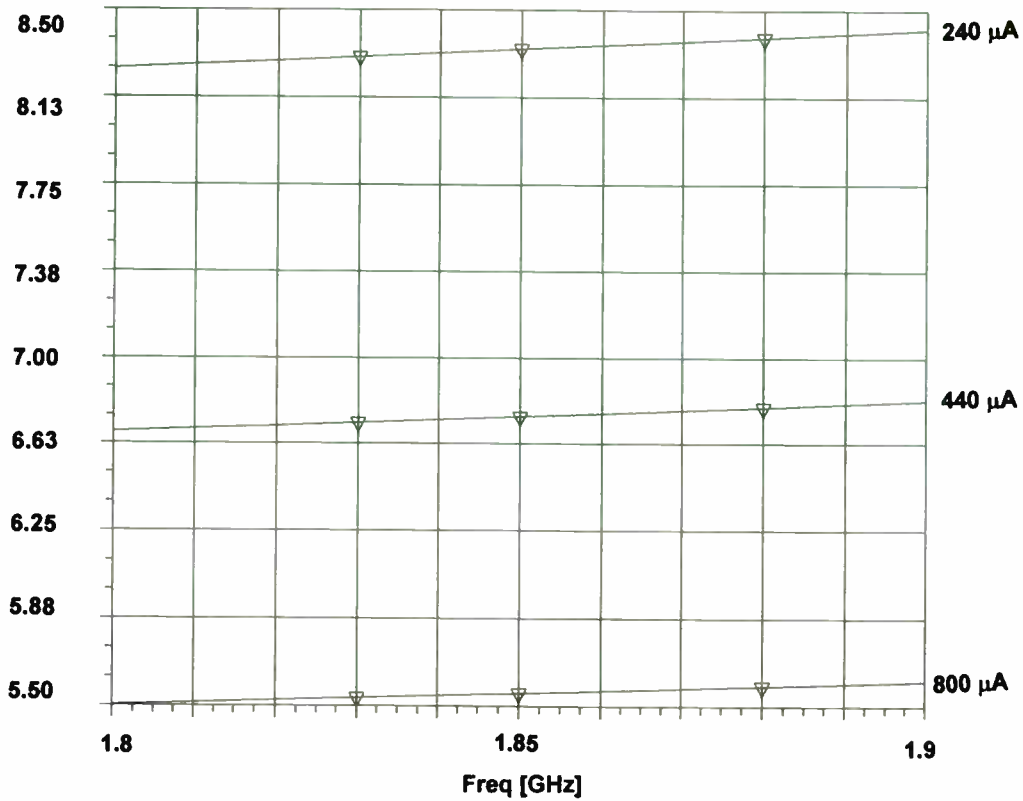


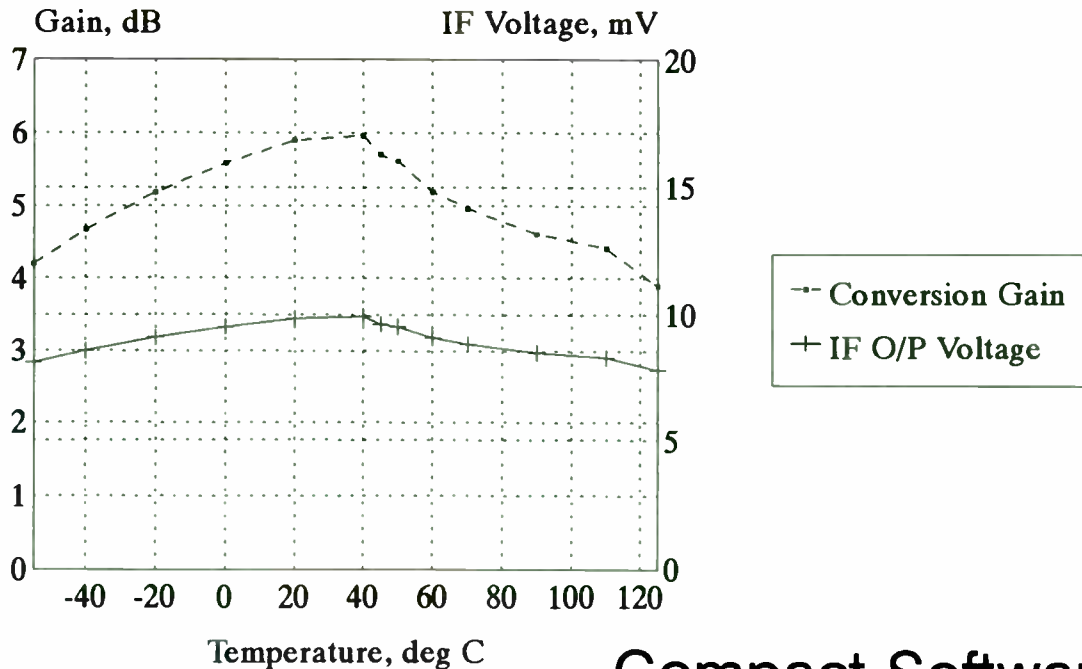
FIGURE 15: COM solutions for an IDT

Noise Figure of Balanced BJT Mixer versus Quiescent Current for LO = 300 mV

▽ NF [dB] MYMIX



Simulated Variations in Performance of Balanced BJT Mixer versus Temperature



Compact Software

This rect function $V(x)$ is the sum of all mode profiles $f_m(x)$, where $f_m(x)$ is defined separately for symmetric modes as

$$f_m(x) = a_m \cos \frac{(2m-1)\pi x}{L + \delta_m} \quad (48)$$

and for the antisymmetric modes as

$$f_m(x) = b_m \sin \frac{2m\pi x}{L + \delta_m} \quad (49)$$

where, 'L' is the width of the transducer region, 'm' is the mode number, a_m and b_m are the normalized mode amplitudes and δ_m is the effective widening of the mode shapes as a result of the Goos Haechen effect [7]. Since, $V(x)$ is the sum of all mode profiles,

$$V(x) = \sum_{m=1}^{\infty} a_m \cos \frac{(2m-1)\pi x}{L + \delta_m} + b_m \sin \frac{2m\pi x}{L + \delta_m} \quad (50)$$

The wave number of the guided wave k , is related to that of the unguided wave number by

$$k^2 = \beta_m^2 + \left(\frac{m\pi}{L + \delta_m} \right)^2 \quad (51)$$

In order to use (51), the effective widening parameter δ_m must be known, which can be determined by

$$\delta_m = \frac{L2\theta_m}{m\pi - 2\theta_m} \quad (52)$$

where
$$\sin(\theta_m) = \frac{m\pi - 2\theta_m}{k(L + \delta_m)\sqrt{1 - v_m^2/v_f^2}} \quad (53)$$

The relation between the wavenumber of the guided wave and the unguided wavenumber becomes

$$\frac{\beta_m^2}{k^2} = 1 - \left[\left(1 - \frac{v_m^2}{v_f^2} \right) \sin^2 \theta_m \right] \quad (54)$$

where v_f and v_m are the velocities in the substrate and the metal respectively and β_m is the modal wavenumber. For a transducer electrode region the wave is slowed down by $\Delta v/v$ because of the perturbations of the wave by the electrodes. It is assumed that this velocity ratio does not change for waves at an incident angle to the electrodes, since the effective metallisation ratio of the

electrodes to free space is constant for all waves propagating at different angles to the electrodes. Equation (50) is used to calculate the normalized mode amplitudes, where the transverse excitation function $V(x)$ is expressed for an active fingerpair as the decomposition into a modified non-orthogonal Fourier series with Fourier coefficients a_m and b_m given by

$$a_m = \frac{1}{L + \delta_m} \left\{ \int_{-L/2}^{L/2} |V(x)| \cos \left[\frac{(2m-1)\pi x}{L + \delta_m} \right] dx \right\} \quad (55)$$

$$b_m = \frac{1}{L + \delta_m} \left\{ \int_{-L/2}^{L/2} |V(x)| \sin \left[\frac{2m\pi x}{L + \delta_m} \right] dx \right\} \quad (56)$$

$|V(x)|$ is the amplitude of the rectangular function. The decomposition into modes uses alternate sine and cosine mode shapes which satisfy the boundary conditions. Therefore the antisymmetric modes will have to be close to zero near the edges of the slow region. In order to calculate the number of modes, the simultaneous equations (52) and (53) have to be solved for δ_m and θ_m as suggested in [14]. Once these parameters are determined, the wave numbers can be determined using (54) and the amplitude profiles can be determined from equations (48) and (49). In order to calculate the number of modes in a device structure, the grating aperture and the ratio of the velocities $\Delta v/v$ should be known. Once the number of modes that the device structure can support is known, the corresponding mode velocities can be calculated to analyze the device structure. Each mode propagates with a different velocity and have different COM parameters. The mode velocity for each mode can be determined by solving for the wavenumber associated with that mode using (54) given the substrate velocity is known.

CASCADING COMPONENTS

In order to analyze SAW resonator filter structures, the basic SAW components will have to be cascaded efficiently by modeling them as 3X3 P-matrices, with the appropriate terms forced to zero for the reflective grating and the delay. The delay represents the distance between the reflective grating and the interdigital transducer. For the simple configuration of cascading two structures, each structure can be considered as a separate three port device having two acoustic ports and one electrical port. When cascaded, the acoustic ports are effectively in series and the electrical ports are in parallel as shown in Figure 17. The P-matrix of the cascaded pair becomes [4]

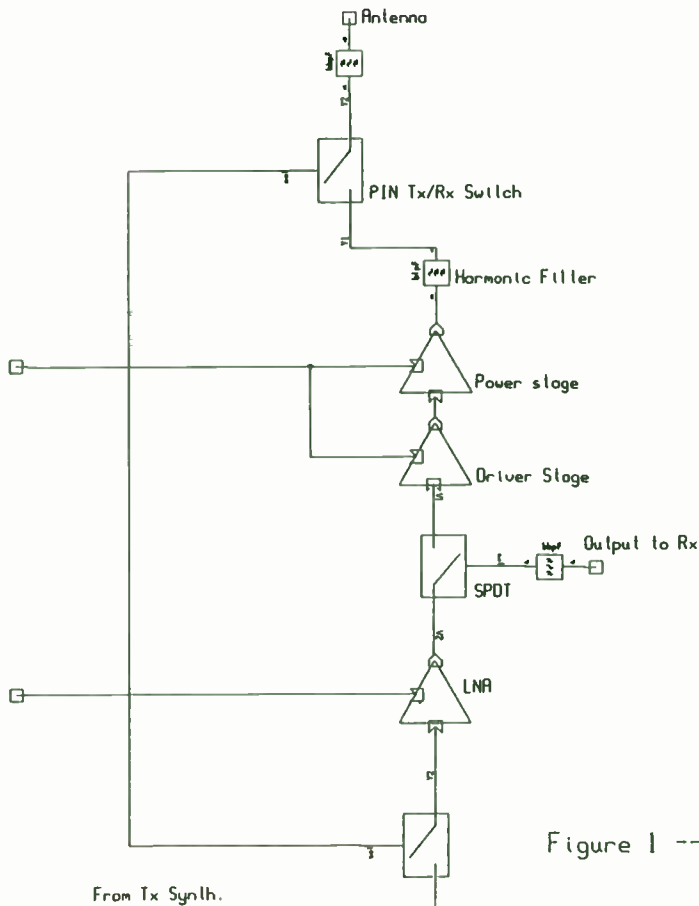


Figure 1 -- Module Architecture

Digital European Cordless Telephone

Typical GaAs Amplifier Performance Specifications Low Noise Amplifier Application

Frequency range:	1880 MHz to 1900 MHz
Gain:	10 dB +/- 1 dB
Noise figure:	< 3 dB
Input two-tone 3rd order intercept point:	> -10 dBm
Quiescent current consumption:	< 10 μ A
Input and output impedances:	50 ohms
Power supply:	Single supply 3.3 to 4.5 volts
Operating temperature range:	-10 $^{\circ}$ C to +50 $^{\circ}$ C
Storage temperature range:	-50 $^{\circ}$ C to +150 $^{\circ}$ C

Compact Software

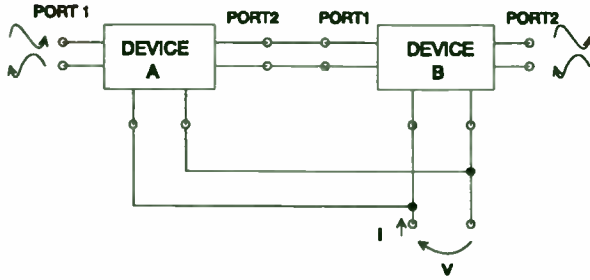


FIGURE 17 : Cascading P matrices

$$P_{11} = P_{11A} + P_{11B} \left[\frac{P_{21A}P_{12A}}{1 - P_{11B}P_{22A}} \right] \quad (57)$$

$$P_{12} = \frac{P_{12A}P_{12B}}{1 - P_{11B}P_{22A}} \quad (58)$$

$$P_{13} = P_{13A} + P_{12A} \left[\frac{P_{13B} + P_{11B}P_{23A}}{1 - P_{11B}P_{22A}} \right] \quad (59)$$

$$P_{22} = P_{22B} + P_{22A} \left[\frac{P_{12B}P_{21B}}{1 - P_{11B}P_{22A}} \right] \quad (60)$$

$$P_{23} = P_{23B} + P_{21B} \left[\frac{P_{23A} + P_{22A}P_{13B}}{1 - P_{11B}P_{22A}} \right] \quad (61)$$

$$P_{33} = P_{33A} + P_{33B} + P_{32A} \left[\frac{P_{13B} + P_{11B}P_{23A}}{1 - P_{11B}P_{22A}} \right] + P_{31B} \left[\frac{P_{23A} + P_{22A}P_{13B}}{1 - P_{22A}P_{11B}} \right] \quad (62)$$

The above technique is used to cascade first the left most grating to the delay of the resonator in Figure 1. The equivalent P matrix is then cascaded with the IDT P-matrix, and so on, until a single equivalent P matrix is obtained for the device. A proximity resonator is analyzed by cascading the SAW components the same way. For the two port resonators shown in Figure 2, the IDT's acoustic ports are in series through a delay representing the distance between the transducers, but their electrical ports are not connected at all. If the outer acoustical port of each IDT is terminated in its characteristic impedance, the device can be reduced to an equivalent two port, with the IDT electrical ports being the ports of interest. The effects of the grating with the associated delay is accounted for by cascading each IDT to its grating as in the case for a one port resonator. The two equivalent P-matrices are converted to an equivalent two port admittance matrix which are then converted to the corresponding S-parameters [15].

$$S_{11} = \frac{(1 - Z_1^* Y_{11})(1 + Z_2 Y_{22}) + Y_{12} Y_{21} Z_2^* Z_2}{(1 + Z_1 Y_{11})(1 + Z_2 Y_{22}) - Y_{12} Y_{21} Z_1 Z_2} \quad (63)$$

$$S_{12} = \frac{-2\sqrt{R_1 R_2} Y_{12}}{(1 + Z_1 Y_{11})(1 + Z_2 Y_{22}) - Y_{12} Y_{21} Z_1 Z_2} \quad (64)$$

$$S_{21} = \frac{-2\sqrt{R_1 R_2} Y_{21}}{(1 + Z_1 Y_{11})(1 + Z_2 Y_{22}) - Y_{12} Y_{21} Z_1 Z_2} \quad (65)$$

$$S_{22} = \frac{(1 - Z_2^* Y_{22})(1 + Z_1 Y_{11}) + Y_{12} Y_{21} Z_1 Z_1^*}{(1 + Z_1 Y_{11})(1 + Z_2 Y_{22}) - Y_{12} Y_{21} Z_1 Z_2} \quad (66)$$

EQUIVALENT CIRCUIT REPRESENTATION

The proximity device structure can be represented by an equivalent circuit keeping in mind that the key element is the admittance parameter at the electrical port. Figure 18 shows the equivalent circuit for a device supporting two modes.

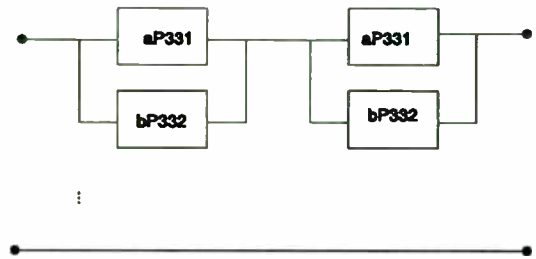


FIGURE 18 : Equivalent Circuit for a 2 mode device structure

The coefficients 'a' and 'b' represent the couplin between the modes and 'P331' and 'P332' represent the admittance's for the first mode and the second mode respectively. Figure 19 shows the equivalent circuit for a structure propagating N modes. The equivalent circuit

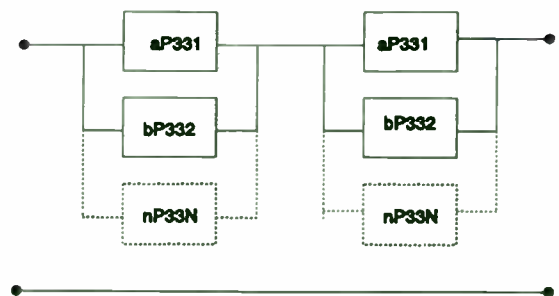


FIGURE 19 : Equivalent Circuit for a 2 mode device structure

Digital European Cordless Telephone Power Amplifier Application

Frequency range:	1880 MHz to 1900 MHz
Gain:	37 dB max.
Output power:	26 dBm max.
Quiescent current consumption:	< 10 μ A
Quiescent forward gain:	< -50 dB
Input and output impedances:	50 ohms
Power supply:	Single supply 3.3 to 4.5 volts
Operating temperature range:	-10 $^{\circ}$ C to +50 $^{\circ}$ C
Storage temperature range:	-50 $^{\circ}$ C to +150 $^{\circ}$ C

An input port is provided to allow the power amplifier to be turned completely off by a standard TTL logic level. The turn-off time must be less than 2 msec and the current consumption must be less than 10 μ A in this quiescent state. A logic input is also required to provide a ramp up/down within 6 to 8 milliseconds of a 20 dB gain increase/decrease.

Compact Software

**GaAs MMIC LNA/ Driver/Power Amplifier
and Switches**

for structures propagating various modes can be represented as a two port admittance parameter network as shown in Figure 20, from which the S-parameters for the proximity device structure of interest can be computed.

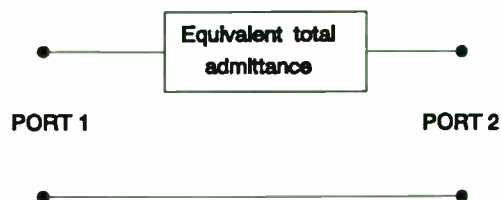


FIGURE 20 : Equivalent Circuit

The two port equivalent network can be shown as a circuit excited by a source and terminated at a normalizing impedance Z_o , as shown in Figure 21.

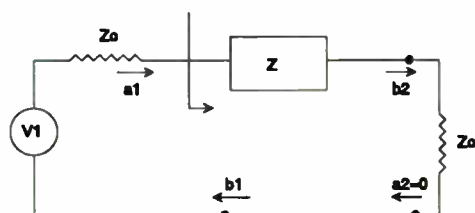


FIGURE 21 : two port network for s-parameter determination

From Figure 21, the S-parameters for the network are determined to be [16]

$$S_{11} = \frac{Z}{Z + 2Z_o} \tag{67}$$

$$S_{21} = \frac{2Z_o}{Z + 2Z_o} \tag{68}$$

Knowing the admittance's of the various modes and the coupling associated with them, the S-parameters for the device can be calculated.

COMPUTER MODEL

A computer program using the C programming language is written to implement the coupling of modes analysis technique. The program is capable of modeling the basic SAW components, the reflective grating and

the interdigital transducer which are essential to model SAW resonator filters. The package "RESCAD" developed at the University of Central Florida is also capable of modeling some resonator structures like the one port resonators, the inline two port resonator structures and a two port SAW guided mode resonator filter. The "RESCAD" architecture is shown in Figure 22. The model sets an upper bound of 10000 data points

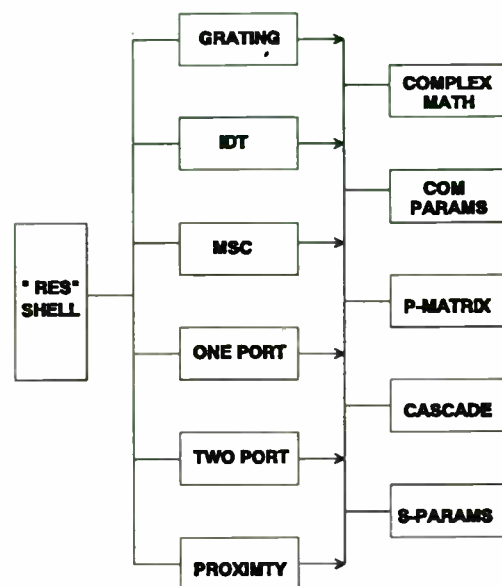


FIGURE 22 : "RESCAD" architecture

for the user specified frequency range. After choosing the structure of analysis, the user is prompted to open a file to store the output data, the geometry of the device and the analysis range. The output of RESCAD, the S-parameter data of the chosen structure. In addition, in order to model proximity resonators, the program takes into account the number of modes the device is capable of supporting, the corresponding mode velocities and the mode coupling coefficients. For each mode, the program cascades the P-matrices of the SAW components including the delay and finally calculates the S-parameters of the overall device structure from the admittance parameters of the various modes. The S-parameter output file can then be easily imported onto a commercially available spreadsheet for plotting.

EXAMPLE

To check the validity of the computer model "RESCAD" written to implement the coupling of modes solutions, a sample example with certain assumed device specifications listed in the following table is executed.

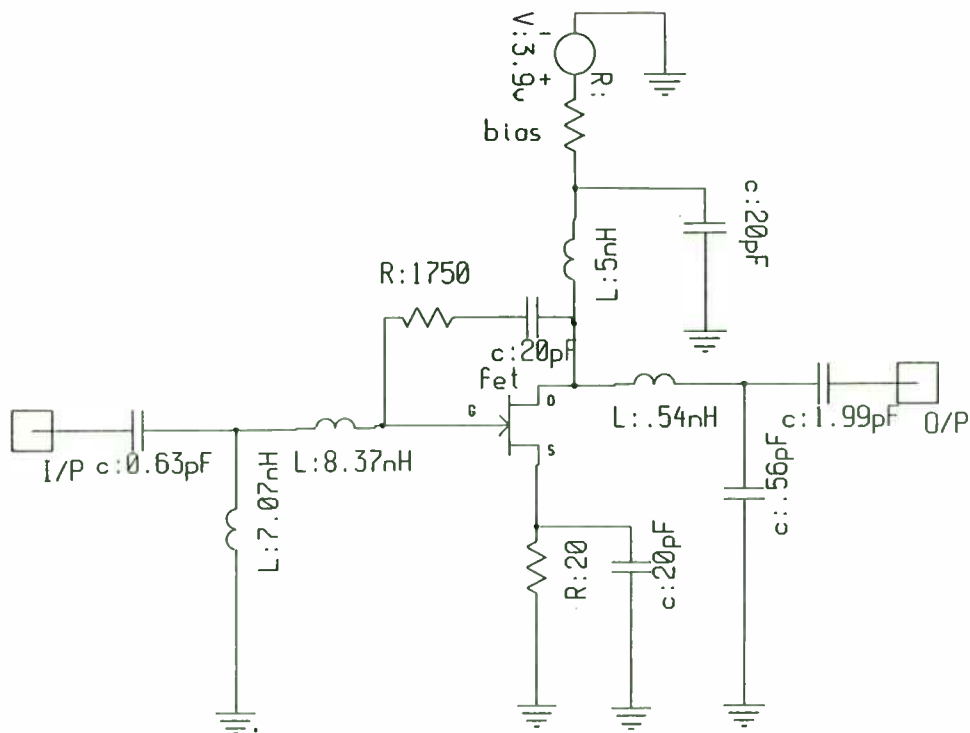


Figure 14 -- Self-Biased Driver Amplifier Stage

21-OCT-92

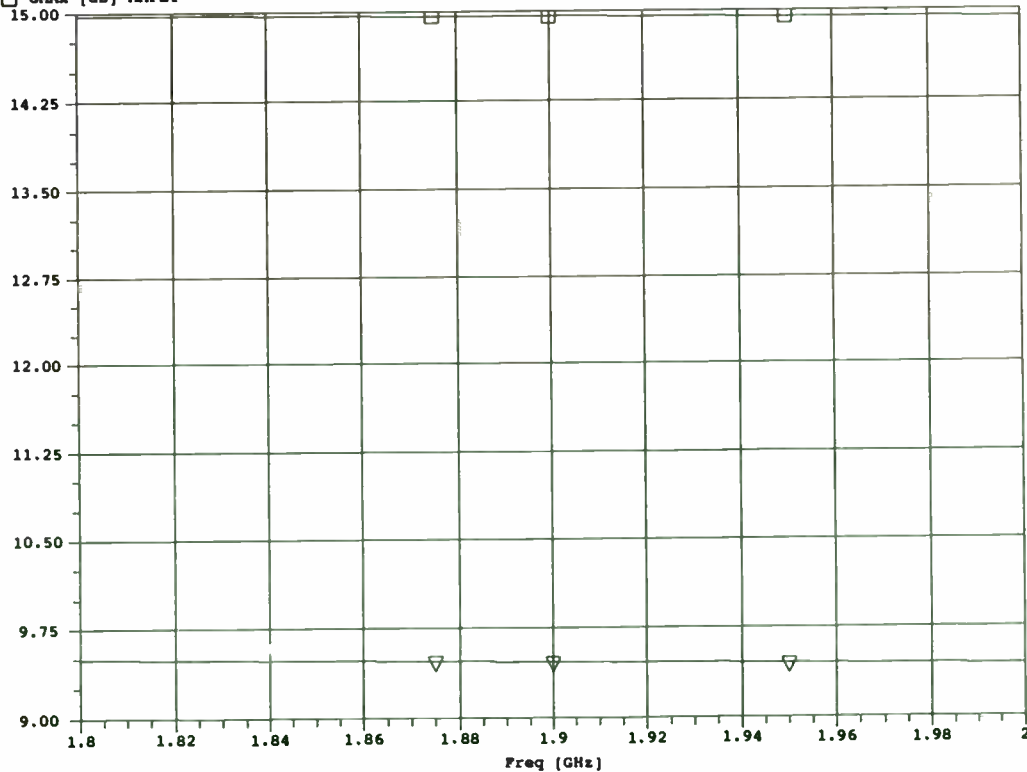
MICROWAVE HARMONICA PC V5.1

17:35:32

File: dect10.ckt

MS21 and MAG of MMC-05 (400um) FET @ 50% Idss with 1500 ohms feedback resistor

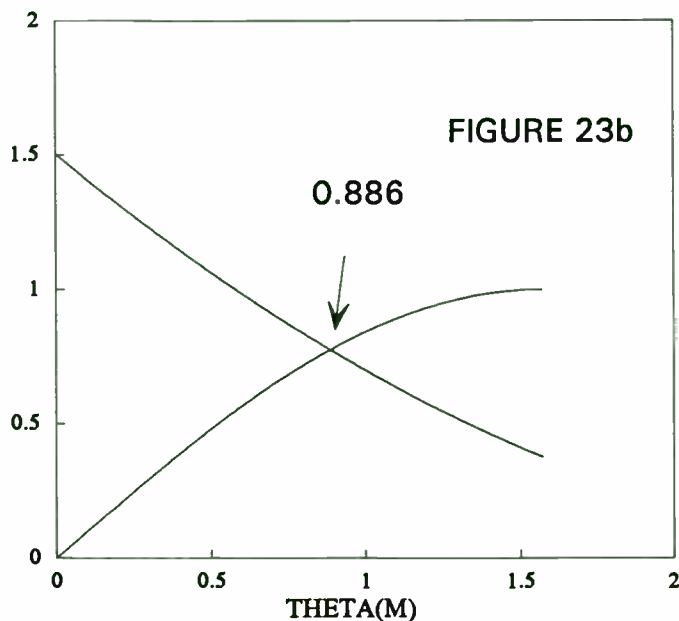
MS21 [dB] MMFET
 GHAX [dB] MMFET



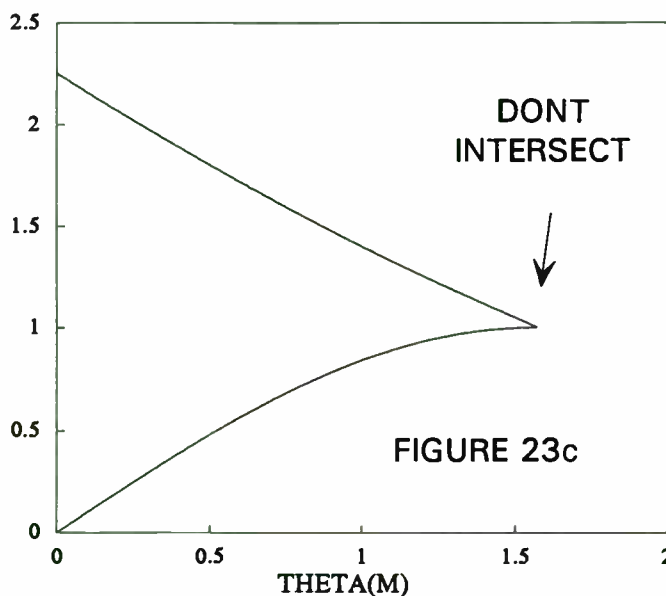
Number of grating strips	650
Number of IDT fingers	45
period of the grating	10.5um
period of the IDT	10.5um
Center Frequency	150MHz
Metal Thickness	1800A
Width of the Grating	405um
Resistivity	0.2
Substrate Assumed	Quartz
Velocity	3157m/s
Delay	13.125um
Width of the electrodes	5.25um

In order to calculate the number of transverse guided modes in the device structure equation (53) has to be solved. One way of solving this is by plotting both the sides of equation (53) from which the number of modes can be determined as shown in Figure 23. Figure 23 shows that there are just two transverse guided modes possible in this proximity device structure.

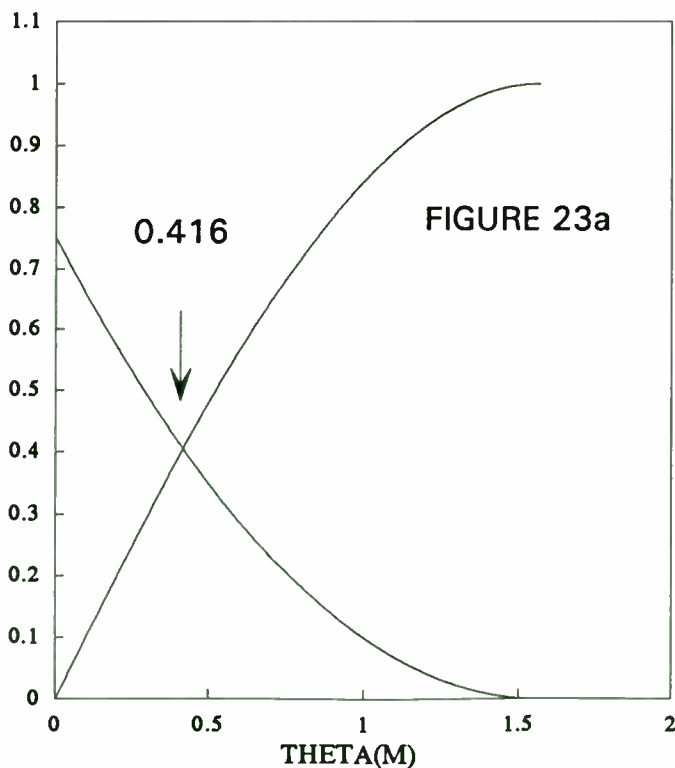
OCCURRENCE OF MODE 2



MODE 3



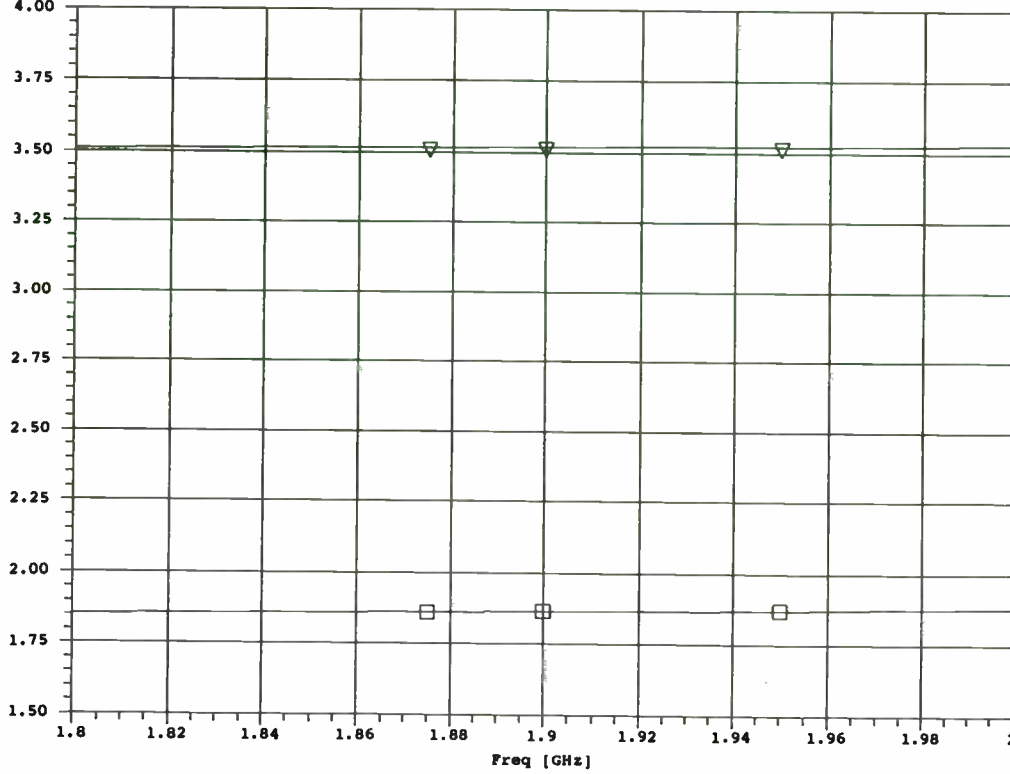
OCCURRENCE OF MODE 1



Once θ_m is known, the wavenumber of the guided modes can be determined from (54). The velocities of the two modes can then be determined knowing the substrate free surface velocity. In addition, the mode coupling coefficients can also be determined using (55) and (56). The mode velocities are found to be 3157.3m/s and 3158.13m/s for the first and second modes respectively. The responses for the various structures are given below in Figure 24.

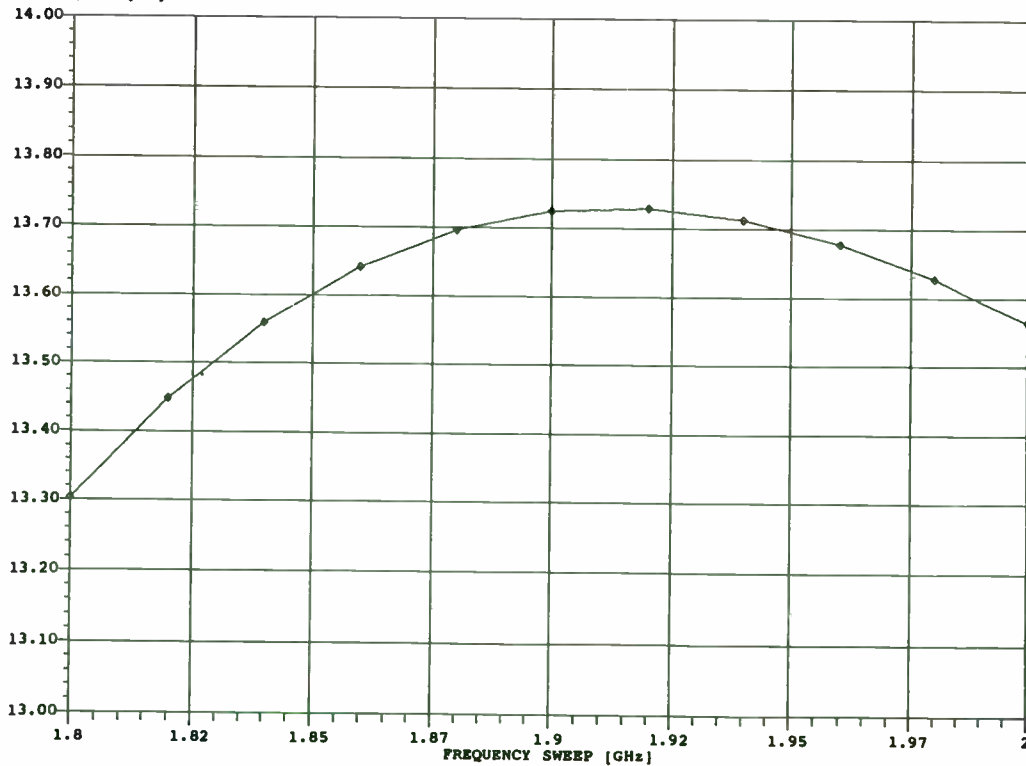
File: dect10.ckt
50 ohm an Minimum Noise Figure of MMC-05 (400um) FET (feedback stabilization)

▽ NF [dB] MMFET
□ FMIN [dB] MMFET

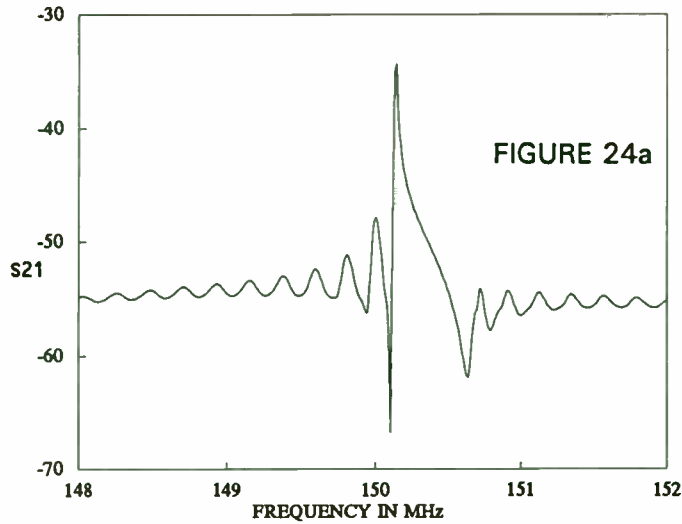


File: DECT17.CKT
Gain of Low-Noise Amplifier versus Freq. @ Pin = -10 dBm
SWEEP OF NETWORK FUNCTION TG21<H1,H1> [dB]

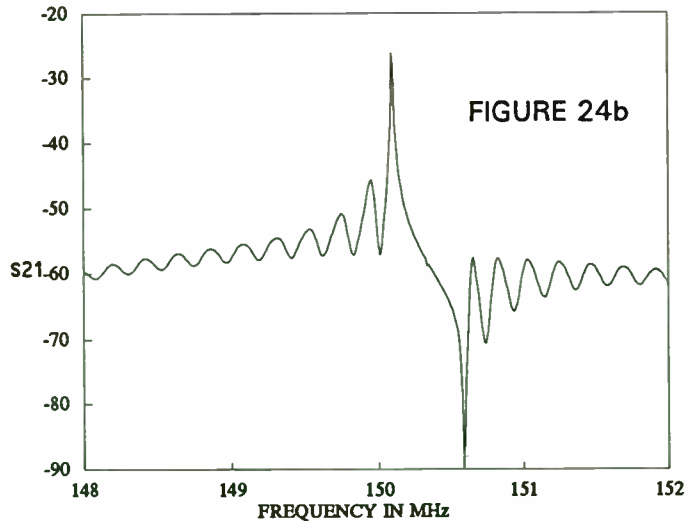
◇ TG21<H1,H1> [dB]



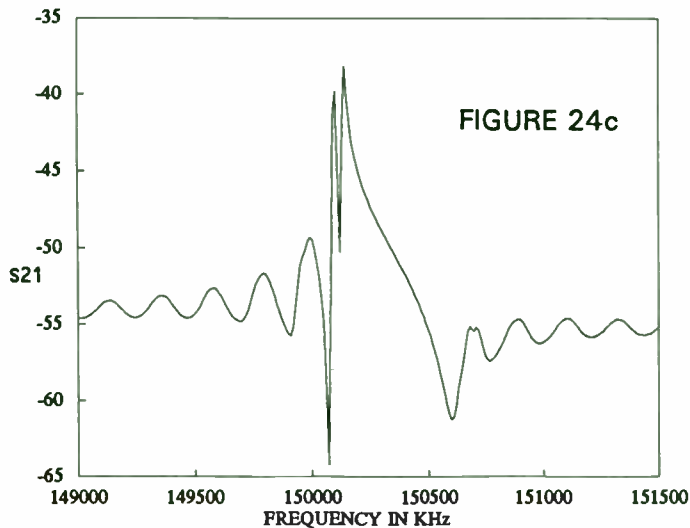
ONE PORT DEVICE



TWO PORT DEVICE



PROXIMITY DEVICE



[1] P.V.Wright "A review of SAW resonator filter technology" 1992 IEEE Ultrason. Symp. Proc.

[2] H.F.Tiersten and R.C.Smythe, " Guided Acoustic surface wave filters", 1975 IEEE Ultrason. Symp. Proc., pp 293-294.

[3] W.R.Smith et al., "Analysis of interdigital transducers by use of an equivalent circuit model", 1979 IEEE Trans.

[4] C.S.Hartmann and B.P.Abbott, " Generalised impulse response model for SAW transducers including effects of electrode reflections", 1988 IEEE Ultrason. Symp. Proc., pp40 - 45.

[5] W.R.Mader, H.R.Stocker, "Extended impulse model for the design of precise SAW filters on quartz", 1982 IEEE Ultrason. Symp. Proc. pp 29-36.

[6] H.A.Haus and P.V.Wright, " Analysis of grating structures by Coupled mode theory", 1980 IEEE Ultrason. Symp. Proc.

[7] N.S.Kappany and J.J.Burke, " Optical waveguides ", Academic Press 1972, pp 74-80.

[8] C.Elachi, "Waves in active and passive periodic structures: A review", Proceedings of the IEEE, Dec 1976.

[9] T.Thorvaldsson, "Analysis of SAW resonators".

[10] B.P.Abbott, " Coupling of modes model for SAW transducers with arbitrary reflectivity weighting", Ph.D. dissertation, University of Central Florida 1989.

[11] D.P.Morgan, "Surface acoustic wave devices for signal processing".

[12] Engan.H., "Excitation of elastic surface waves by spatial harmonics of interdigital transducers", 1969 IEEE Trans on Electron Devices. pp 1014-10

[13] S.Jungling, " The impulse model including waveguiding effects using modal analysis" 1991 IEEE Ultrason. Symp. Proc.

[14] S.Datta, "surface acoustic wave devices", 1986 Prentice Hall, Englewood Cliffs.

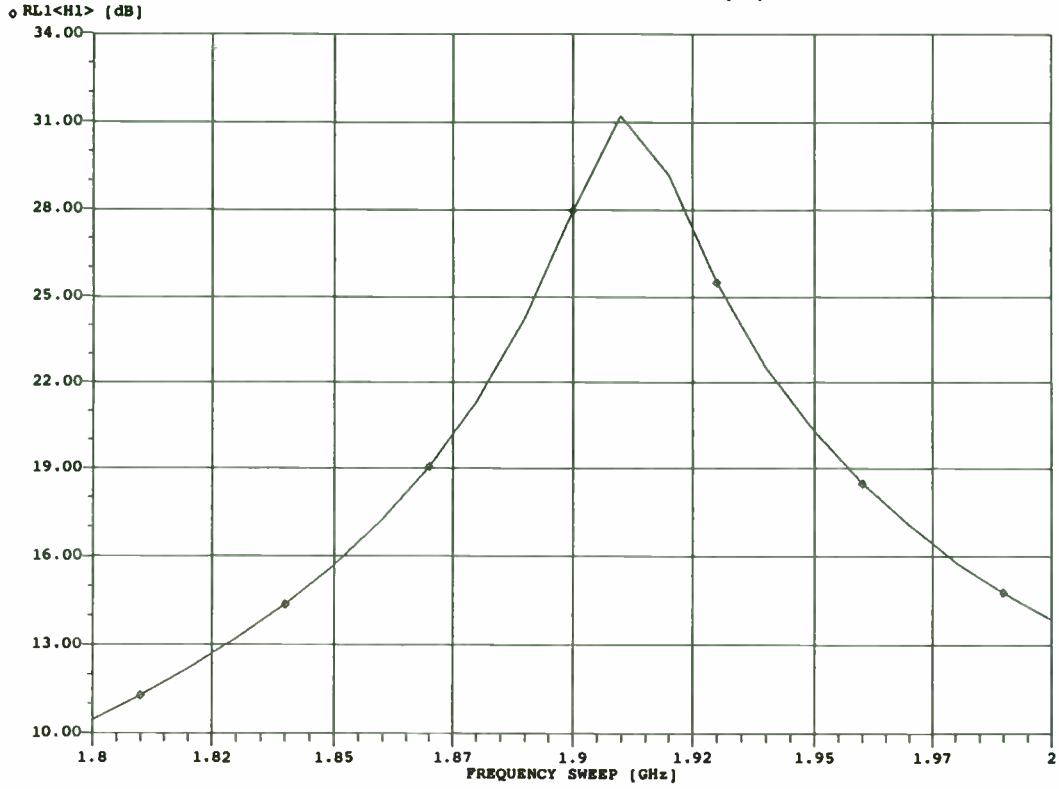
[15] Pozar David .M., "Microwave Engineering" Reading, Mass.: Addison-Wesley, 1990

[16] G.Gonzalez, " Microwave transistor amplifiers, design and analysis", 1984 Prentice Hall, Englewood Cliffs

[17] Robert P.Burke, " A coupling of modes analysis of SAW resonators", University of Central Florida.

[18] M.Tanaka, T.Moriata et al, " Narrow bandpass filter using double mode SAW resonators on Quartz" , IEEE 38th Annual Frequency Control Symposium, 1984.

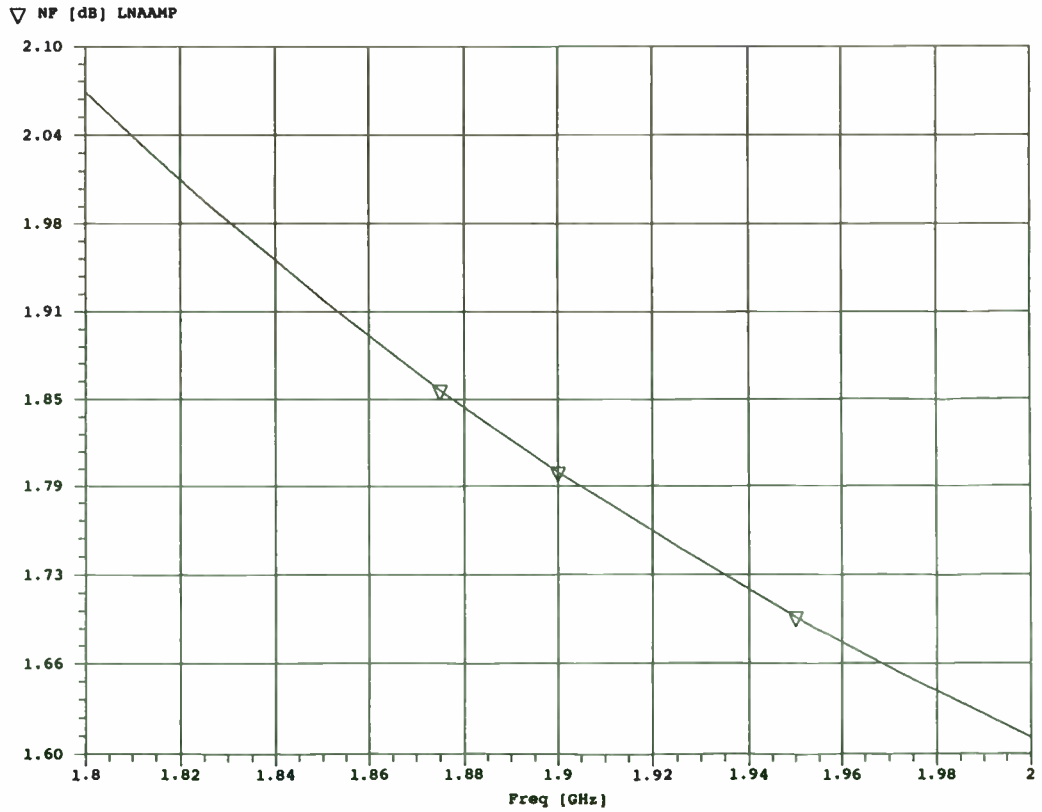
MICROWAVE HARMONICA PC V5.1
 File: DECT17.CKT
 I/P Return Loss of Low-Noise Amp. versus freq. at Pin=-10dBm
 SWEEP OF NETWORK FUNCTION RL1<H1> [dB]



21-OCT-92

MICROWAVE HARMONICA PC V5.1
 File: dect13
 Noise Figure of Low-Noise Amplifier

18:04:25



Designing Microwave Circuits for Geosynchronous Space Applications

Ronald Ogan
TRAK Microwave Corporation
4726 Eisenhower Blvd.
Tampa, Florida 33634

INTRODUCTION

Today's world is a blur of information, some of which is transmitted via microwaves to and from earth stations through satellite electronics systems. Most communication satellites are placed in geostationary orbits, which have a radius of 35,880 km (22,300 miles) in the equatorial plane with a period equal to the rotation of the earth about the poles. A satellite in a geosynchronous orbit appears stationary over one point on the equator. After launch via rocket or Space Shuttle, the satellite is relocated from a low parking orbit into the final orbit by a maneuver called a Hohmann transfer. Thrusters provide 3-axis stabilization over the projected operating life of 10 years or longer (for INTELSAT series). Telemetry and Command/Control beacons provide attitude and data required to efficiently manage the satellite from earth stations. INTELSAT-6, by using advanced digital and modulation techniques can carry 120,000 telephone circuits and 3 television channels. The satellite uses TDMA (Time Division Multiple Access) technique to transmit in the 6-4 GHz (C-Band) and 14-12 GHz (Ku-Band) frequencies.

TECHNICAL OBJECTIVES

Designing microwave circuits for the geosynchronous space application requires pushing the envelope of device and assembly knowledge to the limits. Since the reliability of the design is paramount, the major aspects of the design are carefully analyzed: device selection, materials selection, assembly processes and compliance testing. These areas will be discussed in the sections to follow.

SPACE ENVIRONMENT

Space is a harsh mistress which includes radiation hazards, materials outgassing, and the severe limitation that electronics must function flawlessly for 10 or more years without repair. Also, another prerequisite to operating in a stable orbit in space is the survival of launch vibrations. Temperature variations are typically controlled

by the satellite rotation from -25 C to +65 C. Exposure of the electronic circuits to temperature variations and radiation depends upon the location on the spacecraft platform. Microwave beacons which are mounted on the external sections are subjected to the environmental extremes.

DEVICE SELECTION/ QUALIFICATION

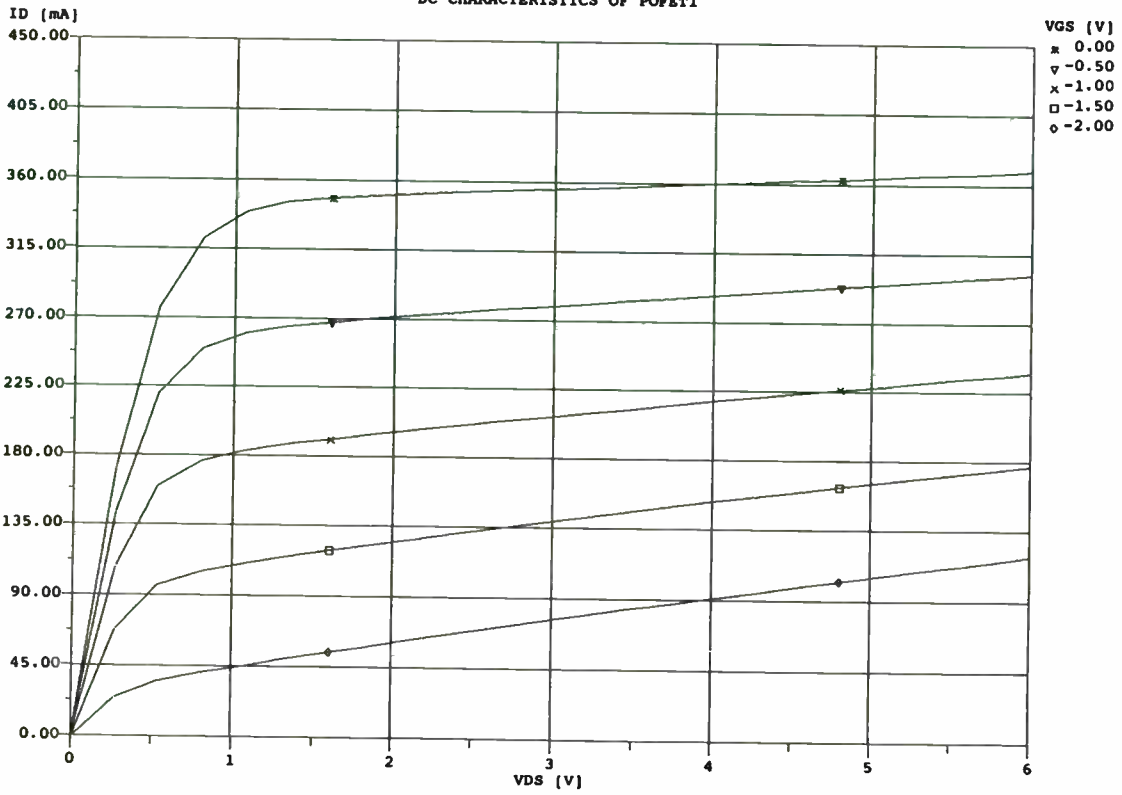
Active and passive components are selected to the maximum extent possible from established reliability devices as listed in MIL-STD-975. However, few microwave components appear in the military standard so the next choice is to find devices with space heritage. Semiconductor vendors such as NEC, Motorola, and National Semiconductor have listings of space programs on which their devices have been flown. The device selection process proceeds interactively through the initial design process. The initial target device specifications are defined in the initial design and changes are made as required based upon a combination of the worst case circuit analysis and the breadboard testing of the circuits.

Devices are qualified for use on flight circuits by passing Environmental Stress Screening (depending upon the starting reliability of the devices: "R" .1% failure rate, or "S" .01% failure rate) and a Destructive Part Analysis (such as per MIL-STD-1580). Other inspection criteria may be imposed depending upon the specific program requirements such as Scanning Electron Microscope, SEM, examination of the device wafer, Particle Impact Noise Detection, PIND, of the packaged devices, and radiography of each packaged device. Additional lot sample tests may be required such as destructive testing of lead strength and lead solderability.

DESIGN CRITERIA

Designing microwave circuits to meet stringent End-of-Life Tolerances requires determination of the circuit variables, their effect on the circuit output parameters and the

MICROWAVE HARMONICA PC V5.1
 File: DECT01.CKT
 I-V CHARACTERISTICS OF MMC-05 PROCESS POWER FET (1200um)
 DC CHARACTERISTICS OF POFET1

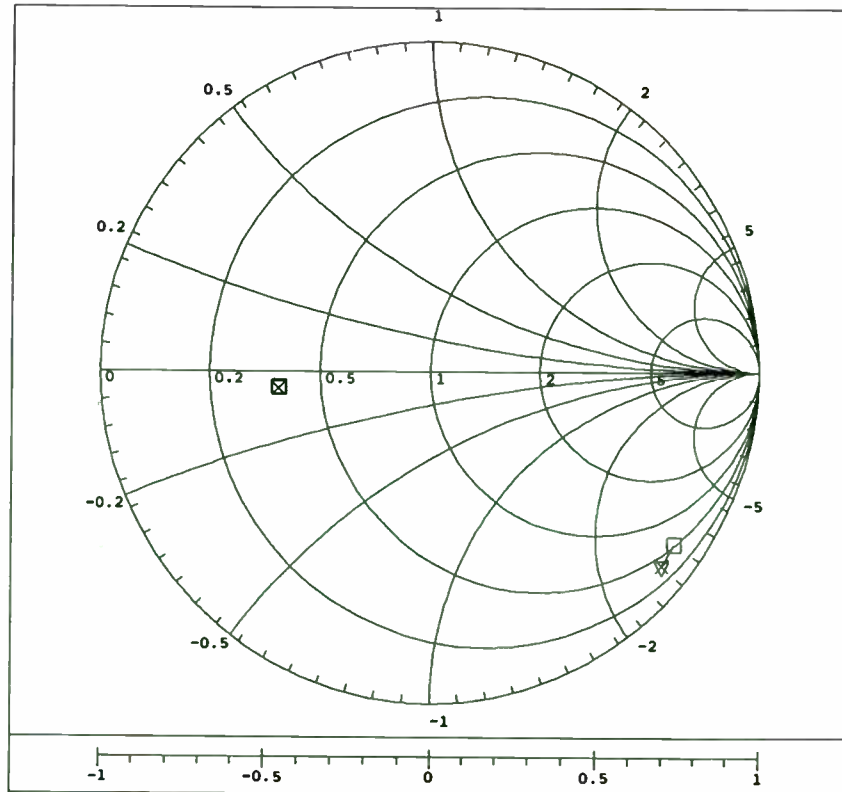


21-OCT-92

MICROWAVE HARMONICA PC V5.1
 File: dect02.ckt
 S11 and S22 of MMC-05 FET @ Vdd=3.9volts Vgs=-1volt; RF I/P power = 10dBm

16:57:38

□ S11 MMFET
 x S22 MMFET



□ 1.800 GHz
 x 2.000 GHz

predicted aging variations over the environmental conditions. For oscillator circuits, the worst case analysis can be divided into the following sections: Frequency Stability, Amplitude Stability, Spurious frequencies, radiation effects and EMI/EMC effects. The circuit configuration which will be discussed is shown in Figure 1 and is typical of microwave circuits used in satellites for command receivers and telemetry beacons.

For oscillator circuits, the components which can directly affect the frequency are usually limited to the first three stages of the chain. Amplifier and multiplier stages which follow can affect the amplitude but cannot affect the oscillator frequency. In designing long life (10 year life), microwave circuits, strict derating guidelines must be met such as limiting the transistor power dissipation to 20% of the manufacturer's rating. When the impedance match between stages is tuned during the initial alignment process, amplitude peaking occurs. Worst case circuit analysis must be performed to establish limits for the transistor bias currents, capacitor, and inductor values as required for achieving the specific RF output limits. Figure 2 shows a non-linear simulation using EESOF™ Libra™ for Windows for a X3 multiplier with +13 dBm input at 452 MHz. Note that the 3rd harmonic is approximately at 0 dBm and the 2nd harmonic is at -2 dBm, 904 MHz. Figure 3 shows the variation of the first and second harmonic for the output amplifier with different RF input levels. Bandpass filters are used to reject the unwanted harmonics and spurious signals which result from the multiplication process.

EOL changes must be calculated for each component parameter to determine the effect upon the circuits critical parameters such as frequency stability, RF power stability and minimal spurious at the output port. EOL drift characteristics are often stated as guidelines by the program. Device manufacturer's collect and report aging data that is taken during qualification tests to the National Aeronautics and Space Administration, NASA in addition to reporting to other government agencies. Component changes over life effectively detune the resonant and impedance matching circuits which degrades the output waveform. Aging effects on the bandpass filters which are used to reject spurious frequencies result in broader skirts with higher insertion losses. As the inductors and capacitors age as a result of time and exposure to the space environment, the transfer characteristics are shifted and flattened (Q of the filters is reduced). The total parameter variation, P_{EOL} is determined:

$$P_{EOL} = P_o + \Delta P_m + \Delta R$$

where:

P_o = the initial Beginning-of-Life tolerance

ΔP_m = the calculated parameter change based on mission life and operating temperature

ΔR = the effects of radiation upon the device parameter.

Figure 4 shows a typical transistor multiplier configuration. Using Libra™, a sensitivity may be performed manually or by Monte Carlo simulation to determine how variations of each component within the tolerance range can effect the harmonic power levels. The multiplier circuits are biased class B to allow them to turn on with the application of the input RF signal. The Libra™ simulator performs reasonably well against measured data but caution must be exercised when the multiplier output power increases directly as a function of the DC bias condition.

Crystal oscillators have aging characteristics that are set by the stability of the crystal. Recent advances in SC-cut crystals have resulted in frequency variations < .5 ppm per year for 100 MHz, fifth overtone crystals. The factors affecting frequency stability are as shown:

Initial set accuracy (may be adjusted out)	± 1.0 ppm
Aging over 10 years in space	± 5.0
Temperature variations	± .5 ppm
Power Supply variation	± .1 ppm
Shock/vibration	± .1 ppm
Radiation exposure	± .1 ppm
TOTAL	± 6.8 ppm

The initial set accuracy may be eliminated during the alignment tuning process by pulling the crystal on frequency using the circuit resonant components. However, SC-cut crystals, because of their excellent long term aging characteristics, have a limited pulling range. Preconditioning of the crystal and monitoring of the aging trends is very important to insure long term stability. Initially, the crystal frequency rate of change is rapid until a stable plateau is reached.

CONCLUSION

Microwave circuits have been used in low altitude space programs such as the weather satellites for over 30 years beginning with TIROS-1 in 1960. Circuit complexity has increased steadily and now includes many requirements for telecommunication satellites in geosynchronous orbits.

21-OCT-92

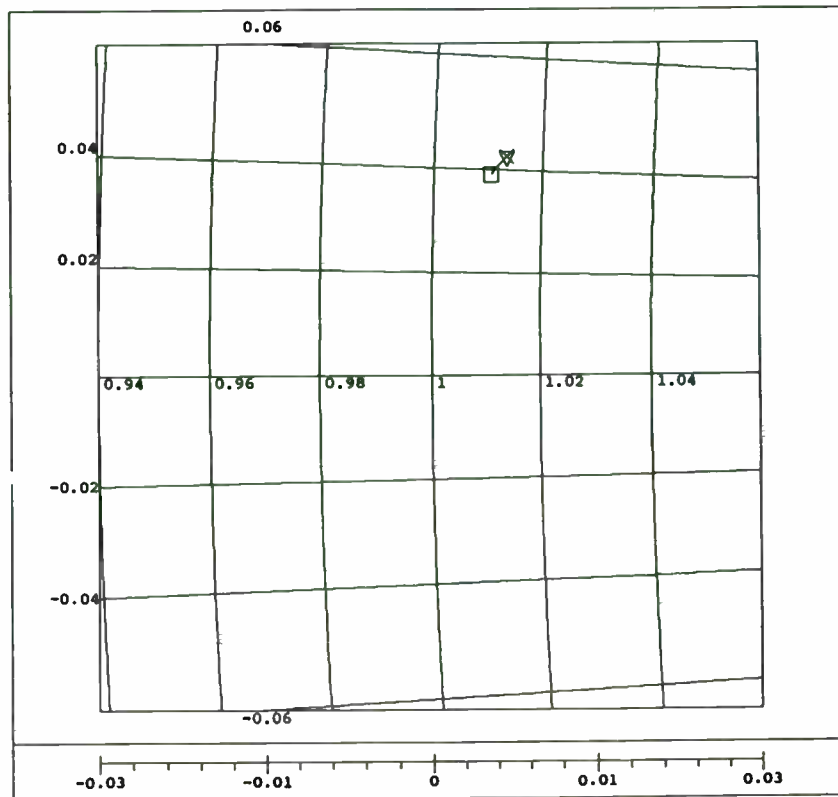
MICROWAVE HARMONICA PC V5.1

16:56:21

File: dect02.ckt

S12 of MMC-05 FET @ Vdd=3.9volts Vgs=-1volt; RF I/P power = 10dBm

▽ S12 MMFET



□ 1.800 GHz
 × 2.000 GHz

21-OCT-92

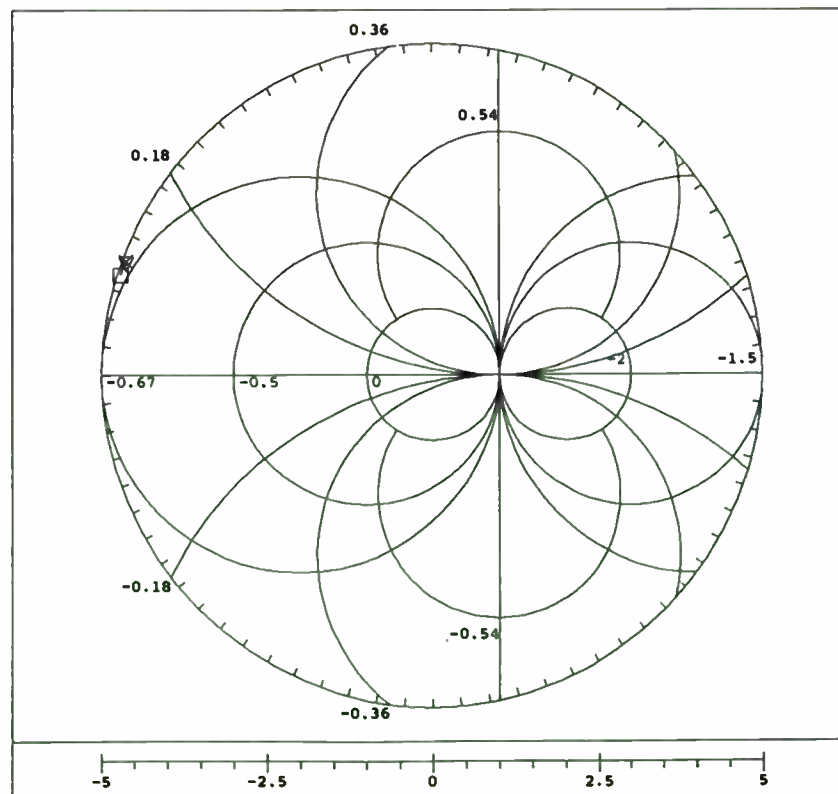
MICROWAVE HARMONICA PC V5.1

16:58:51

File: dect02.ckt

S21 of MMC-05 FET @ Vdd=3.9volts Vgs=-1volt; RF I/P power = 10dBm

▽ S21 MMFET



□ 1.800 GHz
 × 2.000 GHz

Time Division Multiple Access technology has driven the need for more accurate clock oscillators to control the frequency channels. The future for geosynchronous applications such as Global Positioning Systems is a bright rising star in today's relatively flat technological landscape.

Non-linear circuit analysis tools such as EESOF™, Libra™ provide insight into how the circuits can be analyzed and improved to meet the stability demands. Device, materials, and assembly processes are improving reliability for missions that are now approaching 20 years in length. Long life programs require methodical approaches to device and material selection with the emphasis on reliability and design margins. Device environmental screening and strict operational derating further enhance the mission performance.

[Figure 1 appears on the following page. Ed.]

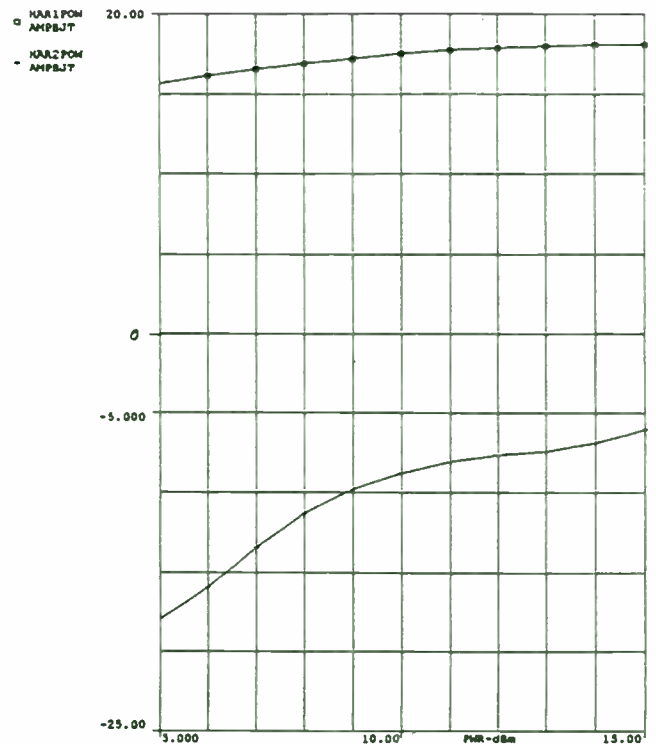


Figure 3: Output Amplifier First and Second Harmonics with varying inputs

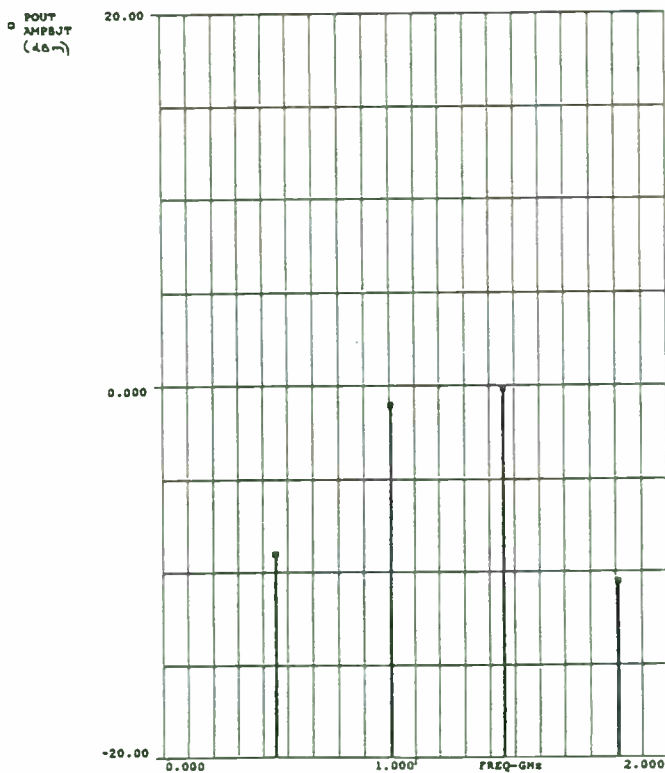


Figure 2: Non-linear Libra™ plot of X3 multiplier

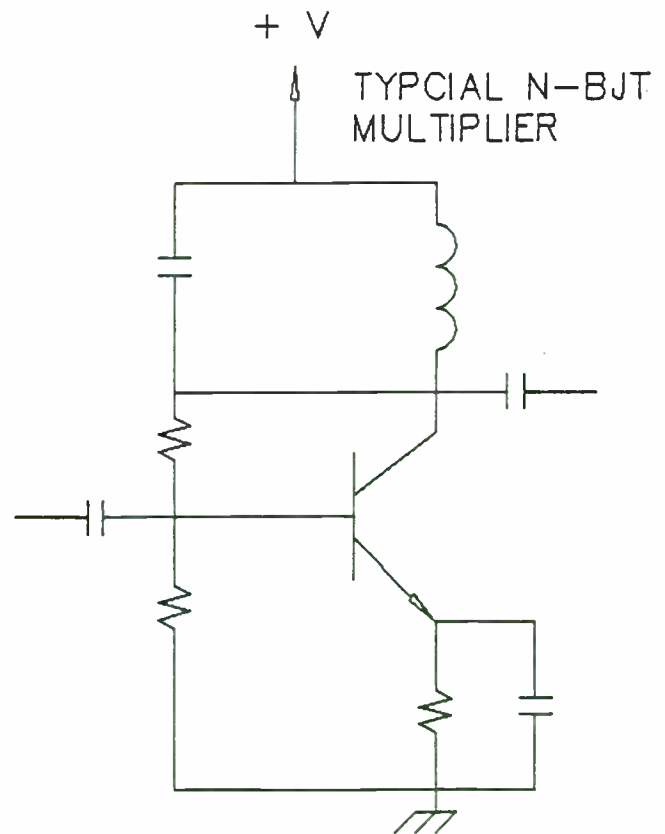


Figure 4: Typical Multiplier Stage

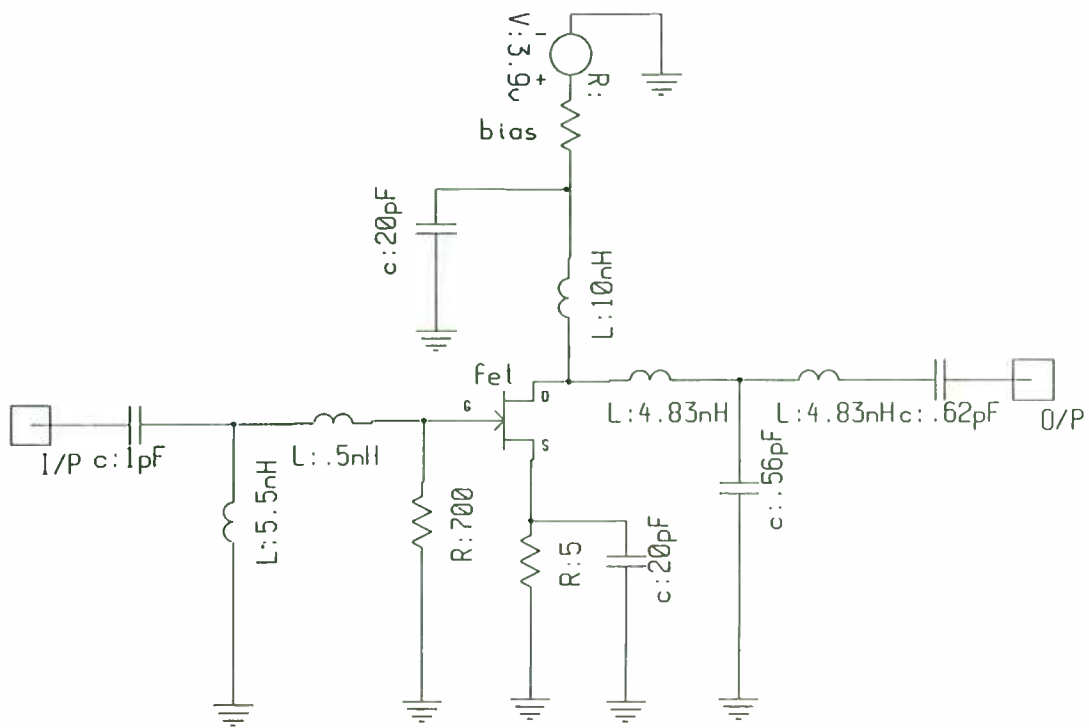
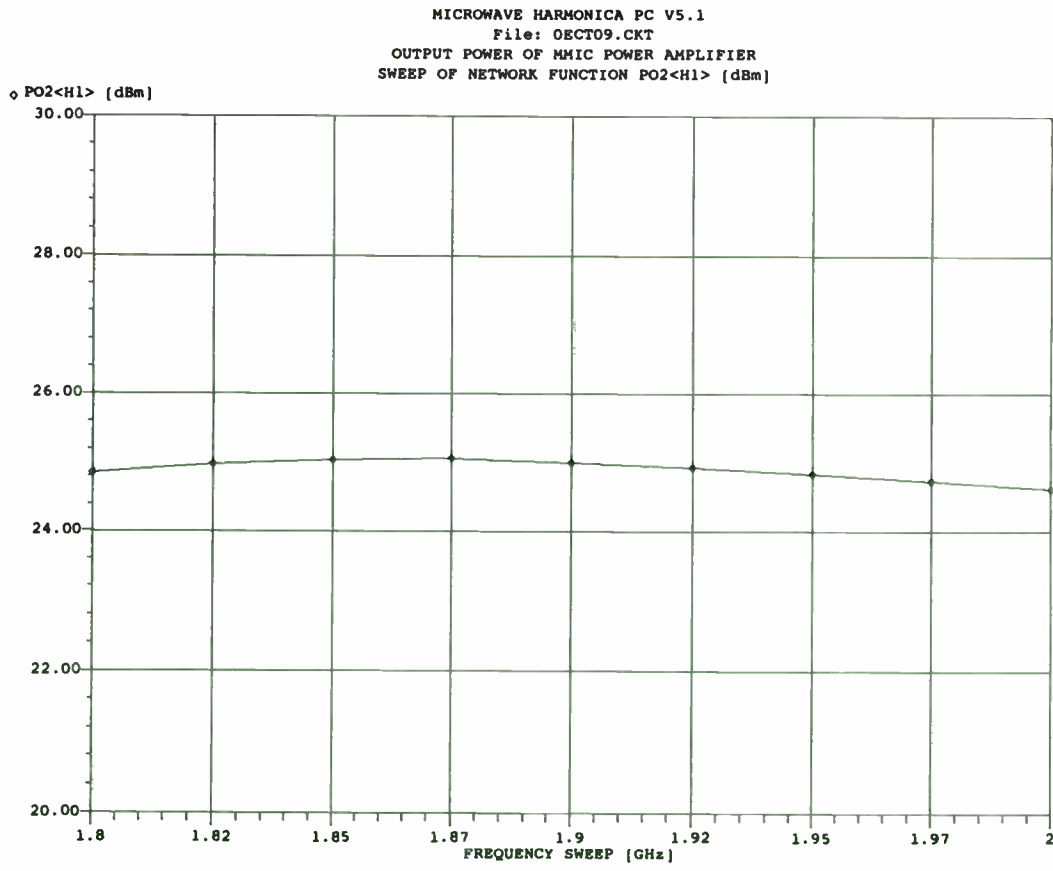


Figure 4 -- Self-Biased Power Amplifier Stage



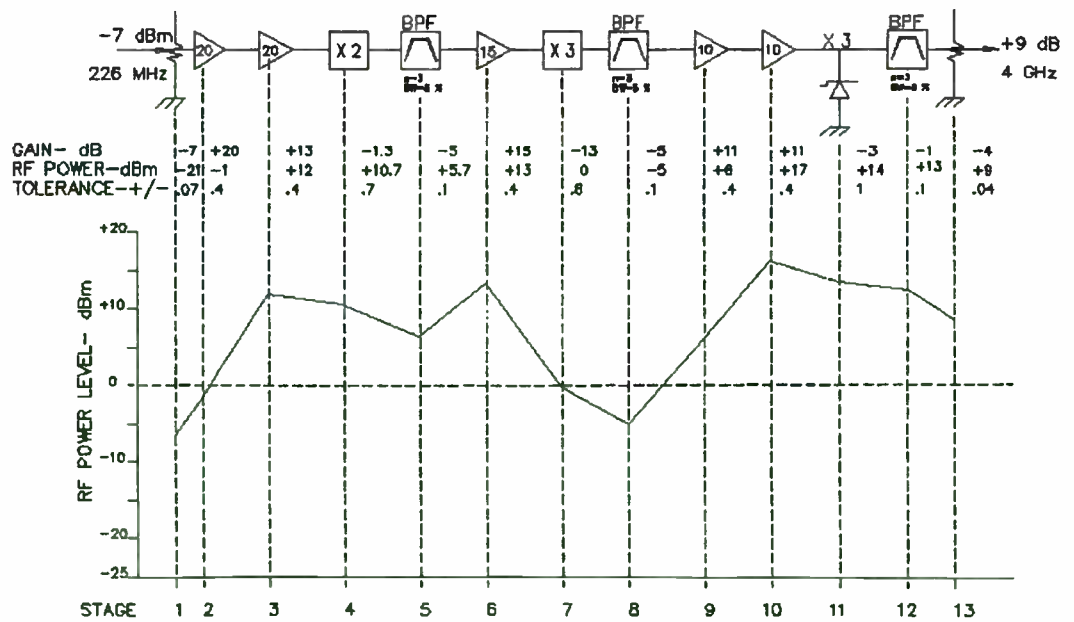
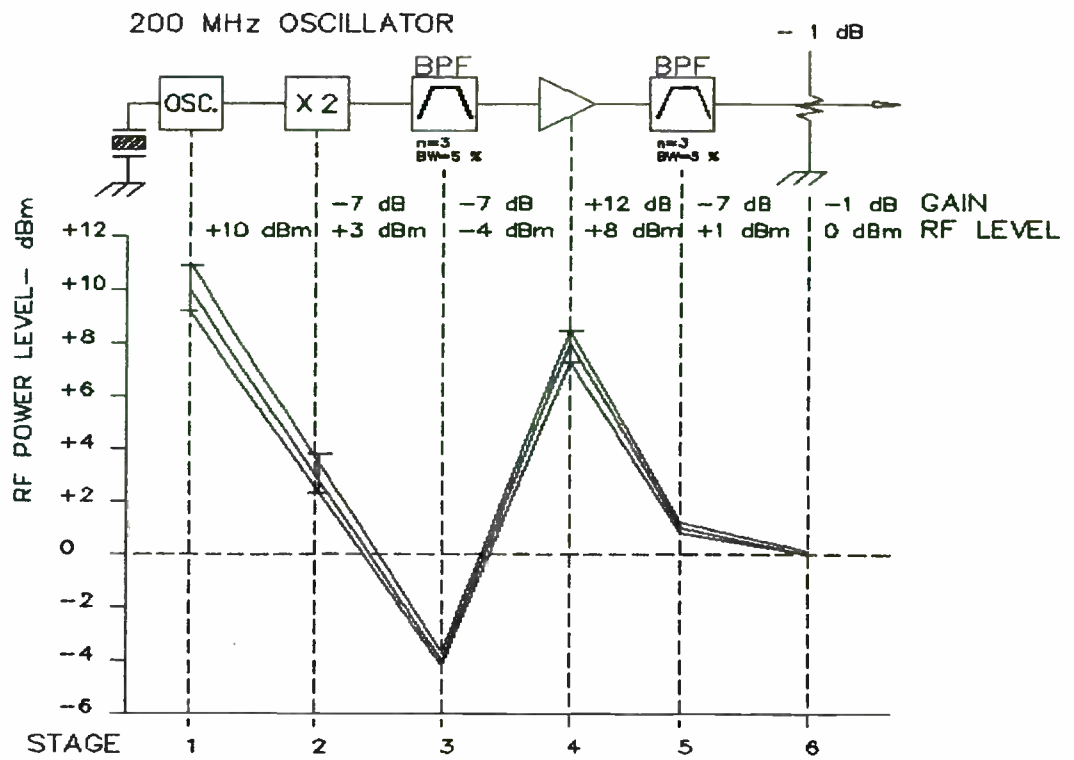
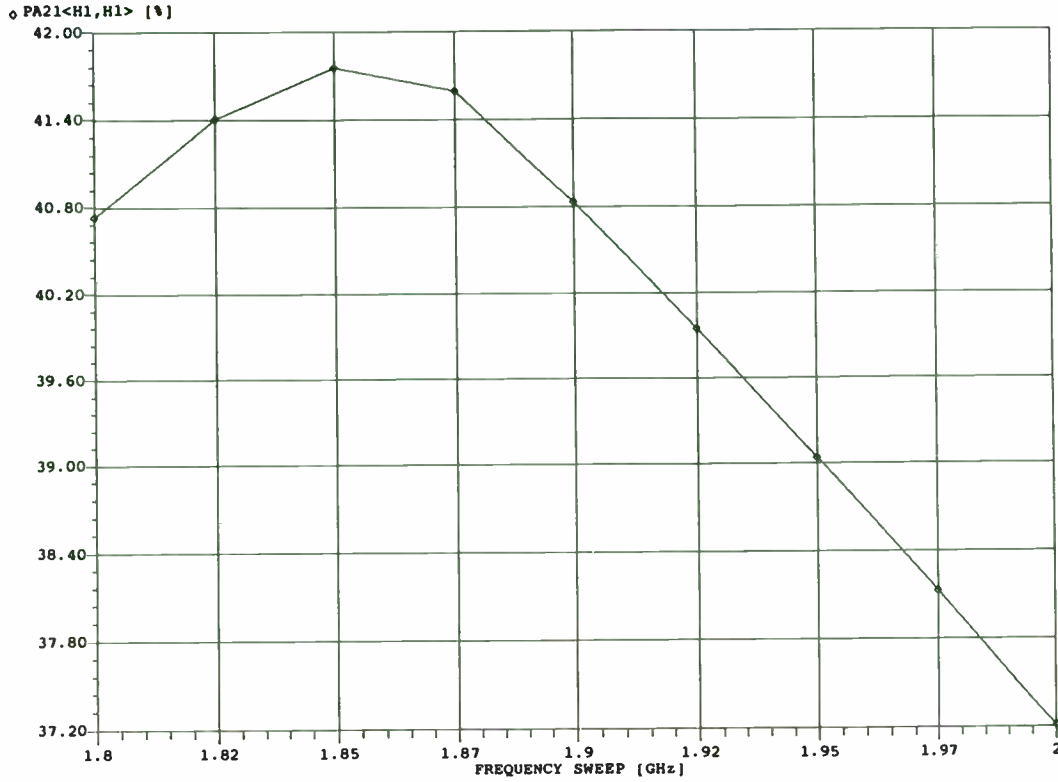
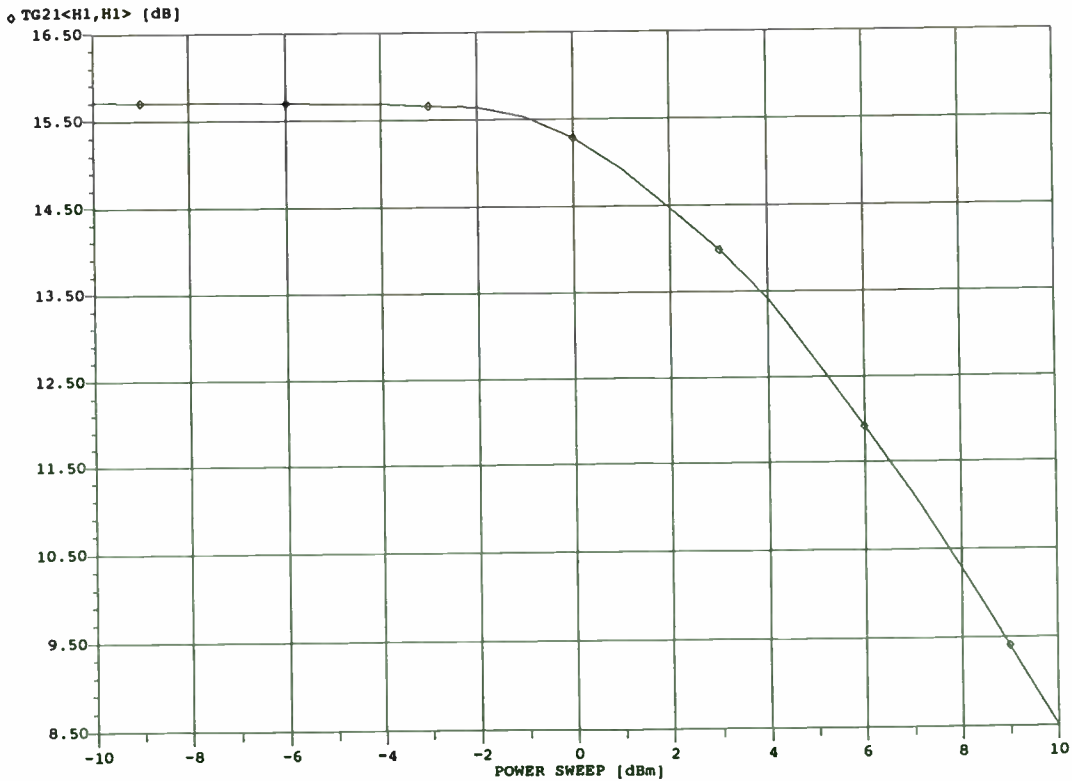


Figure 1: Oscillator and X18 multiplier block diagram

MICROWAVE HARMONICA PC V5.1
 File: DECT09.CKT
 Power-Added Efficiency of MMIC Power Amplifier
 SWEEP OF NETWORK FUNCTION PA21<H1,H1> [%]



MICROWAVE HARMONICA PC V5.1
 File: DECT16.CKT
 Gain of Driver Amplifier versus Pin at F = 1.89 GHz
 SWEEP OF NETWORK FUNCTION TG21<H1,H1> [dB]



Low Cost Plated Plastic Diplexers For Use In Commercial Mobile Satellite Communications

Chip Scott
Teledyne Electronic Technologies
Microwave Products
1290 Terra Bella Avenue
Mountain View, CA 94043

Global satellite communications are growing at an astounding rate. Never before has the need for rapid and reliable telecommunications been so vital for professional and private success. Over the last several years a tremendous amount of design activity, as well as financial investment, has been placed on the latest generations of light weight, low cost mobile communication systems. As the demands for this market increase we can expect to see substantial pressure placed on cost reduction and enhanced performance.

As with most of today's state-of-the-art communication systems, the proper filtering technology is critical to both cost and performance. In the past, system designers have had basically two options; focus on low cost and sacrifice performance or incorporate the preferred solution, i.e. cavity filters and minimize costs as best as possible. However, until recently the latter option still represented considerable costs due to associated machining processes.

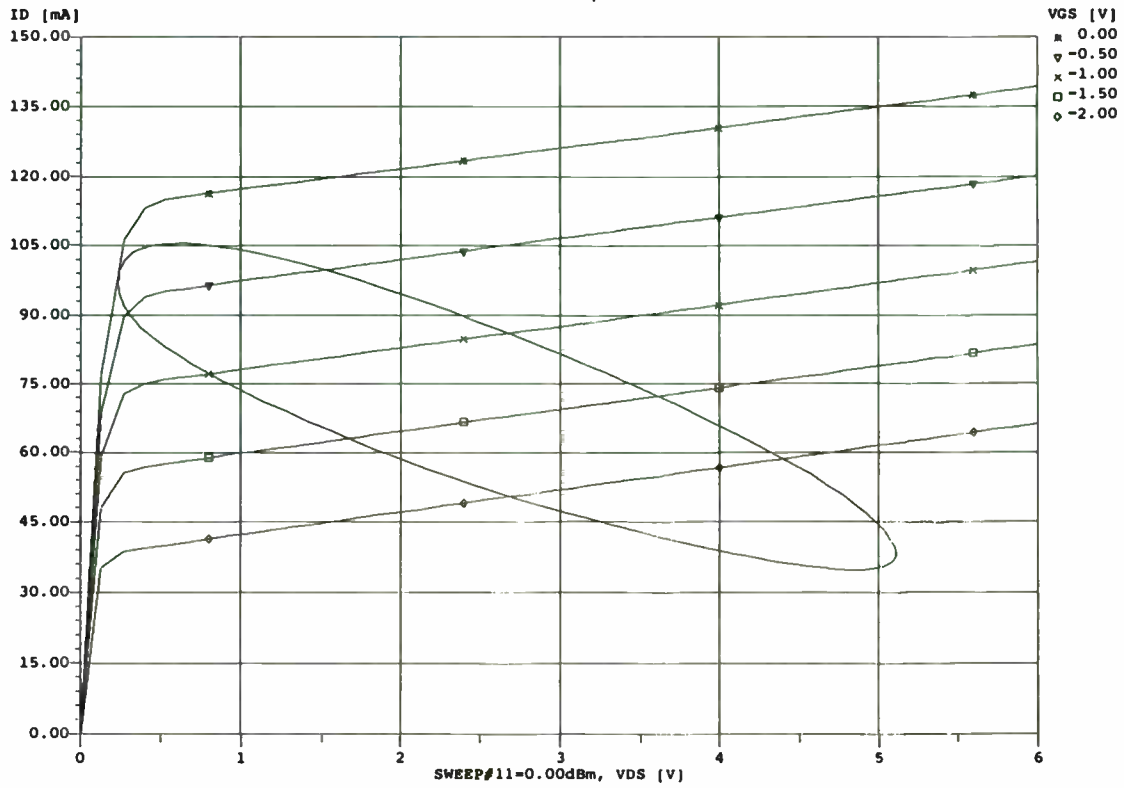
High performance cavity type filters are often used in many communications systems. High performance cavity filters reduce the performance demands of associated system components in areas such as; the noise figure of Low Noise Amplifiers, the gain of antennas and even critical battery life for portable applications. In many of today's commercial applications, cavity type filters are not common, primarily due to their relatively high costs. However, the latest in high performance engineering thermo-plastics can be

injected molded and plated to replace the conventional metal housing. The use of plastic significantly reduces the cost of the housing and opens the door to alternative assembly and tuning techniques. An additional benefit of replacing the aluminum housing with plastic is a considerable reduction in weight of approximately 35%.

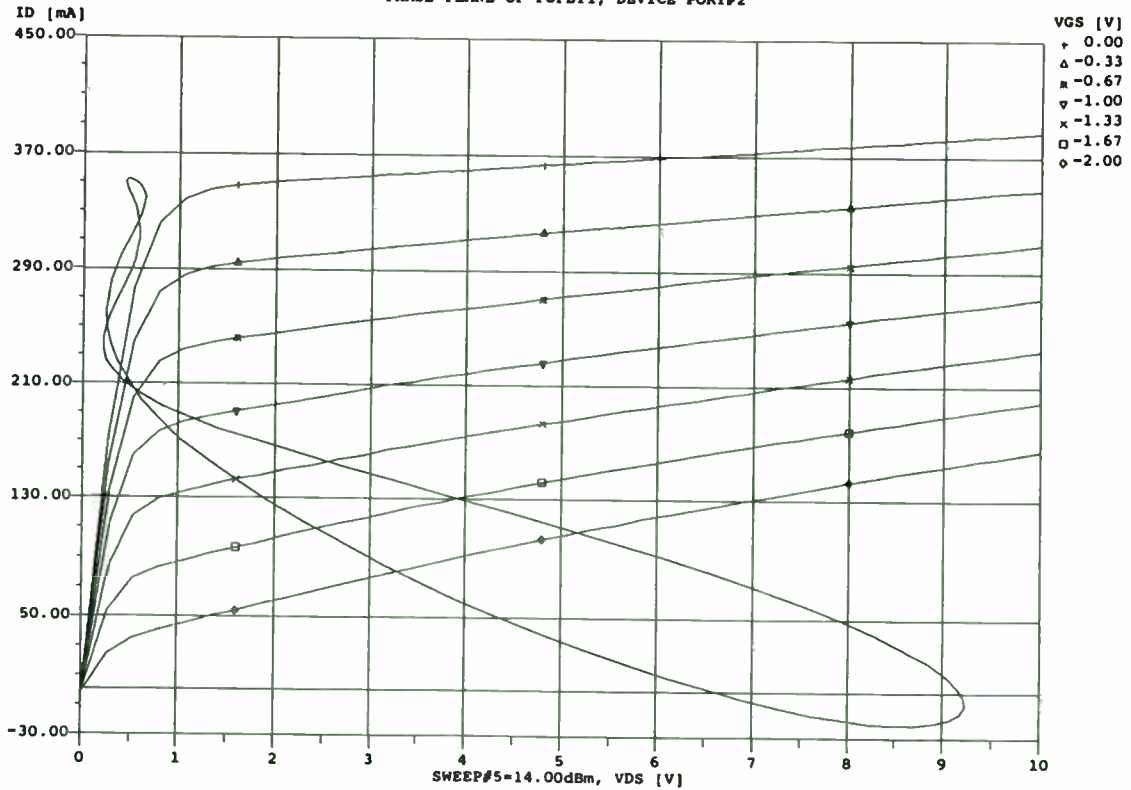
This product was originally developed to fill a need for a high performance, low cost diplexer for a mobile earth terminal application. Extensive review of the specifications of available engineering thermo-plastics led us to choose a filled Polyetherimide (PEI) material. A block of the candidate material was purchased and machined for evaluation. A duplicate housing was machined out of aluminum for direct comparison purposes. Both filters were silver plated, assembled and tuned in the same manner. Surprisingly, the plastic filter exhibited a more stable electrical performance over temperature than the aluminum housing. Figures 1 and 2, aluminum and plastic filters respectively, show the electrical performance over the temperature range of -35 to +85°C. Note that the plastic filter was tuned slightly narrower than the aluminum filter. Note also that the insertion loss droop of the plastic filter at ambient and hot temperatures is associated with excessively thin plating in this sample unit. The initial success of this test led us to continue development.

The plastics industry in the last decade has seen

MICROWAVE HARMONICA PC V5.1
 File: DECT16.CKT
 Dynamic Load Line at Driver FET Drain @ Pin = 0 dBm
 PHASE-PLANE OF POPET1, DEVICE PORT#2



MICROWAVE HARMONICA PC V5.1
 File: DECT09.CKT
 Dynamic Load Line at FET Drain at Pin=14 dBm
 PHASE-PLANE OF POPET1, DEVICE PORT#2



an explosion in the development of so called engineering thermo-plastics. Engineering thermo-plastics are plastics used for their performance characteristics and are used as alternatives to glass, metal and wood. Every large plastics manufacturer has a complete line of them. Early on we developed a set of criteria that we used to cull the choices. An important consideration for a microwave filter application was that the plastic must be platable, preferably with silver. Equally important was that the plastic had to be injection moldable. For the filter to perform over a large temperature range we needed a plastic that had a coefficient of linear thermal expansion that was less than aluminum (our usual housing material). This requirement is what led to the choice of a filled material. Fillers in plastics include wood flour, Kaolin (clay), cotton/cloth, mica, and glass. Special care must be taken when specifying a filler since filler can have a considerable impact on the mechanical properties of the molded part (as can color!). Since the original application was for a transmit/receive diplexer the final criterion was the plastic must be dimensionally stable even at high temperatures.

The cost benefit is where the shift to plastic really shines. In quantities of 1000 the cost of a machined diplexer housing is about \$30. The equivalent cost of the plastic housing is only \$3- even though the plastic that we have chosen is relatively expensive compared to other plastics. The cost of the plating is comparable for the aluminum and plastic housings. The tooling (mold) cost must be considered. The tooling cost for the diplexer is on the order of tens of thousands of dollars. Even so, the non-recurring cost of the mold can be easily amortized over the piece part price on large production runs. The tooling cost can be recovered in part volumes as small as 1000 pieces.

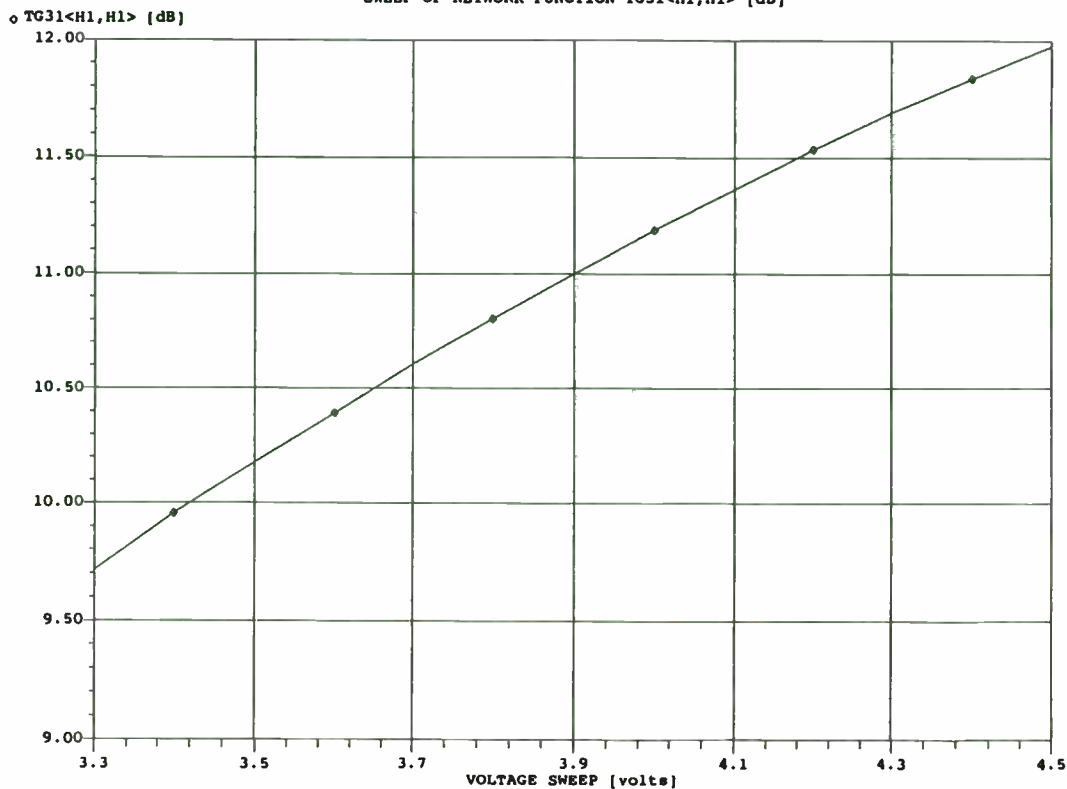
The original diplexer design was an L band diplexer. Due to the skin effect the housing material below about five skin depths is completely arbitrary. The fact that the plastic is a good dielectric has no effect on the electrical performance of the filters. And, since the coefficient of linear thermal expansion is lower than that of aluminum the filters are more stable (less band edge drift) than equivalent aluminum filters.

For high power applications, such as a transmit/receive diplexer there were some concerns about the ability of the plastic parts to dissipate heat. The thermal conductivity of the plastic is only about one one thousandth the thermal conductivity of aluminum. The major concern was the long term and thermal integrity of the silver plating. The original machined and plated parts were subjected to elevated temperatures. The plating was found to adhere without blistering up to about 200°C. At 200°C the plastic undergoes a phase change and the plating blisters. Since the plastic is essentially an insulator the silver plating plays a major role in the dissipation of internally generated heat (due to the insertion loss of the filter). The original machined and plated part was subjected to high power testing. With an insertion loss of 1 dB the plastic part was capable of passing 18 watts with no degradation or damage. The filters are capable of handling higher power levels utilizing specially developed techniques to dissipate the internal heat. An extensive thermal analysis was performed and verified the laboratory results.

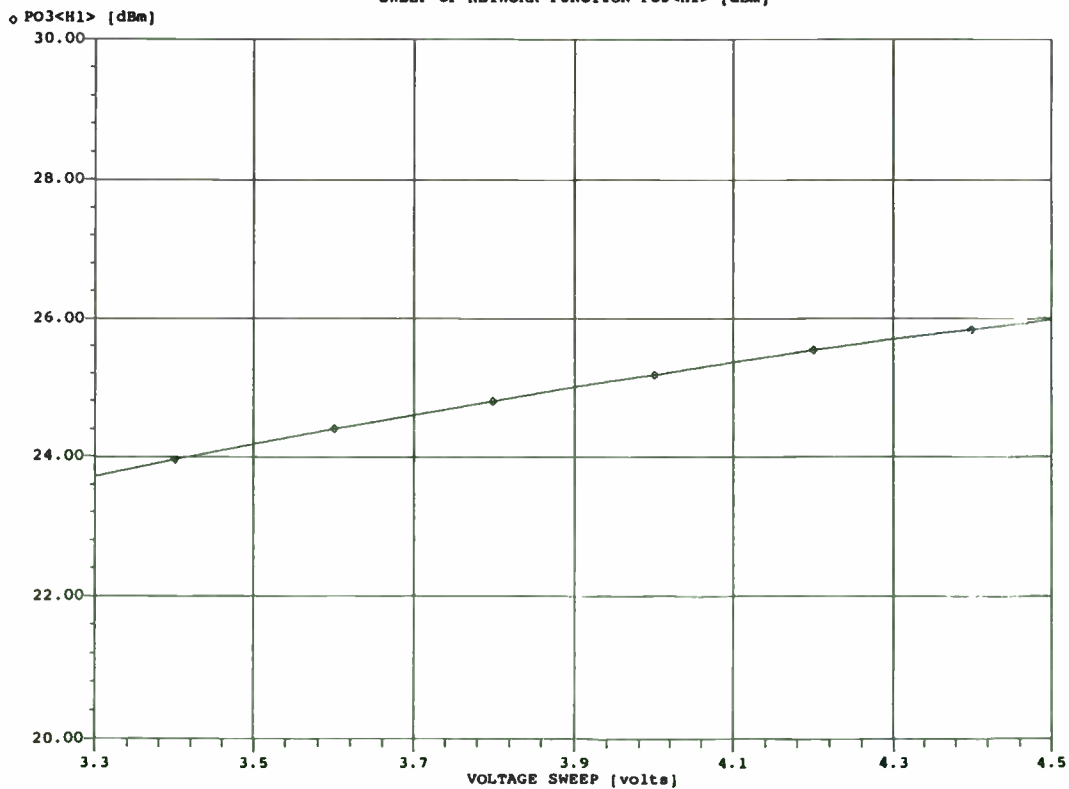
An important side effect in the switch from aluminum to plastic is the reduction in weight of the parts by about 35%. The density of the plastic is so low that the weight of the filter is driven by the weight of the aluminum cover. The reduced weight has become a major attraction for manufacturers of portable equipment. One other potential application where reduced weight is important is space (High-Reliability) applications where it costs approximately \$30,000 per pound to launch a payload into space. To test the feasibility of utilizing plated plastic filters in space the original plated plastic parts were subjected to a vacuum to test for survivability and passed with no blistering or degradation in performance. The plastic itself exhibits very low outgassing characteristics. The potential use of plastic plated parts in space is still being investigated.

There are still many areas in low cost and plated plastic filters that need to be and are being investigated. One of these areas is to take advantage of the properties of plastic parts and incorporate advanced assembly techniques, such as, snap together parts, ultrasonic welding, and/or solvent bonding. Another area to be investigated is solderless 'tapping' techniques. (A tap point is the electrical connection between the coaxial connectors and the filter input and output

MICROWAVE HARMONICA PC V5.1
 File: DECT09.CKT
 Power Gain of Amplifier v. Power Supply Voltage @ Pin=14dBm
 SWEEP OF NETWORK FUNCTION TG31<H1,H1> [dB]



MICROWAVE HARMONICA PC V5.1
 File: DECT09.CKT
 Output Power versus Power Supply Voltage @ Pin=14 dBm
 SWEEP OF NETWORK FUNCTION PO3<H1> [dBm]



resonators.) And of course, the dream of every filter engineer, automated tuning, which would also go a long way in further reducing filter cost. And finally the low cost of plated plastic filters coupled with higher levels of integration including: low noise amplifiers, power monitors, SWR detectors and even horn antennas can have a significant impact on system performance and reliability while at the same time minimizing costs, size and weight.

Conclusions: Through the utilization of engineering thermo-plastic material and a proprietary plating process, the adhesion and mechanical problems of the past with plated plastic parts have been eliminated. Adding up all the features; light weight, high performance, large volume production and low costs equals an excellent value. With few exceptions this new, *patent pending*, plated plastic technology is the ideal solution for low cost high performance commercial filtering requirements.

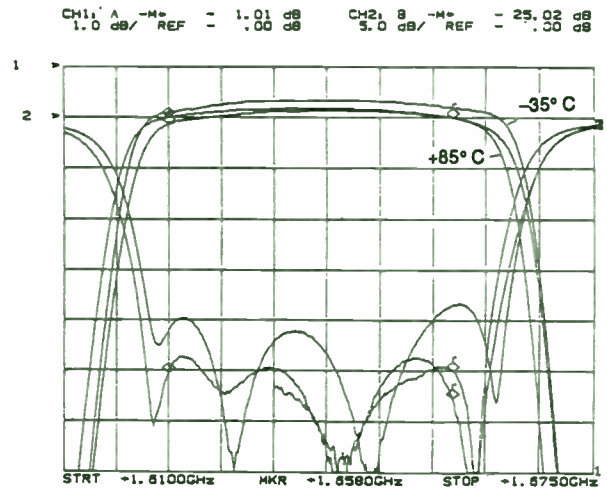


Figure 2
Temperature Performance of Rased Plastic (PEI) Diplexer
-35°C to +85°C
6.5 Mhz/Div.

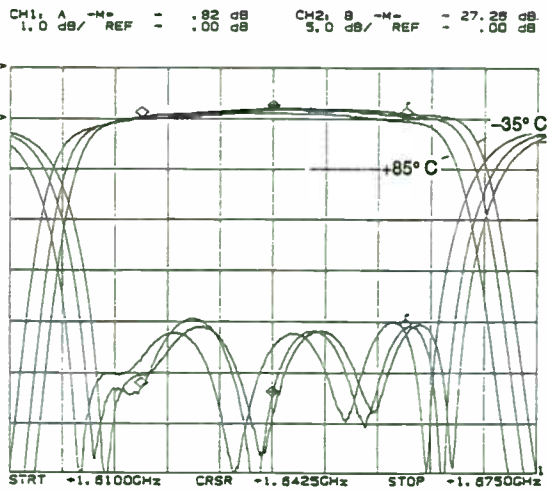
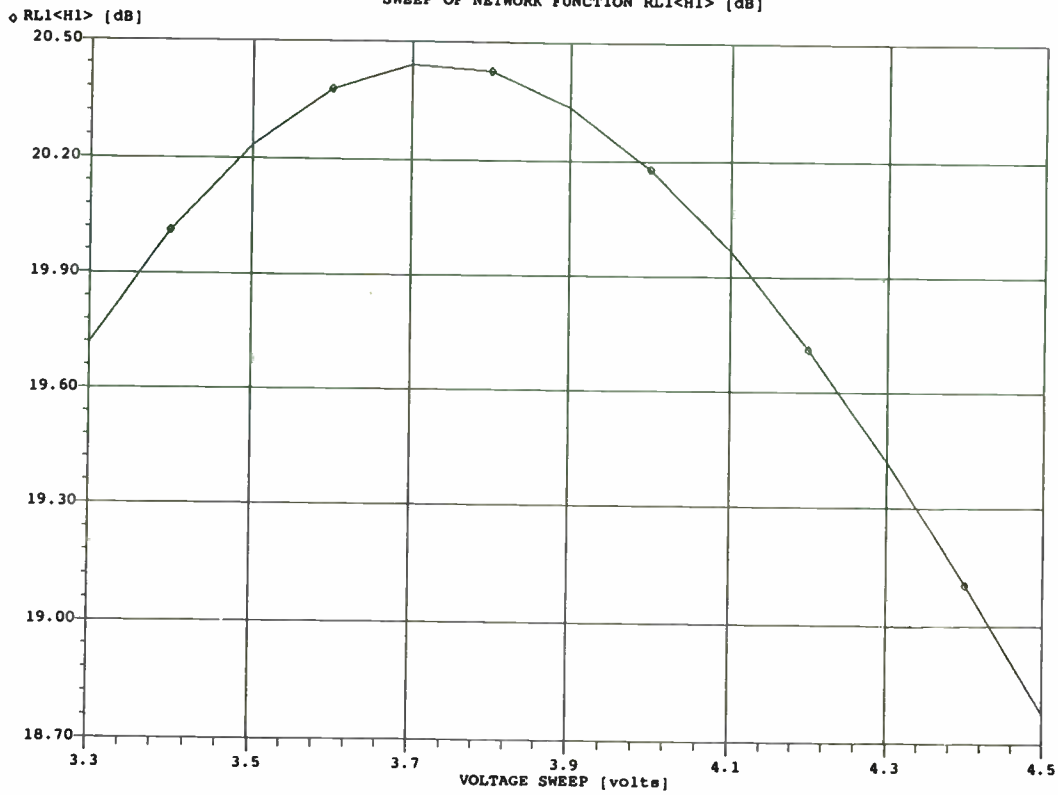


Figure 1
Temperature Performance of Aluminum Diplexer
-35°C to +85°C
6.5 Mhz/Div.

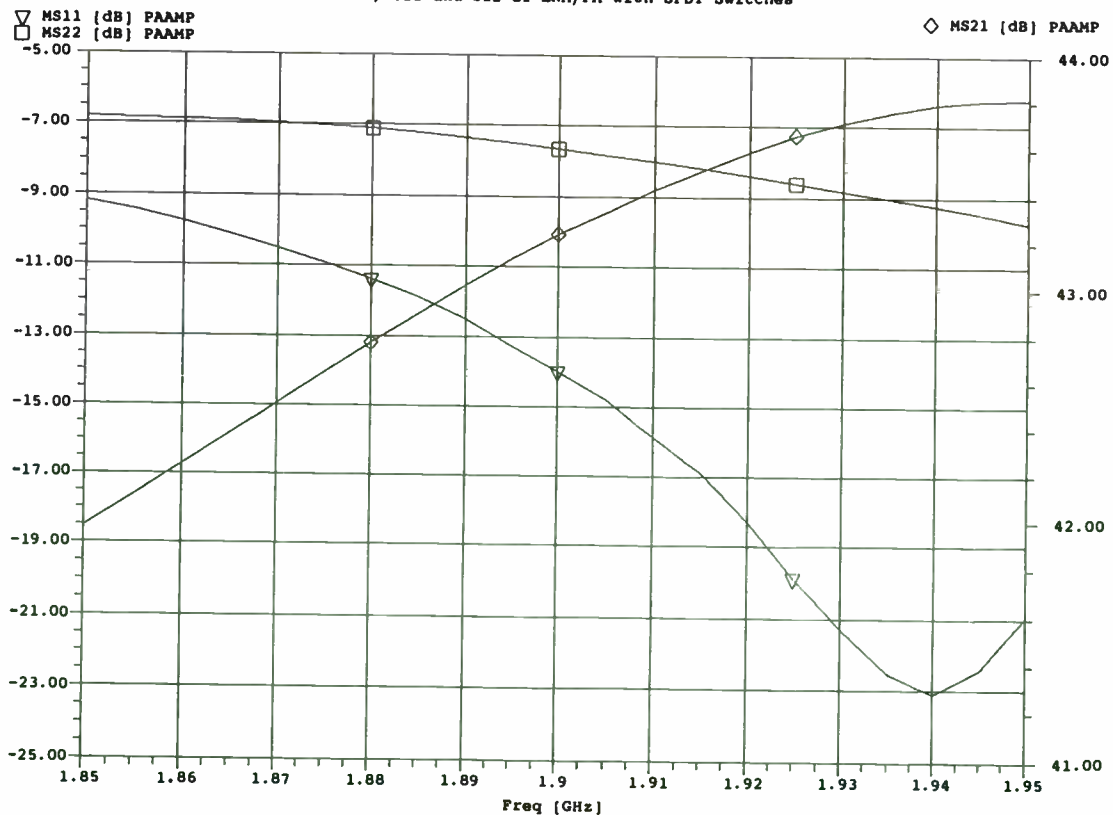
MICROWAVE HARMONICA PC V5.1
 File: DECT09.CKT
 I/P Return Loss of Amp. v. Power Supply voltage @ Pin=12 dBm
 SWEEP OF NETWORK FUNCTION RL1<H1> [dB]



21-OCT-92

MICROWAVE HARMONICA PC V5.1
 File: dect20
 Gain, S11 and S22 of LNA/PA with SPDT Switches

18:08:46



Satellite Channel Utilization in the Presence of Rain Attenuation

Kaivan Karimi and Valentine Aalo

Electrical Engineering Department

Florida Atlantic University

Boca Raton, FL 33431

Phone: (407) 367-3485

ABSTRACT

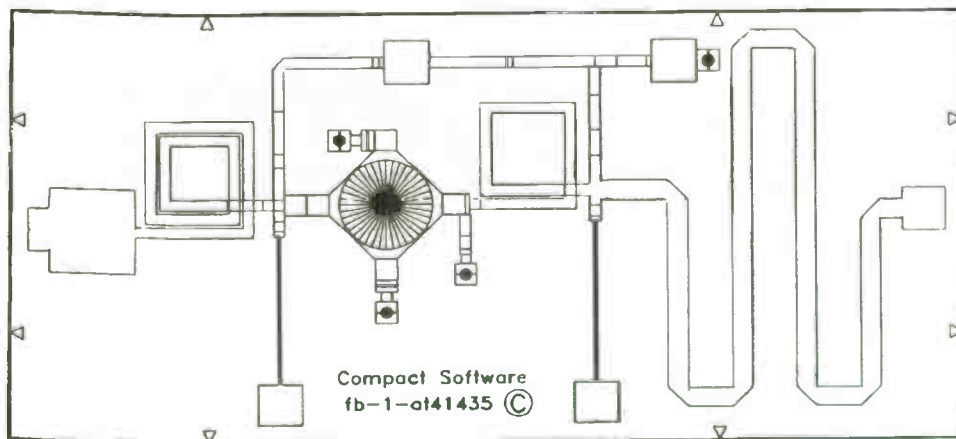
The most dominant cause of signal degradation in satellite links operating at Ka-band is attenuation due to rain. Presently most rain compensation algorithms are based on the use of a fixed, large fade margin to combat occasional deep fades. However the use of a fixed margin results in an inefficient use of channel capacity for a high percentage of the time. In this paper an adaptive rain fade counter-measure based on the effective utilization of the channel capacity is used for a typical satellite link operating in the Ka-band. Manning's rain attenuation prediction model, based on the rain history of the transmitting and receiving stations is used to determine outage rates both in terms of channel capacity and BER.

Integration of Simulation with Layout is MOST important even at the relatively low frequencies of present-day wireless communication circuits and subsystems.

Vendors now supplying so-called Layout-Driven Simulation

EXAMPLE

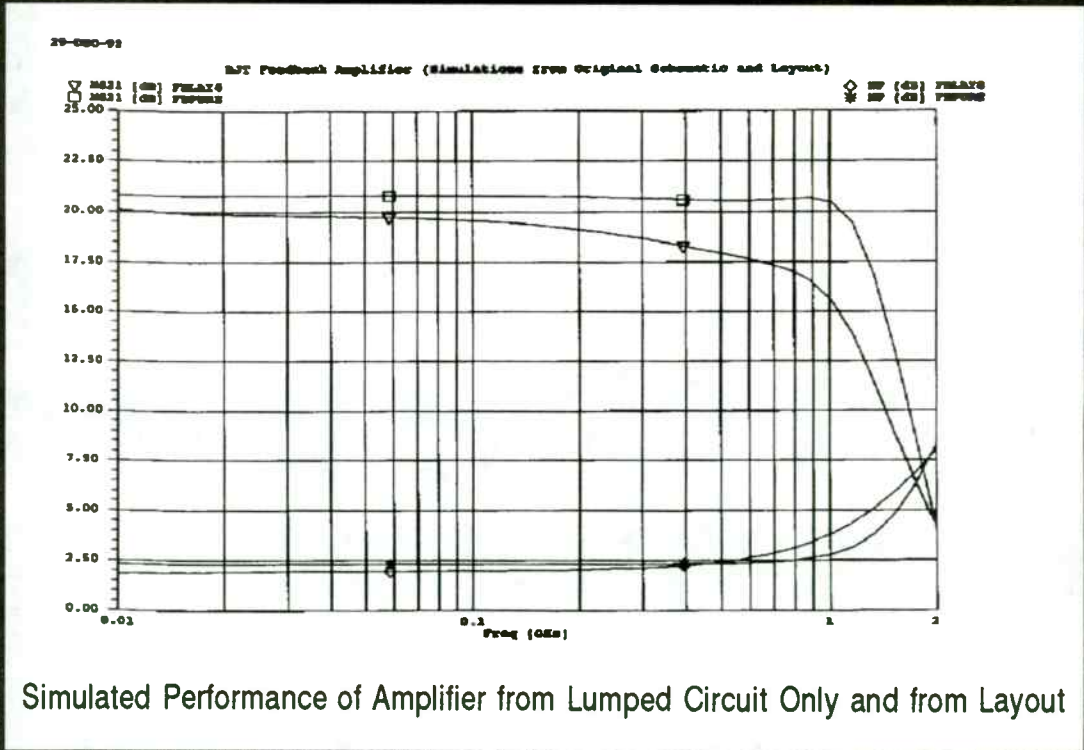
Broadband BJT Feedback Amplifier with a frequency range of 10 MHz to 1 GHz has performance which is markedly changed by layout.



Layout of BJT Amplifier generated with Serenade

I. Introduction

Satellite communications form an essential part of global telecommunication systems, carrying large amounts of data, voice and video, and offer a number of features not readily available with other means of communications. As demand for telecommunication services increases, spectrum congestion forces system planners to use higher frequencies [1]. Currently, most satellite links operate at C-band, but as time passes, there will be increased use of earth-space links operating at Ka-band. The Advanced Communications Technology Satellite (ACTS), which is scheduled to be launched into orbit in 1993, has several experiments on board related to the utilization of earth-space link at Ka-band with downlink frequencies from 19.2 to 20.2 GHz and uplink frequencies from 29.1 to 30.0 GHz [2]. ACTS mobile terminal program will explore the potentials of Ka-band to meet the needs of future mobile satellite services. The Ka-band, with the promise of less congestion, may also offer increased bandwidth and, therefore, the expansion of system capacity and user services. Also, the accompanying significantly smaller ground terminal equipment are expected to reduce system cost [3]. However, one of the major concerns of the investigators is that satellite channels at Ka-band are subject to severe performance degradations due to propagation effects that occur at this band. For a mobile satellite link, the attenuation factors involved include scintillation, shadowing, multipath fading, and the most dominant factor of all, rain attenuation. In the design of such a link maintaining a fixed,



large fade margin to combat occasional deep rain fades as done in most rain compensation algorithms, results in severe reduction in communication capacity [4]. Traditional fade countermeasures concentrate on the use of power, bandwidth, and site diversity and pay very little attention to the optimum use of channel capacity. In this paper we use the adaptive rain fade counter measure, based on the effective utilization of the channel capacity proposed in [4] to study the performance of a typical ACTS communication link.

II. Rain Attenuation On Satellite Link

Figure 1 illustrates a typical satellite link. Currently, almost all of the satellites in operation have no onboard processing. For a conventional frequency translation satellite, the total system carrier-to-noise density ratio $(C/N_0)_{s,c}$ for clear air (no attenuation) is given by [5]

$$\left(\frac{C}{N_0}\right)_{s,c} = \frac{\left(\frac{C}{N_0}\right)_u \cdot \left(\frac{C}{N_0}\right)_d}{\left(\frac{C}{N_0}\right)_u + \left(\frac{C}{N_0}\right)_d} \quad (1)$$

where $(C/N_0)_u$ and $(C/N_0)_d$ are the carrier-to-noise density ratio for the uplink and downlink transmissions for clear air, respectively. Note that the quantities in (1) are not in units of dB. Now, let

$$S_u = 10 \log \left(\frac{C}{N_0}\right)_u, \quad S_d = 10 \log \left(\frac{C}{N_0}\right)_d \quad (2)$$

Then the total equivalent attenuation due to rainfade for the system (up and down link), is given by

An Integrated Microwave Radio Transceiver For WLAN Applications

David Williams
GEC Plessey Semiconductors

1. Introduction

The FCC regulations permit un-licensed operation of radio transmitting equipment in the 2.4 to 2.483 GHz band provided that the spectrum of the transmitted signal is spread in a prescribed manner.

This paper describes the design of a Frequency Hopping radio transceiver intended for use in a Wireless Local Area Network system.

2. Discussion

In any design for a frequency agile radio it is essential to minimise the number of oscillators whose frequency must change when the radio changes channel, since the radio will be required to be capable of transmitting or receiving data in the shortest time possible after a command to change frequency.

This requirement is particularly important where Frequency or Phase modulation schemes are used to impart Data on to the carrier signal. If the phase of the carrier signal was changing after a frequency hop any frequency modulated Data would remain corrupted until the rate of change of carrier phase fell below that representing a Data bit.

2a. Radio System Design

A schematic diagram of the basic Radio is shown in Figure 1. The design is fundamentally that of a Radio MODEM or Up/Down Converter.

The Frequency Synthesised Master Oscillator (MO) feeds both an up-converter mixer (For Transmit) and a down-converter mixer (For Receive). The Master Oscillator is designed to switch frequency in a short time (100

$$A(dB) = \left(\frac{C}{N_0}\right)_{s,c}|_{dB} - \left(\frac{C}{N_0}\right)_{s,att}|_{dB} \quad (3)$$

where

$$\left(\frac{C}{N_0}\right)_{s,c}|_{dB} = 10 \log\left\{\frac{10^{\frac{S_u}{10}} \cdot 10^{\frac{S_d}{10}}}{10^{\frac{S_u}{10}} + 10^{\frac{S_d}{10}}}\right\} \quad (4)$$

$$\left(\frac{C}{N_0}\right)_{s,att}|_{dB} = 10 \log\left\{\frac{10^{\frac{S_u-A_u}{10}} \cdot 10^{\frac{S_d-A_d}{10}}}{10^{\frac{S_u-A_u}{10}} + 10^{\frac{S_d-A_d}{10}}}\right\} \quad (5)$$

In (5), A_u and A_d (in dB) are the uplink and downlink attenuations due to rain, respectively. The over-all system attenuation expressed in dB given in (3) can be shown to be

$$A(dB) = A_u + A_d + 10 \log\left\{\frac{10^{\frac{S_u-A_u}{10}} + 10^{\frac{S_d-A_d}{10}}}{10^{\frac{S_u}{10}} + 10^{\frac{S_d}{10}}}\right\} \quad (6)$$

It is well known that the attenuations A_u , A_d , and A are approximately log-normally distributed random variables [4], [6]. Therefore, the overall long-term probability density function (pdf) of rain attenuation along the link has the form

$$P_A(a) = \frac{1}{a\sigma\sqrt{2\pi}} \exp\left(-\frac{(\ln a - m)^2}{2\sigma^2}\right) ; a \geq 0$$

$$P_A(a) = 0 ; a \leq 0 \quad (7)$$

The median and standard deviation of A can be determined by anyone of two methods described in [4].

micro seconds) and is locked to the system reference oscillator (A Crystal Oscillator running at 10 MHz).

The Radio is designed to operate in the 2.4-2.483 GHz Industrial, Scientific & Medical Band and has a first Intermediate Frequency of 350 MHz. The MO therefore operates between 2.05 GHz and 2.133 GHz. The Radio channels are spaced 1 MHz apart.

A Major problem with Up/Down Converter systems is the fact that both the Transmit and Receive IFs are at the same frequency and steps must be taken to prevent leakage of the transmit signal into the Receiver IF chain. This design employs a frequency divider in the Transmitter IF system which is disabled when the Radio is configured to receive. The transmit IF signal is generated at 700 MHz with DATA being imposed by Frequency Modulation of the Voltage Controlled Oscillator (VCO) within the 700 MHz Phase Locked Loop (PLL).

A block schematic of the complete Phase Two (Non-Integrated) radio is shown in Figure 2.

2b. The Receiver Section

The Receiver is a classical double conversion superhetrodyne design. Signals entering the receiver via either antenna port are fed via a Band Defining Filter to the transmit/receive switch, then to a low-noise signal amplifier. A second band-pass filter is inserted after the amplifier to suppress noise generated at the image frequency (1.7 to 1.783 GHz) by this device. Signals are then fed to the first down-converter mixer together with Local Oscillator (LO) drive from the fast hopping synthesiser. Intermediate Frequency signals at 350 MHz are amplified and fed to a Surface Acoustic Wave Filter whose purpose is to restrict the IF band-width in order to maximise signal to noise ratio at this point. An Integrated circuit amplifier/mixer device (GPS SL6444) is used to down-convert the signals to the second IF of 38 MHz, further filtering is provided by a second SAW filter. The Frequency Modulated IF signal is de-modulated in an Integrated Circuit FM Receiver device (MOTOROLA MC 13055). This device provides a digital DATA output together with an analogue output which is used to monitor receiver signal strength. The LO drive for the second down-converter at 312

III. Efficient Satellite Channel Utilization

Due to particular constraints of modulation, coding, and throughput, and the absence of onboard processing, in most cases satellite communications system designers implement a fixed link budget margin. For very small aperture terminals (VSAT), this implies insufficient utilization of the channel capacity for a considerably high percentage of the time, especially for a satellite communications system operating at 20/30 GHz band which is subject to severe performance degradations due to rain attenuation [4]. A good performance measure of such a communications system is channel capacity which gives the maximum rate of signal transmission over the channel.

A. Channel Capacity

For a continuous channel with additive white Gaussian noise, Shannon defines the channel capacity in bits per sec. (b/s) by [7]

$$C = B \log_2 \left(1 + \frac{S}{N} \right) \quad (8)$$

where B is the channel bandwidth in Hz, and S/N is the signal-to-noise power ratio in the channel. The capacity per unit bandwidth may be written as

$$\frac{C}{B} = \log_2 \left(1 + \frac{S}{N} \right) \quad \left(\frac{\text{b/s}}{\text{Hz}} \right) \quad (9)$$

Due to propagation fading, the term S/N in (9) is a random variable with arbitrary but known distribution which depends on the characteristics and type of the fading process. This implies that

MHz is generated using a Frequency Synthesiser Integrated Circuit (GPS NJ8820) which is locked to the 10 MHz system reference oscillator.

2c. The Transmitter section

Serial digital DATA is taken from the DATA input and fed to a Low Pass Filter having a Gaussian transfer response, this has the effect of limiting the bandwidth occupied by the Frequency Modulated carrier and ensures that transmissions comply with the requirements of the FCC.

The "shaped" digital signal is used to Frequency Modulate the VCO within a Phase Locked Loop operating at 700 MHz. The Frequency Modulated signal is amplified before being fed to a high speed divide-by-two circuit which is gated on and off by the Transmit/Receive control. The divider output is in the form of a 350 MHz Frequency Modulated "square-wave". It is necessary to Low-Pass filter this signal before it is amplified and fed to the Up-Converter mixer. This is done to reduce the level of the harmonic energy within the signal at this point.

The Upper-Sided output signal from the Up-Converter is selected by the use of a Band-Pass filter at the output of the mixer. This filter provides adequate suppression of the carrier and un-wanted sideband signals from the mixer. The wanted signal is of low amplitude and it is necessary to amplify at this point to a level sufficiently large to drive the output amplifier.

The output power level may be selected to be either 10 mW or 100 mW by use of the "Power Set" control, this switches an attenuator in the output amplifier causing the output level to change.

The output signal from the transmitter is fed to the Transmit/Receive switch and band defining filter before reaching the antenna selector switch and Output/Input ports.

2d. Radio Performance

The Radio described in the previous section has been tested and its performance is summarised in the table shown in Figure 3.

the channel capacity is also a random variable and therefore imposes performance degradation on the system. Using standard transformation of random variables, the pdf of C/B can be written in terms of that of S/N [4].

In the presence of rain attenuation, the received signal-to-noise power level is given by

$$\left(\frac{S}{N} \right) = \left(\frac{S}{N} \right)_{s,c} - A \quad (\text{dBW}) \quad (10)$$

where $(S/N)_{s,c}$ is the unfaded signal-to-noise power level (in dB) for clear air condition, and A is the total equivalent rain attenuation on the link. The cumulative distribution function (cdf) of channel capacity is given by

$$\begin{aligned} F_{C/B}(y) &= \text{Prob} \left\{ \frac{C}{B} \leq y \right\} = \text{Prob} \left\{ \frac{S}{N} \leq 2^y - 1 \right\} \\ &= \text{Pr} \left\{ A \geq \left(\frac{S}{N} \right)_{s,c} - 10 \log (2^y - 1) \right\} \\ &= \text{Prob} \left\{ \ln A \geq \ln \left[\left(\frac{S}{N} \right)_{s,c} - 10 \log (2^y - 1) \right] \right\} \\ &= Q \left\{ \frac{1}{2} \left(\frac{\ln \left[\left(\frac{S}{N} \right)_{s,c} - 10 \log (2^y - 1) \right] - m}{\sigma} \right)^2 \right\} \quad (11) \end{aligned}$$

where the variable $y = C/B$, $(S/N)_{s,c}$, A are all expressed in units of dB, and

$$Q(x) = \int_x^{\infty} \frac{1}{\sqrt{2\pi}} e^{-\frac{t^2}{2}} dt \quad (12)$$

The long-term cdf of channel capacity in the presence of rain

3. The Integrated Transceiver

The radio design has been developed further to a stage where the complete transceiver may be realised using only four integrated circuits.

A block schematic of the new radio is shown in Figure 4. It can be seen that integrated design makes use of the same basic architecture as the previous design but the various radio functions have been "absorbed" into Radio Frequency Application Specific Integrated Circuits (ASICs).

3a. The Microwave Front-End

This section of the Radio is realised as a Gallium Arsenide Microwave Monolithic Integrated Circuit (GaAs. MiMIC) and comprises the following circuit functions:-

- Antenna Selector (Diversity) Switch
- Transmit/Receive Switch
- Receiver Low Noise Amplifier
- Down-Converter Mixer
- IF Pre-amplifier
- Up-Converter Mixer
- Power Amplifier
- Microwave VCO (for fast hopping synthesiser)

GEC Plessey Semiconductors has developed the design of this device with a GaAs foundry and has received first article devices which are being used in prototype integrated radios.

3b. The IF Receiver

The IF Receiver comprises:-

- The first IF amplifier
- The second down-converter
- The RSSI circuitry
- The second Local Oscillator
- The frequency discriminator and DATA buffer

attenuation, for the various unfaded signal-to-noise ratio values is plotted in Figure 1.

B. BER Degradations

Another measure of the performance of a satellite communication system is the bit error rate (BER). For a given modulation scheme, the system BER is a function of S/N, and in the presence of fading, is also a random variable. By following a procedure similar to the channel capacity analysis presented above, it is possible to determine the cdf of BER performance in the presence of propagation fading. This gives the measure of the availability of the communications link, since it gives the percentage of the time for which the specified BER will be exceeded. For a digital communications system using M-PSK modulation scheme, the probability that any M-ary symbol will be received in error, P_s , is given by [7]

$$P_s = \frac{M-1}{M} - \frac{1}{2} \operatorname{erf}\left(\sqrt{\frac{E_s}{N_0}} \sin \frac{\pi}{M}\right) - \frac{1}{\sqrt{\pi}} \int_0^{\sqrt{\frac{E_s}{N_0}} \sin \frac{\pi}{M}} e^{-y^2} \operatorname{erf}\left(y \cot \frac{\pi}{M}\right) dy. \quad (13)$$

where

$$\operatorname{erf}(x) = 1 - 2Q(\sqrt{2}x)$$

For $P_s < 10^{-3}$, a useful approximation of (13) is given by [7]

$$P_s = 2Q\left[\left(\sin \frac{\pi}{M}\right) \sqrt{\frac{2E_s}{N_0}}\right] \quad (14)$$

where E_s is the energy per M-ary symbol, and N_0 is one-sided power

The IF receiver is fabricated using the GEC Plessey Semiconductors "HE" Advanced Silicon bipolar process and contains transistors having a transition frequency in excess of 14 GHz.

3c. The Triple Synthesiser

This device is fabricated using the GEC Plessey Semiconductors 1.0 micron CMOS process and comprises all the PLL components required to control the three frequency synthesisers in the radio.

3d. The Oscillator/Divider

The final RF ASIC contains the 700 MHz oscillator circuit together with the high speed, variable-modulus, pre-scaler which is used in conjunction with the microwave oscillator in the fast hopping synthesiser. This device is also fabricated using the "HE" bipolar process.

4. Radio Construction

The Phase two (non-integrated) radio contains approximately 40 Integrated Circuits and 200 various passive components and is fabricated on a multi-layer Printed Circuit card having an area 7.0 inches by 5.0 inches. The new integrated radio contains only 4 integrated circuits and 50 passive components and occupies a much-reduced area of 3.0 inches by 2.0 inches. The Phase two and Phase three radios are shown in Figures 5 and 6 respectively.

5. Conclusions

A radio transceiver has been designed and produced whose performance meets the requirements of a frequency agile transmission scheme for Local Area Network applications.

The spectral properties of the radio transmitter are compliant with the requirements of the FCC.

spectral density. The equivalent energy per data bit E_b is given by

$$E_b = \frac{E_s}{\log_2 M} \quad (15)$$

The relationship between probability of bit-error and signal-to-noise may be denoted by

$$P_b = f\left(\frac{S}{N}\right) \quad (16)$$

The long-term cdf of BER in the presence of overall rain attenuation A is then given by

$$\begin{aligned} \text{Prob}\{BER > x\} &= \text{Prob}\left\{\left(\frac{S}{N}\right)_{s,c} - f^{-1}(x) > A\right\} \\ &= 1 - Q\left\{\frac{1}{2} \left(\frac{\ln\left[\left(\frac{S}{N}\right)_{s,c} - 10 \log(f^{-1}(x))\right] - m}{\sigma}\right)^2\right\} \quad (17) \end{aligned}$$

Figure 2 illustrates the long-term cdf of BER in the presence of over-all rain attenuation for a given M-ary modulation scheme. One can see that based on the fading characteristics of the channel, along with relaxation of the BER requirements for applications that are more error tolerant (voice as oppose to data), assuming that the modulation schemes available are limited to uncoded M-PSK, the availability can be improved. Thus during deep fades, the transmission rate may be reduced, or equivalently, the modulation scheme may be changed accordingly.

The Phase two radio designated DE6002 has been delivered to "BETA-Site" Customers.

A new fully, integrated radio designated DE6003 containing only four high-performance ASICs has been designed and is being developed.

The device will be commercially available early in 1993.

C. Advanced Communications Technology Satellite (ACTS)

With the launch of the Advanced Communications Technology Satellite (ACTS) into orbit, a new door into the optimum utilization of earth-space link at Ka-band will be opened to us. The Space Communications Technology Center (SCTC) at Florida Atlantic University is one of the several centers with propagation experiments on board ACTS. The rain attenuation prediction model which will be used at the center, is a model based on annualized rainfall statistics developed by R.M. Manning of the Lewis Research Center [6]. According to this model, based on the past rain history of a given location, the link (up or down) attenuation due to rain can be predicted. The exceedance curve for the link between two of the locations involved in ACTS propagation studies (Cleveland, Ohio and West Palm Beach, Florida) using R.M. Manning's model are given in Figure 3. We assume NASA Lewis in Cleveland as the transmitting station (uplink), and FAU-SAT terminal located at Florida Atlantic University's Boca Raton campus (Southern Palm Beach County) as the receiving station (downlink). Table 1 is a typical "Statistics of Rain Attenuation" Table showing the percentage of time for which a certain level of rain attenuation is exceeded for the two links involved. Data for the uplink are taken from past rain history of Cleveland, and similarly data for the downlink are taken from past rain history of West Palm Beach. The last column represents the over-all link attenuation (A) based on an uplink and downlink carrier-to-noise ratio of 45.2 dB and 42.7 dB respectively [2]. The International Station Meteorological

Climate Summary (ISMCS) CD-ROM was used to obtain past rain history of West Palm Beach, and Cleveland. ISMCS is a reliable and accurate source of rain history for over 5800 locations throughout the world, dating back to 1948 [8]. Data from ACTS collected at a receive-only terminal at FAU, will be used to compare our prediction model with the actual levels of attenuation. This will enable us to validate R. M. Manning's Rain Attenuation Model for use in Ka-band.

IV. Summary and Conclusion

Spectrum congestion has forced satellite system planners to consider the use of earth-space links operating at Ka-band. However satellites operating at these high frequencies are subject to severe performance degradations due to the propagating medium. The most dominant factor contributing to signal degradations is the attenuation due to rain. To combat occasional deep rain fades, currently most satellite system designers use a fixed large fade margin budget, which reduces the link capacity greatly. In order to utilize the channel more efficiently, an adaptive technique based on the characteristics of the channel and the fading process associated with it needs to be implemented. A long-term statistical analysis of the channel capacity based on the fading statistics of the channel can help the system designers to implement an adaptive modulation scheme, in order to use the channel more efficiently. Figure 2 is the illustration of such analysis. Using the statistical rain data for Cleveland (transmitting station) and West

Palm Beach (receiving station) the cdf of channel capacity in the presence of rain attenuation as a function of unfaded signal-to-noise ratio values is graphed.

Figure 3 illustrates the cdf of BER of several uncoded PSK schemes in the presence of rain attenuation. One can see that for a given unfaded signal-to-noise ratio value, by relaxation of the BER for more error tolerant applications, the capacity of the communications can be increased drastically. For example by lowering the BER from 10^{-6} to 10^{-3} , we can use 16-PSK instead of 8-PSK and still stay under 0.01% of the time for BER exceedance. Thus we can stay with in our BER requirements for over 99.99% of the time.

Using Figure 3, once an acceptable level of BER and modulation scheme are chosen, one can then go back to Figure 2 and choose the appropriate rate of transmission. Using such adaptive technique based on the stochastic characteristics of the fading process of the channel, the utilization of the channel capacity may be done more efficiently.

V. References

- [1] J. H. Lodge, "Mobile Satellite Communications Systems: Toward Global Personal Communications," IEEE Communications Mag., Vol. 29, pp. 24-30, November 1991.
- [2] D. Chakraborty, F. Davarian, and W. L. Stutzman, "The Ka-

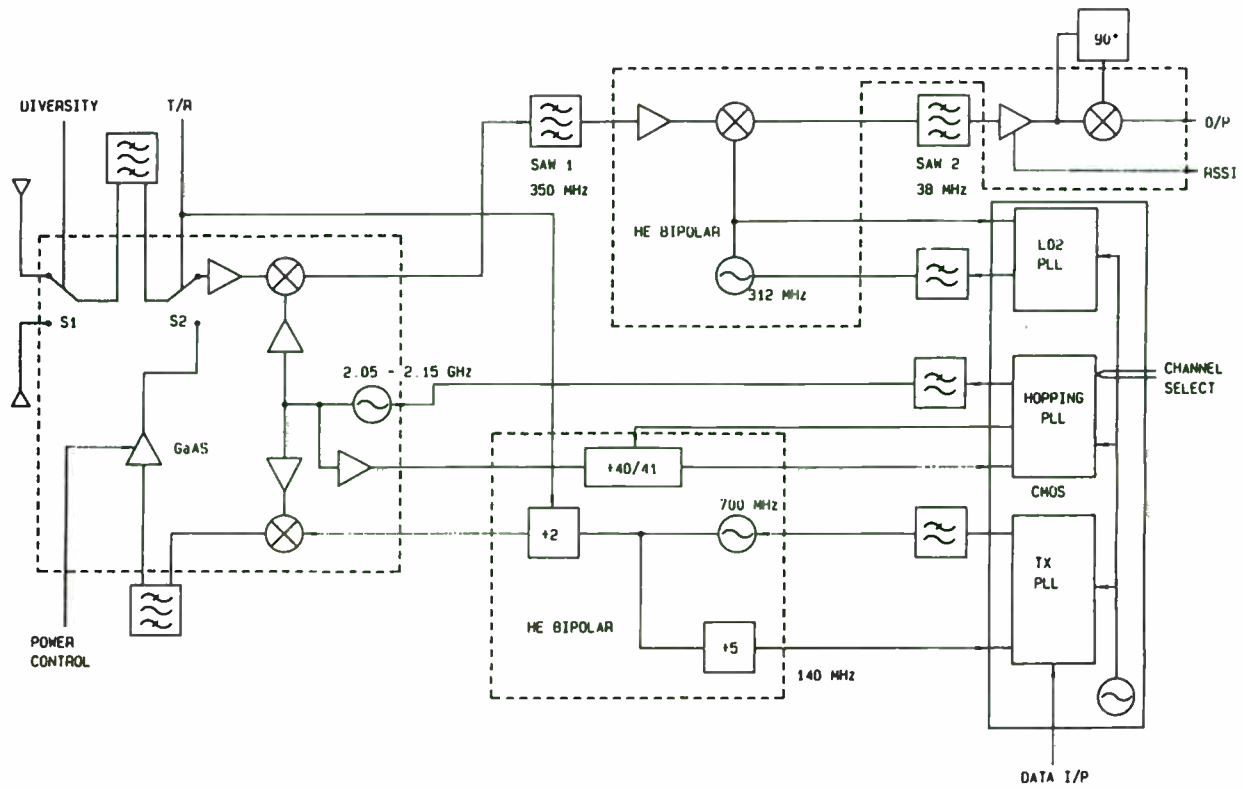


FIG. 4 PHASE III TRANSCEIVER

H29991A3-32
ISSUE 8

- band Propagation Measurement Campaign at JPL," *IEEE Antennas and Propag. Mag.*, Vol. 35, pp. 7-13, February 1993.
- [3] B. K. Levitt, "Rain Compensation Algorithm for ACTS Mobile Terminal," *IEEE Journal On Sel. Areas In Comm.*, Vol. 10, pp. 358-363, February 1992.
- [4] M. Filip, and E. Vilar, "Optimum Utilization of the Channel Capacity of a Satellite Link in the Presence of Amplitude Scintillations and Rain Attenuation," *IEEE Trans. On Comm.*, Vol. 38, pp. 1958-1965, November 1990.
- [5] L. J. Ippolito Jr., *Radiowave Propagation in Satellite Communications*, Van Nostrand Reinhold Co., New York, NY, 1986.
- [6] R. M. Manning, "A unified statistical rain attenuation model for communications link fade predictions and optimal stochastic fade control design using a location-dependent rain statistics database," *Int. J. Satel. Comm.*, Vol. 8, pp. 11-30, 1990.
- [7] V. K. Bhargava, D. Haccoun, R. Matayas, and P. P. Nuspl, *Digital Communications by Satellite: Modulation, Multiple Access and Coding*, Wiley, New York, NY, 1981.
- [8] T. Jarret, "The International Station Meteorological Climate Summary CD-ROM," *Bulletin of the American Meteor. Soc.*, Vol. 73, pp. 1578-1580, October 1992.

Planar Mixers For PCN Applications Utilizing GMIC Technology

Paul J. Schwab, Timothy A. Murphy

IC Design Center

M/A-Com Inc.

Abstract -- The investigation of planar mixers for use in communications applications will be discussed. These mixers were developed for use in a block converter or other similar applications where small size and weight are crucial system requirements. Two mixers which utilize separate design approaches are presented. The first approach is a lumped element [1] ratrace mixer which measures 0.150 X 0.120 inches. The second approach is a sub harmonically pumped mixer utilizing lumped element resonators and covering an area of 0.191 X 0.100 inches.

The Ratrace Mixer

This mixer consists of a ratrace coupler, a "beam lead tee" with its associated matching structure, and a low pass filter. The beam lead is the only external part to be assembled onto the GMIC circuit.

The ratrace coupler [2] is configured of three "pi" networks for the 90 degree sections and a "tee" network for the 270 degree section. The networks are transmission line equivalents for the appropriate sections. These equivalents are truly valid only at the exact center frequency, but still provide enough bandwidth for this application. The high pass "tee" was chosen for the 270 degree section to minimize the number of inductors (which are relatively lossy) in the realization of the network. The circuit schematic is shown in Figure 1. Simulated as well as actual performance of the coupler is shown in Figure 2.

The two isolated ports of the coupler are used for the RF and IF signals of the mixer [3]. The coupler isolation therefore provides the isolation between these two signals. The RF and IF signals are then passed through the remaining two ports of the coupler and are matched to the diodes with lumped element matching networks.

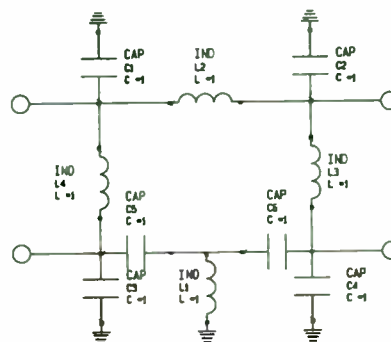


Figure 1. Lumped element equivalent for the ratrace coupler.

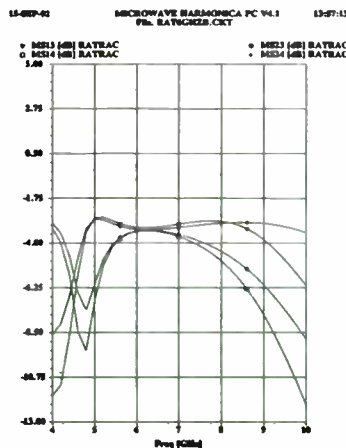


Figure 2a. Simulated coupling vs frequency for the ratrace coupler.

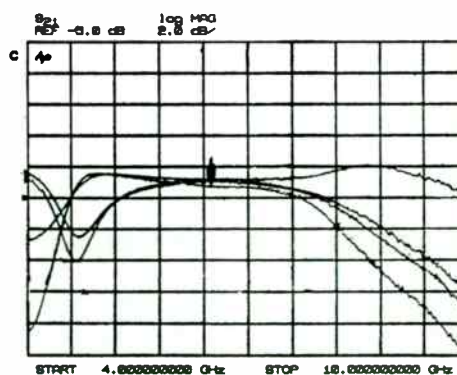


Figure 2b. Measured coupling vs frequency for the ratrace coupler.

Table 1- Statistics of Rain Attenuation on Uplink (Cleveland), Downlink (West Palm Beach), and the Over-all link through ACTS ($S_u = 45.2\text{dB}$, $S_d = 42.7\text{dB}$).

% time	$A_u(\text{dB})$	$A_d(\text{dB})$	$A(\text{dB})$
0.001	90.29	143.39	141.45
0.002	73.31	115.13	113.19
0.003	64.54	100.60	98.66
0.005	54.61	84.21	82.27
0.010	42.95	65.06	63.13
0.02	33.15	49.08	47.21
0.03	28.19	41.05	39.24
0.05	22.67	32.17	30.50
0.1	16.36	22.12	20.79
0.2	11.24	14.06	13.24
0.3	8.74	10.16	9.70
0.5	6.03	5.95	5.98
1.0	3.05	0.73	1.71

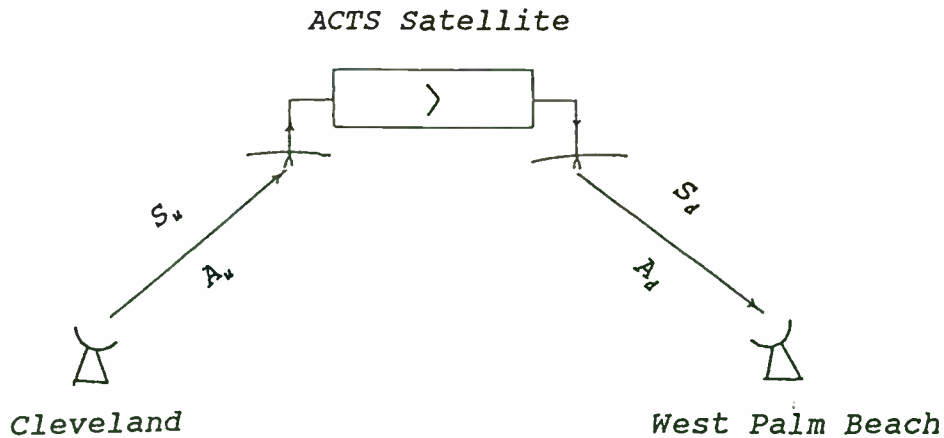


Figure 1. A typical ACTS satellite link.

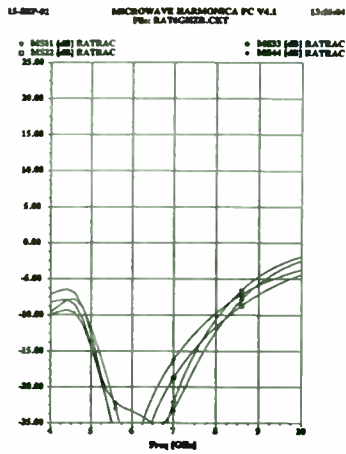


Figure 2c. Simulated return loss vs frequency for the ratrace coupler.

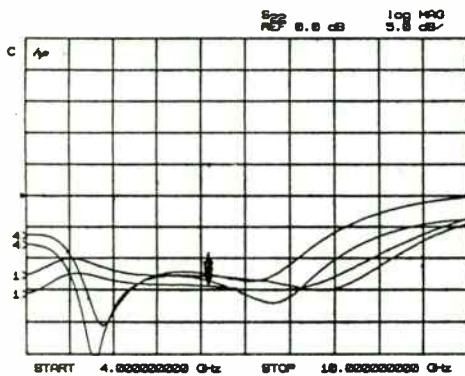


Figure 2d. Measured return loss vs frequency for the ratrace coupler.

The mixing products resulting from the two signals are passed through a three element filter to reject any unwanted signals which might be present. The simulated and measured performance of the mixer is shown in Figure 3. A schematic and a GMIC layout of the mixer are shown in Figure 4 and 5 respectively. A performance summary is presented in Table 1.

Frequency: RF 5 - 8 GHz
 LO 5 - 8 GHz
 IF 750 - 950MHz

Conversion Loss 8 dB

Isolation: RF-LO 18 dB
 RF-IF 45 dB
 LO-IF 45 dB

Table 1. Performance Summary.

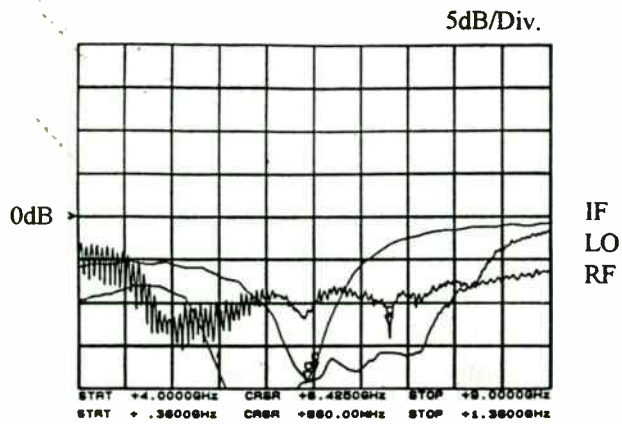


Figure 3a. Return loss of the ratrace mixer.

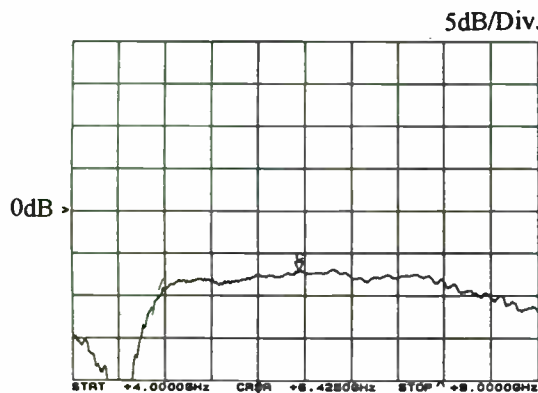


Figure 3b. Conversion loss of the ratrace mixer.

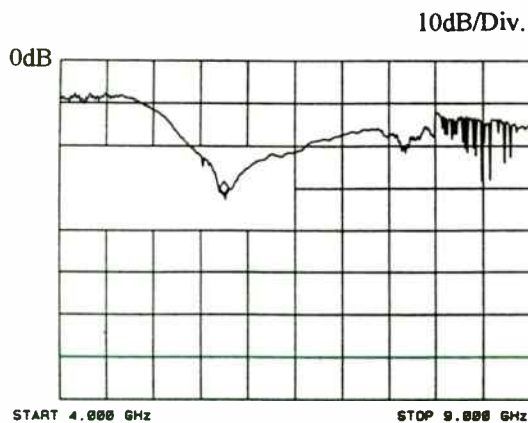


Figure 3c. Isolation of the ratrace mixer.

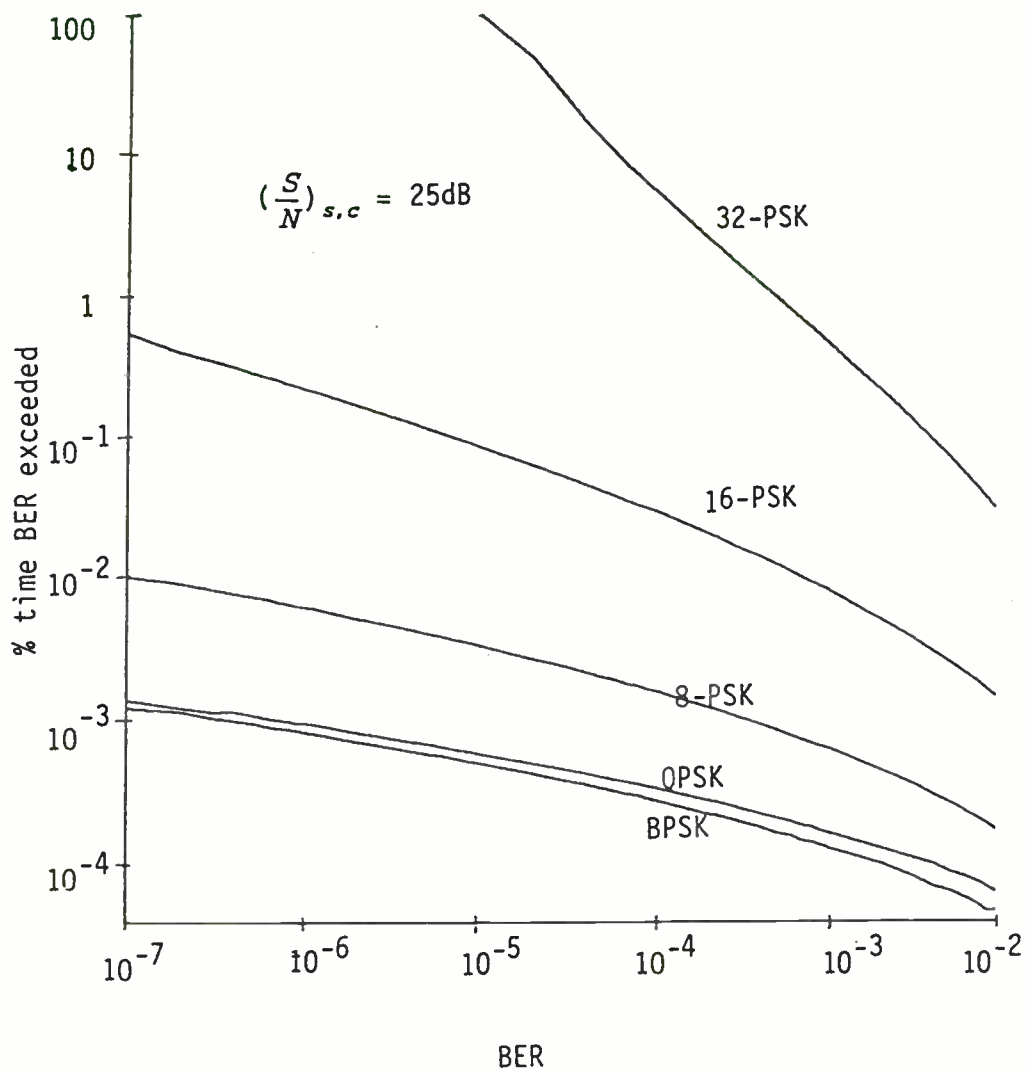


Figure 3. Complementary cdf of BER for uncoded M-PSK scheme in the presence of rain attenuation on the Cleveland - ACTS - W. Palm Beach link.

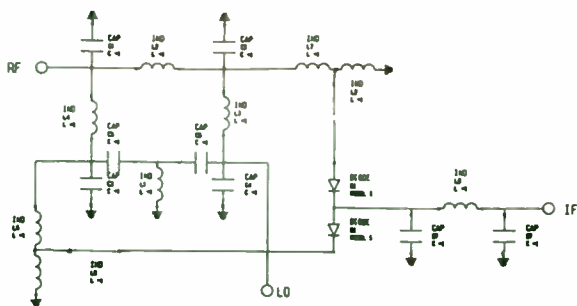


Figure 4. Schematic for the ratrace mixer.

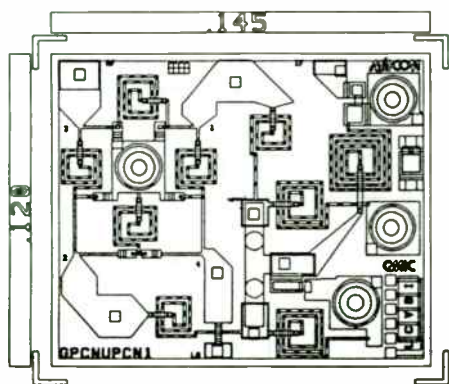


Figure 5. GMIC layout of the ratrace mixer.

Sub Harmonically Pumped Mixer

The sub harmonically pumped mixer was designed around an anti-parallel Schottky diode pair. Figure 6 shows the schematic for this mixer. Lumped element transformers provide matching from the diodes to the appropriate ports.

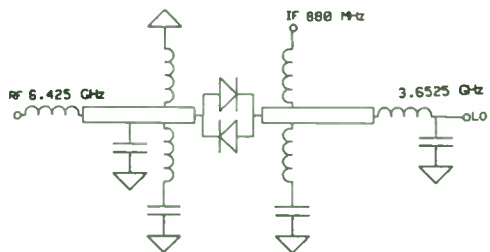


Figure 6. Sub harmonically pumped mixer schematic.

Shunt resonators are used on either side of the diode pair to provide AC ground for the LO and RF signals. The basic design approach is to deliver maximum RF and LO power to the diode pair with minimal leakage to the IF port. The power level of the LO signal typically needs to be about 10 dB greater than that of the RF signal. This insures that the diodes are driven by the LO signal and not the RF. At any given moment the LO signal is driving one of the two diodes in the pair to conduct while the other is being back biased at the same time. Since the LO signal is conducting for both the positive and negative halves of the wave form, the RF signal mixes with each half equally. The resulting IF signals are at the same frequency but are 180 degrees out of phase thereby canceling each other. The desired IF signal is a product of the RF signal mixing with twice the LO frequency.

The GMIC mask layout for the sub harmonically pumped mixer is shown in Figure 7. The measured performance of a fixtured mixer is shown in Figure 8. Return loss at the RF and IF ports are 8dB and 14dB respectively. The return loss of the LO port is 2.5 dB causing a large portion of the LO power to be reflected. The LO drive level has to be increased somewhat to compensate for this. The optimum power level required for the best conversion loss is +11 dBm. This is higher than originally expected, but can be explained by the poor return loss. The conversion loss of this mixer is 7.6 dB while the RF to IF isolation is 13 dB

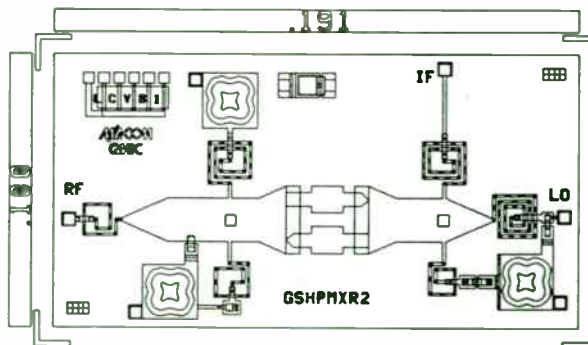


Figure 7. GMIC layout for the sub harmonically pumped mixer.

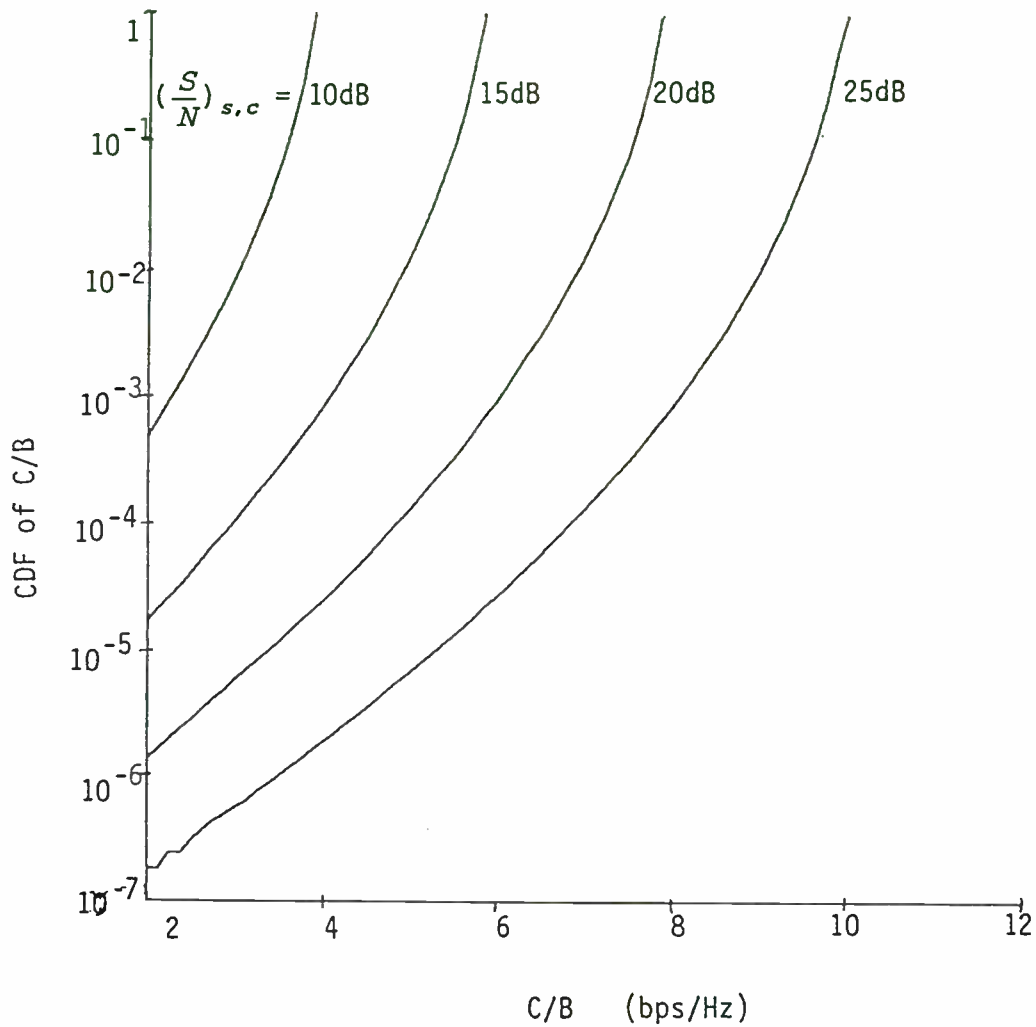


Figure 2. Cumulative distribution of channel capacity in the presence of rain attenuation on the Cleveland - ACTS - W. Palm Beach link.

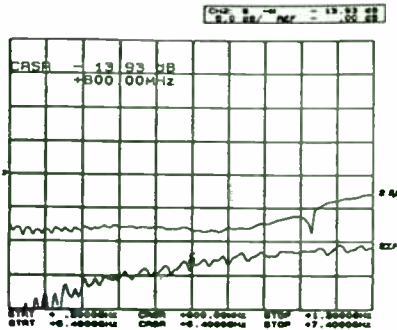


Figure 8. Return loss for the sub harmonically pumped mixer.

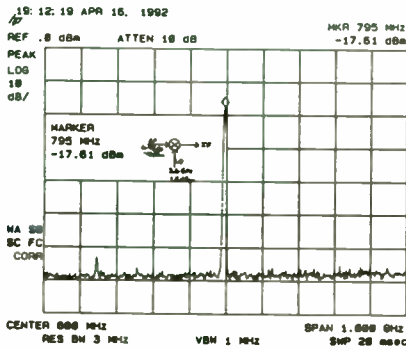


Figure 9. Conversion loss of the sub harmonically pumped mixer.

CONCLUSION

The mixers described in this paper are an example of the types of mixers which can be manufactured with the use of planar technology. This technology offers compact mixers at a very economical cost to the customer. Each of the two mixers has different performance characteristics and tradeoffs.

The ratrace mixer performance is consistent with the simulated results. It's 45% bandwidth makes it a useful circuit for a fairly wide range of applications. This circuit could also be designed and produced in other frequency ranges where the lumped element approach has advantages.

The sub harmonically pumped mixer also performs within the expected design parameters with the exception that the LO return loss resonates at a higher frequency than expected causing a poor return loss at the design frequency. This effect could be resolved with a mask revision to adjust the resonant frequency.

ACKNOWLEDGMENTS

The authors would like to thank all of the people involved in the design and fabrication of the mixers in this paper. Specifically, Scott Doyle and Renato Pantoja for their design expertise and assistance. Also, the GMIC processing and test groups for all their time and effort which they put into this work.

REFERENCES

- [1] Joseph Staudinger and Warren Seely, "An Octave Bandwidth 90 Degree Coupler Topology Suitable For MMIC's", Microwave Journal, November 1990, pp. 117-130.
- [2] Samuel J. Parisi, "A Lumped Element Rat Race Coupler", Applied Microwave, August/September 1989, pp. 84-93.
- [3] Stephen A. Maas, "Microwave Mixers", pp. 264-266, Artech House Inc., 1986.

HARDWARE VERIFICATION OF COMMUNICATION SYSTEM SIMULATIONS

Henry F. Helmken
Florida Atlantic University
500 NW 20th Street
Boca Raton, Florida 33431

Introduction

The Space Communications Technology Center (SCTC), a NASA sponsored Center for the Commercial Development of Space (CCDS), at Florida Atlantic University is developing systems for digital satellite communication. The increasing cost of fabricating hardware prototypes is placing greater emphasis on computer simulations of proposed systems. Signal Processing Workshop (SPW) software from COMDISCO is being used to generate baseband signal files of proposed hardware designs. These files are downloaded to an arbitrary waveform generator which generates real-time baseband signals that can be transmitted over a satellite link. The received satellite signal is down-converted to baseband and digitized for subsequent analysis by SPW. This methodology permits flexibility and speed in system design and performance evaluation.

Mission of SCTC

The Centers for the Commercial Development of Space (CCDS) are non-profit consortia of industry, academia and government that conduct space-based, high technology R & D in areas such as communications, materials processing, biotechnology, remote sensing, automation and robotics, space power and space propulsion. This program was created by NASA in 1985 to maximize U.S. industry leadership in commercial space related activities.

In 1991, a CCDS dedicated to satellite communications was established and headquartered at Florida Atlantic University. Associated with the

center are the University of Florida, the University of South Florida, the University of Central Florida and several industrial partners i.e. Harris Corp., Motorola Inc., Cablelabs, Honeywell and Electromagnetic Sciences. The specific mission of this CCDS, the Space Communications Technology Center (SCTC), is to assist U.S. industry in developing the use of digital techniques for transmitting video, audio and data to earth via satellite.

One specific focus of center investigation is the area of modulation and propagation. The goal is to develop propagation models capable of spanning satellite communication links from L-band to Ka-band and use these models for "hardware-in-the-loop" system studies. At Ka band, a series of experiments are planned using the Advanced Communications Technology Satellite (ACTS) satellite. Supporting these experiments will be one of the seven NASA ACTS propagation terminals that has been established at the University of South Florida and a transportable receive only terminal.

System Modeling

Cost of developing prototypes of potential communication systems can be very expensive and time consuming. An alternate approach to an all hardware prototype is to software model, at baseband, the transmitter and receiver characteristics and use general purpose hardware to transmit and receive the modeled baseband signals through a satellite system.

Figure 1 illustrates an implementation of this

GMIC Interdigital Filters for Microwave Applications by Holly A. LaFerrara M/A-COM, Inc.

Abstract -- The design of interdigital filters utilizing Glass Microwave Integrated Circuitry is presented. The advantages and disadvantages of the interdigital structure are examined. Four interdigital filter designs are discussed, and comparisons are made between predicted results and measured data. Various applications for these filters are investigated. The issues of high-volume production and integration into larger modules are also addressed.

INTRODUCTION

As microwave applications such as cellular telephones, global positioning systems, and bar code readers develop there is more need for small, repeatable, low-cost microwave circuits than ever before. Filters are an essential component in each of these systems. Glass Microwave Integrated Circuits (GMIC) provide an excellent medium for the production of passive filters. The high yields for GMIC filters, along with the ability to combine discrete FETs, MMICs, or other GMIC circuits onto a single piece of substrate provide a path toward low-cost, high-volume production. The interdigital filters discussed in this paper were designed for use in a 6GHz frequency converter.

HIGH-VOLUME PRODUCTION

A GMIC wafer can contain a single circuit that has been stepped and repeated hundreds of times. This allows

for mass production once a design is established. Also, several circuits that are intended to form one module can be masked on the same wafer. This allows for testing each component of the module as well as having parts handy to build and test an entire module at once. These filters were included on GMIC wafers containing other circuitry such as amplifiers and multipliers. By utilizing VAP (Volume Automated Processing) techniques and on-wafer testing, the filters can be both tested and tuned on wafer. This eliminates the losses incurred during fixturing and gives a better picture of the actual filter performance.

Filters done on GMIC are ideal candidates for integration into larger modules. It is possible to fabricate entire modules such as T/R modules on a single piece of substrate, because the filters can be attached to other components.

DESIGN ADVANTAGES/DISADVANTAGES

There are several common structures used in the design of microwave filters. For filters designed in microstrip, special care must be taken when choosing a design that gives both low loss and good stopband rejection. Several filter structures were examined, but many were simply too large for use in every location where a filter was needed. Others did not give results that were predictable enough to use in high-volume production. In the trade-off between performance and size, there are several advantages to using GMIC interdigital filters. Figures 1a through 1d show the GMIC CAD layouts of the four interdigital filters used in this

process. The Signal Processing Software (SPW) from COMDISCO has been selected for both baseband modeling and analysis software. The current host is a SUN IPX SPARC workstation. Using the block Diagram Editor (BDE) of SPW, a representative transmitting site comprising a data source, an encoding scheme, carrier modulation type, bandpass filtering, Doppler, output power, and transmission plan (i.e. TDMA, CDMA etc.) can be modeled at baseband. Replication of a single transmission site can be used to model a multiple transmitter scenario.

For the selected transmitting scenario, the SPW software is used to generate integer Inphase and Quadrature (I & Q) baseband data files. These baseband waveforms are oversampled, typically 4 to 8 times Nyquist. The I & Q data sets are downloaded via IEEE-488 bus into 2 channels of an Arbitrary Waveform Generator (AWG). The AWG clock is set to produce I & Q baseband signals at the required real time rates. A typical AWG such as the Tektronix 2020 has an internal sampling clock extending to 250 MHz and thus can produce waveforms with a maximum bandwidth of 20 MHz. Each channel has a storage capacity of 256k 12 bit words which can be operated in a continuously looping mode. For example, a CDMA system with a 1 Mhz chip rate, sampled at a 8 Mhz rate, produces a continuously looping 32 millisecc baseband I & Q data stream.

Both channels of the AWG are clocked synchronously at the real time rate determined by the bit or chip rate of interest. Each channel is connected to the respective I & Q inputs of a vector modulator which generates the desired complex transmission signal at a specified IF frequency (typically 70 MHz). The IF signal is upconverted and transmitted to the satellite. The received signal undergoes the reverse process i.e. downconverted to IF and vectored demodulated into baseband I & Q components. Each component is sampled via an A/D converter and stored as raw I & Q baseband data for off line analysis.

For the analysis, the data is loaded back into the

computer and SPW software is used to model a candidate receiver design which will have to acquire and track the carrier, remove Doppler, and recover the original bit stream. Storing raw I & Q baseband data allows different receiver designs and analysis methods to be applied to the same data set, permitting realistic comparisons (e.g. generate Bit Error Rate (BER) curves) to be made on data acquired under different propagation conditions.

ACTS Satellite

The Advanced Communications Technology Satellite was launched into orbit on August 1, 1993 and achieved operational status on August 1993.

ACTS operates in the Ka band with downlink frequencies from 19.2 to 20.2 GHz and uplink frequencies from 29.1 to 30.0 GHz. These frequency bands are high susceptible to rain fades and hence, for commercial use, robust transmissions schemes will have to be developed. In the Microwave Switch Matrix (MSM) mode, the satellite operates in a wideband "bent pipe" mode and thus suitable for testing a variety of transmission schemes.

ACTS Demonstration Plan

The proposed scheme shown in Figure 1 is now under development and will be tested using ACTS in the MSM mode. Opportunities will also be sought on Low Earth Orbiting (LEO) transponder satellites. Software models of both transmitter and receiver designs and transmission schemes (TDMA, CDMA, etc.) have been developed I & Q baseband data files have been generated by both SPW and special communication software code. These files have been successfully down-loaded to a Tektronix 2020 AWG and coupled to an HP 8782B Vector Modulator and IF performance verified via a Vector demodulator.

The main area of current effort is selecting and testing hardware for an IQ vector demodulator, interfacing I & Q data streams to A/D converters and storing several Gbytes of data at a high sampling rate. The choice for the A/D converter is the Analog

application.

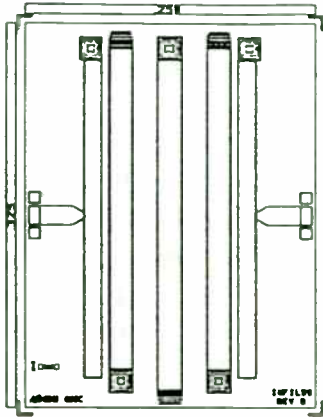


Figure 1a. Layout of GMIC interdigital filter for the transmit chain.

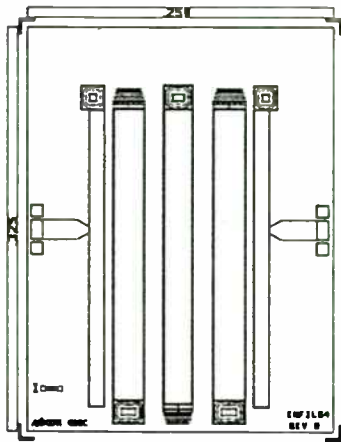


Figure 1b. Layout of GMIC interdigital filter for the receive chain.

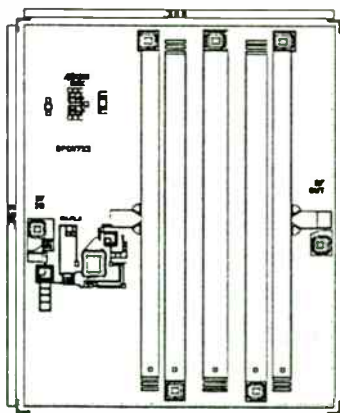


Figure 1c. Layout of GMIC multiplier/filter combination for transmit chain.

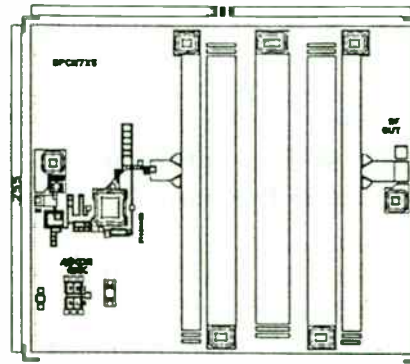


Figure 1d. Layout of GMIC multiplier/filter combination for receive chain

The interdigital structure is the most compact of all distributed filter designs. This makes the interdigital design an outstanding candidate for use in situations where space is at a premium. This design also possesses excellent rejection of the filter's second harmonic. Most filters will resonate at the second harmonic, but the interdigital structure does not resonate until the third harmonic. Thus, a second passband will still appear, but it will be very far out and spurious responses close to the fundamental frequency will be eliminated.

Another advantage of the interdigital design is the ability to vary the impedance of the structure by varying the location of the tap points on the input and output of the filter. By varying the tap point of either side or both sides of the filter, the need for an impedance transformer in a non-50 ohm system is eliminated.

The interdigital filter also possesses low insertion loss. The insertion loss tends to rise with

Devices AD872, a 12 bit A/D capable of running at 10 MSPS. For the data recording system, the goal is to have the capability of storing 10 minutes of continuous data at a 10 MBytes/sec sampling rate. The initial storage device will be a video tape recorder, a Panasonic D3 unit, which can accept digital data in NTSC timing format. An alternate high data rate storage device is the Storage Concepts Model 71 RAID system. This latter system employs parallel transfer disk technology and can accommodate 5 GByte storage at continuous transfer rate up to 20 MByte/sec. The probable host for this latter system will be a VME based controller interfaced to a SUN Sparc Workstation. Data will be transferred and stored on 5 Gbyte tape cartridges for subsequent analysis.

Conclusions

As part of the effort to help U.S. industry develop competitive digital satellite system, SCTC is developing a combination software-hardware concept for testing new communication systems. The concept

relies on the capabilities of COMDISCO SPW software to model and generate baseband signals of complex transmission scenarios and analyze the received raw baseband I & Q data.

Test baseband I & Q data files have been generated by SPW models and successfully downloaded into an Tektronix 2020 AWG. The AWG has been run at a real time data bit rate of 1 Mb/s, (8 Mhz sampling rate) into a vector modulator generating an IF signal at 70 MHz. This latter signal is available for upconversion to a satellite frequency. The received baseband signal will be vector demodulated and raw baseband data stored via a 12 bit A/D. Data recording will be either via a Panasonic D3 video tape recorder or a Storage Concepts parallel disk array. SPW receiver designs are under development to acquire and track the signal and recover the original bit stream for BER analysis.

References

Advanced Communications Technology (ACTS) Experiments Application Guide. NASA TM-100265 (January, 1990)

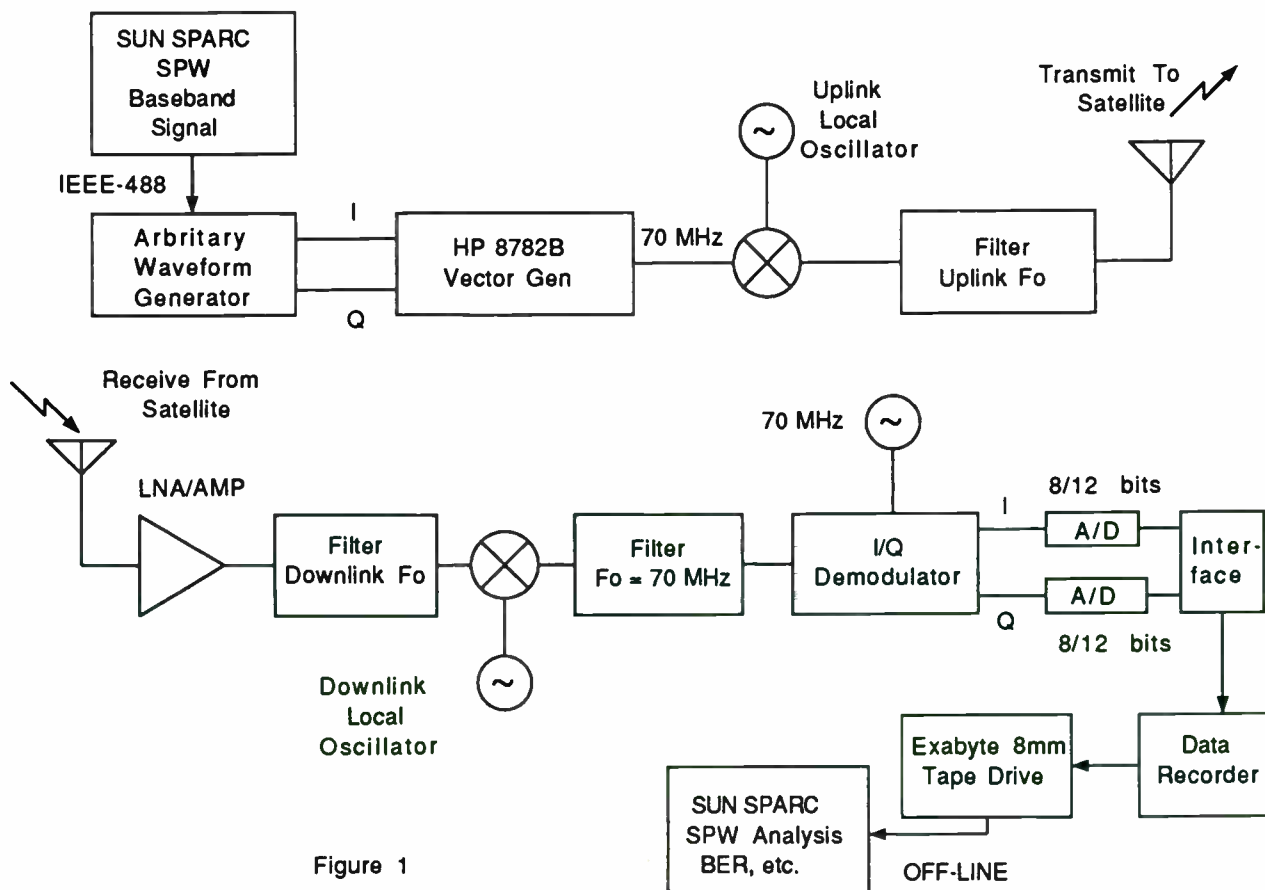


Figure 1

decreasing bandwidth; however, with careful modelling an optimal structure can be found having an insertion loss of 2.4 dB to 2.6 dB in a fixture. When on-wafer probing techniques are used, the interdigital filter will have losses of 1.7dB to 2 dB due to elimination of losses incurred during fixturing.

One disadvantage of interdigital filters is that they are thought to be lossy due to the effects of dispersion and coupling between lines. For designs having many resonators, loss can be a problem, but for designs with few resonators (here a three-resonator design was used) the insertion loss is comparable to that of other filter structures.

An apparent disadvantage lies in the grounding of alternate ends of the lines. In cases where the grounds are not well characterized, this could be a problem; however, with GMIC, the vias are well characterized and very repeatable. The via element can be modelled as a series resistor and inductor to ground, and can be included in a simulation to give a more accurate response than an ideal ground. This is especially important for filters needing very low loss, because the resistance of the via hole must be accounted for in order to have an accurate model.

Another disadvantage lies of the interdigital structure appears when trying to accurately predict the higher-order coupling effects between lines. Most CAD packages do not have accurate models for more than three coupled line sections. This presents a problem due to the fact that even a basic, three-resonator interdigital filter contains five coupled lines when you

include the input and output coupling sections. Ideally, a full electromagnetic simulation should be done to thoroughly understand these effects; however, software availability and time constraints prevented a full-wave analysis. Sonnet¹ simulations were done on some of the crucial junctions, and then the rest of the frequency converter was structured so that there was minimal interference from other chips.

For these filter designs, the Super Compact² software package was used to analyze the structure. The Super Compact program contains a multiple-coupled line model which will analyze up to ten coupled line segments. This model proved to be accurate in its predictions of the filter performances.

DESIGN AND ANALYSIS

The initial design equations³ for interdigital filters of narrow bandwidth are used in conjunction with mapping equations⁴ to select a low-pass prototype filter. A low-pass-to-band-pass transformation⁵ is then used to estimate the attenuation characteristics of the interdigital filter. The design equations are as follows:

$$\theta_1 = \pi/2 * (1-\pi/2)$$

$$J_{01}/Y_A = 1/\sqrt{(g_0 g_1 \omega_1')},$$

$$J_{k,k+1} \Big|_{k=1 \text{ to } n-1} = 1/((\omega_1') * \sqrt{(g_k g_{k+1})})$$

$$J_{n,n+1}/Y_A = 1/\sqrt{g_n g_{n+1} \omega_1'}$$

GFO Water Vapor Radiometer

Muhammad A. Malik, P.E.
E-SYSTEMS, Inc., ECI Division
1501 72nd Street North,
P.O. Box 12248
St. Petersburg, FL 33733-2248
Phone: 813-381-2000 ext. 3419
Fax: 813-381-2000 ext. 4810

ABSTRACT

GEOSAT Follow-On (GFO) is the latest Navy altimetry satellite for determining sea surface topography. The required precision is about 3 centimeters in a range measurement of 800 kilometers. Various error sources have to be accounted for to achieve this precision. One error source is the variation of the RF propagation velocity through the atmosphere depending on the moisture content. A total power Ka-band radiometer is provided on-board for atmospheric water vapor delay correction, sharing a broad-band antenna with the Ku-band altimeter.

The radiometer will measure the radiometric brightness temperature of the earth at two frequencies, 22 and 37 GHz, in the approximate footprint of the altimeter return signal. Due to the low level of signal measured, the radiometer receiver design pays special attention to gain stability, and the supply voltage stability. During the radiometer operation, regular calibrations are made using hot and cold sources to maintain the output accuracy. The antenna is required to have very high main beam efficiency and very low sidelobes.

A description of the GFO radiometer and antenna, including the system requirements, correction algorithms and performance projections, is presented in this paper.

INTRODUCTION

Satellite altimetry is a unique tool for understanding and predicting changes in the ocean which have a significant effect on the climate and the life on earth, including the ocean circulation, sea-level and the polar ice sheet volume. There are three major scientific objectives for satellite altimetry [1]:

- * Measure the global ocean circulation
- * Observe the mean sea-level change; and
- * Monitor the polar ice sheet volume

A number of altimeter-carrying satellites have been launched or are being planned as shown in Figure 1.

The current satellite altimeter program, GEOSAT Follow-on (GFO), will provide operational, continuous, global altimeter data on mesoscale sea-surface topographic fronts, eddies, and other oceanographic phenomena to meet U.S. Navy requirements [2].

Under the management of the Space and Naval Warfare Systems Command (SPAWAR) of the Department of the Navy, the GFO program was awarded in 1992 with an anticipated launch in the 1995-1996 time frame, and a specified 8 year mission life.

Ball Corporation, Space and Systems Engineering Division (BSSSED), located in Boulder, Colorado, is the prime contractor for GFO, responsible for the payload, spacecraft and launch vehicle, as well as all required ground system modifications. As Ball's team member, E-Systems, ECI Division (ECI), located in St. Petersburg, Florida, is responsible for the Radar Altimeter and other payload systems engineering services. AIL Systems, located in Deer Park, New York, is developing the radiometer hardware and Ball Communications Systems Division, located in Broomfield, Colorado is responsible for the antenna.

GFO PAYLOAD

The GEOSAT Follow On (GFO) Radar Altimeter is a 13.5 GHz, nadir looking, pulse compression radar [3]. It is designed to provide all-weather global monitoring of sea surface wave height, radar cross-section, and range between itself and its nadir point on the sea surface with great precision.

The variability of atmospheric water vapor column abundance produces an unpredictable variation in altimeter range measurements which can be as large as tens of centimeters, and which must be accounted for in order to achieve meaningful results [4]. This variability cannot be accurately dealt with by models. An on-board nadir-looking radiometer is the most viable approach to accurately measure the tropospheric range delay.

$$N_{k,k+1} \Big|_{k=1 \text{ to } n-1} = \sqrt{((J_{k,k+1}/Y_A)^2 + (\tan^2 \theta_1)/4)}$$

$$M_1 = Y_A((J_{01}/Y_A)\sqrt{h} + 1)$$

$$M_n = Y_A((J_{n,n+1}/Y_A)\sqrt{h} + 1)$$

where h is a dimensionless admittance scale factor to be specified arbitrarily so as to give a convenient admittance level in the filter.

For this application, four three-resonator interdigital filter designs were selected. The three-resonator structure was chosen for its small size and low insertion loss characteristics. After the initial parameters were generated from the equations, the design was simulated using Super Compact PC. The resonator lengths, widths, and spacings were then optimized to obtain the desired performance. Figures 2, 3, 4, and 5 provide comparisons between the simulated and measured data for the four interdigital filters that were designed.

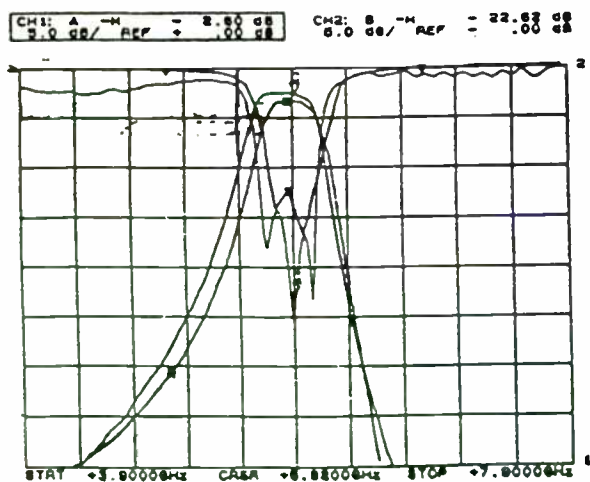


Figure 2. Comparison between simulated and measured data for GMIC interdigital filter at f=5.9 GHz.

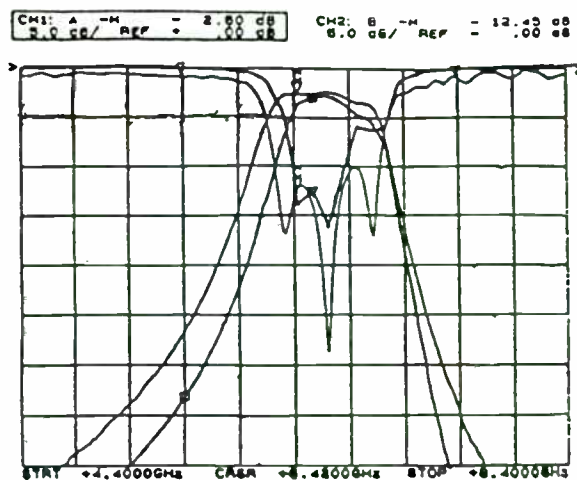


Figure 3. Comparison between simulated and measured data for GMIC interdigital filter at f=6.4 GHz.

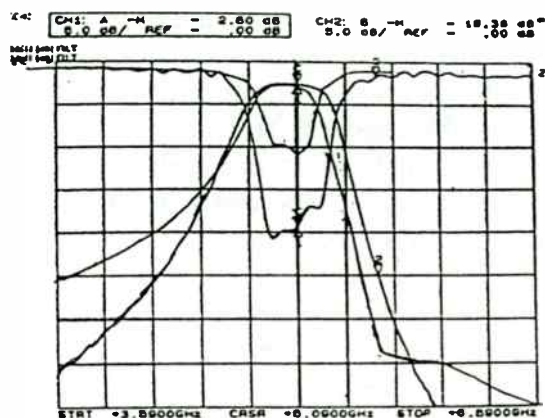


Figure 4. Comparison between simulated and measured data for GMIC interdigital filter at f=5 GHz.

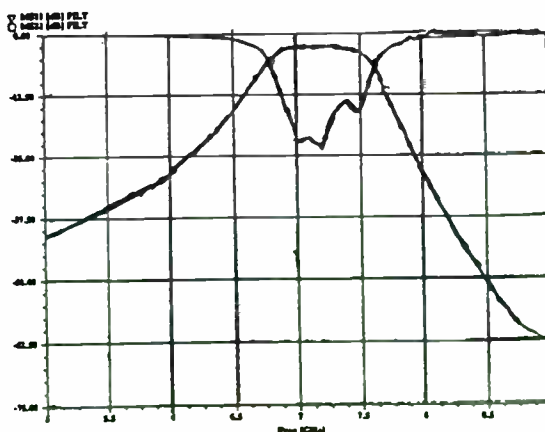
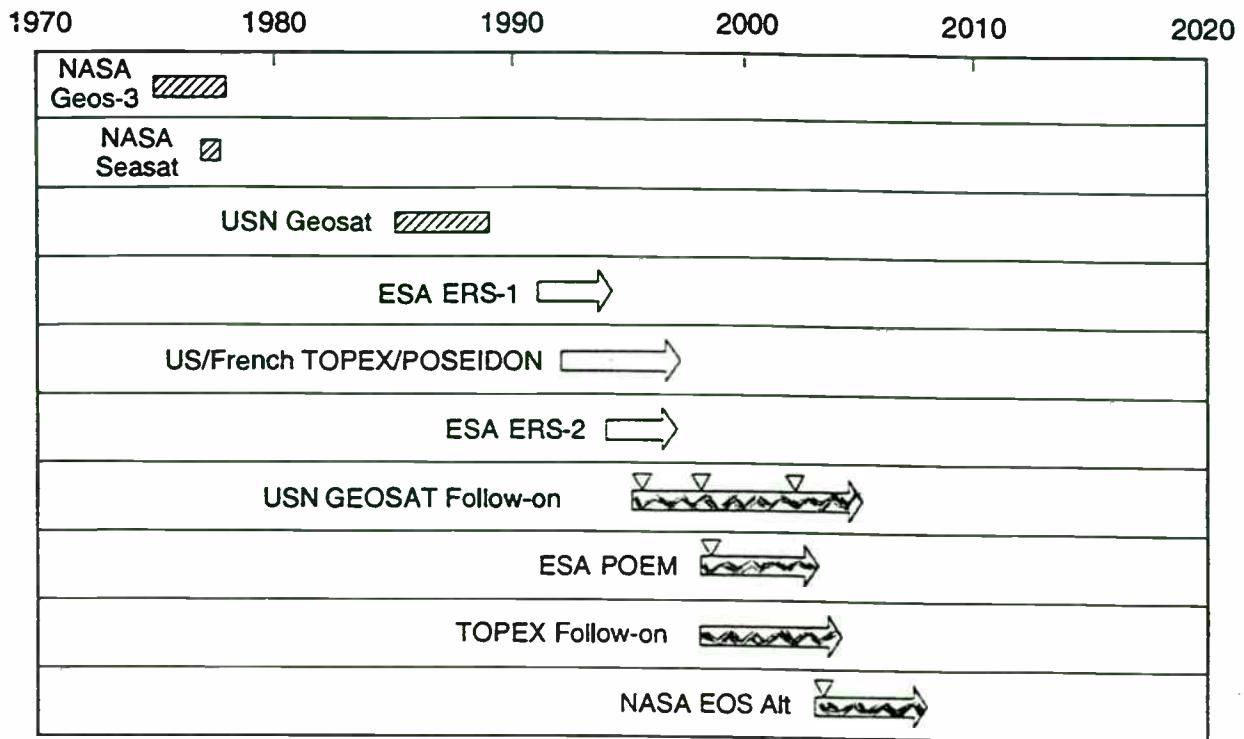


Figure 5. Predicted data for GMIC interdigital filter at f=7.3 GHz.






-  Completed Mission
-  Supported (In space or under construction)
-  Tentative (Proposed or in early stages of development)

Figure 1. Altimetry Spacecraft: 1970-2020

Excellent results were achieved for these filters. The measured data corresponds well to the software's predictions, and the insertion loss is approximately 2.6dB in a fixture. The filter passband can easily be shifted to achieve better high side or low side rejection. The structure can also be tuned to a slightly lower insertion loss of 2.4dB by adjusting the length of the middle resonator if a lower loss filter is needed.

CONCLUSION

GMIC interdigital filters are excellent for applications where highly reliable, predictable, and small filters are needed. Through careful modelling of the coupled-line structure, an optimal design may be obtained. With the addition of on-wafer probing capability, these filters are excellent candidates for high-volume production using VAP techniques.

ACKNOWLEDGEMENT

The author wishes to thank Paul Schwab, Tim Murphy, and Scott Doyle for their guidance and advice. Thanks also go to Bill Foley and Rick Gibson for help with fixturing and testing these designs.

REFERENCES

- [1] Sonnet Software, Inc., Liverpool, NY, Sonnet is a registered trademark.
- [2] Compact Software, Patterson, NJ, Super Compact is a registered trademark.
- [3] G.L.Matthei, L.Young, and E.M.T.Jones, *Microwave Filters, Impedance-Matching Networks, and Coupling Structures*, p. 617. New York:

McGraw-Hill, 1964.

[4] G.L.Matthei, L.Young, and E.M.T.Jones, pp. 617-627.

[5] G.L.Matthei, L.Young, and E.M.T.Jones, pp. 617-627.

The GFO Water Vapor Radiometer (WVR) is a two frequency, 22 GHz and 37 GHz, total power radiometer to measure the brightness temperature of the earth. Hot and cold calibrations are regularly performed to maintain the measurement accuracy. The radiometer outputs digital data, which is telemetered to the ground processing center.

The GFO altimeter and radiometer share a tri-band, nadir looking, offset-fed parabolic antenna. This antenna is designed to have 97% main beam efficiency and very low side lobes.

RADIOMETER DESIGN FUNDAMENTALS

The theory of microwave radiometry is described in the literature [5],[6]. In essence, the received power at the radiometer is proportional to the radiation intensity, which is related to the water vapor content. In the microwave region, the Rayleigh-Jeans form of Planck's law can be used to relate the power received to the apparent temperature in the following direct linear form:

$$P = \frac{1}{2} A \int \int_{4\pi} \frac{2k}{\lambda^2} T(\theta, \phi) \Delta f F(\theta, \phi) d\Omega$$

where P = Power received
 A = Receiving aperture
 k = Boltzmann's constant
 λ = Wavelength
 T = Apparent temperature
 Δf = Bandwidth
 F = Normalized radiation pattern
 θ = Azimuth angle
 φ = Elevation angle
 dΩ = Differential solid angle

As indicated by the above equation, the radiometric temperature is obtained by measuring the incident power with a well calibrated antenna and receiver.

There are several tradeoffs involved at the system level to satisfy the mission requirements with a minimum size, weight and cost package. These include the frequency selection, radiometer type, number of operating channels, and RF bandwidth.

The radiometric temperature of the atmosphere with respect to frequency, as shown in figure 2 [7], can be exploited for different purposes. The water vapor spectral line centered at 22.2 GHz is suitable for studying properties that depend on the total amount of water vapor present in the atmosphere, and is typically used for radiometry. The liquid water also emits strong radiations. Separate measurements are needed at two

frequencies to properly determine the water vapor and the liquid water. For this reason, the frequencies of 22.2 GHz and 37 GHz were chosen.

There are two basic types of radiometers; total power and Dicke, as shown in Figures 3 and 4, respectively. Both of them produce an output voltage proportional to the received signal power. The main difference between them is the Dicke switch which alternates the receiver connection between the antenna and the calibration reference to minimize the time interval available for gain fluctuation.

To appreciate the importance of gain fluctuation, consider a case of antenna temperature of 300 K, a bandwidth of 100 MHz and a measurement interval of one second. For a total power radiometer, the measurement uncertainty (proportional to $1/\sqrt{Bt}$, where B is the signal bandwidth and t is the measurement interval) in this case is 0.03 K or one part in 10^4 of the total noise power. The stability of the radiometer would have to be held to better than one part in 10^4 , over a period of one second, so that gain fluctuations do not dominate the sensitivity of the instrument. Historically, Dicke radiometers have been used to circumvent this problem. If the switching time between calibrations is much smaller than the time period of the gain fluctuations, the effect of gain fluctuations becomes almost negligible.

The component technology is advancing, however, such that with a careful circuit design, the receiver gain can be stabilized enough to enable the use of a total power radiometer. The elimination of the Dicke switch results in size and cost reduction. Another consideration is the comparatively higher measurement uncertainty of the Dicke radiometer, which is proportional to $2/\sqrt{Bt}$ because of the time evenly divided between the antenna and the calibration reference. The total power radiometer concept was chosen for GFO because of better measurement accuracy and design economy.

The number of radiometer frequencies or channels is another important consideration. More channels would provide information in different areas of the spectrum about the atmospheric contents but will increase the size and weight also. For the GFO, a two-frequency design was chosen because it satisfied the water content measurement requirements in a compact package.

As shown above, greater RF bandwidth would increase the measurement accuracy, but it can adversely impact the noise figure. Electromagnetic interference (EMI) is another important consideration. For the GFO, the RF bandwidth was specified as 220 MHz for

Dual-Use Technologies

Session Chairperson: David Sprague, *The Strategy Group* (Martinez, CA)

Affordable Intelligence/Direction-Finding Systems for Military and Civil Enforcement Missions, Dr. Nicholas Cianos, Delfin Systems (Santa Clara, CA).....N/A

Microwave Instrumentation: In Transition from All Bells and Whistles to Just Enough for the Job, John Minck, Hewlett-Packard Co. (Palo Alto, CA).....324

Applications of Microwave Power Tubes, Glen Hoffman, Varian Microwave Tube Products (Palo Alto, CA).....N/A

Affordable MMIC Power Amplifier for 2.4 and 5.8 GHz Spread Spectrum Applications, T. Apel, R. Bhatia, H. Sun, and S. Ludvik,* Teledyne Microwave (Mountain View, CA).....327

Affordable Dual-Use Direction-Finding (DF) Receiver, Toshikazu Tsukii, Raytheon Co., Electromagnetic Systems Division (Goleta, CA).....N/A

**Paper presented by Ratan Bhatia.*

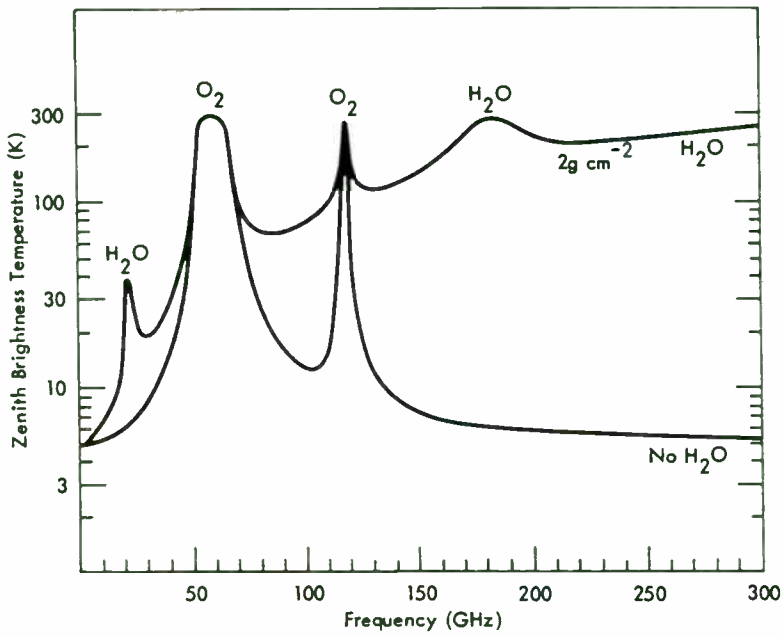


Figure 2. Sky radiometric temperature in the upward zenith direction

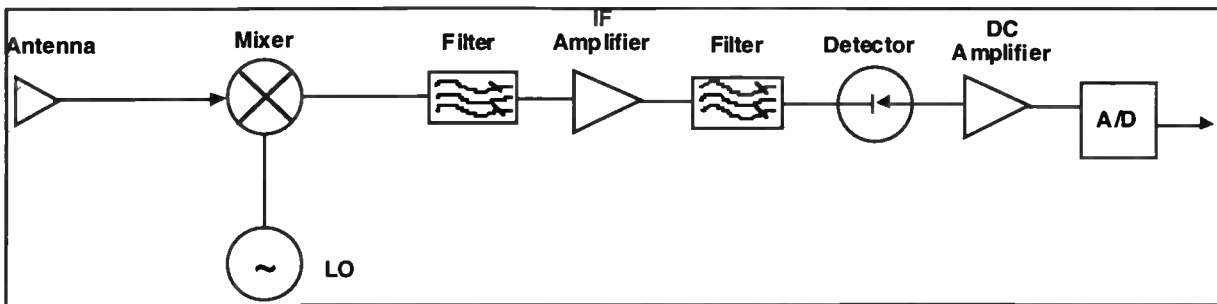


Figure 3. Total Power Radiometer

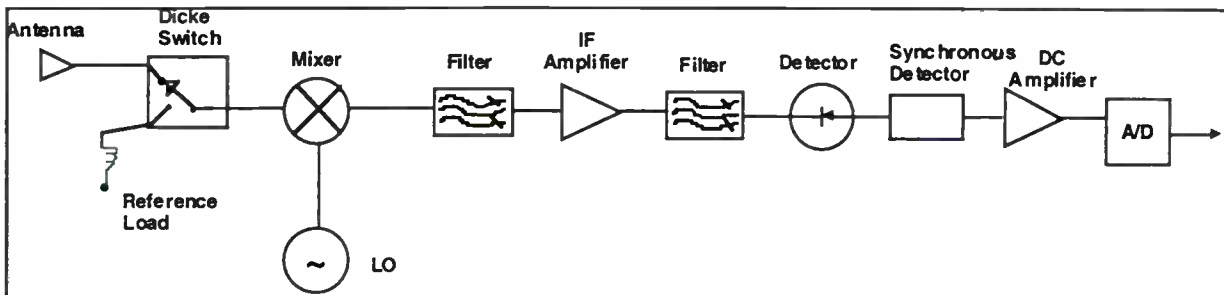


Figure 4. Dicke Radiometer

An Evolving Strategy for Dual-Use Microwave Instrumentation

John Minck
Stanford Park Division
Hewlett-Packard Co.

Presented at
Wireless Symposium
and Exhibition



Outline

- The 1950-1990 microwave era
- The historical bias toward DOD
- The evolving impact on MW product strategies
- Some observations & examples for 1990-onward

The 1950-1990 Microwave Era

- The post-WWII decades
- Commercial microwave systems technology lagged Aerospace
 - Communications, radar, navigation
- Influence of strategic weapons race (Korean/Vietnam conflicts)
- Commercial systems became somewhat dependent on DOD technologies and funding
- Instrumentation tended to lag system test needs

Slide 2



Today I hope to offer a few comments and observations about the evolution of microwave instrumentation product strategies. Certainly, many if not most people would acknowledge that the "golden age" of MW systems and instrumentation occurred during the decades of the '50s to '90s.

The microwave business situation outlook today is partly the result of the DOD dominance through the last 40 years. And the big surge of the '80s further warped the balance. I'll try and emphasize what we will need to do to succeed in the decade of the '90s and onward.

Slide 3



Looking backward doesn't help much with business, other than to realize how the "easy" microwave years owed a lot to the pervasive DOD funding windfalls of those years. Component technology, system capabilities, computer and communication breakthroughs pioneered by the military sector helped in the emerging commercial sectors.

While MW system technology drivers would come from both the DOD and commercial sector, DOD tended to dominate, if for no other reason than its considerable funding power. Given that model, the instrument manufacturers usually found that product definitions which favored DOD requirements were virtually always successful.

At the same time, many of the instrument introductions tended to lag the system requirements, partly because the designers wanted to build the highest-performance they could manage. "Good enough" wasn't as likely to hit a product home run as the highest stability or agility.

both the 22 GHz and 37 GHz channels to satisfy the sensitivity and EMI requirements.

RADIOMETER DESCRIPTION

The GFO WVR is a two-frequency, linearly polarized, total power, double sideband, super-heterodyne radiometer. The operating frequencies were selected on the basis of the best path delay error performance and to minimize cost, size and weight. Path delay calculation is based on the emission from atmospheric water vapor which is peaked around 22 GHz. The signal level at 37 GHz is used to indicate liquid water in clouds and rain columns due to microwave absorption and to support the overall water vapor measurement.

The WVR requirements flowdown is shown in Figures 5 and 6. The overall performance requirement is to provide path delay corrections to an accuracy of 1.9 centimeters over the temperature range on-orbit and 8 year life time. These requirements have been related to the system observables and translated into RF subsystem design parameters and component specifications.

WVR Design

The WVR functions to receive the RF energy, downconvert it to baseband, and detect and digitize it in a redundant design for reliability. WVR also includes thermal sensors at selected locations to measure physical temperatures and correct the antenna brightness temperature.

The WVR operating modes are standby, normal and calibrate. It enters the normal state after power-up is complete. Normal mode outputs digital data in a 7-second frame format that includes: brightness temperature measurements at a 2 Hz rate synchronized to the space craft time reference, calibration measurements, physical temperature sensor data, and WVR status and telemetry information. In the calibrate mode, brightness temperature measurements are halted and continuous calibration of the WVR is performed. The WVR can be commanded to the normal or calibrate modes via a data control word from the space craft IAP (integrated avionics processor). All analog outputs are multiplexed and converted to digital data before being output.

WVR Receiver

The WVR receiver, as shown in the block diagram, Figure 7, accepts the RF energy from the antenna at two frequencies, 22 GHz and 37 GHz, each having a prime and a redundant channel for reliability.

Switching between the antenna and the two calibration sources is provided by internally latched ferrite switches with greater than 30 dB isolation. The receiver front-end incorporates a double-sideband mixer. The receiver gain fluctuations are minimized by operating well below the device 1 dB compression point and incorporating amplifiers and detectors with low 1/f noise. DC power regulated to 5% level is supplied to the radiometer where it is further regulated to achieve an overall line regulation of 0.1%.

The receiver design includes pre-detection channel bandwidths of 110 MHz at both 22 GHz and 37 GHz. The local oscillators are designed to minimize the frequency drift. The dynamic range is designed to operate over a brightness temperature range of 3 K to 350 K with a system noise temperature due to the receiver electronics of 640 K at 22 GHz and 670 K at 37 GHz. An AGC circuit with a long time constant (minutes) keeps the operating point of the detector constant over long-term gain/temperature changes. Potential frequency interference below waveguide cut-off, such as altimeter frequency of 13.5 GHz, is attenuated to negligible levels before it impacts the RF front-end components. Final filtering occurs in the highly selective low pass IF filter which provides greater than 80 dB attenuation to out-of-band signals. The integration interval is set at 0.5 second, resulting in a 2 Hz output rate. The output voltage is digitized and provided for down link telemetry.

The radiometer weighs 20 pounds, occupies 600 in³, and dissipates 18 watts.

Cold Horn Assembly

The cold source assembly consists of a 22 GHz and a 37 GHz cold horn, interconnecting waveguide, and redundant thermal sensors that monitor the temperature of each horn and associated waveguide. The cold horns are linearly polarized corrugated horns with approximately 62.5 degree half-power beamwidths. They have maximum sidelobes of -25 dB, a loss of 0.04 dB, and a beam efficiency of 98%. The cold source horns are mounted to provide an unobstructed field of view when looking at deep space, while minimizing the waveguide runs to the receiver front-end.

Antenna

The GFO antenna is a space borne three-frequency, (13.5, 22 and 37 GHz) offset-fed parabolic reflector design that interfaces with the altimeter and the radiometer. The aperture is 41.5 inches diameter and the focal length is 26 inches. The feed is pointed at the central angle of the reflector to minimize spill-over

The Evolving Impact on MW Product Strategy

- The "Ideal" MW instrument product strategy
- Full-feature sets
- All bells and whistles
- Inelastic demand (Aerospace Funding)
- High performance/high price

Slide 4



When there are legends of customers ready to take high-performance instruments off your hands at high prices, limited R&D resources push the decision-maker to favor a feature set which does it all. Wider frequency spans, more comprehensive modulation, higher stabilities and agilities, and more importantly, a horsepower race on accuracies all sold products.

The thinking prevailed that as long as a commercial customer, who only needs a subset of the full feature set, can get the capability with a higher-priced product, let's take those who can scrape up the money, and forget those who can't because the optimum return still looks good. I don't want to overdo the DOD argument, because there were many companies who targetted the commercial niche well. Bird power meters, IFR test sets, and others are just a few which come to mind.

Catagories of Instruments

DUAL-USE "Generic" Instruments	SINGLE-USE Application-Oriented
Vector Network Analyzers	Signal Generators
Oscilloscopes	Counters
Sweepers	Test Sets
Scalar Network Analyzers	Agile-Simulators
Spectrum Analyzers	"Personality" Spectrum Analyzers

Slide 5



It seems to me that an important distinction can be made between instrument types, which might be divided into two groups. Most "general purpose" instruments such as oscilloscopes, spectrum analyzers, power supplies, and others serve both commercial and DOD markets with little need for differentiation. In addition, component design tools, specifically vector network analyzers (VNAs), scalar network analyzers (SNAs), and the multi-band sweepers that drive them also have fitted into buying plans of both user sectors.

I'm begging the question a bit on instrument pricing. It is true that VNAs that cost \$200,000 (without wheels), often were not cost justified by customers working on purely commercial components. But typically the component manufacturers were also working both sides of the user street, and were able to fill commercial and DOD needs.

It is in the RF and microwave-system test instruments that single-use was most noticed, and most confining. Conventional signal generators which tried to directly match radar and EW needs tended to outprice themselves for pure commercial. DOD-use instruments often had frequency ranges that split commercial bands like 3.9 to 4.4 GHz. Same story for DOD test sets. Recent additions to product lines such as fast-agile-simulators and vector modulation generators also directly focused on DOD applications, as revealed by their high prices.

3

Dual-Use Requirements for the Decade of the 90's

- Support Time-to-market initiatives
- Software re-configurable
- Hardware re-configurable (VXI, MMS)
- Real-life simulations
- Instrumentation strategies that lead system needs

Slide 6



In the '90s, business will divide into the nimble and the dead. Time-to-market is not just a catchy phrase rolling off our lips, but a new culture for design engineers. Fast-track design projects will dominate, and design engineers will need to bring real-life complex/impaired signal environments right down to the design bench to stress-test circuits and equalizers before they get to field testing environments.

Test equipment, as it is, will need to be highly-reconfigurable, both for hardware, and for software. VXI and MMS are vehicles which do some of this in hardware terms. Large, highly-capable signal systems such as agile simulators are the other example, which can reconfigure the entire signal environment instantly.

Finally, most marketing departments have gotten the message. No more technology horsepower races. Even DOD wants "just enough." And they are also buying "from-the-shelf" by directive.

Swords to Plowshares

- Turning modern DOD technologies to commercial success
- Cellular and PCN—agilities and spread spectrum
- Video and HDTV revolution—compression and coding
- Digital revolution continues—DSP
- MTBFs going up, BITE for digital circuitry

Slide 7



This conference and others are trying to figure out where we go from here? Not an easy task. There are intriguing success stories of military technology invading the commercial sector. These are just a couple of examples. We've all heard of the Pacific Rim making successes of US initial breakthroughs, and it is up to us to extend from those examples.

There are many non-intuitive things going to happen before 2000. When you can now buy a TV set which has not been tested in the conventional sense, because of sophisticated TQM and statistical quality control, you had better realize that test instrumentation can't be very far behind. The ideal instrument would be self testing. (Perhaps some traceable links to national standards will be allowed.)

As digital continues to invade the systems and the test instruments, abbreviated testing will be the norm. After all, you now buy complex computers in pieces, and assemble them at home. Digital interfaces make a BIG difference.

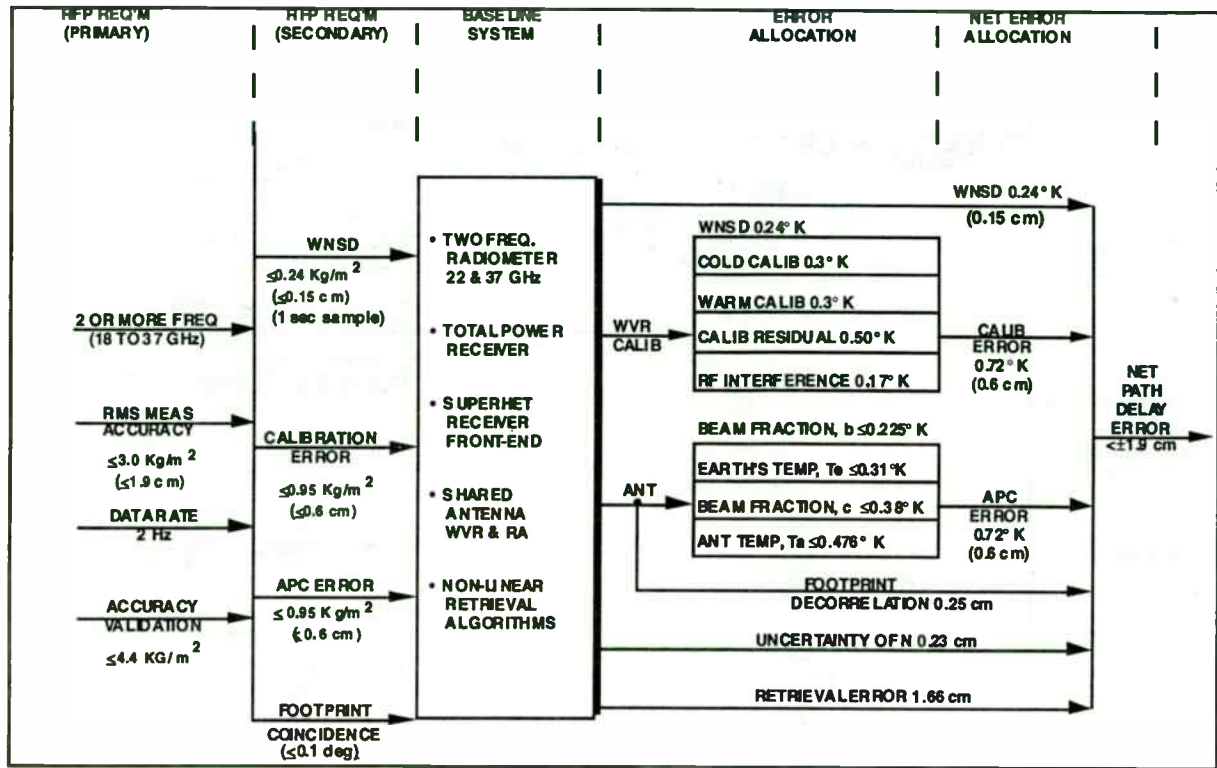


Figure 5. WVR Requirements Flowdown

Impact on Instrumentation Strategies

- John Young statement to SIA
- Fast-track projects
- Simulation capabilities
- New paradigms

Slide 8



The simple message is that everyone needs to start writing on a clean sheet. Don't expect things to be the same, as they were under DOD cultures. Expect big discontinuities in testing strategies and test equipment

Is there any reasonable future for those of use with 40 years in instruments and measurements? Absolutely. I have appended a summary of some comments made recently by John Young just before his retirement as CEO of HP. John has an exciting vision. It is up to us to fill in the blanks.

Young at SIA

November 3, 1992

In his last public address prior to retiring as HP president and chief executive officer, John Young told a Semiconductor Industry Association (SIA) audience in San Jose, California, on October 28 that despite very real problems, the glory days are not gone: "Our industry's prospects can be even more exciting than its past."

Predicting that the Information Age will come during the lifetime of those in the room ("even for those of us who are retiring"), Young said three important technological trends are driving this change:

- The accelerating performance of technology — which has already made it possible to provide 50 to 75 percent more hardware performance every year — and the likelihood that by the end of this decade, software applications will be able to tap that potential. The cost of a computer cycle at the end of the decade will be about one-hundredth of what it is today, Young predicted. "Information technology will be as pervasive as electricity," he said.
- A trend under way toward development of an "information utility" as telecommunications and broadcasting move to digital technology and datacom, telecom and entertainment converge. Young sees ahead a network of networks stacked with services, intelligent directories, the Library of Congress on-line, the expertise of the world's best doctors, and far more.
- Information appliances. "The hundreds and thousands of new information appliances that tap into the utility will capitalize on U.S. strengths — sophisticated software solutions, multimedia, microprocessors and specialized ICs, and the willingness of countless entrepreneurs to exploit the almost infinite opportunities that will exist." This will offer opportunities for collaboration and "for bridging the distances and disciplines that divide us." Young sees the government's role as facilitator, not builder, with public funding focussed on research into architectures, switching and security. Public policy should smooth the way in such areas as standards, protection of intellectual property and the allocation of communication frequencies.

The High Performance Computing and Communications Initiative (HPPI), a government-backed network tying together the U.S. supercomputer centers, is a good start, Young believes. It addresses "grand challenges" for technical cooperation such as cancer, air pollution, energy conservation and superconductors.

Young was a founding member of the Computer Systems Policy Project (CSPP) made up of the heads of the largest U.S. computer companies. CSPP supports HCCI and believes further that the U.S. should aim for an expanded network with millions of nodes that would be widely accessible to the public. "Such a national information infrastructure would spur economic development — creating high value-added and high-paying jobs — in ways we can't even foresee," Young declared.

Requirement	System Element	Requirements Flowdown
Two Freq. 22/37 GHz (Allocation)	22 GHz Receiver Channel	F _o (22.235 GHz)
		F _o stability (±25 MHz)
		Bandwidth, ±1 dB (<220 MHz)
		VSWR (<1.2:1)
		Sample period (0.50 sec) (Sync 1.25 MHz Ref.)
WNSD 0.24° K (1 sec sample)	22 & 37 GHz WVR Calibration	WNSD (<0.3° K, 0.50 sec)
		Dynamic Range (2.7-350°K)
Data Rate 2 Hz	22 & 37 GHz Cold Source Horns	Residual Non-Linearity (<0.5°K)
		Warm/cold calib accuracy (±0.2°K)
WVR Calb. (Allocation)	37 GHz Receiver Channel	RF Interference (<0.04° K)
		Thermal warm source temp accuracy (±0.05°K)
		Instrum. thermal temp sensor accuracy (±0.05°)
		Thermal sensor traceability (to NBS)
		Beam efficiency (≥98%)
		Sidelobe level (>25 dB)
		Horn loss (<0.1 dB)
		Polarization (linear)
		Horn window (IR)
		F _o (37.0 GHz)
		F _o stability (±25 MHz)
		Bandwidth, ±1 dB (<220 MHz)
		VSWR (<1.2:1)
		Sample period (0.50 sec) (Sync 1.25 MHz Ref.)

Figure 6. WVR Receiver Requirements/Flowdown

AFFORDABLE MMIC POWER AMPLIFIERS FOR 2.4 AND 5.8 GHz SPREAD-SPECTRUM APPLICATIONS

T. Apel, R. Bhatia , H. Sun and S. Ludvik
Teledyne Microwave
1274 Terra Bella Ave.
Mountain View, CA. 94043.

ABSTRACT:

This paper describes the design and performance of fully integrated, low-cost MMIC power amplifiers for 2.4 and 5.8 GHz commercial Spread-Spectrum applications. Both MMIC amplifier designs deliver high gain and high-power in a modest chip area of only 3.0 x 1.7 mm with integrated bias networks, thereby providing an affordable solution to general purpose power amplifiers required in unlicensed commercial spread-spectrum transceivers. These PAs are optimized for +5V supply operation. The 2.4 GHz chip is discussed in greater detail, since same issues, tradeoffs and topology considerations apply to the 5.8 GHz amplifier.

INTRODUCTION:

In applications above L-band where Silicon devices are used, GaAs MMIC technology offers improved gain per stage and better multistage power added efficiency . In addition , MMIC technology also provides size reduction, improved reliability, lower parts count, lower cost and simpler component assembly. The amplifiers discussed here are designed to provide affordable solutions to the need for general purpose power amplifiers in unlicensed commercial spread-spectrum transceivers [1]. The FCC authorized frequency bands for Spread-Spectrum systems are 902 to 928 MHz, 2400 to 2483 MHz. and 5725 to 5850 MHz. The requirements for transmitter power output are +30 dBm EIRP with spread-spectrum modulation. With typical antenna gains in 0 to 3 dBi range , the maximum power output is in the + 27 to +30 dBm range. The two PAs described here are designed to provide greater than +27 dBm power output @ 1dB Gain Compression with +5 V drain supply.

CIRCUIT DESIGN:

Based on the requirements of an existing direct-sequence spread-spectrum system, the following minimum design goals were established for 2.4 and 5.8 GHz power amplifiers

Frequency Band	2.4 GHz +/-50 MHz	5.8 GHz +/-75MHz
Gain	25 dB	20 dB
Power Ouput @ 1dBGC.	+27 dBm	+27 dBm
Power Added Efficiency, η_{add} .	20 %	20 %
Input VSWR, max.	2:1	2:1
Output Third Order Intercept Point	35 dBm	35 dBm
Operating Temperature Range	0 to +70 °C	0 to +70 °C

Based on these electrical specifications the circuit topology chosen includes 3-stages with lossy-reactive , lumped-element matching networks for high-gain, high power, high efficiency and small size. The power loading was based on +5 V drain operation . The FETs are biased in Class-AB mode for improved efficiency. Based on measured load-pull data on discrete FETs the optimum power loading is obtained by matching an equivalent source admittance of 47.6 ohms + j5.9 mS per mm of gate-width. The output power density @ 1dB gain compression is about 0.26 watts per mm. Accordingly, a 3mm FET device was chosen for the output stage. For the 2.4 GHz. PA , the stage 1 and stage 2 device sizes

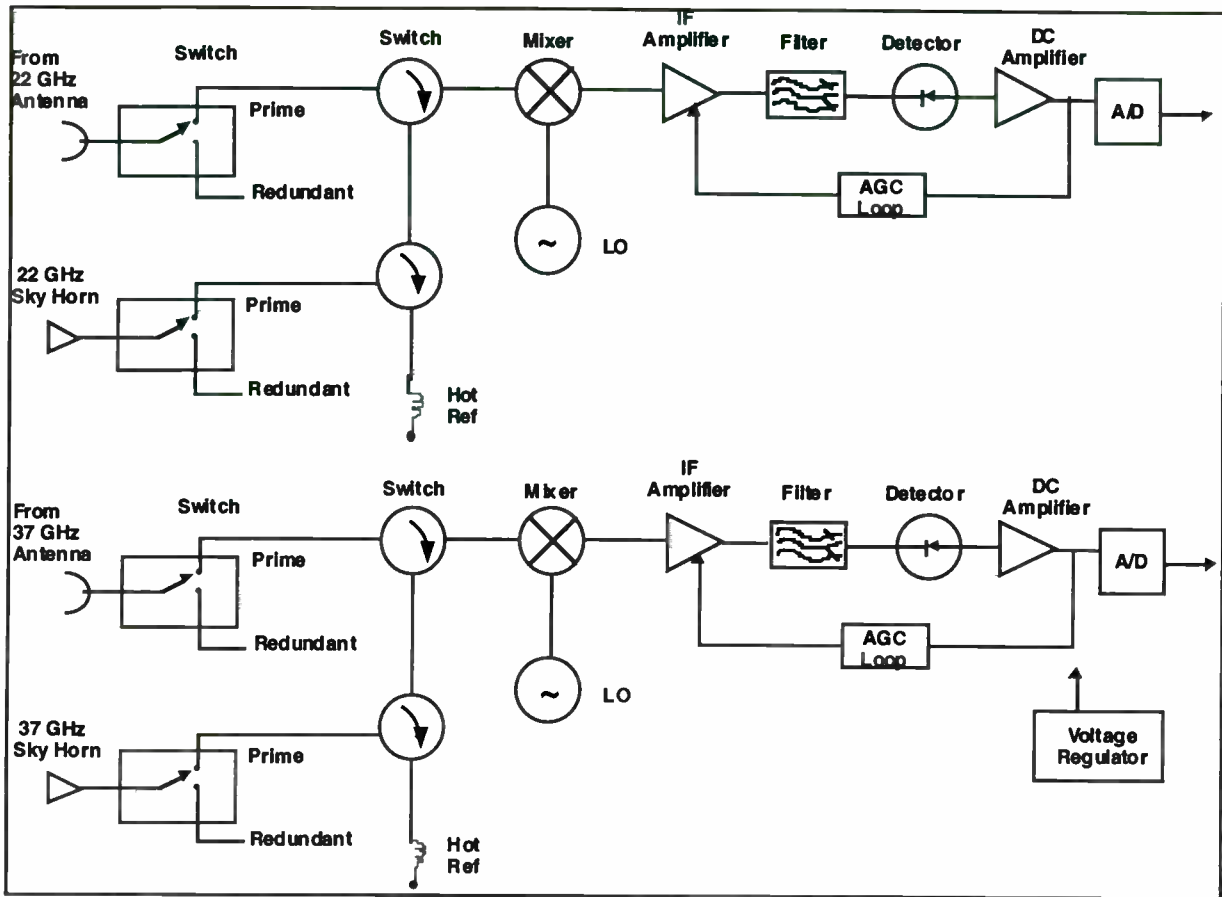


Figure 7. GFO Radiometer Block Diagram

were selected as 0.3 mm and 0.6 mm , whereas for the 5.8 GHz PA the stage 1 and 2 device sizes were 0.3 mm and 0.72 mm respectively. This choice was based on achieving high efficiency and ensuring that the first two stages are linear over the operating bandwidth and temperature range. The input, output and interstage matching network topologies were selected to provide optimum power match and flat gain. Other considerations were unconditional stability, minimum number of elements, bias application and realizability. Further, the output matching on final stage also included 2nd harmonic tuning to increase efficiency. Gate and drain bias networks included sufficient bypass and resistive loading to ensure stable operation. Both PAs are unconditionally stable. The circuit schematics of the two PA designs are shown in Figures 1 and 2.

The circuit analysis included both linear and non-linear simulations in Libra. The large-signal model used was the Curtice-Cubic FET. The model parameters were provided by the MMIC foundry. Modeled amplifier power and efficiency were within 1 dB of measured levels.

FABRICATION:

The MMICs were fabricated at a commercial foundry. The active devices are supported by a standard 0.5 micron GaAs MESFET ion-implanted process. Gates are written in E-beam lithography and realized in a double recess. The process includes silicon nitride MIM capacitors, tantalum nitride and GaAs resistors, and low-loss transmission line elements. Low-inductive paths are provided through 50 micron diameter via holes. Typical DC parameters for a 1 mm device are $I_{dss}=320\text{mA}$, $V_p= -3.5\text{V}$, $G_m=135\text{mS}$ and $V_b=15\text{V}$. Chip area is conserved by distributing bypass MIM capacitors around via pads. This technique has been previously presented in [2].

MEASURED RESULTS:

The first-pass results on these MMICs have met all the design specifications. The photo of the MMICs is shown in Figures 3 and 4. The chip size of the 2.4 GHz MMIC is 3.0 x 1.7 x 0.1 mm and that of the 5.8 GHz MMIC is 3.0 x 1.9 x 0.1 mm. The measured data is taken in a low-cost surface-mount package. The only external components required are two 0.1 μF bypass capacitors for the positive and negative bias leads placed close to the chip to prevent any bias induced oscillations. The packaged chip assemblies are shown in Figures 5 and 6 . The measured gain and return loss for the 2.4 GHz MMIC is shown in Figure 7 and that for 5.8 GHz MMIC in Figure 8. Clearly, the 2.4 GHz PA has typical small-signal gain of 28 to 30 dB and less than -12 dB input return loss over a bandwidth in excess of the desired 2.4 to 2.483 GHz . The 5.8 GHz PA provides a typical gain of 23 dB and less than -12 dB of input return loss over a bandwidth in excess of the desired 5.725 to 5.850 GHz. Small-signal data is taken @ 25 ° C at a bias of +5 V, 422 mA quiescent current .

The measured output power and efficiency of the 2.4 GHz chip is displayed in Figures 9 through 12. Figure 9 shows the 1dB gain compression output power vs frequency for a 35% I_{dss} bias. The 1dB gain compression power performance trade-off with operating point (drain bias and quiescent current) is illustrated in Figure 10. Similarly, the efficiency impact of operating point is shown in Figure 11. It can be seen that power output greater than 1 watt and associated power-added efficiency above 32% has been typically achieved from this MMIC. Power and efficiency at $V_{ds}=+5\text{V}$ are typically +28dBm and 25% respectively. Since the primary application of this chip is for direct sequence spread-spectrum modulated signals, Figure 12 has been included to illustrate the effect of operating point on spectral regrowth of the second (5th order) side-lobes. The power levels displayed are associated with a 3 dB degradation in the second (5th order side-lobes). Typical 3rd order output intercept point for the 2.4 GHz PA at 2.45GHz is about 36dBm at $V_{ds}=+5\text{V}$.

losses. Illumination taper is used to reduce the sidelobes.

The feed is designed for a hybrid HE11 mode. The feed will be located such that the 37 GHz phase center is at the focus of the parabolic reflector. The phase center offset, therefore, exists only at 22 and 13.5 GHz. The antenna requirements are listed in Figure 8. The simulations and test results indicate that these requirements will be met.

WVR PERFORMANCE ANALYSIS

Analyses have been conducted to verify that the radiometer performance shall meet all the specified requirements. The major performance parameters are discussed in this section.

White Noise Standard Deviation

A key GFO WVR performance parameter is the radiometer sensitivity, measured by the output white noise standard deviation (specified as less than 0.15 cm for a one second sample period). This requires a radiometer temperature sensitivity of < 0.24 K. This requirement has been incorporated in the WVR design.

Calibration Accuracy

Radiometer calibration is very important because even small measurement errors, in the range of a tenth of a degree Kelvin, have a significant impact on the wet path delay calculations. For this reason, the radiometer will be thoroughly calibrated on the ground using black body targets and other calibrated instruments. The WVR calibration algorithm accounts for losses, physical temperatures, and re-radiation in the microwave components, as well as non-linearities in the receiver. The on-orbit calibration technique uses a cold source (cosmic space at about 3 K) and a hot source (internal ambient of about 285 K). Both hot and cold calibration measurements are made at uniform 7-second intervals. The net precision of the on-orbit instrument calibration is an rss (root sum square) combination of significant individual error sources, including the white noise standard deviation, cold calibration, hot calibration, calibration residual and RF interference.

Antenna Pattern Correction Accuracy (APC)

Radiation is received by the WVR from antenna sidelobes, reflections from the space craft, and direct spillover into the feed horn. This spurious radiation must be accounted for by the APC algorithm to obtain the mean brightness temperature from the scene averaged over the main-beam solid angle. The net

precision of the antenna pattern correction (APC) is an rss combination of the energy received from the regions outside the main beam efficiency region. The APC algorithms, based on the TOPEX microwave radiometer (TMR) heritage [4], are depicted in Figure 9.

Footprint

The altimeter and WVR beam centers are co-boresighted to less than 0.07 degrees. The GFO antenna beamwidths are 1.6 degree for 13.5 GHz, 1.0 degree for 22 GHz, and 0.63 degree for 37 GHz, which provide an effective footprint for the (pulse limited) altimeter of 2 km, and 14 km and 9 km for the WVR. This ensures that the altimeter and WVR footprints are highly correlated and the path delay uncertainty is minimized.

Refractive Index

In space, the energy propagates in a straight line. In the earth's atmosphere, the rays are bent depending on the refractive index of the medium. The determination of refractive index is needed to calculate the difference between the straight line distance and actual distance traveled, or the delay.

Retrieval Algorithms

The retrieval algorithms, relating the measurements to delay calculations, are based on atmospheric models using the radiative transfers and incorporating the satellite radiometry data base. These algorithms represent the results of a significant scientific effort but are still the largest source of uncertainty due to the nature of variables involved.

Path delay Measurement Accuracy

The overall path delay measurement accuracy is an rss combination of the individual error sources including calibration, APC, footprint decorrelation, uncertainty of the refractive index of the air, and the retrieval algorithms. The analyses and test data indicate that the overall radiometer accuracy will satisfy the requirements.

CONCLUSIONS

This paper has presented the requirements and design considerations on the GFO radiometer and antenna. The system level requirements have been allocated to the lower level design specifications and the flight hardware is in development. The GFO design experience is applicable to future space missions.

Under similar bias conditions the 5.8 GHz PA delivers a minimum output power of 26 dBm with associated power-added efficiency of 18 % as shown in Figure 13 and 14. At appropriate bias levels, 1 watt power output and associated power added efficiencies above 20% are typically measured. The third-order intercept point at 5.85 GHz is typically 35 dBm at $V_{ds}=+5V$.

CONCLUSIONS:

The design and performance results of 2.4 GHz and 5.8 GHz MMIC power amplifiers for spread-spectrum applications have been presented. These PAs provide a very compact, reliable, simple, stand-alone, and low-cost alternative to conventional hybrid and discrete power amplifiers. Power and efficiency performance is quite good for a fully integrated power MMIC. Both PAs provide useful gains in excess of 20 dB and P-1dB power output of 0.5 W, compatible with the typical requirements of unlicensed spread-spectrum systems. Further, these results were achieved on a first-pass with an overall design, fabrication and test cycle time of about 2.5 months.

REFERENCES:

- [1] A. Ward, " Survey of Component Technologies for 900, 2400 and 5700 MHz Unlicensed Spread Spectrum Transceivers," RF Expo-West Proceedings, pp197-208, March 1992.
- [2] T. Apel & S. Ludvik, " A Compact, High Gain, 2-20 GHz MMIC Amplifier," 1992 IEEE Journal of Solid State Circuits, Vol.27, No.10, pp. 1463-1469, Oct. 1992.

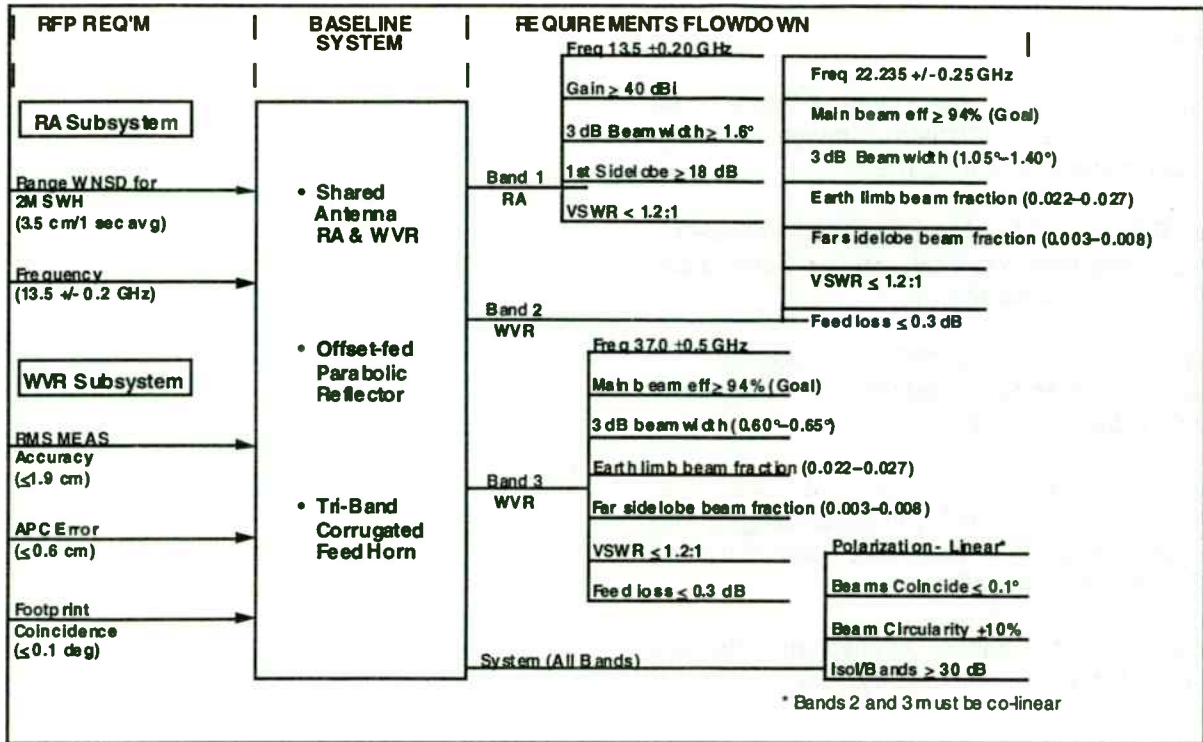


Figure 8. GFO Antenna Requirements Flowdown

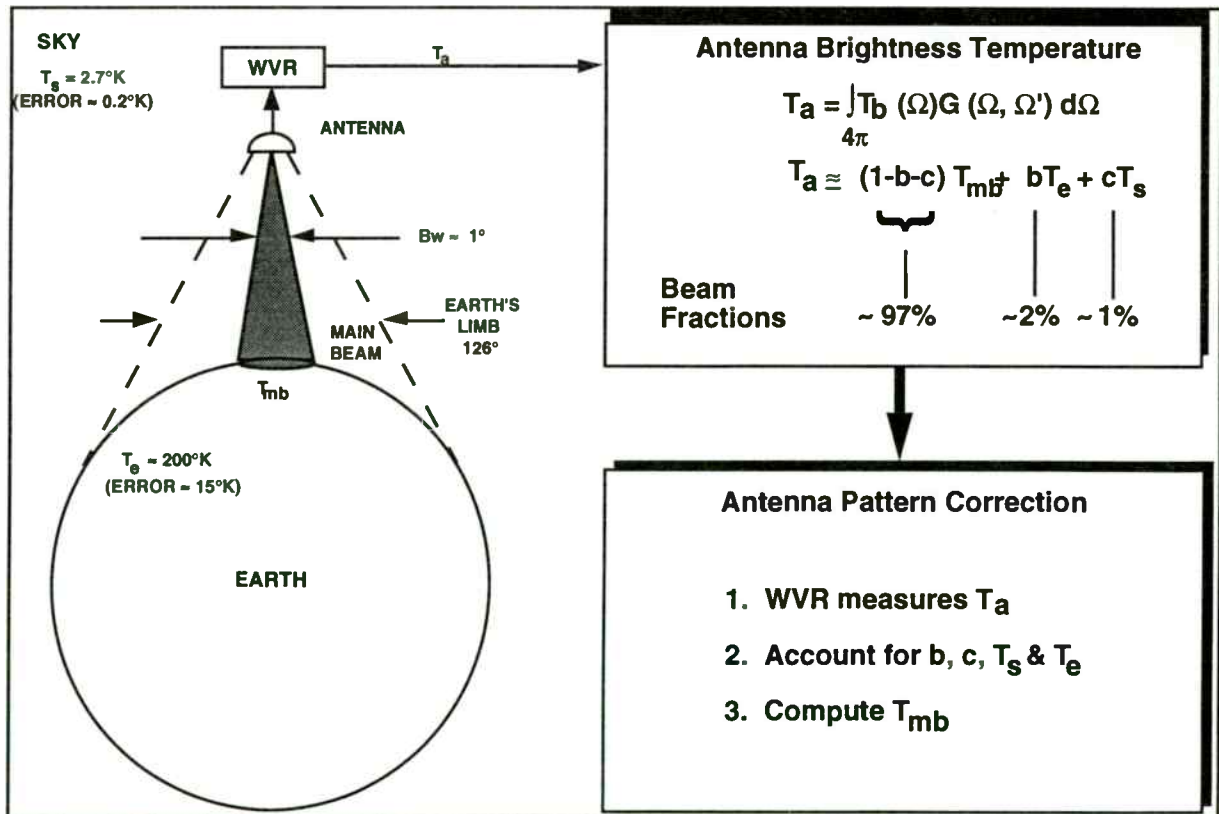


Figure 9. Antenna pattern Correction (APC)

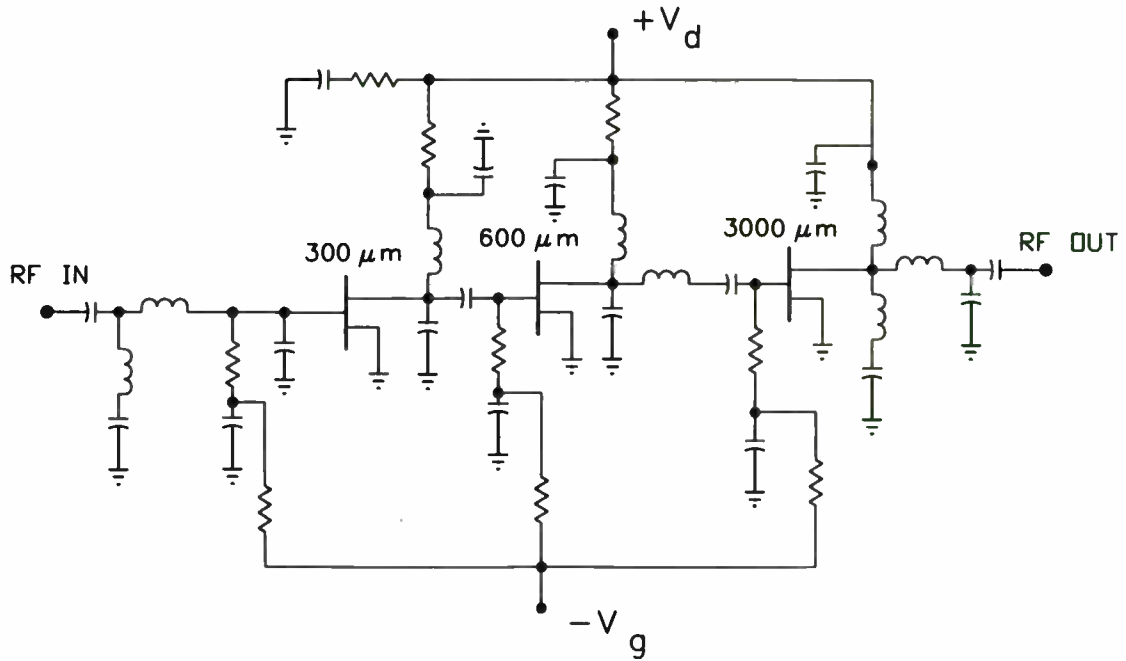


Figure 1. 2.4 GHz MMIC Schematic

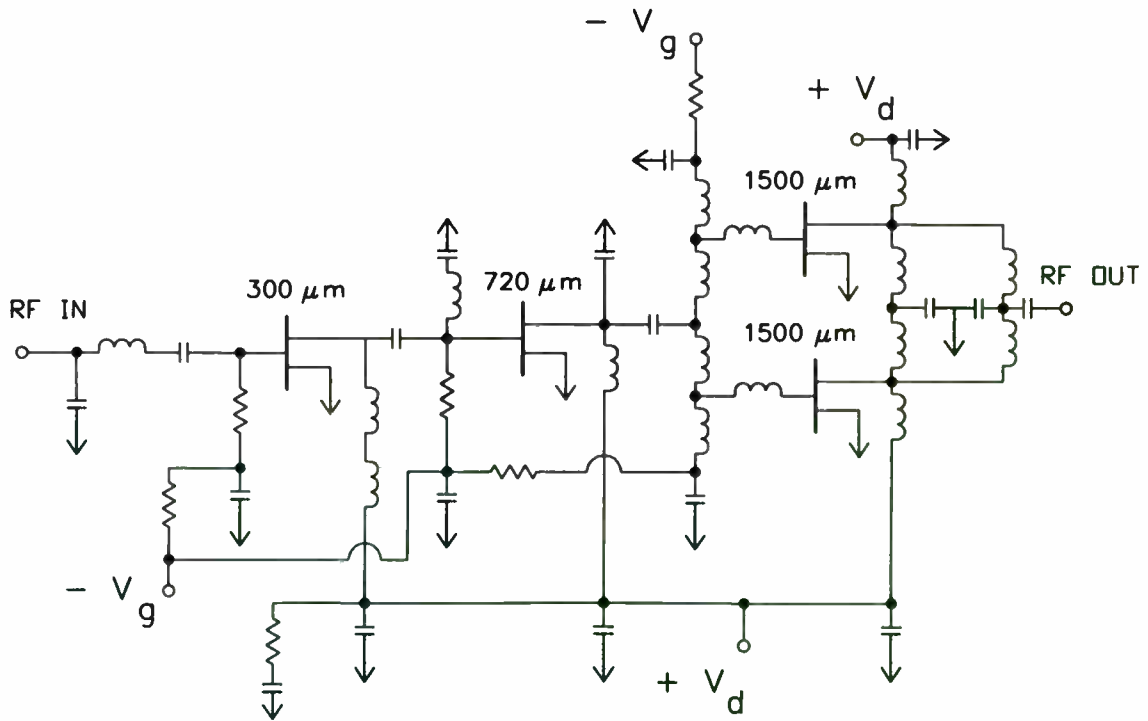


Figure 2. 5.8 GHz MMIC Schematic

REFERENCES:

- [1]. Koblinsky, C. J. et al, " The Future of Space borne Altimetry: Ocean and Climate Change", Joint Oceanographic Institutions Inc., 1992
- [2]. Quinn, P.F. et al, "U.S. Navy GEOSAT Follow-on", AIAA Space Programs and Technologies Conference, March 24-27, 1992, Huntsville, AL
- [3]. Walker, D. M. et al, " The GEOSAT Follow-on (GFO) Altimeter", AIAA Small Satellites Conference, Salt Lake City, September 1993
- [4]. Janssen, M. A., Keihm, S.J., and Ruf, C. S., "The TOPEX Microwave Radiometer", In Proceedings of the Third Specialist Meeting on Microwave Radiometry and Remote Sensing, Boulder, 1992
- [5]. Janssen, M. A., editor: Atmospheric Remote Sensing by Microwave Radiometry; John Wiley & Sons, Inc., 1993
- [6]. Skolnik, M. I., editor: Radar Handbook, McGraw-Hill Book Company, 1970
- [7]. Ulaby, Moore and King: Microwave Remote Sensing, Volume 1, Artech House, 1981

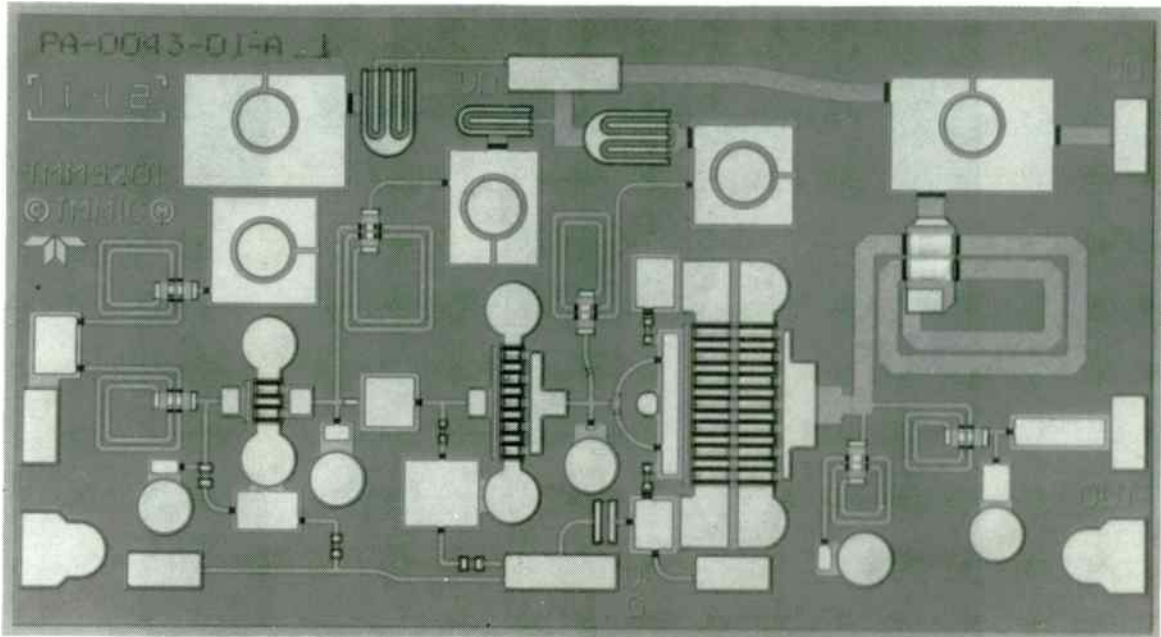


Figure 3. Photo of the 2.4 GHz MMIC PA

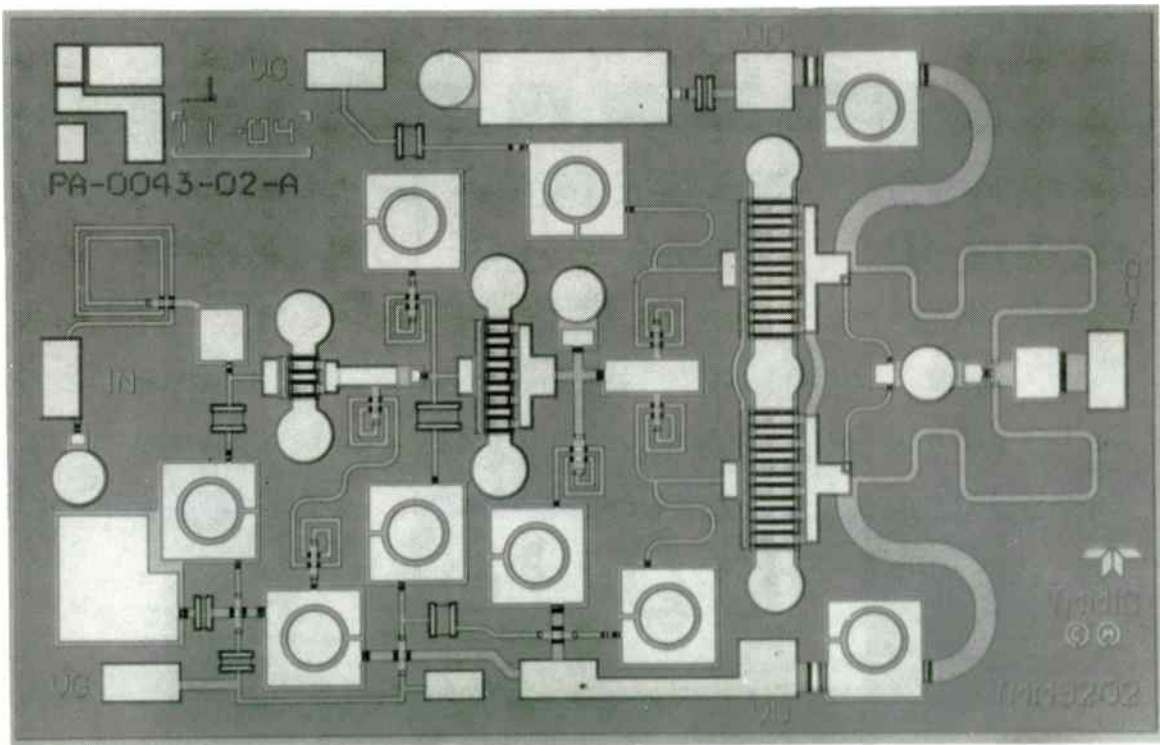


Figure 4. Photo of the 5.8 GHz MMIC PA

High Power, Low Frequency Microstrip Switches

Sharyn Irons
Eric Higham
M/A-COM MED

Abstract

This paper will describe how low thermal resistance substrates and PIN diodes have been used to produce compact high power switches in the UHF frequency range. These switches, an SPDT and SP3T, are 2.0" x 0.75" x 0.25" and can be used in drop-in or open substrate configurations. Data will be presented for operation at 150W CW input power in the 30-88 MHz frequency range.

Introduction

Switches may perform a variety of different functions in electronic systems. Depending on the system and the desired function, these switches may be located anywhere from the antenna to the receiver or transmitter. The performance parameters required from the switch will be determined, in part, by this location. To best meet this broad range of requirements, switches are fabricated from many different technologies. PIN diode technology offers several advantages to system designers.

PIN diode switches can be faster, smaller and more reliable than electromechanical or ferrite switches. They can handle more power than GaAs FET switches. The need is arising for switches that are small, compact and can handle transmit powers in the UHF communication bands of 100-200 watts.

Mechanical

Switches meeting these requirements do already exist. These conventional electrical and mechanical designs result in large devices. A primary goal of this new design was to minimize package size.

This switch was part of a switch filter in a .062" microstrip multifunction assembly. The package could occupy a 2.00" x .750" area. The electrical connections were .035" x .200" x .002" gold plated copper tabs.

The biggest concern with high power switches is the removal of heat. The major source of this heat is power dissipated in the PIN diodes. The RF design incorporated series diodes to satisfy the size and frequency constraints. With the diodes mounted in series, the thermal resistance path for removal of heat includes the PIN diode and its attachment material, the substrate and its attachment

material, and finally the carrier. Low power PIN diode switches are generally manufactured using soft substrates or Alumina (Al_2O_3) for the transmission media. A thermal analysis would show these materials to have a thermal resistance of greater than $200^\circ C/W$. This is much higher than what can be tolerated for this application. For high power applications where thermal properties of the substrate material are critical, the substrate selection usually narrows to Beryllium Oxide (BeO) or Aluminum Nitride (AlN). The primary reason for considering these materials is a significant increase in thermal conductivity. Both substrate materials will satisfy the thermal requirements, but AlN offers some additional advantages.

Some of the advantages of AlN are higher and more stable thermal conductivity, lower coefficients of thermal expansion (CTE) and non-toxicity. The thermal conductivity values range from 70-320 W/m^2K . This property remains more stable than BeO over normal operating temperatures, as shown below[2].

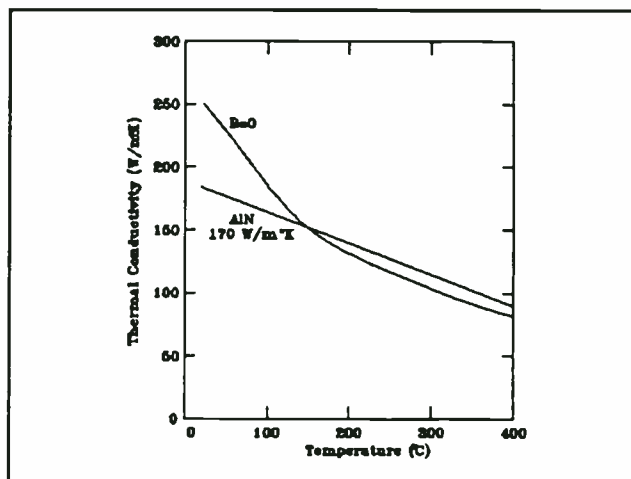


Figure 1 Thermal Conductivity of BeO and AlN vs Temperature

The CTE of AlN ($4.5 \text{ ppm}/^\circ C$) is a better match than BeO ($8 \text{ ppm}/^\circ C$) to Si ($3.5 \text{ ppm}/^\circ C$). Since Silicon PIN diodes and driver IC chips will be used in the switches, the likeli-

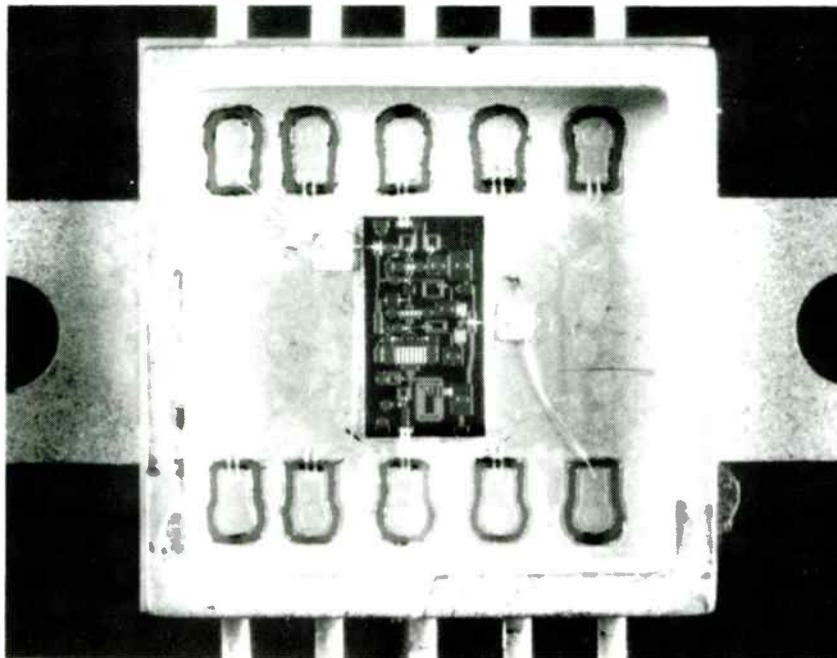


Figure 5. Photo of 2.4 GHz MMIC Assembly in Package

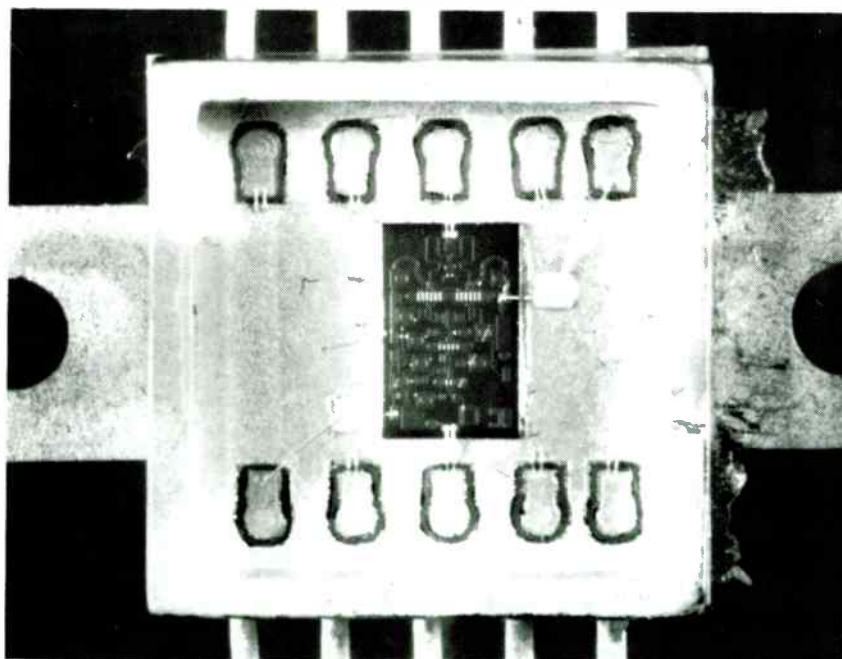


Figure 6. Photo of 5.8 GHz MMIC Assembly in Package

hood of cracking, caused by unequal expansion rates is greatly reduced.

The final component in the thermal resistance path is the carrier. The most significant factor in the selection of the carrier material is high thermal conductivity. This is important for transporting heat away from the PIN diode during high power operation. Another very important thermal property to consider is Coefficient of Thermal Expansion. Large CTE mismatches between substrate and carrier can cause damage when subjected to temperature excursions. Solder attachment, for example, will mechanically restrict displacement, and force the materials to bow upon cooling. This bowing can create an uneven ground plane, degrading RF performance, or cause cracking throughout the ceramic.

For this design, Molybdenum was chosen for the carrier material. Thermal properties of some other possible materials are listed below. Kovar and Aluminum have serious deficiencies and cannot be used in this application.

<u>Material</u>	<u>CTE</u> (ppm/°c)	<u>Thermal</u> <u>Conductivity</u> (W/m°K)
W/Cu	6.5	190
MCX-622™	6.2	170
Mo	5.0	140
Kovar ^R	5.9	14
Al	23.0	171
AlN	4.5	170

To minimize the combined component to substrate to carrier thermal resistance path, the attachment method was chosen to be Au80/Sn20 solder. Other lower temperature solders were considered but discarded to avoid solder reflow during installation. Electrical connections are made with Sn62 or Sn63.

The materials in the thermal resistance path have been chosen in order to insure proper heat transfer from the PIN diodes. AlN was selected as the substrate material, based on the thermal properties. Processing techniques need to be investigated.

AlN ceramic is a mixture of AlN powder, organic additives and sintering agents. The composition of the mixture can be varied to result in a range of practical thermal conductivities from 70 W/m°K to 270 W/m°K. The highest AlN thermal conductivity, 320 W/m°K [3], is a theoretical value which could be obtained only if there were no impurities in the process. However, the sintering process is more difficult for "pure" AlN because it does not densify well. For this application, a thermal conductivity of 170W/m°K was selected.

The chemical structure of a nitride, such as AlN, differs from that of common oxides (Al₂O₃, BeO). Fewer grain boundaries in high thermal conductivity AlN inhibit good adhesion of thin film metallization. Thick film processing does not completely eliminate concern, either.

Thick film pastes contain glass particles which are not CTE compatible with AlN. This mismatch causes cracking of the pastes upon drying. Development of thick film pastes which improve adhesion has been reported [4], but they have not been widely used. In either case, the adhesion may also be affected by processing. Chemical processing agents can cause a reaction which alters the chemical structure of the surface of the AlN substrate. Laser processing can also cause chemical reactions which will disassociate the AlN substrate into Aluminum around the lasered area. This will create a conductive path through the substrate.

Observing these precautions can simplify the processing of AlN. This substrate was manufactured with laser drilled vias and square cut-outs. The circuit was sputtered with nichrome, nickel (1500 angstroms avg) and gold (3000 angstroms avg), using thinfilm technology. To improve solderability and bondability, 100 μin. of gold was electroplated onto the circuit. A final layer of silicon dioxide was deposited for handling protection and insulation between the driver lines with high voltage potential.

The final switch assembly can be used in open substrate or packaged form. A cover provided protection for the bond wires and components and allowed the device to meet the gross leak requirements. Because of space constraints, the cover rested on the substrate. This dictated the cover material to be non-metallic. A plastic with a low CTE would have been ideal, but the CTE of plastic is high. Because of the CTE mismatch, a flexible epoxy seal was used to meet gross leak requirements. Prototype units incorporated ME7155-AN, stress-free epoxy with a Torlon^R 4203 cover. Production units used a glass-fibre filled plastic cover, with a silastic (silicone-rubber type) epoxy.

Electrical

To minimize space for the required bandwidth, an all series diode design was selected. The switches required only 37 dB isolation. This is achievable with two series diodes. The all series RF design resulted in bias current from a single supply. The PIN diodes were oriented with cathode to ground at the common junction. This allowed the forward bias current to be generated by the positive supply. Since this supply is much smaller in magnitude (+5V versus -100V), the DC dissipation of the switch is minimized.

Having decided on the topology, a diode was selected to meet these demands. An important consideration for a high power switch is heat dissipation. In the all series topology, the diode, substrate and attachment methods all contribute to the thermal resistance path. If this path is not low enough, the PIN diode junction will reach too high a temperature and fail.

The thermal resistance path from the diode (80Au/20Sn solder, Aluminum Nitride substrate and carrier) has a calculated thermal impedance of 4°C/W. To determine the maximum allowable diode thermal resistance, the expected power dissipation and maximum junction temperature rise must be determined.

The device had to survive a load VSWR of 4.5:1.

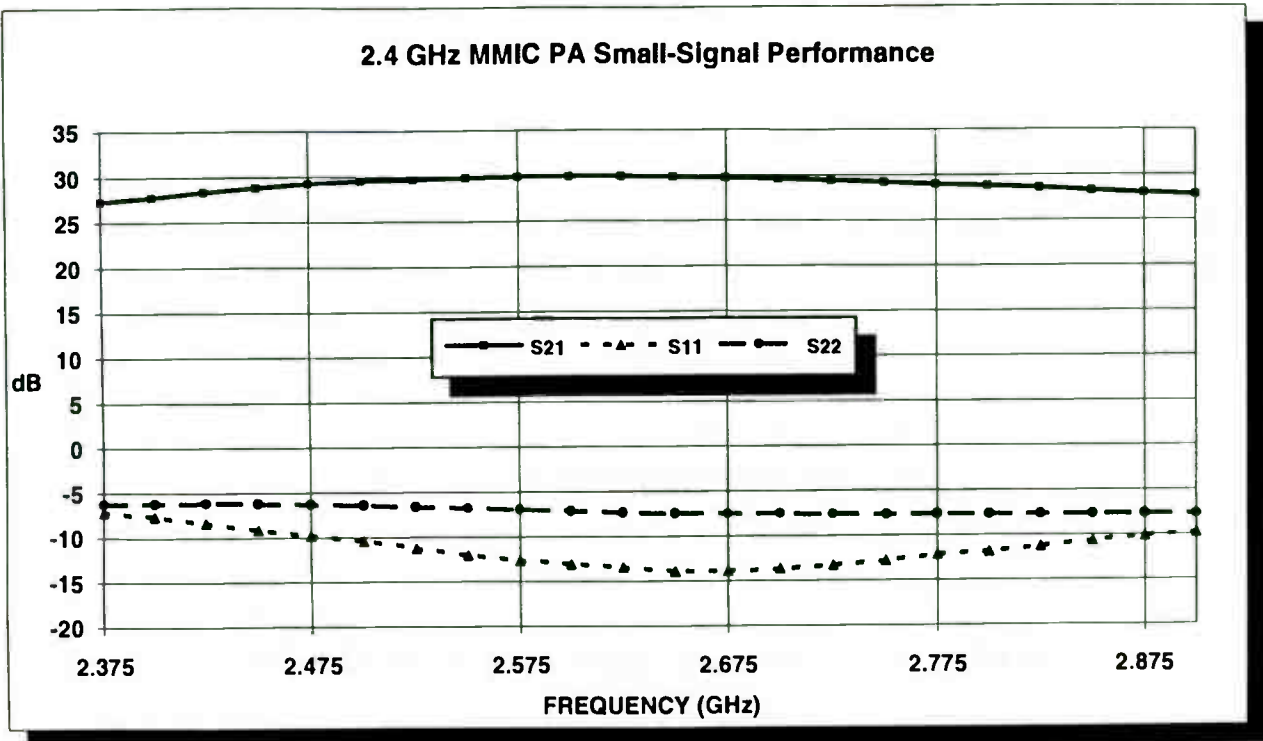


Figure 7. Measured Gain & Return Loss of 2.4 GHz PA

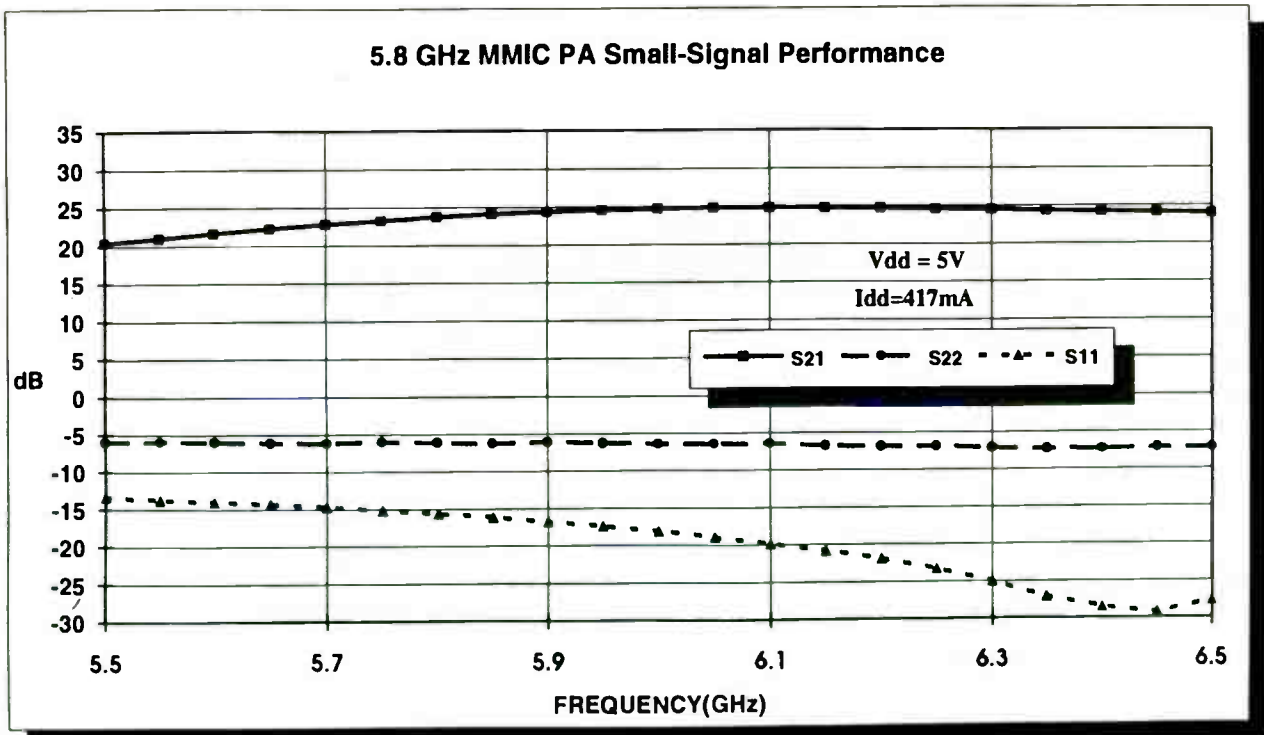


Figure 8. Measured Gain & Return Loss of 5.8 GHz PA

This, coupled with a 1.25:1 maximum VSWR for the switch, results in a standing wave pattern with maximum power of:

$$P_{max} = P_{inc} \cdot [2VSWR/VSWR + 1]^2$$

$$= 150W \cdot [(2 \cdot 5.625)/(5.625 + 1)]^2$$

$$= 432W$$

This worst case power represents a peak RF voltage of $\approx 208V$. Since $-100V$ back bias voltage is used, the breakdown voltage of the PIN diode must be specified as greater than $600V$. PIN diodes with this breakdown voltage routinely have forward resistances of 1Ω or less at forward bias levels of 100 mA .

For a series mounted diode:

$$P_d = 200R/(100 + R)^2 \cdot P_{max}$$

R = Diode resistance.

For a 1Ω diode with $P_{max} = 432W$,

$$P_d = 8.47W$$

For this particular requirement, the maximum operating temperature is specified as $100^\circ C$. The maximum junction temperature of PIN diodes is conservatively specified at $175^\circ C$. This allows a $75^\circ C$ junction temperature increase.

$$\theta_{total} = 75^\circ C / 8.47W \approx 9^\circ C/W$$

With the remainder of the thermal resistance path being $4^\circ C/W$, the PIN diode must be less than $5^\circ C/W$ for the design to accommodate the worst case power conditions.

For this device to be useful in communications applications, harmonic and intermodulation performance also needs to be considered. It has been shown[1] that, at low frequency, the intercept point of a switch can be calculated as:

$$IP_2 = 34 + 20 \cdot \log(F \cdot I_0 \cdot \tau / R_f)$$

where: IP_2 = Second order intercept point

F = Frequency (MHz)

I_0 = Bias Current (mA)

τ = Lifetime (μsec)

R_f = Diode resistance

The requirement was for harmonics less than 65 dBc . Second order intermodulation products are 6 dB higher than a second order harmonic, so this implies:

$$IP_2 = \text{Intermod Level(dBc)} + P_{inc}$$

$$= 71 \text{ dBc} + 51.7 \text{ dBm}$$

$$= 122.7 \text{ dBm}$$

Using the quantities we have discussed ($R_f = 1\Omega$, $I_0 = 100 \text{ mA}$, $F = 30 \text{ MHz}$, $IP_2 = 122.7 \text{ dBm}$), the equation for IP_2

can be solved to give:

$$\tau_{min} = 9.1 \mu\text{sec}$$

Once the desired switch performance was related to the diode parameters, M/A-COM's Burlington Semiconductor Operation was able to supply a CERMACHIP™ PIN diode to meet the following requirements:

$$\theta \leq 5^\circ C/W @ 100 \text{ mA}$$

$$\tau \geq 10 \mu\text{sec} @ 100 \text{ mA}$$

$$C_j \leq 0.5 \text{ pF} @ -100V$$

$$R_f \leq 1.0\Omega @ 100 \text{ mA} @ 100 \text{ MHz}$$

$$V_b \geq 600V$$

The RF circuit is composed of transmission line with $060" \times .060"$ pads to mount the diodes on. The bias is injected and returned for each arm through discrete inductor chips. The DC blocking and RF bypass capacitors are ceramic parallel plate chips.

DC blocking and bias network components (RF bypass capacitors and inductors) will define a filter structure. Ordinarily, the values of these components are selected to result in a filter with a lower cut-off extending well below the lowest frequency of operation. This ensures low insertion loss and VSWR in the operating band, but results in large values of capacitance and inductance for operation in the $30\text{-}88 \text{ MHz}$ band. As inductance value increases, the self resonant frequency (SRF) decreases. For the device to behave as predicted, the SRF must be above the highest frequency of operation

Designing the filter to have a cut-off frequency below 30 MHz minimized component value, and physical size. The reactances of the components in an "on" arm were modeled and optimized. The final component values were selected to be industry standard values with SRFs above 88 MHz .

The schematic and modeled results are presented below.

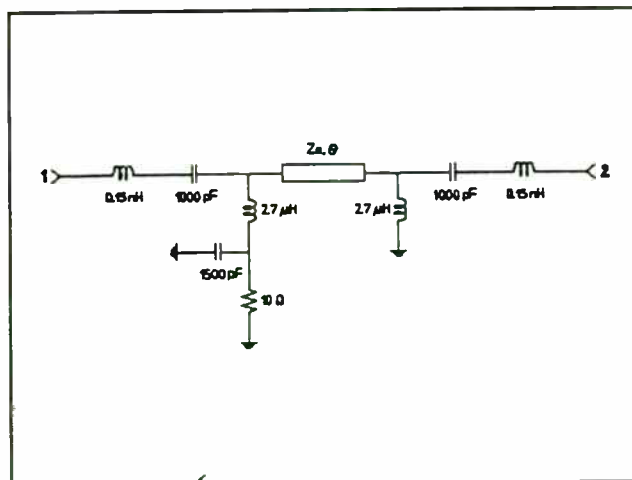


Figure 2 Bias Network Model

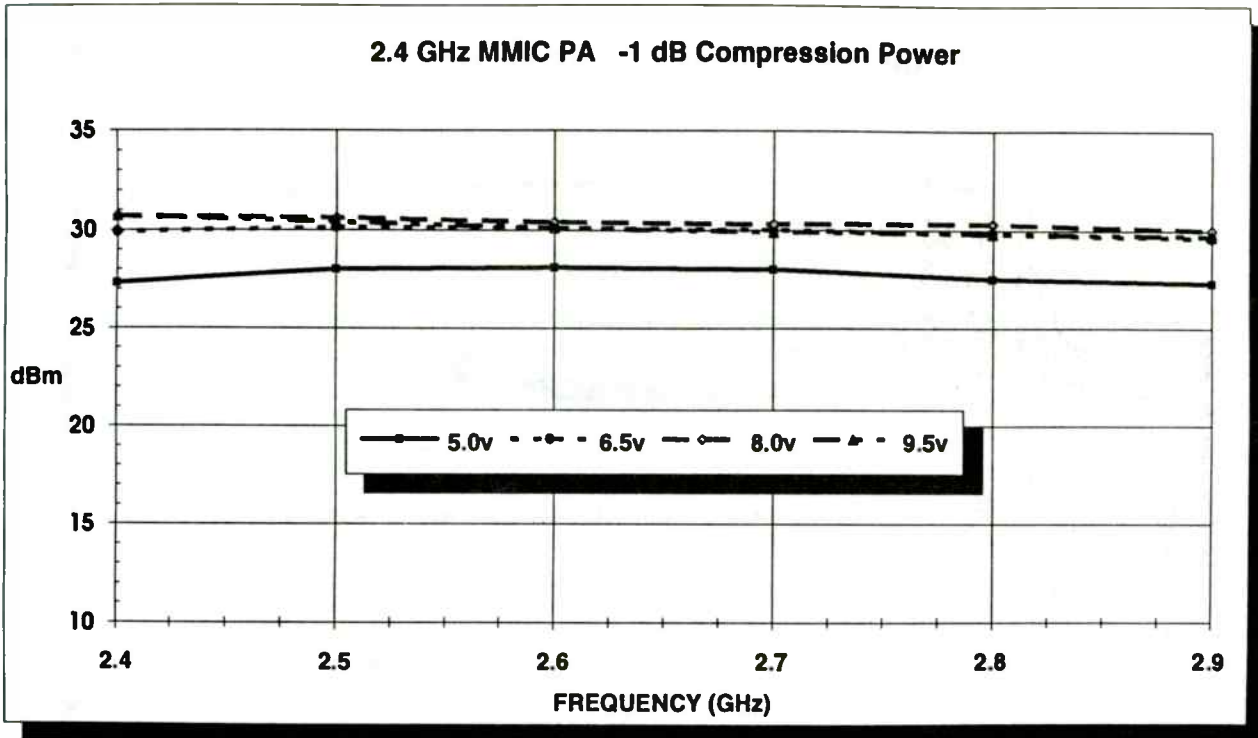


Figure 9. Measured Output Power Response of 2.4 GHz PA

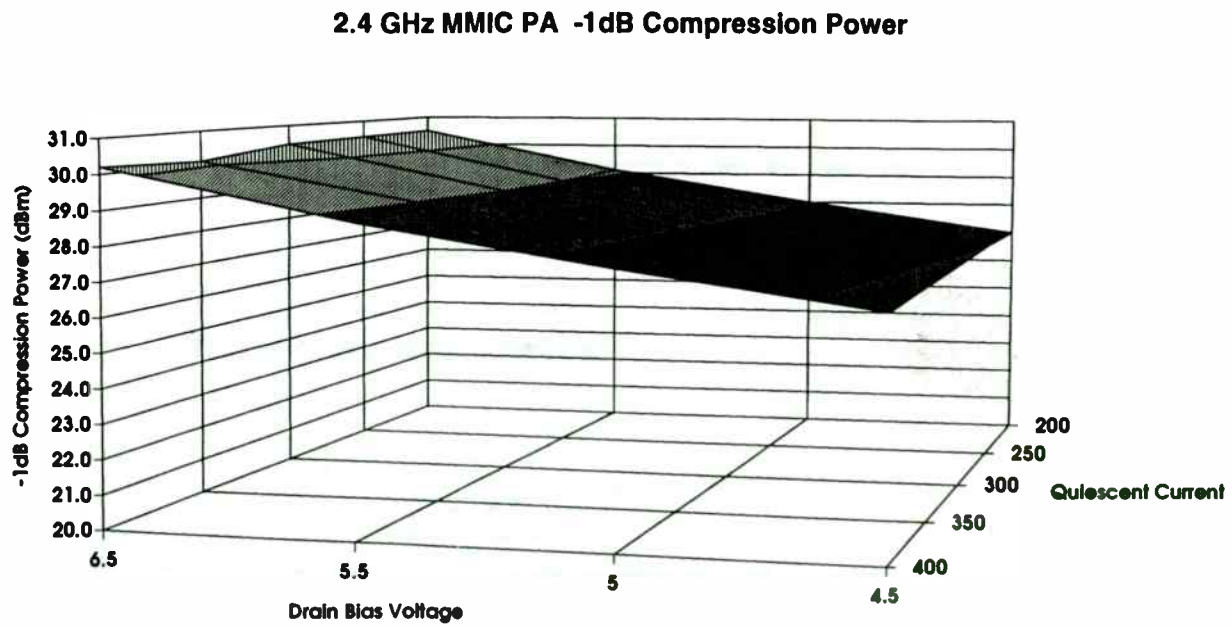


Figure 10. Measured Output Power Vs Drain Bias & Current of 2.4 GHz PA

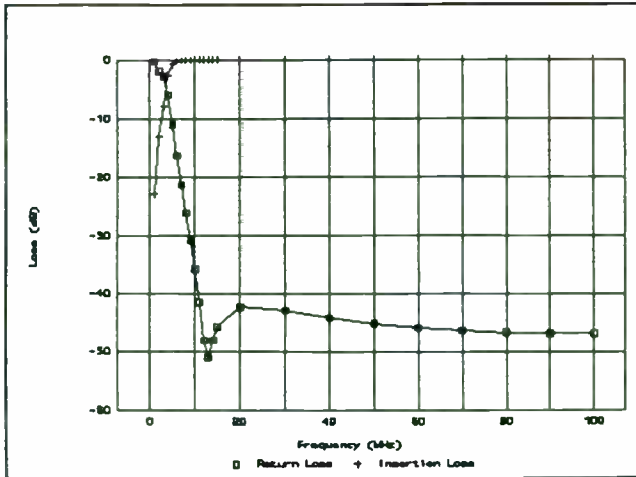


Figure 3 Filter Response of Bias Network

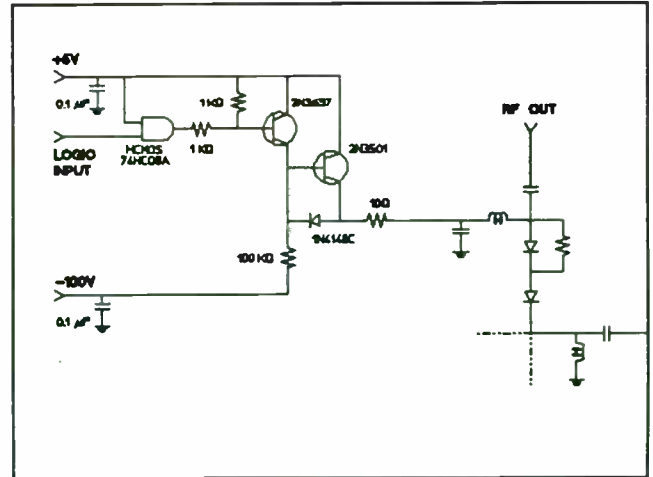


Figure 4 Driver Schematic (One Channel)

Driver

The driver, shown schematically with the RF section below, was designed to provide forward current of 100 mA for insertion loss and reverse voltage of -100V for isolation. The slow switching speed (50 μ sec) requirement allowed a design which minimized driver components.

There is a potential drawback to this approach. A provision must be made to back bias the common junction diode. If the reverse bias signal is applied at the anode of the second diode, the first diode will see little or no back bias. The incident RF charge will be high enough to cause the junction diode to compress, or change state.

This problem is solved by the addition of a bypass resistor around the second RF diode. Under reverse bias conditions, there is very little current flow, and the -100V bias is applied to the diode at the junction. Of the two off arm diodes, the junction diode will have the highest incident power, and therefore needs the highest back bias voltage. The second diode is isolated from the input power and needs little or no back bias.

During forward bias, the PIN diode becomes a very low resistance ($\approx 1\Omega$). The bypass resistor is chosen to be large enough so that the parallel resistance of the network is essentially the PIN diode resistance. Over the 30-88 MHz frequency range, this technique causes very little impact to the RF performance.

Conclusion

A design has been outlined for low frequency, high power switches. These design techniques, coupled with Aluminum Nitride substrate and processing technology, and CERMACHIP™ diode technology have enabled the development of small, high power switches that can be configured to meet a variety of packaging requirements. Present devices have a plastic cover which allows the seal to meet gross leak requirements. This design can be used as a building block for drop-in, connectorized or surface mount

applications. The design, processing and packaging techniques presented here offer a smaller, more reliable solid-state approach to lower frequency switches.

The RF performance of the completed device is summarized below:

Requirement	Performance	Comments
Input power:	150W CW	4.5:1 Load VSWR
Switching Time :	34 μ sec	50% HCMOS to 10% RF
	1.5 μ sec	50% HCMOS to 90% RF
VSWR :	1.25:1	
Harmonics :	-70 dBc	
Intermod Distortion :	-25 dBc	2nd
	-22 dBc	3rd
	-30 dBc	5th
	-45 dBc	7th
Isolation :	-40 dB	
Noise Floor:	-155 dBm/Hz	
DC Supply :	+5Vdc @ 200 mA	
	-100Vdc @ 5 mA	
Temperature:	-40°C to +100°C	

The finished switches are shown below.

2.4 GHz MMIC PA Efficiency at -1dB Compression

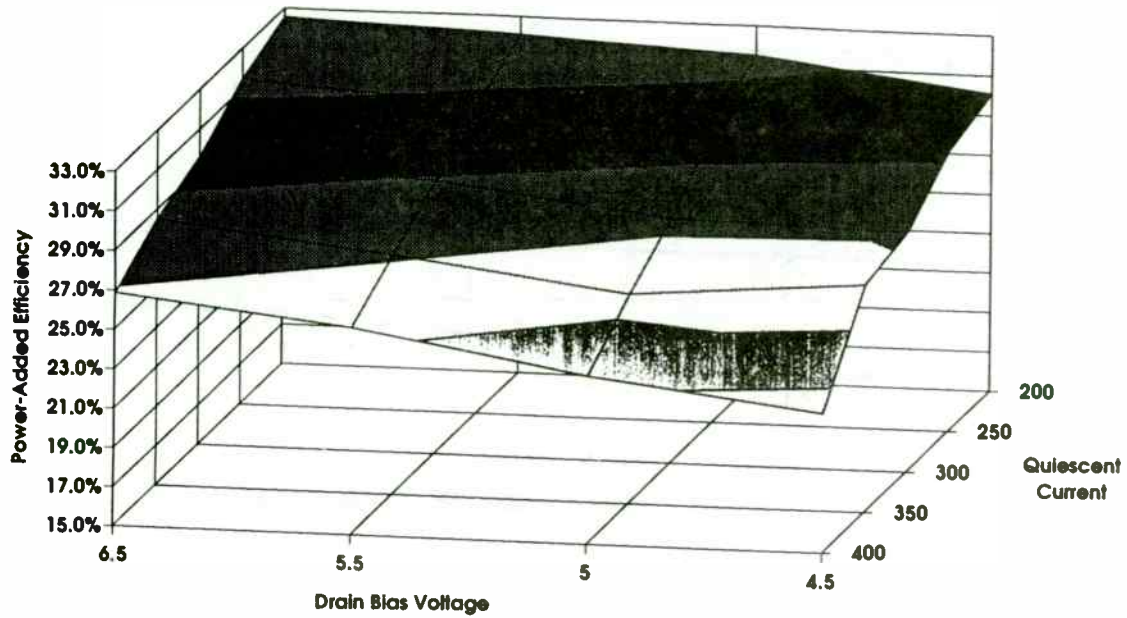


Figure 11. Measured Efficiency Vs Drain Bias & Current of 2.4 GHz PA

2.4 GHz MMIC PA Spread Spectrum Output Power

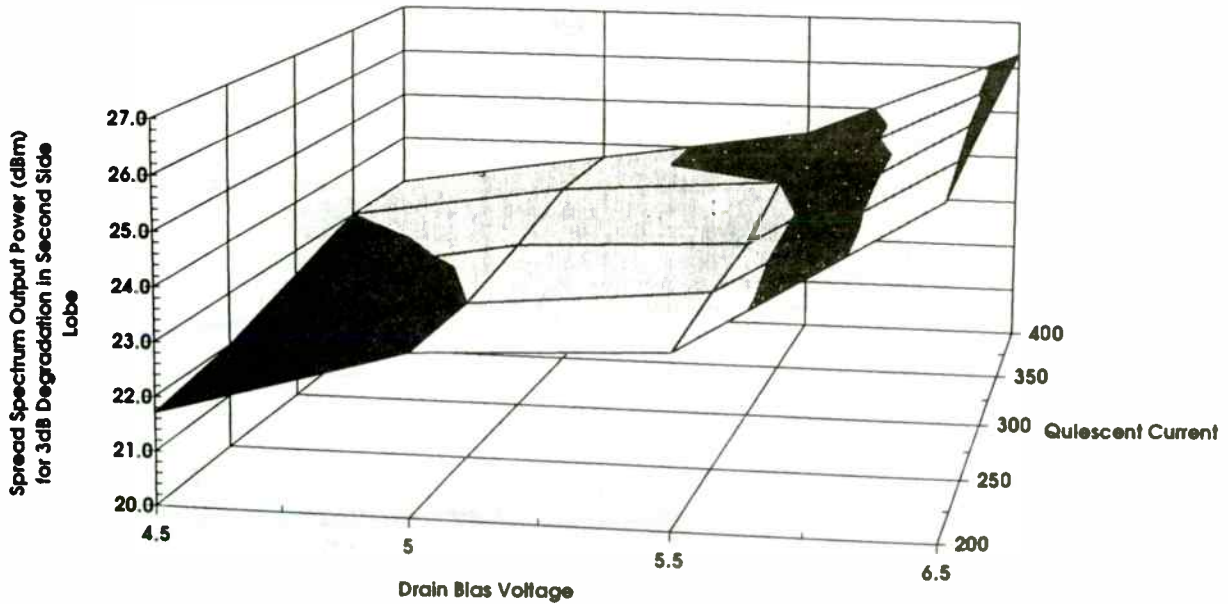


Figure 12. Spread Spectrum Output Power for 3dB Degradation in side-lobe Vs Drain Bias and Current of 2.4 GHz PA

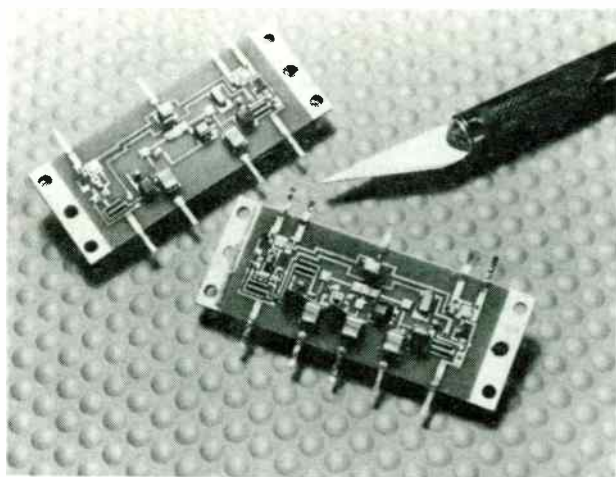


Figure 5

References

[1] R. Caverly and G. Hiller, "Predict PIN-diode switch distortion," *Microwaves & RF*, p. 8, January, 1986.

[2] J. B. Blum and K. Anzai, "Aluminum Nitride Substrates for Hybrid Microelectronic Applications," CeraTronics Application Note.

[3] G. A. Slack, "Nonmetallic Crystals with High Thermal Conductivity", *J. Phys. Chem Solids*, vol. 34, 1973, 321-335.

[4] Yamamoto *et.al*, *39th Electron. Comp. Proceedings*, pp. 23-28, May 1989.

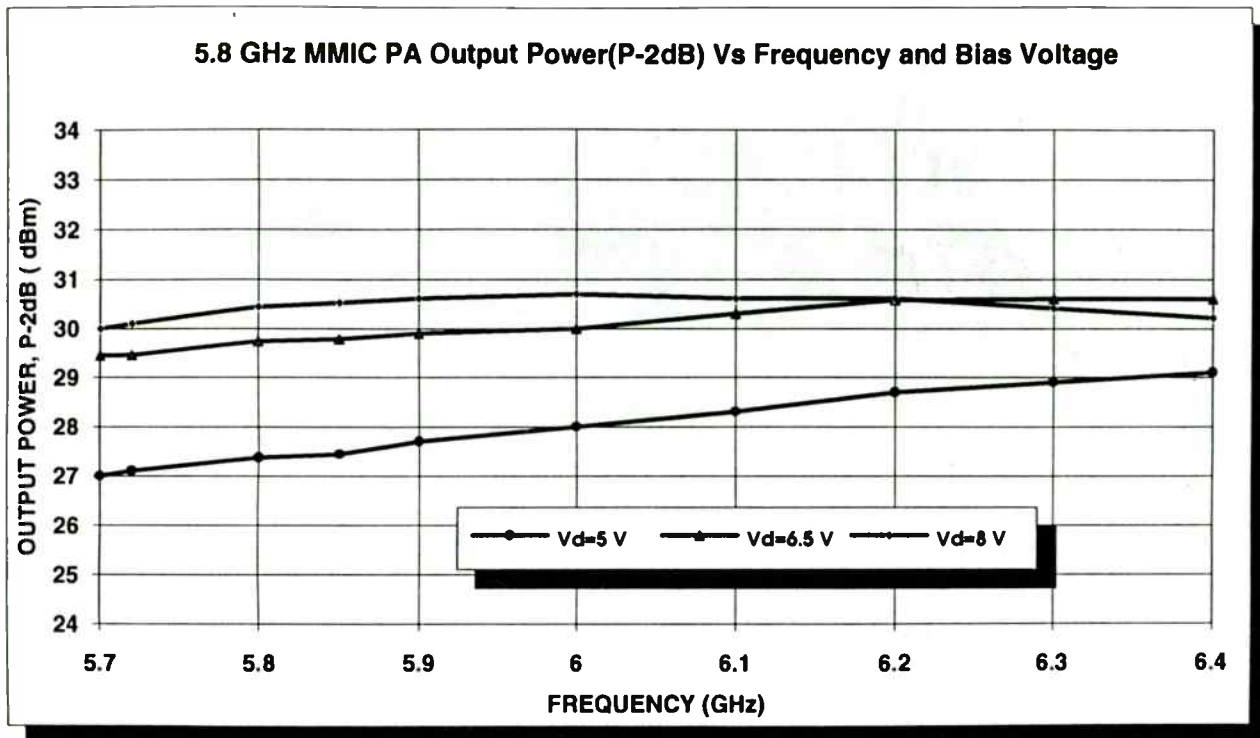


Figure 13. Measured Output Power Response of 5.8 GHz PA

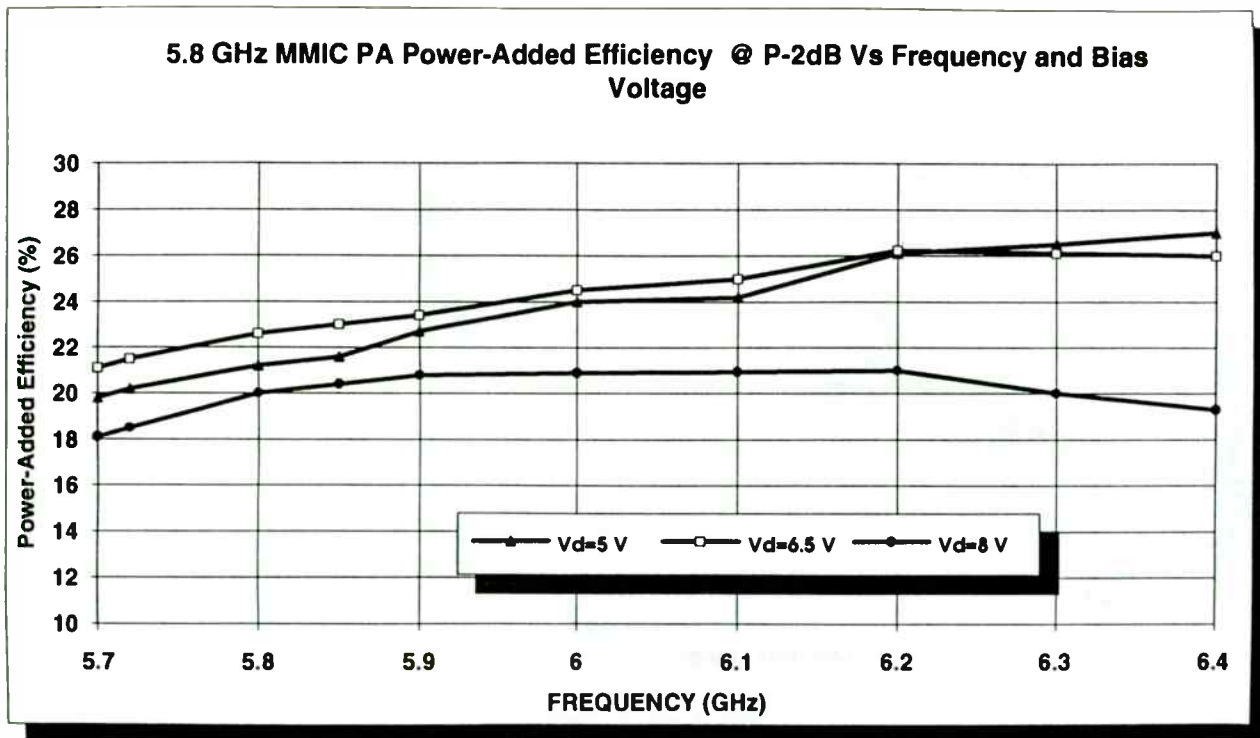


Figure 14. Measured Efficiency of the 5.8 GHz PA

FMCW RADAR ARCHITECTURE

K. V. PUGLIA
M/A-COM, INC.
MICROELECTRONICS DIVISION
LOWELL, MA 01853-3295

1.0 INTRODUCTION

The paper presents the results of a program to develop a low cost, general purpose FMCW radar set. The program was conducted to investigate and to determine those elements of system design as they relate to RF components and subsystems and to demonstrate the hardware effectiveness as a more general purpose range measurement instrument.

The general purpose nature of the hardware is emphasized as applications are limited only by the imagination and awareness of potential users who are confronted with a problem. In addition to obstacle detection, the hardware is suitable for stand alone ranging or positioning applications, traffic control and monitoring, and perimeter security or surveillance. The various applications would require changes to the processor algorithm (software); the algorithm being unique to each application.

The system architecture and many of the system parameters were based upon an earlier M/A Technical Memorandum by M. Hines (reference 1). In the development cycle, it was decided to employ a digital signal processor so that a more general purpose device could be constructed.

The program objectives included the manufacture of an engineering model with the attendant requirements of a microwave assembly, operator display, and packaging and mounting considerations.

The program was conducted over a one year period and included the following tasks:

1. system architecture development
2. component development
3. prototype manufacture
4. algorithm development
5. operational laboratory and field tests.

The tasks are reviewed and results are presented with respect to those tasks.

A summary is presented which delineates the more significant events of the program and offers some

suggestions for future study or hardware feature improvement.

2.0 THEORETICAL CONSIDERATIONS

The discussion of the theoretical aspects FMCW radar is quite elementary and is offered only to acquaint the reader with the basic principles necessary to understand the hardware implementation. The interested reader is referred to reference 2 for a more comprehensive presentation.

2.1 FMCW Radar Operation

FMCW radar are amongst the first types employed in low cost ranging applications. Their low cost was primarily the result of a simplified architecture which eliminated some of the components required in pulsed type ranging radar; specifically, the local oscillator, automatic frequency control, etc. The FMCW radar may be visualized as the electronic dual of the pulsed type radar where the timing mark is changing frequency as contrasted with changing amplitude (PAM). The question of range resolution is, nonetheless, determined by the width of the transmitted frequency spectrum; a wider transmitter spectrum resulting in better range resolution.

For the elementary FMCW radar depicted in Figure 2.1, the frequency at the output of the mixer is related to range of a fixed target, i.e. zero relative velocity, in accordance with the formula:

$$f_s = 2R (\Delta F/\Delta t)/c ,$$

where,

f_s is the output frequency,
 R is the target range,
 $\Delta F/\Delta t$ is the transmitter frequency rate of change, and
 c is the speed of light.

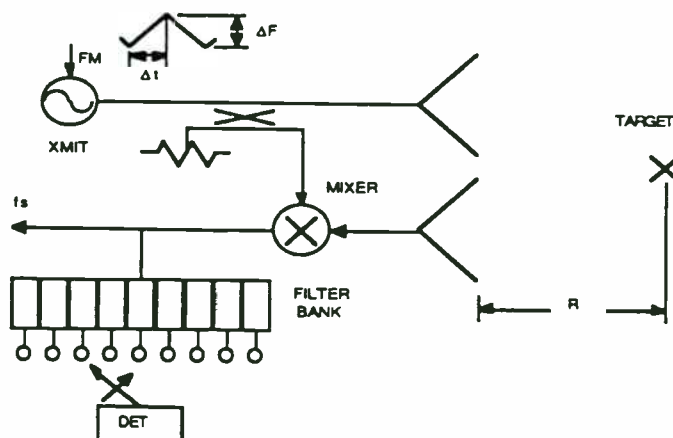


Figure 2.1 Simple FMCW Radar

Measurement Techniques for Wireless Systems

Session Chairperson: Ben Zarlingo, Hewlett-Packard Co., Lake Stevens Instrument Division (Everett, WA)

A Better Way to Design Tomorrow's Wireless Communications Systems Using RF Analyzers with Advanced Digital Signal Processing (DSP) **Ben Zarlingo, Hewlett-Packard Co., Lake Stevens Instrument Division (Everett, WA)**.....338

Applying the Modulation Domain to Wireless Communication Testing, **Barry Dropping, Hewlett-Packard Co., Santa Clara Div. (Santa Clara, CA)**.....344

Measuring the Peak-to-Average Power of Digitally-Vector-Modulated Signals, **Charles Meyer, Boonton Electronics (Randolph, NJ)**.....351

Delay-Spread Measurements and Feher's Bound for Digital PCS and Mobile Cellular Systems, **Dr. Kamilo Feher, DIGCOM, Inc. (El Macero, CA) and University of California at Davis (Davis, CA)**.....355

A filter bank, corresponding to respective range bins, and detector is employed to sequentially sample the energy within each range bin; if the detected energy within a particular filter exceeds a set threshold, then a target is determined to be present with a certain probability. There are several methods to implement the filter bank. With the recent advances in digital signal processing hardware and software, one technique is to structure an algorithm using filter coefficients which are stored within the processors data or program memory.

The determination of range is considerably more complex when relative motion between radar and target is considered. The equation representing the output frequency in this case is: (see appendix A for derivation)

$$f_s = 2f_0 v/c + 2(\Delta F/\Delta t)R/c + 2(\Delta F/\Delta t)vt/c,$$

where,

- v is the normal component of relative velocity,
- f₀ is the operating frequency, and,
- t is time.

The first term is a frequency component contributed by the Doppler effect; the second component is contributed by the range; and the third component is contributed by the change in range, or the velocity component. Note that with no relative motion between radar and target, i.e. v = 0, The equation reduces to $f_s = 2(\Delta F/\Delta t)/c$ as previously presented; if the radar frequency is not changed, i.e. $\Delta F/\Delta t = 0$, only the Doppler component remains, $f_s = 2f_0 v/c$. This provides a convenient method of measuring the target velocity and possibly some processing options.

2.2 Radar Range Equation

For either a pulsed or FMCW type radar, the maximum range of operation may be determined from a number of system and target parameters when entered into the radar range equation. Due to the statistical nature of the target cross section, weather conditions, minimum detectable signal level, propagation path variations and operational environment, the accuracy of the predicted range when compared with field experiments is generally poor. Notwithstanding the poor accuracy, the radar range equation does provide a basis for parameter comparison and trade studies as well as a model for the system operation.

The power at the radar receiver input is the product of the transmitted power, P_t, the

transmitter antenna gain, G_t, the two way path loss, $(1/4\pi R^2)^2$, the effective target cross section, σ, and the effective area or aperture of the receive antenna, A_e. This relationship may be deduced thru the following reasoning:

The power density at a given range from a transmitter = $P_t G_t / 4\pi R^2$.

The power reflected from a target = $P_t G_t \sigma / 4\pi R^2$.

The power density of the target at the receiver = $P_t G_t \sigma / (4\pi R^2)^2$.

The power intercepted by the receiving antenna, P_r = $P_t G_t A_e \sigma / (4\pi R^2)^2$.

This is the basic form of the radar range equation. The minimum detectable signal at the receiver is designated P_{rmin}, and occurs at the maximum operational range, R_{max}. Substituting into the equation, one may determine the maximum operational range:

$$R_{max} = [P_t G_t A_e \sigma / 4\pi P_{rmin}]^{1/4}.$$

There are a number of forms of this equation which make use of the following expression for antenna gain in terms of aperture and operating wavelength, λ, and the antenna physical area, A, and efficiency, η:

$$G = 4\pi A_e / \lambda^2 = 4\pi A \eta / \lambda^2.$$

Equations which are of some interest are repeated here:

$$R_{max} = [P_t A_e^2 \sigma / 4\pi \lambda^2 P_{rmin}]^{1/4}$$

or

$$R_{max} = [P_t G^2 \lambda^2 \sigma / (4\pi)^3 P_{rmin}]^{1/4}.$$

The minimum detectable signal may be approximated as that signal level which engenders a signal-to-noise ratio at the receiver output of 0 dB. The test equipment configuration required to perform this measurement is shown in Figure 2.2.

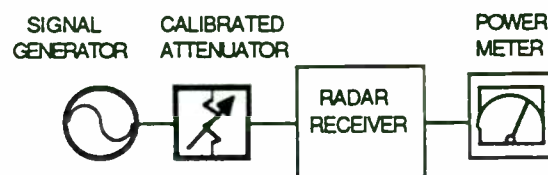


Figure 2.2 Minimum Detectable Signal Measurement

A Better Way to Design Tomorrow's Wireless Communications Systems Using RF Analyzers with Advanced DSP

Ben Zarlingo, Hewlett-Packard Co.

Abstract: Designing tomorrow's wireless communications equipment means working with burst and vector modulated signals. These signals are difficult to characterize using traditional instruments. This paper discusses real world measurements on these signals and systems, made with analyzers that combine traditional approaches and advanced DSP (Digital Signal Processing).

While the RF spectrum that we all must share is limited, the demands for use of this spectrum are growing exponentially. That situation, and the factors driving it are well known to everyone in the industry. It is a situation containing both good news and bad news for RF design engineers.

The good news is the expanded need for RF design expertise to develop these new systems. New systems to transmit more of the same information (such as voice and video) and new systems to transmit an ever-larger quantity of new information (mostly data of one type or another). In any event, more and more information is being sent in digital form, whether it is data or just voice. This increase in the use of digital techniques is often a result of the need to send more information in the same "space"--to make the most efficient use of the RF spectrum.

But of course this is where the bad news comes in. Designing tomorrow's digital wireless communications systems involves working with signals that are burst, transient (or non-repeating), and complex modulated. A far cry from the past, where the information was usually encoded as continuous AM or FM, and where high performance signal analysis could be done with tools such as spectrum analyzers, counters, power meters and so on.

On today's complex signals, performing even the simplest traditional measurements is a difficult challenge. The process of RF design involves nearly countless measurements of simple parameters such as frequency, power, distortion, noise, etc. But as engineers have discovered, making these measurements with speed and precision on complex modulated and/or time-varying signals is next to impossible.

Designers long to reach for traditional tools such as oscilloscopes and spectrum analyzers, and to make the

traditional measurements that will give them the insight to be able to use accumulated judgment, experience and talent and established design techniques to quickly and efficiently design circuits and systems that meet stringent requirements.

But many measurement tools have not been able to keep up with these new signals. While today's digital oscilloscopes are excellent tools for viewing complex and time-varying signals, their 8-bit A/D converters do not have the resolution and accuracy to take over the functions traditionally performed by spectrum analyzers.

And swept spectrum analyzers offer high performance, but are designed for continuous signals. Any signal that is time-variant--that is, a signal that changes during a spectrum analyzer's sweep time--demands new tools and techniques.

For the designer, several approaches have emerged. Traditional tools have been enhanced. Some spectrum analyzers now have time-gated signal analysis capability, allowing them to measure certain time-variant signals which repeat consistently, and where an external trigger signal is available. However burst signals of short duration may limit the frequency resolution and dynamic range of these measurements, due to the need to use wide, fast-settling RBW filter settings.

New tools have been developed, such as modulation domain analyzers. These analyzers can measure the frequency behavior of rapidly time-varying signals by implementing very fast zero-dead-time counters. Their analysis is limited to frequency and phase, since they cannot measure amplitude or distortion, and cannot separate multiple signals from one another.

But what designers need are tools that give them traditional measurement functions and insight and allow them to make tests throughout the block diagram of communication systems--all frequencies, including baseband through IF and RF. Tools with the performance and broad capability that a spectrum analyzers offer in traditional RF design. Tests that correspond with those they have developed for simpler signals and systems.

The measurement procedure consists of reducing the input signal level such that the power meter reads only the receiver output noise level. Next, the attenuator is decreased until the power meter reads 3 dB above the noise level. At this input power level, the signal-to-noise ratio is 0 dB and the minimum detectable input power level has been established. The procedure is somewhat more complicated when measuring pulsed radar receivers.

The equivalent input noise level in dBm, which is the same as the minimum detectable signal, may be written mathematically (see appendix B):

$$N_i = K T_0 B L_c (F_{if} + T_r - 1),$$

where,

$K T_0$ is Boltzman's constant times absolute temperature,

B is the receiver bandwidth,

L_c is the mixer conversion loss,

F_{if} is the IF amplifier noise figure, and,

T_r is the mixer diode noise temperature ratio.

3.0 SYSTEM IMPLEMENTATION

The system implementation is presented below commencing with a brief discussion of the block diagram and the component development.

3.1 System Block Diagram

The system block diagram is illustrated in Figure 3.1 and depicts the basic elements of the FMCW radar:

- WIP or waveguide integrated package;
- Preamplifier/Filter PCB Assembly;
- Gunn Voltage Controlled Oscillator or VCO;
- Digital Signal Processor PCB Assembly;
- +/- 12 V DC/DC Converters;
- Display Assembly;
- Pyramidal Horn Transmit and Receive Antennas.

The Gunn VCO is employed as both transmit and receiver local oscillator source; a coupler (6 dB) samples the transmit power and applies it to the Schottky diode, quadrature mixer. The receive signal enters the system thru a pyramidal horn and is then applied to the other port of the quadrature mixer. A preamplifier (60 dB gain) boosts the converted signal and applies it to the band pass

filter. The amplified/filtered signal then becomes the input to the digital signal processor (DSP) where further filtering and amplification take place. Initially, two algorithms were employed in the digital signal processor: a feedthru mode and a Fast Fourier Transform (FFT) mode. The feedthru mode routes the input signal thru the codec where both filtering and A/D conversion are performed; the signal is then applied to the digital signal processor (ADSP-2101) where the sampled value from the codec is stored/retrieved and subsequently routed back to the codec, processed via D/A conversion and output. In the FFT mode, the codec again supplies the A/D samples to the DSP where the sequence of values (256 values of the sampled input signal) are stored and subsequently multiplied by stored coefficients in accordance with a radix four, complex, FFT algorithm. The output sequence represents the spectral content of the input signal with a resolution bandwidth of approximately 30 Hz (approximately 4 KHz/128).

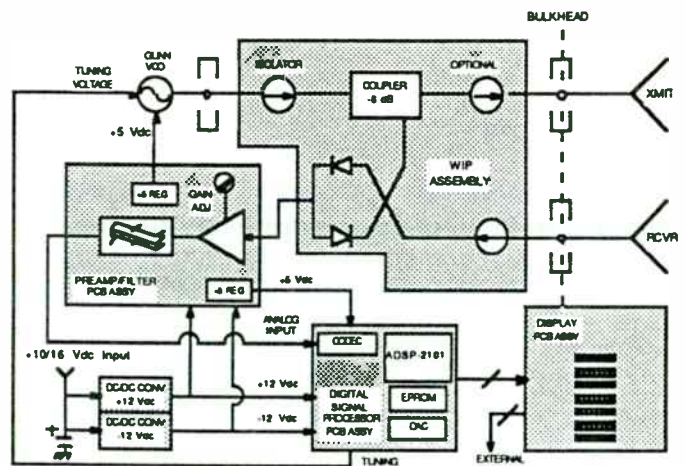


Figure 3.1 System Block Diagram

Each frequency bin of the FFT represents a target range. The values of FFT are sequentially strobed to a D/A converter and oscilloscope. The resulting display is the classic 'A' scope of target amplitude on the vertical axis and target range on the horizontal axis.

Two DC/DC converters have been employed to facilitate operation from a single positive voltage source over a range of input voltages from 10 Vdc to 16 Vdc.

The Unit is housed within an extruded and brazed aluminum enclosure and fitted with a conventional camera attachment for tripod mounting. A low cost LCD portable oscilloscope was utilized for information display purposes. The entire assembly weighs a total of less than 12 pounds.

3.2 Component Development

Fortunately the digitizing and digital signal processing technologies that have created these complex and time-varying signals have also made new measurement solutions possible--both new tools and new measurements to go along with them. This paper will demonstrate several new or enhanced measurements that are useful in the design of digital wireless communications systems.

These measurements are made with the HP 89440A Vector Signal Analyzer. It covers the baseband-through-RF frequency range of DC to 1.8 GHz with broad measurement capability in the frequency, time and modulation domains. Key innovations of the analyzer include:

- An A/D subsystem with state-of-the-art performance of up to 16 bits linearity and up to 22 bits resolution at 25.6 million samples/second
- A high performance digital signal processing subsystem using both proprietary and off-the-shelf elements to produce complex measurement results at up to 60 traces/second
- Advanced digital signal processing techniques including a universal AM/FM/PM demodulator, digital modulation analysis, correlation and coherence functions
- A flexible stimulus source covering the analyzer's entire frequency range with narrowband signals such as sinewaves, chirps, random noise and arbitrary waveforms.

Transient or Burst Signal Measurement

Designing systems using burst or time-varying signals is complicated by the difficulty of making simple, traditional signal quality measurements such as frequency, power, signal/noise, distortion, etc. Any signal which changes during the measurement time of a signal analyzer will prevent the user from obtaining reliable measurements. The same is true for transient signals of insufficient duration for a complete measurement or sweep.

An example of such a signal is shown in the time domain in figure 1a. It is composed of two alternating frequency bursts, with noise and harmonic distortion. Several spectrum measurements (made at slightly different times) of this signal are shown as figures 1b-1d. These spectra are not useful for making the signal quality measurements described above, since the actual spectra are obscured by the burst artifacts and the presence of two different signals at different times

during the spectrum measurement.

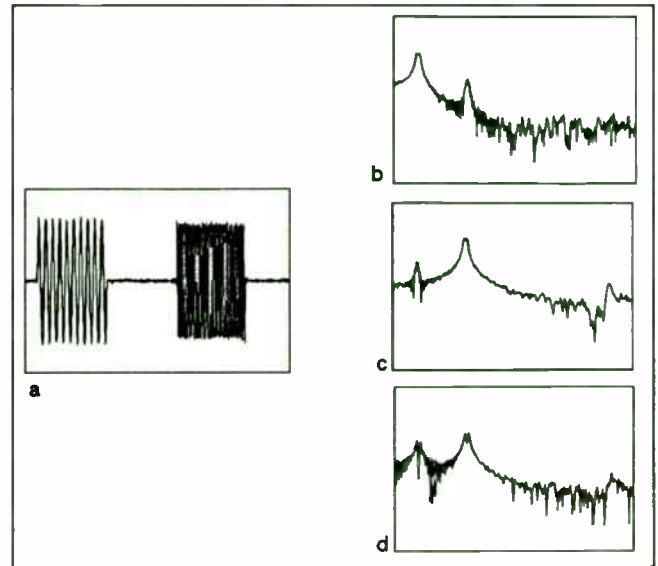


Figure 1: Burst measurements without time-gated spectrum analysis

When the signal is digitized with high resolution and accuracy, DSP techniques can be used to isolate the different components of the signal and perform spectrum analysis. This is shown in figures 2a-2c. In each figure the upper trace is the time domain signal and the lower trace is the spectrum measurement. The "gate" markers are shown on the upper trace as vertical bars, with the spectra (lower trace) corresponding to the part of the signal selected between the gate markers.

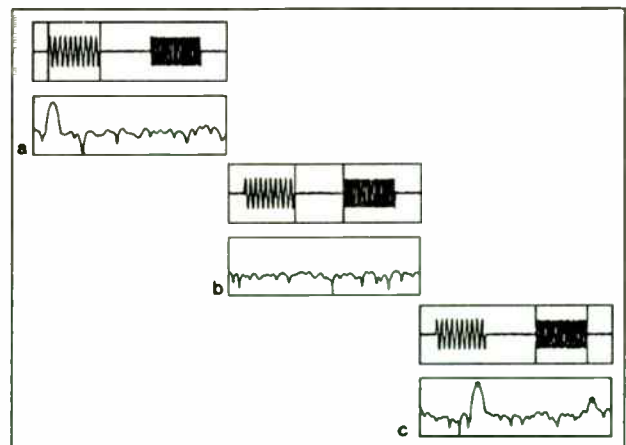


Figure 2: Burst measurements with time-gated spectrum analysis

Though they came from a challenging, time-variant signal, these spectra are as easy to interpret as similar

A number of components were developed for the prototype hardware and for special tests to be conducted on other components and the prototype hardware. In order to provide a comprehensive understanding of the prototype operation, all components of the system will be reviewed and test data will be presented. In some cases, the component parameter data will be discussed relative to the performance of the prototype hardware.

3.2.1 Voltage Controlled Oscillator (VCO)

The VCO is the most critical component of prototype hardware. The VCO supplies both transmitter and local oscillator signals and ultimately, via tuning linearity, determines the radar range resolution performance. A VCO which exhibits a nonlinear tuning characteristic spreads the spectrum of the IF signal. One may immediately discern this through examination of the equation for the IF signal developed earlier. The instantaneous frequency of the IF signal was found to be linearly proportional to the rate of change of frequency with time. Although no evidence was found in the prototype hardware, the VCO PM noise will also contribute to noise in the IF band.

The VCO employed within the prototype hardware was a high quality, waveguide cavity, Gunn oscillator with electronic tuning via hyperabrupt GaAs varactor diode. The equivalent circuit of the VCO is illustrated in Figure 3.2. The Gunn diode is a negative resistance device which is coupled to the waveguide cavity resonator; the varactor diode is similarly coupled. The net loop resistance is negative and thereby becomes a source of energy at the resonator frequency. A positive load resistance is coupled to absorb a portion of the energy. If the load coupling increases to the point where the net loop resistance becomes positive, the oscillation is extinguish.

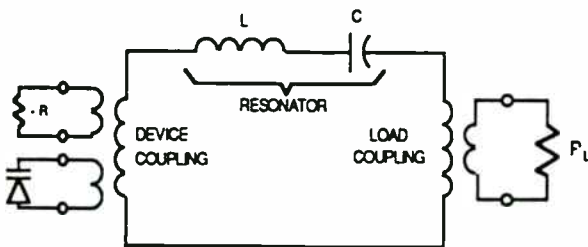


Figure 3.2 VCO Equivalent Circuit

The mechanical configuration of the Gunn oscillator is depicted in Figure 3.3. The waveguide cavity is approximately $\lambda/2$ long at the operating frequency.

Both the Gunn and varactor diodes are coupled to the cavity by posts thru the top wall of the waveguide. This configuration has been successfully employed for many years and is the topology of choice for the commercial sources group at M/A-COM. The VCO operates from well regulated +5 Vdc supply at a current of approximately 300 ma.

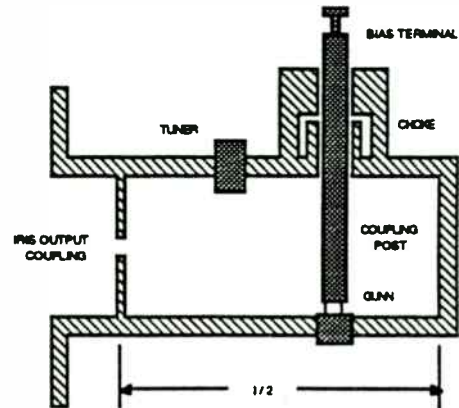


Figure 3.3 Gunn Oscillator Configuration

The power output and voltage tuning characteristic of the VCO is shown in Figure 3.4. Analysis of the data indicates that the deviation from linear tuning is less than one percent over the four to seven volt range.

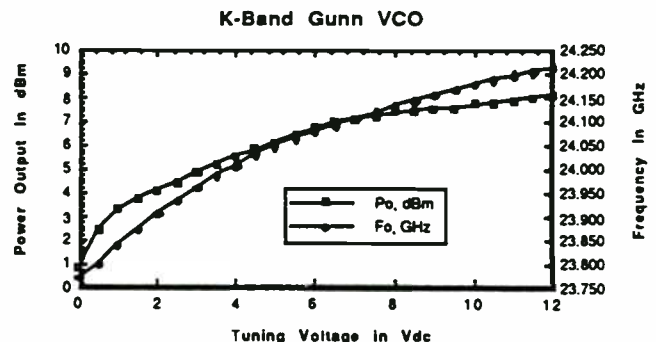


Figure 3.4 VCO Power Output and Voltage Tuning

3.2.2 Waveguide Integrated Package

The Waveguide Integrated Package or "WIP" is a construction medium used at M/A-COM for several years to achieve optimum component and subsystem performance within a planar physical realization which supplies both the microwave transmission medium and the mechanical housing. The WIP configuration makes use of the extensive numerically controlled machinery and lends itself well to low cost investment or die casting. The WIP construction technique is illustrated in Figure 3.4. The channels are machined or cast and permit the propagation of the TE₁₀ rectangular waveguide mode. Semiconductor devices are coupled to the waveguide transmission medium by means of posts;

CW signals. Frequency, power, distortion and noise or signal/noise can be measured directly. The third, highest frequency, component of the signal can be tracked down as harmonic distortion on the higher frequency burst. The relative power of the signal bursts can be measured, along with on/off ratio and other parameters.

A measurement architecture with DSP operations performed on a digitized signal has other advantages for time-gated signal analysis:

- The signal to be tested need not repeat consistently, since the spectrum analysis can be performed from a stored single record.
- An external trigger signal is not required, since the signal to be measured can be selected from storage using gate markers.
- The IF filters used to perform spectrum analysis can be implemented digitally, providing better selectivity, shape factor and accuracy.
- The digital IF filters can be implemented with any arbitrary resolution bandwidth, allowing the user to select the best combination of gate width and frequency resolution, whether or not it fits the traditional 1-3-10 sequence.
- Additional dynamic range can be obtained when measuring repetitive signals by using time-domain averaging of the input signal. Noise and other components uncorrelated with the trigger will tend to average themselves out of the measurement, revealing lower level coherent spectral components.

This combination of benefits allows the designer to extract the maximum amount of information and insight from time-varying signals.

Transmitter Turn-On Analysis

Time-division multiple-access (TDMA) and other burst or frequency-agile communication schemes place special demands on many of the components of the transmission chain. For example, transmitters must turn on quickly and in a well-controlled fashion to avoid disturbing adjacent channels. In addition, their amplitude and frequency or phase must rapidly achieve stable (final) values so that these parameters may be used for modulation.

Time spent in turn-on is time lost for transmitting the data that is the fundamental purpose for the system, so designers must carefully optimize this behavior.

Traditional swept analyzers are good tools for measuring the frequency and power level of stable signals, but designers often must use other tools to characterize these rapidly changing characteristics of transmitters at turn on. Peak power meters and modulation domain analyzers are used to measure instantaneous power and frequency, respectively. However these tools give up some of the advantages that narrowband swept analyzers brought to such measurements. Specifically, broadband power meters do not have the wide dynamic range of spectrum analyzers and modulation domain analyzers do not have the frequency selectivity that allows one signal to be characterized among many others.

Here again the flexibility and power of advanced DSP can provide direct, intuitive measurements on dynamic signals combined with the benefits of traditional approaches used on simpler signals. Figure 3 is an example of a transmitter burst with amplitude and frequency variations at turn on. The lower trace is a spectrum analysis of the entire burst, indicating that there are probably multiple frequencies present in the burst. The amplitude variations can be roughly seen from the upper (time domain) trace.

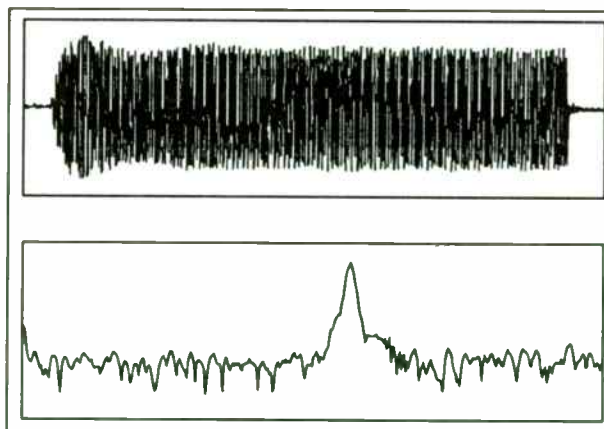


Figure 3: Transmitter turn-on and spectrum

If a trigger signal was available and if the signal consistently repeated itself, time gated spectrum analysis might be used to characterize the parameters of this signal. The advanced time gated spectrum analysis described in the example above could also be used, even if the signal was a transient or if no trigger was available.

But since any variation in amplitude, frequency or phase can be treated as modulation, we can use DSP to implement precision demodulation and display the desired characteristics of this burst directly. This is

similar to the Gunn diode mounting discussed in the previous section. The WIP packaging technique allows the integration of a number of components within a single chassis which also serves as a mounting platform or enclosure for various electronic functional controls such as PIN diode drivers, VCO tuning circuits, IF and video amplifiers, voltage regulators, etc.

The WIP package which was developed for the FMCW radar program is illustrated schematically in Figure 3.5. The integrated functions are the LO isolator, the LO coupler, optional transmit and receive port isolators, and a balanced mixer. The transmit and receive port isolators are configured such that a single antenna or separate transmit and receive antennas may be utilized. The balanced mixer employs a 'short slot' quadrature hybrid for the separation of the local oscillator and signal ports. The 6 dB local oscillator coupler is also implemented using a similar narrow waveguide wall coupling aperture. The ferrite isolator originated from a previous design at a slightly lower operating frequency. The isolators are constructed with a teflon-ferrite-teflon 'sandwich' which is placed upon impedance matching triangles at waveguide junctions formed at 120 degrees. The loads for the isolators are simple polyiron material with a machined taper transition in two planes.

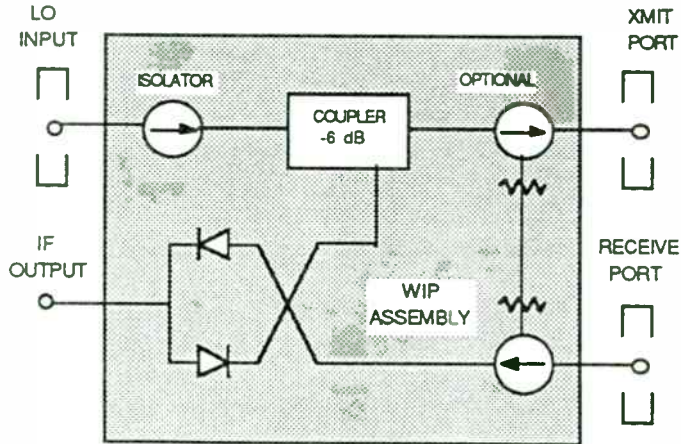


Figure 3.6 WIP Schematic

The performance of the WIP assembly is illustrated in Figures 3.6 and 3.7. Note that the operating bandwidth of the WIP assembly is significantly wider than the required 24.125 +/- 0.10 GHz.

To summarize the performance: the VSWR at all ports is less than 1.20:1, the transmitter to antenna loss is less than 3 dB, and the single sideband noise figure is less than 10 dB over a frequency range from 23.0 to 25.0 GHz. No attempt

has been made to improve the noise figure thru diode selection; anticipated improvement is 1.0 to 2.0 dB.

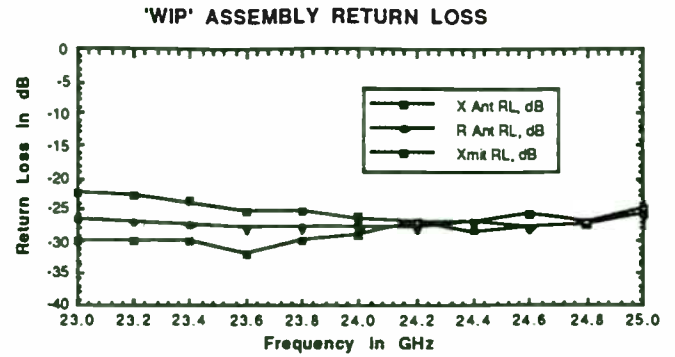


Figure 3.7 WIP Assembly Return Loss

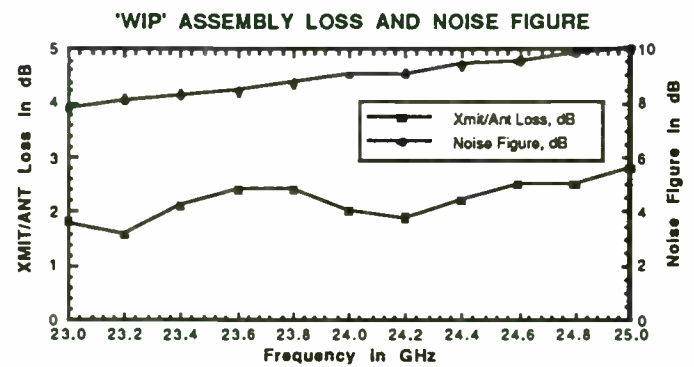


Figure 3.8 WIP Assembly Loss and Noise Figure

3.2.3 Pre-amplifier/Filter

The pre-amplifier is required to raise the signal level at the mixer output prior to application to the processor, while the filter is required to limit extraneous signals and noise. Specifically, the filter has a low frequency cut-off of approximately 1.0 KHz to attenuate those signals generated from the frequency sweep. These signals are the result of variations in the mixer output voltage over the sweep frequency. The upper frequency limit of the filter is approximately 5.0 KHz. The CODEC within the digital signal processor also has a fifth order switched capacitor bandpass filter with low and high frequency cut-offs of 200 Hz and 3.4 KHz, respectively. A schematic of the pre-amplifier filter is illustrated in Figure 3.8.

shown in figure 4a as instantaneous amplitude and in figure 4b as instantaneous frequency. The measurement is made by selecting the desired center and span frequencies, along with the modulation type. If desired, an "auto-carrier" function can be implemented in the signal processing as well.

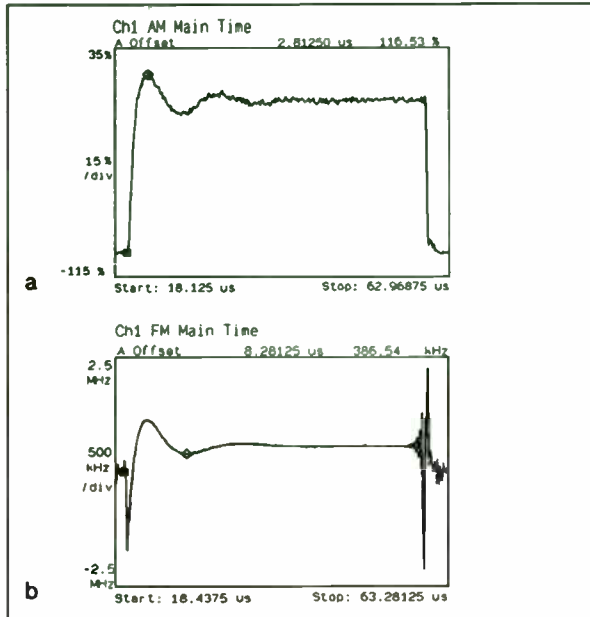


Figure 4: Amplitude and frequency at turn-on

For the designer this measurement technique offers several benefits:

- Direct display of the desired parameters--The amplitude demodulation result can be displayed as percent modulation, and the frequency variations displayed as deviation in Hz.
- No AM/FM/PM interaction--DSP technology allows the AM demodulator to be insensitive to PM, the PM demodulator to be insensitive to AM, and so on.
- Wide dynamic range and frequency selectivity--By using a narrowband analysis technique, the noise floor is kept low and no extraneous signals or adjacent channels interfere with the measurement.
- Real-time results for tuning--Modern DSP hardware allows this demodulation to be performed inside the instrument at a rate of tens of measurements/second rather than off-line in an external general purpose computer. Circuits can be adjusted and performance optimized in real time.

- Design with a single analyzer--Only one piece of measurement hardware is necessary to perform both general purpose signal analysis and precision demodulation.

Baseband-RF Coherence Measurement

Phase modulation techniques are increasing in number and variety, and are used more and more frequently in advanced communications systems. Whether a system uses phase modulation alone or in combination with other modulation, oscillator phase stability is a critical design parameter. Unfortunately it can also be a difficult parameter to measure, and the sources of phase noise or spurious sidebands can be very tough to track down. Both the sources and coupling mechanisms are many and varied.

Precision phase demodulation using DSP is an obvious tool to use to attack these measurement problems. It offers all the measurement benefits described in the example above. In addition, a signal processing function called coherence can be used with demodulation to great benefit in examining the relationship between baseband noise or discrete signals and troublesome phase noise or spurious sidebands at RF.

An example of this technique is shown schematically in figure 5.

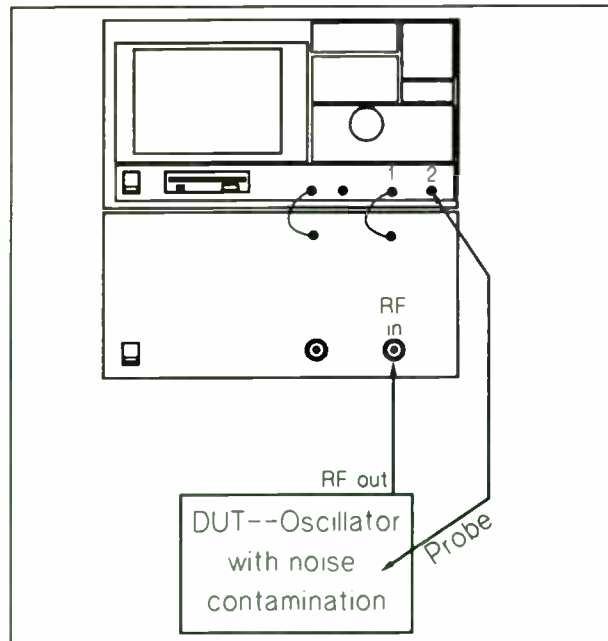


Figure 5: Baseband--RF coherence measurement

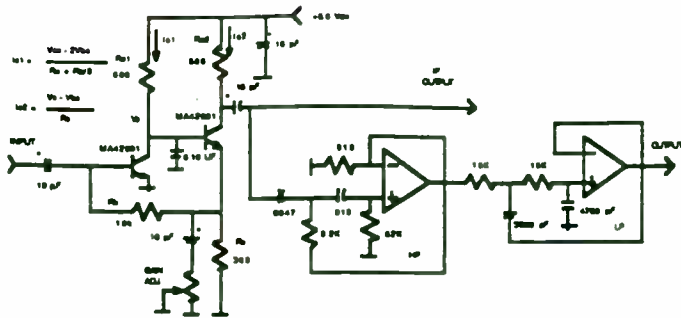


Figure 3.9 Preamplifier/Filter Schematic

The passband response of the amplifier/filter is displayed in Figure 3.9. The gain at 1.0 KHz is 60 dB and the noise figure is estimated at 2.0 dB.

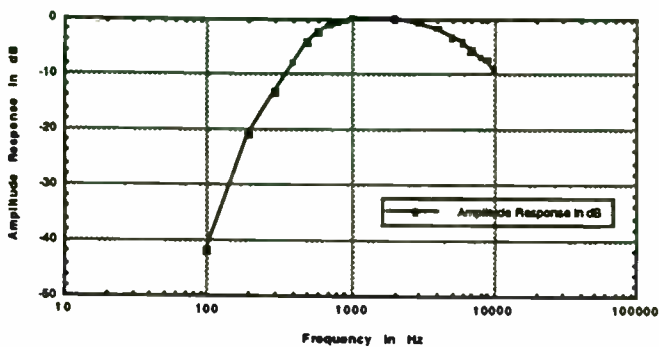


Figure 3.10 Preamplifier/Filter Frequency Response

3.2.4 Digital Signal Processor

To avoid the cost of developing an integrated digital signal processor, it was decided to purchase a general purpose board which incorporates a digital signal processing integrated circuit and the necessary peripheral functions such as sampling, A/D conversion, filtering, D/A conversion, program and data storage, etc. The selected board is the Analog Devices EZ-LAB. The EZ-LAB is a low cost evaluation and demonstration tool for the ADSP-2101 DSP microcomputer. It permits the testing of coded digital signal processing applications on the ADSP-2101. The EZ-LAB is equipped with a 27C512 EPROM containing several prepared processing algorithms. The EPROM is socket mounted and may be replaced with another EPROM containing user created algorithms. The DSP board measures 4.5 X 6.0 inches and is functionally illustrated in Figure 3.10 below.

The DSP board contains a processor controlled CODEC (TP3054) which samples (8 KHz rate) and digitizes (8 bit) the input signal; the resulting data is converted to serial mode and enters the ADSP-

2101 digital signal processor. The data is processed in accordance with the algorithm in the program memory of the DSP.

Currently, we have made use of two of the 'canned' algorithms (firmware) supplied as boot pages on the 27512 EPROM. The first algorithm is a feedthru mode whereby the digitized signal enters the DSP serial port from the CODEC. The signal is output from the DSP to the CODEC, back to a D/A converter and fed to the LM388 for amplification and sent to the analog output of the DSP board. It should be mentioned that the CODEC contains a fifth order switched capacitor bandpass filter (200-3400 Hz).

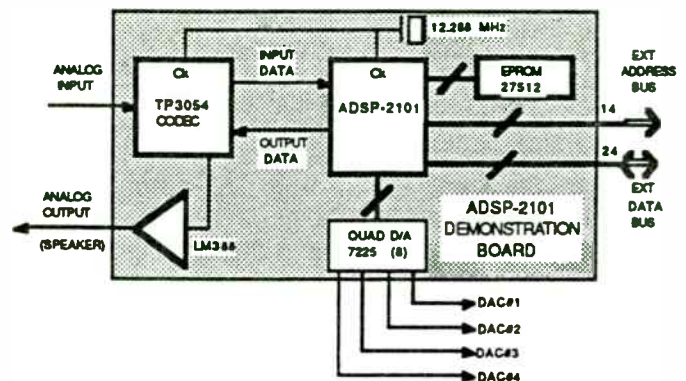


Figure 3.11 Digital Signal Processor Functional Schematic

Another algorithm utilized is a 256 point, radix-4, complex Fast Fourier Transform or FFT algorithm. A frame of data (256 sampled points) is processed and stored in a results buffer; the results buffer is then scanned and displayed on an oscilloscope at 40 frames per second. The timer function of the DSP continuously scans and displays the results and allows updates to the changes in the spectrum. The display driver generates a negative sync pulse to allow proper operation of the oscilloscope. The resulting display resembles a radar 'A' scope type display, i.e., target amplitude and range. The 256 point FFT display presents the frequency or range bins sequentially in a spectrum analyzer or magnitude-squared format.

The DSP board has an operational limitation; the relatively low (8 KHz) sampling rate permits processing signals over a relatively narrow frequency band, i.e., 4 KHz, or half the sample rate. Although this is not a severe restriction for general purpose applications, processing signals with wider bandwidths or Doppler components is not possible without consideration of a more complex algorithm. An alternate DSP board could be obtained with a CODEC operating at a higher sampling rate.

First, a direct RF spectrum measurement is made of the carrier with its close-in phase noise sidebands. This narrowband spectrum measurement is shown in figure 6, where the noise sidebands can be clearly seen.

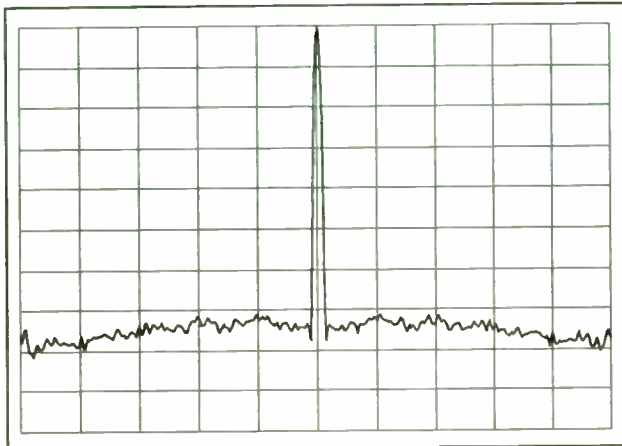


Figure 6: Narrowband spectrum with phase noise

Phase demodulation can be used on this RF carrier to recover and display the actual noise modulating signal in the time domain. This is the top trace in figures 7a and 7b.

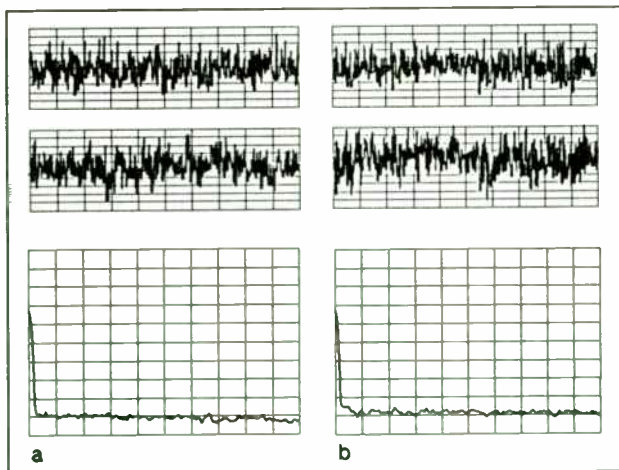


Figure 7: Phase demodulation in frequency and time

A second, baseband input channel of the vector signal analyzer can be used to probe various locations in the oscillator circuit to uncover noise sources which may be contaminating the RF carrier. This is shown schematically in figure 5. But in examining the resulting noise sources in both the time and frequency domains, the analysis problem is readily apparent: One source of noise often looks identical to another, whether examined in the time or frequency domains.

The bottom two traces in figures 7a and 7b represent time and frequency domain analysis of two different baseband noise sources. They are indistinguishable, and thus the source of the undesirable phase modulation (phase noise) remains unknown.

A powerful solution to this analysis problem is the DSP coherence function. Coherence is a measure of causality or the "relatedness" of two signals. It is a function of frequency, and is expressed as a value between zero and one. A value of zero indicates that two signals are unrelated, while a value of one indicates that two signals are exclusively related through a linear system.

We can use the coherence function in this example to compare the phase noise demodulated from the RF carrier with the noise sources which have been probed and measured directly at baseband. The results are shown in figures 8a and 8b.

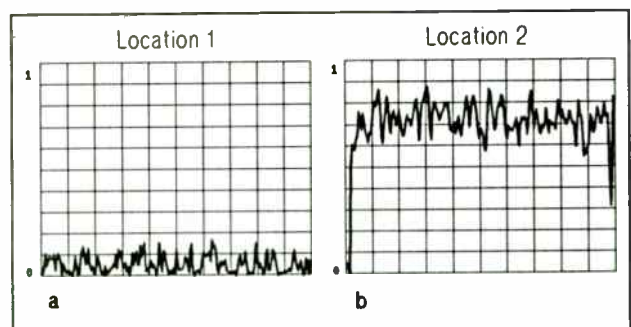


Figure 8: Baseband-RF coherence measured at two locations

The low coherence of figure 8a indicates that the baseband signal probed at that location is not responsible for the phase noise on the RF transmitter. The high coherence result in figure 8b shows that this signal is indeed the source of the phase noise, and that the baseband-to-RF coupling is broad and flat, with no obvious filtering characteristics.

This is a powerful and productive result for the RF designer. A principal source of phase noise can be discovered easily and attacked directly. In addition to the source of the phase noise, the strength and frequency response of the baseband-to-RF coupling function is revealed. This knowledge can help the designer better understand the phenomena and perhaps provide alternative solutions. If the noise source cannot be eliminated, the problem may still be fixed by defeating the newly-understood coupling mechanism through the use of filtering, active

This is one of the recommendations for a possible next phase. Many of the field tests employed this algorithm to obtain data on the FMCW equipment.

3.2.5 Horn Antenna

The transmit and receive antennas were low cost, cast pyramidal horns with E-plane and H-plane aperture dimensions of 1.29 X 1.72 inches, respectively. Using the formulae of Braun (reference 3), the antenna gain was calculated to be 16.5 dB. Subsequent gain measurements of 16.8 db sustained the calculation within acceptable accuracy limits. The antenna beamwidths (H and E plane) were calculated using the formulae of Stimson (reference 4): $\theta_h = 20^\circ$, and, $\theta_e = 27^\circ$.

3.2.6 DC/DC Converter

Two DC/DC converters were procured to produce +12 and -12 Vdc for operation of the FMCW equipment. The negative converter permitted field operation of the equipment from an automobile battery via the cigarette lighter plug. Two separate +5 Vdc supplies were developed to operate the Gunn oscillator and the logic devices.

3.2.7 Ramp Voltage Generator

In order to utilize the inherent linearity of the VCO, a swept voltage must be generated which has both a symmetrical and linear up/down sweep. A nonsymmetrical or nonlinear ramp voltage will limit target resolution and accuracy.

A circuit capable of the required linearity and symmetry is illustrated in Figure 3.11. The circuit makes use of a stable oscillator and digital counters with up and down mode control. The counter numeric outputs are cycled through the up and down counts and applied to a D/A converter. The converter output is offset and buffered in order to be compatible with the required VCO control voltage. The circuit further permits ramp frequency control by variation of the modulus of the input counter. The ramp frequency control is required to display full scale ranges of 30, 60, 120, and 240 meters. These ranges are related to ramp frequencies of 100, 50, 25, and 12.5 Hz, respectively.

It is not anticipated that the digital ramp generator be utilized in the final equipment because the DSP is to be programmed to generate the required ramp voltage. However, the linear ramp generator was required for test purposes prior to algorithm development.

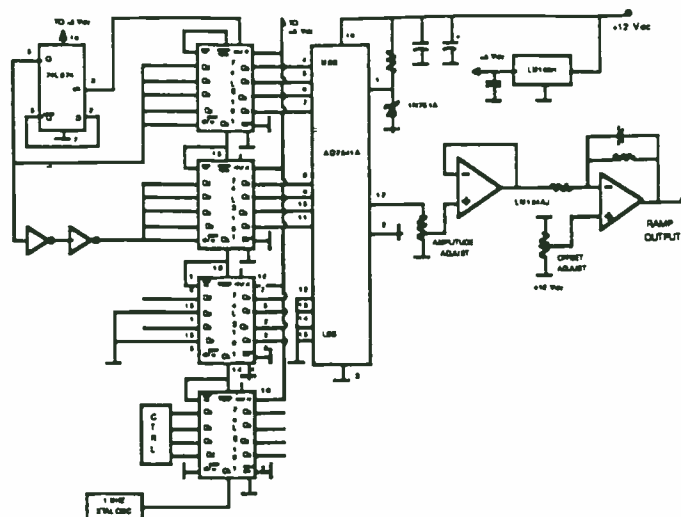


Figure 3.12 Digital Ramp Generator

3.2.8 Display

The display employed during equipment test phase was a purchased portable oscilloscope, Leader Instruments model 100P. The Model 100P is a battery powered combination DMM/oscilloscope with an LCD display. A companion battery powered thermal printer (Model 710) provides hard copies of stored waveform data. The unit measures 5.5 X 4.0 X 1.5 inches and attaches to the FMCW radar equipment back panel.

4.0 SYSTEM TEST

Following assembly and system alignment, both laboratory and field tests were conducted. The test description, conditions and results are presented in this section.

4.1 Laboratory Test

Two configurations of test equipment were utilized to determine the operational quality of the engineering model. The configurations and test results are presented.

4.1.1 Sensitivity measurements

The sensitivity measurement test employed a double sideband generator to offset the transmitter output of the FMCW module; the transmitter frequency was not swept during these tests. An audio oscillator was used to vary the sideband frequency to permit testing of minimum detectable signal, equivalent input noise and IF bandwidth.

The test equipment configuration of Figure 4.1 was utilized to conduct the tests. The transmit frequency was held constant for these measurements.

cancellation, shielding, etc.

Digital Modulation Analysis

If sufficient processing power and signal memory is available, DSP algorithms can be written to extract information from, and perform tests on digitally modulated carriers. Engineers dealing with digital modulation can then have access to test techniques designed specifically for their systems.

The process begins with AM/FM/PM demodulation such as that described above. An example is shown in figure 9. This is a plot of a digitally modulated signal using the pi/4 DQPSK scheme, which is here phase demodulated and plotted in continuous phase vs. time.

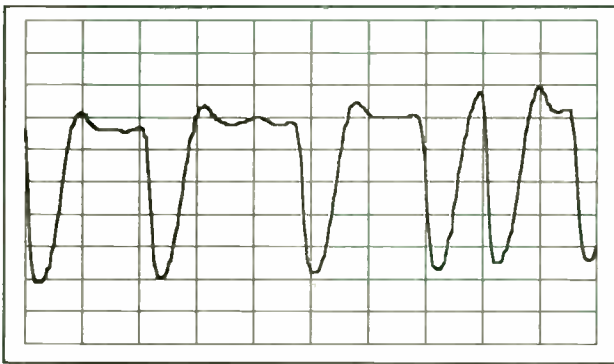


Figure 9: Phase-demodulated pi/4 DQPSK

To perform digital demodulation the DSP engine must perform extra processes in parallel. After the time data is processed by a digital filter, algorithms must perform carrier and symbol lock functions. The timing and phase reference information is then provided to a DSP process performing demodulation to generate I and Q outputs. This parallel processing is shown schematically in figure 10.

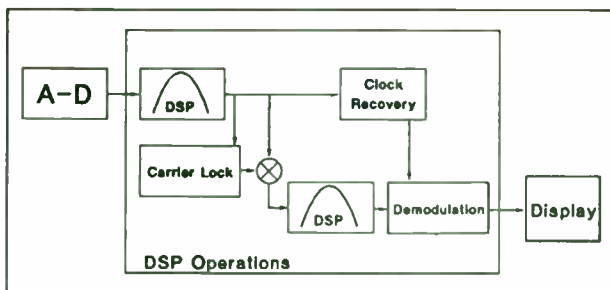


Figure 10: Digital modulation analysis with clock recovery, carrier lock

Results of these operations are displayed in two different formats in figures 11a and 11b, for a QPSK

signal. Constellation diagrams allow the designer to isolate the signal at the instants when the data is valid, while vector diagrams permit examination of the signal trajectory between valid states.

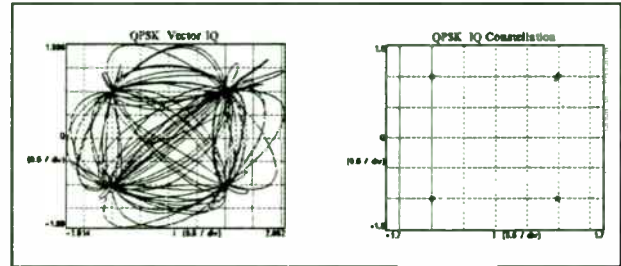


Figure 11: Vector and constellation diagrams

In addition to the graphs, measurement data can be presented in quantitative form such as Error Vector Magnitude.

Other DSP Measurement Benefits

DSP-based techniques such as this can provide a number of other measurements and measurement benefits. Several, beyond the scope of this paper include:

- True RMS detector and selectable band power measurements--Digital signal processing can be used to implement a bank of parallel filters with true RMS detection. This permits direct and accurate measurements of average power over arbitrary bandwidths.
- Direct phase noise measurements--Combining a precision phase demodulator with spectrum analysis using true RMS detection allows some phase noise measurements to be made in real time without external hardware or correction factors.
- PLL closed-loop frequency response--Comparing baseband stimulation of a PLL control loop with the phase-demodulated PLL output yields the amplitude and phase frequency response of the PLL in real time. This is a powerful design tool for tuning PLL response.
- Determining center frequency of modulated signals--This often-difficult task can be performed using techniques such as phase demodulation or computed frequency centroids.
- Correlation functions--DSP auto- and cross-correlation functions are a useful method for comparing different signals (or time-delayed versions of the same signal) to determine their similarity.

Using calibrated attenuators and having previously measured the transmitter output power and the sideband conversion loss, one may reduce the power at the input to the receiver and monitor the IF power with the RMS voltmeter and thereby determine the signal to noise ratio within the IF bandwidth for any input power.

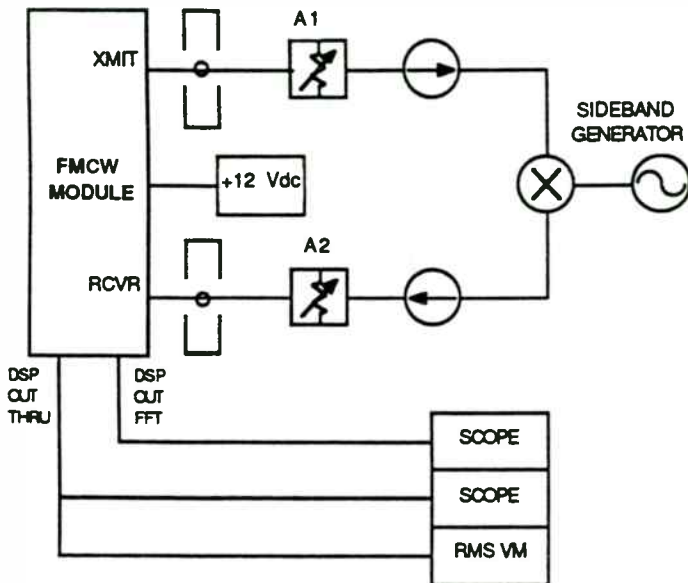


Figure 4.1 Sensitivity Measurement Test Equipment

The IF bandwidth was measured by varying the offset generator frequency while observing the RMS voltmeter and noting the -3 dB points. The following data was recorded:

Transmitter Power	+8 dBm
Sideband Conversion Loss	-10 dB
Attenuator A1	-50 dB
Attenuator A2	-70 dB

Received Power for S/N=0 dB -122 dBm
(IF BW = 3 KHz)

Recalling the mathematical expression for equivalent input noise (appendix B):

$$N_{ie} = L(F_i + T_r - 1)kTB = E-12.2$$

The diode noise ratio may be calculated; $T_r=7.39$, or 8.5 dB excess noise.

4.1.2 Operational Test

Operational testing of the engineering model was conducted using the test equipment configuration depicted in Figure 4.2.

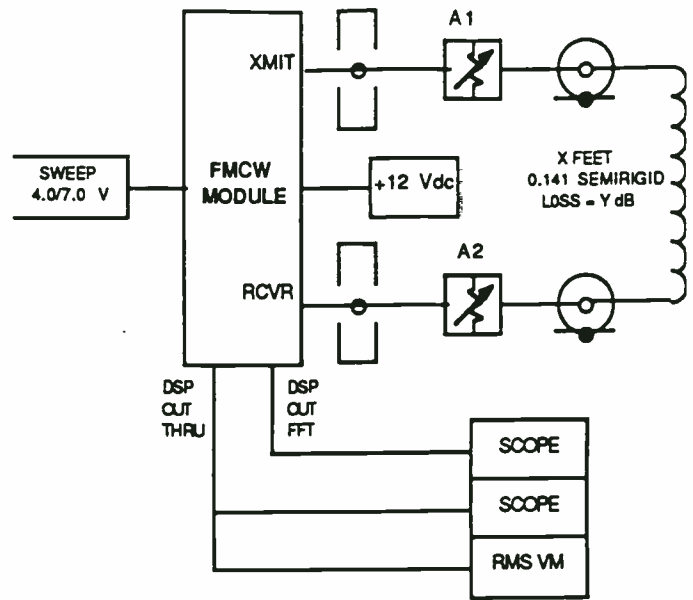


Figure 4.2 Operational Test Equipment Configuration

The operational mode testing simulated targets at various ranges and cross sections by inserting different path attenuations and lengths of 0.141 inch diameter semirigid cable between the transmitter and receiver ports. Documentation consisted of through mode and FFT mode photographs of the IF signal and 256 point FFT spectral output. The FFT spectral output was via frequency (range) bin sequential strobing.

The assorted conditions are set forth in Table 4.1. The oscillograph data is displayed in Figure 4.3.

Table 4.1 Operational Test Conditions

CONDITION NO	PH CABLE LENGTH M	EL CABLE LENGTH M	RANGE SCALE M	SWEEP RATE HZ	XMIT ATTN dB	RECEIVE ATTN dB	RECEIVE POWER dBm
1	3.05	4.42	30	100	35.0	35.4	-79.4
2	9.14	13.25	30	100	35.0	28.4	-79.4
3	9.14	13.25	60	50	35.0	28.4	-79.4
4	18.29	26.50	30	100	11.7	35.4	-85.1
5	18.29	26.50	60	50	11.7	35.4	-85.1
6	18.29	26.50	120	25	6.1	28.4	-72.5
7	18.29	26.50	240	12.5	0.4	25.5	-63.9
8	27.43	39.75	30	100	8.7	23.0	-93.7
9	27.43	39.75	60	50	8.7	23.0	-93.7
10	27.43	39.75	120	25	1.0	23.0	-86.0

4.2 Field Test

Field testing of the engineering model was conducted using the pyramidal horn antennae and calibrated attenuators at both transmit and receive ports. Two triangular trihedrals of known target cross section were employed. A diagram of the triangular trihedrals is shown in Figure 4.3. The triangular trihedral is quite popular as a radar target cross

Applying the Modulation Domain to Wireless Communication Testing

Barry Dropping
Hewlett Packard
Santa Clara, CA USA

Introduction

Wireless RF communications is a dynamic worldwide market. Technologies are rapidly changing as cellular and cordless systems move from analog to digital transmission. New digital systems promise improved voice and data quality as well as more efficient use of the frequency spectrum. Time Division Multiple Access (TDMA) formats will solve capacity limitations that users and operators of cellular systems are currently experiencing in many of the large metropolitan areas.

These fast emerging digital modulation and accessing methods present tough new challenges for test equipment. New test equipment is required to bring designs to market quicker, and to perform manufacturing testing in a fast and efficient manner. This paper discusses recently introduced Modulation Domain Analysis techniques which have greatly simplified the analysis of dynamic frequency signals used in modern wireless communications systems.

Applying the Modulation Domain to Wireless Communication Testing.

The days of simple continuous wave transmission techniques are passing. Wireless communication system designers are utilizing various spread spectrum and time division accessing techniques to develop more reliable and efficient systems.

These techniques make analysis of carrier frequency and modulation much more difficult. For example, in the case of a frequency hopping spread spectrum system, the carrier is switching frequencies hundreds or thousands of times each second. Designers need a method to characterize the frequency switching behavior of such a system.

The Modulation Domain provides a new way of looking at your signals. Figure 1 shows a three dimensional view of a dynamic signal. You are probably familiar with the time and frequency domains. The time domain is a view of voltage versus time (oscilloscope). The frequency domain shows amplitude versus frequency (spectrum analyzer). The modulation domain is the missing

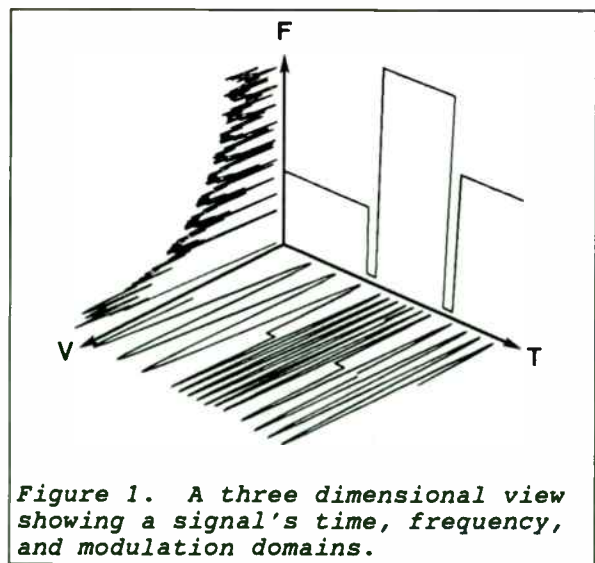


Figure 1. A three dimensional view showing a signal's time, frequency, and modulation domains.

section because the azimuth and elevation lobes are wide, i.e. constant cross section over angular deviations, and therefore exhibit large skew tolerance.

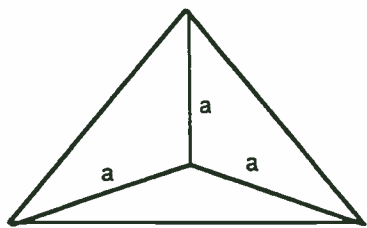


Figure 4.4 Triangular Trihedral

The radar cross section is calculated from the formula (reference 5):

$$\sigma = 4\pi a^4/3\lambda^2.$$

The target cross sections are 3.344 and 33.078 square meters.

The photographic documentation of the field test are displayed in Figure 4.4.

5.0 SUMMARY AND CONCLUSIONS

The program, as originally proposed, was conducted to determine feasibility of the reference 1 system architecture to function as a general purpose ranging. The program objectives were altered to include the manufacture of an engineering prototype FMCW radar system with more general operational capability.

The engineering model exhibited excellent operational characteristics as evidenced by the data reported herein and demonstrated the requirement for further study and feature enhancement in the following areas:

- system display
- advanced DSP algorithm
- receiver automatic gain control

One conclusion that may be declared without reservation is that the FMCW radar concept is appropriate for a wide range of potential applications and that the RF architecture is simple and cost effective; the addition of digital processing techniques and algorithm development will likely be the vehicle which generates broad market acceptance to the product.

6.0 APPENDICES

Appendix I FMCW IF Signal Development

Appendix II Noise Figure Development

7.0 REFERENCES

1. M/A Technical Memorandum of 10 February 1991
2. Skolnik, M.I.: "Radar Handbook," McGraw-Hill Book Co, New York, 1970
3. Braun, E.H., Data for the Design of EM Horns, IRE Transactions on A & P, January, 1956.
4. Stimson, G.W., "Introduction to Airborne Radar," Hughes Aircraft Co, El Segundo, CA, 1983.
5. Currie, N.C. and Brown, C.E., "Principles and Applications of Millimeter-Wave Radar," Artech House, Norwood, MA, 1987.

APPENDIX A IF SIGNAL DEVELOPMENT

Consider the equipment configuration of Figure A.1 where a VCO is swept at the rate of K Hz/sec by the applied sawtooth signal. The VCO signal is radiated toward a target X at range R and normal component of velocity, v. A portion of the VCO signal is coupled to a mixer LO port; the mixer receives the reflected VCO signal at the RF port. The difference frequency is available at the IF port of the mixer.

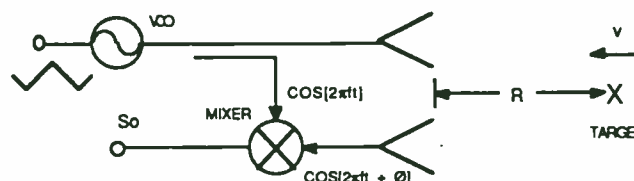


Figure A.1 FMCW Radar IF Signal

The signal, S_o , at the mixer IF port is the filtered product of the cosinusoidal signals entering the LO and RF ports of the mixer, and may be written:

$$S_o = A \cos[\theta],$$

where, θ is the total phase shift associated with the two way range, R, i.e., $\theta = 2[2\pi R/\lambda]$, and A is the attenuation associated with the two way path loss and the target cross section. λ is the transmission wavelength, $\lambda = c/f$. Substituting, one may write:

$$\theta = 4\pi Rf/c.$$

Now remember that the frequency is linearly changing at the rate K, and that the sawtooth starts at frequency, f_o , and therefore θ may be written:

$$\theta = [4\pi R/c] * [f_o + Kt], \text{ or,}$$

$$\theta = 4\pi Rf_o/c + 4\pi RKt/c.$$

From FM theory, the instantaneous frequency is defined as:

$$f_i = [1/2\pi] * [\partial\theta/\partial t].$$

Performing the differentiation:

third dimension - frequency versus time. The modulation domain reveals things that you have not been able to see before. Signal parameters that are not readily available in the time or frequency domains are now apparent. The Hewlett Packard HP 53310A and HP 5372A are the first instruments that let you see your signals in the modulation domain. All measurement results shown in this paper were taken with the HP 53310A Modulation Domain Analyzer.

The modulation domain analyzer can be thought of as a "frequency oscilloscope" when viewing a signal's frequency versus time. It also provides histograms showing the probability distribution of millions of continuous frequency measurements.

Lets examine how a modulation domain analyzer makes frequency versus time measurements. The measurement technology breakthrough is called continuous counting. A patented

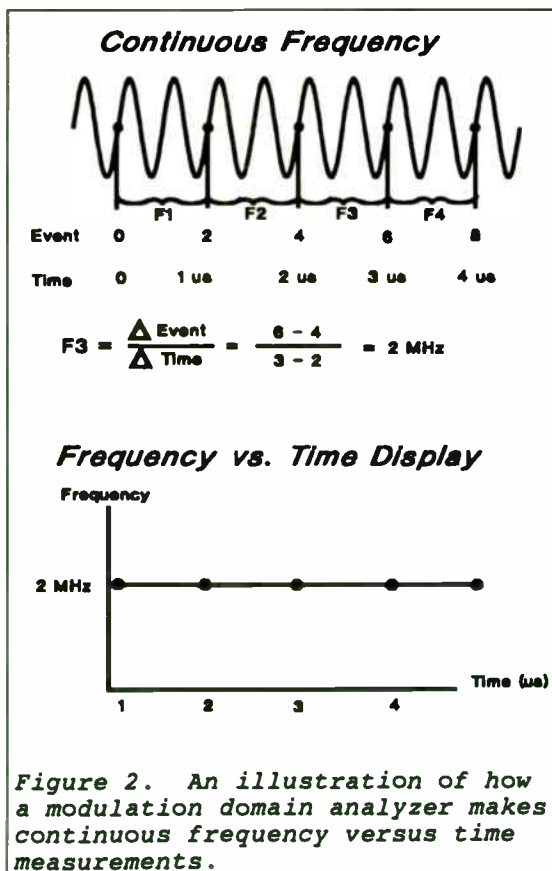
technique of reading high speed event and time counters on the fly without disturbing the counting process makes single-shot continuous frequency measurements possible. Figure 2 shows how continuous frequency samples are taken. Continuous event and time counters monitor zero threshold crossings of the input signal. The point-to-point frequency is equal to delta events divided by delta time. The time of each sample is known, so the input signal's frequency can be plotted as a function of time.

The modulation domain analyzer's frequency versus time and histogram displays are very useful in analyzing synthesizer settling time, turn-on/off frequency behavior, frequency hopping, and FSK center frequency and peak deviation. Now we will examine many of these measurements in detail.

Measuring Synthesizer Settling Time.

The synthesizer is a key part of the RF design effort for today's digital RF communication systems. The synthesizer is constantly switching frequencies in many systems for a variety of reasons including cell hand-offs, frequency division duplexing, or frequency hopping. Measuring synthesizer settling time is critical to design verification. Indirect measurement methods such as delay line discriminators, zero beat mixing, or spectrum analyzers in zero span have been used in the past. These indirect techniques are difficult to use and prone to a variety of errors. A fast and accurate method is needed to characterize synthesizer settling time.

Figure 3 is a time domain view of a frequency step. The step command edge is also shown. Settling time measurements must be time referenced to the step command edge. The modulation domain analyzer can measure the frequency continuously during the step to provide a direct view of synthesizer settling (figure 4). The measurement is triggered by, and time referenced to, the step command edge. The display is



$$f_i = [2f_0/c] \cdot [\partial R/\partial t] + [2K/c] \cdot [R + t\partial R/\partial t].$$

Rewriting the equation with the substitution, $\partial R/\partial t = v$:

$$f_i = 2f_0 v/c + 2KR/c + 2Kvt/c.$$

Note that there are three discrete terms which describe the instantaneous frequency at the mixer output:

1. $2f_0 v/c$, the 'Doppler' frequency component;
2. $2KR/c$, the frequency component associated with target range, R;
3. $2Kvt/c$, the frequency component associated with the change in range.

The following points should be noted:

If there is no relative motion between the radar and target, i.e. $v = 0$, then $f_i = 2KR/c$, f_i is range dependent only.

and,

if the radar frequency is not changing, i.e. $K = 0$, $f_i = 2f_0 v/c$, the 'Doppler' component and f_i is velocity dependent only.

APPENDIX B NOISE FIGURE DEVELOPMENT

Consider the equipment block diagram of Figure B.1. A mixer with conversion loss, L_c , and diode noise temperature ratio, T_m , is connected to an amplifier of gain, G , noise figure, F_i , and noise temperature, T_i . The mixer is driven by an ideal local oscillator, i.e., one that contributes no additive noise to the system. A power meter measures the total output noise in a bandwidth, B , under the input conditions of connection to a termination at temperature, T_a , or a termination at temperature, T_b .

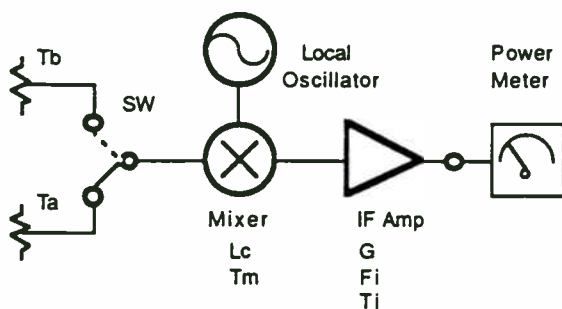


Figure B.1 Noise Figure Measurement

The Y-factor is defined as the ratio of the total noise power output under the two switch conditions, i.e., $Y = N_b/N_a$. Now, one may write,

$$N_a = F_i k T_a B G + k(T_m - T_a) B G, \text{ and,}$$

$$N_b = L k(T_b - T_a) B G + F_i k T_a B G + k(T_m - T_a) B G,$$

where, k is Boltzman's constant, 1.38×10^{-23} Joules/ $^{\circ}$ K.

Forming the Y-factor and eliminating the common multiplier, kBG , one obtains:

$$Y = [L(T_b - T_a) + F_i T_a + (T_m - T_a)] / [F_i T_a + (T_m - T_a)].$$

Subtracting -1 from both sides of the equation, one obtains:

$$Y - 1 = [L(T_b - T_a) + F_i T_a + (T_m - T_a)] / [F_i T_a + (T_m - T_a)] - 1.$$

Performing some algebraic manipulation:

$$Y - 1 = L(T_b - T_a) / [F_i T_a + (T_m - T_a)].$$

Remember that F_s , system noise figure, has the following mathematical relationship:

$$F_s = (T_b - T_a) / (Y - 1) T_a, \text{ and } (T_b - T_a) / T_a = ENR.$$

Substituting into the equation for F_s , one obtains:

$$F_s = (F_i + T_m / T_a - 1) / L.$$

T_m / T_a is called the diode noise temperature ratio, T_r , and upon substitution and exchange of the conversion loss, L , from a numeric which is less than one to an inverse which is greater than one, the formula may be written in the more conventional manner:

$$F_s = L(F_i + T_r - 1)$$

The noise figure represents the degradation in signal to noise ratio as a signal progresses thru a system; the formal definition is:

$$F_s = [S_i / N_i] / [S_o / N_o].$$

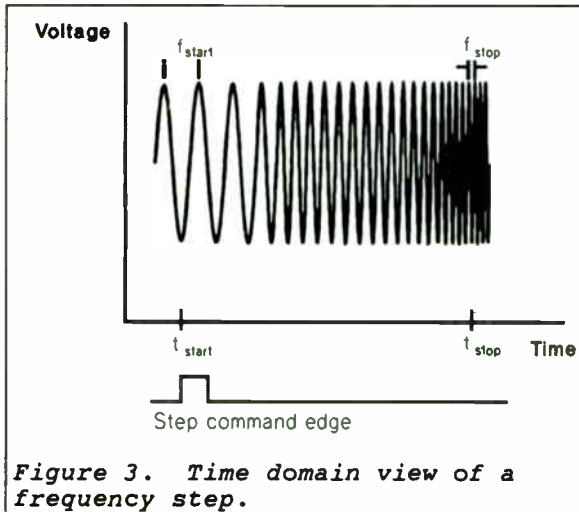
Rearranging terms and with the following substitutions: $N_i = kTB$ and $S_o / S_i = G$, yields:

$$F_s = N_o / kTBG.$$

The equation leads to another (equivalent) noise figure definition:

Noise figure is the ratio of total output noise power to that output noise power engendered by the input.

The total output noise power, N_o , may be written in terms of the system noise figure:



zoomed-in on the final part of the settling transient for optimum resolution. The settling time is measured automatically by analyzing the trace. The user enters the target frequency and tolerance band using the horizontal frequency markers. The analyzer then automatically searches backwards in time from the right edge of the display to find the point where the trace last entered the "pass band". This time is indicated with the vertical time marker, and the settling time result is shown at the bottom of the display.

Another consideration for synthesizer performance is amplitude pulling. Amplitude pulling can occur as a result of power

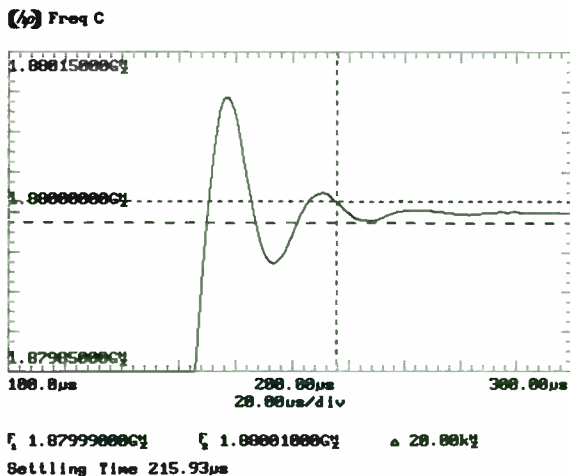


Figure 4. Synthesizer settling time measurement.

variations as the TDMA burst is turned on. The power ramp can cause a temporary shift in the synthesizer's frequency. The modulation domain analyzer makes it easy to analyze pulling effects (figure 5). You can quickly see how far off frequency it is pulled and how long it takes to relock.

Direct frequency versus time displays make it easy to measure synthesizer settling time and pulling. The automatic measurement of settling time speeds your analysis. Accuracy of better than 100 Hz is typically achieved at RF frequencies.

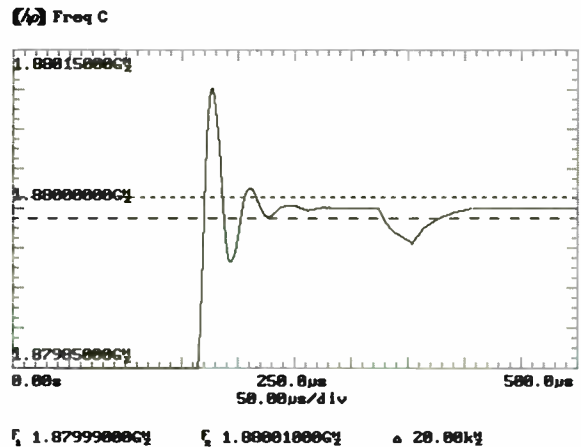


Figure 5. Synthesizer frequency pulling measurement.

Transmitter Turn-on and Turn-off Frequency Behavior

Manufacturers of RF communications systems must characterize transmitter turn-on and turn-off behavior to comply with various new international test standards (e.g. ETS 300 113 & 162). The intent of the new test standards is to assure that the device is not transmitting "out of channel" during power on/off. Many people are searching for an easy and reliable test method to comply with the new standards. The Modulation Domain Analyzer makes it easy to measure transmitter turn-on and turn-off transients.

$$N_o = F_s kTBG.$$

The equivalent input noise is:

$$N_{ie} = F_s kTB.$$

Substituting the expression developed for the system noise figure, F_s , the equivalent input noise, or minimum detectable signal, is:

$$N_{ie} = L(F_1 + T_r - 1)kTB.$$

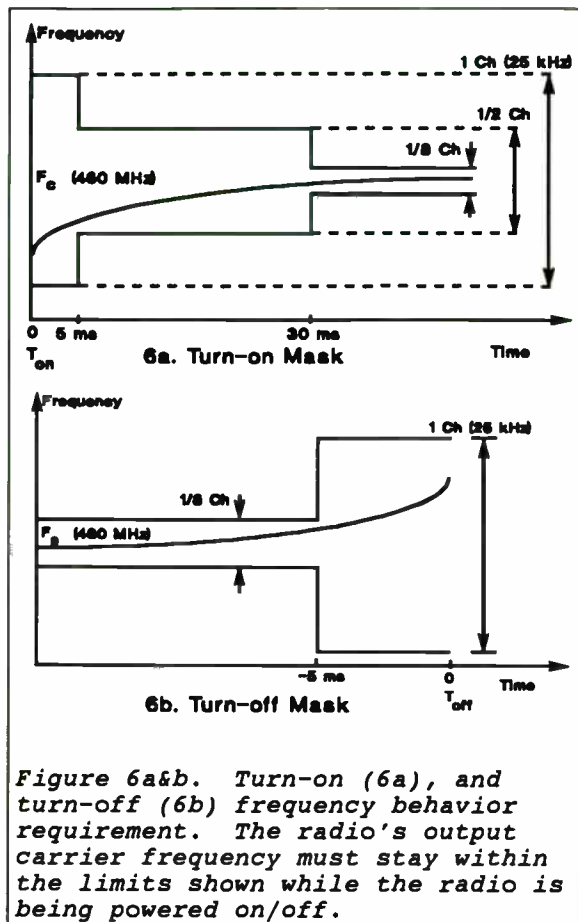


Figure 6a&b. Turn-on (6a), and turn-off (6b) frequency behavior requirement. The radio's output carrier frequency must stay within the limits shown while the radio is being powered on/off.

Figure 6a&b provide a quick graphical view of a typical set of transmitter turn-on and turn-off frequency behavior requirements. These requirements apply to a 460 MHz emergency services radio.

The modulation domain analyzer provides a direct frequency versus time view of the transmitter's frequency behavior during turn-on and turn-off. Accurate triggering is the key to turn-on/off frequency transient measurements. The preferred method is to trigger on the -30 dBc point. This is the point on the power ramp where the transmitter's output power is 30 dB below its average carrier power level. It is referred to as the T(on) or T(off) point. This is the preferred method because it assures that the frequency is being measured when it is important - when the transmitter is transmitting above -30 dBc. The modulation domain

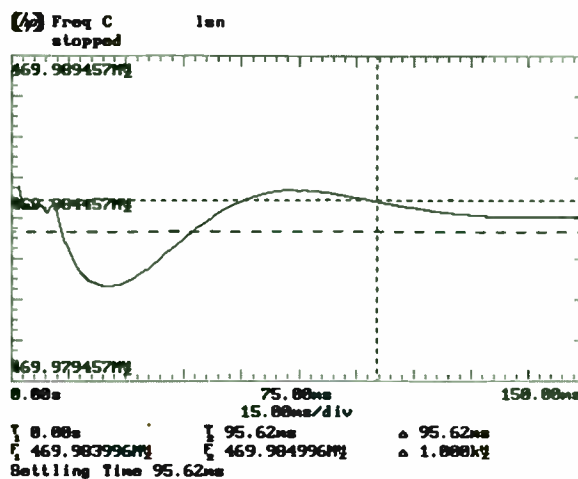


Figure 7a

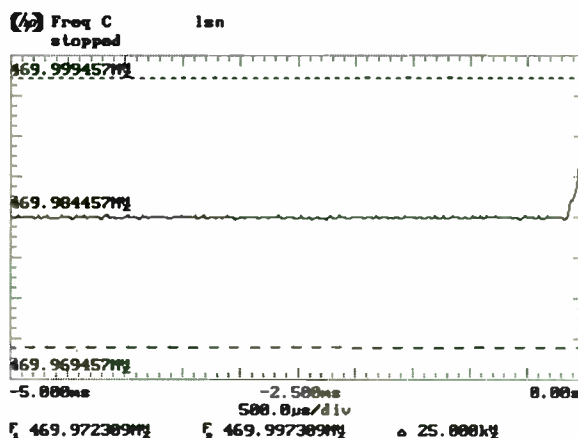


Figure 7b

Figure 7a&b. Turn-on (7a) and turn-off (7b) frequency behavior of a 460 MHz emergency services radio.

analyzer can be calibrated to trigger a measurement at the -30 dBc point. An alternate method is to trigger the measurement with an external sync pulse. This sync pulse should have a fixed timing relationship to the -30 dBc point.

Figure 7a shows a single shot measurement of a radio's frequency behavior during turn-on. The time zero trigger for this was the -30 dBc point on the power ramp up. The radio must settle to within the limits shown in figure 6a. The horizontal markers can be easily

Designing RF Circuits and Modules using Modern CAD Tools

Raymond S. Pengelly
Compact Software, Inc.
Paterson, New Jersey,
USA

Session E-3: Practical RF CAD
RF Expo East, Tampa, FL
October 21

SUMMARY

- ◆ CAD tools for the RF community have reached a high level of sophistication during the last few years
- Design complex sub-systems using a software suite, like Compact Software's Serenade[®], without leaving the CAD tool environment.
 - ⇒ Modular combination of schematic entry, simulation engine and (semi)-automatic layout preparation available in either PC or workstation-based formats.
- Use a System Level Simulator, like Microwave Success[®], with a circuit-level linear/nonlinear simulator, like Microwave Harmonica[®]
 - ⇒ Inputs to the simulators are defined using the Serenade Schematic Editor and the planar integrated/hybrid circuits are defined using the Layout Editor.
 - ⇒ Schematic entry, via Serenade, provides a fast, comprehensive and error-free method of entering circuit and system-level information to the simulators and the layout editor.

positioned to define the target frequency and tolerance bands. This radio passes the 30 ms requirement. The 1 channel (25 kHz) and 1/2 channel (12.5 kHz) settling times are easily measured by changing the timebase setting.

Figure 7b shows a measurement of the radio's frequency behavior during turn-off. This measurement is made by looking at the pretrigger information. The trigger is the -30 dBc point on the power ramp down as the radio is keyed off. The markers show a peak frequency deviation of less than 7 kHz during the turn-off. This is well within the 1 channel (25 kHz) allowance for this radio.

Frequency Hopping Measurements

Many wireless communication systems employ frequency hopping. The GSM Pan-European Digital Cellular system can use a frequency hopping mode to overcome multipath fading problems. When frequency hopping is used, the carrier frequency is switched for each TDMA burst of the mobile (figure 8). The modulation domain analyzer can provide a direct view of the frequency hopping pattern in a single pass measurement (figure 9). Frequency and time markers can be used to verify the hopping sequence.

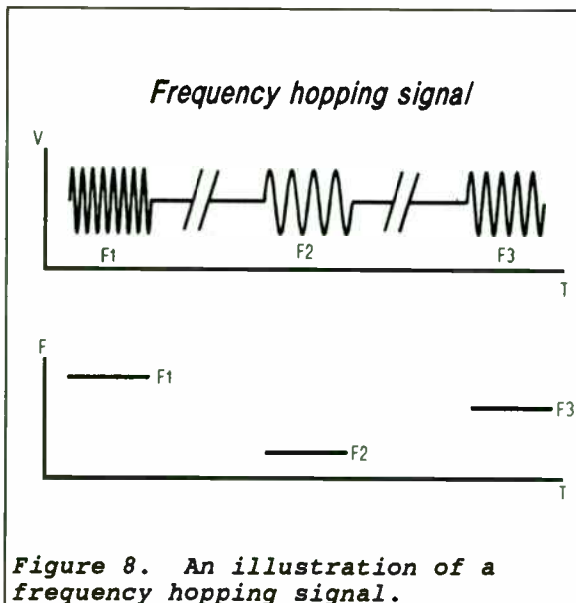


Figure 8. An illustration of a frequency hopping signal.

(A) Freq C

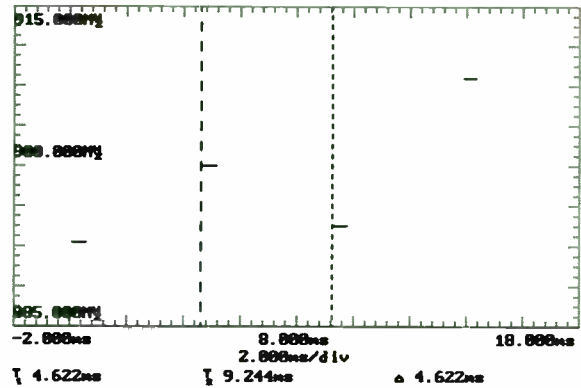


Figure 9. Frequency hopping measurement on a GSM transmitter.

FSK Center Frequency and Peak Deviation

Lets now look at modulation measurements on the RF carrier. Advanced cordless telephone systems such as CT2, CT3 and DECT require that carrier center frequency and peak deviation be measured in order to meet the regulatory standards. The TDMA bursting of the carrier makes this a very difficult measurement. Figure 10 provides a view of a typical TDMA carrier. The mobile only transmits in a given time slot. Center frequency and peak deviation of the filtered FSK modulation must be accurately measured in the presence of the on-

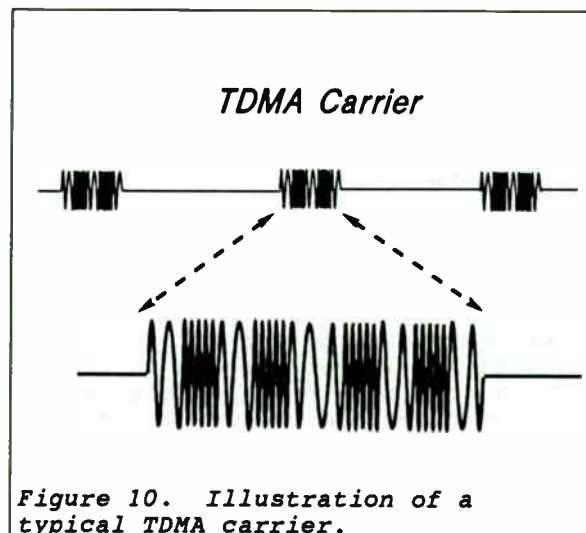
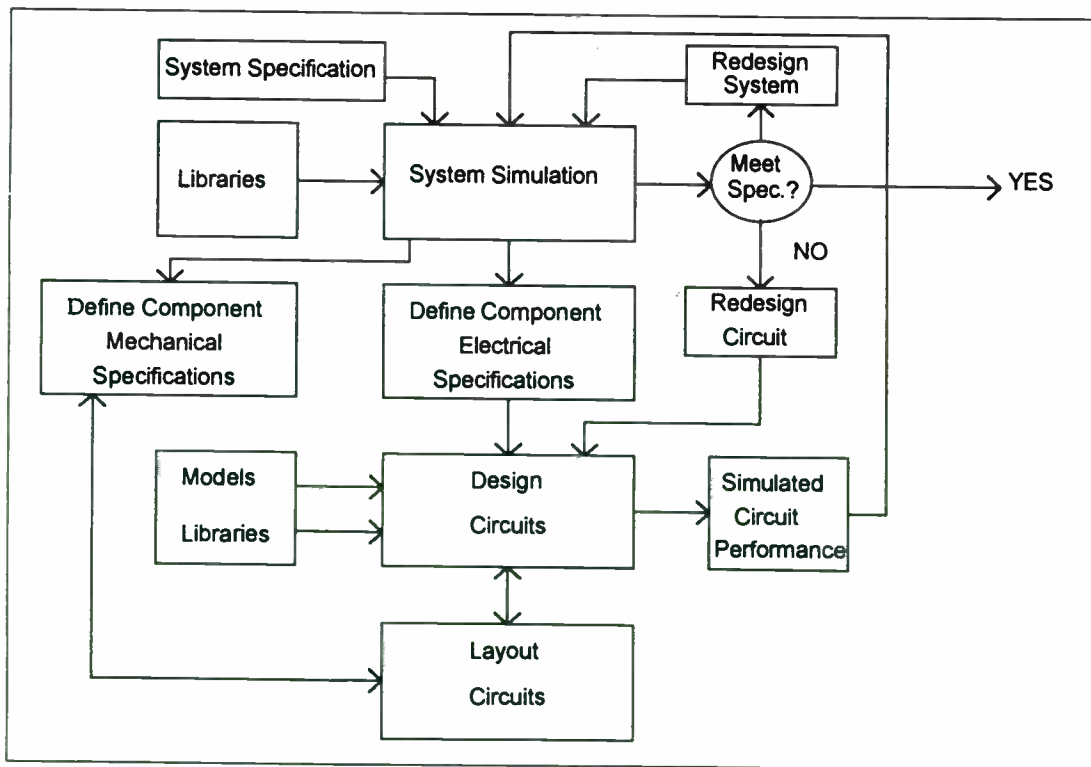


Figure 10. Illustration of a typical TDMA carrier.

◆ **System simulation allows the design engineer to investigate a complete range of parameters including:**

- ✓ **Gain**
- ✓ **Noise performance**
- ✓ **Group delay**
- ✓ **Power compression characteristics**
- ✓ **Intermodulation distortion**
- ✓ **Degradation to modulated carriers such as 64-QAM**
- ✓ **Bit-Error Rate**
- ✓ **Eye-Diagrams**
- ✓ **Constellation Plots**
- ✓ **Phase Noise**



Designing Modules and Systems using Modern CAD Tools

off TDMA bursting. The modulation domain analyzer gives a direct view of the modulation on a TDMA carrier.

Figure 11 is an example of a frequency versus time display of the 0.5 GMSK modulation used on the new Digital European Cordless Telephone (DECT) system. You can quickly verify the bit pattern, bit rate, frequency deviation, and filtering profile on the RF signal.

The measurement data can also be displayed as a histogram (figure 12). The histogram display shows the probability distribution of thousands of fast frequency measurements on a DECT carrier. The filtered BFSK modulation peaks are revealed directly in the histogram. The center frequency is the midpoint of the deviation peaks. The modulation domain analyzer automatically calculates the center frequency and peak deviation from the histogram display. Measurement results are presented at the bottom of the display.

The modulation domain is well suited to measuring center frequency and deviation on TDMA carriers. The automatic measurements simplify bench use and make it easy to automate in a manufacturing test system. Automatic center frequency and peak deviation measurements make it easy to verify conformance to regulatory standards.

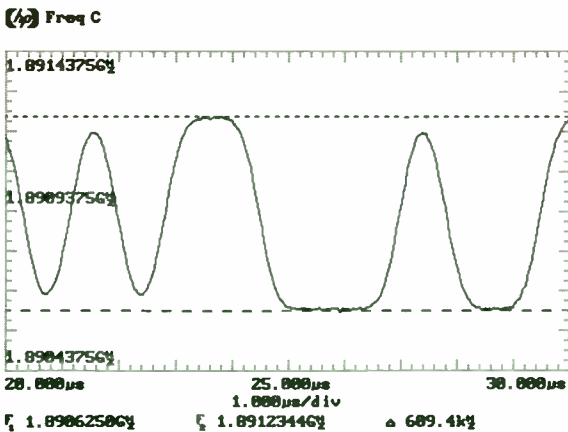


Figure 11. Frequency versus time measurement of 0.5 GFSK modulated DECT carrier.

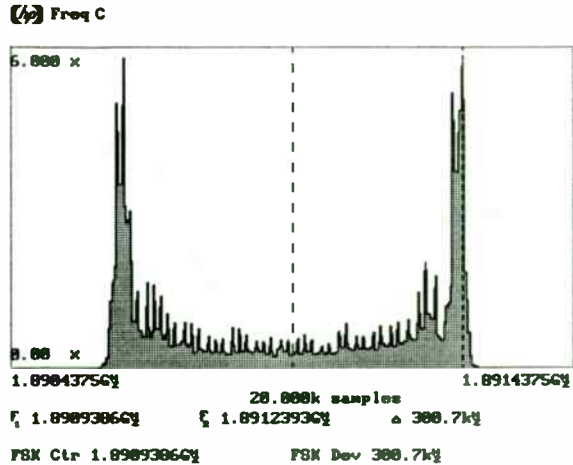


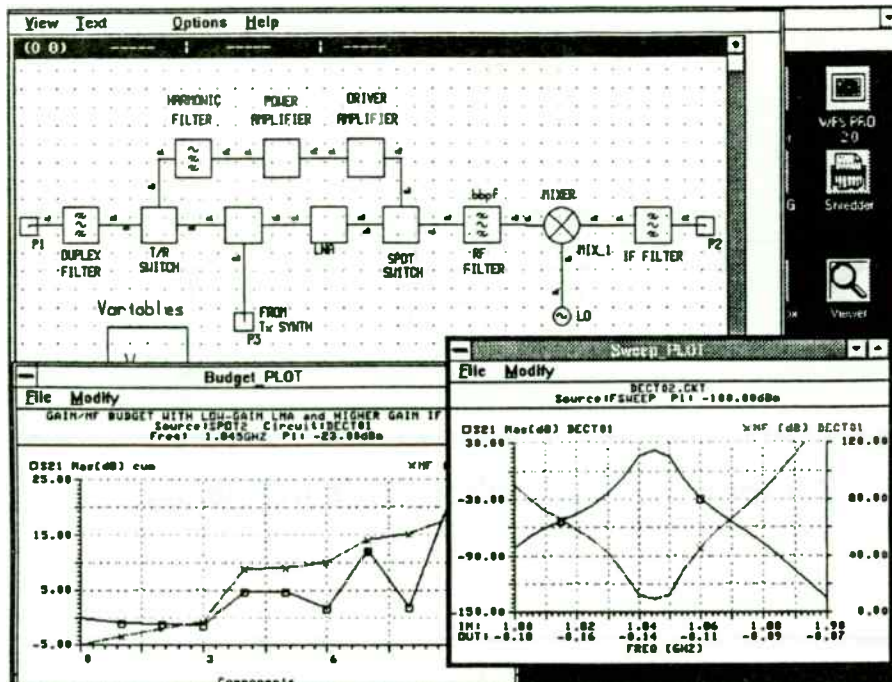
Figure 12. Center frequency and deviation are automatically calculated from the frequency histogram.

Jitter Measurements and RF Eye Diagrams

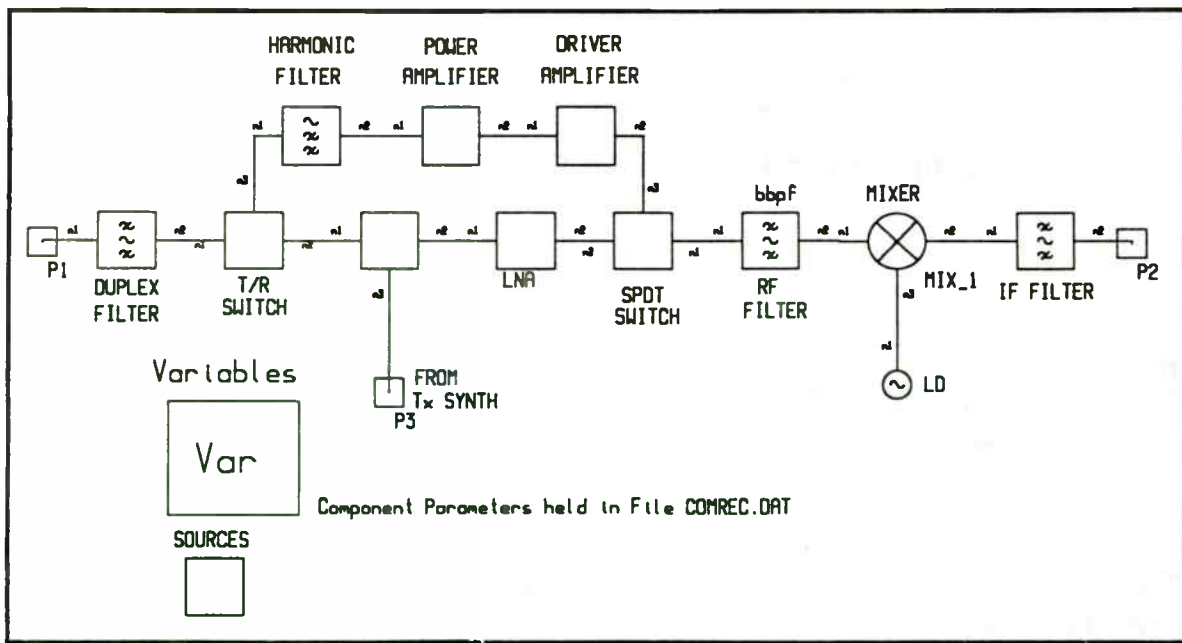
Let's now examine jitter measurements on the RF carrier. It is very common to measure jitter on a baseband signal using a digital oscilloscope. To do so, you trigger on a reference edge and repetitively trace the bit transition edge of interest. Infinite display persistence allows you to build up a history of bit transition positions. The width of the infinite persistence trace at the midpoint is the peak-to-peak jitter.

A key limitation of the digital oscilloscope method is that you must have a baseband signal available. Many people either do not have a convenient baseband signal available or would prefer to measure jitter directly on the RF carrier. A modulation domain analyzer can use the same method described above for a digital oscilloscope to provide an infinite persistence frequency versus time trace of a bit transition directly on the RF carrier.

Figure 13 shows an infinite persistence frequency versus times display of the first bit transition in a TDMA burst. The peak-to-peak jitter can now be measured directly on the modulated RF carrier.



- Serenade Schematic Editor and Microwave Success System Simulator running concurrently under Windows 3.1 on PC



Typical System Diagram for the Transmit/Receive Section of a Digital European Cordless Telephone -- DECT 1800

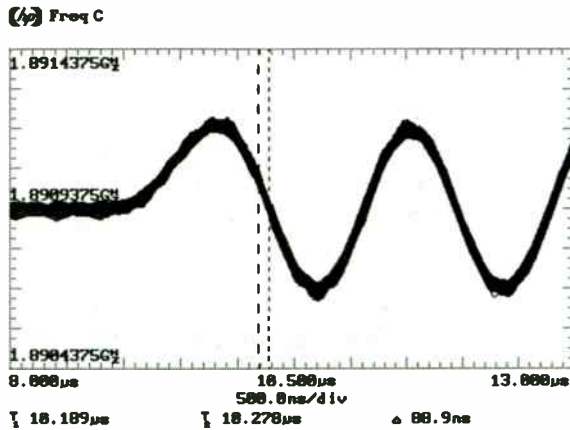


Figure 13. Peak-to-peak jitter measurement on the RF carrier.

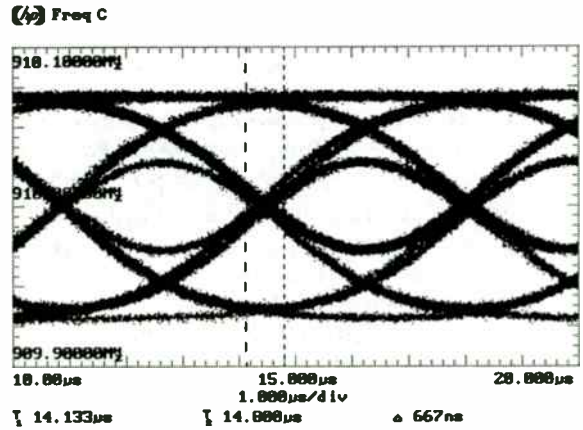


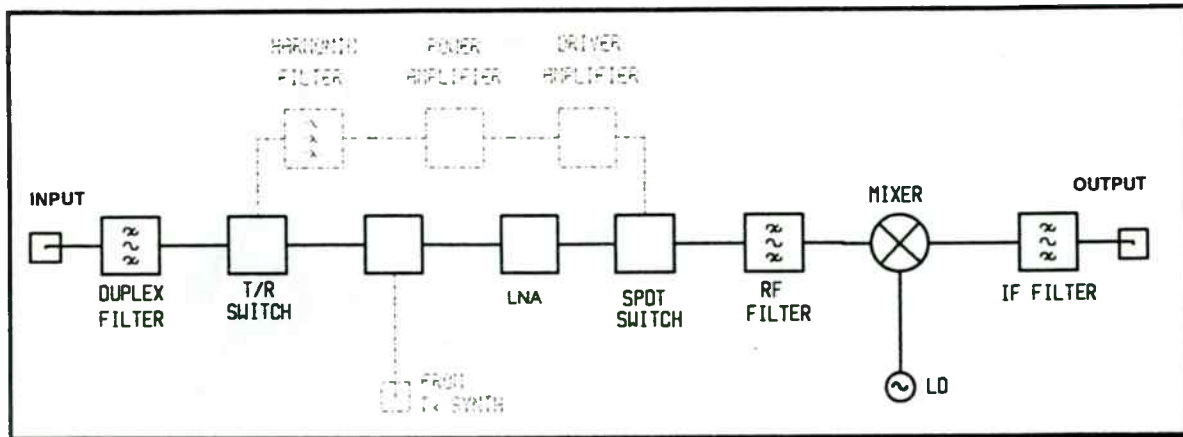
Figure 14. Frequency versus time eye diagram of a GSM carrier.

The modulation domain analyzer can also provide frequency versus time eye diagrams when measuring a carrier with live data. Figure 14 is an example of the unique eye pattern of a 0.3 GMSK modulated GSM signal. Frequency versus time eye diagrams provide a quick qualitative view of transmitter performance.

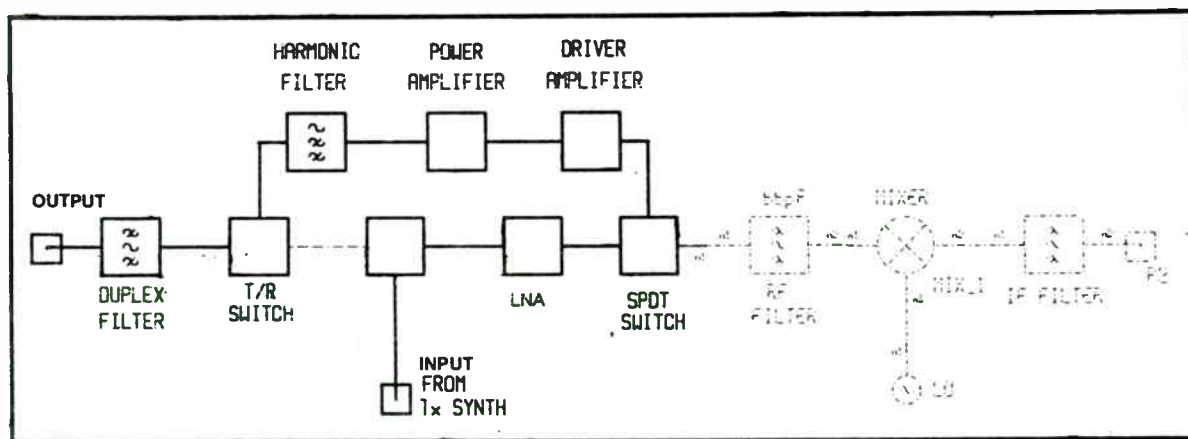
Eye patterns allow you to view the effects of bit jitter and inter-symbol interference directly on an RF carrier. The frequency versus time eye diagram can be compared to a conventional baseband eye diagram of an oscilloscope. Comparing the RF eye diagram with the baseband eye diagram allows you to quickly isolate problems with the RF chain.

Summary

We have seen that the modulation domain analyzer can provide many new measurements for wireless communications systems. It is a powerful new tool for design characterization and manufacturing test. Its ability to provide direct frequency versus time views provide insights not previously available. The automatic measurements of FSK center frequency and peak deviation on TDMA carriers provide an easy way for engineers to automate their test systems.



Components Used when CT is in Receive



Components Used when CT is in Transmit

Parameter	Specification
Dynamic Range at the antenna	-100 to -23 dBm
Signal-to-Noise Ratio at the Output	min. 9 dB
Noise Figure	max. 12 dB
Third Order Intercept Point at the input	min. -20.5 dBm
In-band Blocking	min. 80 dB
Out-of-band Blocking	min. 106 dB

Specifications for DECT 1800 Front End

MEASURING THE PEAK-TO-AVERAGE POWER OF DIGITALLY VECTOR MODULATED SIGNALS

Charles J. Meyer, Senior Applications Engineer, Boonton Electronics

Digital vector modulation has become the preferred method of modulation for wireless digital communication today. The need to have the capacity and robustness of a high speed digital communication channel with the versatility of a wireless transmission has resulted in considerable advancement of this area in recent years. However, system designers continue to be challenged by the high peak-to-average power ratios and large linear dynamic ranges that this type of modulation requires. The Boonton 4400 is an advanced Peak Power Meter that can be used to accurately measure these requirements.

Digital Vector Modulation

Digital vector modulation is being utilized in a wide variety of technologies such as digital cellular radio, high definition television (HDTV), satellite and microwave links, military communication, and numerous spread spectrum applications.

Digital vector modulation is a modulation scheme whereby a signal's phase and/or amplitude are altered to represent digital bit patterns called symbols. Specific phase/amplitude combinations are called symbol states and valid symbol states are defined on a vector map called an I-Q (in-phase - quadrature) diagram (Fig. 1).

Schemes which modulate only a signal's phase are often referred to as Phase-Shift Keying (PSK) modulations, whereas when amplitude and phase are both used to encode data it is usually referred to as Quadrature Amplitude Modulation (QAM).

Variations of these basic schemes continue to emerge. A variation of PSK called pi/4 differential quadrature phase-shift keying (pi/4-DQPSK), is used by the North American Digital Cellular (NADC) and Japanese Digital Cellular (JDC) formats, while another PSK variant called minimum shift keying (MSK) is used by the GSM European digital cellular format.

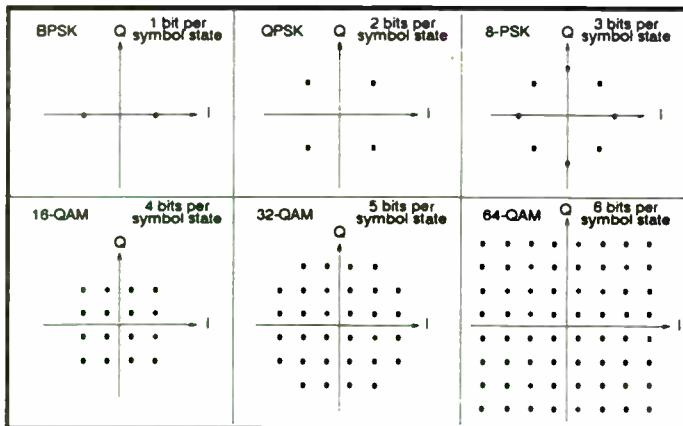


Figure 1 - Typical I-Q Diagrams

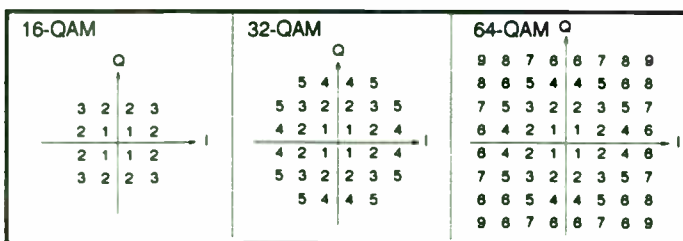


Figure 2 - Symbol Power Levels

Power Analysis of Digital Vector Modulation

The high peak (envelope) power of a digitally vector modulated signal is the result of three primary factors: the existence of multiple symbol power levels (caused by the multiple amplitude levels that exist in a QAM type scheme), compound ringing (caused by filtering of the baseband I&Q signals), and multiple carrier power addition (caused by the vectorial summation of the voltages of multiple carriers).

Digitally vector modulated schemes that modulate a signal's amplitude (such as QAM), have multiple symbol power levels. Vectorial analysis of an I-Q diagram will reveal these levels (Fig. 2). Since each symbol power level represents multiple symbol states (and all of the data associated with those states), any system non-linearities that could alter one of the symbol power levels (such as AM/AM or AM/PM distortions) would also affect the system bit error rate (BER). An impairment of this type could easily generate BER's high enough to disable an entire system. PSK modulations have only one symbol power level, but they are still vulnerable to amplifier nonlinearity distortions (especially AM/PM).

Assuming that all of the symbol states are occupied equally over time, then it is possible to calculate the relative peak-to-average symbol power and dynamic range requirements of a complex signal (Tables 1 and 2)¹. Discrete symbol power levels can be easily seen and measured on a QAM signal that employs little or no baseband filtering (Fig. 3).

Symbol Power Level Number	Power Vector Magnitude (a)	Number of occurrences (b)	Weighted Symbol Power (a) ² (b)
1	1	4	4
2	5	8	40
3	9	4	36
Total weighted symbol power :			80
divided by total number of symbol states :			16
Average symbol power magnitude :			5
Peak symbol power magnitude :			9
Peak/Average Power Ratio = 9/5 = 1.80 = 2.55 dB			
Dynamic Range = 9/1 = 9.54 dB			

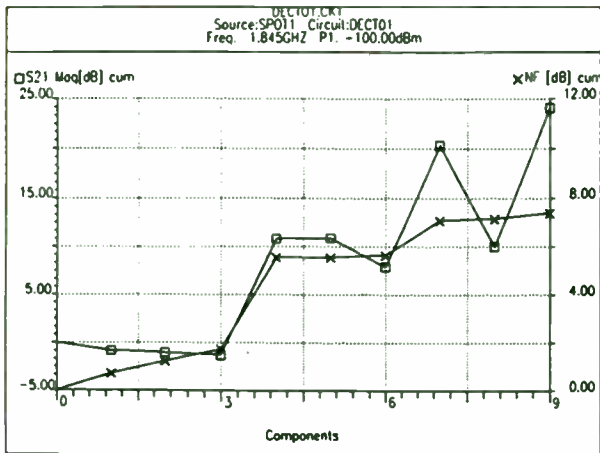
Table 1 - Calculation of Symbol Power for 16-QAM

Type of Vector Modulation	Number of Symbol Power Levels	Peak-to-Avg Symbol Power ratio	Dynamic Range	Percent of Data in highest power level	Percent of Data above average power level
16-QAM	3	1.8:1 2.55	9:1 9.54	25.0 %	25 %
32-QAM	5	1.7:1 2.30	17:1 12.31	25.0 %	50 %
64-QAM	9	2.3:1 3.88	49:1 16.90	6.3 %	50 %
256-QAM	32	2.7:1 4.23	225:1 23.52	4.8 %*	45 %
256-SSQAM	30	1.9:1 2.85	157:1 21.98	25.0 %*	52 %

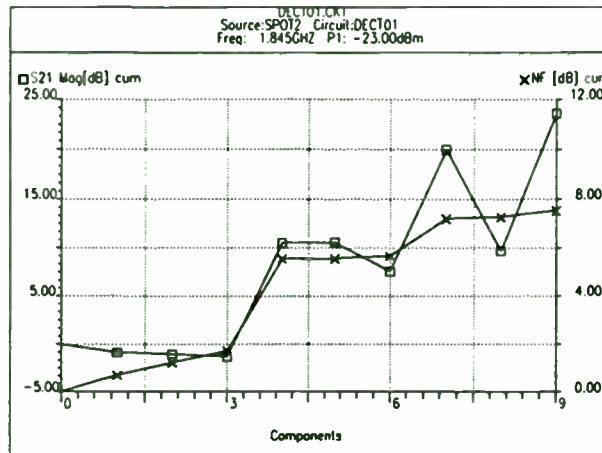
* Highest 1dB of power

Table 2 - Symbol Power requirements of various schemes

As published in the Wireless Symposium Proceedings, San Jose, CA, January 1993,
Also published in abridged form in Microwaves & RF Magazine, January 1993



(a)

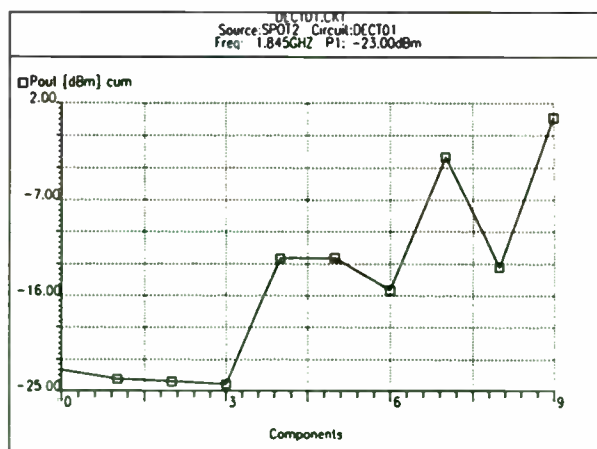
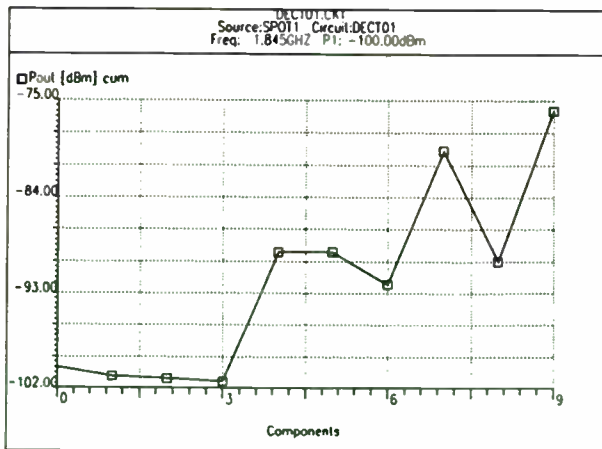


(b)

■ **The Microwave Success System Simulator is used to investigate design specification trade-offs.**

■ (a) shows, for example, the results of calculating the system budget at a received signal level of -100 dBm at a frequency of 1845 MHz. The cumulative budget plot shows the way in which the overall gain and noise figure of the front-end "build-up" through the various components. The overall gain of the front-end in this case is 22 dB with a SSB noise figure of 7.6 dB.

■ The same front-end, operating with a received signal level of -23 dBm (the specification maximum), has an overall gain of 21.7 dB with a noise figure of 7.7 dB (Figure (b)).



■ **Microwave Success calculates the overall performance of the system and displays the results using a variety of graphic displays. Shown above is the output power of a DECT mobile station on receive displayed as a cumulative budget plot at two different receive levels, -100 dBm and -23 dBm.**

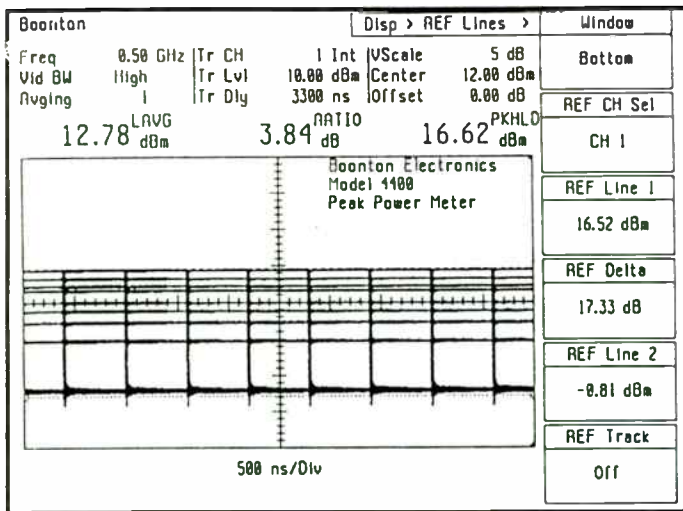


Figure 3 - Nine symbol power levels of a 64-QAM (unfiltered)

Baseband filtering will introduce an additional peak power contribution in the form of compound ringing (Fig. 4). Digitally vector modulated signals require baseband filtering because they have a theoretically infinite bandwidth (as defined by the function $(\sin x)/x$). To limit the occupied signal bandwidth, the I&Q modulator signals must be filtered so that the digitally driven modulator does not have to instantly transition to the next symbol state. A digitally produced symbol change causes an impulse response that has an infinite Fourier series. This series becomes truncated when it is convoluted with a bandwidth limiting filter. Whenever a Fourier series is truncated, ringing results (known as Gibbs phenomena)².

The amplitude of the ringing will vary from symbol to symbol because certain phase/amplitude changes will be more drastic than others. This is compounded by residual ring voltages that are still decaying from previous symbol changes. Although well designed baseband filters will keep this effect to a minimum, peak power transitions will occur in proportion to the square of the compounded ring voltage.

The effect of symbols transitioning across multiple power levels combined with the compound ringing from the baseband filters will produce a power spectrum that resembles white noise (Fig. 5). The highest (peak) power levels of this signal must be preserved within the linear region of an amplifier. Failure to do this has serious consequences since compression of the peak power could result in significant data loss as well as the generation of unacceptable intermodulation distortion products (IMD). Thus, QAM amplifiers are usually operated with average power levels of about 7 to 15 dB below their 1 dB compression points. PSK amplifiers usually require 3 to 7 dB of output "backoff" as well.

Accurate measurement of the peak power is necessary since only 3 dB of error equates to 50% linear error. This could be the difference between choosing either a 500 watt or a 1000 watt amplifier for the same system.

Multiple Carrier Transmissions

Transmitters that support multiple simultaneous carriers are further challenged due to the peak power effect that results from the vectorial addition of the voltage waveforms of each individual carrier. Each time that the number of carriers (with equal power) in a system are doubled, the average power level will increase by 3 dB, and the peak power level will increase by 6 dB (Table 3). In PSK and QAM schemes, the peak power will always be higher due to the

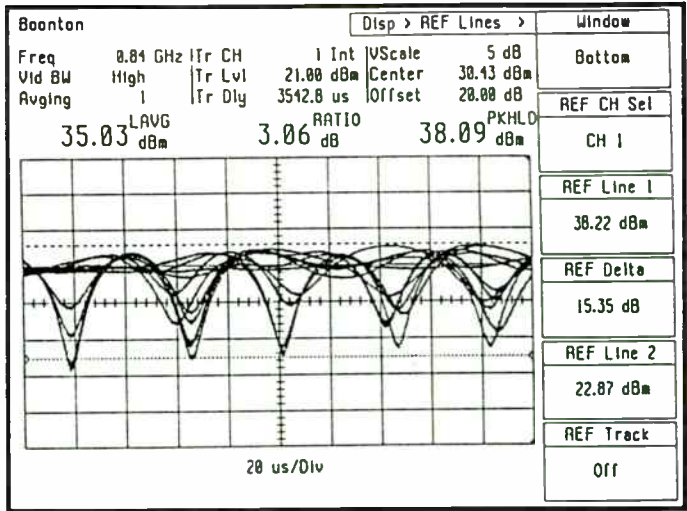


Figure 4 - Compound ringing caused by baseband filtering

peak power components of the individual carriers (symbol power and baseband filter ringing contributions).

In an example situation of 32 carriers, each being QPSK modulated and having an individual average power of 10 Watts with a peak-to-average power ratio of 3 dB, the combined average power would be 320 Watts (55 dBm), but the combined instantaneous peak power would reach to over 20,000 Watts (73 dBm) (Table 4). Assuming that the amplifier was rated for linear operation to 5 kW, all peak power occurrences greater than 5 kW would drive the amplifier toward saturation.

If we constructed a histogram of the power levels, totaling all random occurrences of peak power by level, we would see a statistical distribution with a diminishing number of occurrences as we approached the highest levels. If these were FM carriers, the number of peak power occurrences at and above the power amplifier's compression level would represent the amount of crosstalk and IMD being tolerated. But with a digital vector modulation scheme such as QPSK, this may also be representing instantaneous occurrences of symbol destruction on every carrier at the same time.

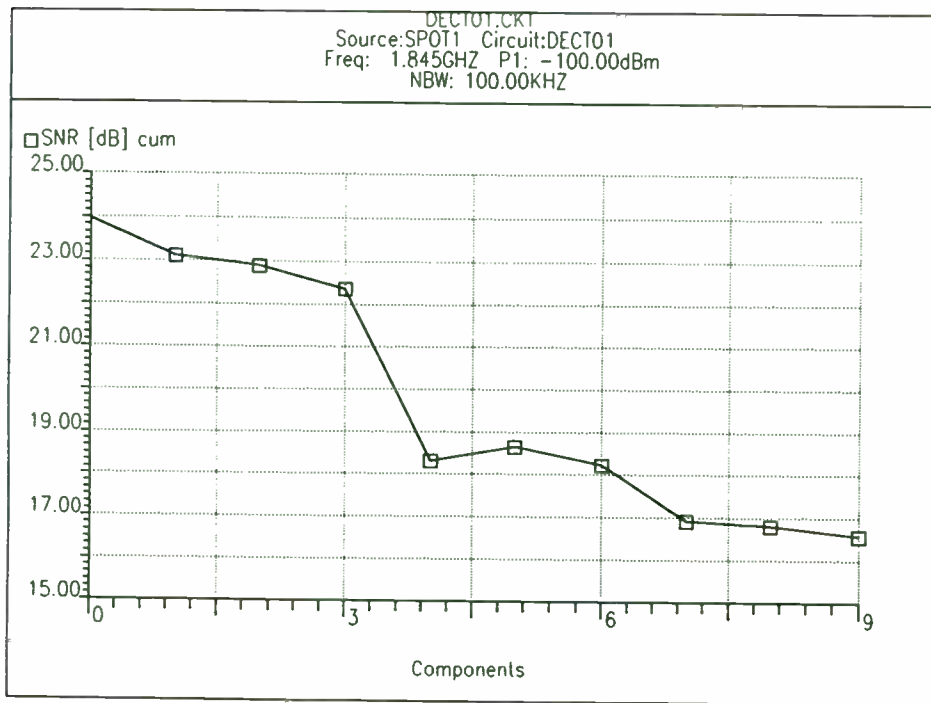
Assuming that the peak power occurrences are of a very small duration compared to the symbol rate and that the amplifier can quickly recover from these occurrences, the symbol information may be recoverable and the transient IMD

Number of Carriers (1W each)	Combined Average Power		Maximum Peak Power		Peak-to-Average Power	
	dBm	Watts	dBm	Watts	dB	ratio
1	30	1	30	1	0	1:1
2	33	2	36	4	3	2:1
4	36	4	42	16	6	4:1
8	39	8	48	64	9	8:1
16	42	16	54	256	12	16:1
32	45	32	60	1024	15	32:1
64	48	64	66	4096	18	64:1
128	51	128	72	16.4 k	21	128:1

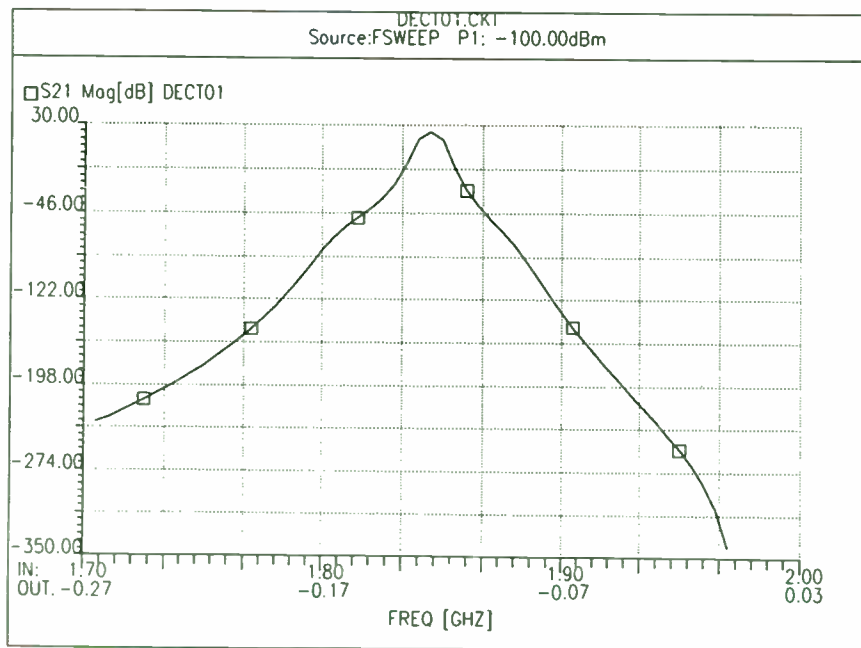
Table 3 - Peak-to-Average Power of Multiple FM Carriers

Number of Carriers (10W each)	Combined Average Power		Maximum Peak Power		Peak-to-Average Power	
	dBm	Watts	dBm	Watts	dB	ratio
1	40	10	43	20	3	2:1
2	43	20	49	80	6	4:1
4	46	40	55	320	9	8:1
8	49	80	61	1280	12	16:1
16	52	160	67	5120	15	32:1
32	55	320	73	21 k	18	64:1
64	58	640	79	82 k	21	128:1
128	61	1280	85	328 k	24	256:1

Table 4 - Peak-to-Average Power of Multiple QPSK Carriers



- The overall signal-to-noise ratio (SNR) for DECT 1800 must be greater than 9 dB. With an input signal of -100 dBm the SNR is 16.2 dB



- The overall response of the front-end at a fixed local oscillator frequency of 1975 MHz is shown. The plot clearly shows the effects of the various band-pass filters in the front-end which aid in meeting the in-band blocking and out-of-band blocking specifications.

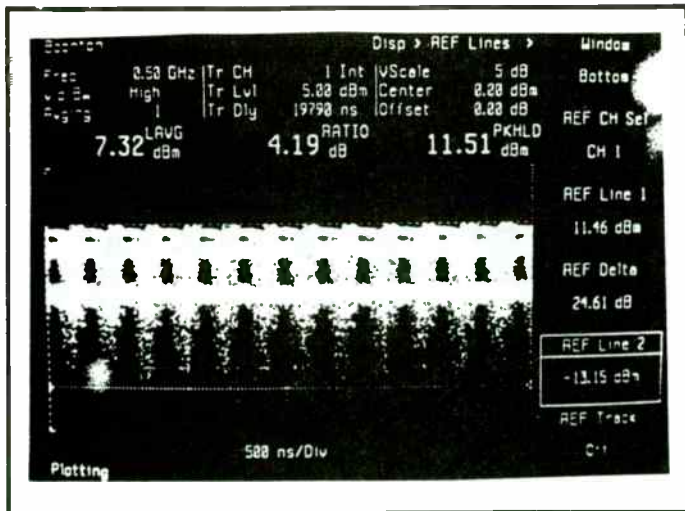


Figure 5 - The "white-noise" power spectrum of a QAM signal

may be able to be tolerated. Yet, if the peak power was known on a continuous basis (by monitoring), the amplifier loading could be regulated to allow for maximum linear output performance while protecting against saturation.

Power Domain

Successful implementation of a digitally vector modulated system requires an analysis of the peak and RMS average power response of a system. What is needed is a power domain analysis, or an ability to analyze instantaneous peak power occurrences as a function of time. Power domain analysis requires measuring scalar power as it occurs in the time domain.

This can be viewed in contrast to traditional scalar analyzers that measure scalar power in the frequency domain. This type of analysis was first defined by commercial and military requirements to analyze pulsed power transmitters. They needed to accurately measure specific pulsed power envelope parameters in the time domain. The peak power meter was developed to meet those needs.

Traditional instruments used for power measurement are not suitable for power-domain analysis. Spectrum analyzers, for example, have bandwidth and mixer limitations and lack the accurate power level measurement capability of a power meter. Conventional averaging power meters are also not suitable for this type of analysis since they are designed to average all instantaneous peak power occurrences. They can, however, provide true RMS average power information.

Thermocouple sensors thermally derive the measurement of true average power, while averaging diode sensors use long resistive-capacitive (R-C) time constants to provide an average voltage response proportional to the average RF power input level. Averaging diode sensors also cannot be used to measure the true RMS power of complex waveforms unless the peaks of the complex waveform exist completely within the square-law limits of the diodes³.

Peak Power Meters

Power domain analysis of a digitally vector modulated signal requires a peak power meter with advanced features. The peak power sensor must be a fast, average-responding diode type, providing instantaneous voltage output proportional to instantaneous RF power input. This is to accurately follow the details of the power envelope of a signal and to capture all instantaneous power occurrences to the fre-

Dynamic Range	Digitizing Bits	Percent Bit Resolution	Power Measurement Resolution
45 dB	8	0.391 %	0.176 dB
45 dB	10	0.098 %	0.044 dB
45 dB	12	0.024 %	0.011 dB
45 dB	14	0.006 %	0.003 dB
45 dB	16	0.002 %	0.001 dB

Table 5 - Power Measurement Resolution

quency limit of its video bandwidth.

The sensor's video bandwidth specification should be sufficient to capture all power transitions related to a symbol change. Any power transitions occurring above the limit of a sensor's video bandwidth will be averaged by the diode's video load. These sensors typically use diodes in a full-wave rectification method to insure accurate detection of both positive and negative voltage transitions.

The sensor diode's video output must be supported by a wide dynamic range amplifier such as a logarithmic amplifier. This is necessary to accurately track a signal through large peak-to-average power levels and to preserve the details of large power transitions. The amplifier's output must then be digitized at high speed with high resolution. High speed sample and hold circuits and flash type A/D converters are often used to perform this type of digitization.

The number of bits used to digitize the signal will determine the power measurement resolution. When the percent bit resolution is applied across the full dynamic range of the logarithmic amplifier, the quantization level resolution is established (Table 5). This resolution must be fine enough to discern the smallest power level of interest.

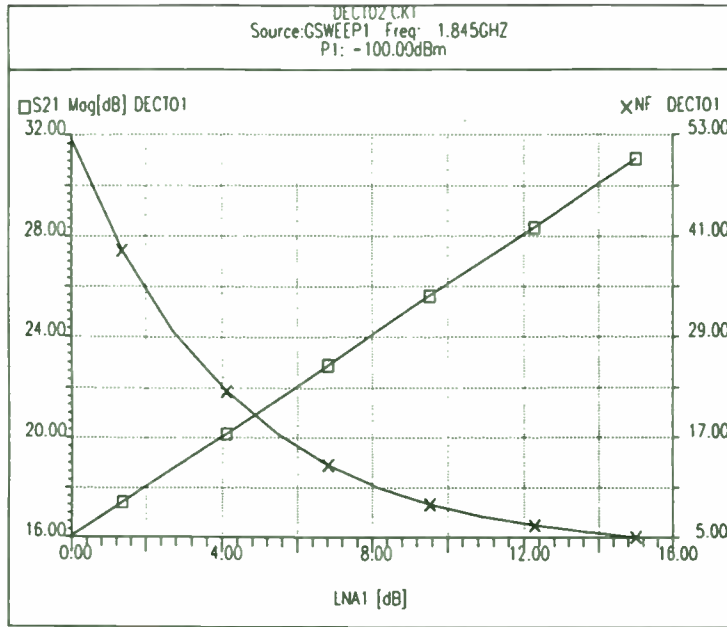
Video averaging is often used to interpolate the area between the quantization levels. This has an effect as if the number of bits of resolution could be increased and it is usually referred to as "averaging the signal". By averaging a PSK/QAM signal in this way, peak power information is lost. This is because the power envelope is not repetitious with time, but changing continuously from symbol to symbol. So signal averaging cannot be used.

The acquisition system must use very high speed sampling, or else use a technique such as random repetitive sampling to provide true statistically random sampling. The system should also acquire power data with or without a repetitive trigger event. This is important in situations where a symbol trigger is not available or with multiple carrier transmissions.

Finally, consideration also must be given to the processing system since acquisition speed (samples per second) does not take into account how effectively the processing system can utilize these samples. When significant mathematical processing is required, a weak processing system may be forced to ignore a significant percentage of the available samples because it will not have the time to process them.

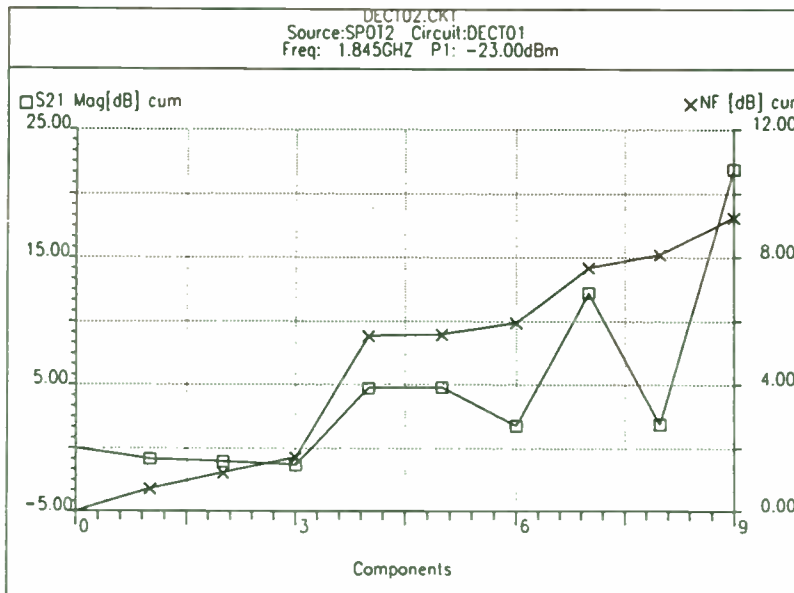
Boonton 4400 Peak Power Meter

The Boonton 4400 is an advanced peak power meter designed to support extensive power domain analysis. It combines powerful signal acquisition and digital signal processing with a versatile set of user interface features. It can accurately analyze instantaneous peak power occurrences on either continuous or pulsed signals, whether repetitive or not, from 30 MHz to 40 GHz (depending on sensor) with NIST traceable accuracy.



Methods of achieving the required system specification that result in rather different (and, perhaps, unrealistic) specifications for the single-pole, double-throw switch, LNA, filters and mixer can be investigated. For low-cost production it is mandatory that the performance of each circuit is reproducible and easy to achieve resulting in high yield.

■ **DECT 1800 System Trade-Off Analysis using Microwave Success**



In order to achieve a front-end noise figure of 12 dB, an amplifier with a gain of 6 dB is needed (mixer noise figure and gain of 10 dB). Increasing the gain of the amplifier to 14 dB gives the required overall front-end gain but may not be the most cost-effective method.

- Above we show the case where the front-end gain is mainly concentrated after the mixer in the first IF amplifier -- in both cases the noise figure of the LNA was 4 dB. In this case the noise figure of the mixer was made 6 dB, which is easily achievable with active mixers.
- ◆ **DECT 1800 System Trade-Off Analysis using Microwave Success**

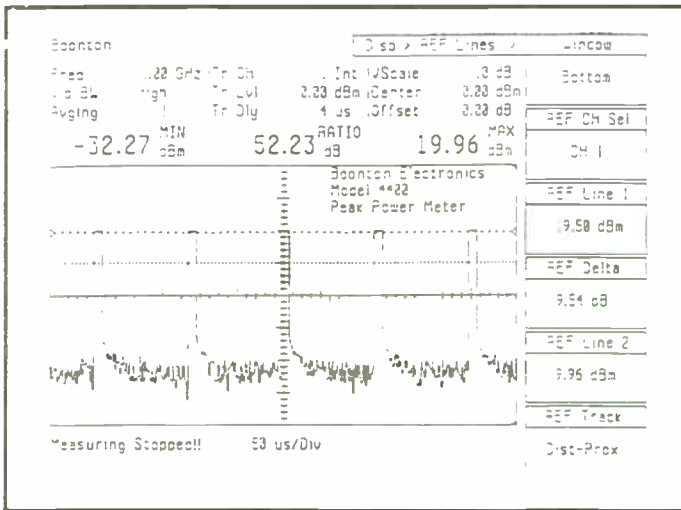


Figure 6 - The 4400 tracks power over a large dynamic range

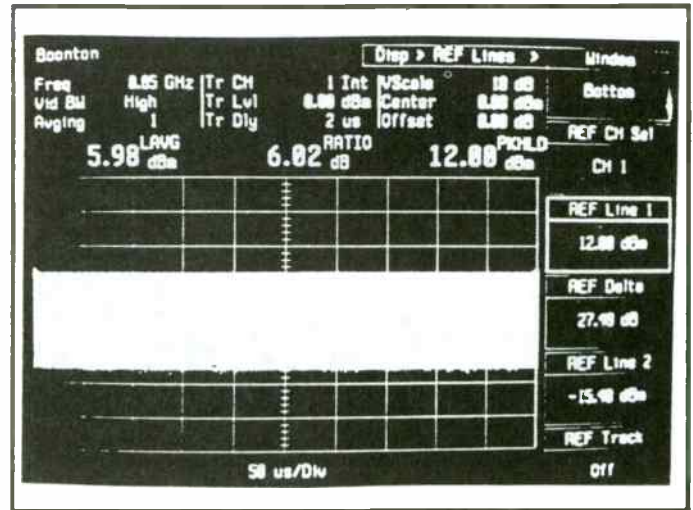


Figure 8 - Multiple carriers requiring 28dB of dynamic range

It's 56318 peak power sensor can accurately track all instantaneous power events up to 35 MHz (video bandwidth limit). Power occurrences (or white noise effects) that are faster than this, are averaged down to the video bandwidth limit. Pulse rise/fall time measurements are possible to less than 15ns. Diode response is tracked with a logarithmic amplifier having a dynamic range of over 47 dB (Fig. 6). The logamp's output is random-repetitively sampled by a 12-bit flash acquisition system digitizing at 1 Msamples/sec (1 MSample/s for timebase settings of 50us or faster, else .5 MSample/s).

A dedicated 32 bit floating point digital signal processor (DSP) continually process this data and execute all mathematically related analyses with negligible sample decimation. The DSP system can perform true integral RMS averaging on any portion of a waveform by simply positioning the area of concern between two time markers. These markers can be positioned to integrate an area within a pulse or across the whole screen (the DSP converts all data to linear values for RMS integration). The area between these markers also can be analyzed to indicate max/min power occurrences, long-term peak occurrence (peak-hold), long-term RMS average (LAVG), and peak-to-average power ratio (Fig. 7).

The DSP performs all trigger and measurement analysis directly on the acquired data (not on the displayed data), and it does not require that the operator have the display set in

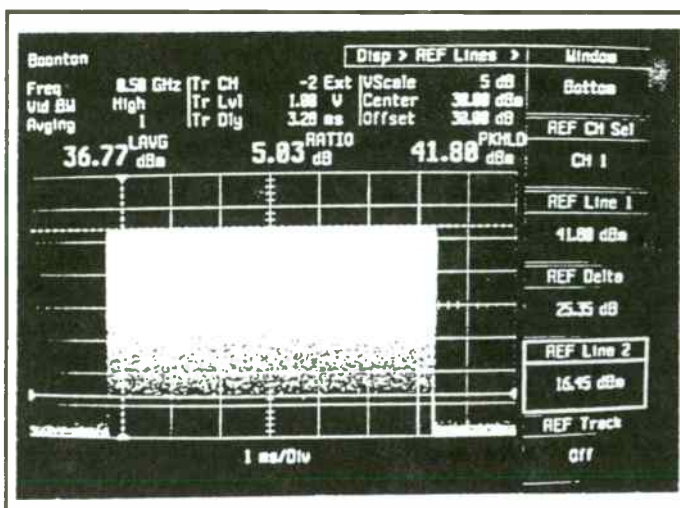


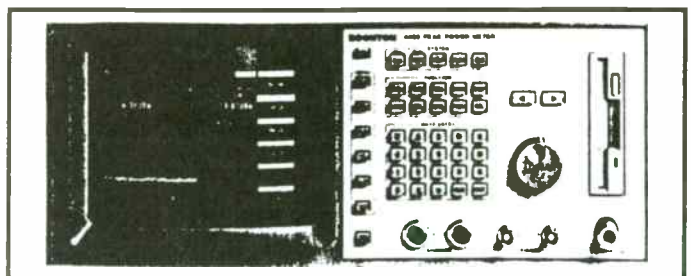
Figure 7 - RMS integration of area between time markers

any particular way for proper operation. A dedicated video graphics processor continually processes the peak power data for display on an integral high resolution 256 color VGA compatible display. Both logarithmic and linear display modes are available for analysis. The screen display can be plotted or printed to a variety of supported devices.

Amplitude reference lines are provided to index absolute power levels on the VGA display. This feature, combined with display persistence, allows the large dynamic range requirements of a signal (or multiple signals) to be easily measured (Fig. 8).

On slower timebase settings (10 msec/div and slower), the DSP can process many more samples than can be displayed. In this situation, the DSP will over-sample to determine a pixel's value. The user can select whether the DSP will average a set of samples (normal mode) or select the highest value of the set (peaking-mode) to represent a pixel's value. With peaking-mode enabled, the DSP can peak-detect up to 5 million continuously acquired samples in one sweep.

Peak power data can also be continuously transferred to a host computer via the IEEE-488 GPIB port. This feature can be used to support extensive user analyses such as transmitter power histograms and peak power monitoring.



Boonton 4400 Peak Power Meter

For more information contact Boonton Electronics, USA, at (201) 584-1077.

References

- 1 "Measuring Peak and Average Power of Digitally Modulated Advanced Television Systems", C.W.Rhodes & P.Crosby, IEEE Transactions on Broadcast Technology, December 1992
- 2 Digital Filters R.W.Hamming, Prentice-Hall, 1977
- 3 "Diode Sensors for the Measurement of True Power" R.E.Lafferty, Microwave Journal, November 1987

Component	Gain	NF	IP3 (input)	Power
Duplex Bandpass Filter	-3.0 dB max.	<3.0 dB	150 dBm	---
SPDT T/R Switch	-0.5 dB	0.5 dB	>0 dBm	---
SPDT T/R Switch	-0.5 dB	0.5 dB	>0 dBm	---
Low-Noise Amplifier	14.0 dB	<6.0 dB	>0 dBm	---
SPDT Switch	-0.5 dB	0.5 dB	> 0 dBm	---
RF Filter	-4.0 dB max	<4.0 dB	150 dBm	---
Mixer	10.0 dB	10.0 dB	> 0 dBm	---
Local Oscillator	---	---	---	-10 dBm
IF Filter	-10.0 dB max	<10.0 dB	150 dBm	---

List of the important parameters for the components in a DECT front-end (for Receive)

Parameter/Component	Value	Gain	Noise Figure	1 dB O/P Power	Third Order Intercept Point @ Input
Frequency range	1880MHz to 1900MHz	---	---	---	---
Power Amplifier	---	37 dB min.	---	26 dBm	---
Low-Noise Amplifier	---	12 dB	4 dB	---	-10 dBm
T/R SPDT Switch	---	-0.5 dB	---	>27 dBm	---
Power from TX Synth.	-10 dBm	---	---	---	---
Power Supply	3.3 to 4.5 volts, three NiCd batteries	---	---	---	---
Temperature range	-10C to +50C	---	---	---	---

List of the important parameters for the Components in a DECT Front-End (for the Transmitter)

DELAY SPREAD MEASUREMENTS AND FEHER'S BOUND FOR DIGITAL PCS AND MOBILE CELLULAR SYSTEMS

DR. KAMILO FEHER

President, Digcom Consulting Group
Director, Digital Communications Research Laboratory
Professor, Department of Electrical and Computer Engineering
University of California, Davis; Davis, CA 95616
916-752-8127 or 916-752-0583; FAX 916-752-8428

ABSTRACT

A simple and powerful technique and apparatus for delay spread measurements and analytical predictions is presented. Delay spread (τ) is one of the most critical practical radio propagation parameters in the design of US digital cellular standard, Japanese digital cellular and GSM European systems. Delay spread may also control the performance of several high data rate PCS/PCN systems.

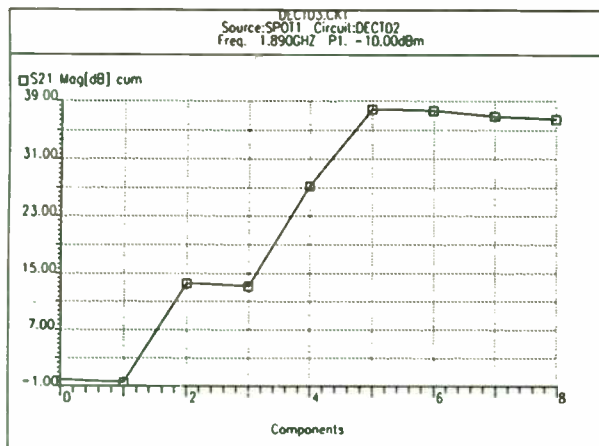
The described measurement technique is suitable for laboratory and factory measurements, as well as for field measurements. A simple CW burst generator, spectrum analyzer and graphic plotter are configured to provide measurement accuracy within 5%. This accuracy is significantly higher than is required for most practical applications. We compare this measurement apparatus with considerable more sophisticated and unnecessarily complex test instrumentation. We highlight the advantages of the bursted RF method. Several field measurement results of indoor (up to 1 km), cellular (up to 10 km) and Public Land Mobile Radio (PLMR-up to 70 km) have been performed with the described method.

For analytical predictions of the maximal worst case delay spread bound τ_{\max} , we introduce "Feher's delay spread bound" and compare it to numerous experimental data. We demonstrate that this simple bound " τ_{\max} " requires only a knowledge of RF frequency and of transmit and receive (threshold) power. It is useful as a practical design tool for delay spread estimation of wireless systems.

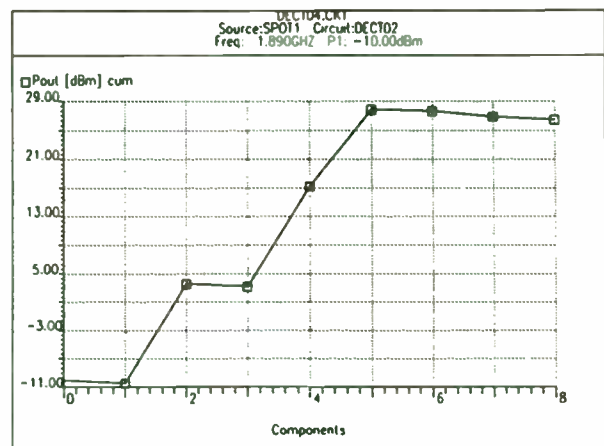
Proceedings of the WIRELESS Symposium and Exhibition, San Jose, CA, Jan. 12-15, 1993.

Component	Gain	Noise Figure	Return Losses	P 1 dB comp.	O/P IP3
Duplex Filter	-0.5 dB	0.5 dB	>15 dB	>150 dB	>150 dBm
SPDT Switches 1 & 2	-0.5 dB	0.5 dB	>15 dB	>10 dBm	>20 dBm
LNA	14 dB	4 dB	>20 dB	11 dBm	23 dBm
Driver Amplifier	15 dB	4 dB	>20 dB	16 dBm	28 dBm
Power Amplifier	12 dB	4 dB	>15 dB	>25 dBm	37 dBm
T/R Switch	-0.5 dB	0.5 dB	>15 dB	>30 dBm	>37 dBm
Harmonic Filter	-0.5 dB in band -20 dB at 1900 MHz	0.5 dB	>15 dB	>150 dBm	>150 dBm

Parameters of Components used in system level simulation of DECT Transmitter



(a)



(b)

- (a) shows a budget plot of the gain of the transmit section when the input power level is set at -10 dBm. The overall gain is close to 40 dB.
- (b) shows the corresponding power cumulative budget plot for the transmitter. The power output from the power amplifier is 26.7 dBm. At the antenna the power output level is 25.4 dBm.

1. DELAY SPREAD: THEORETICAL CONCEPTS AND TERMINOLOGY

The physical cause of delay spread is illustrated in Fig. 1. As an illustrative example we assume that at $t = 0$ one very short RF burst is transmitted from the base station located on the 70 m rooftop of a high-rise building. The “direct” LOS (line-of-sight) signal path has a length of d_0 (m) and a propagation time (delay) of τ_0 . The LOS path is obstructed by several buildings and has an obstruction caused signal attenuation of 60 dB. If $d_0 = 1000 \text{ m} = 1 \text{ km}$, then the free space LOS loss at 150 MHz, as shown in Fig. 2, is 101 dB. Thus, the total path loss of the direct signal path is 60 dB + 101 dB = 161 dB, see Table 1. The reflected multipath RF signals travel along of

$$d_1 + d_2, d_3 + d_4, \dots, d_k + d_L$$

If the signal obstruction caused attenuation along these longer signal paths is not very large, e.g., assume 7 dB and 10 dB in Table 1, then the received reflected signals, having a considerably longer propagation delay than the LOS signal in the d_0 path, arrive to the mobile with received powers of comparable magnitude to the power of the LOS signal path. In this example, we assume that the signal received by the mobile, through the reflected delayed path $d_1 + d_2$, having a propagation delay of $\tau_1 + \tau_2$ is -119 dBm , that is, 2 dB higher than the obstructed LOS signal.

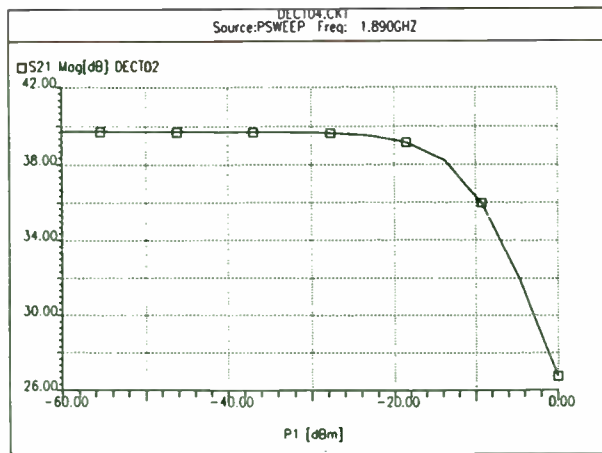
The reflected signal path $d_1 + d_2$, arriving at $\tau_1 + \tau_2$ has a delay, relative to the direct LOS signal of $\tau_A = \tau_1 + \tau_2 - \tau_0$. It is known as the first arrival delay (or delay spread). The second reflected signal, path $d_3 + d_4$, arrives at $\tau_3 + \tau_4$ and has a delay spread, relative to the d_0 direct signal path of $\tau_B = \tau_3 + \tau_4 - \tau_0$ and a received power of -138 dBm , that is, the received power of this delayed signal is 17 dB lower than the power of the direct path signal. In a real multipath environment a very large number, practically infinite, of delayed components are added. These components form a power delay profile.

2. DELAY SPREAD MEASUREMENTS

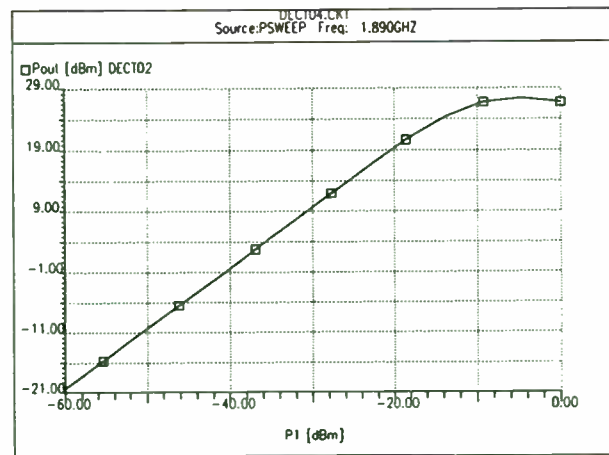
The impact of delay spread (τ) on the performance of mobile systems can be analytically evaluated, predicted by means of computer simulations and measured in the laboratory and/or in the field in a real multipath propagation environment. In this section laboratory and field measurement concepts are presented.

2.1 LABORATORY - DELAY SPREAD MEASUREMENT SET-UP

For laboratory delay spread measurements the delay model, profile, and/or amount of the delayed signal path and received levels are specified. System specifications are developed from field propagation experimental data and are based on overall cellular/mobile system network studies. A frequently used specification and model, illustrated in Fig. 3, is the radio and delay spread propagation model adopted by the TIA and EIA committees for the North American Digital Cellular (NADC) standard, known as TIA-IS 54. In this measurement set-up the transmitted modulated RF signal is fed to the direct path Rayleigh simulator, $R_0 e^{j\phi_0}$ and also to a delayed path Rayleigh simulator, having a simulated propagation delay of τ_1 [μs] and the same average power as the direct path. In Fig. 3 the second transmitter Tx2, transmits a modulated interfering signal, having the same center frequency as the main and delayed signal path. This interfering signal is simulating co-channel interference (CCI) C/I_c . It is passed through an independent Rayleigh simulator $R_i e^{j\phi_i}$ and a variable attenuator which sets the specified desired carrier power to CCI ratio, i.e. C/I_c . In these set-ups the individual Rayleigh fade simulators



(a)



(b)

- ◆ The compression characteristics of the transmitter are shown in (a) and (b).
- In (a) the Input Power to port P3 is swept from -60 dBm to -10 dBm. The Output Power at -10 dBm input is 26.5 dBm with an overall Gain Compression of 3 dB.
- (b) shows the Power Compression curve for the Transmitter.

Linear and Nonlinear Circuit Design

- ◆ Super-Compact provides state-of-the-art linear circuit simulation facilities
 - ◆ *Fast Nodal Analysis on both Workstations and PCs*
 - ◆ *Unrestricted Nodal Noise Analysis*
 - ◆ *Very Accurate Active and Passive Component Models*
 - ◆ *Quasi-Full Wave Analysis Module for Multiple-Coupled Lines*
 - ◆ *Complete Libraries of commonly-used components including*
Bipolar and Field-Effect Transistors
 - ◆ *"Electronic" Smith Chart for easy impedance matching*
 - ◆ *Circuit Optimization and Tuning*
 - ◆ *Statistical Yield Analysis and Circuit Design Centering*
 - ◆ *Voltage "Probing" of the internal nodes of circuits*

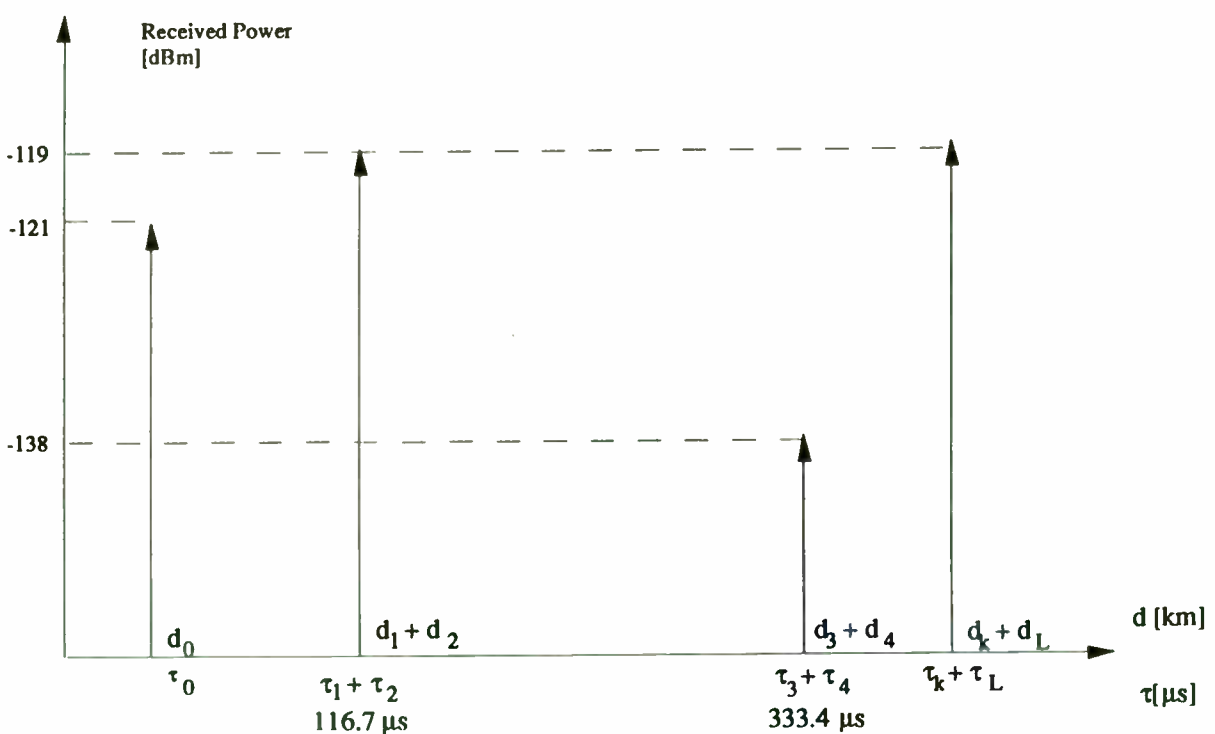
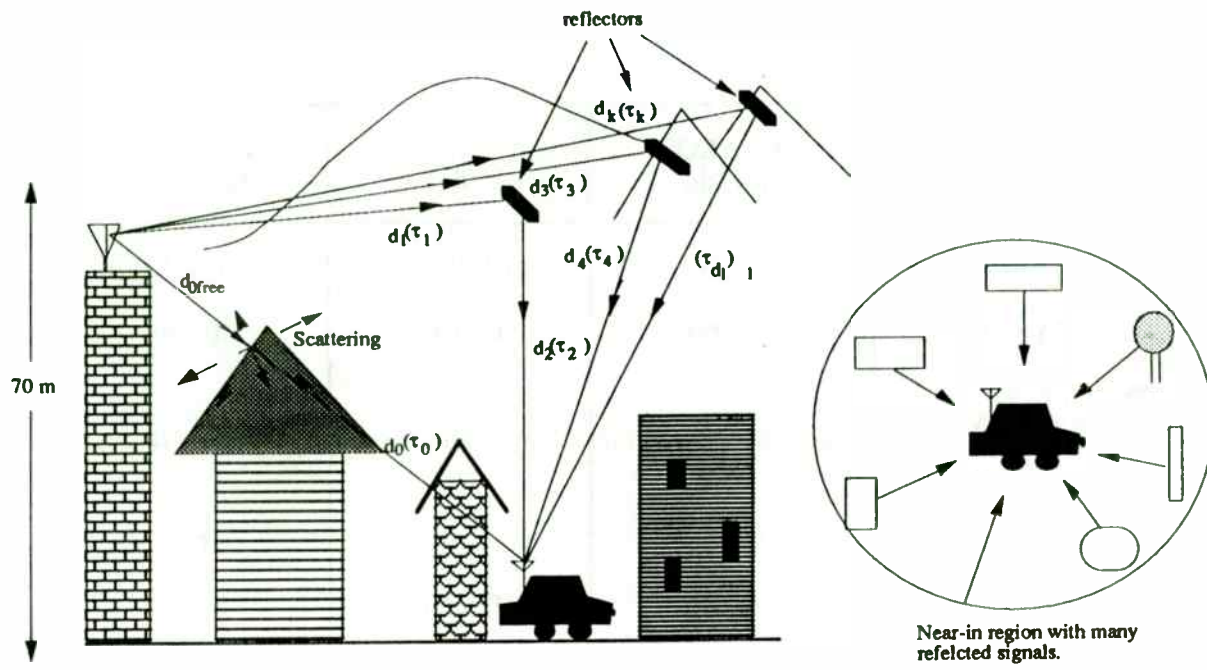
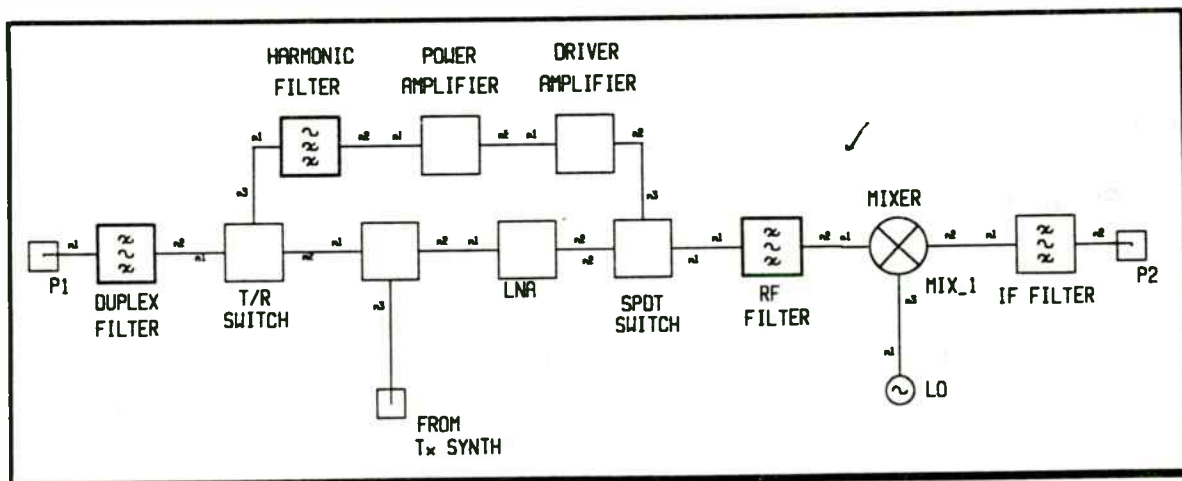


Fig. 1 Propagation environment of a land-mobile Line-of-Sight (LOS) and Non-Line-of-Sight (NLOS) radio system. The base station antenna in this illustrative example is at a height of 70 m. The direct LOS free space path “ d_{0free} ” is between the base antenna and the first building. Afterwards the direct d_0 path is attenuated. The distant mountains reflect the signals. The reflected delayed signals could be received at a comparable power level to the attenuated direct path signals. Ref. K. Feher [FE-B6].

Linear and Nonlinear Circuit Design

◆ Microwave Harmonica provides state-of-the-art nonlinear circuit simulation facilities

- ◆ *Fast Harmonic Balance Technique on both Workstations and PCs -- many times faster than Spice.*
- ◆ *Very Accurate Active and Passive Component Models*
- ◆ *Superior Large-Signal Models such as modified Gummel-Poon for Bipolar Transistors; modified Materka and Triquint-Own-Model (TOM) for FETs and Charge-Conservation Model for MOSFETs*
- ◆ *Complete Libraries of commonly-used components including Bipolar and Field-Effect Transistors*
- ◆ *Circuit Optimization and Tuning*
- ◆ *Statistical Yield Analysis and Circuit Design Centering*
- ◆ *Voltage "Probing" of the internal nodes of circuits*
- ◆ *Many display types including spectral and time domain, power, harmonics, DC voltages and currents*



Designing Filters for the CT

	Direct LOS Path "d ₀ "	1st Reflected Path "d ₁ +d ₂ "	2nd Reflected Path "d ₃ +d ₄ "
Total Propagation Distance	d ₀ =1km	d ₁ +d ₂ =36km	d ₃ +d ₄ =101km
Transmit Power P _T =10 Watt	40dBm	40dBm	40dBm
Propagation Path Loss (based on Fig. 2 at 150MHz)	101dB	152dB	168dB
Path loss due to buildings and other obstructions	60dB	7dB	10dB
Total path loss (L _T)	161dB	159dB	178dB
Received Power P _R = P _T - L _T (dBm)	-121dBm	-119dBm	-138dBm
Total Propagation Delay	τ ₀ = 3.3μs	τ ₁ + τ ₂ = 120μs	τ ₃ + τ ₄ = 336.7μs
Delay Spread "τ" of Reflected Signal τ=(τ _N +τ _m)-τ ₀	0 μs	116.7 μs	333.4 μs

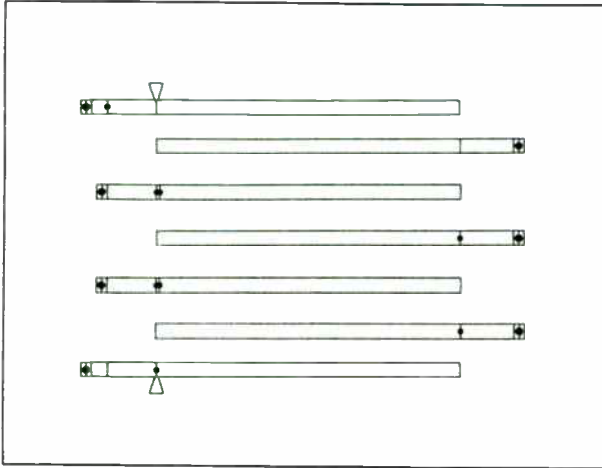
Computation of τ₁ + τ₂ and τ₃ + τ₄:

$$\tau_1 + \tau_2 = \frac{d_1 + d_2}{c} = \frac{36 \times 10^3 \text{m}}{3 \times 10^8 \text{m/s}} = 120 \mu\text{s}$$

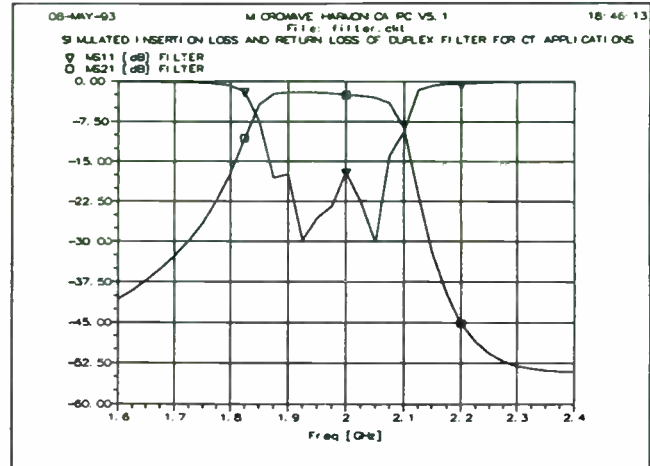
$$\tau_3 + \tau_4 = \frac{d_3 + d_4}{c} = \frac{101 \times 10^3 \text{m}}{3 \times 10^8 \text{m/s}} = 336.7 \mu\text{s}$$

Table 1 Delay spread "τ" and illustrative propagation loss values of a 3kHz narrowband 150MHz radio frequency Public Land Mobile Radio (PLMR) system. Values in this Table correspond to Fig. 1, Ref. [FE-B6].

- In order to reduce size and keep manufacturing costs low design engineers are adopting novel techniques to realize circuits and sub-systems.
- As RF circuits are packed closer together parasitic, unwanted coupling and cross-talk can take place between components.
- Filters are used to define signal bandwidths, produce image rejection as well as prevent transmission signal harmonics from reaching antennas. These filters need to be physically small and often need high rejection close to the operating signal band.



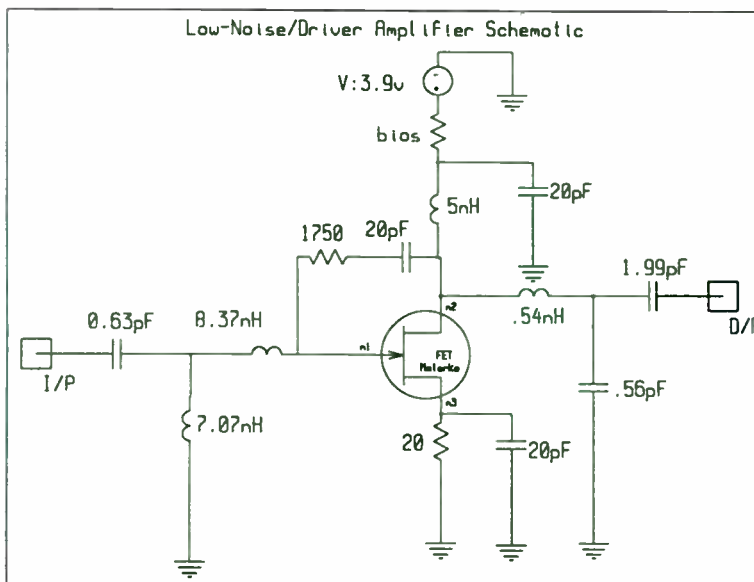
Layout of a Typical Interdigitated Filter



The Simulated response of such a Filter in the 1.8 to 2.0 GHz frequency range.

Linear and Nonlinear Circuit Design

- ◆ Use of Frequency Domain Circuit Simulators, like Super-Compact, for Small-Signal, Linear Design
- ◆ Use of Frequency/Time Domain Circuit Simulators, like Microwave Harmonica, for Large-Signal, Nonlinear Design



EXAMPLE -- The Low-Noise Amplifier shown aside is used as a small-signal amplifier, on receive, as well as a pre-driver amplifier on transmit. This requires that the amplifier not only have the required GAIN and NOISE FIGURE (simulated using Super-Compact) but also have the necessary 1 dB GAIN COMPRESSION and OUTPUT POWER (simulated using Microwave Harmonica)

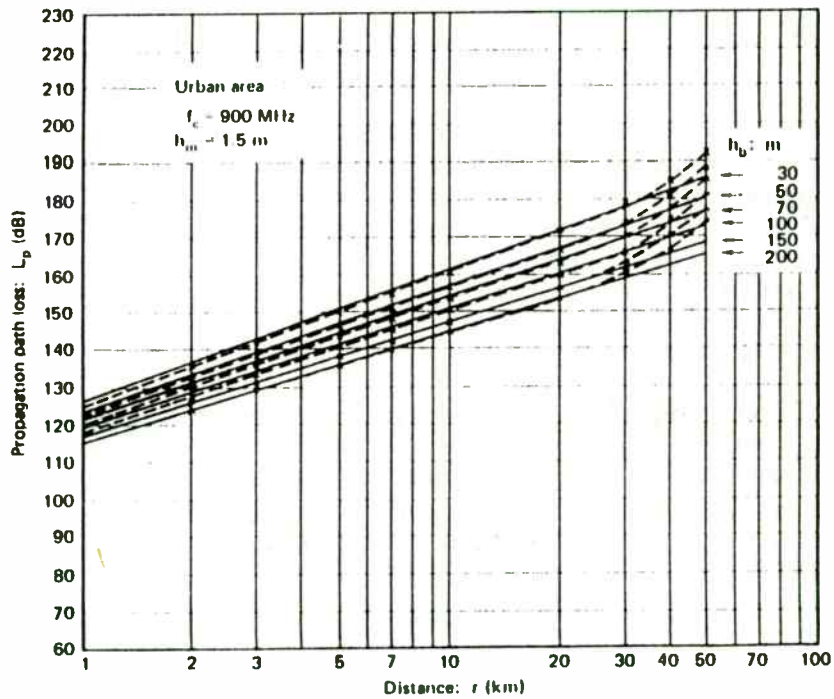
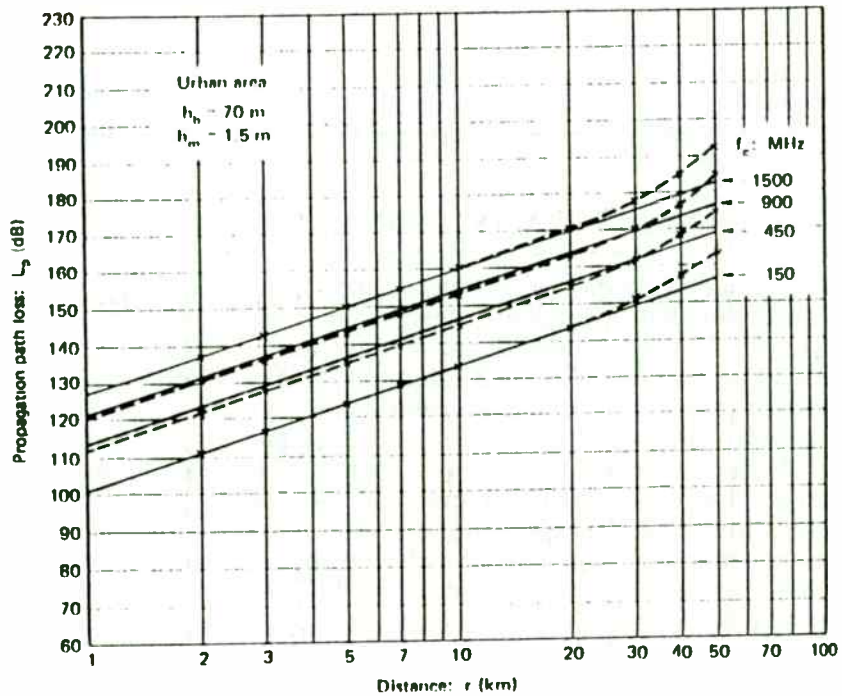
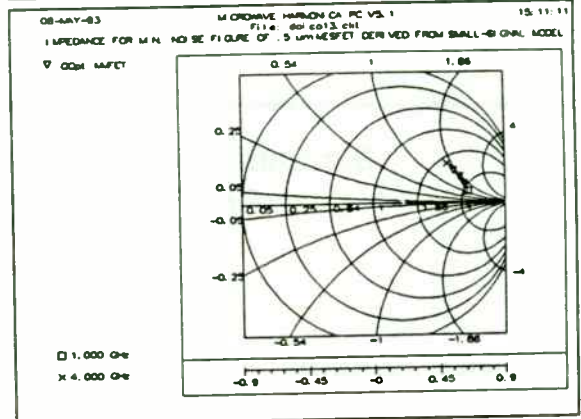
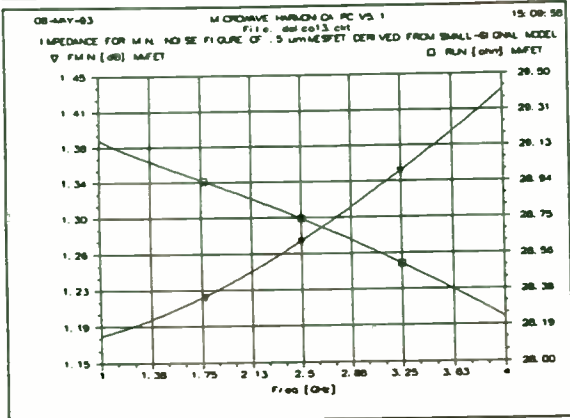
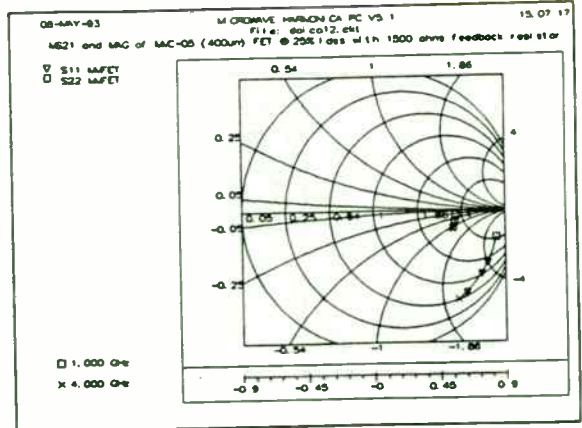
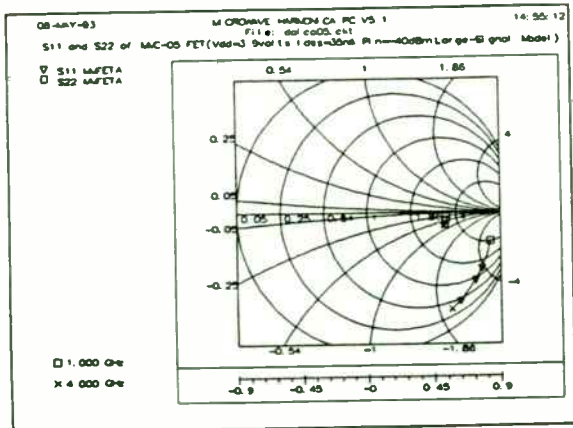
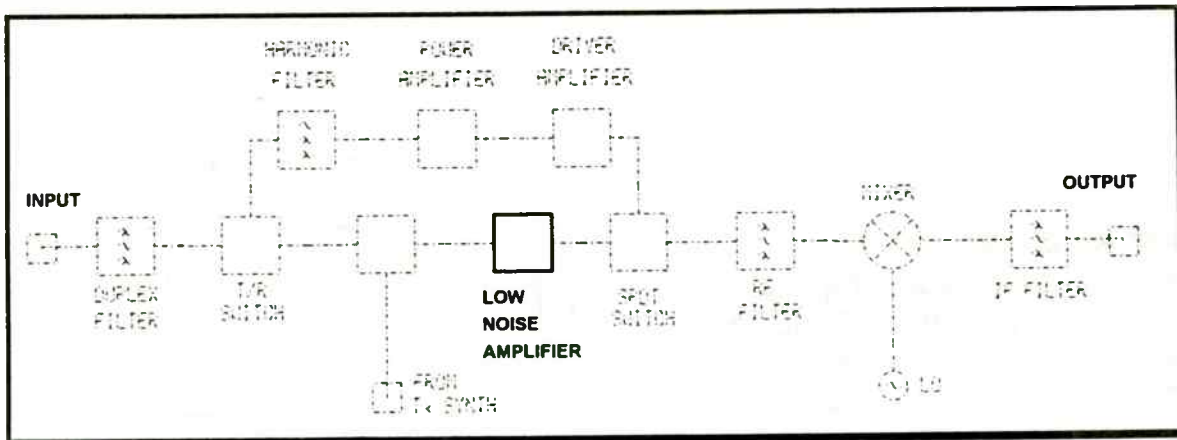


Fig. 2 Propagation path loss in urban area. Solid lines are obtained by empirical formula, dashed lines by Okumura's prediction method [FE-B5].



S-Parameters of Foundry GaAs MESFET Transistor (Large and Small-Signal Models) and Derived Noise Parameters for the Device at Low-Noise Bias (Raytheon)



Designing the Low-Noise Amplifier on Receive

have adjustable Doppler frequencies. A considerably more complex laboratory delay spread simulator is illustrated in Fig. 4. In this simulator, adopted by the European GSM standardization committee, up to twelve delayed Rayleigh faded "taps" simulate the multipath Rayleigh delay spread environment.

2.2 DELAY SPREAD - FIELD MEASUREMENT APPARATUS

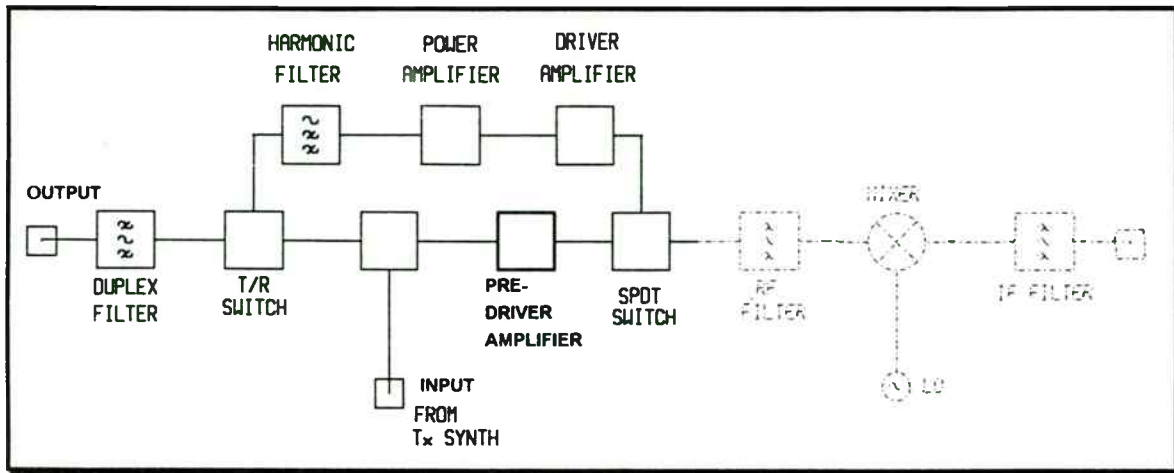
A simple and powerful delay spread field measurement concept and apparatus is shown in Fig. 5. In this set-up an RF oscillator (frequently designated as LO = local oscillator or CW = carrier wave generator) provides an unmodulated carrier wave to an "on-off" - RF switch. The amplified RF signal is illustrated at point A in the timing diagram. Note that the RF signal is turned "on-off" at a periodic rate, e.g., every 5 ms, and has a very short "on" duration, e.g., 100 ns. Practically a periodic RF impulse stream is generated and transmitted [DR-1]. The mobile receiver amplifies the received signal by a low-noise amplifier (LNA) and down converts it to a suitable intermediate frequency (IF), for example 140 MHz. The LNA and down converter could be part of a low-noise RF spectrum analyzer. By setting the RF-IF spectrum analyzer to a "zero IF" the spectrum analyzer envelope detects the received burst carrier wave. The "resolution" bandwidth also known as "noise bandwidth" of the spectrum analyzer has to be sufficiently wide in order to preserve the "impulse nature" of the received signals. At the same time this bandwidth should not be too wide because the "noise floor" of the set-up increases with increased resolution bandwidth [FE-B4]. For a time resolution of approximately 5 μ s a spectrum analyzer resolution (noise) bandwidth of about 300 kHz leads to acceptable measurement accuracy. To calibrate the time delay spread in the laboratory you may wish to add a calibrated delayed path " τ_{cal} " attenuated by 0 dB, 10 dB to 50 dB. This "pre-field" laboratory calibration assures that the set-up handles the amplitude dynamic range of interest and the required resolution accuracy of the time delay spread. The falling edge of the direct path corresponds to the $\tau=0$ reference point.

More advanced delay spread field test sets have been developed by several engineers. The apparatus described by A. Zogg [ZO-1] utilizes a wideband RF signal obtained by an 8 bit length pseudo-random sequence ($2^8 - 1 = 255$ bits) having a 4.9 MHz clock rate. This baseband data stream modulates the RF carrier. The received modulated signal is coherently demodulated to the in-phase and quadrature signal components. The difference between the received multipath-delay spread signals and the reference signal is caused by propagation reflections "echoes". By obtaining the Fourier transforms and the inverse Fourier transforms the delay path/profile/spread characteristics are computed.

In summary, the simple set-up of Fig. 5 provides reasonable accurate measurements. The more advanced (and unfortunately more complex) set-up described by Zogg [ZO-1] requires considerably wider RF bandwidth. It leads to more data and somewhat increased field measurement accuracy.

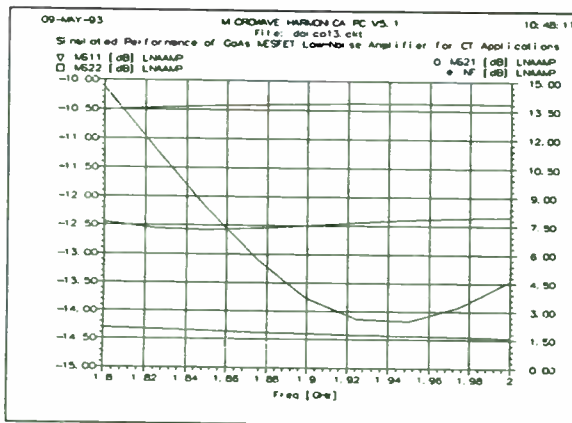
3. DELAY SPREAD FIELD MEASUREMENT RESULTS

Delay spread has a tremendous impact on the performance of digital mobile radio systems and in particular on relatively high bit rate systems. If the rms delay spread τ exceeds about 10% of the bit duration, T_b then the BER performance degradation becomes significant. For a $\tau_{rms}/T_b = 0.25$, a high BER floor of about 3×10^{-2} has been observed. This severe impact of delay spread on the performance of digital cellular and PCS systems led to large scale global research and delay spread field measurement efforts. Hundreds of publications and reports contain delay spread field measurement data and analysis. Most IEEE conferences in mobile



Simulating the Low-Noise Amplifier used as a Pre-Driver Amplifier on Transmit

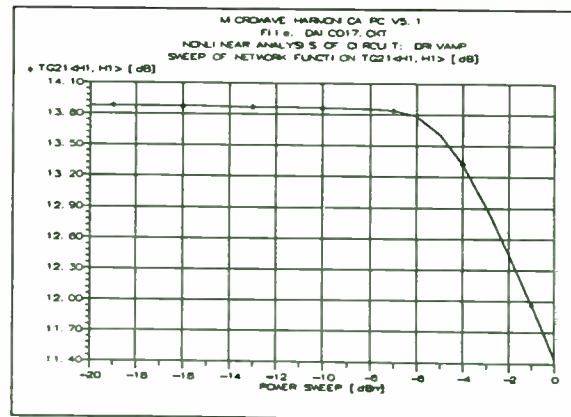
Low-Noise Amplifier



Raytheon MMC-05 400 μm gate width FET used in the low-noise/pre-driver amplifier design. The FET is operated at 25% I_{dss} i.e. at 35 mA. Self-bias used for single-rail operation. Gain is > 13 dB with noise figure of < 2 dB.

Pre-Driver Amplifier

Used as the pre-driver amplifier on transmit the circuit has a 1 dB gain compression point of + 10 dBm at its output. Power consumption is 70 mW.



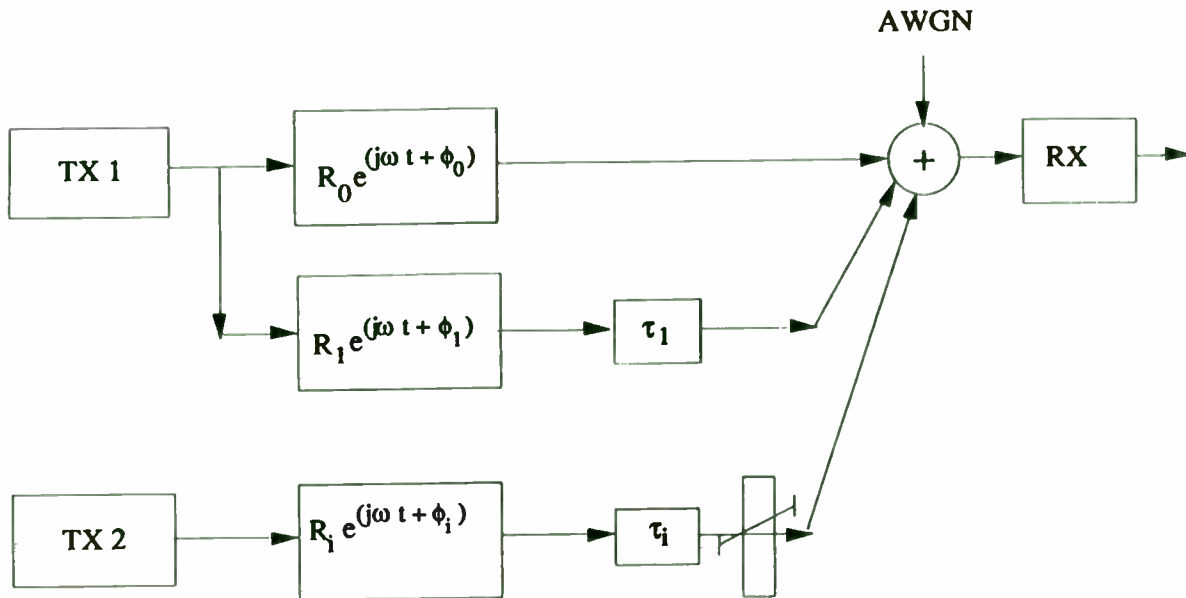


Fig. 3 Radio Propagation Simulator Model Specified by TIA and EIA committees for the North American Digital Cellular (NADC) standard. Co-channel interference comes from the adjacent cell transmitting at the same frequency. R_x is an independent Rayleigh fade simulator, with a given rms power gain. The specified rms delay τ_x is smaller than the symbol duration T_s , i.e., $\tau_x < T_s$ Ref. [FE-B6].

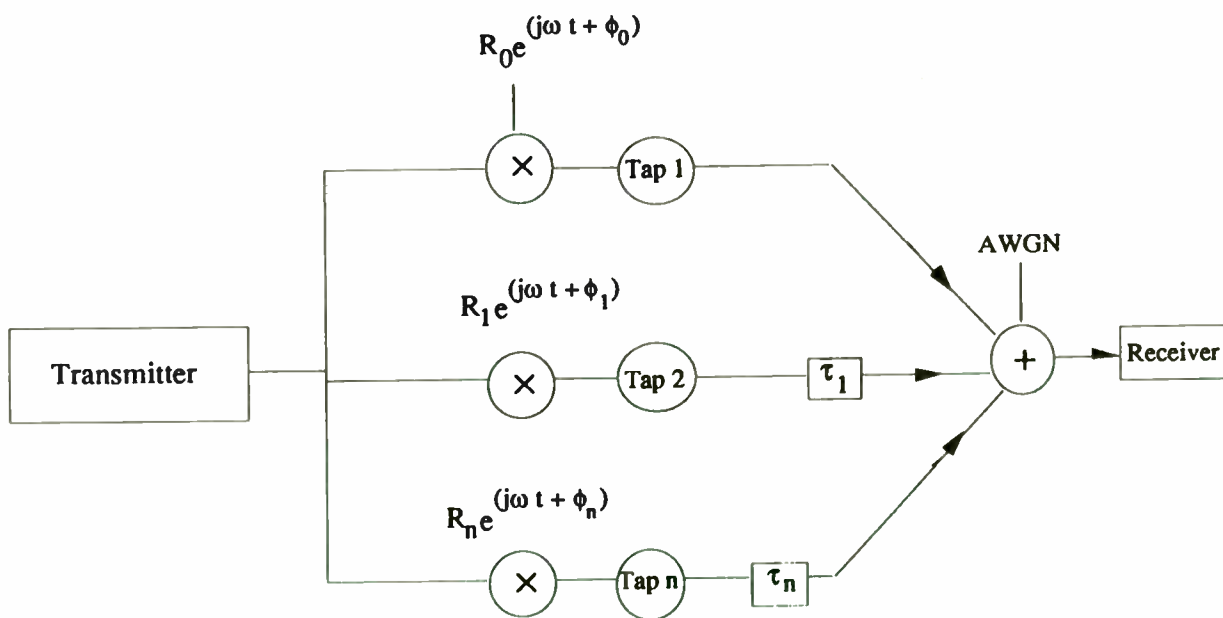
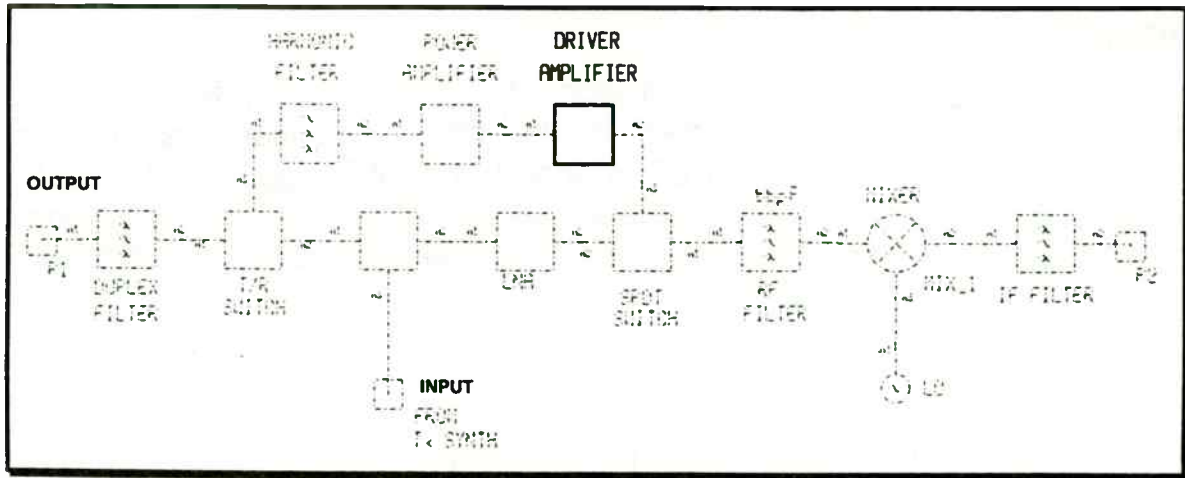
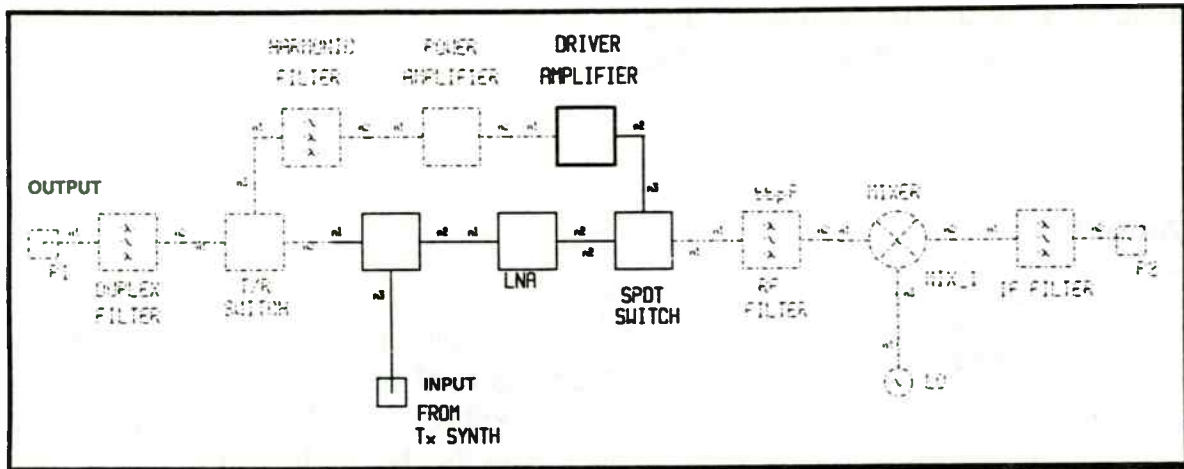


Fig. 4 Multi-tap Rayleigh/Rician fade simulator Conceptual-Implementation Diagram. In the GSM system specifications up to 12 taps have been specified. For the NADC (North American Digital Cellular) system, only two taps (worst case two taps) have been simulated. In this diagram, each tap represents a Rayleigh faded signal [FE-B6].



Simulating the Driver Amplifier on Transmit



Simulating the Pre-Driver/Driver Amplifier Combination on Transmit

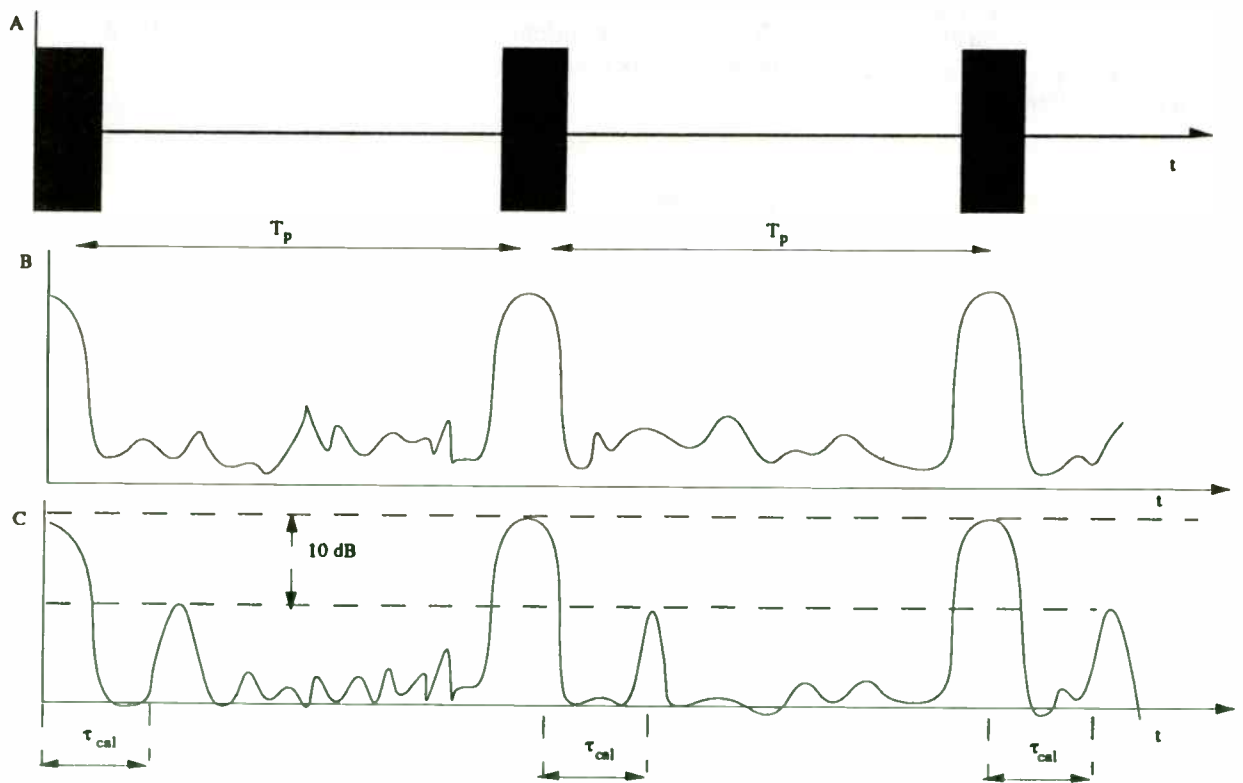
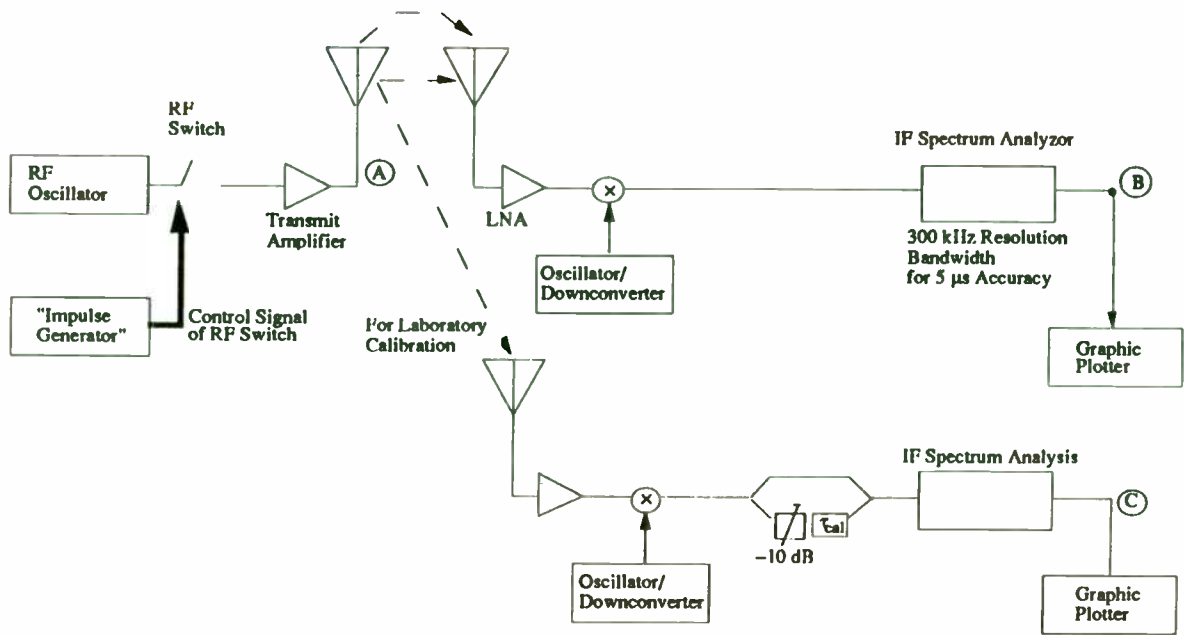
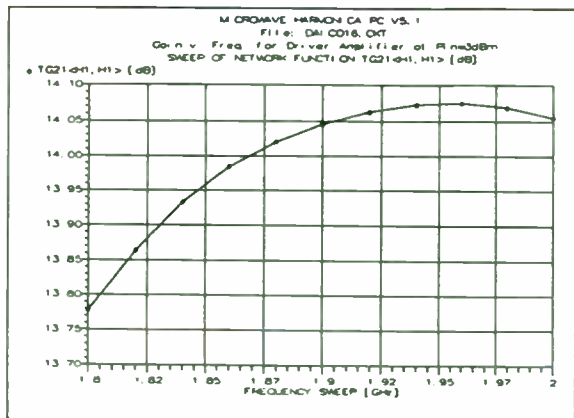


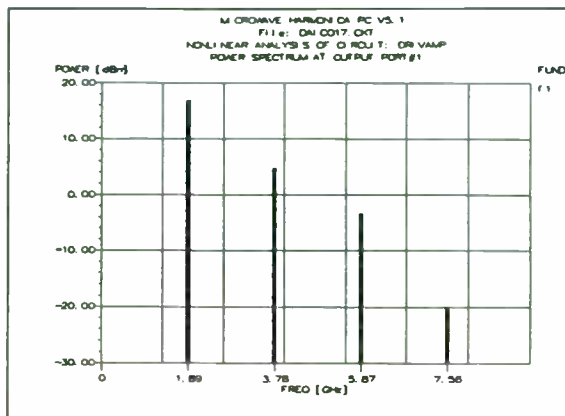
Fig. 5 Delay spread-measurement apparatus for simple field measurements. At point A, a wide-band short burst, having a repetition time of T_p is illustrated. At point B, a bandlimited pulse pattern with noise floor is measured. At point C, 10 dB attenuated and delayed signals are observed.

Driver Amplifier

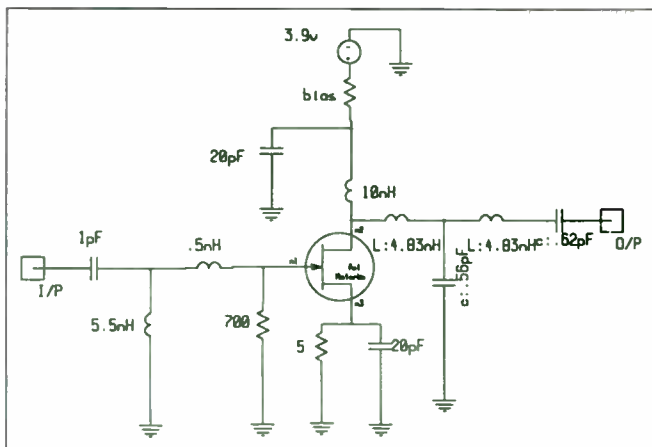


Raytheon MMC-05 400 μm gate width FET used in the driver amplifier design. The FET is operated at 50% I_{DSS} i.e. at 70 mA. Self-bias used for single-rail operation. Gain is > 13 dB with noise figure of 2.5 dB.

The harmonic performance of the driver amplifier driven by the output signal from the pre-driver is shown aside. Power consumption is 250 mW. The second harmonic is only 12 dB below the wanted signal -- hence the need for harmonic filtering.



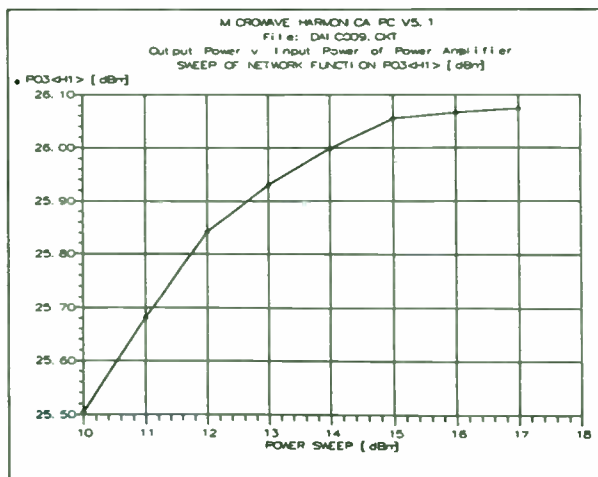
Power Amplifier



Power Amplifier required to provide 25 to 26 dBm of output RF power from a single voltage rail that can be as low as 3.3 volts. Need for high DC to RF conversion efficiency.

Class A/B design used with a quiescent current of 225 mA.

Power gain of > 12.5 dB achieved at 26 dBm output power.



communications fields contain about 20 papers per conference proceedings and there are about 5 to 10 conferences per year in this area.

Instead of a comprehensive literature survey, which could require several hundred pages, we list illustrative delay spread measurement results for:

- cellular systems coverage up to 10 km: delay up to 100 μ s
- land mobile radio coverage up to 70 km: delay up to 350 μ s
- PCS indoor/outdoor coverage up to 30 m: delay up to 300 ns.

4. FEHER'S THEORETICAL DELAY SPREAD BOUND

A powerful and simple theoretical upper bound of worst case delay spread is introduced and derived in this section. Maximal delay spread, abbreviated as τ_{\max} , is one of the most difficult measurement and estimation parameters. It can have a devastating effect on the BER (Bit-Error-Ratio) floor and overall mobile system performance.

This theoretical delay spread bound, introduced by Feher, leads to a simple estimation of "worst case" delay spread, based on knowledge of basic system parameters: transmit power (P_T), receive power at threshold ($P_{R\min}$) and radio frequency (f_c). **It is an unexpected new discovery that, based on "Feher's bound-theoretical model", the environment, that is, surroundings, including urban or suburban, flat terrain, hills, or mountains, indoor short distance, e.g., up to 100m, or outdoor distance of up to many hundreds of km or even larger distances, have no impact on the delay spread bound, τ_{\max} . Our theoretical limit applies to all mobile and all radio/wireless communications and broadcast systems applications.**

To derive the delay spread upper bound, we take a closer look at Fig. 1. In this "physical-engineering derivation" (contrary to sophisticated mathematical analysis and complex derivations of upper bounds), we assume that the " d_k " and " d_l " signal paths having " τ_k " and " τ_l " propagation delays are the longest line-of-sight (LOS) signal paths and that the reflection coefficient is 100%, that is, the total signal energy is reflected. Furthermore, we assume that the "direct" or shortest path is LOS for a short distance d_{ofree} and afterwards scattering and severe signal attenuation occurs in this direct path. For our upper bound derivation we assume that the delayed signal energy could have a significant impact on the system performance, e.g., $\text{BER} = f(S/N)$ if the received power of the delayed path is at threshold level, that is,

$$P_{R\min} = P_{R\text{ threshold}}$$

Thus, we have

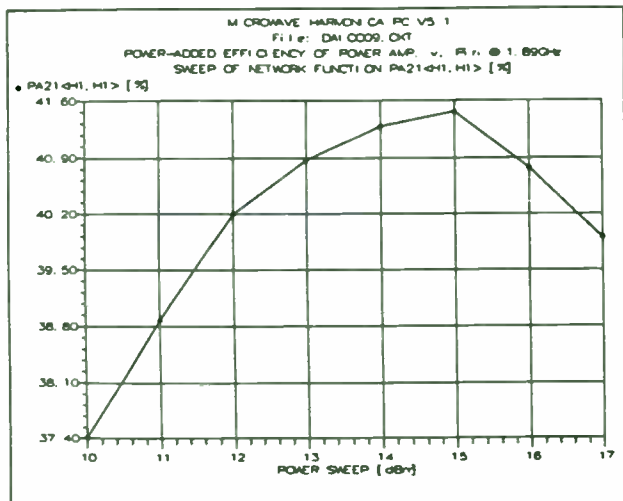
$$d_{\max} = r_{\max} = d_k + d_l$$

and for LOS propagation, the path loss is given as the ratio of $P_{R\min}/P_T$ that is,

$$\frac{P_{R\min}}{P_T} = G_T G_R \left(\frac{\lambda}{4\pi r_{\max}} \right)^2$$

From this expression, we obtain

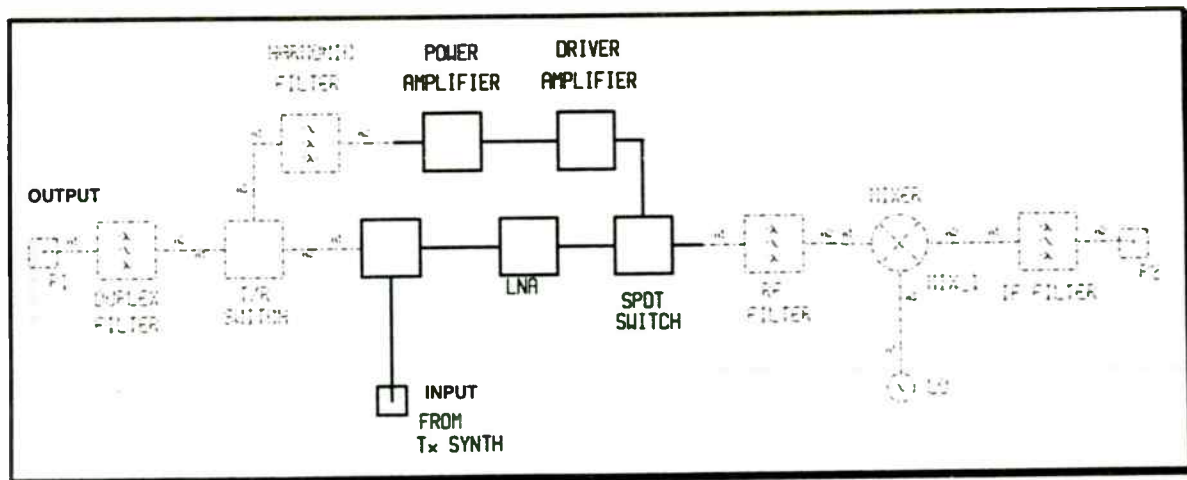
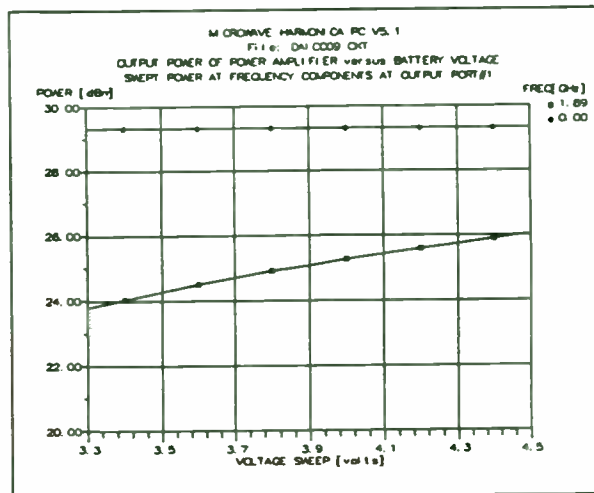
Power Amplifier Design



← **Power Added Efficiency**
Power-Added Efficiency is maximized at the required Output Power. DC to RF Conversion Efficiency is close to 40%.

Output Power must vary with battery voltage as little as possible over the "working range" of the battery.

Battery Range →



Simulating the Complete CT Transmitter

$$d_{\max} = \left[\frac{P_T G_T G_R (\lambda/4\pi)^2}{P_{R\min}} \right]^{1/2}$$

The delay spread bound of the propagation delay, that is, delay spread is given by

$$\tau_{\max} = \frac{d_{\max}}{c}$$

where P_T = transmit power, G_T and G_R represent the transmit and receive antenna gains and λ and c the wavelength ($\lambda = c/f$) and velocity of light respectively, f = radio carrier frequency.

Feher's maximal delay spread bound can be further simplified if omnidirectional unity gain ($G_T = G_R = 1$) transmit and receiver antennas are assumed. This simplified delay spread bound is

$$\tau_{\max} = \frac{d_{\max}}{c} = \left[\frac{P_T}{P_{R\min}} \right]^{1/2} \frac{\lambda}{4\pi} \frac{1}{c} = \left[\frac{P_T}{P_{R\min}} \right]^{1/2} \frac{c}{f} \frac{1}{4\pi c}$$

$$\tau_{\max} = \frac{1}{4\pi} \frac{1}{f} \sqrt{\frac{P_T}{P_{R\min}}}$$

The following examples illustrate the simple and powerful estimation method offered by this bound:

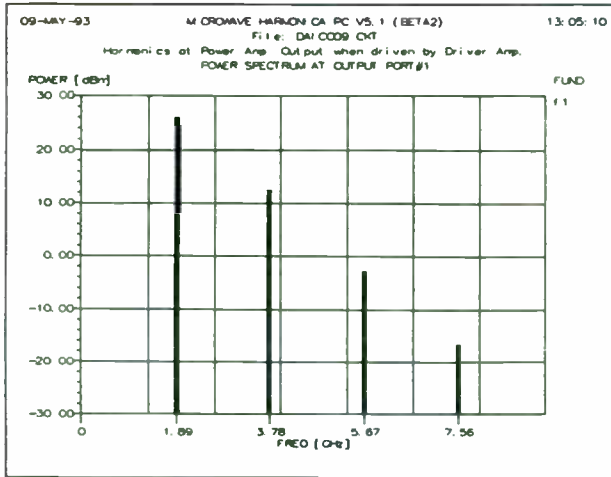
Example 1: How much is Feher's delay spread bound τ_{\max} of a 220 MHz Public Land Mobile Radio (PLMR) system if $P_T = 1$ Watt (+ 30 dBm) and $P_{R\min} = -90$ dBm?

We use Feher's bound with unity gain omnidirectional antennas and the specified parameters:

$$\tau_{\max} = \frac{1}{4\pi} \frac{1}{f} \sqrt{\frac{P_T}{P_{R\min}}}$$

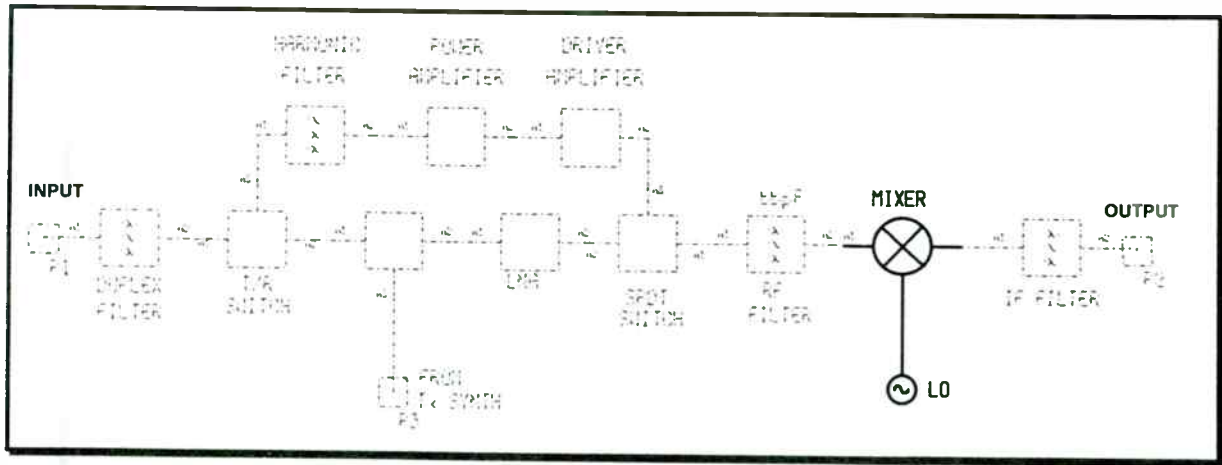
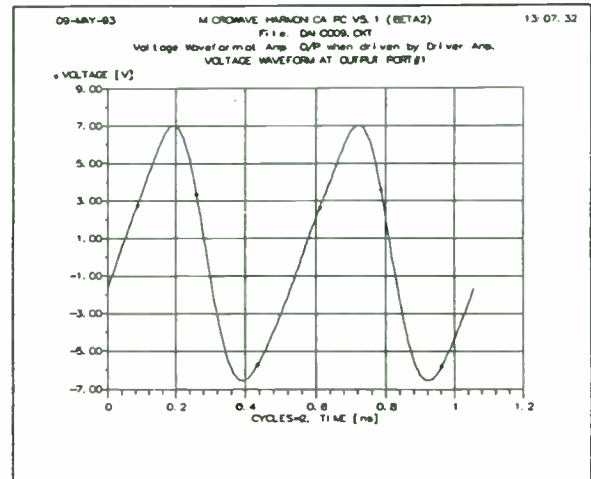
For $P_T = 1$ Watt = 10^3 mW and $P_{R\min} = -90$ dBm = 10^{-9} mW, we have $P_T/P_R = 10^{12}$, thus

Power Amplifier Design



↩ **Harmonics Generated by Amplifier**
 Although Class A/B operation has high DC to RF Efficiency the amplifier generates significant harmonics.

RF voltage waveforms at Power Amplifier Output show high 2nd and 3rd harmonic content. These waveforms are "cleaned up" by the harmonic filter that follows the amplifier. Spectral Plots ↩



Designing the Mixer on Receive

$$\tau_{\max} = \frac{1}{4\pi} \frac{1}{220 \cdot 10^6} \sqrt{10^{12}} = 361.7 \mu\text{s}$$

Thus, the delay spread theoretical bound in this example is 362 μs .

Example 2: How much is Feher's delay spread bound for the European standard "DECT" system, having a transmit power of $P_T = +24 \text{ dBm}$ (250 mW) a receiver bandwidth of 1.1 MHz and a carrier frequency of $f_c = 1.8 \text{ GHz}$. The receiver sensitivity is controlled by the receiver noise figure (F). This low cost system is designed for an $F = 11 \text{ dB}$ overall noise figure and requires a threshold (minimum) C/N of 23 dB.

To use the theoretical delay spread bound, first we have to compute $P_{R\min}$. It is given by

$$P_{R\min} = P_{R \text{ threshold}} = kTBF + C/N$$

where

$$kT = -174 \text{ dBm/Hz}$$

B = Receiver noise bandwidth

F = Noise figure of the receiver

C/N = required carrier-to-noise ratio in the receiver bandwidth

First we obtain the total noise N_T in the receiver

$$\begin{aligned} N_T = kTBF &= -174 \text{ dBm/Hz} + 10\log 1.1 \cdot 10^6 \text{ Hz} + 11 \\ &= -174 \text{ dBm/Hz} + 60.041 + 11 = -103 \text{ dBm} \end{aligned}$$

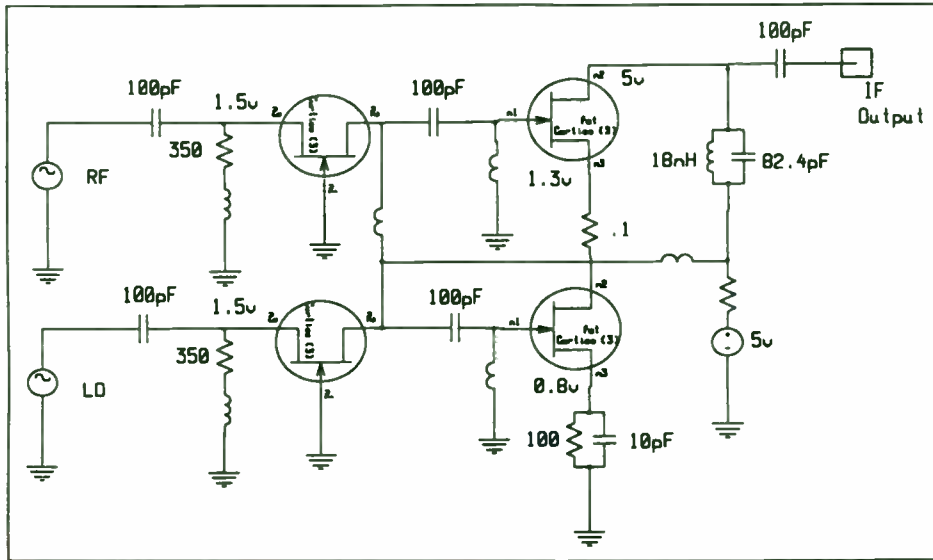
$$P_{R\min} = N_T + C/N = -103 \text{ dBm} + 23 \text{ dB} = -80 \text{ dBm} (10^{-8} \text{ mW})$$

Thus,

$$\begin{aligned} \tau_{\max} &= \frac{1}{4\pi} \frac{1}{f} \sqrt{\frac{P_T}{P_{R\min}}} = \frac{1}{4\pi \cdot 1.8 \cdot 10^9} \sqrt{\frac{250 \text{ mW}}{10^{-8} \text{ mW}}} \\ \tau_{\max} &= 6.99 \mu\text{s} \end{aligned}$$

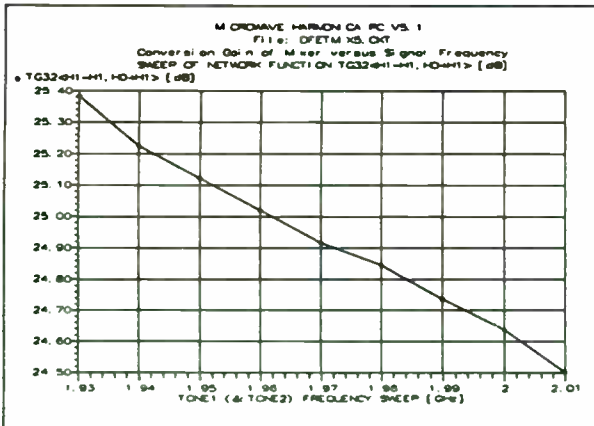
Note: the computed Feher's delay spread upper bound $\tau_{\max} = 6.99 \mu\text{s}$ is about 20 times higher than typical indoor measurement results having a coverage of about 30 m. For systems having a coverage in the 1 km to 5 km range, a 7 μs delay spread is a typical measured result.

MESFET Active Mixer Design



- ◆ **Dual Gate MESFET Mixer**
 - ◆ Dual-Gate FET is driven by Common-Gate FETs at RF and LO
 - ◆ Uses a minimum of passive components to reduce circuit size
 - ◆ LO level is -10 dBm – Average mixer current is 8 mA
 - ◆ Mixer has high (25 dB) gain from RF to IF

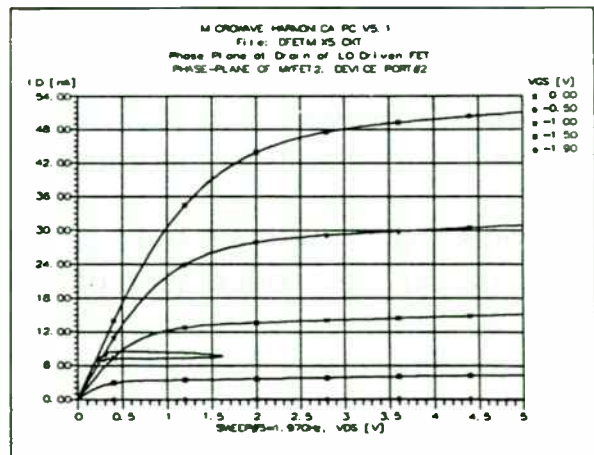
MESFET Active Mixer Design



Microwave Harmonica allows the investigation of both DC and AC performances. The voltage and current excursions at the drain of the mixer FET are shown aside plotted on top of the I-V characteristics of the transistor. Current is 8 mA with a voltage swing of 1.5 volts.

RF to IF Conversion Gain v. Signal Frequency

- ◆ Use Microwave Harmonica to design mixer
- ◆ Conversion Gain of Mixer varies by only 1 dB over the 1.93 to 2.01 GHz band



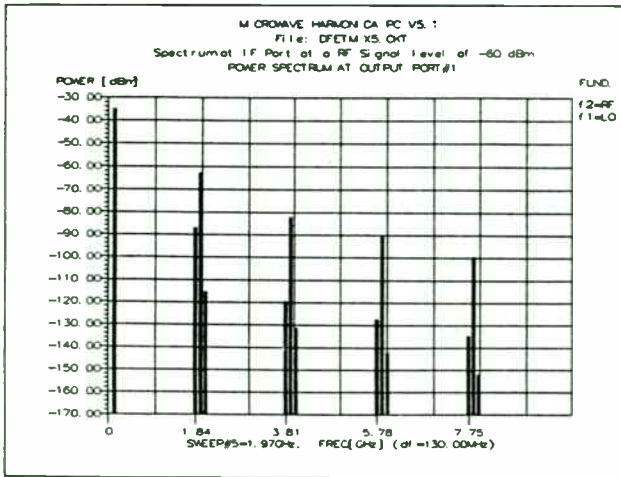
COPYRIGHTED REFERENCE MATERIAL

Most of the material contained in this paper is based on and is closely related to the copyrighted material by Dr. K. Feher, Reference [FE-B6]. This material will appear in a forthcoming book and also in a journal/magazine publication.

REFERENCES

- [FE-B1] K. Feher: "Digital Modulation Techniques in an Interference Environment," Encyclopedia on EMC, Vol. 9, Don White Consultants, Inc., Gainesville, Virginia, (1977-178 pages).
- [FE-B2] K. Feher: "Digital Communications: Microwave Applications," Prentice Hall, Inc., Englewood Cliffs, New Jersey 07632 (1981-282 pages).
- [FE-B3] K. Feher: "Digital Communications: Satellite/Earth Station Engineering," Prentice-Hall, Inc., Englewood Cliffs, New Jersey 07632 (1983-480 pages).
- [FE-B4] K. Feher and Engineers of Hewlett-Packard: "Telecommunications Measurements, Analysis and Instrumentation," Prentice-Hall, Inc., Englewood Cliffs, New Jersey 07632 (1987-415 pages).
- [FE-B5] K. Feher, Ed.: "Advanced Digital Communications: Systems and Signal Processing Techniques," Prentice-Hall, Inc., Englewood Cliffs, New Jersey 07632 (1987-710 pages).
- [FE-B6] K. Feher: "Cellular Digital PCS-Mobile Radio Communications," a forthcoming book, copyright K. Feher, 1993.
- [ZO-1] A. Zogg: "Multipath delay spread in a hilly region at 210 MHz," IEEE Transactions on Vehicular Technology, Vol. VT-36, No. 4, pp. 184-187, Nov. 1987.

MESFET Active Mixer Design

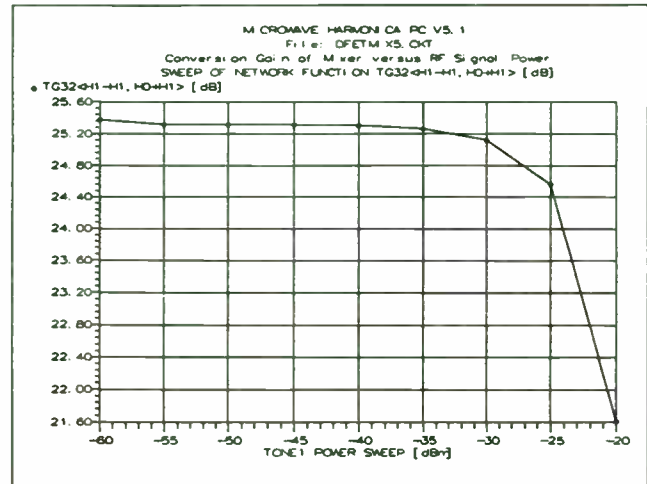


Compression of the mixer is plotted aside. The 1 dB compression occurs at -25 dBm RF input power corresponding to a -2.5 dBm (approx. 0.5 mW) output power.

Compression Characteristics of Mixer →

↩ Spectrum at the IF port at an RF signal Level of -60 dBm

◆ Rejection of LO and RF signals at the IF port is greater than 50 dB.



Simulation from Layout is important at RF

- ◆ At low frequencies simulations are usually derived from electrical representations of the circuits
- ◆ At higher frequencies the ACTUAL layouts of the circuits influences the performances obtained
 - ◆ Layout effects include coupling between components; electrical length of interconnections; parasitic elements; discontinuities
- ◆ Schematics used to derive circuit description
 - ◆ Provides connectivity check
 - ◆ Provides documentation
- ◆ Layouts are auto-generated from schematics that contain "layout-linked" information -- e.g. orientation of bends, tees, component footprints, material layers

Personal Communications Systems (PCS)

Session Chairperson: Randy Roberts,
Spread-Spectrum Scene (El Granada, CA)

GaAs MMICs for PCS Applications, **Charles Huang,**
ANADIGICS, Inc. (Warren, NJ).....368

A High-Efficiency GaAs MMIC Power Amplifier for 1.9 GHz
PCS Applications, **John Wachsman,** Pacific Monolithics, Inc.
(Sunnyvale, CA).....372

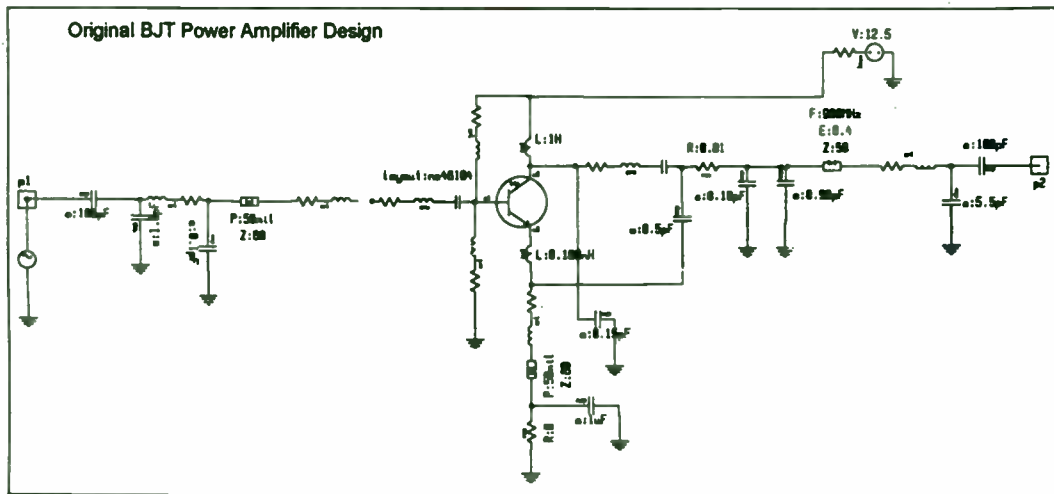
Low-Cost Surface-Mount Mixer for PCS Applications, **Shankar R.
Joshi,** Synergy Microwave Corp. (Paterson, NJ).....378

Frequency Synthesizer Strategies for Wireless, **Bar G. Goldberg
and Henry Eisenson,*** Sciteq Electronics (San Diego, CA).....387

A 2.4-GHz Single-Chip Transceiver, **L. M. Devlin, B. J. Buck, J. C.
Clifton, A. W. Dearn, and A. P. Long,** GEC-Marconi Materials
Technology Limited (Caswell, Towcester, Northands, United
Kingdom).....395

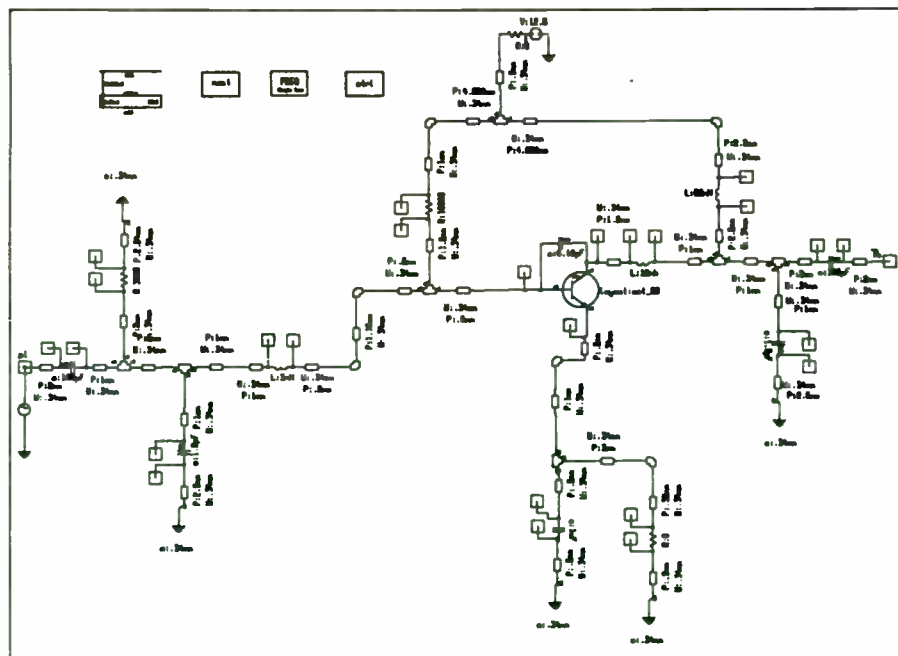
**Paper presented by Henry Eisenson.*

Simulation from Layout



- ◆ In the original BJT Power Amplifier design no account of layout features are taken. The design consists of simple lumped and distributed elements together with the transistor.

Simulation from Layout



- ◆ The schematic representing the circuit as laid out on the PCB contains many more elements than the original design including bends, tees, bond pads etc..

GaAs MMICs FOR PCS APPLICATIONS

Charles Huang
ANADIGICS, INC.
35 Technology Drive
Warren, New Jersey 07059

Introduction

When personal communication services (PCS) were first proposed in 1989-1990, the objective was to develop a system that is more versatile and cheaper than the existing cellular mobile telephone (CMT) services.

The proposal was to divide existing CMT cells into hundreds of small cells and use a small, inexpensive handset that would work inside buildings and tunnels. The proposed frequency spectrum would be around 1.8 - 2.0 GHz in order to avoid serious background noise problems encountered by CMT services at between 800 - 900 MHz.

Although most of the original concept for PCS has been kept as the development moved forward, there might be a time in the future that PCS will encompass CMT services and become the ubiquitous single wireless phone for everyone, everywhere. People will carry phones with them and would be able to be reached at any time.

System Technology

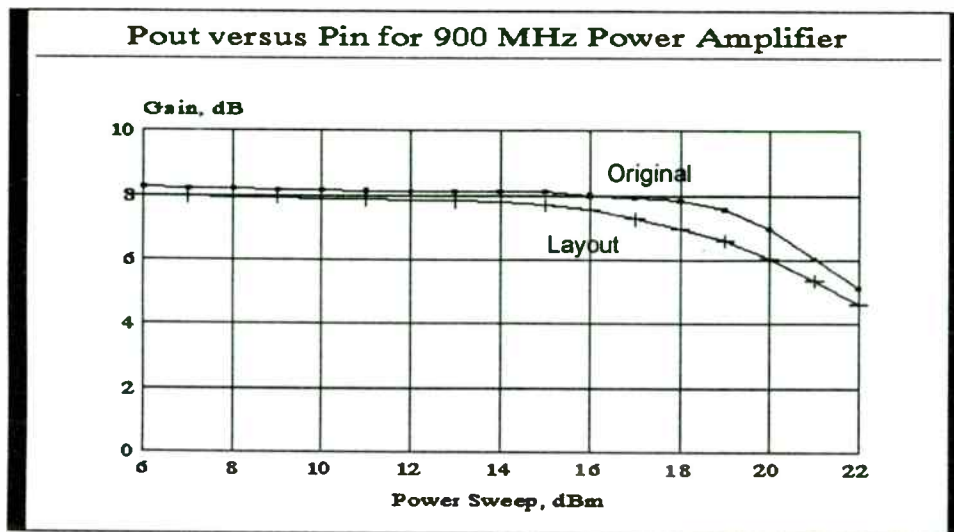
Many competing systems are vying for dominance in the PCS market. It is not the scope of this paper to review every system proposed [1, 2]. In this paper, the discussion will be focused on the code division multiple access (CDMA) system proposed by Qualcomm and the DCS-1800, which is a Pan-European time division multiple access (TDMA) system. Key parameters for these systems are listed in Table I.

Table I

SYSTEM PARAMETERS

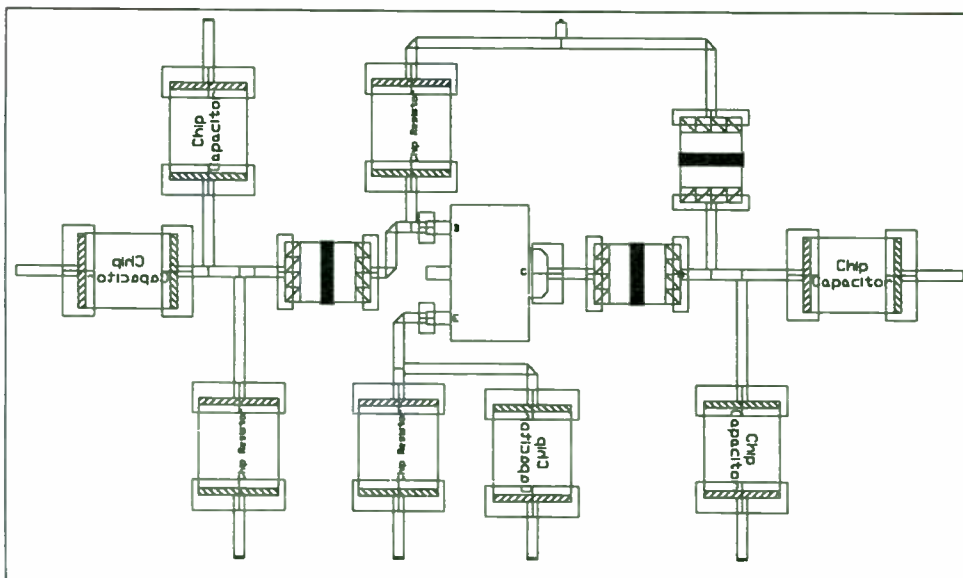
	Qualcomm	DCS-1800
Frequency Spectrum	1850 - 1900 MHz	1710 - 1880 MHz
Multiple Access	CDMA	TDMA
Duplexing	FDD	FDD
Channel Bandwidth	1.25 MHz	200.0 KHz
Traffic Channel on One RF Channel	32	8
Speech Rate	8.0 KB/S	13.0 KB/S
Modulation	QPSK	GMSK
Portable Transmit Power, Peak/Average	500 mW	1.0 W/125 mW

Simulation from Layout



- ◆ The above response shows the effect circuit layout has on the gain compression characteristics of a Class A BJT Power Amplifier at 900 MHz

Simulation from Layout



- ◆ The BJT Amplifier Layout is derived automatically from the circuit schematic. The amplifier shown above consists entirely of surface mounted devices. Individual layers for solder attach, drill holes, transmission lines are created.

RF Systems for Portable Handsets

A generic block diagram of the RF system for portable handsets is provided in Figure 1 [2]. The present receiver and transmitter circuits are mostly homemade products made with discrete devices. This is because there are no cost effective, application specific MMICs available.

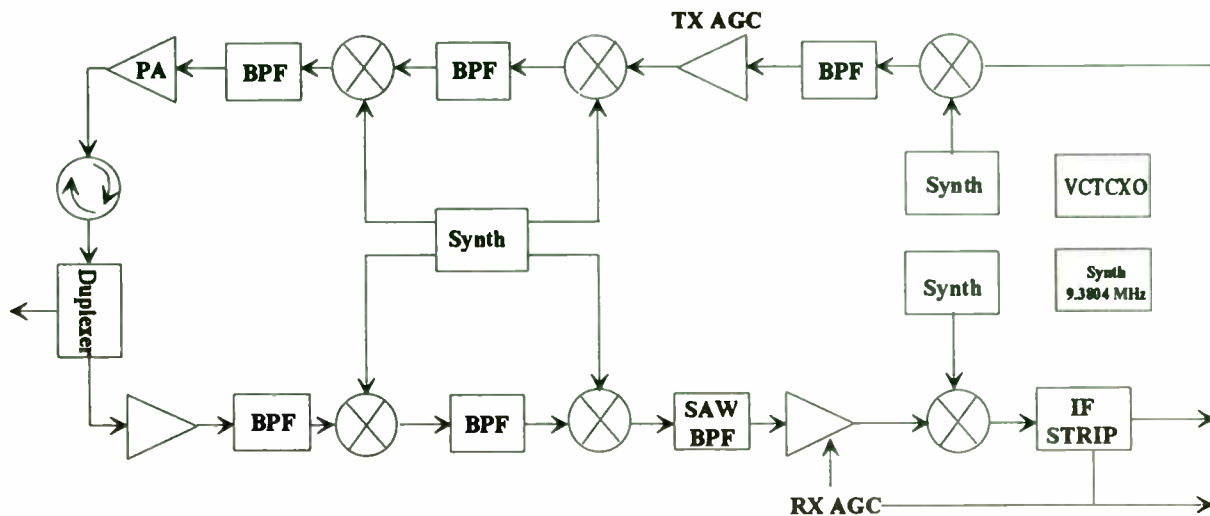


Figure 1. An RF System Block Diagram for Portable Handsets

GaAs MMICs for PCS Applications

Since 1989, cost effective GaAs MMICs for high volume production have become available for direct broadcast satellites (DBS), global position systems (GPS) and cable television systems [3]. GaAs MMICs are ideally suited for PCS applications because of the following performance advantages:

- A. High Intercept Point
- B. Low Noise Figure
- C. Low Voltage operation
- D. Low Current Consumption
- E. High Power Added Efficiency

In Figures 2 through 4, block diagrams for GaAs MMICs currently under development for PCS are provided. The receiver circuit, as shown in Figure 2, will replace a low noise amplifier transistor, a mixer diode, a bulky image rejection filter, and also provide a local oscillator and a buffer drive to the mixer. All of these functions will be integrated on a single GaAs chip. It will use a tiny (0.4 mm) square plastic surface mount package. The power supply for the receiver MMIC is 3.0V and 13 mA, which is comparable to the best results achievable by using discrete devices.

Additional CAD Tools for RF Design

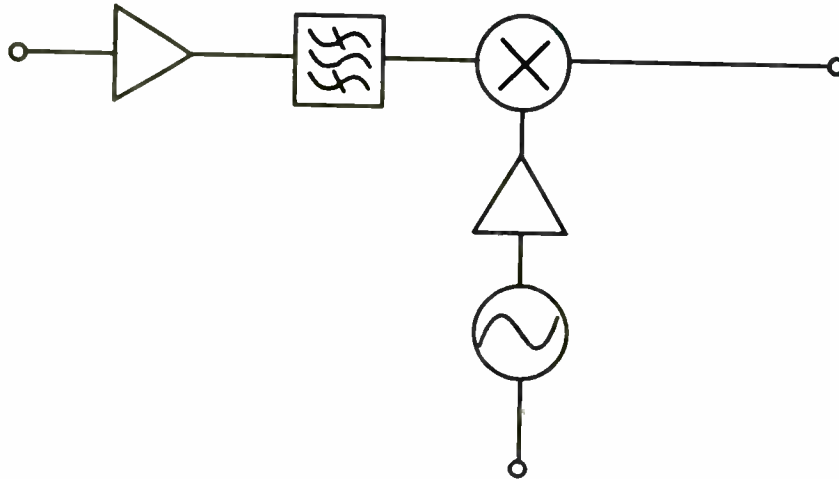
◆ Time Domain Simulation with RF/Microwave Components

- ◆ *Conventional SPICE programs only contain "low frequency" models*
- ◆ *To overcome these problems new versions of SPICE are being introduced that contain microwave component models:*
 - *Models developed using the Method of Lines*
 - *Models that are "translated" from the frequency to the time domain using "convolution"*
- ◆ *Compact Software has produced new time domain simulator called Super-Spice® using an X-Windows/Motif Interface on Workstations*
- ◆ *Multi-layer circuits such as multi-level PCBs and MCMs can be analyzed. Transient as well as steady-state analysis can be performed*
- ◆ *Super-Spice allows RF design engineers to investigate mixed-signal sub-systems e.g. Phase-Locked Loops at high RF frequencies*

Additional CAD Tools for RF Design

◆ Electromagnetic Simulation

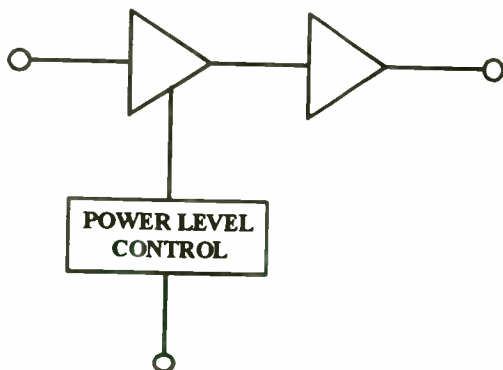
- ◆ *Many circuit structures cannot be analyzed using conventional circuit simulators*
- ◆ *To overcome these problems ElectroMagnetic (EM) Simulators based on the Method of Moments have been developed*
- ◆ *Compact Software has produced an efficient EM simulator called Explorer® using an X-Windows/Motif Interface on Workstations*
- ◆ *Multi-layer circuits such as multi-level PCBs and MCMs can be analyzed. S-Parameter data is then transferred to Super-Compact and/or Microwave Harmonica for incorporation in other sub-systems*
- ◆ *Today, EM simulators are much slower than nodal-based circuit simulators – that situation will change with new mathematical techniques and faster CPUs*



RF Frequency	1900 MHz
IF Frequency	150 MHz
Conversion Gain	20 dB
Noise Figure	2.5 dB
Image Rejection	15 dB
Input Intercept Point	-10 dBm
Power Supply	3 V, 13 mA

Figure 2. Receiver MMIC Specification

The power amplifier MMIC, as shown in Figure 3, will use a 16 pin surface mount SOIC package and will operate with a 3.0V power supply. The linearity and power added efficiency of this MMIC is comparable to the much larger discrete hybrid power modules.



FREQUENCY	1900MHz
Output Power	500mW
Gain	30dB
Power Efficiency	45%
Power Supply	3V

(Spurs at -30dBc)

Figure 3. Power Amplifier MMIC Specification

◆ **Conclusions**

- **CAD Tools for the Design of Circuits and Systems at RF are Commercially Available and Mature Products**
- **There is a Continuing Growth in the Supply of Component Libraries for both Circuit and System Level Simulation**
- **Products for the Layout of Circuits and Systems at RF with Direct Links to Performance, Yield and Manufacturing Costs are being Developed and some are Available Commercially**
- **Examples have been given of Circuit and System Level Designs and the Importance of New CAD Tools such as Electromagnetic Simulation**

The transceiver circuit, as shown in Figure 4, will be customarily optimized for each application in order to maximize the benefits of the monolithic integration.

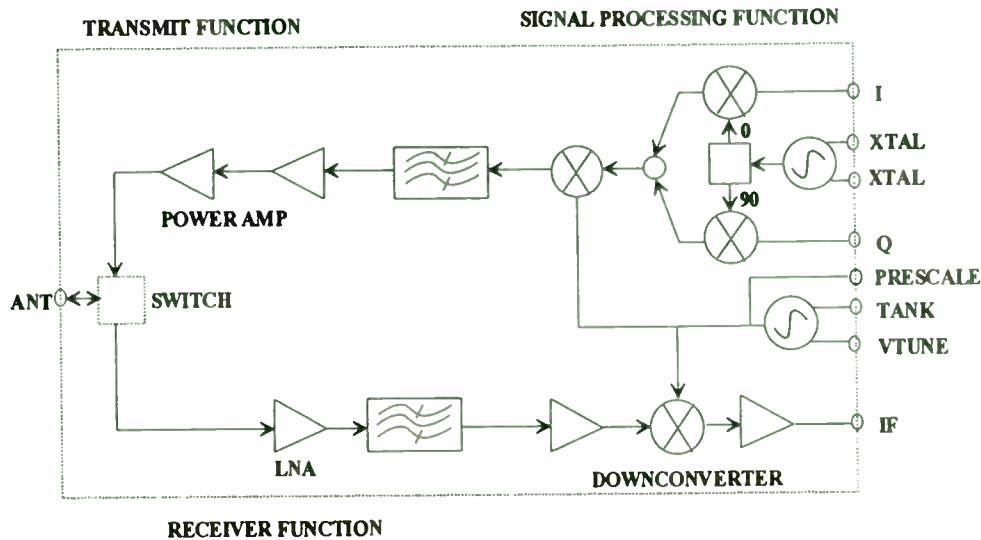


Figure 4. A Transceiver MMIC Architecture

These MMICs should prove very successful in the marketplace because they offer size and weight advantages when compared to discrete device solutions. Furthermore, the MMIC reduces the engineering development effort and simplifies the manufacturing process. Consequently, the quality and reliability of the final product is improved, while the cost of manufacturing is reduced.

Summary

GaAs MMICs for PCS applications should become available in 1993 and the market prospects for these products is bright.

References

1. D. Cox, "Wireless Network Access for Personal Communications," IEEE Commun. Mag., p. 96, Dec. 1992.
2. Qualcomm, "RF Vendor's Forum, CDMA and PCN," San Diego, Aug. 1992.
3. C. Huang, "MMICs Move Into New Marketplaces," Microwaves & RF, p. 134, Sept. 1992

1. The first part of the document discusses the importance of maintaining accurate records of all transactions and activities. It emphasizes that this is crucial for ensuring transparency and accountability in the organization's operations. The text highlights that without proper record-keeping, it becomes difficult to track expenses, revenues, and other financial data, which can lead to mismanagement and potential legal issues.

2. The second part of the document focuses on the role of the management team in overseeing the organization's performance. It states that the management team is responsible for setting strategic goals, allocating resources, and monitoring progress. The text suggests that regular communication and reporting are essential for the management team to stay informed about the organization's current status and to make timely adjustments as needed.

3. The third part of the document addresses the issue of employee performance and motivation. It notes that employees are the backbone of any organization, and their performance directly impacts the organization's success. The text recommends implementing a fair and transparent performance evaluation system that provides constructive feedback to employees. Additionally, it suggests offering incentives and training opportunities to motivate employees and help them develop their skills.

4. The fourth part of the document discusses the importance of maintaining a strong relationship with the organization's stakeholders. It identifies key stakeholders such as customers, suppliers, and the community, and emphasizes the need to engage with them regularly. The text suggests that organizations should strive to provide high-quality products and services, communicate openly, and address any concerns or complaints promptly. Building trust and loyalty among stakeholders is essential for long-term success.

5. The fifth part of the document concludes by summarizing the key points discussed and reiterating the organization's commitment to excellence and continuous improvement. It encourages all employees to work together to achieve the organization's goals and to maintain the highest standards of integrity and ethical conduct. The text ends with a statement of confidence in the organization's future and a call to action for all stakeholders to support the organization's mission.

A High-Efficiency GaAs MMIC Power Amplifier for 1.9 GHz PCS Applications

John Wachsman

Pacific Monolithics, Inc.
245 Santa Ana Court
Sunnyvale, California 94086
(408) 732-8000

Abstract

A high-efficiency 1.9 GHz GaAs MMIC power amplifier has been developed for emerging PCS applications. Operating at 3V of DC supply, the module achieves a typical RF output power of +27.5 dBm at 1890 MHz with an RF input power of 3 dBm and an overall DC-RF efficiency of 50%.

I. Introduction

Emerging PCS applications such as DECT (Digital European Cordless Telephone) and PHP (Personal Handy Phone) place stringent demands on RF component designers. Aggressive size and cost targets require highly integrated solutions. In addition, to maximize talk time, these next generation systems require high DC power efficiency at low supply voltage.

The RF power amplifier is a particularly challenging piece of the overall PCS system, since traditional silicon bipolar or BiCMOS approaches fall well short of the needed performance. We report here on a novel 2-stage power amplifier which sets new standards for DC power efficiency, accomplished through a GaAs MMIC (monolithic microwave integrated circuit) approach. The MMIC approach is ideal for consumer electronics because of its ability to be mass produced at a low cost.

II. Design Approach

The power amplifier was designed to meet the following objectives:

1. Low DC voltage, 3.0V nominal, 2.7V minimum.
2. +27 dBm output power and 50% efficiency
3. High gain, 30 dB goal, 25 dB minimum
4. Manufacturable low cost design
5. Ability to reconfigure to 2.4 GHz.

The performance criteria of objectives 1 through 3 dictated a relatively low pinch off, high f_t GaAs process. Additionally, the desired efficiency required that the output match be external to the chip as the Q of MMIC matching structures are relatively low. The ability to reconfigure the module to 2.4 GHz also required the input, output, and interstage matching to be external.

The functional schematic diagram, Figure 1, indicates the portion of the circuit which is included on the MMIC and the additional external components required. The MMIC itself uses 0.5 μm gate length technology and has 2 stages of amplification with associated bias circuitry. The driver stage and the output stage are 600 μm and 5000 μm gate widths, respectively. The MMIC is 0.036 x 0.036 inches in area. The external L-C matching structures are a combination of standard 0603 surface-mount capacitors and printed transmission line inductors. The PCB used in the module is standard 0.031 inch thick FR-4 board.

The module, shown in Figure 2, is 0.810 x 0.515 x 0.160 inches in size. It requires a Vdd of +3V and negative bias of -1.2V and -1.5V for the driver stage and output stage respectively. The negative voltage can be generated by a simple switched capacitor design as the required negative current is less than 2 mA.

III. Measured Performance

The small signal gain, input, and output VSWR are shown in Figure 3. The output power vs. input power is shown in Figure 4. The measurements show that reasonable power is achieved even at 0 dBm but to achieve 50% efficiency it is necessary for the input power to be +3 dBm. Another important requirement is the ability to control the output power of the amplifier. This is accomplished by controlling the negative bias to the amplifier. Figure 5 shows the reduction in power and efficiency as a function of this control. In actual use it is not possible to create the -3.1V required to pinch off the device from a 3V battery. Therefore, external circuitry was developed that switches off the +3V Vdd line when the transmitter is not in use. This has been possible due to the graceful degradation in output power as Vdd is reduced. Figure 6 indicates that at 2.7V the module achieves 26 dBm and degrades to 23 dBm at 2.0V.

IV. Conclusion

A small, high-efficiency 1.9 GHz GaAs power amplifier has been demonstrated. The GaAs MMIC based design will meet the stringent demands of performance, size, and cost in the PCS market.

V. Acknowledgment

The author would like to acknowledge the technical contributions of Steve Cripps, Gary Lizama, and Fernando Aguilar.

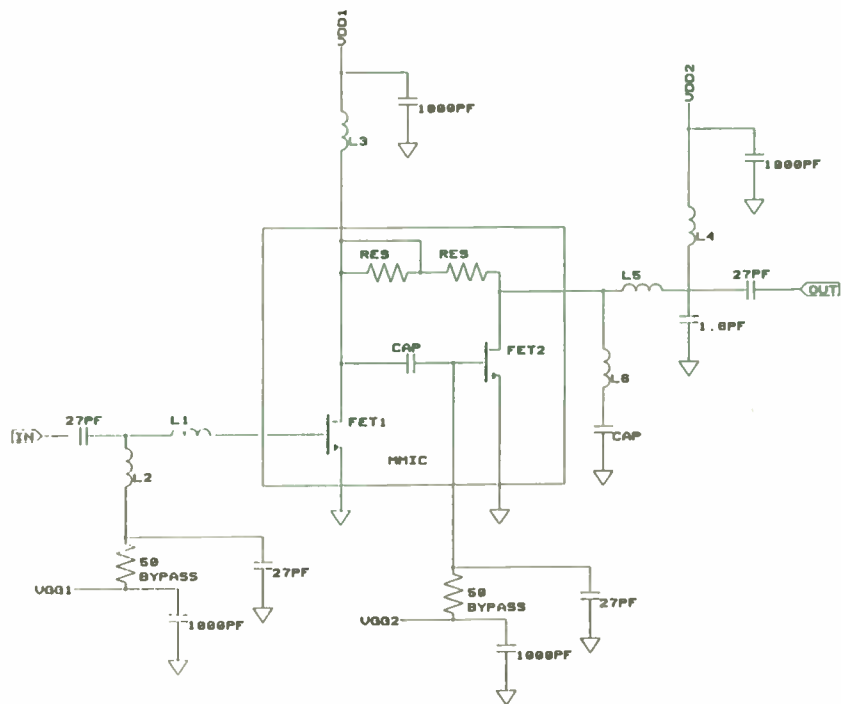


FIGURE 1. POWER AMPLIFIER MODULE SCHEMATIC

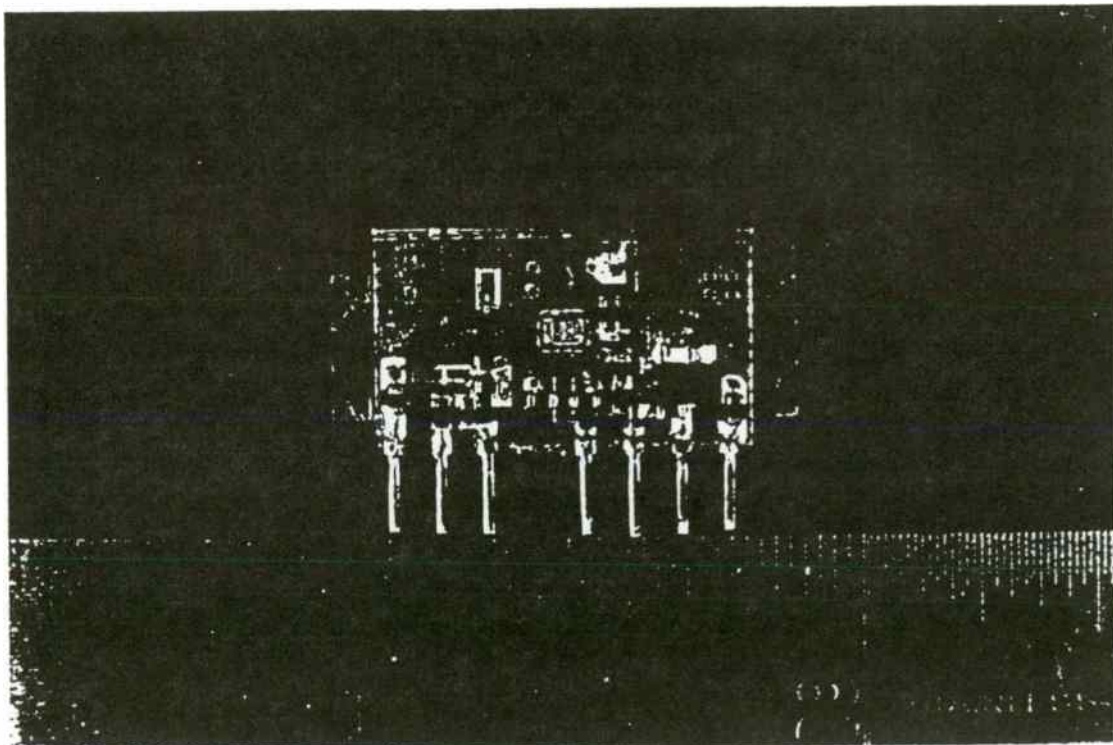


FIGURE 2. POWER AMPLIFIER MODULE

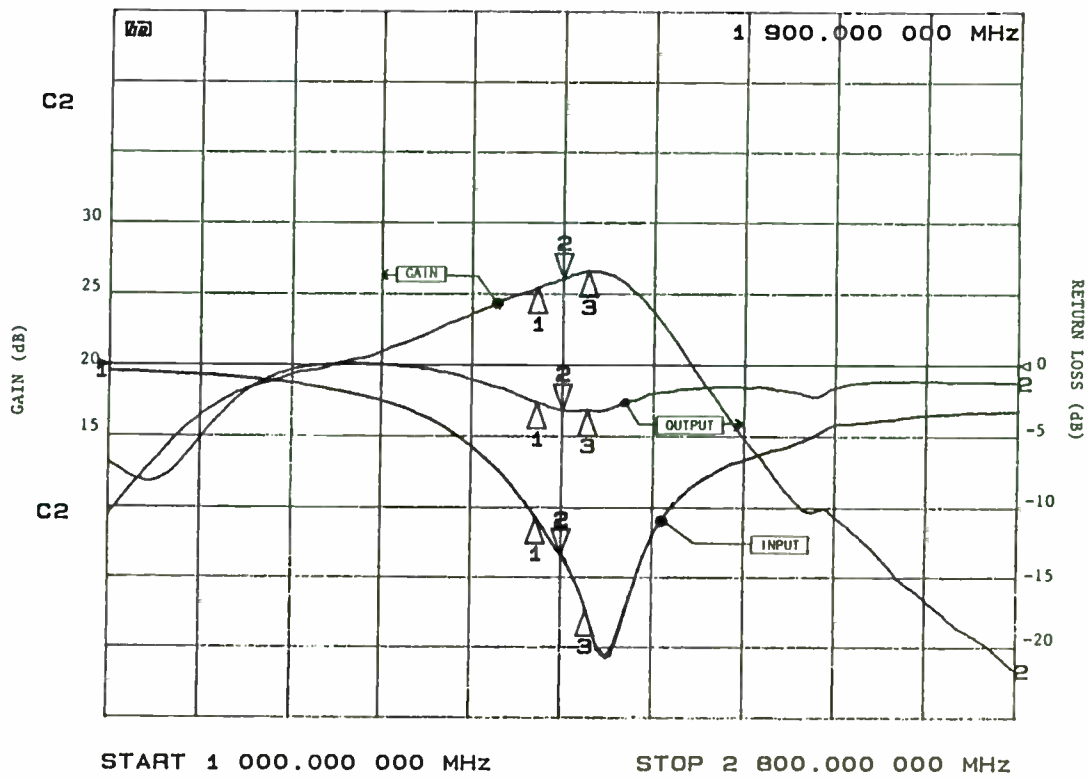


FIGURE 3. SMALL SIGNAL CHARACTERISTICS

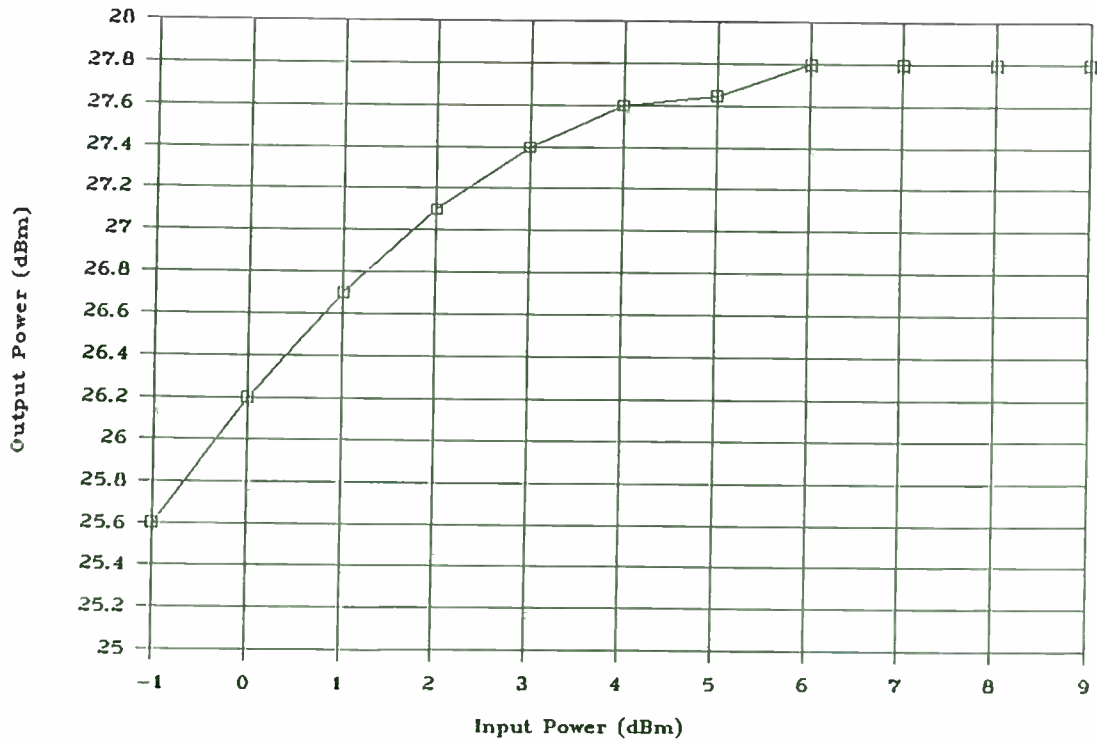


FIGURE 4. OUTPUT POWER vs. INPUT POWER

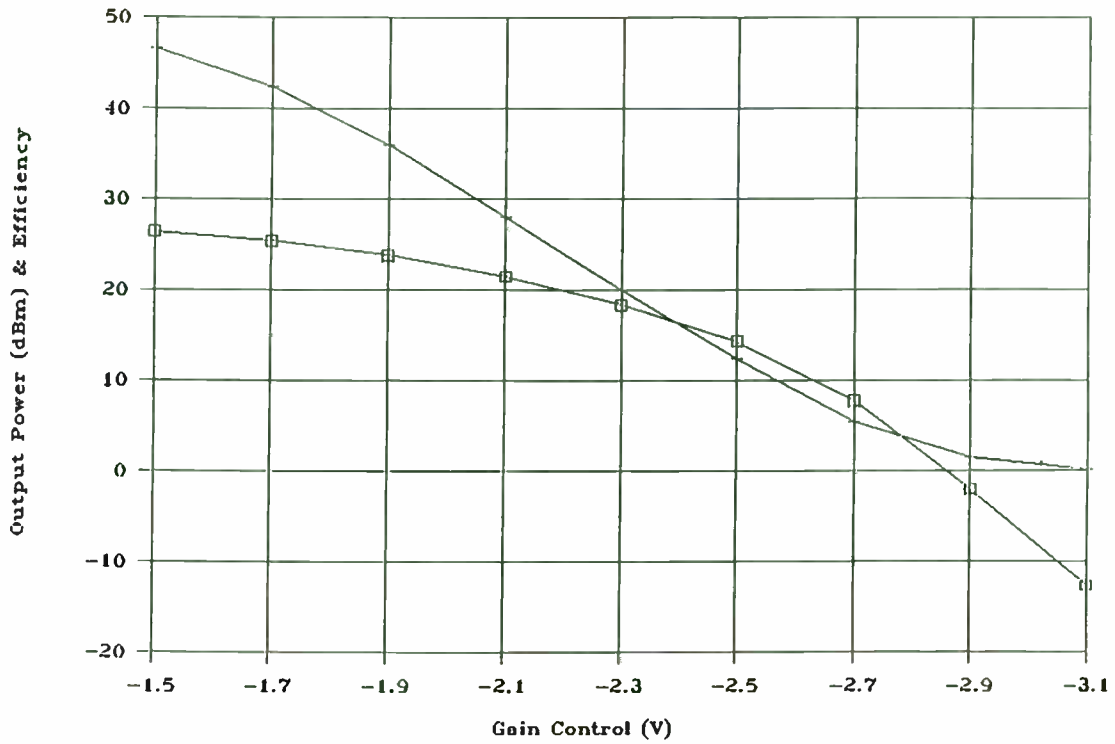


FIGURE 5. OUTPUT POWER EFFICIENCY vs. GAIN CONTROL

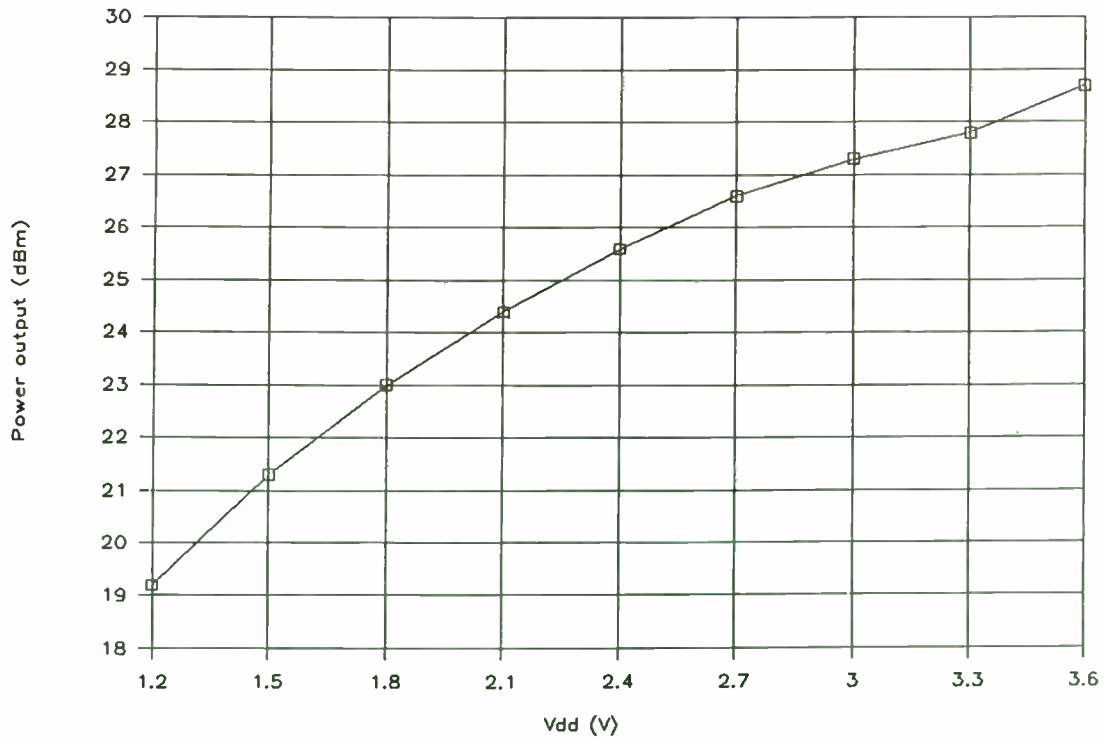


FIGURE 6. POWER OUTPUT vs. DRAIN VOLTAGE

LOW COST SIGNAL PROCESSING COMPONENTS FOR THE CELLULAR MARKET

by
Shankar Joshi
Synergy Microwave
483 McLean Boulevard
Paterson, New Jersey 07504

INTRODUCTION

In the last few years, the cellular telephone market, the market for global position systems, and the cordless telephone have expanded dramatically. While this new technology offers greater advantages for the users, it is very cost sensitive. Typical components for signal processing are mixers, power dividers, hybrid transformers, switches, various types of attenuators, phase shifters and even modulators. Construction of these components reveals instantly that there are a number of labor costs affecting the production price and, therefore, there is a critical need to find manufacturing methods to reduce these labor related costs. The traditional method of handling this has been to employ off-shore production facilities with low labor costs, but this is only a temporary fix as costs will increase there in the future as well. Synergy Microwave has successfully looked into changes in the physical design of the components with a goal to automate production in the USA, eliminate manual wiring and thereby reduce costs.

APPROACH

Radio Frequency (RF) components, commonly referred to as signal processing components, require ferrite cores and twisted (bifilar, trifilar and quadrafililar) wires for their construction, which makes it difficult for automated assembly. Since most of the ferrite cores are either in the form of a toroid or a balun, manual operation is required. This automatically means a labor intensive process. Figure 1 shows the traditional way of manufacturing an RF cellular mixer, which serves as an example of using toroidal transformers and Schottky quad rings. These toroids are usually hand-wound and secured in place prior to being connected to the diode ring. The following assembly steps are required:

1. By using epoxy or epoxy adhesive, the diode ring has to be secured to the mounting base of the assembly.

* **Patent pending**

2. The hand-wound transformers have to be placed in the appropriate locations and secured.
3. All connections have to be made with hand-wiring.
4. The assembly has to be cleaned with a combination of chemical treatment and forced air.
5. In order to obtain a sturdy and rugged design, either epoxy or potting compound is used.
6. Finally, the cover is either soldered or welded to the base assembly.

In reviewing this process, it becomes obvious that it is time-consuming and labor intensive.

Synergy Microwave has developed an innovative method* which drastically reduces the assembly time, improves and maintains constant performance. This new method of assembly is shown in Figure 2. The layout consists of an SMD printed/bonded diode ring which will become part of the assembly. Instead of using toroid or balun cores, ferrite rods (marked T1 and T2 in Figure 2) have been selected. By incorporating the winding on the cores as part of the assembly process (interconnection between the diodes and transformer), an economical way of assembling an array of these mixers at one time is achieved. Encapsulation and sealing are also done in one step. This manufacturing process incorporates repetition and consistency as key features since the tedious, awkward and expensive manufacturing process of winding wires around the toroid and baluns is streamlined. In these instances, the wire must be repeatedly looped in and out of central hole or holes. As the holes become much smaller, these windings become more difficult to achieve. It also becomes difficult to affix a toroidal transformer to the mounting base where there are insufficient flat edges. In the case of a balun structure, the windings are exposed on the flat surface. In the case of RF transformers the typical diameter of the central holes for a balun is approximately .020 inches and generally AWG36 to AWG30 sized wire is used. Unlike the toroid and balun cores, rods can more easily be placed and the windings can be handled more conveniently. The most effective method of attaching the rods to the surface is to provide a recess of the proper size on the mounting base, which is referred to as a base. Using the base as a substrate, Schottky diodes, either in ring or cross-over configuration, can be cost effectively mounted and the leads of the diodes will be brought out in the form of pads as interconnection to the transformers using either a bonding, welding or soldering technique. The ferrite rods are then firmly secured to the substrate as shown in Figure 2. The same basic design can be used for

various frequency ranges which require different numbers of turns or diodes with different characteristic performance.

The substrates are available in standard panel sizes either 8" x 8" for alumina or 24" x 24" for epoxy, fiberglass material or Teflon. Figure 3 shows such a panel assembly. Individual substrates are scribed so that each of the components can be separated easily by snapping. Diodes are assembled on the substrates while on the panel. The required amount of glue is dispensed into the recesses of the substrate and rods are placed into these recesses by a pick and place machine. After proper baking, at a specific temperature for a precise period of time, the panel is ready for further assembly. After winding the required number of turns of the twisted wires on the first ferrite rod, the transformer leads are connected to the diodes and package leads. This same procedure will be used for the second core. All the units on the substrate are assembled utilizing the above-described method. Therefore, the complete panel can be cleaned at one time and then it is ready for the next manufacturing operation. It is recommended that an inspection be conducted following each production step.

Special molds are used and hold the required quantity of encapsulating compound for each device. Molds in the form of an array are designed in such a way that -- with the exception of the package leads -- the rest of the assembled material is fully covered by the encapsulating material. This material is then baked at the appropriate temperature sufficiently long enough to achieve the proper consistency. Once the mold is removed, the individual components are then snapped apart. This process of manufacturing for RF components can be automated by using the above outlined procedure. The same basic procedure can be applied to different types of RF signal processing components using this new and innovative technique. Therefore, even modulators and other complex assemblies are available in smaller sizes. **CELLULAR & PCN BAND MODULATORS CAN BE PRODUCED INEXPENSIVELY.**

To highlight this new manufacturing method, we are now looking at two components, namely a double-balanced mixer and power divider. Depending on the number of required turns in the transformer, the design can be optimized for certain frequency ranges and bandwidth. To achieve the optimized design, parasitics are kept to a minimum. The advantages of this new approach by Synergy Microwave are best demonstrated by comparing measured data. Figure 4 shows the plot of conversion loss as a function of intermediate frequency (IF) for two fixed RF signals. These plots are the results of mixing fixed RF signals with a variable local oscillator (LO). Figure 5 shows the isolation

between the LO and RF ports and the LO and IF ports as a function of frequency. For the purpose of this discussion, the plots cover the cellular radio frequency band. In the case of a second example, we looked at an in-phase (zero degree) two-way power divider. The theoretical loss for such a two-way power divider is 3dB. Any loss in excess of 3 dB is called the insertion of the power divider. Typical parameters for the power dividers are insertion loss, amplitude and phase imbalance between the outputs, and isolation between the output ports when the input port is terminated in proper impedance (generally 50 Ω). To see the differences between various frequency ranges, two power dividers with different numbers of turns are compared.

Figures 6 and 7 describe the two-way power divider with two turns and whereas Figures 8 and 9 describe the power divider with three turns. The power divider with two turns has a better high frequency response whereas the one with three turns has better lower frequency response.

SUMMARY

As the cellular radio, global position systems (GPS) and cordless telephone markets require both high performance and low cost signal processing components, Synergy Microwave has successfully demonstrated a new and innovative manufacturing method which allows one to obtain and maintain high performance at greatly reduced costs. The process detailed herein is also subject to various patents pending for Synergy Microwave.

2544 Rev 1/8993

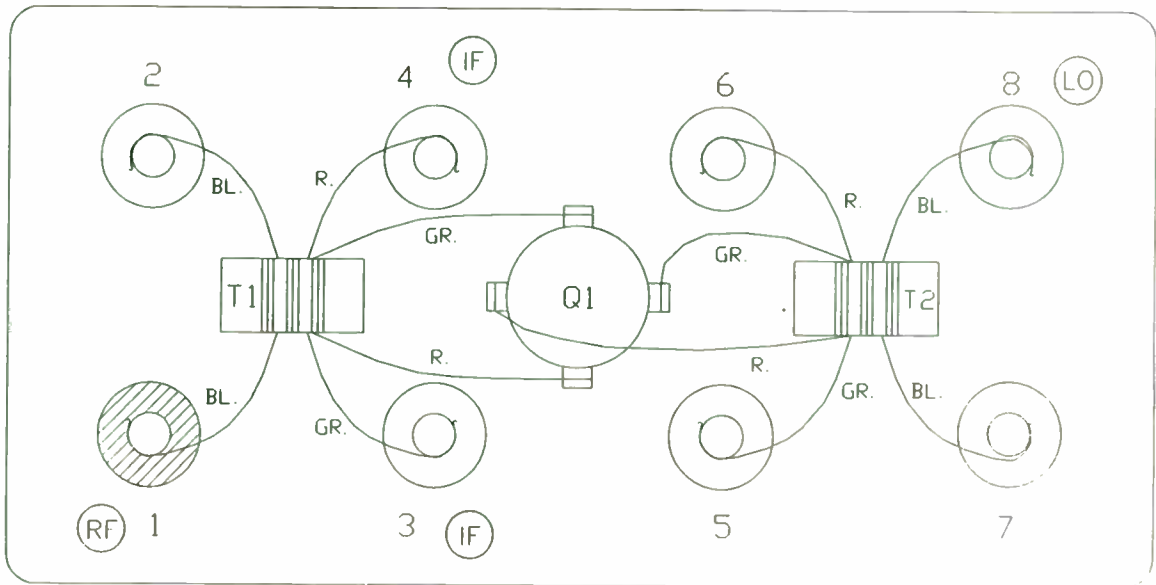


Fig.1 Typical assembly of a double balanced mixer using conventional technique.

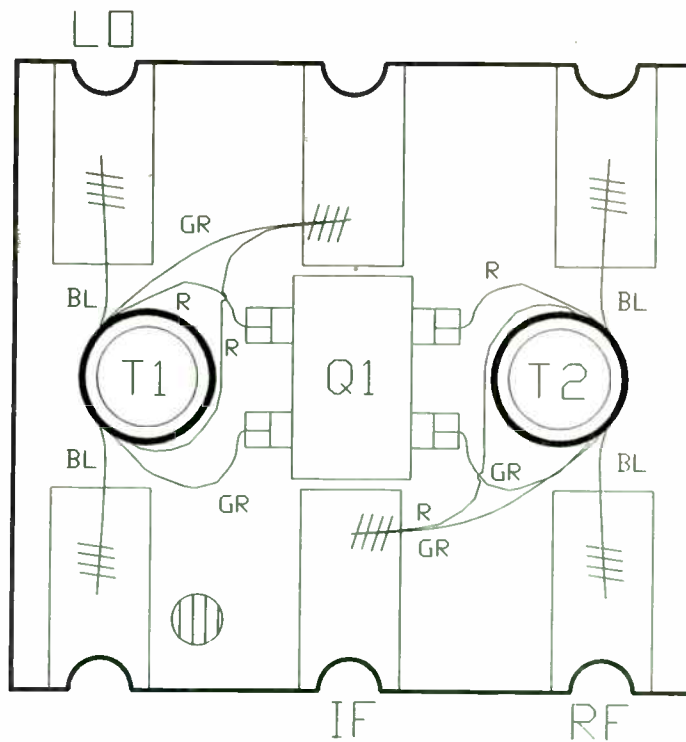


Fig.2 Typical assembly of a double balanced mixer using the new method.

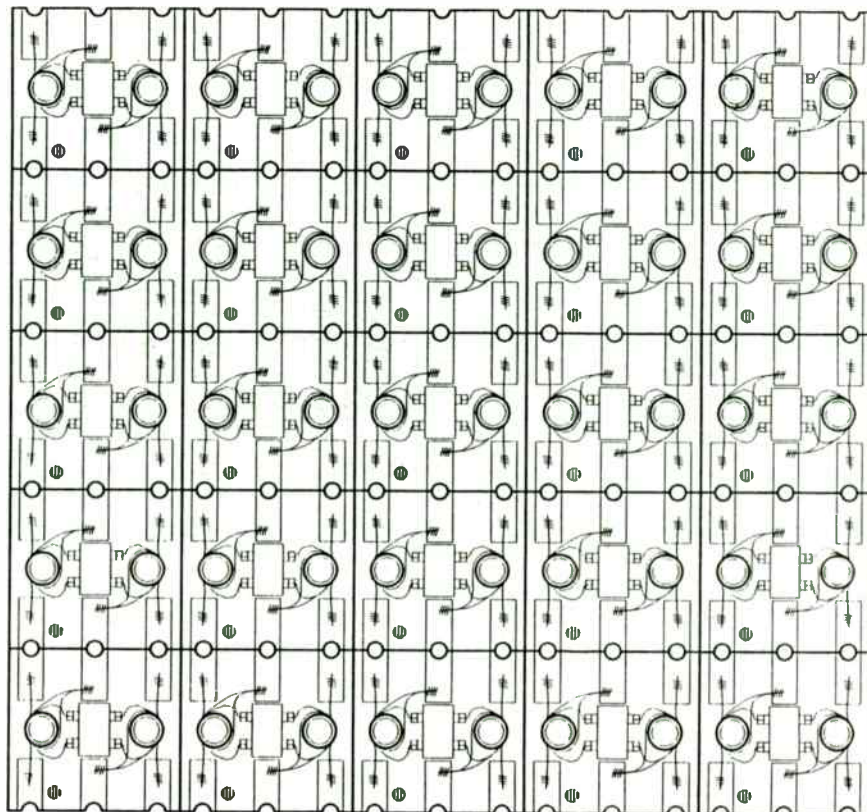
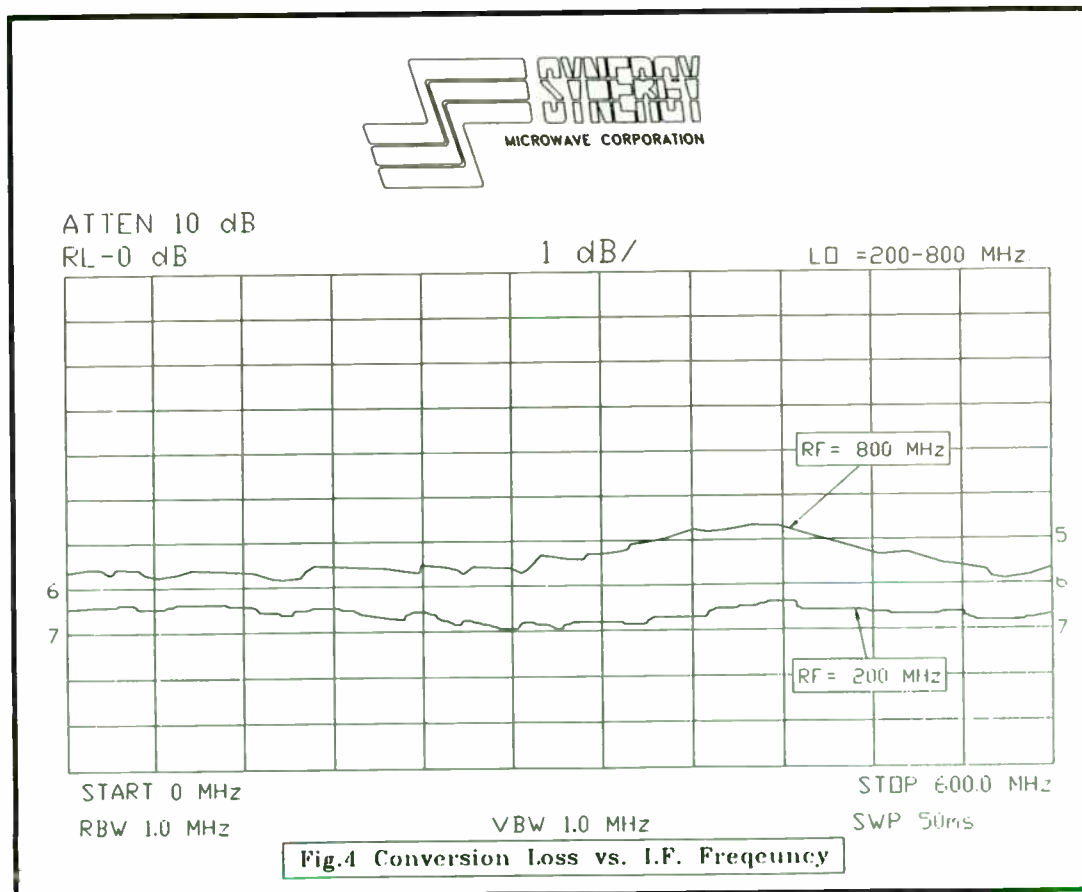


Fig.3 Panel Assembly



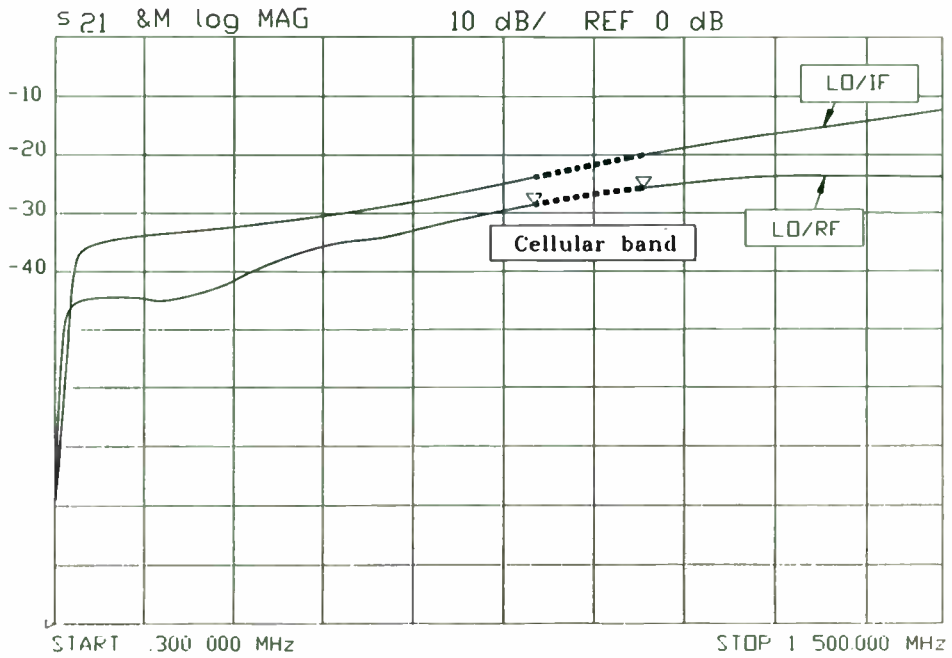


Fig.5 Isolation vs. Frequency

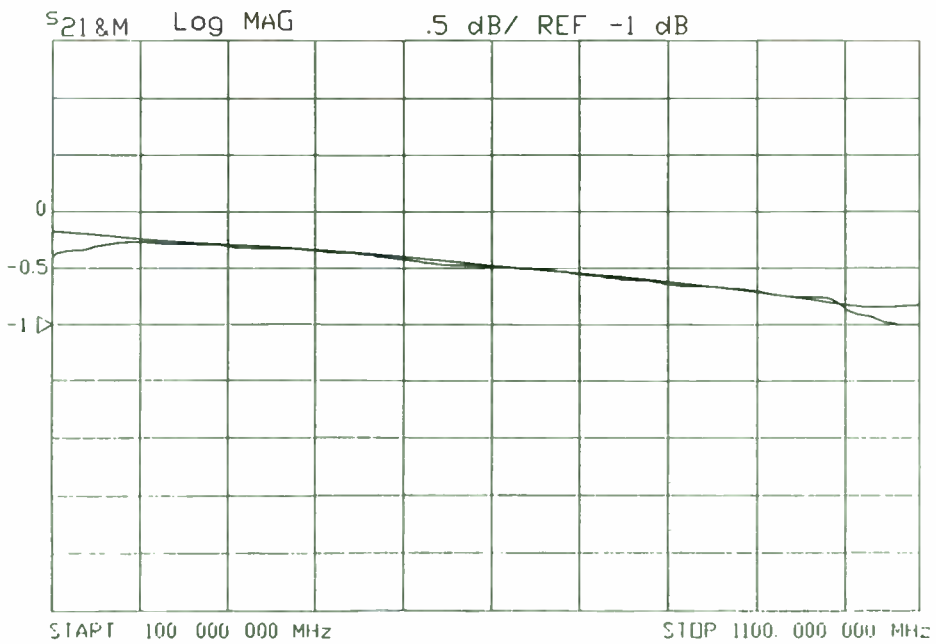


Fig.6 Insertion Loss vs. Frequency for 2-way power divider with 2 turns.

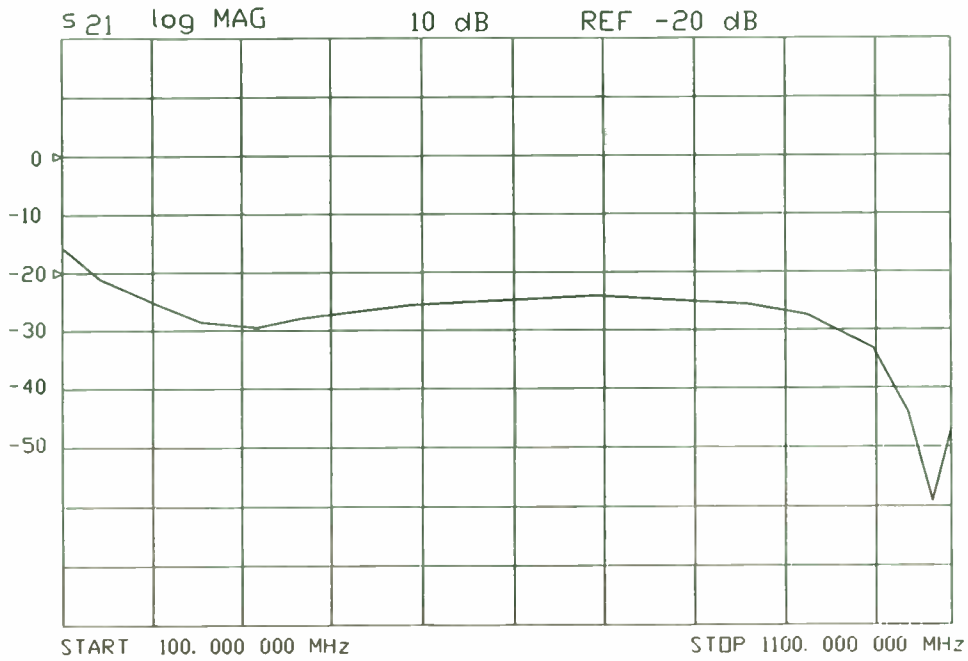


Fig.7 Isolation vs. Frequency for 2-way power divider with 2 turns

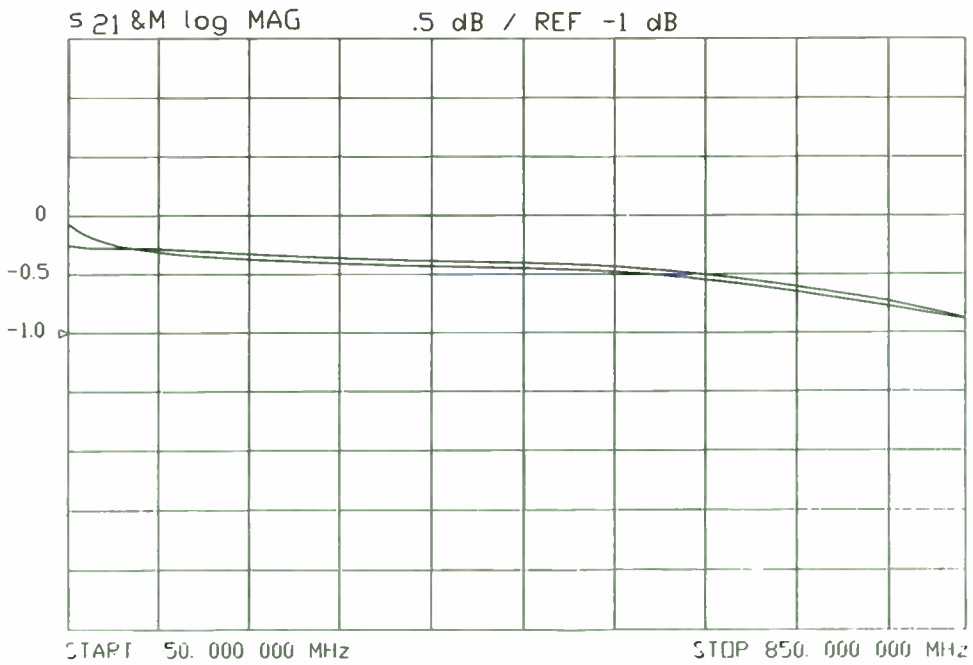


Fig.8 Insertion Loss vs. Frequency for 2-way power divider with 3 turns

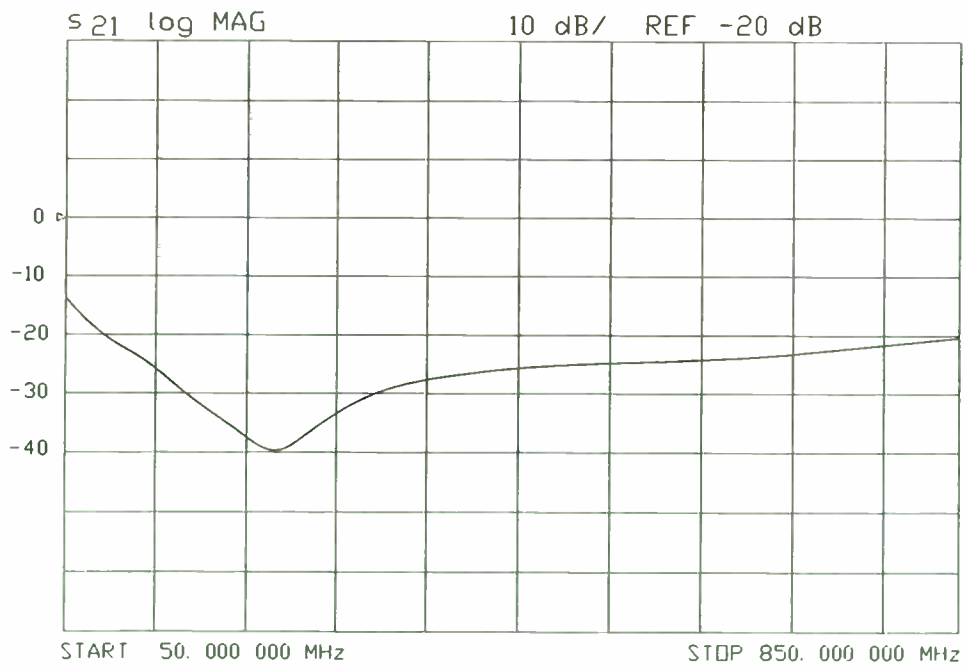


Fig.9 Isolation vs. Frequency for 2-way power divider with 3 turns

FREQUENCY SYNTHESIZER STRATEGIES FOR WIRELESS

Bar-Giora Goldberg, MSEE
Henry Eisenson
Scitcq Electronics, Inc.
December, 1992

PURPOSE

This presentation was prepared to illustrate some of the challenges posed by emerging wireless/PCN/PCS industries (hereafter "wireless"), particularly as they apply to a key subsystem: the frequency synthesizer. Wireless creates a spectrum of opportunity and technical challenge, as well as risk, and since the frequency synthesizer is one of the most difficult developments in any analog system this document will seek to present some potential strategies for meeting those requirements.

Optimistically, the authors have written to two audiences. The first includes design and system engineers, who may be very competent at designing the RF systems of five years ago but with the advent of wireless are encountering new arrays of challenges based on economic, production engineering, and performance factors. The second target audience includes program managers and company executives, who may have limited technical knowledge yet must listen to the engineer's explanations as to why the strategies of yesterday simply don't work in this new technical and marketing environment.

DEFINITIONS

One of the problems facing many designers of systems and subsystems for the wireless businesses is a lack of structure. Operating bands, modulation schemes, protocols, power limitations, and – surprisingly – even applications, are all poorly defined. Firms developing systems and making investments in this new market, and particularly those who are aggressively working to establish a position early in the evolution of the industry, are very much at risk because of the lack of structure, protocols, spectrum allocations, and – of course – definitions. It is beyond the scope of this paper to attempt to generate such a set of data, however, so this statement is presented only as a warning to those investing money and engineering, and a plea to those involved in the establishment and standardization of protocols and definitions.

Regarding frequency synthesizers, for the purpose of this document historical definitions apply. Though they will not be listed in this paper, they correspond with those appearing in many publications.

INTRODUCTION

Radio systems are tuned by generating a frequency reference, and the quality of that reference determines the performance of the radio circuit. Accuracy is critical; both transmitters and receivers must be at the same frequency for communication to occur. When the energy of the signal appears only at the desired frequency, phase noise is considered perfect, and as that energy spreads to nearby frequency, phase noise is described as less perfect. A good reference generates no discrete uncommanded signals (spurs). Together, accuracy, phase noise and spurious signals define the performance of a reference.

By far, the best way to tune a radio or any RF system is with a crystal, and when multiple frequencies are necessary, multiple crystals and a switch can be used. Eventually, however, it becomes first impractical and then impossible to use complex arrays of crystals, as shown in Figure 1.

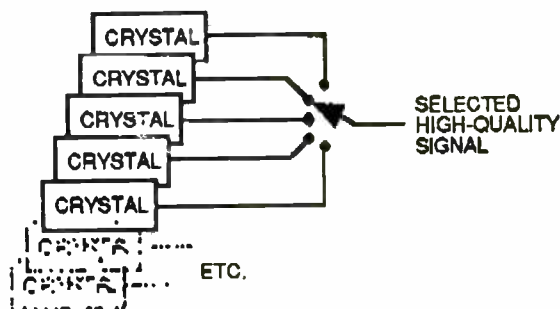


Figure 1

A "frequency synthesizer" is a device or circuit that synthesizes a new frequency based upon an original one (reference), retaining the stability, accuracy, and spectral purity of the reference though at a new point in the spectrum. It can generate one frequency (beyond that of the crystal reference) or multiple frequencies, as selected by a control mechanism (Figure 2).

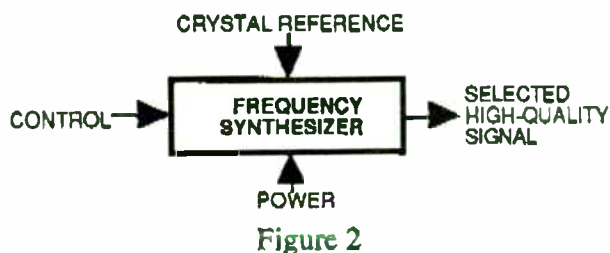


Figure 2

Like shoreline, spectrum is limited and precious, and the synthesizer (among other factors) determines how efficiently spectrum is used and how many channels can be compressed into any given operating band. Frequency synthesis is always a challenge, and the characteristics of the synthesizer have long defined the performance of the system that employs it.

Though there are as many synthesizer designs as there are designers, only three synthesizer techniques can be described as fundamental; all others are variations or combinations of one or more of them.

DIRECT-ANALOG

This (mix/filter/divide) is the oldest frequency synthesis method. The first time an engineer amplified a reference sufficiently to saturate a diode and used a filter to pick out a new frequency derived from the original, direct-analog was born. Today, many direct-analog techniques exist for multiplying, dividing, adding and subtracting an array of references, all locked to a common reference, to produce new frequencies.

This process supports very high spectral purity, since there is no correction circuit's "seeking" (that corrupts phase noise in a PLL), and careful planning can achieve frequency manipulation that avoids spurious signals. An important advantage of this technique is fast switching. The major drawback of direct-analog is the cost of the array of references required to cover the desired frequency range, plus the cost of one echelon of mix/filter/divide circuitry for each decade of resolution (step size) required.

Nevertheless, the finest synthesizer performance achieved by the industry employs direct-analog techniques, and appears in the Comstron FS-5000. Expensive, but there is no better method for generating a fast-switching, high spectral purity, broad bandwidth signal. Obviously, while this may be interesting to the designer of a simulator or radar system, the direct-analog approach is of little interest to a designer of wireless systems.

DDS

In one sense, the only true "synthesizer" is a DIRECT-DIGITAL SYNTHESIZER (DDS), since it literally constructs the waveform from the ground up (synthesizes the frequency) rather than combining or controlling existing oscillators.

A "vanilla" DDS appears in Figure 3, which also shows the signals generated by each circuit element.

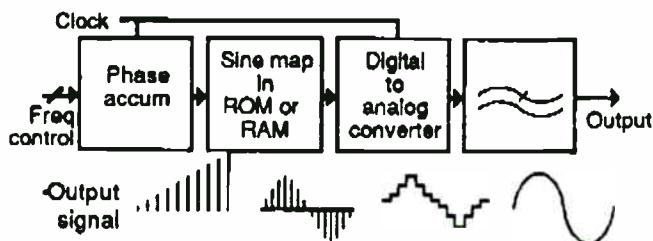


Figure 3

Though each of the blocks can be broken into many smaller ones (even down to the transistor level), the arrangement shown permits understanding of the means by which a DDS constructs a waveform.

The PHASE ACCUMULATOR correlates the clock with a control word, defining a "ramp" from 0° to 360° within some time period, and therefore the output frequency. A MEMORY maps the phase data in that ramp to a series of digital amplitude words, and a digital-to-analog converter DAC converts those digital data to an analog sinusoid (or any waveform stored in memory). That process must comply with sampled data rules, and therefore any frequency to be produced must be sampled *at least* twice each 360° (cycle), and the highest frequency that can be digitally generated is exactly one half the clock rate – though filter realities make the available output closer to 45%.

The DDS is also a supreme modulator. Digital shifting of frequency supports FM and toggling between two frequencies supports MSK/FSK; in fact, the DDS is a theoretically perfect FSK modulator. By placing an adder between the accumulator and the memory, the output can be shifted in time (phase), and a multiplier between the memory and the DAC permits scaling of the output, and therefore amplitude control. Both phase and amplitude modulation is therefore possible with a DDS, and with digital precision not possible with analog circuitry. Finally, SSB implemented using DDSs approaches theoretical perfection.

The advantages of the DDS include inexpensive high resolution (fine step size), fast switching speed, excellent phase noise, and while the signal is in the digital domain it can be manipulated/modulated with exceptional accuracy. The disadvantages include the fundamental limit of bandwidth (maximum frequency output is less than one half the clock rate, and logic has limits), and discrete spurious signals at a higher level than with other techniques. Nevertheless, in only twenty years the DDS has grown from an engineering novelty to a serious design tool.

There are many DDS products on the market today, and they're generally divided into two categories based upon a combination of price and performance. The "commodity DDS," typically in CMOS and from Analog Devices, Harris, Qualcomm, and Stanford Telecommunications, is characterized by low price, performance that is most often exploited as part of a much more complex synthesizer, and a high level of integration. Such DDS products often offer waveform manipulation capabilities, modulation, and other features sought by the wireless designer, but do not operate in the frequency ranges of most wireless systems.

High performance DDS products are often executed using very fast silicon or gallium arsenide logic so they can be clocked at a much higher rate than the commodity-level products. These DDS products cover a band much broader than that of the commodity DDSs. Expanded bandwidth requires higher clock rates, and therefore faster logic and more critical manufacturing and testing processes, hence higher prices. Even the fastest of the high performance DDSs operate only at about 400MHz, and that plus their relatively higher prices make the DDS unsuited to the needs of wireless systems.

While there are many specifications and architectures that differentiate one DDS from another, in general, a DDS can be characterized by a combination of bandwidth and spurious signals. By that simple standard, the state of today's DDS art will not meet the needs of wireless. The DDS should not be ignored by the wireless system designer, however, because as will be seen there are techniques by which the performance of the DDS can be translated to the frequency ranges of interest.

PLL

The PHASE LOCKED LOOP (PLL) is the single most commonly used synthesis technique, and is unquestionably the most flexible and adaptable. Perhaps more than ninety-nine percent of all synthesizers use one variant or another of the PLL. It appears in countless automobile radios and television sets, yet variants of the same architecture are used in exotic satellite transponders.

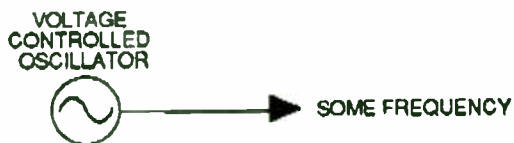


Figure 4

In Figure 4, a free-running oscillator generates a signal, the frequency of which varies (drifts) over time, according to circuit anomalies, temperature, etc.

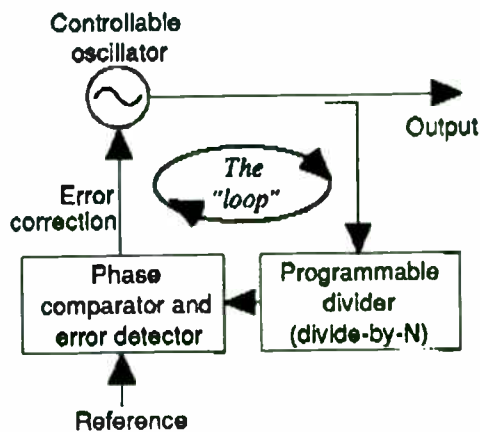


Figure 5

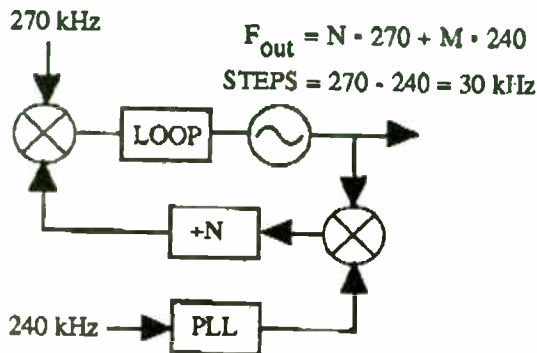
Figure 5 adds feedback and a phase detector, a correction mechanism that completes a loop to lock the output to some reference (thus "phase locked loop" or PLL), in accordance with some numeric ratio set by the frequency control command.

The PLL does not synthesize a waveform; rather, it controls the oscillator to the desired output frequency by dividing the output of the oscillator by some number, and then comparing the result with a reference. When errors are detected, they produce correction signals that return the oscillator to the correct operating frequency. For that reason, the system is always "seeking perfection," and the effectiveness of that seeking process determines the performance of the synthesizer. As that seeking occurs, the greater the deviation from the commanded frequency the worse the purity of the output signal. Such deviations are called "phase noise."

The advantages of PLL are low cost and excellent spurious suppression. The major disadvantage is that *both* fine steps *and* good phase noise can be achieved only in expensive implementations. In fact, the primary deficiency of PLL is that inverse relationship between step size and phase noise, because as step size decreases, division ratios in the system must increase, and the higher the division ratio the worse the phase noise within the loop bandwidth (close to the carrier). There is another drawback to PLL: switching speed. While the direct approach (DDS and direct analog) can be very fast, the PLL is slow because there is a certain electrical inertia involved before the system settles at a new frequency. The finer the required steps (the higher

the division ratio) the longer it takes a typical PLL design to reach a new commanded frequency.

Phase noise can be reduced by using two PLLs wherein a primary loop generates the required operating band but in coarse frequency steps, therefore with low division ratios and acceptable phase noise. A second loop, also doing coarse steps, is combined with the first to generate fine steps (a difference). See Figure 6.



TYPICAL TWO-LOOP SYNTHESIZER

Figure 6

Switching speed can be improved by generating a tuning signal to the VCO early in the change process. That's usually done by generating a digital change word, and converting it to an analog voltage applied to pre-tune the VCO. This approach can increase speed, but it also increases circuitry, cost, power dissipation, etc.

Another approach is to simply use two PLLs, with a switch to select between them. Assuming only that the system "knows" the next frequency, it can tune PLL-2 to that frequency while PLL-1 dwells at the prior frequency. When the time comes to change, a digital command switches to PLL-2. This obviously requires two PLLs, with twice the power, etc.

As can be seen, the PLL is a very useful technique, but a conventional single PLL cannot achieve aggressive combinations of fine steps, fast switching, and good phase noise.

COMBINATION DESIGNS

Many systems combine two or more of the basic techniques, and this approach is constantly being explored for wireless applications. To cover a limited band in fine steps, above the range of a DDS, the output of a DDS can be mixed with an LO and a filter used to select the desired sideband. In direct-

analog systems, a PLL might be used to generate some of the required references. PLLs are often successfully combined with DDS to achieve fine frequency steps with reasonable phase noise. Ever more inventive combination designs appear every year, and some include elements of all three building blocks: PLL, DDS, and direct analog.

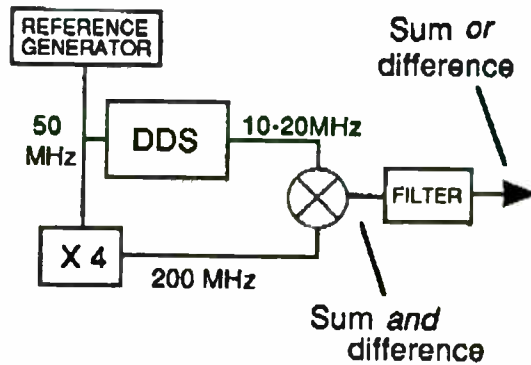
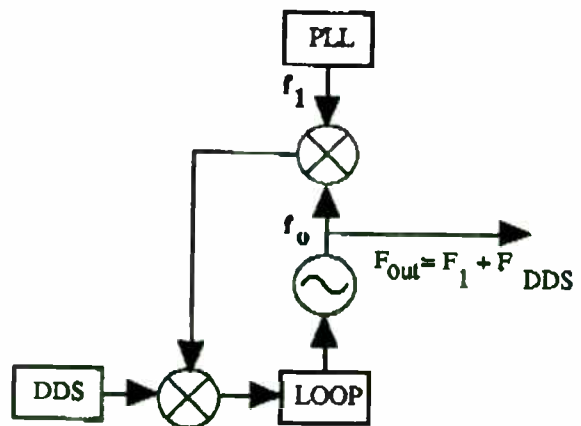


Figure 7

When a system concept dictates operation over a relatively narrow band but at a higher center frequency, a DDS can be upconverted to that range so as to exploit the DDS' fine steps, modulation capabilities, and fast switching. An example of such an architecture appears in Figure 7. In the example shown, 10 MHz of the DDS' output is translated or upconverted to the 200 MHz range. Obviously, the same architecture can be used to achieve a wide variety of goals, limited by DDS bandwidth and the physics of the filter.

It is sometimes useful to upconvert the DDS with a PLL, and, again, there are many ways to accomplish this. One mechanism (developed in 1984) uses a DDS as a reference to the phase detector of the PLL, though multiplication seriously degrades spurious performance.



TYPICAL DDS+PLL SYNTHESIZER

Figure 8

Another (also from that period) uses a DDS, a PLL, plus a combining loop. A typical DDS+PLL approach is shown in Figure 8. These techniques are useful, but involve cost and power compromises.

There are other interesting PLL mechanisms, which will be discussed as the needs of the emerging wireless market are analyzed.

GENERAL REQUIREMENTS OF WIRELESS SYSTEMS

The wireless industry will be filled with cell or base stations, of which each interacts wirelessly with dozens, hundreds, or even thousands of portable stations. The consumer purchases the wireless portable but the price of the cell/base radio is usually buried in service charges by the network owner. Also, because power, cost, and size are less important in immobile cell/base radios, this paper addresses only the requirements of portable systems.

It also considers only frequency-agile systems. The synthesizer for a typical wireless system (for instance a TDMA-based wireless PBX) will operate near 900 MHz with steps under 50 kHz, spectral purity that supports digital modulation, and power dissipation that ensures reasonable battery life. CDMA-based designs can trade frequency agility for complex coding circuitry, but TDMA, N-AMPS, AMPS, GSM, and most other cellular/PCS/PCN wireless systems require channel selection, hence agility.

Throughout wireless, once the basic function is accomplished price becomes paramount. Few engineers are experienced in designing products for the volumes involved in the wireless market. When millions of units will be made, savings of a few cents on each can have a profound effect upon the profitability of the enterprise. There is a spectrum of companies addressing every emerging opportunity in wireless, hence competition is fierce and will only grow tougher as the industry evolves. The relationship between price and performance, therefore, determines corporate success and failure.

Required performance is established by marketers who determine what the end user needs and wants, and what limits are acceptable. Once that information is collected and integrated, it is the engineer's task to achieve that performance at the lowest possible price. The most general assumption is that parts count will affect price, particularly when assembly effort is considered, and therefore the simplest (or more highly integrated) product will probably be lowest in cost and most competitive.

In wireless, reliability and durability are only barely behind price in relative importance. Historically, our industry has defined quality as either "military" or "commercial," and the assumption was that "military quality" produced the highest reliability. There are two reasons why production methodologies that define "military" quality won't work for wireless. Military quality standards require training programs, a wall full of diplomas, constant inspections, intensive testing, and reams of documentation. Like the ubiquitous pager, wireless products are measured only by the simplest standard of all; they must work nearly forever.

Generally, in the electronics industry, parts count and reliability are inversely related, and the more parts the more opportunities for manufacturing defects, so the simplest (or more highly integrated) product will be the most reliable.

Size is an issue because all wireless system developers are driven toward exceptional portability, and small size always complicates RF/analog design problems, involves higher levels of integration, and generally raises the cost of engineering the final product.

Some system architects have described requirements that include rapid settling. GSM (the European standard), for instance, establishes timing standards that dictate a fast switching solution. Designers of PBX and security systems have also asked for fast switching. A generic wireless synthesizer solution must, therefore, include the ability to switch at rapid rates. By extension, that seems to demand either multiple synthesizers with a selector and supporting software, or some implementation of a direct design.

"Wireless" implies exactly that, so not only is the communication by radio rather than coaxial cable, there are no extension cords and portable elements of the system run on batteries. Power consumption determines battery life, and one of the major engineering challenges of the wireless industry is efficiency of power utilization.

Marketing defines the needs of the end user and ensures that the product will have salable competitive advantages. The engineering group must develop a product that first attains those goals, but also costs little to make and works forever.

The needs of the wireless industry, in general, can best be met by simple, highly integrated, physically small, low-power designs. That is true in general,

and it is especially valid for the frequency synthesizer engine that drives the system.

FREQUENCY SYNTHESIS FOR WIRELESS

The frequency synthesizer subsystem of a wireless product does exactly the same job as a synthesizer does for any RF system. It is the system's tuning mechanism, and its performance determines the product's compliance with many marketing-driven requirements. Channel spacing determines step size, and in a PLL that establishes a mathematical relationship between operating band and division ratios that also dictates phase noise performance. Spurious signals can fool the system, lack of reliability can kill it, and excess cost makes everything else insignificant. This is valid for all RF systems and subsystems, including the synthesizer.

We've learned that the frequency synthesizer "menu" offers many alternatives from which the system designer can select, and we've also covered some of the needs of marketable wireless systems. Perhaps one valid method for identifying the best approach for wireless is to eliminate those techniques that will not work. The problem would be solved if a wireless portable end-user would pay for – and carry around – a Comstron FS-5000, or if the industry knew how to clock a cheap DDS at 2 GHz and still get good spurious suppression from the result. For reasons of cost, bandwidth, size, or spectral purity, therefore, pure-direct (analog or digital) synthesizers do not work for wireless.

What about a DDS upconverted using mix/filter circuitry – in other words, one of the "combination" designs? One advantage is the ability of the DDS to generate a modulated signal derived from digital manipulation of the waveform, and a second advantage is switching speed. At first glance, this approach looks inviting, but what are the disadvantages?

Make the estimate. Assume that the system demands 10 MHz bandwidth at a final operating frequency near 900 MHz. If reasonable filters are to be used, then there must be either two upconversions or substantial bandwidth in baseband. Two upconversions are expensive, since two good LOs must be generated and that greatly increases complexity.

For a single upconversion the required baseband coverage might be 50 MHz, which implies a clock rate for the logic near 110 MHz. Consider Figure 9,

which illustrates the limitations imposed by filter issues.

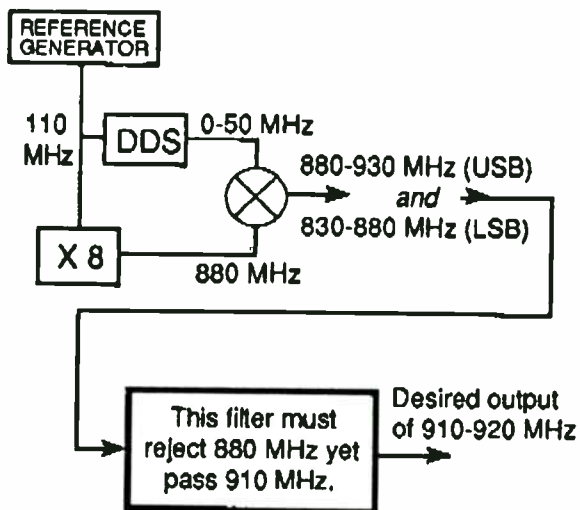


Figure 9

Depending upon the required suppression of the undesired sideband, the filter requirements shown are not impossible to meet. They are, however, difficult, very expensive, labor intensive, and impractical for inexpensive portable equipment.

Power is another issue that probably disqualifies the DDS. Even an advanced-technology, fractional-micron CMOS, fully integrated DDS will occupy a die of about 100 x 100 mils, and assuming a clock rate of 100 MHz the most optimistic dissipation estimate is 0.5W. Wireless portables will probably use a tenth of that for the entire design, hence the likely disqualification of DDSs using today's technology.

For these reasons, neither two conversions nor a 100 MHz DDS clock rate are practical. The designer must look beyond the direct approach. That leaves indirect, or PLL, which works for nearly all RF applications throughout the electronics industry.

In today's wireless, synthesizers are almost all PLL and use either one or two loops. Both have been implemented with very high levels of integration, and single chip PLL ASICs are available at \$5 or less, with operation from 6-15 mA. These devices include all functions and require only an external VCO plus a few discrete devices for the loop filter.

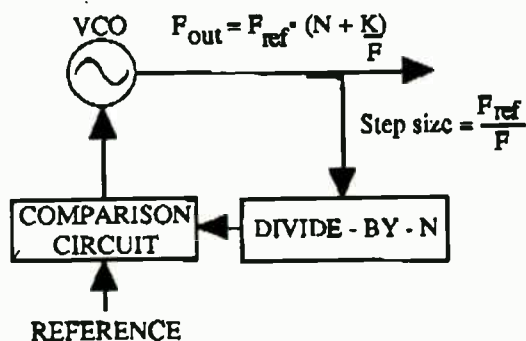
The single loop iteration of such a design is simple, economical, reliable, and small, but it does not meet the requirements of digital modulation techniques.

For many years, a broad variety of simple single loop synthesizers have used inexpensive PLL chips by Fujitsu, Plessey, Motorola, etc. to meet the requirement of early wireless, including FM/analog cellular. Close channel spacing of agile wireless requires fine tuning steps and therefore high division ratios, yet digital modulation demands phase noise better than conventional PLL architectures can achieve.

Designers have therefore used two loops to achieve the combination of phase noise and step size needed by digital modulation schemes, which means two synthesizers with two VCOs, etc., and all the baggage a double circuit implies. The two-loop solution therefore implies higher power, complexity, cost, and likelihood of failure – everything the successful wireless system designer was directed to avoid. Nevertheless, state of the PLL art for wireless has been two loops, which achieve the required phase noise. In some systems, the requirement is for two such assemblies with a switch, to support fast switching. That's four loops, with four VCOs and associated circuitry; it's expensive, large, power hungry, and in general is an array of compromises.

FRACTIONAL N

There's a relatively little-known derivative of PLL that can address many such requirements with only one loop; it's called fractional n . Though mysterious to many engineers, it is not a true innovation because some fractional designs have been used for years. Fractional n synthesis can best be understood by examining the conventional block diagram for a PLL, but with one twist. The divide-by- N circuit appears where it always has, but additional circuitry changes the value of N from an integer to some fraction. Consider the impact, as suggested by Figure 10.



Conventional PLL: N is an integer
 Fractional: N can be a fraction

Figure 10

N is programmable, of course, to define the relationship between the output and the reference. Suppose the requirement is to operate at about 1 GHz in 30 kHz steps. In conventional PLL designs, the output (1000 MHz) is divided by 33,000 to reach a value that can be compared to the reference (30 kHz), and that division imposes a phase noise degradation of $20 \log N$, or 90 dB. That degradation can be cut by 20 dB with a good fractional design, and there are several ways to achieve the desired result. Fractional division can be used to *increase* the reference by an order of magnitude, or to *reduce* the division ratios, and in any case the effect is to reduce the division ratio for a given combination of output frequency and step size, thus improving phase noise.

Fractional at first appears to be an aspirin for all forms of PLL headaches, but that hasn't been the case. Conventional implementations of fractional require major increases in circuitry, and that implies increased power dissipation, parts count, complexity, labor costs, and therefore overall costs – again, all the things the designer was told to avoid.

Naturally, fractional division generates a new periodicity within the divide-by- N circuitry, and therefore introduces spurious signals. For the above example, if the reference goes from 30 to 300 kHz, for 30 kHz steps there will be 30kHz/60/90...etc. spurs in addition to the 300 kHz spurs. Those spurs are at the frequency of the new periodicity or its harmonics, but in either case they can produce a major degradation of spurious suppression. In a way, fractional has been largely ignored because those who have experimented with it consider the improvement in phase noise to be virtually a trade off for spurs.

Yet another problem with fractional is that the fractionality of conventional circuits is fixed, hence a given design has little flexibility and new applications imply new designs. For these and allied reasons, fractional n synthesis has been largely ignored. This situation is about to change, as market factors drive engineering to examine every alternative.

An important derivative of fractional is Sciteq's Arithmetically Locked Loop (ALL), which combines aggressive digital signal processing (DSP) with fractional to overcome all of the disadvantages outlined above. ALL is a simple – and patented – design that increases overall gate count (compared, for instance, to the Fujitsu or Plessey PLL chips) by about 3%, so complexity is not an obstacle. The effect of the new periodicity is minimized, hence spurious signal level is also not an obstacle. Finally,

spurious signal level is also not an obstacle. Finally, fractionality is programmable, making one design suitable to a spectrum of applications.

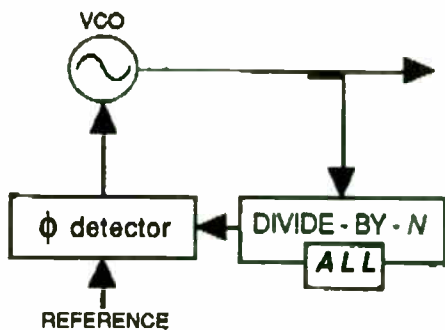


Figure 11

Adding ALL to a synthesizer design is simple, as implied by Figure 11. There is no change to the existing design except for I/Os in the divider circuit; the ALL block adds simple DSP that does the actual job of managing the division process and reducing the required ratios.

ALL APPLICATIONS IN WIRELESS

The ALL can operate over all wireless segments of the spectrum up to C-band. Comparisons are best made by examining any of the standard single-chip solutions (Fujitsu, National Semiconductor, Plessey, etc.) and adding about 3% in gate count and power while reducing close-in phase noise by about 20 dB.

That performance level support digital modulation scenarios with a single loop. Even close-in, phase noise is competitive with levels ordinarily achieved using two loop designs.

Frequency switching is far faster than conventional PLL designs, even without pretuning, since the reference frequency can be much higher for a given step size.

ALL has been in full production for two years, executed with discrete components to build modular synthesizer products. These designs have been very successful, and constitute one of Sciteq's most important product line. Potential users can today support system development using prototypes built with discrete devices, in the expectation that a fully integrated solution will be available during summer 1993.

Now that the U. S. Patent Office has allowed Sciteq's patent, a full-custom chip development

contract has been let to a U. S. semiconductor firm. Because the design is based on existing hardware (that uses discrete devices), risk is viewed as low.

The new low-power Sciteq design has a 2.5 GHz front end, integrated dual modulus, integrated ALL, low spurious levels, and programmable fractionality. It is suitable to all wireless applications, as well as other systems where competitive posture requires new levels of cost-effectiveness. Projected cost of the new single-loop integrated synthesizer, designated the SCX-180, is under \$10 in commercial quantities.

Some derivative of ALL will be used in many future cellular and other wireless products requiring agility, so Sciteq invites inquiries from system developers, who are invited to contact Sciteq in San Diego, at 619-292-0500.

A 2.4GHz Single Chip Transceiver

L M Devlin, B J Buck, J C Clifton, A W Dearn, A P Long,

GEC-Marconi Materials Technology Limited
Caswell, Towcester, Northants
NN12 8EQ
Telephone: 0327 50581
Facsimile: 0327 54775

Introduction

The Industrial, Scientific and Medical (ISM) frequency band includes the frequency range 2.4 - 2.5GHz. In the USA, unlicensed operation using spread spectrum modulation at transmitter powers of 1W is permitted over this band. This paper describes a transmit/receive front end for a 2.4GHz wireless communications transceiver, the entire circuit of which has been integrated onto a single GaAs Microwave Monolithic Integrated Circuit (MMIC). A photograph of the 3.3mm x 5.2mm chip, which is available in an SSOP28 style plastic package, is shown in figure 1. Low receive current of 30mA from a +5V supply and a standby current of less than 0.5mA, make this an ideal component for battery powered operation.

Transceiver Architecture

A block diagram of the complete transceiver is shown in figure 2. The circuit can be switched between receive, transmit and standby states. In receive mode, input signals are down converted to differential IF signals. Although designed specifically for the 2.4-2.5GHz band, RF signals between 1.9GHz and 2.6GHz could be utilised. The off chip filters can be selected to suit the band of interest.

In transmit mode, the IF input signal, either balanced or single ended, is between 200MHz and 500MHz. The IF input is up converted to a single ended signal at the RF frequency. The circuit has been designed to provide a constant output power for a wide range of IF signal levels. A switched attenuator has been included to allow a 10dB step in the output power level.

The frequency of the VCO, and hence the IF frequency, is selected by appropriate choice of an off-chip resonator. Local oscillator frequencies of between 1.4GHz and 2.7GHz are available. A diversity switch has also been included to allow antenna selection. DC supply to the chip is +5V and -5V, with complementary 0V/-5V switching. The -5V supply takes less than 0.5mA of current, regardless of transceiver operating mode. Typical current requirements from the +5V supply are 30mA in receive mode and 220mA in transmit mode. A standby state is also available and requires a current of less than 0.5mA.

In addition to the complete transceiver chip, all of the sub-circuits have been manufactured as individually measurable components. The design and measured performance of these subcircuits is described below. The circuits were realised on the standard GMMT F20 GaAs MMIC process.

Sub-Circuit Design and Measurements

LNA

The Low Noise Amplifier (LNA) is a two stage design with series inductive feedback to allow good noise figure performance with a well matched input[1]. A stacked bias arrangement is used to help reduce current consumption. Instead of biasing the drain of each FET at +5V and the source at 0V, the arrangement shown in figure 3 is used. This allows the +5V to be shared between the FETs and the current to be re-used.

The RF On Wafer (RFOW) measured s-parameters of a typical LNA are shown in figure 4. Gain is 17.5dB \pm 0.5dB from 2 - 3GHz. The input match is better than 15dB and the output match is better than 13dB. Measured noise figure is 2.5dB at 2.4GHz. Total current consumption is 6mA from a +5V supply.

Switches

T/R and diversity switches all use simple series mounted FETs[2]. The FETs are biased at zero volts DC and the control signal is applied to the gates. One common design of Single Pole Double Throw (SPDT) switch is used throughout. The measured "on" case insertion loss is typically 0.7dB with an "off" case isolation of 20dB.

Mixers

A quad ring of zero biased FETs is used to realise a balanced conductance mixer[3]. When driven with differential inputs, excellent balance is achieved with a conversion loss of 6dB.

VCO

A Clapp type Voltage Controlled Oscillator (VCO) is used[4]. The oscillation frequency can be set between 1.4GHz and 2.7GHz by an external resonator. For operation with an IF of, say 250 MHz, the nominal LO frequency is 2.15GHz. An on chip inductor/capacitor combination was included on the sub-circuit, for use as an alternative to the off-chip coaxial resonator. This allows testing of the oscillator on wafer. Figure 5 shows the output power and tuning voltage versus oscillation frequency. Output power varies by less than \pm 0.2dB across the tuning range.

VCO Balun

A common gate stage and a common source stage of amplification are used to provide an equal amplitude split with 180° phase difference[5]. The inputs of each stage are common and the two outputs are used to provide the differential drive to the balanced mixer. Figure 6 shows the RFOW measured s-parameters of a typical device and figure 7 shows the insertion phase between the input and each of the two outputs. A gain of 1dB at 2.1GHz and terminal matches of better than 20dB are achieved. The amplitude difference is only 0.15dB and the phase difference is 186°. Stacked bias has been used to allow operation with only 6mA of current from a +5V supply.

RF Balun

The RF balun is very similar to the LO balun but at a slightly higher frequency. The RFOW measured s-parameters are shown in figure 8 and the insertion phases in figure 9. A gain of 1dB with terminal matches of better than 20dB is achieved at 2.4GHz. Amplitude difference between the outputs is 0.45dB and the phase difference is 189°.

Buffer Amplifier

The buffer amplifier is used to provide a low level VCO output for phase locking of the LO. It must present minimal loading to the VCO, provide high isolation and be able to operate into any load from 50Ω to an open circuit. This has been achieved by using a small single finger FET, biased through a 50Ω resistor in the drain. Figure 10 shows the measured s-parameters of a typical amplifier. S_{11} is close to unity, which is indicative of the high input impedance presented to the VCO. The reverse isolation is more than 40dB at 2.4GHz and the output match is better than 14dB. An insertion loss through the buffer of 12.5dB ensures the required low level of output power is delivered. Current consumption of this component is only 1.5mA.

Differential Amplifier

With the chip in transmit mode, the IF input is into a differential amplifier[6,7]. A long-tailed pair at the input of the amplifier allows single ended or balanced input. Each of the differential outputs from this first stage is then amplified by identical common source stages of amplification. Active biasing is used throughout in order to minimise chip area. The differential input impedance to the circuit is 800Ω . When driven with differential signals from a source of the same impedance, the gain of the amplifier is 20dB over a frequency range of 200MHz to 500MHz.

Pre-amplifier

The output of the transmit mixer is amplified by the pre-amplifier prior to passing off chip, through the transmit filter and into the power amplifier. A low level of gain is required to balance the gain budget through the transmit chain. The input to the pre-amp is resistivity matched with reactive matching at the output. Figure 11 shows the measured s-parameters of a typical pre-amp. The amplifier exhibits a flat 5dB of gain from 2 - 3GHz. Input return loss is greater than 12dB and output return loss is greater than 17dB.

Power Amplifier

A two stage power amplifier is used to increase the level of the transmit signal[4]. Figure 12 shows the small signal s-parameters of the amplifier. The gain is 23dB at 2.4GHz with input and output return losses of greater than 13dB.

Switched Attenuator

A 10dB switched resistive attenuator[8] is positioned before the common T/R output, in the transmit path. This allows the output power level to be switched by 10dB. The small signal gain through the power amplifier, attenuator and T/R switch on the complete transceiver chip has been measured with the attenuator in both states. Figure 13 is a plot of this and the 10dB gain difference shows the accuracy of the switched attenuator. Because the attenuator is positioned after the power amplifier this gives an accurate 10dB step in output power level, regardless of amplifier compression.

Transceiver Measurements

Measurements have been made on the complete transceiver chip. These were made on an unpackaged device in a purpose built jig. A spectral plot of the buffer amplifier output is shown in figure 14. The output power level is -12dBm with a phase noise of -122dBc/Hz at 1MHz off carrier. This signal is used to drive the phased lock loop of the transmit/receive circuit.

Figure 15 shows the measured receiver conversion gain and double sideband noise figure versus IF frequency. This is for a fixed LO frequency of 2.035GHz with the IF varying from

50MHz to 500MHz. The slight roll off with increasing IF frequency is a result of on chip IF path losses and the off chip balun used to combine the differential IF signals developed by the chip.

The power transfer characteristic through the power amplifier, attenuator and T/R switch chain has been measured and is shown in figure 16. A 1dB compression point of +18.5dBm with a saturated output power capability of +21dBm is demonstrated. Figure 17 shows the gain versus IF frequency through the entire transmit chain from differential IF input to T/R common port output. This is also measured with the LO frequency fixed at 2.035GHz and shows a gain of 38dB \pm 1dB for IF frequencies between 200MHz and 500MHz.

Conclusions

A single chip GaAs transceiver to cover the 2.4 - 2.48GHz ISM band has been described. Receive gain is 13dB with differential IF outputs and a double sideband noise figure of 4dB. Current consumption in receive mode is just 30mA from a +5V supply. A standby mode is available with a current consumption of less than 0.5mA. Transmit mode offers a constant output power level switchable by 10dB, for a large range of IF input levels. These features combine to give a component which is ideally suited to spread spectrum Wireless LAN applications.

Acknowledgements

Numerous staff at GEC-Marconi Materials Technology have helped with the development of this chip, the authors would like to thank all concerned and in particular: Arthur Bradley, Rod Conlon, Ian Davies, Alistair Frier, Mike Geen and Barry Roberts.

References

1. Murphy, M.T., "Applying the Series Feedback Technique to LNA Design", Microwave Journal, November 1989, pp 143 - 152.
2. Ayasli, Y., "Microwave Switching With GaAs FETs". Microwave Journal, November 1982, pp 61 - 74.
3. Boulouard, A., "Simple Analysis Method Simulates Switching Mixers", Microwaves & RF, June 1989, pp 103 - 107.
4. Vendelin, G.D., Pavidio, A.M. and Rohde, U.L., "Microwave Circuit Design", John Wiley & Sons, Inc 1990.
5. Hiraoka, T. et al, "A Miniaturized Broad-Band MMIC Frequency Doubler", IEEE Transactions On Microwave Theory and Techniques, Vol 38 No 12, December 1990, pp 1932 - 1936.
6. Gray, P.R and Meyer, R.G. "Analysis and Design of Analog Integral Circuits", Second Edition, John Wiley & Sons, Inc 1984.
7. Robertson, I.D and Aghvami, A.H "Ultrawideband Biasing of MMIC Disturbed Amplifiers Using Improved Active Load", Electronics Letters Vol 27, No 21, 10th October 1991, pp 1907 - 1909
8. Clifton J.C and Arnold J., "Digitally Controlled GaAs MMIC Attenuator For Active Phase Arrays", Proceedings of the 22nd European Microwave Conference 1992, Vol 1, pp 231 - 235.

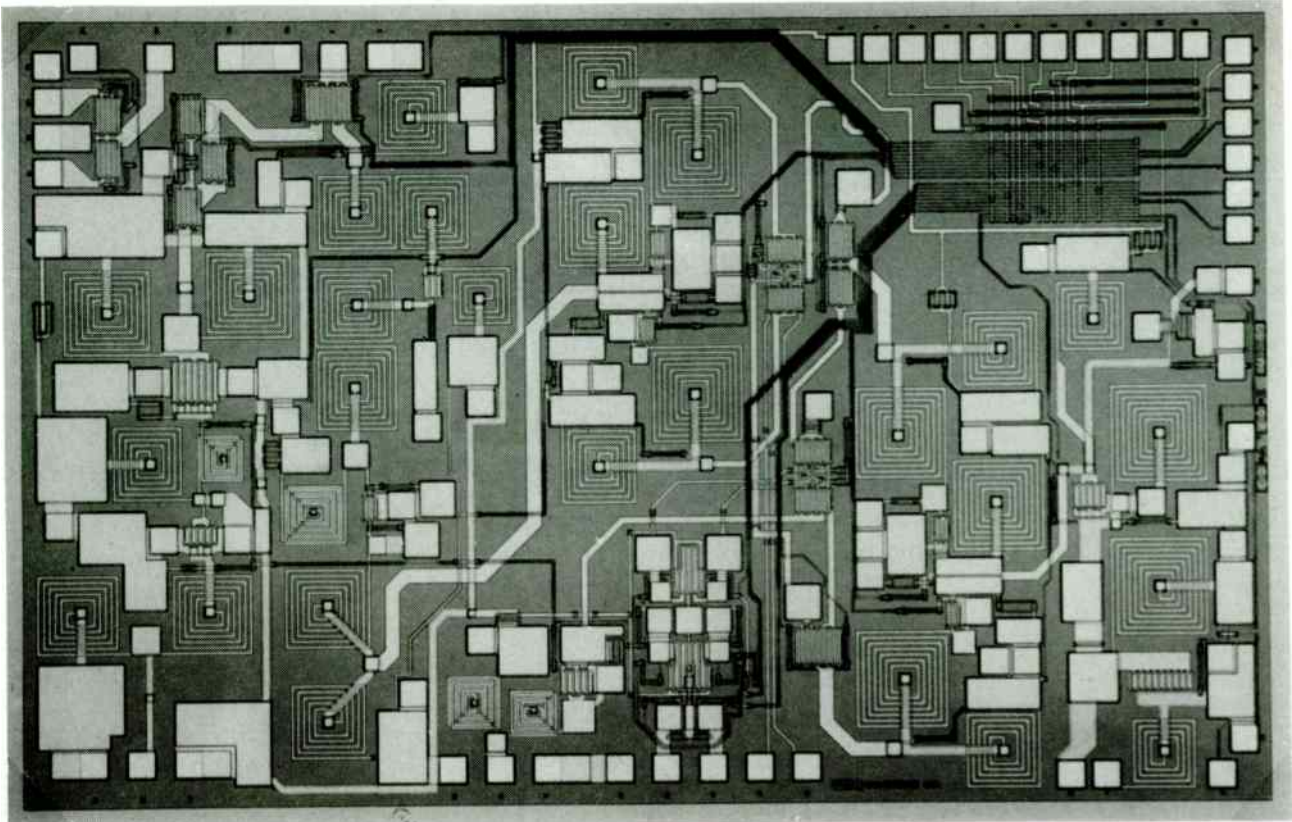


Figure 1 Photograph Of The Transceiver MMIC

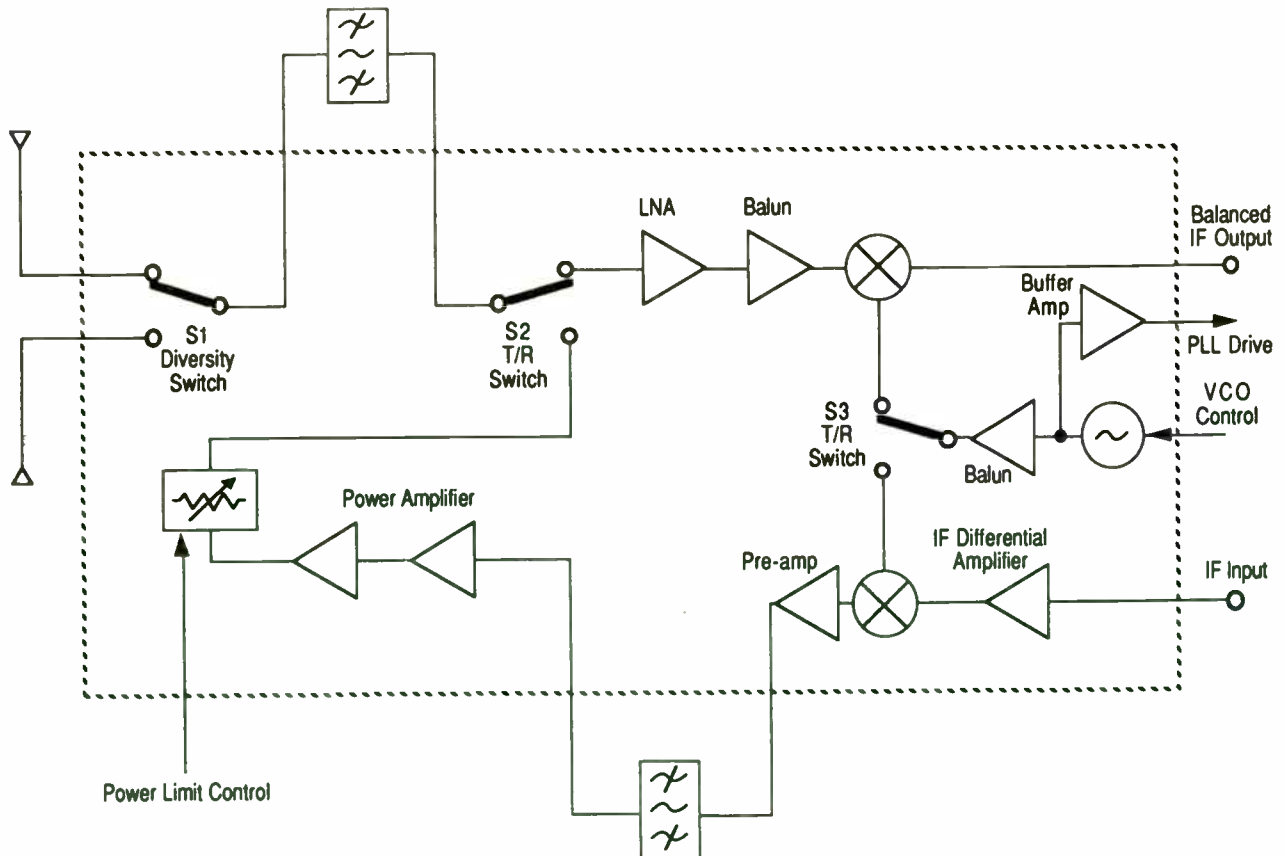


Figure 2 Block Diagram Of The Transceiver
399

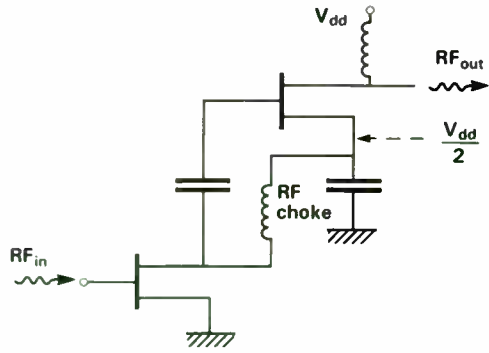


Figure 3 Stacked Biasing Arrangement

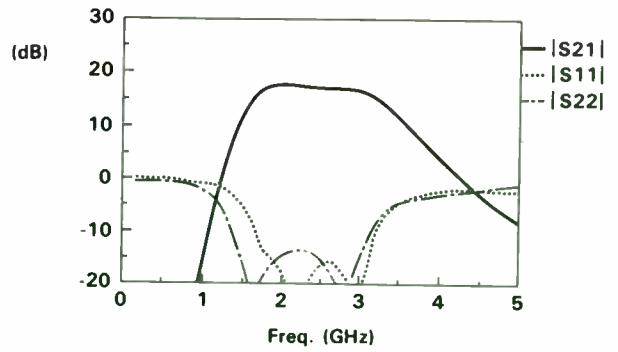


Figure 4 RFW Measured Performance Of the LNA

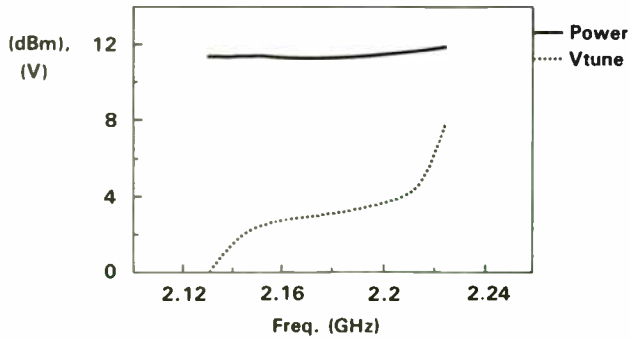


Figure 5 RFW Measured Performance Of The VCO

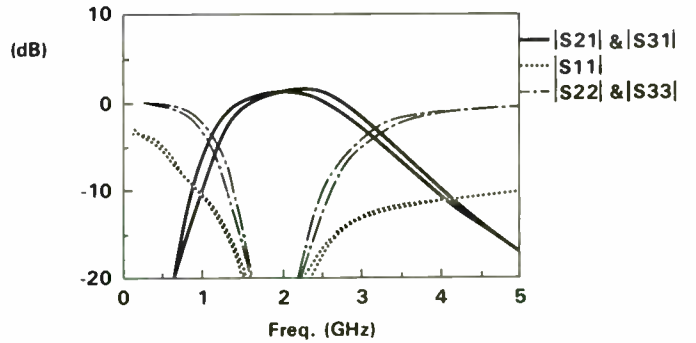


Figure 6 RFW Measured Performance Of The VCO Balun

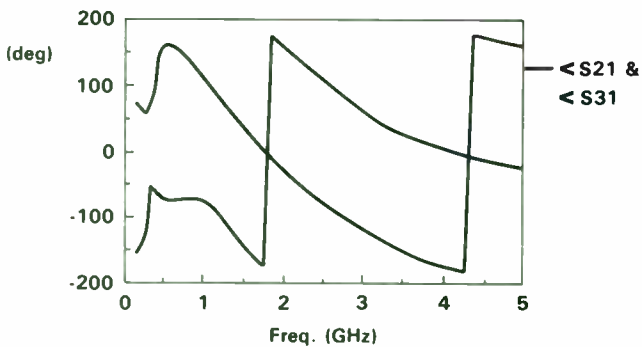


Figure 7 RFW Measured Performance Of The VCO Balun

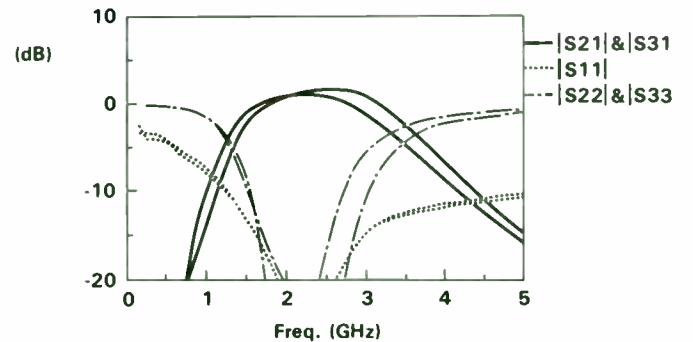


Figure 8 RFW Measured Performance Of The RF Balun

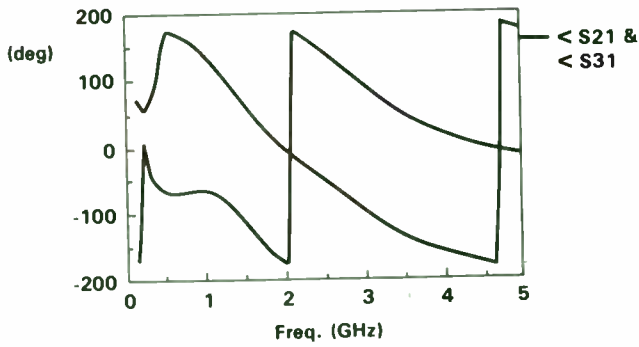


Figure 9 RFW Measured Performance Of The RF Balun

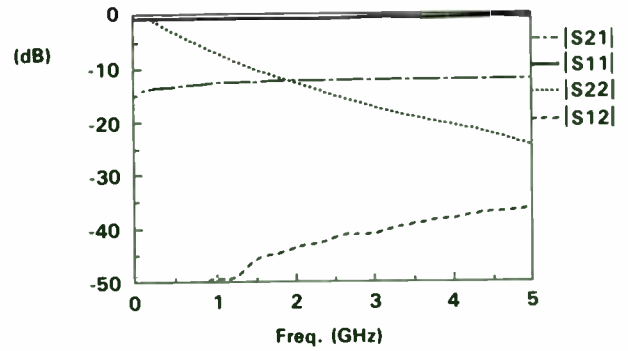


Figure 10 RFW Measured Performance Of The Buffer Amplifier

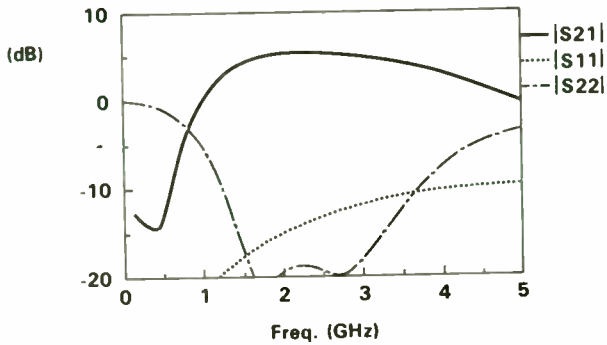


Figure 11 RFW Measured Performance Of The Pre-Amplifier

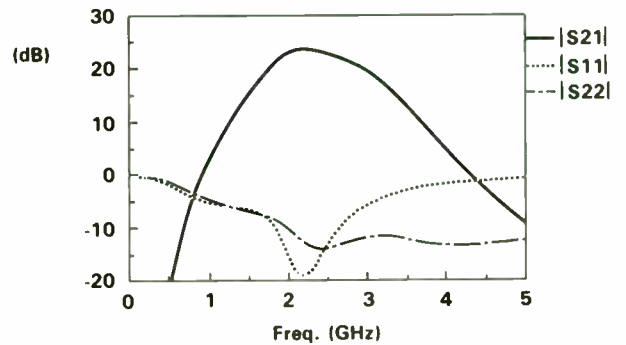


Figure 12 RFW Measured s-parameters Of The Power Amplifier

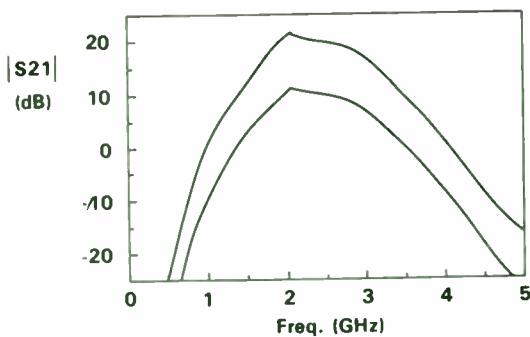


Figure 13 Measured Gain Through The Power Amplifier, Attenuator and T/R Switch Chain. Two States.

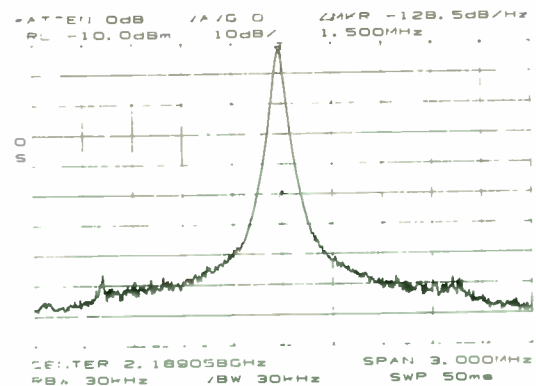


Figure 14 Spectral Output From The Buffer Amplifier

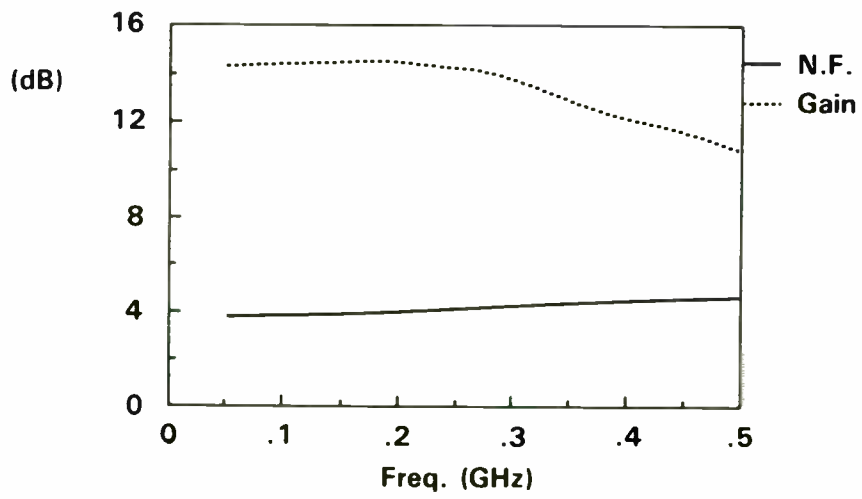


Figure 15 Measured Receive Gain And Noise Figure

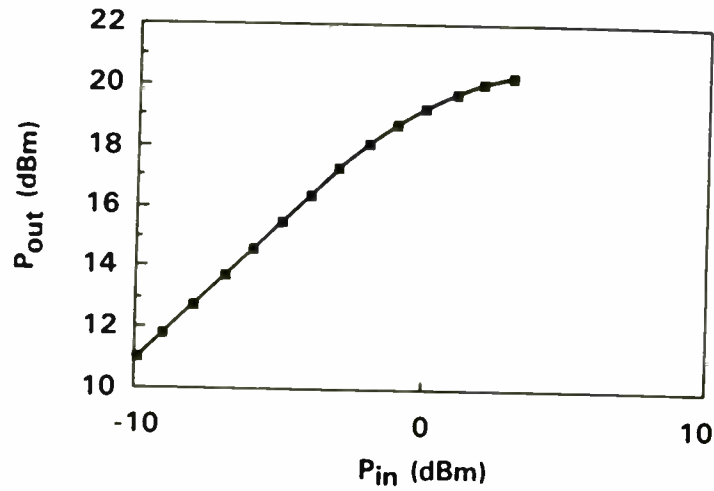


Figure 16 Measured Power Transfer Through The Power Amplifier, Attenuator And T/R Switch Chain

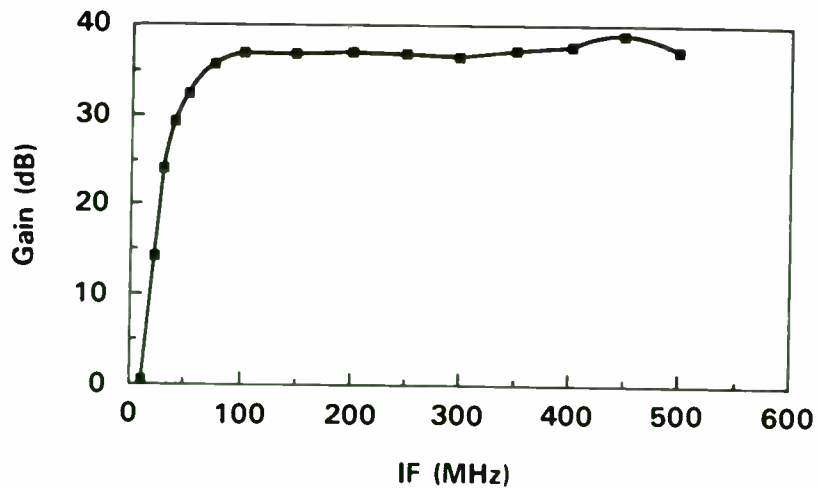


Figure 17 Transmit Up-Converter Gain Versus Intermediate Frequency

Wireless Data and Personal Communications

Session Chairperson: Jack Browne,
Microwaves & RF (Hasbrouck Heights, NJ)

Demodulating at 10.7 MHz IF with the NE/SA605/625, **Alvin K. Wong,** Philips Semiconductors-Signetix (Sunnyvale, CA).....**404**

Review of Technologies and Key Issues for Wireless Local Area Networks, **Greg Hopkins,** Windata, Inc. (Northboro, MA).....**415**

A Low-Current UHF Remote-Control System Using a SAW-Based Superhet Receiver, **Matthias Bopp,** TEMIC Telefunken Electronic GmbH (Heilbronn, Germany).....**424**

Comparison of Path Loss Performance of a Leaky Feeder Cable vs. a Distributed Antenna, **Jim Ford, Robert Perelman, and D. Lang,** Times Microwave Systems (Wallingford, CT).....**435**

Low-Cost F-QPSK Modem Radio Solutions for Doubling the Capacity of European Standard Cellular/PCS Systems, **P.S.K. Leung,** Digital Communications Laboratory, Department of Electrical and Electronic Engineering, Victoria University of Technology (Footscray, Melbourne, Victoria, Australia) and **Kamilo Feher,** DIGCOM, Inc. (El Macero, CA) and The University of California at Davis (Davis, CA).....**443**

Author: Alvin K. Wong

INTRODUCTION

The need for high speed communications is increasing in the market place. To meet these needs, high performance receivers must demodulate at higher IF frequencies to accommodate for the wider deviations in FM systems.

The standard 455kHz IF frequency, which is easier to work with, and thus more forgiving in production, no longer satisfies the high speed communication market. The next higher standard IF frequency is 10.7MHz. This frequency offers more potential bandwidth than 455kHz, allowing for faster communications.

Since the wavelength at 10.7MHz is much smaller than 455kHz, the demand for a good RF layout and good RF techniques increases. These demands aid in preventing regeneration from occurring in the IF section of the receiver. This application note will discuss some of the RF techniques used to obtain a stable receiver and reveal the excellent performance achieved in the lab.

BACKGROUND

If a designer is working with the NE/SA605 for the first time, it is highly recommended that he/she reads AN1994 and AN1995.

These two application notes discuss the NE/SA605 in great detail and provide a good starting point in designing with the chip.

Before starting a design, it is also important to choose the correct part. Philips Semiconductors offers an extensive receiver line to meet the growing demands of the wireless market. Table 2 (see end of app note) displays the different types of receivers and their key features. With the aid of this chart, a designer will get a good idea for choosing a chip that best fits their design needs.

If low voltage receiver parts are required in a design, a designer can choose between a NE/SA606, SA607, SA608, or SA626. All of these low voltage receivers are designed to operate at 3V while still providing high performance to meet the specifications for cellular radio. All of these parts can operate with an IF frequency as high as 2MHz. However, the SA626 can operate with a standard IF frequency of 10.7MHz and also provide fast RSSI speed. Additionally the SA626 has a power down mode to conserve battery power.

A close look at Table 2 will also show that there are subtle differences between the 3V receivers. The main differences between the NE/SA606, SA607, and SA608 can be seen

in the audio and RSSI output structure. Additionally the SA607 and SA608 provide a frequency check pin which can aid in locking in the desired received frequency over temperature.

OBJECTIVE

The objective of this application note is to show that the NE/SA605 can perform well at an IF frequency of 10.7MHz. Since most Philips Semiconductors receiver demo-boards are characterized at RF = 45MHz/IF = 455kHz, we decided to continue to characterize at this frequency. This way we could compare how much degradation (for different IFs) there was with a RF = 45MHz/IF = 455kHz vs RF = 45MHz/IF = 10.7MHz. As we will discuss later, there was minimal degradation in performance.

We also tested at RF = 240MHz/IF = 10.7MHz. The 240MHz RF is sometimes referred to as the first IF for double conversion receivers. Testing the board at RF=83.16MHz (which is also a common first IF for analog cellular radio) and IF = 10.7MHz was not done because the conversion gain and noise figure does not change that much compared to 45MHz input. Therefore, we can probably expect the same type of performance at 83.16MHz.

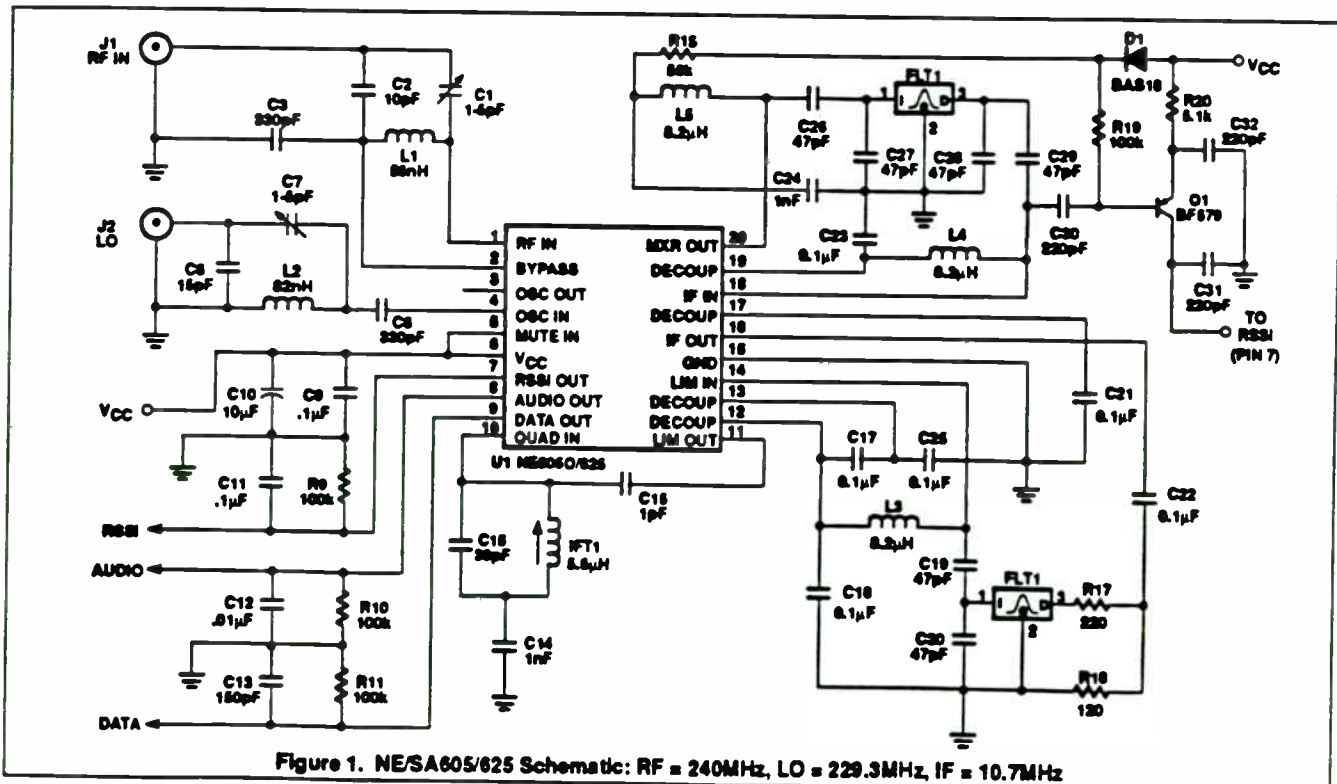


Figure 1. NE/SA605/625 Schematic: RF = 240MHz, LO = 229.3MHz, IF = 10.7MHz

Demodulating at 10.7MHz IF with the NE/SA605/625

AN1996

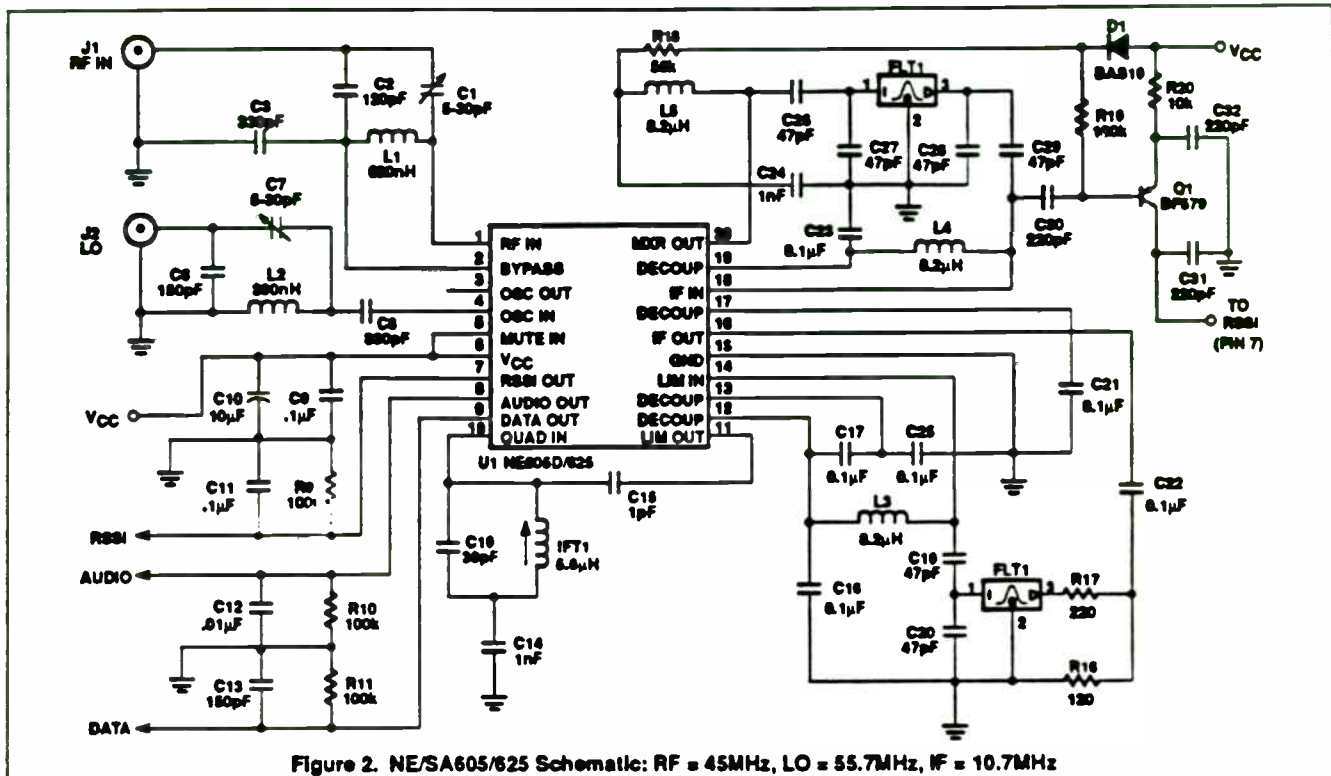


Figure 2. NE/SA605/625 Schematic: RF = 45MHz, LO = 55.7MHz, IF = 10.7MHz

The RF = 240MHz/IF = 10.7MHz demo-board is expected to perform less than the RF = 45MHz/IF = 10.7MHz demo-board because the mixer conversion gain decreases while the noise figure increases. These two parameters will decrease the performance of the receiver as the RF frequency increases.

With the new demands for fast RSSI time, Philips Semiconductors has also designed receiver chips with fast RSSI speed: The NE/SA624, NE/SA625 and SA626. The NE/SA625 can also be used in this layout because it is pin-for-pin compatible with the NE/SA605. The RSSI circuitry was the only change done for the NE/SA625, so performance will be similar to the NE/SA605. Performance graphs shown in this application note will reveal the similarities.

For systems requiring low voltage operation, IF=10.7MHz and fast RSSI speed, the SA626 will be the correct choice, however, this application note does not address the performance of the SA626 because the SA626 was not available at this writing.

Board Set-Up and Performance Graphs

Figures 1 and 2 show the NE/SA605/625 schematics for the 240MHz and 45MHz boards, respectively. Listed below are the basic functions of each external components for both Figures 1 and 2.

SO Layout Schematic List

- U1- NE/SA605 or NE/SA625
- FLT1-10.7MHz ceramic filter Murata SFE10.7MA5-A (280kHz BW)
- FLT2-10.7MHz ceramic filter Murata SFE10.7MA5-A (280kHz BW)

Note: If a designer wants to use different IF bandwidth filters than the ones used in this application note, the quad tank's S-curve may need to be adjusted to accommodate the new bandwidth.

- C1- Part of the tapped-C network to match the front-end mixer
- C2- Part of the tapped-C network to match the front-end mixer
- C3- Used as an AC short to Pin 2 and to provide a DC block for L1 which prevents the upsetting of the DC biasing on Pin 1
- C6- part of the tapped-C network to match the LO input
- C7- part of the tapped-C network to match the LO input
- C8- DC blocking capacitor
- C9- Supply Bypassing
- C10-Supply bypassing (this value can be reduced if the NE/SA605/625 is used with a battery)
- C11- used as a filter, cap value can be adjusted when higher RSSI speed is preferred over lower RSSI ripple
- C12-used as a filter

- C13-used as a filter
- C14-used to AC ground the quad tank
- C15-used to provide the 90° phase shift to the phase detector
- C16-quad tank component to resonant at 10.7MHz with IFT1 and C15
- C17-IF limiter decoupling capacitor
- C18-DC block for L3 which prevents the upsetting of the DC biasing on Pin 14
- C19-part of the tapped-C network for FLT2
- C20-part of the tapped-C network for FLT2
- C21-IF amp decoupling cap
- C22-DC blocking cap
- C23-IF amp decoupling cap and DC block for L3 which prevents the upsetting of the DC biasing on Pin 14
- C24-provides DC block for L5 which prevents the upsetting of the DC biasing on Pin 20
- C25-IF limiter decoupling capacitor
- C26-part of the tapped-C network for FLT1
- C27-part of the tapped-C network for FLT1
- C28-part of the tapped-C network for FLT1
- C29-part of the tapped-C network for FLT1
- R9- used to convert the current into the RSSI voltage
- R10-converts the audio current to a voltage
- R11-converts the data current to a voltage
- R16-used to kill some of the IF signal for stability purposes
- R17-used in conjunction with R16 for a matching network for FLT2

Demodulating at 10.7MHz IF with the NE/SA605/625

AN1996

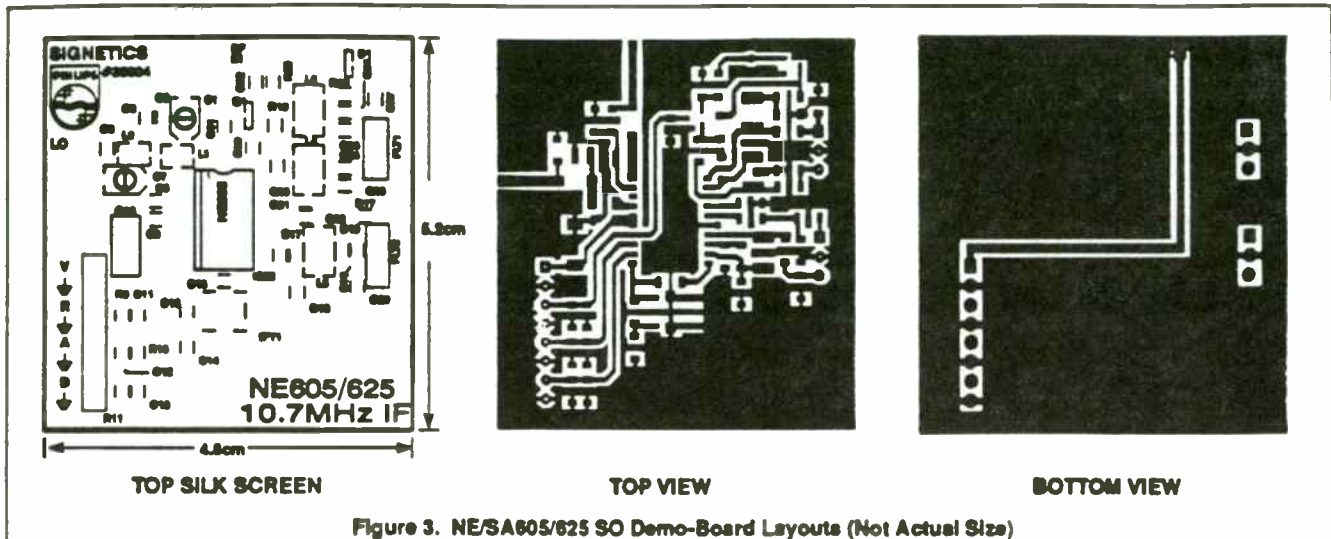


Figure 3. NE/SA605/625 SO Demo-Board Layouts (Not Actual Size)

- L1 - part of the tapped-C network to match the front-end mixer
- L2 - part of the tapped-C network to match the front-end mixer
- L3- part of the tapped-C network to match the input of FLT2
- L4- part of the tapped-C network to match the input of FLT1
- L5- part of the tapped-C network to match the input of FLT1

RSSI Extender Circuit

- R18-provides bias regulation, the gain will stay constant over varying Vcc
- R19-for biasing, buffer RF DC voltage
- R20-provides the DC bias, RSSI gain (when R20 increases, RSSI gain decreases)
- C30-DC blocking capacitor which connects the ceramic filter's output to the PNP transistor's input
- C31-decoupling capacitor, and should be removed for measuring RSSI systems speed
- C32-peak detector charge capacitor
- D1- diode to stabilize the bias current
- Q1- Philips BF579 PNP transistor
- IFT1-part of the quad tank circuit

There are minor differences between Figures 1 and 2. The RF and LO tapped-C component values are changed to accommodate for the different RF and LO test frequencies (RF=240MHz and 45MHz and LO = 229.3MHz and 55.7MHz). The other difference is the value of R20. This resistor value was changed to optimize the RSSI curve's linearity (see RSSI extender section in this application note for further details).

The recommended NE/SA605/625 layout is shown in Figure 3. This layout can be integrated with other systems.

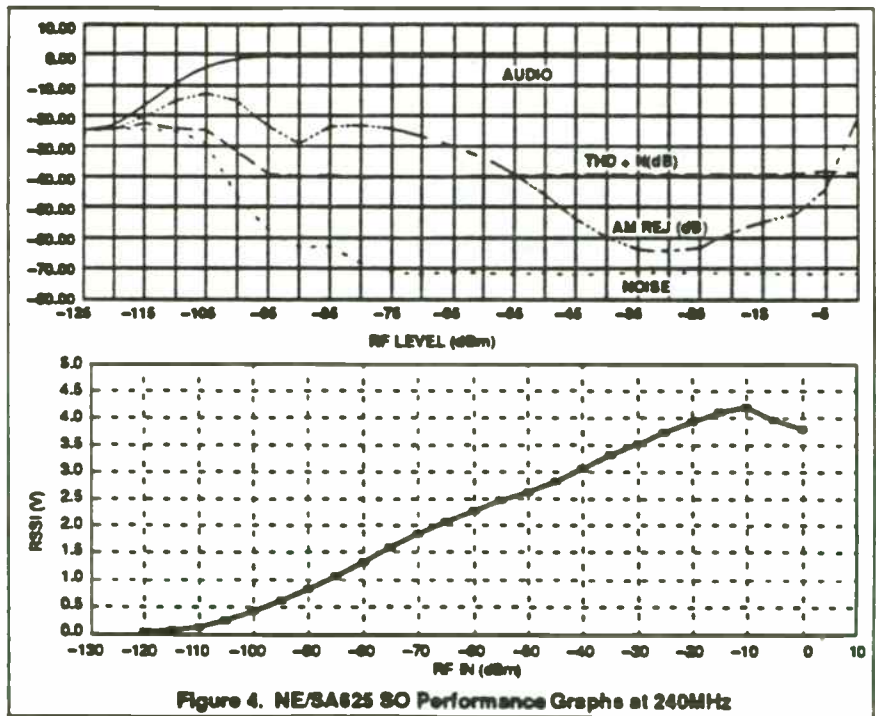


Figure 4. NE/SA625 SO Performance Graphs at 240MHz

Figures 4 through 7 show the performance graphs for the NE/SA605 & NE/SA625 at 240MHz and 45MHz RF inputs. There was no real noticeable difference in performance between a NE/SA605 or NE/SA625 except for AM rejection. The NE/SA605 appears to have a little better AM rejection, but from the end user's point of view, there is no difference between the receiver. All the other measurements were perfect, including SINAD.

RF Input

The NE/SA605/625 board is set up to receive an RF input of 240MHz (see Figure 1). This is achieved by implementing a tapped-C network. The deviation should be set to ±70kHz to achieve -110dBm to -112dBm for -12dB SINAD. However, the deviation can be increased to ±100kHz, depending on the bandwidth of the IF filter and the Q of the quad tank.

Demodulating at 10.7MHz IF with the NE/SA605/625

AN1996

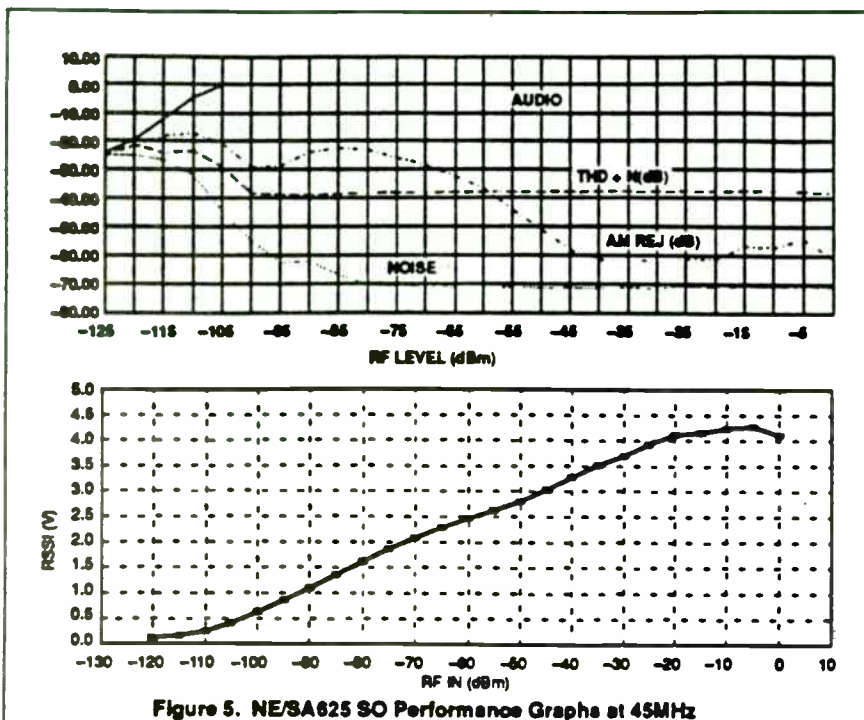


Figure 5. NE/SA625 SO Performance Graphs at 45MHz

frequency. It should be noted that if a designer purchases a stuffed NE/SA605/625 demo-board from Philips Semiconductors its set up will be for an RF input frequency of 240MHz. AN1994 will aid the designer in calculating the tapped-C values for other desired frequencies, while AN1995 will be of value for making S11 bench measurements. Just remember that the input impedance will differ for different RF frequencies.

LO Input

The LO frequency should be 229.3MHz for the RF = 240MHz demo-board and have a drive level of -10dBm to 0dBm (this also applies for the RF = 45MHz and LO = 55.7MHz). The drive level is important to achieve maximum conversion gain. The LO input also has a matched tapped-C network for efficiency purposes which makes for good RF practices.

If a designer wanted to change the matching network to inject a different LO frequency, he/she could follow the steps in AN1994 and assume that the input impedance is around 10kΩ for low frequency inputs. The main goal is to get maximum voltage transfer from the signal generator to the inductor.

An external oscillator circuit was used to provide greater flexibility in choosing different RF and LO frequencies; however, an on-board oscillator can be used with the NE/SA605/625. New high frequency fundamental crystals, now entering the market, can also be used for high LO frequency requirements. Most receiver systems, however, will use a synthesizer to drive the LO port.

10.7MHz Ceramic Filters

The input and output impedance of the 10.7MHz ceramic IF filters are 330Ω. The NE/SA605/625's input and output impedances are roughly 1.5KΩ. Therefore, a matching circuit had to be implemented to obtain maximum voltage transfer. Tapped-C networks were used to match the filters input and output impedance.

But in this case, we decided to go with non-tuning elements to reduce set-up time. Figure 6 shows the values chosen for the network.

Although our total deviation is 140kHz, we used 280kHz IF bandwidth filters to maximize for fast RSSI speed. The SINAD performance difference between using 180kHz BW filter versus 280kHz BS filter was insignificant.

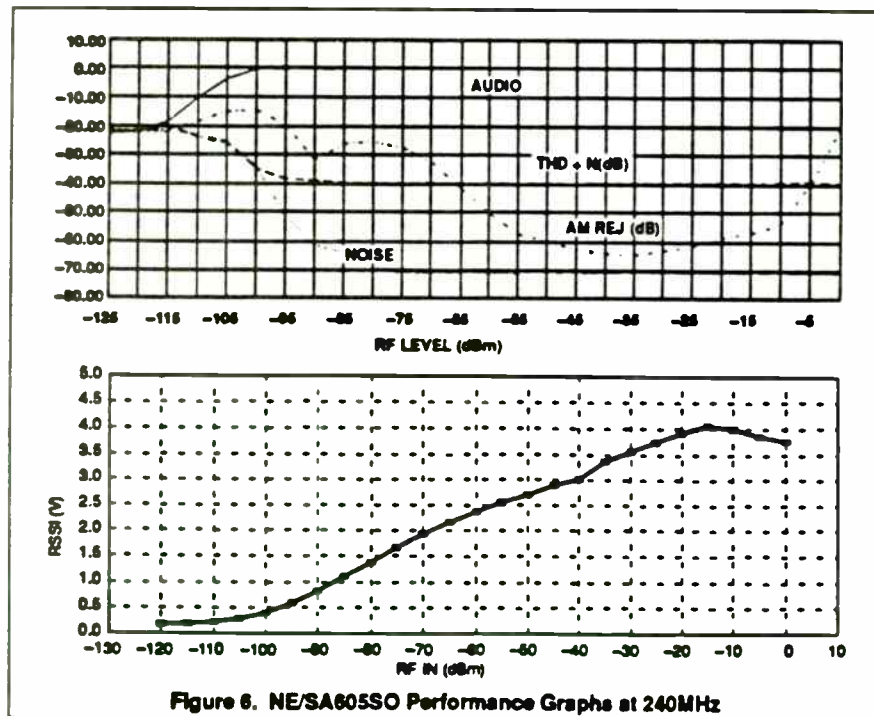


Figure 6. NE/SA605SO Performance Graphs at 240MHz

Because we wanted to test the board at 45MHz, we changed the values of the tapped-C network for the RF and LO ports (see Figure 2). We found that a -116dBm to -118dBm for -12dB SINAD could be achieved. With these results, we were pretty

close to achieving performance similar to our standard 455kHz IF board.

A designer can also make similar RF and LO component changes if he/she needs to evaluate the board at a different RF

Demodulating at 10.7MHz IF with the NE/SA605/625

AN1996

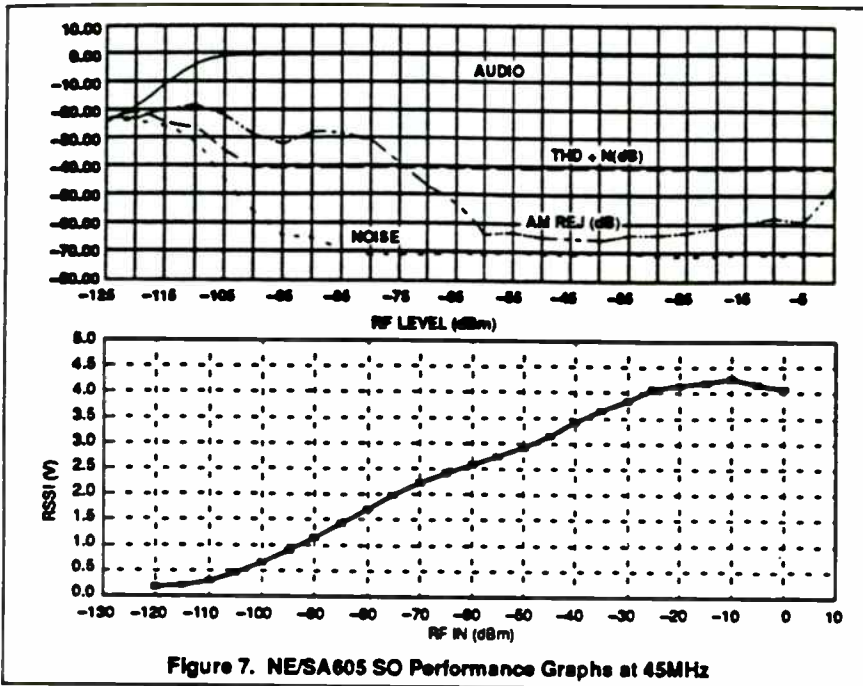


Figure 7. NE/SA605 SO Performance Graphs at 45MHz

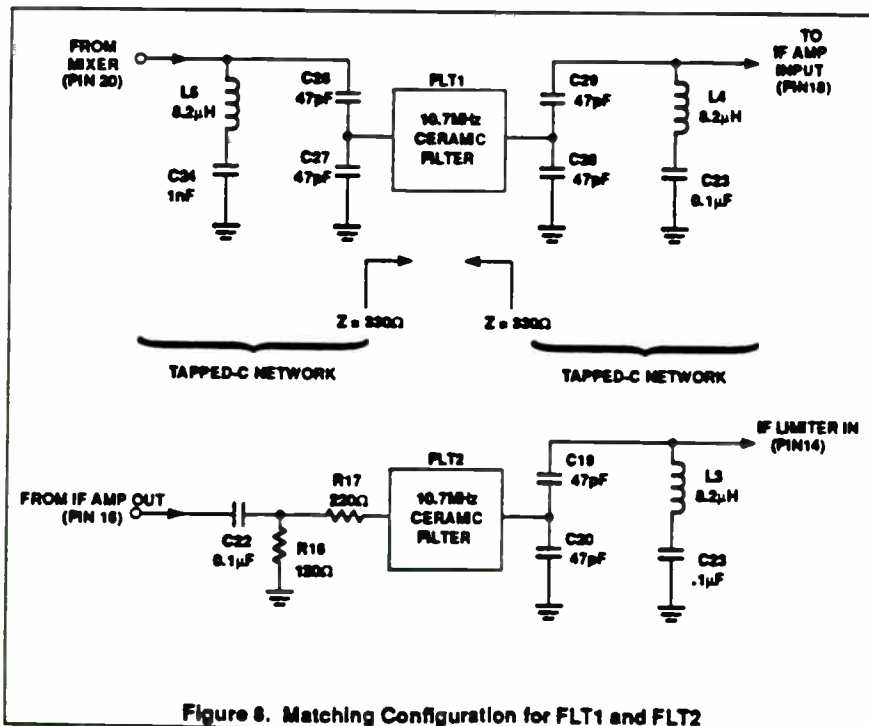


Figure 8. Matching Configuration for FLT1 and FLT2

Stabilizing the IF Section From Regeneration

Because the gain in the IF section is 100dB and the wavelength for 10.7MHz is small, the hardest design phase of this project was to stabilize the IF section.

The steps below show the methods used to obtain a stable layout.

1. The total IF section (IF amp and limiter) gain is 100dB which makes it difficult to stabilize the chip at 10.7MHz. Therefore,

a 120Ω (R16 of Figure 1) resistor was used to kill some of the IF gain to obtain a stable system. (NOTE: Expect AM rejection performance to degrade as you decrease the IF gain externally.)

2. Since the tapped-C inductors for FLT1 and FLT2 are not shielded, it is important not to place them too close to one another. Magnetic coupling will occur and may increase the probability of regeneration.
3. It was also found that if the IF limiter bypass capacitors do not have the same physical ground, the stability worsens. Referring to Figure 1, the IF limiter bypass capacitors (C17, C25) are connected to assure a common ground.
4. The positioning of ground feedthroughs are vital. A designer should put feedthroughs near the IF bypass capacitors ground points. In addition, feedthroughs are needed underneath the chip. Other strategic locations are important for feedthroughs where insufficient grounding occurs.
5. Shielding should be used after the best possible stability is achieved. The NE/SA605/625 demo-board is stable, so shielding was not used. However, if put into a bigger system, shielding should be used to keep out unwanted RF frequencies. As a special note, if a good shield is used, it can increase the R16 resistor value such that there is less IF gain to kill to achieve stability. This means the RSSI dynamic range is improved. So if a designer does not want to implement the RSSI extender circuit, but is still concerned with SINAD and RSSI range, he/she can experiment with R16 and shielding because there is a correlation between them (see RSSI extender section in this application note for more information). In addition, AM rejection performance will improve due to the greater availability of the total IF gain.

The key to stabilizing the IF section is to kill the gain. This was done with a resistor (R16 in Figure 8) to ground. All the other methods mentioned above are secondary compared to this step. Lowering the value of this resistor reduces the gain and the increasing resistor value kills less gain. For our particular layout, 120Ω was chosen to obtain a stable board, but we were careful not to kill too much gain. One of the downsides of killing too much gain is that the SINAD reading will become worse and the RSSI dynamic range is reduced.

Demodulating at 10.7MHz IF with the NE/SA605/625

AN1996

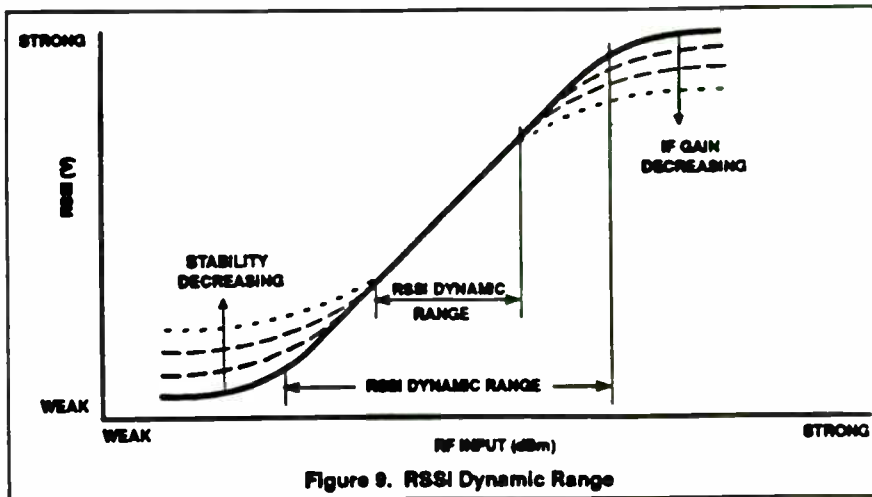


Figure 9. RSSI Dynamic Range

linear dynamic range when the RSSI modification is used.

Referring to Figure 10, one can see that one transistor is used with a few external components. The IF input signal to the PNP transistor is tapped after the ceramic filter to ensure a clean IF signal. The circuit then senses the strength of the signal and converts it to current, which is then summed together with the RSSI output of the chip.

The PNP transistor stage has to be biased as a class B amplifier. The circuit provides two functions. It is a DC amplifier and an RF detector. The gain of the RSSI extender can be controlled by R20 and R9 (Gain = R9/R20). Adjusting R20 is preferable because it controls the upper half of the RSSI curve, whereas adjusting R9 shifts the whole RSSI curve.

If a different RF frequency is supplied to the mixer input, it is important to set the external RSSI gain accordingly. When the RF input was changed from 240MHz to 45MHz, the conversion gain of the mixer increased. Therefore, the earlier gain settings for the RSSI extender was too much. A lower gain setting had to be implemented such that a smoother transition would occur.

Quad Tank

The quad tank is tuned for 10.7MHz ($F = 1/2\pi \sqrt{LC}$). Figure 1 shows the values used (C14, C15, C16, IFT1) and Figure 11 shows the S-curve. The linear portion of the S-curve is roughly 200kHz. Therefore, it is a good circuit for a total deviation of 140kHz. It is possible to deviate at 200kHz, but this does not leave much room for part tolerances.

If more deviation is needed, a designer can lower the S-curve with a parallel resistor connected to the quadrature tank. A designer should play with different value resistors and plot the S-curve to pick the best value for the design. To key in on the resistor value with minimum effort, a designer can put a potentiometer in parallel with the quad tank and tune it for best distortion. Then the designer can use fixed value resistors that are close to the potentiometer's value.

Fixed quad tank component values can be used to eliminate tuning, but a designer must allow for part tolerances and temperature considerations. For better performance over temperature, a resonator/discriminator can be used. Thus, no tuning is required for the quad tank section, which will save on production costs.

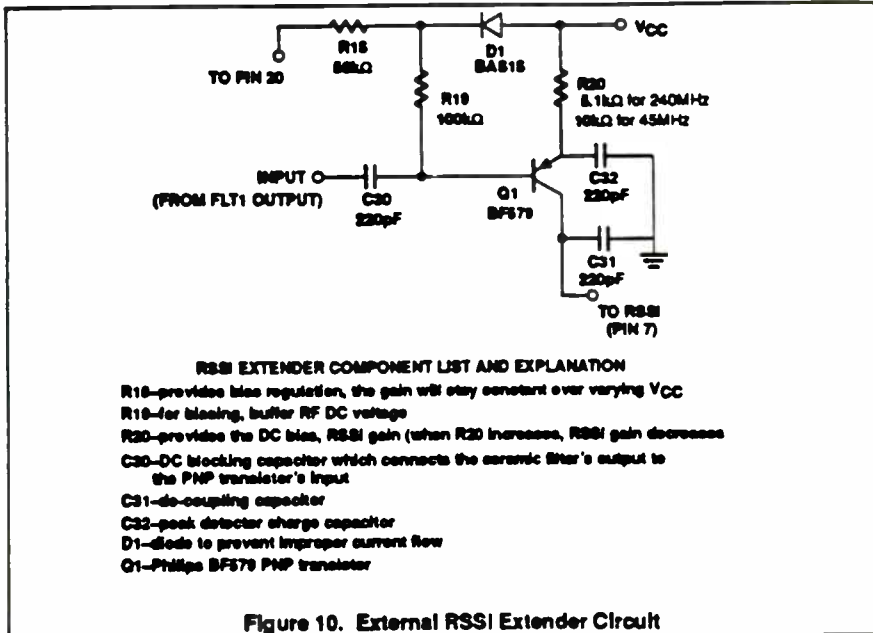


Figure 10. External RSSI Extender Circuit

RSSI Dynamic Range

There are two main factors which determine the RSSI dynamic range. These two factors are 1.) how stable is the board, and 2.) how much gain is killed externally. If the board is unstable, a high RSSI voltage reading will occur at the bottom end of the curve. If too much gain is taken away, the upper half of the curve is flattened. Thus the dynamic range can be affected. Figure 9 shows how the linear range can be decreased under the conditions mentioned above.

It is important to choose the appropriate resistor to kill enough gain to get stability but not too much gain to affect the upper RSSI curve dynamic range. Because we had to kill some IF gain to achieve good board stability and good SINAD readings, our RSSI overall

dynamic range was reduced on the upper end of the curve.

Because SINAD and the RSSI dynamic range are two important parameters for most of our customers, we decided to add an "RSSI extender" modification to the board to get the best of both worlds. Together with the RSSI external modification and the "stability resistor", we can now achieve excellent SINAD readings and maintain a wide RSSI dynamic range.

RSSI Extender Circuit

The RSSI extender circuit increases the upper dynamic range roughly about 20-30dB for the 240MHz demo-board. The NE/SA605/625 demo-board has 90-100dB of

Demodulating at 10.7MHz IF with the NE/SA605/625

AN1996

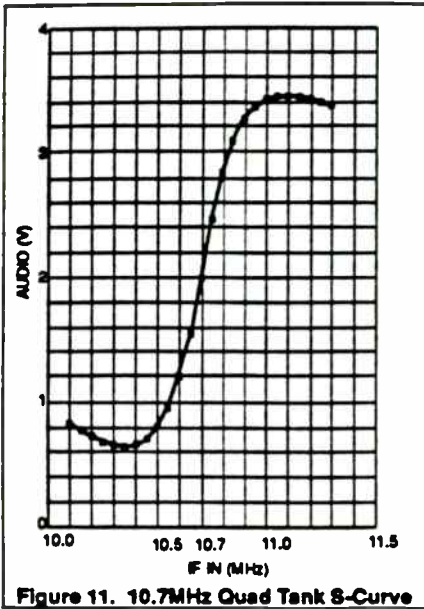


Figure 11. 10.7MHz Quad Tank S-Curve

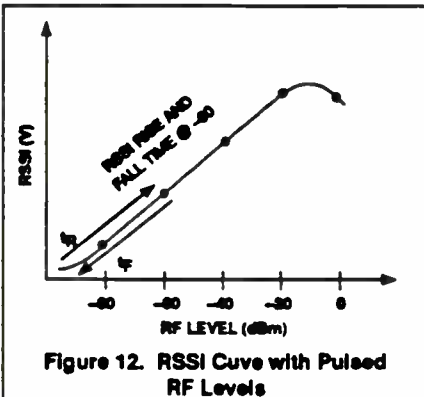


Figure 12. RSSI Curve with Pulsed RF Levels

RSSI System Speed

The RSSI rise and fall times are important in applications that use pulsed RF in their design. The way we define the speed is how fast the RSSI voltage can travel up and down the RSSI curve. Figure 12 shows a representation of this. Five different pulsed RF levels were tested to get a good representation of the RSSI speed. One can predict that the stronger the pulsed signal, the higher the RSSI voltage and the longer it will take for the fall time to occur. Generally speaking, the rise time is determined by how long it takes to charge up an internal capacitor. The fall time depends on how long it takes to discharge this capacitor.

It is also important to understand that there are two types of RSSI speeds. The first type is the RSSI chip speed and the second is the RSSI system speed. The RSSI chip speed will be faster than the system speed. The bandwidth of the external filters and other

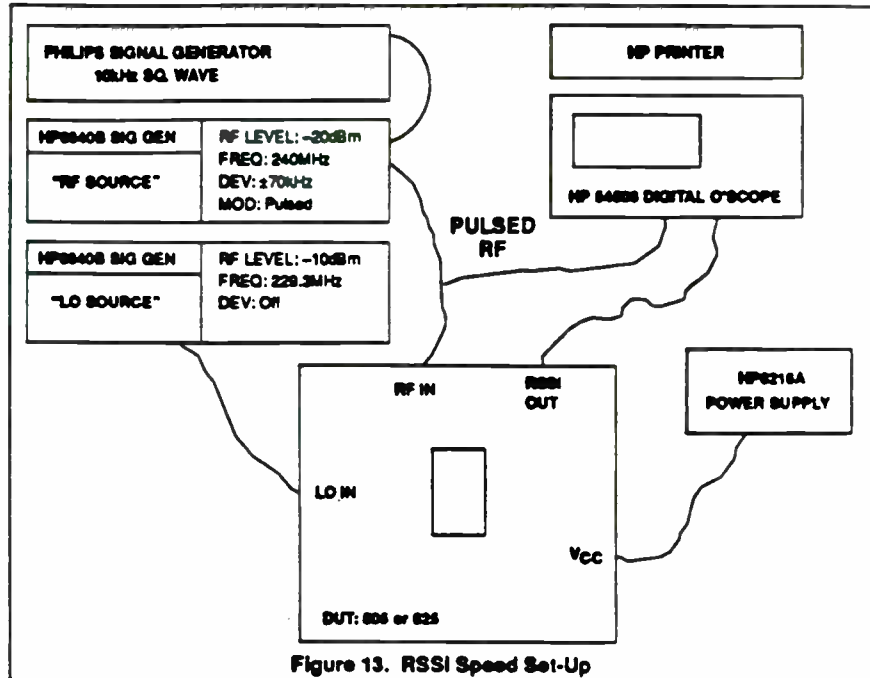


Figure 13. RSSI Speed Set-Up

external parts can slow down the RSSI system speed dramatically.

Figure 13 shows the bench set up for the RSSI system speed measurements. The pulsed RF was set for 10kHz and the RSSI output was monitored with a digital oscilloscope. Figure 14 shows how the rise and fall times were measured on the oscilloscope.

The modifications done on the NE/SA625 board are shown in Figure 15. The RSSI caps C11 and C31 were eliminated, and the RSSI resistor values were changed. We wanted to see how much time was saved by using a smaller RSSI resistor value.

The RSSI system speed for the 240MHz NE/SA625 demo board is shown in Figure 16. Again, the only modification was that the RSSI caps (C11 and C31) were taken out and the RSSI resistor value (R9) was varied. For different RF levels, the speed seems to vary slightly, but this is expected. The higher the RSSI voltage, the longer it will take to come back down the RSSI curve for the fall time.

Looking more closely at Figure 16, one can note that the 0dBm input level has a faster fall time than the -20dBm level. This occurs because of the limited dynamic range of the test equipment. The equipment does not have sufficient on/off range, so at 0dBm the 'off' mode is actually still on. Therefore, you don't get a true reading.

At 0dBm the RSSI voltage is lower than -20dBm. The reason why this happens is because the RSSI linearity range stops at -10dBm. When the RF input drive is too high (e.g., 0dBm), the mixer conversion gain decreases, which causes the RSSI voltage to drop.

QUESTION AND ANSWER SECTION

Q. What should the audio level at Pin 8 be?

A. The audio level is at 580mV_{rms} looking directly at the audio output pin and does not include a C-message filter. However, the audio output level will depend on two factors: the "Q" of the quadrature tank and the deviation used. The higher the quadrature tanks "Q", the larger the audio level. Additionally, the more deviation applied, the larger the audio output. But the audio output will be limited to a certain point.

Q. Am I required to use the 10µF supply capacitor?

A. No, a smaller value can be used. The 10µF capacitor is a suggested value for evaluation purposes. Most of the time a power supply is used to evaluate our demo boards. If the supply is noisy, it will degrade the receiver performance. We have found that a lower value capacitor can be used when the receiver is powered

Demodulating at 10.7MHz IF with the NE/SA605/625

AN1996

by a battery. But it is probably safer to stay at a reasonable capacitor size.

Q. Can I use different IF filters for my required bandwidth specifications?

A. Yes, you can order different IF filters with different bandwidths. Some of the standard manufacturers have 180kHz, 230kHz, and 280kHz bandwidths for 10.7MHz ceramic filters. Just be sure that the quad tank "S-curve" is linear for your required bandwidth. The NE/SA605/625 demo-board has a 200kHz linearity for the quad tank. So ± 70 kHz deviation is perfect.

We have also found that even though the IF filter's bandwidth might be more than our requirements, it does not really degrade overall receiver performance. But to follow good engineering practices, a designer should order filters that are closest to their requirements. Going with wider bandwidth filters will give you better RSSI system speed.

Q. I want to use part of your demo board for my digital receiver project. Can you recommend a good 10.7MHz filter with accurate 10.7MHz center frequency which can provide minimum phase delay?

A. At the present time, I only know of one manufacturer that is working on a filter to meet digital receiver requirements. Murata has a surface mount 10.7MHz filter. The number is FX-6502 (SFECA 10.7). It was specifically designed for Japanese digital cordless phones. You

can adapt these filters to our NE/SA605/625 demo board.

We also used these filters in our layout and got similar SINAD and RSSI system speed performance compared to the standard 10.7MHz filters (280kHz BW). I believe the difference between the filters will be apparent for digital demodulation schemes.

Q. If the system RSSI time is dependent on the external components used, like the IF filters, then what is the difference in using the NE/SA605 vs the NE/SA625?

A. The difference comes in the fall time for high IF frequencies. You are correct that for IFs like 455kHz, there is probably little delta difference because the filter's bandwidth prohibits the speed dramatically. However, for 10.7MHz IFs, there will be a difference in the fall time between the chips because the bandwidths are much wider. Therefore, the chips will play a role in the RSSI system speed. The chip difference in RSSI speed will depend on your overall system configuration.

Q. Why does the AM rejection performance look better on the NE/SA605, 455kHz IF board than the NE/SA605/625 10.7MHz IF demo-board?

A. For the 455kHz IF demo-board there is more IF gain available compared to the 10.7MHz IF board. Recall that for the 10.7MHz IF board, some of the IF gain was killed externally for stability reasons.

Since the IF gain helps improve AM rejection performance, by killing IF gain, AM rejection is decreased.

Q. The NE/SA605/625 10.7MHz IF demo-board is made for the SO package. Can I use your SSOP package and expect the same level of performance?

A. We have not done a SSOP layout yet. But if the same techniques are used, I am sure the SSOP package will work. The SA626 demo-board will be done in SSOP, and probably be available in the future.

Q. I tried to duplicate your RSSI system reading measurements using your demo-board and I get slower times. What am I doing wrong?

A. The RSSI system speed measurements are very tricky. Make sure your cable lengths are not too long. I have found that when making microsecond measurements, lab set-up is of utmost importance. Also, make sure the RSSI caps (C11 and C31) are removed from the circuit.

Also be sure that the bandwidth of your IF filters is not slowing down the RSSI system speed (Cf: section on RSSI system speed).

Q. I am going to use your design in my NTT cordless digital phone. Can you recommend a 240.05MHz filter?

A. Murata SX-4896 (SAMAFC 240.05) is a filter you can use for your application.

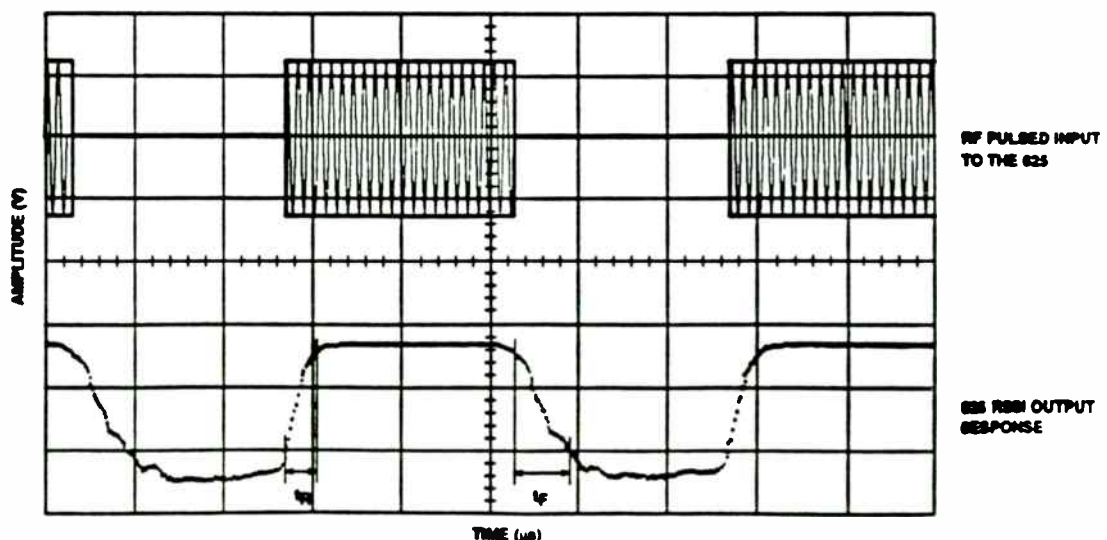


Figure 14. Oscilloscope Display of RSSI System Rise and Fall Time

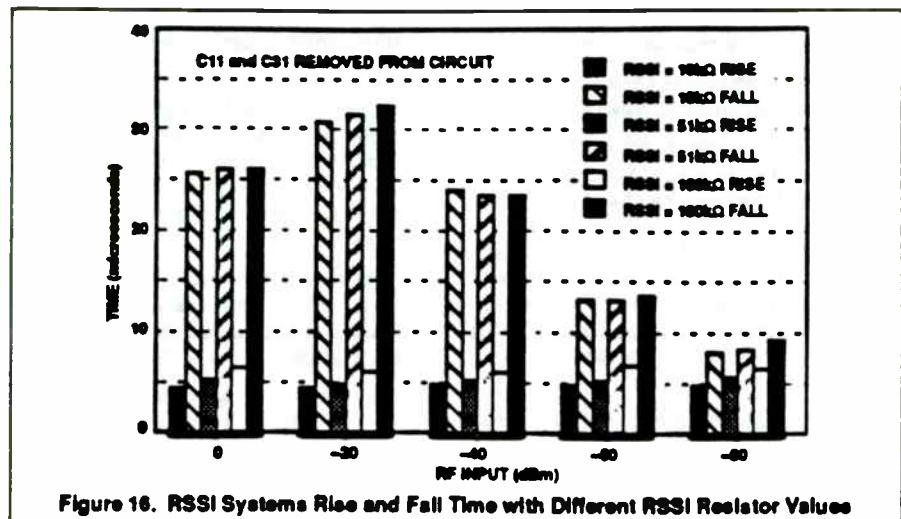
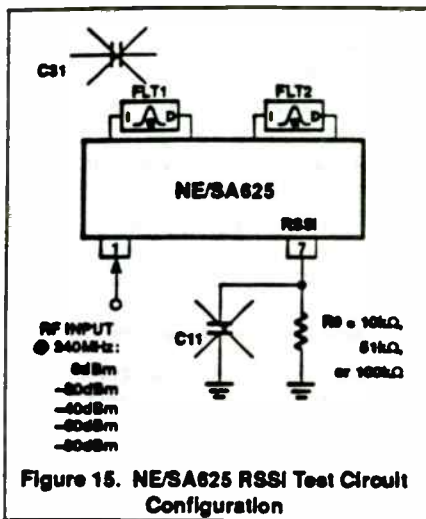


Table 1. FM/IF Family Overview

	NE602A/604A		NE605	NE606	SA607	SA608	NE624	NE625	SA626	NE627	
V _{CC}	4.5-8V	4.5-8V	4.5-8V	2.7-7V	2.7-7V	2.7-7V	4.5-8.0V	4.5-8.0V	2.7-6.5V	4.5-8.0V	
I _{CC}	2.4mA @ 8V	3.3mA @ 8V	5.7mA @ 8V	3.5mA @ 3V	3.5mA @ 3V	3.5mA @ 3V	3.4mA @ 8V	5.8mA @ 8V	6.5mA @ 3V	5.8mA @ 8V	
Number of Pins	8	16	20	20	20	20	16	20	20	20	
Packages NE: 0 to +70°C SA: -40 to +85°C N: Plastic DIP D: Plastic SO FE: Ceramic DIP DK: SSOP	NE602AN NE602AD NE602AFE SA602AN SA602AD SA602AFE	NE604AN NE604AD SA604AN SA604AD	NE605N NE605D NE605DK SA605N SA605D SA605DK	NE606N NE606D NE606DK SA606N SA606D SA606DK	SA607N SA607D SA607DK	SA608N SA608D SA608DK	NE624N NE624D SA624N SA624D	NE625N NE625D NE625DK SA625N SA625D SA625DK	SA626D SA626DK	NE627N NE627D NE627DK SA627N SA627D SA627DK	
-120dB SINAD (RF = 455kHz), IF = 455kHz 1kHz Tone, 8kHz Dev.	-120dBm / 22µV		-120dBm / 22µV	-117dBm / 31µV	-117dBm / 31µV	-117dBm / 31µV	-120dBm / 22µV	-120dBm / 22µV	-112dBm / 54µV (RF = 240MHz) (IF = 10.7MHz) 1kHz Tone, ±70kHz Dev.	-120dBm / 22µV	
Process f ₁	8GHz		8GHz	8GHz	8GHz	8GHz	8GHz	8GHz	8GHz	8GHz	
For lower cost version and less performance	612A & 614A		615	616	617	—	—	—	—	—	
Features	<ul style="list-style-type: none"> - Audio & Data pins - IF BW of 25MHz - No external matching required for standard 455kHz IF filter 		<ul style="list-style-type: none"> - Audio & Data pins - IF BW of 25MHz - No external matching required for standard 455kHz IF filter 	<ul style="list-style-type: none"> - Low voltage - Internal RSSI and audio op amps - No external matching required for standard 455kHz IF filter - IF BW of 2MHz 	<ul style="list-style-type: none"> - Freq check pin - Low voltage - Internal RSSI and audio op amps - Unity gain RSSI output - No external matching required for standard 455kHz IF filter - IF BW of 2MHz 	<ul style="list-style-type: none"> - Freq check pin - Low voltage - Internal RSSI and audio op amps - Unity gain audio output - No external matching required for standard 455kHz IF filter - IF BW of 2MHz 	<ul style="list-style-type: none"> - Fast RSSI Time - Pin-to-Pin compatible with 604A - No external matching required for standard 455kHz IF filter 	<ul style="list-style-type: none"> - Fast RSSI Time - Pin-to-Pin compatible with 605 - No external matching required for standard 455kHz IF filter 	<ul style="list-style-type: none"> - Power down mode - Low voltage - Fast RSSI Time - IF BW of 25MHz - Internal RSSI & audio op amps - No external matching required for standard 10.7MHz IF filter 	<ul style="list-style-type: none"> - Fast RSSI Time - Freq check pin - IF BW of 25MHz - Internal RSSI & audio op amps - No external matching required for standard 455kHz IF filter 	
RSSI OUTPUT SECTION	Dynamic Range		90dB	90dB	90dB	90dB	90dB	90dB	90dB	90dB	
	Accuracy		±1.5dB	±1.5dB	±1.5dB	±1.5dB	±1.5dB	±1.5dB	±1.5dB	±1.5dB	
	455kHz IF	Rise Time	—	1.4µs	—	—	—	1.1µs	1.2µs	—	1µs
		Fall Time	—	21.3µs	—	—	—	1.3µs	2.1µs	—	1.7µs
10.7MHz IF	Rise Time	—	1.5µs	—	—	—	1.2µs	1.2µs	1.2µs	0.9µs	
	Fall Time	—	19.4µs	—	—	—	1.9µs	2µs	2µs	1.4µs	

*NOTE: No IF filter in the circuit

Table 1. (cont.) FM/IF Family Overview

	NE602A/604A	NE605	NE606	SA607	SA608	NE624	NE625	SA626	NE627
Misc. Conversion Power Gain (RF = 45MHz; IF = 455kHz)	17dB	13dB	17dB	17dB	17dB	—	13dB	13dB	13dB
3rd Order Intercept Point (Input)	-13dBm	-10dBm	-8dBm	-8dBm	-8dBm	—	-10dBm	-11dBm I1 = 240.05 I2 = 240.35	-10dBm
1 st = 45MHz I2 = 45.05MHz									
Noise Figure @45MHz	5dB	5dB	6.2dB	6.2dB	6.2dB	—	5dB	11dB @ 240MHz	5dB
RF Input Resistance and Capacitance @45MHz	1.5k 3pF	4.7k 3.5pF	1k 3pF	1k 3pF	1k 3pF	—	4.7k 3.5pF	4.7k 3.5pF @ 240MHz	4.7k 3.5pF
Output Resistance	1.5k	1.5k	1.5k	1.5k	1.5k	—	1.5k	300	1.5k
Input Impedance	—	1.5k	1.5k	1.5k	1.5k	1.5k	1.5k	300	1.5k
Output Impedance	—	1.5k	300	300	300	1.5k	1.5k	300	1.5k
Gain	—	40dB	44dB	44dB	44dB	40dB	40dB	44dB	40dB
BW	—	41MHz	5.5MHz	8.5MHz	5.5MHz	41MHz	41MHz	40MHz	40MHz
Input Impedance	—	1.5k	1.5k	1.5k	1.5k	1.5k	1.5k	300	1.5k
Output Impedance	—	300	300	300	300	300	300	300	300
Gain	—	60dB	56dB	56dB	56dB	40dB	60dB	60dB	60dB
BW	—	28MHz	4.5MHz	4.5MHz	4.5MHz	28MHz	28MHz	28MHz	28MHz
Total IF Gain	—	100dB	100dB	100dB	100dB	100dB	100dB	86dB (includes -6dB pad)	100dB
Total IF BW	—	28MHz	28MHz	28MHz	28MHz	28MHz	28MHz	28MHz	28MHz

NOTE: *Not designed to drive a matched load

Windata Inc.

WIRELESS INFORMATION NETWORKS

Greg Hopkins

Chairman & CEO

10 Bearfoot Road

Northboro, MA 01532

508-393-3330

11/11/92

Agenda

- Wireless LANs - Why all the fuss?
- Market Opportunities
- Technology Options
- Standards, The FCC, and International
- Technology Trends

What is a Wireless LAN?

- Systems operating at >1 Mbps
- Broadcast packet communications
- Indoor / In-building applications
- 30-100 meter distance coverage
- Current technology focus is radio in unlicensed frequency bands

RD 1.1

Why all the fuss?

- **The LAN connection of choice for portable computers**
- **Augmentation to existing wired LANs**
 - **Rapid deployment**
 - **Construction limitations**
 - **Aesthetics**
 - **Labor intensive adds and changes**
- **Wiring alternative for interbuilding links**

RD 1.1

Wireless LAN Market Forecast

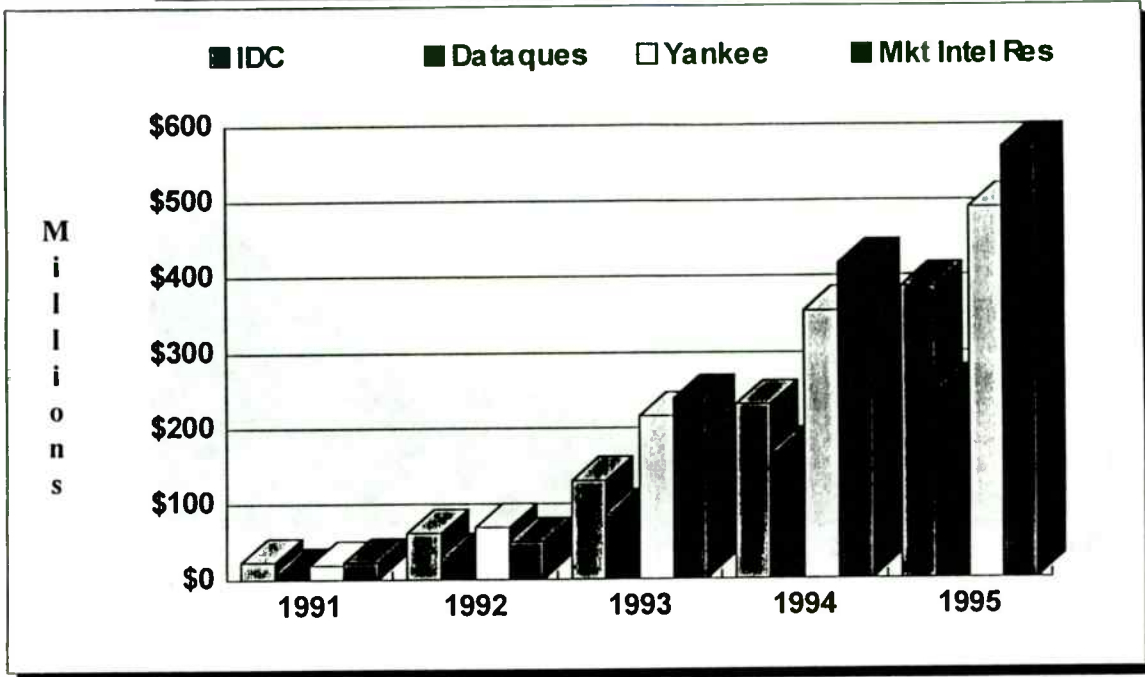


FIG. 5

WLAN Market Size - \$

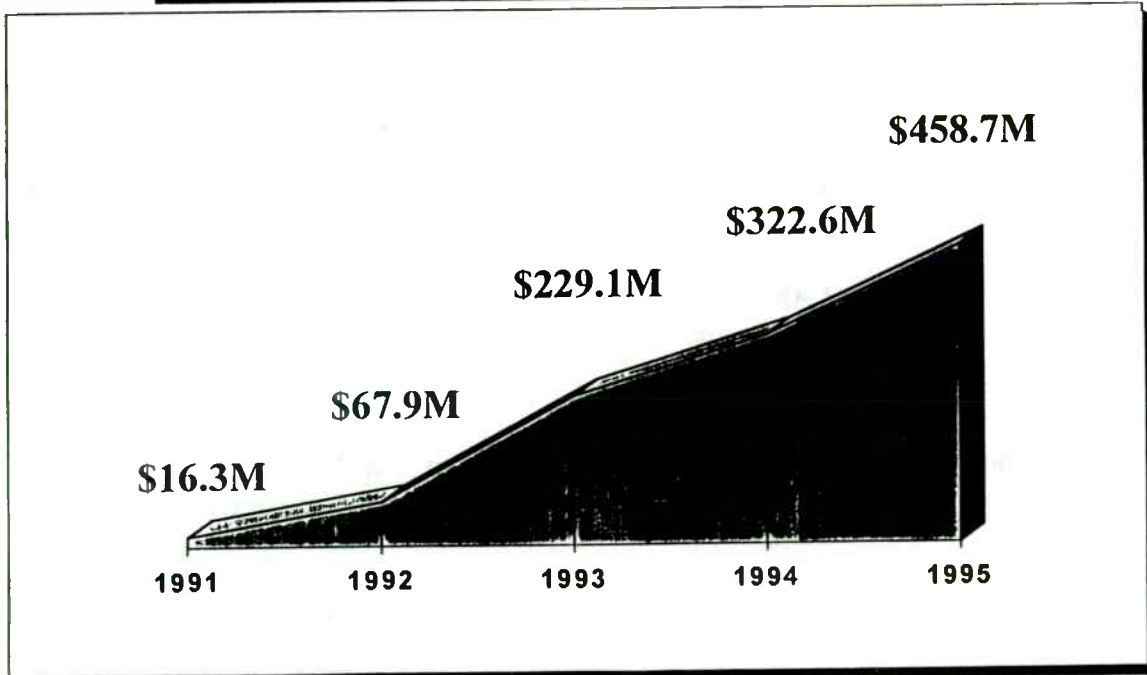
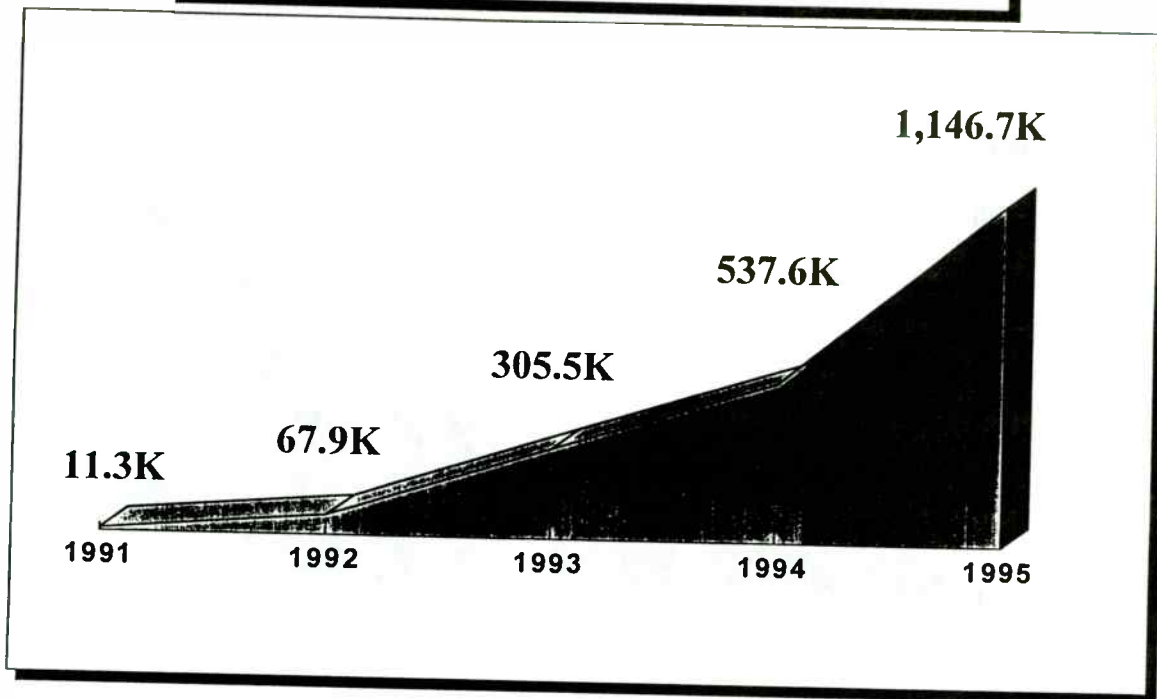


FIG. 6

WLAN Market Size - Units



914 7

Market Segmentation

Wireless Data Network Market Segmentation

<u>Attribute</u>	<u>In-Business</u>	<u>Outdoor/Mobile</u>	<u>Home</u>
License?	no	maybe	equipment certified
Data Rate	LAN speeds	< 50 Kbps	< 1 mbps (ISDN?)
Distance	<100 meters	>> 100 meters	< 100 meters
Voice & Data	maybe	yes	yes
\$/bit or \$/sec	no	yes	no
Typical Application?	Your portable connected to the Corporate LAN	Your PDA in your car with digital voice (PCS)	High quality digital voice, message storage, LAN, and phone line/cable connection for your in-house network

What are the market drivers?

- **Product cost**
 - > \$1000 - rapid deployment/harsh environments
 - \$500-1000 - wired LAN augmentation
 - <\$500 - portables/general usage/why use wire?
- **Growth of networked portables**
- **Killer applications**
 - Enterprise network services for portables
 - Wireless classroom
 - Wireless business meeting

R01.0

Infrared Transmission

- **Infrared**

Point-to-point	10 Mbps, 1km, LOS
Focused Shared Beam	1 Mbps, 100 ft, reflected
Diffuse	1 Mbps, 20 ft, diffuse
- **Diffuse Infrared is the most promising infrared option**
- **Laser and High Power Infrared**

R01.10

Radio Transmission

- **Four Radio choices:**
 - **Licensed (Motorola at 18 GHz)**
 - **Unlicensed Part 15(902-928, 2400-2485, 5700-5825 MHz)**
 - Direct Sequence**
 - Frequency Hopped**
 - **Low Power**
 - **New Part 15 Allocation(1910-1930 MHz)**

RF 11

Windata's Solution

- **Spread Spectrum "radio" based family of products**
 - **Offer family of products in three major categories:**
 - Ethernet and token ring* products that integrate transparently to enterprise structured wire at LAN speed and performance
 - Inter-building* wireless products
 - Portable computing* battery operated wireless LANs
- All systems focused on high performance, easy connection to wired systems, and SNMP network management**

The Indoor Radio Problem

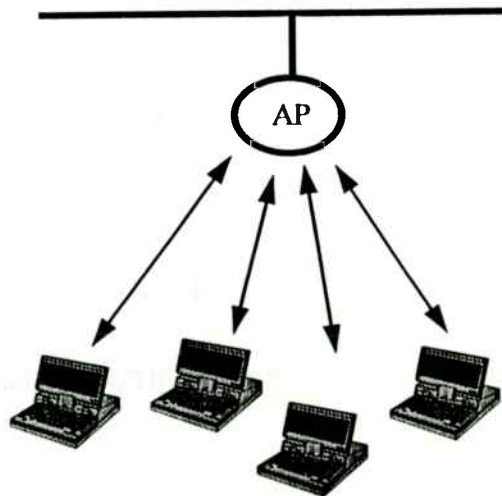
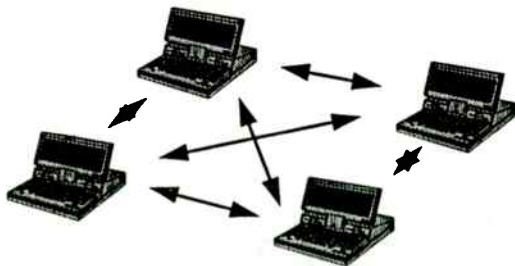
- **Multipath**
Reflections
- **Outages**
Difficult locations disrupting system operation
- **Propagation path changes**
Doors closing, people moving, etc.

Surprisingly, signal power is not the major problem!

2014.11

The Architectural Question

Is the system peer to peer
or controller based?



2014.11

Why a Hub or Access Point?

- Consistent with structured wire installations
- Doubles service area over peer to peer
- Solves near-far problem
- Simplifies and reduces cost of transceiver
- Provides focus for network management
- Provides logical interface point to wired LANs
- Provides wake-up capability for reduced power consumption

Reliable wireless data communications systems cannot be built without a hub or access point

801.14

The FCC & Standards

- **IEEE-802.11**
- **FCC and DATA-PCS**
- **The WINForum**
- **Motorola and 18 GHz licensing**

International Activities

- Europe is looking at 2.4 and 5.2 GHz (lower power than US)
- Japan at 2.4 GHz, 300 Mhz, but 30 milliwatts
- Many companies are building 2.4 GHz spread spectrum systems because of potential international opportunity
- Data-PCS band is a very appealing because it is a clear channel(?), capable of being a silicon radio, and without spread spectrum restrictions

804-17

A Low Current UHF Remote Control System using a SAW based superhet receiver

M. Bopp, J. Strohal
TEMIC
TELEFUNKEN microelectronic GmbH
7100 Heilbronn
Germany

ABSTRACT

This paper presents a new technical approach to a low current UHF remote control system. This system is universal with regard to modulation systems (AM or FM), different transmission coding and a wide range of data rates. After a description of the system's boundary conditions and the SAW (surface acoustic wave resonator) stabilized single stage transmitter, we are focusing on the receiver. The superheterodyne receiver is likewise SAW based with a very low average current consumption of approximately 1 mA. This outstanding feature is achieved by a standby concept in conjunction with a special circuit arrangement and an application specific Integrated Circuit.

The standby concept minimizes the current consumption of the receiver by utilizing the fact, that some functions are not permanently required. Therefore two receiver modes exist. First in the standby mode only those parts are turned on which are needed to detect the presence of a relevant signal, and if necessary to switch the receiver to the active mode. In this second mode the remaining components, which are needed for further signal processing, are enabled and current consumption is consequently increased.

The special circuit arrangement consists in the stacking of circuit stages for current reduction. This DC stacking appears on the one hand inside the tuner, which is realized using special discrete UHF transistors, and on the other hand in the cascading of the entire tuner with the remaining IF and baseband parts, which are covered by a single IC.

This monolithic IC in bipolar technology includes all necessary parts from IF signal processing to data output. In detail these are standby power control, IF amplifier, FM demodulator with adjustable discriminator bandwidth, logarithmic received signal strength indicator suited as an AM demodulator, high performance operational amplifier to realize a signal adapted baseband filter and a clamping comparator for additional noise suppression and data regeneration.

The performance of the described system is discussed by using measurement results of realized universal 433.92 MHz transmitter and receiver modules. A prospect of possible further developments will round off this presentation.

INTRODUCTION

In the present age of modern communication and increasing mobility we recognize a raising need for remote control systems. Reasons for using wireless systems are numerous and can not only be for comfort, versatility and flexibility but also for safety and cost savings. This is valid for various applications, as keyless entry systems for cars and buildings, alarm and security systems, domestic installation and wireless data transfer systems.

Recently in some areas low-power radio links are replacing infrared systems. Especially in the car market, which was the initial target for us, infrared systems experienced transmission problems due to dirt, ice and snow. Nowadays often the car's windows are additionally shaded to reduce excessive heating of the car interior. Unfortunately the shading attenuates the IR transmission of the remote control systems just as much as the emission from the sun.

RF systems operating in the UHF band are not restricted to the line-of-sight coverage of optical systems due to diffraction and reflection of radio waves at edges and conductive surfaces, as well as their capability to penetrate dielectric materials. This becomes apparent in an even illumination of space under complicated spatial circumstances as in buildings. Also the necessity to aim with the transmitter at the receiver is removed, because the commonly used small low gain aerials show an almost perfect omnidirectional radiation pattern. The range of the RF system can not be well defined because of the said propagation characteristic and due to additional polarization losses. These may vary from zero up to approximately 20 dB depending on the relative orientation of the transmitter and the receiver antennas.

As has been shown, IR as well as RF systems have advantages and drawbacks and therefore they are likely to co-exist. A more detailed comparison of the two systems can be found in [1].

SYSTEM CONTEMPLEMENTATIONS

To be able to appraise a system, one needs to know the boundary conditions and objectives, it is based upon. So every developer of a remote control system must be aware of his special requirements. The mere attempt to expound all possible requirements would be beyond the scope of this paper. Nevertheless we will not fail to mention some marked points, which seem to be relevant for most applications. Customers usually keep their eyes on range, safety in operation, current consumption, response time, size of the system's components and last but not least of course the price. Additionally the legal regulations in the particular country has to be considered.

From the boundary conditions technical attributes can be derived such as used frequency band, transmitter power, receiver sensitivity, modulation system, data rate and coding techniques. Most of these aspects depend on each other and some of them will be discussed in the subsequent explanations.

To get an overview let us first look at the block diagram (see figure 1). To simplify matters we consider an uni-directional transmission system. Therefore we need only one transmitter and a single receiver. Nevertheless most of the following considerations apply also to multi-directional systems.

Both transmitter and receiver can be subdivided into a digital and an analog section. The digital part of the transmitter encodes the information to a serial bit stream which can be modulated upon a RF carrier. This is done in the RF transmitter unit.

Vice versa in the receiver module the serial data signal is recovered and the subsequent decoder makes the transmitted information available at its control outputs. The frequency of the radio link in our example is 433.92 MHz but any other frequency in the UHF range can be used after minor modifications of the RF part of the transmitter and the tuner of the receiver.

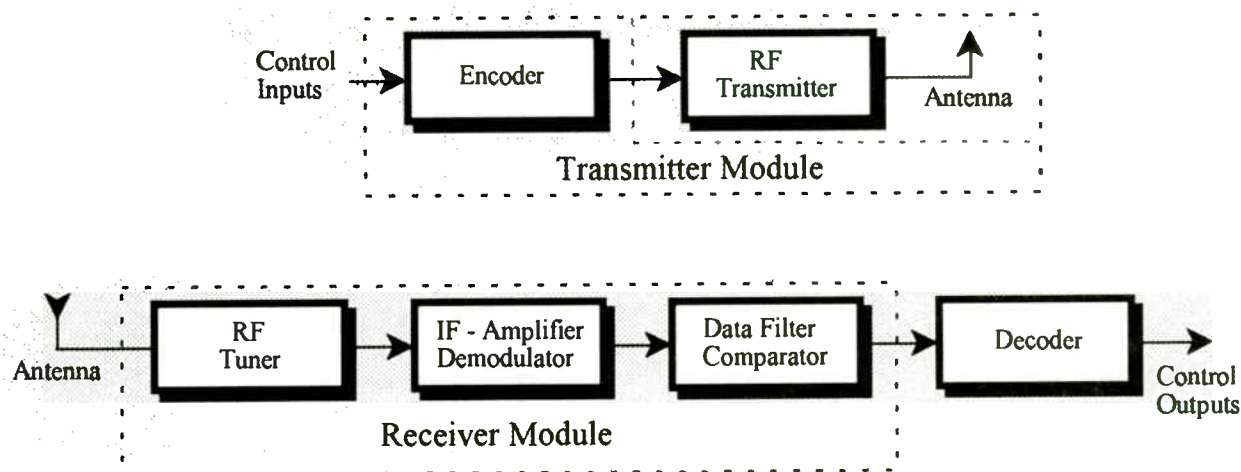


Figure 1: UHF - Remote Control System

The benefits of the UHF range become obvious by a study of the radio wave propagation versus frequency. For simplification we assume free space propagation and consider only the far field region. Referring to a transmission at a frequency f , respectively a wavelength λ , the received power P_R in a distance d from the transmitter, with output power P_T and an antenna gain G_T referred to an isotropic radiator, respectively G_R on the receiver side is according to reference [2]

$$P_R = P_T \cdot \frac{\lambda^2}{(4 \cdot \pi \cdot d)^2} \cdot G_T \cdot G_R \quad (1)$$

The logarithmic attenuation ratio L_0 for free space propagation is defined as

$$\begin{aligned} \frac{L_0}{dB} = & -10 \cdot \log \frac{P_R}{P_T} = 32.5dB + 20 \cdot \log \frac{d}{km} + \\ & + 20 \cdot \log \frac{f}{MHz} - 10 \cdot \log G_T - 10 \cdot \log G_R \quad (2) \end{aligned}$$

Taking the widespread demand for small size into account, a small loop antenna seems to be a good choice. The pattern of such an antenna is equal to that of a Hertzian dipole with a gain of $G = 1.5$. Supposing the transmitter, as well as the receiver antennas, are to be of that kind ($G_T = G_R = 1.5$), we obtain from equation (2)

$$\frac{L_0}{dB} = 29.0dB + 20 \cdot \log \frac{d}{km} + 20 \cdot \log \frac{f}{MHz} \quad (3)$$

Next the total radiated power P_T of such a small loop of w turns tuned with a parallel capacitor is deduced

analogically to that of an electrical Hertzian dipole [3]. Assuming a spherical coordinate system, electric and magnetic intensities are

$$H_{\vartheta} = H_{\max} \cdot \sin \vartheta = \frac{2 \cdot \pi \cdot w \cdot A}{\lambda} \cdot \frac{I}{2 \cdot \lambda} \cdot \frac{\sin \vartheta}{r} \cdot e^{-j \frac{2 \cdot \pi \cdot r}{\lambda}} \quad (4)$$

and

$$E_{\varphi} = E_{\max} \cdot \sin \vartheta = -\frac{\pi \cdot w \cdot A \cdot I}{\lambda^2} \cdot \frac{\sin \vartheta}{r} \cdot Z_0 \cdot e^{-j \frac{2 \cdot \pi \cdot r}{\lambda}} \quad (5)$$

related by the free-field characteristic impedance Z_0

$$E_{\varphi} = -Z_0 \cdot H_{\vartheta} \quad (6)$$

The surface integral of the power density S yields the total radiated power P_T

$$P_T = \iint S \cdot dO = \frac{1}{2} \cdot \iint E_{\varphi} \cdot H_{\vartheta} \cdot dO = \frac{1}{2} \cdot \iint \frac{E_{\varphi}^2}{Z_0} \cdot dO \quad (7)$$

Substitution of the electric intensity (5) and solving the integral yields

$$\begin{aligned} P_T &= \frac{E_{\max}^2}{Z_0} \cdot \int_0^{\pi} \sin^2 \vartheta \cdot 2 \cdot \pi \cdot r \cdot \sin \vartheta \cdot r \cdot d\vartheta = \\ &= 2 \cdot \pi \cdot r^2 \cdot \frac{E_{\max}^2}{Z_0} \cdot \int_0^{\pi} \sin^3 \vartheta \cdot d\vartheta = \frac{8}{3} \cdot \pi \cdot r^2 \cdot \frac{E_{\max}^2}{Z_0} \quad (8) \end{aligned}$$

with

$$E_{\max} = \frac{2 \cdot \pi \cdot w \cdot A}{\lambda} \cdot \frac{I}{2 \cdot \lambda} \cdot \frac{1}{r} \cdot Z_0 \cdot e^{-j \frac{2 \cdot \pi \cdot r}{\lambda}} \quad (9)$$

and

$$|E_{\max}| = \frac{\pi \cdot w \cdot A}{\lambda^2} \cdot \frac{I}{r} \cdot Z_0 \quad (10)$$

Hence

$$P_T = \frac{8 \cdot \pi^3 \cdot w^2 \cdot A^2 \cdot I^2 \cdot Z_0}{3 \cdot \lambda^4} \quad (11)$$

The Quality Q of the resonant circuit determines the resonance step-up of the loop current. With the impressed output current I_T from the transmitter to the antenna the effective loop current is equal to

$$I = I_T \cdot Q \quad (12)$$

Furthermore the area A of the circular loop with a diameter D is

$$A = \frac{\pi \cdot D^2}{4} \quad (13)$$

Herewith we get

$$P_T = \frac{\pi^5 \cdot w^2 \cdot Z_0}{6} \cdot \left(\frac{D}{\lambda}\right)^4 \cdot I_T^2 \cdot Q^2 \quad (14)$$

Substituting P_T from (14) in (1) we derive

$$P_R = \frac{\pi^5 \cdot w^2 \cdot Z_0}{6} \cdot \left(\frac{D}{\lambda}\right)^4 \cdot I_T^2 \cdot Q^2 \cdot \frac{\lambda^2 \cdot G_T \cdot G_R}{(4 \cdot \pi \cdot d)^2} \quad (15)$$

and with the assumption $G_T = G_R = 1.5$ (two small single turn loop aerials) finally

$$P_R = \frac{3 \cdot \pi^3 \cdot w^2 \cdot Z_0}{128 \cdot d^2} \cdot \frac{D^4}{\lambda^2} \cdot I_T^2 \cdot Q^2 \quad (16)$$

As we can see from this formula, received power is directly proportional to Q^2 and D^4 , whereas inversely proportional to λ^2 . This equation is only valid, if the diameter D of the loop is small compared to the wavelength λ . Furthermore Q is not independent of D and λ . Particularly losses due to skin effect increase with frequency and reduce Q . Therefore owing to circumstances a practical optimum does exist.

Exemplary the total transmitted and received power will be calculated at 40 MHz, 433.92 MHz and 2400 MHz, because these are frequently used bands. The corresponding Q values are roughly estimated to 100, 60 and 10. Assuming $D = 1$ cm and $I_S = 2$ mA, the transmitted power P_T at the above mentioned frequencies is -56, -19 and -5 dBm whereas the received power P_R in a distance $d = 20$ m will be -83, -67 and -68 dBm respectively. This applies to free space propagation and shows that higher frequencies are favourable when using such a small antenna.

In practical operation some additional factors influence the propagation characteristic. Diffraction and reflection of radio waves at edges and conductive surfaces as well as their capability to penetrate dielectric materials is frequency dependent. RF is shielded by metallic structures if the size of the gaps and slots of the structure are small compared to the wavelength. This fosters higher frequencies as well. On the other side, if one bears in mind, that propagation losses due to H_2O absorption and reflections by dielectric layers (e.g. window panes) are increasing rapidly at frequencies above 2 GHz, the UHF range reveals to be the best frequency choice for our purposes. Moreover the low absorption of radio waves in the UHF band by H_2O molecules is beneficial because this pays regard to human protection.

However, the formulae from above can be used to get a course impression of the required receiver sensitivity for a

given transmitter design and a claimed minimum operating range. The conformity of the levels, calculated according to the above valuations (15,16), with experimental results is good. Under the given circumstances, among others the operating frequency of

433.92 MHz, and considering additional losses due to antenna shielding problems and polarisation mismatch a typical operation sensitivity of -80 dBm is marginal for a reliable and trouble free operation.

TRANSMITTER

The transmitter module contains not only the RF transmitter but also either a data and control interface or even a μC or μP for encoding (see fig.1). Concerning the transmitter we will not go into details because one can find several realization proposals in various application notes for instance of SAW resonator suppliers [4],[5].

In a simple design it consists only of one single stage, a SAW based oscillator whose inductance of the tank circuit is realized as a loop and acts also as antenna. When designing the RF transmitter equation (14) is important. Let us direct our attention to the parameter Q. A doubling of Q yields a four times larger total transmitted power.

Another benefit of high Q is less obvious but as least as important. The higher the quality, the greater the ratio of the effective current of the fundamental wave compared to the current of the harmonics, because the resonance step-up appears only at the resonance frequency of the antenna circuit. Therefore the suppression of radiated harmonics is essentially determined by the quality of the aerial.

The RF transmitter can be amplitude modulated by switching the base voltage of the transistor as well as frequency modulated by the help of a varicap in the tank circuit (see fig. 2 and 3).

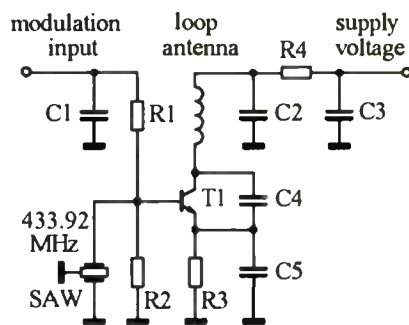


Figure 2: UHF - Transmitter, AM version

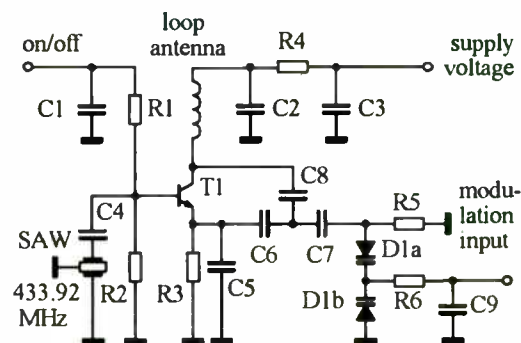


Figure 3: UHF - Transmitter, FM version

RECEIVER

One of the most stringent requirements is the very low current consumption of the receiver. At first claimed out of the quarter of car manufacturers the demand for an average current consumption of maximal 1 mA was adopted in several other fields of application, for instance to supply the receiver from a mains independent solar buffered accumulator.

Principle of operation

To realize such a receiver two principles of operation are favourable:

Using the polling method, the receiver is periodically switched on for short times. During the active periods, current consumption can be higher than 1 mA whereas in the interim the receiver is entirely turned off. Herewith the average current consumption depends on the duty

cycle, which is the ratio of times when the receiver is active compared to when it is switched off. Unfortunately this duty cycle determines also the reaction time of the system. This means, that the non active intervals can not be enlarged over the maximal permissible response time of the system. In addition the active period can not be made arbitrary short, because during this time the receiver has to decide whether a relevant signal is being received. In that case the receiver remains in the active mode, at least for the expected duration of a potential transmitted signal. This method is very favourable with respect to system sensitivity, because the receiver has its maximum sensitivity when it is active.

If the reaction time is a critical parameter, a second conception called wake up method, is more advantageous. Also here two modes exist. In the low power standby mode with a current consumption of about 1 mA only those parts are turned on, which are necessary to detect

the presence of a possibly relevant signal. If such a signal is detected, which means that the received signal strength exceeds a given threshold, the receiver itself switches on (wakes up) the remaining parts which are necessary for signal processing. In this active mode, current consumption is increased. After an adjustable hold-time, in the course of which the signal strength is below the threshold, the receiver automatically switches back to the standby mode. The distinctive feature of this system compared to the polling system lies in a reduced sensitivity in the standby mode. To avoid false alarms, which raise the average current consumption for no purpose, the wake up circuit shall not be triggered by noise or weak interference. Therefore the wake up threshold, respectively the time constant of the integrator in the wake up circuit which determines the necessary energy of a trigger signal, must not be too small. A reduction of the false alarm probability implies unfortunately a decrease of the detection probability.

A decoder, receiving permanently a random bit sequence, will sometime detect a valid telegram. The statistic probability of such an event, caused by noise, interference or similar signals, increases with the frequency and duration of the times, when the receiver is in the active mode. The wake up concept therefore helps

to reduce redundancy in the transmitted code.

The TEMIC receiver modules can support both conceptions. It is possible to use the wake up concept alone or to poll the receiver additionally. Of course it is also possible to switch the receiver to continuous operation, if the increased current consumption can be permitted. Therefore an application dependent optimization of response time and sensitivity of the system can be done. A less obvious benefit of this feature is the possibility to implement a distance dependent functionality.

Constructional details of the receiver

Our approach to the low current receiver is not only the previously commented standby concept but also a special circuit arrangement consisting of the stacking of circuit stages for current reducing. This DC stacking appears on the one hand in the cascading of the entire tuner with the remaining IF and baseband parts, and on the other hand in the tuner itself (see fig. 4). In the subsequent sections we will describe the circuitry of the receiver. Corresponding to the signal flow, first of all we will present the design of the RF tuner followed by an introduction into the IF and baseband parts.

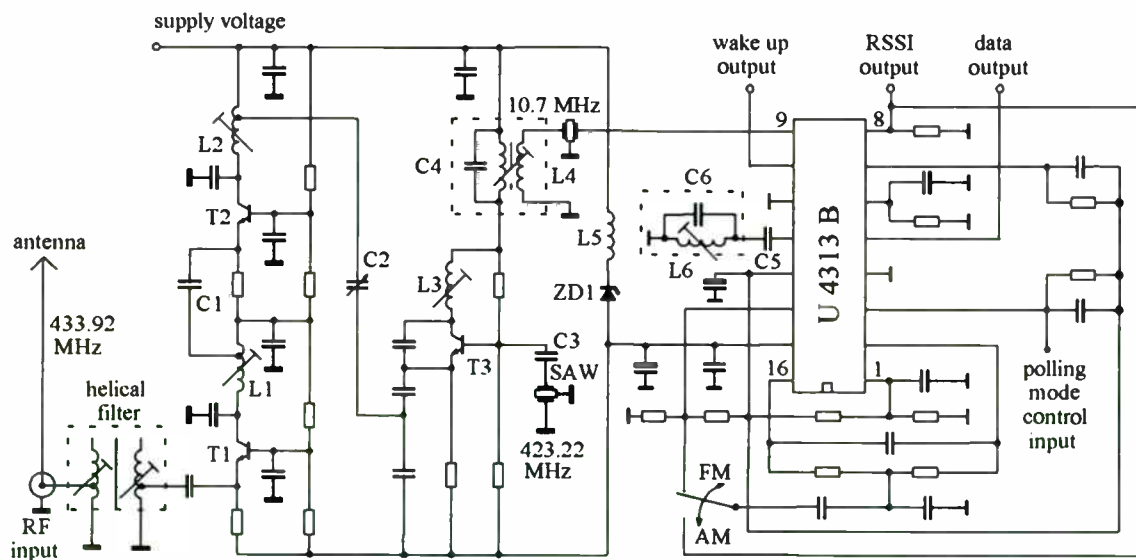


Figure 4: Low current UHF - Remote Control Receiver

Coming from the antenna input with a characteristic impedance of 50Ω the received signal passes a double-tuned miniature helical filter. This preselector provides good far-off selectivity, improves image rejection and makes the subsequent prestage insensitive to deviations of the antenna impedance. The two preamplifiers in common base circuit are DC cascaded. The grounded base amplifiers are distinguished by a high reverse isolation and guarantee a good suppression of the local oscillator

signal to the antenna input. The LO level as well as spurious response and harmonics are less than -65 dBm at any port of the receiver module, which is encased in a tin plate cabinet for shielding. In the tuner special low noise, low current, low voltage bipolar transistors are applied. The transition frequency of the used S 852 T is 3 GHz for a given collector current of 0.5 mA , which provides a gain of about 10 dB per stage at 433.92 MHz .

In the following self-oscillating mixer the signal is converted to the sole intermediate frequency (IF). The large-signal characteristic of the receiver can be improved by using a master-excited mixer whereby the complexity of the circuitry and its power consumption are slightly increased. By means of a SAW resonator as frequency-determining element, the local oscillator is oscillating at a high frequency in the UHF band and therefore no frequency multiplication is necessary. This results in a tuner free of spurious resonances at a minimal expense.

The IF is chosen to 10.7 MHz as there are various low cost components such as transformers, resonators and filters available. The filter bandwidth should be chosen with regard to the tolerances of the SAW resonators in transmitter and receiver. A worst case appraisal of the frequency tolerance yields ± 130 kHz for one SAW, taking into account manufacturing tolerances of ± 75 kHz, temperature variations ($-40^{\circ}\dots+80^{\circ}\text{C}$) of ± 50 kHz and a drift due to component ageing of ± 5 kHz. The frequency tolerance assessment of SAW based oscillators must include

additionally the effects of battery-voltage variations, hand capacitance and shock. We recommend to use ceramic filters with a bandwidth of 350 kHz, as used for instance in large number of pieces in US stereo broadcasting receivers.

As shown in fig.4, the voltage drop at the tuner is clamped to approximately 5.1 V by a zener diode. This diode keeps the operating points of the transistor stages in the tuner constant although the total current consumption depends on the mode of the receiver. In fact the diode takes over the differential current between active and standby mode.

The tuner works without automatic gain control (AGC) to avoid settling time problems especially in AM systems. Therefore the dynamic range of the subsequent stages must be kept in view.

Special care has to be taken when designing the layout of the printed-circuit board. This is necessary to avoid parasitic oscillations and coupling by ground lines.

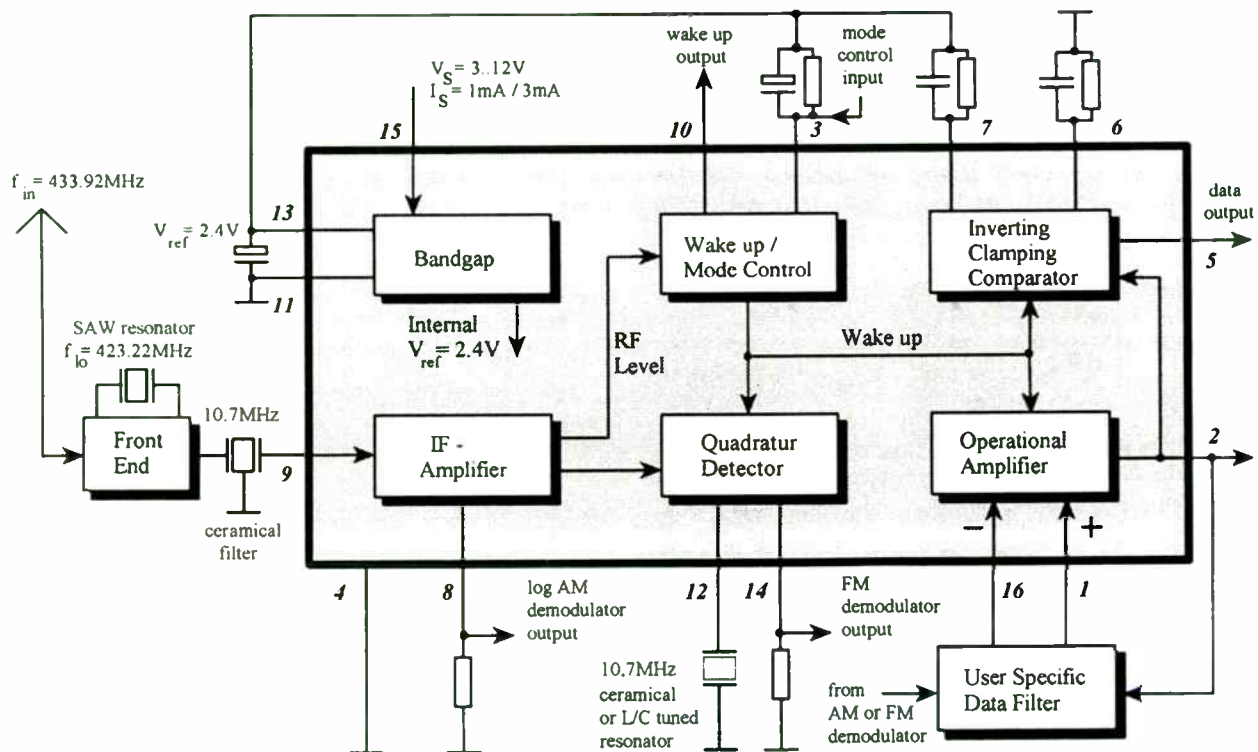


Figure 5: U 4313 B in a superhet receiver concept

We will now concentrate on the remaining IF signal processing, demodulation and data shaping. All these functions including the wake up / mode control circuitry are carried through by a single integrated circuit. For this purpose TEMIC provides a family of ICs in bipolar technology, which are available in DIP as well as in SO

case. We will take as an example the U 4313 B, which is very universal as will be shown. The presentation will be confined to the principle operation and we will not discuss all electrical parameters. These can be found in great detail in the corresponding data sheets and application note [6].

As described earlier, the tuner voltage is clamped to about 5.1 V. Assuming the claimed voltage range of the power supply to be from 9 to 15 V, the remaining voltage for the IF and baseband parts varies from 3.4 to 9.4 V. The operating range of the used integrated circuit IC is 3 to 13 Volts and therefore the claimed power supply range can be guaranteed. The reference currents and voltages of the various parts of the IC are controlled by a bandgap circuit. This is the basis for a largely voltage and temperature independent performance. The very stable reference voltage of 2.4 V is externally available and can be used to supply peripheral components such as the decoder.

The IF signal comes from the tuner through a ceramic filter to the integrated IF amplifier, whose input impedance is 330 Ω and therefore well matched to most ceramic filters.

The U 4313 B is suited for FM as well as AM demodulation. The dynamic range of the logarithmic received signal strength indicator (RSSI) is more than 60 dB (see figure 6), which is enough as has been proved in practical investigations. This RSSI current output is predestined to act as an AM detector and so an AM receiver without any gain control and settling time problems can be realized. The FM demodulator stage needs either a single ended ceramic resonator or a LC tank circuit. At the latter the S-shaped demodulator characteristic can be aligned with respect to center frequency, steepness and bandwidth (compare with figure 8). Therefore tolerances of the receivers SAW resonator can be equalized to some extent and additionally the demodulator can be easily matched to the bandwidth of the IF filter just as to the deviation of the transmitter.

The additional expenditure of the FM receiver compared to the AM is low and consists in the described discriminator filter plus two resistors.

The FM demodulator is only switched on, if the received signal strength is above the threshold of the wake up circuit. The threshold referred to the input of the IF amplifier is typically 40 dB μ V and temperature independent. The delay time as well as the hold time of the

wake up function can be externally adjusted. Peripheral components as the decoder can be controlled by the wake up output and thereby incorporated into the standby concept. Jointly with the FM demodulator two other functions of the IC, an operational amplifier and a clamping comparator are turned on.

With the internal high performance operational amplifier a signal adapted active filter can be realized. The amplifier's power-gain-product is about 4 MHz. Therefore even second order filter for high data rates can be realized to reduce the basebands system bandwidth. Important for the dimensioning of the data filter is not only the data rate but also the code to be transmitted. Recommendable is a code without DC component. This is a code with an equal probability of high and low states, as for instance a Manchester code, which can be generated by a logical exclusive-or operation of the data signal with a clock of doubled frequency.

When the received signal is as far as possible cleared of distortion and noise it has to be converted to a digital bit stream. Therefore a binary quantization has to be carried out. For this data shaping a clamping comparator is implemented. The reference level, which is needed as decision threshold, is generated as follows. Positive and negative peaks of the received signal are stored in two RC circuits. The arithmetical mean of these two voltages forms the threshold. By this clamping to peak values an effective suppression of low frequency interference as hum can be achieved. An optimization of the suppression is possible by the proper adaption of the time constants. The difference of the peak values controls the hysteresis of the comparator. This provides an amplitude depending noise suppression. The open collector output of the comparator delivers a binary data signal with very steep flanks and a level, which can be easily adapted to that of the subsequent decoder. The pin compatible U 4311 B-C delivers a data signal, which is inverted compared to that of U 4313 B. So respective customer demands can be accomplished instantaneously and the designer of the data filter is free whether to choose an inverting or non-inverting type.

EXPERIMENTAL PROCEDURE

We will now look at the experimental investigation of the system performance. First the AM version of the receiver is examined, then the FM receiver is studied and finally a comparison of the two systems is made.

Figure 6 shows the temperature dependence of the static RSSI characteristic. Especially at low levels, which is the area of the wake up threshold, as good as no temperature dependence is evident. This region determines the sensitivity of the receiver, which is therefore almost independent of temperature variations. The straight part of the characteristic extends to approx. 95 dB μ V. Compression effects, occurring at higher levels, do not

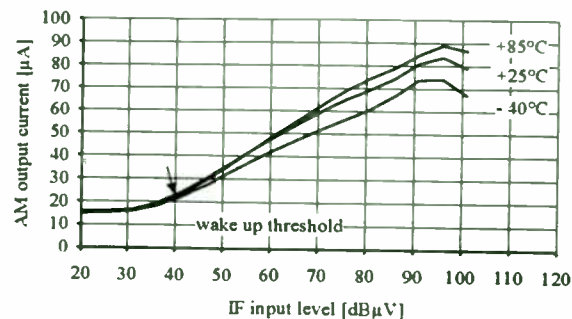


Figure 6: RSSI / AM output current versus IF input level and temperature

disturb the digital system because at such high signal levels the signal-to-noise ratio usually is very high. This is proved by the corresponding measurement and can be seen in figure 7, which will be discussed later.

The RSSI output follows variations of the receiver's input level virtually without any delay. Therefore the data rate can be raised up to several hundred kBauds. At such high rates merely the IF filter has to be replaced by one with a larger bandwidth. However the operational amplifier is still well suited to realize an effective data filter.

In the tested AM receiver a data filter with a voltage gain of 20, a high-end cutoff frequency of 2 kHz and a low frequency cutoff of approx. 20 Hz is applied. The large gain is necessary to provide a signal amplitude, which is sufficient to overcome the hysteresis of the subsequent clamping comparator, when weak signals are received. Diagram 7 reveals the results of a signal-to-noise measurement referred to the output of the operational amplifier, which is simultaneously the output of the data filter. We assume the modulation depth to be 100%, which means that the low bit of the data signal is characterized by no RF signal and the high bit by the corresponding RF input level.

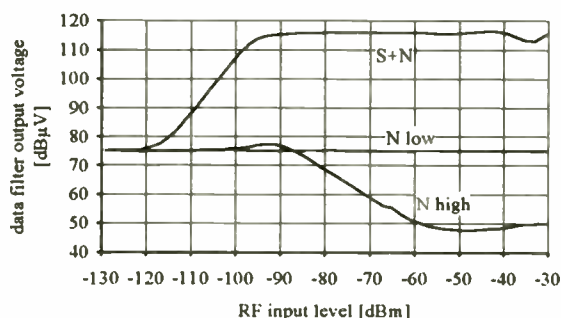


Figure 7: (S+N) / N ratio at the 2 kHz data filter output of the AM receiver. RF is 433.92 MHz, AM modulation depth is 100 %, AF is 1 kHz sinus

To define a signal-to-noise ratio in a digital AM system, it is necessary to distinguish between two different amounts of noise. The noise in the low state N_{low} results from the thermal noise at the receiver input plus the noise originated from the receiver, when no input signal is applied and the gain of all stages is maximal. The noise N_{high} , which appears if a high bit of the data signal is transmitted, can be measured with an unmodulated carrier. While raising the level of the carrier from -105 dBm to approx. -95 dBm, noise increases slightly due to the level dependent directivity of the logarithmic AM detector. With higher values of the input level the gain of the IF amplifier and therefore also the noise decreases. The signal plus noise curve S+N is measured while a RF carrier, which is amplitude modulated with a 1kHz sinusoidal signal, is applied to the RF input. The noise floor of the used Audio Analyzer is 30 dBµV and herewith its influence to the accuracy of the measurement can be neglected.

The S+N/N ratio is the difference between the S+N and the N curves. This ratio is a standard of the signal quality. It increases from 0 at the limiting sensitivity of -120 dBm to more than 60 dB referred to N_{high} , respectively 40 dB referred to N_{low} , at an input level of -55 dBm. In fact the effective S+N/N ratio lies between those two values and depends on the probability of the low and the high bits. The maximum signal-to-noise ratio is limited by the noise respectively the dynamic range of the receiver. At all S+N/N measurements only thermal noise which can be considered as white Gaussian noise is present. Therefore the sensitiveness of AM systems to pulse noise as for example ignition noise becomes not evident.

As has been discussed previously, the FM discriminator filter should be tunable. The discriminator output voltage varies with the input frequency between 0.1 V and 2.3 V with its mean value of 1.2 V at the centre frequency. The demodulator bandwidth depends mainly on the difference of the series and the parallel resonance frequency of the discriminator filter. Hence the bandwidth can be adjusted by changing the series capacitor C5 and retuning the center frequency with L6 (labels according to figure 4). The S-shaped curves for two different filter configurations are plotted in figure 8.

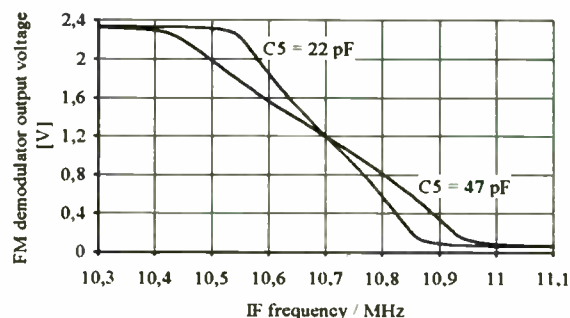


Figure 8: FM demodulator frequency response for different values of C5

The next figure 9 presents the signal-to-noise ratio of the FM receiver versus the RF input level. The measuring was carried out in analogy to that at the AM receiver. The bandwidth of the used data filter was chosen equal to that of the AM system. Its gain was reduced to a value of 3 because the FM demodulator delivers a higher signal amplitude, which is additionally almost independent of the RF input level. The limiting sensitivity is -110 dBm and therefore worse compared to that of the AM system, but the S+N/N ratio increases more rapidly with the input level due to the threshold effect of the FM system. Here one benefit of the FM system becomes obvious: the level of the RF signal and therefore also the noise is independent of the transmitted information. Therefore the S+N/N ratio at higher input levels is better than that of the AM receiver.

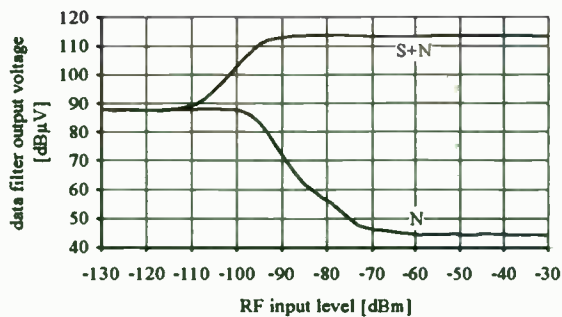


Figure 9: (S+N) / N ratio at the 2 kHz data filter output of the FM receiver, RF is 433.92 MHz, FM deviation is 22.5 kHz, AF is 1 kHz sinus

To characterize the quality of a digital data transmission the specification of a bit error rate (BER) is very common. This is the probability of a wrong bit at the output of the receiver. At systems with a limited bandwidth (what applies to every real system), the BER depends on the transmitted bit stream. In systems with bandpass characteristic not only the data rate is limited by the system's high-end cutoff frequency but also the low frequency cutoff is important. The latter limits the maximum number of successive equal bits. Therefore the use of a 0-1-0-1 sequence as a test signal does not reveal the real performance of the system. A pseudo random sequence (PRS) is recommended to be used instead. This is a sequence of a given length of 2^n-1 bits which is transmitted periodically. The distribution of the bits in the sequence are quasi random and the maximum number of successive equal bits is n . The probability of occurrence of the low and the high bit is almost equal but never identical, because the sequence has an odd number of bits.

If the complete baseband signal processing functions are DC coupled, the optimal threshold of a binary decision element is the mean value of the low and the high bits' amplitude. This applies as long as no interference is present. In an AC - coupled system in particular the transmission of many successive equal bits leads to a so-called baseline wandering in the decision element, what means that the optimal threshold shifts. The amount of this baseline wandering depends on the the low-end cutoff frequency in proportion to the ratio of data rate to number of successive equal bits. The carrying out of a BER measurement by using a PRS as test signal is well suited to determine the influence of the baseline wandering on the receiver performance. In our case the low-end cutoff frequency can be adapted by the value of the coupling capacitor which connects the datafilter to the output of the demodulator. An optimization of the complete data filter should be done by the help of the eye pattern at its output.

The data filter and the subsequent clamping comparator are DC coupled. The time constants of this comparator must be large compared to n times the length of one bit. The purpose of its gliding threshold is to suppress only low frequency distortions.

The time of decision, whether a right or wrong bit was decoded is set to the middle of the bits. The BER measurement equipment compares the modulation signal of the transmitter with the signal at the output of the clamping comparator and counts the number of faults per time.

With this BER measurement equipment the dependence of the receivers' sensitivity referred to the modulation depth of the AM transmitter respectively the deviation of the FM transmitter is examined. A fixed BER of 10^{-3} is taken as a basis. The RF input level corresponds to the carrier peak level at the output of a signal generator, which must be independent for all values of modulation depth respectively frequency deviation. This means, that the AM modulator must be clamped to the high level of the modulation signal, as done for instance at the transmission of TV signals.

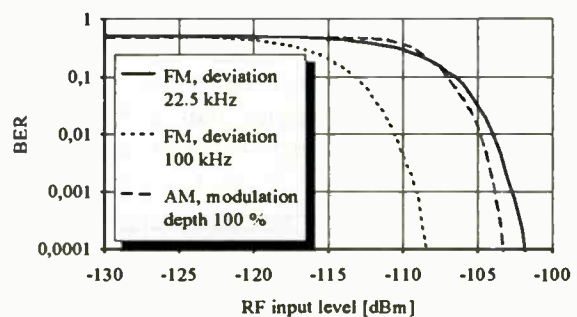


Figure 10: Bit Error Rates of a 2 kbit/s PRS of length 2^5-1

As can be seen in fig. 11 and 12, the AM System using a modulation depth of 100% achieves the claimed BER at lower input levels than the FM system using 22.5 kHz deviation. The FM system is superior to the AM system if the used deviation is more than 35 kHz. At a deviation of 100 kHz, the margin is about 5 dB. This does not surprise because the FM system exploits the system's IF bandwidth of 350 kHz much better than the AM system. Further the FM is superior to AM by principle. The derivation of this theoretical 3 dB margin can be found in [7].

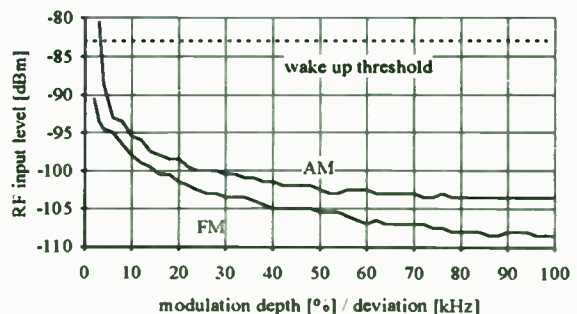


Figure 11: Sensitivity of the AM and FM systems for a 2 kbit/s PRS of length 2^5-1 and a given BER = 10^{-3}

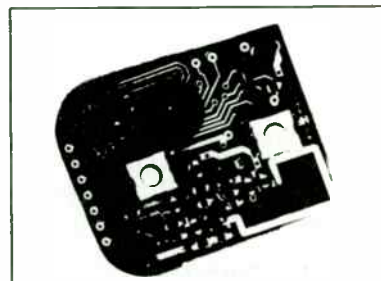
SUMMARY OF THE SYSTEM PERFORMANCE

General:

- ⇒ RF characteristics according to FTZ 17TR2100, will fulfill the regulations of most countries, please request corresponding specifications
- ⇒ Operating frequency 433.92 MHz (can be adapted to other frequencies in the UHF range)
- ⇒ Modulation FM or AM
- ⇒ Ambient operation temperature -40 °C to +85 °C
- ⇒ Fulfills requirements of international car manufacturers

Transmitter:

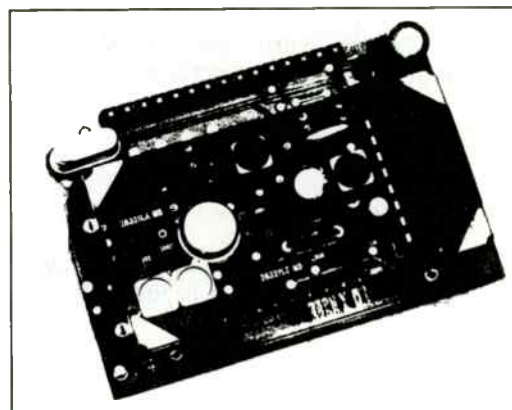
- ⇒ Custom designed, characterized by performance and outlines
- ⇒ Example incl. antenna, 4 bit μ Controller and battery see picture 1 (6V, standby current of max. 0.5 μ A, active current of max. 8 mA)
- ⇒ Radiated power: approx. -20 dBm
- ⇒ Spurious response / harmonics:
 - less than -65 dBm up to 1 GHz
 - less than -55 dBm above 1 GHz
- ⇒ AM or FM operation depending on component assembling.
 - AM: modulation depth approx. 90 %
 - FM: Deviation approx. \pm 15 kHz
- ⇒ Size: approx. 38 mm • 32 mm • 10 mm, custom specific solution with a reduced size of 38 mm • 25 mm • 8 mm exists



Picture 1: UHF - Transmitter, FM version

Receiver:

- ⇒ Power supply: DC 9 V - 16 V, typical currents:
 - 1.0 mA using U 4311 B / U 4313 B standby mode (AM / FM)
 - 3.2 mA using U 4311 B / U 4313 B active mode (AM / FM)
 - 0.9 mA using U 4312 B standby mode (only AM)
 - 2.7 mA using U 4312 B active mode (only AM)
- ⇒ AM or FM operation depending on component assembling
- ⇒ Wake-up function: threshold approximately -83 dBm referred to the 50 Ω antenna input, delay and hold time adjustable
- ⇒ Polling mode supported
- ⇒ Output to activate peripheral circuitry e.g. decoding system
- ⇒ Antenna jack makes customs specific antenna design and location feasible
- ⇒ Data output for individual external data processing or optional μ Controller on accessory board (see picture 2)
- ⇒ Spurious response and harmonics less than -65 dBm (at any port of the RF module in a tin plate cabinet)
- ⇒ Input sensitivity: AM: better than -100 dBm (see figure 7 and figure 10)
 - FM: better than -100 dBm (see figure 9 and figure 10)
- ⇒ Good out-of band rejection due to double tuned helical filter at RF input
- ⇒ Size of the RF module: approx. 55 mm • 30 mm • 18 mm



Picture 2: UHF - Receiver, FM version, RF module on accessory board

FUTURE CONSIDERATIONS

Finally we give a prospect of possible further development. Due to the limited modulation capability of the actual SAW-based FM transmitter design, deviation is limited to less than \pm 20 kHz. Unfortunately the tolerance of the SAWs demand an IF-band-width of more than 250kHz. For this reason an increase of FM-deviation to about 100kHz will result in an improvement of the system-sensitivity of approximate 6dB (see figure 11). We intend to develop an PLL-based transmitter with better frequency tolerance and improved modulation capability [8]. Certainly semiduplex and fullduplex radio links will be needed for special applications and we intend to include this also in our future activities.

ACKNOWLEDGEMENT

The authors would like to thank the TEMIC subassembly division for making available receiver and transmitter modules and Dr. Sapotta and Mr. Bürgerhausen for general technical assistance and helpful comments. Moreover we would like to express our sincere appreciations to the colleagues in the development and application groups who gave us unlimited encouragement.

REFERENCES

- [1] Sapotta, Bürgerhausen
Infrared or high-frequency transmission for car locking systems ?
TEMIC internal paper 1992
- [2] Meinke, Gundlach
Taschenbuch der Hochfrequenztechnik
Springer-Verlag Berlin 1986, Vol. 1, H4
- [3] Zinke, Brunswig
Lehrbuch der Hochfrequenztechnik
Springer-Verlag Berlin 1986, Vol. 1, pp. 339-346
- [4] Niestroj, Zapsky, Lang
Kostengünstige und zuverlässige Fernsteuerungen durch OFW-Resonatoren
Siemens Components 4/90, pp. 142-145
- [5] Vollers jr.
General-purpose SAW resonator oscillator for 300 MHz to 1000 MHz
RF Monolithics Inc. 1984, Application Note No.3
- [6] Strohal, Bopp
UHF Remote Control System
TEMIC Application Note No.10
- [7] Lüke
Signalübertragung
Springer-Verlag Berlin, 4th edition 1990, pp.167-197
- [8] Boese, Gebauer
Kombiniertes Funksende- und -empfangsgerät mit einer PLL-Schaltung
Patent pending, reference P4201415.8

Matthias Bopp was born in Mosbach, Germany, on May 6th, 1964. He received his Dipl.-Ing. degree in electrical communication engineering from the University of Kaiserslautern in 1990. His Dipl.-Ing. research was the development and investigation of a coherent optical PSK homodyne receiver at ANT Bosch Telecom in Backnang. In the same year he joined the TELEFUNKEN electronic GmbH, meanwhile reorganized to TEMIC TELEFUNKEN microelectronic GmbH. He is engaged in the development of RF remote control systems and advanced Integrated Circuits. Mr. Bopp holds a radio amateur licence and is member of AMSAT.

Jürgen Strohal was born in Aalen, Germany, on June 17th, 1963. He studied electrical engineering, concentrating on communication techniques, at the University of Stuttgart. His diploma research was the improvement of an UV sensitive sensor read out by a CCD. He obtained the diploma in 1991 and joined the TELEFUNKEN electronic GmbH, where he is engaged in the application group and is involved in the application of RF circuits. He is fond of languages and increases his knowledge on periodical journeys.

Comparison Of Path Loss Performance of a Leaky Feeder Cable vs. A Distributed Antenna

J. Ford, R. Perelman, D. Lang
Times Microwave Systems

Abstract

The use of a wireless system in an enclosed area may be inhibited by the lack of signal propagation through walls or in and around metal structures. This paper will compare the measured values of path loss for two systems of signal distribution designed to be part of a larger signal distribution system. The measurements were performed at 900 MHz. This paper will present relative parameters for the design engineer to use to configure an indoor wireless system.

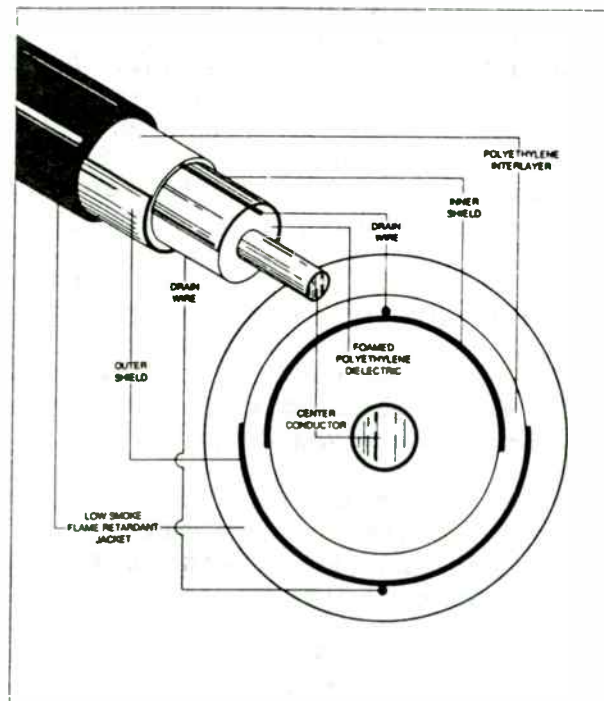
Introduction

A leaky feeder or radiating cable is an RF transmission line which is designed to couple the RF energy propagating its length to the environment. In so doing, it functions as a continuous antenna and is useful for providing RF coverage in enclosed environments, where point source antennas may have been used. A distributed antenna is a set of antennas fed by a single source used to provide RF coverage in enclosed areas. Examples of environments which cannot be effectively covered with point source antennas include tunnels, mines, metal hulled ships and metal framed buildings.

The low levels of energy emitted by radiating cables make them ideal for achieving coverage in limited areas, allowing frequency re-use. This is important because of the many competing demands for RF spectrum which makes efficiency of spectrum use an ever more pressing concern. The creation of mini-cells within buildings and coverage of limited areas for Wireless Local Area Networks are examples of applications where this characteristic of radiating cable can be usefully exploited. The purpose of this paper is to aid the designer of in-building communications systems by providing a comparison of the coverage performance of radiating cable and point source antennas within a building environment.

Types of radiating cables

Radiating cables are of two basic types--coaxial and triaxial. Coaxial types consist of coaxial cables with openings in the outer shield to allow coupling of RF energy to the environment. Within this category many different techniques are used by different manufacturers for forming openings in the outer conductor. One of the most common is to take a corrugated copper outer conductor and mill a continuous slot along the length of the cable. Another construction utilizes a foil outer conductor which is pre-punched with the coupling apertures. Another common cable utilizes loose braids or leaves off carriers on standard braided coaxial constructions. The radiating cable used in this comparison is a triaxial type where the outer conductor is in two sections separated by a polyethylene interlayer, Shown in figure 1.



Schematic for nu-Trac Triaxial Antenna Cable

Patent Number 4339733

Figure 1.
Triaxial Radiating Cable

Applications of radiating cables

Radiating cables have been used in many different environments for many different types of communications systems. They have been installed in subway systems for two-way voice communications for public safety, for train control systems and to relay video information to the conductors to help in door control at stations. In hospitals, radiating cables have been installed to extend paging systems to underground tunnels and parking garages and to allow patients wearing monitoring equipment equipped with RF outputs to move about freely. The US Navy has installed radiating cables on virtually all of its ships as part of a system called Damage Control-Wire Free Communications (DC-WIFCOM) and for a shipboard

security system. Radiating cable was used for communications during the construction of the English Channel Tunnel and will be installed for the permanent communications system. Long road tunnels such as the Sumner and Calahan Tunnels in Boston are being furnished with radiating cable in order to allow the use of cellular phones by motorists traveling through them.

Experimental design

One of the areas where radiating cable has the greatest potential for contributing to productivity enhancement and cost savings is in manufacturing. In both office and plant environments, the use of Local Area Networks is allowing the transmission of data, correspondence and voice messages rapidly and efficiently between work stations. One recent trend is to make these interconnections without the requirement for hard wiring. This allows reconfiguration and relocation of equipment and personnel to be achieved more quickly and at lower cost. Wireless connections also allow equipment to be used in a portable fashion, while remaining interconnected to the network.

One of the problems in achieving a truly wireless network is the difficulty in achieving adequate RF coverage throughout a building. This study compares the coverage achieved with point source antennas and radiating cables in a factory environment. The results show that more complete coverage is achieved using radiating cable, which would result in more reliable operation of a wireless network.

Figure 2 shows the positions of two quarter wave monopoles that were mounted near the ceiling at P1 and P2 and the radiating cable location.

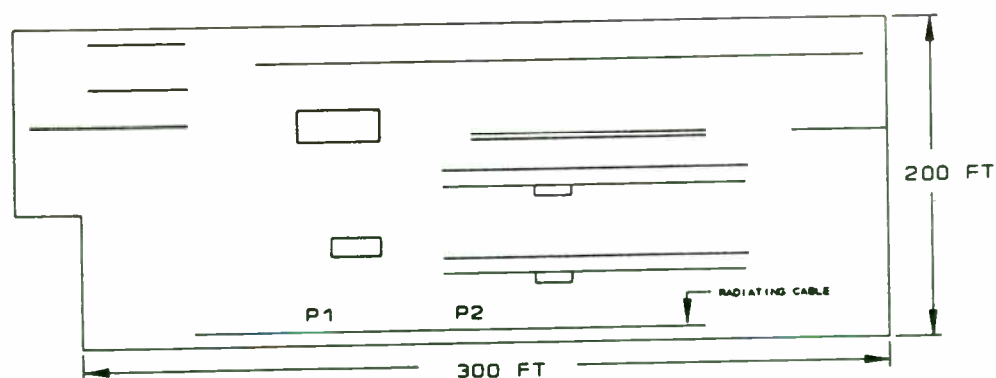


Figure 2
Test Area and Source Layout

The monopoles were fed by a $\frac{1}{2}$ " aluminum-foam cable which is commercially available. The monopoles were fed by coupling power off the $\frac{1}{2}$ " coax with taps. The lengths of coax used were 130ft. to the first tap 150ft between taps in the test area and 300ft after the second tap to feed a third tap in a separate building. For a total length of 480ft. The monopoles were connected to the feed line by a 16dB and a 10dB tap. The attenuation between the first two taps is 5.4dB. The monopoles were configured this way to function as part of a distributed antenna system that would also feed an area beyond our test area with equivalent signal strength. A loss budget is shown in Figure 3 giving the cable losses and the signal strength delivered to the quarter wave monopole.

Tx	→ 4dB	→ -16dB Tap	→ 5.4dB	→ -10dB Tap	→ 10dB	→ 0dB Tap
	cable loss		cable loss		cable loss	
+30.0dBm		+10.0dBm		+10.6dBm		+10.6dBm
		monopole		monopole		monopole

Figure 3.
Loss Budget for Distributed Antennas

The coupling values of the taps were selected to provide equivalent radiated power at each of the monopoles. Only the first two antennas were in the area that was evaluated. The third tap was in an adjacent building and was terminated in a 50 Ohm load for this test. The power level measured at the third tap was +10.6dBm.

The radiating cable ran along side the feed cable for the monopoles. The installation crew that installed both the Aluminum sheathed coax and the radiating cable had experience installing electrical conduit, phone lines, and datacom lines. The only special instructions given was that both cables for our test could not be bundled with any existing cables and would need to be clamped in place separately. A loss budget for the radiating cable is shown in figure 4.

Tx	-----	13.2dB	-----	500hm
		loss		Load
+30.0dBm				+16.8dBm

Figure 4.
Loss Budget for Radiating Cable

The signal received by a half wave dipole was measured at 17 locations around the manufacturing area. The technique used to generate the path loss values is similar to that used by previous investigators¹. The value used is the average of ten values taken evenly over a 20ft. length. The locations of the measurements were identical for each signal distribution technique. The receive dipole was held with horizontal polarization. Recent investigations in wireless communications have compared polarizations for antennas and showed linear vertical to be optimal². Since we are comparing two signal distribution techniques in the presence of many conducting bodies, horizontal polarization was used for convenience. A comparison of optimal receive antenna polarizations for radiating cables is forthcoming.

Results

The average measured values of path loss for the monopoles and the radiating cable are shown in figures 5 and 6 respectively. The received signal strength fades predictably as the measurement point is taken a distance away from the sources. Figure 7 shows a plot of the path loss of each point, the points are randomly located.

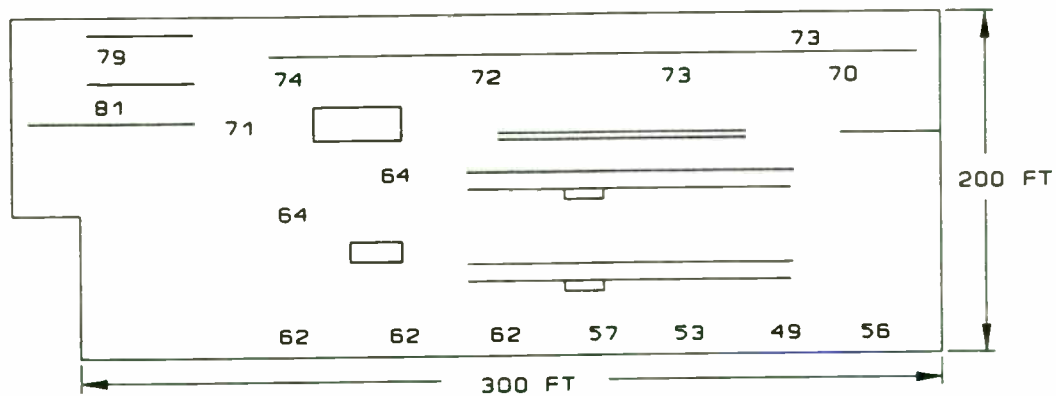


Figure 5.
Path Loss in dB for Distributed Antennas

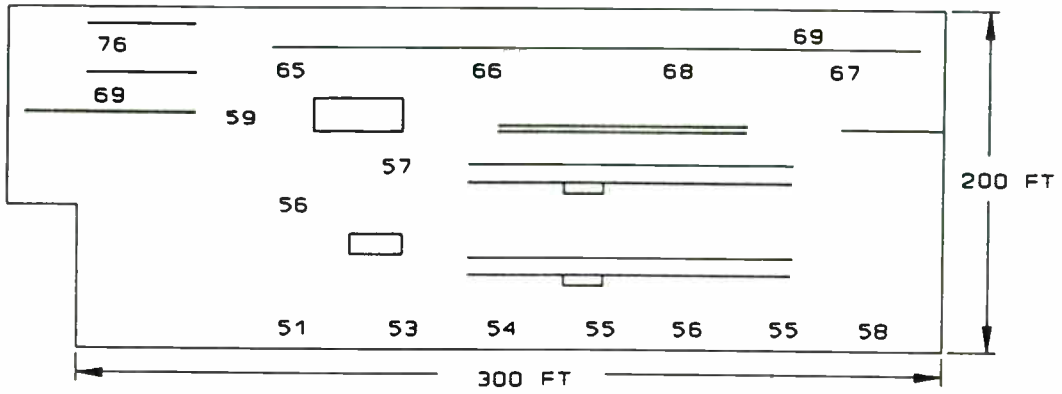


Figure 6.
Path Loss in dB for Radiating Cable

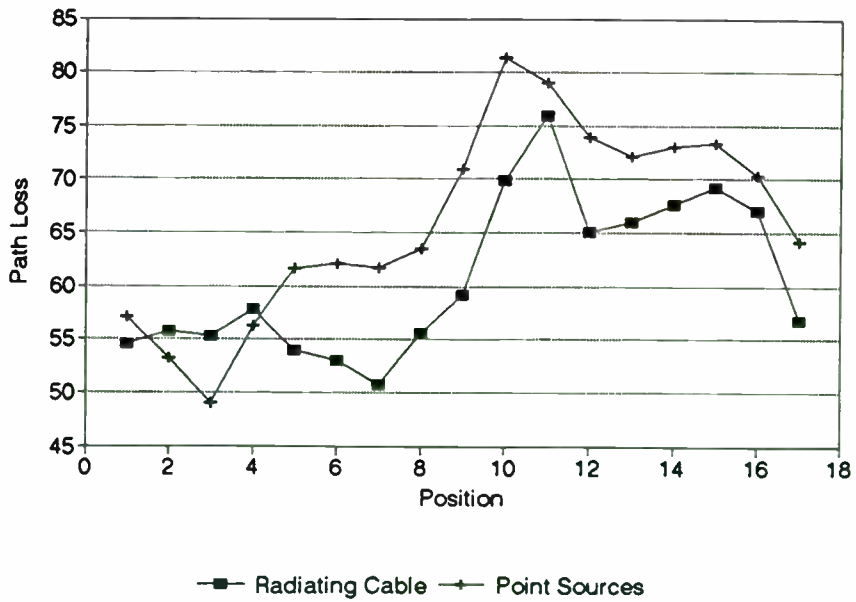


Figure 7.
Relative Path Loss Values (dB)

Figure 8 shows the difference in dB between the two distribution techniques where a positive value would favor the monopoles. The values given for the difference in RF coverage range from 12dB in favor of the radiating cable to 6dB in favor of the two quarter wave monopoles.

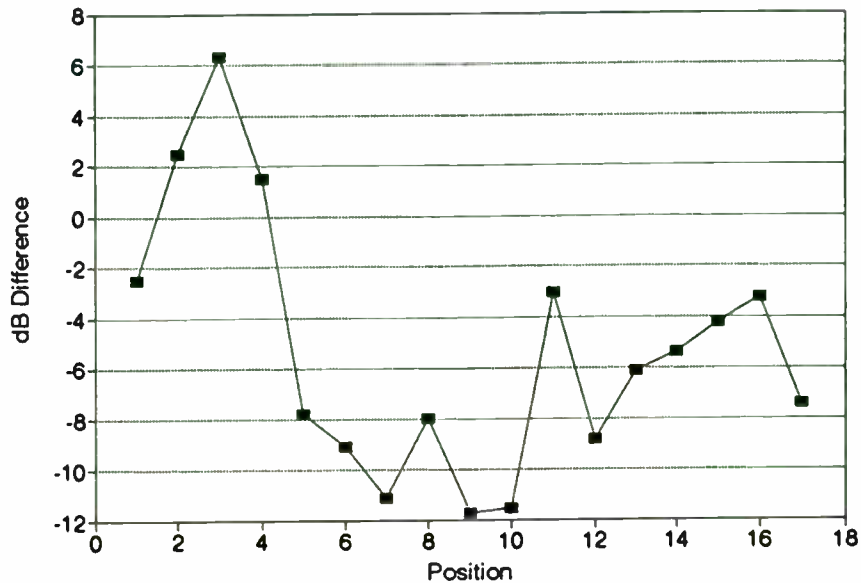


Figure 8
Difference in Path Loss (dB)

If the covered area were smaller the RF distribution would more conveniently be covered by a single source antenna like a monopole. In fact if all of the available power was distributed through the two monopoles there would be an additional 10dB at each of the two monopoles and would therefore reduce the path loss by the same value. The average difference between the path loss values for the two systems is 5.3dB with the advantage going to the radiating cable system. The relative power available at the output of each system shows the advantage of radiating cables in larger systems. An additional benefit of the radiating cables was the ease of installation. Installing the cables on the factory ceiling took twice as long for the aluminum sheathed coax as it did for the radiating cable. The aluminum sheathed coax was used because it is intended to have the best performance with the available taps. Also there was additional labor required installing the taps, mounting plates, and monopoles that was not required with the radiating cable.

Conclusion

For the particular 900 MHz system demonstrated we have shown that radiating cable provided better RF coverage using path loss evaluation. For 14 of the 17 locations in the factory, a higher signal level was measured with the radiating cable and will have a greater advantage when used in larger systems. This point is emphasized by the available power at the output of each system. The available power for an additional area was 16.8dBm for the radiating cable and 10.6dBm for the point source system, Both systems being supplied the same 30dBm input power. Future work will include polarization performance, comparison of performance in larger and smaller systems, and development of design values for general system use.

Radiating cable is a desirable alternative to discrete antennas because of improved RF coverage achieved and because of the ease of installation of this type of system.

1. Seidel, S.Y. and Rappaport, T.S.: "914 MHz Path Loss Prediction Models for Indoor Wireless Communications in Multifloored Buildings" IEEE AP-40
2. Ho, C.M.P. and Rappaport, T.S.: "Effects of Antenna Polarization and Beam Pattern on Multipath Delay Spread and Path Loss in Indoor Obstructed Wireless Channels", "ICUPC '92" Proceedings.

LOW COST F-QPSK MODEM RADIO SOLUTIONS FOR DOUBLING THE CAPACITY OF EUROPEAN STANDARD CELLULAR/PCS SYSTEMS

P.S.K. Leung

Digital Communications Laboratory
Dept. of Electrical & Electronic Engineering
Victoria University of Technology
Footscray, Melbourne, Victoria 3011,
Australia

Dr. Kamilo Feher

President, Digcom Consulting Group
Director, Digital Communications Research Laboratory
Professor, Electrical and Computer Engineering
University of California, Davis; Davis, CA 95616
916-752-8127 or 916-752-0583; FAX 916-752-8428

Abstract

A low cost combined modulation radio technique **F-QPSK** is proposed for cellular/mobile and personal communications. The F-QPSK technique invented by Feher [18] belongs to an original power and spectrally efficient family of radio/modems developed and used for satellite communications. Similar to GMSK modulation used in the European DECT and other wireless land mobile standards, F-QPSK has constant envelope. This allows it to operate with class C power amplifier without output backoff (OBO). F-QPSK is thus 4 to 8 dB more power efficient than $\pi/4$ DQPSK as currently adopted in the US IS-54 standard for land mobile and in the Japanese Digital Cellular (JDC) systems.

Our experimental hardware and computer generated results demonstrate that F-QPSK has a 51% higher spectral efficiency than the European standard GMSK system having a $BT=0.5$. Additionally, F-QPSK has superior BER performance characteristics. Our research shows that F-QPSK is 5.5 dB better than noncoherent GMSK in E_b/N_0 over Rayleigh fading channels, and it is 2.5 dB more robust in a CCI controlled environment. We demonstrate that the combined spectral efficiency and C/I advantage of our proposed F-QPSK modem radio could nearly double (95% increase) the capacity of DECT.

1 Introduction.

Over the last few years, the worldwide demand for wireless communications has grown spectacularly. This is particularly evident in the cellular mobile communications markets that have been enjoying 33% to 50% annual growth rates [3]. As a parallel development, there is also a strong surge of interest in the emerging micro-cellular personal communications services (PCS) [1,2,3] that allow people to communicate anywhere, anytime. The worldwide demand for PCS services is expected to be huge and annual revenues of between \$33 billion to \$55 billion by the year 2000 in the United State alone have been projected by

some analysts [3]. However, successful exploitation of such huge potential market requires coordination and efficient industrial standards.

Currently, the most well-known standards for the emerging PCS are the European "Digital European Cordless Telecommunications" (DECT) [11] and CT-2. DECT is a low power microcellular system that uses TDMA/TDD (Time Division Multiple Access/Time Division Duplex) access method in the 1.8GHz band. CT-2, on the other hand, is designed mainly for telepoint services and is less versatile. But both standards use Gaussian Minimum Shift Keying (GMSK) for digital modulation. In this paper, we propose an alternative coherent F-QPSK (or Feher's QPSK [18,14]) modem radio solution for PCS that is significantly more efficient. Our investigation shows that the proposed scheme can nearly double (95% increase) the capacity of DECT.

F-QPSK is a power efficient digital modulation that belongs to the Intersymbol-interference-and-Jitter-Free Offset Quad-Phase-Shift-Keying (IJF-OQPSK) family originally introduced for satellite communications [9,13,14,18]. Our experimental hardware and computer generated results demonstrate that it is also more spectrally efficient than GMSK as used in European PCS standards. In addition, we find that F-QPSK has superior BER performance to noncoherent GMSK in both additive Gaussian and Rayleigh fading channel. More importantly, it is also more robust in cochannel interference (CCI) controlled environments typically encountered in microcellular PCS operations. **It is the combined spectral efficiency and C/I advantage of our proposed F-QPSK modem radio solution that leads to the significant improvement of capacity over DECT.**

The organization of this paper is as follows. After the introduction in Section 1, the principles and properties of F-QPSK are briefly reviewed in Section 2. The spectral efficiency and adjacent channel interference (ACI) characteristics of F-QPSK are compared with GMSK as used in DECT in Section 3. Section 4 analyses the BER performance of F-QPSK and finds it better than noncoherent GMSK in both Gaussian and Rayleigh fading environment. Finally, the capacity of F-QPSK in a cellular mobile environment is compared with DECT in Section 5. We summarize our results and present the conclusions in Section 6.

2 F-QPSK modulation.

The block diagram of our F-QPSK modulator is shown in Fig.1. It consists of a serial-to-parallel converter, pulse shaping filter $p(t)$, I/Q modulator and a hardlimiter.

The input binary data sequence $\{\alpha_n\}$ is first converted into 2 independent I/Q channel

symbol streams $\{a_n\}$, $\{b_n\}$ before being processed by the pulse shaping filter with impulse response:

$$p(t) = \begin{cases} 0.5[1 + \cos(\frac{\pi t}{T_s})] & \text{for } |t| \leq T_s \\ 0 & \text{otherwise.} \end{cases} \quad (1)$$

where T_s is symbol duration. After the quadrature modulator and hardlimiter, we obtain the F-QPSK signal $S_o(t)$:

$$S_o(t) = \frac{x(t)\cos 2\pi f_c t}{\sqrt{x^2(t) + y^2(t)}} + \frac{y(t)\sin 2\pi f_c t}{\sqrt{x^2(t) + y^2(t)}} \quad (2)$$

where $x(t) = a_n p(t - nT_s) + a_{n-1} p[t - (n-1)T_s]$ and $y(t) = b_n p[t - (n-0.5)T_s] + b_{n-1} p[t - (n+0.5)T_s] + b_{n-2} p[t - (n+1.5)T_s]$ are the I and Q channel baseband signals respectively [4,9].

It is interesting to note from Fig.1 and equation (2) that F-QPSK is a power efficient modulation. Like GMSK as used in DECT, F-QPSK is also a constant envelope modulation capable of operating with class C power amplifier without output backoff (OBO). This is in contrast with the nonconstant envelope $\frac{\pi}{4}$ DQPSK that typically requires 4 to 8 dB OBO to avoid spectral spreading. F-QPSK is thus 4 to 8 dB more power efficient than the popular $\frac{\pi}{4}$ DQPSK used in the US IS-54 [10] standard for digital cellular mobile communications and in the Japanese Digital Cellular system.

Another advantage of F-QPSK is the simplicity of its implementation. The pulse shaping function in equation (2) can readily be realized using simple transversal filter technique [14]. Fig.2 shows the circuit diagram of the pulse shaper in a F-QPSK prototype modem [17] built in our Digital Communications Research Laboratory at University of California, Davis. The resulting I/Q channel eye diagrams are shown in Fig.3.

3 Spectral efficiency and ACI characteristics.

The power spectral density of F-QPSK is compared with GMSK in Fig.4. We notice that F-QPSK has a narrower main spectral lobe than GMSK although its tail decays less rapidly at high frequency. This indicates that F-QPSK is more spectrally efficient.

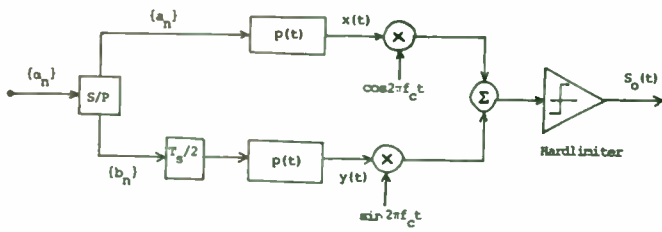


Fig. 1. Block diagram of F-QPSK modulator.

Fig. 1 Block diagram of F-QPSK modulator.

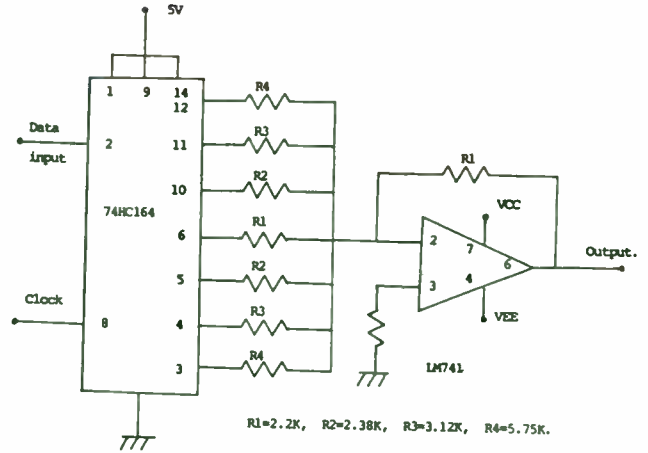


Fig. 2 Circuit diagram of F-QPSK pulse shaper.

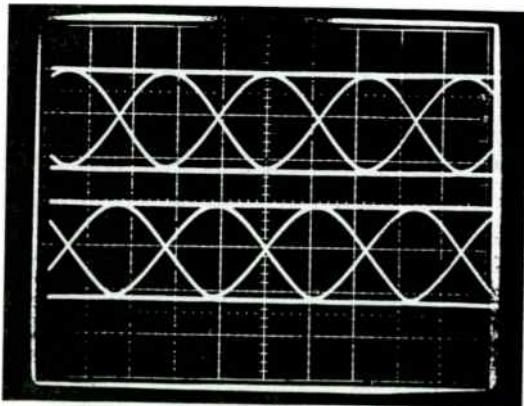


Fig. 3 Measured eyediagram of the experimental 180 Kb/s prototype F-QPSK modem, 5 μs/Div, 1v/Div.

P.S.D. of F-QPSK & GMSK.
(Hard-limited Channel).

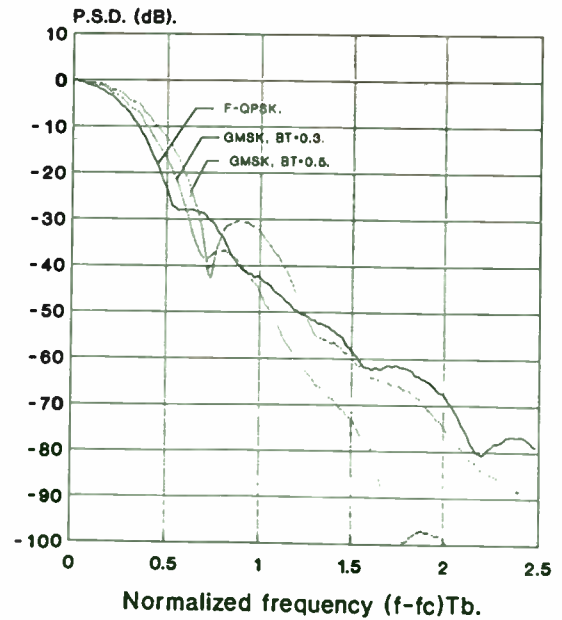


Fig. 4 Power spectrum of F-QPSK and GMSK as a function of the normalized frequency $(f-f_c)T_b$.

Spectral efficiency η_f (b/s/Hz) of a digital modulation is defined as $\eta_f = \frac{1}{WT_b}$ where W is the channel spacing and $\frac{1}{T_b}$ is the data bit rate. In a multicarrier system, normalized channel spacing WT_b is usually determined by the maximum acceptable adjacent channel interference (ACI) level. In this study, we calculate the ACI ratio $A(W)$ as :

$$A(W) = \frac{\int_{-\infty}^{\infty} G(f)|H(f-W)|^2 df}{\int_{-\infty}^{\infty} G(f)|H(f)|^2 df} \quad (3)$$

where $G(f)$ is the PSD of the signal and $H(f)$ the receive BPF transfer function in their baseband equivalent forms. This definition is adopted because it reflects accurately the impact of $H(f)$ on the ACI level.

The ACI characteristics of F-QPSK and GMSK are computed using (3) and the result plotted in Fig.5. It shows that F-QPSK causes significantly less ACI than GMSK and hence is spectrally more efficient in multicarrier systems. In this study, the BPF used for F-QPSK is 4th order Butterworth [7] with normalized 3dB bandwidth $B_i T_b = 0.55$,

$$H(j\omega) = \frac{1}{(\omega^4 - 3.4142\omega^2 + 1) - j2.6131\omega(\omega^2 - 1)} \quad (4)$$

And the BPF used for GMSK is 4th order Gaussian [7] with $B_i T_b = 0.6$,

$$H(j\omega) = \prod_{i=1}^2 \frac{\omega_i^2}{\omega_i^2 + 2j\xi_i\omega_i\omega - \omega^2} \quad (5)$$

where $\omega = 2\pi f$, $\omega_1 = 1.9086$, $\omega_2 = 1.6768$, $\xi_1 = 0.7441$, $\xi_2 = 0.9721$. These filters are chosen for their good performance in Gaussian noise channel [5,6].

The spectral efficiency η_f of F-QPSK and GMSK in b/s/Hz are listed in Table 1 for four different ACI levels. For convenience, we also include the modulations' relative spectral efficiency using GMSK BT=0.5 as reference base (100%). This table shows that for ACI=-20 dB, F-QPSK has a spectral efficiency of 1.42 b/s/Hz which is 51% more efficient than GMSK BT=0.5 as used in DECT. Also, the spectral efficiency of F-QPSK could jump up to 1.63 b/s/Hz if -15 dB ACI can be tolerated.

	ACI=-15dB	ACI=-20dB	ACI=-26dB	ACI=-30dB
F-QPSK	1.63 (147%)	1.42 (151%)	1.23 (156%)	1.10 (155%)
GMSK BT=0.3	1.16 (105%)	0.98 (104%)	0.83 (105%)	0.74 (104%)
GMSK BT=0.5	1.11 (100%)	0.94 (100%)	0.79 (100%)	0.71 (100%)

Table 1. Spectral efficiency η_f in b/s/Hz.

4 BER performance.

The BER performance of our coherent F-QPSK scheme in Gaussian noise channel is obtained using computer simulation and the result plotted in Fig.6. This is compared with GMSK BT=0.5 with noncoherent detection as in typical DECT receiver [15]. In this study, the detection method employs frequency discriminator [16] with a Gaussian predetection BPF ($B_b T_b=0.6$) and a 4th order Butterworth postdetection LPF ($B_b T_b=0.4$). Fig.6 shows that in Gaussian noise channel, F-QPSK has a 3 dB Eb/No gain over noncoherent GMSK BT=0.5 at BER $P_e = 10^{-4}$.

Fig.7 compares the BER performance of coherent F-QPSK and noncoherent GMSK in slow Rayleigh fading (normalized Doppler frequency $f_D T \approx 0$). It shows that F-QPSK performs better than GMSK BT=0.5 by a wide 5.5 dB Eb/No margin in this environment. The performance of GMSK BT=0.3 is similarly obtained and is found to be within 0.5 dB of the BT=0.5 case.

Finally, F-QPSK's performance in a cochannel interference (CCI) controlled environment with Rayleigh fading is also obtained (see Fig.8). This performance is of considerable interest to system designer since CCI is known to limit the cellular system's performance rather than Gaussian noise [8]. Our study shows that coherent F-QPSK is 2.5 dB more robust than noncoherent GMSK in a cellular mobile environment. Fig.8 shows that while F-QPSK requires only C/I=15.7dB for BER $P_e = 10^{-2}$, GMSK BT=0.5 requires C/I=18.2dB.

5 Capacity in cellular environment.

In microcellular PCS systems, frequencies are reused in geographically separate cells to achieve greater network capacity [8]. In this environment, we need to include the frequency reuse factor K [9] when comparing modulations. Suzuki and Hirade's definition of the overall spectral efficiency η_T (b/s/Hz/m²) of a modulation in a cellular environment is given by [9]:

$$\eta_T = \eta_f \times \frac{1}{K} \times \frac{1}{S} \quad (6)$$

where η_f is the modulation's spectral efficiency with respect to frequency (in b/s/Hz) and S is the coverage area of a cell (m²).

ACI of F-QPSK & GMSK.
 F-QPSK: Butterw'th BPF (4 ord), $BiT_b=0.55$
 GMSK: Gaussian BPF (4 ord), $BiT_b=0.6$.

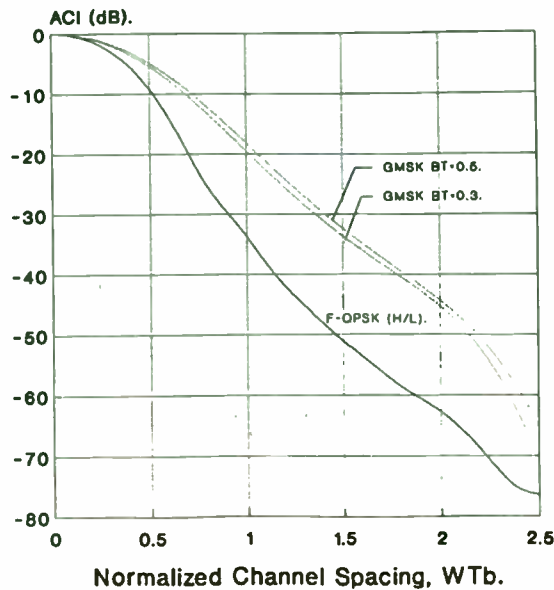


Fig. 5 ACI characteristics of F-QPSK and GMSK as function of normalized channel spacing WT_b . F-QPSK employs Butterworth (4th order) receive BPF with $BiT_b = 0.55$. GMSK employs Gaussian (4th order) receive BPF with $BiT_b = 0.6$.

B.E.R. of coherent F-QPSK & noncoherent GMSK BT=0.5 (DECT) in AWGN.

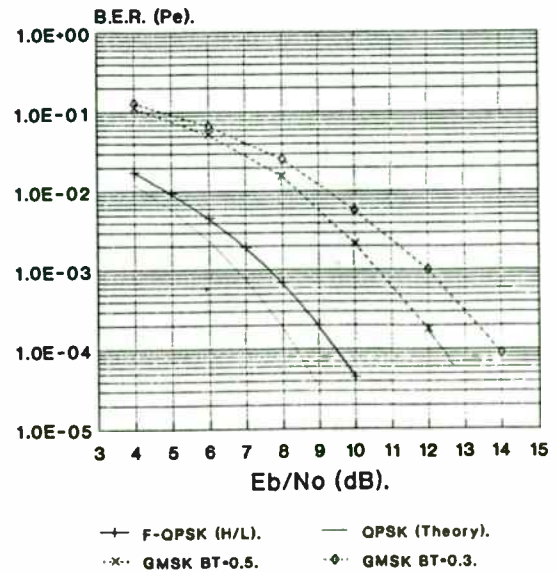


Fig. 6 BER performance of coherent F-QPSK and noncoherent GMSK in Gaussian noise channel.

B.E.R. of coherent F-QPSK & noncoherent GMSK BT=0.5 (DECT) in Rayleigh fading.

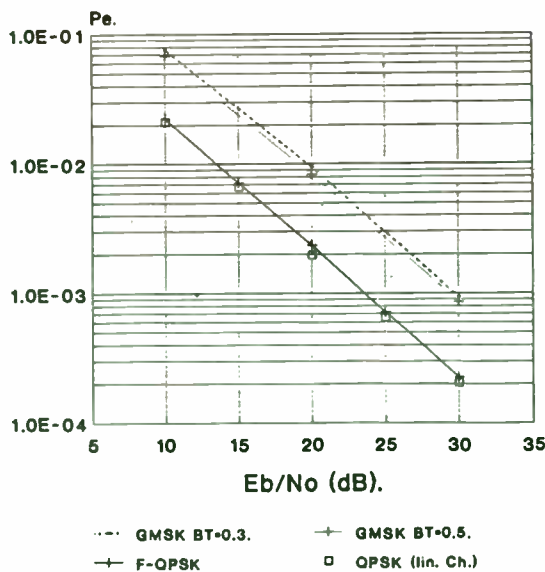


Fig. 7 BER performance of coherent F-QPSK and noncoherent GMSK in slow Rayleigh fading.

C/I characteristics of coherent F-QPSK and noncoherent GMSK BT=0.5 (DECT).

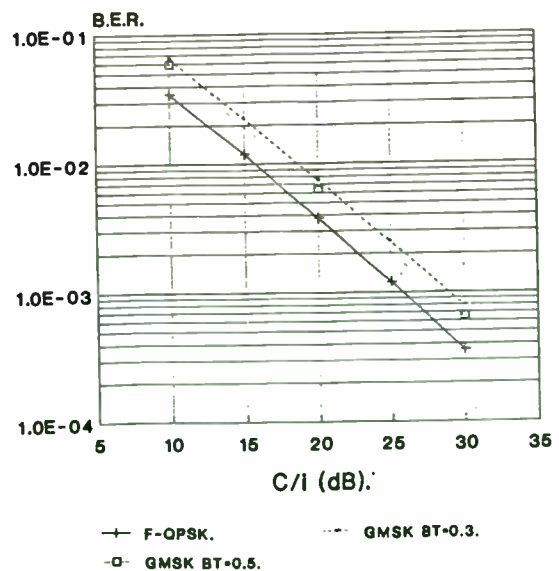


Fig. 8 C/I performance of coherent F-QPSK and noncoherent GMSK in slow Rayleigh fading.

The frequency reuse factor K (cells/cluster) is an integer [9]:

$$K = \frac{1}{3}[1 + (M_f \Lambda)^{\frac{1}{\gamma}}]^2 \quad (7)$$

where Λ is the C/I ratio required for a given BER performance. γ is the propagation constant whose value ranges between 2 and 4, and M_f is the C/I margin. The value of K is related to the normalized frequency reuse distance D by the formula $K = \frac{D^2}{3}$ although only some discrete values of K are possible. The allowable values are $K = (i + j)^2 - ij$ where i and j are positive integers including zero (ie. $K=1,3,4,7,9,12$ etc.) [12,8].

In this analysis, we assume (i) a BER of 10^{-2} for acceptable quality voice, (ii) $\gamma = 0.35$ and (iii) a fade margin of $M_f=3$ dB. This margin corresponds to a geographical outage probability of approximately 10% [9]. Furthermore, without loss of generality, we let $S=1$ m^2 .

The total spectral efficiency η_T of the proposed F-QPSK scheme and GMSK in a micro-cellular mobile PCS communications environment are compared in Table 2. For ease of comparison, we also list the modulations' relative total spectral efficiency, using GMSK BT=0.5 as used in DECT for reference base (100%). This comparison serves as an indicator of the network's capacity.

	η_f	Λ for $P_e=10^{-2}$	K	η_T
F-QPSK	1.42	15.7 dB.	7	0.203 (195%)
GMSK BT=0.3	0.98	18.9 dB.	12	0.082 (79%)
GMSK BT=0.5	0.94	17.7 dB.	9	0.104 (100%)

Table 2, η_T in b/s/Hz/ m^2 .

Table 2 shows that the combined spectral efficiency η_f of F-QPSK and its CCI advantage over the noncoherent GMSK leads to a 95% increase of the overall spectral efficiency η_T in a cellular mobile environment. This demonstrates that our proposed F-QPSK modem radio solution can nearly double (95% increase) the capacity of DECT.

6 Conclusion.

In this paper, we propose a low-cost coherent F-QPSK modem radio technique that is ideal for the emerging personal communications services (PCS) standard. F-QPSK is a power efficient digital modulation. Being with a constant signal envelope, it can operate

with class C power amplifier without output backoff (OBO) and hence is 4 to 8 dB more power efficient than the $\frac{\pi}{4}$ DQPSK as used in the current US IS-54 and the Japanese Digital Cellular standards.

The ACI characteristics, spectral efficiency in b/s/Hz/m^2 and BER performance of F-QPSK in mobile communications environment have been investigated using computer simulation. The results are compared with GMSK. We show that F-QPSK has an attainable spectral efficiency of 1.42 b/s/Hz, based on the ACI = -20dB criterion. This is up to 51% more spectrally efficient than the GMSK BT=0.5 as used in DECT. Coherent F-QPSK also has superior BER performance characteristics. Our research shows that it is 5.5 dB better than noncoherent GMSK in E_b/N_0 over Rayleigh fading channels, and it is 2.5 dB more robust in a CCI controlled environment.

The impact of using F-QPSK in a microcellular PCS environment is also investigated. We show by numerical example that coherent F-QPSK is up to 95% more spectrally efficient than noncoherent GMSK BT=0.5. This means that our F-QPSK modem radio solution could nearly double (95% increase) the capacity of DECT.

We conclude that F-QPSK's high spectral efficiency and superior BER performance in both Rayleigh fading and CCI controlled channels make it an excellent choice for the future generation high capacity microcellular mobile PCS networks.

Acknowledgement.

Financial supports from Ericsson/GE, NASA, TRW, the University of California, Davis MICRO program and other industrial sponsors to our research are gratefully acknowledged.

Copyrighted reference material.

Most of the material contained in this paper is based on and is closely related to the copyrighted material by the authors, reference [19,20]. This material will appear in a forthcoming book [19] and also in journal/magazine publications.

References

- [1] S. Ginn, "Personal Communications Services: Expanding the freedom to communicate", *IEEE Communications Magazine*, Vol.29, No.2, pp.30-39, February 1991.
- [2] J.S. Bryan, "PCN: prospects in United States", *Telecommunications*, Vol.25, No.1, pp.54-56, January 1991.
- [3] T. Rappaport, "The wireless Revolution", *IEEE Communications Magazine*, pp.52-71, Nov. 1991.
- [4] T. Le-Ngoc, S. Slimane, "IJF-OQPSK modulation schemes with MLSE receivers for portable/mobile communications," *Proc. IEEE 42nd. Veh. Tech. Conference*, pp.676-680, Denver 1992.
- [5] K. Murota, K. Hirade. "GMSK modulation for digital mobile radio telephony", *IEEE Trans. on Comm.* Vol. COM-29, No.7, pp.1044-1050, July 1981.
- [6] J. Seo, K. Feher. "SQAM: A new superposed QAM modem technique", *IEEE Trans. on Comm.* Vol. COM-33, N0.3, pp.296-300, March 1985.
- [7] C.S. Lindquist. "Active network design with signal filtering applications", *Steward and Sons* 1977.
- [8] W.C.Y. Lee. "Mobile cellular telecommunications systems", McGraw Hill, 1989.
- [9] K. Feher. "Advanced Digital Communications Systems and Signal Processing Techniques.", Prentice-Hall, Englewood Cliff, NJ, 1987.
- [10] EIA IS54 Dual-mode subscriber equipment - Network equipment compatibility specification. December 1989.
- [11] DECT Specification. Physical Layer, CI SPEC Part 1, Rev 06.0.
- [12] R.C. French. "The effect of fading and shadowing on channel reuse in mobile radio". *IEEE Trans. on Vehicular Technology*, Vol. VT-28, No.3, pp.171-181, Aug. 1979.
- [13] T. Le-Ngoc, K. Feher, H. Phamvan, "New modulation techniques for low-cost power and bandwidth efficient satellite earth stations", *IEEE Trans. Comm.* Vol. COM-30, No.1, pp.275-283, Jan. 1982.
- [14] K. Feher, "Digital communications satellite/earth station engineering", Prentice-Hall 1983.
- [15] D. Fague, "Integrated circuit solutions - Design considerations for DECT", *Proc. IEEE Vehicular Technology Conference*, pp.101-103, Denver 1992.

- [16] K. Ohno, F. Adachi, "Half-bit offset decision frequency detection of differentially encoded GMSK signals", *Electronics Letters*, Vol.23, no.24, pp.1311-1312, Nov. 19, 1987.
- [17] Y. Guo, K. Feher, "Frequency hopping F-QPSK for power and spectrally efficient cellular systems", submitted to IEEE Vehicular Technology conference, 1993.
- [18] K. Feher, "Filter: Nonlinear Digital", U.S. Patent No. 4,339,724, issued July 13, 1982; Canada No. 1130871, August 31, 1982.
- [19] K. Feher, "Cellular Digital PCS-Mobile Radio Communications", forthcoming book. Copyrighted.
- [20] P.S.K. Leung, "GMSK and F-QPSK for high capacity cellular mobile and microcellular personal communications systems", forthcoming Ph.D. thesis, University of California, Davis, 1993.



